NUREG/CP-0097
Vol. 4
R4

Proceedings of the U.S. Nuclear Regulatory Commission

# Sixteenth Water Reactor Safety Information Meeting

Volume 4
- Code Uncertainty for ECCS Rule
- International Code Assessment Program
- Thermal Hydraulics
- 2D/3D Data Applications

Held at
National Institute of Standards and Technology
Gaithersburg, Maryland
October 24-27, 1988

Date Published: March 1989

Compiled by: Allen J. Weiss

**Office of Nuclear Regulatory Research**
**U.S. Nuclear Regulatory Commission**
**Washington, DC 20555**

Proceedings prepared by
Brookhaven National Laboratory

ABSTRACT

This five-volume report contains 141 papers out of the 175 that were presented at the Sixteenth Water Reactor Safety Information Meeting held at the National Institute of Standards and Technology, Gaithersburg, Maryland, during the week of October 24-27, 1988. The papers are printed in the order of their presentation in each session and describe progress and results of programs in nuclear safety research conducted in this country and abroad. Foreign participation in the meeting included twenty different papers presented by researchers from Germany, Italy, Japan, Sweden, Switzerland, Taiwan and the United Kingdom. The titles of the papers and the names of the authors have been updated and may differ from those that appeared in the final program of the meeting.

PROCEEDINGS OF THE
16th WATER REACTOR SAFETY INFORMATION MEETING

October 24-27, 1988

Published in Five Volumes

## GENERAL INDEX


VOLUME 1
- Plenary Session
- Decontamination and Decommissioning
- License Renewal
- Human Factors
- Generic Issues
- Risk Analysis/PRA Applications
- Innovative Concepts for Increased Safety of Advanced Power Reactors

VOLUME 2
- Industry Safety Research
- Non-Destructive Evaluation
- Materials Engineering
  - Pressure Vessel Research
  - Radiation Effects
  - Degraded Piping

VOLUME 3
- Nuclear Plant Aging
- Structural and Seismic Engineering
- Mechanical Research
- Environmental Effects in Primary Systems

VOLUME 4
- Code Uncertainty for ECCS Rule
- International Code Assessment Program
- Thermal Hydraulics
- 2D/3D Data Applications

VOLUME 5
- NUREG-1150
- Accident Management
- Recent Advances in Severe Accident Research
- TMI-2
- BWR Mark I Shell Failure

REGISTERED ATTENDEES (NON-NRC)
16th WATER REACTOR SAFETY INFORMATION MEETING

J. A. ADAM
STONE & WEBSTER
245 SUMMER ST
BOSTON MA 02107
USA

S. L. ADDITON
TENERA
2011 EYE STREET N.W., SUITE 300
WASHINGTON DC 20006
USA

M. J. ADES
SAVANNAH RIVER LABORATORY
BLDG. 773-43A
AIKEN SC 29808
USA

D. W. AKERS
EG&G IDAHO INC.
P.O. BOX 1625
IDAHO FALLS ID 83415
USA

H. AKIMOTO
JAPAN ATOMIC RESEARCH INST.
TOKAI-MURA, NAKA-GUN
IBARAKI-KEN 319-11
JAPAN

N. S. AKSAN
PAUL SCHERRER INSTITUTE
WUERENLINGEN CH5303
SWITZERLAND

R. P. ALLEN
PACIFIC NORTHWEST LABORATORY
P.O. BOX 999
RICHLAND WA 99352
USA

R. A. ALLEN
SAVANNAH RIVER LABORATORY
AIKEN SC 29808
USA

K. ALMENAS
UNIVERSITY OF MARYLAND
COLLEGE PARK MD 20742
USA

A. ALONSO
MADRID POLYTECHNIC UNIVERSITY
JOSE GUTIERREZ ABASCAL,2
MADRID 28006
SPAIN

H. ALSMEYER
KERNFORSCHUNGSZENTRUM, IRB/PRS
POSTFACH 3640
7500 KARLSRUHE 1
FRG

J. G. ANDERSEN
GENERAL ELECTRIC CO.
175 CURTNER AVE
SAN JOSE CA 95125
USA

J. M. ANDERSON
BECHTEL POWER CORP.
15740 SHADY GROVE ROAD
GAITHERSBURG MD 20874
USA

K. B. ANDERSSON
SWEDISH NUCLEAR POWER INSPECTORATE
BOX 27016
STOCKHOLM SW S-10252
SWEDEN

C. E. APPERSON
SAVANNAH RIVER LABORATORY
1635 ALPINE DR.
AIKEN SC 29801
USA

K. J. ARAJ
BDM
7915 JONES BRIDGE DRIVE
MCLEAN VA 22102
USA

W. C. ARCIERI
ENSA
15825 SHADY GROVE ROAD
ROCKVILLE MD 20850
USA

W. W. ASCROFT-HUTTON
HMNI
BAYNARDS HOUSE/WESTBOURNE GROVE
LONDON ENGLAND W2 4TF
UK

B. ATEFI
SCIENCE APPLICATIONS INT'L CORP.
1710 GOODRIDGE DR.
MCLEAN VA 22102
USA

N. I. AVDOSHKIN
USSR EMBASSY
1125 16TH ST NW
WASHINGTON DC 20036

S. M. BAJOREK
WESTINGHOUSE POWER SYSTEMS DIVISION
P.O. BOX 355
PITTSBURGH PA 15230-2728
USA

K. K. BANDYOPADHYAY
BROOKHAVEN NATIONAL LABORATORY
BLDG 129
UPTON NY 11973
USA

R. A. BARI
BROOKHAVEN NATIONAL LABORATORY
BLDG. 197C
UPTON NY 11973
USA

G. P. BAROIS
FRAMATOME
TOUR FIAT - CEDEX 16
PARIS LA DEFENSE FR 92084
FRANCE

J. H. BARON
MADRID POLYTECHNICAL UNIVERSITY
JOSE GUTIERREZ ABASCAL,2
MADRID 28006
SPAIN

B. R. BASS
OAK RIDGE NATIONAL LABORATORY
PO BOX 2003
OAK RIDGE TN 37831
USA

J. A. BAST
GENERAL ELECTRIC CO.
P.O. BOX 1072, BLDG. F3-8
SCHENECTADY NY 12301
USA

P. D. BAYLESS
EG&G IDAHO INC.
P.O. BOX 1625
IDAHO FALLS ID 83415
USA

P. BEDNARIK
SCIENCE & TECHNOLOGY
3900 LINNEAN AVE., NW
WASHINGTON DC 20008
CZECHOSLOVAKIA

K. D. BERGERON
SANDIA NATIONAL LABS.
P.O. BOX 5800
ALBUQUERQUE NM 87185
USA

R. F. BEYER
WESTINGHOUSE
206 NAVAJO RD.
PITTSBURGH PA 15241
USA

V. M. BHARGAVA
VIRGINIA POWER
5000 DOMINION BLVD.
GLEN ALLEN VA 23060
USA

W. BINNER
AUSTRIAN RESEARCH CENTER
SEIBERSDORF A-2444
AUSTRIA

D. P. BIRMINGHAM
BABCOCK & WILCOX CO.
1562 BEESON STREET
ALLIANCE OH 44601
USA

D. BIZZAK
CARNEGIE-MELLON UNIVERSITY
386 HUNTINGDON AVENUE
N. HUNTINGDON PA 15642
USA

R. J. BOHL
LOS ALAMOS NATIONAL LABORATORY
P.O. BOX 1663, MS K560
LOS ALAMOS NM 87545
USA

T. C. BORDINE
CONSUMERS POWER COMPANY
1945 WEST PARNALL RD.
JACKSON MI 49201
USA

R. B. BORSUM
BABCOCK & WILCOX CO.
1700 ROCKVILLE PIKE, #525
ROCKVILLE MD 20852
USA

B. E. BOYACK
LOS ALAMOS NATIONAL LAB
PO BOX 1663
LOS ALAMOS NM 87545
USA

D. R. BRADLEY
SANDIA NATIONAL LABS.
P.O. BOX 5800
ALBUQUERQUE NM 87185
USA

R. J. BRANDON
GE NUCLEAR CORP
6728 LOOKOUT BEND
SAN JOSE CA 95120
USA

P. A. BRATBY
NATIONAL NUCLEAR CORP.
BOOTHS HALL, CHELFORD ROAD
KNUTSFORD
UK

R. J. BREEDING
SANDIA NATIONAL LABS., DIV. 6410
P.O. BOX 5800
ALBUQUERQUE NM 87185
USA

S. J. BRETT
CEGB, GENERATION DEV. & CONSTRUCTION
GEN. DEV. & CONST. DIV., BARNWOOD
GLOUCESTER GL47RS
UK

I. BRITTAIN
UKAEA/AEE WINFRITH
DOERCHESTER
DORSET DT28DH
UK

J. M. BROUGHTON
EG&G IDAHO INC.
P.O. BOX 1625
IDAHO FALLS ID 83415
USA

S. BRYANT
CENTRAL ELECTRICITY GENERATING BD.
BOOTHS HALL, CHELFORD RD
KNUTSFORD, CHESHIRE WA168QG
UK

C. E. BUCHHOLZ
GENERAL ELECTRIC CO.
175 CURTNER AVE
SAN JOSE CA 95125
USA

B. BUESCHER
EG&G IDAHO INC.
P.O. BOX 1625
IDAHO FALLS ID 83415
USA

L. C. BUFFARDI
GEORGE MASON UNIVERSITY
4400 UNIVERSITY DRIVE
FAIRFAX VA 22030
USA

J. D. BYRON
ELECTRIC POWER RESEARCH INSTITUTE
3412 HILLVIEW AVE.
PALO ALTO CA 94303
USA

J. I. CALVO
CONSEJO SEGURIDAD NUCLEAR
SOR ANGELA DE LA CRUZ 3
MADRID 28020
SPAIN

A. L. CAMP
SANDIA NATIONAL LABS. DIV. 6412
P.O. BOX 5800
ALBUQUERQUE NM 87185
USA

D. D. CARLSON
SANDIA NATIONAL LABS, DIV. 6513
P.O. BOX 5800
ALBUQUERQUE NM 87185
USA

R. CARO
CONSEJO DE SEGURIDAD NUCLEAR
C/SOR ANGELA DE LA CRUZ, 3
MADRID 28020
SPAIN

D. E. CARROLL
SANDIA NATIONAL LABS.
P.O. BOX 5800
ALBUQUERQUE NM 87185
USA

R. CARUSO
NUCLEAR ENERGY AGENCY
38 BLVD. SUCHET
PARIS 75016
FRANCE

D. A. CASADA
OAK RIDGE NATIONAL LABORATORY
PO BOX 2009, BLDG. 9104-1
OAK RIDGE TN 37831
USA

J. H. CHA
KOREA ADVANCED ENERGY RESEARCH INST.
PO BOX 7, DAEDUK-DANJI
TAEJON CHUNG-NAM
KOREA

S. CHAKRABORTY
PAUL SCHERRER INSTITUTE
WUERENLINGEN CH5303
SWITZERLAND

R. CHAMBERS
EG&G IDAHO INC.
P.O. BOX 1625
IDAHO FALLS ID 83415
USA

Y. I. CHANG
ARGONNE NATIONAL LABORATORY
9700 S. CASS AVE.
ARGONNE IL 60439
USA

D. CHAPIN
MPR ASSOCIATES, INC.
1050 CONNECTICUT AVENUE, N.W.
WASHINGTON DC 20036
USA

S. C. CHENG
TAIWAN POWER COMPANY
TAIPEI

ROC

L. Y. CHENG
BROOKHAVEN NATIONAL LABORATORY
BLDG 703
UPTON NY 11973
USA

R. D. CHEVERTON
OAK RIDGE NATIONAL LABORATORY
PO BOX 2009
OAK RIDGE TN 37831
USA

W. G. CHOE
TU ELECTRIC
400 N. OLIVE STREET
DALLAS TX 75201
USA

O. K. CHOPRA
ARGONNE NATIONAL LABORATORY
9700 S. CASS AVE., BLDG 335
ARGONNE IL 60439
USA

B. CHUNG
KOREA ADVANCED ENERGY RESEARCH INST.
NSC, DAE DUK DAN-JI, BOX 7
CHOONG-NAM
KOREA

D. T. CHUNG
SCIENTECH
11821 PARKLAWN DR.
ROCKVILLE MD 20878
USA

H. CHUNG
ARGONNE NATIONAL LABORATORY
9700 S. CASS AVE.
ARGONNE IL 60439
USA

J. P. CHURCH
SAVANNAH RIVER LABORATORY
BLDG. 773-41A
AIKEN SC 29808
USA

D. B. CLAUSS
SANDIA NATIONAL LABS. DIV. 6442
P.O. BOX 5800
ALBUQUERQUE NM 87122
USA

M. COLAGROSSI
ENEA/DISP
VIA VITALIANO BRANCATI, 48
ROME 00144
ITALY

M. W. CONEY
CENTRAL ELECTRICITY GENERATING BD.
C.E.R.L., KELVIN AVENUE
LEATHERHEAD SURREY KT227SE
UK

W. R. CORWIN
OAK RIDGE NATIONAL LABORATORY
PO BOX 2009
OAK RIDGE TN 37831
USA

D. CROUCH
BROOKHAVEN NATIONAL LABORATORY
BLDG. 130
UPTON NY 11973
USA

W. H. CULLEN
MATERIALS ENGINEERING ASSOCIATES
9700-B M. L. KING HIGHWAY
LANHAM MD 20706
USA

G. E. CUMMINGS
LAWRENCE LIVERMORE NATIONAL LAB
P.O. BOX 808, L-198
LIVERMORE CA 94526
USA

H. D. CURET
ADVANCED NUCLEAR FUELS
2101 HORN ROAD
RICHLAND WA 99352
USA

B. D. CURRY
PHILADELPHIA ELECTRIC CO.
PO BOX A SARATOGA BR.
POTTSTOWN PA 19464
USA

R. A. CUSHMAN
NIAGRA MOHAWK POWER CORP
301 PLAINHELD ROAD
SYRACUSE NY 13212
USA

D. A. DAHLGREN
SANDIA NATIONAL LABS., ORG. 6440
P.O. BOX 5800
ALBUQUERQUE NM 87123
USA

J. DALLMAN
EG&G IDAHO INC.
P.O. BOX 1625
IDAHO FALLS ID 83415
USA

R. DAMERON
ANATECH
10975 TORREYANA RD., SUITE 301
SAN DIEGO CA 92121
USA

J. DARLASTON
CENTRAL ELECTRICITY GENERATING BD.
BERKLEY NUCLEAR LABS
GLOUCESTER GL139PB
UK

W. L. DAUGHERTY
SAVANNAH RIVER LABORATORY
PO BOX A
AIKEN SC 29808
USA

N. W. DAVIES
UKAEA, RISLEY LABORATORY
WARRINGTON
CHESHIRE WA3 6AT
UK

M. A. DAYE
BECHTEL POWER CORP.
15740 SHADY GROVE RD.
GAITHERSBURG MD 20877
USA

J. A. DE MASTRY
FLORIDA POWER AND LIGHT CO.
BOX 14000
JUNO BEACH FL 33408
USA

L. O. DelGEORGE
COMMONWEALTH EDISON
P.O. BOX 767
CHICAGO IL 60690
USA

L. V. DeWITT
SAVANNAH RIVER LABORATORY
1313 WILLIAMS DR.
AIKEN SC 29801
USA

M. DIMARZO
UNIVERSITY OF MARYLAND
MECHANICAL ENGINEERING DEPT.
COLLEGE PARK MD 20016
USA

M. R. DINSEL
BECHTEL POWER CORP.
15740 SHADY GROVE ROAD
GAITHERSBURG MD 20874
USA

S. R. DOCTOR
PACIFIC NORTHWEST LABORATORY
P.O. BOX 999
RICHLAND WA 99352
USA

C. V. DODD
OAK RIDGE NATIONAL LABORATORY
PO BOX 2008
OAK RIDGE TN 37831
USA

T. F. DORIAN
DOUB, MUNTZING & GLASGOW, CHARTERED
808 17TH STREET, N. W., SUITE 400
WASHINGTON DC 20006
USA

J. DRCEC
NPP KRSKO
PO VRBINA 12
KRSKO 68270
YUGOSLAVIA

S. S. DUA
GENERAL ELECTRIC
M/C 769, 175 CURTNER AVE.
SAN JOSE CA 95125
USA

S. W. DUCE
EG&G IDAHO INC.
P.O. BOX 1625
IDAHO FALLS ID 83415
USA

J. J. DUCO
CEA FRENCH ATOMIC ENERGY COMMISSION
DAS/SASC,CEN/FAR, BP NO. 6
FONTENAY-AUX-ROSES 92265
FRANCE

R. B. DUFFEY
EG&G IDAHO INC.
P.O. BOX 1625
IDAHO FALLS ID 83415
USA

K. K. DWIVEDY
VIRGINIA POWER
5000 DOMINION BLVD.
GLEN ALLEN VA 23060
USA

J. L. EDSON
EG&G IDAHO INC.
P.O. BOX 1625
IDAHO FALLS ID 83415
USA

G. R. EIDAM
BECHTEL/GPUN
P.O. BOX 72
MIDDLETOWN PA 17057
USA

D. M. EISSENBERG
OAK RIDGE NATIONAL LABORATORY
PO BOX 2009, BLDG. 9104-1
OAK RIDGE TN 37831
USA

Z. J. ELAWAR
ARIZONA NUCLEAR POWER PROJECT, 7202
P.O. BOX 52034
PHOENIX AZ 85072
USA

G. ELETTI
ENEA/DISP
VIA VITALIANO BRANCATI, 48
ROME 00144
ITALY

F. A. ELIA
STONE AND WEBSTER
PO BOX 2325
BOSTON MA 02014
USA

G. T. EMBLEY
GENERAL ELECTRIC
BOX 1092
SCHENECTADY NY 12301
USA

T. C. ENG
DEPARTMENT OF ENERGY
EH-35, MAIL STOP F-137
WASHINGTON DC 20545
USA

R. G. ESPEFALT
SWEDISH STATE POWER BD.
VATTENFALL
VALLINGBY S-16287
SWEDEN

C. R. FARRAR
LOS ALAMOS NATIONAL LAB.
MS J576
LOS ALAMOS NM 87545
USA

H. E. FILACCHIONE
SCIENTECH
11821 PARKLAWN DR.
ROCKVILLE MD 20878
USA

S. R. FISCHER
MIDDLE SOUTH UTILITIES
188 E. CAPITOL STREET, SUITE 600
JACKSON MS 39201
USA

R. G. FITZPATRICK
BROOKHAVEN NATIONAL LABORATORY
BLDG 130
UPTON NY 11973
USA

C. W. FORSBERG
OAK RIDGE NATIONAL LABORATORY
P.O. BOX 2008, BLDG 4500N
OAK RIDGE TN 37831
USA

E. FOX
OAK RIDGE NATIONAL LABORATORY
P.O. BOX 2009
OAK RIDGE TN 37831-8063
USA

G. FREI
SIEMENS
HAMMERBACHERSTR. 12
ERLANGEN 852
FRG

B. C. FRYER
ADVANCED NUCLEAR FUELS
1930 CYPRESS
RICHLAND WA 99352
USA

H. FUJIMOTO
COMPUTER SOFTWARE DEVELOPMENT CO.
4-1,SHIBAKOUEN 2-CHOME,MINATO-KU
TOKYO 105
JAPAN

P. J. FULFORD
NUS CORPORATION
910 CLOPPER ROAD
GAITHERSBURG MD 20878
USA

R. R. FULLWOOD
BROOKHAVEN NATIONAL LABORATORY
BLDG 130
UPTON NY 11973
USA

F. M. GANTENBEIN
CEA FRENCH ATOMIC ENERGY COMMISSION
CEN-SACLAY DEMT/SMTS/EMSI
GIF-SUR-YVETTE 91191
FRANCE

F. GELBARD
SANDIA NATIONAL LABS.
P.O. BOX 5800
ALBUQUERQUE NM 87185
USA

D. I. GERTMAN
EG&G IDAHO INC.
P.O. BOX 1625
IDAHO FALLS ID 83415
USA

T. GINSBERG
BROOKHAVEN NATIONAL LABORATORY
BLDG 820
UPTON NY 11973
USA

T. GINZBURG
APPLIED BIOMATHEMATICS INC.
100 NORTH COUNTRY ROAD
SETAUKET NY 11733
USA

B. GITNICK
ENSA, INC.
15825 SHADY GROVE RD., STE. 120
ROCKVILLE MD 20850
USA

H. G. GLAESER
GESELLSCHAFT FUR REAKTORSICHERHEIT
FORSCHUNGSGELANDE
D-8046 GARCHING
FRG

J. GLEASON
WYLE LABORATORY
7800 GOVERNORS DRIVE WEST
HUNTSVILLE AL 35807
USA

D. W. GOLDEN
EG&G IDAHO INC.
P.O. BOX 1625
IDAHO FALLS ID 83415
USA

M. GOMOLINSKI
CEA FRENCH ATOMIC ENERGY COMMISSION
CEN/FAR, BP NO. 6
FONTENAT-AUX-ROSES 92265
FRANCE

C. GONZALEZ
MADRID POLYTECHNICAL UNIVERSITY
JOSE GUTIERREZ ABASCAL,2
MADRID 28006
SPAIN

E. D. GORHAM-BERGERON
SANDIA NATIONAL LABS.
P.O. BOX 5800
ALBUQUERQUE NM 87185
USA

T. C. GORRELL
SAVANNAH RIVER LABORATORY
RX TECH, DU PONT (SRP)
AIKEN SC 29808
USA

G. A. GREENE
BROOKHAVEN NATIONAL LABORATORY
BLDG. 820M
UPTON, NY 11973
USA

P. GRIFFITH
MIT
ROOM 7-044
CAMBRIDGE MA 02139
USA

F. GRIMM
SIEMENS
HAMMERBACHERSTR. 12
ERLANGEN 852
FRG

C. GRIMSHAW
BROOKHAVEN NATIONAL LABORATORY
BLDG. 130
UPTON NY 11973
USA

W. W. GUNTHER
BROOKHAVEN NATIONAL LABORATORY
BLDG 130
UPTON NY 11973
USA

S. HABER
BROOKHAVEN NATIONAL LABORATORY
BLDG. 130
UPTON NY 11973
USA

D. R. HAFFNER
WESTINGHOUSE HANFORD CO.
P.O. BOX 1970 A3-30
RICHLAND WA 99352
USA

F. M. HAGGAG
OAK RIDGE NATIONAL LABORATORY
P.O. BOX 2008, BLDG 4500-S
OAK RIDGE TN 37831-6151
USA

A. N. HALL
HM NUCLEAR INSTALLATIONS INSPECTORATE
ST PETER'S HOUSE, BALLIOL RD
BOOTLE,MERSEYSIDED L203LZ
UK

R. J. HAMMERSLEY
FAUSKE & ASSOCIATES
16W070 WEST 83RD STREET
BURR RIDGE IL 60521
USA

A. M. HASHIMOTO
JAPAN INST. OF NUCLEAR SAFETY
3-17-1 TOYANOMON
MINATOKU, TOKYO 105
JAPAN

Y. A. HASSAN
DEPT OF NUCL ENERGY, TEXAS A & M
COLLEGE STATION TX 77843
USA

J. R. HAWTHORNE
MATERIALS ENGINEERING ASSOCIATES
9700-B M. L. KING HIGHWAY
LANHAM MD 20706
USA

H. D. HAYNES
OAK RIDGE NATIONAL LABORATORY
PO BOX 2009, BLDG. 9201-3
OAK RIDGE TN 37831
USA

J. HAZELTINE
WYLE LABORATORY
7800 GOVERNORS DRIVE WEST
HUNTSVILLE AL 35807
USA

R. E. HENRY
FAI
16W070 WEST 83RD STREET
BURR RIDGE IL 60521
USA

G. F. HEWITT
UKAEA/HARWELL LABORATIRY
THERMAL HYDRAULICS DIV, BLDG 392
OXON OX11 ORA
UK

J. HIBBARD
MPR ASSOCIATES, INC.
1050 CONNECTICUT AVENUE, N.W.
WASHINGTON DC 20036
USA

D. E. HIDINGER
GENERAL ELECTRIC
14 CORONET CT.
SCHENECTADY NY 12309
USA

J. C. HIGGINS
BROOKHAVEN NATIONAL LABORATORY
BLDG 130
UPTON NY 11973
USA

C. J. HIGGINS
APPLIED RESEARCH ASSOCIATES, INC.
4300 SAN MATEO NE, STE B 380
ALBUQUERQUE NM 87111
USA

P. R. HILL
PENNSYLVANIA POWER & LIGHT CO.
2 N. NINTH STREET
ALLENTOWN PA 18101
USA

J. E. HINTON
DU PONT DE NEMOURS
SRP 707-C, RM. 329
AIKEN SC 29808
USA

T. J. HIRONS
LOS ALAMOS NATIONAL LABORATORY
P.O. BOX 1663, MS E561
LOS ALAMOS NM 87545
USA

M. HIROSE
NUCLEAR POWER ENG'G TEST CTR
FUJITA KMKO BLDG., TORANOMON, MINATO-
TOKYO 105
JAPAN

S. A. HODGE
OAK RIDGE NATIONAL LABORATORY
PO BOX 2009, BLDG. 9104-1
OAK RIDGE TN 37831
USA

P. G. HOFMANN
KERNFORSCHUNGSZENTRUM, IMF
POSTFACH 3640
7500 KARLSRUHE
FRG

C. H. HOFMAYER
BROOKHAVEN NATIONAL LABORATORY
BLDG 129
UPTON NY 11973
USA

G. S. HOLMAN
LAWRENCE LIVERMORE NATIONAL LAB
P.O. BOX 808, L-197
LIVERMORE CA 94550
USA

K. R. HOOPINGARNER
PACIFIC NORTHWEST LABORATORY
P.O. BOX 999
RICHLAND WA 99352
USA

R. G. HOPPE
WESTINGHOUSE ELECTRIC CORP
P.O. BOX 79
W MIFFLIN PA 15122
USA

K. G. HORNBERGER
OAK RIDGE NATIONAL LABORATORY
P.O. BOX 2009
OAK RIDGE TN 37831-8056
USA

P. J. HOSEMANN
PAUL SCHERRER INSTITUTE
WUERENLINGEN CHS303
SWITZERLAND

B. J. HSEIH
ARGONNE NATIONAL LABORATORY
9700 SO CASS AVE.
ARGONNE IL 60439
USA

A. H. HSIA
URA
240 MONROE STREET
ROCKVILLE MD 20854
USA

H-N HSIAU
TAIWAN POWER COMPANY
TAIPEI TAIWAN
ROC

K. HU
BROOKHAVEN NATIONAL LABORATORY
BLDG. 475B
UPTON NY 11973
USA

D. S. HUMPHRIES
SCIENTECH
11821 PARKLAWN DR.
ROCKVILLE MD 20852
USA

M. L. HYDER
SAVANNAH RIVER LABORATORY
AIKEN SC 29808
USA

C. R. HYMAN
OAK RIDGE NATIONAL LABORATORY
PO BOX 2009, BLDG. 9104-1
OAK RIDGE TN 37831
USA

T. IGUCHI
JAPAN ATOMIC RESEARCH INST.
TOKAI-MURA, NAKA-GUN
IBARAKI-KEN 319-11
JAPAN

R. L. IMAN
SANDIA NATIONAL LABS. DIV 6415
P.O. BOX 5800
ALBUQUERQUE NM 87185
USA

J. R. IRELAND
LOS ALAMOS NATIONAL LAB
PO BOX 1663, MSK 551
LOS ALAMOS NM 87544
USA

M. ISHII
PURDUE UNIVERSITY
WEST LAFAYETTE ID
USA

S. K. ISKANDER
OAK RIDGE NATIONAL LABORATORY
P.O. BOX 2008
OAK RIDGE TN 37831-6151
USA

R. IVANY
COMBUSTION ENGINEERING, INC.
1000 PROSPECT HILL RD.
WINDSOR CT 06095
USA

J. M. IZQUIERDO
CONSEJO SEGURIDAD NUCLEAR
SOR ANGELA DE LA CRUZ 3
MADRID 28020
SPAIN

M. J. JACOBUS
SANDIA NATIONAL LABS., DIV. 6447
P.O. BOX 5800
ALBUQUERQUE NM 87185
USA

J. F. JANSKY
BTB-LEONBERG
RILKESTRASSE 5
LEONBERG D-7250
FRG

D. B. JARRELL
PACIFIC NORTHWEST LABORATORY
P.O. BOX 999
RICHLAND WA 99352
USA

G. W. JOHNSEN
EG&G IDAHO INC.
P.O. BOX 1625
IDAHO FALLS ID 83415
USA

A. B. JOHNSON
PACIFIC NORTHWEST LABORATORY
P.O. BOX 999
RICHLAND WA 99352
USA

E. R. JOHNSON
WESTINGHOUSE ELECTRIC CORP.
P.O. BOX 2728
PITTSBURGH PA 15230-2728
USA

H. V. JULIAN
VOLIAN ENTERPRISES, INC.
PO BOX 410
MURRYSVILLE PA 15668
USA

J. E. KALINOWSKI
SAVANNAH RIVER LABORATORY
AIKEN SC 29808
USA

P. S. KALRA
ELECTRIC POWER RESEARCH INSTITUTE
3412 HILLVIEW AVE.
PALO ALTO CA 94303
USA

F. B. KAM
OAK RIDGE NATIONAL LABORATORY
PO BOX 2008
OAK RIDGE TN 37831
USA

H. KAMATA
JAPAN ATOMIC RESEARCH INST.
TOKAI-MURA, NAKA-GUN
IBARAKI-KEN 319-11
JAPAN

D. D. KANA
SOUTHWEST RESEARCH INSTITUTE
6220 CULEBRA ROAD
SAN ANTONIO TX 78284
USA

L. D. KANNBERG
PACIFIC NORTHWEST LABORATORY
P.O. BOX 999
RICHLAND WA 99352
USA

S. KARIMIAN
BROOKHAVEN NATIONAL LABORATORY
BLDG. 130
UPTON NY 11973
USA

W. Y. KATO
BROOKHAVEN NATIONAL LABORATORY
BLDG 197C
UPTON NY 11973
USA

K. R. KATSMA
EG&G IDAHO INC.
P.O. BOX 1625
IDAHO FALLS ID 83415
USA

G. KATZENMEIER
KERNFORSCHUNGSZENTRUM, PHDR
POSTFACH 3640
7500 KARLSRUHE 1
FRG

W. R. KEANEY
GENERAL ASSOCIATES CORP.
1314 OAKVIEW DR.
WORTHINGTON OH 43085
USA

J. E. KELLY
SANDIA NATIONAL LABS. DIV. 6418
P.O. BOX 5800
ALBUQUERQUE NM 87185
USA

C. R. KEMPF
BROOKHAVEN NATIONAL LABORATORY
BLDG. 197-C
UPTON NY 11973
USA

W. L. KIRK
LOS ALAMOS NATIONAL LABORATORY
P.O. BOX 1663, N-DO, MS E561
LOS ALAMOS NM 87545
USA

E. KNOGLINGER
PAUL SCHERRER INSTITUTE
WUERENLINGEN CH5303
SWITZERLAND

A. KOHSAKA
JAPAN ATOMIC RESEARCH INST.
TOKAI-MURA, NAKA-GUN
IBARAKI-KEN 319-11
JAPAN

M. J. KOMSI
IMATRAN VOIMA OY
P.O. BOX 112
VANTAA 01601
FINLAND

C. A. KOT
ARGONNE NATIONAL LABORATORY
9700 S. CASS AVE., BLDG 335
ARGONNE IL 60439
USA

G. S. KRAMER
BATTELLE COLUMBUS
505 KING AVE.
COLUMBUS OH 43201
USA

T. S. KRESS
OAK RIDGE NATIONAL LABORATORY
P.O. BOX 2009
OAK RIDGE TN 37831-8063
USA

C. A. KROPP
ENEA/DISP
VIA ANGUILLARESE K 1+300
ROME 00060
ITALY

G. A. KRUEGER
PHILADELPHIA ELECTRIC
2301 MARKET ST., N2-1
PHILADELPHIA PA 19101
USA

R. C. KRYTER
OAK RIDGE NATIONAL LABORATORY
P.O. BOX 2008
OAK RIDGE TN 37831-6010
USA

R. KUBOTA
HITACHI
SAIWAICHO 3-1-1
IBARAKI-KEN 317
JAPAN

C. A. KUKIELKA
PENNSYLVANIA POWER & LIGHT CO.
2 N. NINTH STREET
ALLENTOWN PA 18101
USA

D. S. KUPPERMAN
ARGONNE NATIONAL LABORATORY
9700 S. CASS AVE
ARGONNE IL 60439
USA

K. F. KUSSMAUL
UNIVERSITY OF STUTTGART
PFAFFENWALDRING 32
STUTTGART 80 7000
FRG

P. S. LACY
URA
51 MONROE STREET
ROCKVILLE MD 20854
USA

T. K. LARSON
EG&G IDAHO INC.
P.O. BOX 1625
IDAHO FALLS ID 83415
USA

D. LEAVER
TANERA
1340 SARATOGA-SUNNYSIDE ROAD, SUITE 2
SAN JOSE CA 95129
USA

R. E. LECKENBY
UKAEA, RISLEY LABORATORY
WARRINGTON
CHESHIRE WA36AT
UK

M. LEE
BROOKHAVEN NATIONAL LABORATORY
BLDG. 130
UPTON NY 11973
USA

N. E. LEE
COMBUSTION ENGINEERING
1000 PROSPECT HILL RD
WINDSOR CT 06095
USA

J. R. LEHNER
BROOKHAVEN NATIONAL LABORATORY
BLDG. 130
UPTON NY 11973
USA

K. M. LEIGH
UKAEA/SRD
WIGSHAW LANE, CULCHETH
WARRINGTON WA34NE
UK

S. J. LEVINSON
BABCOCK & WILCOX CO.
3315 OLD FOREST RD
LYNCHBURG VA 24506
USA

P. M. LEWIS
PACIFIC NORTHWEST LABORATORY
P.O. BOX 999
RICHLAND WA 99352
USA

K. LIESCH
GESELLSCHAFT FUR REAKTORSICHERHEIT
FORSCHUNGSGELANDE
D-8046 GARCHING
FRG

J. N. LILLINGTON
UKAEA/AEE WINFRITH
DOERCHESTER
DORSET DT28DH
UK

C. L. LIN
ELECTRIC POWER RESEARCH INSTITUTE
3412 HILLVIEW AVE.
PALO ALTO CA 94303
USA

L. LINDSTROM
SWEDISH NUCLEAR POWER INSPECTORATE
BOX 27016
STOCKHOLM SW S-10252
SWEDEN

Y. Y. LIU
ARGONNE NATIONAL LABORATORY
9700 S. CASS AVE.
ARGONNE IL 60439
USA

R. LOFARO
BROOKHAVEN NATIONAL LABORATORY
BLDG. 130
UPTON NY 11973
USA

J. P. LONGWORTH
CENTRAL ELECTRICITY GENERATING BD.
COURTNEY HSE., WARWICK LA
LONDON
UK

F. J. LOSS
MATERIALS ENGINEERING ASSOCIATES
9700-B M. L. KING HIGHWAY
LANHAM MD 20706
USA

A. L. LOWE, JR
BABCOCK & WILCOX CO.
PO BOX 10935
LYNCHBURG VA 24506
USA

T. S. LUBNOW
MPR ASSOCIATES
1050 CONNECTICUT AVE., NW
WASHINGTON DC 20036
USA

W. J. LUCKAS, JR.
BROOKHAVEN NATIONAL LABORATORY
BLDG. 130
UPTON NY 11973
USA

H. L. MAGLEBY
EG&G IDAHO INC.
P.O. BOX 1625
IDAHO FALLS ID 83415
USA

A. P. MALINAUSKAS
OAK RIDGE NATIONAL LABORATORY
P.O. BOX 2008
OAK RIDGE TN 37831-6135
USA

R. M. MANDL
SIEMENS
HAMMERBACHERSTR. 12
ERLANGEN 852
FRG

C. F. MARKUS
WESTINGHOUSE ELECTRIC CORP.
P.O. BOX 79
W. MIFFLIN PA 15122-0079
USA

C. W. MARSCHALL
BATTELLE COLUMBUS
505 KING AVE.
COLUMBUS OH 43201
USA

P. MARSILI
ENEA/DISP
VIA VITALIANO BRANCATI, 48
ROME 00144
ITALY

B. MAVKO
J. STEFAN INSTITUTE
JAMOVA 39
LJUBLJANA 61000
YUGOSLAVIA

D. E. MC CABE
MATERIALS ENGINEERING ASSOCIATES
9700-B M. L. KING HIGHWAY
LANHAM MD 20706
USA

L. D. McCANN
WESTINGHOUSE ELECTRIC CORP.
P.O. BOX 79
W MIFFLIN PA 15122-0079
USA

R. K. McCARDELL
EG&G IDAHO INC.
P.O. BOX 1625
IDAHO FALLS ID 83415
USA

D. J. McCLOSKEY
SANDIA NATIONAL LABS.
P.O. BOX 5800
ALBUQUERQUE NM 87122
USA

K. P. McKAY
WESTINGHOUSE ELECTRIC CORP.
P.O. BOX 79
W MIFFLIN PA 15228
USA

N. R.H. McMILLAN
UKAEA/SRD
WIGSHAW LANE, CULCHETH
WARRINGTON WA34NE
UK

C. MEDICH
SIET
VIA NINO BIXIO 27
PIACENZA ITALY 29100
ITALY

H. B. MEIERAN
H B MEIERAN ASSOCIATES
458 SOUTH DALLAS AVENUE
PITTSBURGH PA 15208
USA

M. MERILO
ELECTRIC POWER RESEARCH INSTITUTE
3412 HILLVIEW AVE.
PALO ALTO CA 94303
USA

J. G. MERKLE
OAK RIDGE NATIONAL LABORATORY
P.O. BOX 2009
OAK RIDGE TN 37831-8049
USA

J. F. MEYER
SCIENTECH
11821 PARKLAWN DRIVE
ROCKVILLE MD 20852
USA

A. MEYER-HEINE
CEA FRENCH ATOMIC ENERGY COMMISSION
CEN CADARACHE-DERS/SEMAR BP NO. 1
SAINT PAUL LEZ DURANCE 13108
FRANCE

S. M. MIHAIU
YANKEE ATOMIC ELECT. CO.
508 MAIN ST.
BOLTON MA 01740
USA

J. S. MILLER
GULG STATES UTILITIES
P.O. BOX 220
ST. FRANCISVILLE LA 70775
USA

A. MINATO
ENERGY RESEARCH LAB., HITACHI LTD.
1168 MORIYAMA-CHO
HITACHI-SHI IBARAKI-KEN 316
JAPAN

S. M. MODRO
FZS-AUSTRIA C/O EG&G
P.O. BOX 1625
IDAHO FALLS ID 83415
USA

T. MOMMA
JAERI C/O GENERAL ELECTRIC SAPS
RT. 168 S.
BEAVER PA 15077
USA

F. J. MOODY
GE NUCLEAR ENERGY
175 CURTNER AVE. MAIL CODE-769
SAN JOSE CA 95125
USA

R. J. MOORE
SAVANNAH RIVER LABORATORY
BLDG. 707C
AIKEN SC 29808
USA

F. I. MOPSIK
NAT'L INST. OF STDS. & TECH.
GAITHERSBURG MD 20899
USA

M.J. MOREAU
GENERAL ELECTRIC
P.O. BOX 1072
SCHENECTADY NY 12301
USA

V. MUBAYI
BROOKHAVEN NATIONAL LABORATORY
BLDG. 130
UPTON NY 11973
USA

Y. MURAO
JAPAN ATOMIC RESEARCH INST.
TOKAI-MURA, NAKA-GUN
IBARAKI-KEN 319-11
JAPAN

S. A. NAFF
SIEMENS AG.UB.KWU.U8S
POSTFACH 3220
ERLANGEN 8520
FRG

C. NAKAMURA
JAPAN ATOMIC RESEARCH INST.
TOKAI-MURA, NAKA-GUN
IBARAKI-KEN 319-11
JAPAN

R. K. NANSTAD
OAK RIDGE NATIONAL LABORATORY
PO BOX 2008, MS 6151
OAK RIDGE TN 37831
USA

A. NATLIZIO
ATOMIC ENERGY OF CANADA
SHERIDAN PARK RSCH. COMM.
MISSISSAUGA ONTARIO L5K1B2
CANADA

D. J. NAUS
OAK RIDGE NATIONAL LABORATORY
P.O. BOX 2009, BLDG 9204-1
OAK RIDGE TN 37831-8056
USA

E. NEGRENTI
ENEA/DISP
V. ANGUILLARESE, 301
ROME 00060
ITALY

D. B. NEWLAND
NATIONAL NUCLEAR CORP.
BOOTHS HALL, CHELFORD ROAD
KNUTSFORD ENGLAND
UK

L. Y. NEYMOTIN
BROOKHAVEN NATIONAL LABORATORY
BLDG 475B
UPTON NY 11973
USA

Y. NOGUCHI
CHUBU ELECTRIC POWER CO. INC
900 17TH ST. N.W., SUITE 714
WASHINGTON DC 20006
USA

P. NORTH
EG&G IDAHO INC.
P.O. BOX 1625
IDAHO FALLS ID 83415
USA

H. NOURBAKHSH
BROOKHAVEN NATIONAL LABORATORY
BLDG. 130
UPTON NY 11973
USA

S. P. NOWLEN
SANDIA NATIONAL LABS.
PO BOX 5800, DIV. 6447
ALBUQUERQUE NM 87185
USA

E. I. NOWSTRUP
CONSULTANT
17605 PARK MILL DR
ROCKVILLE MD 20855
USA

A. NUHM
TECHNICATOME
CEN CADARACHE
CADARACHE 13115
FRANCE

J. O'HARA
BROOKHAVEN NATIONAL LABORATORY
BLDG. 130
UPTON NY 11973
USA

K. R. O'KULA
SAVANNAH RIVER LABORATORY
BLDG. 773-41A
AIKEN SC 29808
USA

C. F. OBENCHAIN
EG&G IDAHO INC.
P.O. BOX 1625
IDAHO FALLS ID 83415
USA

T. OHNO
NUCLEAR POWER ENG'G TEST CTR
BLDG. 4-3-13, TORANOMON, MINATO-KU
TOKYO 105
JAPAN

M. OHUCHI
JAPAN SYSTEMS CORP.
NOMURA BLDG., 4-8 YOMBANCHO, CHIYODA
TOKYO 102
JAPAN

T. OKUBO
JAPAN ATOMIC RESEARCH INST.
TOKAI-MURA, NAKA-GUN
IBARAKI-KEN 319-11
JAPAN

R. C. OLSON
BALTIMORE GAS & ELECTRIC CO.
CCNPP-NGF PO BOX 1535
LUSBY MD 20657
USA

A. OMOTO
TOKYO ELECTRIC POWER
1901 L ST., NW, STE. 720
WASHINGTON DC 20036
USA

N. R. ORTIZ
SANDIA NATIONAL LABS., DIV. 6410
P.O. BOX 5800
ALBUQUERQUE NM 87185
USA

J. PAN
UNIVERSITY OF MICHIGAN
2250 G. G. BROWN BLDG., MECH. ENG.
ANN ARBOR MI 48108
USA

R. K. PAPESCH
BECHTEL-KWU ALLIANCE
15740 SHADY GROVE RD.
GAITHERSBURG MD 20877
USA

C. PARK
BROOKHAVEN NATIONAL LABORATORY
BLDG. 130
UPTON NY 11973
USA

W. R. PEARCE
CONSULTANT
6846 GLENBROOK ROAD
BETHESDA MD 20814
USA

G. A. PERTMER
UNIVERSITY OF MARYLAND
DEPT. OF CHEMISTRY & NUCLEAR ENGR.
COLLEGE PARK MD 20742
USA

G. PETRANGELI
ENEA/DISP
VIA VITALIANO BRANCATI, 48
ROME 00144
ITALY

J. L. PIERREY
CEA FRENCH ATOMIC ENERGY COMMISSION
CEN/FAR, BP NO. 6
FONTENAT-AUX-ROSES 92265
FRANCE

A. PINI
ENEA/DISP
VIA VITALIANO BRANCATI, 48
ROME 00144
ITALY

M. G. PLYS
FAUSKE & ASSOCIATES
16W070 WEST 83RD STREET
BURR RIDGE IL 60521
USA

M. Z. PODOWSKI
RENSSELEAR POLYTECHNIC INSTITUTE
TROY NY 12180-3590
USA

A. Y. PORRACCHIA
CEA FRENCH ATOMIC ENERGY COMMISSION
CEN CADARACHE-DERS/SEMAR BP NO. 1
SAINT PAUL LEZ DURANCE 13108
FRANCE

D. A. POWERS
SANDIA NATIONAL LABS.
P.O. BOX 5800
ALBUQUERQUE NM 87185
USA

N. PRASAD
WESTINGHOUSE POWER SYSTEMS DIVISION
P.O. BOX 2728
PITTSBURGH PA 15230-2728
USA

T. PRATT
BROOKHAVEN NATIONAL LABORATORY
BLDG. 130
UPTON NY 11973
USA

D. A. PRELEWICZ
ENSA, INC.
15825 SHADY GROVE RD. (SUITE 170)
ROCKVILLE MD 20850
USA

J. G. PRUETT
OAK RIDGE NATIONAL LABORATORY
P.O. BOX 2008
OAK RIDGE TN 37831-6135
USA

J. PUGA
UNITED ELECTRICIA, S. A. (UNESA)
FRANCISCO GERVAS, 3
MADRID 28020
SPAIN

C. E. PUGH
OAK RIDGE NATIONAL LABORATORY
P.O. BOX 2009
OAK RIDGE TN 37831
USA

W. J. QUAPP
WESTINGHOUSE HANFORD CO.
PO BOX 1970
RICHLAND WA 99352
USA

P. J. QUATTRO
MBZ, INC.
1175 HERNDON PKWY., STE. 150
HERNDON VA 22070
USA

Z. H. QURESHI
SAVANNAH RIVER LABORATORY
786-5A
AIKEN SC 29808
USA

H. J. REILLY
IDAHO NATIONAL ENGINEERING LAB
PO BOX 1625
IDAHO FALLS ID 83402
USA

L. RIB
LNR ASSOCIATES
8605 GRIMSBY CT.
POTOMAC MD 20854
USA

B. RIEGEL
GESELLSCHAFT FUR REAKTORSICHERHEIT
FORSCHUNGSGELANDE
D-8046 GARCHING
FRG

D. E. ROBERTSON
PACIFIC NORTHWEST LABORATORY
P.O. BOX 999
RICHLAND WA 99352
USA

S. B. RODRIGUEZ
EG&G IDAHO INC.
1646 GRANDVIEW #1
IDAHO FALLS ID 83402
USA

U. S. ROHATGI
BROOKHAVEN NATIONAL LABORATORY
BLDG 475B
UPTON NY 11973
USA

B. ROSENSTROCH
EBASCO SERVICES INC.
2 WORLD TRADE CENTER 89E
NEW YORK NY 10048
USA

S. T. ROSINSKI
SANDIA NATIONAL LABS, DIV. 6513
P.O. BOX 5800
ALBUQUERQUE NM 87185
USA

J. C. ROUSSEAU
CEA FRENCH ATOMIC ENERGY COMMISSION
CEN/GRENOBLE
GRENODLE 38000
FRANCE

D. RUBIO
ELECTRIC POWER RESEARCH INSTITUTE
3412 HILLVIEW AVE.
PALO ALTO CA 94303
USA

K. A. RUSSELL
EG&G IDAHO INC.
1520 SAWTELLE
IDAHO FALLS ID 83415
USA

J. RUTHERFORD
CENTRAL ELECTRICITY GENERATING BD.
BOOTHS HALL, CHELFORD ROAD
KNUTSFORD CHESHIRE WA16 806
UK

B. F. SAFFELL
BATTELLE COLUMBUS DIVISION
505 KING AVENUE
COLUMBUS OH 43201
USA

R. T. SAIRANEN
TECHNICAL RSCH CTR OF FINLAND
POB 169
HELSINKI SF-00181
FINLAND

K. SAKANA
JAPAN INST. OF NUCLEAR SAFETY
FUJITA KANKOU TORANOMON MINATO
TOKYO 105
JAPAN

K. SAKANO
JAPAN INSTITUTE OF NUCLEAR SAFETY
FUJITA KANKON TOR. BLDG. 3-17-1
TOKYO 105
JAPAN

A. SALA
HIDROELECTRICO ESPANOLA
HERMOSILLA 3
MADRID 28001
SPAIN

J. SALUJA
VIKING SYSTEMS INTERNATIONAL
2070 WM PITT WAY
PITTSBURGH PA 15238
USA

L. SCHOR
YANKEE ATOMIC ELECT. CO.
508 MAIN ST.
BOLTON MA 01740
USA

D. G. SCHRAMMEL
UFK
WEBERSTR. 5
KARLSRUHE
FRG

S. SETH
MITRE CORP.
7525 COLSHIRE DR.
MC LEAN VA 22102
USA

W. J. SHACK
ARGONNE NATIONAL LABORATORY
BLDG. 212
ARGONNE IL 60439
USA

V. N. SHAH
EG&G IDAHO INC.
P.O. BOX 1625
IDAHO FALLS ID 83415
USA

R. H. SHANNON
CONSULTING ENGINEER
P.O. BOX 2264
ROCKVILLE MD 20852
USA

R. S. SHARMA
AMERICAN ELECTRIC POWER
ONE RIVERSIDE PLAZA
COLUMBUS OH 43017
USA

D. A. SHARP
SAVANNAH RIVER LABORATORY
AIKEN SC 29801
USA

D. L. SHAW
BALTIMORE GAS & ELECTRIC COMPANY
CALVERT CLIFFS NPP, P.O. BOX 1535
LUSBY MD 20657
USA

L. SHEN
ATOMIC ENERGY COUNCIL, ROC
NO 67, LANE 144, KEELUNG RD. SEC. 4
TAIPEI TAIWAN 107
ROC

G. L. SHERWOOD
U.S. DEPT. OF ENERGY
GERMANTOWN MD 21701
USA

P. SHEWMON
ACRS
2477 LYTHAM ROAD
COLUMBUS OH 43220
USA

K. SHIBATA
JAPAN ATOMIC RESEARCH INST.
TOKAI-MURA, NAKA-GUN
IBARAKI-KEN 319-11
JAPAN

K. SHIMIZU
HITACHI, LTD.
1-1 SAIWAI-MACHI
HITACHI
JAPAN

A. SHIMIZU
OHBAYASHI CORP.
777 RIVERVIEW DR., APT. 9
ROCHESTER PA 15074
USA

J. J. SHIN
EBASCO SERVICES, INC.
2 WORLD TRADE CENTER
NEW YORK NY 10048
USA

M. S. SHINKO
EMERGENCY RESPONSE TEAM
PO BOX 129
WASHINGTON GROVE MD 20880
USA

B. S. SHIRALKAR
GENERAL ELECTRIC CO.
175 CURTNER AVE (M/C 186)
SAN JOSE CA 95125
USA

D. A. SIEBE
LOS ALAMOS NATIONAL LABORATORY
P.O. BOX 1663, MS K555
LOS ALAMOS NM 87545
USA

E. G. SILVER
OAK RIDGE NATIONAL LABORATORY
P.O. BOX 2009, BLDG 9201-3
OAK RIDGE TN 37831-8065
USA

F. A. SIMONEN
PACIFIC NORTHWEST LABORATORY
P.O. BOX 999
RICHLAND WA 99352
USA

F. B. SIMPSON
EG&G IDAHO INC.
P.O. BOX 1625
IDAHO FALLS ID 83415
USA

L. SLEGERS
SIEMENS KWU
BERLINER STR 295-303
OFFENBACH 6000
FRG

G. L. SMITH
WESTINGHOUSE HANFORD CO.
P.O. BOX 1970 X0-44
RICHLAND WA 99352
USA

A. W. SNYDER
SANDIA NATIONAL LABS., ORG. 6500
P.O. BOX 5800
ALBUQUERQUE NM 87185
USA

P. SOO
BROOKHAVEN NATIONAL LABORATORY
BLDG 830
UPTON NY 11973
USA

H. SPECTER
NEW YORK POWER AUTHORITY
123 MAIN STREET
NEW YORK NY 10601
USA

J. E. SPEELMAN
ECN
3 WESTERDUINWEG, P.O. BOX 1
PETTEN NEW HOLLAND 1755 ZG
THE NETHERLANDS

K. E. ST. JOHN
YANKEE ATOMIC ELECTRIC CO.
1671 WORCESTER RD
FRAMINFHAM MA 01701
USA

H. STADTKE
JOINT RESEARCH CENTRE-ISPRA ESTABLISH
ISPRA 21020
ITALY

D. D. STEPNEWSKI
WESTINGHOUSE HANFORD CO.
P.O. BOX 1970 NI-31
RICHLAND WA 99352
USA

E. J. STUBBE
TRACTABEL
31 RUE DE LA SCIENCE
BRUSSELS 1040
BELGIUM

P. K. SUNDARAM
YANKEE ATOMIC ELECT. CO
508 MAIN ST
BOLTON MA 01740
USA

J. D. SUTTON
YANKEE ATOMIC ELECTRIC CO
580 MAIN ST
BOLTON MA 01740
USA

T. SUZUKI
TOSHIBA
SHINSUGITA ISOGO-KU
YOKOHAMA
JAPAN

I. SZABO
C.E.A.
C.E.N CADARACHE
ST PAUL LES DURAN 43
FRANCE

A. TAKAGI
TOSHIBA
4921 NORWALK DR., APT V202
SAN JOSE CA 95125
USA

K. TASAKA
JAPAN ATOMIC RESEARCH INST.
TOKAI-MURA, NAKA-GUN
IBARAKI-KEN 319-11
JAPAN

J. H. TAYLOR
BROOKHAVEN NATIONAL LABORATORY
BLDG 130
UPTON NY 11973
USA

B. J. TOLLEY
COMM. OF THE EUROPEAN COMMUNITIES (CI
200 RUE DE LA LOI
BRUSSELS 1049
BELGIUM

J. S. TONG
ATOMIC ENERGY CONTROL BOARD
PICKERING NGS OPERATIONS
PICKERING ONTARIO L1V2R5
CANADA

L. S. TONG
TAI
9733 LOOKOUT PLACE
GAITHERSBURG MD 20879
USA

F. M. TOUBOUL
CEA FRENCH ATOMIC ENERGY COMMISSION
CEN-SACLAY DEMT/SMTS/RDMS
GIF-SUR-YVETTE 91191
FRANCE

H. E. TRAMMELL
OAK RIDGE NATIONAL LABORATORY
104 OGLETHORPE PL.
OAK RIDGE TN 37830
USA

J. D. TROTTER
GROVE ENGINEERING
15215 SHADY GROVE RD.
ROCKVILLE MD 20878
USA

C-K TSAI
WESTINGHOUSE POWER SYSTEMS DIVISION
P.O. BOX 355
PITTSBURGH PA 15230-2728
USA

T. TSUJINO
JAPAN ATOMIC RESEARCH INST.
TOKAI-MURA, NAKA-GUN
IBARAKI-KEN 319-11
JAPAN

B. D. TURLAND
UKAEA CULHAM
CULHAM LABORATORY
ABINGDON
UK

G. TYROR, DIRECTOR
UKAEA/SRD
WIGSHAW LANE, KNUTSFORD
WARRINGTON WA34NE
UK

R. E. UHRIG
OAK RIDGE NATIONAL LABORATORY
113 CONNORS DRIVE
OAK RIDGE TN 37830
USA

R. A. VALENTIN
ARGONNE NATIONAL LAB - BLDG. 208
9700 S. CASS AVE
ARGONNE IL 60439
USA

G. L.C.M. VAYSSIER
MINISTRY OF SOCIAL AFFAIRS
P.O. BOX 69
VOORBURG 2270MA
THE NETHERLANDS

O. VESCOVI
SIET
VIA NINO BIXIO 27
PIACENZA 29100
ITALY

G. L. VINE
ELECTRIC POWER RESEARCH INSTITUTE
3412 HILLVIEW AVE.
PALO ALTO CA 94303
USA

D. S. WALLS
OAK RIDGE NATIONAL LABORATORY
P.O. BOX 2009, MS-8057
OAK RIDGE TN 37831-8065
USA

S. F. WANG
INST. OF NUCLEAR ENERGY RSCH.
PO BOX 3-3, LUNG TAN
TAIPEI TAIWAN 32500
ROC

O. J. WANG
WESTINGHOUSE HANFORD CO.
P.O. BOX 1970 XO-14
RICHLAND WA 99352
USA

R. WANNER
PAUL SCHERRER INSTITUTE
WUERENLINGEN CHS303
SWITZERLAND

E. A. WARMAN
STONE & WEBSTER
245 SUMMER ST.
BOSTON MA 02107
USA

K. E. WASHINGTON
SANDIA NATIONAL LABS.
P.O. BOX 5800
ALBUQUERQUE NM 87185
USA

W. L. WEAVER
EG&G IDAHO INC.
P.O. BOX 1625
IDAHO FALLS ID 83415
USA

E. O. WEINER
WESTINGHOUSE HANFORD CO.
P.O. BOX 1970, L2-57
RICHLAND WA 99352
USA

P. A. WEISS
SIEMENS AG / UB KWU
HAMMERBACHERSTR. 12+14
ERLANGEN 8520
FRG

H. J. WELLAND
EG&G IDAHO INC.
442 JOAN AVENUE
IDAHO FALLS IDAHO 83401
USA

E. T. WESSEL
CONSULTANT
312 WOLVERINE STREET
HAINES CITY FL 33844
USA

H. WESTPHAL
GESELLSCHAFT FUR REAKTORSICHERHEIT
SCHWERTNERGASSE 1
D-5000 COLOGNE 1
FRG

A. M. WHITE
SAVANNAH RIVER LABORATORY
BLDG. 773-11A
AIKEN SC 29808
USA

J. D. WHITE
OAK RIDGE NATIONAL LABORATORY
P.O. BOX 2008
OAK RIDGE TN 37831-6009
USA

G. M. WILKOWSKI
BATTELLE COLUMBUS
505 KING AVE.
COLUMBUS OH 43201
USA

W. K. WINEGARDNER
PACIFIC NORTHWEST LABORATORY
P.O. BOX 999
RICHLAND WA 99352
USA

F. J. WINKLER
SIEMENS
RINGSTRASSE 19
SPARDORF
FRG

L. WOLF
KERNFORSCHUNGSZENTRUM, PHDR
POSTFACH 3640
7500 KARLSRUHE 1
FRG

A. J. WOLFORD
EG&G IDAHO INC.
P.O. BOX 1625
IDAHO FALLS ID 83415
USA

D. N. WOODY
SAVANNAH RIVER LABORATORY
AIKEN SC 29808
USA

R. O. WOOTON
BATTELLE COLUMBUS
505 KING AVE.
COLUMBUS OH 43201
USA

J. WREATHALL
SAIC
2929 KENNY RD.
COLUMBUS OH 43221
USA

D. W. WRIGHT
ANCHOR/DARLING VALVE
701 FIRST ST.
WILLIAMSPORT PA 17701
USA

W. WULFF
BROOKHAVEN NATIONAL LABORATORY
BLDG 475B
UPTON NY 11973
USA

H. XU
BROOKHAVEN NATIONAL LABORATORY
BLDG. 130
UPTON NY 11973
USA

Y. YAMAMOTO
TAKENAKA CO.
21-1 8CHOME CHUO-KU
TOKYO
JAPAN

H. YASOSHIMA
JAPAN ATOMIC RESEARCH INST
TOKAI-MURA, NAKA-GUN
IBARAKI-KEN 319-11
JAPAN

M. YOKOTA
JAPAN ATOMIC RESEARCH INST.
TOKAI-MURA, NAKA-GUN
IBARAKI-KEN 319-11
JAPAN

Y. YOSHIMOTO
HITACHI, LTD.
SAIWAI-CHO 3-H
HITACHI-SHI 316
JAPAN

R. W. YOUNGBLOOD
BROOKHAVEN NATIONAL LABORATORY
BLDG 130
UPTON NY 11973
USA

R. ZIPPER
GESELLSCHAFT FUR REAKTORSICHERHEIT
SCHWERTNERGASSE 1
D-5000 COLOGNE 1
FRG

P. C. ZMOLA
C&P ENGINEERING
5409 NEWINGTON RD.
BETHESDA MD 20816
USA

R. ZOGRAN
MPR ASSOCIATES, INC.
1050 CONNECTICUT AVENUE, N.W.
WASHINGTON DC 20036
USA

PROCEEDINGS OF THE
FIFTEENTH WATER REACTOR SAFETY INFORMATION MEETING

October 24-27, 1988

TABLE OF CONTENTS - VOLUME 4


Page

ABSTRACT . . . . . iii
GENERAL INDEX . . . . . v
REGISTERED ATTENDEES . . . . . vii

CODE UNCERTAINTY FOR ECCS RULE
Chairman: N. Zuber (NRC)

Quantifying Reactor Safety Margins - Part 1: An Overview of the Code Scaling, Applicability, and Uncertainty Evaluation Methodology . . . . . 1
Technical Program Group

Quantifying Reactor Safety Margins - Part 2: Characterization of Important Contributors to Uncertainty . . . . . 19
Technical Program Group

Quantifying Reactor Safety Margins - Part 3: Assessment and Ranging of Parameters for the Uncertainty Analysis of LBLOCA Codes . . . . . 45
Technical Program Group

Quantifying Reactor Safety Margins - Part 4: Uncertainty Evaluation of LBLOCA Analysis Based on TRAC-PF1/MOD1 . . . . . 101
Technical Program Group

INTERNATIONAL CODE ASSESSMENT PROGRAM
Chairman: G. Rhee (NRC)

Summary of ICAP Assessment Results for RELAP5/MOD2 . . . . . 161
W. E. Driskell and R. G. Hanson (INEL)

RELAP5/MOD3 Development Plan and Status . . . . . 173
W. L. Weaver III (INEL)

TRAC-PF1/MOD2 Status and Plans . . . . . 179
J. W. Spore et al. (LANL)

Status of ICAP Activities in Japan . . . . . 199
Y. Murao (JAERI)

## INTERNATIONAL CODE ASSESSMENT PROGRAM (Cont'd)


Page

JRC ISPRA Contribution to the Improvement of RELAP5/MOD2. . . . . 219
H. Stadtke (CEC, JRC)

Switzerland's Code Assessment Activities in Support of the International Code Assessment Program (ICAP). . . . . 245
S. N. Aksan, G. Th. Analytis and D. Lubbesmeyer (PSI)

TRAC and RELAP5 Code Development Within the UK. . . . . 275
I. Brittain (UKAEA) and M. Coney (CEGB)


## THERMAL HYDRAULICS
Chairman: R. Lee (NRC)


MIST Program: Summary of Key Results . . . . . 299
J. R. Gloudemans and D. P. Birmingham (B&W)

UMCP 2x4 Loop Observations Regarding the Behavior of an Integral System During SB-LOCA. . . . . 313
K. Almenas et al. (U. of Md.)

TRAC PF1/MOD1 Calculations and Data Comparisons for MIST Feed and Bleed and Steam Generator Tube Rupture Experiments. . . . . 331
D. A. Siebe, B. E. Boyack and J. L. Steiner (LANL)

Results and Analysis of the INEL Once Through Steam Generator Air-Water and Steam-Water Experiments . . . . . 359
T. K. Larson, K. G. Condie and G. E. McCreery (INEL)

Two-Phase Flow Characteristic of Inverted Bubbly, Slug and Annular Flow in Post-Critical Heat Flux Region. . . . . 387
M. Ishii (Purdue U.) and J. P. Denten (ANL)

Loop Seal Clearing and Refilling During a PWR Small-Break LOCA: Results of ROSA-IV LSTF Experiments. . . . . 413
K. Tasaka et al. (JAERI)

PKL III Investigation of PWR Off-Design Conditions. . . . . 431
R. M. Mandl, B. Brand and K. Umminger (Siemens)

Boron Mixing in the Lower Plenum of a BWR . . . . . 445
T. G. Theofanous and E. A. Shabana (UCSB)

Admitting Cold Water Into Steam Filled Pipes Without Water Hammer Due to Steam Bubble Collapse . . . . . 463
Y. Chou (INER) and P. Griffith (MIT)

## 2D/3D DATA APPLICATIONS
Chairman: G. Rhee (NRC)


Page

UPTF Upper Plenum Injection (UPI) Test Results and Application to PWR . . . . . 485
A. Russell and P. Damerell (MPR Assoc.) and G. Ahrens and P. Weiss (Siemens)

Use of 2D/3D Data to Scale Up Liquid Carryover/DE-Entrainment (Steam Binding) Behavior to a PWR . . . . . 511
G. Rhee (NRC), and P. Damerell and J. Simons (MPR Assoc.)

Use of 2D/3D Data for Peak Cladding Temperature Uncertainty Studies . . . . . 533
B. E. Boyack (LANL)

UPTF Experiment - Principal Experimental Results to be Used for Improved LBLOCA Understanding . . . . . 543
P. A. Weiss (Siemens)

Recent Results of Analytical Study on SCTF-III Tests for Reflood Phenomena of PWR with Combined Injection-Type ECCS Under Cold-Leg-Large-Break LOCA . . . . . 557
T. Iguchi et al. (JAERI)

Assessment of J-TRAC Code with CCTF/SCTF Test Data. . . . . 583
H. Akimoto et al. (JAERI)

# QUANTIFYING REACTOR SAFETY MARGINS
# PART 1: AN OVERVIEW OF THE CODE SCALING, APPLICABILITY, AND UNCERTAINTY EVALUATION METHODOLOGY*

by

B. E. Boyack
Nuclear Technology and Engineering Division
Los Alamos National Laboratory

and

R. B. Duffey (INEL), P. Griffith (MIT), K. R. Katsma (INEL), G. S. Lellouche and S. Levy (S. Levy, Inc.), U. S. Rohatgi (BNL), G. E. Wilson (INEL), W. Wulff (BNL), and N. Zuber (USNRC)

## ABSTRACT

In August 1988, the Nuclear Regulatory Commission (NRC) approved the final version of a revised rule on the acceptance of emergency core cooling systems (ECCS) entitled "Emergency Core Cooling System; Revisions to Acceptance Criteria." The revised rule states an alternate ECCS performance analysis, based on best-estimate methods, may be used to provide more realistic estimates of plant safety margins, provided the licensee quantifies the uncertainty of the estimates and includes that uncertainty when comparing the calculated results with prescribed acceptance limits.

To support the revised ECCS rule, the NRC and its contractors and consultants have developed and demonstrated a method called the Code Scaling, Applicability, and Uncertainty (CSAU) evaluation methodology. It is an auditable, traceable, and practical method for combining quantitative analyses and expert opinions to arrive at computed values of uncertainty.

This paper provides an overview of the CSAU evaluation methodology and its application to a postulated cold-leg, large-break loss-of-coolant accident in a Westinghouse four-loop pressurized water reactor with 17 x 17 fuel. The code selected for this demonstration of the CSAU methodology was TRAC-PF1/MOD1, Version 14.3.

---

* This work was funded by the US Nuclear Regulatory Commission (NRC), Office of Nuclear Regulatory Research, Division of Accident Evaluation.

## I. INTRODUCTION

In August 1988, the Nuclear Regulatory Commission (NRC) approved the final version of a revised rule on the acceptance of emergency core cooling systems (ECCS) entitled "Emergency Core Cooling System; Revision to Acceptance Criteria" (Ref. 1). The revised rule contains three key features. First, the current acceptance criteria related to peak cladding temperature, clad oxidation, hydrogen generation, coolable core geometry, and long-term cooling are retained. Second, evaluation model (EM) methods based on Appendix K (Ref. 1) may continue to be used as an alternative to the best-estimate (BE) methodology. Third, an alternate ECCS performance analysis, based on BE methods, may be used to provide more realistic estimates of plant safety margins, provided the licensee quantifies the uncertainty of the estimates and includes that uncertainty when comparing the calculated results with prescribed acceptance limits (Ref. 2).

To support the revised ECCS rule, the NRC and its contractors and consultants have developed and demonstrated a method called the Code Scaling, Applicability, and Uncertainty (CSAU) evaluation methodology. The objective of this paper is to provide an overview of this methodology and a brief summary of its application to a large-break loss-of-coolant accident (LBLOCA). More detailed descriptions of specific features of the CSAU method and its demonstration for a Westinghouse four-loop pressurized water reactor (PWR) with 17 x 17 fuel are presented in companion papers (Refs. 3–5).

## II. BACKGROUND

Recent review papers concerning the history and content of the ECCS rules are found in Refs. 6–8. The background material provided here was summarized from these papers. The acceptance criteria for ECCS performance for light-water-cooled nuclear power plants are found in the Code of Federal Regulations, Title 10, Section 50.46 (10CFR50.46) (Ref. 9). Included is the requirement that analysis models used to calculate the thermal-hydraulic performance of the ECCS conform to the requirements specified in Appendix K (Ref. 1) to 10CFR50, Section 50.46 and Appendix K were finalized after extensive public hearings in 1973, and the rule was implemented in January 1974. The basic criteria for evaluating ECCS performance focus on a peak cladding temperature (PCT) limit (2200°F or 1477 K), a limit on the maximum cladding oxidation (cannot exceed 17% of the cladding thickness before oxidation), a limit on the hydrogen generation from the chemical reaction of the cladding with water or steam (1% of potential), a requirement that a coolable core geometry be retained, and a requirement that acceptable long-term cooling be provided. These criteria were re-evaluated as part of the rule revision process and were found, in the judgement of the NRC, to be appropriate for continued use. Appendix K contains required and acceptable features of evaluation models to be used for loss-of-coolant accident (LOCA) analysis.

Several features of the Appendix K requirements have been found to have a significant effect on PWR design and operation. These are requirements related to initial stored energy, use of 1.2 times the 1971–73 American Nuclear Society standard decay heat, the emergency core coolant (ECC) bypass prescription, the prohibition on a return to nucleate boiling, reactor coolant pump modeling, and calculation of reflood rates (Ref. 10). Other features of Appendix K were found to have smaller impacts on plant design and operation. A summary of an early study (Ref. 11) to quantify the conservatisms associated with a particular set of

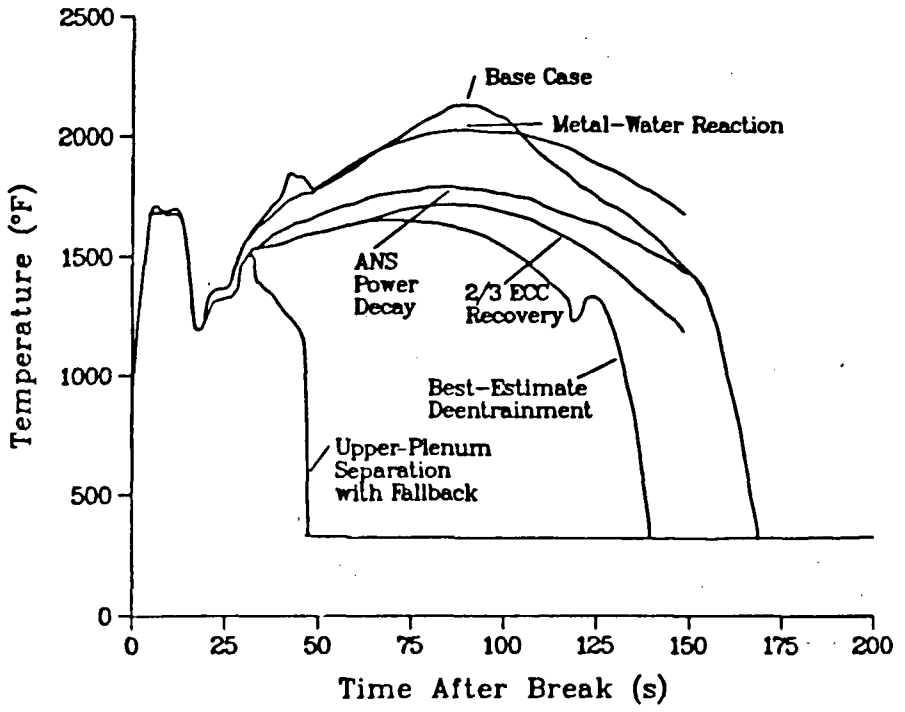


**Fig. 1.**
Effect of selected conservative assumptions on PCT.

Appendix K requirements is provided in Fig. 1. Following the base-case code calculation using EM conditions, selected conservatisms were removed one at a time and the transient recalculated. Taken in the order below, the conservatisms accounted for a reduction in the reflood PCT of about 700°F (390 K); the order in which the selected Appendix K conservatisms were treated was (1) metal-water reaction, (2) decay heat, (3) ECCS bypass, (4) upper-plenum de-entrainment, and (5) upper-plenum separation with fallback. The blowdown PCT was only slightly affected by treatment of the listed conservatisms.

There appear to be many areas of possible benefit available to licensees as increased margin is demonstrated under the revised ECCS rule. Possible benefits for PWR plants include increased discharge burnup, low leakage loading patterns, longer fuel cycles, use of advanced fuel designs, power uprating, improved load-following capabilities, more flexible burnup windows, use of axial blankets, and technical specification relaxation (Ref. 12). Similar insights related to potential benefits for boiling-water reactors (BWRs) are found in Ref. 13. In 1985, a BE licensing approach based on the SAFER/GESTR codes was licensed by the NRC for application to BWRs. This approach has subsequently been used to identify areas where this licensed technology could be used to relax ECCS performance requirements for BWR/4 (Ref. 14).

## III. CSAU EVALUATION METHODOLOGY

### A. Objectives of CSAU

The objectives of the CSAU evaluation methodology developed by NRC and its contractors and consultants are to:

1. provide a technical basis for quantifying uncertainties within the context of the revised ECCS rule;
2. provide an auditable, traceable and practical method for combining quantitative analyses and expert opinion to arrive at computed values of uncertainty; and
3. provide a systematic and comprehensive approach for:
   - defining scenario phenomena
   - evaluating code applicability
   - assessing code scale-up capabilities, and
   - quantifying code uncertainties concerned with:
     - code and experiment accuracies
     - code scale-up capabilities
     - plant state and operating conditions.

Additional objectives of the CSAU activities described in this and the companion papers were to "demonstrate feasibility of the methodology, to develop an audit tool, and to provide the necessary experience to audit licensee submittals" (Ref. 1).

### B. Elements of CSAU

In developing CSAU, the emphasis was placed on providing a **practical engineering approach** that could be used to quantify code uncertainties. Consequently, for a specified nuclear power plant (NPP) and a given scenario, the CSAU method focuses only on important processes and/or phenomena, assesses the code capability to scale them up, and evaluates the accuracy with which the code calculates them.

The CSAU evaluation methodology consists of three primary elements as shown in Fig. 2.

- The first element, **Requirements and Code Capabilities**, contains steps 1–6. In this element, scenario modeling requirements are identified and compared against code capabilities to determine the code's applicability to the particular scenario in a given plant type. In addition, an effort is made to identify potential code limitations.

  The modeling requirements are established by identifying and ranking problems and phenomena important to the particular scenarios. The need for such a screening process arises from the fact that the resources required to quantify the uncertainty for **every** process and phenomenon occurring during the selected transient are **too** large. Furthermore, although many processes and phenomena occur during a given transient, the overall plant behavior is not influenced equally by each. Consequently, a sufficient and more efficient (cost-effective) approach is to rank process and phenomena by evaluating their importance relative to the primary safety criteria so that **only** the significant contributors need to be evaluated. A list of the processes and phenomena occurring during the selected transient is compiled following examination of experimental data and code simulations.

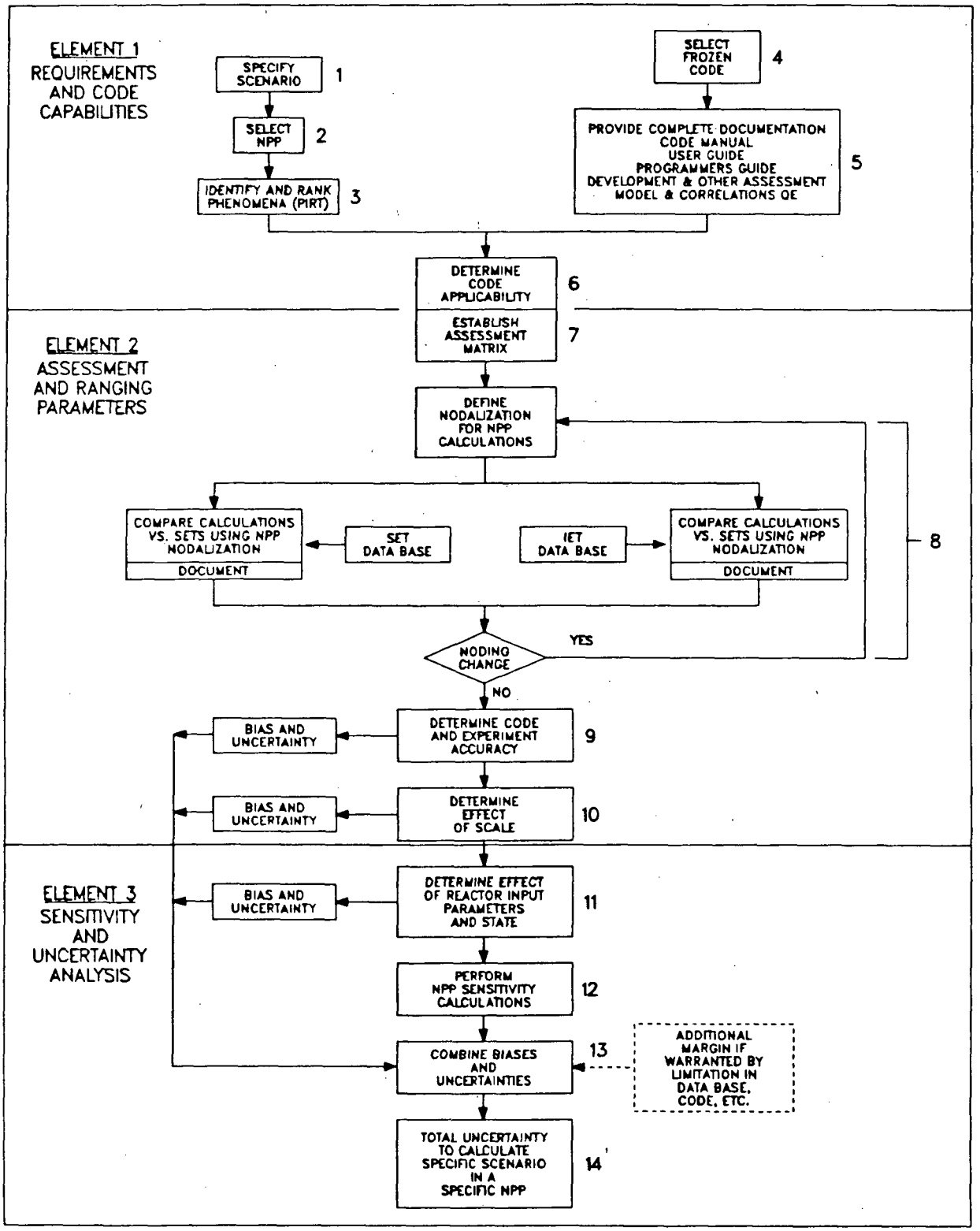


**Fig. 2.**
Code scaling, applicability, and uncertainty evaluation methodology.

The phenomena and processes are then ranked according to importance using one or more techniques.

The evaluation of code applicability to the selected transient is based on a complete set of code documents (specified in step 5). It is conducted by reviewing the adequacy of code models to calculate the important processes and phenomena identified above. Code deficiencies and/or limitations are also identified and evaluated as to their potential affects on uncertainties to calculate primary safety criteria. A more detailed description of this element and its demonstration for a LBLOCA is provided in Ref. 3.

- The second element, **Assessment and Ranging of Parameters**, contains steps 7–10. In this element there are activities to assess the capability of the code to calculate processes important to the scenario by comparing calculations against experimental data to determine code accuracy, to determine scale-up capability, and to specify ranges of parameter variations needed for sensitivity studies. In addition, bounding analyses can be performed and, in such cases, code calculations may not be required. A more detailed description of this element and its demonstration is provided in Ref. 4.
- The third element, **Sensitivity and Uncertainty Analyses**, contains steps 11–14. The total uncertainty in a safety analysis includes contributors that arise from code limitations, scaling inaccuracies embedded in the experimental data (and therefore the code), and uncertainties associated with the state of the reactors at the initiation of a transient. The ultimate objective of the CSAU process is to provide a simple and direct statement of the calculated uncertainty in the primary safety criteria (e.g., the PCT) used as the basis for assessing safety and making licensing decisions relative to the revised ECCS rule. This objective is accomplished when the magnitudes of individually important contributors are determined, collected, and subsequently combined to provide the desired summary statement. This element contains the activities to calculate, collect, and combine individual contributors to uncertainty into the required total mean and 95% probability statements including separately identified and quantified biases. A more detailed description of this element and its demonstration is provided in Ref. 5.

### C. Prescriptive Steps of CSAU

A brief description of each of the steps (numbered to conform to Fig. 2) in the CSAU evaluation methodology follows.

1. **Specify Scenario**: Code applicability and uncertainty are transient dependent because processes and safety parameters of interest may change from one scenario to another. Consequently, it is necessary to specify the scenario to order to establish the parameters that need to evaluated.
2. **Select Nuclear Power Plant (NPP)**: The scenario definition depends on both the type of transient to be analyzed, and the particular plant in which it is postulated that it occurs. Consequently, the NPP for which the calculations are to be performed should be specified.

3. **Identify and Rank Processes**: The CSAU methodology focuses only on phenomena/processes that are important to the particular scenario and plant design. Consequently, physical processes need to be first identified (together with relevant plant components) and then ranked to establish process identification and ranking tables (PIRT) appropriate to the particular scenario and plant design. The identification and ranking should be justified and documented.
4. **Select "Frozen" Code**: The methodology emphasizes the use of a "frozen" code version. This ensures that changes to the code after an evaluation has been completed do not impact the conclusions, and that changes occur in an **auditable** and **traceable** manner.
5. **Provide Code Documentation**: Complete documentation should include: the user manual, the user guide, the model and correlations quality evaluation (MC/QE) document, assessment reports, and other relevant supporting evidence. The MC/QE is a new kind of document that NRC's contractors have been requested to provide for each BE code. It provides detailed information on closure relations as implemented in the code, that is, information on their source, data base, accuracy, scale-up capability, and applicability to NPP conditions.
6. **Determine Code Applicability**: Steps 1 through 3 establish the requirements for modeling a specific scenario, whereas steps 4 and 5 provide information on code capabilities. By comparing requirements and capabilities in step 5, one determines whether the code can be used to calculate the scenario and whether the data base, accuracy, and scale-up capabilities of closure relations are adequate to model processes important to the scenario.
7. **Establish an Assessment Matrix**: Test data should be selected for a) assessing code accuracy to calculate dominant phenomena/processes identified in PIRT (step 3) and b) addressing any code inadequacy identified in step 6. Both separate effects tests (SET) and integral effects tests (IET) are to be used in establishing the assessment matrix.
8. **Define NPP Nodalization**: The plant model should be nodalized with enough detail to capture the important phenomena and design characteristics of the NPP. The iterative process shown in the flow diagram (Fig. 2) makes use of the Assessment Matrix to support the rationale for the choice of nodalization. The same nodalization should be used in performing NPP and code assessment calculations.
9. **Determine Code and Experiment Accuracy**: Simulations of experiments from step 7 with the frozen code, using the nodalization defined above, should lead to a statement of code accuracy. Differences between code and experiment should be quantified for bias and uncertainty (deviation). Individual contributors to uncertainties in modeling important phenomena/processes should be identified and cast in terms of bias and distribution (to be used in step 12 for sensitivity calculations). In addition, separate biases should be evaluated as appropriate.

   SET data from facilities up to full scale when available should be used to evaluate code scale-up capability and accuracy to model important phenomena, whereas IET test data should be used to evaluate **overall** code accuracy.

10. **Determine Effect of Scale**: Differences for similar physical processes, but at different scales, should also be quantified for bias and deviation to establish a statement of potential scale-up effects. In addition, separate biases should be evaluated as appropriate.
11. **Determine Effect of Reactor Input Parameters and State**: The effect upon uncertainty because of an imprecise knowledge of the reactor state and operating conditions at the initiation of the transient should be quantified. A typical example of these contributors is the potential variability of the fuel state that arises from the assumed condition of the fuel as a function of the burn-up cycle and the original manufacturing tolerances. Realistic variations are determined by examination of the most probable reactor state and the distribution around this condition using both experimental data and analytical studies. In addition, separate biases should be evaluated as appropriate.
12. **Perform NPP Sensitivity Calculations**: The influence of the individual contributors to uncertainty, determined in steps 9, 10, and 11, upon the primary safety criteria should be determined by performing NPP sensitivity calculations. That is, the individual variabilities cast in terms of bias and distribution are input to the NPP model and are used to determine their effect upon the uncertainty of simulating the primary safety parameters. These results are used in combining the biases and uncertainties for a singular statement regarding total uncertainty in steps 13 and 14.
13. **Combine Biases and Uncertainties**: Uncertainties determined in the above steps should be combined in a statement of total uncertainty. As there are several ways of combining them (addition, root mean square, response surface, etc.), a justification should be provided for selecting a particular method. Separate biases must also be added to produce total mean and 95% probability values of the appropriate parameter(s) including combined biases.
14. **Determine Total Uncertainty**: A statement of total uncertainty for the code may be given as an error band or statement of confidence about the code calculation with respect to the primary safety criteria (for example, PCT during a LBLOCA).

It is important to note that the CSAU methodology outlined above is not fully prescriptive regarding the details of its implementation. Rather, the CSAU methodology provides a complete and logical structure to which the details of alternative implementation approaches can and must be referenced and evaluated for completeness. In the following section, the approach selected by the NRC-organized Technical Program Group (TPG) to demonstrate the CSAU methodology is briefly described. During the process of developing the demonstration, the TPG explored many approaches; some proved fruitful and some did not. However, valuable lessons were learned in each case. The lessons learned are documented in the CSAU final report (Ref. 15) and should prove useful to those interested in alternative implementation approaches.

## IV. CSAU DEMONSTRATION

An application of the CSAU methodology has been demonstrated by the TPG for a cold-leg LBLOCA in a Westinghouse four-loop PWR with 17 x 17 fuel. The demonstration conformed to the requirements of the revised 10CFR50.46 (Ref. 1). The BE PCT and uncertainty in predicting PCT were quantified. Only one of the acceptance criteria was evaluated, the PCT.

This focus was warranted as long as the total mean PCT including combined biases at the 95% probability level remained below the initiation temperatures for cladding oxidation and hydrogen generation from chemical reaction of the cladding with water or steam. Activities and results related to this demonstration are summarized below.

**Element 1: Requirements and Code Capabilities (Steps 1–6, Fig. 2)**

For the specified scenario (LBLOCA) and selected power plant, key phenomena and processes were first identified and then ranked by expert opinion and a subjective decision-making process, the Analytical Hierarchical Process (Ref. 16). The results were then summarized in a PIRT. The key phenomena and processes identified as important during the entire LBLOCA transient were break flow, stored energy and fuel response, reactor coolant pump two-phase flow, steam binding, ECCS bypass, and non-condensible gas (NCG). The steam binding and ECCS bypass phenomena are of importance only during the reflood phase of a LBLOCA.

The frozen code selected was TRAC-PF1/MOD1, Version 14.3. Exclusive of the many assessment reports, only one of which is cited here, the applicable code documents are Refs. 17–20. These documents were reviewed and the ability of the code to simulate these key processes was confirmed. As this effort was completed, available parameters and processes within the code related to the highly ranked phenomena were identified. For example, the parameters available within the code for modeling stored energy and fuel response were the gap conductance, peaking factor, fuel conductivity, surface heat transfer, initial power, clad conductivity, fuel and clad heat capacity, and pellet power distribution. Several code-related deficiencies were identified, e.g., the code does not provide models for dissolved NCG. The processes and outcomes associated with the first CSAU evaluation methodology element, requirements, and code capability are summarized in Fig. 3.

**Element 2: Assessment and Ranging of Parameters (Steps 7–10, Fig. 2)**

The processes and outcomes associated with the second CSAU evaluation methodology element, assessment, and ranging of parameters, are summarized in Fig. 4. A test data matrix was established to a) assess code accuracy to calculate the important processes shown in Fig. 3, and b) address code deficiencies identified in step 6.

The nodalization of the NPP was guided by past experience, by the need to capture the important phenomena and the design characteristics of the plant, and by the desire to perform NPP calculations in a timely and cost-effective manner. Subsequent assessment using SET and IET data were performed using the same nodalization.

Where possible, auxiliary calculations not requiring application of TRAC-PF1/MOD1 were used to further reduce the number of uncertainty parameters associated with the highly ranked phenomena identified in step 3, Fig. 2. For example, a closed-form fuel-rod model was developed at Brookhaven National Laboratory (BNL) and used to further reduce the set of stored energy and fuel response related parameters requiring evaluation to quantify individual contributions to uncertainty (Ref. 21): the reduced set of parameters was the gap conductance, peaking factor, fuel conductivity, surface heat transfer coefficient, and the minimum homogeneous nucleation temperature ($T_{min}$). This process is illustrated in Fig. 4. For these remaining parameters, uncertainty ranges were determined and used later in the NPP calculations (step 12, Fig. 2). Where such simplified models could not be identified, code

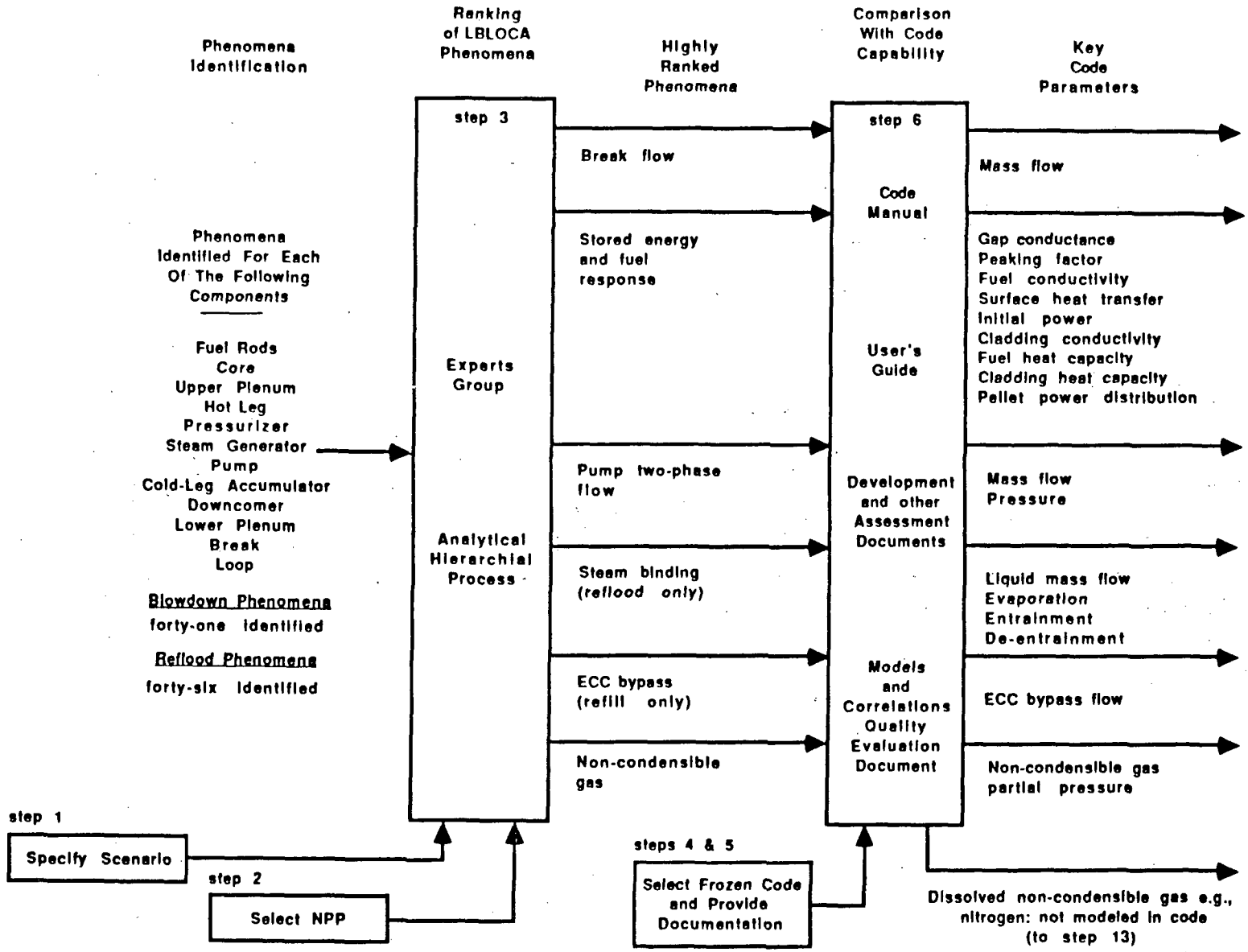


**Fig. 3.**

Illustration of Element 1, Requirements and Code Capabilities, of the CSAU Methodology as applied to a LBLOCA and TRAC-PF1/MOD1.

assessments were performed using the SET and IET data. Such assessments proved useful in two ways, one direct and one indirect.

First, data were used directly to develop uncertainty ranges for the selected code parameters. The individual uncertainty contributions of previously identified parameters relative to selected data were determined (steps 9 and 10, Fig. 2) and later input to the NPP model so that the effect upon the primary safety criteria (PCT in the demonstration) could be evaluated (step 12, Fig. 2). For example, the scale-related bias in the TRAC-PF1/MOD1 prediction of ECC bypass as measured by the lower-plenum filling rate was examined at BNL (Ref. 22). BNL examined the data from Creare 1/15 and 1/5 scale downcomer tests, the Battelle Columbus Laboratory 2/15 downcomer tests, and UPTF 1/1 scale downcomer tests. Based on these studies, it was demonstrated that a scale effect exists in the code when modeling the ECC bypass. TRAC was shown to overpredict the delivery of ECC to the lower plenum at smaller scales and underpredict the delivery of liquid at full scale. The BNL work provided convincing evidence of a scale-related bias in TRAC regarding the prediction of ECC bypass phenomena. This code bias was subsequently quantified using a bounding argument and the result factored into the overall quantification of uncertainty as an additional margin (step 13).

Second, the data were used in a supportive role to provide insight into the accuracy of code calculations and to confirm conclusions that were being drawn regarding specific CSAU studies. LBLOCA transients have been run in reduced-scale integral and separate effect facilities such as Semiscale, the Loss-of-Fluid Test Facility, the Cylindrical Core Test Facility, and the Slab Core Test Facility. Numerous assessment calculations have been performed using the data from these tests. From such calculations it is possible to state that a given code, e.g., TRAC-PF1/MOD1, will predict a selected parameter in the sub-scale facility, such as PCT or cladding quench time, with a stated bias and within a stated uncertainty band. In addition, the level of confidence related to such calculations can be provided. Although such results provide insight into the ability of the code to calculate similar phenomena in operating plants, they do not, in themselves, transfer directly to the full-size plant. Therefore, such results are considered to be supportive within the context of the CSAU methodology. It is important to emphasize, however, that the availability of such supportive results is important. In addition to increasing confidence that the dominant phenomena are modeled in the code, the quantified uncertainty for full-size plants can be checked for both trends and magnitudes as insurance that problems in application of the CSAU method at full scale do not go unrecognized.

**Element 3: Sensitivity and Uncertainty Analysis (Steps 11–14, Fig. 2)**

The approach taken to quantifying the total mean and total 95% probability PCTs, including margins, is illustrated in Fig. 5. Inputs for NPP calculations come from several sources. One source of uncertainty is related to code, scale, and experimental data contributors to uncertainty (e.g., pump and break flow characterization, core heat transfer coefficient calculation, and $T_{min}$ calculation), which are evaluated as part of the second CSAU evaluation methodology element (steps 9–10, Fig. 2); the ranges and distributions of these parameters were used to specify one set of NPP calculations. Another source of uncertainty is the range and distribution of plant operating conditions and process variations that arise from imprecise knowledge about the reactor state during the transient. For example, the ranges and distributions of the fuel conductivity, gap conductance, and peaking factor as a function of the

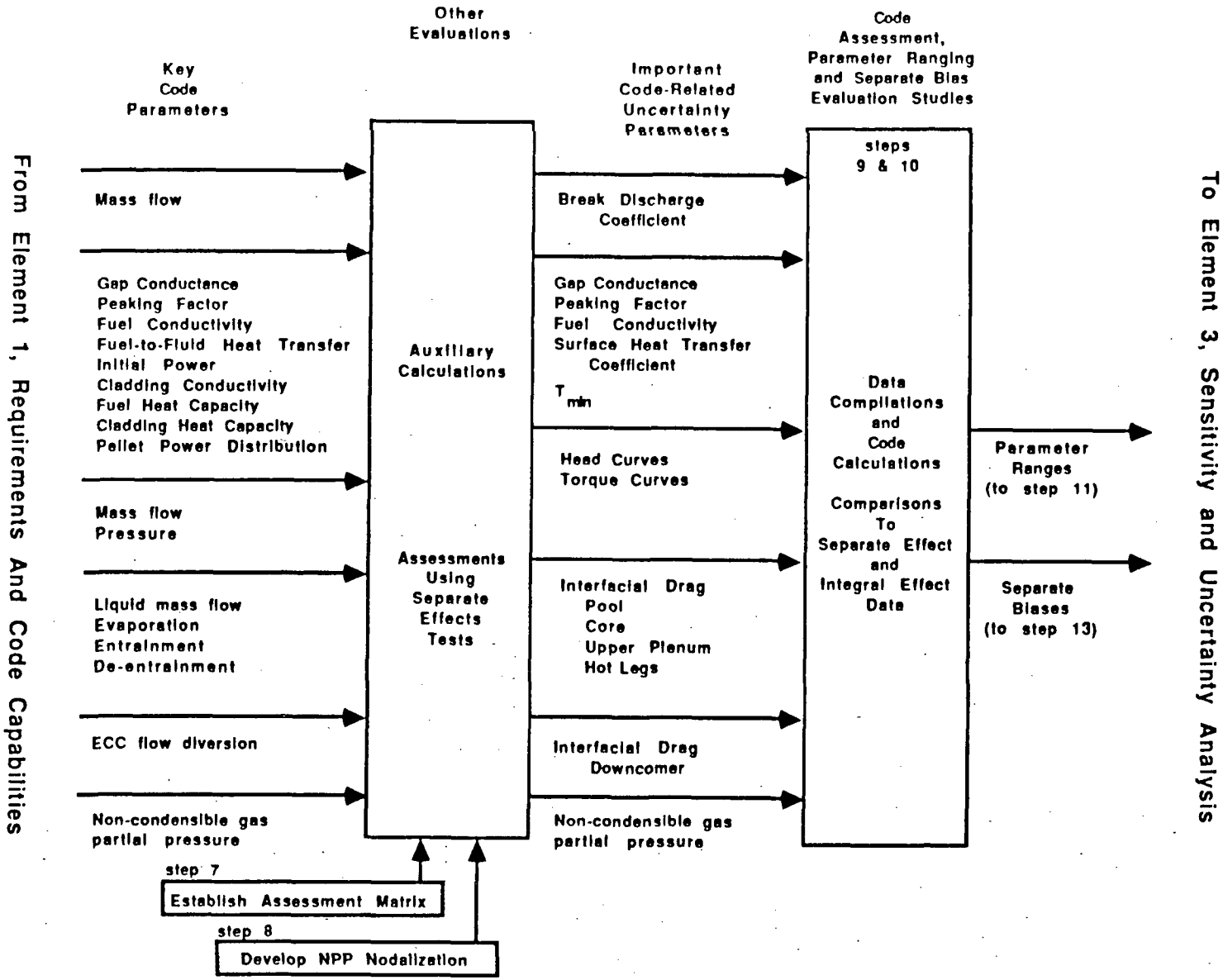


**Fig. 4.**
Illustration of Element 2, Assessment and Ranging of Parameters, of the CSAU Methodology as applied to a LBLOCA and TRAC-PF1/MOD1.

burn-up cycle and the original manufacturing tolerances were determined and used to specify a second set of NPP calculations (step 11, Fig 2). The result of each NPP run was a PCT related to the particular parameters specified.

To combine these individual uncertainties (step 12, Fig. 2), a probability distribution function (pdf) was generated from Monte Carlo sampling of a response surface representing the code output from the NPP calculations described above. The response surface methodology requires that a pdf be specified for each of the significant parameters; a uniform distribution was chosen because investigation of the literature does not indicate that the uncertainty of any of the parameters exhibits a particular distribution in its experimental data. Also, a uniform distribution requires the least prior knowledge (Ref. 23). For the CSAU demonstration, 184 calculated PCT total points arising from TRAC-PF1/MOD1 calculations were used to construct response surfaces. Many of the points arose from cross-product calculations; 22 of the 184 points were single parameter variations, 98 were double, 57 triple, and 7 quadruple. For the blowdown peak, response surfaces were constructed for seven significant LOCA parameters: peaking factor, gap conductance, fuel conductivity, fuel-to-fluid heat transfer coefficient, break discharge coefficient, pump characteristic, and $T_{min}$. For each response surface, a process of random sampling or Monte Carlo was used to get the values of mean PCT, the standard deviation, and the PCT at the 95th percentile probability level. A 50,000 history Monte Carlo sample appears to provide an acceptable degree of convergence. The statement of combined uncertainty by pdf includes the specification of a mean PCT and the PCT at 95% probability. For the CSAU demonstration, it has been concluded that a TRAC-PF1/MOD1 prediction of the PCT during a cold-leg LBLOCA in a Westinghouse four-loop PWR with 17 x 17 fuel will be equal to or less than 1447°F (1059 K) 95% of the time. This PCT occurs during blowdown.

However, this is not a final statement of the total uncertainty (mean and 95% probability PCT) until appropriate separate biases are incorporated. As the effects of some contributors to uncertainty were not quantified by means of sensitivity calculations and response surface (because of limited data base, considerations of cost effectiveness and/or scheduling, etc.), separate biases were evaluated based on bounding calculations. These separate biases are included in the total uncertainty as shown in Fig. 5. For the CSAU demonstration, five separate biases were evaluated in this manner.

First, a bias was quantified to account for hot channel effects that could be modeled with the code but were not modeled for economic reasons. Second, a bias was estimated for uncertainty related to modeling phenomena associated with the presence of NCG. The TRAC-PF1/MOD1 code includes the capability for modeling NCG as a separate fluid component, e.g., following the movement of the accumulator cover gas before and following accumulator injection. However, the code does not include models for dissolved NCG. Because the code lacked this modeling capability, the bias associated with dissolved NCG was analyzed and bounded. Third, a bias was taken for a code error, a nonconservative implementation of a heat transfer correlation that did not adequately represent scale effects. Fourth, a bias was taken by bounding ECC bypass effects to account for code correlations that did not adequately represent scale effects. Fifth, a bias was taken for steam binding effects because the code did not adequately model core entrainment processes.

The total uncertainty in PCT is obtained by adding the combined uncertainty by pdf and the additional separate biases described above. For the CSAU demonstration, the contributors

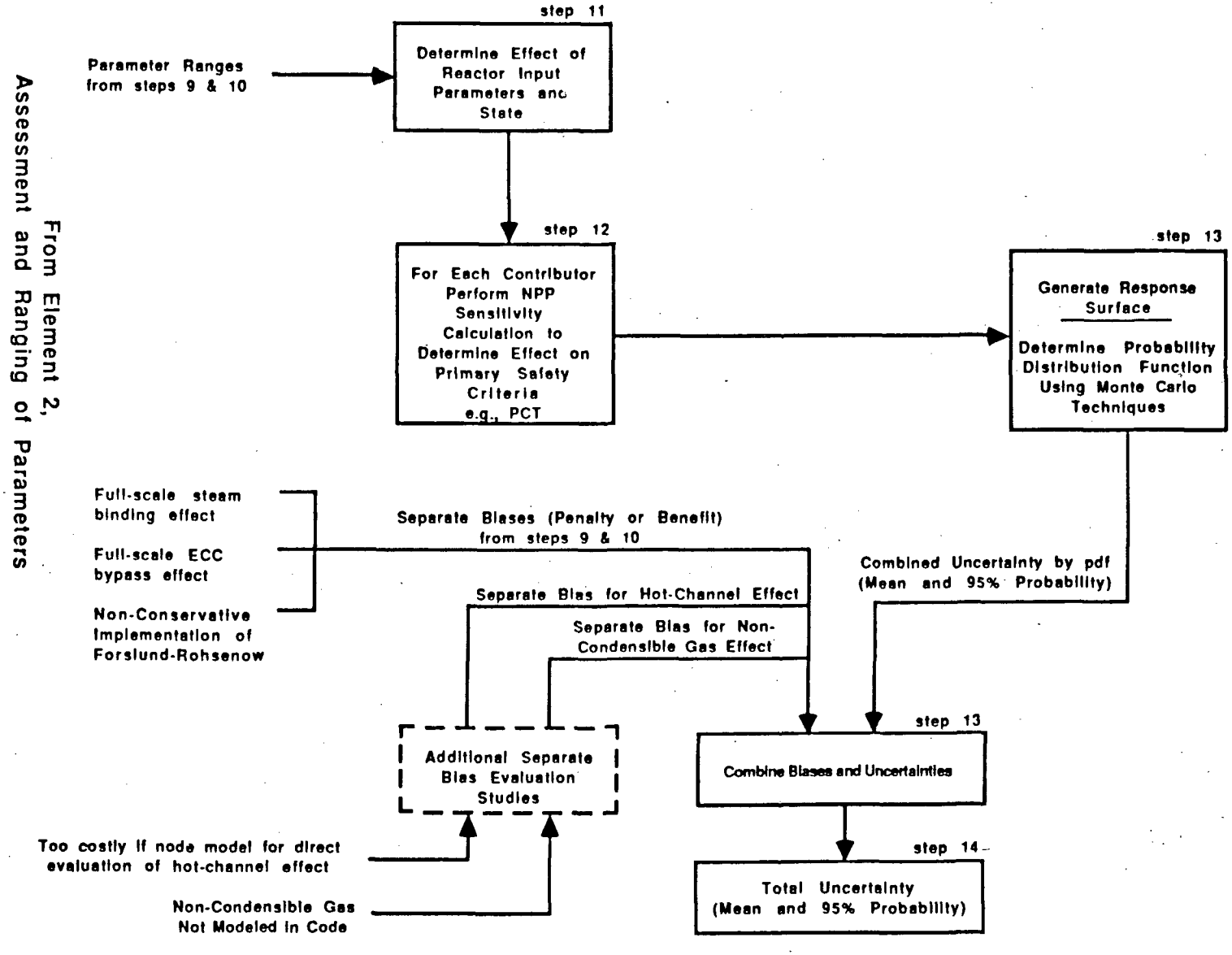


**Fig. 5.**
Illustration of Element 3, Sensitivity and Uncertainty Analysis, of the CSAU Methodology as Applied to a LBLOCA and TRAC-PF1/MOD1.

to the total uncertainty are presented in Table I. From Table I it can be seen that the mean and 95% probability PCTs, excluding separate biases, reach maximums during the blowdown, and lesser peaks are predicted for the first and second reflood peaks. After including the combined biases, the total mean PCT still occurs during reflood. However, the total 95% probability PCT including the combined margins occurs during the second reflood peak and is 1572°F (1129 K). This shift in the peak to the latter part of the LBLOCA transient is a reflection of the increasing uncertainty in PCT as time increases and the increasing importance of several separate biases later in the transient. In this regard, the two key contributors are the nonconservative implementation of the Forsland-Rohsenow correlation and steam binding effects. Each of these margins is related to code model and correlation defects and could be eliminated by improving the appropriate code models and correlations.

## SUMMARY

The commissioners of the NRC recently approved the final version of a revised rule for the acceptance of ECCS. The revised rule permits alternate ECCS performance analysis, based on BE methods, to be used provided the licensee quantifies the uncertainty of the estimates and includes that uncertainty when comparing the calculated results with prescribed acceptance limits. Under NRC sponsorship, a CSAU evaluation methodology has been defined and a demonstration completed for a Westinghouse four-loop PWR with 17 x 17 fuel. The demonstration considered a cold-leg LBLOCA and calculated the total uncertainty associated with use of the thermal-hydraulic systems code, TRAC-PF1/MOD1, Version 14.3.

The demonstration effort showed that uncertainties in the complex phenomena occurring during accident conditions in NPPs can be quantified. The demonstrated methodology is auditable, traceable, and practical in the sense that sound engineering judgment, accompanied by external peer review, is an integral part of the process. The demonstration results confirm the existence of a significant margin in current plant operating conditions for the demonstration NPP.

## ACKNOWLEDGMENTS

Development and demonstration of the CSAU evaluation methodology was a team effort by the TPG-member authors of this paper and their co-workers at the participating institutions. The lead author of this paper wishes to acknowledge that much of the information presented in this paper was extracted from CSAU documentation prepared by other members of the TPG. In particular, the significant contributions by Idaho National Engineering Laboratory staff members G. E. Wilson and K. R. Katsma are gratefully acknowledged.

## TABLE I

## TOTAL UNCERTAINTY FOR THE CSAU DEMONSTRATION*

| | PCT (F)** | | |
|---|---|---|---|
| | BLOWDOWN | REFLOOD | |
| | | 1st Peak | 2nd Peak |
| Mean PCT (combined uncertainty by pdf) | 1162(901) | 978(799) | 758(676) |
| 95% probability PCT (combined uncertainty by pdf) | 1447(1059) | 1399(1032) | 1336(997) |
| Mean separate biases added for: | | | |
| Hot-channel effects | 63(35) | 25(14) | -14(-8) |
| NCG effect (dissolved nitrogen) | N/A | 18(10) | 18(10) |
| Nonconservative implementation of Forsland-Rohsenow correlation in code | 47(26) | 84(47) | 160(89) |
| Full-scale steam binding effects | N/A | -9(-5) | 106(59) |
| Full-scale ECC bypass effects | N/A | -34(-19) | -34(-19) |
| Combined mean biases | 110(61) | 84(47) | 236(131) |
| Total mean PCT (including combined biases) | 1272(962) | 1062(845) | 994(807) |
| Total 95% probability PCT (including combined biases) | 1557(1120) | 1483(1079) | 1572(1129) |

*Application to a four-loop Westinghouse PWR for a cold-leg LBLOCA and using TRAC-PF1/MOD1, Version 14.3.

**Numbers shown in parenthesis are PCT in K.

## REFERENCES


1. "Emergency Core Cooling Systems; Revisions to Acceptance Criteria," Federal Register V53, N180, pp 35996-36005 (September 16, 1988).
2. B. W. Sheron and N. Zuber, "Treatment of Uncertainties in the Regulatory Process," Transactions of the American Nuclear Society, **56**, 364–365 (1988).
3. G. W. Wilson, B. E. Boyack, R. B. Duffey, P. Griffith, K. R. Katsma, G. S. Lellouche, U. S. Rohatgi, W. Wulff, and N. Zuber, "Quantifying Reactor Safety Margins, Part II: Characterization of Important Contributors to Uncertainty," Proceedings of the 16th Water Reactor Safety Information Meeting, October 24–27, 1988, Gaithersburg, Maryland (to be published).
4. W. Wulff, B. E. Boyack, R. B. Duffey, P. Griffith, K. R. Katsma, G. S. Lellouche, U. S. Rohatgi, G. E. Wilson, and N. Zuber, "Quantifying Reactor Safety Margins, Part III: Assessment and Ranging of Parameters," Proceedings of the 16th Water Reactor Safety Information Meeting, October 24–27, 1988, Gaithersburg, Maryland (to be published).
5. G. S. Lellouche, B. E. Boyack, R. B. Duffey, P. Griffith, K. R. Katsma, U. S. Rohatgi, G. E. Wilson, W. Wulff, and N. Zuber, "Quantifying Reactor Safety Margins, Part IV: Uncertainty Evaluation of LBLOCA Analysis Based on TRAC-PF1/MOD1," Proceedings of the 16th Water Reactor Safety Information Meeting, October 24–27, 1988, Gaithersburg, Maryland (to be published).
6. C. E. Slater and R. T. Jensen, "LOCA/ECCS Analysis-Historical Development of Appendix K and Implementation of EM Models," Electric Power Research Institute workshop on Appendix "K" Relief Using Best Estimate Methods: The Revised LOCA/ECCS Rule, Cambridge, Massachusetts (August 11–12, 1988).
7. R. K. House and S. P. Kalra, "Interpretation of Proposed LOCA/ECCS Rule Change - Focus on Requirements and Options," Electric Power Research Institute workshop on Appendix "K" Relief Using Best Estimate Methods: The Revised LOCA/ECCS Rule, Cambridge, Massachusetts (August 11–12, 1988).
8. L. H. Sullivan, "Uncertainty in LOCA Analysis Historical Discussion," Los Alamos National Laboratory document LA-UR-88-2631 (August 1988).
9. 10 CFR Part 50, "Acceptance Criteria for Emergency Cooling Systems for Light-Water-Cooled Nuclear Power Plants," Federal Register **39** (3) (January 4, 1974).
10. R. E. Collingham, "Impact of Appendix K on Fuel Designs," Electric Power Research Institute workshop on Appendix "K" Relief Using Best Estimate Methods: The Revised LOCA/ECCS Rule, Cambridge, Massachusetts (August 11–12, 1988).
11. R. Steiger, "Extended BE/EM Study," Idaho National Engineering Laboratory letter STIG-177–77 (1977).
12. F. F. Cadek, L. E. Hochreiter, and M. Y. Young, "Best Estimate Approach for Effective Plant Operation and Improved Economy," Electric Power Research Institute workshop on Appendix "K" Relief Using Best Estimate Methods: The Revised LOCA/ECCS Rule, Cambridge, Massachusetts (August 11–12, 1988).

13. G. L. Sozzi, "On the Development of New BWR LOCA Models - Technology Application and Results," Electric Power Research Institute workshop on Appendix "K" Relief Using Best Estimate Methods: The Revised LOCA/ECCS Rule, Cambridge, Massachusetts (August 11–12, 1988).

14. K. Cornwell, G. Sozzi, and B. Chexal, "Basis for Relaxing ECCS Performance Requirements for BWR/4s," Electric Power Research Institute document NSAC-130 (September 1988).

15. Technical Program Group, "Quantifying Reactor Safety Margins-Application of CSAU Methodology to a LBLOCA," EG&G Idaho, Inc. report NUREG/CR-5249 (to be published).

16. R. A. Shaw, T. K. Larson, and R. K. Dimenna, "Development of a Phenomena Identification and Ranking Table (PIRT) for Thermal-Hydraulic Phenomena During a PWR LBLOCA," EG&G Idaho, Inc. document NUREG/CR-5074 (August 1988).

17. D. R. Liles, et. al., "TRAC-PF1/MOD1: An Advanced Best Estimate Computer Program for PWR Thermal-Hydraulic Analysis," Los Alamos National Laboratory report NUREG/CR-3858 (July 1986).

18. B. E. Boyack, H. Stumpf, and J. F. Lime, "TRAC User's Guide," Los Alamos National Laboratory report NUREG/CR-4442 (November 1985).

19. M. S. Sahota and F. L. Addessio, "TRAC-PF1/MOD1 Developmental Assessment," Los Alamos National Laboratory report NUREG/CR-4278 (August 1985).

20. D. R. Liles, et. al., "TRAC-PF1/MOD1 Correlations and Models," Los Alamos National Laboratory report NUREG/CR-5069 (Draft) (to be published).

21. W. Wulff, "Uncertainties in Modeling and Scaling in the Prediction of Fuel Store Energy and Thermal Response," Brookhaven National Laboratory report NUREG/CR-5232 (June 1988).

22. U. S. Rohatgi, L. Y. Neymotin, and W. Wulff, "PCT Uncertainty from Downcomer Modelling and UPTF Experiments," Brookhaven National Laboratory report NUREG/CR (to be published).

23. S. Levy, G. Lellouche, R. May, B. E. Boyack, R. B. Duffey, P. Griffith, K. R. Katsma, U. S. Rohatgi, G. E. Wilson, W. Wulff, and N. Zuber, "Elements of Uncertainty and Meaning of 95LOCA/ECCS Analysis," Electric Power Research Institute workshop on Appendix "K" Relief Using Best Estimate Methods: The Revised LOCA/ECCS Rule, Cambridge, Massachusetts (August 11–12, 1988).

# QUANTIFYING REACTOR SAFETY MARGINS PART 2 - CHARACTERIZATION OF IMPORTANT CONTRIBUTORS TO UNCERTAINTY

by

Gary E. Wilson
EG&G Idaho, Inc.
Idaho National Engineering Laboratory
and
B. E. Boyack(LANL), R. B. Duffey(INEL), P. Griffith(MIT),
K. R. Katsma(INEL), G. S. Lellouche(SLI), S. Levy(SLI), U. S. Rohatgi(BNL),
W. Wulff(BNL), and N. Zuber(NRC)

## ABSTRACT

The NRC has issued a revised ECCS rule which allows the use of best estimate computer codes for safety analysis, providing the uncertainty of the calculations are quantified and compared with acceptance limits contained in 10 CFR Part 50. To support the revised rule, the NRC and its contractors and consultants have developed and demonstrated a methodology to quantify uncertainty called CSAU (Code Scaling, Applicability and Uncertainty). The methodology consists of three primary elements containing 14 Steps. The first element, "Requirements and Capabilities", which contains the first six steps, is described and demonstrated in this paper. The objective of this element is to characterize the important contributors to uncertainty. The objective is accomplished by determining the applicability of a code to analysis of a transient in a Nuclear Power Plant through comparison of the scenario- and plant-dictated requirements with the simulation capabilities of the code.

## INTRODUCTION

An overview of the complete CSAU methodology, including its background, objectives and general structure, is given in a companion paper (Reference 1). The information contained in Reference 1 is considered a preface to this paper.

The CSAU methodology emphasizes a practical engineering approach that can be used to quantify code uncertainty. The CSAU procedure can be most easily conceptualized as consisting of fourteen primary

---

* Work supported by the U.S. Nuclear Regulatory Commission, Office of Nuclear Regulatory Research, under DOE Contract No. DE-AC07-76ID01570.

steps which can be grouped in three key elements:

Requirements and Capabilities, in which scenario modeling requirements are identified and compared against code capabilities to determine the code's applicability to the particular scenario and to identify potential limitations.

Assessment and Ranging of Parameters, in which code capabilities to calculate processes important to the scenario are assessed against experimental data to determine code accuracy, scale-up capability and ranges of parameter uncertainties needed for sensitivity studies.

Sensitivity and Uncertainty Analysis, in which the effects of individual contributors to total uncertainty are obtained, and for which the propagation of uncertainty through the transient is properly accounted.

The elements and steps of the methodology are diagramed in Figure 1. This paper addresses only the Requirements and Capabilities element. The Assessment and Ranging of Parameters element and the Sensitivity and Uncertainty Analysis element are addressed in companion papers, (References 2 and 3, respectively).

The Requirements and Capabilities element consists of Steps 1 through 6 (see Figure 1). The applicability of a code to the analysis of a transient in a NPP is determined by comparison of the scenario- and plant-dictated requirements with the simulation capabilities of the code. The steps needed to achieve this objective are the selection of a specific scenario (Step 1) and power plant (Step 2), the identification and ranking of phenomena (Step 3), the selection of computer code (Step 4), the documentation of the computer code (Step 5), and a determination of the code applicability (Step 6). These steps are now discussed individually; first at the general process level, followed by a typical application to a large break loss of coolant accident (LBLOCA).

## SCENARIO SPECIFICATION (STEP 1)

### Process Description

Determination of a code's applicability and uncertainty is scenario-dependent because the dominant processes and safety parameters change from one scenario to another. The transient scenario therefore dictates the processes that must be addressed. Once the scenario has been selected, the most important phenomena may be identified. In this process, it is advantageous to subdivide the scenario into phases. By doing so, the complexity of analyzing the components and phenomena is reduced. The subdivision allows reduction of the analysis to only those processes and components that are important during each phase. By carefully defining the scenario and its phases, the groundwork for the identification and ranking of the components and processes is laid.

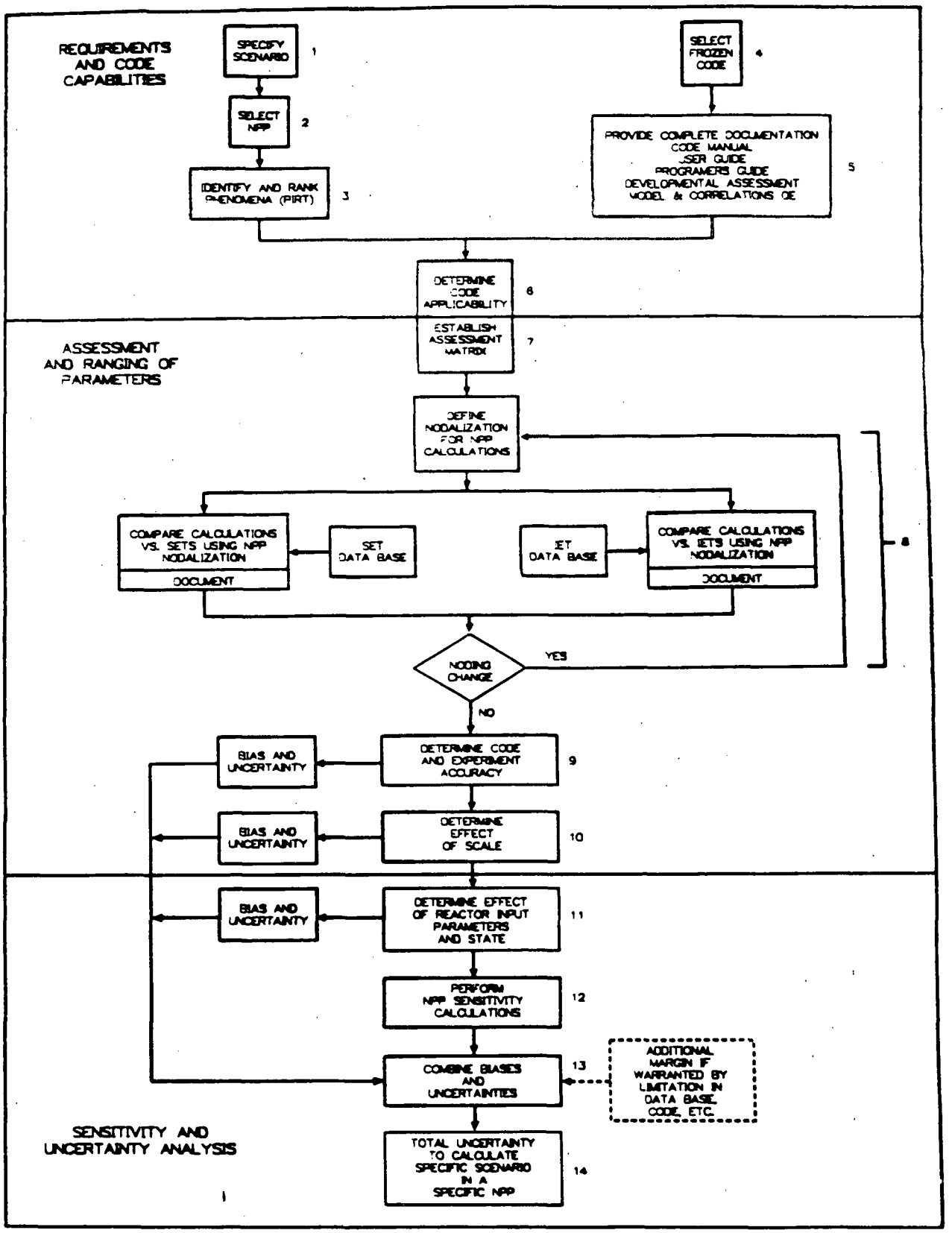


NSE0105

Figure 1. Code scaling, applicability and uncertainty (CSAU) methodology.

Typical Application to LBLOCA

The scenario used to demonstrate the methodology is a hypothesized double-ended cold leg break between the emergency core coolant (ECC) injection nozzle and the reactor vessel. This hypothesized break is a design basis accident for Pressurized Water Reactors (PWRs) and is expected to produce the maximum fuel rod clad temperature. In accordance with 10 CFR part 50 the primary safety criteria, and their limits, for this accident are:

Peak Clad Temperature (PCT) - 2200 $^{0}F$
Cladding Oxidation - 17 percent of local potential
Hydrogen Generation - 1% of the total potential

As shown in the companion papers, the threshold values of clad temperature where significant oxidation and hydrogen generation result were never encountered. Thus, PCT remained the important primary safety criteria for the LBLOCA demonstration case.

To facilitate analysis, the Large Break Loss of Coolant Accident (LBLOCA) scenario is subdivided into three time periods that characterize events during the sequence. These time periods, termed blowdown, refill, and reflood, are defined by the core and lower plenum liquid mass fraction behaviors shown in Figure 2. A comprehensive discussion of LBLOCA thermal-hydraulic phenomena is found in the Compendium of ECC Research for Realistic LOCA Analysis (Reference 4). A comprehensive discussion of the LBLOCA sequence of events is found in the process identification and ranking document (Reference 5).

During the LBLOCA transient, two or more peaks are noted in the clad temperature. Figure 3 illustrates three peaks for one of the fuel rods in the LOFT L2-2 experiment that realistically simulated a PWR LBLOCA (Reference 6). The first peak is associated with the blowdown time period and is caused by the initial stored energy in the fuel rods and degraded fuel rod-to-coolant heat transfer. The second and third peaks occur during refill and reflood when the rod temperatures increase due to decay heat and poor fuel rod-to-coolant heat transfer. The following sections briefly summarize the thermal-hydraulic phenomena and sequence of events for PWR LBLOCA blowdown, refill, and reflood.

The blowdown period is the result of the break in the coolant system through which the primary coolant is expelled. Blowdown physical processes include critical flow at the break, fluid flashing and depressurization, and heating of the fuel rods due to degraded heat transfer. During blowdown, some components are affected more than others. In particular, the heat generated in the core may not be adequately removed due to decreased heat transfer resulting from the loss of fluid. The performance of the reactor coolant pumps will degrade as the coolant flashes. The steam generator heat transfer degrades because primary system temperatures are lower than secondary system temperatures during this period. Important phenomena and processes for blowdown are:

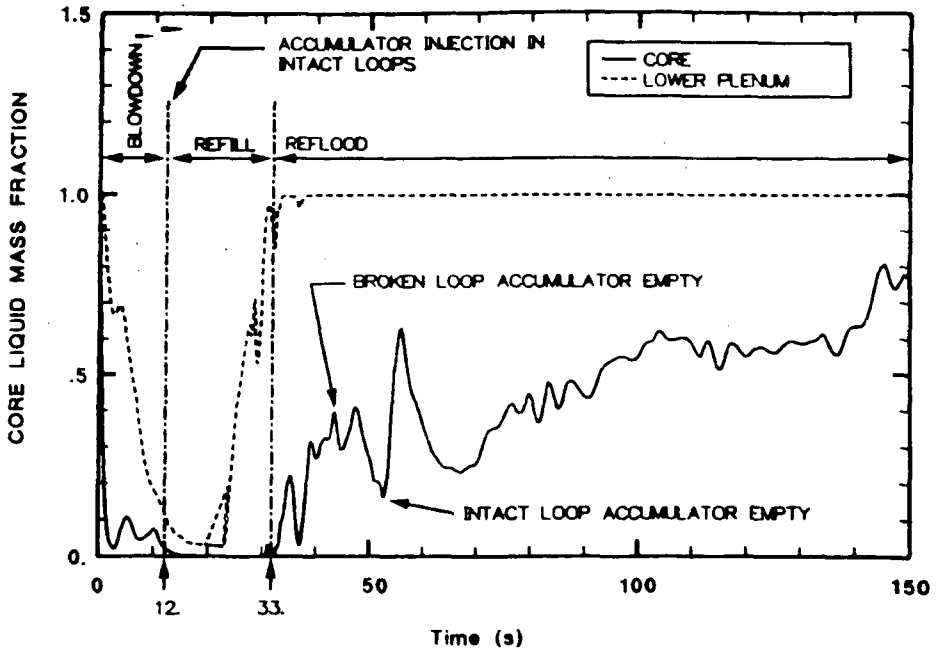


Figure 2. Calculated liquid fractions in core and lower plenum, showing blowdown, refill and reflood phases.

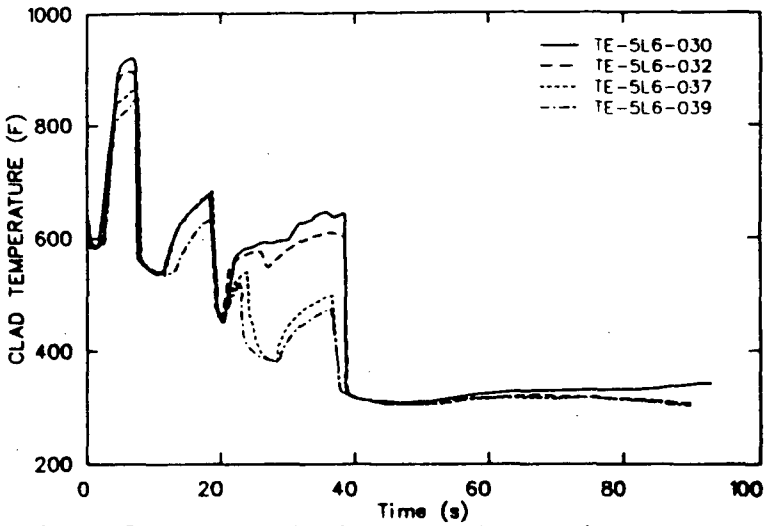


Figure 3. Measured cladding temperatures during blowdown in LOFT.

- o Subcooled and saturated critical flows at the break
- o Flashing and voiding in all volumes
- o Depressurization
- o Release of stored and decay heat in the fuel
- o Boiling and DNB on the cladding surface

During the refill period the reactor system starts to recover as the safety systems inject ECC into the primary system. Refill physical processes are the operation of the ECC systems, the penetration of ECC water into the lower plenum, and potential ECC bypassing through the broken cold leg to the containment. The important refill components and processes therefore concern the distribution of water in the reactor vessel, and include:

- o CCFL and ECC bypass in the downcomer
- o Decay heat in the fuel
- o Heat transfer in the core and lower plenum
- o ECC penetration into the lower plenum

Finally, when ECC water has filled the lower plenum, core recovery is initiated during the reflood period as the hot fuel rods are recovered with water. The reflood process may be quite slow because much of the water is boiled and transported as steam and entrained droplets into the upper plenum and hot leg regions. If sufficient water is entrained, carried to the steam generator, and boiled within the tubes, then a back pressure may develop that reduces the flooding rate. During reflood the important process and phenomena include:

- o Decay heat
- o Heat conduction in the gap and cladding
- o Liquid entrainment in the steam at the quench front
- o Deentrainment of liquid in the upper plenum
- o Droplet evaporation in the steam generator U-tubes
- o Pool boiling in the core
- o Quenching of the heated rods by the rising liquid level and by the falling film

## SELECT THE NUCLEAR POWER PLANT (STEP 2)

Process Description

A complete scenario definition depends on the particular plant in which it occurs because the dominant phenomena and their interactions differ to varying degrees with the reactor design. The various U. S. reactor vendors of pressurized water reactor systems have individual designs. Although, overall, PWR systems are similar, individual components differ significantly. As examples, fuel rod design, core loading, steam generator tubes, number of loops, safety injection, and control systems differ significantly from plant to plant. The selection of a particular plant is crucial to the CSAU process because the resulting uncertainty is highly dependent on the phenomena and components identified.

Typical Application to LBLOCA

In this demonstration of the CSAU methodology, a generic Westinghouse four loop RESAR-3S plant model is selected. For this plant the core consists of 193 fuel bundles containing 264 fuel pins, in a 17 x 17 array, which generate 3411 $MW_t$ at normal full-power operation. The core for this application has an assumed operating history based on a burnup of 16000 MWD/T, representing midlife in the second fuel cycle. In the RESAR-3S plant, each of the four coolant loops consists of a steam generator, reactor coolant pump, associated piping, and emergency core cooling systems (ECCS). The steam generators are of the vertical U-tube Westinghouse configuration containing inconel tubes, and the reactor coolant pumps are of single-stage, centrifugal design. An electrically heated pressurizer is connected to one of the loops. Additional details of the plant are given in the plant modeling discussions of a companion paper (Reference 2).

## IDENTIFY AND RANK PHENOMENA (STEP 3)

Process Description

Plant behavior is not equally influenced by all processes and phenomena that occur during a transient. The most cost efficient, yet sufficient analysis reduces all candidate phenomena to a manageable set by identifying and ranking the phenomena with respect to their influence on the primary safety criteria. Each phase of the scenario is separately investigated. The processes and phenomena associated with each component are examined. Cause and effect are differentiated. After the processes and phenomena have been identified, they are ranked with respect to their effect on the safety criteria for the scenario. A phenomena identification and ranking table (PIRT) is established to guide the subsequent uncertainty quantification.

The processes and phenomena that the codes must simulate are found by examining experimental data and code simulations related to the specified scenario. Independent techniques to accomplish the ranking include expert opinion, subjective decision making methods (such as Analytical Hierarchical Process [AHP]) and selected calculations. Examples of the first two of these are found in Reference 5, and the last in a companion paper (Reference 2). Comparison of the results of these techniques provides assurance of the accuracy and sufficiency of the process.

Typical Application to LBLOCA

The U. S. Nuclear Regulatory Commission (NRC) has completed a Phenomena Identification and Ranking Table (PIRT) project for the thermal-hydraulic phenomena during a LBLOCA in a Westinghouse 4-loop PWR (Reference 3). In the report on this project the phases of the transient are described, along with a detailed description of the potentially-important phenomena during each phase. Figures 4, 5, and 6 portray these potentially-important phenomena for the blowdown, refill, and reflood phases, respectively.

The phenomena were then ranked in importance by two independent

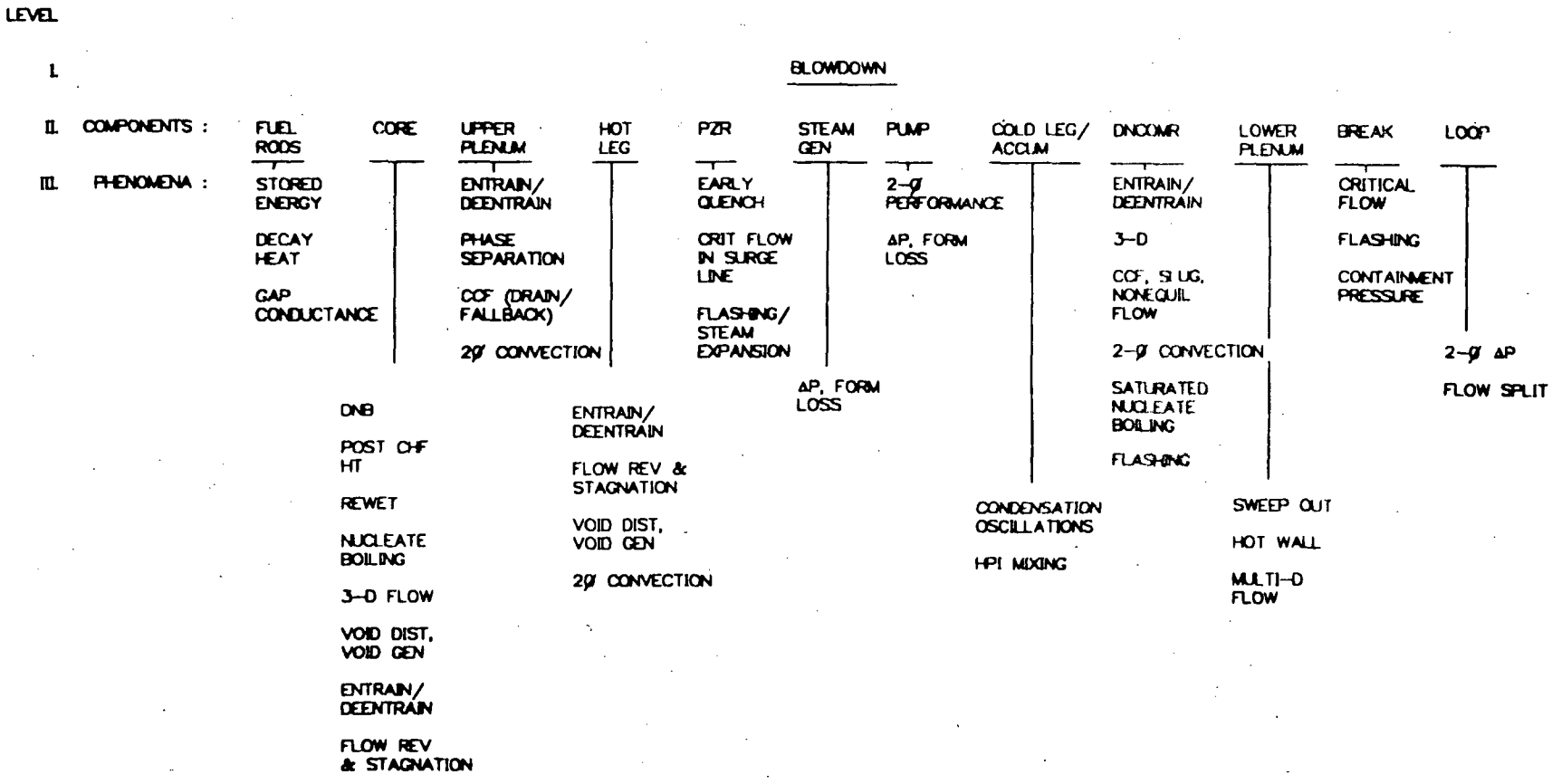


Figure 4. Component and Phenomena Hierarchy during LBLOCA blowdown.

NSL00638

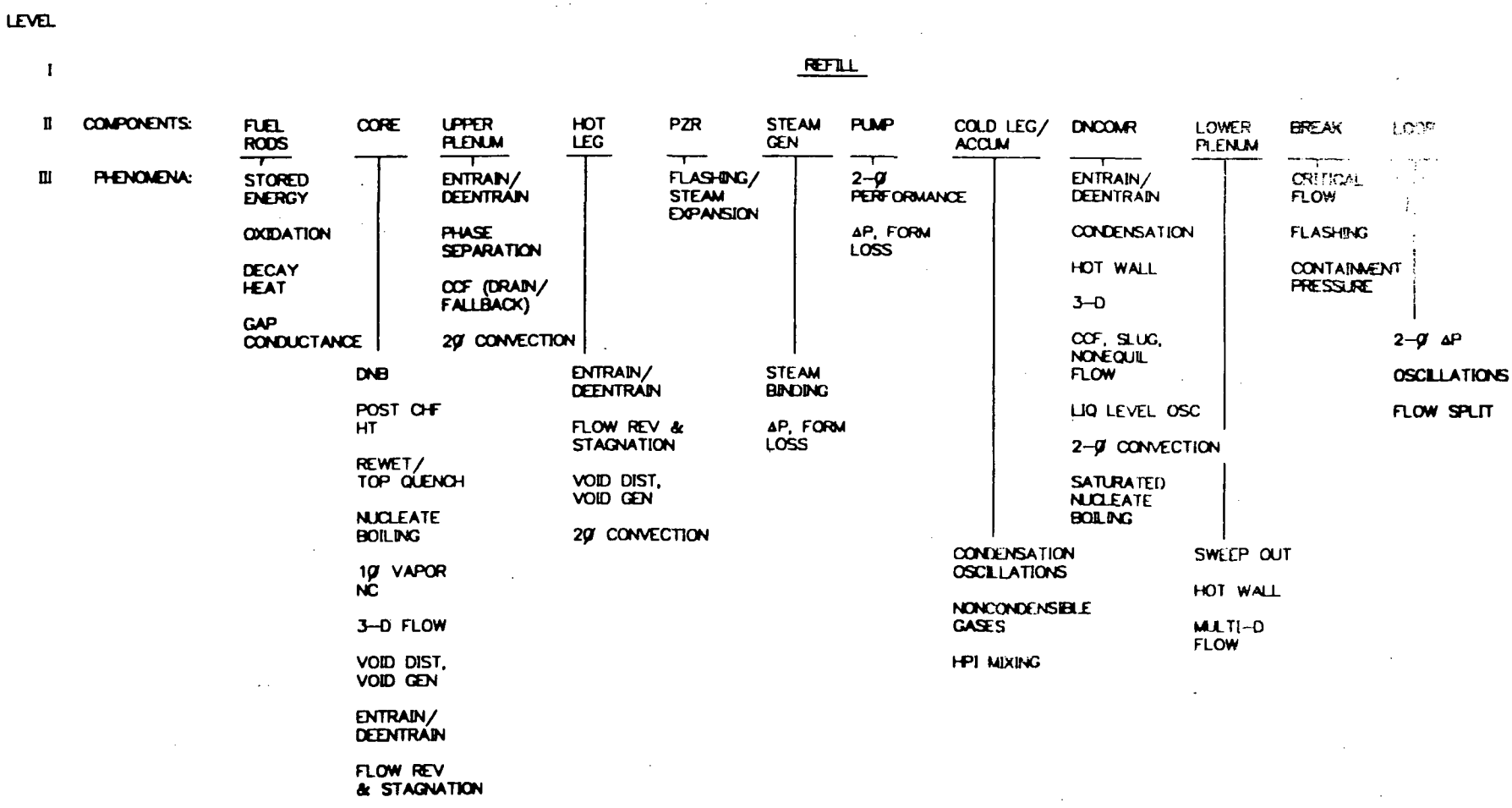


Figure 5. Component and Phenomena Hierarchy during LBLOCA refill.

NSL00639

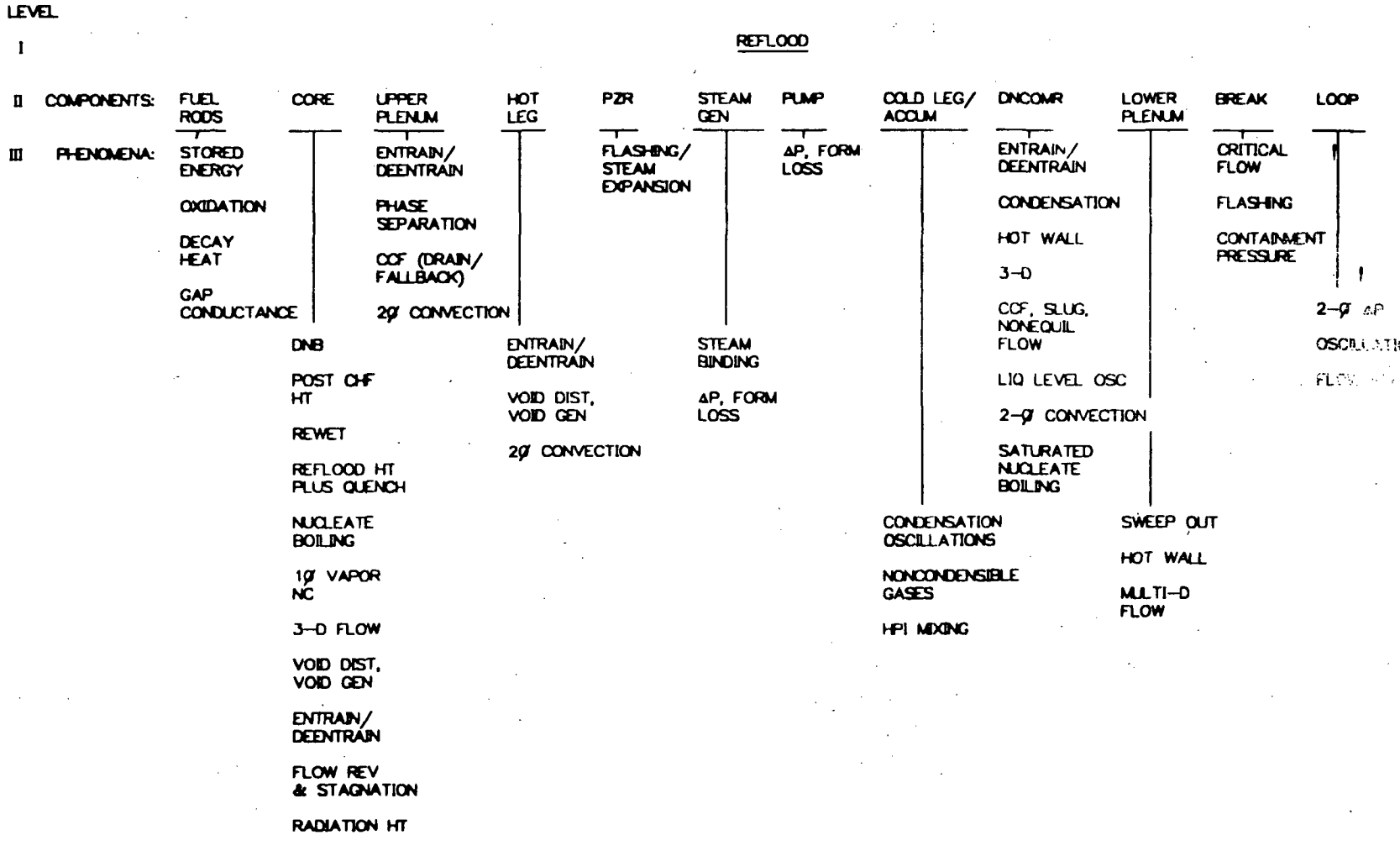


Figure 6. Component and Phenomena Hierarchy during LBLOCA reflood.

NSL00640

panels: (1) a group of experts, and (2) by a group of thermal-hydraulic analysts at the Idaho National Engineering Laboratory (INEL). The INEL effort employed an Analytical Hierarchical Process (AHP). The results of the independent rankings were compared to confirm the findings. A comparison summary of the rankings of both committees is provided in Table 1. The phenomena were ranked from 9, the highest rank, to 1, the lowest. Only the higher ranked phenomena (9, 8, and 7) are listed in the expert rankings. As shown, the thermal-hydraulic analysts found many of the physical phenomena had little impact on the primary safety criteria, the peak clad temperature.

The findings from the independent committees agree very well. The numerical ratings of the two committees for all higher ranked phenomena differ by at most a value of 2.

The important phenomena in each LBLOCA phase are summarized as follows. For blowdown, the fuel rod stored energy, break flow, and RCP degradation have the highest rank. During refill, the highest ranked phenomena are cold leg and downcomer condensation, and downcomer multi-dimensional flow. For reflood, the core reflood heat transfer, void generation, three-dimensional flow, entrainment and deentrainment in the upper plenum and hot legs, steam binding, and the effect of non-condensible gases in the cold legs receive the highest rating.

## SELECTION OF A "FROZEN" CODE VERSION (STEP 4)

### Process Description

For consistency, the methodology emphasizes the use of a "frozen" code version. A frozen computer code version is rigorously maintained, with changes allowed for corrections only. Model enhancements and code improvements are not allowed during the analysis period. This ensures that changes to the code after an evaluation has been completed do not impact the conclusions, and that changes occur in an auditable and traceable manner.

### Typical Application to LBLOCA

For this CSAU demonstration application, the code selected is TRAC-PF1/MOD1, Version 14.3 (Reference 7). The Nuclear Regulatory Commission requested the code developer, Los Alamos National Laboratory, to freeze this version of the code on September 11, 1987. This version has been preceded by many code versions, and the current version is demonstrated to be mature. A broad assessment effort has been completed and the code version is supported by a complete set of documentation, as described in the following section.

TABLE 1. SUMMARY OF EXPERTS RANKINGS AND AHP CALCULATED RESULTS

| | BLOWDOWN | | REFILL | | REFLOOD | |
|---|---|---|---|---|---|---|
| | Experts | AHP | Experts | AHP | Experts | AHP |
| Fuel rod | | | | | | |
| stored energy | 9 | 9 | | 2 | | 2 |
| oxidation | | - | | 1 | 8 | 7 |
| decay heat | | 2 | | 1 | 8 | 8 |
| gas conductance | | 3 | | 1 | 8 | 6 |
| Core | | | | | | |
| DNB | | 6 | | 2 | | 2 |
| post-CHF | 7 | 5 | 8 | 8 | | 4 |
| rewet | 8 | 8 | 7 | 6 | | 1 |
| reflood heat transfer | | - | | - | 9 | 9 |
| nucleate boiling | | 4 | | 2 | | 2 |
| 1-phase vapor natural circulation | | - | | 6 | | 4 |
| 3-D flow | | 1 | | 3 | 9 | 7 |
| void generation & distribution | | 4 | | 6 | 9 | 7 |
| entrainment/deentrainment | | 2 | | 3 | | 6 |
| flow reversal/stagnation | | 3 | | 1 | | 1 |
| radiation heat transfer | | | | | | 3 |
| Upper plenum | | | | | | |
| entrainment/deentrainment | | 1 | | 1 | 9 | 9 |
| phase separation | | 2 | | 1 | | 2 |
| CCF drain/fallback | | 1 | | 2 | | 6 |
| 2-phase convection | | 2 | | 1 | | 5 |
| Hot leg | | | | | | |
| entrainment/deentrainment | | 1 | | 1 | 9 | 9 |
| flow reversal | | 2 | | 1 | | - |
| void distribution | | 1 | | 1 | | 4 |
| 2-phase convection | | 2 | | 2 | | 3 |
| Pressurizer | | | | | | |
| early quench | 7 | 7 | | - | | - |
| critical flow in s.l. | | 7 | | - | | - |
| flashing | | 7 | | 2 | | 2 |
| Steam generator | | | | | | |
| steam binding | | - | | 2 | 9 | 9 |
| delta-p, form losses | | 2 | | 2 | | 2 |
| Pump | | | | | | |
| 2-phase performance | 9 | 9 | | 5 | | |
| delta-p, form losses | | 3 | | 3 | 8 | 8 |

TABLE 1. (CONT'D)

| | BLOWDOWN | | REFILL | | REFLOOD | |
|---|---|---|---|---|---|---|
| | Experts | AHP | Experts | AHP | Experts | AHP |
| Cold leg/accum | | | | | | |
| condensation | | 2 | 9 | 9 | | 5 |
| noncondensible gases | | - | | 1 | 9 | 9 |
| HPI mixing | | - | | 3 | | 2 |
| Downcomer | | | | | | |
| entrainment/deentrainment | | 2 | 8 | 8 | | 2 |
| condensation | | - | 9 | 9 | | 2 |
| countercurrent, slug, noneq | | 1 | | 8 | | 2 |
| hot wall | | - | 5 | 4 | 7 | 3 |
| 2-phase convection | | 2 | | 3 | | 2 |
| saturated nucleate boiling | | 1 | | 2 | | 2 |
| 3-D effects | | 2 | 9 | 7 | | 2 |
| flashing | | 1 | | - | | - |
| liquid level oscillations | | - | | 3 | | 7 |
| Lower plenum | | | | | | |
| sweep out | | 2 | 7 | 6 | | 5 |
| hot wall | | 1 | | 7 | 7 | 6 |
| multi-dimensional effects | | 1 | | 2 | | 7 |
| Break | | | | | | |
| critical flow | 9 | 9 | 7 | 7 | | 1 |
| flashing | | 3 | | 2 | | 1 |
| containment pressure | | 2 | | 4 | | 2 |
| Loop | | | | | | |
| 2-phase delta-p | 7 | 7 | | 7 | | 6 |
| oscillations | | - | 7 | 7 | 9 | 9 |
| flow split | | 7 | 7 | 7 | | 2 |

## PROVIDE COMPLETE CODE DOCUMENTATION (STEP 5)

Process Description

The documentation supporting the code must be consistent with the frozen code version. Adequate documentation allows evaluation of the code's application to a postulated scenario for a specific plant. The documentation should include, at a minimum, the user manual, user guide, developmental assessment reports, and most importantly the models and correlations quality evaluation (MC/QE) report. The MC/QE report provides a basis for the traceability of the models in the code and detailed information on the code closure relations. Information on correlation and

model sources, data bases, accuracy, scale-up capability, applicability to NPP conditions, and ideally the results of a line by line coding check is also documented. The MC/QE report represents a quality evaluation document that provides a blueprint as to what is in the code, how it got there, and where it came from. References 7 through 12 are typical examples of the required information.

Typical Application to LBLOCA

The relevant TRAC-PF1/MOD1 documentation consists of References 7 through 10 and the additional independent assessments given in the Appendix. The theory manual contains the computer program outline and basic methods (hydrodynamics, structural heat transfer, reactor kinetics, and solution strategy). Descriptions of the component models and user information (including input requirements) are also given. The TRAC users guide lists prerequisites for input model preparation, plus generated and detailed guidelines for preparing TRAC input models. The TRAC models and correlations document provides information on the original source, data base, accuracy, an applicability of models in the code. It also describes how the models are implemented in the code, any modifications, and assessment of effects due to modification and implementation. The developmental assessment report details the application of the code in the analysis of various experiments.

## DETERMINE CODE APPLICABILITY (STEP 6)

Process Description

Steps 1 through 3 identify the important transient and plant requirements for a code simulation. Steps 4 and 5 reveal the code's capability. Integration of the requirements and capabilities results in an understanding of the applicability of the code to the subject simulations. The desired goal is a statement of applicability regarding why a code is applicable for the scenario and plant and furthermore identifies the areas of deficiencies or limitations important to its computational accuracy. The stated limitations then become a part of the uncertainty determination, to the extent they are important.

By comparing the scenario and phenomena with the code and its documentation, an evaluation is made to determine if the code is applicable for the simulation. Codes typically are written for a specific task so generally the first response is that the code is applicable. However the applicability statement is more quantitative; the eventual outcome of the analysis is to state that the safety criteria is calculated accurately with a high probability.

If inadequacies are noted, they should be fully documented and, if possible, quantified. If the code deficiency cannot be quantified at this time, it should be further investigated in later steps.

Typical Application to LBLOCA

With the requirements specified, and the analysis tools documented, a qualitative evaluation is made to determine if:

(1) The TRAC-PF1/MOD1 code is applicable to the scenario and plant system,

(2) The TRAC-PF1/MOD1 code is applicable with reservation (particular models and correlations require further investigation to quantify uncertainty or further assessment and documentation is necessary),

or (3) The TRAC-PF1/MOD1 code is not applicable due to shortcomings that preclude its use to model the scenario, plant, dominant phenomena, or to evaluate the uncertainty in calculating the safety parameter.

The evaluations required to determine which of the above three conditions apply are described as follows.

Global Processes

The ability of TRAC-PF1/MOD1 to simulate the three distinct phases of a LBLOCA (blowdown, refill, reflood) is first determined by the governing field equations. These equations must have the basic ability to model single-phase subcooled flow (during steady-state and early blowdown), two-phase flow (throughout the transient), and single-phase vapor flow (within portions of the reactor vessel and coolant loops late in the transient). The evaluation and decision making as to the applicability of the TRAC-PF1/MOD1 field equations to address the global flow processes is summarized in Table 2.

Closure Equations

To support the basic field equations, a large number of closure equations (constitutive models, and correlations) are required to model many of the processes and phenomena previously discussed. To provide confidence that the TRAC-PF1/MOD1 code has the capability to simulate the LBLOCA scenario, the closure equations require an adequate data base. The models and correlations document supports the closure models used in the code. The document defines the uses of the models, the data ranges, accuracies, and abilities to scale-up.

The closure equations are needed for simulation of wall-to-liquid and wall-to-vapor drag, interfacial drag, wall-to-liquid and wall-to-vapor energy exchange, interphase energy exchange, and pressure changes due to expansion, contraction, and other flow losses. The various models require flow regime maps, boiling curves, and fluid and material properties for completeness. The selection, use, and evaluation of the correlations are based on experiments and code assessment.

TABLE 2 FIELD EQUATIONS IN TRAC-PF1/MOD1

| Scenario and PIRT Requirements | Modeled In TRAC-PF1/MOD1 | Field Equations/Model |
|---|---|---|
| Non-equilibrium two-phase flow | Yes | Six equation unequal velocity, unequal temperature |
| Non-condensable gas flow | Yes | Gas mass balance in vapor flow field |
| Solute tracking for boron | Yes | Solute mass balance liquid flow field |
| Multidimensional flow capability | Yes | Vessel only, 1-D, 2-D, 3-D flow field |
| Separation due to gravity | Yes | Gravity pressure differential in flow field equations |
| Interphase exchange terms | Yes | Mass and energy transfer between phases, vaporization and condensation |

The capabilities of the TRAC-PF1/MOD1 code closure relationships to model the LBLOCA are summarized in Table 3.

Numerical Solution

The capability of the numerical solution scheme to provide stable, accurate, and reliable solutions of the field equations and closure relationships has been demonstrated through the assessment of the code. The TRAC-PF1/MOD1 code has been assessed against many separate and integral effects experiments.

Components and Control

NPP modeling requires the capability to accurately describe the geometric detail, flow paths, fluid and metal masses, heat generation, and plant operations. The TRAC-PF1 code is designed on a component basis, and the interconnection of the components determines the system. Each component has the capability to describe the geometric detail, heat transfer surfaces,

TABLE 3 PHENOMENA/PROCESS MODELS IN TRAC-PF1/MOD1

| Component | Phenomena | Modeled In TRAC | Model |
|---|---|---|---|
| Fuel rod | Stored energy | Yes | Fuel rod conduction model |
| | decay heat | Yes | Kinetics or power-time models |
| | oxidation | Yes | Rossi-Stout model |
| | Gap Conductance | Yes | Dynamic gap width and gas conductivity models |
| Core | Post-CHF | Yes | Full boiling curve |
| | Rewet/top quench | Yes | Quench front tracking model in conduction solution, axial conduction |
| | Reflood heat transfer | Yes | Full boiling curve, 2-d conduction solution, quench front modeling |
| | Multidimensional flow | Yes | Vessel only, 1,2,3d flow field |
| | Void generation and | Yes | Vaporization and condensation, mass exchange, two fluid field equations |
| Pressurizer | Early Rewet | Yes | Flow distribution, pressurizer to upper plenum via flow paths. |
| Steam Generator | Steam Binding | Yes | Primary-secondary heat transfer, vaporization of liquid. |
| Pump | Two phase performance loss coefficient | Yes | Full four-quandrant homologous curves with head and torque two-phase degradation, geometric description for loss coefficient. |
| Cold leg/ Accumulator | Condensation | Yes | Vaporization/condensation closure models, mass balance for gas field. |
| | Non-condensible gas | Yes | |
| | Dissolved nitrogen | No | |
| Lower plenum | Sweepout, hot walls | Yes | Interphase drag, wall-fluid energy exchange. |
| Break | Critical flow | Yes | Subcooled, two phase, and vapor choke flow model. |
| Loops | Two phase pressure drop, flow split oscillations | Yes | Wall to liquid, wall to vapor, interphase drag models, tee model with angle dependence, effect of pressure gradients due to vaporization/condensation in field equations |

and control operations associated with the component. Control systems and trip logic allow for control actions to be included in the plant model. A list of required component modeling requirements for a PWR system and the corresponding TRAC-PF1 code capabilities is presented in Table 4.

TRAC-PF1/MOD1 Capability to Model PWR LBLOCA

The preceding sections developed several checklists for the capabilities of TRAC-PF1/MOD1 to model the LBLOCA transient for a four-loop Westinghouse PWR. The purpose of these evaluations was to prepare a statement of the applicability of the TRAC-PF1/MOD1 code to calculate the PCT and simulate the processes for the LBLOCA scenario in the selected NPP. At this stage of the evaluation, the checklists yield no identifiable reasons why the TRAC code is not suitable for use in this application. Moreover, it can be stated that the code is applicable for the analysis, because:

1. The code can address the entire scenario for a LBLOCA (blowdown, refill, and reflood) in a continuous calculation.

2. A three-dimensional fluid modeling capability is present for the reactor vessel region.

3. The non-equilibrium (UVUT) field equations and added non-condensible gas and solute balance equations are sufficient to address the important phenomena: critical flow at the break, pump characteristic dynamics and degradation, blowdown heat transfer, ECC penetration and bypass, multiple quench fronts, liquid entrainment, upper plenum pool formation, steam binding, and two phase flow and pressure drops.

4. The code contains a complete set of flow regime dependent closure relationships.

5. A large data base and assessment evaluation are available.

6. Qualitatively and quantitatively satisfactory comparisons to experiments have been demonstrated.

7. Because many different-scaled experiments have been successfully simulated, no evidence exists that would preclude applying the code to a full-scale NPP simulation.

8. The code is fully capable of describing all pertinent geometric and control characteristics of the plant.

9. The code is frozen and supported by complete documentation.

Providing a defensible statement of code applicability was the primary objective of this section. A secondary objective was to state which code models, and their associated uncertainty, would have the major effect on the primary safety related variables. The primary phenomena and processes were given in the PIRT process. The comparison of the dominant phenomena with the code capability is summarized in Figure 7, which satisfies the objective of this element in the methodology.

TABLE 4. COMPONENT MODELING REQUIREMENTS FOR PWR

| Requirement | Component In TRAC | Code Component |
|---|---|---|
| Pressure vessel | Yes | Vessel: models upper head, upper plenum, core, lower plenum, downcomer, structure, flow paths, elevations, resistances, volumes. |
| Hot leg | Yes | Pipe; models flow area, volume, geometry, elevations. |
| Steam generator | Yes | Steam generator; models flow areas, volumes for primary/secondary heat transfer, boiling, phase separation, recirculation, feedwater, steam flow, etc. |
| Pump suction | Yes | Pipe; models flow areas, volumes, elevation. |
| Pumps | Yes | Pump; models homologous curves, degradation, flow area, volumes, losses. |
| Cold leg | Yes | Pipe or Tee; models flow areas, volumes, elevations, branches. |
| Pressurizer | Yes | Pressurizer; models volumes, flow areas, separation, heating. |
| Surge line | Yes | Pipe; models volumes, flow areas, elevations, choked flow. |
| Accumulators | Yes | Accumulator; models volumes, flow areas, liquid, gas head. |
| ECC systems | Yes | Fills; model flow rates, pressure dependence. |
| Valves | Yes | Valve; model areas, volumes, control. |
| Pressure boundary | Yes | Break; models pressure boundary, control. |

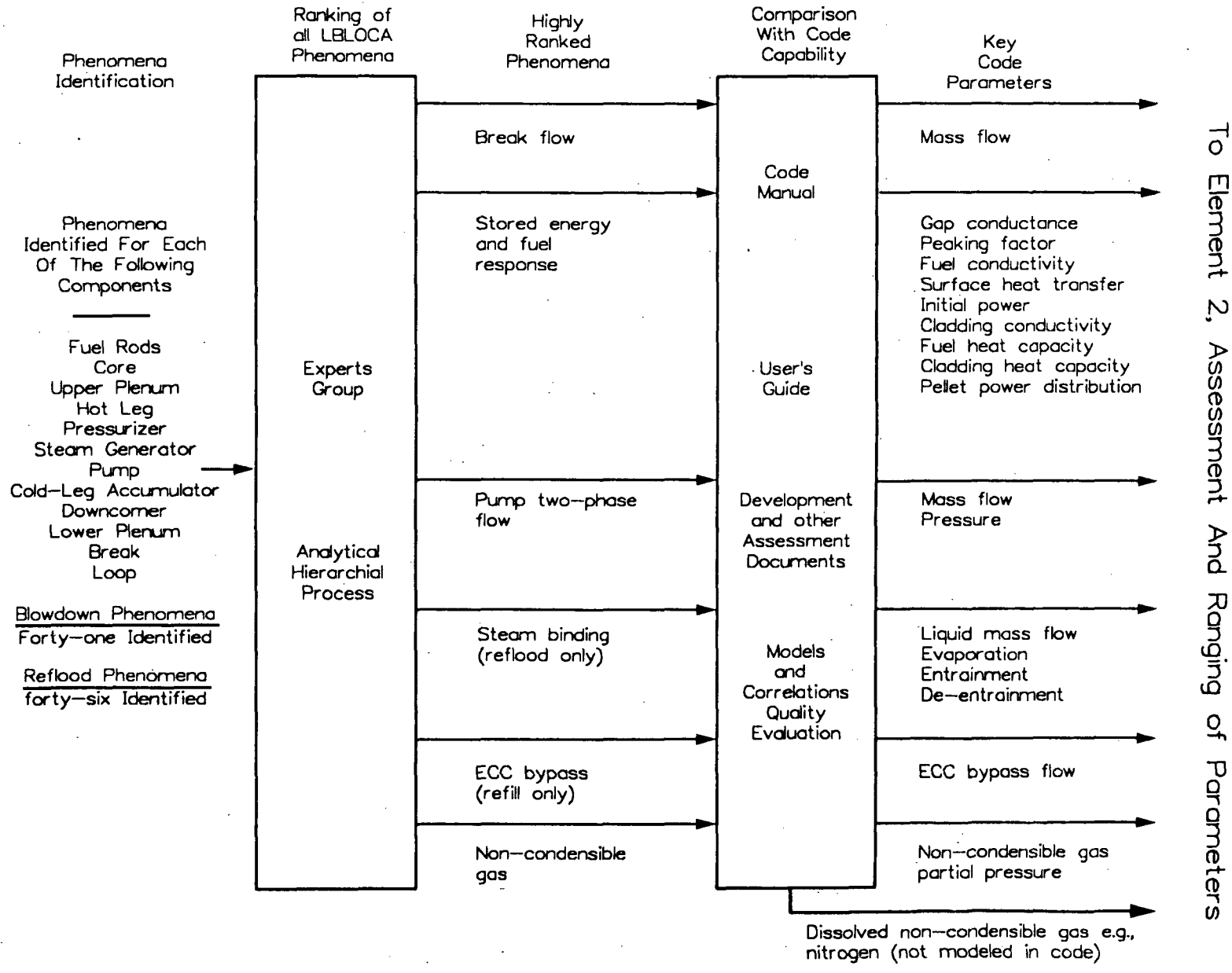


Figure 7. Illustration of CSAU application to determine potential contributors to uncertainty in a TRAC-PF1/MOD1 simulation of a LBLOCA.

NSL01070

## SUMMARY AND CONCLUSIONS

From the process perspective, the CSAU methodology contained in the Requirements and Capabilities Element is:

- Systematic and comprehensive as it addresses and integrates the scenario, experiments, code, and plant,
- Made both efficient and sufficient by combining a "top-down" approach to define the dominant phenomena with a "bottom-up" approach to quantify uncertainty,
- General, and therefore applicable to a variety of scenarios, plants, and codes.

A typical application of the methodology to a large cold leg break in a Westinghouse 4-loop PWR using TRAC-PF1/MOD1 has:

- Demonstrated the scenario is well understood
- Identified the phenomena which are likely to dominate the response in the primary safety criteria
- Shown the code can generally model the scenario and plant
- Identified the candidate uncertainty parameters which must be addressed in the subsequent two elements in the methodology

The important results of the demonstration case are summarized in Figure 7. In addition, a checklist of items, which the TPG believes are sufficient to quantify code uncertainty for LBLOCA has been developed. Because these steps are general in nature, the are considered equally applicable to other accident scenarios. The checklist for the total process is given in Reference 13.

## REFERENCES


1. B. E. Boyack, et. al., "Quantifying Reactor Safety Margins - Part 1 An Overview of the Code Scaling, Applicability and Uncertainty Evaluation Methodology", Proceedings of the 16th Water Reactor Safety Information Meeting, October 24-27, 1988, Gaithersburg, Maryland (To be published).

2. W. Wulff, et. al., "Quantifying Reactor Safety Margins - Part 3 Assessment and Ranging of Parameters", Proceedings of the 16th Water Reactor Safety Information Meeting, October 24-27, 1988, Gaithersburg, Maryland (To be published).

3. G. S. Lellouche, et. al., "Quantifying Reactor Safety Margins - Part 4 Uncertainty Evaluation of LBLOCA Analysis Based on TRAC-PF1/MOD1", Proceedings of the 16th Water Reactor Safety Information Meeting, October 24-27, 1988, Gaithersburg, Maryland (To be published).

4. Compendium of ECCS Research for Realistic LOCA Analysis, NUREG-1230, USNRC, August 1988.

5. R. A. Shaw, et al, Development of a Phenomena Identification and Ranking Table (PIRT) for Thermal-Hydraulic Phenomena During a PWR LBLOCA, NUREG/CR-5074, EG&G Idaho, Inc., August 1988.

6. M. McCormic-Barger, Experiment Data Report for LOFT Power Ascension Test L2-2, EG&G Idaho, Inc., NUREG/CR-0492, February 1979.

7. D. R. Liles, et al, "TRAC-PF1/MOD1: An Advanced Best Estimate Computer Program for PWR Thermal-Hydraulic Analysis," NUREG/CR-3858, Los Alamos National Laboratory, July 1986.

8. B. E. Boyack, H. Stumpf and J. F. Lime, TRAC User's Guide, NUREG/CR-4442, LANL, November 1985.

9. M. S. Sahota and F. L. Addessio, TRAC-PF1/MOD1 Developmental Assessment, NUREG/CR-4278, LANL, August 1985.

10. D. R. Liles, et al, TRAC-PF1/MOD1 Correlations and Models, NUREG/CR-5069 (Draft), LANL, (To be published).

11. V. H. Ransom, et al, RELAP5/MOD2 Code Manual - Volumes 1, 2 and 3, NUREG/CR-4312, EG&G Idaho, Inc., August 1985.

12. R. A. Dimenna, et al, RELAP5/MOD2 Models and Correlations, NUREG/CR-5194, EG&G Idaho, Inc., August 1988.

13. TPG, et al, Quantifying Reactor Safety Margins: Application of CSAU Methodology to a LBLOCA, NUREG/CR-5249, EG&G Idaho, Inc. (To be published).

## APPENDIX

TRAC-PF1/MOD1 ASSESSMENT REPORTS

An asterisk (*) indicates the assessment was performed with frozen Version 14.3. For documents listed "to be issued," the analysis has been completed and a draft document prepared, however a final report has not been issued.

Cylindrical Core Test Facility

1. M. W. Cappiello, "TRAC-PF1/MOD1 Analysis of CCTF Combined Injection Test Run 79," Los Alamos National Laboratory Group N-9, LA-2D/3D-TN-86-20, December 1986.

2. B. D. Boyer and D. A. Siebe, "The Analysis of CCTF Run 58 with TRAC-PF1/MOD1," (to be issued).

3. M. Roberts, "TRAC-PF1/MOD1 Upper Plenum Nodalization Studies of CCTF UPI Test C2-AA1 (Run 57)," Los Alamos National Laboratory Group N-9, LA-2D/3D-TN-86-14, March 1986.

4. B. E. Boyack, "TRAC-PF1/MOD1 Analysis of CCTF UPI Test C2-AA1 (Run 57)," Los Alamos National Laboratory Group N-9, LA-2D/3D-TN-86-11, August 1986.

5. H. Stumpf and G. J. Wilcutt, "CCTF Run 71 TRAC-PF1/MOD1 Analysis," Los Alamos National Laboratory Group N-9, LA-2D/3D-TN-86-8, May 1986.

6. M. W. Cappiello, "TRAC-PF1/MOD1 Analysis of CCTF No-Failure UPI Test C2-13 (Run 72)," Los Alamos National Laboratory Group N-9, LA-2D/3D-TN-86-7, July 1986.

7. H. Stumpf, "CCTF Run 76 TRAC-PF1/MOD1 Analysis," Los Alamos National Laboratory Group N-9, LA-2D/3D-TN-86-6, March 1986.

8. H. Stumpf, "CCTF Run 78 TRAC-PF1/MOD1 Analysis," Los Alamos National Laboratory Group N-9, LA-2D/3D-TN-86-5, February, 1986.

Slab Core Test Facility (SCTF)

1. S. C. Harmony and B. E. Boyack, "A Posttest Analysis of SCTF Run 703 Using TRAC-PF1/MOD1," (to be issued).*

2. P. R. Shire, "TRAC-PF1/MOD1 Analysis of SCTF Core-III Test S3-02 (Run 713), Los Alamos National Laboratory, LA-CP-88-11, 1988.

3. B. E. Boyack and P. L. Mascheroni, "A Posttest Analysis of SCTF Run 704 Using TRAC-PF1/MOD1," Los Alamos National Laboratory, LA-CP-88-131, 1988.

4. S. C. Harmony and B. E. Boyack, "A Posttest Analysis of SCTF Run 714 Using TRAC-PF1/MOD1," Los Alamos National Laboratory, LA-CP-88-234, 1988.

5. M. W. Cappiello, et al, "CCTF Core-II Upper-Plenum Injection TRAC-PF1/MOD1 Analysis Summary," Los Alamos National Laboratory Group N-9, LA-2D/3D-TN-86-16, March 1987.

6. P. R. Shire and B. E. Boyack, "Upper Plenum Studies of SCTF Run 605," Los Alamos National Laboratory Group N-9, LA-2D/3D-TN-86-15, August 1986.

7. J. Gilbert, "TRAC-PF1/MOD1 Calculation of SCTF-II Test S2-12 (Run 617)," Los Alamos National Laboratory Group N-9, LA-2D/3D-TN-86-13, March 1987.

8. J. Gilbert, "TRAC-PF1/MOD1 Calculation of SCTF-II Test S2-06 (Run 611)," Los Alamos National Laboratory Group N-9, LA-2D/3D-TN-86-9, March 1987.

9. J. C. Lin, "TRAC-PF1/MOD1 Calculation of SCTF Core-II Supply Test S2-03 (Run 608)," Los Alamos National Laboratory Group N-9, LA-2D/3D-TN-85-13, July 1985.

10. Y. Abe, et al, "TRAC-PF1/MOD1 Calculation of SCTF Core-II Steam Supply Test S2-05 (Run 610)," Los Alamos National Laboratory Group N-9, LA-2D/3D-TN-85-9, July 1985.

11. J. Gilbert, "TRAC-PF1/MOD1 Calculation of SCTF Core-II Test S2-SH1 (Run 604)," Los Alamos National Laboratory Group N-9, LA-2D/3D-TN-85-6, March 1985.

12. J. Gilbert, "TRAC-PF1/MOD1 Calculation of SCTF Core-II Test S2-09 (Run 614)," Los Alamos National Laboratory Group N-9, LA-2D/3D-TN-85-4, March 1985.

Multiple-Loop Integral System Test (MIST) Facility

1. B. E. Boyack, "Postest Analysis of MIST Test 330302 Using TRAC-PF1/MOD1," Los Alamos National Laboratory, LA-UR-88-1937, June 1988.*

2. J. L. Steiner and D. A. Siebe, "Posttest Analysis of MIST Test 3109AA Using TRAC-PF1/MOD1," (to be issued).

3. D. A. Siebe and J. L. Steiner, "Posttest Analysis of MIST Test 320201 Using TRAC-PF1/MOD1, (to be issued).*

Large-Scale Test Facility (ROSA-IV)

1. H. J. Stumpf and F. E. Motley, "Results of TRAC Analysis of Run ST-NC-02 from the Large-Scale Test Facility," Los Alamos National Laboratory, LA-CP-87-131, 1987.

2. F. E. Motley and R. R. Schultz, "Comparison of a TRAC Calculation to the Data from LSTF Run SB-CL-05," Los Alamos National Laboratory, LA-UR-86-3692, 1986.

3. R. R. Schultz, et al, "Core Liquid Level Depression in 5% Small-Break LOCAs: An Investigation Using Subscale Data," Los Alamos National Laboratory, LA-UR-2839, 1987.

Loss of Fluid Test Facility

1. T. D. Knight, "TRAC Analyses of LOFT LP-02-6," Los Alamos National Laboratory, LA-UR-85-3723, October 17, 1985.

2. L. D. Buxton, "Summary of TRAC-PF1/MOD1 Independent Assessment using LOFT Large Break Test L2-5," Sandia National Laboratories, letter report to H. S. Tovmassian (USNRC), March 30, 1987.

Semiscale Facility

1. L. N. Kmetyk, "TRAC-PF1/MOD1 Independent Assessment: Semiscale Mod-2A Intermediate Break Test S-IB-3," Sandia National Laboratories, SAND85-2563, NUREG/CR-4465, February 1986.

Loop Blowdown Investigations (LOBI) Test Facility

1. L. N. Kmetyk, "TRAC-PF1/MOD1 Independent Assessment: LOBI Intermediate Break Test B-R1M," Sandia National Laboratories, SAND85-2264, NUREG/CR-3970, February 1986.

2. L. N. Kmetyk, "TRAC-PF1/MOD1 Independent Assessment: LOBI Small Break Transient A1-04R," Sandia National Laboratories, SAND85-0442, NUREG/CR-4171, December 1985.

Dartmouth College Air-Water Counter-Current Flow Tests

1. D. Dobranich, "TRAC-PF1/MOD1 Independent Assessment: Dartmouth College Air-Water Counter-Current Flow Tests," Sandia National Laboratories, SAND85-1594, NUREG/CR-4337, December 1985.

Northwestern University Perforated-Plate CCFL Tests

1. D. Dobranich, "TRAC-PF1/MOD1 Independent Assessment: Northwestern University Perforated-Plate CCFL Tests," Sandia National Laboratories, SAND85-0172, NUREG/CR-4155, February 1985.

Davis-Besse Loss-of-Feedwater Event of June 9, 1985

1. J. F. Lime, et al, "Rapid-Response Analysis of the Davis-Besse Loss-of-Feedwater Event on June 9, 1985," Los Alamos National Laboratory, LA-UR-85-3083, 1987.

Ginna SGTR Event of January 25, 1982

1. J. F. Lime and R. P. Jenks, "A TRAC-PF1/MOD1 Analysis of the Ginna Tube-Rupture Event on January 25, 1982," Los Alamos National Laboratory, LA-11094, NUREG/CR-4988, October 1987.

## ASSESSMENTS WITH OTHER TRAC CODE VERSIONS

1. M. E. Waterman, "Overview of TRAC-PD2 Assessment Calculations," Idaho National Engineering Laboratory, EGG-2380, NUREG/CR-4195, November 1985.

2. T. D. Knight and V. Metzger, "TRAC-PD2 Developmental Assessment," Los Alamos National Laboratory, LA-9700-MS, NUREG/CR-3208, January 1985.

3. T. D. Knight, "TRAC-PD2 Independent Assessment," Los Alamos National Laboratory, LA-10166-MS, NUREG/CR-3688, December 1984.

# QUANTIFYING REACTOR SAFETY MARGINS: APPLICATION OF CSAU METHODOLOGY TO LBLOCA

## Part 3
## Assessment and Ranging Of Parameters for the Uncertainty Analysis of LBLOCA Codes*

W. Wulff (BNL)
Department of Nuclear Energy
Brookhaven National Laboratory
Upton, NY 11973

and

B.E. Boyack (LANL), R.B. Duffey (INEL), P. Griffith (MIT),
K.R. Katsma (INEL), G.S. Lellouche (SLI), S. Levy (SLI),
U.S. Rohatgi (BNL), G.E. Wilson (INEL) and N. Zuber (USNRC),
as members of the Technical Program Group

ABSTRACT

Comparisons of results from TRAC-PF1/MOD1 code calculations with measurements from Separate Effects Tests, and published experimental data for modeling parameters have been used to determine the uncertainty ranges of code input and modeling parameters which dominate the uncertainty in predicting the Peak Clad Temperature for a postulated Large Break Loss of Coolant Accident (LBLOCA) in a four-loop Westinghouse Pressurized Water Reactor. The uncertainty ranges are used for a detailed statistical analysis to calculate the probability distribution function for the TRAC code-predicted Peak Clad Temperature, as is described in an attendant paper (Part 4 of the presentation).

Measurements from Separate Effects Tests and Integral Effects Tests have been compared with results from corresponding TRAC-PF1/MOD1 code calculations to determine globally the total uncertainty in predicting the Peak Clad Temperature for LBLOCAs. This determination is in support of the detailed statistical analysis mentioned above.

The analyses presented here account for uncertainties in input parameters, in modeling and scaling, in computing and in measurements. The analyses are an important part of the work needed to implement the Code Scalability, Applicability and Uncertainty (CSAU) methodology. CSAU is needed to determine the suitability of a computer code for reactor safety analyses and the uncertainty in computer predictions. The results presented here are used to estimate the safety margin of a particular nuclear reactor power plant for a postulated accident.

Specifically, this paper describes, first in principle and then through their application, Steps No. 7 through 10 of the fourteen-step CSAU methodology.

*Work performed under the auspices of the U.S. Nuclear Regulatory Commission.

# 1. INTRODUCTION

## 1.1 Background

This paper is the third in a four-part sequel of reports on the implementation of the Code Scalability, Applicability and Uncertainty (CSAU) methodology [1]. All four papers are published together in the proceedings of the meeting. The first paper (Part 1 [2]) presents an introductory overview of the CSAU methodology. The second paper (Part 2 [3]) describes the assessment of the computer code's capabilities of meeting the analysis requirements. This paper (Part 3) presents the determination of uncertainty ranges for those parameters which have been identified to impact on the uncertainty with which the selected TRAC-PF1/MOD1 computer code predicts the Peak Clad Temperature. The fourth paper [4] presents the detailed statistical analysis to estimate the probability distribution function for the uncertainty in predicting PCT, particularly its mean and 95 percentile values.

The CSAU methodology [1] was developed by the USNRC in response to the needs arising from the proposed revision of ECCS acceptance criteria (52FR6334, March 3, 1987). It is designed to determine (i) whether or not a selected code has the capability to simulate a particular transient of interest, (ii) whether or not the code has the capability to model and scale the processes occurring during that transient, from test facility subscale to full scale nuclear power plants, and (iii) the uncertainty with which the code predicts particular parameters important to that transient.

In the work presented here, and in the attendant papers [2,3 and 4], the CSAU methodology has been implemented to estimate the uncertainty of Peak Clad Temperature (PCT) predictions with the TRAC-PF1/MOD1, Version 14.3 computer code for the postulated Large Break Loss of Coolant Accident (LBLOCA) in a generic four-loop Westinghouse Pressurized Water Reactor (PWR).

The CSAU methodology has been described, in general, in Part 1 [2] of this paper sequel. It is carried out in fourteen major steps as shown in Figure 1. CSAU Element 1, or Steps 1 through 6, are described in detail in Part 2 [3] of this report sequel and serve to identify the transient of interest (LBLOCA), the power plant of interest (four-loop W PWR), and the code to be used for the analysis (TRAC/PF1/MOD1, Version 14.3). Furthermore, the first six steps lead to the identification of all processes relevant to the transient of interest, and to their ranking in the Priority Identification and Ranking Table (PIRT). This priority ranking is essential to focus resources and achieve efficiency in carrying out the uncertainty analysis. Finally, the first six steps serve also to determine the code applicability, based on the complete code documentation.

This paper builds upon the results presented in Part 2 [3] and describes CSAU Element 2, or Steps No. 7 through 10, shown in Figure 1, inside the bold frame. Specifically, the summary of test facilities shown in Table 1* and the List of Candidate Parameters shown in Table 2 are used as the starting point for this paper. The summary of test facilities identifies the available Separate Effects Test (SET) and Integral Effects Test (IET) data which are used to

*Table 1 is an incomplete sample of the full listing shown in Reference 5.

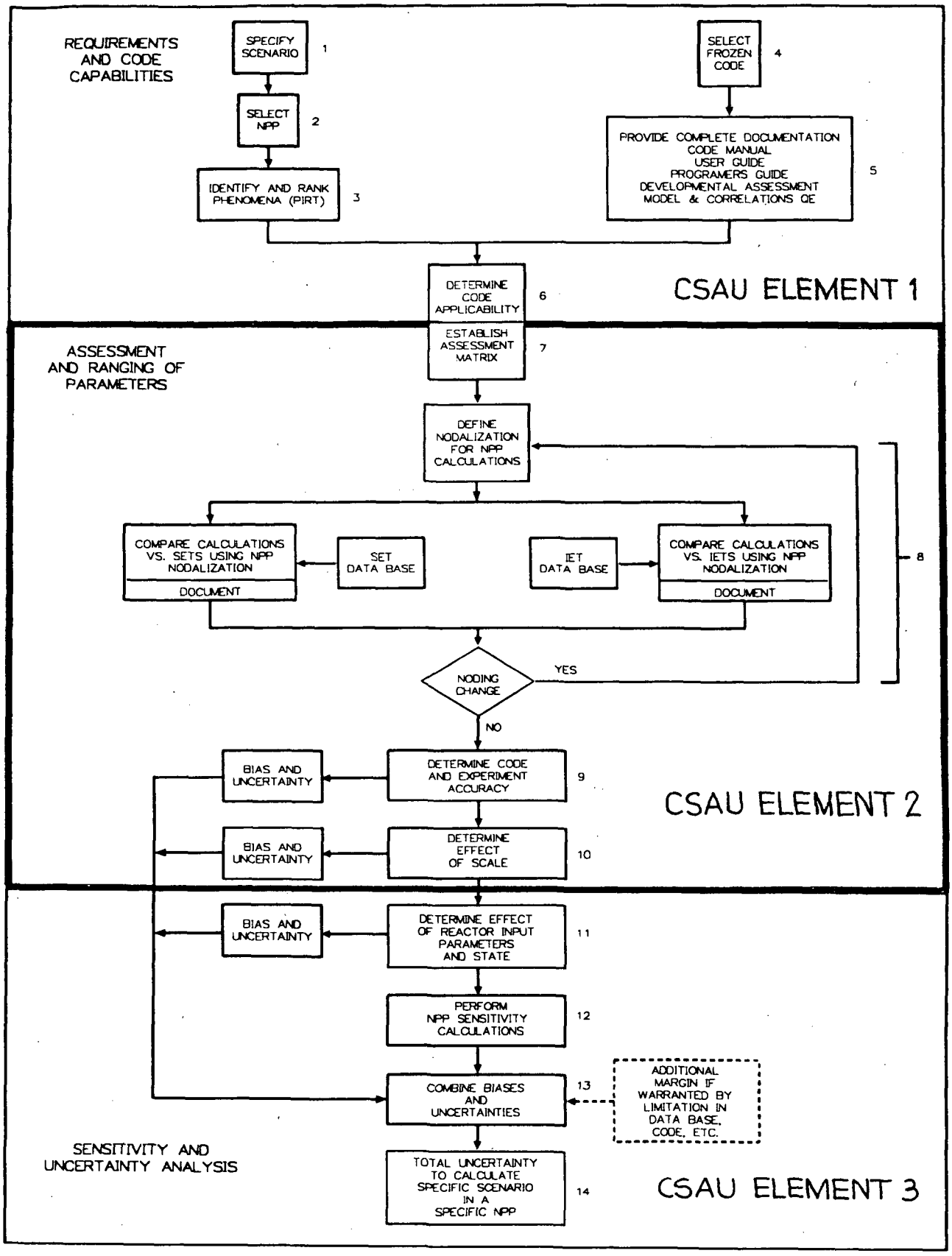


Figure 1. Schematic for the Code Scaling, Applicability and Uncertainty (CSAU) Methodology

# Table 1. Summary of SET and IET Facilities

TABLE 1 IET Experimental Data Bases For LBLOCA

| SET/IET | PRINCIPLE PHENOMINA INVESTIGATED | FACILITY | TEST | PHASE OF INTEREST | DATA REFERENCE | COUNTERPART TESTS | TRAC-PF1/MOD1 ASSESSMENT | REFERENCES OTHER BE CODE ASSESSMENTS | FACILITY AND TEST |
|---|---|---|---|---|---|---|---|---|---|
| IET | ALL THERMAL HYDRAULIC | LOFT | L2-2 | FULL TRANSIENT | NRC DATA BANK | SEMISCALE S-06-2 | | T.D. Knight and V. Metzger,"TRAC-PD2 Developmental Assessment", NUREG/CR-3208, LA-9700-MS, January 1985. | S.M Modro, S.N. Aksan, V.T. Berta, A.B. Wahba, "Review Of Loft Large Break Experiments," OECD LOFT-T-3900 (MARCH 1988). |
| IET | ALL THERMAL HYDRAULIC | LOFT | L2-3 | FULL TRANSIENT | NRC DATA BANK | SEMISCALE S-06-6/S-06-3 | | T.D. Knight, TRAC-PD2 Independent Assessment, NUREG/CR-3866, LA-10166-MS, December 1984. | S.M Modro, S.N. Aksan, V.T. Berta, A.B. Wahba, "Review Of Loft Large Break Experiments," OECD LOFT-T-3900 (MARCH 1988). |
| IET | ALL THERMAL HYDRAULIC | LOFT | L2-5 | FULL TRANSIENT | NRC DATA BANK | | L.D. Buxton, Summary of TRAC-PF1/MOD1 Independent Assessment Using LOFT LBLOCA L2-5, Sandia National Laboratories Letter Report to H.S. Tovmassian (USNRC), March 30, 1987. | T.D. Knight, TRAC-PD2 Independent Assessment, NUREG/CR-3866, LA-10166-MS, December 1985. | S.M Modro, S.N. Aksan, V.T. Berta, A.B. Wahba, "Review Of Loft Large Break Experiments," OECD LOFT-T-3900 (MARCH 1988). |
| IET | ALL THERMAL HYDRAULIC | LOFT | LP-02-6 | FULL TRANSIENT | NRC DATA BANK | | T.D. Knight, "TRAC Analysis of LOFT LP-02-6," LA-UR-85-3723, October 17, 1985, PP. 59-56. | T.D. Knight, "TRAC Analysis of LOFT LP-02-6," LA-UR-85-3723, October 17, 1985, P.P. 13-17. | S.M Modro, S.N. Aksan, V.T. Berta, A.B. Wahba, "Review Of Loft Large Break Experiments," OECD LOFT-T-3900 (MARCH 1988). |
| IET | ALL THERMAL HYDRAULIC | SEMISCALE | S-04-5 | FULL TRANSIENT | NRC DATA BANK | | | M.E. Waterman, Overview of TRAC-PD2 Assessment Calculations, NUREG/CR-4195, EGG-2380, November 1985. | "Quick Look Report On Semiscale MOD-1 Test S-04-5, (Baseline ECC Test Series)," J.M. Cozzuol, October 1976. |
| IET | ALL THERMAL HYDRAULIC | SEMISCALE | S-06-3 | FULL TRANSIENT | NRC DATA BANK | LOFT L2-3 | | T.D. Knight and V. Metzger, TRAC-PD2 Developmental Assessment, NUREG/CR-3208, LA-9700-MS, January 1985. | "Quick Look Report On Semiscale MOD-1 Test S-06-3, (LOFT Counterpart Test Series)," M.A. Langerman, May 1978. |
| IET | ALL THERMAL HYDRAULIC | LOBI | A1-4R | BLOWDOWN/REFILL | | | L.N. Kmetyk, "TRAC-PF1/MOD1 Independent Assessment: LOBI Large Break Transient A1-04R," Sandia National Laboratories report SAND85-L0442 (NUREG/CR-4171) | L.N. Kmetyk, "RELAP5 Assessment: LOBI Large Break Transients," NUREG/CR-3075, SAND82-2525, March 1983. | L. Piplies and W. Kolar, "Quick Look Report on LOBI Test A1-04R," Communication LOC 80-03, Commission of the European Communities, J.R.C.-Ispra, CC-3802, December 1980. |
| IET | COLD LEG INJECTION | UPTF | 2 | REFILL/REFLOOD | | CCTF C2-4 | | | TO BE PUBLISHED |
| IET | COLD LEG INJECTION | UPTF | 17 | REFLOOD | | SCTF S3-10 | | | TO BE PUBLISHED |

Table 1. Summary of SET and IET Facilities (Cont.)

TABLE 1 IET Experimental Data Bases For LBLOCA - CONTINUED

| SET/IET | PRINCIPLE PHENOMINA INVESTIGATED | FACILITY | TEST | PHASE OF INTEREST | DATA REFERENCE | COUNTERPART TESTS | TRAC-PF1/MOD1 ASSESSMENT | REFERENCES OTHER BE CODE ASSESSMENTS | FACILITY AND TEST |
|---|---|---|---|---|---|---|---|---|---|
| IET | COLD LEG INJECTION | UPTF | 27 | REFILL/REFLOOD | | CCTF C2-SH2 | | | TO BE PUBLISHED |
| IET | CORE HEAT TRANSFER | SEMISCALE | S-02-8 | BLOWDOWN | | | | T.D. Knight, TRAC-PD2 Developmental Assessment, NUREG/CR-3208, LA-9700-MS, January 1985. | "Quick Look Report On Semiscale Mod-1 Test S-02-8," T.K. Larson, G.M. Johnson, M.A. Langeraan, August 1976. |
| IET | REFLOOD HEAT TRANSFER | PKL | K9 | REFILL/REFLOOD | | | | T.D. Knight, "TRAC-PD2 Independent Assessment," NUREG/CR-3866, LA-10166-MS, December 1984. | B. Brand, R. Mandl and H. Schmidt, "PKL Refill and Reflood Experiment-Selected Results From Test K9," Kraftwerk Union report R51/22/79, December 14, 1979. |

Table 1. Summary of SET and IET Facilities (Cont.)

TABLE 2 SET Experimental Data Bases For LBLOCA

| SET/IET | PRINCIPLE PHENOMINA INVESTIGATED | FACILITY | TEST | PHASE OF INTEREST | DATA REFERENCE | COUNTERPART TESTS | TRAC-PF1/MOD1 ASSESSMENT | REFERENCES OTHER BE CODE ASSESSMENTS | FACILITY AND TEST |
|---|---|---|---|---|---|---|---|---|---|
| SET | ALL THERMAL HYDRAULIC | SEMISCALE | S-07-4 | REFLOOD | NRC DATA BANK | FLECHT SEASET 3105B | | M.E. Waterman, Overview of TRAC-PD2 Assessment Calculations, NUREG/CR-4195, EGG-2380, November 1985. | "Experiemental Data Report For Semiscale MOD-3 Reflood Heat transfer Test S-07-4," R. Gillins, K. Sackett, K. Stanger, NUREG/CR-0254, August 1978. |
| SET | ALL THERMAL HYDRAULIC | SCTF | S1-13 (519) | REFLOOD | NRC DATA BANK | FLECHT SEASET 43716C | | Suzanne T. Smith, "Analysis of the SCTF FLECHT Counterpart Test Using TRAC-PF1 (RUN 519)," Los Alamos National Lab. doc. LA-2D/3D-TN-83-02 (JAN 1983). | "Data Report on Large Scale Reflood Test, SCTF Test S1-13 (Run 519)," JAERI-aeea-57-401, December 1982. |
| SET | ALL THERMAL HYDRAULIC | SCTF | S2-08 (613) | REFLOOD | NRC DATA BANK | FLECHT SEASET 27148 | J.C. Lin "TRAC-PF1/MOD1 Calculation of SCTF Core II FLECHT- SET Coupling Test S2-08(run 613)," Los Alamos National Lab. doc.LA-2D/3D-TN-85-2 (FEB 1985). | | "Data Report on Large Scale Reflood Test, SCTF Test S2-08 (Run 613)," JAERI-aeea-59-437, February 1985. |
| SET | ALL THERMAL HYDRAULIC | SCTF | S3-10 (714) | REFLOOD | NRC DATA BANK | UPTF Test 17 | S.C. Harmony and B.E. Boyack, "A Posttest Analysis of SCTF Run 714 Using TRAC-PF1/MOD1," (to be issued). | | "Data Report on Large Scale Reflood Test, SCTF Test S3-10 (Run 714)," JAERI-aeea-62-125, March 1987. |
| SET | ALL THERMAL/ HYDRAULIC | CCTF | C1-06 (015) | REFLOOD | NRC DATA BANK | FLECHT SEASET 3015B | | Tsutomu Okubo, "An Analysis of A TRAC-PD2 Core Calculation for CCTF Test C1-06 (run 015)," Los Alamos National Lab. Document LA-2D/3D-TN-82-8, (MARCH 1982). | "Quick Look Report On Large Scale Reflood Test-06 - CCTF Test C1-06 (Run 015)," JAERI-aeea-8990, July 1980. |
| SET | ALL THERMAL/ HYDRAULIC | CCTF | C1-16 (025) | REFLOOD | NRC DATA BANK | FLECHT SEASET 3105B | | J. Sugimoto, "TRAC-PD2 Reflood Code Assessment for CCTF Test C1-16," LA-2D/3D-TN-81-9, FEB 1981. | "Quick Look Report On Large Scale Reflood Test-16 - CCTF Test C1-16 (Run 025)," JAERI-aeea-9349, March 1981. |
| SET | ALL THERMAL/ HYDRAULIC | CCTF | C2-06 (064) | REFLOOD | NRC DATA BANK | SCTF S2-04 (run 619) | | Jonathon F. Kotas, "The Effect of the Radial Power Upon the Reflood Phase of a Loss of Coolant Accident: TRAC Analysis of CCTF Test C2-05(run 63) and CCTF Test-06(run 64)," Los Alamos | "Quick Look Report On CCTF Core-II Reflood Test, C2-6 (Run 64)," JAERI-aeea-59-012, February 1984. |
| SET | ALL THERMAL/ HYDRAULIC | CCTF | C2-15 (075) | REFLOOD | NRC DATA BANK | FLECHT SEASET 27148 | | Christopher J. Crowley and Paul H. Rothe, "TRAC-PF1 Calculations of CCTF Core II Reflood Test 75 (C2-15), "Los Alamos National Lab. doc. LA-2D/3D-TN-86-1 (APRIL 86). | "Quick Look Report On CCTF Core-II Reflood Test, C2-15 (Run 75)," JAERI-aeea-60-255, September 1985. |
| SET | CORE THERM- HYDR AND CHF | THTF | 154R | BLOWDOWN | NRC DATA BANK | | | | G.S. Massengill,M.D. White,R.A. Hendrick,"PWR Blowdown Heat Transfer Seperate Effects Program Thermal-Hydraulic Test Facility Experimental Data Report for Test |

Table 1. Summary of SET and IET Facilities (Cont.)

TABLE 2 SET Experimental Data Bases For LBLOCA - CONTINUED

| SET/IET | PRINCIPLE PHENOMINA INVESTIGATED | FACILITY | TEST | PHASE OF INTEREST | DATA REFERENCE | COUNTERPART TESTS | TRAC-PF1/MOD1 ASSESSMENT | REFERENCES OTHER BE CODE ASSESSMENTS | FACILITY AND TEST |
|---|---|---|---|---|---|---|---|---|---|
| SET | CORE THERM- HYDR AND CHF | THTF | 153 | BLOWDOWN | NRC DATA BANK | | | | D.M. Leon,M.D. White,R.A. Hendrick,"PWR Blowdown Heat Transfer Separate Effects Progra Thermal-Hydraulic Test Facility Experimental Data Report for Test |
| SET | CRITICAL FLOW | MARVIKEN | 22 | BLOWDOWN | NRC DATA BANK | | | T.D. Knight, "TRAC-PD2 Independent Assessment," NUREG/CR-3866, LA-10166-MS, December 1984. | "Results From Test 22, The Marviken Full Scale Critical Flow Tests," Joint Reactor Safety Experiment in the Marviken Power Station, Sweden, Marviken report MXC-222, September |
| SET | CRITICAL FLOW | MARVIKEN | 24 | BLOWDOWN | NRC DATA BANK | | | T.D. Knight, "TRAC-PD2 Independent Assessment," NUREG/CR-3866, LA-10166-MS, December 1984. | "Results From Test 24, The Marviken Full Scale Critical Flow Tests," Joint Reactor Safety Experiment in the Marviken Power Station, Sweden, Marviken report MXC-224, September |
| SET | ECC BYPASS | BCL | 29111 | REFILL | | | | T.D. Knight, "TRAC-PD2 Independent Assessment," NUREG/CR-3866, LA-10166-MS, December 1984. | "Baseline Plenum Filing Behavior In a 2/15 Scale Model of a Four Loop PWR, Topical Report," R.A. Cudnit, L.J. Flanigan, R.C. Dykhuizen, W.A. Carbiener, J.S. Liu, NUREG/CR-0069, |
| SET | ECC BYPASS | CREARE | 2.5032 thru 2.5046 | REFILL | | | | | "1/5 Scale Counter Current Flow Data Presentation and Discussion," C.J. Crowley, P.H. Rothe, R.G. Sae, NUREG/CR-2106, November 1981. |
| SET | ECC BYPASS | CREARE PF | Runs D1 THRU D21 | REFILL | | | | | "ECC Delivery Study: Experimental Results and Discussion," Crowley, C.T., Block, J.A., CREARE TN-217, October 1975. |
| SET | ECC BYPASS | UPTF | 5, 6 | REFILL | | | | | TO BE PUBLISHED |
| SET | PUMP PERFORMANCE | CREARE | 524,526,13 13,1452 | BLOWDOWN | | | | | "Model Pump Performance Program," W.L. Swift, EPRI-NP-2379 (MAY 1982). |
| SET | PUMP PERFORMANCE | CREARE | 1145 | STEADY STATE STEAM-WATER,FWD SFD. | | | | | "Model Pump Performance Program," W.L. Swift, EPRI-NP-2379 (MAY 1982). |
| SET | PUMP PERFORMANCE | CE | 403-406 | STEADY STATE TWO PHASE REV FLOW | | | | | "PUMP TWO-PHASE PERFORMANCE PROGRAM," Combustion Engineering, Inc., ERPI NP-1556, September 1980. |

Table 1. Summary of SET and IET Facilities (Cont.)

TABLE 2

SET Experimental Data Bases For LBLOCA - CONTINUED

| SET/IET | PRINCIPLE PHENOMINA INVESTIGATED | FACILITY | TEST | PHASE OF INTEREST | DATA REFERENCE | COUNTERPART TESTS | TRAC-PF1/MOD1 ASSESSMENT | REFERENCES OTHER BE CODE ASSESSMENTS | FACILITY AND TEST |
|---|---|---|---|---|---|---|---|---|---|
| SET | REFLOOD HEAT TRANSFER | FLECHT-SS | 31504 | REFLOOD | NRC DATA BANK | | | T.D. Knight, "TRAC-PD2 Independent Assessment," NUREG/CR-3866, LA-10166-MS, December 1984. | M.J. Loftus et al., "PWR FLECHT-SEASET Unblocked Bundle Forced and Gravity Reflood Task Data Report," NUREG/CR-1532, Vols. 1 and 2, WCAP-9699, Westinghouse, 1981. |
| SET | STEAM BINDING | UPTF | 10 | REFLOOD | | | | | TO BE PUBLISHED |

Table 2. Candidate Parameters Affecting PCT Uncertainty

| | | | |
|---|---|---|---|
| A. | Fuel-Related Parameters (Fuel Stored Energy Modeling) | | |
| | 1. | Fission Power | $P$ |
| | 2. | Peaking Factors (local axial and radial) | $F$ |
| | 3. | Pellet Radius | $R_1$ |
| | 4,5. | Cladding Radii | $R_2, R_w$ |
| | 6,7. | Neutron Flux Depression Parameters | $m,n$ |
| | 8. | Fuel Thermal Conductivity | $k_f$ |
| | 9. | Cladding Thermal Conductivity | $k_c$ |
| | 10. | Fuel Heat Capacity | $c_{p,f}$ |
| | 11. | Cladding Heat Capacity | $c_{p,c}$ |
| | 12. | Gap Gas Thermal Conductivity | $k_g$ |
| | 13. | Effective Gap Width | $t$ |
| | 14. | Pellet Emissivity | $\epsilon_f$ |
| | 15. | Cladding Emissivity | $\epsilon_c$ |
| | 16. | Convective Heat Transfer Coefficient | $h_c$ |
| B. | Pump Model Parameters | | |
| | 17. | Pump Head | $H_{2\phi}$ |
| | 18. | Pump Torque | $T_{2\phi}$ |
| C. | Break Flow-Related Parameters | | |
| | 19. | Break Flow Bias $W_{comp.}/W_{exper.}$ | $R_m^{\cdot}$ |
| D. | ECC Bypass Model Parameters | | |
| | 20. | Interfacial Drag, Entrainment, 3-d Effects | $c_d$ |
| | 21. | Condensation Rate, Noncondensable Gases | $\Gamma_v$ |
| E. | Modeling Parameters for Steam Binding | | |
| | 22. | Entrainment in Core | $e_{CR}$ |
| | 23. | Entrainment in Upper Plenum | $e_{UP}$ |
| | 24. | Entrainment in Hot Legs | $e_{HL}$ |
| | 25. | Entrainment in S.G. Inlet Plena | $e_{SG}$ |

determine the ranges of uncertainty for the Candidate Parameters in Table 2. The parameters listed in Table 2 are called Candidate Parameters because their uncertainties can have significant influence on the Peak Clad Temperature uncertainty. The parameters in Table 2 were obtained [3] by identifying from the code documentation all the input and modeling parameters needed to predict the high-priority processes listed in the PIRT for the transient of interest. The Candidate Parameters will be further screened for relevance to PCT uncertainty, as described in Section 2 below, so as to reduce the list of Candidate Parameters to the list of nine Relevant Parameters whose uncertainty alone affects significantly PCT uncertainty.

## 1.2 Purpose of this Paper

The objectives of this paper are to explain the purpose of Steps 7 through 10 of the CSAU methodology and to present the work performed for implementing these four CSAU steps. Particularly, the analyses carried out for the implementation were needed:

a. to assess the relative significance on PCT uncertainty of the sixteen fuel-related candidate modeling parameters and to identify among these the Relevant Parameters for fuel modeling uncertainty.

b. to specify the range of uncertainties for all Relevant Parameters of fuel, pump, critical break flow and ECC bypass modeling in TRAC-PF1/MOD1,

c. to estimate the possible biases in modeling the effects of steam binding and of nitrogen on steam condensation during ECC bypass,

d. to identify the scale dependence of uncertainty ranges and modeling biases, and the scale effects on PCT measurements.

e. to estimate code and experimental accuracies through the comparison of PCT predictions by TRAC-PF1/MOD1 with PCT measurements from Separate Effects Test (SET) and Integral Effects Test (IET) facilities, which provide an estimate of the total PCT uncertainty.

Items a. through d. are needed for the detailed statistical analysis of PCT uncertainty, leading to the uncertainty distribution function [4]. Item e. produces a total uncertainty estimate in support of the detailed uncertainty analysis.

Separate analyses are performed for the blowdown PCT, for the early and for the late reflood PCTs.

## 1.3 CSAU Steps of Element 2: Parameter Assessment and Ranging

Figure 2 below illustrates the process of parameter assessment and ranging which constitutes the second CSAU Element of Steps 7 through 10, as shown earlier in the bold frame of Figure 1. In Figure 2 are shown inputs, activities and results for Steps 7 and 8 and for Steps 8, 9 and 10, the latter serving in turn as inputs to CSAU Element 3 [4]. Notice the overlapping of the generic activities in Step 8. The CSAU steps in Figure 1 are activities identified as steps for didactic reasons, while Figure 2 explains the processing

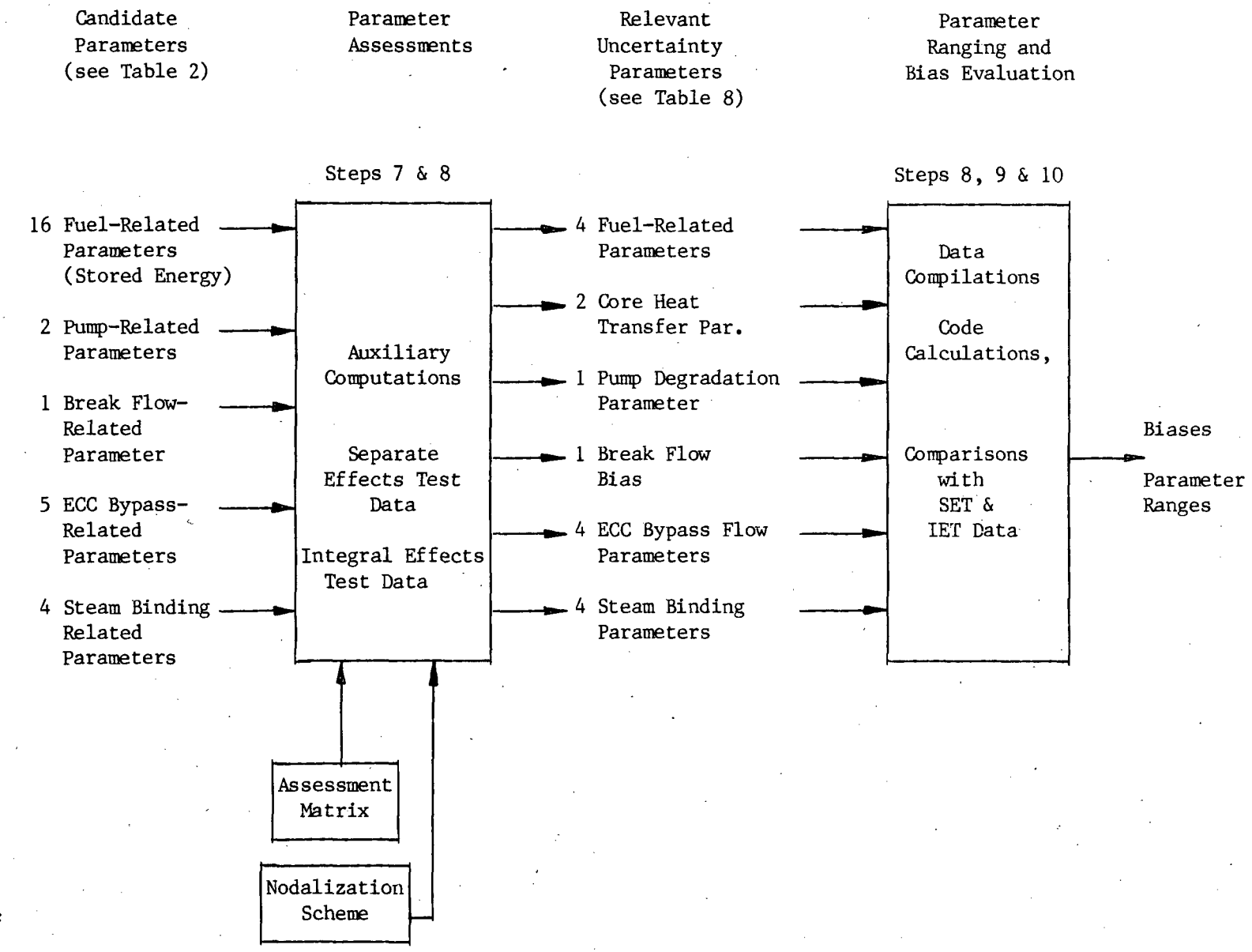


Figure 2. CSAU Element 2: Assessment and Ranging of Parameters

From CSAU Element 1: "Requirements and Code Capabilities"

To CSAU Element 3: "Sensitivity and Uncertainty Analysis"

of the output information from CSAU Element 1, namely, of the Candidate Parameters, to obtain the input information for CSAU Element 3, namely, the range of parameters and of biases which affect significantly the Peak Clad Temperature.

Below are explained in principle the four steps, Steps 7 through 10 of the CSAU methodology. Chapters 2 through 5 present then the specific applications of the four CSAU steps to the Large Break LOCA in the generic Westinghouse four-loop PWR power plant, analyzed with TRAC-PF1/MOD1, Version 14.3. The presentation follows the schematics in Figures 1 and 2, but only to the extent possible. Since each parameter in Table 2 must be analyzed in accordance with all four steps and in Figure 1, one would have to repeat the descriptions of Steps 7 through 10 for each parameter. Instead, we present the applications of Steps 7 through 10, as applicable, to groups of parameters and simply indicate the steps involved in the processing of each group of parameters.

Step No. 7 is carried out to establish the Assessment Matrix which pairs the test facilities with the Relevant Parameters affecting PCT uncertainties. The test facilities available for estimating the ranges of parameter uncertainties and of modeling biases are the Separate Effects Test (SET) and Integral Effects Test (IET) facilities contained in Tables 4.1 and 4.2, respectively, of Appendix 4.1 in Reference 5; a short extract of these complete and detailed tables was presented Section 1.1 as Table 1. The Relevant Parameters are those parameters among the Candidate Parameters which are determined by detailed analysis to have significant influence on PCT uncertainty. The Candidate Parameters are shown in Table 2 and were taken from Figure 7 of Reference 3, they were obtained by identifying from the code documentation all the code input and modeling parameters needed to predict the high-priority processes listed in the Priority Identification and Ranking Table (PIRT). High-priority processes which are either inadequately modeled in TRAC, or not modeled at all, are represented by appropriate bias parameters (ratios of computed over calculated process parameters (see Item 19 in Table 2).

Applications of Step 7 are found in Section 2.4. Detailed hand calculations [6] are used to identify the 13 Relevant Parameters from among the 25 Candidate Parameters in Table 2. Four modeling biases are identified and used to shift the PCT uncertainty probability distribution function as described in Part 4 [4].

Step No. 8 is carried out to obtain a standard nodalization scheme for all SET, IET and Nuclear Power Plant (NPP) code calculations needed for Items b, c and d in Section 1.2 above. The nodalization scheme is developed by comparing results from code calculations with experimental results from SET and IET facilities. As indicated in Figure 1, the development requires iterating until a nodalization scheme is obtained which enables the code to simulate all important processes without needing an excessively large number of computational cells or discretization nodes. The uncertainty of code results arising from nodalization is obtained through nodalization studies and estimates of computing errors or, as in the case of the TRAC code, as described in Sections 3.2 and 3.3 below.

Step No. 9 is the central process of quantifying individual contributions to PCT uncertainty by comparing code predictions with results primarily from Separate Effects Tests and possibly from Integral Effects Tests, further by comparing code correlations with test data for thermophysical properties or heat transfer coefficients, and by carrying out auxiliary (hand) calculations for uncertainty estimates. The purpose is to find standard deviations between code calculations and measurements for the relevant parameters and to set the range of parameter uncertainty equal to two sample standard deviations, corresponding to the 95 percentile of uncertainty. Where the code has systematic modeling errors, one seeks the bias and the 95 percentile of the bias range.

Applications of Step No. 9 are given in Chapter 4. The uncertainty ranges of thermophysical properties, namely, Parameters A.8 through 12 and A.14 and 15 in Table 2 are obtained from the statistics of thermophysical property measurements [6]. Uncertainty ranges for parameters which describe plant conditions (see A.1 through 7) are estimated from published data on operating experience.

The uncertainty ranges for parameters of heat transfer, pump, break and ECC bypass modeling are obtained from the comparison of TRAC-PF1/MOD1 calculations and SET measurements. The comparison cover facilities with a wide range of scale to assess the effects of scale on PCT uncertainty.

Step No. 10 is the extrapolation of uncertainty ranges, or of biases and bias uncertainties, from laboratory subscale to full scale, by identifying the trends of uncertainty and bias dependencies on scale, and by deriving and utilizing scaling laws. This activity is intimately connected to the activities described as Steps No. 8 and 9.

Applications of Step 10 are presented in Sections 4.2, 4.3, 4.4, 4.5 and 5.5. Scale effects are investigated primarily by separate hand calculations [6], by the use of SET facilities of differing scales, and by an assessment of scale on PCT as measured in a large number of widely differing test facilities (see Section 5.5).

Supporting evidence for the PCT uncertainty estimates obtained in Part 4 [4] is obtained by independently comparing predicted and measured PCT data. TRAC-PF1/MOD1 post-test predictions of PCT are compared with test data from the Loss of Fluid Test (LOFT) facility, the Slab Core Test Facility (SCTF) and the Cylindrical Core Test Facility (CCTF) to obtain an additional estimate of uncertainty in PCT prediction, which can serve to support the detailed uncertainty analysis present in Part 4 [4].

## 1.4 Organization of Report

Section 2 summarizes first the results obtained from the ranking of thermohydraulic processes and from the code documentation and then it presents the Assessment Matrix. The selection of the nodalization scheme is presented in Section 3. The parameter ranging and the use of SET data are described in Section 4. Section 5 presents the global estimate of PCT uncertainty, based on the comparison of SET and IET data with code predictions. The results of the work presented here and needed for the detailed statistical analysis are summarized in Section 6.

## 2. RESULTS FROM PIRT AND CODE DOCUMENTATION

### 2.1 Relevant Processes (PIRT)

As shown in Figure 1, Step 3 of the CSAU methodology calls for the screening of phenomena or processes, for the purpose of reducing the extremely large number of modeling parameters in a computer code to the much smaller number of parameters, the uncertainties of which can affect significantly the uncertainty of predicting PCT, and therefore justify inclusion in the detailed uncertainty analysis. The screening process (described in detail in References [5] and [7]) requires the basic understanding of the physics involved in the reactor transient of interest. It was performed in two ways. First, a group of experts ranked all the phenomena in all the components according to their importance in affecting PCT. A second group of experts, which was independent of the first group, ranked all the phenomena in an independently established list, by comparing two phenomena at a time and by using then the so-called Analytical Hierarchical Process (AHP) [7]. The result of the two ranking processes are organized in the Priority Identification and Ranking Table (PIRT) [7, Table 3], which lists the following top ranking phenomena for blowdown and refill phases of an LBLOCA:

Table 3. PIRT Results (Excerpt)

| LBLOCA Phase | Top Priority Phenomena |
|---|---|
| Blowdown | Fuel Stored Energy,<br>Pump, Two-Phase Flow Performance,<br>Critical Flow through Break |
| Refill | Downcomer Mass Transfer,<br>3-D Bypass Flow in downcomer,<br>Effects from noncondensable gas ($N_2$) in ECC injection<br>Entrainment in Downcomer |

### 2.2 Candidate Input and Modeling Parameters Affecting PCT Uncertainty

Once the important phenomena affecting Peak Clad Temperature (PCT) have been identified, one needs to determine from the code documentation first whether or not the code can simulate these phenomena, and then one needs to identify all the parameters appearing in the code for modeling the above important phenomena. The uncertainty of either specifying as input, or of computing in the code each one of the above modeling parameters contributes in principle to the uncertainty of predicting PCT, because the important phenomena themselves affect PCT. Therefore, the parameters identified by combining PIRT and code documentation are called the Candidate Parameters for PCT uncertainty analysis.

The Candidate Parameters related to fuel-stored energy (first entry in Table 3) are the first sixteen parameters in Table 2 presented earlier in Section 1.1. Similarly, the Candidate Parameter for pump performance modeling

under two-phase flow conditions, for critical break flow modeling, for downcomer bypass modeling and for modeling of effects from noncondensable gases are listed in Table 2 as parameters No. 17 through 21. Steam binding effects are characterized by liquid entrainment coefficients, the ratios $e = W_\ell/W_m$ of entrained liquid over mixture mass flow rates. These ratios are listed in Table 2 as parameters No. 22 through 25 for four components affected by liquid entrainment.

The above total of twenty-five input and modeling parameters still contains parameters which have either very small uncertainties themselves or only a week impact on PCT, or both. Such parameters need to be eliminated from considerations in the detailed statistical analysis in order to conserve resources. After sorting out the parameters important for the uncertainty analysis, one reduces the set of Candidate Parameters to the set of Relevant Parameters, as discussed below in Section 2.3. The possible effects from unimportant parameters combined with important parameters was investigated also for the sake of completeness [4].

## 2.3 Parameter Assessment by Analysis (CSAU Step No. 7)

Stored energy in the fuel before the LBLOCA initiation was identified as an important phenomenon in Section 2.2 [7]. Fuel stored energy is modeled in TRAC-PF1/MOD1 by the first sixteen parameters listed in Table 2 (cf. Sect. 1.1). A detailed analysis, based on closed-form integrations and hand calculations [6], was used to determine the relative importance of the sixteen fuel-related parameters on fuel stored energy and on PCT uncertainty. The analysis was carried out in three parts, which are:

(i) The identification of parameter uncertainty ranges.

(ii) The calculation of fuel-stored energy in terms of the sixteen fuel-related parameters, and calculation of the changes of stored energy caused by changing the fuel-related parameters, one at a time, in the range of their respective uncertainty ranges.

(iii) The calculation of PCT in terms of boundary conditions as prescribed by a TRAC-PF1/MOD1 computer calculation for the nuclear power plant, and in terms of the fuel related modeling parameters, varied one at a time over their respective uncertainty ranges.

(i) The ranges of uncertainties for the sixteen fuel-related parameters are presented in Tables 4 and 5 for Input and Modeling Parameters, respectively. Shown are the ranges in terms of standard deviation, the description of the distribution and the source reference. Uniform probability distributions are specified, when the known distribution is approximately uniform or when the distribution is unknown, because equal probability or uniform distribution represents the maximum ignorance about the distribution and leads only to conservative uncertainty estimates. The values in Table 4 reflect operating plant experience. Uncertainties and probability distributions for thermophysical properties in Table 5 are derived from data [10]; for heat transfer coefficients, they come from Separate Effects Tests (cf. Section 4.2.4).

Table 4. Uncertainties in Fuel-Related Input Data [5]

| Parameter | 1-σ Uncertainty | Distribution | Reference |
|---|---|---|---|
| Fission Power | ±2% | Normal | [8], Table 2 |
| Peaking Factors | | | |
| Local Axial | ±0.7% | Normal | [8], Table 2 |
| Local Radial | ±2.5% | Normal | [8], Table 2 |
| Pellet Radius (cold) | ±0.1% | Uniform | [9], Table 2 |
| Clad Radii (cold) | ±0.1% | Uniform | [9], Table 2 |
| Neutron Flux Depression | | | |
| m [5] | ±0.05 | Uniform | Estimated |
| n [5] | ±0.3 | Uniform | Estimated |

Table 5. Uncertainties of Fuel-Related Modeling Parameters [5]

| Parameter | 1-σ Uncertainty | Distinction | Reference |
|---|---|---|---|
| Fuel thermal cond., $k_f$ | ±0.2 W/(mK)* | Uniform | [10], p. 24 |
| Clad thermal cond., $k_c$ | ±1.01 W/(mK) | Normal | [10], p. 218 |
| Fuel heat capacity, $(\rho c)_f$ | ±30.035 kJ/($m^3$K) | Uniform | [10], p. 10† |
| Clad heat capacity, $(\rho c)_c$ | ±64.875 kJ/($m^3$K) | Uniform | [10], p. 211 |
| Gas thermal cond., $k_g$ | ±0.0131 W/(mK) | Uniform | [10], p. 485,† [11], p. 15 |
| Effective gap width, t | ±20.98 μm | Skewed | [12], pp. 31 & 92 |
| Pellet emissivity, $\varepsilon_f$ | ±7% | Uniform | [10], p. 48.6 |
| Clad emissivity, $\varepsilon_c$ | ±0.10 | Uniform | [10], p. 237 |
| Convective heat transf., single-phase, forced, turb. | -5% to +35% | Uniform | [5], p. 18; [13] |

*Notice that Hobson's data listed in Table A-2.VII [10], are incorrectly plotted in Figure A-2.4 [10].
†Revision 8/81.

The uncertainties of all modeling parameters in Table 5, which affect the gas gap conductance, namely $k_g$, t, $\varepsilon_f$, $\varepsilon_c$, and the uncertainties of calculating clad and pellet radii under operating conditions, have been combined into one uncertainty for gap conductance. The gap conductance uncertainty was determined from separate effects tests [6,8,14,15] and is listed in the first line and third column of Table 6.

(ii) The initially (steady-state) stored energy in the fuel at the location of the highest clad temperature was computed to be $E_{ref}$ = 67.991 kJ/m (19.643 Btu/ft). Table 6 below ranks the fuel-related parameters in accordance with their significance on fuel-stored energy. Column 1 in Table 6 shows the fuel related parameters which are left after the gap conductance parameter has replaced all gap conductance-related parameters. The second column shows the reference values [6], the third column the parameter variations by one standard deviation, while the fourth column lists the extreme values used to compute the positive change $E - E_{ref}$ of fuel stored energy. The last two columns show stored energy values corresponding to the values listed in the fourth column and the change in stored energy, $E - E_{ref}$, relative to the reference value $E_{ref}$.

Table 6 shows that gap conductance, peaking factors and fuel thermal conductivity are the modeling parameters which dominate the uncertainty in fuel stored energy calculations. The next most important parameter is total fission power. It is considered an input parameter and therefore not included in the detailed PCT uncertainty analysis.

(iii) Transient conduction calculations [6] have shown that the blowdown Peak Clad Temperature is dominated by the same three modeling parameters as the stored energy and in addition by the convective heat transfer, since it has a greater range of uncertainties during the transient. Table 7 shows blowdown Peak Clad Temperatures and their changes relative to the reference value in the last line, and obtained by varying the fuel-related parameters by the uncertainty range values listed in the third column of Table 6.

Summarizing the results of the fuel analysis, one recognizes that only four of the sixteen Candidate Parameters in Table 2 contribute significantly to PCT uncertainty. These four Relevant Parameters related to fuel modeling are:

1. Gap Conductance,
2. Peaking Factors,
3. Fuel Thermal Conductivity, and
4. Convective Heat Transfer Coefficient (initial single-phase flow).

It will be seen in Section 4.2.4 below that the convective heat transfer modeling uncertainty introduces a fifth fuel-related parameter, the minimum stable film boiling temperature, $T_{min}$.

The results of the fuel analysis [6] also show the important benefit from separate thermal and hydraulic analyses in support of code assessment and uncertainty analyses. The analyses, based on closed-form solutions and hand calculations, serve to:

Table 6. Contributions to Stored Energy Uncertainty

| Parameter | Reference Value | 1σ Change† | Max./Min. Values | E, Stored Energy kJ/m | $E - (E)_{ref}$ kJ/m |
|---|---|---|---|---|---|
| Gap Conductance | 10.960 $kWm^{-2}K^{-1}$ | -5.028 $kWm^{-2}K^{-1}$ | 5.932 $kWm^{-2}K^{-1}$ | 84.928 | 16.937 |
| Peaking Factors | 1.41736 | x1.03218 | 1.46297 | 70.675 | 2.685 |
| Fuel Thermal Cond. | 4.392 $Wm^{-1}K^{-1}$ | -0.2 $Wm^{-1}K^{-1}$ | 4.186 $Wm^{-1}K^{-1}$ | 70.475 | 2.484 |
| Power | 486.49 $MW/m^3$ | +2% | 496.22 $MWm^{-3}$ | 69.655 | 1.664 |
| Fuel Heat Capacity | 3.028 $MJm^{-3}K^{-1}$ | +30.035 $kJm^{-3}K^{-1}$ | 3.059 MJ $m^{-3}K^{-1}$ | 68.651 | 0.661 |
| Cladding Thermal Cond. | 16.735 $Wm^{-1}K^{-1}$ | -1.01 $Wm^{-1}K^{-1}$ | 15.728 $Wm^{-1}K^{-1}$ | 68.455 | 0.464 |
| Burn-Up m<br>n | 0.4034<br>3.9167 | -0.05<br>-0.30 | 0.3534<br>3.6167 | 68.346 | 0.355 |
| Convective Film Coeff. | 40.05 $kWm^{-2}K^{-1}$ | -50% | 38.05 $kWm^{-2}K^{-1}$ | 68.304 | 0.318 |
| Cladding Heat Capacity | 2.145 $MJm^{-3}K^{-1}$ | +64.875 $kJm^{-3}K^{-1}$ | 2.210 MJ $m^{-3}K^{-1}$ | 68.033 | 0.042 |

†cf. Tables 4 and 5.

a. detect systematic code errors and code biases,
b. identify, and focus upon, important parameters affecting code uncertainties (e.g., PCT uncertainty),
c. combine the uncertainties of several parameters into the uncertainty of one parameter (see gap conductance),
d. settle, on a quantitative basis, whether or not a parameter under dispute is relevant to code uncertainty.

The last item is extremely important to confirm expert opinions and engineering judgment.

Table 7. Change in Peak Clad Temperature Due to Parameter Uncertainties

| Parameter | Peak Clad Temp. K | Change in Peak Clad Temp. K |
|---|---|---|
| Gap conductance | 884.8 | 52.4 |
| Peaking factor | 843.0 | 10.6 |
| Fuel thermal conductivity | 847.5 | 15.1 |
| Power | 839.0 | 6.6 |
| Fuel heat capacity | 833.3 | 0.9 |
| Cladding thermal cond. | 833.9 | 1.5 |
| Convective heat trans. coef. | 836.7 | 4.28 |
| Cladding heat capacity | 833.5 | 1.1 |
| Reference case | 832.4 | --- |

The analyses of pump, break flow and ECC bypass modeling uncertainties lead also to combinations of uncertainties, similar to Item c above. Pump head and torque modeling uncertainties are found to be dominated by one parameter, namely two-phase flow pump degradation. Break flow modeling uncertainties were combined into a single measure of modeling bias, the ratio of predicted over measured break mass flow rates. The uncertainties in modeling interfacial drag and condensation during ECC bypass in the downcomer were combined directly into PCT uncertainty contributions. This was achieved by analyzing SET data and comparing these with code calculations, yet it would have been impossible to realize the simplification involved without supporting hand calculations.

## 2.4 Relevant Modeling Parameters and the Assessment Matrix (CSAU Step No. 7)

The assessment of modeling parameters as discussed in Section 2.3 above lead to this list of Relevant Parameters which have significant impact on blowdown and reflood Peak Clad Temperature uncertainties (cf. Figure 2):

Table 8. Relevant Parameters Affecting PCT Uncertainty

| | |
|---|---|
| a. Fuel Stored Energy | 1. gap conductance<br>2. peaking factors<br>3. fuel thermal conductivity<br>4. convective heat transfer of single-phase flow |
| b. Core Heat Transfer | 5. boiling and post-CHF heat transfer coefficients<br>6. minimum stable film boiling temperature |
| c. Pump Performance | 7. two-phase flow pump degradation |
| d. Critical Break Flow | 8. break flow bias coefficient |
| e. ECC Bypass Flow | 9. interfacial drag, entrainment<br>10. 3-D effects<br>11. interfacial mass transfer, noncondensable gas effects ($N_2$ dissolved in ECC fluid)<br>12. hot wall effects |
| f. Steam Binding | 13. entrainment in core, upper plenum, hot legs and steam generator inlet plena |

Any one particular of these thirteen parameters affects PCT uncertainty strongly because PCT is very sensitive to the particular parameter and either because the prediction of the parameters has itself a large uncertainty, or because the computer code (TRAC-PF1/MOD1) has serious modeling errors in predicting the parameter. The range of uncertainties and, where applicable the modeling bias of these parameters is ascertained in Step 9 of the CSAU methodology, by comparing computed results with Separate Effects Tests (SET) data (see Figure 1). A list of available SET facilities is given in Table 1 in Section 1.1. Table 9 below is the Assessment Matrix and associates in general the data resource with specific CSAU actions in Steps 8 through 10 in Figure 1.

The Assessment Matrix has three sets of rows, one each for SET facilities, for IET facilities and for published data compilations. The acronyms designating SET and IET facilities are explained in Table 1.

The matrix has also two sets of columns. The first set contains the groups of Relevant Parameters listed in Table 8 and shows which SET and IET data and which source of published thermophysical property data were used to determine the range of uncertainties for the parameters in the second column of Table 8. Also, the first column in the second set of columns, labelled "Contribution to CSAU," indicates which of the test facilities served for identifying the ranges of parameter uncertainties.

In the second column under "Contribution to CSAU" are marked the test facilities which had been simulated with TRAC, and the simulation results of which contributed to the selection of the NPP nodalization scheme [5,16]. The third column under "Contribution to CSAU" mark the test facilities which were

Table 9. Assessment Matrix [16]

| | Parameter Groups | | | | | | Contribution to CSAU | | | |
|---|---|---|---|---|---|---|---|---|---|---|
| SET Test Facilities | a. Fuel Stored Energy | b. Core Heat Transfer | c. Pump Performance | d. Critical Break Flow | e. ECC Bypass Flow | f. Steam Binding | Range of Parameter Uncertainty | Nodalization | Scale Effects | Overall PCT Uncertainty |
| UPTF | | | | | • | • | • | | • | |
| CE (PUMP | | | • | | | | • | | | |
| NORTHWESTERN | | | | | | | | • | | |
| CRBTF | | | | | | | | | | |
| BCL (2/15) | | | | | • | | • | • | • | |
| BCL (1/15) | | | | | | | | | • | |
| DARTMOUTH | | | | | | | | • | | |
| LEHIGH UNIVERSITY | | • | | | | | • | | | |
| ORNL | | • | | | | | • | | | |
| BENNETT | | • | | | | | • | | | |
| BECKER | | • | | | | | • | | | |
| JANSSEN | | • | | | | | • | | | |
| DHIR | | • | | | | | • | | • | |
| CREARE (1/15) | | | | | • | | • | | | |
| CREARE (1/30) | | | | | • | | • | | | |
| CREARE (1/5) | | | | | | | | | • | |
| CREARE (PUMP) | | | • | | | | • | | • | |
| CREARE (TF) | | | | | | | | | | |
| FLECHT | | • | | | | | • | • | • | |
| FLECHT-SEASET | | • | | | | | • | • | • | |
| MARVIKEN | | | | • | | | • | • | | |
| THTF | | | | | | | | | • | |
| NEPTUNUS | | | | | | | | • | | |
| W PUMP (1/3) | | | • | | | | • | | | |
| CCTF | | | | | | | | • | • | • |
| SCTF | | | | | | | | • | • | • |
| IET Test Facilities | | | | | | | | | | |
| LOFT | | | | | • | | • | • | • | • |
| LOBI | | | | | | | | | • | |
| POWER BURST FAC | | | | | | | | | • | |
| PKL | | | | | | | | • | • | |
| SEMISCALE | | • | | | | | • | • | • | |
| DATA COMPILATIONS | | | | | | | | | | |
| MATPRO[9] | • | | | | | | • | | | |
| INAYATOV | | • | | | | | • | | | |
| WEISMAN | | • | | | | | • | | | |
| INEL POST-CHF | | • | | | | | • | | | |

used for scaling up from test scale to full-scale the bias and uncertainties of Relevant Parameters in Table 8, and for demonstrating the weak scale dependence of blowdown PCT, as discussed later in Section 5.5. The last column in Table 9 marks the three test facilities used for generating the scatter diagrams which depict the overall uncertainty of PCT predictions as obtained from post-test calculations with TRAC-PF1/MOD1. This is described in Sections 5.3 and 5.4 below.

The Assessment Matrix reflects the importance of assessing uncertainty in parallel independent activities, which support each other and the final results. The relevance of individual parameter uncertainties is assessed from SET data as well as by separate analysis, without code calculations. Scaling effects are assessed by hand calculations, by use of SET and IET data for specific phenomena followed by detailed statistical analyses, and also by global comparisons of test data alone (see Section 5.5). Finally, PCT uncertainty is estimated not only from the detailed statistical analysis, but it is also estimated from comparing systems calculations with IET PCT measurements. All of these activities strongly support the detailed analysis of PCT uncertainty, the determination of its probability distribution function and its 95 percentile margins.

## 3. SELECTION OF NODALIZATION SCHEME (CSAU STEP NO. 8)

The nodalization scheme for the TRAC computer code is the arrangement of computational cells or control volumes to which are applied the conservation principles. The TRAC code developers [17] call the control volumes for mass and energy conservation simply "volumes" and for momentum conservation "junctions". "Junction" cells are staggered relative to the "volume" cells. Under nodalization we understand the process of developing a nodalization scheme. A nodalization scheme is needed for all TRAC code applications and must be specified by the user. Being part of the input data specifications, the nodalization scheme affects Peak Clad Temperature (PCT) predictions and PCT uncertainty, as explained in Section 3.2 below.

### 3.1 Need of Code Calculations for Parameter Ranging

Figure 1 shows that Step 8 begins with nodalization. A nodalization scheme must be established because code calculations are needed for (a) ranging of parameter uncertainties based on the comparison of code calculations with SET data, (b) for estimating systematic modeling errors or modeling bias, (c) for the global assessment of PCT uncertainty, based on the comparison of code calculation with IET data, and (d) for generating the response surface which is needed for the detailed statistical analysis of PCT uncertainty as described in Part 4 [4].

All but the fundamental thermophysical property parameters in Table 8 require code calculations for the determination of their uncertainties, because they model reactor-specific phenomena, and the modeling uncertainty must therefore be determined by comparing code calculations against results from reactor-related experiments. The code calculations must be performed for test facilities which cover a range of facility scales, so as to facilitate extrapolations of uncertainties, of biases and of associated standard deviations, from small-scale facilities to full-scale power plants [1].

The particular parameters for PCT prediction under LBLOCA conditions, for which the uncertainty range is determined from code calculations simulating SET facilities, are the parameters for pump performance, for critical flow, for ECC bypass flow, including the effects from noncondensable gases, and for steam binding (see Items c through f in Table 8).

Parts of determining the uncertainties in core heat transfer (Item b in Table 8) required calculations with some of the TRAC-PF1 heat transfer subroutines [5]. However, these calculations were unaffected by the nodalization scheme, because they did not involve the integration of conservation equations.

The uncertainty ranges for fuel-related parameters (Items a in Table 8) were determined by the hand calculations described in Section 2.3. The hand calculations utilized also TRAC-PF1/MOD1 calculations. Specifically, TRAC calculations provided the boundary conditions for transient fuel temperature predictions. Therefore, the nodalization scheme indirectly affected the uncertainty range estimates of fuel-related parameters.

All SET and IET computer simulations and the development of the response surface [4], all carried out as part of the PCT uncertainty analysis, are affected by the nodalization scheme.

### 3.2 Rationale for Selecting the TRAC Nodalization Scheme for LBLOCA

Computer simulations are normally independent of the discretization or nodalization schemes used, because such schemes are chosen so that the simulation results approximate the solution to the governing modeling equations with a sufficiently small convergence error that is insignificant relative to measurement errors. Simulation errors and uncertainties arise then only from modeling uncertainties and not from computational errors which could be related to the nodalization scheme.

The TRAC code, however, is not used in a manner that lends itself to such numerical testing. The complexity of the system being modeled has led to a number of compromises in the procedure to accommodate special features of a nuclear plant and to yield reasonable results when the nodalization is very coarse. Many years of experience starting with early work at INEL have yielded the present nodalization and confidence in its effectiveness.

Therefore the following three principles have been adopted to deal with the associated issues of nodalization and computational error impact on PCT uncertainty.

1. A standard nodalization scheme for Nuclear Power Plant (NPP) calculations was developed which meets all the requirements for nodalization detail known from the past ten years of NPP, SET and Integral Effects Test (IET) simulations. This nodalization scheme was selected [5].

   a. to accommodate, with the specific TRAC model formulations, all relevant processes according to the PIRT listing,

   b. to satisfy all the noding requirements known not only from TRAC simulations of SET, IET and NPP (LBLOCA) transients, but from simulations with similar codes (RELAP5) as well,

   c. to result in affordable computer execution times for TRAC-PF1/MOD1.

   As Figure 1 clearly shows, the nodalization scheme must be selected in an iterative process, involving refinements of the scheme until a compromise is reached between needed detail and affordable cost [5].

2. The standard nodalization scheme, developed according to the first principle above, was adopted as the standard scheme for all SET and IET code simulations carried out for the purpose of estimating the ranges of uncertainty, the systematic code biases and their uncertainty ranges (standard deviations). The same standard nodalization scheme was also used later to develop the response surface for the detailed statistical analysis of PCT uncertainty [4]. In short, all computations needed to estimate the uncertainty of predicting PCT with TRAC-PF1/MOD1 were performed with one and the same standard nodalization scheme and the uncertainty estimates apply only when that standard nodalization scheme is used.

3. Modeling uncertainties and modeling biases are combined with computational errors from nodalization, into compound uncertainties and compound biases, respectively. Thus, discrepancies which are observed in comparing SET and IET results against code results contain contributions from modeling errors, computing errors and code tuning. The compound error is then the basis for estimating code uncertainties and biases in predicting PCT.

Since all SET and IET facilities except UPTF are in part small-scale facilities, the acceptance of the above three principles is based upon the supposition that the composite of modeling, computing and tuning errors can be scaled up from laboratory test scale to full-scale of NPP conditions, by extrapolating uncertainties from small-scale predictions to uncertainties of full-scale predictions. As will be seen in Sections 4.3 through 4.4, whenever this supposition cannot be demonstrated to be valid, one must determine a suitable upper bound for uncertainty estimates and accept the penalty of a large contribution to PCT uncertainty.

Figures 3, 4, and 5 were taken from Reference 5 and show the standard nodalization scheme as used for both NPP systems and SET component simulations with TRAC-PF1/MOD1.

The standard nodalization scheme has 180 vessel volumes (for mass and energy balances; cf. beginning of Chapter 3) and the total of 380 volumes to represent four loops of a W PWR.

A detailed description of the reasons, the data base and the component by component arrangement of computational cells can be found in Reference 5.

## 3.3 Impact of Nodalization on PCT Uncertainty

As explained in Section 3.2 above, the contribution to PCT uncertainty from nodalization and associated computational errors are assessed indirectly in CSAU. The uncertainties arising from nodalization are included in the composite uncertainties from modeling, computing and code tuning.

The strongest nodalization effect on PCT should come from core nodalization because core nodalization affects the calculation of cell-averaged power peaking factors which are fuel-related Relevant Parameters (cf. Table 8). Therefore, two computer calculations were performed, one each with two and three radial subdivisions in the core [4,20]. Each computer calculation involved a large number of different hot rod calculations. Forty PCT calculations from the two computations were used to determine a nodalization bias of

$$\Delta PCT_N = 35°K\ (63°F) \quad \text{for the mean}$$

$$\delta PCT_N = 25°K\ (45°F) \quad \text{for the 95 percentile}$$

for the blowdown PCT uncertainty. The details of this bias estimation and its extension to reflood Peak Clad Temperatures are given in References 4 and 5.

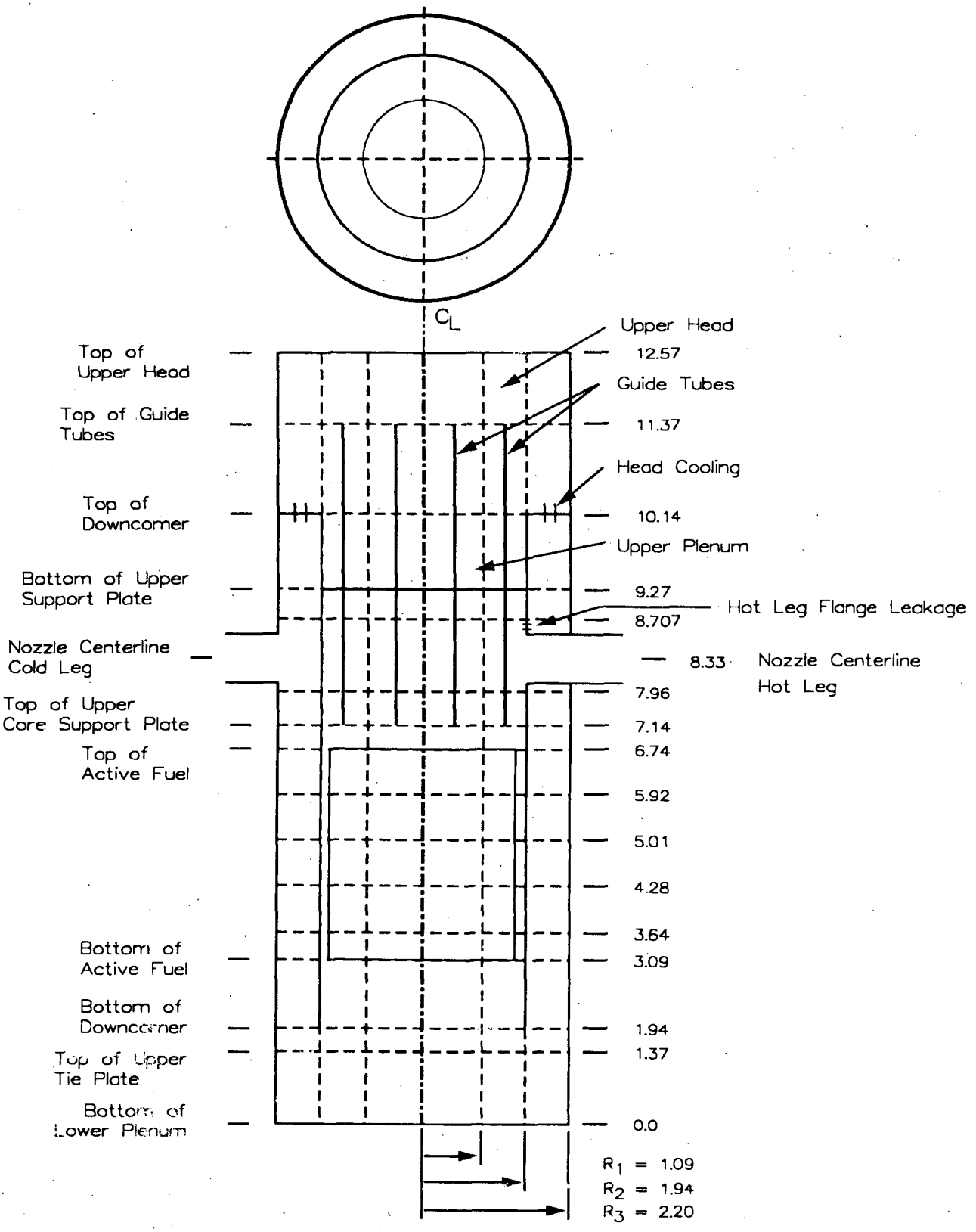


Figure 3. Vessel Nodalization Scheme

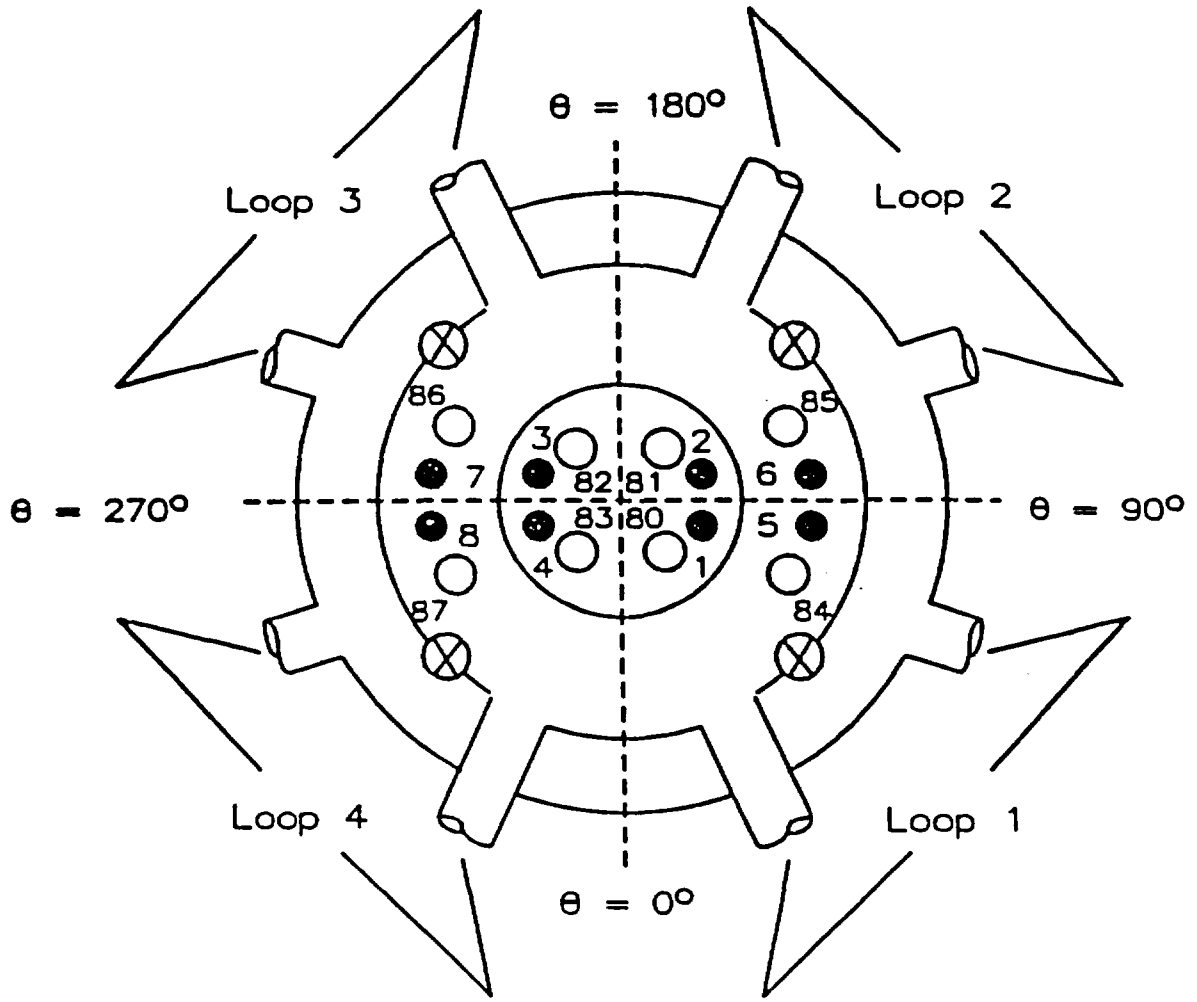


Vent valves (simulates hot leg nozzle leakage path)

Guide tubes (with component numbers)

Average fuel rod

Figure 4. Vessel Nodalization Scheme, Top View

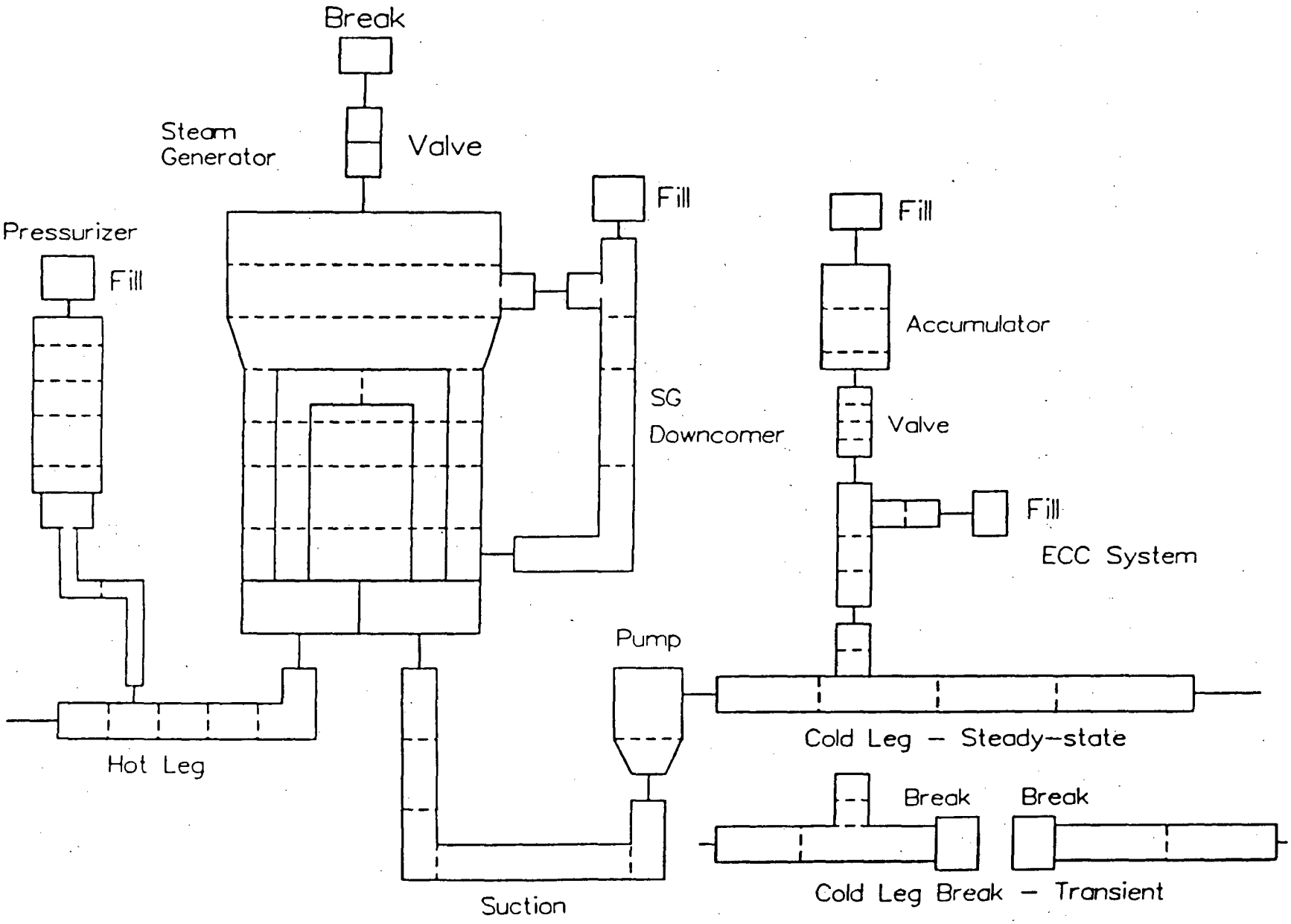


Figure 5. Loop Nodalization Scheme

## 4. PARAMETER RANGING AND MODELING BIAS, CSAU STEPS NO. 8, 9 AND 10

### 4.1 Methods and Resources

No single method provides the uncertainty range or bias for all the input and modeling parameters which affect PCT uncertainty. Instead, the Relevant Parameters in Table 8 should be grouped and assessed by methods which apply to the individual parameter categories:

a. Parameters which describe the condition of the plant, such as initial power, manufacturing tolerances or peaking factors, must have their uncertainties determined from manufacturing and from plant operating experiences. Sample populations must be evaluated to estimate probability distributions and sample standard deviations.

b. Parameters describing thermophysical data must have their uncertainties evaluated in terms of standard deviation from the original experiments [10]. Standard deviation and distribution functions are computed from the difference between the experimental data and the modeling correlation used in the subject computer code [6].

c. Parameters describing component-specific processes, such as heat transfer coefficients, pump performance parameters, etc., must have their uncertainties estimated from the comparison between Separate Effect Test (SET) data and computer code simulations of such SETs. The computer simulations are to be carried out with the standard NPP nodalization scheme applied to the subject component. The comparisons between measurements and code predictions are to be evaluated to yield either the distribution function of differences, or the mean bias and the standard deviation of the bias. The comparisons must encompass data from a range of test facility scales, to facilitate extrapolation to full NPP scale. Otherwise it is necessary to adopt conservative estimates of parameter uncertainties and to accept the penalties from correspondingly large PCT uncertainty (cf. Sect. 4.3.4).

It is always desirable to represent phenomena whose modeling uncertainty is to be estimated by a single, leading parameter (cf. Sect. 2.3, Item c and Sect. 4.3 below) or to introduce a single measure of modeling bias which combines the effects from all modeling parameters. Such a single measure of uncertainty simplifies the development of the response surface, and it then reduces the number of Monte Carlo calculations, both of which are needed for the statistical uncertainty analysis (cf. Sect. 4.4 below).

Data resources are listed, with references, in Table 1. The detailed selection of data resources for all the specific Relevant Parameters as listed in Table 8 is shown in the Assessment Matrix, given as Table 9.

### 4.2 Fuel-Related Parameters Affecting PCT Uncertainty (CSAU Steps No. 8, 9 and 10)

The fuel-related Relevant Parameters are the first four parameters listed under (a) in Table 8. Table 10 below lists these parameters along with their ranges of uncertainty and probability distributions. The ranges constitute the span of two standard deviations (first moment) for the parameters listed with a normal probability distribution. For the parameters listed with

uniform distributions, the ranges constitute extreme margins outside of which no data are expected. The uncertainty ranges listed in Table 10 were used to generate the response surface and the PCT uncertainty probability distribution [4].

Table 10 Uncertainty Ranges and Probability Distributions for Fuel-Related Relevant Parameters

| Parameter | Uncertainty Range | Probability Distribution | Reference Value at Initial Conditions |
|---|---|---|---|
| Gap Conductance | -80% to +80% | uniform | 10.96 kW/($m^2$K) |
| Power Peaking Factor | -5.6% to +5.6% | normal | 1.545 |
| Fuel Thermal Conductivity | -10% to +10% | normal | 4.39 W/(mK) |
| Convective Heat Transfer Coefficient: | | | |
| operating conditions | -25% to +50% | uniform | 40.05 kW/($m^2$K) |
| LBLOCA transient | -25% to +75% | uniform | --- |
| Min. Stable Film Boiling Temperature | -20°K to +100°K | uniform | --- |

The gap conductance uncertainty range in Table 10 equals approximately two times the standard deviation found by Wulff [6] (cf. first entry in Table 6) on the basis of SET data correlated by Lassmann and Hohlefeld [14], by Cunningham et al. [15] and by Steck et al. [12], and also on the basis of estimates of gap width uncertainties. Lassmann and Hohlefeld [14] obtained in their laboratory-controlled environment an approximately normal probability distribution of gap conductance, relative to their URGAP code model. We adopted the uniform distribution, because the ideal laboratory conditions do not exist in a power plant, and no information exists for the actual fuel conditions.

The power peaking factor uncertainty is taken from the code uncertainty study published by Sheron [8] and it is based upon manufacturing and operating experiences.

The fuel thermal conductivity has its uncertainty range determined from fundamental measurements published in MATPRO [10]. The value listed in Table 10 equals twice the standard deviation of the difference between calculated and measured values of thermal conductivity. This implies that 95% of all measurements fall within the range of uncertainty for fuel thermal conductivity.

For the convective heat transfer coefficient the uncertainty range was determined from SET versus code comparisons. For steady-state, single-phase, turbulent forced convection, the standard deviation of ±25% for the Dittus Boelter correlation was corrected according to Lellouche [see Ref. 5] to account for the difference between tube and bundle heat transfer, and for the

effect of grid spacers. The range of uncertainty for boiling heat transfer coefficients was also obtained from the standard deviation of measurements from the code model, and corrected for spacer effects. The range of uncertainty for the minimum stable film boiling temperature, a parameter used in TRAC for computing post-CHF heat transfer coefficients, was estimated by Shumway [19 and also 5].

The TRAC-PF1/MOD1 code has a modeling bias arising from the systematic error of superposing two mixture heat transfer coefficients as if they were phasic heat transfer coefficients [6, Sect. 2.8.3, Item 4]. Based on the comparisons between measured and TRAC-computed heat transfer coefficients, carried out by Shumway [19] for the most important regime of post-CHF heat transfer, the bias on PCT from post-CHF heat transfer modeling was estimated [4,5] to be:

$$\Delta PCT_{PCHF} = 26°K \ (47°F) \quad \text{for blowdown peak,}$$

$$= 47°K \ (84°F) \quad \text{for first reflood peak,}$$

$$= 89°K \ (160°F) \quad \text{for second reflood peak.}$$

These biases are added to the mean and the 95 percentile PCT [4].

## 4.3 Pump Modeling Uncertainties (CSAU Steps No. 9 and 10

Modeling uncertainties for the Reactor Coolant Pump performance have been published earlier [21] and are summarized here.

### 4.3.1 Pump Modeling Parameters

The TRAC-PF1/MOD1 code models pump head H and hydraulic pump torque T by "interpolation" between single-phase liquid and single-phase vapor components to obtain the general head and torque relations

$$H_{2\phi} = \Delta p_{Pump}/(\rho_m)_{in} = H_{1\phi} + M(\alpha)[H_D - H_{1\phi}]$$

$$T_{2\phi} = T_{1\phi} + N(\alpha)(T_D - T_{1\phi}) \ ,$$

where $\Delta p_{pump}$ = pressure rise across the pump

$(\rho_{min})_{in}$ = inlet mixture density

M, N = interpolants, dependent on

$\alpha$ = average void fraction

and subscripts $1\phi$ and D denote single-phase liquid and fully degraded, respectively.

All the parameters, $H_{1\phi}$, $T_{1\phi}$; $H_D$, $T_D$, M and N, are supplied as input data by the user in tabular form. Thus, the user can accommodate in principle any pump size and design (specific pump speed). Single-phase data $H_{1\phi}$ and $T_{1\phi}$ are furnished as homologous curves with good precision and insignificant uncertainty ($\approx \pm 2\%$) by the pump supplier. Pump performance degradation under two-phase flow conditions are obtained from small scale (up to 1/3-scale) SET data and encompass all the relevant pump uncertainties.

The uncertainties in the pump model of TRAC-PF1/MOD1 arise from the fact that

(a) The model does not account for the effects of pressure (phasic densities), which are recognized as being important [21].

(b) There are no full-scale pump data available for reactor pressure conditions on $H_D$, $T_D$, M and N, and TRAC is unable to account through mechanistic modeling for pump size, or specific speed, or pressure.

(c) Two-phase pump performance is stochastic; precise measurements and predictions are difficult when two-phase flow conditions exist.

The TRAC-PF1/MOD1 pump model is based upon data for $H_{1\phi}$, $T_{1\phi}$; $H_D$, $T_D$, M and N from the Westinghouse 1/3-size pump, having the same specific speed $n_s$ = 5,200 $[gpm^2/ft^3]^{1}/^{4}$ as the full-size Reactor Coolant Pump. The data cannot be reproduced here because they are proprietary.

### 4.3.2 Measure of Pump Modeling Uncertainty

The uncertainties of pump modeling are the differences between predicted and measured pump head and torque values for the full-scale reactor pump. These differences consist of two parts [21].

The first part is the set of sample standard deviations $s_H$ and $s_T$ of measured from predicted values of pump head, $M(\alpha)$, and of pump torque degradation, $N(\alpha)$, respectively. The pump head degradation $M(\alpha)$ varies between -0.2 and +0.8, the pump torque degradation varies between -0.3 and +0.8, both in the void fraction range between 0 and 1.

The second part of the pump modeling uncertainty arises from the omission of high-pressure modeling and the lack of high-pressure data, and also from scale effects, since no degradation data are available for the full-scale reactor pump. This uncertainty is estimated by extrapolation of $M(\alpha)$, $N(\alpha)$, $s_H$ and $s_T$ from 1/3-scale, low-pressure data to full-scale, high-pressure data, using small-scale pump data.

### 4.3.3 SET Data Base for Pump Modeling Assessment

For 1/3-scale, lower-pressure pump performance data, we used proprietary measurements from the Westinghouse pump.

For the purpose of extrapolations, we used data from the 1/20-scale CREARE pump [22] $(n_s = 4{,}200\ (gpm^2/ft^3)^{1}/^{4})$ and from the 1/5-scale CE pump [23] $(n_s = 4{,}200\ (gpm^2/ft^3)^{1}/^{4})$, because they have the same specific speed $n_s$. For further details on available pump models, pump data and their evaluation, see Reference 21.

The total of 127 pump head degradation data points was used for the extrapolation. We covered the range of void fractions from zero to one, and the range of normalized flow rates, divided by normalized* pump rotational speeds from zero to two [21].

### 4.3.4 Pump Model Uncertainty in TRAC-PF1/MOD1

The sample standard deviations for pump head and torque are listed in Table 11 below. The listed values were obtained from the Westinghouse Pump data. A uniform distribution of the discrepancies between modeled pump degradation $\bar{M}(\alpha)$ and measurements was adopted because the actual probability distribution is not known (cf. Sect. 2.3, Item (i)).

Table 11. Pump Modeling Uncertainty in TRAC-PF1-MOD1

| Void Fraction $\alpha$ | Sample Standard Deviation for | |
|---|---|---|
| | Pump Head $s_H$ | Pump Torque $s_T$ |
| 0 | 0 | 0 |
| 0.01 | 0.078 | - |
| 0.05 | 0 | - |
| 0.09 | - | 0 |
| 0.10 | 0.032 | - |
| 0.17 | 0.083 | - |
| 0.20 | 0.083 | - |
| 0.21 | - | 0.104 |
| 0.30 | 0.097 | - |
| 0.50 | 0.144 | - |
| 0.57 | - | 0.104 |
| 0.63 | - | 0.225 |
| 0.69 | - | 0.346 |
| 0.70 | 0.202 | - |
| 0.80 | 0.238 | 0.351 |
| 0.90 | 0.299 | 0.310 |
| 0.98 | 0.115 | 0.159 |
| 1.00 | 0 | 0 |

The uncertainty range is taken to be twice the standard deviation listed in Table 11. The values given in Table 11, and the multipliers, are added to, and subtracted from the (proprietary) modeling values $\bar{M}(\alpha_i)$ and $\bar{N}(\alpha_i)$. The result is then entered in TRAC-PF1/MOD1 in tabular form and linearly interpolated during the transient to generate the response surface [4].

It is clear that the values in Table 11, as well as the proprietary data for $\bar{M}(\alpha)$, $\bar{N}(\alpha)$, $H_D$ and $T_D$, apply only to the 1/3-scale pump and at low-pressure conditions. Figure 6 below shows, however, that pump degradation

*Normalized with respect to rated operating conditions.

decreases as the pump size increases. This was recognized not only from the extrapolation of small-scale pump data, but also from the observation that two-phase flow pump degradation is the stronger the larger the scale is of the internal structure of the flow, relative to the dimensions of the flow channels in the pump. Thus, it was concluded that extrapolation of Westinghouse pump data from 1/3 to full scale would only decrease degradation and uncertainty of degradation.

Since there are insufficient data to estimate this decrease of uncertainty, however, the full range of uncertainty as obtained from the 1/3-scale Westinghouse pump, and listed in Table 11 above, was used to analyze PCT uncertainty.

## 4.4 Break Flow Modeling Uncertainty (CSAU Steps No. 8, 9 and 10)

Uncertainty estimates for modeling critical flow through breaks have been published earlier [21] and are summarized briefly below.

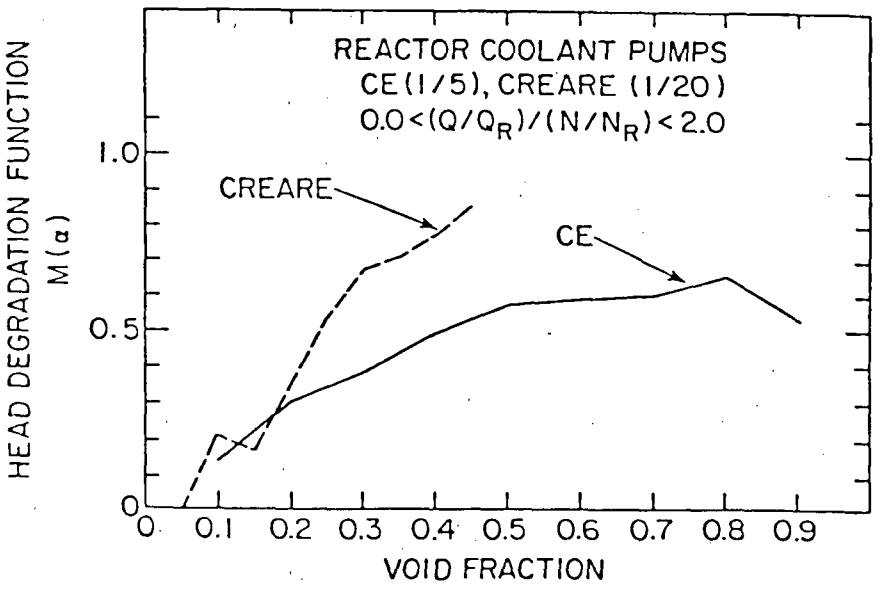


Figure 6 Comparison of Head Degradation Functions Developed from CREARE and CE Pump Data, Showing a Decrease in Pump Degradation with Increasing Pump Size

### 4.4.1 Break Flow Modeling Parameters

The TRAC-PF1/MOD1 code has three models for critical flow, of which only two are relevant for LBLOCA analyses. One model is for subcooled critical flow and contains more than 18 parameters [21], most of which depend in turn on state variables of the flow at the break and upstream of the break. The model computes the critical velocity $v_c$ from

$$v_c = \text{Max}\{a_{HE}, v_B\} ,$$

where $a_{HE}$ is the sound speed of homogeneous flow and $v_B$ is a velocity which is computed from the Bernoulli equation, in total disregard both for the limitations of Bernoulli's equation and for the need of a choking criterion. Since this model has no basis in physics, there is also no basis for estimating an uncertainty range for any of the parameters appearing in the model. Any relation between parameter uncertainty and break mass flow uncertainty is without rational basis. Therefore, we assess break flow uncertainty directly by comparing measurements with "predictions" from TRAC (cf. Sect. 4.4.2 below).

The other model deals with two-phase flow and employs the criterion that the maximum value of the real part of the characteristic roots $\lambda_i$ of the two-phase flow field equations

$$\underset{\approx}{A}\, \partial\underset{\sim}{U}/\partial t + \underset{\approx}{B}\, \partial\underset{\sim}{U}/\partial z = \underset{\sim}{C}$$

is zero for chocked flow [17]. The characteristic roots $\lambda_i$ are computed from the characteristic equation

$$\det\left[\underset{\approx}{A}\, \underset{\sim}{\lambda} + \underset{\approx}{B}\right] = 0 .$$

Unfortunately, this criterion, which is valid if supplemented with standard compatibility criteria (see NUREG-tr-0002, Vol. 1, p. 75), is made to compete in TRAC-PF1/MOD1 with another, independent choking criterion, based on the flow maximization at the break location. Thus, as for subcooled critical flow, the model for two-phase critical flow has no basis in physics. The modeling uncertainty cannot be obtained by methods which require a rational relation between parameter uncertainty and break flow uncertainty.

### 4.4.2 Measure of Break Flow Uncertainty

For the reasons given in Section 4.2.1 above, no relation is sought between parameter uncertainties and break flow uncertainty. Instead, the ratio

$$R_m = \frac{(W_c)_m}{(W_c)_P}$$

of measured critical mass flow rate $(W_c)_M$ over predicted critical mass flow rate $(W_c)_P$ is determined from SET measurements and TRAC-PF1/MOD1 predictions, and its scale dependence is obtained to predict critical break flow rates at

full-scale reactor conditions. The data comparison is carried out to yield the statistical mean $\bar{R}_m$ and the sample standard deviation $s_R$ of $R_m$, in the pressure and temperature range that is actually encountered under full-scale LBLOCA conditions.

The bias ratio $R_m$ is found to depend upon upstream conditions, namely pressure and temperature, and possibly void fraction, and upon upstream geometry [21]. It has also been determined that geometric effects are fully described by the ratio L/D, i.e. of upstream pipe length L over pipe diameter D. The ratio L/D is specified as input parameter. It is the dominant scale parameter for break flow predictions and used as argument in the expression for the mean bias ratio $\bar{R}_m(L/D)$. Modeling uncertainties of the TRAC code in predicting fluid conditions upstream of the break, and in predicting critical break flow from upstream conditions, are then characterized by the sample standard deviation $s_R$ of $R_m$.

### 4.4.3 SET Data Base for Break Flow Uncertainty

The ratio $R_m$ was determined from Marviken test data [21], carried out with different nozzle lengths and diameters, and with variations in inlet subcooling. Marviken test data were used because Marviken can accommodate pipe diameters of up to 0.5 m, requiring the least amount of extrapolation to the full-scale diameter of 0.7 m.

The dependence of $R_m$ on L/D was determined from Marviken tests by using break nozzle geometries with $0.3 \leq L/D \leq 3.7$ [21]. Inlet subcooling was varied between 5 and 50°K. The Marviken tests and their TRAC simulations were depressurizing transients, covering the pressure range from 50 to 1 bar. For the purpose of data reduction for critical break flow, the transients were considered as a sequence of quasi-steady transients. Each transient provided a large number of bias ratios $R_m$.

Twelve different Marviken tests were used to provide the total of 151 critical mass flow pairs $\{(W_c)_M, (W_c)_p\}$, i.e. 151 bias ratios $R_m$; of these 111 are for subcooling and 40 for two-phase flow conditions.

### 4.4.4 Uncertainty of Modeling Break Flow in TRAC-PF1/MOD1

The mean $\bar{R}_m$ of the bias ratio $R_m$ was calculated [21] for each nozzle geometry of the Marviken tests and represented, through least-square fitting, by

$$\bar{R}_m = 0.696 \exp\left[0.649\left(\frac{L}{D}\right)^{-0.168}\right] \quad \text{for subcooled conditions, and}$$

$$= 0.778 \exp\left[0.679\left(\frac{L}{D}\right)^{-0.25}\right] \quad \text{for two-phase flow conditions}$$

upstream of the break area. The uncertainty in $\bar{R}_m$, caused by the shortcoming in the TRAC-PF1/MOD1 model to predict upstream conditions and break flow for a given scale (L/D) is expressed by the sample standard deviation $s_R$ of $R_m$ about $\bar{R}_m$ which also depends on scale (L/D)

$$s_R = 0.90 \exp\left[-1.737\left(\frac{L}{D}\right)^{0.227}\right] \text{ for subcooled conditions}$$

$$= 2.03 \exp\left[-2.160\left(\frac{L}{D}\right)^{0.25}\right] \text{ for two-phase flow conditions.}$$

If TRAC-PF1/MOD1 accommodated scale effects on break flow properly, both $\bar{R}_m$ and $s_R$ would be constants. If TRAC modeled break flow accurately, and if experiments were accurate $\bar{R}_m$ would be equal to one and $s_R$ equal to zero. $R_m$ varies between 1.11 and 1.92 in the range of $0.3 \leq (L/D) \leq 3.0$ and subcooling temperatures between 5°K and 50°K.

## 4.5 Downcomer Modeling Uncertainty (CSAU Steps No. 8, 9 and 10)

The estimate of uncertainties in modeling ECC bypass phenomena in TRAC-PF1/MOD1 was carried out by Rohatgi and Neymotin [24] and is briefly summarized here.

### 4.5.1 Bypass Modeling, Reflood Timing and Effects on PCT

The standard method of estimating the uncertainties of all the parameters appearing in the TRAC-PF1/MOD1 downcomer model and then calculating the propagation of parameter uncertainties through the model, to obtain the resulting PCT uncertainty is not possible because

(i) without significant code modifications, TRAC-PF1/MOD1 does not facilitate variations of parameters which are related to downcomer models; needed code modifications would violate the CSAU requirement to "freeze" the code which is being assessed,

(ii) the computational effort needed to carry out the necessary TRAC-PF1/MOD1 calculations with all the downcomer-related parameter changes is prohibitively expensive.

Therefore, the contribution to PCT uncertainty from downcomer modeling of ECC phenomena was estimated directly as a code bias. The code bias was then used to shift the PCT probability distribution function [4] so as to accommodate the downcomer modeling uncertainty in the overall PCT uncertainty.

To estimate the uncertainty contribution from downcomer modeling, it was recognized first that the downcomer phenomena control the time period of nearly adiabatic fuel heating and clad temperature rise. The time period controlled by the downcomer thermohydraulics during refill and reflood begins with the beginning of ECC injection at the time $t_{ECCi}$ and ends at the time $t_{LPf}$, when the lower plenum has been refilled, and liquid water begins to enter the core, thereby cooling the fuel and terminating the clad temperature rise. Any uncertainty in predicting this period $\delta t_{if} = t_{LPf} - t_{ECCi}$ results in the PCT uncertainty according to

$$\Delta PCT_{ECC} \approx \frac{dT_c}{dt} \cdot \delta t_{if} \quad , \tag{4.1}$$

where $dT_c/dt$ is the time rate of clad temperature rise at the location in the core where PCT occurs. The time rate of clad temperature rise is obtained from NPP calculations carried out with reference conditions. The uncertainty $\delta t_{if}$ of the time period between start of ECC injection and completion of Lower Plenum refill is obtained by comparing TRAC-PF1/MOD1 calculations with SET test data [24].

### 4.5.2 SET Data Base for ECC Phenomena in Downcomer

The uncertainty estimate for downcomer thermohydraulics is based on UPTF Test Runs 131, 132, 133, and 136 [24].

The Upper Plenum Test Facility (UPTF) is a full-scale reactor vessel testing facility with cold leg injection nozzles, four cold legs, the downcomer, the lower plenum and the core barrel, i.e. all the components important to ECC phenomena. There is no geometric scale distortion or scaling uncertainty, because UPTF has full-scale geometry and geometric similarity with the nuclear power plant (NPP).

UPTF Test Runs 131, 132, 133, and 136 are blowdown transients. The important difference between UPTF blowdown tests and the NPP blowdown phase during LBLOCA is that the steam flow rate from the core to the lower plenum and downcomer is maintained to be nearly constant in UPTF, while in NPP transients it is governed by decreasing flashing rates in the core and in the lower plenum. This difference is accounted for in the estimate for the uncertainty $\delta t_{if}$.

### 4.5.3 Analysis of PCT Bias Due to ECC Bypass Modeling Uncertainty in TRAC-PF1/MOD1

The time period $(t_{LPf} - t_{ECCi})$ between the start of ECC injection and the completion of downcomer refill is divided into two parts, the bypass and the refill periods. The partition is at the time $t_{LPm}$, when the liquid inventory in the lower plenum reaches its minimum. The three points in time, $t_{ECCi}$, $t_{LPm}$ and $t_{LPf}$, are obtained from TRAC calculations for NPP reference conditions. The uncertainties in predicting the two time spans between the three points in time are estimated by comparing TRAC simulations of UPTF tests with UPTF test data [24].

The first or bypass period begins with the holdup phase during which all the injected liquid escapes through the break, allowing no accumulation in the downcomer nor any flow through the downcomer, and it ends with the delay phase, where liquid accumulates in the downcomer before entering the lower plenum. UPTF data show no holdup phase, but TRAC predicts a holdup or an initial complete bypass phase. The complete bypass phase ends when the steam flow up the downcomer, opposing liquid downflow, decreases to some critical value $(W_v)_{crit}$. Even the largest UPTF steam flow was less than $(W_v)_{crit}$, as there was no bypass observed in UPTF. By taking the pessimistic assumption that the holdup phase lasts as long in a power plant as it takes during a

blowdown to reduce the steam flow to the largest measured UPTF steam flow rate, one extends the holdup phase beyond the time where holdup stops. The real holdup phase in the power plant can only be shorter. Therefore the uncertainty must be negative. Because of the UPTF steam flow limitations, it is impossible to know how large the negative uncertainty for the holdup phase is. Thus, the uncertainty in predicting the end of the holdup phase is taken to be the largest negative value, namely zero.

The uncertainty for predicting the time span of the delay phase is obtained [24] from the ratio of TRAC-predicted over measured time spans in UPTF tests, between the end of complete holdup in the downcomer and the time at which the lower plenum liquid inventory reaches its minimum. Adding up this uncertainty with the above upper estimate of zero uncertainty, one obtains the uncertainty in predicting the time span of the whole bypass period, namely

$$\delta t_1 = \delta\{t_{LPm} - t_{ECCi}\} = \delta t_{holdup} + \delta t_{delay} = 0\text{-}3.4s = -3.4s \; . \qquad (4.2)$$

The uncertainty $\delta t_1 = \delta t_{delay}$ is negative because TRAC-PF1/MOD1 predicts consistently longer delay phases than can be observed in UPTF.

The second or refill period begins with the countercurrent flow phase and ends with the phase of no bypass flow [24]. The two phases are separated at the time when the steam flow at the lower end of the downcomer reaches zero. The uncertainty of predicting the time span of the countercurrent flow phase is estimated by comparing TRAC-predicted and experimentally obtained filling rates for the lower plenum and by using the known volume of the lower plenum to predict the changes in filling time, caused by changes in filling rate. For the phase of no bypass flow, i.e. no steam flow up through the downcomer, there are no UPTF data available. By comparing the trend of the ratio of predicted over measured filling rates for decreasing steam flow rates in UPTF, one can conclude, however, that TRAC consistently underpredicts the filling rate. The uncertainty in predicting the time span for the phase of no bypass is therefore negative but unknown in magnitude. An upper bound for that uncertainty is zero. Thus the uncertainty for predicting the time span of the refill period is [24]

$$\delta t_2 = \delta\{t_{LPf} - t_{LPm}\} = \delta t_{ccflow} + \delta t_{no\ bypass} = -0.25s + 0 = -0.25s \; . \qquad (4.3)$$

By adding the uncertainties from the first and second periods, one obtains the uncertainty $\delta t_{if}$ of predicting the entire time period $(t_{LPf} - t_{ECCi})$ between the start of injection and the completion of lower plenum refill

$$\delta t_{if} = \delta t_1 + \delta t_2 = -3.65s \; . \qquad (4.4)$$

### 4.5.4 TPC Bias from TRAC-PF1/MOD1 Modeling of ECC Phenomena

The time rate of clad temperature rise in Eq. (4.1), averaged over the time frame from $t_{ECCi}$ to $t_{LPf}$ was obtained from TRAC NPP calculations, carried out with reference conditions. It was found to be

$$\frac{dT_c}{dt} = 5.2°K/s \ . \qquad (4.5)$$

By substituting this value and that of Eq. (4.4) into Eq. (4.1), one obtains the contribution to PCT uncertainty from the uncertainty of predicting ECC bypass phenomena

$$\Delta PCT_{ECC} = -19°K(-34°F) \ .$$

This means that the TRAC-code is conservative relative to PCT in its modeling of ECC bypass phenomena. The modeling of bypass phenomena during LBLOCA causes the predicted PCT to be too high by at least 19°K. The bias $\Delta PCT_{ECC}$ is used to shift both the mean PCT and the 95 percentile of the uncertainty probability distribution [4].

## 4.6 Effects from Noncondensable Gases (Steps No. 9 and 10)

The noncondensable gas affecting ECC bypass flow processes is the nitrogen used as the pressurant gas in the accumulators to drive the emergency coolant through the cold leg injection nozzles into the vessel. There is nitrogen gas dissolved in the ECC water and there is free nitrogen above the ECC water in the accumulator tanks.

The flow of the free nitrogen entering the vessel, after all the ECC water has been discharged into the vessel, is modeled in TRAC-PF1/MOD1. The associated modeling uncertainty, however, has no impact on the blowdown PCT uncertainty because the free nitrogen enters the vessel only late in the reflood phase. The uncertainty of modeling the effects from the free nitrogen has also no significant impact on refill and reflood PCTs because the nitrogen itself has only minor effects on ECC thermohydraulics: (a) the free nitrogen cannot affect condensastion when it arrives in the vessel because condensation is already terminated by the nitrogen that came out of solution earlier, (b) momentum effects from the nitrogen expanding behind the ECC water are insignificant because the expansion is absorbed in the downcomer and it is over before the flow is accelerated in the core and, (c) the nitrogen arrives in the vessel only after the second peak of the clad temperature.

It is the dissolved nitrogen in the ECC water, however, that affects the reflood PCT because it enters the vessel at the beginning of ECC injection, at the time $t_{ECCi}$ (cf. Eq. 4.2), and immediately interferes with condensation and break flow. TRAC-PF1/MOD1 does not model the dissolved nitrogen in the ECC water.* Rohatgi [24] has estimated the change $\delta t_{NC}$ in time span $t_{LPf} - t_{ECCi}$ between the start of ECC injection and the completion of lower plenum filling, that is caused by nitrogen as it comes out of solution in the ECC water. This

*Artificial nitrogen injection through a "fill junction" may be possible but this method is undocumented and unreviewed; therefore it cannot be considered in the implementation of the CSAU methodology.

change $\delta t_N$ alters the period ($t_{LPf} - t_{ECCi}$) of nearly adiabatic clad heating and must be multiplied, as $\delta t_{if}$ in Eq. (4.1) to obtain the nitrogen-related contribution to PCT uncertainty (cf. Section 4.5.1), or PCT bias,

$$\Delta PCT_{NC} = \frac{dT_c}{dt} \delta t_{NC} ,$$

where the subscript NC denotes a noncondensable gas in general.

The nitrogen coming out of solution inhibits condensation, it increases the mass of gas in the vessel and it retards the break flow. These three actions retard the rate of vessel depressurization which, in turn, prolongs the bypass period (cf. Section 4.5.3). Rohatgi [24] estimated the change of depressurization rate, arising from dissolved nitrogen coming out of solution and he derived the estimate $\delta t_{NC} = 1.91$ s. By using the rate of adiabatic temperature rise from Eq. (4.5), one finds for the estimate $\Delta PCT_{NC}$ of PCT bias due to noncondensable gas

$$\Delta PCT_{NC} = 9.9°K \ (17.9°F) .$$

This bias is used, as $\Delta PCT_{ECC}$, to shift the mean and the 95 percentile of the PCT probability distribution.

## 4.7 Effects from Steam Binding (CSAU Steps No. 9 and 10)

Steam binding denotes the generation of backpressure in the steam generators by the evaporation of droplets which were entrained by steam from the liquid in the core, upper plenum, in cold legs and steam generator entrance plena (cf. E., Table 2). The droplet evaporation causes volume expansion, which requires vapor acceleration and causes back pressure.

Steam binding is dominated by entrainment and deentrainment in the reactor core and steam generator entrance plena and in the components connecting these. Consequently, the contributions to PCT uncertainty from steam binding is dominated by uncertainties in the models for entrainment and deentrainment. Specifically, the uncertainties of modeling liquid entrainment at the mixture level in the core, of modeling liquid entrainment from films on component structures by interfacial shear and of modeling deentrainment on component structures, which is caused by the mismatch of liquid and vapor inertia, are the most important contributing factors impacting PCT uncertainty.

Similarly to the modeling of ECC bypass phenomena in TRAC (cf. Section 4.5.1 above), the entrainment and deentrainment models in TRAC make it impossible to use the standard method of estimating first all the parameter uncertainties in these models and then their probabilistic propagation through the model and to the PCT uncertainty. It is impossible because

(i) the entrainment model for the core is not physical in TRAC-PF1/MOD1 as it has been used to tune the code, i.e. to compensate for deficiencies in heat transfer and mixture level motion* models; thus there is no basis for relating modeling parameters to PCT uncertainties, and

(ii) the computational effort needed to analyze the error propagation from all relevant parameter uncertainties by statistical methods is prohibitively expensive with TRAC-PF1/MOD1.

Therefore, the contributions to PCT uncertainty from steam binding effects, i.e. from entrainment and deentrainment modeling uncertainties, were computed directly as a code bias. The code bias was calculated as the change in computed PCT that is caused by multiplying, in the TRAC-PF1/MOD1 code, the relevant entrainment coefficients E and interfacial shear coefficients $C_i$ with such constant multipliers as are necessary to achieve agreement between computed and measured entrainment. This work was performed by Boyack of LANL.

It has been determined that the relevant entrainment and interfacial shear coefficients are the entrainment coefficient E of Rozen's entrainment correlation [19], the core interfacial shear coefficient $(C_i)_{CR}$ and the upper plenum interfacial shear coefficient $(C_i)_{UP}$.

Measurements of entrainment, namely the liquid accumulation in the upper plenum (indicative of the amount first entrained just below the mixture level in the core, and then transported into the upper plenum) and the liquid mass flux through the cold leg (indicative of deentrainment in the upper plenum), were obtained from SET data. To resolve issues of scale, the SET data were obtained from the Slab Core Test Facility (SCTF).

It was determined by Boyack [5] that for the best match between SCTF test data and TRAC-PF1/MOD1 results, obtained with the standard NPP nodalization scheme (cf. Chapter 3), one has to multiply the

| | | |
|---|---|---|
| Rozen entrainment coefficient | E | by 20, |
| core interfacial shear coefficient | $(C_i)_{CR}$ | by 10, and |
| upper plenum interf. shear coeff. | $(C_i)_{UP}$ | by 1.0. |

These three multipliers were used for one NPP calculation with TRAC-PF1/MOD1. The differences ($\Delta PCT_{SB}$) between the PCT obtained with the above three multipliers and the PCT obtained in the standard reference NPP calculation (all multipliers set equal to one) were found to be

for blowdown PCT: $\Delta PCT_{SB} = 0$ (no steam binding effect)
for cavity reflood PCT: $\Delta PCT_{SB} = -5°K(-9°F)$
for rate reflood PCT: $\Delta PCT_{SB} = 59°K(106°F)$.

The three code bias values of $\Delta PCT_{SB}$ which arise from TRAC-PF1/MOD1 modeling uncertainties of steam binding effects, are used in Part 4 to shift the PCT uncertainty probability distribution functions [4]. That accounts for steam binding contributions to PCT uncertainty.

*Nonphysical "level sharpener."

# 5. GLOBAL ASSESSMENT OF PCT UNCERTAINTY (CSAU STEPS 9 AND 10)

## 5.1 Purpose

The objective of the global PCT uncertainty assessment is to support the detailed PCT uncertainty analysis with the comparison of direct PCT measurements in Separate Effects Test (SET) and Integral Effects Test (IET) facilities with TRAC-PF1/MOD1 predictions of the LBLOCA transients in SET and IET facilities.

Whereas the detailed PCT uncertainty analysis is built upon the component uncertainties associated with every modeling parameter and whereas the overall PCT uncertainty is then related to the parameter uncertainties through probabilistic superposition, the global assessment of PCT uncertainty involves experimental uncertainties and code uncertainties from modeling and computing. The detailed uncertainty probability analysis yields the probability distribution function; the global assessment of PCT uncertainty yields the scatter diagram of measured versus predicted peak clad temperatures.

Since all SET and IET simulations with TRAC-PF1-MOD1 were post-test simulations, it must be expected that the above comparisons produce smaller values of code bias and of standard deviation than would be obtained from pre-test or blind test simulations, where code tuning* could not influence the comparisons between computed and measured results.

Special care is to be exercised to avoid systematic errors from experiments (such as early quenching of external thermocouples, etc.).

The comparisons are to be made separately for blowdown and for reflood PCT, because different phenomena govern the two different LBLOCA phases, and compensating errors would corrupt the results if no distinction were made.

The objective is also to assess the scale effect on PCT by correlating the normalized peak clad temperature, as obtained from experiments on facilities of widely varying scale, with scaling parameters. It will be shown that the blowdown PCT depends only weakly on facility scale.

## 5.2 SET and IET Data Bases

### 5.2.1 IET Data Base for Blowdown PCT Comparisons with TRAC

The blowdown Peak Clad Temperature (PCT) measurements were obtained from the LOFT Test LP-02-6 and published by Knight [25, Appendix C].

Measurements were taken from 11, 1, 1 and 14 thermocouples, located on Fuel Rod Nos. 1, 2, 3 and 4, respectively, at different elevations. The peak

*Code tuning that affected the results consisted of nodalization changes, and changes in friction factors, condensation rates and entrainment.

clad temperatures were read from temperature traces, obtained from temperature recorders at the LOFT facility and from continuous plots generated by TRAC. The results are shown in Subsection 5.3 below.

PCT measurements from THTF blowdown experiments, i.e. from Test Series I (ORNL/NUREG-19 & 45) and Test Series II (ORNL/NUREG-053) and from those reported in NUREG/CR-3208, have also been evaluated concerning their usefulness of PCT uncertainty assessment. It has been found however, that the test data are not accurate and sufficiently reliable for the assessment, and that experimental boundary conditions are not adequately documented to facilitate TRAC calculations. Also, the TRAC documentation does not reveal how THTF-type boundary conditions are implemented in TRAC.

### 5.2.2 SET Data Base for Reflood PCT Comparisons with TRAC

The reflood PCT measurements were obtained from the Cylindrical Core Test Facility (CCTF) and from the Slab Core Test Facility (SCTF). The experimental and computed PCT data were collected by Los Alamos National Laboratory (LANL) and transmitted to Brookhaven National Laboratory. The total of 220 data points were used, namely

36 data from CCTF Run No. 71, Report No. LA-2D/3D-TN-86-8,
36 data from CCTF Run No. 72, Report No. LA-2D/3D-TN-86-7,
36 data from CCTF Run No. 76, Report No. LA-2D/3D-TN-86-6,
36 data from CCTF Run No. 78, Report No. LA-2D/3D-TN-86-5, and
12 data from CCTF as reported in Report Nos.:
LA-2D/3D-TN-83-10 & 12,
84-6 (two data pairs),
85-1 & 7,
86-1,2,5,6,7 &8;

12 data from SCTF Run No. 604, Report No. LA-2D/3D-TN-85-6,
12 data from SCTF Run No. 605, Report No. LA-CP-87-103
12 data from SCTF Run No. 611, Report No. LA-2D/3D-TN-86-9
12 data from SCTF Run No. 613, Report No. LA-2D/3D-TN-2
12 data from SCTF Run No. 614, Report No. LA-2D/3D-TN-85-4, and
4 data from SCTF as reported in Report Nos.:
LA-2D/3D-TN 85-2,7,13 and 15.

These reports were written by H.J. Stump, G.J. Willcut, M.W. Cappiello, J.S. Gilbert, and J.C. Lin of Los Alamos National Laboratory.

The four sets of 36 data from CCTF Runs Nos. 71, 72, 76 and 78 were obtained from 12 fuel rods with thermocouples at three elevations: 1,015; 1,830 and 2,440 mm above core entrance.

The five sets of 12 data from SCTF Runs Nos. 604, 605, 611, 613 and 614 were obtained from four selected fuel rods with thermocouples at three elevations, namely at 950, 1,905 and 2,760 mm above core entrance.

## 5.3 Blowdown PCT Data Reduction and Results

The 27 data points obtained from the LOFT facility, Test No. LP-02-6 [25, Appendix C] are plotted in Figure 7, showing measured vs. post-test computed PCTs.

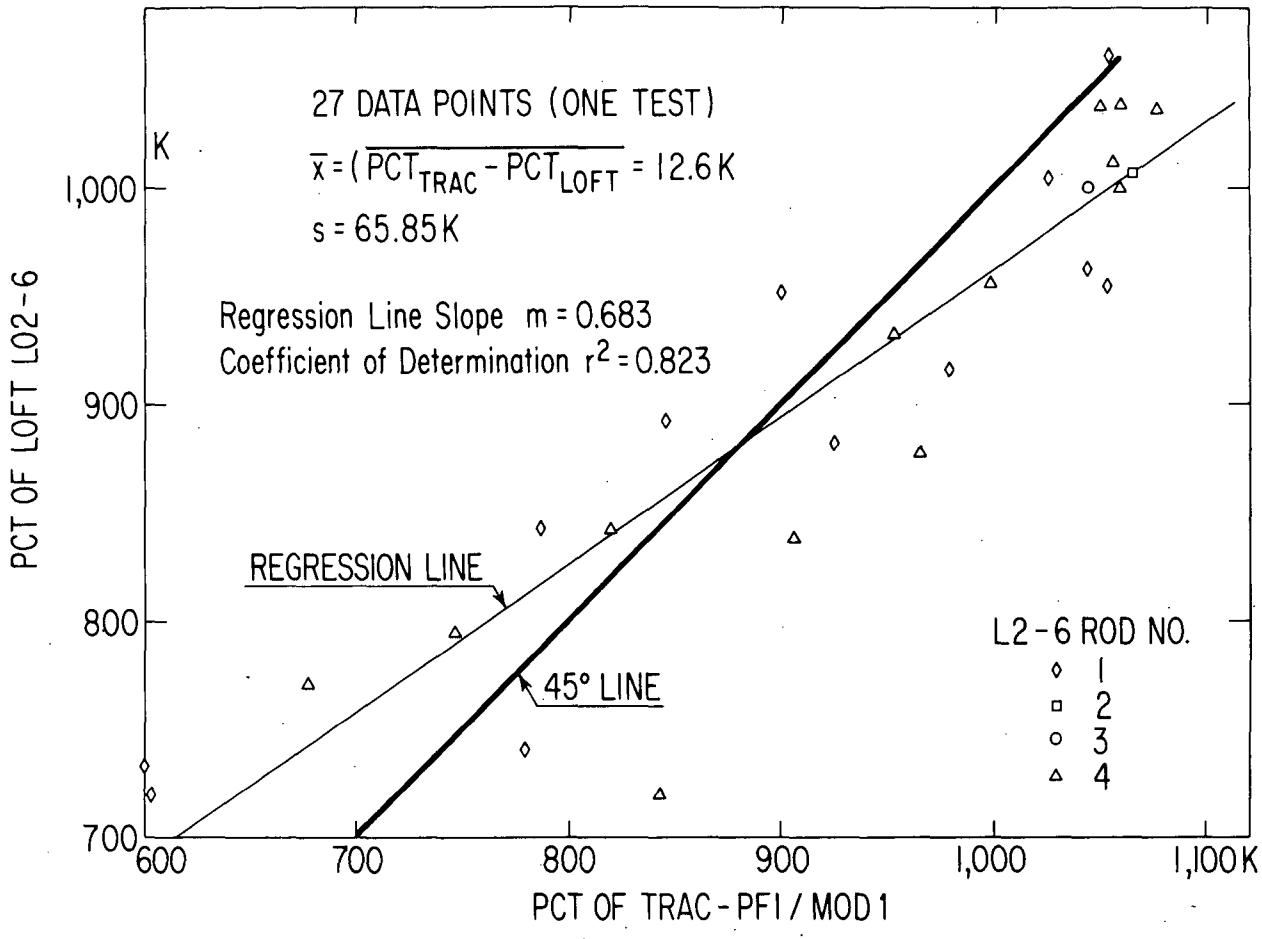


Figure 7 Blowdown Peak Clad Temperature - TRAC-PF1/MOD1 vs LOFT L02-6

The combined bias from TRAC code and experiments equals the arithmetic mean $\bar{x}$ of the differences $(PCT_{TRAC} - PCT_{LOF})$, i.e.

$$\bar{x} = (1/N) \sum_{i=1}^{N} [PCT_{TRAC} - PCT_{LOF}]_i = 12.6°K \ (22.7°F)$$

and is conservative. The sample standard deviation s is

$$s = \sqrt{\{\sum_{i=1}^{N} [PCT_{TRAC} - PCT_{LOF}]_i^2 - N\bar{x}^2\}/(N-1)} = 65.9°K \ (118.6°F) \ .$$

This means that 95% of all TRAC vs. LOFT comparisons fall within the uncertainty range of approximately ±132°K (273°F).

Figure 7 shows also the straight regression line through all points. Since the slope of the regression line is less than one, it can be concluded that TRAC is conservative for high values of PCT, PCT > 885°K (1,133°F), and nonconservative for low PCT values below 885°K. No credit should be taken for the conservative bias $\bar{x}$ at low PCT values!

## 5.4. Reflood PCT Data Reduction and Results

### 5.4.1 Data Reduction

All CCTF, SCTF and TRAC-PF1-MOD1 data were provided by LANL as clad temperatures versus time and then scanned at BNL by computer to yield the maxima or PCT values. The TRAC calculations were executed with non-standard nodalization schemes, but the deviation is not serious. The core nodalization scheme is as follows:

| | CCTF | SCTF | Standard NPP |
|---|---|---|---|
| Axial segments in core | 6 | 6 | 5 |
| Radial segments in core | 3 | 4 | 2 (+ hot assy) |
| Azimuthal segments | 4 | - | 4 |

The highest temperature computed by TRAC for any computational cell was paired with the highest temperature measured in that computational cell. Between two and four thermocouples shared each computational cell in the TRAC calculations for CCTF simulations, two thermocouples were in each TRAC-computational cell for SCTF simulations.

It should be pointed out that higher temperatures may have been reached in any computational cell then were recorded by the thermocouples in that cell, and the difference between the TRAC-computed cell-average temperature and the maximum temperature obtained from the exact solution to the field equations in TRAC is not known. The comparisons of computed with measured data reveal therefore only a composite of the uncertainties associated with measurement, modeling and computing.

### 5.4.2 Results for Reflood PCT

The 220 pairs of measured and computed PCT values are plotted in the scatter diagram of Figure 8. The mean of differences $[PCT_{TRAC} - PCT_{EXP}]$ between computed and measured peak clad temperatures (PCT) is

$$\bar{x} = 10.3°K \ (18.6°F)$$

while the sample standard deviation from the mean is

$$s = 49.8°K \ (89.6°F) \ .$$

Thus, an approximation to the PCT uncertainty range for reflood, i.e. the deviation range of 95% of all data pairs, is ±97°K (±179°F). However, it must be pointed out that this uncertainty range does not account for the uncertainty of predicting with TRAC the initial conditions for the refill period, that is the uncertainty of predicting the events of the blowdown. To obtain an approximation to the uncertainty range for reflood PCT in a complete LBLOCA simulation, one should add the uncertainty ranges of 132°K and 97°K. The result would be the uncertainty range of ±229°K (±412°F) for predicting PCT in an LBLOCA calculation with TRAC, based on IET data comparisons.

It will be shown in Part 4 [4] that the uncertainty range, based upon the probabilistic superposition of parameter uncertainties and of modeling biases, is considerably larger than the above values. The chief reason for the small sample deviations obtained from the above comparisons with SET and IET data is code tuning. Blind test calculations would most likely produce uncertainty ranges as large as those obtained in Part 4. Also, SET results cannot account for uncertainty contributions from loop components. This is a second reason for the lower results from SET versus code comparisons.

## 5.5 Scale Effects on Blowdown PCT (CSAU Step No. 10)

The implementation of the CSAU methodology requires the careful assessment of scale effects on PCT uncertainty, because almost all SET and IET facilities are small-scale facilities and one must estimate the errors between code calculations and all available parameters from the full-scale Nuclear Power Plant (NPP). The methods used to account for scaling effects have been described in Sections 4.3 and 4.4.

It was also shown by the analysis described in Sections 2.3 and 4.2 [6], that the blowdown peak clad temperature measurements are not affected by systems scale distortions as long as the fuel elements have full-scale geometry and nuclear fuel pellets. It was shown that fuel-stored energy or, equivalently, linear heating rate, dominates peak clad temperature. This section leads to the same conclusion by comparing experimental PCT data from a wide range of test facility designs and sizes. The comparison was carried out at INEL [5].

### 5.5.1 Data Base and Results

Figure 9 below shows measured blowdown peak clad temperatures, PCT, plotted versus linear heating rates, $q'_w$.

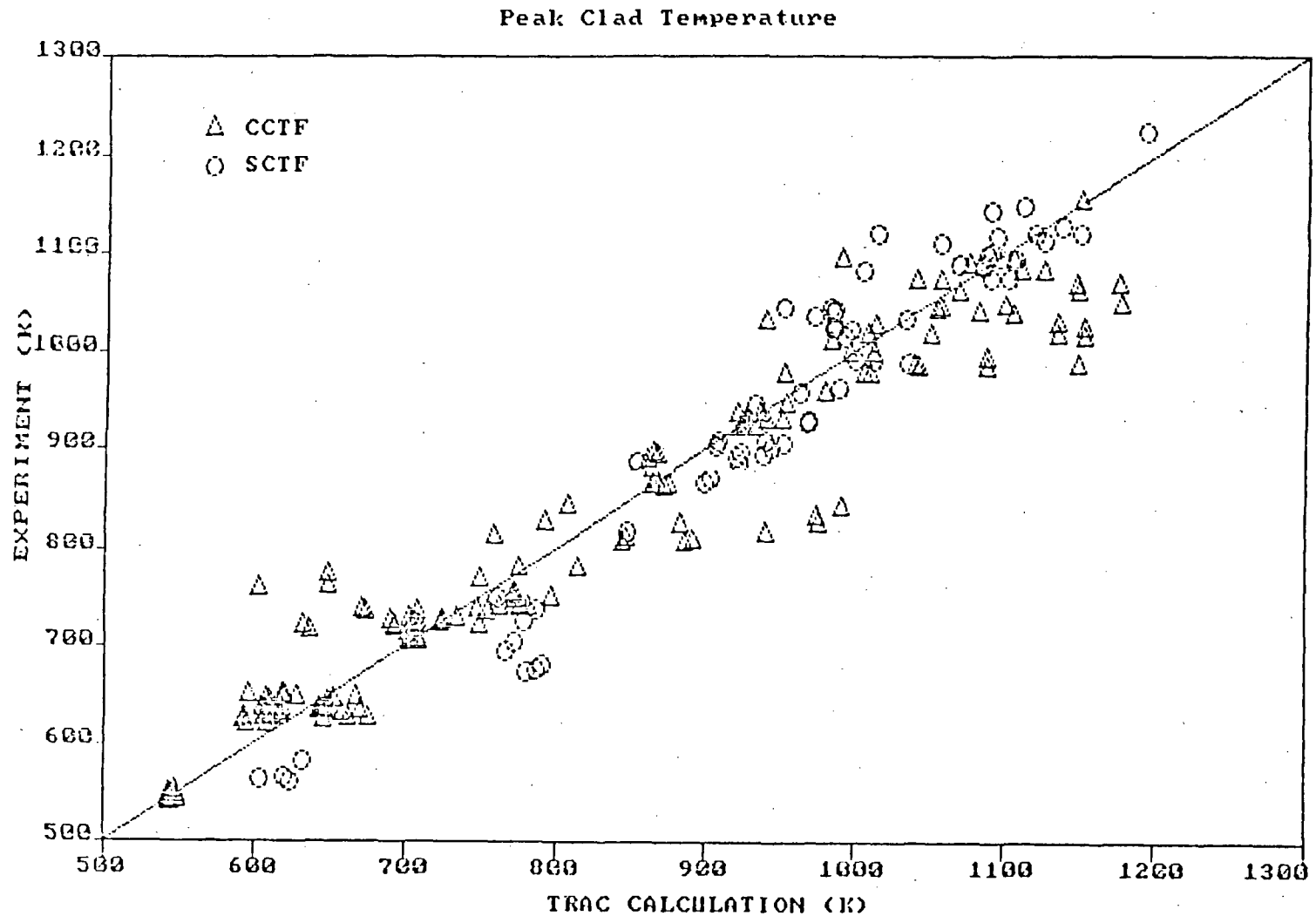


Figure 8 Comparison of TRAC-PF1/MOD1 Computed PCT with CCTF and SCTF Data

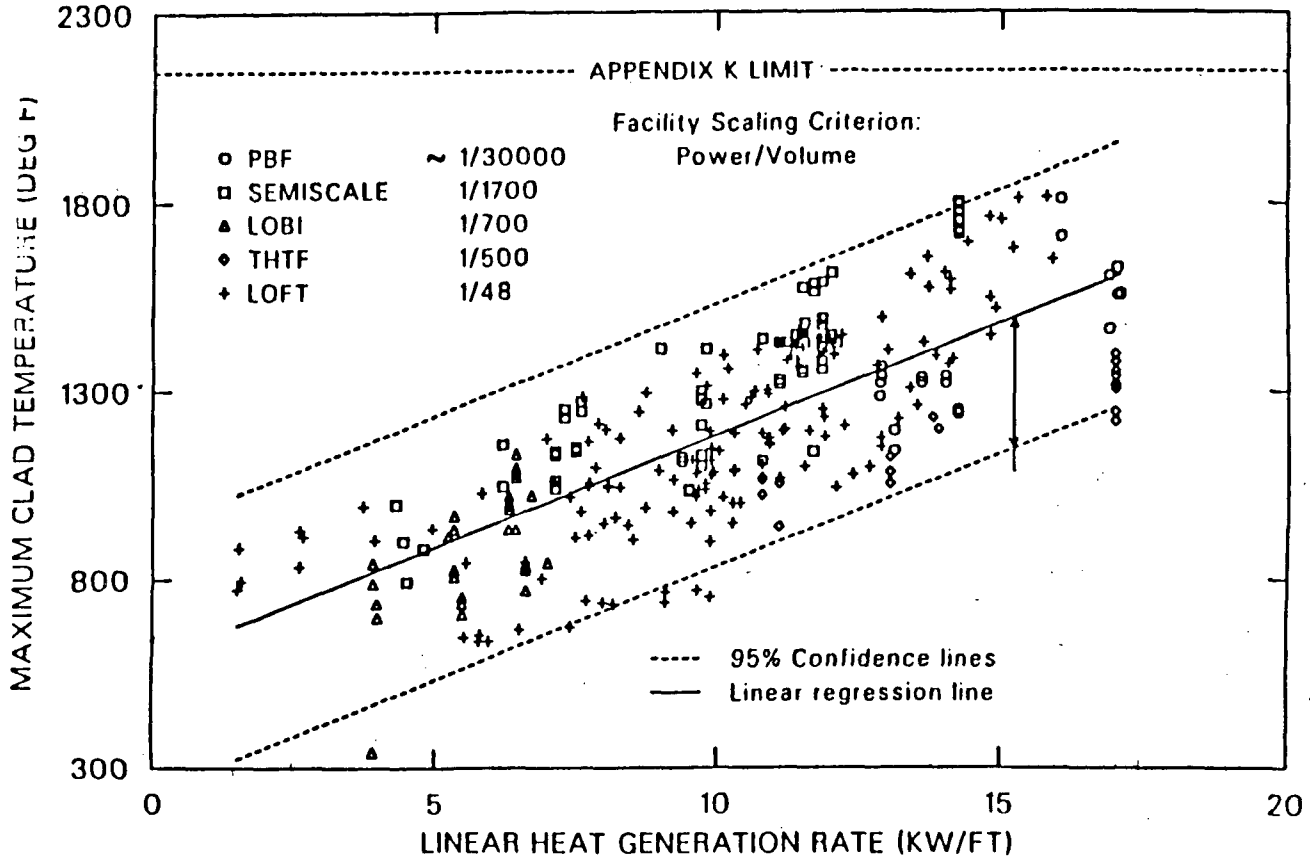


Figure 9 Scaling Effects on Blowdown PCT

The measurements were taken from five widely different test facilities with nuclear heating, indirect electrical heating by a heating element in ceramic and covered with cladding, and with direct ohmic heating of an empty cladding. The volume scale ratios of the test facilities involved varies from 1/30,000 to 1/48 as shown in Figure 8. The linear heating rate varied from 6.5 to 56 kW/m (or 2 to 17 kW/ft). The total of 301 data points are shown in Figure 9.

The coordinates of Figure 9 were chosen on the basis of an energy balance in an analysis by Duffey and Catton [5, Appendix XV]. The diagram in Figure 9 is preliminary because it is not cast in nondimensional form. In fact, it can be shown that if the transient conduction in the fuel is governed by local core hydraulics and not strongly dependent on loop hydraulics, then the following scaling groups govern PCT of nuclear fuel elements:

$$N_{q'} = \left(\frac{s}{R_1}\right) \cdot C \cdot \frac{q'_{w,o}}{\bar{k}_c (PCT - T_o)} \tag{5.1}$$

$$(N_{Bi})_{gp} = \frac{\bar{h}_{gp} s}{\bar{k}_c}, \quad C = \frac{(\overline{\rho c})_c}{(\overline{\rho c})_f} \cdot \frac{s}{R_1} \tag{5.2,3}$$

$$(N_{Bi})_c = \frac{\bar{h}_c \cdot s}{\bar{k}_c}, \tag{5.4}$$

where $s$, $R_1$, $q'_{w,o}$, $T_o$ and $\bar{k}_c$ stand for, respectively, clad thickness, pellet radius, initial linear heating rate, initial clad temperature, and mean fuel thermal conductivity, while $(\overline{\rho c})_c$ and $(\overline{\rho c})_f$ denote volumetric heat capacity for clad and fuel, respectively, and $\bar{h}_{gp}$ and $\bar{h}_c$ are the average gap conductance and convective film coefficient, respectively. It should be expected that the linear heating number, $N_{q'}$, depends on the gap and clad Biot numbers $(N_{Bi})_{gp}$ and $(N_{Bi})_c$, and on the heat capacity ratio C. The converse of the statement above Eq. (5.1) is, that if $N_{q'}$ depends only on $(N_{Bi})_{gp}$, $(N_{Bi})_c$ and C, the PCT is governed only by local core hydraulics, and PCT measurements on full-scale fuel elements are undistorted by scale effects of the plant components outside the core. This should be confirmed by reevaluating the data in Figure 9, using governing scaling groups as shown above.

For reflood PCT, the governing scaling groups listed above must be supplemented by the groups which characterize the primary system, accounting for the variation of fuel boundary conditions. Duffey and Catton [5, Appendix XV] have shown that the temperature rise in the clad can be correlated with the ECC injection flow rate, divided by the core cross-sectional flow area, or "cold flooding velocity" $U_r$. Figure 10 shows the correlation in logarithmic coordinates. Regression analysis yields the best-fit line $PCT - T_{init.} = 339/U_r^{1.14}$.

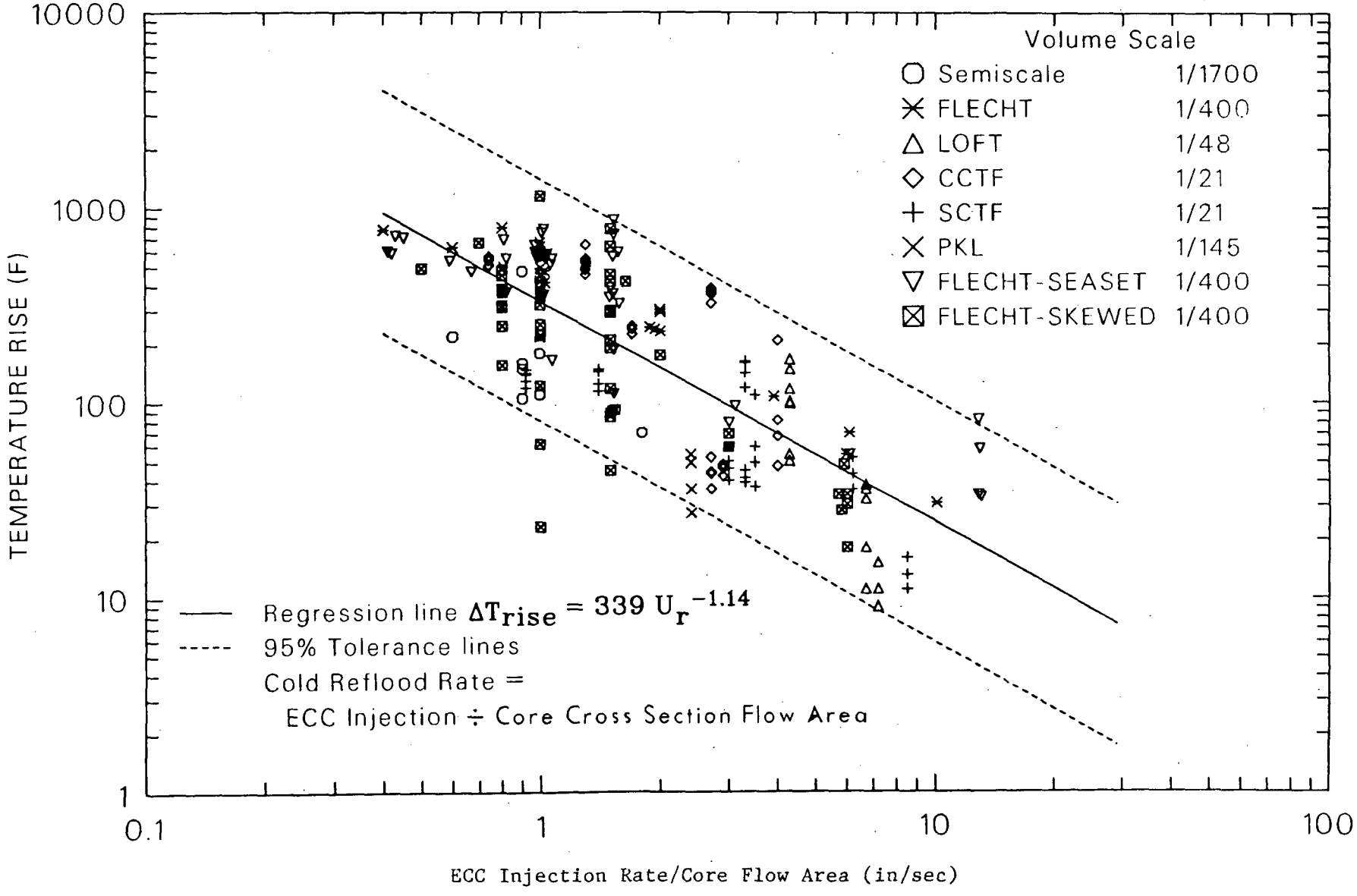


Figure 10 Measured Temperature Rise Data from Scaled Experimental Facilities (217 points) During Reflood

### 5.5.2 Conclusions and Recommendations

Even without having completed the above exploration of scaling groups, one can conclude from Figures 9 and 10:

a) Blowdown PCT is governed by fuel-stored energy, or equivalently, by initial linear heating rate. The linear regression line corresponds to a constant $N_q$, and a fixed value of $\overline{k_c} \cdot C \cdot (s/R_l)$.

b) Within the range of PCT uncertainty of ±194°K (±350°F), there are no strong scale effects detectable which could impact on blowdown PCT.

c) Reflood PCT depends primarily on the ratio $U_r$ of ECC injection rate over core flow area. Data available so far near the typical NPP value of $U_r$ = 10 cm/s (≈4 in/sec) indicate that scaling affects PCT by approximately ±165°K (±297°F). However, scaling effects are significantly stronger at lower values of $U_r$.

This observation lessens the need of computer codes to be able to scale blowdown phenomena taking place outside the reactor core. Small-scale SET and IET facilities with full-scale fuel elements can be used to assess the uncertainty in predicting blowdown PCT predictions. This cannot be said for reflood PCT predictions, because reflood PCTs are affected by primary system component processes outside the core. One must resort to the techniques described in Sections 4.3 and 4.4 for assessing PCT uncertainty.

It is recommended that scaling groups be derived from appropriate field or lumped-parameter equations and that the dominant groups be selected from blowdown and refill/reflood PCT measurements. The results would provide scaling groups for extrapolating bias and uncertainty ranges (cf. Sect. 4.3 and 4.4) from SET and IET scale to NPP scale.

## 6. SUMMARY AND CONCLUSIONS

Peak Clad Temperature (PCT) uncertainties are derived in Part 4 [4] from the ranges of parameter uncertainties and from code modeling biases (systematic code errors) as presented in this paper. Parameter uncertainty ranges and code modeling biases are quantified primarily on the basis of statistics from basic property measurements and Separate Effects Test (SET) data.

The results from the analysis of PCT uncertainty are supported by comparisons of code calculations with Integral Effects Test (IET) data.

This paper describes the determination of parameter uncertainty ranges and modeling biases and it presents the comparisons of code results with IET data. The paper describes CSAU Element 2, i.e., Steps 7 through 10.

### 6.1 Ranges of Parameter Uncertainty

The ranges of parameter uncertainties are given in Table 10 of Section 4.2. They are listed for the relevant fuel-related parameters of gap conductance, power peaking factors, fuel thermal conductivity and convective heat transfer coefficients. Convective heat transfer coefficients contribute to PCT uncertainty through both parameter uncertainty and modeling bias.

### 6.2 Modeling Biases

The contributions to PCT uncertainty from the modeling in TRAC-PF1/MOD1 of all the relevant phenomena not represented in Table 10 by parameter uncertainty ranges, are assessed as modeling biases as follows:

For post-CHF heat transfer modeling uncertainties, the bias is expressed directly as $\Delta PCT_{NC}$ = 26, 47, and 89°K, (47, 84, and 160°F) respectively, for blowdown, refill and reflood peaks (cf. Sect. 4.2).

For pump modeling uncertainties, the pump head and torque biases $s_H$ and $s_T$ are given in Table 11 as functions of void fraction $\alpha$ in the pump. The effects from $s_H$ and $s_T$ on PCT are determined by the TRAC code [4].

For break flow modeling uncertainties, the bias $\overline{R}_m$ and its uncertainty $s_R$ are given in Section 4.4.4 as functions of the scale parameter (L/D).

For the modeling of ECC phenomena, the PCT uncertainty is determined directly as $\Delta PCT_{ECC}$ = -19°K (-34°F), i.e. the code is too conservative by that amount (cf. Sect. 4.5.4).

The PCT uncertainty contribution from TRAC's modeling of noncondensable gas effects was found to be $\Delta PCT_{NC}$ = 9.9°K (17.9°F) and to affect only the reflood PCT.

Steam binding effects are modeled in TRAC with an uncertainty of 59°K (106°F), affecting the second reflood PCT.

The effects of nodalization have been estimated to contribute to PCT uncertainty with $\Delta PCT_N$ = 35°K (63°F) to its mean and with $\delta PCT_N$ = 25°K (45°F) to its 95 percentile value; this is in addition to contributions from nodalization on uncertainties determined by simulating SET phenomena.

## 6.3 Importance of Analysis, SET and IET Data

As explained at the end of Chapter 2, PCT uncertainty is determined in parallel activities. Code calculations and SET data provide the detailed probability distribution function of PCT uncertainty. Code calculations and IET data provide an independent confirmation of PCT uncertainty estimates (cf. Sections 5.3 and 5.4.2).

These parallel actives must rely on the Priority Identification and Ranking Table (cf. Section 2.1) and on independent analyses (hand calculations, cf. Section 2.3). In fact, separate analyses are needed to resolve any contested claim in any phase of the CSAU methodology (expert opinion, etc.). Separate analyses are needed in assessing uncertainty ranges (cf. Section 2.3) and modeling biases (cf. Sections 4.3, 4.4, 4.5 and 4.6).

## 6.4 Check List of Requirements for CSAU

The CSAU methodology, as shown schematically in Figure 1, constitutes a set of necessary requirements but contains no criteria to establish sufficiency. Sufficiency must be established by supporting the uncertainty estimates through independently obtained results which confirm each other. There is no single rigorous method to obtain PCT uncertainty, or code uncertainty in general. Instead code uncertainty results are justified by evidence obtained from analysis, SET and IET data. The less a selected computer code is derived from first principles, the more one has to rely upon nonstandard methods of analysis and on upper bound estimates of uncertainty, and the greater will be the code uncertainty.

However, a Check List of Requirements for the CSAU methodology is presented in Reference 5. The list contains the minimum necessary requirements for all three elements of the CSAU Methodology. An application of the CSAU methodology will be deemed incomplete unless all requirements in the check list are met.

References


1. "Compendium of ECCS Research for Realistic LOCA Analysis," Draft Report, NUREG-1230, Division of Reactor Plant Systems, U.S. Nuclear Regulatory Commission, Washington, DC (1987). See Section 4.3.4.

2. B. E. Boyack et al., "An Overview of the Code Scaling, Applicability and Uncertainty (CSAU) Evaluation Methodology," Part 1, 16th Water Reactor Safety Information Meeting, National Bureau of Standards, Gaithersburg, MD, Oct. 1988.

3. G. E. Wilson et al., "Characterization of Important Contributors to PCT Uncertainty," Part 2, 16th Water Reactor Safety Information Meeting, National Bureau of Standards, Gaithersburg, MD, Oct. 1988.

4. G. S. Lellouche et al., "Uncertainty Evaluation of LBLOCA Analysis Based Upon TRAC-PF1-MOD1, Part 4, 16th Water Reactor Safety Information Meeting, National Bureau of Standards, Gaithersburg, MD, Oct. 1988.

5. TPG and K. Katsma, D. Hall and C. D. Fletcher, "Quantifying Reactor Safety Margins: Application of CSAU Methodology to SBLOCA," NUREG/CR-5249, Idaho National Engineering Laboratory, EG&G Idaho, Idaho Falls (1989) (in press).

6. W. Wulff, "Uncertainties in Modeling and Scaling in the Prediction of Fuel Stored Energy and Thermal Response," 15th Water Reactor Safety Information Meeting, National Bureau of Standards, Gaithersburg, MD, Oct. 1987, NUREG/CR-0091, Vol. 4, p. 23, and BNL-NUREG-52164, NUREG/CR-5232 (June 1988).

7. R. A. Shaw, T. K. Larson and R. A. Dimenna, "Development of a Phenomena Identification and Ranking Table (PIRT) for Thermohydraulic Phenomena During a PWR Large Break LOCA (in press, 1988), Idaho National Engineering Laboratory, EG&G, Inc., Idaho Falls, ID 83415.

8. B. W. Sheron, "Bases and Criteria for the Selection of Response Surface Parameters for the Statistical Assessment of LOCA," Enclosure 7, GEW-38-87, U.S. Nuclear Regulatory Commission, Division of Safety, Washington, DC 20555, (301) 492-7588 (1987).

9. E. T. Laats, "FRAPCON-2 Model Uncertainty Study," EGG-CAAD-5584, EG&G Idaho, Idaho National Engineering Laboratory, Idaho Falls, ID (1981).

10. D. L. Hagrman et al., "MATPRO-Version II (Revision 1), A Handbook of Materials Properties for Use in the Analysis of LWR Fuel Rod Behavior," NUREG/CR-0497, TREE-1280, Rev. 1, EG&G Idaho, Inc., Idaho Falls, ID (February 1980).

11. R. Chambers, W. E. Driskell and S. C. Resch, "Assessment of FRAP-T6 Code Capabilities During Large Break Loss of Coolant Accidents," EGG-CAAD-5829, Idaho National Engineering Laboratory, Idaho Falls, ID (1982).

12. G. P. Steck, M. Berman, R. K. Byers, "Uncertainty Analysis for a PWR Loss-of-Coolant Accident: 1. Blowdown Phase Employing the RELAP4/MOD6 Computer Code," NUREG/CR-0940, SAND79-1206, Sandia National Laboratories, Albuquerque, NM 87185 (1980).

13. F. W. Dittus and L. M. K. Boelter, "Heat Transfer in Automobile Radiators of Tubular Type," Publications in Engineering, University of California, Berkeley; p. 443 (1930).

14. K. Lassmann and F. Hohlefeld, "The Revised Urgap Model to Describe the Gap Conductance Between Fuel and Cladding," Nuclear Engineering and Design, 103 (1987), p. 215.

15. M. E. Cunningham et al., "Stored Energy Calculation: The State of the Art," PNL-2581, Pacific Northwest Laboratory, Richland, WA 99352, operated by Battelle Memorial Institute (1978).

16. G. S. Wilson et al., "Achieving 95% Probability Level Using Best Estimates Codes and the Code Scaling, Applicability and Uncertainty (CSAU) Methodology," EPRI Workshop, Cambridge, MA (Aug. 1988).

17. Safety Code Development Group, "TRAC-PF1/MOD1: An Advanced Best Estimate Computer Program for Pressurized Water Reactor Thermal-Hydraulics Analysis," NUREG/CR-3858, LA-10157-MS, Los Alamos National Laboratory, Los Alamos, NM 87545 (1986).

18. U. Graf et al., "Zur Absicherung der Ergebnisse Technisch-Wissenschaftlicher Rechnungen" (on the validation of the results from technical and scientific computations), GRS-A-1274 (Sept. 1986), Gesellschaft fuer Reaktor Sicherheit (GRS) mbH, Forschungsgelaende, 8046 Garching, FRG.

19. M. W. Cappiello et al., "TRAC-PF1 Models and Correlations," Draft Q.A. Documentation (Nov. 1987), LANL, Los Alamos, NM; and D. R. Liles et al., "TRAC-PF1/MOD1 Correlations and Models," Draft NUREG/CR-5069, LA-11208 MS.

20. S. Levy, G. S. Lellouche and R. May, "Elements of Uncertainty and Meaning of 95% Probability Level for LOCA/ECCS Analysis," EPRI Workshop, Cambridge, MA (1988); S. Levy, Inc. 3425 S. Bascom Ave., Campbell, CA 95008.

21. U. S. Rohatgi and W-S. Yu, "Uncertainties in Modeling and Scaling of Critical Flows and Pump Model in TRAC-PF1-MOD1," 15th Water Reactor Safety Information Meeting, National Bureau of Standards, Gaithersburg, MD, Oct. 1987, NUREG/CR-0091, Vol. 4, p. 1.

22. W. L. Swift, "Model Pump Performance Program - Data Report," EPRI NP-2379, May 1982.

23. W. C. Kennedy et al., "Pump Two-Phase Performance Program," EPRI Reports, NP-1556, Vol. 1-8, September 1980.

24. U. S. Rohatgi, "Bias in Predicting Peak Clad Temperature Due to Uncertainty in ECC Bypass Modeling," NUREG/CR-5254, BNL-NUREG-52168, Brookhaven National Laboratory, Upton, NY 11973 (in press).

25. T. Knight, "TRAC Analysis of LOFT LP-02-6," LA-UR-85-3728, Los Alamos National Laboratory, Los Alamos, NM, October 1985.

SLI-8816

# QUANTIFYING REACTOR SAFETY MARGINS

## PART 4

## UNCERTAINTY EVALUATION OF LBLOCA ANALYSIS

## BASED ON TRAC-PF1/MOD 1*


Prepared by

G. S. Lellouche
and
S. Levy

S. Levy Incorporated
3425 S. Bascom Ave.
Campbell, CA 95008

With Contributions from

B. E. Boyack (LANL), R. B. Duffy (INEL),
P. Griffith (MIT), K. R. Katsma (INEL), R. May (SLI),
U. S. Rohatgi (BNL), G. Wilson (INEL)
W. Wulff (BNL), N. Zuber (NRC)



## ABSTRACT

The NRC has issued a revised ECCS rule allowing the use of best estimate computer codes for safety analysis. The rule also requires an estimation of the uncertainty in the calculated system response and a comparison of the resulting bound with the acceptance limits of 10CFR Part 50. To support this revised rule the NRC and its consultants and contractors have developed and demonstrated the Code Scaling, Applicability and Uncertainty Methodology (CSAU). The last of the three elements of the methodology - Uncertainty Evaluation - is described in this paper.



*Work supported by the USNRC office of Nuclear Regulatory Research, under DOE Contract No. DE-AC07-76D01570.

## INTRODUCTION

This paper summarizes the results of an uncertainty evaluation of a PWR LBLOCA analysis and completes the presentation on the CSAU methodology started with the preceding papers. This paper is in four parts:

I. Calculation of TRAC Uncertainty (CSAU Step 3-12)

This section discusses the establishment of the TRAC calculational matrix and reprises some of the work presented earlier (1, 2). It considers how to reduce the number of TRAC calculations to a feasible number and how we develop the Response Surface (RS) using Regression Analysis (RA). Finally, it discusses the establishment of a probability distribution function.

II. Calculation of Biases (CSAU Step 8-10)

This section deals with a number of phenomena which are considered significant but are not modeled or mismodeled in TRAC. We also consider the effect of various parameters not considered individually significant which, because of large uncertainties in their variation, could become so, or which in combination may become so.

III. Combining the Uncertainties and Biases (CSAU Step 13-14)

In this section we present the conditions under which the biases and the TRAC pdf may be combined and establish the final LBLOCA uncertainty table.

IV. Comparison with Experimental Data (CSAU Step 13)

In this final section we consider the direct comparison of TRAC with data. This is done at the individual transient level and for blowdown and late reflood at the level of the distribution functions.

## CONCLUSIONS

This uncertainty evaluation for a PWR LBLOCA analysis shows that:

*The peak clad temperature of a four-loop Westinghouse NPP undergoing a double-ended LBLOCA modeled by TRAC-PF1/MOD1 using the specific nodalization discussed in 2 and accounting for all phenomena identified as significant, including those not modeled by TRAC, is bounded at the 95$^{th}$ percent probability level by 1572°F; that is:*

$$Pr\ (PCT < 1572°F) = 0.95$$

Another important result of this study is related to the timewise propagation of uncertainties.

*The uncertainty in the PCT (defined here as the difference between the 95$^{th}$ percentile and the mean), at any point or within any interval in time is a consequence of the preceding time behavior. It is not constant with time and generally tends to increase with time. The most significant consequence of this condition is to require uncertainty evaluations for each major phase of a scenario.*

This can be seen in Table 16 where this uncertainty varies from 285°F in the blowdown period to 578°F in the late reflood period. This observation is equally true of uncertainties in the mean or in the 95$^{th}$ percentile.

Thus we observe that uncertainties determined early in time do not propagate unchanged as time increases and that uncertainties established for one statistic (the mean for example) cannot be applied indiscriminately to another statistic (the 95$^{th}$ percentile for example).

A final conclusion is that: *Conservative approximations were made in the study particularly with respect to establishing some of the biases; as such there is a strong likelihood that there is at least a 100°F reduction that could be made in the 95$^{th}$ percentile limit.*

## I. TRAC UNCERTAINTIES

This section discusses the preparatory work required to produce a pdf using TRAC. The work includes:

- Establishing the dominant sources of calculational uncertainty;
- Establishing the pdf for each uncertainty parameter;
- Creating the calculational matrix; and
- Determining the structure of the Response Surface.

Dominant Sources of Calculational Uncertainty (CSAU Step No. 3)

The PIRT (1) process had the purpose of identifying which phenomena could be expected to have the greatest effect on the peak clad temperature during a LBLOCA. This process has already been described (1) and has produced seven phenomena which were felt to be dominant; they are found in Table 1.

Although PIRT produces seven phenomena, they are generally not directly treatable with any computerized calculational procedure and must be translated into the specific physical aspects that are contained in a systems code. This process can lead to the seven phenomena becoming many more than seven. For example, stored energy in the fuel pin is a function of the thermophysical properties of the fuel, gap, and clad as well as those of the coolant and the geometry of the pin cell and other more global factors. The number of potential parameters here exceeds twenty.

However, as has also been shown in earlier papers (1,2), this large list can be reduced to a workable size by straightforward, analytically based sensitivity calculations which can be used to order the importance of each parameter. In this case, the stored energy term was expanded initially into seven fuel related input parameters (Table 4 of 2) and nine fuel related physical parameters (Table 5 of 2) but several of these were combined into a gap conductance term leaving thirteen independent parameters. A search of the literature provided sufficient information to estimate standard deviations and distributional shapes (mostly uniform).

Table 6 of 2 then showed the results of a series of calculations which permit an ordering of the sensitivity of the initial stored energy to changes in the parameters from their nominal to the one Sigma values. Thus we end up with the following ordering: gap conductance followed by peaking factors, fuel thermal conductivity, power level, fuel heat capacity, etc. Finally, when translated by transient calculations into changes in peak clad temperature only four have an effect in the blowdown phase of altering the PCT by more than 2°K: Gap Conductance, Peaking Factor, Fuel Thermal Conductivity, and Convective Heat Transfer Coefficient.

When this process is completed the seven phenomena are replaced by ten parameters and one phenomenon (related to noncondensibles). These are shown in Table 2 and are the basic parameters which are assumed to dominate the uncertainty in the PCT. Of these the first four phenomena (comprising seven parameters) will be treated by a direct statistical analysis. The last three will be dealt with as biases and will be discussed in Part II of this paper.

Ranging the Uncertainty Parameters (CSAU Element No. 7-10)

In this portion of the paper we are following a procedure that is consistent with those used in the theory of experimental design (3). We need to specify the range and distributions for the first seven parameters on the right side of Table 2 because we plan to combine all such uncertainties through a response surface for the PCT. Basically a response surface is a fit through a set of data and it replaces the data in subsequent analysis. If this response surface is to have meaning for an uncertainty analysis, the range of the parameters entering it must be related to a probability. That is, we wish to be able to state that these seven parameters have underlying probability distribution functions.

It is well known (4) that real experimental data do not follow any of the classical distribution functions, but in order to proceed we must specify an underlying function. We deal with this problem by using the Uniform Distribution. This choice should not be presumed to imply that we believe

that the data really are uniform. The uniform distribution requires only that the end points (the range) be specified and does not imply that any value of the parameter is more likely than any other value; it is often referred to as the distribution which maximizes lack of knowledge. Under such circumstances the choice of the range is most important. In this study it was made conservatively, and was based on data considerations (2). Table 3 shows the uncertainty range given as relative to the nominal value contained in the TRAC code (2).

The peaking factor variation is based on calculation/experimental comparisons (5) as is the gap conductance; the Fuel Conductivity was taken from MATPRO 11, while the Break $R_m$ and Pump ranges were based on Marviken and proprietary Westinghouse data, respectively.

The heat transfer coefficient is one of the most important uncertainty parameters and for our purposes consists of five parts:

- Single-phase liquid (Dittus-Boelter);
- Two-phase subcooled nucleate boiling (Chen);
- Transition;
- Annular with dispersed droplet field; and
- Single-phase vapor (Dittus-Boelter).

In determining what ranges to use for these heat transfer parameters we note that all of the surface heat transfer correlations in TRAC are "inside" rather than "outside" correlations; that is, they relate to pipe flow rather than flow around a fuel rod (in a bundle of such rods). We must first account for the effect of inside versus outside flows; then we may consider the ranges of uncertainty. The effect of changing from an inside to an outside flow correlation for single-phase liquid or vapor flow has been shown (6) to be simply a multiplication of the single-phase Dittus-Boelter correlation by the pitch to diameter ratio (P/D = 1.32 for a W PWR). On top of this, experimental data indicate that the uncertainty is ±40% around this nominal value. For TRAC as it is this would correspond to

an uncertainty range of 0.79 to 1.85 for the single-phase heat transfer coefficients.

For the subcooled and nucleate boiling regimes where the Chen model is used, there are no studies showing how an inside coefficient must be varied in order to become an outside coefficient. From continuity considerations, the Dittus-Boelter portion of the Chen relation should blend smoothly into the single-phase model but no published evidence for this has been located.

The annular with dispersed flow field model (referred to as Mode 4 in TRAC) implements the Forslund-Rohsenow coefficient. Shumway (7) has shown that, as implemented, this model is significantly optimistic when compared to separate effects rod bundle data. He has also shown that removing the Forslund-Rohsenow coefficient leaves the predictions of data some 30% low. This 30% may be a characterization of the pitch/diameter correction. Alternatively, if we reduce the F-R coefficient by 74%, the comparison to data shows a mean error near zero and a scatter of about -25%/+50% leading to multipliers of .75/1.5.

In our ranging of the complete heat transfer surface we take the multiplicative range to be 0.75/1.75, but in preparing the probability distribution function and the statistics of Tables 8 through 17 we use a sampling range of 0.75/1.50.. Subsequently we account for the F-R effect by means of a bias (see Section II, below). Further, we shall show in Section IV that on average TRAC, without any F-R correction, predicts Reflood experiments conservatively.

The transition heat transfer regime in TRAC makes use of the surface heat flux at CHF and the MODE 4 heat flux defined at a temperature $T_{MIN}$ and interpolates between them. The $T_{MIN}$ data base has been discussed in (2) and the model used in TRAC lies 36°F above the most conservative data bound and 360°F below the other bound. As such, TRAC is considerably conservative in its modeling of $T_{MIN}$. We take the uncertainty range for this parameter as -36°F/+180°F which is still conservative with respect to the data (2).

A complete list of the uniform distribution ranges can be found in Table 3.

Establishing the Calculational Matrix (CSAU Step 9-11)

The purpose of this study - in the end - is to estimate the uncertainty in a best-estimate calculation of a LBLOCA. The word "uncertainty" has, however, not yet been defined. The new Rule and Regulation Guide points out that the $95^{th}$ percentile of the probability distribution (presumably the cumulative distribution of the PCT) is sufficient, and although the $95^{th}$ percentile is itself not an uncertainty, we shall accept it as an indication that any important uncertainties have been accounted for.

There are a number of ways to establish the underlying probability distribution function (pdf) for this PCT. Some require more calculational effort than others. The one we have chosen requires the establishment of a Response Surface (RS, 8). For our purposes an RS is established by Regression Analysis (RA, 12) and this can be viewed simply as a multinomial least squares fitting process of the calculated PCT in terms of the important parameters selected above. The purpose of the RS is to replace the code by a fit to the output of interest (here the PCT). A number of underlying assumptions have to be made concerning the behavior of the output relative to that of the input (e.g., the output is a continuous function of the input) and as we shall discuss below the order of the polynomials is restricted by considerations of the amount of data available and the structure of the calculational matrix.

The amount of data needed to describe an RS is discussed in the standard texts (3, 8), specialized publications (13, 14) and the general technical literature (9, 10). In the present case with seven parameters, a complete description at a three-level polynomial formulation using a central composite design (8) would require more than 2000 TRAC calculations! Similarly, for a five-level polynomial formulation more than 70000 calculations would be needed! Clearly we are not able to provide such a level of data input. Equally important was the need to be aware of the realistic constraints imposed by finite financial resources.

With an expectation that only about 10-15 computer runs were possible any "unnecessary" runs had to be eliminated. As a result, the pump and break calculations were limited to only those runs which would increase the PCT (i.e. be conservative) and the effect of the other side of the nominal point was treated probabilistically. That is, 50% of the probability would be absorbed at the nominal point. Similarly, while intermediate levels were chosen for some parameters on the conservative side, such intermediate levels were excluded on the other side. Table 4 shows the final matrix which will generate close to 200 peak clad temperatures.

Fortunately TRAC has a capability for carrying along a set of "supplementary rods," which can be allocated to any sector. These rods carry the thermal hydraulics of that sector (mass flow rate, temperature, void fraction, etc.) and permit different fuel and clad properties (including heat transfer coefficient) to be assigned. Thus in Table 4 the vertical column describes the changes in fuel and clad properties while the horizontal row describes the variations which alter the thermal hydraulic behavior. Specifically, there are eight TRAC runs listed here and 23 supplemental rods per run yielding 184 clad temperature traces. These 184 traces consist of one nominal point, 21 linear variations, 98 double crossproducts, 57 triple crossproducts, and seven quadruple crossproducts; they provide the basis for the RA which produces the RS.

Having defined the conditions under which TRAC will be run, the actual runs were made and Tables 5 through 7 exhibit the PCT for three more or less distinct portions of the time trace of PCT: Blowdown, Early Reflood, and Late Reflood. From a time interval point of view these comprise (for this Westinghouse model) the intervals: 0-20 seconds, 20-60seconds, 60-150 seconds. Figures 2 through 6 show several time traces for a number of the parameter variations. Of interest is the failure of the pump variations to have any significant effect on PCT (max $\approx$ 50°F at blowdown); not shown but similar conclusions can be found for the fuel thermal conductivity variations.

The Response Surface (CSAU Step 12)

Because we are dealing with a computer code certain fundamental problems arise concerning a determination of the quality of the RS, i.e. concerning the question of Lack-of-Fit. In normal experimental design this is resolved by providing redundant experiments at the nominal point; these provide information that can be used to prepare quantitative statements about Lack-of-Fit if the underlying, not modeled, background uncertainties meet certain statistical requirements (3, 12). When the information comes from a computer code there are no background uncertainties and no statement can be made concerning Lack-of-Fit; that is, a computer code always gives the same answer with 100% reliability (voltage failures do not count). Some discussion of an equivalent problem is found in Plackett and Burman (10) but generally the question of Lack-of-Fit reduces to an examination of the RMS between calculation and fit. It is important to note that the RMS does not directly indicate a good or poor fit since it can always be driven to zero by taking a sufficiently elaborate fit! There does not appear to be any general theory available here to guide us and we follow Box and Behnken (7) who state that, "the highest degree of polynomial that may be fitted to the observations from a p-level factorial is p-1."

An examination of Table 4 shows that the design we have implemented is a seven-factor, mixed (three to five) level design and the maximum polynomial order is different for the various factors:

- Peaking factor — $4^{th}$ order
- Heat Transfer Coefficient — $4^{th}$ order
- Gap Conductance — $4^{th}$ order
- Break, Pump, $T_{MIN}$ — $2^{nd}$ order
- Fuel Conductivity — $3^{rd}$ order

In performing our analyses we find that different mixes of $3^{rd}$ and $4^{th}$ order terms produce a minimum RMS depending on which phase of the transient we are dealing with; this can be seen in Table 8. We note here that the

quartic fits produce an RMS which is in all cases less than 5% of the mean PCT, hence can be considered small and provides little incentive for further improvement. It is also clear from this table that the data becomes more difficult to fit with a polynomial as we move out in time. This is not unexpected.

Within the ranges of the underlying parameters, the RS can be looked at as defining a surface of the form PCT=f ($X_1$,---, $X_7$). We are interested in knowing what fraction of the surface exceeds any given value for PCT; this produces the cumulative distribution function. If the surface is a linear one, there are analytical tools to provide this information; for a complex surface the usual procedure is to randomly pick values of the $X_1$---,$X_7$ (seven at a time) and calculate the PCT. If we do this many times we can prepare a histogram defining the frequency response (so many calculated values of the PCT between 1000 and 1050, etc.). Normalized, this produces an estimate of the pdf.

In order to produce a decent estimate of the probability distribution function (pdf) from an RS we must sample the surface in a statistically acceptable way. Because the surface is only algebraic we use a crude Monte Carlo sampler. The SLI code RAM-CAM (Regression Analysis Monte Carlo Analysis Module) was used in this analysis. Statistical sampling of a surface contains as a free parameter the number of sampling histories. For each sample set a pdf can be produced and the behavior of the pdf with increasing sample size examined. Figures 7 through 9 show a study varying between 2000 and 50,000 histories for each of the three surfaces. While there is still some variation around 50,000 histories it is considered acceptably small and we take the 50,000 history pdf's as converged.

Although we speak about the 50,000 history case being converged it is clear that there is still some variability (but only 10-20°F) in the result. Indeed at $10^5$ or $10^6$ histories there would still be some variability. It is at this point that we might ask how sure are we that the mean or 95th percentile value is what we say it is. One could introduce additional studies at this point to determine a tolerance or confidence band about the

50,000 history values using the non-parametric methods of (4), but this seems to us to be unnecessary. Using the central limit theorem on the mean value shows convergence within ±2-4°F at the 95$^{th}$ percent (one-sided) level.

The question of robustness can be also considered from the viewpoint of the RS polynomial order. Thus Tables 9 through 11 show the results of 50,000 history studies for each of the surfaces previously considered in Table 8. These studies lead us to believe that the pdfs we have established quite reasonably describe the response of the TRAC code to variation of the seven parameters of Table 3, and the complete uncertainty distribution functions for each phase of the transient can be found in Figure 10. It will be noticed that the width of the pdfs increase with time and that the structure becomes more complex. For the Late Reflood pdf it appears as if we have a double peak. There is clear evidence that there is an early rewetting portion to the parameter space characterized most nearly by heat transfer coefficients larger than nominal, and a late rewetting portion characterized by those less than nominal (none of the other parameters seem to be important in this regard). We noted at the beginning of this paper that uncertainties do not generally propagate unchanged in time. Studies show that tolerance bands often tend to widen as time increases. In our situation we have another aspect which is also important. The space-time interval included in each of the three phases increases with time hence may be presumed to tend to broaden the pdf.

Although we have spent a great deal of time running TRAC and grinding up a lot of numbers, it appears prudent to ask whether there is any relationship between these numbers and experimental data. We discuss this topic in Section IV where we conclude from comparisons with experimental data that the overall heat transfer process in TRAC adequately accounts for the blowdown and reflood phenomena during a LBLOCA. It is important to stress the word "overall" because we now need to deal with certain specific aspects of the TRAC-PF1/MOD 1 code which are in a separate effects sense, less than adequate.

Before proceeding we establish a first view of the final uncertainty table. Table 12 shows the means and 95$^{th}$ percentile values for the three phases of the NPP LBLOCA.

## II. CALCULATION OF BIASES (CSAU Elements 8-10)

There are three types of effects which were not dealt with when we constructed the test matrix shown in Table 4 and defined the system nodalization:

- Phenomena requiring more extensive nodalization than available resources could support: a fourth radial ring describing a central hot channel;
- Phenomena which are incorrectly modeled in the code: the implementation of the Forslund-Rohsenow correlation;
- Phenomena which require multiple simultaneous variations of the relevant CRC or which have insufficient experimental data available to justify even a uniform pdf range; these are labeled as "Other Modeling Uncertainties" but may also imply "incorrect" modeling ab initio.

The numbers we present in this section are temperature increments which must be (see Section III) combined with the results of Section I.

### The Hot Channel

Questions were raised concerning the degree of radial nodalization--should we model the hot assembly directly or only as a hot rod? The decision--discussed in previous papers (1,2)--was to remain with the standard nodalization (two radial powered rings, one downcomer ring). The question of hot channel effects would be treated separately. Among the reasons for this choice was a 30% increase in resource allocation to directly treat the hot channel.

It has been pointed out that the use of the supplementary rod as a hot channel may be less accurate than we might expect because the hydraulics are incorrect. To utilize a more elaborate nodal model containing a fourth

radial zone in the core was beyond the practical resource capability of the project. As such, it was decided to do a simplified calculation which would only require two TRAC runs with four rings. We would create a mini data base and determine the mean and 95$^{th}$ percentile differences between the two 4-ring and the appropriate 3-ring runs. We would then use these results as a bias to be combined with the results of Table 12. This set of calculations was carried out and the results are found in Table 13. It can be seen that the variation is nearly linear with time period and leads to a strongly decreasing penalty (becoming a benefit) as time unfolds.

Modeling Limitations

There are a number of modeling limitations in the code. We have earlier addressed the fact that the heat transfer surface is only valid for inside flows while the dominant area of need (in the core) is for external flows. This is a potential benefit worth 30-50°F at the 95$^{th}$ percentile as the LOCA proceeds through its phases, but because of our inability to validate the p/D correction in the pre CHF two-phase regime, we do not deal further with it.

The implementation of the Forslund-Rohsenow (F-R) correlation in the mode 4 heat transfer regime has been criticized for some time. Shumway (7) has shown that the TRAC-PF1/MOD1 Mode 4 heat transfer modeling is considerably but non-uniformly optimistic, and that when the F-R correlation is removed, the result is quite conservative. However, from the viewpoint of an integrated test comparison a completely different view is found: TRAC-PF1/MOD1 as currently formulated and using the F-R correlation is conservative in both blowdown (LOFT Figure 14) and reflood (CCTF/SCTF Figure 12) comparisons. Shumway has shown that if a multiplier of 0.26 is applied to the F-R correlation that a comparison with experimental data shows a zero mean error. When a series of eight supplemental rods carrying various F-R multipliers is examined, the effect of a 0.26 multiplier is found to be worth between 47°F and 160°F as we proceed from Blowdown to Late Reflood. These results can be quantified as shown in Table 14. Because of the difficulty of being sure that the slightly conservative TRAC

comparison to experiment exhibited by the LOFT/SCTF/CCTF experiments will hold at full scale, it has been decided to accept the use of a F-R multiplier of 0.26 and use the difference between FR=1 and FR=0.26 as a bias. This is also shown in Table 14.

Other Modeling Uncertainties

There are three "other" uncertainties that we believe must be dealt with; they are:

- The effect of $N_2$ arising from the Accumulator injection process;
- Steam binding phenomena; and
- ECCS bypass phenomena.

The Effect of $N_2$ Addition from the Accumulators

Two aspects are of potential importance here; the first relates to the $N_2$ pressure in the Accumulator, the second to the effect on condensation heat transfer. While the details of the analyses and calculations may be found elsewhere (1,2), the results may be stated as follows:

- The allowed operating range for $N_2$ pressure in an Accumulator has been determined to be sufficiently small that it would not affect our calculations;
- The time necessary for the depressurizing (fizzing) accumulator liquid to reach the downcomer and the momentum change at the downcomer are felt to be sufficiently great that most of the dissolved $N_2$ would separate out and leave the vessel via the by-pass route. However, the effect on condensation is so large that we calculate a 3.7 second delay in the time to reach peak temperature which corresponds to an 18°F bias on the early reflood PCT. While the $N_2$ condensation effect is complete before the start of the Late Reflood time period, it is not clear that the effect does not carry over into the Late Reflood interval. In order to avoid arguments it was decided to account for this bias in both reflood periods.

Steam Binding Phenomena

It is clear from an examination of the modeling of interphase friction existing in TRAC that some disagreement between predicted and experimental entrainment can be expected. This means that upper plenum levels, entrainment into the steam generators, and various other interphase drag related phenomena can be expected to be uncertainly predicted.

In order to estimate the importance of this aspect of the code, a series of calculations was undertaken to determine what modifications (in the form of multipliers to existing correlations) would be necessary in order to reasonably predict two SCTF (601, 602) tests. LANL investigated:

- The Rozen entrainment correlation;
- Core entrainment; and
- Upper plenum entrainment.

A series of calculations led to a set of multipliers which adequately allowed prediction of these two transients. Using these multipliers, a single otherwise nominal TRAC run was restarted at the end of blowdown to determine an additive bias. The results indicate a slight (-9°F) benefit during early reflood and a substantial (106°F) penalty during the late reflood phase. The size of this last bias indicates the desirability of a more realistic modeling in TRAC.

ECCS Bypass Phenomena

An additional entrainment phenomena concerns bypass and downcomer modeling. Specifically, the questions relate to

- Delay in the initiation of refill; and
- Lower plenum filling rate.

To estimate the effect of these uncertainties a study of UPTF Test 6 data as well as a bounding analysis (11) indicates that the TRAC calculation is uniformly conservative during the refill/reflood process by 34°F.

These four biases are exhibited in our second look at the final uncertainty table (Table 16).

The Effect of Unmodeled Parameters

Under this heading we wish to examine several effects of the process which led to the final calculational matrix (Table 4). The PIRT process only allowed items labeled "most important" to leave CSAU element 3 and, as we pointed out earlier, not all of the component parameters entering a class 9 item were carried through to Table 4. We can then ask questions concerning what impact some of the items left out might have, whether a large uncertainty or a low impact item might make it into (perhaps) a marginally high impact item, and finally we might ask whether a combination of low impact items (or low impact with high impact items) might create synergisms resulting in significantly greater than expected results. Mathematically, we are asking whether the sum of small effects become large and whether significant nonlinearities exist.

Even the briefest of examinations of the Expert Ranking Table in (1) shows that a detailed answer to these questions is impossible; there are simply too many parameters. We cannot provide closure on such questions with mathematical rigor; all we can do is provide evidence which we believe offers a reasonable level of surety on an "engineering judgement" level.

A series of extra supplementary rods was carried along which provides us with information concerning:

1. The effect of an extreme value (50% reduction) of the clad thermal conductivity on PCT.

2. The effect of compounded 2nd level (end of range) values of clad conductivity and specific heat and fuel specific heat on PCT.

3. The effect of compounded thermal hydraulic runs were made through blowdown between the pump (medium impact) and the break (high impact) to investigate synergisms at this level (rather than only at the low impact levels).

4. The effect of setting the pump form loss coefficient to zero.

Except for item 3, none of these studies show any unexpected results:

1. 50% variations in the clad conductivity (5 times the full range variation) is worth less than 36°F (whether by itself or compounded with pump, break, or $T_{MIN}$ variations) during Blowdown and progressively less as time unfolds.

2. The compounded end of range (2nd level) study is worth less than 13°F (whether by itself or further compounded with pump, break, or $T_{MIN}$ variations) in Early Reflood and less in the other phases of the transient.

3. In all cases the Break 2nd level and Pump 1st level variation had the largest effect and this was carried as the dominant crossproduct through Reflood. However there is a negative interaction between the Pump and Break which reduces rather than increases the effect of the compounded variation. Thus the order of the PCT is nominal<Pump<Pump+Break<Break as can be seen in Tables 5 through 7.

4. The effect of setting the pump loss coefficient to zero had no effect on the PCT at all (pump effects are dominated by the two phase degradation curves).

Except for the Pump, Break crossproduct all these and any other parameter variations have been excluded from further consideration (except for those dealt with earlier as biases) and we have concluded that there is no need for further justification of Table 4.

## III. COMBINING THE UNCERTAINTIES AND BIASES (CSAU Element 13, 14)

Table 16 shows two types of numbers. The first type comes from a pdf with a specific statistical pedigree. Even the first bias (for the hot channel) has a statistical pedigree, but the others do not. By pedigree we mean that these are statistically viable means for combining them.

It is well known that it is "allowable" to add mean values although the underlying rules which permit such addition are seldom understood. Misconceptions also abound as to what the various central limit theorems mean. In order to combine the biases and the pdf results of Table 16 two assumptions have to be made.

1. The biases (stated as ΔPCT) are independent of the TRAC pdf results and independent of each other.

2. The bias is constant over the time interval of the LBLOCA phase under consideration.

These two assumptions permit the last three biases to be algebraically added and combined with both the mean and $95^{th}$ percentile of the appropriate phases. Clearly assumption 2 is incorrect since the bias would have to "jump" between phases; but in general it appears to be reasonable since most of these effects are based (2) on analytical considerations of physical phenomena, not on statistical procedures; that is, we have used bounding analyses to provide maximum effects.

The major problem lies in how to deal with the hot channel bias since we have distributional information. Properly speaking, one can combine the hot channel results with the TRAC pdf. The problem lies in the large benefit biases. There is little doubt that the large benefit biases implied by the $\Delta 95^{th}$ values will appear as nearly as large benefits after combination, but it is not felt by the TPG that such large benefits are easily justifiable on physical grounds. The same thing is true of course for the large penalty biases (106, 160) in Table 15, but from a regulatory perspective, penalties are easier to justify on the grounds of conservatism. Thus the majority viewpoint of the TPG is to disregard the distributional aspects and utilize the mean value, assume it meets the two assumptions and add it to the other biases.

This permits us to use the Summed Bias line in Table 15. Before proceeding further, we wish to show just how conservative our estimation really is by reconsidering the Forslund-Rohsenow (F-R) correction from a statistical viewpoint. A series of supplementary rods were carried along with the F-R correlation multiplied by various values; interpolation produced the specific results for a multiplier of 0.26. For each base CSAU case we could then compare the PCT with and without F-R fully activated. The eight values were averaged and the difference provides an indication of the effect of setting the F-R multiplier to 0.26. Table 16 shows the PCT

calculated with TRAC for the Late Reflood phase of the transient along with the cumulative probability up to that value of PCT. The difference between the two averages (1117-957°K) = 160°F is a difference without a firm statistical location except that all values (except one) are well above the mean hence should not be simply added. The final addition of 160°F is a number that is perhaps one half too large and indicates a significant degree of conservatism in our treatment of this bias.

Final Table of Uncertainties

Table 17 indicates our estimate of the combined LBLOCA uncertainties at the mean and at the 95th percentile. These are obtained by simple addition of the Summed Biases to the results obtained from the 50,000 history studies of the "Best Quartic" response surfaces (RS).

There are several things unlikely about the final numbers if we inter-compare them. The RS analyses show that both the mean and 95$^{th}$ percentile values move to smaller numbers as time increases, and after addition of the summed biases while the mean continues to move to smaller numbers the 95$^{th}$ percentile hardly moves at all. This implies a fracturing of the time dependent pdf in a way that seems unlikely--if not unreal, and indicates to us that we should further compare these "final" uncertainties with whatever experimental data we have available.

## IV. COMPARISONS TO EXPERIMENTAL DATA (CSAU Element 8-10, 13)

The question we wish to pursue here is whether TRAC PF1/MOD1 with the specific nodalization chosen is - as it stands - a conservative estimator of both the blowdown and reflood peaks; that is, should we have added the biases at all. To address this we consider first a series of predictions of experiment of LOFT blowdowns and CCTF/SCTF/LOFT/PKL/etc. reflood experimental data.

Blowdown

In earlier papers (1, 2) two scatter plots of data from various experimental facilities were presented and extensive discussion took place concerning the significance of those plots relative to scaling. At this time we should like to use the blowdown scatter plot (Figure 15) to prepare histograms around the value of 9.5 kw/ft. This value is valid for the full scale NPP calculations we have just discussed. Then we shall superimpose the TRAC blowdown pdf from Figure 10. This composite is found in Figure 11. We note first that the two LHGR ranges shown are essentially similar and that the TRAC pdf nicely rides on top of the experimental data and fits a little to the conservative side. We take this correspondence between experiment and calculation as a reasonable confirmation of the adequacy of the TRAC-PF1/MOD 1 prediction for the blowdown portion of an LBLOCA at full scale.

Figure 16 shows the same results with the TRAC pdf shifted by the summed biases of Table 17; the singular increase in conservatism attributable to the simple addition of the biases is evident. Several questions can be raised here relative to tuning and to the adequacy of the LOFT thermocouple measurements. Figure 14 shows a direct TRAC/LOFT blowdown comparison for 27 maximum clad data points. TRAC predictions are on average 23°F higher than the experimental values indicating the general adequacy and slight conservatism of TRAC relative to (at least) this LOFT test. Indeed, were we to add the summed biases, TRAC would be 133°F too high. But the LOFT measurements have been called into question as being low by as much as 100°F. In this case, the TRAC + summed biases would still be 33°F too high. Consider however what would happen to Figure 16. We took the 301 point blowdown data base and added 100°F to each LOFT point and then plotted the 7.5-10.5 kw/ft histograms with and without the 100°F addition; this is shown in Figure 17. The result is only a slight shift in the histogram. When we now superimpose the TRAC calculations with and without the bias addition in Figure 18 we see that the added biases still produce a significantly conservative aspect. We conclude then that the addition of the summed biases makes the TRAC 95$^{th}$ percentile estimate of the blowdown

PCT conservative by approximately 100°F compared to experiment and that the addition of the biases may be unwarranted.

Reflood

Although TRAC shows the occurrence of two major reflood peaks, the experimental data available does not consistently exhibit such phenomena, as such we have a problem in knowing whether the reflood experiments apply to the first, or second peak. In what follows we show that it applies to the last peak and that it is unlikely to apply to the first (Early) reflood peak because the initial conditions for the early peak do not generally correspond to those of the extent experimental data base.

First we note that in a direct comparison of 220 CCTF and SCTF experiments TRAC predictions (Figure 12) yielded statistics as follows:

Sample Mean Difference (Calc - Exp) = 10.3°C (18.5°F)

Sample Standard Deviation = 49.8°C (89.6°F)

indicating TRAC's capability to calculate the subscale experiments given the correct initial conditions. This implies that - on average - the Forslund-Rohsenow biases are not required to make the TRAC results match (again on average) experiments. The problem lies in the fact that these and all other reflood subscale facilities contain distorted plena and downcomers relative to what could be expected in full size plants and that although TRAC models these facilities on average questions remain concerning scaleup. It is possible however to remove the questions of the downcomer and plena effects and only consider the core heatup.

Figure 13 shows some 213 reflood CCTF/SCTF/LOFT/etc. data points. These show the core temperature rise as a function of the cold reflood rate (total coolant injected divided by core flow area). The base temperature is the clad temperature at the start of core recovery at the elevation which will ultimately be the hot spot. Because the reflood rate used is independent of bypass or other phenomena, the resulting multi-facility data plot is - within its bounds - a scaleless representation of the reflood

temperature rise process. That is we expect about 95% of all experimental data points to fall inside these bounds independently of scale. Analysis indicates that a plot of this sort would be expected with a negative $U_R$ slope hence we believe that within experimental uncertainty this display can accurately be expected to be a scale free representation of the reflood data. Unfortunately, in the range of most interest ($4<U_R<5$ inch/sec) there are only 12 experimental data points and this makes direct comparisons of the type done for Blowdown (where we had more than 50 data points in the intervals of interest) less than adequate. Therefore we proceed differently and utilize two different methods of comparison between calculation and experiment.

Figure 13 shows a data display with a relatively stable band width over a range of a factor of 30 in $U_R$. We infer from this that the underlying pdf has the same form independently of the magnitude of $U_R$ but that the parameters will be functions of $U_R$. Consequently, we rescale each of the experimental data points multiplying them by $(U_{Ri}/4.5)^{1.14}$. The 4.5 inch/sec value is a compromise on the TRAC Late Reflood cold injection rate which varies between 4.27 and 5.09 inches/sec. The plot in Figure 13 will be rotated around the regression line at $U_R$=4.5 inches/sec and the mean regression line will be a constant ($61°F=339/(4.5)^{1.14}$) as will the upper 95% line (at about 225°F). Now we have produced 213 pseudo data points at 4.5 inches/sec from which we create a frequency histogram in Figure 20.

The matrix in Table 4 provides a nearly uniform covering of all the important interactions and nearly uniformly covers each underlying parameter. As such the raw TRAC output, by itself, provides a basis for the direct establishment of a histogram. Figure 19, for example, shows the TRAC data as a histogram and the pdf derived from a fourth order RA through the TRAC data (the smooth line). While the RA derived pdf does not capture the 3% of the data at the right side, it does show that the histogram is a very reasonable approximation to the pdf (and vice versa); indeed within one degree F both representations have the same $95^{th}$ percentile (PR ($\Delta T <$ 350°F) = 0.95). We use the TRAC histogram in place of the derived pdf to compare with the 213 experimental data points discussed in the previous

paragraph. This is done in Figure 20 where both frequency histograms are overlayed. What is novel here is that these histograms have very similar properties except for an offset between 105°F and 125°F. From a probabilistic viewpoint they describe - within a constant offset - the same phenomena. One could use nonparametric analysis (3, Chapter 9) to determine a confidence interval for this offset. It suffices here to say that this comparison between the TRAC calculations and the experimental data shows that TRAC is conservative in predicting the Late Reflood temperature rise by approximately 105°F at the mean and 125°F at the 95$^{th}$ percentile before the addition of any biases.

The above demonstration of TRAC conservatism compared to experiment made use of a scaled set of experimental data points in comparing with the TRAC calculated values for Late Reflood. Another comparison would be to simply plot all the TRAC calculated results on the experimental data plot. Figure 21 reprises Figure 13 without the experimental data display, instead we display all the TRAC calculated points for both parts of reflood.

If we examine Table 4 in conjunction with Tables 5 through 7 we will see that all important maximal crossproducts are included. That is, Tables 5 through 7 contain about all the maximum values that can be expected within the underlying parameter ranges. Since the test matrix is a nearly uniform overlay on the parameter space (test points are nearly evenly spaced on a percent of range basis) we can expect (as we saw in Figure 19) that the TRAC results are themselves a reasonable representation of the underlying pdf.

The 95% experimental data bound indicates that only 5% of any new data should (on average) fall outside the lines. Based on the raw TRAC data some 19% of the Late Reflood data falls above the upper 95$^{th}$ percentile bound. However, if we subtract the scale factor then only between 4.3 and 6.2% would lie above. We see this as a reasonable match (the expected "tail" would be 2.5% for a symmetric distribution).

Although the Late Reflood TRAC calculations can rationally be related to the reflood experimental data, this is not true of the Early Reflood TRAC results. Figure 21 shows some 61% of the TRAC data exceeds the 95% bound, but more importantly there are a significant number of TRAC data points below the mean value. We do not prepare any histograms here, there is little doubt that the TRAC Early Reflood peak is not represented by the subscale facility reflood data display. The cause of this is quite simply that the initial conditions in TRAC at the start of the Early Reflood period are not representative of the initial conditions at the start of the reflood experiments; the TRAC conditions are strongly transient, those in the experiment are nearly static. For the Late Reflood TRAC cases the starting point is near the minimum between the two peaks hence appears to correspond more closely to the conditions of the experiments.

As a result of these considerations we can conclude that the Late Reflood TRAC results statistically correspond well (within a scale factor) with the experimental data. We can say that the Early Reflood TRAC results are conservative compared to the experimental data but this correspondence may not be meaningful. As a result, while the addition of the biases due to Forslund-Rohsenow and the others only make the TRAC results still more conservative, the lack of validation for the Early Reflood situation makes their addition reasonable.

References


1. G.E. Wilson, et al., "Characterization of Important Contributors to Uncertainty-Code Scaling, Applicability and Uncertainty Methodology," Proc. 16th WRSIM Oct. 24-27, 1988 Gaithersburg, Maryland (to be published).

2. W. Wulff, et al., "Assessment and Ranging of Parameters," Proc. 16th WRSIM Oct. 24-27, 1988, Gaithersburg, Maryland (to be published).

3. N. L. Johnson and F. C. Leone, Statistics and Experimental Design, Vol. 2, 2nd Edition, J. Wiley & Sons.

4. W. J. Conover, Practical Nonparametric Statistics, 2nd Edition, Wiley.

5. R. D. Mostellar et al., "Benchmarking of the ARMP Gadolinium Model Against Large-Scale Mockup Experiments," Trans AMS 44, 559 (1983).

6. A. YA. Inaytov, "Correlations of Data on Heat Transfer Flow Parallel to Tube Bundles at Relative Tube Pitches $1.1 < {}^{s}/_{d} < 1.6$," Heat Transfer, Sov. Res. 7, 3 (1975).

7. R. Shumway, Discussion of INEL Post-CHF Data Relative to TRAC-PF1/MOD1 Mode 4 Heat Transfer Modeling.

8. R. H. Myers, Response Surface Methodology, Allyn and Bacon Inc.

9. G.E.P. Box and D. W. Behnken, "Some New Three Level Designs for the Study of Quantitative Variables," Technometrics 2, 4 (1960).

10. R. L. Plackett and J. P. Burman, "The Design of Optimum Multifactor Experiments," Biometrica 33, 305-325 (1946).

11. U. S. Rohatgi, et al., "PCT Uncertainty from Downcomer Modeling," BNL NUREG in preparation.

12. N. R. Draper and H. Smith, Applied Regression Analysis, 2nd Edition, Wiley (1981).

13. W. S. Conner and M. Zelen, "Fractional Factorial Experiment Designs for Factors at Three Levels," NBS COM-73-11111 (1959).

14. W. H. Clatworthy et al., "Fractional Factorial Experimental Designs for Factors at Two Levels," NBS PB176119 (1962).

15. B. L. Raktoe et al., Factorial Designs, Wiley.

Table 1

DOMINANT PHENOMENA FROM THE PIRT PROCESS

| | |
|---|---|
| Break Flow | Pump 2 - Phase Flow |
| Stored Energy | Steam Binding |
| Fuel Rod to Fluid Heat Transfer | ECCS Bypass |
| Non-condensibles | |

Table 2

TREATABLE UNCERTAINTY PARAMETERS

| | |
|---|---|
| Break Flow | $R_M$ |
| Stored Energy | Gap Conductance<br>Peaking Factor<br>Fuel Conductivity |
| Surface heat transfer | Heat transfer coefficient<br>$T_{MIN}$ |
| Pump 2 - Phase Flow | Head and Torque Curves |
| Steam Binding | Interfacial Drag in: Pool, Core, Upper Plenum and Hot Legs |
| ECCS Bypass | Interfacial Drag in the Downcomer |
| Non Condensibles | Non condensibles |

Table 3

TRAC PARAMETER RANGES

| Parameter | Range |
|---|---|
| Peaking Factor | ±5.6% |
| Gap Conductance | ±80% |
| Fuel Conductivity | ±10% |
| Heat Transfer Coefficient | -25%/+50% |
| Break $C_D$ (1) | $0/+2S_B$ |
| Pump (2) | $0/+2S_p$ |
| $T_{MIN}$ | -20°C/+100°C |

Notes

1 $S_B$ is based on Marviken data.

2 $S_p$ is based on proprietary Westinghouse data.

## Table 4

### Calculational Test Matrix

| Major Run | Nominal | Break +1L | Break +2L | Pump +1L | Pump +2L | Pump+L Break+2L | TMIN -20°C | TMIN +100°C |
|---|---|---|---|---|---|---|---|---|
| Supplemental Rod Status Nominal | As built code | → | → | → | → | → | → | → |
| Peaking Factor | -5.6%<br>-2.8%<br>+2.8%<br>+5.6% | | → | → | → | → | → | → |
| Gap Conductance (HG) | -80%<br>-46%<br>+46%<br>+80% | | → | → | → | → | → | → |
| Fuel Conductivity (KF) | -10%<br>-5%<br>+10% | | → | → | → | → | → | → |
| Heat Transfer Coefficient (HC) | -25%<br>+25%<br>+50%<br>+75% | | → | → | → | → | → | → |
| Cross Products | | | | | | | | |
| HG, KF | -46%, -10% | | | | | | | |
| HG, HC | -46%, -25% | | | | | | | |
| HG, HC | -80%, +50% | | | | | | | |
| HG, HC | -80%, -25% | | → | → | → | → | → | → |
| HG, HC | -80%, +25% | | | | | | | |
| HG, HC | -80%, +75% | | | | | | | |
| HG, HC | +46%, -25% | | | | | | | |

TABLE 5. BLOWDOWN PEAK CLAD TEMPEATURES (°F) FOR CSAU RODS (0-20 S)

| Rod # | | CSAU Variation | Nominal | CFM One Level | CFM Two Level | Pump One Level | Pump Two Level | $T_{MIN}$ -36°F | $T_{MIN}$ +180°F | Core Entrainment | X-Product CF, Pump |
|---|---|---|---|---|---|---|---|---|---|---|---|
| 9 | | Nominal | 1103 | 1285 | 1321 | 1121 | 1166 | 1090 | 1125 | -- | 1290 |
| 11 | Pf | -5.6% | 1080 | 1252 | 1283 | 1096 | 1139 | 1069 | 1099 | -- | 1258 |
| 12 | | -2.8% | 1092 | 1269 | 1299 | 1108 | 1153 | 1080 | 1112 | -- | 1274 |
| 13 | | +2.8% | 1114 | 1299 | 1332 | 1135 | 1180 | 1103 | 1137 | -- | 1305 |
| 14 | | +5.6% | 1126 | 1315 | 1348 | 1148 | 1193 | 1114 | 1150 | -- | 1321 |
| 16 | Hg | -80% | 1276 | 1562 | 1576 | 1335 | 1398 | 1265 | 1337 | -- | 1558 |
| 17 | | -46% | 1175 | 1409 | 1438 | 1218 | 1269 | 1162 | 1209 | -- | 1413 |
| 18 | | +46% | 1062 | 1218 | 1249 | 1069 | 1112 | 1049 | 1078 | -- | 1224 |
| 19 | | +80% | 1040 | 1186 | 1216 | 1045 | 1089 | 1029 | 1054 | -- | 1191 |
| 20 | Kf | -10% | 1114 | 1308 | 1337 | 1144 | 1189 | 1101 | 1137 | -- | 1310 |
| 21 | | -5% | 1108 | 1296 | 1326 | 1134 | 1179 | 1096 | 1130 | -- | 1301 |
| 22 | | +10% | 1094 | 1263 | 1296 | 1101 | 1146 | 1083 | 1114 | -- | 1270 |
| 23 | Hc | -25% | 1216 | 1386 | 1429 | 1258 | 1294 | 1305 | 1251 | -- | 1411 |
| 24 | | +25% | 982 | 1182 | 1206 | 982 | 1029 | 975 | 1013 | -- | 1198 |
| 25 | | +50% | 853 | 1045 | 1081 | 860 | 909 | 838 | 799 | -- | 1078 |
| 26 | | +75% | 626 | 867 | 871 | 626 | 664 | 626 | 640 | -- | 896 |
| 27 | Hg,Kf | -46%, -10% | 1195 | 1423 | 1449 | 1234 | 1285 | 1166 | 1225 | -- | 1423 |
| 28 | Hg,Hc | -46%, -25% | 1328 | 1522 | 1553 | 1377 | 1414 | 1416 | 1373 | -- | 1537 |
| 29 | Hg,Hc | -80%, +50% | 923 | 1184 | 1227 | 972 | 1035 | 891 | 905 | -- | 1225 |
| 30 | Hg,Hc | -80%, -25% | 1481 | 1674 | 1695 | 1530 | 1566 | 1548 | 1531 | -- | 1679 |
| 31 | Hg,Hc | +46%, -25% | 1162 | 1312 | 1357 | 1197 | 1233 | 1249 | 1188 | -- | 1337 |
| 32 | Hg,Hc | -80%, +25% | 1116 | 1409 | 1431 | 1175 | 1242 | 1072 | 1135 | -- | 1427 |
| 33 | Hg,Hc | -80%, +75% | 626 | 882 | 921 | 626 | 702 | 626 | 644 | -- | 919 |

TABLE 6. FIRST REFLOOD PEAK CLAD TEMPERATURES (°F) FOR CSAU RODS (20-60 S)

| Rod # | | CSAU Variation | Nominal | CFM One Level | CFM Two Level | Pump One Level | Pump Two Level | $T_{MIN}$ -36°F | $T_{MIN}$ +180°F | Core Entrainment | X-Produc CF, Pum |
|---|---|---|---|---|---|---|---|---|---|---|---|
| 9 | | Nominal | 997 | 1233 | 1240 | 988 | 981 | 995 | 721 | 988 | 1188 |
| 11 | Pf | -5.6% | 968 | 1197 | 1204 | 961 | 955 | 968 | 693 | 959 | 1153 |
| 12 | | -2.8% | 981 | 1215 | 1222 | 975 | 968 | 981 | 707 | 973 | 1171 |
| 13 | | +2.8% | 1011 | 1251 | 1258 | 1002 | 993 | 1008 | 736 | 1000 | 1206 |
| 14 | | +5.6% | 1024 | 1267 | 1276 | 1015 | 1006 | 1022 | 748 | 1015 | 1222 |
| 16 | Hg | -80% | 1288 | 1562 | 1567 | 1274 | 1276 | 1285 | 1121 | 1269 | 1530 |
| 17 | | -46% | 1080 | 1341 | 1346 | 1069 | 1065 | 1078 | 901 | 1071 | 1294 |
| 18 | | +46% | 963 | 1182 | 1123 | 954 | 945 | 963 | 676 | 957 | 1141 |
| 19 | | +80% | 946 | 1159 | 1173 | 939 | 934 | 950 | 658 | 945 | 1119 |
| 20 | Kf | -10% | 1015 | 1258 | 1265 | 1004 | 999 | 1011 | 739 | 1002 | 1213 |
| 21 | | -5% | 984 | 1245 | 1252 | 995 | 988 | 1002 | 729 | 995 | 1200 |
| 22 | | +10% | 984 | 1213 | 1220 | 975 | 966 | 982 | 707 | 977 | 1168 |
| 23 | Hc | -25% | 1206 | 1441 | 1470 | 1211 | 1216 | 1254 | 1224 | 1220 | 1441 |
| 24 | | +25% | 1033 | 1033 | 1029 | 700 | 680 | 835 | 585 | 669 | 981 |
| 25 | | +50% | 592 | 849 | 847 | 604 | 615 | 642 | 536 | 594 | 806 |
| 26 | | +75% | 615 | 788 | 756 | 628 | 610 | 624 | 507 | 613 | 707 |
| 27 | Hg,Kf | -46%, -10% | 1098 | 1364 | 1369 | 1087 | 1083 | 1096 | 916 | 1089 | 1317 |
| 28 | Hg,Hc | -46%, -25% | 1312 | 1562 | 1587 | 1312 | 1306 | 1353 | 1326 | 1314 | 1555 |
| 29 | Hg,Hc | -80%, +50% | 828 | 1045 | 1053 | 835 | 813 | 837 | 738 | 801 | 1018 |
| 30 | Hg,Hc | -80%, -25% | 1542 | 1792 | 1816 | 1549 | 1526 | 1567 | 1553 | 1528 | 1774 |
| 31 | Hg,Hc | +46%, -25% | 1157 | 1384 | 1414 | 1166 | 1175 | 1211 | 1177 | 1175 | 1386 |
| 32 | Hg,Hc | -80%, +25% | 1072 | 1299 | 1312 | 1063 | 1067 | 1071 | 910 | 1056 | 1267 |
| 33 | Hg,Hc | -80%, +75% | 709 | 851 | 824 | 725 | 705 | 711 | 590 | 702 | 819 |

TABLE 7. SECOND REFLOOD PEAK CLAD TEMPERATURES (°F) FOR CSAU RODS (60-150 S)

| Rod # | | CSAU Variation | Nominal | CFM One Level | CFM Two Level | Pump One Level | Pump Two Level | $T_{MIN}$ -36°F | $T_{MIN}$ +180°F | Core Entrainment | X-Product CF, Pump |
|---|---|---|---|---|---|---|---|---|---|---|---|
| 9 | | Nominal | 959 | 1098 | 1141 | 943 | 950 | 981 | 464 | 1065 | 1126 |
| 11 | Pf | -5.6% | 928 | 1062 | 1103 | 912 | 921 | 948 | 451 | 1024 | 1089 |
| 12 | | -2.8% | 939 | 1080 | 1123 | 928 | 936 | 964 | 457 | 1045 | 1107 |
| 13 | | +2.8% | 973 | 1116 | 1161 | 959 | 966 | 997 | 471 | 1085 | 1144 |
| 14 | | +5.6% | 990 | 1134 | 1182 | 973 | 981 | 1013 | 480 | 1105 | 1164 |
| 16 | Hg | -80% | 1126 | 1308 | 1353 | 1110 | 1128 | 1161 | 1018 | 1189 | 1330 |
| 17 | | -46% | 1004 | 1159 | 1207 | 990 | 999 | 1029 | 567 | 1098 | 1188 |
| 18 | | +46% | 941 | 1069 | 1116 | 923 | 930 | 961 | 442 | 1053 | 1098 |
| 19 | | +80% | 932 | 1056 | 1105 | 916 | 923 | 954 | 435 | 1047 | 1087 |
| 20 | Kf | -10% | 968 | 1112 | 1157 | 952 | 961 | 990 | 471 | 1071 | 1141 |
| 21 | | -5% | 964 | 1105 | 1148 | 948 | 955 | 984 | 468 | 1069 | 1334 |
| 22 | | +10% | 952 | 1087 | 1132 | 936 | 943 | 973 | 460 | 1060 | 1116 |
| 23 | Hc | -25% | 1251 | 1438 | 1504 | 1249 | 1242 | 1303 | 1251 | 1431 | 1481 |
| 24 | | +25% | 441 | 660 | 711 | 408 | 426 | 765 | 403 | 453 | 790 |
| 25 | | +50% | 428 | 471 | 554 | 403 | 392 | 424 | 363 | 433 | 486 |
| 26 | | +75% | 426 | 504 | 576 | 426 | 392 | 520 | 334 | 435 | 486 |
| 27 | Hg,Kf | -46%, -10% | 1013 | 1173 | 1222 | 997 | 1009 | 1036 | 583 | 1105 | 1202 |
| 28 | Hg,Hc | -46%, -25% | 1328 | 1530 | 1593 | 1324 | 1317 | 1378 | 1341 | 1495 | 1575 |
| 29 | Hg,Hc | -80%, +50% | 491 | 563 | 642 | 486 | 460 | 480 | 403 | 504 | 552 |
| 30 | Hg,Hc | -80%, -25% | 1512 | 1704 | 1771 | 1510 | 1504 | 1551 | 1549 | 1647 | 1760 |
| 31 | Hg,Hc | +46%, -25% | 1216 | 1395 | 1458 | 1222 | 1202 | 1269 | 1213 | 1402 | 1436 |
| 32 | Hg,Hc | -80%, +25% | 613 | 847 | 972 | 662 | 707 | 869 | 577 | 757 | 959 |
| 33 | Hg,Hc | -80%, +75% | 457 | 543 | 601 | 462 | 433 | 525 | 334 | 473 | 504 |

Table 8

OPTIMIZING THE RESPONSE SURFACE
BASED ON MINIMIZING THE RMS

| Stage of Transient | Fit | RMS, °F |
|---|---|---|
| Blowdown | Linear | 56.5 |
| | Linear & Crossproducts | 51.7 |
| | Full Second Order | 26.8 |
| | Quartic 1 (52 terms) | 17.4 |
| | Best Quartic (70 terms) | 9.6 |
| Early Reflood | Linear | 91.3 |
| | Full Second Order | 50.6 |
| | Quartic 1 (67 terms) | 46.8 |
| | Quartic 2 (Best, 67 terms) | 24.5 |
| Late Reflood | Linear | 133.2 |
| | Full Second Order | 86.0 |
| | Quartic 1 | 47.2 |
| | Best Quartic (60 terms) | 42.8 |

Table 9

FITTING THE BLOWDOWN DATA

(50000 History Study)

| *FIT* | *Sample Mean, °F* | *95th Percentile, °F* | *RMS °F* |
|---|---|---|---|
| Linear | 1112 | 1418 | 56.5 |
| Linear + Crossproducts | 1128 | 1423 | 51.7 |
| Full Second Order | 1147 | 1430 | 26.8 |
| Quartic 1 (52 terms) | 1159 | 1442 | 17.4 |
| Best Quartic (70 terms) | 1162 | 1447 | 9.6 |

Table 10

EARLY REFLOOD RESPONSE SURFACE DEVELOPMENT

(50000 History Study)

| *FIT* | *Sample Mean, °F* | *95th Percentile, °F* | *RMS °F* |
|---|---|---|---|
| Linear | 904 | 1314 | 91.3 |
| Full Second Order | 961 | 1387 | 50.6 |
| Quartic 1 | 968 | 1394 | 46.8 |
| Quartic 2 (Best Quartic) | 978 | 1399 | 24.5 |

Note: All Quartics contain 67 terms.

Table 11

LATE REFLOOD RESPONSE SURFACE DEVELOPMENT

(50000 History Study)

| *FIT* | *Sample Mean, °F* | *95th Percentile, °F* | *RMS °F* |
|---|---|---|---|
| Linear | 724 | 1219 | 133.2 |
| Full Second Order | 761 | 1319 | 86.0 |
| Quartic 1 | 726 | 1338 | 47.2 |
| Best Quartic (60 Terms) | 758 | 1336 | 42.8 |

Table 12

PRELIMINARY VIEW OF THE FINAL UNCERTAINTIES

| | PCT (°F) | | |
|---|---|---|---|
| | | Reflood | |
| | Blowdown | Early | Late |
| Mean value | 1162 | 978 | 758 |
| 95th percentile | 1447 | 1399 | 1336 |

Table 13

3 Ring/4 Ring: The Hot Channel Bias

| Phase | | Additive Bias, °F |
|---|---|---|
| Blowdown: | mean | 63 |
| | 95th | 45 |
| Early Reflood: | mean | 25 |
| | 95th | -54 |
| Late Reflood: | mean | -14 |
| | 95th | -157 |

Table 14

THE EFFECT OF FORSLUND-ROHSENOW

| | Temperature Difference, °F | | |
|---|---|---|---|
| | | Reflood | |
| | Blowdown | Early | Late |
| Calculation (FR=0.26) - (FR=1.0) | 47 | 84 | 160 |
| LOFT mean (EXP - TRAC) | -23 | | |
| SCTF/CCTF mean (EXP - TRAC) | | | -18.5 |

Table 15

INTERMEDIATE VIEW OF THE FINAL UNCERTAINTIES

| | | PCT (°F) | | |
|---|---|---|---|---|
| | | | Reflood | |
| | | Blowdown | Early | Late |
| TRAC pdf results, | mean | 1162 | 978 | 758 |
| | 95th percentile | 1447 | 1399 | 1336 |
| Biases | | | | |
| Hot Channel: | Δmean | 63 | 25 | -14 |
| | Δ95th percentile | 45 | -54 | -157 |
| Forslund-Rohsenow | | 47 | 84 | 160 |
| Entrainment | | 0 | -9 | 106 |
| ECCS Bypass | | 0 | -34 | -34 |
| Nitrogen | | 0 | 18 | 18 |
| Summed Biases | Mean | 110 | 84 | 236 |

Table 16

ESTIMATING THE PROBABILITY ASSOCIATED WITH THE FORSLUND-ROHSENOW BIAS

| | LATE REFLOOD | | | |
|---|---|---|---|---|
| | FR=1 | | FR=0.26 | |
| Case | PCT, °F | Pr(T<PCT) | PCT, °F | Pr(T<PCT) |
| Nominal | 959 | 0.71 | 1087 | .81 |
| Break 1-L | 1097 | 0.81 | 1251 | .91 |
| Break 2-L | 1141 | 0.83 | 1290 | .93 |
| Pump 1-L | 943 | 0.70 | 1091 | .81 |
| Pump 2-L | 950 | 0.71 | 1051 | .78 |
| $T_{MIN}$ -35° | 981 | 0.74 | 1102 | .82 |
| $T_{MIN}$ +180° | 464 | 0.20 | 779 | .58 |
| Cross Product | 1125 | 0.83 | 1289 | .93 |
| Ave PCT | 958 | 0.71 | 1117 | .82 |

Table 17

ESTIMATE OF TOTAL LBLOCA UNCERTAINTIES

| | | PCT (°F) | | |
|---|---|---|---|---|
| | | | Reflood | |
| Source | | Blowdown | Early | Late |
| TRAC Response Surface | | | | |
| | Mean | 1162 | 978 | 758 |
| | 95th | 1447 | 1399 | 1336 |
| Summed Biases: | | 110 | 84 | 236 |
| Adjusted Mean | | 1272 | 1062 | 994 |
| Adjusted 95th | | 1557 | 1483 | 1572 |

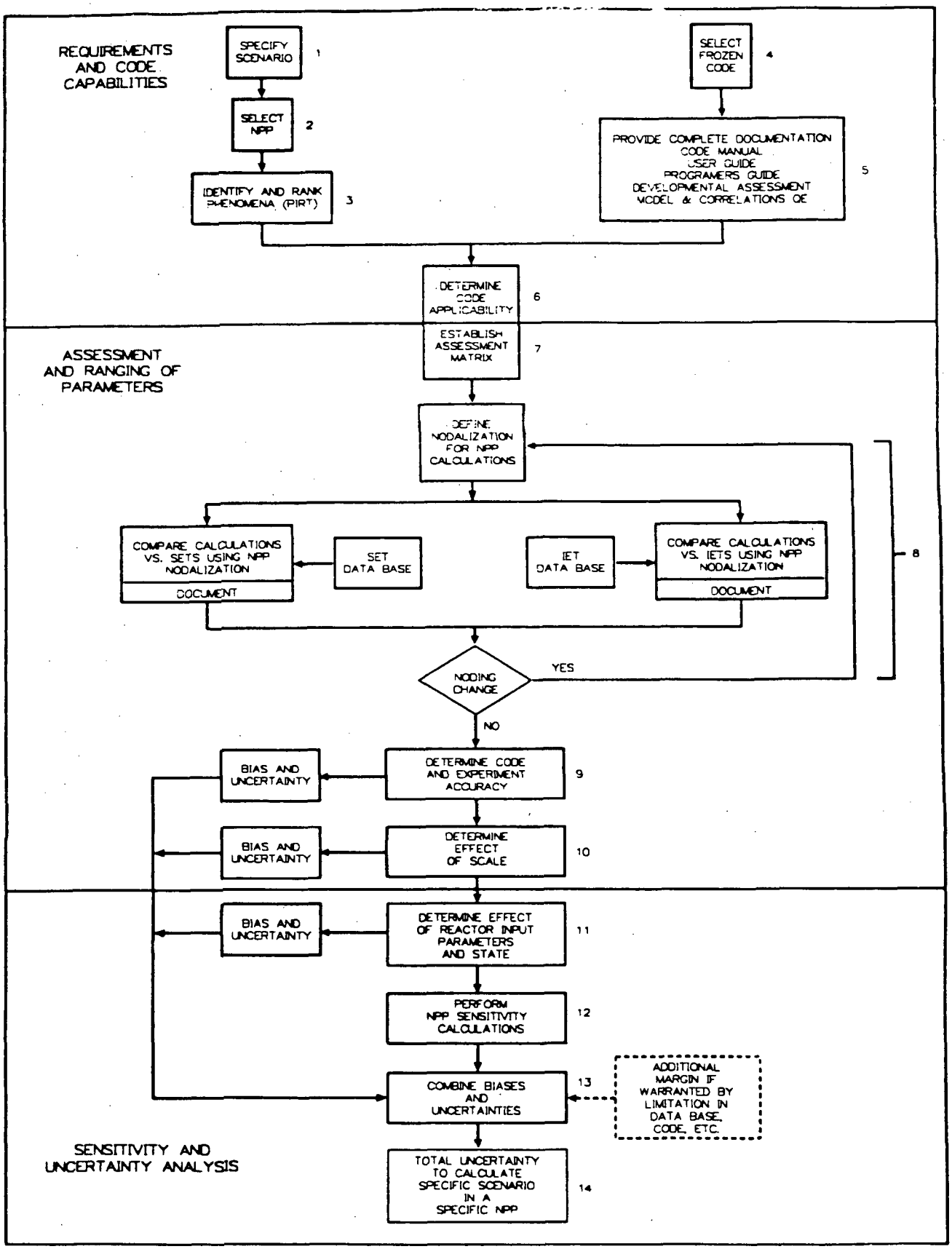


NSL01059

Figure 1. Code scaling, applicability and uncertainty (CSAU) methodology.

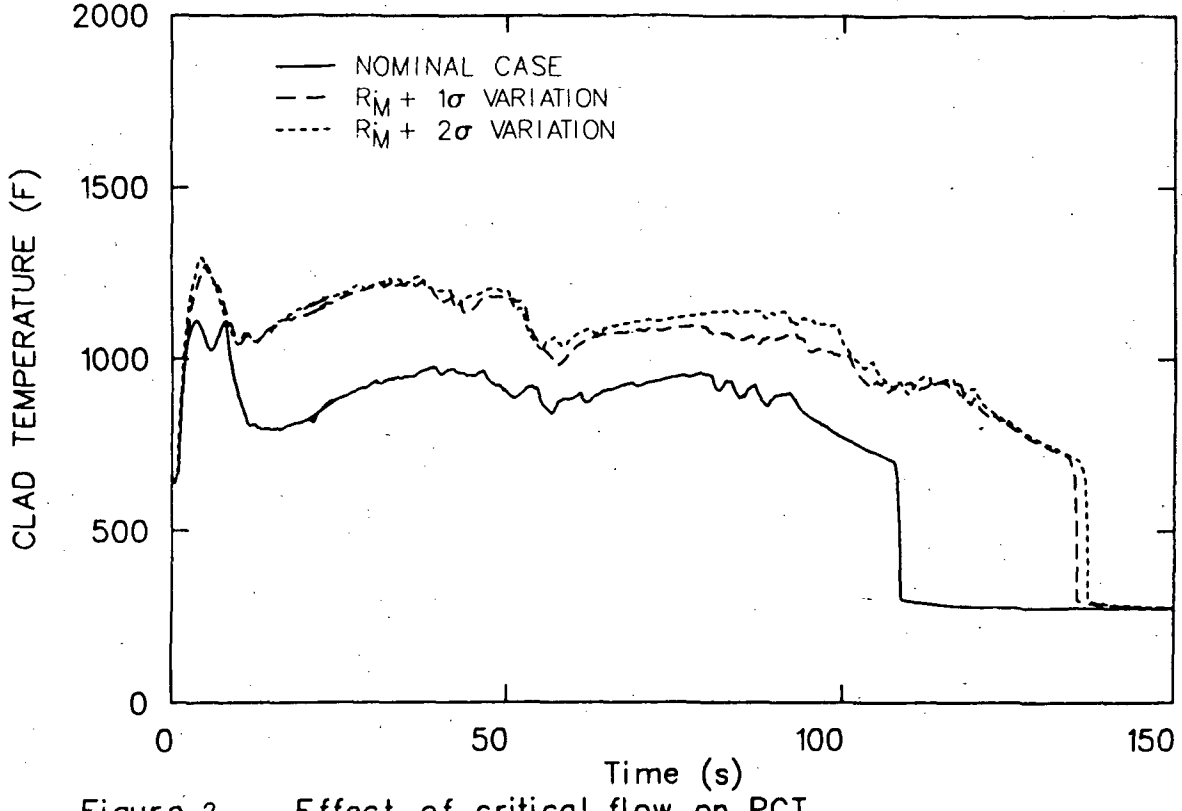


Figure 2 . Effect of critical flow on PCT.

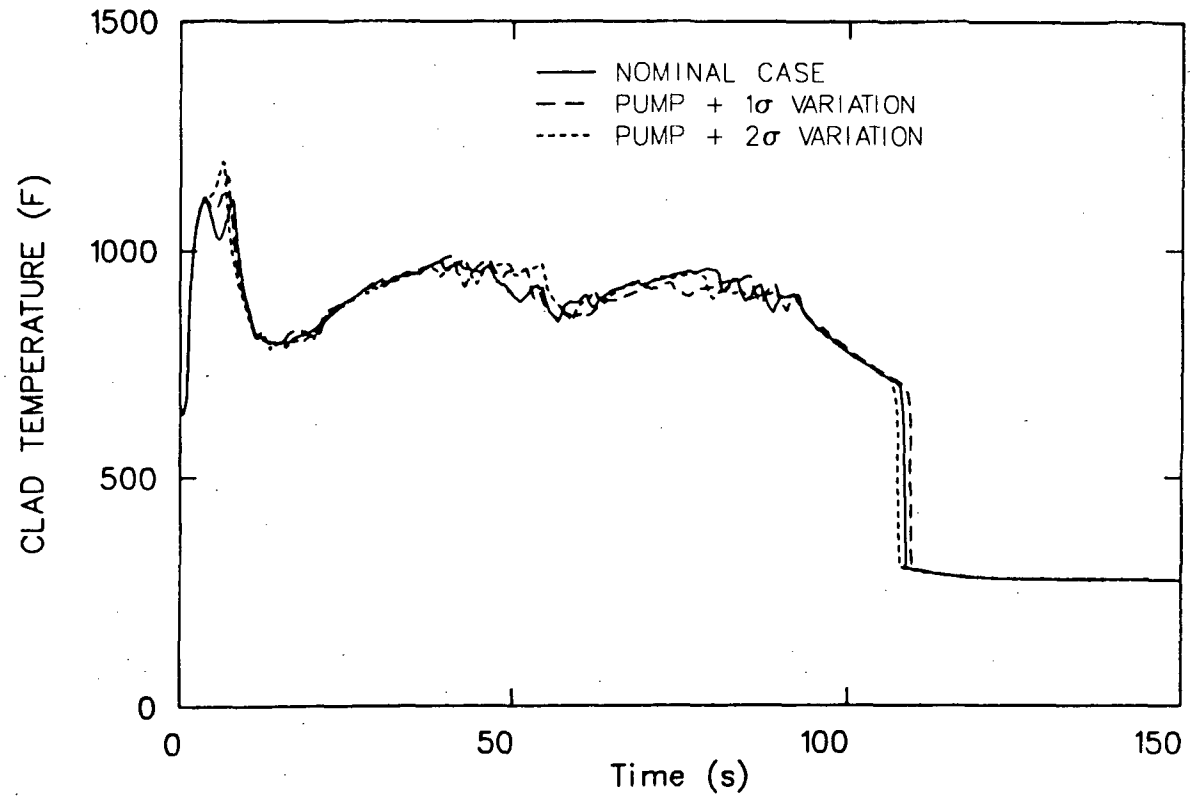


Figure 3 . Effect of pump degradation on PCT.

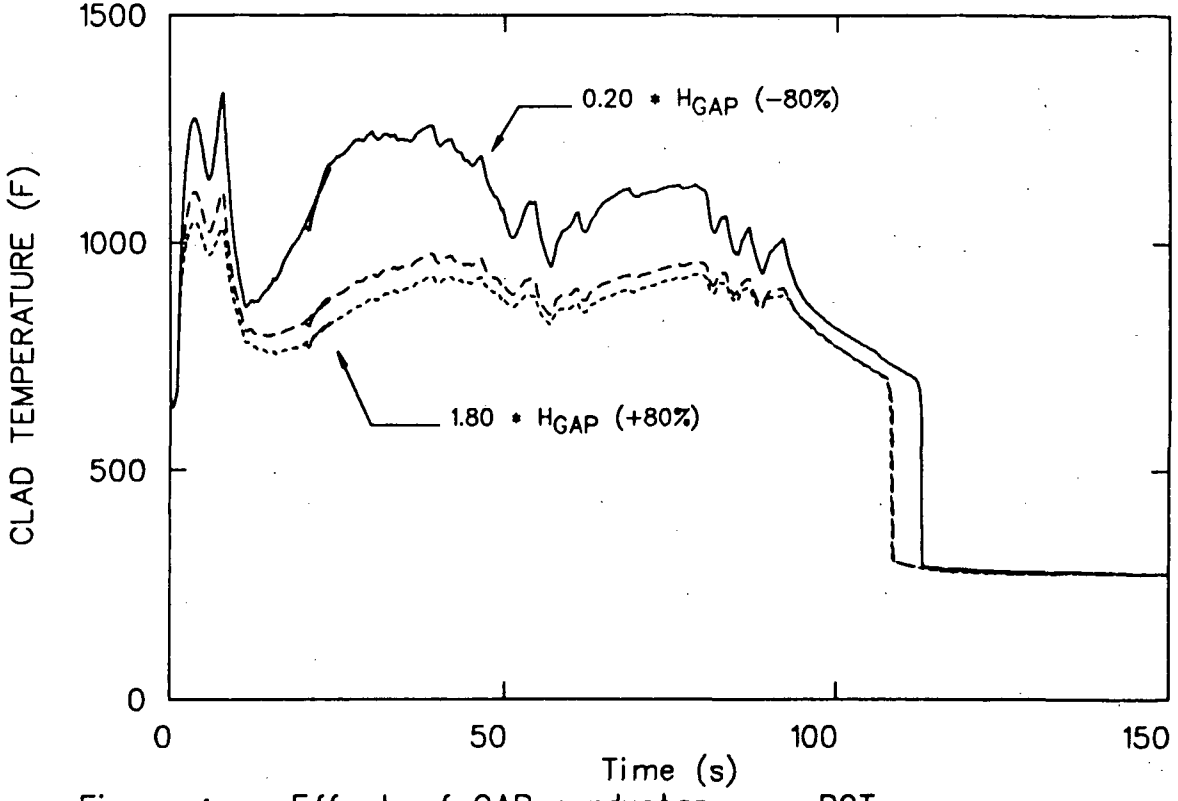


Figure 4 . Effect of GAP conductance on PCT.

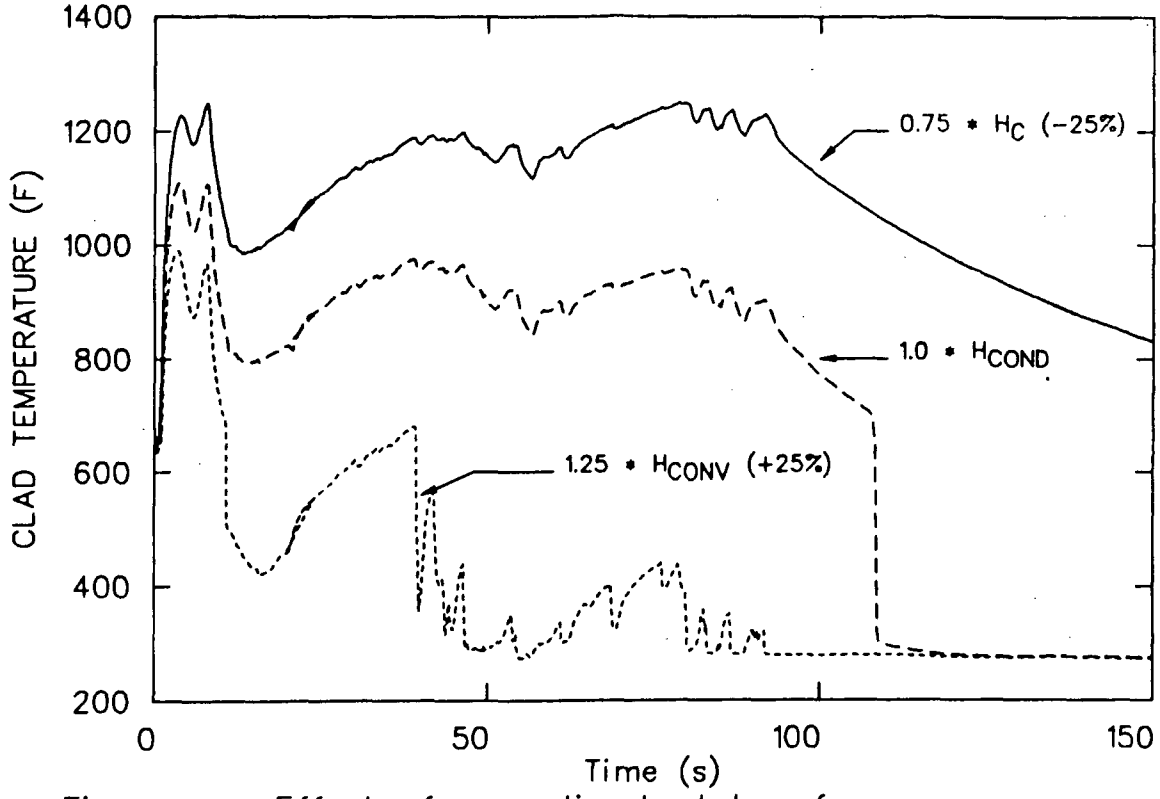


Figure 5 . Effect of convective heat transfer.

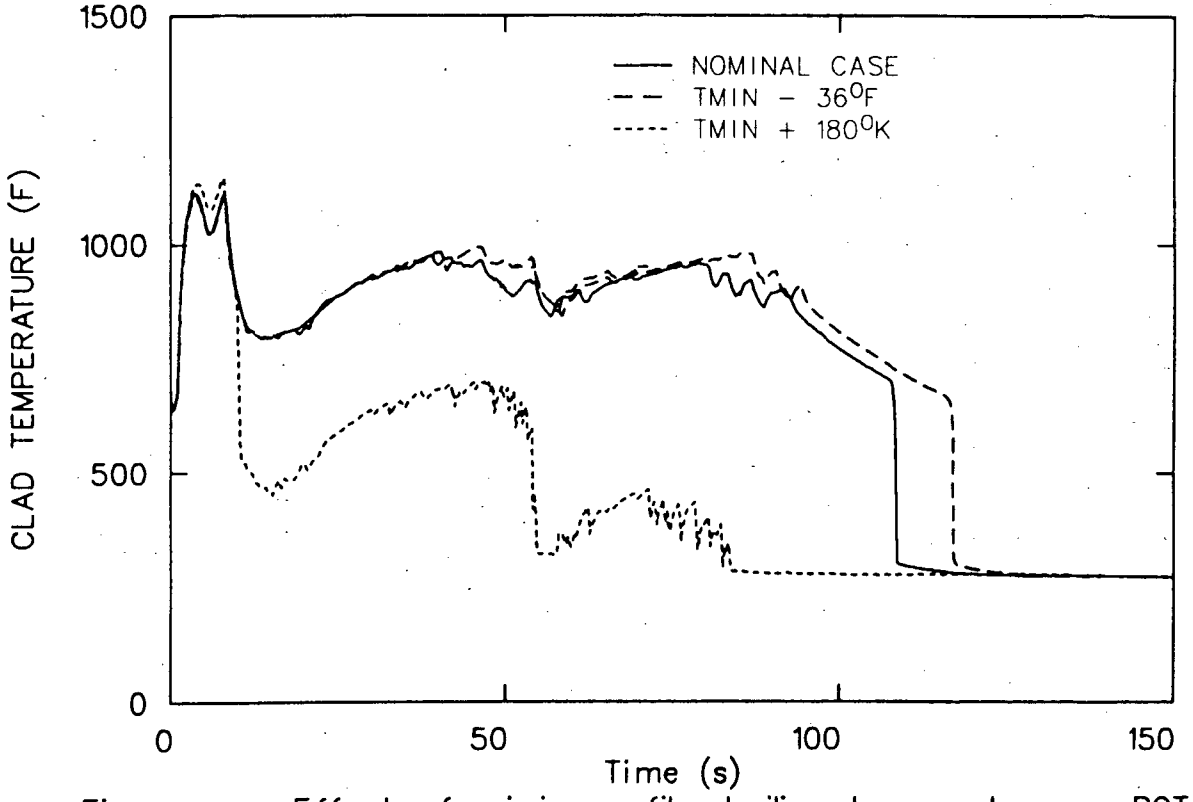


Figure 6 . Effect of minimum film boiling temperature on PCT.

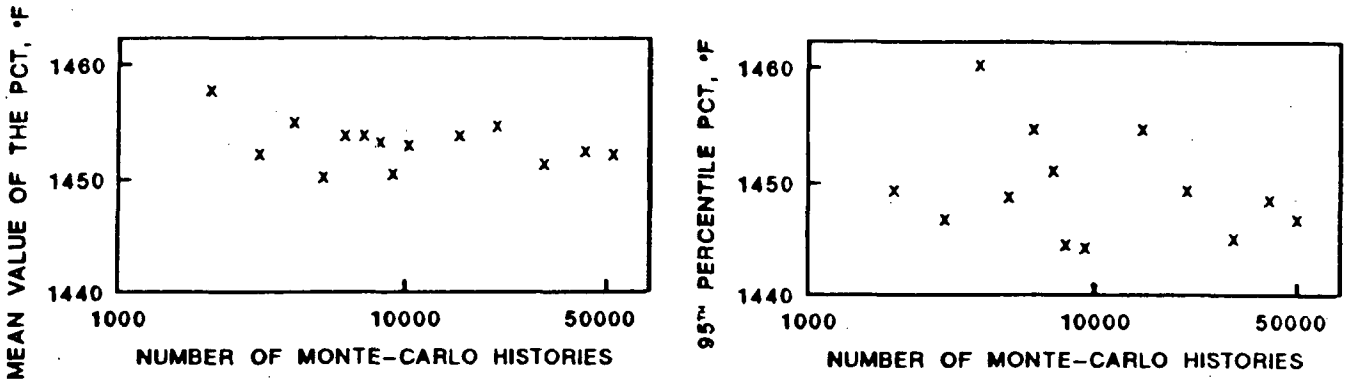


Figure 7. History study for the "Best" fourth order fit to the blowdown data.

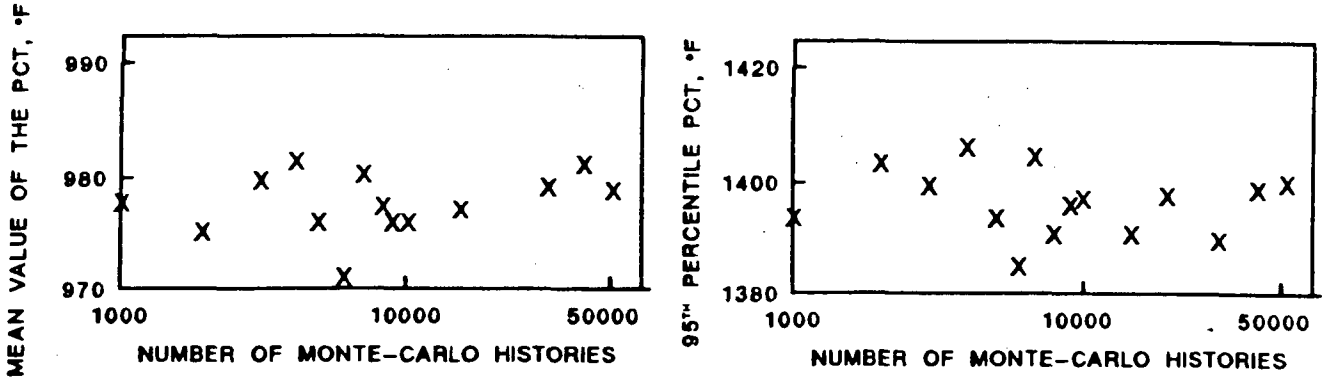


Figure 8. History study for the "Best" fourth order fit to the early reflood data.

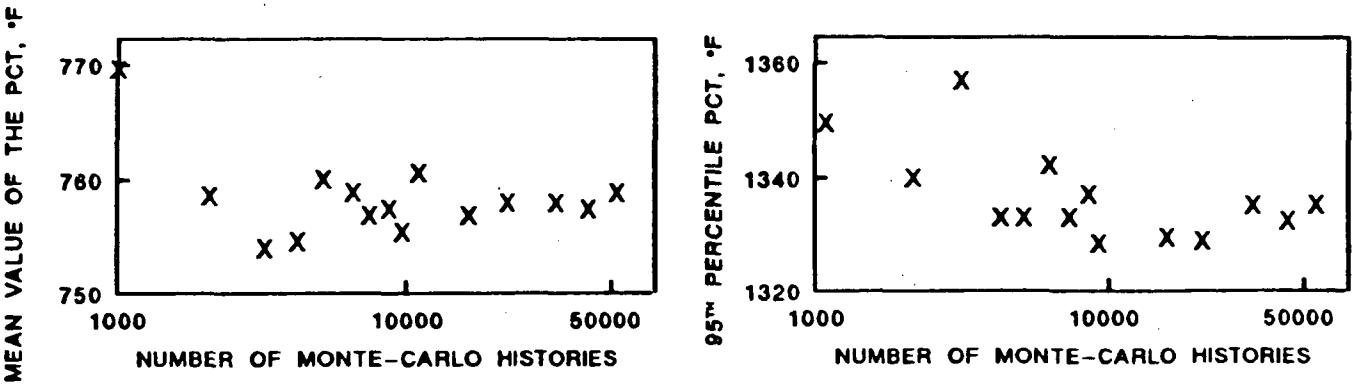


Figure 9. History study for the "Best" fourth order fit to the late reflood data.

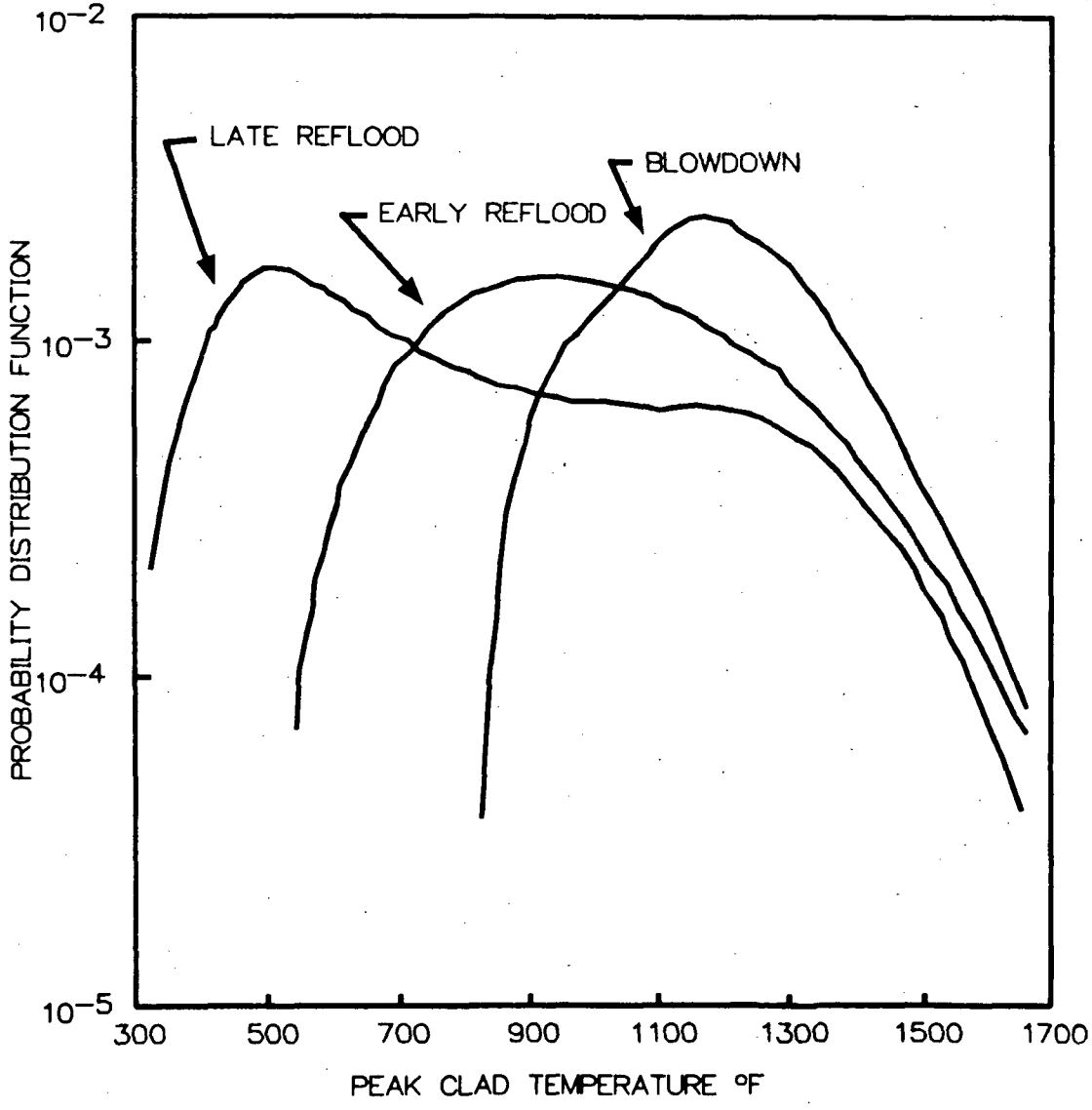


Figure 10. Probability distribution functions for the three phases of the large break LOCA (50000 history study).



NSL01030

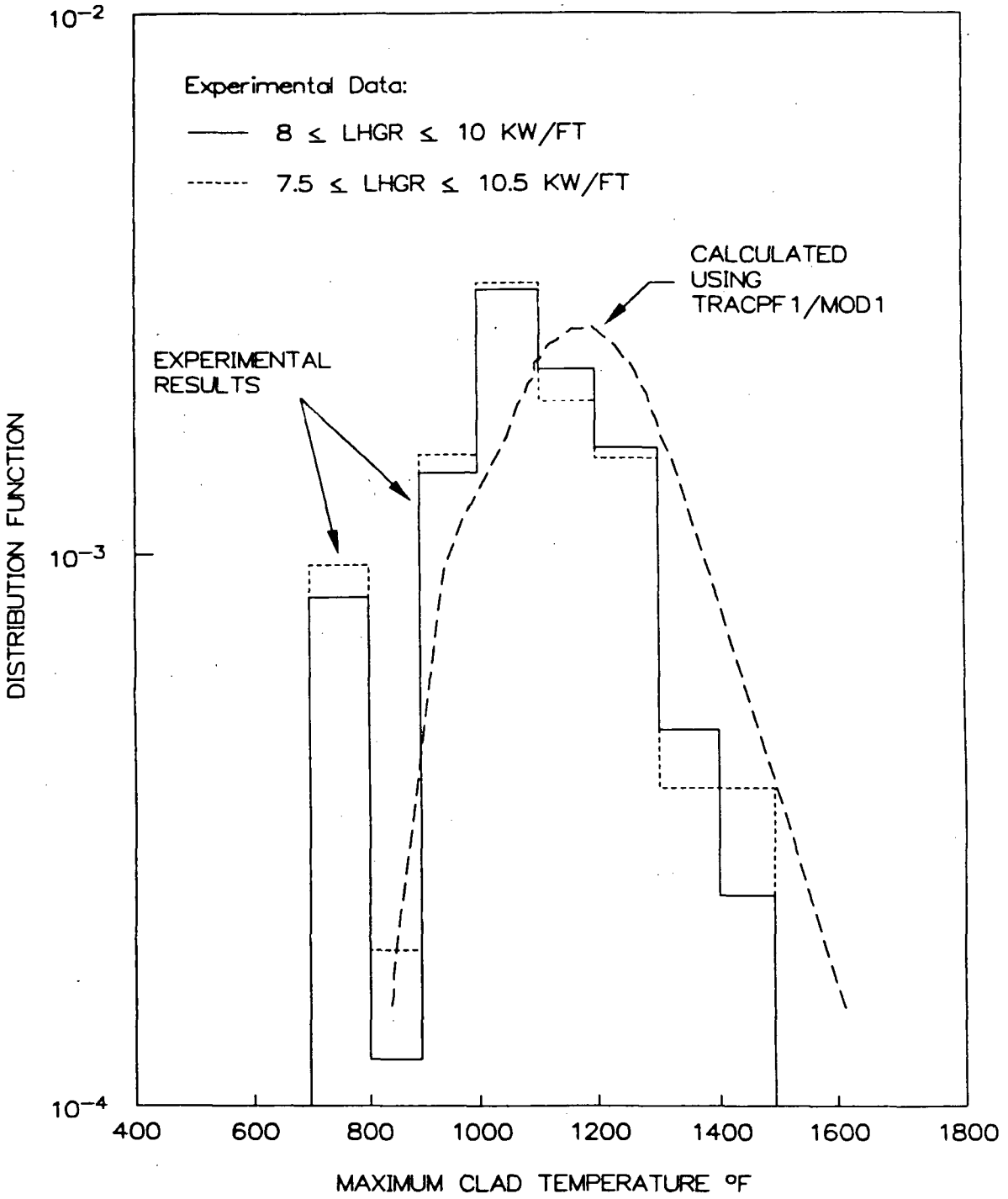


Figure 11. Consideration of the effect of the LHGR range on the distribution function for the maximum clad temperature during blowdown.

NSL01047

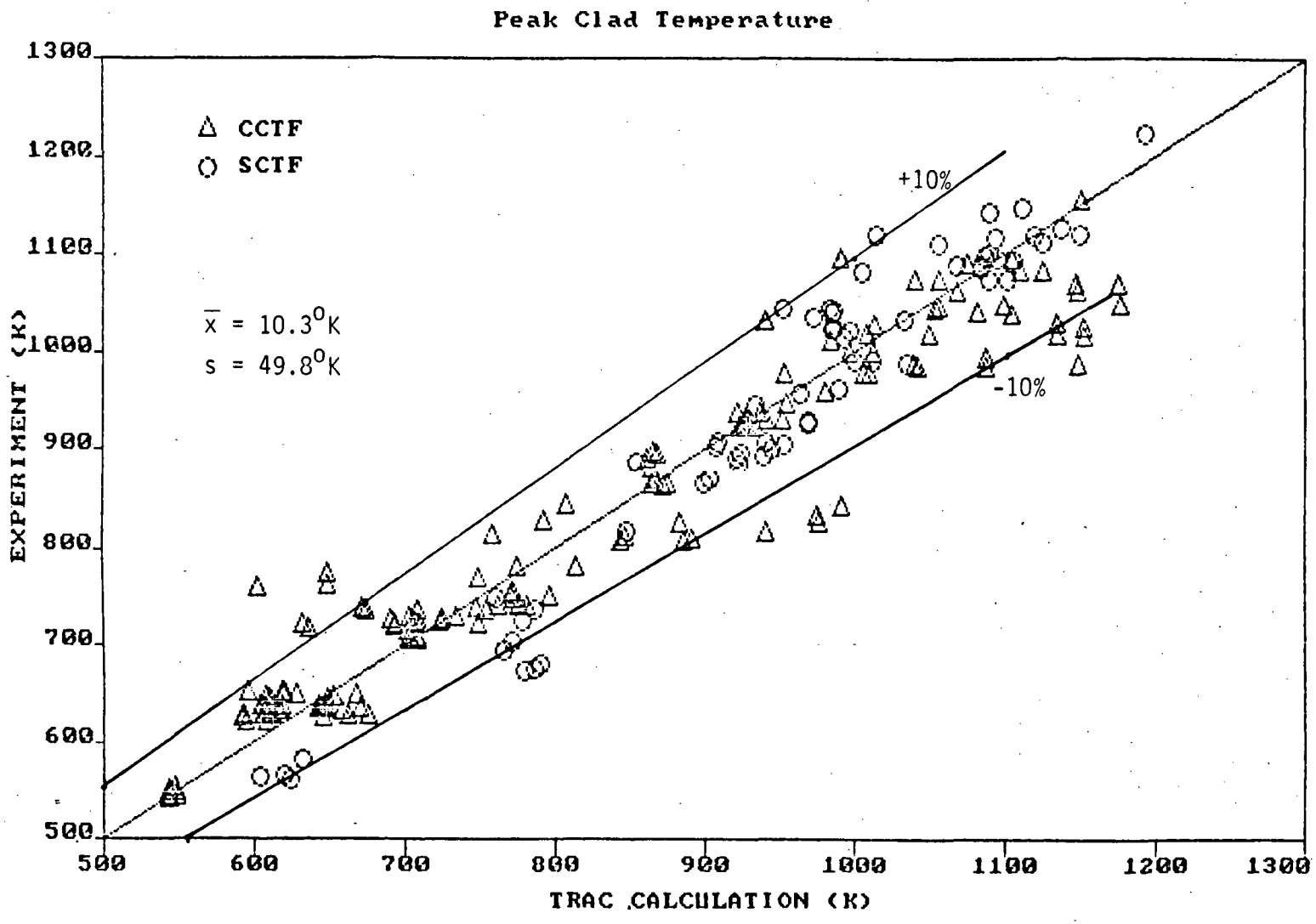
Peak Clad Temperature
CCTF
SCTF
$\bar{x}$ = 10.3°K
s = 49.8°K
+10%
-10%
EXPERIMENT (K)
TRAC CALCULATION (K)
1300
1200
1100
1000
900
800
700
600
500
500
600
700
800
900
1000
1100
1200
1300

FIGURE 12

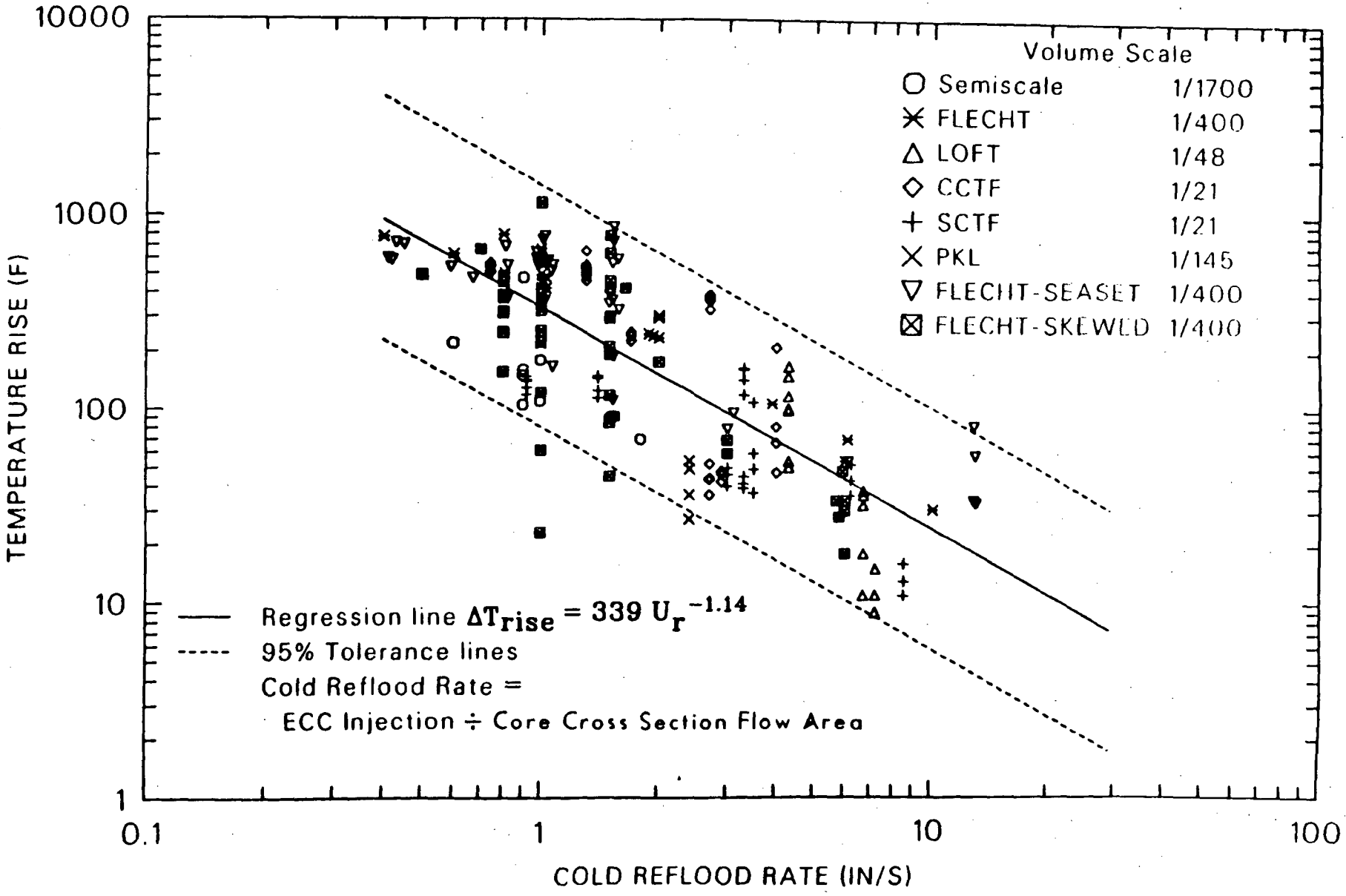


Figure 13. Measured temperature rise data from scaled experimental facilities during reflood.

# ILLUSTRATION OF TEST BY TEST DETERMINTION OF CODE PLUS EXPERIMENT UNCERTAINTY

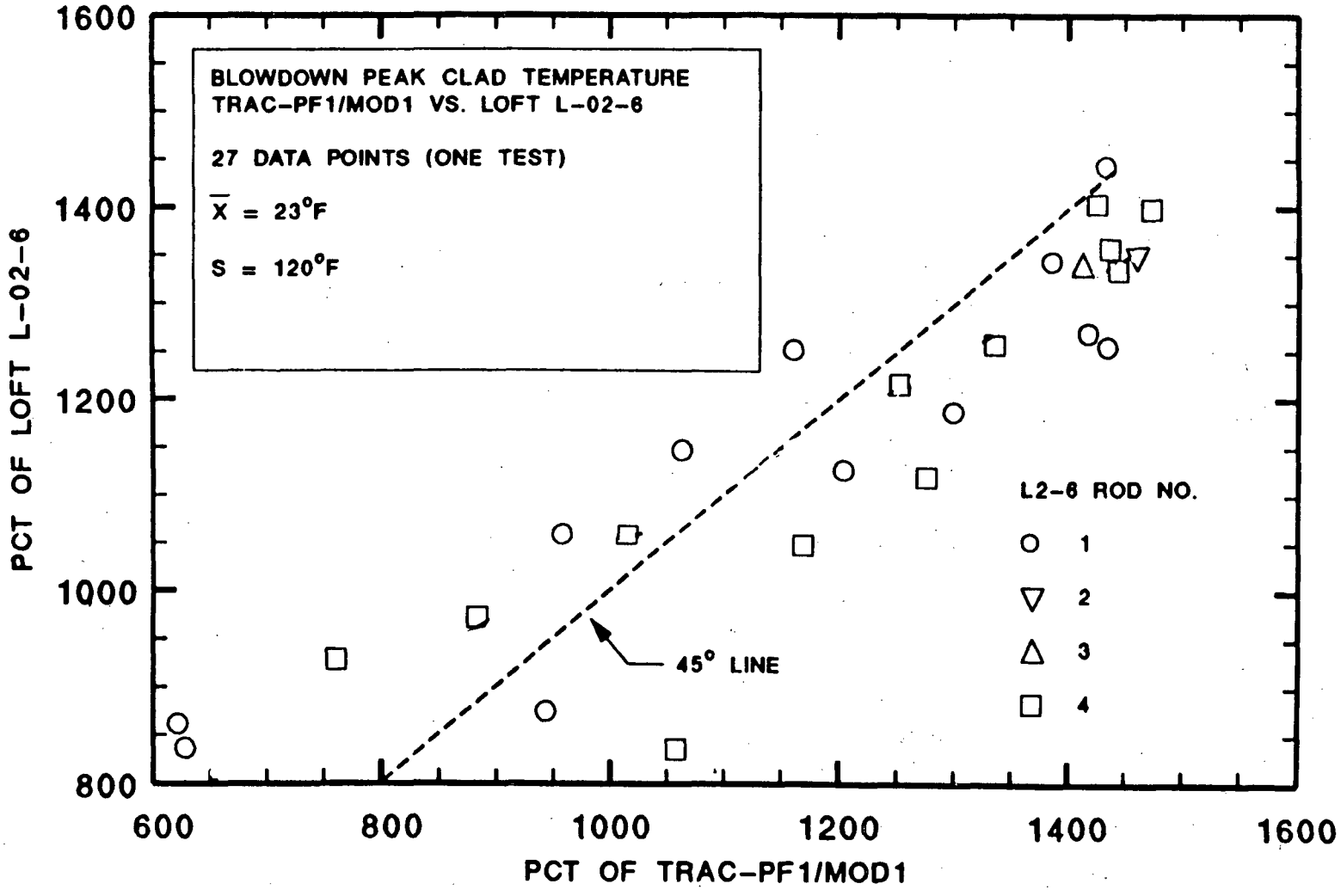


FIGURE 14

NSL00987

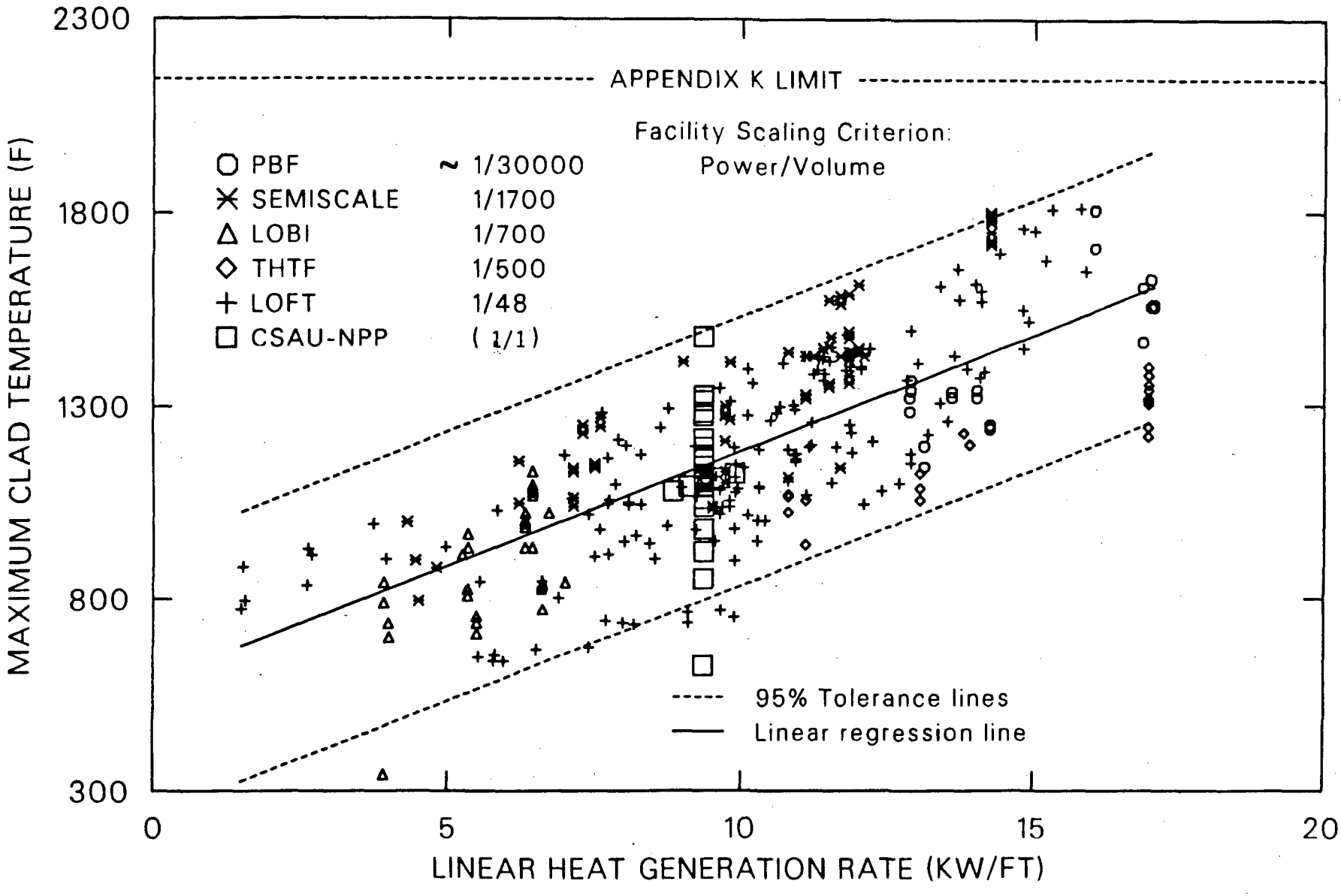


Figure15. Maximum measured clad temperature from several scaled experimental facilities (301 data points) during blowdown

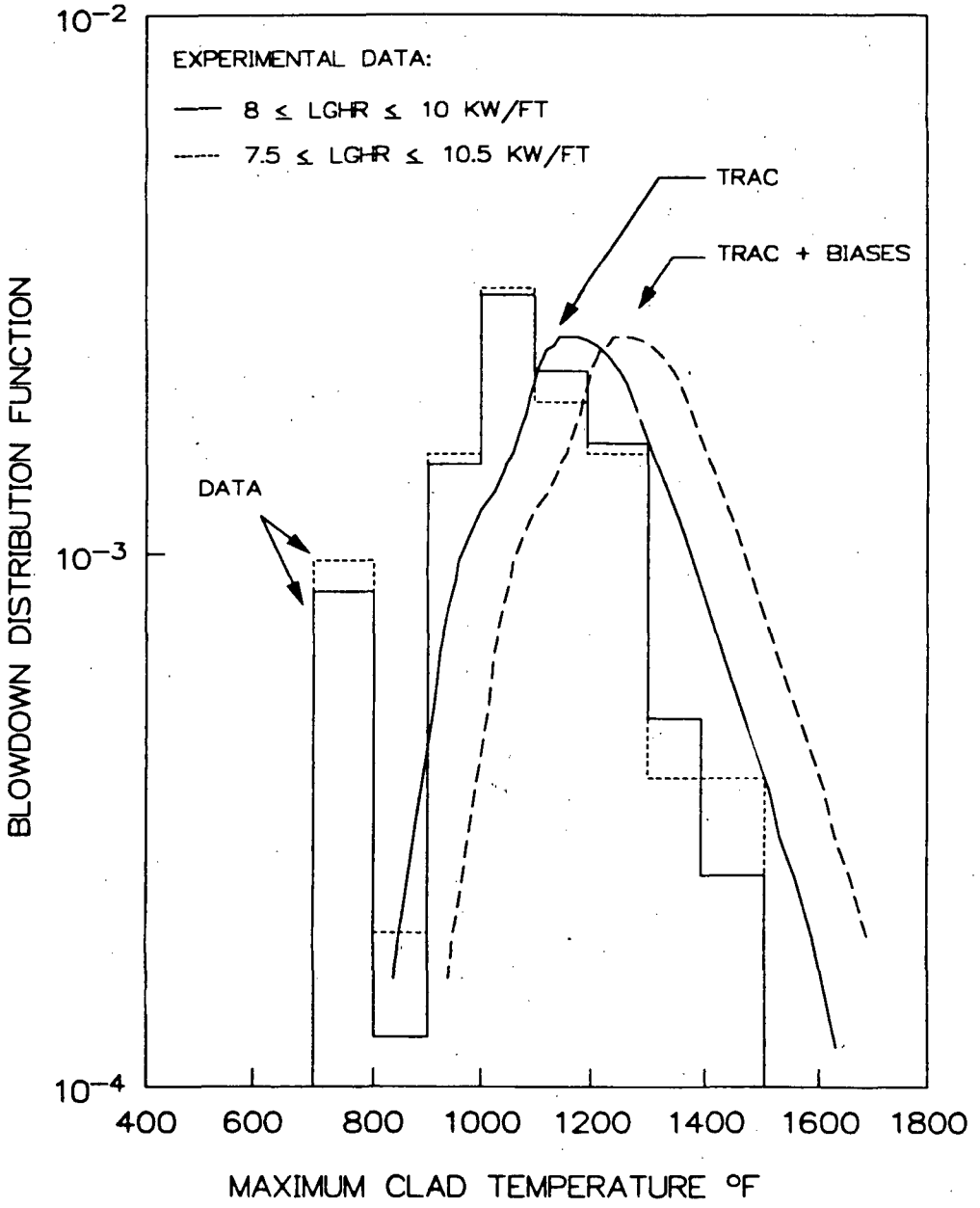


Figure 16. Consideration of the effect of the LHGR range on the distribution function for the maximum clad temperature during blowdown.

NSLO1044

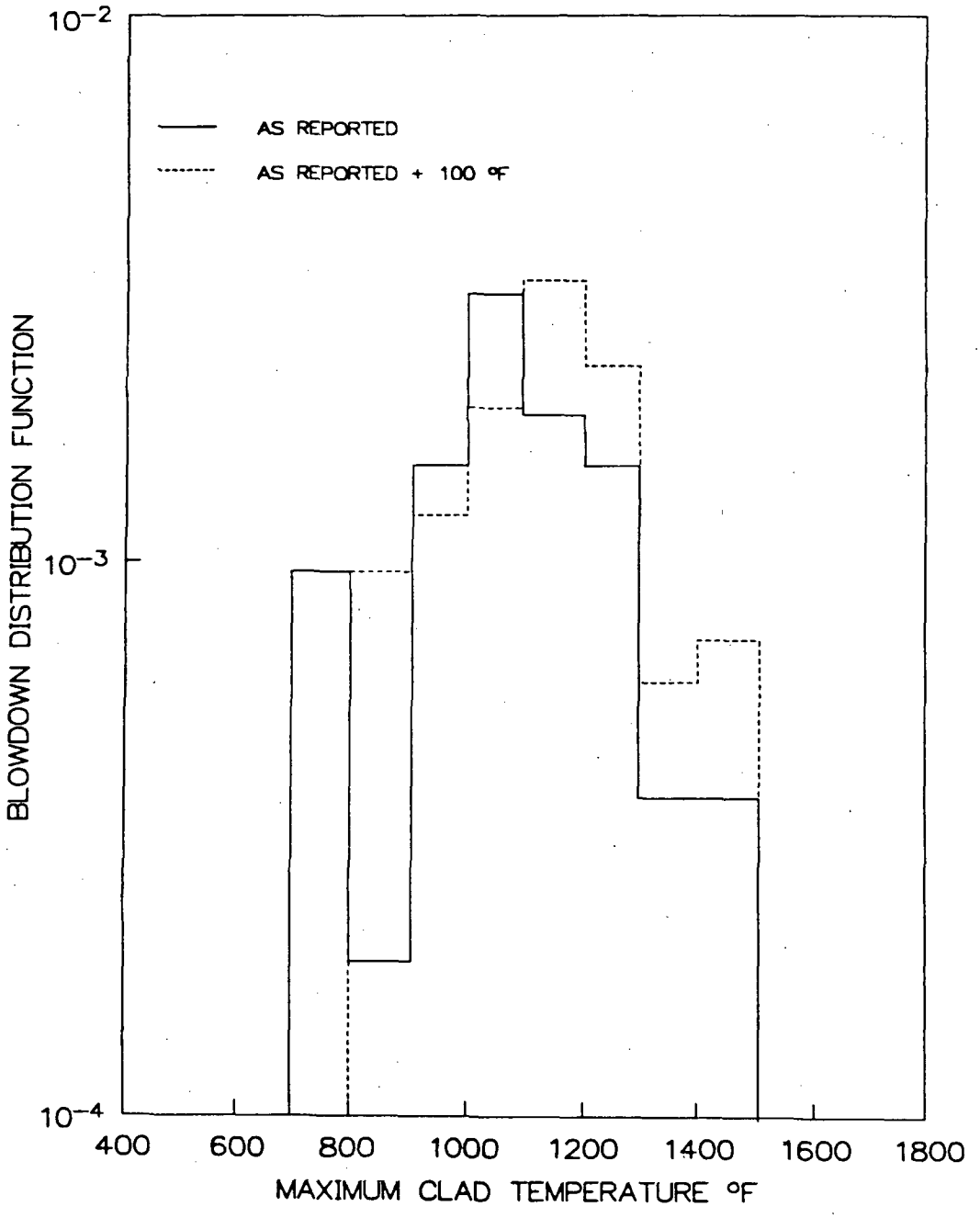


Figure 17. Comparing the effect of a 100°F adjustment to the LOFT data and its affect on the data histogram when compared to the TRAC distribution function.

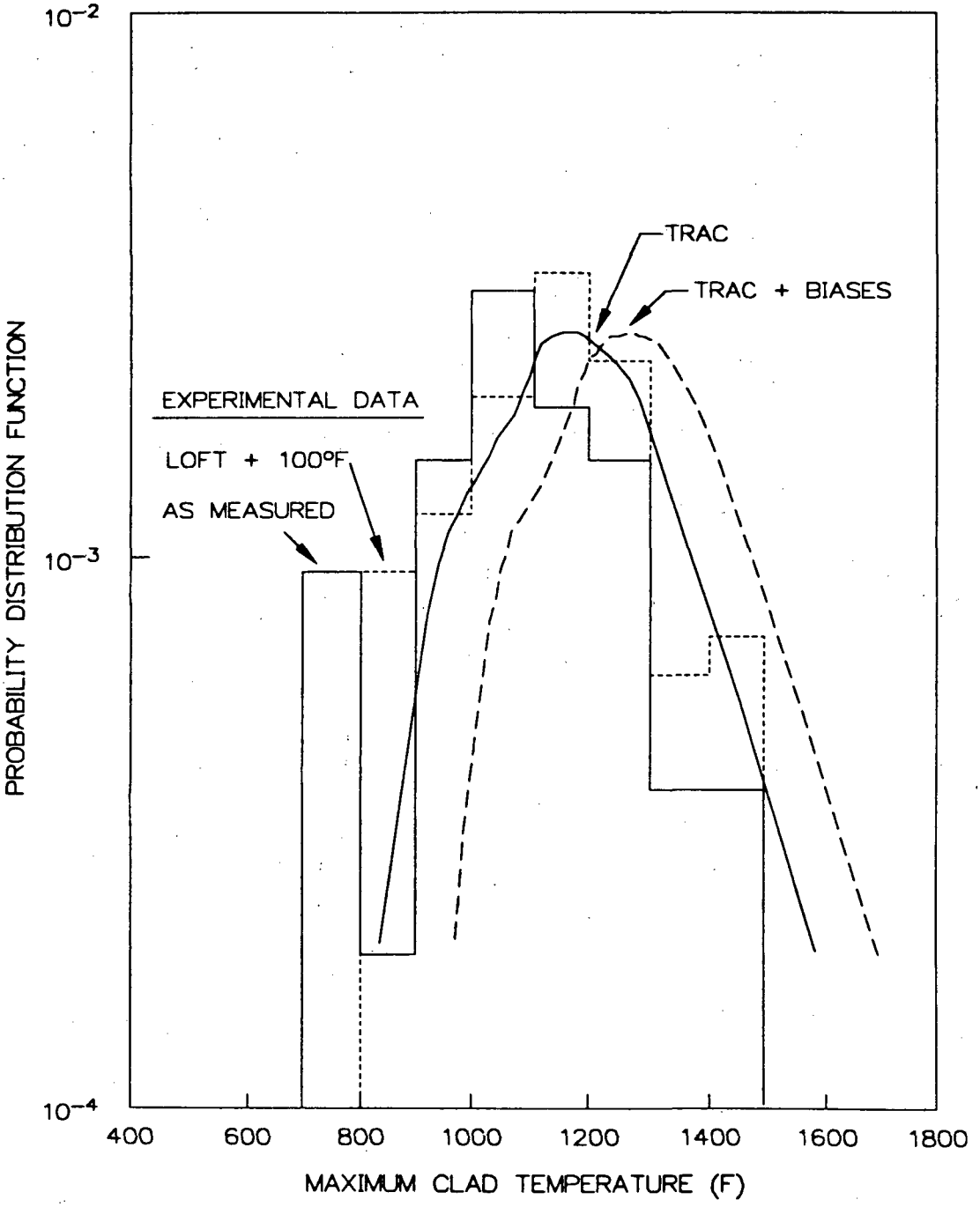


Figure 18. Comparing the effect of a 100°F adjustment to the LOFT data and its affect on the data histogram when compared to the TRAC distribution function during blowdown ($7.5 \leq$ LHGR $\leq 10.5$ KW/FT).

NSL01046

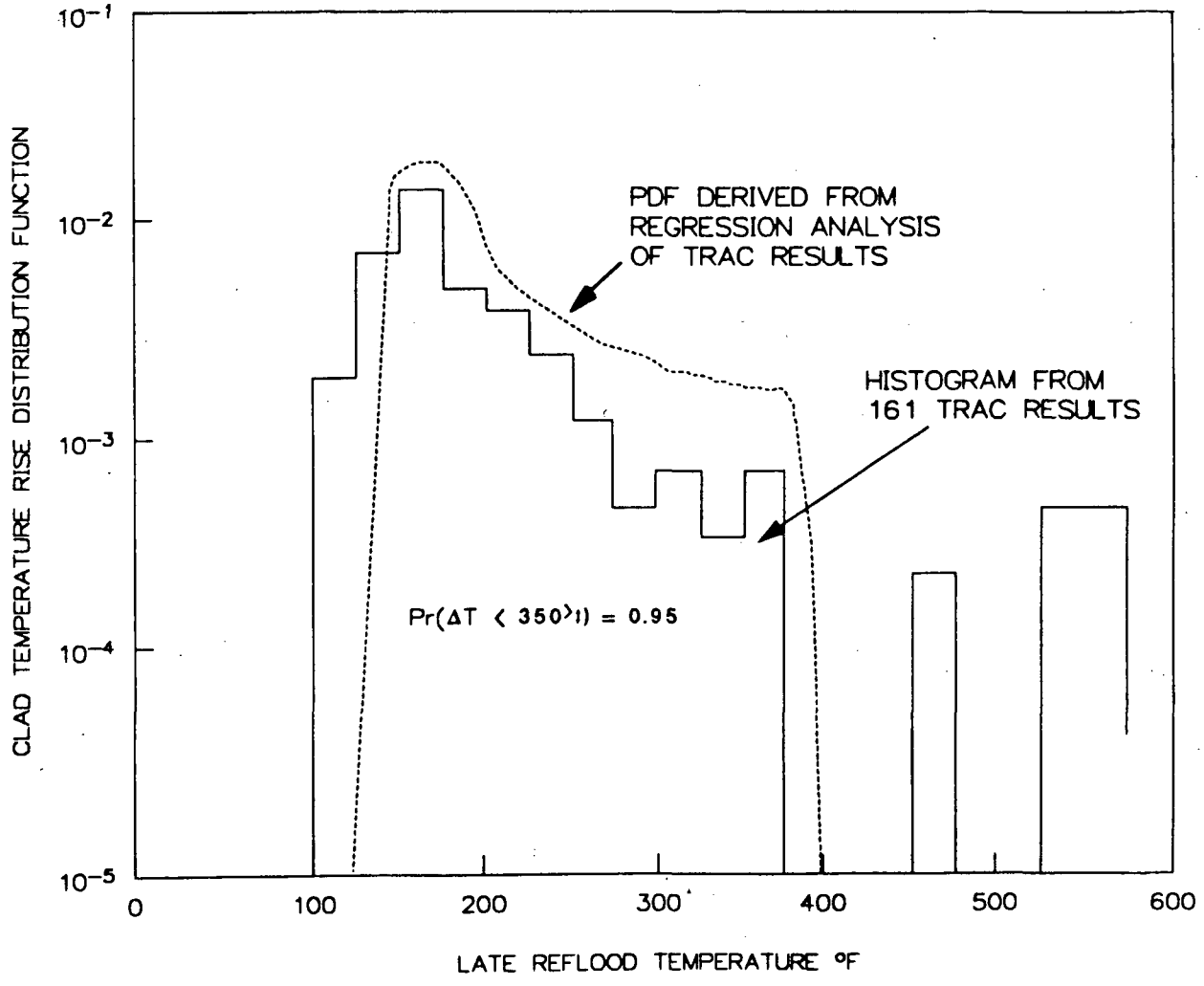


Figure 19. Distribution for the temperature rise during late reflood derived from the TRAC calculations.

NSL01048

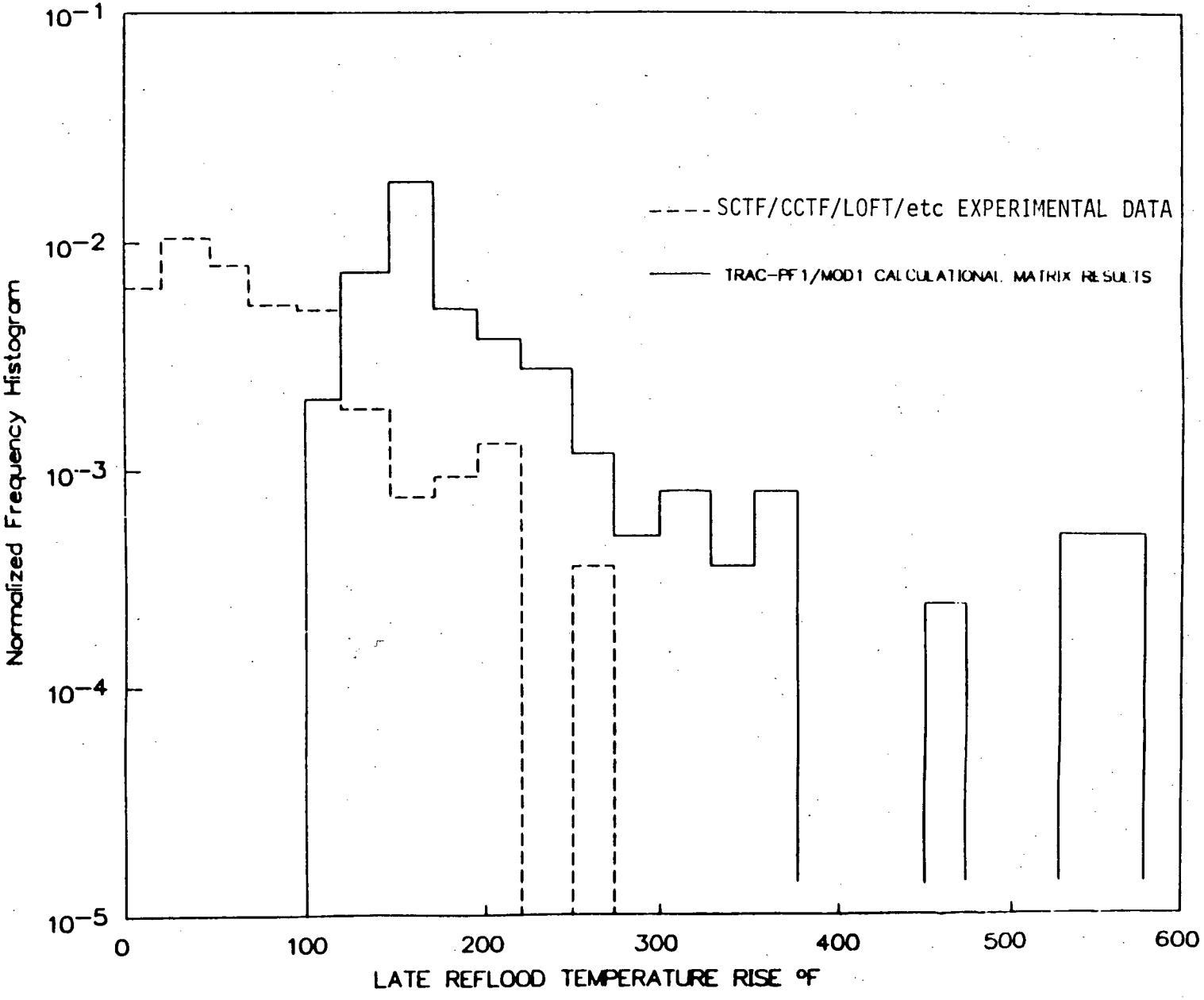


Comparing the calculated and experimental frequency histograms for the late reflood period

NSL01087

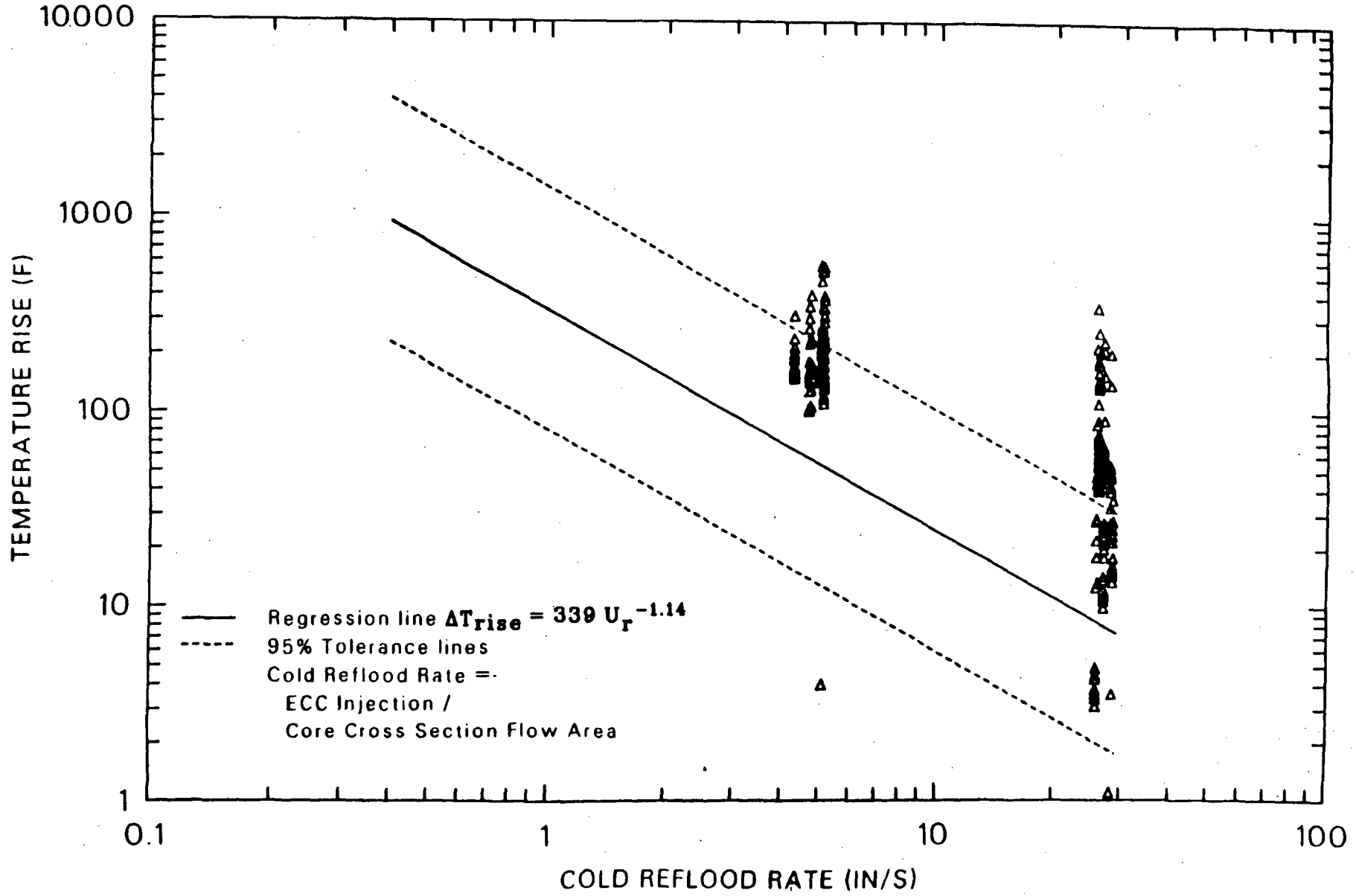


Figure 21. Temperature rise data from TRAC NPP calculation during reflood.

# SUMMARY OF ICAP ASSESSMENT RESULTS FOR RELAP5/MOD2*

W.E. DRISKELL and R.G. HANSON
EG&G Idaho Inc.

Idaho National Engineering Laboratory

ABSTRACT

The International Code Assessment and Applications Program (ICAP) encompasses bilateral agreements between the U.S. Nuclear Regulatory Commission and fourteen nations and/or multinational organizations. One purpose of the ICAP is to provide assessments of the RELAP5 computer code with the intent to identifying code deficiencies and drafting user guidelines. To date, twenty assessment studies have been provided by ICAP assessing the RELAP5/MOD2 code. Of these, ten have been reviewed and evaluated. Based on these ten studies, three code deficiencies were identified and four user guidelines drafted. The code deficiencies are listed and the user guidelines stated. A summary of the information considered and the procedure used in the identification of the code deficiencies and the formulation of user guidelines is given.

## 1. INTRODUCTION

The U.S. Nuclear Regulatory Commission (USNRC) is currently sponsoring the International Code Assessment and Applications Program (ICAP). ICAP encompasses fourteen bilateral agreements between the USNRC and as many nations or multinational organizations. One primary purpose of ICAP is to provide assessment of the RELAP5 and TRAC-PF1 computer codes. These assessments provide an important source of information for the identification of code deficiencies and the formulation of user guidelines. The identification of code deficiencies results in an improved code and that provides an enhanced, more accurate safety analysis tool for the evaluation of light water reactor systems. ICAP assessments have also found errors in the coding. In some cases corrections were provided and code improvements suggested. Hence, ICAP provides direct feedback to the USNRC sponsored code improvement activities and contributes to the enhancement of the analytical capabilities of these codes. Three code deficiencies for the RELAP5/MOD2 code were identified in ICAP code assessment studies: (1) Interphase drag, (2) Critical mass flow, and (3) Critical heat flux. In general, coding errors, corrections and suggested improvements were handled on a one-to-one

* Work sponsored by the US Nuclear Regulatory Commission.

informal basis and are not discussed here. This paper provides a summary of the information considered and procedures used for identifying code deficiencies. Similar information regarding user guidelines is also given.

Currently, ICAP has produced nineteen code assessment studies addressing the RELAP5/MOD2 code. Two studies have been produced addressing the TRAC-PF1/MOD1 code and one study addressing both codes. The twenty assessment studies relating to the RELAP5/MOD2 code were submitted by seven nations and involved the assessment of several areas of the code. RELAP5/MOD2[1] is a best-estimate, full-system, thermal-hydraulic computer code developed at the Idaho National Engineering Laboratory (INEL) and designed for the analyses of pressurized water reactor (PWR) systems. RELAP5/MOD2 calculational models permit the simulation of a wide variety of postulated accidents and have the capability to calculate transient responses through the onset of fuel failure. RELAP5/MOD2, cycle 36 is the latest of the RELAP5 series codes to be released.

To ensure the ICAP code assessment effort has a consistent base, a version of the code is "frozen". Maintaining a frozen version requires that no code development (model improvement) efforts ensue on that version. The only changes permitted are the correction of coding errors or the improvement of user conveniences. The version of the RELAP5 code frozen for these ICAP assessment studies was RELAP5/MOD2, Cycle 36.

The responsibility for evaluating the information contained in the ICAP assessments of RELAP5/MOD2 resides at the INEL. Review of TRAC-PF1/MOD1 related assessments is performed at the Los Alamos National Laboratory. Consequently, assessment activities related to the TRAC-PF1/MOD1 code will not be discussed further here. Review of the ICAP assessment studies for the RELAP5/MOD2 code is based on criteria identified in the "Guidelines and Procedures for the International Code Assessment and Applications Program"[2] and in the "Compendium of ECCS Research for Realistic LOCA Analysis"[3]. In general, the review consists of three parts; (1) potential code deficiencies are identified and user guidelines are extracted, (2) potential code deficiencies and extracted user guidelines are evaluated to ensure they are fully supported by data and/or analyses, and (3) they are consistent with the total body of assessment information. Of the twenty ICAP studies assessing the RELAP5/MOD2 code, ten have been reviewed. The information contained herein is based on those ten assessments.

## 2. IDENTIFICATION AND EVALUATION OF CODE DEFICIENCIES

Assessments were accomplished by comparing code calculated data to a suitable data base. The data base for each study is provided in Table 1. Although these data bases are predominately from subscale experiments, one study was based on plant data recorded during a steam generator tube rupture incident, one was based on critical flow data from a full scale test facility and another was based primarily on a best-estimate void fraction correlation. Two studies were based on data from a test facility simulating a boiling water reactor (BWR). Most studies assessed multiple areas of the

RELAP5/MOD2 code (areas of assessment are included in Table 1). One of the two studies based on data from the BWR type test facility assessed the system initial coolant mass. Since this area of assessment included the initial liquid contained in the separator/condenser component, the assessment may be more applicable to BWR systems. However, the study may have application to calculations of steam generator secondary responses. Other areas of assessment are primarily applicable to PWR systems.

Twenty-eight discrepancies, which were noted by the ten assessment studies reviewed, are listed in Table 2. A discrepancy is noted when a significant difference is observed between the code calculation and the data base. A few of the discrepancies listed were identified by more than one assessment study. Consequently, the list of discrepancies contains less than twenty-eight unique items. Also, some of these discrepancies are related. For example, the discrepancy in the collapsed liquid level and the discrepancy in the vapor fraction profile are related to the same cause, although one was observed in a steam generator downcomer and the other occurred in the core region. A few of the variables with noted discrepancies in Table 2 are not measured directly but are inferred from other measured variables. For example, the time and location of the critical heat flux (CHF) is often inferred from measured fuel/heater rod temperature responses. Figure 1, which compares the heater rod temperature response calculated by the RELAP5/MOD2 code to measured data shows the calculated time of CHF occurring approximately 13 s later than measured. Thus, this set of data show a discrepancy between the calculated and measured time of CHF to be 13 s. Discrepancies in other variables are obtained through the analyses of measured data. Vapor fractions, for example, are obtained from measured coolant conditions. Figure 2 compares a vapor fraction profile calculated by RELAP5/MOD2 with that obtained through analyses of measured differential pressure data in conjunction with measured coolant conditions. The maximum discrepancy among these vapor fraction data is approximately 0.40 occurring at about the 1.5 m elevation (40% of the core height).

Table 2 also contains a list of indicated causes. An indicated cause is the reason given by the assessment study for the noted discrepancy and is generally related to some aspect of the capability of the code to calculate the response observed in the data base. A few studies noted a discrepancy but gave no indicated cause. These are shown on the table. Occasionally, an assessment study suggested more than one possible cause. The one provided in the table, however, was considered to be the primary cause. This list of indicated causes was reviewed for code deficiencies. However, not all indicated causes in Table 2 were considered or evaluated as potential code deficiencies. In a few cases, a selected input or the input model for a particular component was given as an indicated cause. These are identified by footnote and eliminated from consideration. Those remaining were evaluated as potential code deficiencies. The evaluation process considered the following:

(1) Sufficient support to qualifying the cause as a code deficiency,
(2) The frequency that an indicated cause was given, and
(3) Possible interrelationships among indicated causes.

Several of the indicated causes listed in Table 2 were eliminated because the information provided by the assessment study was insufficient to adequately support the item as a code deficiency (these are identified on Table 2 by footnote).

The number of references made to a particular cause was also a consideration in identifying and qualifying code deficiencies. Multiple references to a potential deficiency suggest a higher probability that the deficiency actually exists. For example, CHF correlations were cited on three occasions as the cause for discrepancies observed in fuel/heater rod thermal responses. Although the evaluation of each individual case indicated that additional information would be needed to fully support each as a code deficiency, the CHF correlations in RELAP5/MOD2 were eventually identified as a deficient area. On occasion, conflicting results were observed among assessments. One assessment study provided data showing the critical flow calculated for saturated low-quality conditions was in good agreement with measured data. Another assessment, however, provided data comparisons showing RELAP5/MOD2 calculated critical flows that was approximately 15% lower than measured. (The 15% results after adjusting the calculated data to a discharge coefficient of 1.0.) Although, the data base for these two assessment studies were from different test facilities, the quality of the discharge coolant was essentially the same. System pressures were different. Relatively large uncertainties can occur in measuring coolant flow and it is possible that the uncertainty in the flow data from the two test facilities were significantly different. Consequently, the conflicting results observed in the discrepancies in the critical flow between two assessment studies could possibly be reconciled by considering the uncertainty in the measured data. It was noted, however, that several RELAP5/MOD2 assessment calculations simulating loss of coolant accidents (pipe breaks) found it necessary to input, or recommended the input of, discharge coefficients other than 1.0. The discharge coefficient input to RELAP5/MOD2 modifies the simulated break flow area by a factor equal to the coefficient. Thus, a discharge coefficient other than 1.0 does not represent the true geometry. A discharge coefficient less than 1.0, however, may be justified because of two-dimensional effects, e.g., vena-contracta, which is not considered by the one dimensional RELAP5/MOD2. Discharge coefficients greater than 1.0 represents a nonphysical situation and signifies a possible deficiency in the critical flow models. Consequently, the number of assessment studies using or recommending discharge coefficients other than 1.0 were included with those citing critical flow as the indicated cause and the RELAP5/MOD2 critical flow models and/or correlations were identified as an area of deficiency.

Possible interrelationships among indicated causes were also considered in identifying code deficiencies. This aspect of the evaluation process is similar to item 2 above in that the credibility of a code deficiency increases when a relationship between two or more indicated causes is established. An example is an argument linking the excessive ejection of liquid to interphase drag. The ICAP assessment study citing excessive liquid ejection as a cause was based on boil-off data from a test facility consisting of a bundle of electrically heated rods enclosed in a circular

shroud placed in a vertical cylindrical pressure vessel. The shroud was closed at the bottom but open at the top. Thus, no physical barrier exists to prevent liquid from being carried with the steam flow out of the shroud and removed from the test section. A similar but independent assessment of RELAP5/MOD2[4], also based on boil-off and reflood test data, but from another test facility, showed RELAP5/MOD2 was calculating a collapsed liquid level in the core region to be less than measured and suggested the calculation of excessive liquid entrainment where the liquid was being carried from the test section by vapor flow. The RELAP5/MOD2 interphase drag correlation for the bubbly/slug flow regime was replaced with another and the calculation rerun. The collapsed liquid level obtained from the second calculation was in better agreement with the test data and it was deduced that the standard RELAP5/MOD2 code calculates too much liquid entrainment because of excessive interphase drag in the bubbly/slug flow regime. Based on this, it was concluded that excessive liquid ejection cause indicated by the ICAP assessment study was related to excessive interphase drag.

Based on this review and evaluation process, the following deficiencies in the RELAP5/MOD2 code were identified:

Interphase Drag

Critical Mass Flow

Critical Heat Flux

These identified code deficiencies have strong connections to safety issues. A foremost safety issue is fuel rod cladding integrity during postulated accidents. The three identified areas of deficiency influences the maximum cladding temperature during many accident situations and that influences cladding integrity. Consequently, the three identified code deficiencies are being given special attention in the development of the next version of the RELAP5 code (RELAP5/MOD3). Although RELAP5/MOD2 will form much of the RELAP5/MOD3 code, a development effort will initiated to revise the calculational models and correlations related to these code deficiencies.

The reviewed ICAP studies assessed several aspects of these code deficiencies. For example, one assessment study noted excessive interphase drag in the bubbly/slug flow regimes, whereas another study noted a large drop in the interphase drag when the vertical stratified flow model was implemented. Still another suggested the discrepancy noted in critical flow resulted from a feedback between the input discharge coefficient and the critical flow solution, whereas another suggested the discrepancy resulted from thermal nonequilibrium effects occurring in the discharge nozzle, a phenomena not considered by the RELAP5/MOD2 models. In addition, the time of core dryout discrepancy was noted on three occasions with two different aspects of the CHF correlation given as the indicated cause. It is anticipated, therefore, that the modifications to the RELAP5/MOD2 models necessary to resolve the three identified code deficiencies for the development of RELAP5/MOD3 may involve relatively large areas of the code.

## 3. USER GUIDELINES

Another distinct part of reviewing ICAP code assessment studies is the extraction and evaluation of user guidelines. User guidelines are recommendations intended to improved code usage and are generally based on user experience. For example, a user guideline may recommend an input model that reduces the problem computer time without jeopardizing the quality of the calculated results. One primary criteria was imposed for the selection of user guidelines, i.e., the guideline must be supported by calculated results. Figure 3, an example of a supporting calculation, is a comparison of core dryout response or trajectory (defined as the lowest dryout location in the core as a function of time) calculated with a core model consisting of 6 axial fluid cells versus 24 cells. This data comparison shows that 6 axial fluid cells provides essentially the same dryout response as 24 cells and thus, forms the basis for a user guideline. User guidelines are also evaluated to determine if restrictions or precautions need to be applied. If a calculation is sensitive to a change in an input variable, it would be advisable to restrict the use of the guideline over a limited range of that input variable. Although the data in Figure 3 support using 6 versus 24 axial cells, the discrepancy between the two input models was observed to increase significantly with decreasing system pressure. The system pressure for the data in Figure 3 was 4 MPa. Hence, a guideline based on these data should be restricted over a limited range of system pressure. User guidelines extracted from the ten reviewed ICAP assessment studies are listed below in two categories: (1) those user guidelines confirmed by calculation and evaluation, and (2) suggested user guidelines that have not necessarily been confirmed, i.e., nonconclusive guidelines. Those in category 1 include suggested restrictions on their application.

Category 1 - Confirmed User Guidelines:

1. No benefit is realized by explicitly modeling discharge piping or nozzles with length-to-diameter ratios less than four ($L/D < 4$).

2. Loop pipe connections to the reactor vessel should be modeled using the cross flow option.

3. Two radial nodes in thin (thickness $\leq$ 3 mm) fuel/heater rod cladding produce essentially the same temperatures as models with a greater number of nodes. (Less than 0.5 K difference for two versus ten nodes.)

4. Essentially the same boil-off rates (responses) were obtained with 6 axial fluid cells as with a 24 cell model. Application should not be considered for system pressures < 4 MPa.

Category 2 - Nonconclusive User Guidelines:

1. An acceptable more efficient steady-state calculation may be obtained by relaxing the convergence criteria or using the transient option.

2. A discharge coefficient of approximately 0.8 should be applied for the calculation of critical flow of saturated steam.

## 4. SUMMARY AND ICAP FUTURE

In the time since RELAP5/MOD2, Cycle 36 was released as a frozen version of the code, numerous assessment studies have been carried out under the auspices of the ICAP. These assessments have provided much information in identifying code deficiencies and the formulation of user guidelines. In addition, errors in the coding were found and in some cases corrections provided. Also, some code improvements were suggested. More specifically, as a result of ten ICAP code assessment studies, three areas of the RELAP5/MOD2 code have been identified as being deficient and four user guidelines have been extracted for sharing with the user community.

The review and evaluation of ICAP code assessment studies will continue. The code improvement plan includes, on a prioritized basis, a complete review and reevaluation of the three identified areas of code deficiency. Currently, several ICAP members and the USNRC are co-sponsoring the development of RELAP5/MOD3, with special attention being given to the three identified code deficiencies. As a result, RELAP5/MOD3 will be an improved thermal hydraulic computer code capable of more accurate simulations of postulated reactor accidents and thus, will be an enhanced safety analysis tool for the evaluation of PWR systems.

## 5. REFERENCES


1. V. H. Ransom, et al. RELAP5/MOD2 Code Manual, NUREG/CR-4312, EG&G-2396, August 1985.

2. Guidelines and Procedures for the International Code Assessment and Applications Program, NUREG-1271, April 1987.

3. Compendium of ECCS Research for Realistic LOCA Analysis, NUREG-1230, April 1987.

4. G. Th. Analytis and M. Richner, Implementation and Assessment of a New Bubbly/Slug Flow Interfacial Friction Correlation in RELAP5/MOD2/36.02, EIR Report, TM-32-86-10, January 1986.

TABLE 1. ICAP CODE ASSESSMENT STUDIES (REVIEWED)

| STUDY NO. | BASIS OF ASSESSMENT | AREAS OF ASSESSMENT |
|---|---|---|
| 1. | Steam generator tube rupture incident at the DOEL-2 plant | a. Steam generator liquid level<br>b. Vapor condensation<br>c. Natural circulation |
| 2. | OECD-LOFT Small Break (0.4%) Experiment LP-SB-03 | a. Critical heat flux<br>b. Fuel thermal response |
| 3. | MARVIKEN critical flow data. | a. Critical flow (Subcooled, saturated steam and low-quality two-phase) |
| 4. | FIX-II Loss-of-Coolant (31% split-break) Experiment 3027. | a. Two-phase wall friction<br>b. Critical heat flux<br>c. Flow regime selection process |
| 5. | Royal Institute of Technology dryout experiments | a. Critical heat flux<br>b. Post-CHF thermal response |
| 6. | FIX-II Loss-of-Coolant (200 % double-ended break) Experiment 5061. | a. System depressurization<br>b. Critical heat flux |
| 7. | THETIS boildown experiments. | a. Core boil-off rates<br>b. Interphase drag |
| 8. | Best-estimate vapor fraction correlation and limited test data. | a. Interphase drag |
| 9. | OECD-LOFT Small-Break (0.4%) Experiment LP-SB-03. | a. Steam generator liquid level<br>b. Reflux heat transfer<br>c. Fuel thermal response<br>d. Vapor condensation |
| 10. | OECD-LOFT Small Break (1.0%) Experiment LP-SB-01. | a. Critical mass flow<br>b. Vertical stratified flow |

TABLE 2. ICAP CODE ASSESSMENT STUDIES - SUMMARY OF DISCREPANCIES AND CAUSES

| STUDY NO. | NOTED DISCREPANCY | INDICATED CAUSE |
|---|---|---|
| 1. | a. Liquid level swell in steam generator downcomer | -Excessive interphase momentum transfer (interphase drag) |
| | b. Steam generator pressure response | -Flow regime/heat transfer selection process (1) |
| | c. Erratic natural circulation | -Form-loss coefficients (2) |
| 2. | a. Time of core dryout | -Core modeling limited to one dimension (3) |
| | b. Fuel heat up rate | -No rod-to-rod radiation (1&3) |
| 3. | a. Step increases in critical flow for saturated steam | -Discontinuity in sonic velocity at phase boundaries |
| | b. Critical flow for saturated steam | -Discharge coefficients (2) |
| | c. Atypical critical flow response to input discharge coefficient | -Feedback between discharge coefficient and critical flow solution |
| | d. Critical mass flow for subcooled liquid | -Discharge coefficient (2) |
| 4. | a. Core pressure drop | -Two-phase friction losses (1) |
| | b. Time of core dryout | -Critical heat flux correlations |
| | c. System initial (steady-state) coolant inventory | -Spray droplet diameter and fall velocity (1) |
| 5. | a. Location of CHF | -Critical heat flux correlations |
| | b. Magnitude of CHF | -Critical heat flux correlations |
| | c. Discontinuities in critical heat flux | -Iteration on wall temperature and critical heat flux |
| | d. Transition boiling | -None stated |
| 6. | a. Break flow/system depressurization (system initial coolant mass) | -Spray droplet fall velocity (1) |
| | b. Time of core dryout | -Dryout correlation dependence on vapor fraction |
| 7. | a. Core dryout level response | -Excessive liquid ejection |
| | b. Vapor fraction profiles | -Interphase drag models |
| | c. Oscillation in vapor fraction at steady-state | -Periodic application of vertical stratified flow model |

TABLE 2. (CONTINUED)

| STUDY NO. | NOTED DISCREPANCY | INDICATED CAUSE |
|---|---|---|
| 8. | a. Vapor fraction/two-phase density | -Interphase drag models |
| 9. | a. Steam generator initial liquid level | -Excessive steam entrainment (interphase drag) |
| | b. Fuel thermal response | -Modeling of core (2) |
| | c. Accumulator injection rate | -Excessive vapor condensation (1) |
| | d. Reflux heat transfer | -None stated |
| 10. | a. Subcooled critical mass flow | -Thermal nonequilibrium effect in discharge nozzle |
| | b. Sudden draining of upper plenum and hot leg liquid | -Application of vertical stratified flow model |

1. Insufficient information and/or analyses to support as a code deficiency.
2. Input related.
3. Beyond the intended capability of the code.

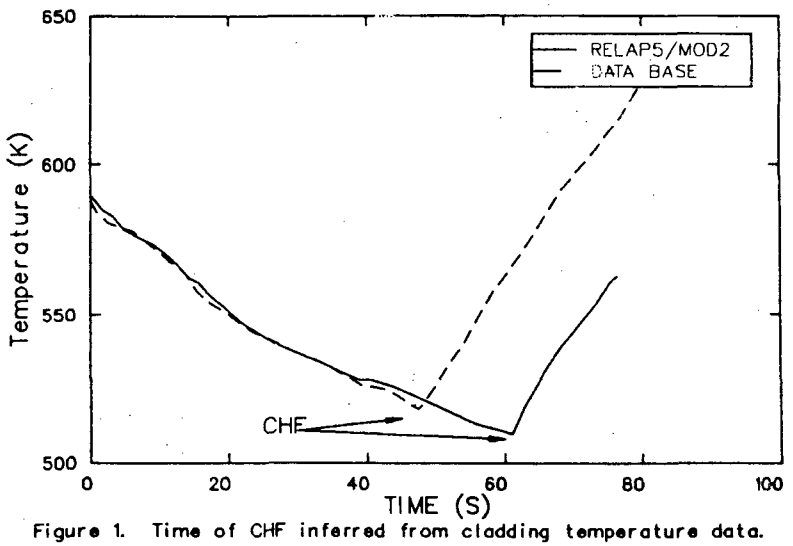


Figure 1. Time of CHF inferred from cladding temperature data.

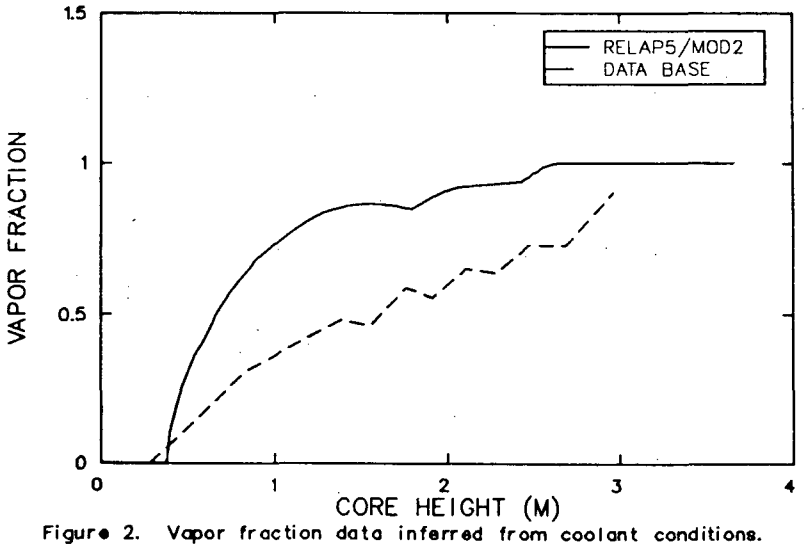


Figure 2. Vapor fraction data inferred from coolant conditions.

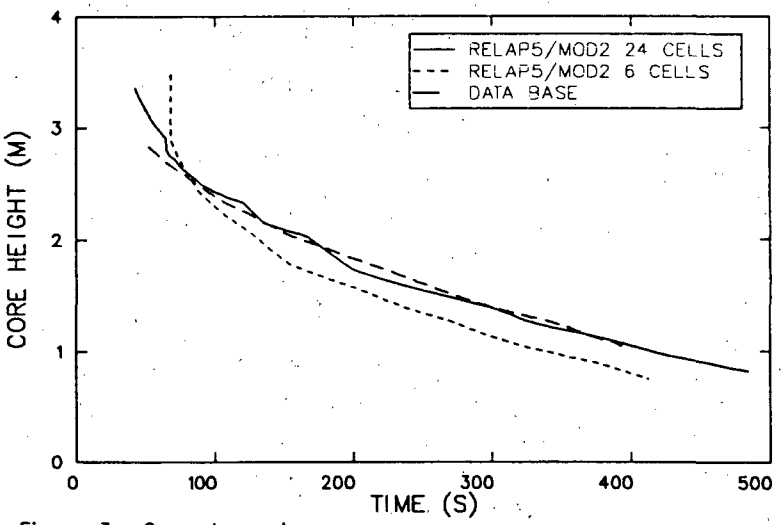


Figure 3. Core dry-out responses.

# RELAP5/MOD3 DEVELOPMENT PLAN AND STATUS

W. L. Weaver III
Idaho National Engineering Laboratory
EG&G Idaho, Inc.

RELAP5/MOD3 is a pressurized water reactor (PWR) system analysis code being developed jointly by the U.S. Nuclear Regulatory Commission (USNRC) and a consortium consisting of several of the countries that are members of the International Code Assessment Program (ICAP). The objective of the RELAP5/MOD3 code development program is to develop a code suitable for the analysis of all transients and postulated accidents in PWR systems including both large and small break loss of coolant accidents (LOCA's) as well as the full range of operational transients.

Prior to forming the RELAP5/MOD3 development consortium, the members of the ICAP program performed assessment calculations using "frozen" versions of the RELAP5/MOD2 code. The results of these assessment calculations were sent to the Idaho National Engineering Laboratory (INEL) for the correction of code errors and for the evaluation of code performance to determine the causes of code deficiencies. In accordance with the rules of the ICAP program, code errors were corrected with the issuance of a new "frozen" code version, while code deficiencies were logged and remained uncorrected in the several "frozen" versions of RELAP5/MOD2. As the list of code deficiencies grew and with the desire of the USNRC and ICAP program members to extend the mission of the RELAP5/MOD2 code to include the analysis of large break LOCA's, the RELAP5/MOD3 code development program was developed and initiated. Table I contains a list of the phenomena and code models that will be addressed by the RELAP5/MOD3 development program. In contrast to the ICAP program, where the participants only performed assessment calculations, several of the RELAP5/MOD3 consortium members will develop, code and test code improvements. Depending upon the particular circumstances, the coding and associated documentation will be sent to INEL for incorporation into RELAP5/MOD3 by personnel at INEL or the individual model developer will come to INEL for incorporation and testing of the model. In addition to listing the areas for code improvement for RELAP5/MOD3, Table I also shows

Work performed under DOE Contract No. DE-AC07-76ID01570 for the U.S. Nuclear Regulatory Commission.

the countries and/or organizations that have proposed to submit code improvements developed by their own staff members. The list of tasks and/or code improvement areas was developed from the results of assessment calculations performed by the ICAP program or as a result of the application of the TRAC-PF1 and TRAC-PF1/MOD1 codes in the 2D/3D Program. Areas where TRAC was weak and where the code models in TRAC and RELAP5 are similar were included as development tasks. In particular, the last three code improvement tasks listed in Table I were identified through this process.

In addition to tasks for the improvement of code accuracy, several other tasks have been included in the RELAP5/MOD3 development plan. These are listed in Table II and include improvements to code performance (i.e. code speed) through vectorization and some parallelization and enhanced code portability to ease the installation of RELAP5/MOD3 on a variety of computer systems. Computers and operating systems that will be supported and on which the RELAP5/MOD3 code will be tested by the INEL staff include CRAY (UNICOS), CYBER (NOS/VE), IBM 3090 (MVS), and VAX (VMS/ULTRIX). Finally, RELAP5/MOD3 development will be governed by a quality assurance plan that will allow the complete documentation of each line of coding added to the program source. This program will be an extension of the QA procedure under which the TRAC-BWR codes were developed at INEL.

The important milestones in the RELAP5/MOD3 development plan are listed in Table III. An interim version of the code containing all of the capabilities listed in Tables I and II will be released along with an updated input description by June 1, 1989. The code will then undergo a period of developmental assessment ending with the release of the "frozen" version of RELAP5/MOD3 by September 30, 1989. The code manuals as well as a revised "models and correlations" document will then be issued in draft form by January 1, 1990.

As shown in Table III, a base version of RELAP5/MOD3 was released to the consortium members on April 1, 1988. This release was to facilitate the development of code improvements by the consortium members. This code version, RELAP5/MOD3, Cycle 0, was based on the latest "frozen" version of RELAP5/MOD2 (Cycle 36.06). Several new process models were included in this code version as well as coding changes related to vectorization and to code portability. This code version was implemented on a VAX (VMS) system by Yankee Atomic Electric Company, on an IBM 3090 (VM) by Northeast Utilities, and on a CYBER 990 (NOS/VE) by KWU of the Federal Republic of Germany. The code modifications generated by each organization to implement RELAP5/MOD3 on these systems have been given to INEL and will be implemented into a single code version to enhance code portability.

The new process models incorporated into the base version of RELAP5/MOD3 address the first two tasks listed in Table I, countercurrent flow limiting (CCFL) and interfacial shear in rod bundles[1]. The countercurrent flow limiting model implements the Bankcoff[2] form of the flooding correlation, which can be specialized into either a Wallis or a Kutatelade form through user input. This model is user activated at each

junction and functions as a flow limit model analogous to the critical flow model, limiting the amount of liquid downflow based on the vapor upflow rate. The model as implemented replaces the difference momentum equation by the CCFL correlation whenever the CCFL criterion is exceeded. Figure 1 shows the results of a simple "thought" problem that was used to check the implementation of the CCFL model. The test case consists of a vertical test section into which liquid is injected at a constant rate at the top, and air is injected at an ever increasing rate at the bottom of the test section. Figure 1 shows the evolution of the flow at a junction in the test section at which the CCFL model is activated. Also shown is the CCFL "flooding" curve as defined by the correlation. The liquid velocity initially increases as the liquid flows down the test section due to gravity. Eventually the air upflow rate reaches a high enough value to limit the downflow rate of liquid (Point 1). As the air flow rate increases further, the correlation limits the downflow rate of liquid, reducing the liquid flow rate as the air flow increases until the liquid downflow velocity goes to zero (Point 2) and then reverses, causing co-current upflow. This simulation demonstrates that the model has been implemented correctly into the code.

The other process model improvement consisted of the implementation of the Bestion[3] correlation for interfacial friction in rod bundle as recommended by Analysis of the Paul Sherer Institute in Switzerland. Since a new interfacial friction model[4] for all types of geometry (i.e., large and small pipes, rod bundles) is being developed by the Central Electricity Generating Board (CEBG) at the United Kingdom (which will replace the Bestion correlation), results from the Bestion correlation as implemented in the base version of RELAP5/MOD3 are not shown. Preliminary results from the new drag package as proposed by the CEGB are shown in Figure 2 which is a reproduction of Figure 3 of Reference 4. Figure 2 shows the axial void profile in the THTF rod bundle test 3.09.10K at steady state conditions. The figure shows the maximum and minimum of the measured data at each elevation as well as two simulations using RELAP5/MOD2 with and without the new interfacial friction model. The figure shows that the new interfacial drag package produces significantly better predictions of the void profile. The simulation of other tests shows similar improvement.

Since the release of the base version of RELAP5/MOD3, several other process model improvements have been received from consortium members. These include a new criterion for the transition between stratified and dispersed flow in horizontal pipes received from JAERI and a pipe offtake model developed by the UK. These models are being implemented and tested at the INEL. Work currently in progress by personnel at the INEL is focusing on problems with the implementation of the critical flow model as described by Studsvik (Sweden) and the JRC (Ispra), the critical heat flux correlation as critiqued by Becker of Sweden as well as others, as well as code implementation problems in the wall condensation regime in the wall heat transfer package.

In summary, a plan for the development of RELAP5/MOD3 has been prepared to address the known shortcomings in RELAP5/MOD2 as well as investigate potential shortcomings in the application of RELAP5/MOD3 to large break LOCA's based on the application of other thermal-hydraulic analysis codes to large break LOCA tests in the full-scale facilities of the 2D/3D Program. The development of RELAP5/MOD3 has begun and is on schedule to release an interim version of RELAP5/MOD3 in June of 1989.

## REFERENCES


1. R. A. Riemke, Report on CCFL and Interphase Drag Models for RELAP5/MOD3, EGG-TFM-8012, EG&G Idaho, Inc., Feb 1988

2. S. G. Bankoff, R. S. Tankin, M. C. Yuen, and C. L. Hsieh, "Countercurrent Flow of Air/Water and Steam/Water Through a Horizontally Perforated Plate", International Journal of Heat and Mass Transfer, Vol 24, 1981 p. 1381 - 1385

3. D. Bestion, "Interfacial Friction Determination for the 1D-6 Equation Two Fluid Model Used in the CATHARE Code," European Two-Phase Flow Group Meeting, Southhampton, England, June 3-7, 1985.

4. J. M. Putney, Proposals for Improving Interphase Drag Modelling for the Bubbly and Slug Regimes in RELAP5, RD/L/3306/R88, PWR/HTWG/p(88)597, Central Electricity Generating Board, United Kingdom, June 1988

TABLE I RELAP5/MOD3 MODEL DEVELOPMENT TASKS

Counter-Current Flow Limiting
Interfacial Shear Modeling (UK)
Critical Heat Flux
Reflood Heat Transfer (PSI)
Critical Flow Modeling
Inception of Vertical Stratification
Inception of Horizontal Stratification (JAERI)
Pipe Offtake Model (UK)
Metal-Water Reaction (Sweden)
Fuel Mechanical Model (Sweden)
Radiation Heat Transfer Model (Sweden)
Improvements to Non-condensible Gas Model
Condensation in Horizontal Pipes
Downcomer Penetration and ECCS Bypass
Upper Plenum Deentrainment

TABLE II RELAP5/MOD3 PERFORMANCE ENHANCEMENT TASKS

Code Speedup
Vectorization (CRAY)
Parallelization (CRAY)

Code Portability
CRAY, CYBER, IBM, VAX

TABLE III RELAP5/MOD3 MILESTONES

| | |
|---|---|
| April 1, 1988 | Release base version of RELAP5/MOD3 (Cycle 0) |
| June 1, 1989 | Release interim "frozen" version of RELAP5/MOD3 |
| September 30, 1989 | Complete Developmental Assessment and release "frozen" version of RELAP5/MOD3 |
| January 1, 1990 | Issue draft code manuals and draft models and correlations document. |

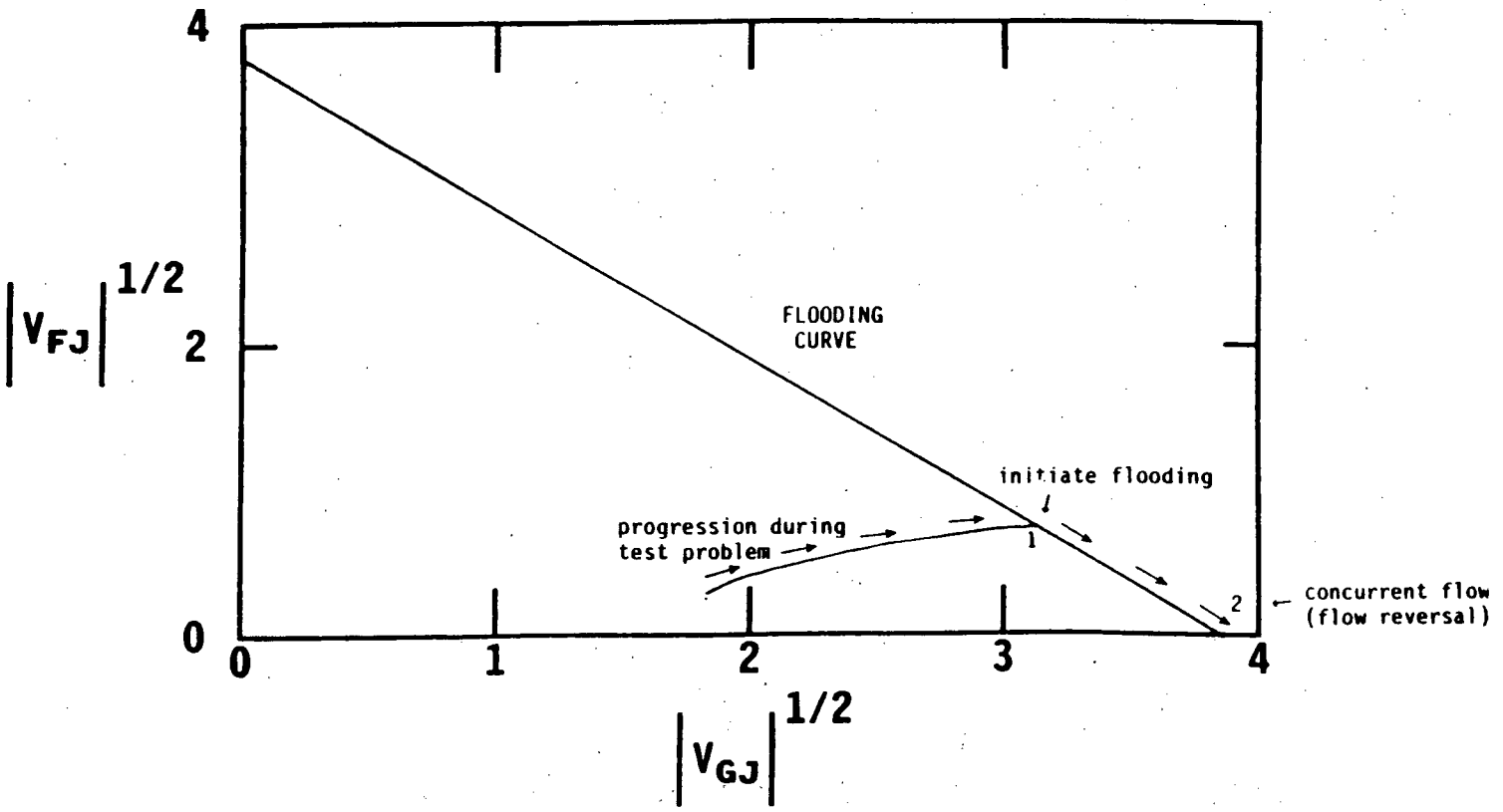


Figure 1. Velocity Trajectory for CCFL Thought Problem

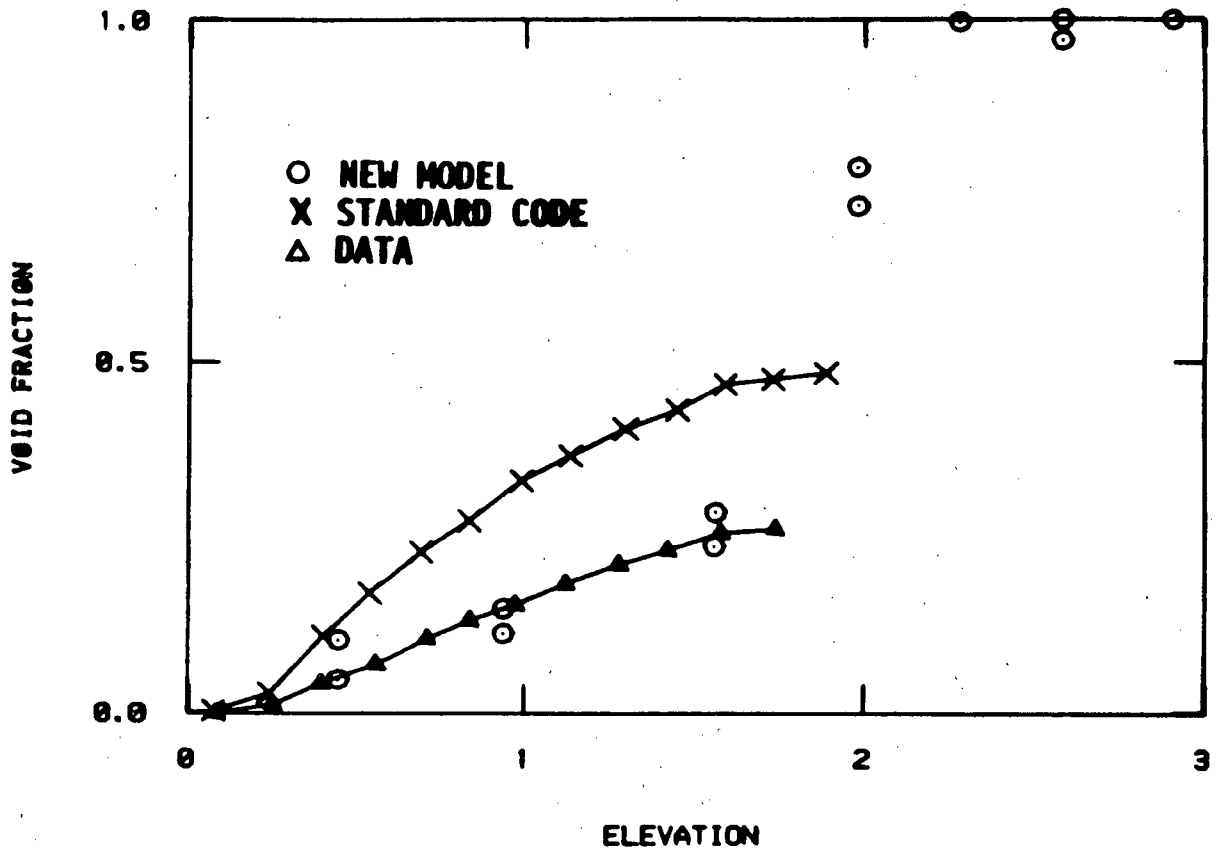


Figure 2. Axial Void Profile for THTF Test 3.09.10K

# TRAC-PF1/MOD2 STATUS AND PLANS

by

J. W. Spore, R. G. Steinke, R. A. Nelson, M. W. Cappiello, and R. Jenks

## ABSTRACT

The development of the TRAC-PF1/MOD1 code was completed in July 1988 with the release of Version 14.4. A TRAC-PF1/MOD2 code deveopment plan addresses code deficiencies identified in the MOD1 code in order to provide an accurate and defensible tool that can be used to simulate large-break loss-of-coolant accidents (LOCAs), small-break LOCAs, and operational transients. The MOD2 code development plan is an international cooperative effort that includes contributions from Los Alamos National Laboratory, Idaho National Engineering Laboratory (INEL), Japanese Atomic Energy Research Institute (JAERI), Cray Research, Central Electricity Generating Board (CEGB), and United Kingdom Atomic Energy Authority (UKAEA).

## INTRODUCTION

Version 14.4 of the TRAC-PF1/MOD1 code was released as the final version of MOD1 in July 1988. The MOD1 interfacial constitutive package in Version 14.4 was improved to provide accurate predictions of downcomer bypass, emergency core coolant (ECC) penetration, upper-plenum modeling, and hot-leg and cold-leg plugging and oscillations. Developmental assessment calculations were performed with Version 14.4 on the Cylindrical-Core Test Facility (CCTF) Run 14; Akimioto's condensation experiment; Upper-Plenum Test Facility (UPTF) Tests 5, 6, 8, 11, and 12; and Small-Core Test Facility (SCTF) Test 703. The MOD2 code development effort has paced the MOD1 maintenance and completion effort by implementing most of the MOD1 error corrections and code improvements into the MOD2 code.

## MOD1 STATUS AND HISTORY

Version 12.1 of the TRAC-PF1/MOD1 code was released in January 1985 as the frozen version for the purpose of independent code assessment. The principal features of the MOD1 code are as follows.

1. A variable-dimension fluid-dynamics model that can analyze three-dimensional (3D) cylindrical geometry flow in the vessel component and one-dimensional (1D) flow in the primary- and secondary-side flow loops. A 1D or two-dimensional (2D) Cartesian-coordinate geometry vessel component can be specified by the user to reduce computational costs.

2. The nonhomogeneous, nonequilibrium, full two-fluid, six-equation hydrodynamics model describes steam-water flow. A horizontal stratified-flow model for 1D flow, a seventh field (mass) equation that evaluates a noncondensable-gas field, and an eighth field equation that tracks solutes in the liquid phase are provided in the TRAC hydrodynamics model.

3. A flow-regime-dependent, constitutive-equation package describes the transfer of mass, momentum, and energy between the steam-water phases and the heat transfer to those fluid phases from the system structure.

4. Flow-regime-dependent wall-to-fluid heat-transfer correlations are obtained from a generalized boiling curve based on local conditions.

5. A two-dimensional, fuel-rod conduction model includes a dynamic fine-mesh rezoning capability that can resolve both bottom-flooding and falling-film quench fronts.

6. Consistent analysis of the entire accident sequence is performed, including initial conditions and blowdown, refill, and reflood phases of a loss-of-coolant accident (LOCA). A complete range of break sizes as well as operational transients can be simulated.

7. Component and functional modularity allow the user to model virtually any PWR design or experimental configuration. There are component models for accumulators, breaks, fills, cores, pipes, pressurizers, pumps, steam generators, tees, turbines, valves, and vessels with associated internals.

8. Signal-variable parameters, control-block function, and action-controlling trips give the TRAC user the flexibility to model virtually any PWR or experimental control and protection system.

Since Version 12.1 was released, additional error-correction/user-convenience update sets have been included. These correction sets contain modifications to the TRAC code that can be grouped into three categories. The first group encompasses error corrections to logic and models less frequently activated by the code or users; the

second group addresses user-convenience changes that deal with input and output; and the third group provides new model options that require user input to activate.

One of the updates in the first group is a major error correction that improves the interfacial-condensation model by limiting its rate of change to what is observed experimentally. This replaces the old method of logrithmic-averaging the old- and new-time values, which yields time-step-size-dependent results. A major user convenience added to TRAC is the multiple-component connections to a single cell of a vessel component. This allows the user to reduce the vessel noding for transients in which multidimensional flow in the vessel is not significant, thereby saving computational costs. Another significant user convenience is the self-initialization capability. This capability allows the user to input user-desired initial conditions (that is, cold-leg fluid temperature, primary- and secondary-side mass flow rates, pressure upstream of a valve, and so on); built-in controllers applied to user-selected component actions force the TRAC steady-state solution to those user-specified conditions.

A major model improvement added to TRAC that is activated by input is the counter-current flow limiting (CCFL) model. The user is given the option of specifying a flooding curve for any location within the vessel component for which there are experimental data. Because the effective interfacial shear for flooding or the CCFL condition is strongly dependent on geometry, TRAC uses this input-specified flooding curve to infer an effective interfacial shear for those locations where the user has flooding data. If no flooding data are available, TRAC uses its default interfacial-shear package, which will predict a typical flooding curve for a straight pipe. In addition, a new separator model has been implemented into the MOD1 code. This new separator model can simulate a separator with a constant efficiency. It uses the GE mechanistic model or user-specified performance curves to predict the carryunder and carryover.

Version 14.3 of TRAC-PF1/MOD1 was released in August 1987. Version 14.3 was used as the base code on which the code scaling applicability and uncertainty (CSAU)[1] methodology was applied. As data became available from the UPTF, it became apparent that additional work on the TRAC constitutive models would be required for large-scale geometries. It was decided that another version of the MOD1 code would be developed and released that addressed some of the large-scale constitutive-model deficiencies.

Version 14.4 of the TRAC-PF1/MOD1 code was released as the final version of MOD1 in July 1988. In Version 14.4, the MOD1 interfacial constitutive package was improved to provide accurate predictions of downcomer bypass, ECC penetration, upper-plenum modeling, and hot-leg and cold-leg plugging and oscillations. Developmental assessment calculations were performed with Version 14.4 on CCTF Run 14; Akimioto's condensation experiment; UPTF Tests 5, 6, 8, 11, and 12; and SCTF Test 703. A comparsion of the TRAC-PF1/MOD1 calculations for Version 14.3 and 14.4 for one of the UPTF downcomer refill tests is shown in Fig. 1. The improvement in the

calculated downcomer-refill is apparent from this figure. The improved model in Version 14.4 forces the interfacial-shear model into the annular-flow regime for the downcomer geometry only. This model is not appropriate for all scales; therefore, additional development is required for a general model that can be applied at all scales for a full range of thermal-hydraulic conditions. The development of a general model for down- comer penetration at all scales and for a full range of thermal-hydraulic conditions is continuing for the MOD2 code.

## MOD2 STATUS

In addition to keeping current with the MOD1 changes, the MOD2 develop- ment effort has resulted in unique enhancements and model improvements. The MOD2 code has the following additional improvements that are not available in the MOD1 code.

1. 3D-Two-Step numerics apply the 1D-Two-Step numerics in MOD1 to the 3D hydro- dynamics solution. The 3D-Two-Step numerics allow the 3D-vessel component to take larger time steps during a relatively slow transient (for example, a small- break or operational transient). The MOD1 3D vessel semi-implicit numerics require smaller time steps and thus a longer computation time for relatively slow transients.

2. Partial vectorization of the vessel-component thermal-hydraulic solution allows the TRAC code to take advantage of the vector-mode computation of Cray or Cray-like computers. Preliminary testing indicated a 10-20% speed-up for a large-break LOCA (LBLOCA) calculation resulting from partial vectorization of the 3D solution.

3. Inversion of the vessel data base results in coding for the vessel component that is easier to read and maintain. In addition, it results in arrays that vectorize computation in the axial direction.

4. A generalized heat-structure component allows the user to couple any hydro cell with any other hydro cell in the TRAC model by way of a heat-transfer path. Also, multiple heat-structure components may be coupled to a given hydro cell. This component provides the capability for increased accuracy in modeling steam generators, vessel internal structures, and so on.

5. Implementation of the Electric Power Research Institute (EPRI) drift-flux correlation results in significant improvements in the axial void-fraction profile when compared with the CCTF Run 14 data. Additional testing and development of improved core-reflood heat-transfer models is in progress.

6. During some recent application work, it was found that the MOD1 momentum-flux solution was inaccurate at smooth flow-area changes. A conserving momentum-flux solution[2] has been developed for the the MOD2 code. The capability to convect momentum flux across a plenum-component cell also has been added.

7. As part of the MOD1 Q/A document[3] development, it was found that the 1D and 3D wall-shear models were inaccurate and inconsistent. The MOD2 wall-shear models were made consistent. In addition, the MOD1 wall-shear model was improved in the MOD2 code with fixes to the laminar-flow model, inclusion of the surface-roughness effect in the turbulent regime, and improvements to the two-phase pressure-drop model.

8. The MOD1 valve model for flow resistance through a partially-closed valve is not based on either theory or experimental data. A new MOD2 valve flow-resist- ance model was developed based on experimental data for partially closed globe valves.

9. The Gauss-Seidel numerical solution for the 3D-vessel pressure-matrix equation was observed to be inaccurate for small breaks and operational transients. This inaccuracy typically would be observed as a mass error in the vessel component. This problem was solved in the MOD2 code by eliminating the Gauss-Seidel method and replacing the remaining full-matrix-inversion algorithm with the more efficient Capacitance-Matrix method[4] for solving the vessel pressure- and stabilizer-matrix equations. The Capacitance-Matrix method is 10 times faster than the vectorized full-matrix-inversion algorithm and faster than the Gauss-Seidel method for a 300- to 400-cell vessel.

10. The MOD1 subcooled-boiling model is inaccurate and has a questionable justification. The subcooled-boiling model was replaced in the MOD2 code with the TRAC-BWR subcooled-boiling model,[5] which has been tested to be accurate and is based on published correlations.

11. The capability to input the magnitude and general orientation of the vessel component for the gravitational-acceleration vector was added to the MOD2 code. This option was developed to address horizontal-tube vessel modeling requirements encountered during a recent application of the MOD2 code.

12. A 60-, 120-, or 180-degree rotational symmetry in cylindrical geometry option was added to the MOD2 code. This option was developed to allow for flexible vessel noding and significantly reduced noding if loop and vessel behavior is rotationally symmetric.

A simple 1D-flow test problem that exercises several of the MOD2 code features is given in Fig. 2. The figure shows a series of pipe and vessel components with

changing flow area and elevation. The capability to orient the vessel component horizontally is required for this simple test problem to be analyzed. In addition, the multiple-vessel capability is required. The results for pipes replacing the vessels and for three different vessel-component orientations in this geometry are given in Fig. 3. This is a plot of the Bernoulli expression vs cell locations down the flow channel. If all of the flow-area changes are smooth with no irrreversible flow losses and if there is no wall friction (by defining the hydraulic diameter large), then the Bernoulli expression should be constant in value according to Bernoulli's equation[6] for single-phase, 1D flow. The MOD2 code with flow-area ratios applied to the momentum-convection term gives a constant-valued Bernoulli expression, whereas the MOD1 code without flow-area ratios produces significant error and nonconservation of momentum as the flow area and elevation change. This calculation was repeated with the 3D-vessel component modeling 1D flow and oriented in the x, y, and z directions to demonstrate that the solution is the same for the vessel component in all three directions. In addition, the calculation was repeated with the vessel components replaced by pipe components of the same geometry to verify that the vessel-component solution is consistent with the pipe-component solution. Consistency between the solutions from the 3D-vessel component and 1D components is not realized with the MOD1 code. In addition, successful consistency calculations for single-phase flow have been performed between the TRAC- PF1/MOD2 pipe, plenum, tee, and vessel components on another parallel-flow-channel test problem. This was possible for the plenum component by applying the new optional capability for convecting momentum flux across the plenum-component cell.

The CSAU MOD1 input-data file was converted to the slightly modified MOD2 input-data format (with an automatic converter program called GOCVRT) to investigate the calculative speed-up of 3D-Two-Step numerics in the MOD2 code in comparison to the MOD1 code without 3D-Two-Step numerics. The peak-clad temperatures (PCT) for the CSAU nominal LBLOCA calculation is given in Figs. 4 to 6. Version 14.3 tends to calculate a lower blowdown PCT because the Version 14.3 steady-state calculation had a cold-leg temperature that was too high. This high cold-leg temperature resulted in early flashing of the cold-leg fluid which resulted in an early blowdown and cooldown of the core from 4 to 7 s. The Version 14.4 and MOD2 steady-state calculations determined an accurate initial cold-leg temperature that resulted in a less significant core blowdown and cooldown and a slightly higher PCT. Because of the improved down- comer models in Version 14.4 and the MOD2 code, the core reflood starts ~10 s earlier than in the Version 14.3 calculation. Both Version 14.4 and the MOD2 code calcula- tions tend to reflood the core faster than the Version 14.3 calculation. The MOD2 core is essentially quenched at 50 s into the transient.

The CPU times for these three calculations is show in Fig. 7. The MOD2 code runs much faster than either of the MOD1 code versions. The major difference between these calculations is the 3D-Two-Step numerics allowing the time-step size to increase significantly over the material-Courant limit. In this input deck, several very small hydro

cells in the vessel component were used to simulate leakage-flow paths between the downcomer and upper-plenum regions. The material-Courant limit in these small hydro cells kept the MOD1 time-step size small, whereas it had no effect on the MOD2 time-step size. The MOD2 time-step size tended to be controlled by how rapidly the LBLOCA transient progressed.

An international cooperative effort to continue development of the MOD2 code through the International Code Assessment and Application Program (ICAP) was started in January 1988. The planned MOD2 development tasks are described in the following section.

## PLANNED MOD2-CODE IMPROVEMENTS

The objective of the MOD2 development plan is to address identified significant code deficiencies in the MOD1 code in order to provide an accurate and defensible tool that can be used to simulate large-break LOCAs, small-break LOCAs, and operational transients. The MOD2 code development plan is an international cooperative effort that includes contributions from Los Alamos, INEL, JAERI, Cray Research, CEGB, and UKAEA. The following MOD2 development contributions are planned.

### 1. Post-CHF Heat Transfer and Quenching

The current TRAC reflood heat-transfer model would be rewritten, removing Forslund-Rohsenow[7] and any nonphysical models or fits. Defensible correlations for inverted annular-film boiling would be included into the TRAC code. These correlations may depend on distance from the quench front or separate thermal-boundary-layer solutions. In addition, improvements in the dispersed-droplet film-boiling heat-transfer regime would be investigated including the possible addition of a cold-surface model. Several organizations currently are developing new TRAC post-CHF models: UKAEA, CEGB, JAERI, and Los Alamos.

### 2. Interfacial Drag Under Wet-Wall Conditons

The CEGB[8] has recommended a set of correlations for use under wet-wall conditions for high flow rates, low flow rates, upflow, downflow, rod bundles, and small-, intermediate-, and large-diameter pipes. Los Alamos has implemented the CEGB recommendations for rod bundles and large-diameter pipes. The other CEBG recommendations are under investigation.

### 3. Improved Offtake Model for Horizontal Pipes

The UK has recommended a model for branching flow at tees. The purpose of the model is to determine the amount of vapor pull through or liquid entrainment that occurs in a horizontal pipe that has a smaller pipe or break located on its side, bottom, or top. This model would be included directly into the TRAC tee component. This same model has been implemented into the RELAP5 code and experience from that implementation and assessment will be used.

### 4. Implicit Axial-Conduction Model

JAERI has agreed to provide to Los Alamos a new fully-implicit axial-conduction model for the MOD2 code. The MOD1 and MOD2 moving-mesh axial-conduction solution is currently explicit. This explicit solution can result in small-time step sizes as the axial-mesh size is reduced in the vicinity of the quench front.

### 5. Code Speed-Up

JAERI has agreed to investigate various methods for speeding-up the TRAC code calculations. For example, smoothing the constitutive correlations between flow regimes has proven successful in speeding up other thermal-hydraulic codes.

### 6. Elimination of Nonstandard Fortran

JAERI has agreed to assist in eliminating nonstandard Fortran. Cray Research developed a set of updates for the MOD1 code that eliminated a significant portion of the nonstandard Fortran. Los Alamos has extended those updates to the MOD2 code.

### 7. Vectorization and Parallelization

Cray Research has agreed to assist in eliminating nonstandard Fortran.

### 8. Documentation on RELAP5/MOD3 Improvements

INEL will provide Los Alamos with documentation on the RELAP5/MOD3 improvements as they become available.

### 9. Improved Critical-Flow Model

Los Alamos plans to investigate improvements in the TRAC critical-flow model for nonequilibrium, two-phase flow conditions.

## 10. Implementation of the ANS 1979 Decay-Heat Standard

Los Alamos plans to develop a simple model for the estimation of nuclear parameters for mixed-oxide fuels. The current model allows for the simulation of power history effects, for the delayed-neutron effect from actinides, and for the recommended decay-heat model. The current model will be modified so that the 1979 standard is the default model.

## 11. Implementation of the CCFL Model Into the MOD2 Code

Los Alamos plans to implement the MOD1 CCFL model into the MOD2 code.

## 12. General Model for Interfacial Heat Transfer

Los Alamos plans to develop a general model for interfacial heat transfer for all flow regimes. The Q/A document and the assessment of TRAC-PF1/ MOD1 Version 14.4 indicate that the current correlations can be modified to predict the dominant phenomena for a few geometries and a few flow regimes. However, to be successful for a wide range of geometries and flow regimes, specific models and correlations must be developed and implemented for specific geometries and flow regimes. For example, the current correlation for condensation assuming St = 0.02 is adequate for cold-leg condensation at high steam-flow rates. However, at lower steam-flow rates, this correlation tends to predict too much condensation.

## 13. Improvements in Time-Step Control

Los Alamos plans to develop new algorithms for the adjustment of time-step size. These algorithms would monitor the rate of change with respect to the important independent variables and the number of outer iterations required to converge a given time-step solution.

## 14. Improved Accumulator Model

Los Alamos plans to set up several test cases for the MOD2 code using the LOFT accumulators and the ROSA-IV separate-effects accumulator tests. Calculations would be performed to determine whether the new models in the MOD2 code still resulted in oscillations and excessive vapor entrainment. It is anticipated that the MOD2 code will not have these same problems; however, if it does, fixes would be proposed.

## 15. Break-Flow Time-Step Sensitivity

The MOD2 interfacial-shear time averaging already has been changed to reduce time-step size dependency on the results. Los Alamos plans to rerun the UPTF- test sensitivity calculations to determine whether any time-step sensitivity is still pre- sent.

### 16. Flexible Vessel Noding

The capability to finely node the downcomer and coarsely node the core region is a code improvement that was identified as being important during the CSAU methodology application to the TRAC-PF1/MOD1 code. The MOD2 code currently has that capability with the exception that the plenum component would have to be improved. With the MOD2 code, the downcomer would be modeled as an eight theta-sector vessel component. Each azimuthal theta sector would have a short-pipe connection to the lower plenum that would be modeled with a plenum component. An additional pipe component would be used to model the lower portion of the lower plenum. The core region would be modeled with one or two theta sectors and with one or two radial rings. A generalized heat-structure capability would have to be programmed for the plenum component. A long-term development effort would be to eliminate the short pipes and connect the vessel component directly to the plenum component.

Current plans for MOD2 development include completing the developmental assessment and draft documentation by the end of October 1989.

## MOD2 ENHANCEMENTS TO BE CONSIDERED FOR FY 1990

### 1. Hot-Channel Option

The capability to model through input a hydraulically coupled hot channel would be developed and tested in the MOD2 code.

### 2. Direct Moderator Heating

The simple model given below would be used to define direct moderator heating as the core-average liquid fraction and fission power change.

$$DMH = a_f \; f_{dmh} \; P_{fp} \; , \tag{1}$$

where

DMH = direct moderator heating (W),
$a_f$ = core-average liquid fraction,
$f_{dmh}$ = input-specified fraction of the total core fission power that is direct moderator heating when the core has no void, and
$P_{fp}$ = total core fission power (W).

The direct-moderator-heating-energy source term would be included in the

liquid-phase energy equation and distributed in the core region according to the power-shape factors that the user inputs.

### 3. Pump-Energy Source Term

Coding would be developed and tested to include the pump-energy source term directly in the PUMP-component energy equations.

### 4. Mechanistic Pump Model

A mechanistic pump model similar to the EPRI pump model would be developed and implemented into the TRAC code. The no-slip assumption at the pump exit would be eliminated.

### 5. Development of a General Model for Downcomer Penetration at All Scales

A general model for predicting the flow regime in the downcomer for both small- and large-scale experiments would be developed and implemented into the TRAC code.

### 6. Improved Fuel-Rod Model (Including Swelling and Rupture Models)

The generalized heat-structure component in the MOD2 code would be modified to keep track of two different gap widths. One gap width ( $Dz_{gap}$) would be a uniform gap width so that the 2D-conduction solution would continue to be solved on an orthogonal 2D-coordinate geometry. The other gap width would be the axial- and time-varying gap width from which $h_{gap}(r,t)$ would be calculated. The $h_{gap}(r,t)$ would be transformed into an effective gap conductance to be used in the fixed geometry of the 2D-conduction solution:

$$k_{gap}(r,t) = h_{gap}(r,t)\ Dz_{gap} \ . \qquad (2)$$

Using Eq. (2) ensures that the heat flux across the uniform gap width is the same as the heat flux across the axial- and time-varying gap width. The heat flux across the uniform gap width is

$$q_{gap} = k_{gap}(r,t)\ \{T_{fuel} - T_{clad}\}/\ Dz_{gap} \ , \qquad (3)$$

and the heat flux across the axiall- and time-varying gap width is

$$q_{gap} = h_{gap}(r,t)\ \{T_{fuel} - T_{clad}\} \ . \qquad (4)$$

Simplified models for swelling and rupture would be investigated for inclusion into the TRAC code.

### 7. Improved Steam-Generator Heat-Transfer Models [Specifically for Babcock & Wilcox (B&W) Steam Generators]

Develop and implement a mechanistic model that estimates the surface area wetted by the auxiliary feed for a B&W steam generator and determines the appropriate wall heat-transfer coefficient.

### 8. Generalized 1D Component

A generalized 1D component would be developed that would allow for vectorization of the 1D routines. The 1D data base would be inverted, and the 1D and 3D data bases would be made consistent.

### 9. Geometry-Dependent Flow-Regime Map

As part of the work on TRAC-PF1/MOD1 Version 14.4, geometry-dependent flow-regime maps already have been developed for the downcomer, lower plenum, upper plenum, and hot leg. This work would continue based on available data and the identification of problem areas.

### 10. Input Preprocessor

As part of a small business contract for the NRC, Energy Incorporated (EI) has developed the capability to generate and modify TRAC input-data files using an IBM/PC. This capability has the user-friendly features of inputting data into prepared forms with data descriptions and screen editing existing input data. Preliminary testing indicates that the software is not ready for release and some debugging is necessary. In addi- tion, the software has to be changed to handle the slightly modified input-data format of the MOD2 code. Los Alamos is proposing that EI be subcontracted to complete this work.

### 11. Improved CHF Model

The results of the RELAP5 work on the development and implementation of an improved CHF model would be used.

## 12. Complete the Implementation of the TRAC-BWR Separator Model Into the MOD2 Code

INEL, Los Alamos, and UKAEA identified numerical problems with the TRAC-BWR separator model. INEL has developed fixes to address these problems. Los Alamos would implement these fixes and test to verify that the separator model is accurate and robust.

## CONCLUSIONS

The list of development tasks described in this presentation will satisfy the objectives of the MOD2 code development plan. Los Alamos is committed to providing a high-quality, accurate, and defensible MOD2 code.

## REFERENCES


1. Technical Program Group, "Quantifying Reactor Safety Margins-Application of CSAU Methodology to a LBLOCA," EG&G Idaho, Inc. report NUREG/CR-5249 (to be published).
2. R. G. Steinke and J. W. Spore, "Conserving Convected Momentum in the TRAC Motion Equation," Proceedings of the 8th Biennial Cube Symposium, Albuquerque, New Mexico (November 1988).
3. D. R. Liles, J. W. Spore, T. D. Knight, R. A. Nelson, M. W. Cappiello, K. O. Pasamehmetoglu, J. H. Mahaffy, L. A. Guffee, H. J. Strumpf, P. J. Dotson, R. G. Steinke, P. R. Shire, S. E. Greiner, and K. B. Sherwood, "TRAC-PF1/MOD1 Correlations and Models," Los Alamos National Laboratory report LA-11208-MS, NUREG/CR-5069 (September 1988).
4. R. G. Steinke and J. F. Dearing, "Capacitance Matrix Method in TRAC and MELPROG," Proceedings of the ANS Topical Meeting on Advances in Nuclear Engineering Computation and Radiation Shielding," Santa Fe, New Mexico (April 1989).
5. P. Saha and N. Zuber, "Point of Net Vapor Generation and Vapor void Fraction in Subcooled Boiling," Proc. of the Fifth International Heat Transfer Conference 4 (1974).
6. R. B. Bird, W. E. Stewart and E. N. Lightfoot, *Transport Phenomena* (New York, John Wiley & Sons, Inc., 1960) 211-3.
7. R. P. Forslund and W. M. Rohsenow, "Dispersed Flow Film Boiling," J. Heat Trans. 90 (6), 399-407 (1968).
8. J. M. Putney, "Implementation of a New Bubbly-Slug Interphase Drag Model in RELAP5/MOD2," RD/L/FTD 005/M88 (August 1988).

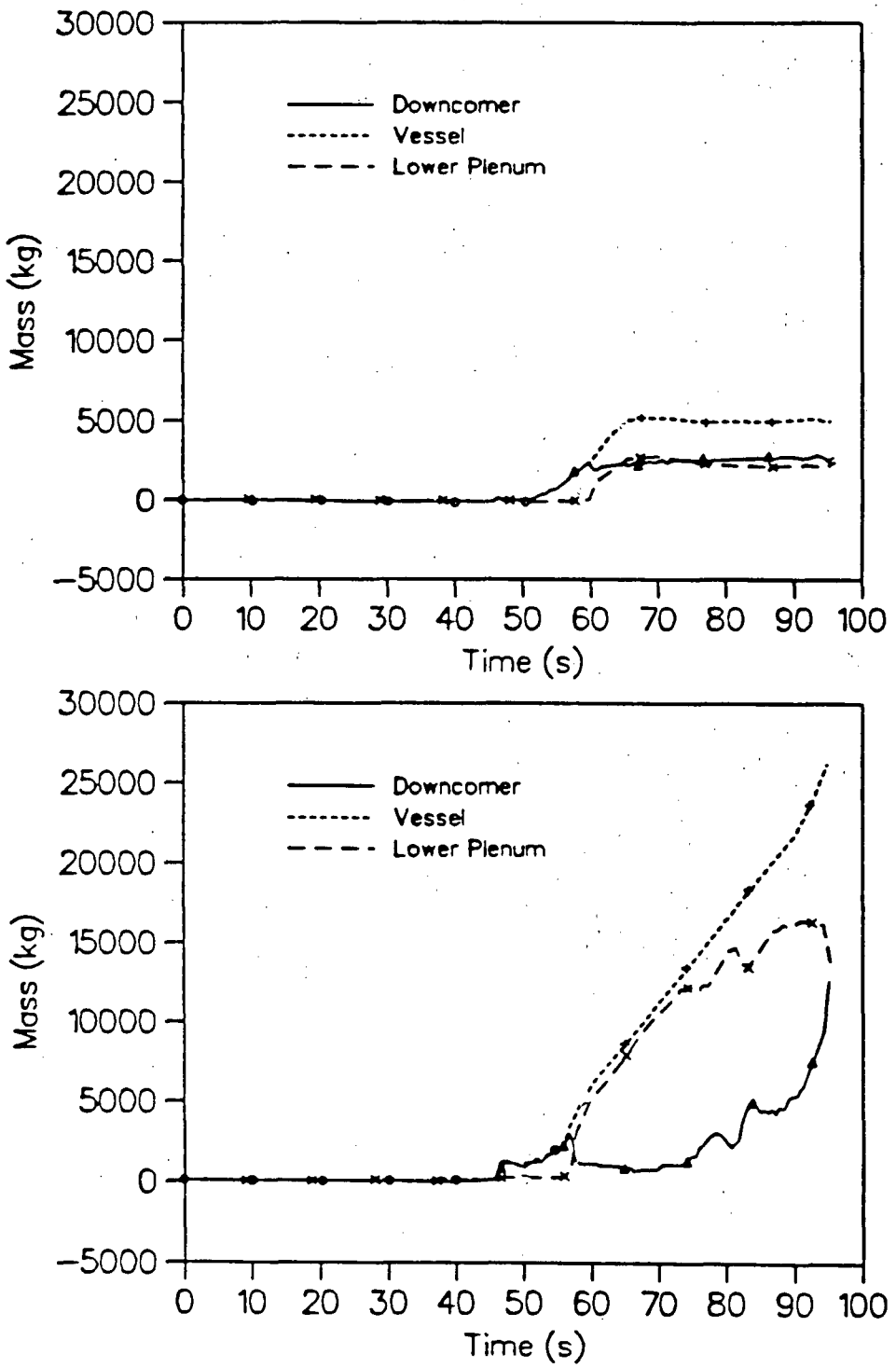


Fig. 1. Comparison of TRAC Versions 14.3 and 14.4 calculations.

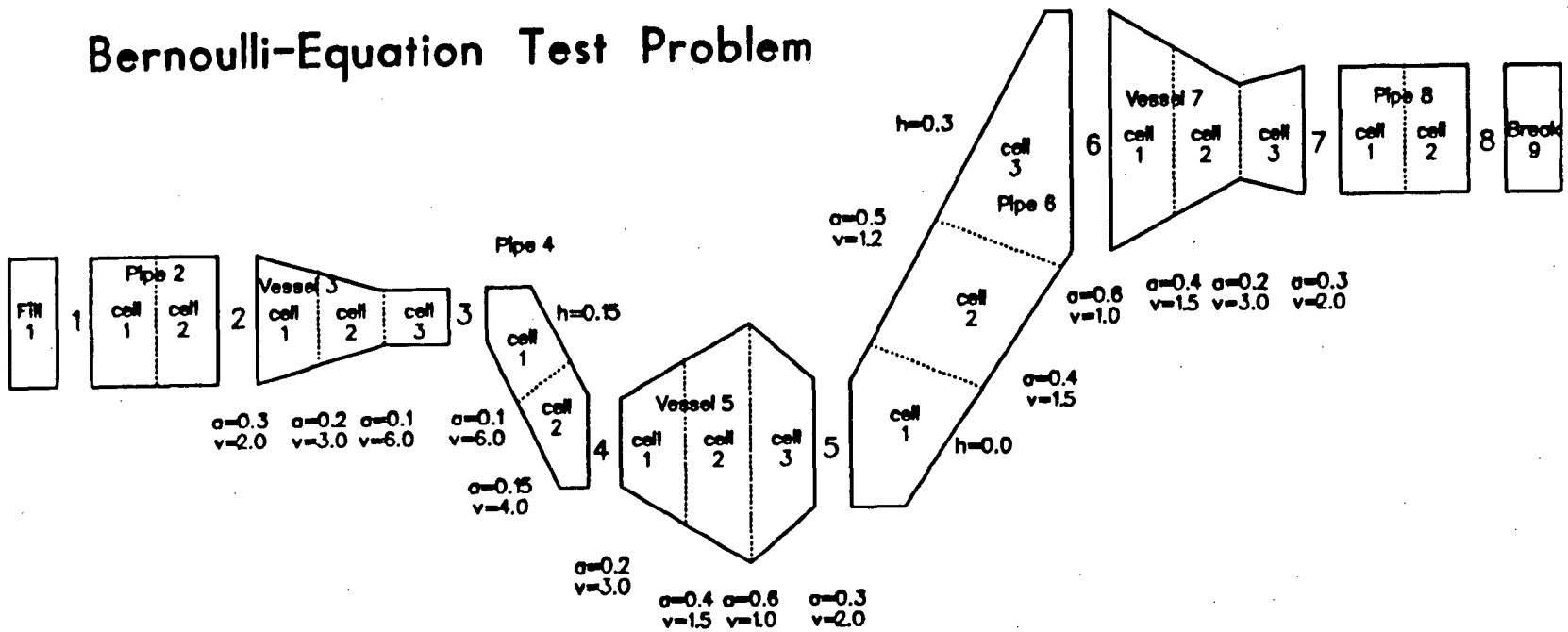


Fig. 2. Simple one-dimensional flow test problem.

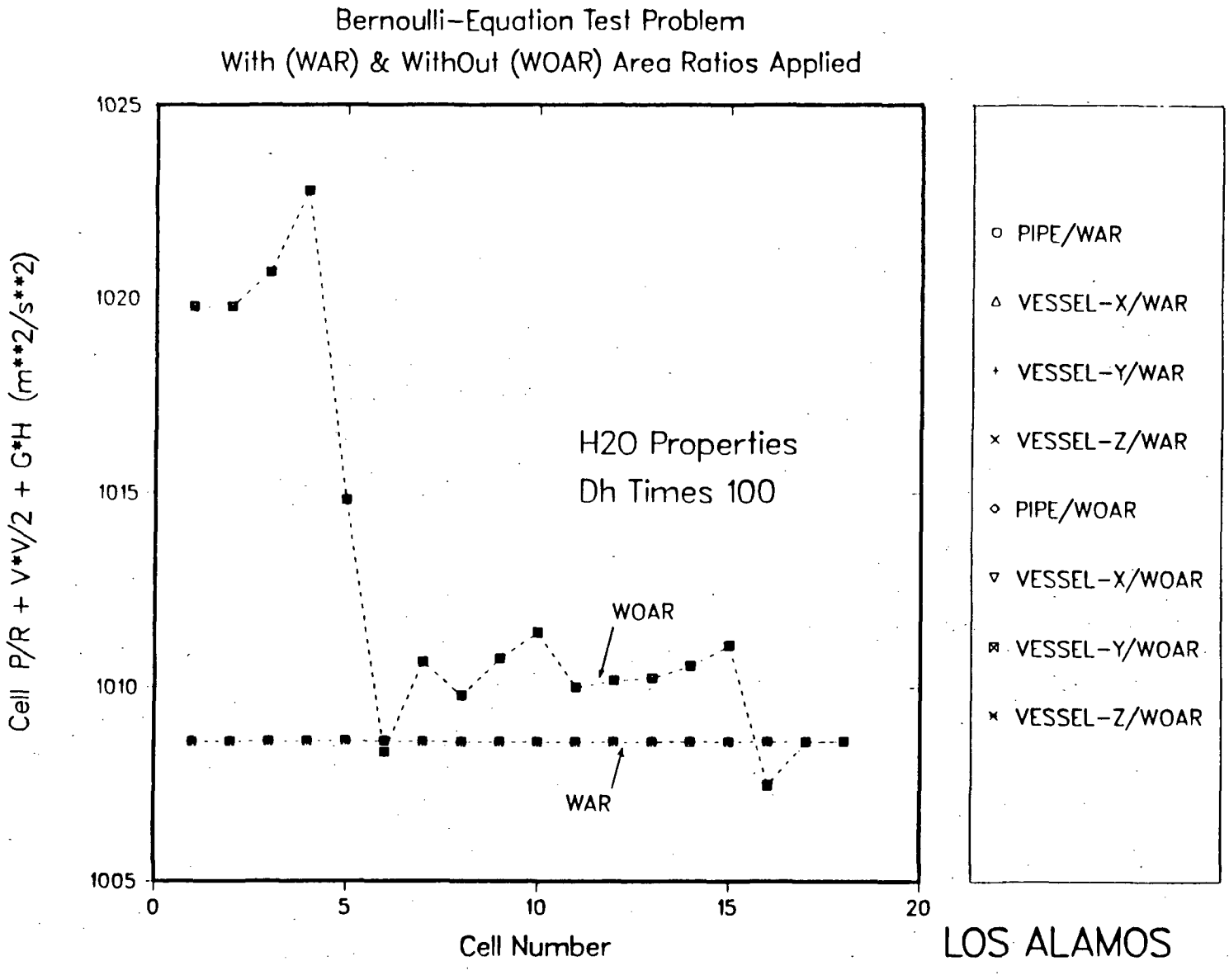


Fig. 3. MOD2 results for simple one-dimensional test problem.

# Mod1 Version 14.3

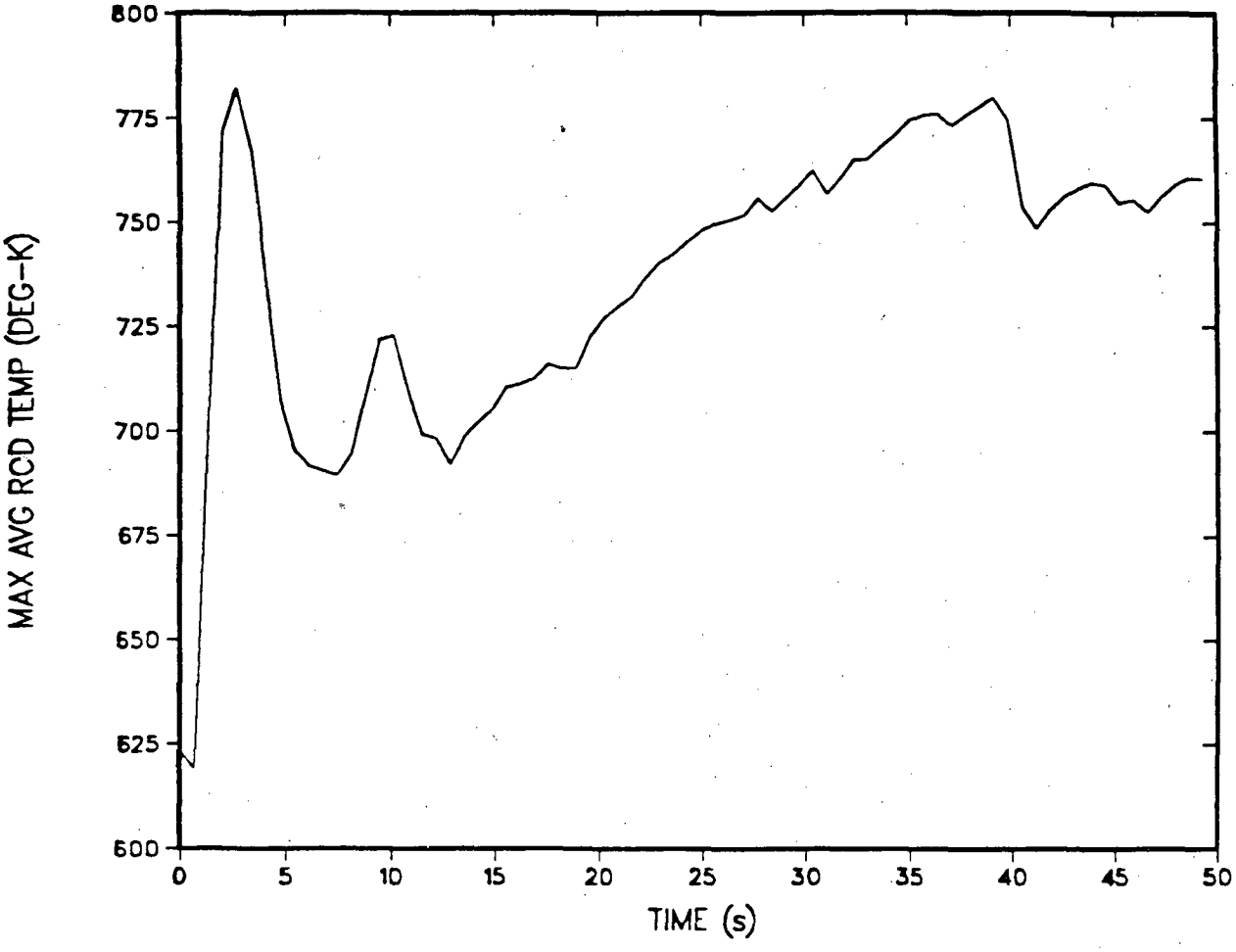


Fig. 4. TRAC-PF1/MOD1 Version 14.3 peak clad temperature for the CSAU LBLOCA calculation.

# Mod1, Version 14.4

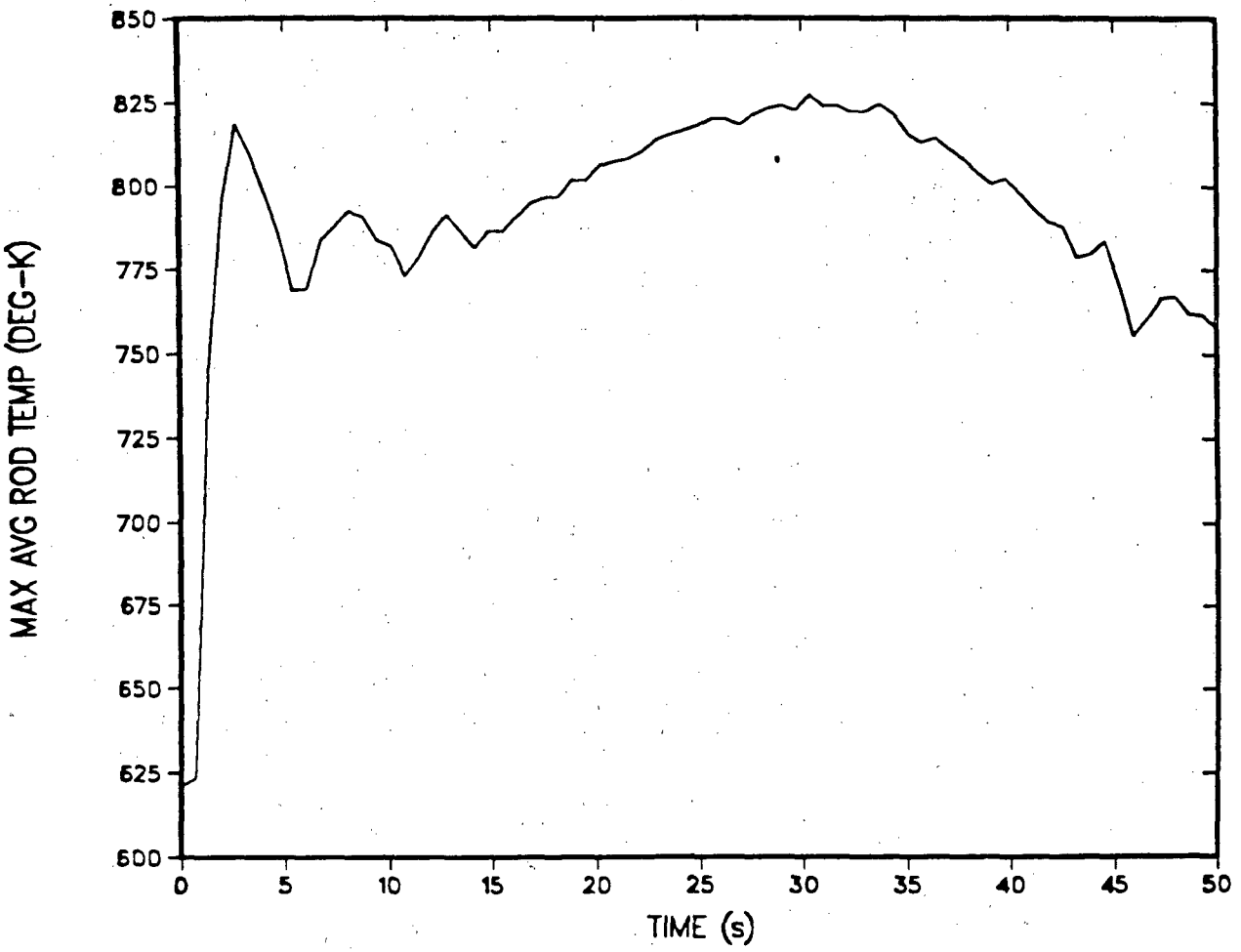


Fig. 5. TRAC-PF1/MOD1 Version 14.4 peak clad temperature for the CSAU LBLOCA calculation.

## Mod2, Version 4.2

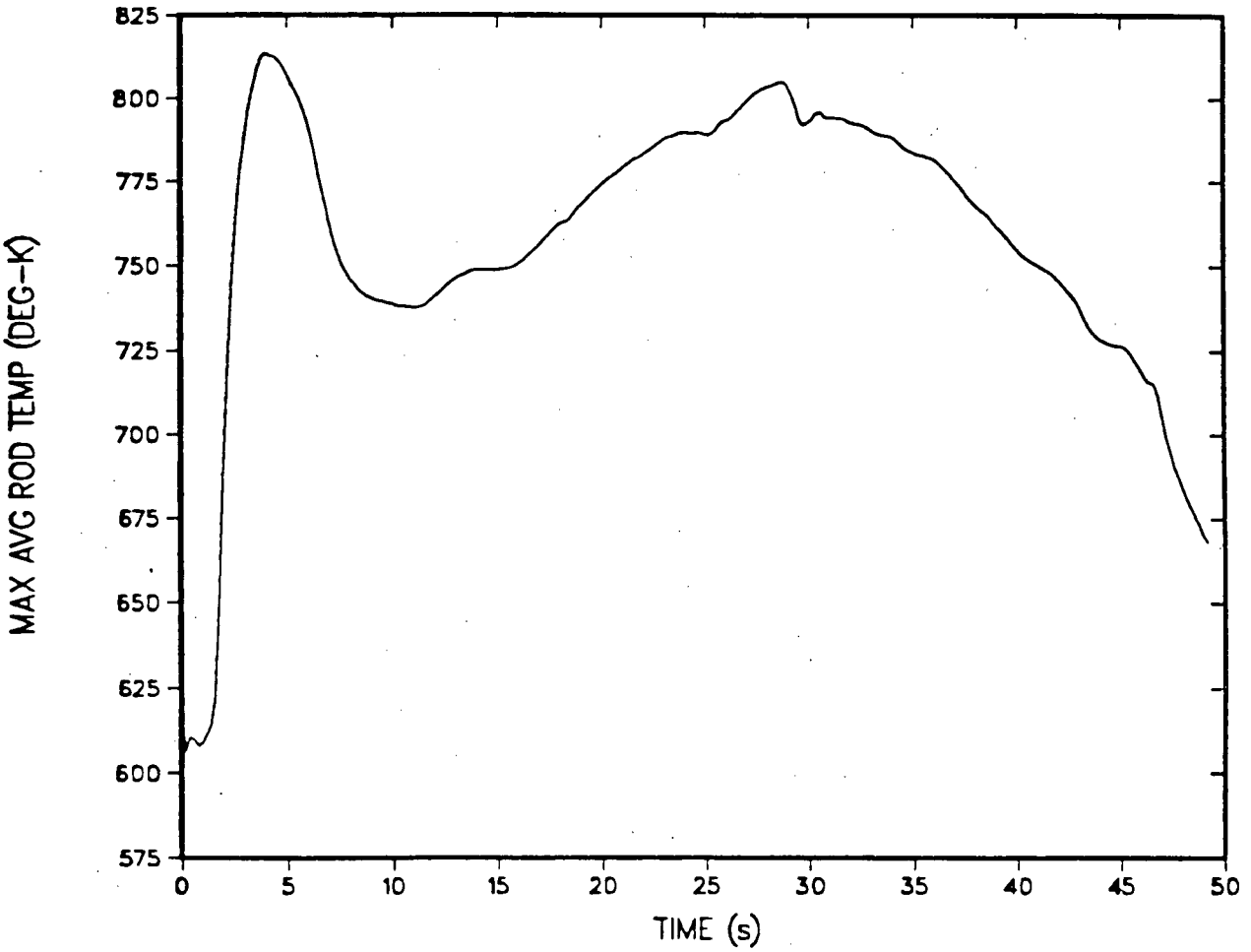


Fig. 6. TRAC-PF1/MOD2 Version 4.1 plus Red Star (~ Version 4.2) peak clad temperature for the CSAU LBLOCA calculation.

## Computer Run Time Comparison

- WPWR LBLOCA, CSAU Input Deck
- 50 Seconds of Transient Time

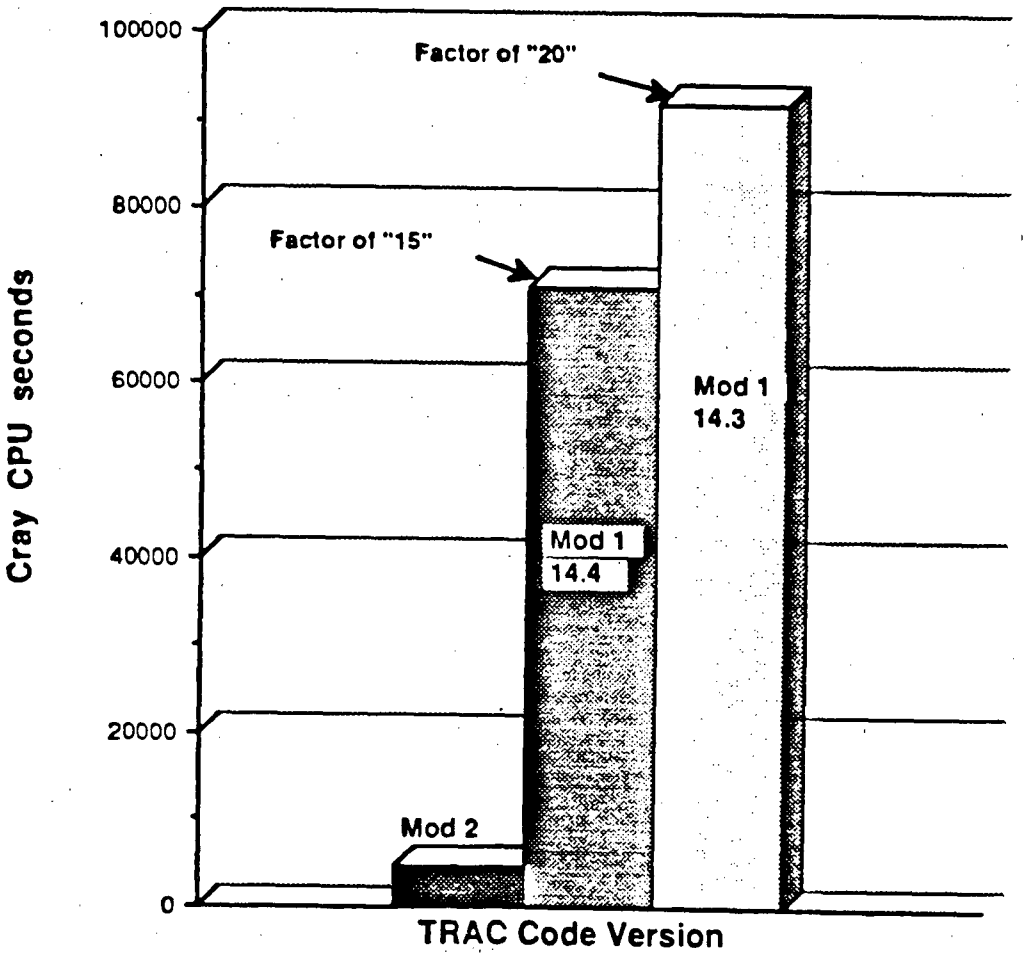


Fig. 7. CPU computer-time comparisons between TRAC-PF1/MOD1 Versions 14.3 and 14.4 and TRAC-PF1/MOD2 Version 4.1.

# Status of ICAP activities in Japan

Yoshio MURAO
Reactor safety research laboratory II
Japan Atomic Energy Research Institute (JAERI)

In Fy 1988, ICAP activities in Japan were started as a cooperative work between JAERI and Japanese industries. Based on the ICAP agreement, forty two assessment calculations are to be performed in Japan by Fy 1991. In Fy 1988, assessment matrix was determined and code installation of USNRC codes was started and almost completed. Eleven assessment calculations were performed with the TRAC-PF1 code. Status of these ICAP activities in Japan will be summarized in this paper.

## 1. Introduction

In Fy 1988, ICAP activities in Japan was started based on the agreement between the USNRC and JAERI. In Japan, forty two assessment calculations will be performed by 1991 for TRAC-PWR, TRAC-BWR and RELAP5 codes with test data from the Cylindrical Core Test Facility(CCTF),[1] the Slab Core Test Facility(SCTF),[2] ROSA-II[3], ROSA-IV[4], ROSA-III[5] and the Two Bundle Loop (TBL).[6] In Japan, the assessment work is performed as a part of the cooperative work between JAERI and Japanese industries listed in Table 1.

Table 1 Participants to ICAP in Japan

PWR group: Kansai Electric Power Co., Kyushu Electric Power Co., Shikoku Electric Power Co., Hokkaido Electric Power Co., Japan Atomic Power Co., Mitsubishi Heavy Industries, Mitsubishi Atomic Power Industries

BWR group: Tokyo Electric Power Co., Hitachi, Ltd. Toshiba Corp.

NFI group: Nuclear Fuel Industries

Japan Atomic Energy Research Institute

As ICAP activities, following works were performed in Japan in Fy 1988:
(1) determination of assessment matrix,
(2) installation of USNRC codes into FACOM and CRAY computers,
(3) preparation of input data for assessment calculations, and
(4) eleven assessment calculations with the TRAC-PF1/MOD1 code.

Status of these ICAP activities will be summarized in this paper.

2. Activities in Fy 1988

Assessment matrix

Based on the ICAP agreement, forty two assessment calculations will be performed in Japan by 1991. The assessment matrix was determined in 1988 as shown in Table 2.

Table 2 Assessment matrix of Japanese calculations

| | LOCA type | TRAC-PWR | | | | RELAP5 | | | | TRAC-BWR | | | | |
|---|---|---|---|---|---|---|---|---|---|---|---|---|---|---|
| | | 88 | 89 | 90 | 91 | 88 | 89 | 90 | 91 | 88 | 89 | 90 | 91 | |
| CCTF | PWR LB | 9 | 1 | | | 5 | | | | 5 | | | | Reflood |
| SCTF | PWR LB | 3 | 5 | 3 | | 1 | | | | 1 | | | | Reflood |
| ROSA-II | PWR LB | | | | | | | 2 | | | | | | Blowdown |
| ROSA-III | BWR LB/SB | | | | | | | | | 1 | 1 | | | Blowdown |
| ROSA-IV | PWR SB | 1 | 1(0) | | | 1 | 0(1) | | | | | | | |
| TBL | BWR LB/SB | | | | | | | | | 1 | 1 | | | Blowdown |
| Total | | 13 | 7(6) | 3 | | 1 | 6(7) | | 2 | 8 | 2 | | | 42 |

With test data from the CCTF and the SCTF, the predictive capability of the TRAC-PWR, RELAP5 and TRAC-BWR codes will be assessed for thermal hydraulic behaviors during reflood, especially for core cooling behaviors. With ROSA-II and ROSA-IV data, the TRAC-PWR and RELAP5 codes will be assessed for the blowdown and integral system behaviors during small-break(SB) or large-break(LB) loss-of-coolant accidents(LOCA) in PWR. With test data from ROSA-III and the TBL, the TRAC-BWR code will be assessed. The assessment matrix covers most of important transients during LOCAs in PWR or BWR.

The assessment work is to be performed by JAERI and Japanese industries. Five assessment calculations are to be performed by PWR group with the TRAC-PWR and RELAP5 codes. Ten assessment calculations are to be performed by BWR group with the TRAC-BWR and TRAC-PWR codes. Five assessment calculations are to be performed by NFI group with the TRAC-PWR and RELAP5 codes. Twenty two assessment calculations are to be performed by JAERI with the TRAC-PWR code, RELAP5 core model and TRAC-BWR core model.

Code installation and input data preparation

In 1988, transmittal magnetic tapes of the TRAC-PF1,TRAC-BF1,RELAP5 and COBRA-TF codes were transferred from the USNRC to JAERI. These magnetic tapes were transferred to Japanese industries by JAERI. The code installation work of USNRC codes was started at JAERI and Japanese industries on CRAY and FACOM computers in 1988. Although several problems were encountered during the installation, the code installation work were completed except for the RELAP5 code on CRAY and the TRAC-BF1 code on CRAY and FACOM computers.

In parallel to the code installation works, input data for assessment calculations are being prepared at JAERI and Japanese industries for CCTF, SCTF, ROSA-III, ROSA-IV and TBL in 1988.

Assessment calculation with TRAC-PF1

Eleven assessment calculations were performed with the TRAC-PF1/MOD1 code in Fy 1988. The assessment calculations include two CCTF 3D system calculations with fine VESSEL model, two SCTF 2D core calculations with 2D fine VESSEL model, six CCTF/SCTF 1D core calculations with coarse VESSEL model and one ROSA-IV system calculation. Analyses of these calculations are being performed through comparisons with test data.

## 3. Preliminary results from assessment calculations

Figure 1 shows the TRAC noding used in CCTF 3D system calculation. Three intact loops of the CCTF are modeled separately as in the facilities. The containment tanks are modeled by two BREAK components by using measured pressure transients. The ECC water injection conditions are specified by FILL components using measured mass flow rates and fluid temperatures. Figure 2 shows a VESSEL noding used in the CCTF 3D system calculation. The pressure vessel of the CCTF is modeled by a VESSEL component with four radial rings, four azimuthal sectors and sixteen levels. The core part corresponds to the axial levels between 2.1 and 5.76 m of the inner three rings.

Figure 3 shows clad temperature transients along a high power rod in a CCTF 3D system calculation for the CCTF base case test. The calculated results show excellent agreement with measured results. The turnaround temperature and quench time are predicted well with the TRAC-PF1/MOD1 code as shown in Fig. 4.

On the other hand, core void fractions showed rather poor agreement with measured results in the TRAC-PF1/MOD1 calculation. Figure 5 shows core void fractions in the CCTF 3D system calculation for the CCTF base case test. The core void fraction is underestimated in the lower part of the core and overestimated in the upper part of the core.

For the system behavior, the TRAC-PF1 code predicted a flow oscillation with a long period, which was not observed in the CCTF tests, as shown in Fig. 6. The flow oscillation seems to be related the boiling in the downcomer and the water carry-over from the upper plenum to hot legs. It is necessary to study more on thermal hydraulic models in downcomer and upper plenum.

Figure 7 shows TRAC noding of the SCTF 2D core calculation. The main objective of the SCTF tests is to study multidimensional thermal hydraulic behaviors during the reflood phase of a PWR LOCA. The SCTF has a full-height, full-radius and one-bundle-width core. The core contains eight 16x16 bundles with about 2000 heater rods in total. The SCTF core is modeled by a VESSEL component with eleven rings, one sector and fifteen levels.

Figure 8 shows clad temperatures at elevation of 1.905 m in a SCTF 2D core calculation for a steep power test. In the steep power test, the highest power was supplied to bundles 3 and 4 with radial peaking factor of 1.2. The radial peaking factor of bundles 7 and 8 was 0.8 in the test. The average power was supplied to the other bundles, that is, bundles 1,2,5 and 6. The TRAC-PF1/MOD1 code predicted excellently the clad temperatures in each power bundle as shown in Fig. 8. The turnaround temperature and quench time are also predicted well by the TRAC-PF1/MOD1 code as shown in Fig. 9.

Figure 10 shows core void fractions at various elevations along a high power bundle in a SCTF 2D core calculation for the SCTF steep power test. The predicted core void fractions show rather poor agreement with measured results.

Figure 11 shows TRAC noding of CCTF 1D calculation. In the calculation, only the core and the upper plenum parts are modeled by a VESSEL component with one ring, one sector and fourteen levels in order to assess the predictive capability of the TRAC-PF1/MOD1 code for parameter effects. In the CCTF 1D code calculation, the core inlet conditions are specified with a FILL component using measured core inlet mass flow rate and fluid temperature. The core power and core outlet pressure are also input as boundary conditions using measured results.

Figure 12 shows a quench envelope from CCTF 1D core calculations for CCTF system pressure effect tests. The calculated results with the TRAC-PF1 code show excellent agreement with measured results. Figure 13 shows a quench envelope from CCTF 1D core calculations for CCTF core power effect tests. The calculated results show excellent agreement with measured results for the core power effect on the quench front propagation. The TRAC-PF1/MOD1 code gives excellent prediction for system pressure and core power effect on clad temperature histories.

Figure 14 shows clad temperatures at various elevations in a CCTF 1D core calculation for the CCTF BE test. BE stands for best-estimate. The CCTF BE test was performed with boundary and initial conditions which were determined based on TRAC calculated results of a Westinghouse PWR using most-probable conditions at Los Alamos National Laboratory.[7] The peak clad temperature at reflood initiation was about 570 K in the CCTF BE test, while it was about 1070 K in the other CCTF tests used in this assessment study. As shown in Fig. 14, very quick quench of heater rods was predicted with the TRAC-PF1 code compared to test results in the CCTF BE test calculation.

Figure 15 illustrates boiling curves and quench behavior.[8] For the boiling transition from film boiling to transition boiling, two limit temperatures are well known; one is homogeneous nucleation temperature and the other is minimum film boiling temperature. In the TRAC code, only the homogeneous nucleation temperature is modeled as a limit temperature for the boiling transition. The limit temperature was calculated to be about 610 K with the correlation in the TRAC-PF1 code. Because of low wall temperature in the CCTF BE test, the quick quench was calculated by the TRAC code. In the CCTF BE test, the low heat transfer due to film boiling was maintained for about 100 s as shown in Fig. 14. It is considered that the clad temperature is higher than the minimum film boiling temperature shown in Fig. 15. It is recommended to model both limit temperatures for boiling transition from film boiling to transition boiling.

## 4. Summary

(1) ICAP activities in Japan were started as a cooperative work between JAERI and Japanese industries in Fy 1988.

(2) In Fy 1988,
  (a) Assessment matrix was determined.
  (b) Code installation of USNRC codes was started and almost completed.
  (c) Eleven assessment calculations were performed with the TRAC-PF1 code.

(3) Total 42 assessment calculations are to be performed in Japan by Fy 1991.

(4) TRAC-PF1 code assessment shows
  (a) excellent PCT prediction,
  (b) excellent prediction of system pressure and core power effects on clad temperature,
  (c) items necessary to be improved:
    - core hydraulic model,
    - quench model at low wall temperature,
    - hydraulic model in downcomer and upper plenum.

## References


(1)Murao,Y.,et al.:Summary of CCTF test results,14-th water reactor safety research information meeting (1986).
(2)Adachi,H.,et al.;Multidimensional effect found in SCTF reflood tests for US/J PWR,15th water reactor safety information meeting (1987)
(3)Adachi,H., et al.:ROSA-II experimental program for PWR LOCA/ECCS integral test,JAERI 1277,March 1982.
(4)For example,Tasaka,K.,et al.:The result of 0.5 % PWR small break LOCA tests in ROSA-IV LSTF break location parameter test series,15th water reactor safety information meeting (1987)
(5)Tasaka,K.,et al.:ROSA-III experimental program for BWR LOCA/ECCS integral simulation tests,JAERI 1307,November 1987.
(6)Naitoh,M.,et al.:Summary of Two-Bundle Loop experimental results, Tenth water reactor safety research information meeting, NUREG/CP-0041,January (1983).
(7)Fujita,R.: Private communication.
(8)Murao,Y.:JAERI-M 10000, March 1982,(in Japanese).

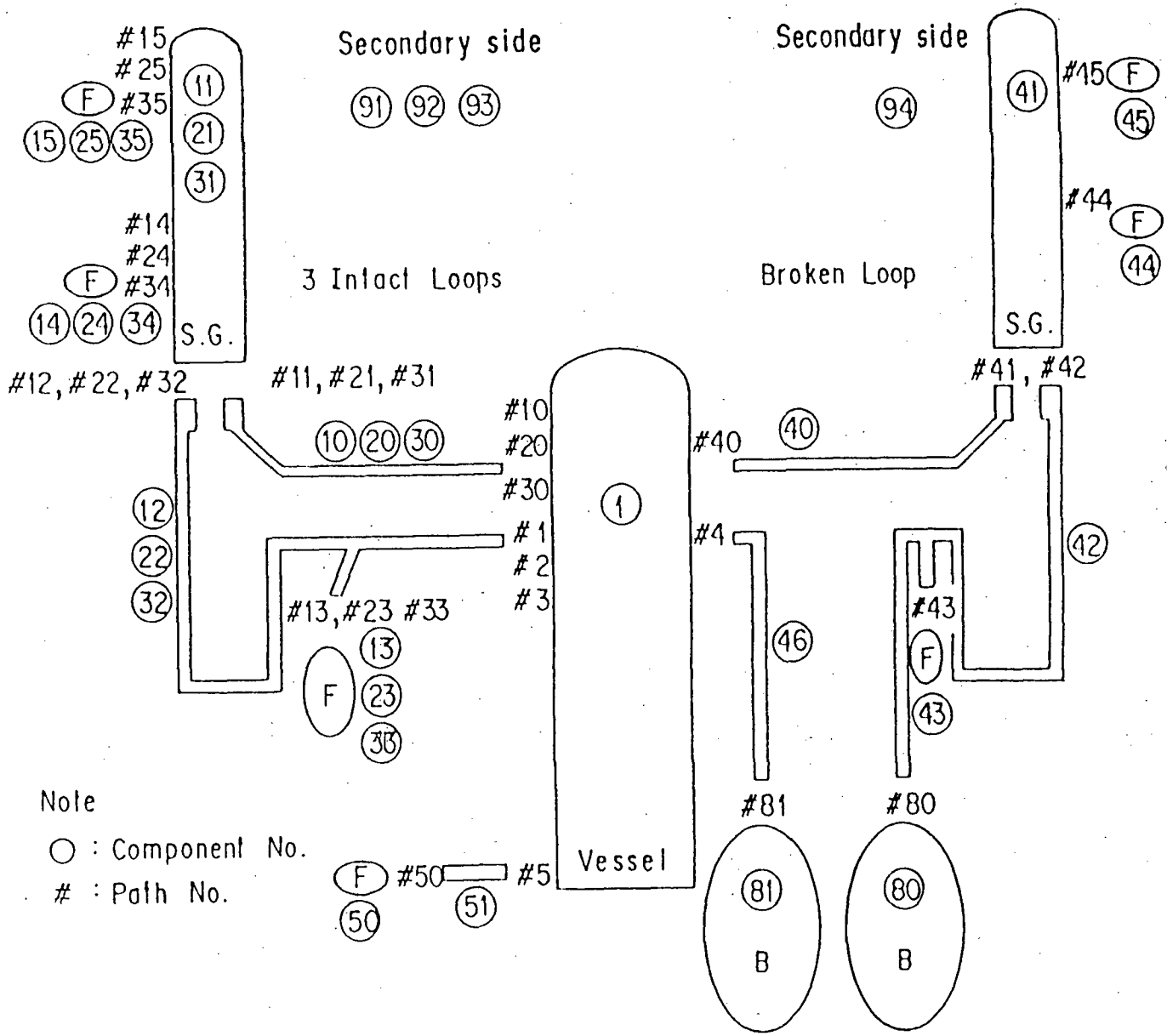


Fig. 1 TRAC noding of CCTF 3D system calculation

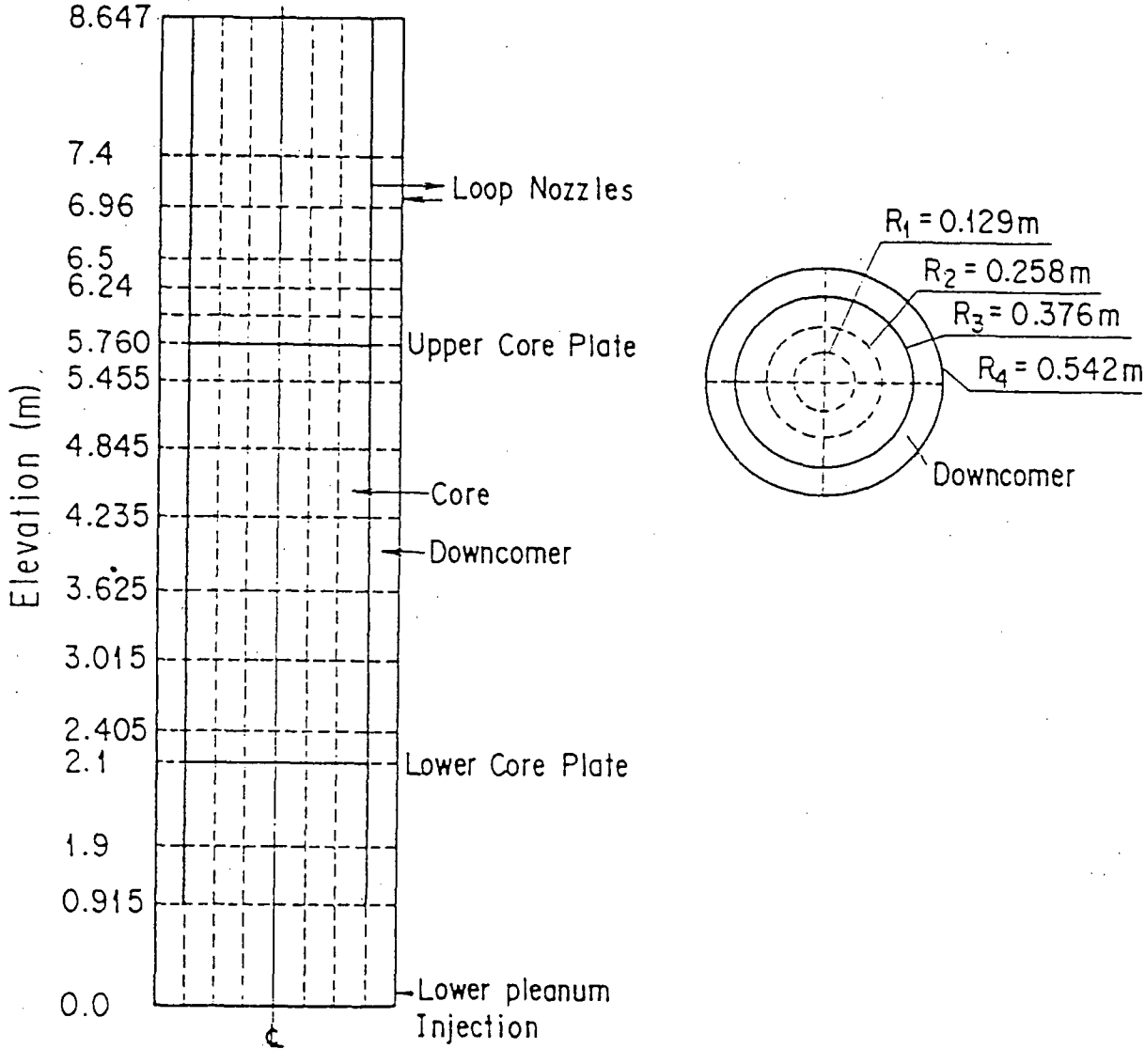


Fig. 2 CCTF VESSEL noding of CCTF 3D system calculation

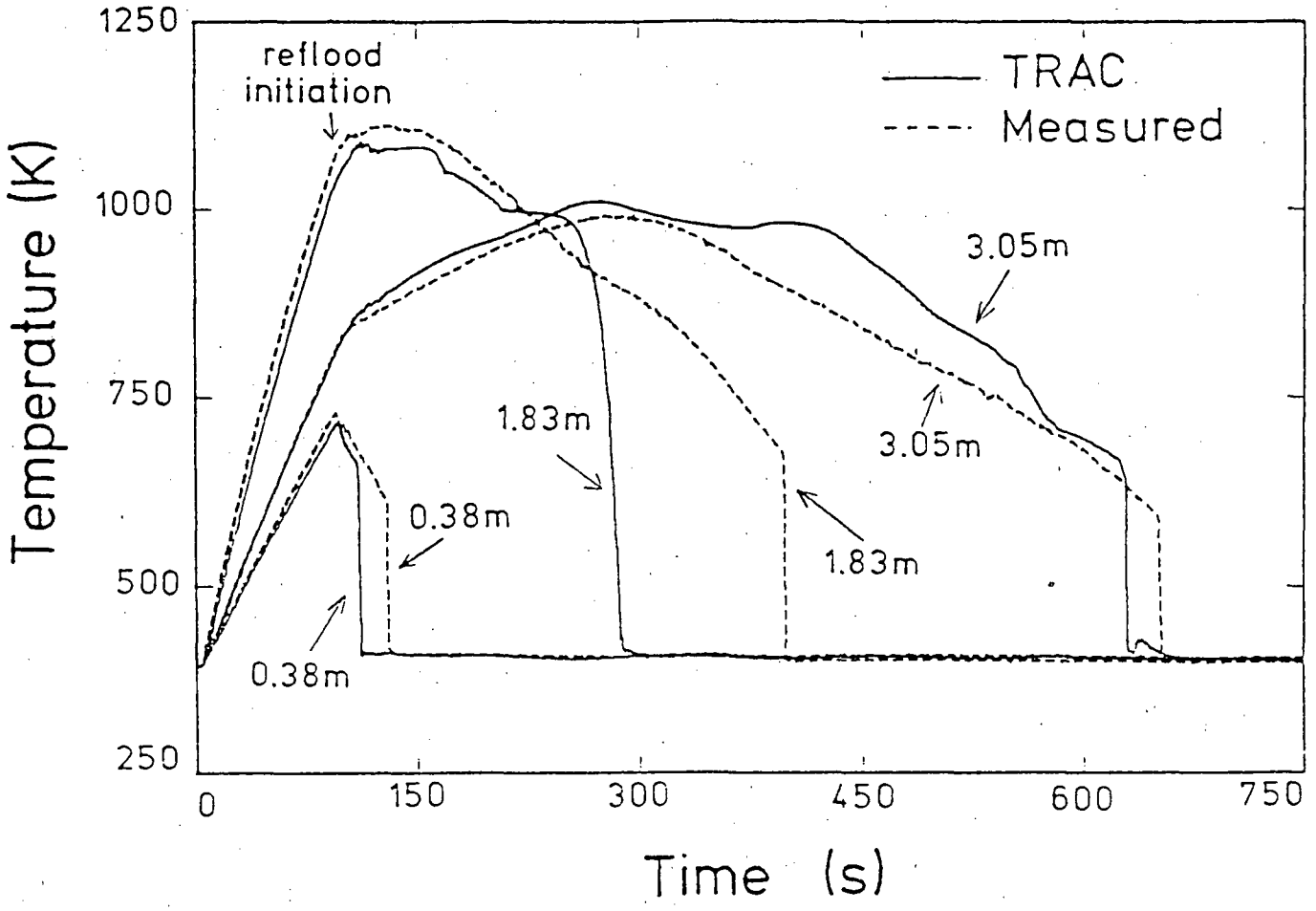


Fig. 3 Clad temperature along a high power rod in a CCTF 3D system calculation

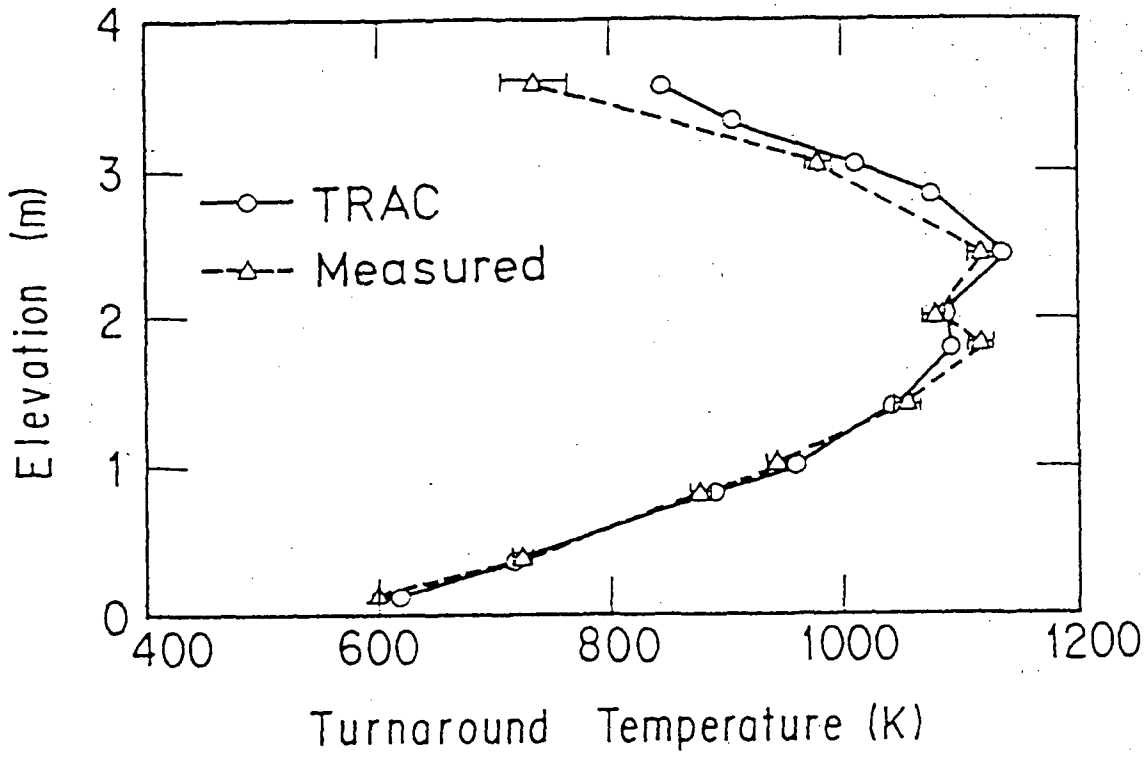


(a) Turnaound temperature

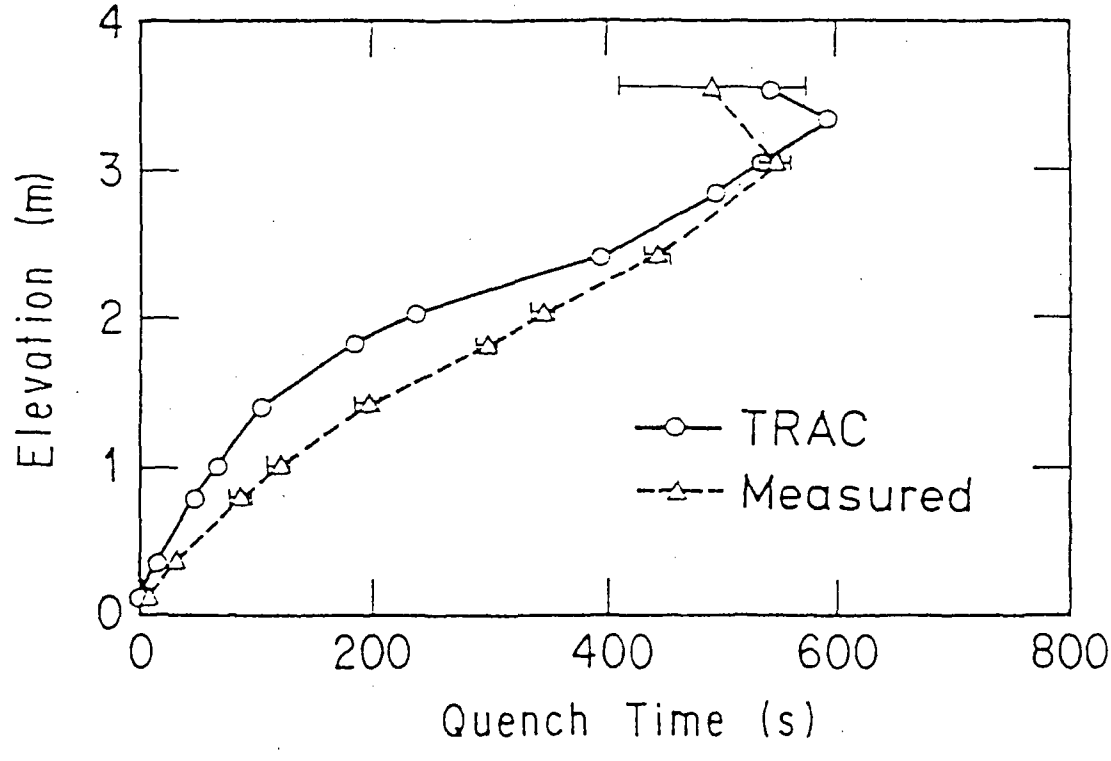


(b) Quench time

Fig. 4 Core cooling behavior in a CCTF 3D system calculation

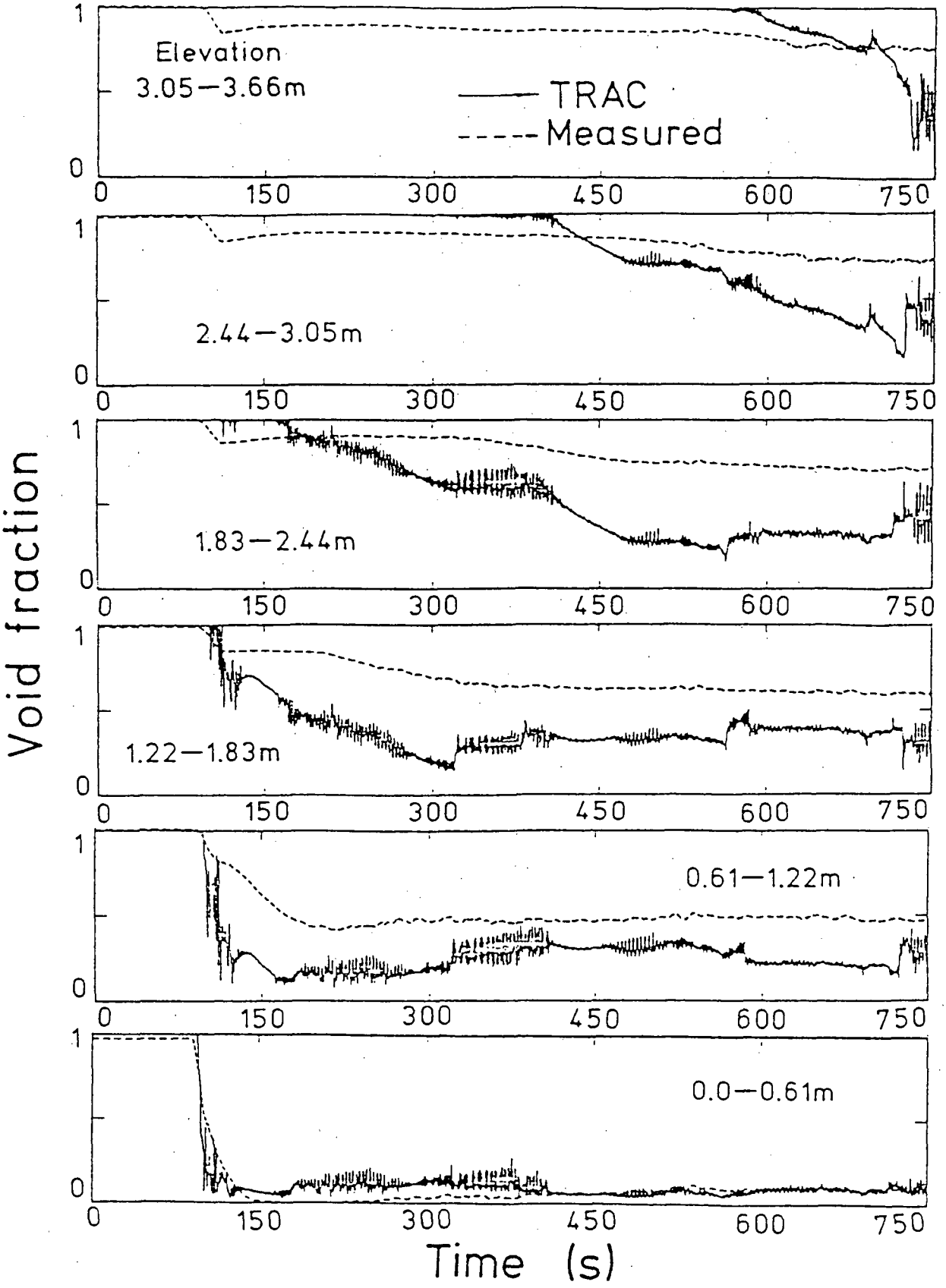


Fig. 5 Core void fractions in a CCTF 3D system calculation

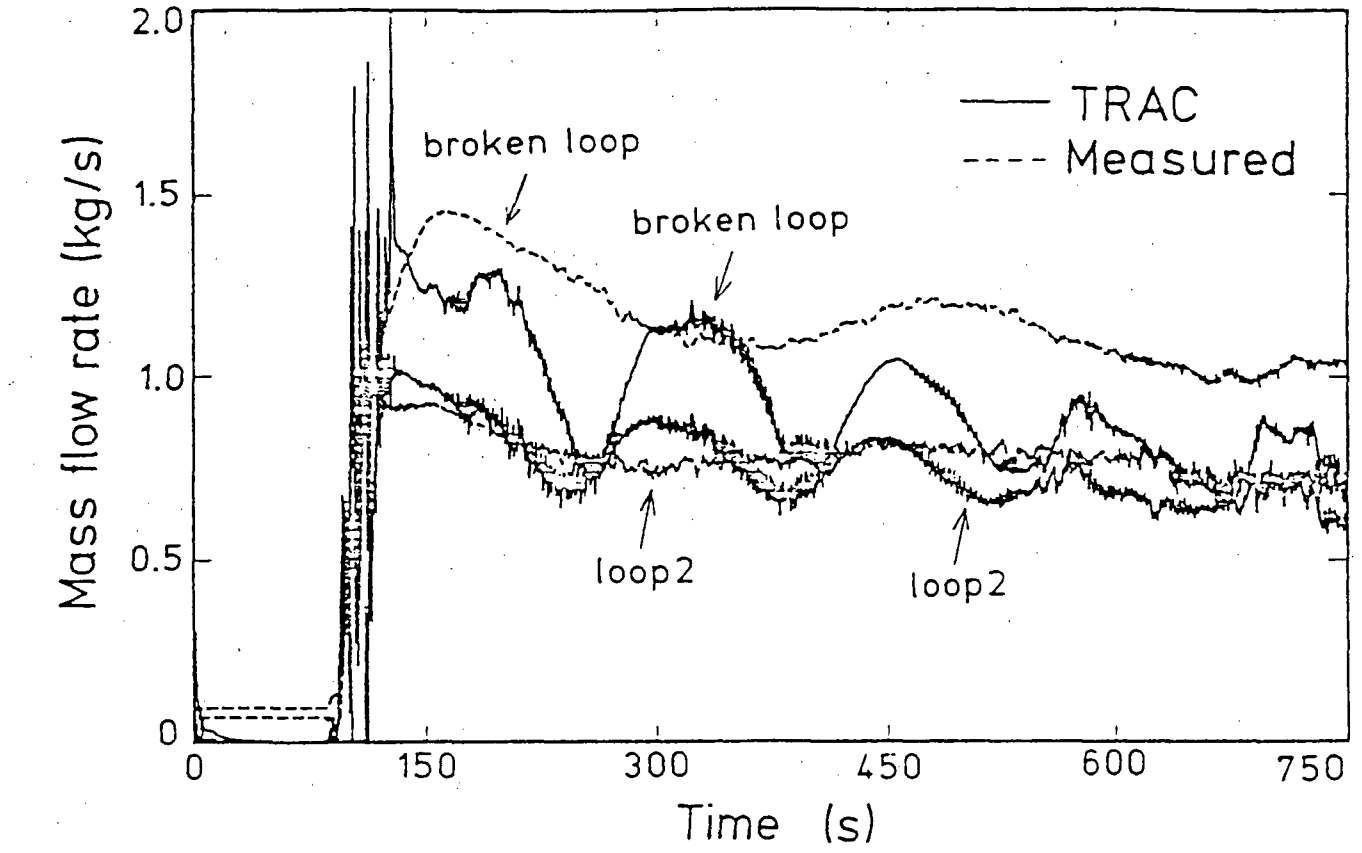


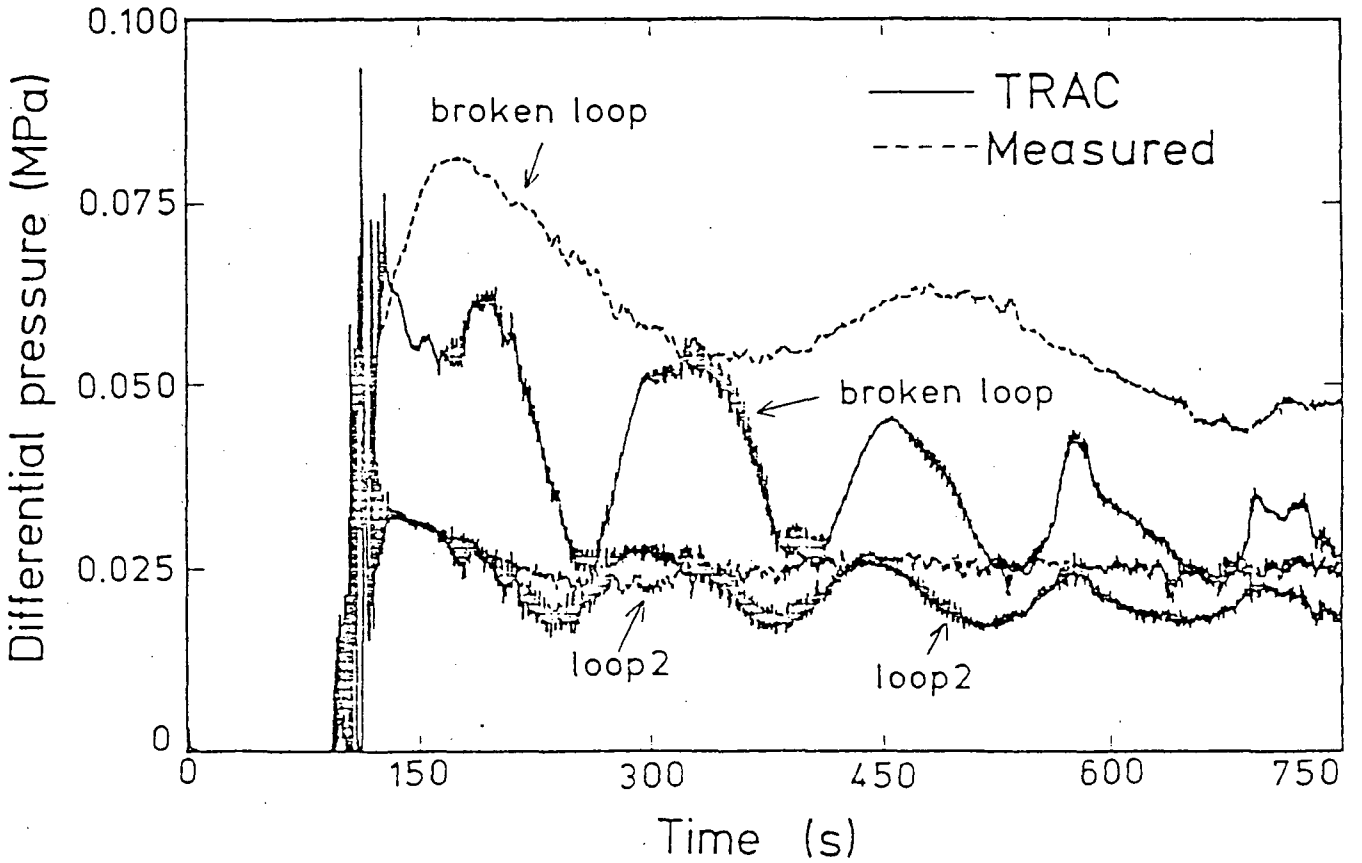


Fig. 6 Loop flow behavior in a CCTF 3D system calculation

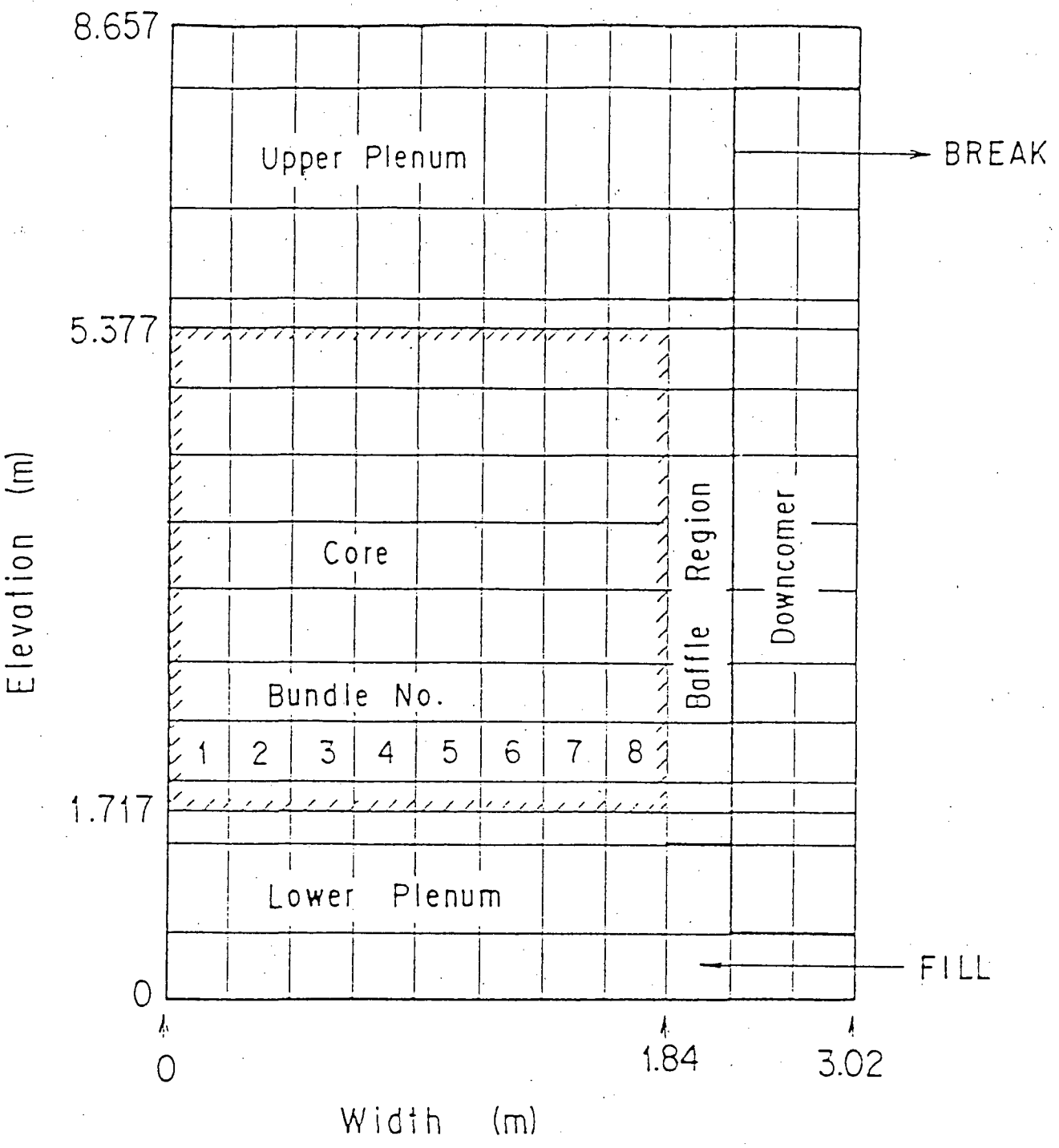


Fig. 7 TRAC noding of SCTF 2D core calculation

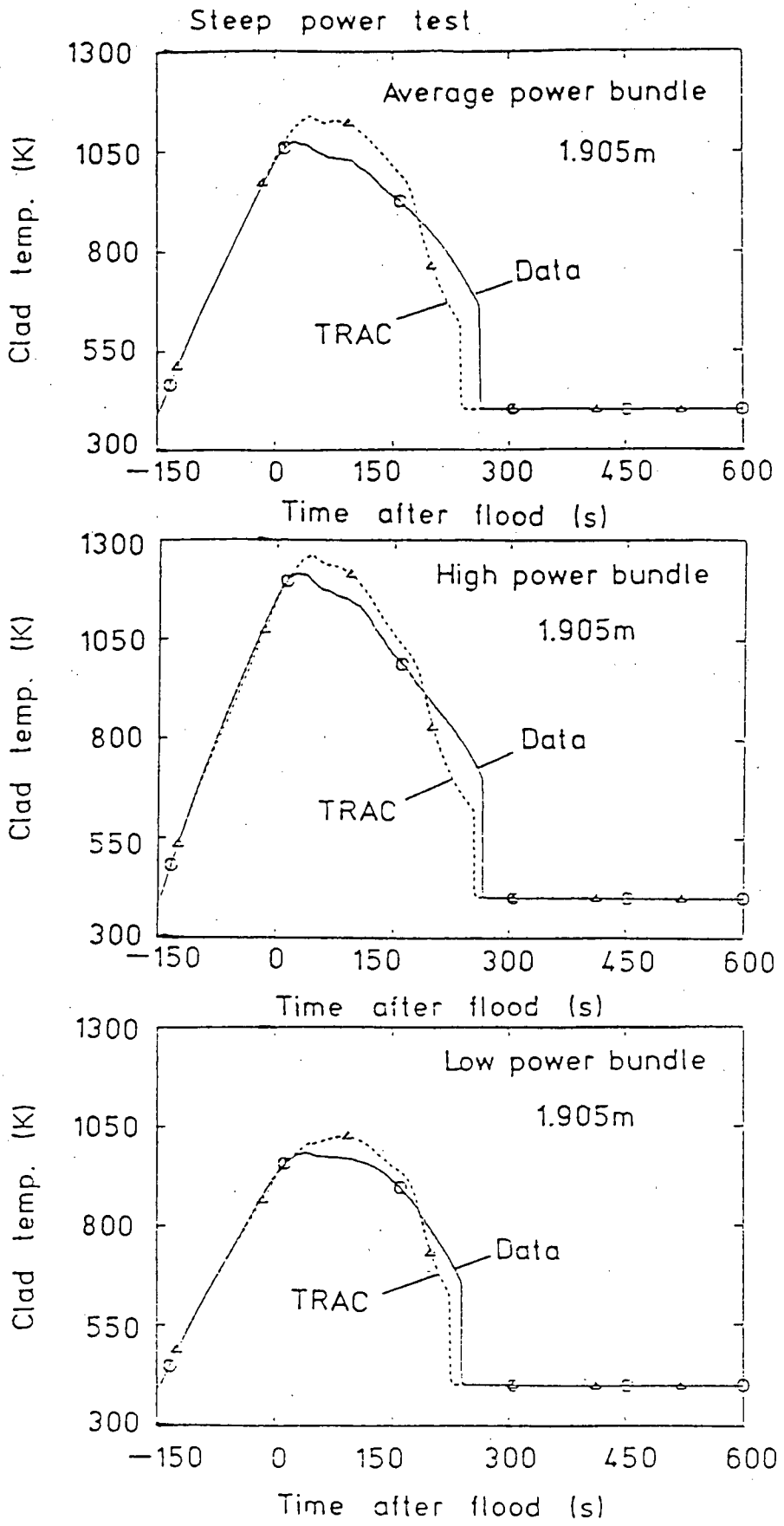


Fig. 8 Clad temperature at elevation of 1.905 m in a SCTF 2D core calculation

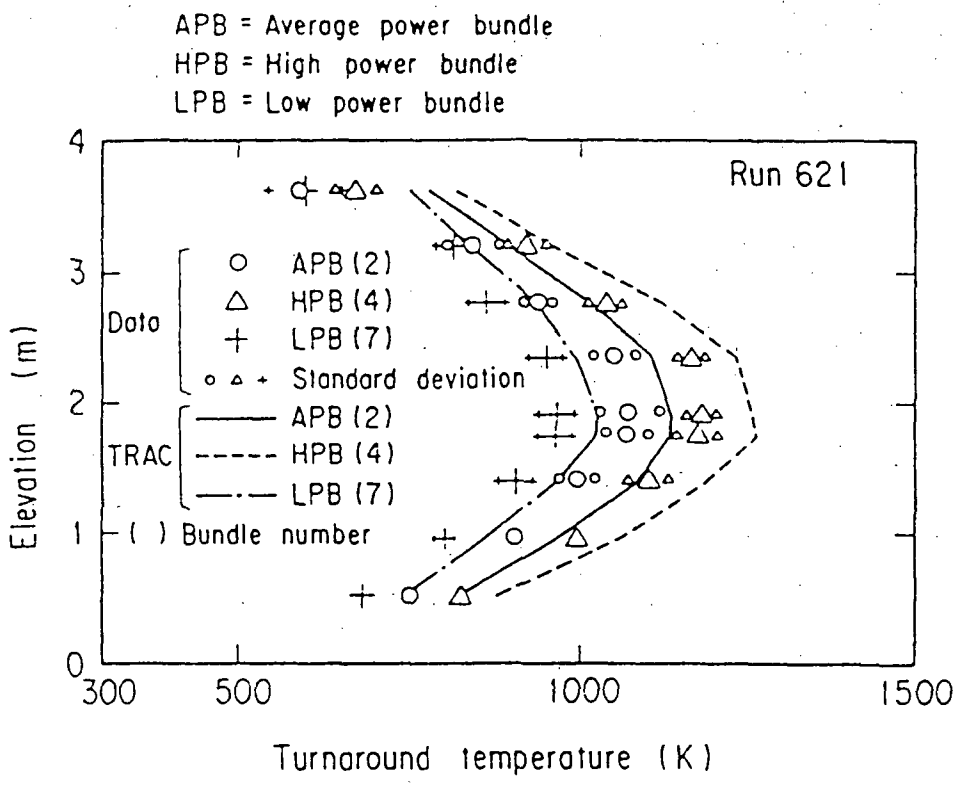


(a) Turnaround temperature

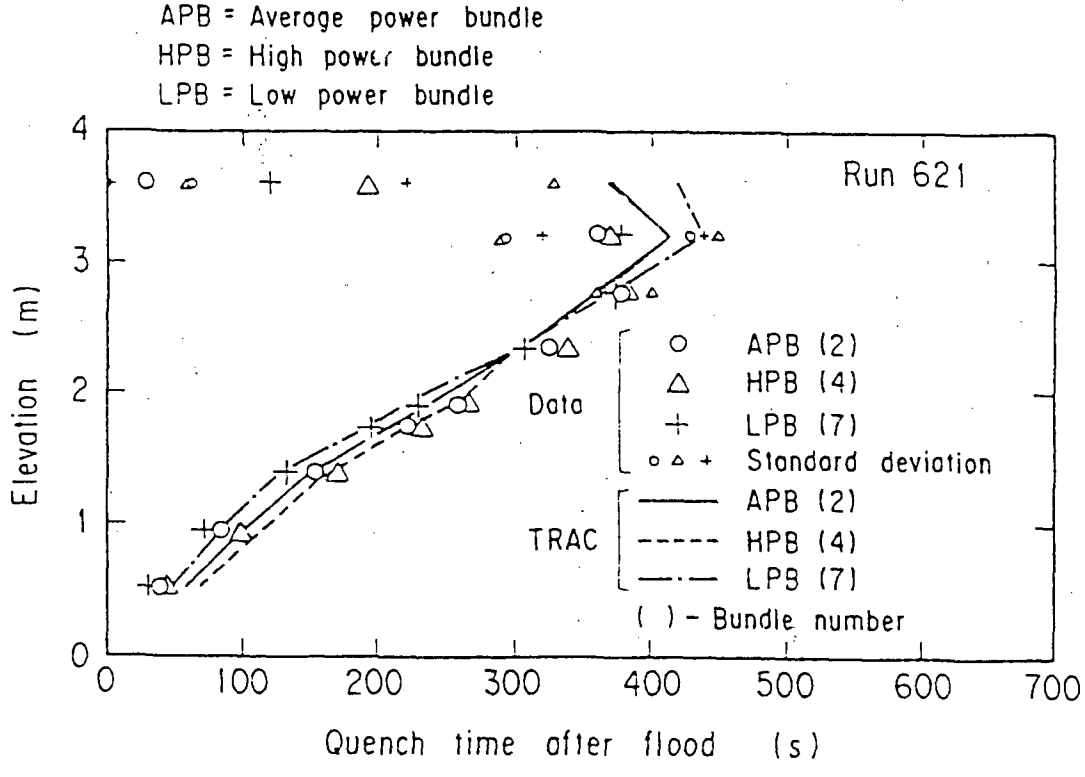


(b) Quench time

Fig. 9 Core cooling behavior in a SCTF 2D core calculation

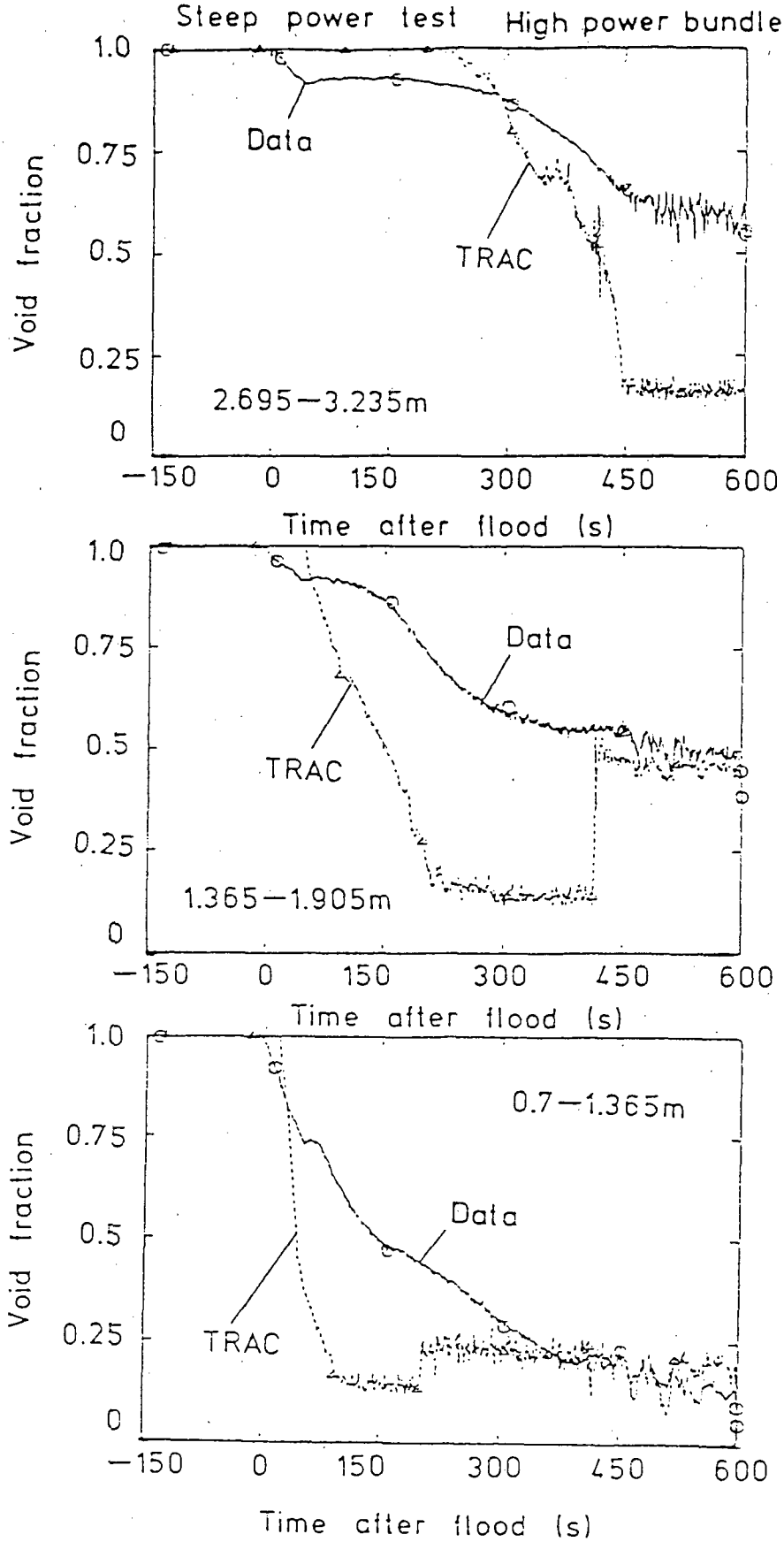


Fig. 10 Core void fractions in a SCTF 2D core calculation

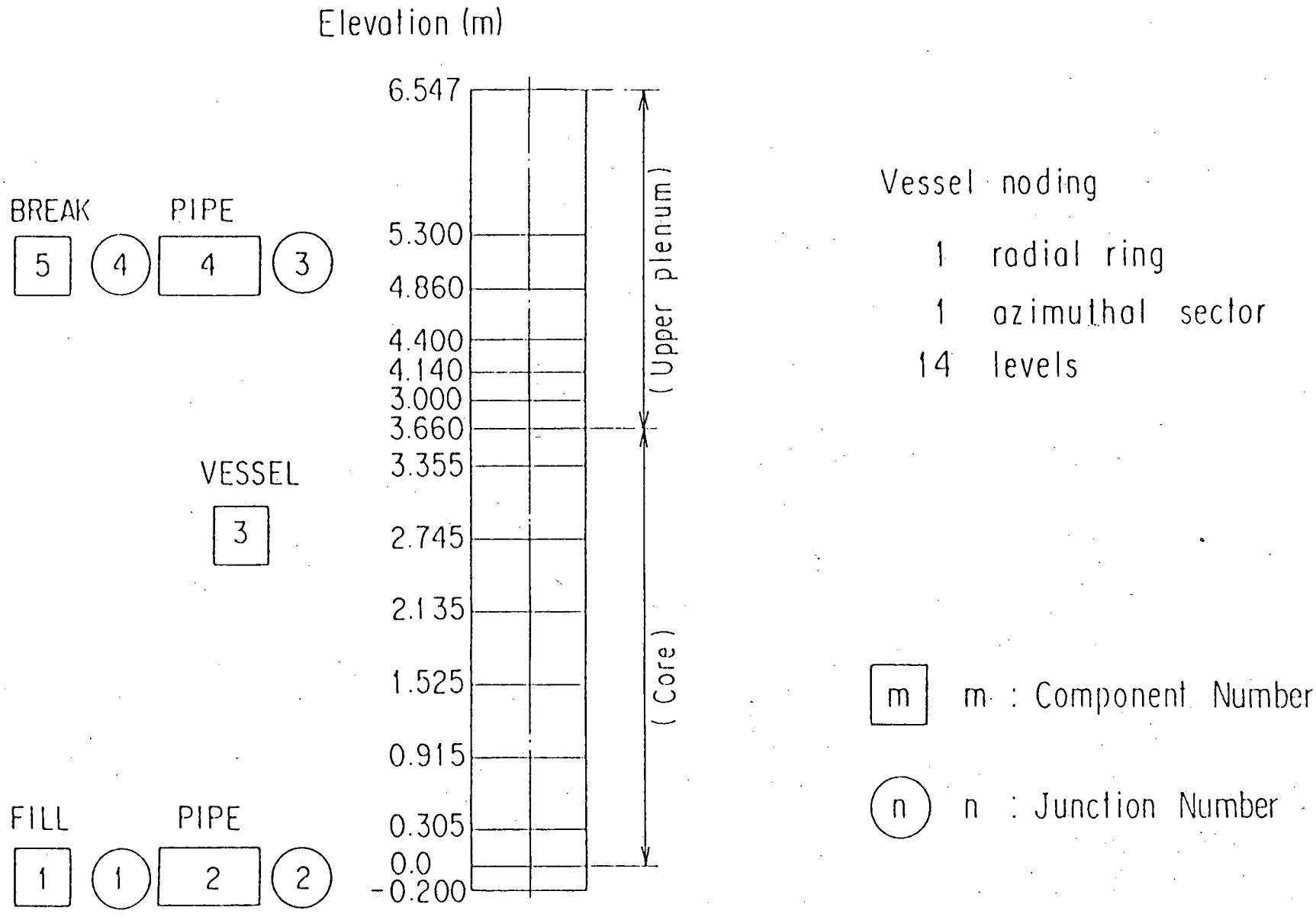


Fig. 11 TRAC noding of CCTF 1D core calculation

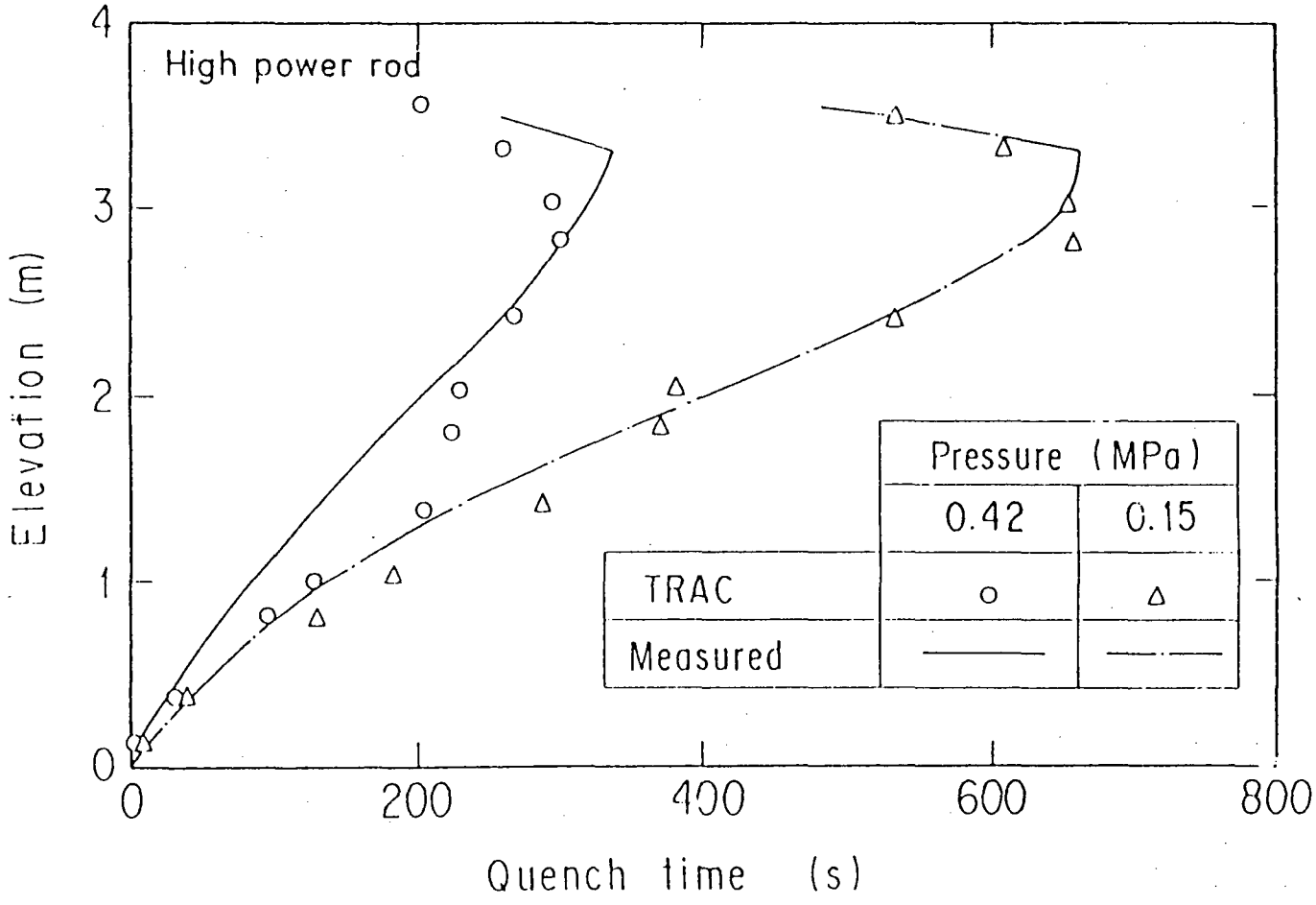


Fig. 12 System pressure effect on quench behavior in CCTF 1D core calculations

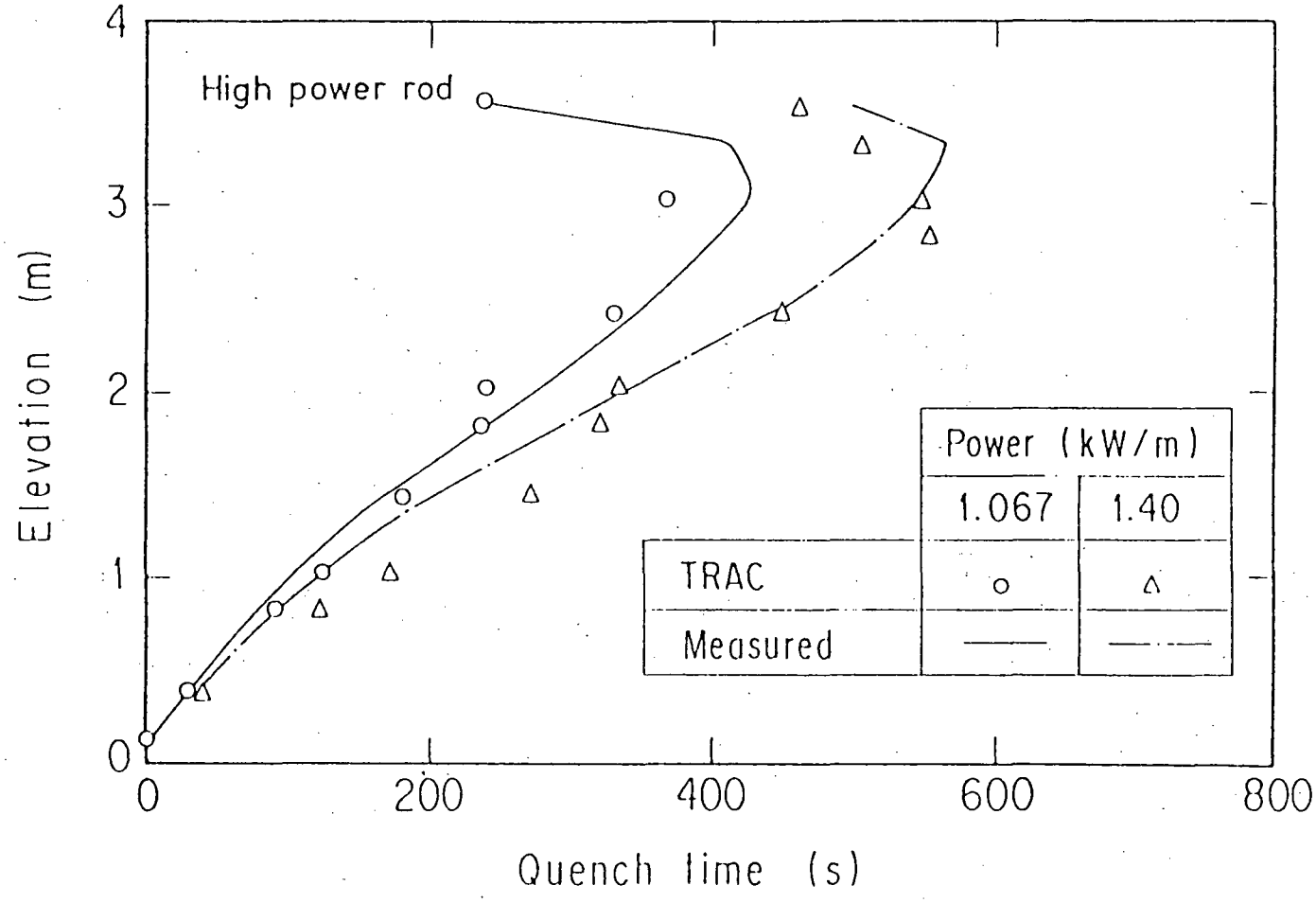


Fig. 13 Core power effect on quench behavior in CCTF 1D core calculation

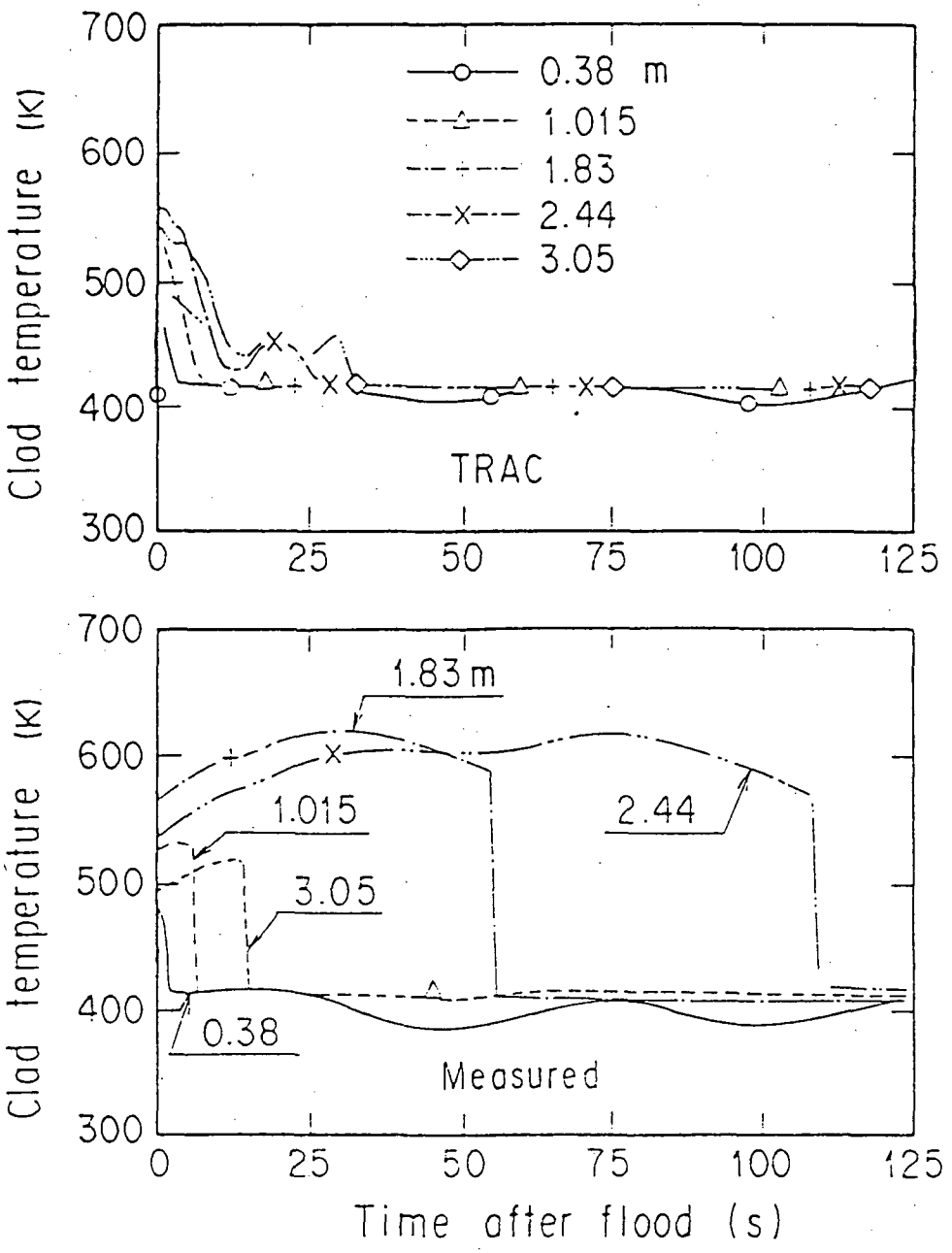


Fig. 14 Clad temperature in CCTF BE test with CCTF 1D core model

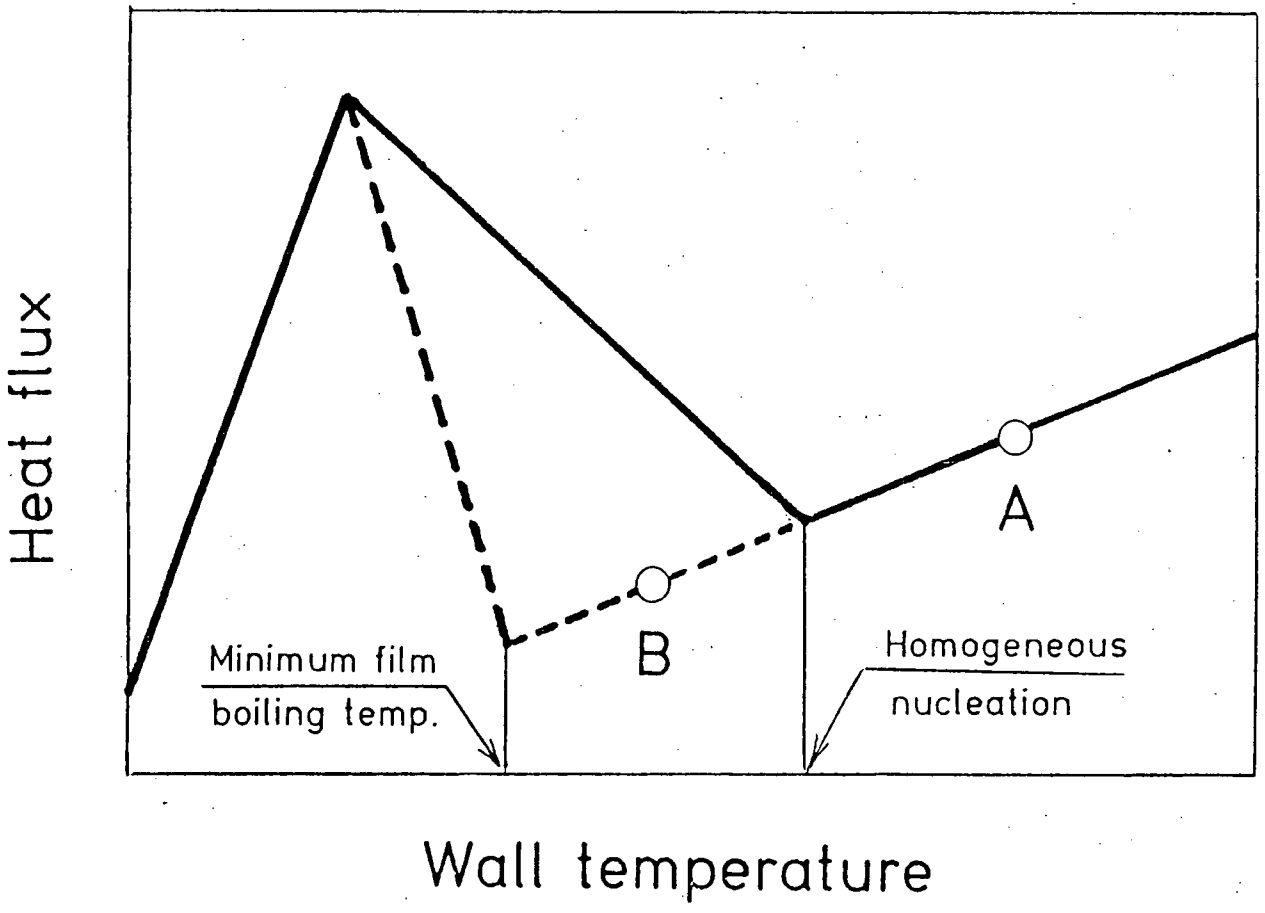


Fig. 15 Boiling curves and quench behavior

# JRC ISPRA CONTRIBUTION TO THE IMPROVEMENT OF RELAP5/MOD2

H. Städtke

Commission of the European Communities
Joint Research Centre, Ispra Establishment
I-21020 Ispra, Italy

ABSTRACT

The assessment of the RELAP5/MOD2 code within the framework of the International Code Assessment and Application Programme has identified various modelling deficiencies and a strong need for a further development of this code. For this reason, a multinational effort, coordinated by the ICAP Technical Programme Group, has been started for the improvement of RELAP5/MOD2. The JRC-Ispra contribution to this activity is based on the experience gained from the improvement of RELAP5/MOD1.

The paper summarizes several modifications and model improvements which have been implemented into a JRC Ispra version of RELAP5/MOD2. This concerns the calculations of state properties for vapour and steam, interphase drag coefficients, occurrence of stratified conditions in horizontal pipes and critical flows for saturated (two-phase) conditions.

The results of these model improvements are demonstrated by the comparison of calculated values using the original and the modified version of RELAP5/MOD2 with separate effect and integral test data.

## 1. INTRODUCTION

In 1985, the LWR system codes RELAP5 and TRAC were 'frozen' in order to provide a common basis for the independent assessment of these codes within the International Code Assessment and Application Programme (ICAP). Since that time, no further code improvements have been included in the officially released code versions apart from error corrections and increased user convinience. The extensive use of the two codes within the ICAP programme during the last three years has identified a number of code deficiencies which are in general common to both codes. The ICAP Technical Programme has established a priority list of about twenty items where further model improvements are felt to

be needed. The list includes all items which have been found also by the use of RELAP5/MOD2 within the LOBI Project at the JRC Ispra / 1 /.

Within the framework of the ICAP programme, a multi-national effort has been started in 1987 for a further improvement of RELAP5 and TRAC. The aim of this activity is the release of new versions denoted RELAP5/MOD3 and TRAC-PF1/MOD2 at the end of 1989.

## 2. OVERVIEW ON MODEL IMPROVEMENTS AND MODIFICATIONS PRESENTLY IMPLEMENTED IN THE JRC ISPRA VERSION OF RELAP5/MOD2

Within the last three years, the main analytical tool used within the LOBI project has been the JRC Ispra version of RELAP5/MOD1, denoted RELAP5/MOD1-EUR. This code, which includes various model improvements compared with the original INEL version, has proven to give reliable predictions for a wide spectrum of accident scenarios as investigated in the LOBI test facility / 2 /. After the conversion of the RELAP5/MOD2 code from the original CDC version into a IBM/AMDAHL compatible form, the intention was to change from RELAP5/MOD1-EUR to RELAP5/MOD2. However, post-test calculations performed with the MOD2 version for selected LOBI tests including large, intermediate and small break LOCA as well as Special Transients tests have indicated several severe code deficiencies which have to be resolved before this code can be used as a reliable predictive tool within the framework of the LOBI experimental programme.

The present RELAP5/MOD2 activities at the JRC Ispra are directed to transfer some of the major model improvements, which have been implemented and tested already in the MOD1 version, into RELAP5/MOD2. The various model changes concern the calculation of properties for water and steam, interphase drag coefficients, occurrence of stratified conditions in horizontal pipes and critical mass flows for saturated (two-phase) conditions.

### 2.1 Calculation of Thermodynamic Properties for Water and Steam

For the use in large LWR system codes a new software package / 3 / has been developed at the JRC Ispra for the calculation of thermodynamic properties of water and steam. The new package is based on the canonical formulation of state equations. All thermodynamic state quantities are derived from a rational equation for the free energy (Helmholtz function) without the need of any table interpolation.

The new property package has been used extensively in the JRC Ispra version of RELAP5/MOD1. The package which has been recently implemen-

ted also in the MOD2 version of the code, provides consistent thermodynamic state properties for liquid and vapour with a high degree of accuracy. It avoids the storage of huge property tables as is needed in the original code. The performance of the new property package with respect to CPU-time is nearly identical with original method based on table interpolations.

## 2.2 Implementation of Interphase Drag Models

The way how the interphase drag coefficients are implemented into the numerical scheme of the code has been drastically changed in RELAP5/MOD2 with respect to the MOD1 version of the code.

In the RELAP5/MOD1 code, the interphase drag coefficients are calculated on the basis of junction flow velocities which results in a direct coupling between interphase friction forces and the difference of phase velocities. In RELAP5/MOD2, however, the interphase drag coefficients are evaluated first for all volumes, using volume average flow velocities. The junction values for the interphase drag coefficients are then calculated as an average of the two corresponding values of the adjacent volumes with the volume size as weighting parameter. For critical flow conditions only the value from the upstream volume is used.

The procedure for the implementation of the interphase drag coefficients in RELAP5/MOD2 can result in the calculation of unrealistic phase velocities in all cases where the flow cross section of the junction considerably deviates from the volume cross section. This especially affects adversely the prediction of critical (break) flow velocities for small and intermediate break LOCA transients with stratified conditions upstream of the break. The extremely low drag coefficient as calculated for stratified conditions in the upstream volume gives, if transferred to the break junction, extremely large differences for the phase velocities (slip) in the break and, as a consequence, results in too low values for the break mass flows.

In order to resolve this problem, the calculation of the interphase drag coefficients has been changed for all junctions with critical flow conditions. If choking has been identified, the interphase drag coefficient is recalculated on the basis of the High Mixing Flow Regime (HMFR) map using directly the junction vapour and liquid flow velocities. The HMFR map includes two basic flow regimes, bubbly flow for void fraction below 0.5 and dispersed droplet flow for void fractions above 0.95. In between these two limits the interphase drag coefficient is interpolated. The HMFR map has been chosen in order to avoid the selection of slug or stratified flow which are unlikely to

exist for critical flow conditions with generally high flow velocities. With these modifications for the calculation of the interphase drag coefficients more realistic phase velocities have been obtained for critical flow conditions, even in the case of small break LOCA calculations with stratified conditions upstream of the break area.

## 2.3 Criterion for Stratified Flow in Horizontal Pipes

In the RELAP5 code, stratified flow conditions with a complete separation of vapour and liquid are assumed to exist when the vapour velocity is smaller than a critical value $(v_g)_{cr}$, as given by a correlation of Taitel and Dukler / 4 /.

$$(v_g)_{cr} = C \frac{(\rho_l - \rho_g) g \alpha_g}{\rho_g d_{hy} \sin\theta} \tag{1}$$

The basic form of this correlation represents the Kelvin-Helmholtz stability criterion for small waves of liquid flowing between horizontal parallel plates. The authors of / 4 / 'speculate' that the coefficient C in equation (1) can be estimated as

$$C = (1 - \cos\theta) \tag{2}$$

where $\theta$ is the angle between the vertical line and the liquid level in pipe cross section.

Using the original correlation with the coefficient as given in equation (2), the RELAP5 code was not able to predict stable stratified conditions for the flow within the cold leg pipes, as was measured over long time periods in most LOBI small break LOCA experiments. For this reason, the coefficient C in equation (1) was set to a value of 0.5 as was done already in the JRC Ispra version of RELAP5/MOD1. With this modification, together with a new choking model as will be described in paragraph 3, stable stratified conditions were calculated for the cold leg pipe upstream of the break and a considerable improvement could be achieved for the prediction of the fluid densities in the horizontal pipes.

## 2.4 Calculation of Critical Flow Velocities for Saturated Upstream Conditions

For the calculation of critical flow velocities, an explicit model is used in RELAP5/MOD2 which, apart from smaller modifications, has been applied already in the MOD1 version of the code. For saturated or two-phase conditions upstream of the throat, the model is known to have the following deficiencies / 5 /: (1) it includes a discontinuity for the transition between upstream subcooled to saturated conditions, and (2) it calculates by far too low mass flows for low vapour qualities, especially in the low pressure region. For this reason, an improved choking model has been developed and implemented into the Ispra modified version of RELAP5/MOD2 which is described in detail in paragraph 3.

## 2.5 Influence of Upstream Stratified Conditions on the Critical Flow Velocities

The mass flows of liquid and vapour in a junction connecting two volumes are calculated as the products of the junction phase velocities, the junction void fractions and the density values. The junction flow velocities are determined on the basis of separate momentum equations evaluated for a region overlapping two adjacent volumes. The junction void fractions and densities, however, are taken from the upstream (donor) volume.

For critical flow conditions (choking) the junction flow velocities for the two phases are recalculated, assuming that the velocities at the throat of the channel cannot exceed a sonic velocity limit. Choking is generally characterized by strong pressure and density gradients which means that the densities in the throat area can differ considerably from the corresponding values in the upstream volume. Since the junction properties are not changed for choking conditions, a correction for the critical flow velocities has been introduced in order to get realistic values for the critical mass flows. This is achieved by multiplying the characteristic (sonic) velocity with a density ratio, calculated from an estimate of the fluid density in the throat and the density in the upstream volume.

In the case of stratified flow conditions upstream of the choked junction, the junction properties (void fractions, phase densities) can largely differ from the corresponding average values in the upstream volume. This fact is not properly taken into account in the present RELAP5/MOD2 choking model, especially if the liquid is subcooled as has been measured upstream of the break in several LOBI small break LOCA tests. To avoid this problem, the correct junction vapour quality as

results from the 'off-take' model is used in the JRC modified code version for the calculation of the final characteristic (sonic) velocity in the throat area.

## 3. IMPROVEMENT OF CRITICAL FLOW MODEL

During Loss of Coolant Accidents in pressurized or boiling water reactors, critical flow or choking conditions exist at the break over long time periods of the transient. For this reason, a large effort has been spent in the past to study critical flow phenomena, especially under two-phase conditions. Today, choking is well understood and a sufficient data base has been generated for the assessment of analytical models. The difficulties which still exist in predicting critical mass flows by the system codes like RELAP5 or TRAC arise from the fact that choking is a local phenomenon occurring in the throat (or downstream of the throat in case of a convergent-divergent channel) of the discharge line. Therefore, the correct prediction of critical flow conditions requires the integration of the governing flow equations along the flow path from the upstream volume into the throat area. In principle, this could be done by the system codes, however, the very steep pressure gradient would demand an extremely fine nodalization and, due to the material Courant limit, to very small time step sizes. To avoid the necessity for such a fine nodalization of the break discharge, explicit choking models have been added to the RELAP5 and TRAC code with the aim to calculate critical flow velocities as a function of upstream (nearly) stagnation conditions.

### 3.1 Present Choking Model in RELAP5/MOD2

In the present version of RELAP5/MOD2 the calculation of critical flow conditions is based on two different models. For subcooled conditions upstream of the throat ($T_1 < T^{sat}$) the flashing is assumed to occur exactly at the throat of the discharge line. The model accounts for a certain delay of the incipient boiling, depending on the depressurization rate during the flow path from the upstream reservoir and on the degree of turbulent fluctuations determined by the flow velocity. Since the flow upstream of the throat is assumed to be single phase liquid, the critical velocity can be calculated by the Bernoulli equation

$$v_{th} = \left[ v_0^2 + 2 \left( \frac{p_0 - p^s(T_0) - \Delta p}{\rho_l} \right) \right]^{1/2} \qquad (3)$$

where $\Delta p$ represents a pressure difference equivalent to thermal non-

equilibrium at the onset of vaporization. The $\Delta p$ value in (3) describing the thermal non-equilibrium effect is calculated from the Alamgir, Lienhard and Jones correlation / 6 / which includes a number of empirical coefficients derived from critical flow experiments of initially subcooled liquids.

For the case of subcooled flow the junction liquid and vapour velocities are set equal to the critical flow velocity as given by equation (3)

$$(v_g)_j = (v_l)_l = v_{th} \tag{4}$$

For saturated (two-phase) conditions upstream of the throat ($X_o \geq 2.5 \cdot 10^{-4}$) choking is assumed to occur when a mean flow velocity of the two-phase mixture, $v_c$, exceeds the thermal equilibrium sound velocity of the two-phase fluid

$$(v_c)_j = (a_{HE})_j \tag{5}$$

where the mean (or mixture) flow velocity is defined as

$$(v_c)_j = \left( \frac{\alpha_g \rho_l v_g + \alpha_l \rho_g v_l}{\alpha_g \rho_l + \alpha_l \rho_g} \right)_j \tag{6}$$

The mean flow velocity is evaluated on the basis of junction quantities which means that in the absence of upstream stratification, the state properties in equation (6) are identical with those of the upstream volume.

The equilibrium sound velocity in (5) which represents a pure thermodynamic quantity is calculated from the properties in the throat of the channel

$$(a_{HE})_{th} = \left[ \left( \frac{dp}{d\rho} \right)_{is}^{1/2} \right]_{th} = f(p_{th}, u_{th}) \tag{7}$$

The pressure $p_{th}$ and the internal energy $u_{th}$ at the throat in equation (7) are estimated from the upstream volume data by means of simplified momentum and energy equations on the basis of old time step values.

In order to make the equilibrium sound velocity (7) comparable with the mixture flow velocity (6), the sound velocity is devided by a density ratio, JCATN, of junction and throat values:

$$(a_{HE})_j = (a_{HE})_{th} / JCATN \tag{8}$$

with $$JCATN = \frac{\rho_j}{\rho_{th}} \ .$$

The final junction flow velocities for vapour and liquid, $(v_g)j$ and $(v_f)j$, are calculated from the choking criteria (5) and from the difference of the two phasic momentum equations.

The transition between subcooled and saturated (two-phase) conditions is assumed for the quality region $1.0 \cdot 10^{-5} < X < 2.5 \cdot 10^{-4}$. In this region the critical flow velocities are calculated as for saturated conditions, however, the sound velocity is taken as the maximum between the two-phase homogeneous sound velocity (7) and the critical throat velocity (3) as used for subcooled conditions upstream of the throat. In addition a heavily old time-step weighted relaxation procedure is applied in order to damp strong phasic flow velocity oscillations.

The RELAP5/MOD2 choking model for saturated (two-phase) conditions upstream of the throat area, as described above, has the following drawbacks:

(1) the use of the thermal-equilibrium sound velocity is inconsistent with the basic two-fluid (unequal temperature, unequal velocity) model of the code

(2) the model does not account for thermal and mechanical non-equilibrium effects which exist also for two-phase conditions upstream of the discharge channel, especially for low vapour qualities and low pressure values

(3) as a result of (1) and (2), the critical mass flow is considerably underpredicted for low vapour qualities; the discrepancy increases with decreasing stagnation pressure

(4) the model includes a discontinuity for the phase velocities (and consequently for the critical mass flow) during the transition from subcooled to saturated (two-phase) upstream conditions. This dis-

continuity together with the (nearly) explicit numerical treatment of the choking model results in heavy flow oscillations which can be reduced only partially with the under-relaxation for the phasic flow velocities.

## 3.2 Improved Choking Model for RELAP5/MOD2

In order to overcome the drawbacks of the original choking model of RELAP5, as described in paragraph 3.1, a new critical flow model has been developed and implemented into the code. The starting point for the new choking model is the set of partial differential equations as used in RELAP5 to describe the conservation of mass, momentum and energy separately for the two phases. These equations can be written in a matrix form as

$$\tilde{A}\frac{\partial \bar{X}}{\partial t} + \tilde{B}\frac{\partial \bar{X}}{\partial x} = \bar{C} \tag{9}$$

The column vector ($\bar{X}$) contains the basic dependent variables used in RELAP5/MOD2: pressure p, void fraction $\alpha$, the phasic flow velocities $v_g$, $v_l$ and the internal energies $u_g$, $u_l$.

For steady state flows, critical or choking flow exists when the determinant of the coefficient matrix for the space derivatives vanishes:

$$Det(\tilde{B}) = 0 \tag{10}$$

Evaluating this equation results in the choking criterion:

$$(v_c)_{th} = (a_{fr})_{th} \tag{11}$$

with

$$(v_c)_{th} = \left[\left(\frac{\alpha_l \rho_l}{\rho} v_l^2 + \frac{\alpha_g \rho_g}{\rho} v_g^2\right)^{1/2}\right]_{th} \tag{12}$$

and

$$\left.\begin{aligned}(a_{fr})_{th} &= \left[\left(\frac{\alpha_l\rho}{\rho_l}\frac{1}{a_l^2}+\frac{\alpha_g\rho}{\rho_g}\frac{1}{a_g^2}\right)^{-1/2}\right]_{th} = f(p_{th},\ X_{th})\\ a_g^2 &= \left(\frac{\partial p}{\partial \rho_g}\right)_{is}\\ a_l^2 &= \left(\frac{\partial p}{\partial \rho}\right)_{is}\end{aligned}\right\} \quad (13)$$

Note that both the expressions for the mixture flow velocity, $v_c$, as well as for the two-phase sound velocity, $a_{fr}$, differ considerably from the corresponding equations of the original choking model.

The two-phase sound velocity given by equation (13), also called 'frozen' sound velocity, is identical with the propagation of high frequency sound waves in a two-phase mixture.

In Fig. 1, both the homogeneous equilibrium and the 'frozen' sound velocities are shown as a function of the mixture void fraction for water at a pressure of 2.0 MPa. The figure indicates the large difference between the equilibrium and the 'frozen' sound velocity for low void fractions ( $\alpha < 0.5$). At the boundaries of the two-phase region ($\alpha \to 0$, $\alpha \to 1.0$) the 'frozen' sound velocity approaches the corresponding values for single phase liquid or vapour, respectively. The thermal equilibrium sound velocity, however, shows large discontinuities for the transition between single and two-phase conditions, especially for zero void fraction.

As for the original choking model, the 'frozen' sound velocity is calculated on the basis of fluid properties at the throat of the flow channel which are extrapolated from the upstream volume data using simplified momentum and energy equations. Contrary to the original model, the vapour quality at the throat, $X_{th}$, is weighted between the quality of the upstream volume, $X_k$, and the equilibrium quality in the throat, $X_{th}^{eq}$, as calculated from the energy equation:

$$X_{th} = X_k + (X_{th}^{eq} - X_k) f(p_o) \quad (14)$$

The weighting function, $f(p_o)$, has been determined from the condition that at the transition between subcooled and two-phase conditions, the

two-phase sound velocity matches the characteristic throat velocity as calculated from the subcooled choking model, given by equation (3).

The implementation of the new choking model follows the same line as was applied in the original model. The 'frozen' sound velocity is corrected by the density ratio JCATN in order to obtain a junction related value

$$(a_{fr})_j = (a_{fr})_{th} / JCATN$$

with

$$JCATN = \frac{\rho_j}{\rho_{th}} \qquad (15)$$

The final phasic flow velocities ($v_g$) and ($v_f$) are calculated from the choking criteria (11) and the difference of the separate momentum equations for liquid and vapour. Since the mixture velocity contains the square of the liquid and vapour velocities, no direct solution is possible as for the original model. Instead, an iteration procedure is applied which converges after a few iteration cycles.

For the transition between subcooled liquid and two-phase conditions upstream of the throat, the same procedure is applied as for saturated two-phase flow. The only difference is that in this case the minimum of the 'frozen' sound velocity (13) and the critical flow velocity for subcooled conditions (3) is used as the characteristic velocity in the choking area.

### 3.3 Assessment of the new Choking Model

As a first check of the new critical flow model for RELAP5/MOD2 the LOBI break nozzle calibration tests have been chosen as were conducted in the hydraulic laboratory of Westinghouse Canada in Hamilton. In these tests four different discharge nozzles as used in the LOBI/MOD1 test rig to simulate 100 %, 50 %, 25 % and 10 % breaks were experimentally investigated. All the four convergent-divergent nozzles, shown in Fig. 2, are of similar geometry and differ only in the throat area. The tests were performed under steady-state conditions. A schematic drawing of the test loop and the RELAP5 nodalization used to represent the test section are shown in Fig. 3. Critical mass flows were measured for four different stagnation pressure values of 2.0 MPa, 4.0 MPa, 6.0 MPa and 8.0 MPa. For each of these pressure values the nozzle inlet conditions were varied between subcooled conditions with a maximum degree of subcooling of 50 K, and saturated conditions with vapour qualitites up to 50 %.

For the assessment of the RELAP5 choking model, the nozzle no. 3 has been selected which simulates a 50 % break in the LOBI test facility.

In Figs. 4 to 11 mass flow rates as calculated by RELAP5/MOD2 with the original choking model and with the improved choking model are compared with the corresponding measured values for all four stagnation pressure values investigated in the test programme. For each pressure, two plots are presented. The first plot shows the critical flow rates as function of the stagnation enthalpy to demonstrate the transition behaviour between subcooled and saturated (two-phase) conditions upstream of the throat. On the second plot critical flow rates are given for saturated (two-phase) conditions with upstream vapour qualities between 0.0 and 1.0. For subcooled inlet conditions the predicted results of the original and the modified code versions are identical since the subcooled choking model has not been changed.

In Fig. 12 and 13 the measured and predicted critical mass flow rates for saturated (two-phase) conditions are shown again, this time as function of the stagnation pressure $p_o$ for different inlet vapour qualities of $X_o$ = 0.02, 0.05, 0.10, 0.20 and 0.50. Fig. (12) includes RELAP5 results calculated with the original choking model. The predicted data in Fig. (13) are obtained with the improved code version.

From the comparison of predicted and measured data the following conclusions can be drawn:

(1) For subcooled conditions upstream of the discharge nozzle, a reasonable agreement exist between measured and predicted data, with a slight tendency of the code to overpredict the critical mass flow rate for large degrees of subcooling.

(2) For saturated (two-phase) conditions the original choking model considerably underpredicted the critical flow, especially for low vapour qualities ($X_o < 0.10$) upstream of the discharge line. The discrepancy between measured and predicted data increases with decreasing stagnation pressure. Only for high vapour qualities are the calculated flow rates in a reasonable agreement with the experimental data.

(3) Although not evident in the figures, the original choking model was unable to predict stable critical flow conditions for very low vapour qualitites in the high pressure range.

(4) The critical mass flow rates calculated by RELAP5 with the improved choking model are in excellent agreement with the measured data

over the whole range of stagnation vapour qualities and for all pressure values investigated in the tests.

(5) With the improved critical flow model no stability problems have been observed.

For the calculation of the blowdown period of the large break LOCA transient, the discrepancies observed with the original choking model of RELAP5 might be less severe, because low vapour qualities upstream of the break generally exist only at high system pressure values, that is in a pressure region where the underprediction of the break mass flow is less significant. For low primary side pressure values, on the other hand, the vapour quality upstream of the break has reached already values above 0.50 for which the model predicted reasonable critical mass flow rates. The deficiencies of the original choking model, however, is expected to have a strong effect for all transients where small vapour qualities upstream of the break exist over long time periods, as for example in small break LOCA or for intermediate and large break LOCA after the refilling of the pressure vessel.

## 4. ASSESSMENT OF RELAP5/MOD2 MODEL IMPROVEMENTS WITH LOBI INTEGRAL SYSTEM TEST DATA

As the first assessment case of the model improvements, introduced into the JRC Ispra version of RELAP5/MOD2, the LOBI test A2-81 / 7 / has been selected. The test which simulates the thermo-hydraulic behaviour of a PWR during 1 % small break LOCA, has been used also for the OECD, International Standard Problem No. 18 (ISP-18). The test is performed starting from nominal PWR conditions. ECC is provided only by the HPIS, where two out of four HPIS pumps are assumed to be available. The secondary side was cooled-down automatically with 100 K/h.

During the experiment the following main phenomena were observed:

(1) A strong thermal coupling between the primary and the secondary system; the primary side pressure remained always slightly higher than the secondary pressure, indicating that the steam generators were at least partially needed for the heat removal from the primary system.

(2) A liquid hold-up in the hot leg pipes, steam generator entrance and in the steam generator U-tubes.

(3) A certain amount of vapour produced in the core was transported directly via by-pass flow paths from the upper plenum into the upper downcomer region and towards the break.

(4) Stratified flow conditions existed over long time periods of the transient in both cold leg pipes; the liquid level upstream of the break largely governed the mass discharge through the break.

(5) The break mass flow was over long time periods nearly compensated by the HPIS flow; the primary side mass inventory never dropped below 67 % of the initial value.

(6) The vessel downcomer and the lower plenum were always filled with subcooled liquid; no loop seal clearance was observed.

(7) No core uncovery occurred during the test and hence the heater rod temperatures always remained close to saturation temperatures.

For the 'blind' test predictions all the codes used in the ISP-18 exercise including RELAP5/MOD2 showed the same deficiencies with regard to the calculation of break mass flows, primary side mass inventory, and mass and temperatures distribution within the primary system.

Results of post-test calculations for the LOBI test A2-81, using the original and the JRC Ispra modified version of RELAP5/MOD2 are compared in Fig. 14 to 21 with measured values for selected key parameters. The figure at the top always shows the calculated parameters from the original RELAP5/MOD2 code, whereas the bottom figure includes the values from the improved code version.

As indicated in the figures, the prediction with the original code failed at about 1400 s into the transient due to numerical instabilities. The problem seems to be connected with the drastic changes of interphase heat transfer coefficients during the transition from saturated to superheated vapour conditions which could not be handled by the (only) partially implicit numerical solution technique in RELAP5. These code failures did not occur in the modified version, probably due to the reduction of sudden changes of the flow parameters.

Apart from the code failures at 1400 s, the original code version shows some large discrepancies with respect to the measured system behaviour. The ECC injection into the intact loop cold leg results in a strong subcooling of the liquid phase upstream of the break and consequently in a decrease of the equilibrium vapour quality. After the equilibrium vapour quality has reached a value near zero, which happened in the prediction at about 700 s into the transient, the calculation of critical flow changes from the saturated to the subcooled choking model. This is accompanied by a drastic increase of the break flow which results for the subsequent time period in a considerable underprediction of the primary side mass inventory as shown in Fig. 14. The

discrepancy as described above is caused by the fact that the present choking model in RELAP5 does not properly account for thermal non-equilibrium effects and horizontal stratification in the main coolant pipe upstream of the break.

The overprediction of the break mass flow has further consequences for the calculation of the mass and temperature distribution in the primary system as shown in Figs. 16 to 21. In the hot leg pipe, for example, a complete voiding is predicted to occur 1200 s into the transient, whereas in the experiment a high density fluid was measured which remained throughout the transient.

With the JRC Ispra modified code version, however, the break mass flow was reasonably calculated, even for upstream stratified and thermal non-equilibrium conditions, as can be concluded from the comparison of measured and predicted primary side mass inventory (Fig. 15). The largely improved agreement for the mass inventory is a result of the model improvements with regard to the criteria for the occurrence of stratified flow, the calculation of interphase drag coefficients for critical flow and the calculation of critical flow velocities. The improved calculation of the mass discharged through the break resulted also in a more realistic prediction for the mass and temperature distribution in the primary system as shown in Figs. 17, 19 and 21.

The large fluctuations shown in some of the calculated parameters from both code versions seem to be caused by the (nearly) explicit treatment of the critical flow and wall heat transfer in the present RELAP5 code.

## 5. CONCLUSION

The extensive use of the RELAP5/MOD2 code within the last three years has identified a number of modelling deficiencies and a strong need for a further development of this code. For this reason, an international effort has been started for the improvement of RELAP5/MOD2 in the framework of the ICAP programme. The JRC Ispra contributions to this activity, as have been summarized in the paper, include a new package for the calculation of thermodynamic properties for water and steam, modifications in the criteria for the occurrence of stratified flow conditions in horizontal pipes, improvements for the calculation of interphase drag coefficient for critical flow conditions, a new choking model for two-phase conditions upstream of the throat and modifications to account for stratified conditions upstream of the break. All these modifications and model improvements have been implemented into the JRC-Ispra version of RELAP5/MOD2.

The new choking model overcomes the severe drawbacks of the original model and provides excellent agreement with separate effects test data for a wide range of inlet vapour qualities and stagnation pressure values. A further verification of this model, including the Marviken critical flow experiments, is planned for the near future.

The modifications implemented in the JRC Ispra version of RELAP5/MOD2 resulted in an improved prediction capability of the code for small break LOCA transients, as has been demonstrated for the LOBI test A2-81 (ISP-18). With the modified code version, all governing phenomena could be calculated with a reasonable agreement between measured and predicted data.

References


/ 1 / H. Städtke, W. Kolar:
JRC Ispra Results from the Assessment of RELAP5/MOD2 on the Basis of LOBI Test Data
15th USNRC Water Reactor Safety Research Information Meeting,
October 24 - 29, 1987, Gaithersburg, Maryland/USA

/ 2 / H. Städtke, W. Kolar:
Predictions Capabilities of RELAP5/MOD1-EUR, an Improved Version of the LWR Safety Code RELAP5/MOD1
European Nuclear Conference (ENC 4),
June 1 - 6, 1986, Geneva, Switzerland

/ 3 / H. Goldammer:
GOST; A Software Package for the Calculation of Thermodynamic Properties of Water and Steam
Final Report on Contract No. 2194-83-10 ED ISP D, November 1984

/ 4 / Y. Taitel, A. Dukler:
A Model for Predicting Flow Regime Transitions in Horizontal and Near Horizontal Flow
AIChE Journal, Vol. 22, No 1, January 1976

/ 5 / H. Städtke, W. Kolar, B. Worth:
Assessment of RELAP5 Choking Model
Third International Topical Meeting on Reactor Thermal Hydraulics,
October 15 - 18, 1985, Newport, Rhode Island, USA

/ 6 / M. Alamgir, J. Lienhard:
Correlation of Pressure Undershoot during Hot Water Depressurization
ASME Journal of Heat Transfer, 103, 1981

/ 7 / J. Sanders, E. Ohlmer:
Experimental Data Report on LOBI-MOD2 Test A2-81
CEC Joint Research Centre, Ispra Establishment,
Communication No. 4019, LEC 84-30, November 1984

/ 8 / L. Piplies, G. Leva:
Quick Look Report on LOBI Test A2-81
CEC-Joint Research Centre, Ispra Establishment,
Communication No. 4022, LQC 85-28, April 1985

/ 9 / H. Städtke:
International Standard Problem No. 18 (ISP-18)
LOBI-MOD2 Small Break LOCA Experiment
Final Comparison Report, OECD/CSNI Report 133, April 1987

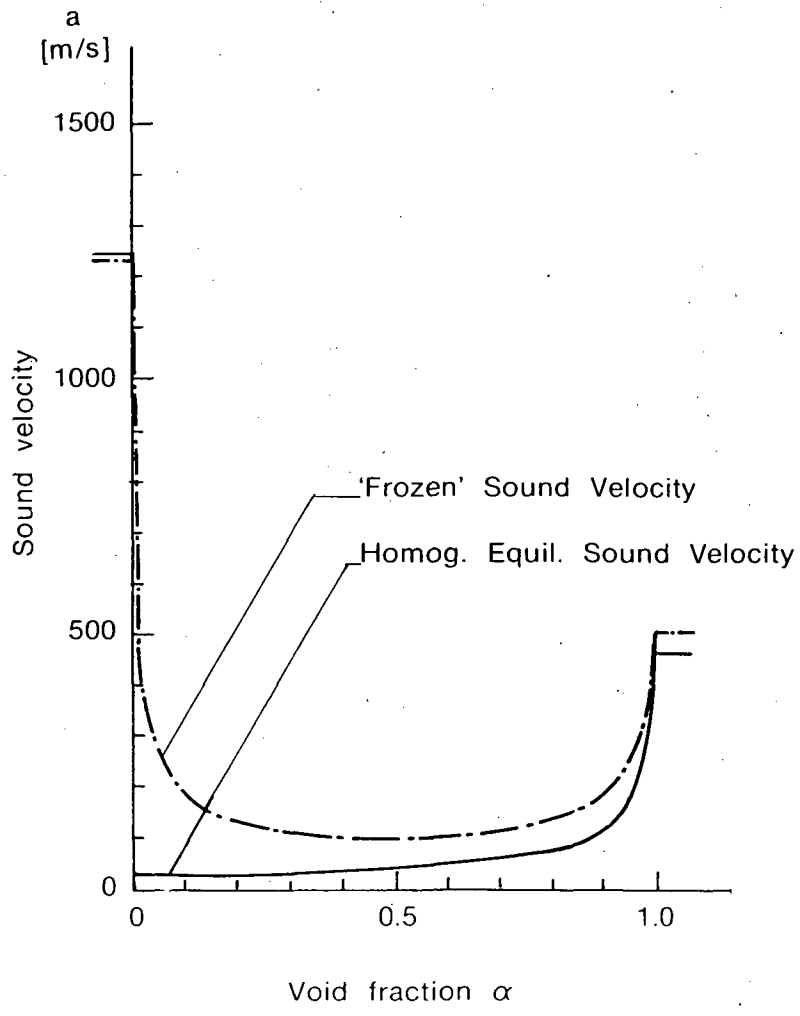


Fig. 1 Homogeneous Equilibrium and 'Frozen' Sound Velocity for Water, Pressure p = 2.0 MPa

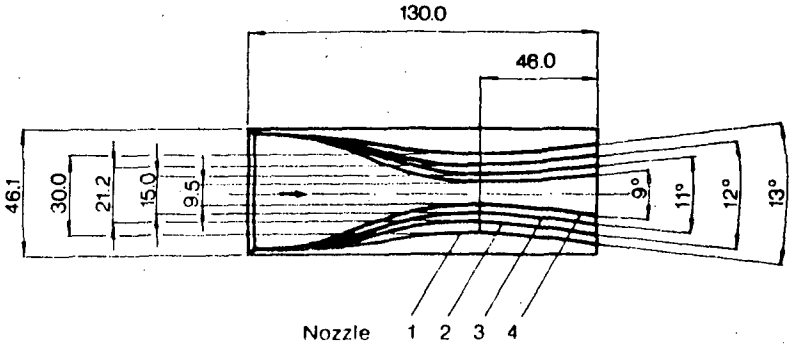


Fig. 2 LOBI Discharge Nozzles for Simulation of 1.0 A, 0.5 A, 0.25 A and 0.10 A Breaks

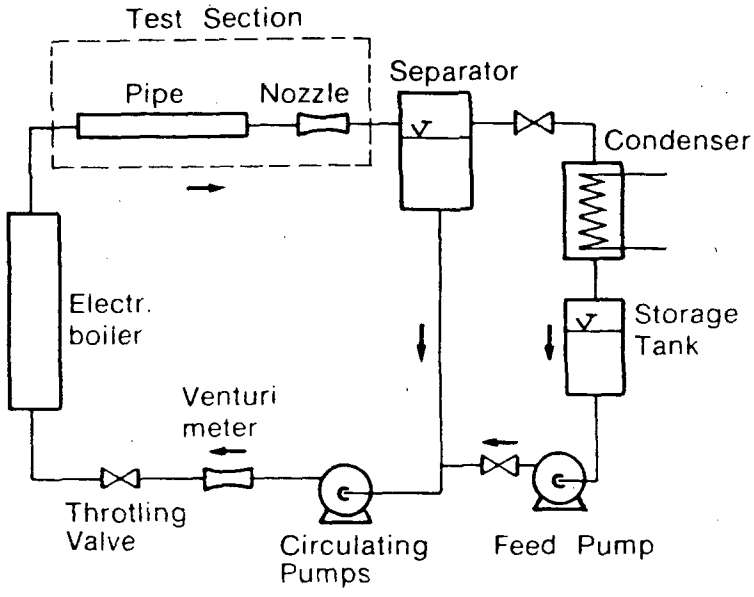


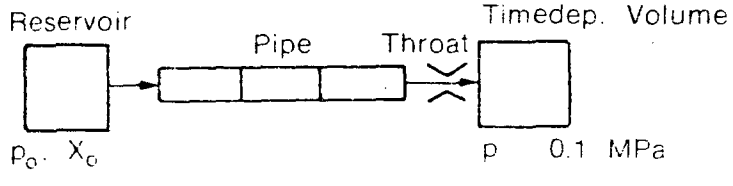


Fig. 3 Schematic of Nozzle Test Loop and RELAP5 Nodalization of Test Section

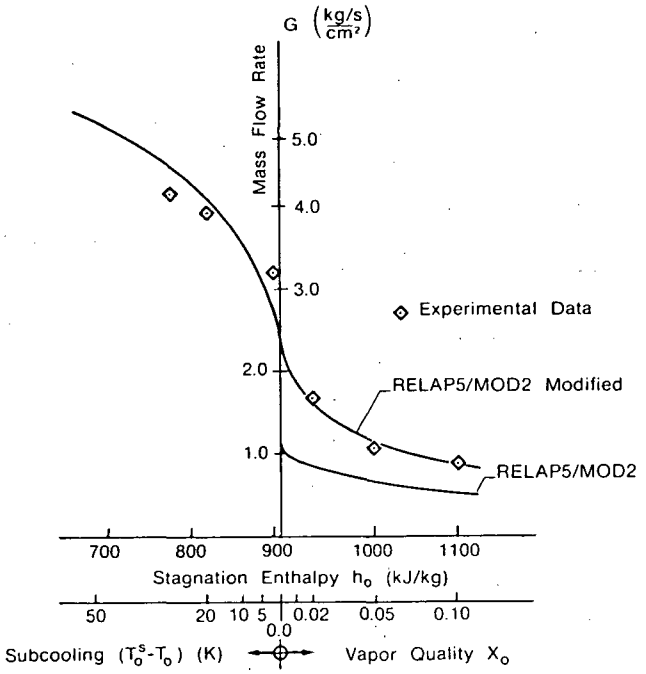


Fig. 4 Critical Mass Flow Rates for LOBI Break Nozzle No. 3, Stagnation Pressure $p_o$ = 2.0x10$^6$ Pa

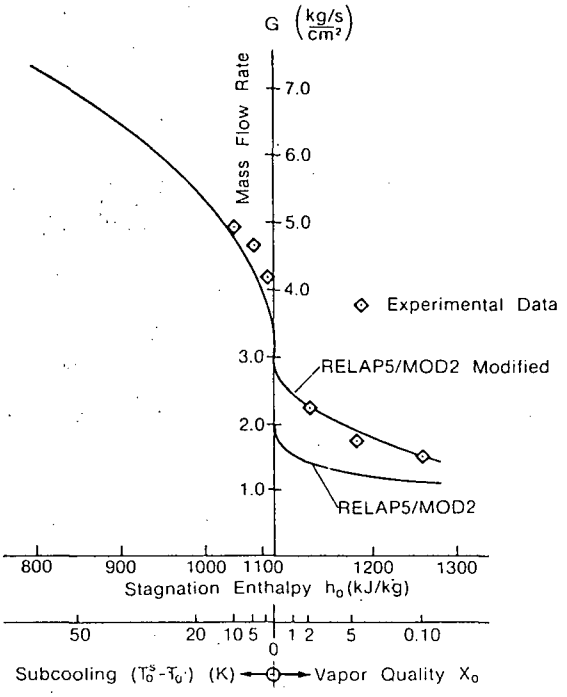


Fig. 6 Critical Mass Flow Rates for LOBI Break Nozzle No. 3, Stagnation Pressure $p_o$ 4.0x10$^6$ MPa

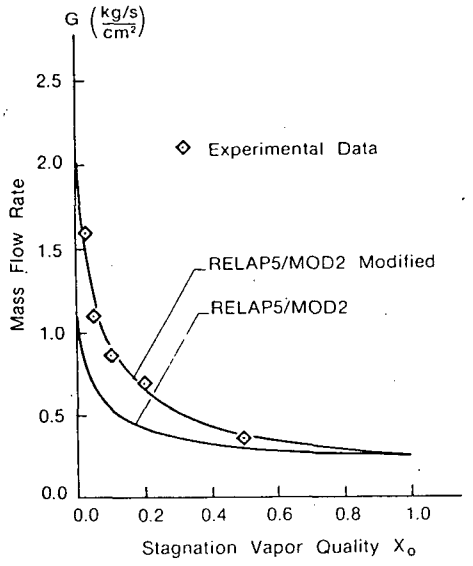


Fig. 5 Critical Mass Flow Rates for LOBI Break Nozzle No. 3, Stagnation Pressure $p_o$ = 2.0 MPa

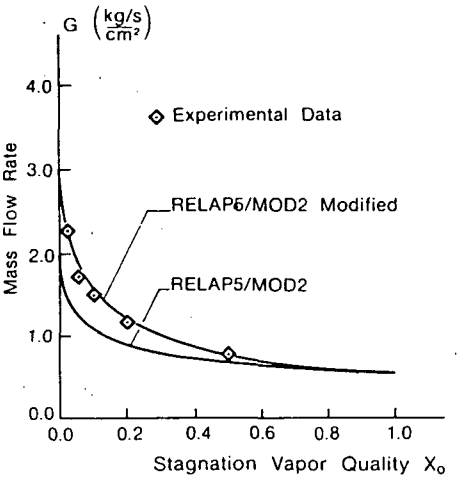


Fig. 7 Critical Mass Flow Rates for LOBI Break Nozzle No. 3, Stagnation Pressure $p_o$ = 4.0x10$^6$ MPa

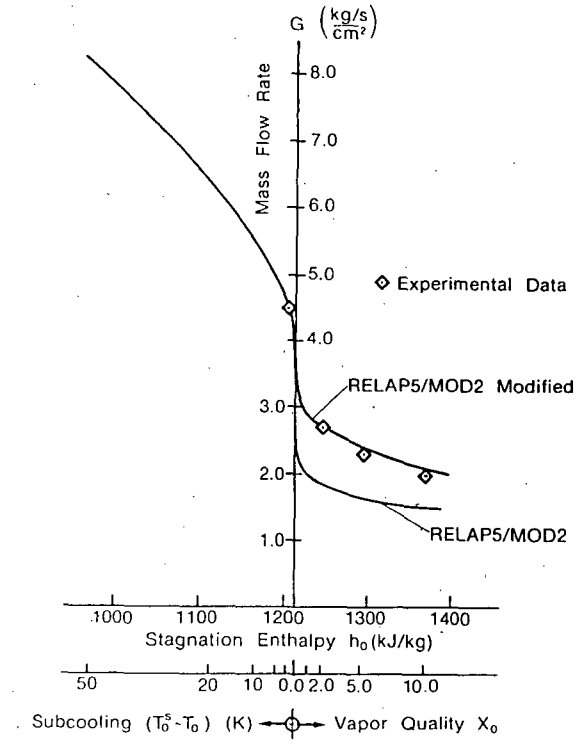


Fig. 8 Critical Mass Flow Rates for LOBI Break Nozzle No. 3, Stagnation Pressure $p_0 = 6.0 \times 10^6$ MPa

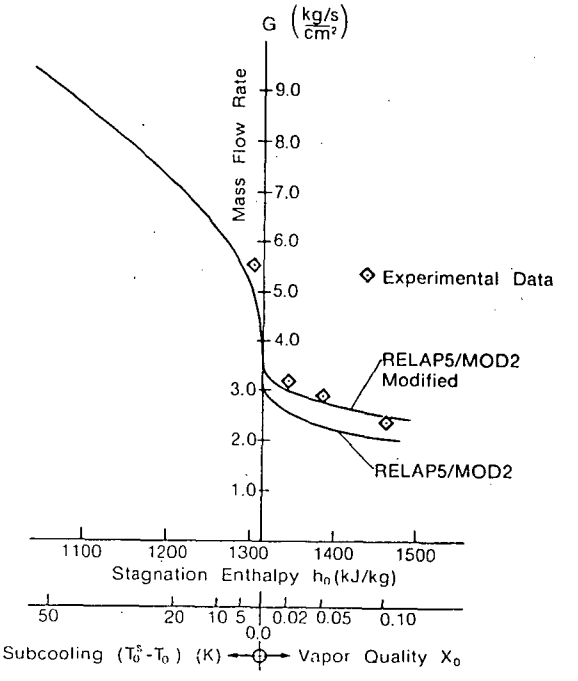


Fig. 10 Critical Mass Flow Rates for LOBI Break Nozzle No. 3, Stagnation Pressure $p_0 = 8.0 \times 10^6$ MPa

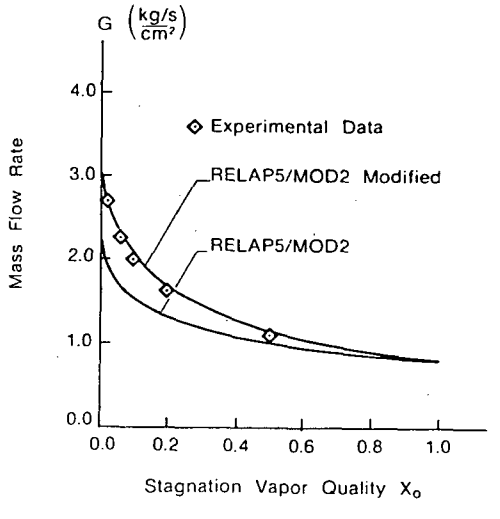


Fig. 9 Critical Mass Flow Rates for LOBI Break Nozzle No. 3, Stagnation Pressure $p_0 = 6.0 \times 10^6$ MPa

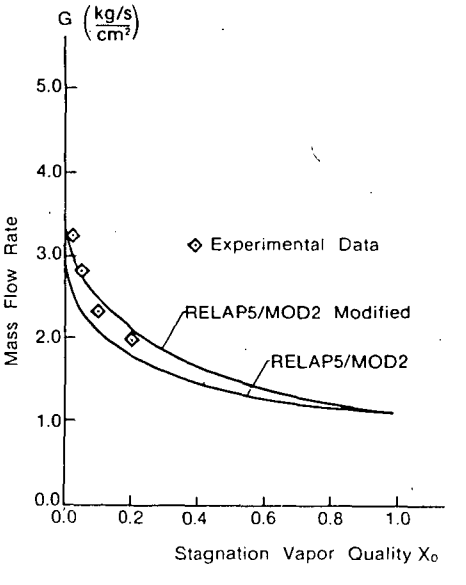


Fig. 11 Critical Mass Flow Rates for LOBI Break Nozzle No. 3, Stagnation Pressure $p_0 = 8.0 \times 10^6$ MPa

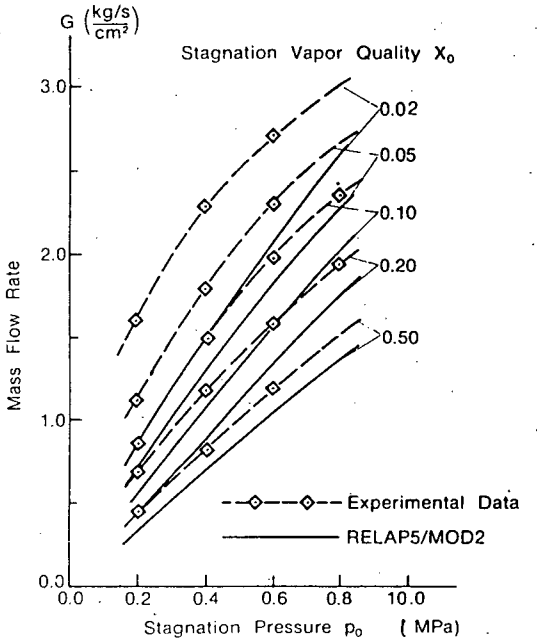


Fig. 12 Critical Mass Flow Rate for LOBI Break Nozzle No. 3, Saturated Inlet Conditions, Original Choking Model

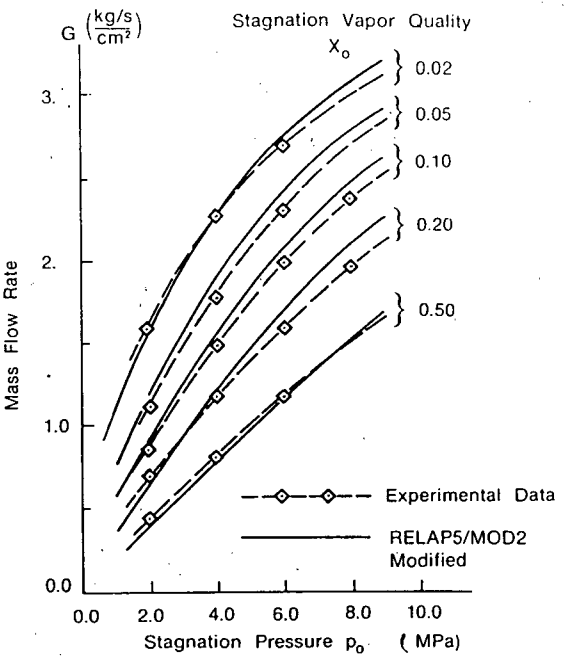


Fig. 13 Critical Mass Flow Rate for LOBI Break Nozzle No. 3, Saturated Inlet Conditions, Improved Choking Model

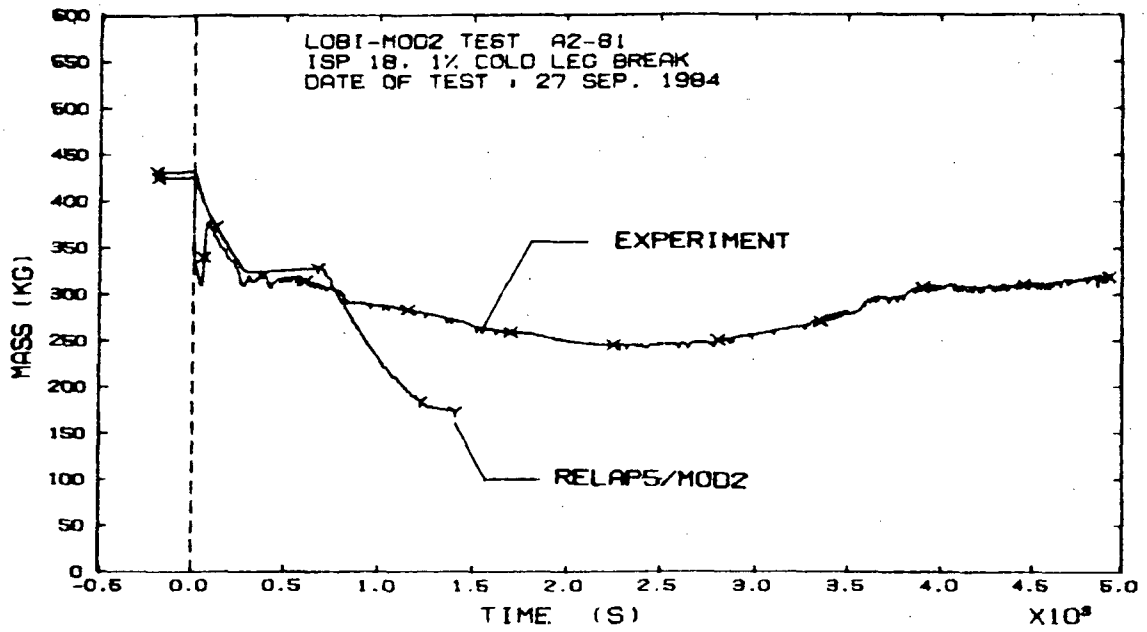


FIG. 14: PRIMARY SIDE MASS INVENTORY
CODE: RELAP5/MOD2

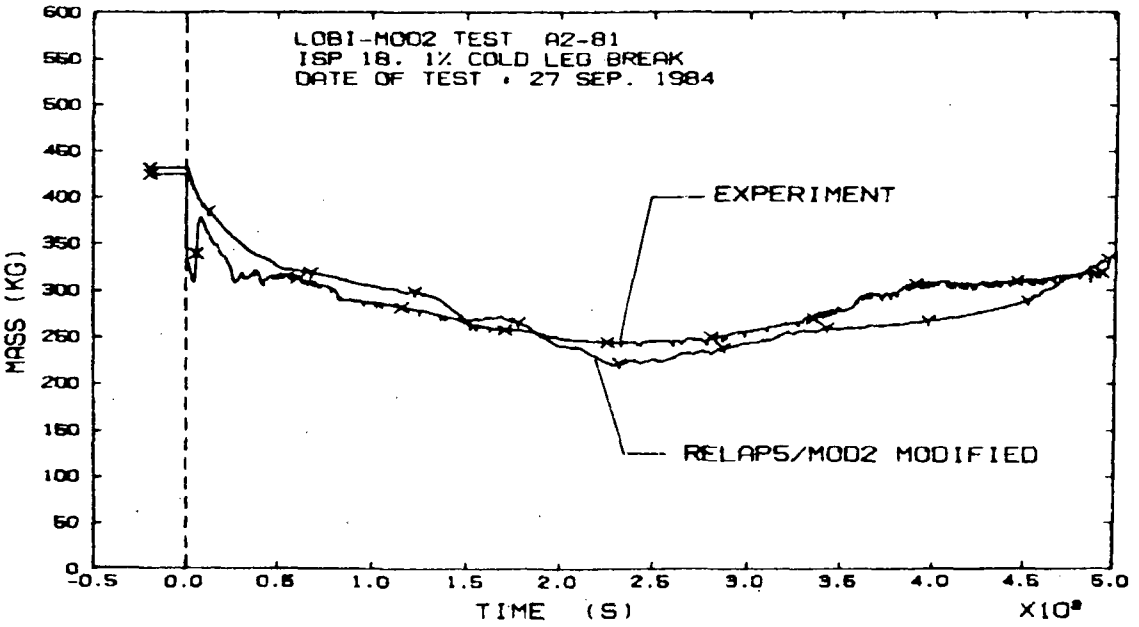


FIG. 15: PRIMARY SIDE MASS INVENTORY
CODE: RELAP5/MOD2 MODIFIED

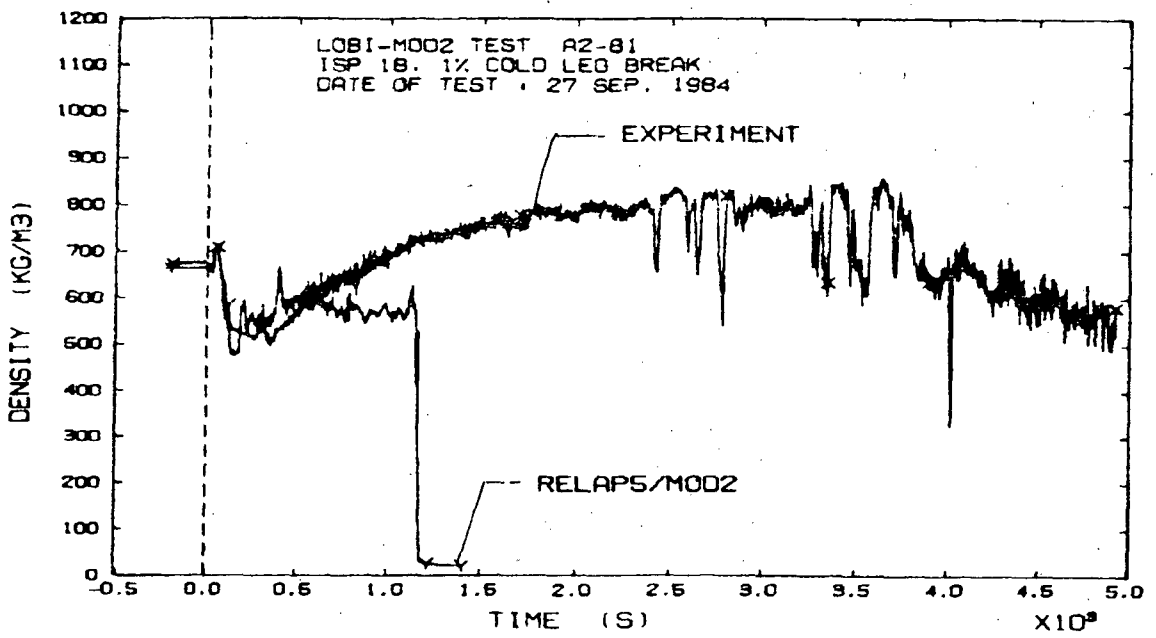


FIG. 16: FLUID DENSITY IN INTACT LOOP HOT LEG. VESSEL OUTLET
CODE: RELAP5/MOD2

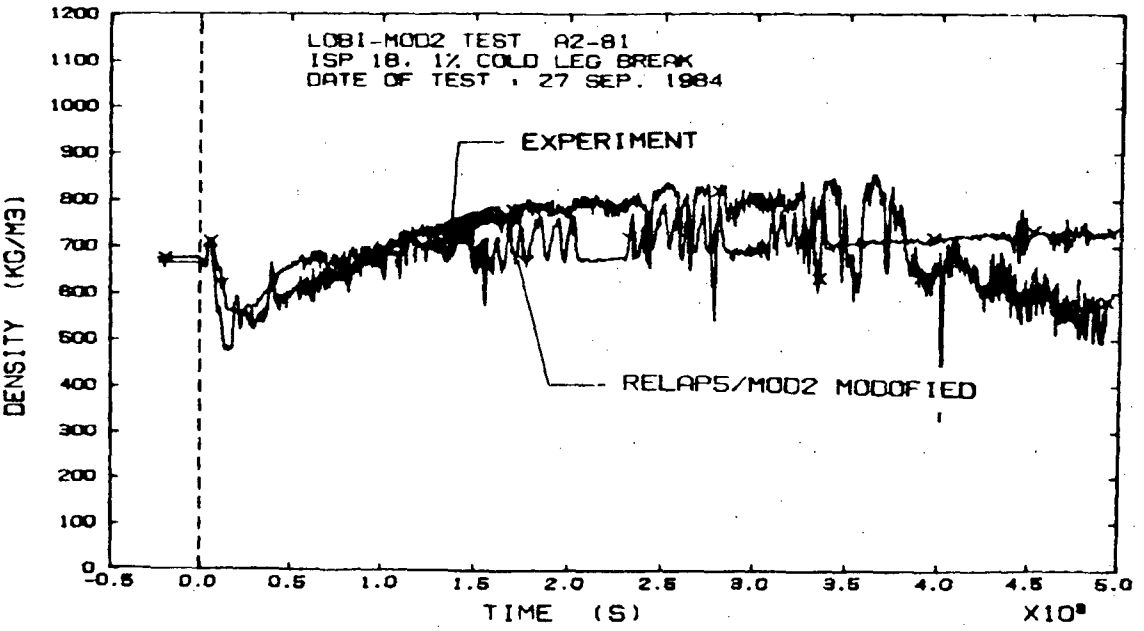


FIG. 17: FLUID DESNSITY IN INTACT LOOP HOT LEG. VESSEL OUTLET
CODE: RELAP5/MOD2 MODIFIED

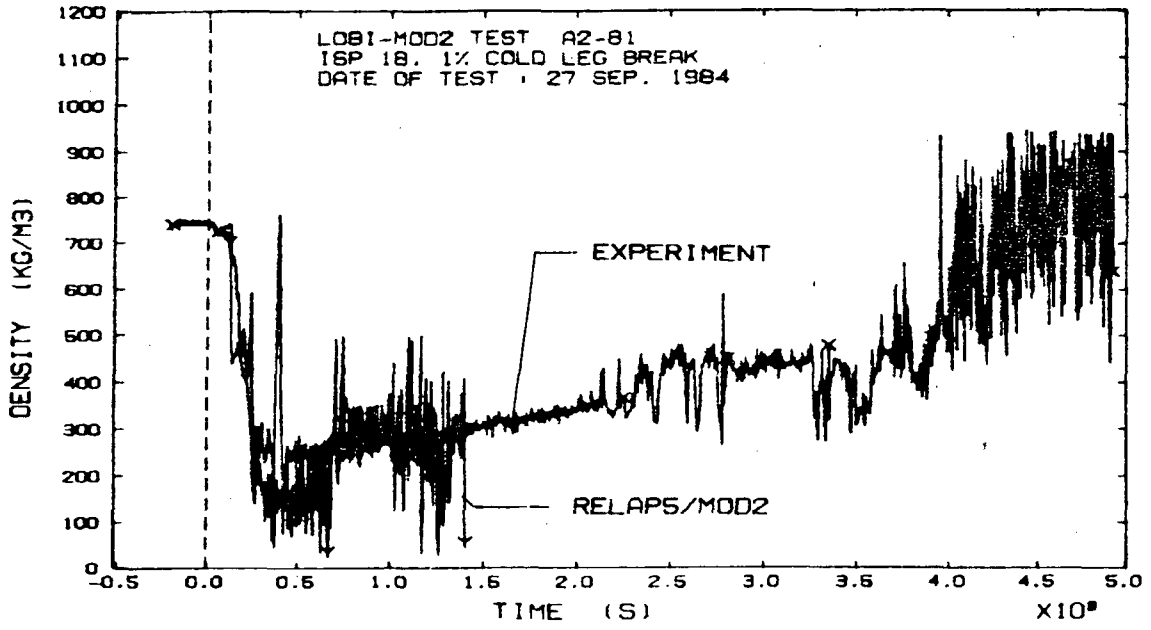


FIG. 18: FLUID DENSITY IN BROKEN LOOP COLD LEG. VESSEL INLET
CODE: RELAP5/MOD2

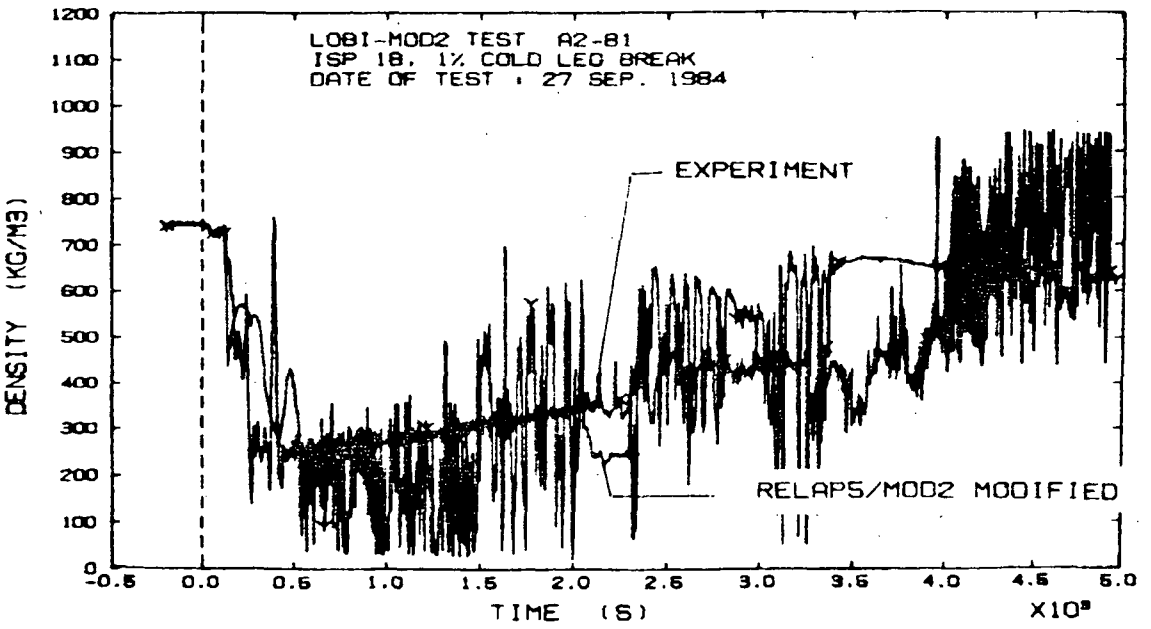


FIG. 19: FLUID DENSITY IN BROKEN LOOP COLD LEG. VESSEL INLET
CODE: RELAP5/MOD2 MODIFIED

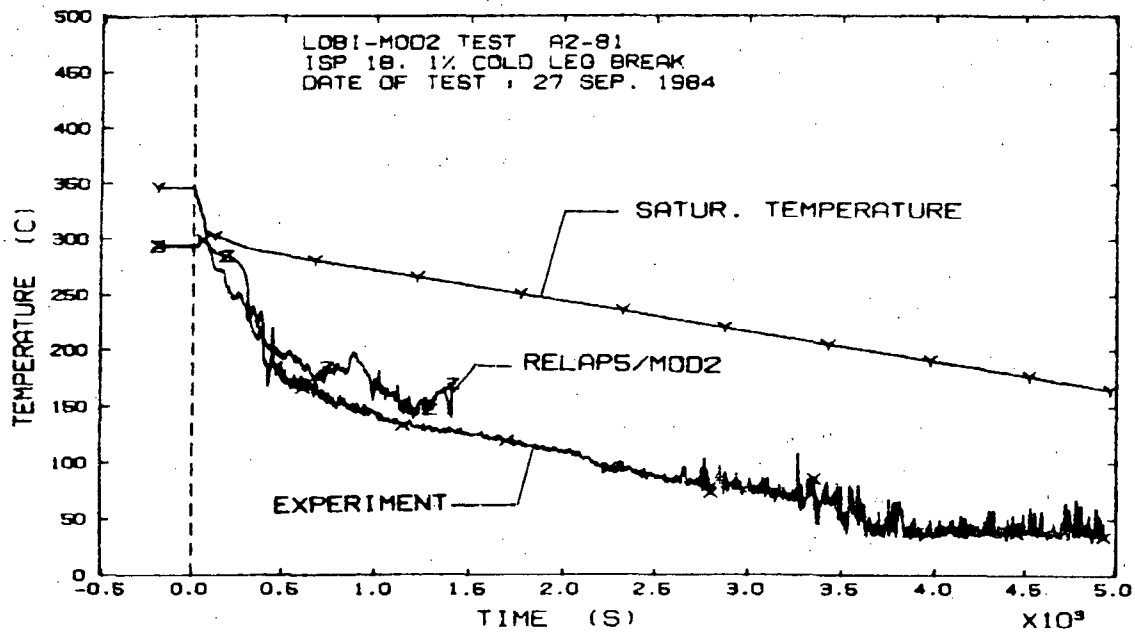


FIG. 20: LIQUID TEMPERATURE IN INTACT LOOP COLD LEG. NEAR ECC INJECTION POINT
CODE: RELAP5 MOD2

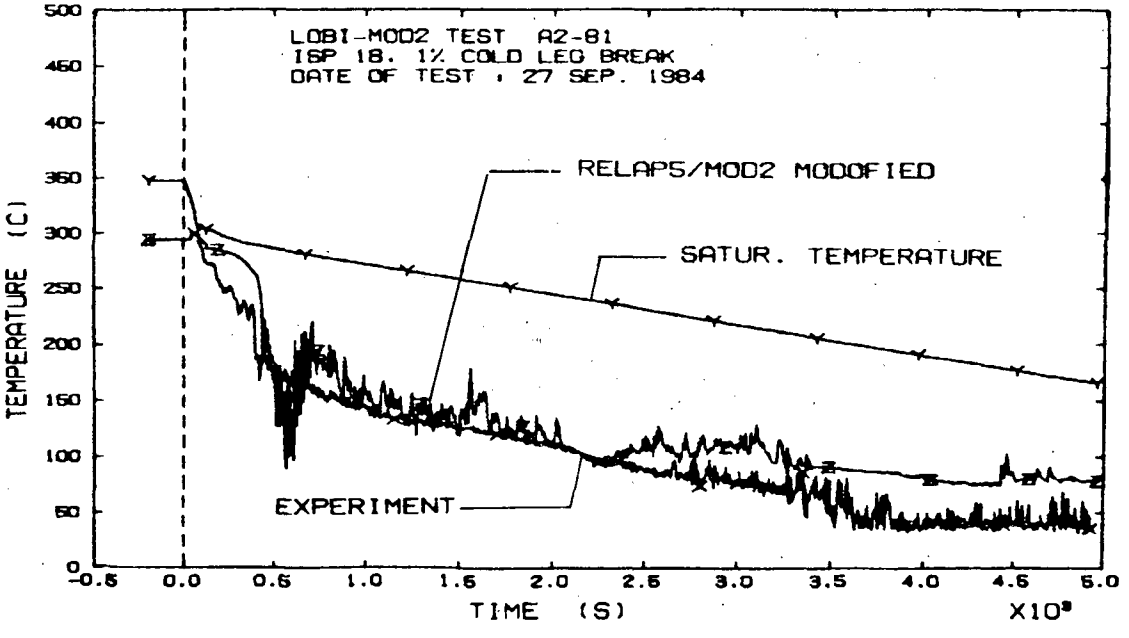


FIG. 21: LIQUID TEMPERATURE IN INTACT LOOP COLD LEG. NEAR ECC INJECTION POINT - BOTTOM OF PIPE
CODE: RELAP5/MOD2 MODIFIED

# SWITZERLAND'S CODE ASSESSMENT ACTIVITIES IN SUPPORT OF THE INTERNATIONAL CODE ASSESSMENT PROGRAM (ICAP)

S.N. Aksan, G. Th. Analytis, D. Lübbesmeyer

Paul Scherrer Institute (PSI) (Formerly EIR)
CH-5303 Würenlingen, Switzerland

**Abstract**

Within the framework of the International Code Assessment Program (ICAP) of the US.NRC, independent code assessment analyses at PSI have been performed using the RELAP5/MOD2 and TRAC–BD1/Mod1 thermal-hydraulic transient codes as part of the agreement. The assessment cases selected include both separate effects and integral tests, e.g. PSI–NEPTUN reflooding and boil-off experiments, FLECHT-SEASET reflooding experiments, OECD/LOFT LP–SB–3 (small break LOCA), LP–LB–1 and LP–02–6 (large break LOCA) experiments and two Leibstadt (BWR-6 plant) startup transient tests.

The calculations and analysis of most of the agreed assessment cases have been completed. In this paper, the main results and conclusions of these calculations are presented. As a result of these calculations and analysis, a number of special models which need to be further improved are identified (e.g. in relation to interfacial shear and heat transfer during boil–off and reflooding phases) and model changes are proposed. Some of these proposals are tested in an experimental version of RELAP5/Mod2 at PSI.

In this assessment work, the rapid cladding cooling and quench during the blowdown phase of a large break loss–of–coolant has also been investigated in some detail. The experimental evidence available from blowdown quench, such as that encountered in the LOFT experiments, is reviewed. Calculations using the RELAP5/Mod2 code have been performed for the OECD/LOFT LP–LB–1 and LP–02–6 tests in order to identify the ability of the code to calculate the blowdown phase quench. To further investigate rapid cladding quenches, separate effects tests conducted in the LOFT Test Support Facility (LTSF) have also been calculated using the frozen version of RELAP5/Mod2. The preliminary results of these calculations and resulting findings are also presented in this paper.

# 1. INTRODUCTION

The research program in the field of thermal-hydraulic transient analysis for the Light Water Reactor (LWR) Safety at the Paul Scherrer Institute (PSI, formerly EIR) is conducted partly in accordance with the bilateral agreement between the United States Nuclear Regulatory Commission (US.NRC) and the Swiss Federal Office of Energy (BEW). PSI has been acting as the executing agent of BEW. From the Swiss side, the purpose of this research is to obtain and to maintain the know–how at PSI for computing and analysing nuclear power plant transients (ranging from operating transients to accidental transients up to severe core degradation) with best–estimate thermal-hydraulic transient computer codes such as RELAP5 and TRAC. Additional to the mentioned purpose, the Swiss participation in the ICAP is also to contribute to establishing internationally assessed and approved computer codes for thermal-hydraulic transient analysis of Light Water Reactors. PSI obtains access to these codes in exchange for contributions as defined in the bilateral agreement.

The PSI research program consists of three main tasks:

(1) computer code assessment,

(2) analytical model development using data from reflooding experiments, and

(3) work in experimental facilities.

In this paper, the main results of the computer code assessment activities using RELAP5/Mod2 and TRAC–BD1/Mod1 will be summarized. The experience gained from the code assessment work is utilized to perform safety analysis and calculations for thermal-hydraulics transients and breaks specific to the Swiss PWR and BWR plants, using RELAP5/Mod2 and TRAC-BF1, respectively.

# 2. PSI–INDEPENDENT CODE ASSESSMENT MATRIX

The PSI independent code assessment matrix shown in figure 1 has been established through discussions with the NRC. In this matrix, there are twenty assessment cases. Fifteen of the assessment cases are devoted to separate-effects tests e.g. boil–off and reflooding experiments in the NEPTUN test facility (Ref. 3) and five of them to integral system tests and plant start-up transients. The assessment calculations are performed using the frozen versions of RELAP5/Mod2 (36.02) and TRAC-BD1/Mod1 (Refs. 1 and 2) as indicated in figure 2. All code assesment cases have been completed with the exception of two BWR6 plant calculations for which the TRAC-BD1 code has been used for input preparation.

# 3. ASSESSMENT OF TRAC–BD1/MOD1

Five of the NEPTUN boil–off experiments have been utilized for assessing the predicting capabilities of the thermal-hydraulics transient analysis code TRAC–BD1/Mod1 (frozen version 22). The results of these assessment calculations have already been reported in the literature (Refs. 4, 5 and 6). In this paper, a short outline of the findings and resulting improvements implemented in Mod1 will be presented. One of these improvements is already included in the TRAC–BF1 version of the code, released in 1987.
The comparison of measured and calculated collapsed liquid level and the rod surface temperature histories at the peak axial power level for one of the typical experimental cases is shown in figure 3, as an example. The conclusions regarding the predicting capabilities of the frozen version of the code can be drawn from the analysis of the five boil–off assessment cases as follows:

(a) TRAC–BD1/Mod1 underpredicts the collapsed liquid level histories and hence, predicts an earlier CHF than the measurements show. Clearly, the code overpredicts the amount of water expelled from the test section. These differences are more pronounced for the 1 bar experiment.

(b) Generally, as mentioned above, TRAC–BD1 predicts an earlier CHF than the measurements actually show; hence as a result, the sudden expulsion of water from the test section is predicted to occur earlier. Also, the predicted rod surface temperatures during nucleate boiling are 8–15 K below the measured ones.

(c) It was noticed that after the rod power was turned off, the slopes of the predicted and measured rod surface temperatures were different, indicating that the calculated steam cooling heat transfer coefficient in this region was overpredicted. This can be seen in figure 3.

To improve the prediction capability of TRAC–BD1/Mod1, the following main modifications were introduced. The resulting comparison of experimental and calculated data shown in figure 4:

- An alternative bubbly/slug interfacial shear correlation based on the work of Bestion (ref. 7), more appropriate for bundles and used in the CATHARE code, is implemented in the code. As a result of this change, the collapsed liquid level histories are correctly predicted by decreasing the interfacial friction in this flow regime.

- The steam cooling heat transfer logic used in TRAC-BD1 version 12 is re-introduced in Mod1, specifically to eliminate the differences during the steam cooling phase after the power was turned off (ref. 4).

Three NEPTUN reflooding experiments were selected for the assessment of TRAC–BD1/Mod1 as shown in figure 2. References 4 and 5 give the details of the frozen version code assessment calculations. The results of these calculations indicated that:

a) There are numerical oscillations on the predicted collapsed liquid level,

b) for high flooding rate cases, the predicted quench temperatures are lower than the measured data and the predicted quench times are always later than the measurements show (fig.5).

c) Calculations for low flooding rates show large differences between measurements and predictions (fig.6).

d) The numerical problems seem to dominate the code predictions especially for the low flooding rate cases. The origin of the oscillations observed on temperature and level calculations was traced back to large steam velocity spikes which result in 'numerical carry–over'.

A number of modifications have been tried in TRAC–BD1 in order to bring improvement to reflooding calculations. As a result of these modifications, the calculations were much more stable and most of the unwanted steam velocity spikes were eliminated. Even so, it seems that there were still some inherent stability problems whose exact origin could not be traced. Considering these findings, further reflooding assessment calculations were not performed with TRAC–BD1/Mod1.

The code assessment analysis of two start-up transients of the Leibstadt nuclear power plant (KKL–BWR6) is in progress. These transients are :

(1) Main Steam Isolation Valve (MSIV) closure
(2) Total loss of feedwater

The first stage of the work, namely the data collection related to the geometrical and functional characteristics of the plant system that play a major role during the transients considered is nearly completed. The prepared input deck for the first of the two start-up transients has been tested with TRAC–BD1/Mod1.

# 4. ASSESSMENT OF RELAP5/MOD2

A limited number of boil–off assessment calculations were also executed with RELAP5/Mod2 (Ref. 5). The results of the calculations for one of the cases are shown in figures 7 and 8. As it can be seen from these figures, the amount of water expelled is overpredicted and consequently, the collapsed liquid level is strongly underpredicted. Dry–out occurs 200 s earlier than in the experiments at the peak axial power level, and as a result the cladding surface temperatures of the rods start increasing earlier, causing a maximum temperature difference between measurements and predictions of 350 K.

TRAC–BD1/Mod1 code calculations of NEPTUN boil–off tests already indicated, as mentioned in section 3, that the interfacial friction correlation in the bubbly and slug flow regimes is one of the main reasons for the deviation between calculations and experimental data. Based on this experience, the bubbly and slug flow regime interfacial friction correlation used in the CATHARE code for bundle geometries (Ref. 7) was implemented into RELAP5/Mod2.

As it can be seen from figures 7 and 8, the results of calculated entrained water, collapsed liquid level and cladding surface temperature compare very well with the experimental data.

All seven NEPTUN reflooding experiments, shown in figure 2 were calculated and analyzed by using RELAP5/Mod2 (frozen version 36.02). Detailed calculations and tests were performed for different nodalization schemes and variation of fine mesh sizes (Ref. 5). On the basis of these studies, the nodalization scheme was established and base case calculations with frozen version of the code were performed for the seven NEPTUN reflooding experiments. The results of these calculations can be summarized for three different flow rate groups:

- For high and medium flooding rate (15–4.5 cm/s) experiments, the code overpredicts the heat transfer for film boiling.
- For almost all cases, RELAP5/Mod2 underpredicts the quench temperatures, sometimes by as much as 150 K.
- For the low flooding rate NEPTUN experiments (2.5–1.5 cm/s), the agreement between calculated and measured surface temperature histories is very good until the measured turnaround temperature point; later on, they deviate considerably. During both dispersed film boiling and film boiling, the calculated heat transfer is lower than in the experiment. Consequently the turnaround-points are calculated at higher temperatures and turnaround-times occur later. Calculated and experimental temperatures differ by as much as 300 K before the quench. The predicted quench-times deviate from the measured ones within a factor of 2.
- The code strongly overpredicts the amount of water expelled and consequently underpredicts the collapsed liquid level (fig. 9). Due to numerical instabilities, steam velocity spikes are produced and these are reflected on entrained water and collapsed liquid level as step increase and decrease, respectively.
- The calculations also show that unrealistic void fraction oscillations are occurring (fig. 11) and especially void fraction discontinuities near the quench front are noticeable. The spikes in void fraction histories were flow regime dependent and mainly due to transition from one regime to another one.

As mentioned above, most of the discrepancies between calculations and measurements are more pronounced in low flooding rate cases. An extensive study has been initiated at PSI to improve the predictive capability of RELAP5/Mod2 for low–flooding rate conditions. Some of the details of this work have already been given in References 5, 8 and 9. The important modifications implemented in the frozen version of RELAP5/Mod2 can be summarized as follows:

- The bubbly/slug interfacial shear correlation (used in the CATHARE code) suitable for rod bundles, was implemented in the code. This improves the liquid carry–over predictions both in boil–off and low flooding rate experiments (fig. 10).
- The Bromley correlation was brought back to its original form; also, the Forslund-Rohsenow correlation was implemented for $\alpha > 0.8$, and the logic of the reflooding

wall heat transfer subroutine was modified. As a result, the film boiling heat transfer of high flooding rate experiments was correctly predicted and steam velocity oscillations in low flooding rate experiments were eliminated.

- Void fraction discontinuities around the quench time were suppressed by modifying the criterion of the code for selection of pre–dry out interfacial shear correlations (fig. 11)
- The Weissmann transition boiling correlation was modified (Ref. 8); as a result, very good agreement between measured and predicted quench temperatures was achieved for all reflooding experiments.

The results of the modifications for both low and high reflooding cases can be seen in figures 12 and 13, where the comparison of measured and calculated data are presented for both the frozen and modified version of RELAP5/Mod2.
In addition to the NEPTUN cases, two FLECHT tests were also selected from RELAP5 developmental code assessment cases, one being a high flooding rate case (31701), and the other a low flooding rate case (34006). Calculations were performed both with the frozen version of RELAP5 and the version with the modifications mentioned above, in order to check their general applicability. The comparison of these calculations also indicated improvement for these cases.

## OECD/LOFT TEST LP–SB–03

The LOFT test LP–SB–03 simulated a small break loss–of–coolant accident (LOCA) which resulted from a 4.67 cm diameter (0.4%) single-ended break in the cold leg of a large commercial PWR with a failure of high pressure emergency core coolant injection capability. Cooldown was achieved by feed and bleed of the secondary system, which was initiated after core uncovering.
This test was calculated by PSI using basically RELAP5/Mod2 (36.01). The details of this calculation are given in Ref. 10. The calculation employed a model of the LOFT facility consisting of 132 fluid cells for the vessel and the rest of the systems. The input deck was developed from an earlier RELAP5/Mod1 model of the LOFT facility.
This calculation showed that many major system variables calculated by RELAP5/Mod2 were in very good agreement with the experimental data, such as primary and secondary system pressures, densities and break flow. Additionally the timing of the draining of the legs, reflux condensation in the steam generator tubes and uncovering of the core were calculated with good accuracy. Typical results are shown in figure 14. The major problem was encountered in calculating the core thermal behavior. An error was observed in the heat-up rate of the fuel cladding as seen in figure 15. Also, the dry-out time was calculated later than in the experiment. This could be due to poor prediction of CHF occurance at high pressure boil–off conditions. The heat-up rate in the calculation was controlled by enhanced cooling, which was due to prediction of drainback of condensate from the hot-legs into the core. This drainback may also have occurred in the test, but is likely to have influenced only the cooling of the peripheral rods in the core. The non-homogeneous liquid distribution in the upper plenum and its asymmetrical fall back into the core could not be properly modeled with one dimensional code.
The calculation was executed at an average CPU-time to real time ratio of 5 on a CDC-176

computer. Considerable improvements could be seen in comparison to a previous PSI calculation of the same test with RELAP5/Mod1, in respect to stability, mass error, capturing the main phenomena observed in the test, and execution speed (ref. 11).

## OECD/LOFT TEST LP–02–6

LOFT experiment LP–02–6 was a cold leg double-ended break loss–of–coolant accident experiment. The initial conditions for this experiment were representative of US.NRC licensing limits in commercial PWR and included loss of offsite power coincident with LOCA initiation and minimum emergency core coolant injection as defined by criteria. The assessment calculations of this experiment at PSI were performed by using the frozen version of RELAP5/Mod2 (version 36.02). The details of the calculations are presented in Refs. 12 and 13.

For modeling the LOFT facility by RELAP5/Mod2, a total of 101 volumes, 103 junctions, and 24 heat structures were used. The nodalization scheme developed at EG&G for the calculation of LOFT small break cases was taken as basis. Main modifications were introduced for the core region, which was modeled by using two channels: a "hot" channel with 219 pins and an "average" channel with 1081 pins: 16% of the flow goes to the hot channel; 79% to the average; and 5% to the bypass. The hot channel was divided into 13 axial nodes of unequal lengths, the smaller ones (0.088 m) in the central region and the larger ones (0.265 to 0.21 m) at the bottom and top, respectively. For the average channel, 5 axial nodes were used. Analysis of the calculations has shown that most of the thermal-hydraulic parameters of the experiment e.g. pressure, broken loop mass flow, etc., are well predicted within an accuracy of approximately $\pm$ 20% with respect to experimental data. Though this was not the case for the blowdown phase early quench behavior of the rods, observed after the mass flow into the core becomes positive at about 5.5 s after the break opens. Consequently, the subsequent heat-up, before the reflooding is initiated, is not predicted at all. Comparisons of the calculated with the measured cladding surface temperature histories in the hot channel at axial elevations of 0.69 m and 0.79 m are shown in figure 16.

Further calculations were performed to investigate the sensitivity of the results to the nodalization scheme. The number of volumes and junctions were reduced especially in the pressurizer, the steam generator secondary side and in the intact loop. Total of nine different nodalization schemes were calculated and the deviations between the results of the different calculations under investigation remain relatively small, with the exception that the significant differences can be observed for cladding surface temperatures (fig. 17).

As will be discussed in section 5, the blowdown phase quench encountered in LOFT LB–02–6 experiment (and also in other LOFT large break experiments) is a very interesting phenomenon for the large break LOCA. Since the frozen version of RELAP5/Mod2 could not predict early quench, further investigations were performed at PSI in this respect (ref. 16). In Particular, the blowdown heat transfer package in RELAP5 was critically examined and it was observed that the return to nucleate and transition boiling is restricted, once the heat transfer regime goes into film boiling (see fig. 16). In the wall heat transfer subroutines of the frozen version of RELAP5/Mod2, the following modifications were made:

1) The logic forces the code to stay in film boiling and prevents it from returning into transition boiling if $T_w > 1350 - T_{sat}$. This restriction was removed.

2) In the subroutine calling the Post or Pre-Dry out subroutines, the code is also prevented from returning to nucleate boiling, if $T_w > 1350 - T_{sat}$; this restriction was also removed.

3) The Chen transition boiling heat transfer correlation was decreased. This is along the lines of the RELAP5/MOD2 quality assurance report (ref. 14) according to which this correlation was developed by assuming the modified Zuber correlation for the CHF. When the Biasi CHF correlation is used (as is the case during the blowdown phase), the Chen correlation will most likely over-predict the transition boiling heat transfer.

4) The film boiling logic was modified in the same way as in the heat transfer subroutine used when the reflood trip is switched on.

With the above modifications, the LP–02–6 large break LOCA test was recalculated using the same nodalization scheme as for the frozen version calculations. The predicted rod surface temperature histories are shown in figure 16 and are compared to the results of the frozen version calculations. The predictions obtained by introducing the modifications in the blowdown heat transfer package are clearly in very good agreement with the experimental data. It can be seen that both the blowdown phase quench and the subsequent heat-up are predicted along the axial length of the hot channel. It should be noted, however, that the frozen version of the code predicts no blowdown phase quench of the central high power regions under the same hydraulic conditions and hence, overpredicts the temperatures reached during the second heat-up phase by as much as 300 K. Here we have a typical case in which the code predictions are dominated by the logic which connects the heat transfer correlations rather than the correlations themselves.

## OECD/LOFT TEST LP–LB–1

LOFT experiment LP–LB–1 simulated a double ended offset shear of one inlet pipe in a four loop a PWR. The experiment was initiated from conditions representative of a PWR operating near its licensing limits. The boundary conditions for this experiment were set to simulate loss of offsite power coincident with LOCA initiation and United Kingdom minimum safeguard emergency core coolant injection (no high pressure injection system). These assumptions resulted in utilization of 70% of the accumulator volume and 50% of the pumped ECC injection of that used in the LP–02–6 experiment which represented the U.S. licensing limits. An early rapid primary coolant pump coastdown was included to attain maximum cladding temperatures by suppression of the blowdown phase quench phenomena. The assessment calculations of this experiment at PSI were performed by using the frozen version of RELAP5/Mod2 (version 36.02). The details of the calculations are presented in Ref. 15. The same nodalization scheme used for the calculation of the LOFT LP–02–6 experiment was applied to the LP–LB–1 calculations. Analysis of the calculations has shown that, in general, thermal-hydraulic behavior of the experiment was predicted satisfactorily, although it failed in describing the top-down quenching which occured between 15 and 20 s at the upper part of the core. As can be seen from figure 18, the cladding surface temperatures were

underpredicted at least about 150 K at the hot spot which during this experiment reached a peak temperature of 1260 K.

Detailed nodalization studies were done by reducing the number of volumes and junctions. Reduction of volumes and junctions did not mean that faster computer runs were obtained. Numerical instabilities were encountered due to increase in the volume sizes.

The code modifications applied to LOFT LP–02–6 experiment, as mentioned above, were tested for analyzing the LP–LB–1 experiment. The modified code also showed no early rewetting as in the experiment case. The predicted rod surface temperature histories around the peak axial power level were in good agreement with the measurements.

# 5. INVESTIGATIONS ON BLOWDOWN PHASE QUENCH

As has already been mentioned, one of the most important phenomena, observed for the first time in the LOFT large break LOCA experiments, is rapid core-wide fuel cladding cooling and quench during the blowdown phase. This phenomenon is very important to the degree of transient severity, because it removes a large part of the stored energy from the fuel during the early phases of the transient. Therefore, an extensive review on the large break loss–of–coolant accident blowdown quench has been done at PSI and elsewhere, and presented in Refs. 17 and 18. A short summary of this review with additional code assessment results obtained at PSI are given in this section.

The blowdown phase quench was determined to be caused by system hydraulics in response to the operational characteristics of the primary coolant pumps relating to the transition from subcooled to the saturated choked flow at the break. These hydraulic processes and the resulting core thermal behavior provide a difficult challenge to the systems codes. Their analysis led to a reevaluation of critical and post-critical heat transfer models. The thermal-hydraulic conditions leading to the rapid cladding cooling and the early quench was primarily a result of low-quality, high upward core flow at a time when the system pressure was still relatively high (7MPa). The rapidly moving density waves through the core had a velocity of approximately 1.8 m/s and caused a quench propagation of approximately 1.0 to 1.5 m/s in the core, It is stated in Ref. 19 that under those conditions (1) no applicable data base exists, and (2) conduction - controlled quenching cannot be the controlling factor. It is apparent that in gerenal currently used correlations in the advanced codes cannot properly handle such blowdown quench phenomena. Though it should be indicated that as reported in section 4, we were able to reproduce the early quenching, observed in the LP-02-6 experiment by modifying the wall heat transfer logic of RELAP5/MOD2 code. This by no means implies that the phenomena physically well understood and rightly modelled in the code.

The research reported in Ref. 20 provides additional non-equilibrium, post-CHF data for the development of fuel rod quenching. The comparison of these data with the wall heat transfer and vapour generation correlations shows that current heat transfer correlations are

in poor agreement with the available data.

Further experiments in a simple geometry (single rod and a nine-rod bundle) with well quantified inlet hydraulics and 7 MPa system pressure were conducted in the LOFT test support facility (LTSF) at INEL. Both of the LTSF high pressure blowdown experiment series provide important information from which to assess the capability of best estimate computer codes to predict blowdown phase quench behavior. One of the LTSF tests from the single rod test series, experiment no. 12 with high inlet flooding velocity of 3.75 m/s was calculated by using the frozen version of RELAP5/Mod2 at PSI (ref. 21). The results are compared to experimental data in figures 19 and 20, at level 1 (34.3 cm from the inlet of the heated section) and level 3 (72.3 cm from the inlet of the heated section) which is the peak power level. As can be observed from these figures, RELAP5/Mod2 slightly underpredicts the heat transfer during the film boiling phase at level 3, even though the agreement at level 1 is very good. But film–to–nucleate boiling transition heat transfer and the resulting quench behavior need additional analytical investigation, and also, require better understanding and description of the physical phenomena during the blowdown phase quench. These code calculations and comparisons also indicate the need for further experimental work. This requires the measurement of factors which will enable the characterization of the phenomena at the quench front, such as entrainment and slip between the phases downstream of the quench front. Such information is needed for advanced codes, in order to model the processes from a phenomenalogical point of view and, to predict the post-CHF heat transfer non–equilibrium and quenching phenomena.

# 6. CONCLUSIONS

The frozen version of the RELAP5/Mod2 (36.02) code has been assessed at PSI against a number of separate-effects and integral system experiments as defined in the PSI-ICAP assessment matrix. The frozen version of TRAC–BD1/Mod1 has also been assessed at PSI (only against boil–off and reflooding separate-effect tests) and the assessment using two start-up transient tests of the Leibstadt nuclear power plant (KKL) is in progress. Some of the characteristic results and specific findings from the code assessment work at PSI have already been mentioned in the text of this paper. Further details of these assessment analyses can be found in the references stated at the end of this paper.

A large number of reflooding experiments in NEPTUN and FLECHT–SEASET and some boil–off experiments in NEPTUN have been analyzed via RELAP5/Mod2-36.02 (frozen version) calculations. Based on the results obtained from the assessment work, specific flow and heat transfer regimes were examined in detail. This led to a number of modifications in the interfacial shear and reflooding heat transfer models of RELAP5/MOD2, so new models have been implemented, resulting in better agreement between measured data and code calculations.

The calculations for two LOFT large break tests (LP–02–6 and LP–LB–1) using RELAP5-/Mod2-36.02 were extended to analyze the sensivity of the results to different nodalizations. Eventhough the cladding temperature results, as shown in figures 17 and 18, are not very

sensitive to different nodalizations, the other calculated parameters given in refs. 12 and 15 showed clearly the need for optimizing the nodalization schemes which are used for the calculations. In respect to integral system calculations performed so far, it has been found that RELAP5/Mod2 is a major improvement over RELAP5/Mod1 in terms of execution speed, stability, mass error and accuracy. RELAP5/Mod2 has calculated the general thermal-hydraulic behavior of these experiments (also the LOFT small break test LP–SB–3) satisfactorily, although failing to predict some of the specific phenomena, e.g. post-CHF heat transfer, early quenching during the blowdown phase and top-down quenching and boil–off at high pressures. But our recent work at PSI summarized in section 5 presents some improvements in predicting LOFT test LP–02–6 blowdown phase quench by changing the selection logic related to nucleate, transition and film boiling in RELAP5/Mod2. However, it should be noted that extensive validation of this modification has not been done in order to draw more general conclusions.

## Acknowledgements

This report is prepared as an account of work partly sponsored by the Swiss Federal Nuclear Safety Authority (HSK) of the Swiss Federal Office of Energy (BEW), within the activities of the International Code Assessment Program (ICAP) of the US Nuclear Regulatory Commission (NRC).

During the course of this work, encouragement and support given by Professor G. Yadigaroglu is gratefully acknowledged. Special thanks are also extended to Mrs. Wemmers for her careful typing of the paper.

# References:

1. D.D. Taylor, et al.: "TRAC-BD1/Mod1: An advanced best estimate computer program for boiling water reactor transient analysis". Volumes 1 and 2, NUREG/CR-3633, 1984

2. Victor H. Ransom, et al.: "RELAP5/Mod2 Code Manual". Volumes 1 and 2, NUREG/CR-4312, 1985

3. Grütter, F. Stierli, S.N. Aksan, G. Varadi: "NEPTUN bundle reflooding experiments: Tests facility description". EIR report No. 386, 1981

4. G. Th. Analytis: "Assessment of TRAC-BD1/Mod1 with boil–off and reflooding experiments: Model improvements and numerical problems"

   Paper presented at the First Specialists Meeting of Code Users ICAP Erlangen, FRG, 9–11 June 1986

5. G. Th. Analytis, M. Richner, M. Andreani, S.N. Aksan:
"Assessment and uncertainty identification for RELAP5/Mod2 and TRAC–BD1/Mod1 codes under core uncovery and reflooding conditions"

Proceedings of the 14th Water Reactor Safety Information Meeting
NUREG/CP-0081, 1986

6. S.N. Aksan, F. Stierli, G. Th. Analytis:
"Boil–off experiments with the EIR–NEPTUN Facility: Analysis and code assessment overview report" EIR–report No. 629, September 1987

7. D. Bestion: "Interfacial friction determination for the 1D-6 equations two fluid model used in the CATHARE code".

European Two–Phase Flow Group Meeting, Southampton, England, 1985

8. G. Th. Analytis, M. Richner, S.N. Aksan:
"Assessment of interfacial shear and wall heat transfer of RELAP5/Mod2/36.02 during reflooding".

European Two–Phase Flow Group Meeting, Trondheim, Norway, June 1–4, 1987

9. G. Th. Analytis: "An 'Experimental' version of RELAP5/Mod2/36.02: Model changes, assessment efforts and, numerical problems".

Paper presented at the third ICAP Specialist Meeting,
Grenoble, France, 1–3 March, 1988

10. S. Güntay: "RELAP5/Mod2 assessment: OECD/LOFT small break experiment LP–SB–3". EIR-Gemeinschaftsreport No. 13, April 1986

11. H. Grütter and M. Andreani: "Post-test analysis of OECD-LOFT experiment LP-SB-3 by RELAP5/MOD1" PSI internal report TM-32-85-18, 1985

12. D. Lübbesmeyer: "Post-test analysis of OECD-LOFT experiment LP–02–6 with RELAP5/Mod2/36.02".
Draft report submitted for NUREG/IA publication, 1988

13. D. Lübbesmeyer: "Post-test analysis and nodalization studies of OECD–LOFT experiment LP–02–6 with RELAP5/Mod2".

Paper presented at the third ICAP specialist meeting, Grenoble, France,
1–3 March, 1988

14. R.A. Dimenna, et al.: "RELAP5/MOD2 models and correlations"
NUREG/CR-5194, August 1988

15. D. Lübbesmeyer: "Post-test analysis of OECD–LOFT experiment LP–LB–1 with RELAP5/Mod2-36.02".
Draft report submitted for NUREG/IA publication, 1988

16. G. Th. Analytis, D. Lübbesmeyer: "Analysis of LOFT experiment LP–02–6 by standard and modified RELAP5/Mod2/36.02"
Transactions of the American Nuclear Society, TRANSAO 56-1-628, Vol. 56, June 1988

17. S.N. Aksan.: "A review of large break loss–of–coolant accident blowdown quench and effect of external thermocouples"

Paper presented at the third ICAP Specialist Meeting, Grenoble, France 1–3 March, 1988

18. S.M. Modro, S.N. Aksan, V.T. Berta, A.B. Wahba
"Review of LOFT Large Break Experiments: Topical Report".
OECD–LOFT–T–3900, August 1988

19. R.A. Nelson: "Forced-convective post-CHF heat transfer and quenching".
Transactions of the ASME, vol. 104, 1982

20. R.C. Gottula, K.G. Condie, R.K. Sundaram, S. Neti, J.C. Chen, R.A. Nelson: "Forced convective, nonequilibrium, post-CHF heat transfer experiment data and correlation comparison report". NUREG/CR-3193, March 1985

21. S.N. Aksan: "Investigations on rapid cladding cooling and quench during the blowdown phase of a large break loss-of-coolant accident using RELAP5/MOD2", paper in preparation, 1989

**Figure 1:** PSI independent code assessment matrix for the ICAP.

| | Facility | Experiment I.D | Description | Parameters | Assessment Cases for Each Code | Computer Code |
|---|---|---|---|---|---|---|
| A | NEPTUN | 5001-5012 (8 Tests) | boil-off experiments | power<br>subcooling<br>initital rod temp. | 3 | TRAC-BD1/MOD1<br>or<br>TRAC-BF1 |
| B | NEPTUN | 5013-5056 (40 Tests) | reflooding experiments | 3* subcooling (low-high)<br>1 flooding rate (low-high)<br>2 initial rod temp. (low-high)<br>or NRC proposals | 6<br><br><br>2 | TRAC-BD1/MOD1<br>or<br>TRAC-BF1<br><br>RELAP5/MOD2 |
| C | heat transfer surface package 3 years program | (flecht-seaset, Oak Ridge, EIR tests, harwell tests, lehigh tests, inel tests) | | | 4-6<br>4 mm+ = 1 code assessment | driver code needed |
| D | OECD/LOFT | LP-LB-1 | large break loca experiment | | 1 | RELAP5/MOD2 |
| E | OECD/LOFT | LP-02-6 | large break loca experiment | | 1 | RELAP5/MOD2 |
| F | OECD/LOFT | LP-SB-3 | small break loca experiment | | 1 | RELAP5/MOD2 |
| G | BWR 6 | input deck for TRAC-BD1/ MOD1 from NRC | standard TRAC-BD sample input large break | check accuracy of the deck and perform parametric calculations | 2 | TRAC-BD1/MOD1<br>or<br>TRAC-BF1 |

* Number indicates the priority

+ mm = man-month

**Figure 2:** Cases to be calculated with RELAP5/Mod2 and TRAC-BD1/Mod1 codes.

Code RELAP5 / MOD2

Boil-Off Experiments A: NEPTUN

| Exp.Nr. | Pressure (bar) | Subcooling (K) | Bundle Power (KW) |
|---|---|---|---|
| 5002 | 1 | 0 | 24.6 |
| 5006 | 5 | 12 | 42.1 |
| 5007 | 5 | 12 | 24.6 |
| 5011 | 5 | 39 | 75.1 |

Reflooding Experiments B: NEPTUN

| Exp.Nr. | Pressure (bar) | Flooding water Velocity (cm/s) | Flooding water Subcooling (°C) | Single rod power (kW) | Initial cladd.temp. (°C) |
|---|---|---|---|---|---|
| 5036 | 4.1 | 1.5 | 11 | 2.45 | 757 |
| 5052 | ↓ | 2.5 | 78 | ↓ | 867 |
| 5051 | ↓ | 4.5 | ↓ | ↓ | ↓ |
| 5025 | ↓ | 10 | ↓ | ↓ | 757 |
| 5050 | ↓ | 15 | ↓ | ↓ | 867 |
| 5049 | 1.0 | 2.5 | ↓ | ↓ | ↓ |
| 5056 | 4.1 | 2.5 | ↓ | 4.19 | ↓ |

Integral system tests:

- OECD/LOFT LP-SB-3
- OECD/LOFT LP-02-6
- OECD/LOFT LP-LB-1

Code TRAC - BD1 / MOD1

Boil-Off Experiments A: NEPTUN

| Exp.Nr. | Pressure (bar) | Subcooling (K) | Bundle Power (KW) |
|---|---|---|---|
| 5002 | 1 | 0 | 24.6 |
| 5006 | 5 | 12 | 42.1 |
| 5007 | 5 | 12 | 24.6 |
| 5008 | 5 | 12 | 10.5 |
| 5011 | 5 | 39 | 75.1 |

Reflooding Experiments B: NEPTUN

| Exp.Nr. | Pressure (bar) | Flooding water Velocity (cm/s) | Flooding water Subcooling (°C) | Single rod power (kW) | Initial cladd.temp. (°C) |
|---|---|---|---|---|---|
| 5036 | 4.1 | 1.5 | 11 | 2.45 | 757 |
| 5025 | ↓ | 10 | 78 | ↓ | 757 |
| 5050 | ↓ | 15 | 78 | ↓ | 867 |

G: BWR 6

2 Start-up transients of Leibstadt NP (BWR 6)

(1) Main Steam Isolation Valve (MSIV) closure
(2) Total loss of feedwater

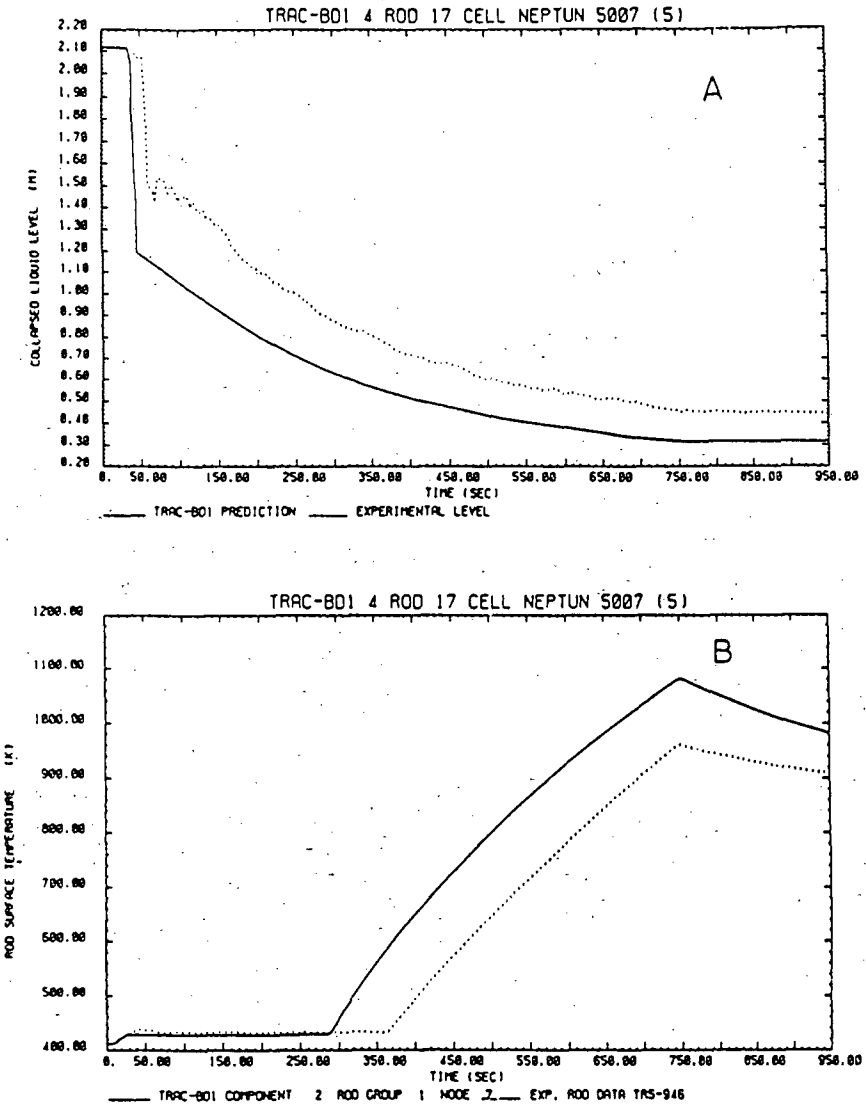


Figure 3: Comparison of measured and calculated collapsed liquid level and peak axial power level rod surface temperature histories, using frozen version of TRAC-BD1 for NEPTUN boil-off experiment 5007.

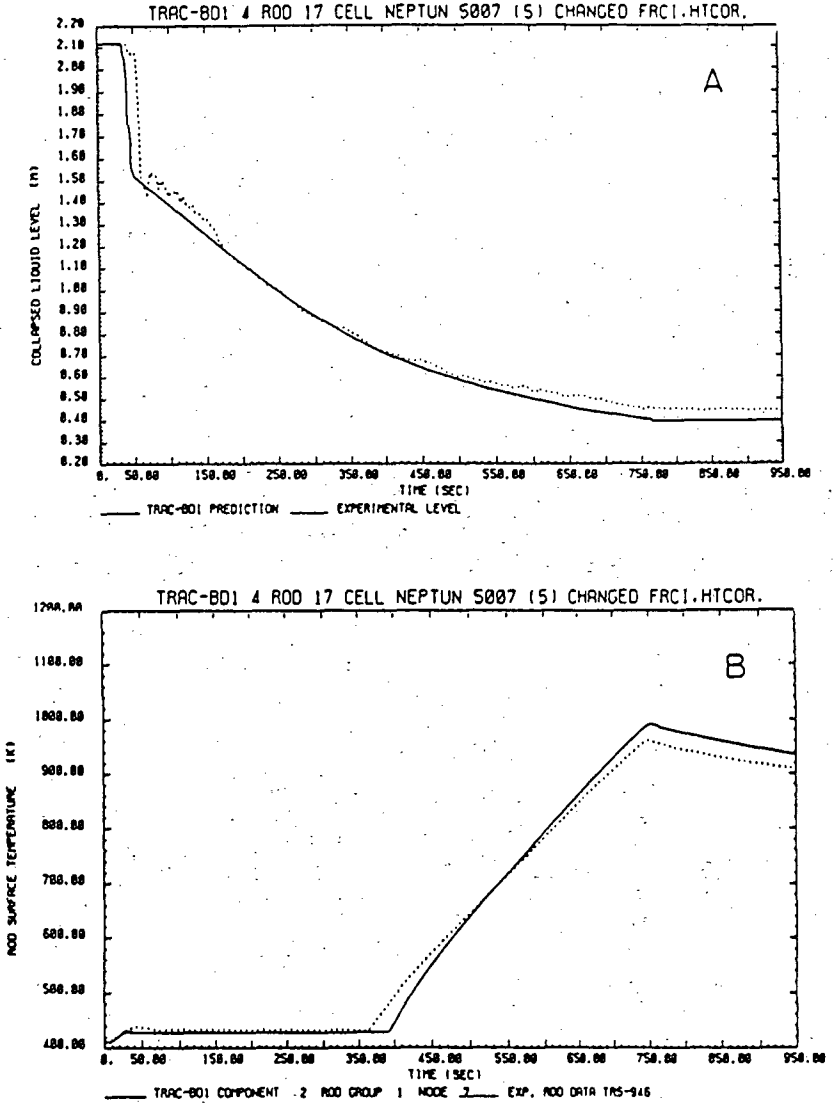


Figure 4: Comparison of measured and calculated collapsed liquid level and peak axial power level rod surface temperature histories, using modified version of TRAC-BD1 for NEPTUN boil-off experiment 5007.

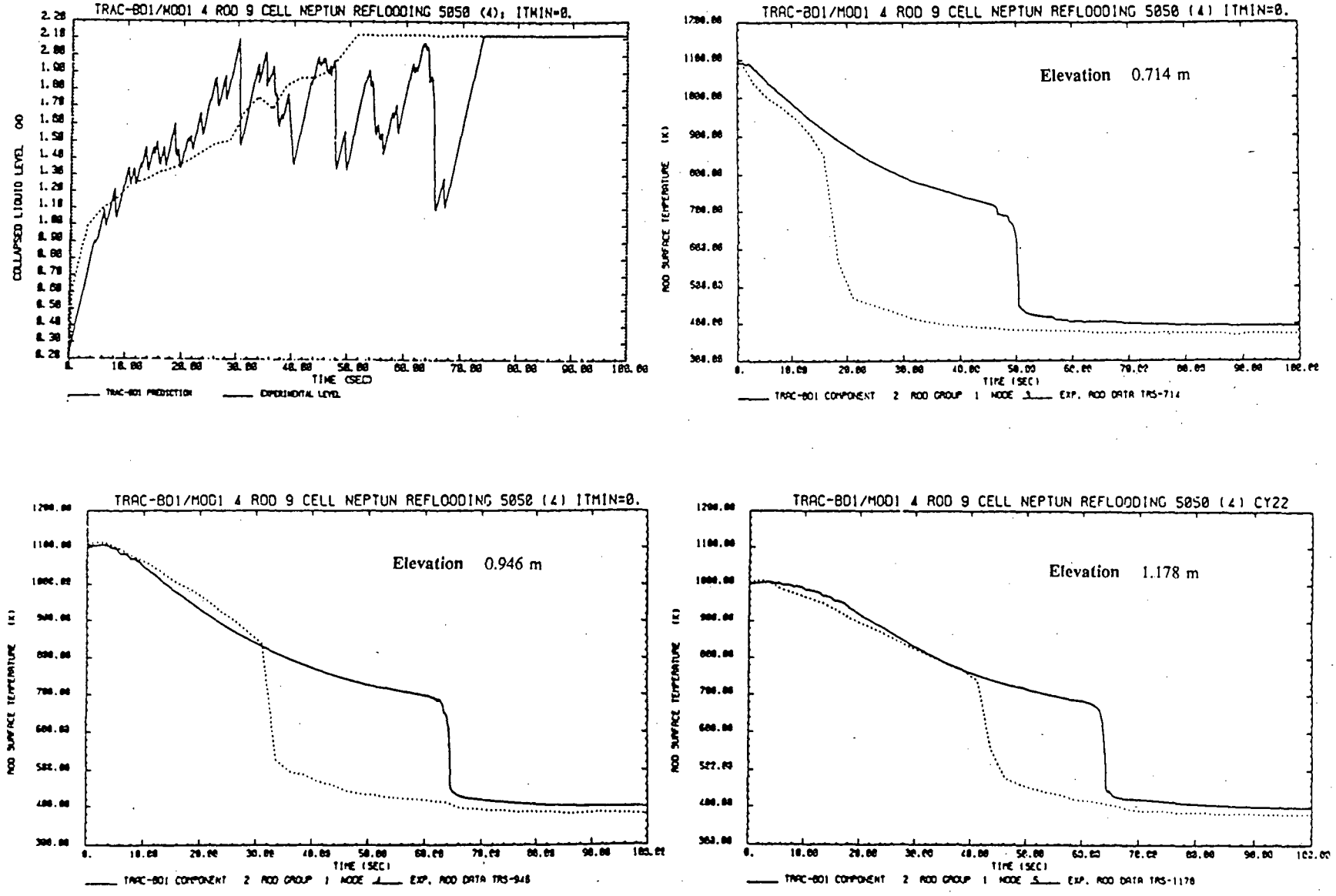


Figure 5: Measured and predicted collapsed liquid level and rod surface temperature histories by TRAC-BD1/Mod 1 for NEPTUN experiment no. 5050.

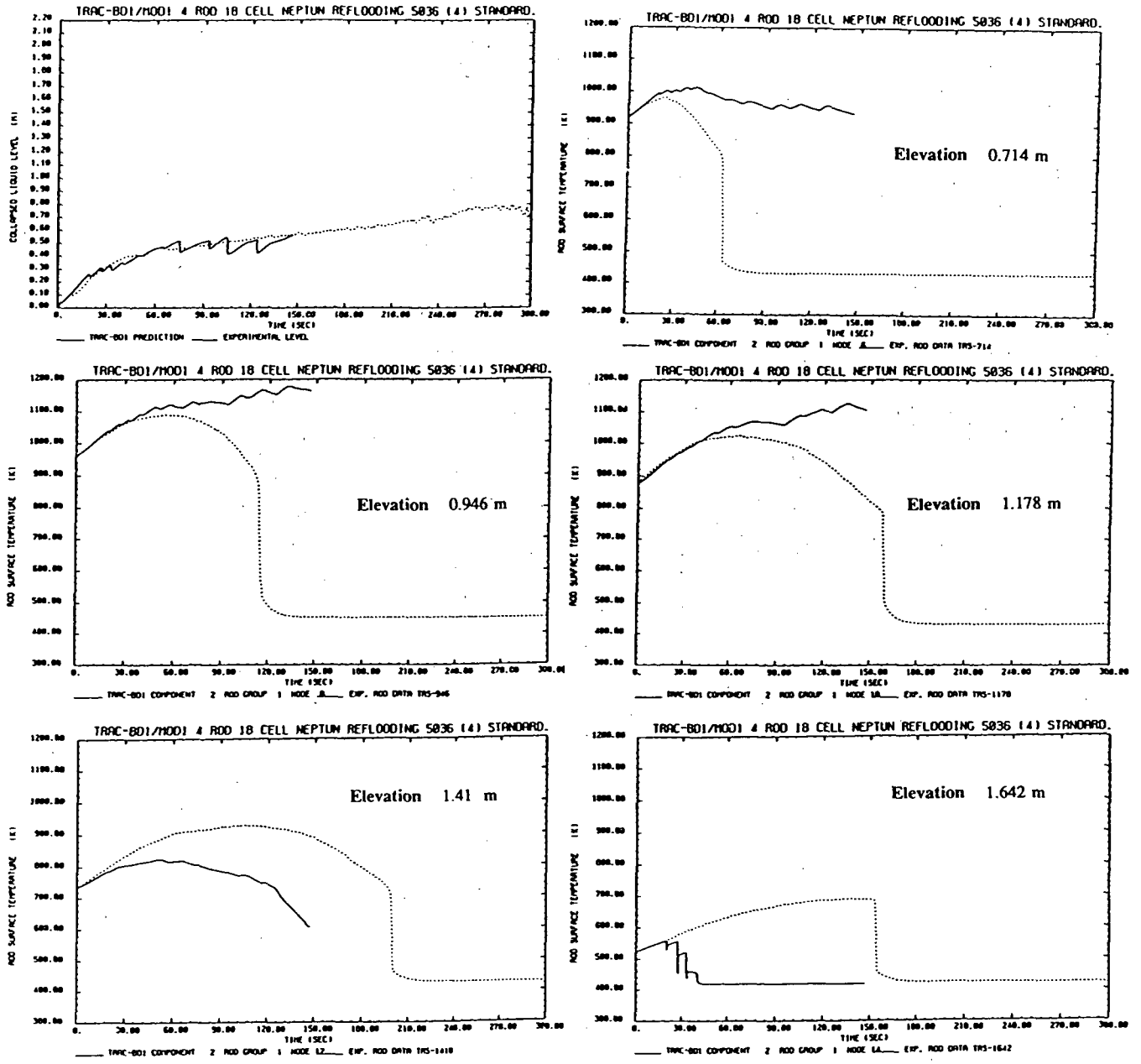


**Figure 6:** Measured and predicted collapsed liquid level and rod surface temperature histories by TRAC-BD1/Mod 1 for NEPTUN experiment no. 5036.

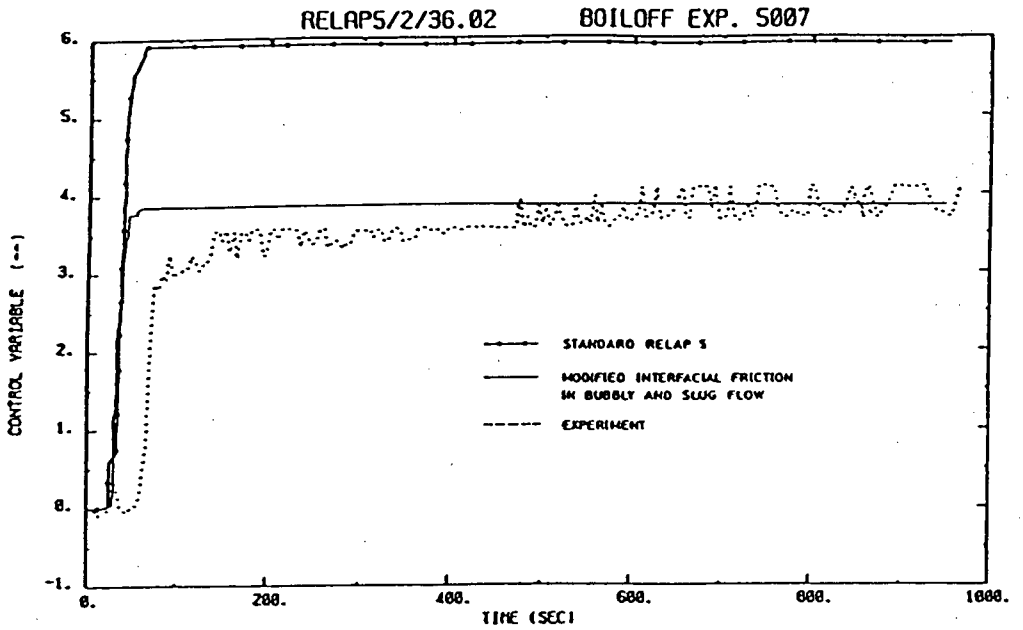


**Figure 7:** Water entrainment in NEPTUN boil-off experiment 5007, calculated by RELAP5/MOD2, with and without new correlation for the interfacial friction in bubbly and slug flow.

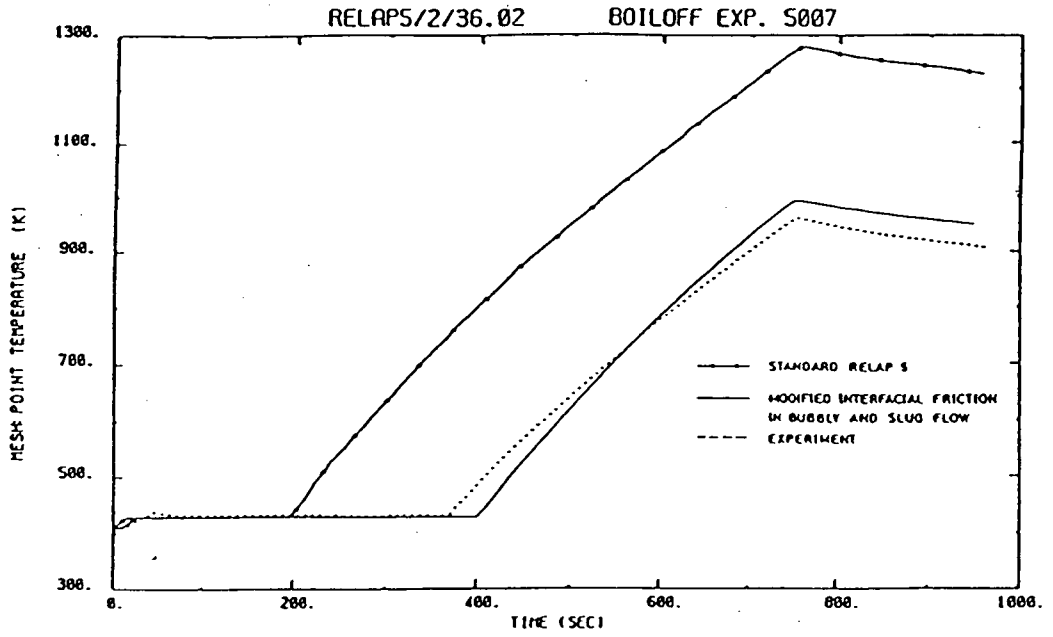


**Figure 8:** Rod cladding temperature at measurement level 4 (0.946 m elevation) in NEPTUN boil-off experiment 5007, calculated by RELAP5/MOD2, with and without Bestion correlation for the interfacial friction in bubbly and slug flow

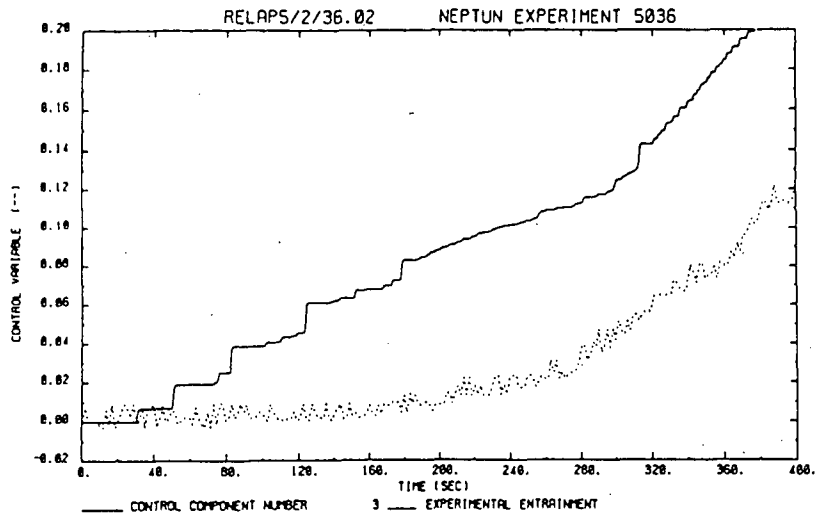


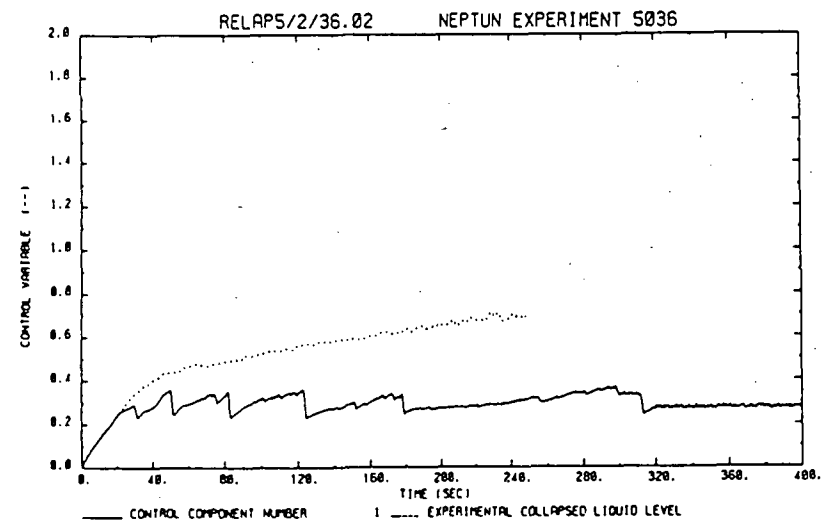


Figure 9: Exp. 5036: Measured and predicted liquid carry-over and collapsed liquid level by standard RELAP5/MOD2

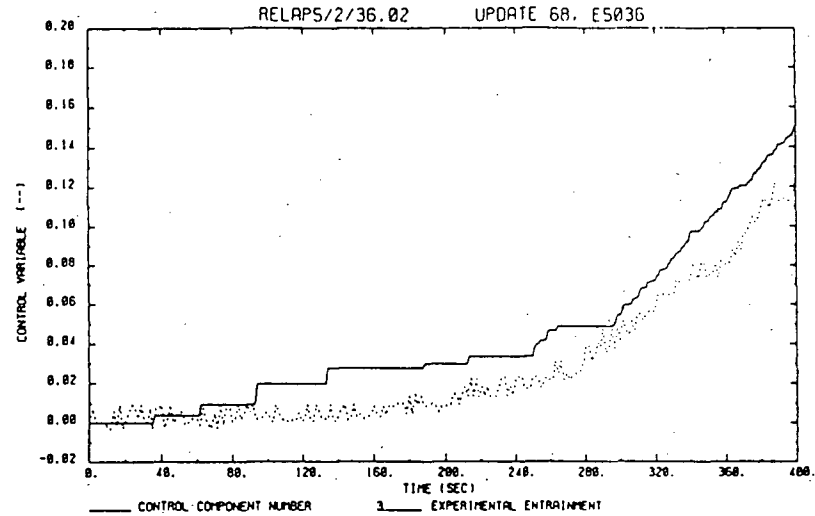


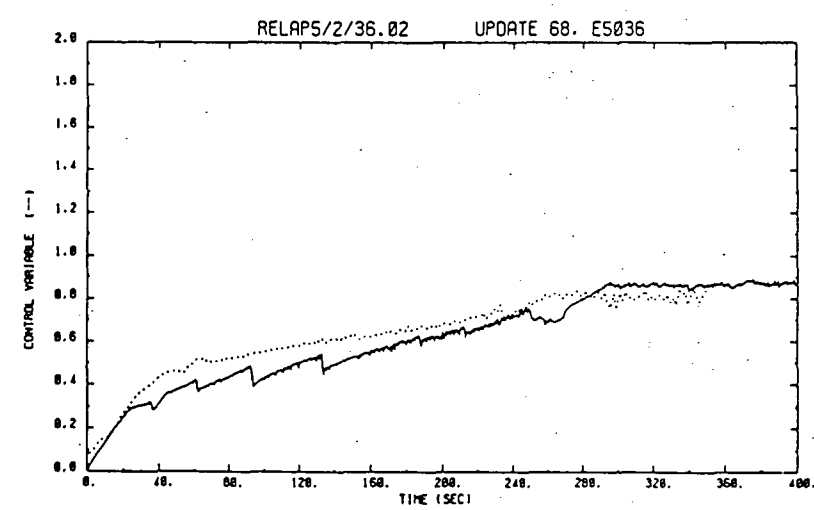


Figure 10: Exp. 5036: Measured and predicted carry-over and collapsed liquid level by RELAP5/MOD2, UPD.68

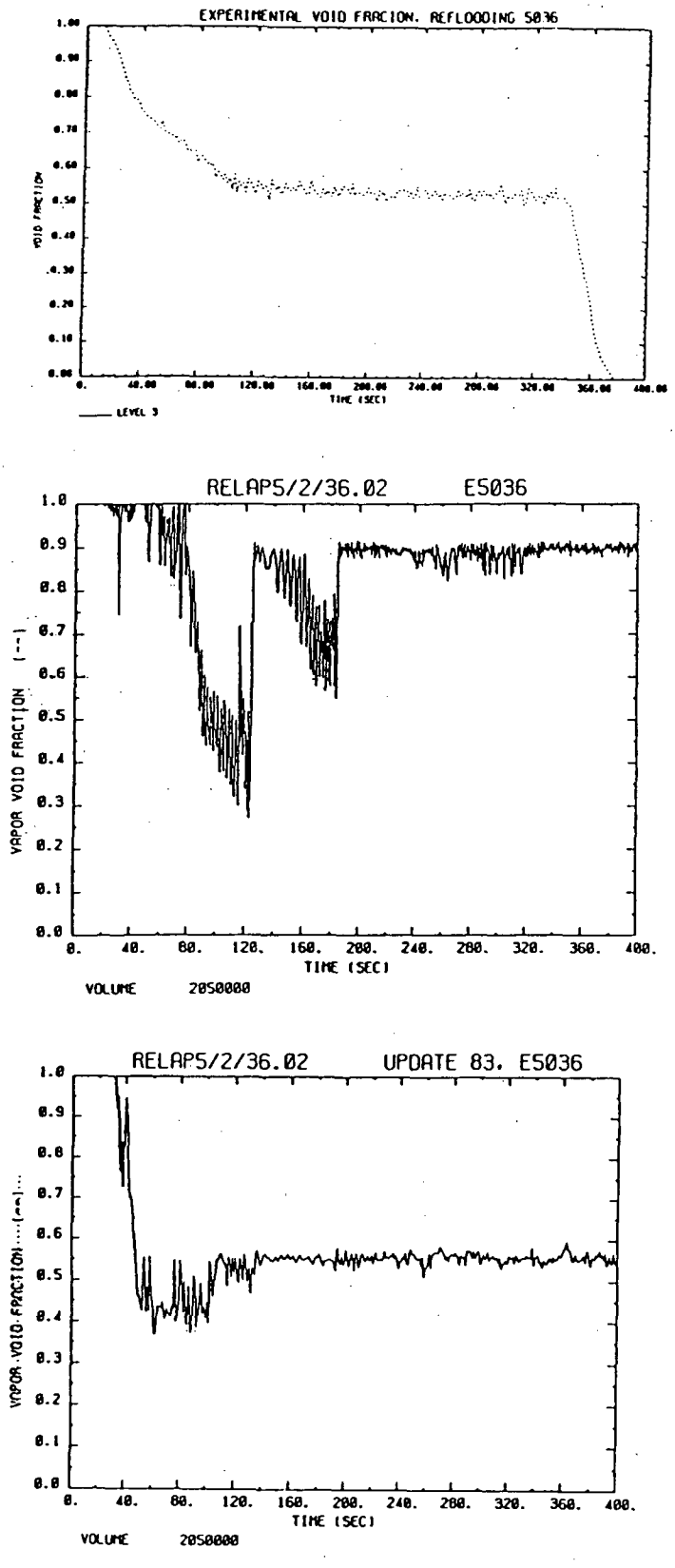


**Figure 11:** Exp. 5036: Measured and predicted void fractions at level 3 (0.714 m elevation) by standard RELAP5/MOD2 and by RELAP5/MOD2 + UPD.83

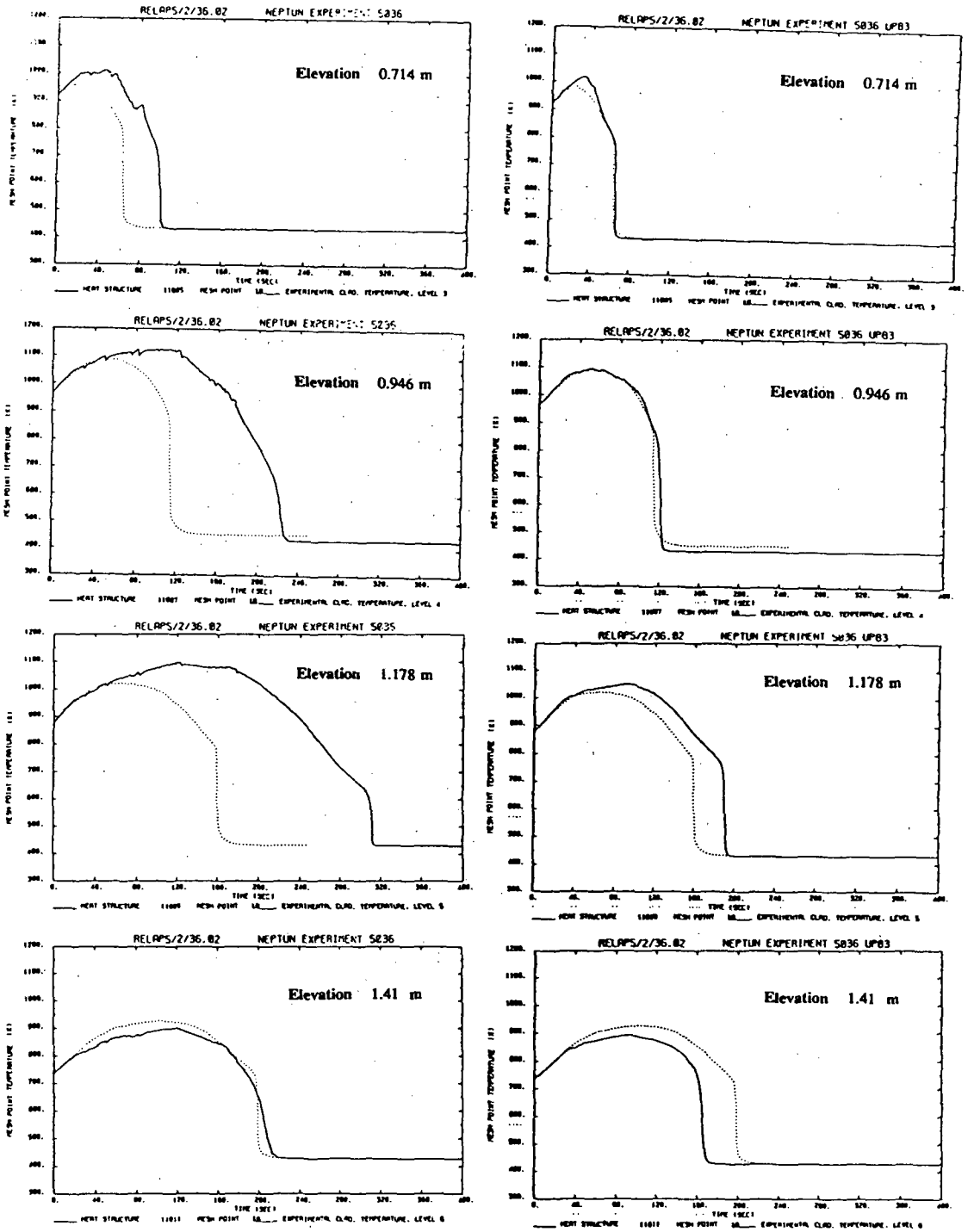


**Figure 12:** Exp. 5036: Measured and predicted rod surface temperature histories by standard RELAP5/MOD2 (left) and by RELAP5/MOD2 + All our modifications (UPD.83)

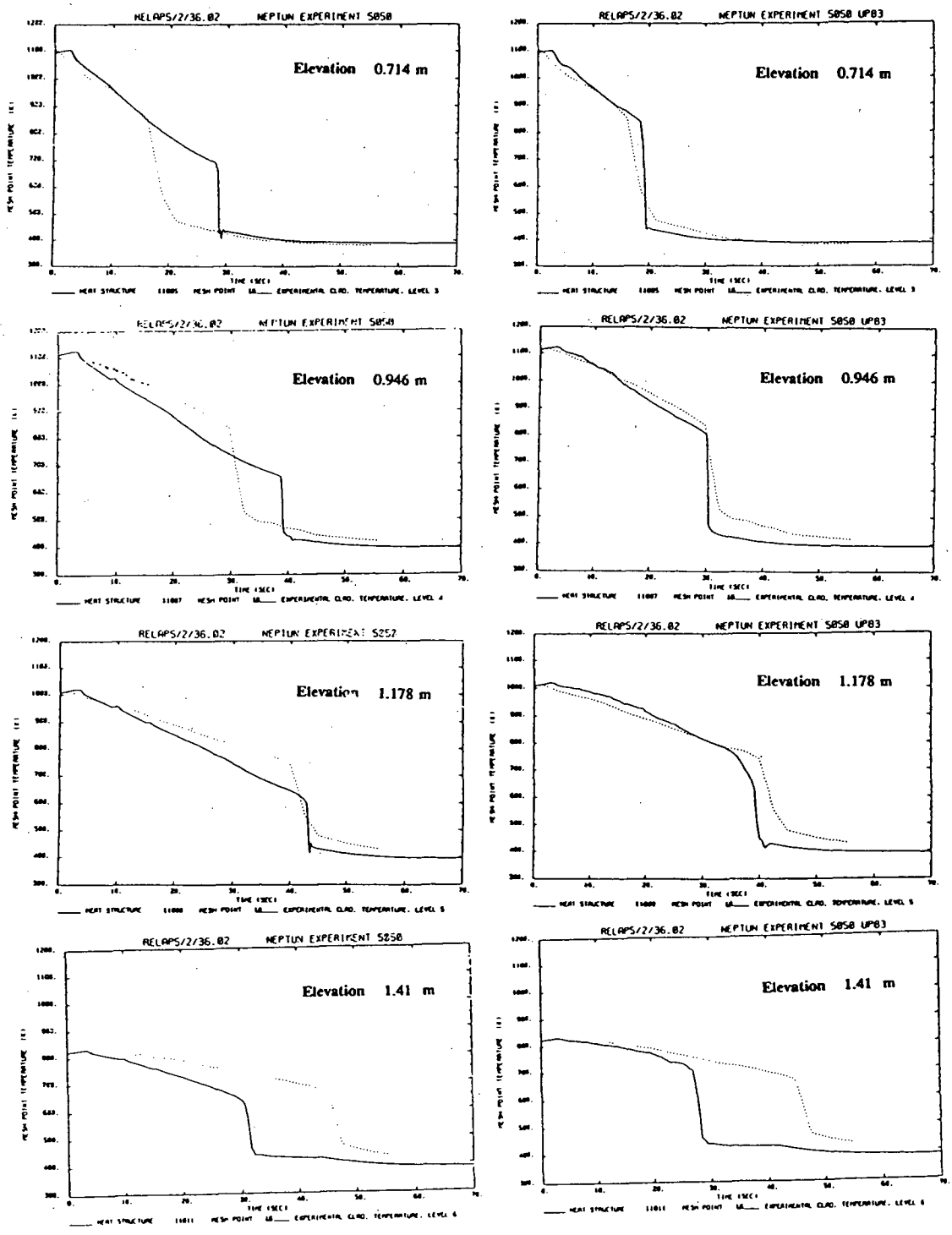


**Figure 13:** Exp. 5050: Measured and predicted rod surface temperature histories by standard RELAP5/MOD2 (left) and by RELAP5/MOD2 + UPD.83 (right)

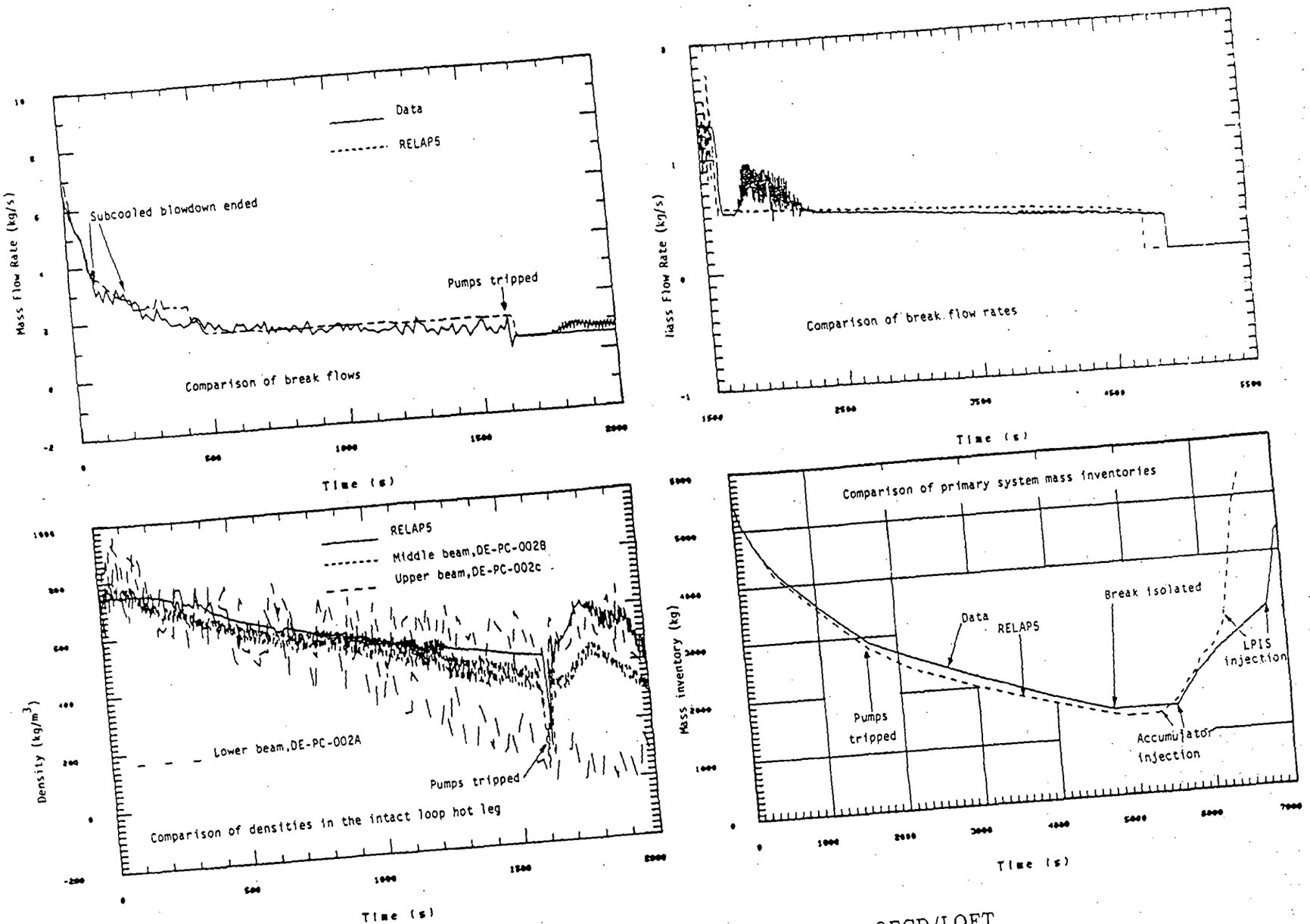


Figure 14: Typical hydraulic parameter results for OECD/LOFT test LP-SB-3.

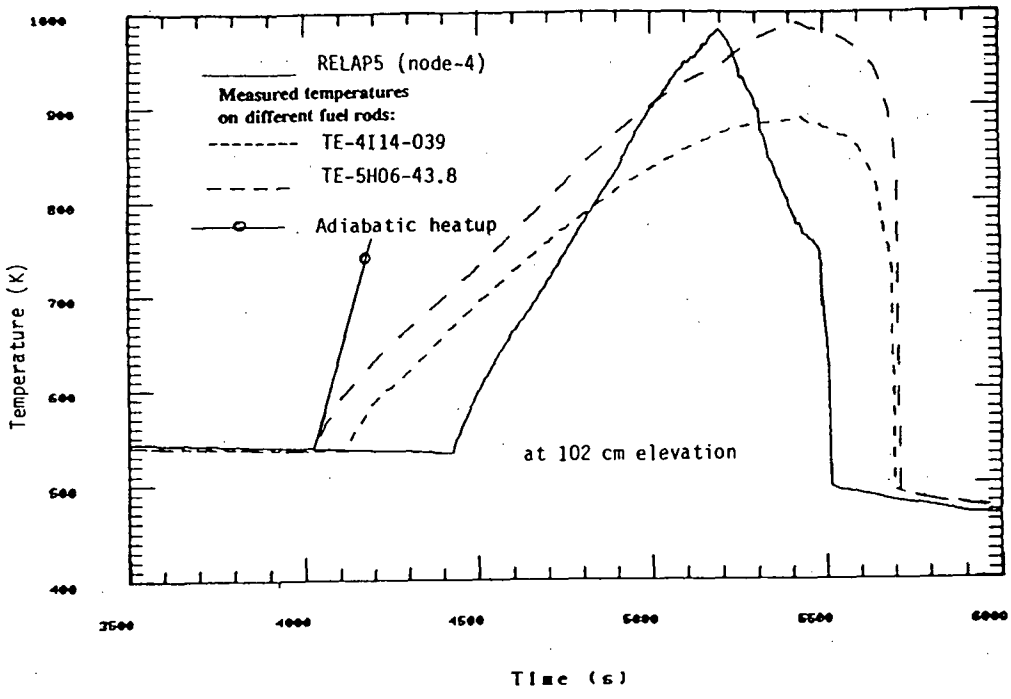


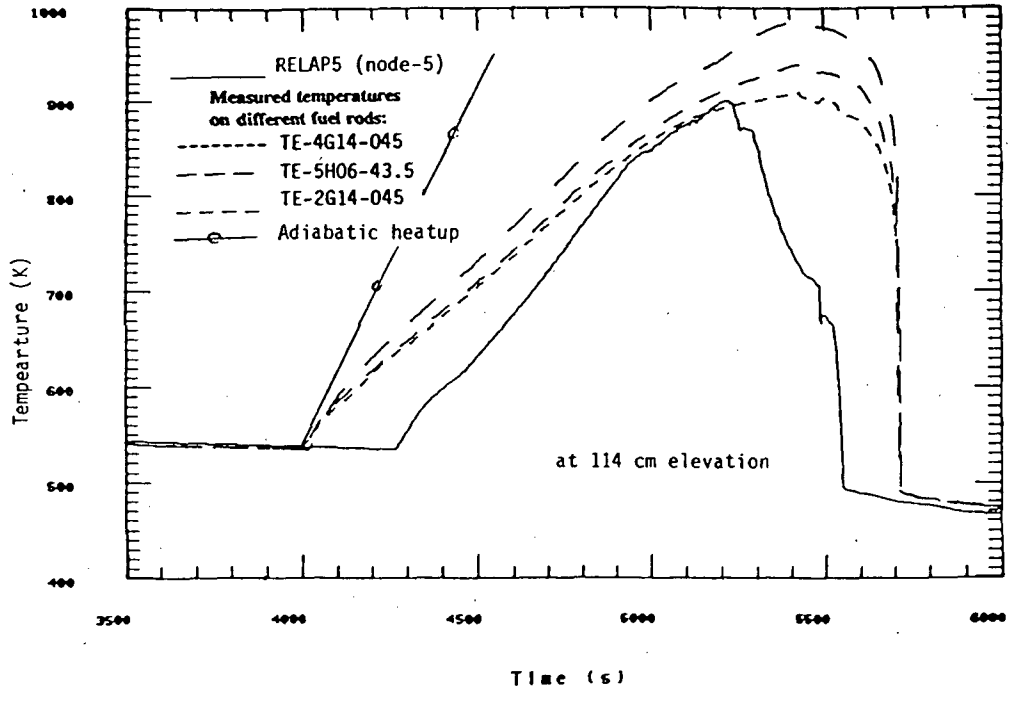


**Figure 15:** Measured and calculated fuel cladding surface temperatures for OECD/LOFT test LP-SB-3.

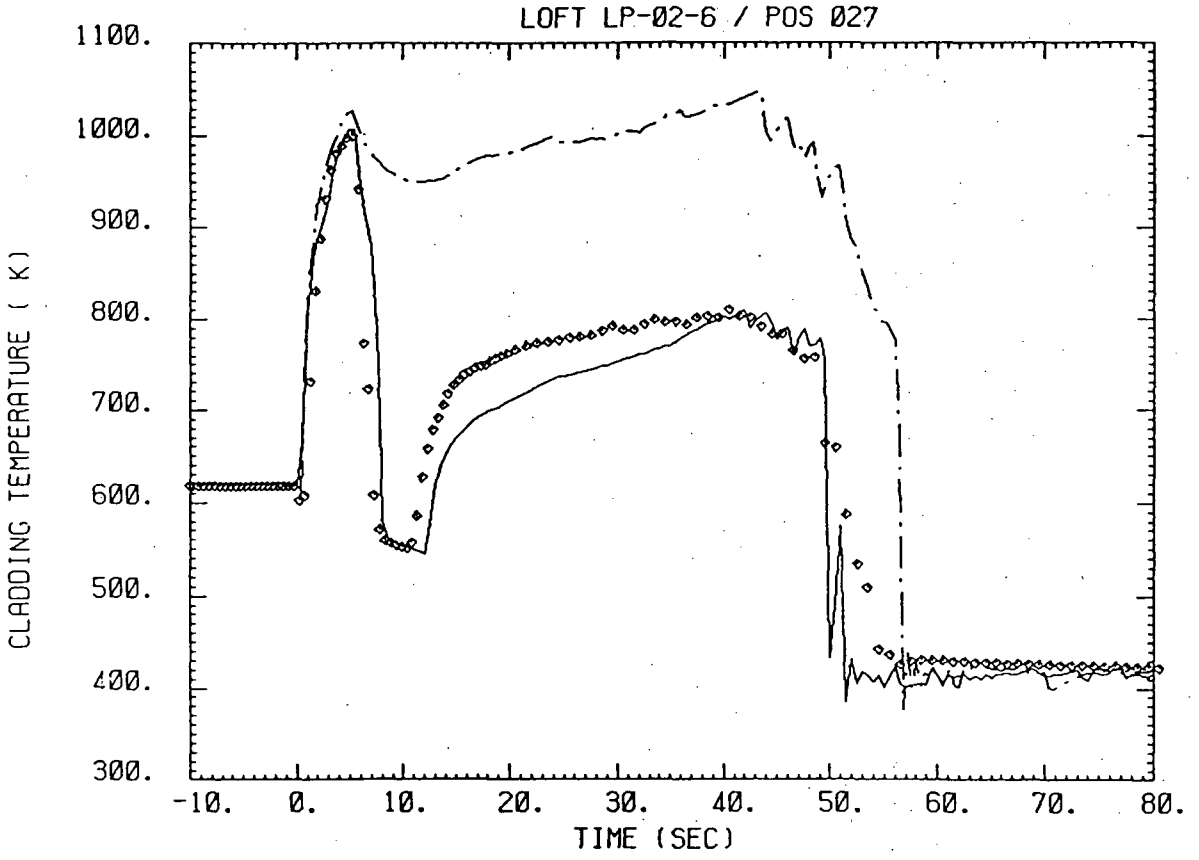


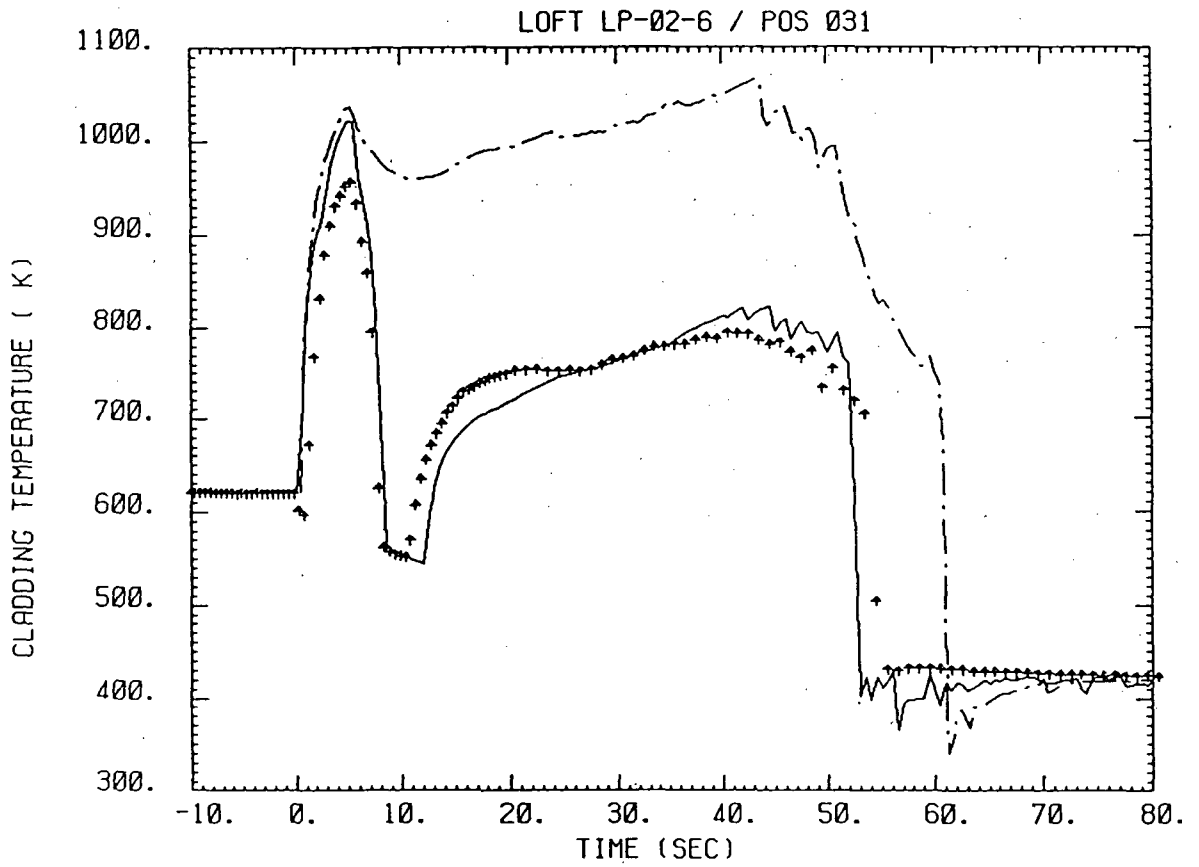


**Figure 16:** Comparison of measured and predicted (–.–.–: Frozen code; ————— : modified code) cladding surface temperature history in hot channel at axial elevations of 0.69 m and 0.79 m for the OECD/LOFT test LP–02–6.

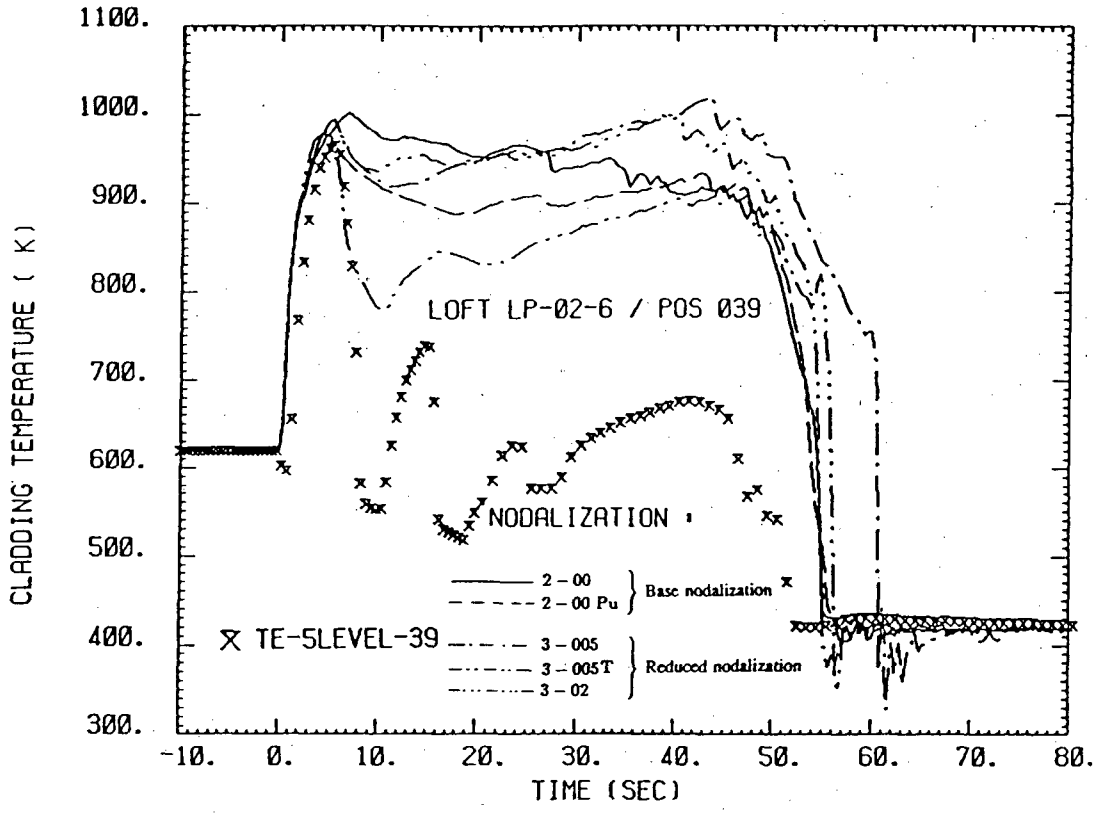


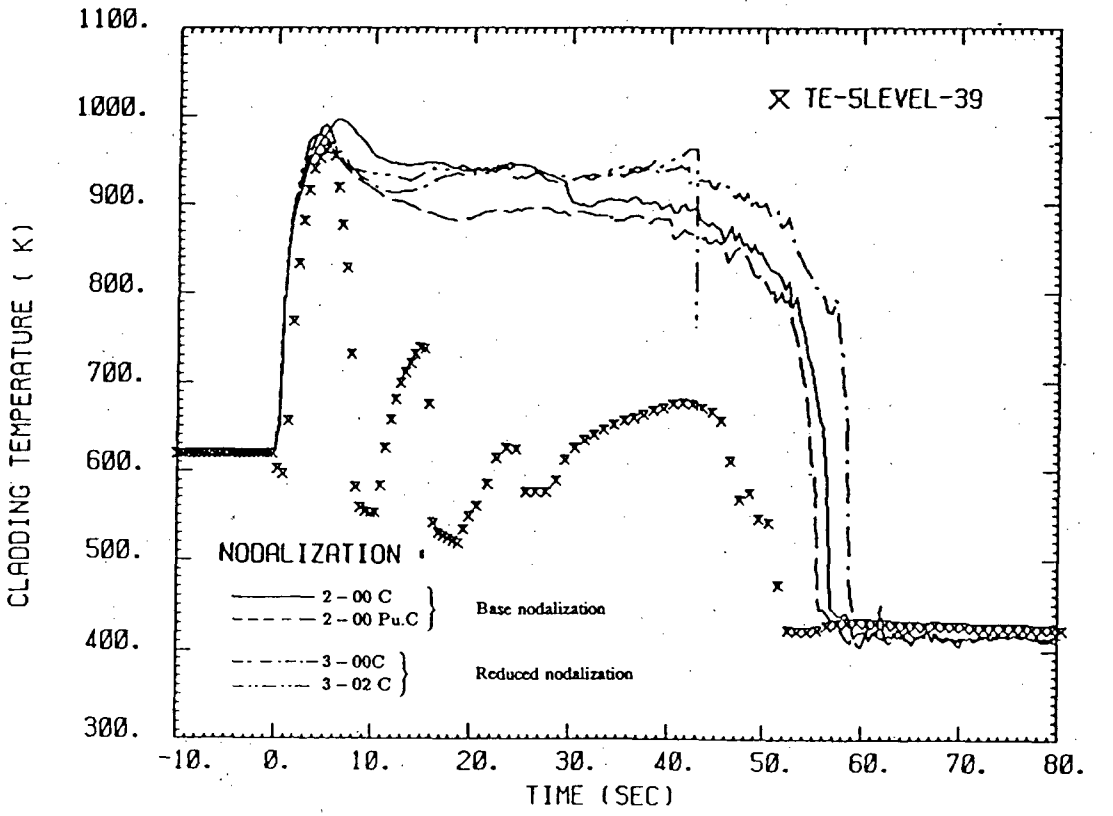


Figure 17: Calculated hot channel cladding surface temperatures for different nodalizations compared with averaged experimental data at elevation of 0.69 m (OECD/LOFT test LP-02-6)

a) Neglecting wall heat capacity (N)

b) Taking wall heat capacity into account (C)

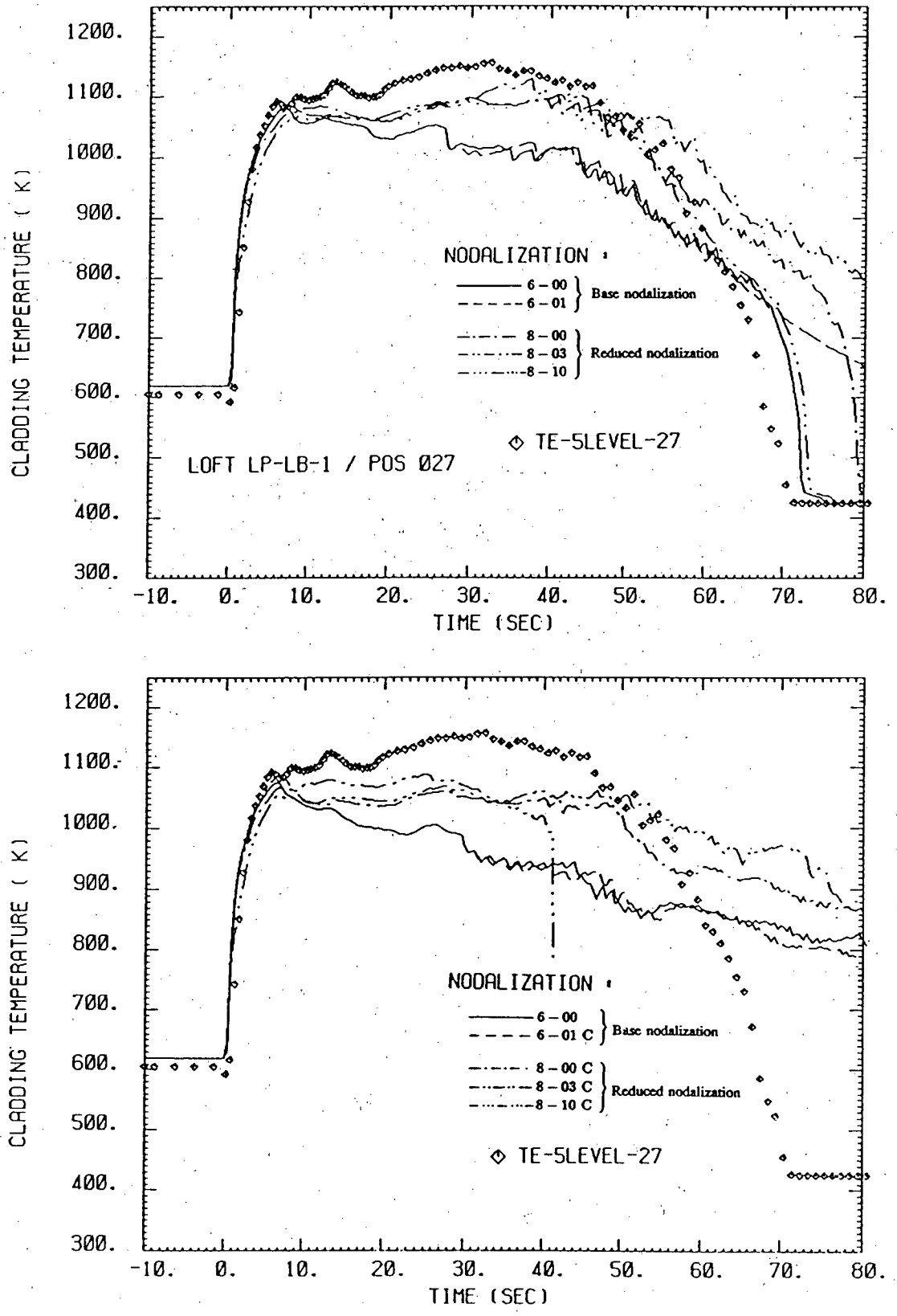


**Figure 18:** Calculated hot channel cladding surface temperature histories using frozen version of RELAP5/Mod2 compared with experimental data at the elevation of 0.69 m (OECD/LOFT test LP-LB-1).

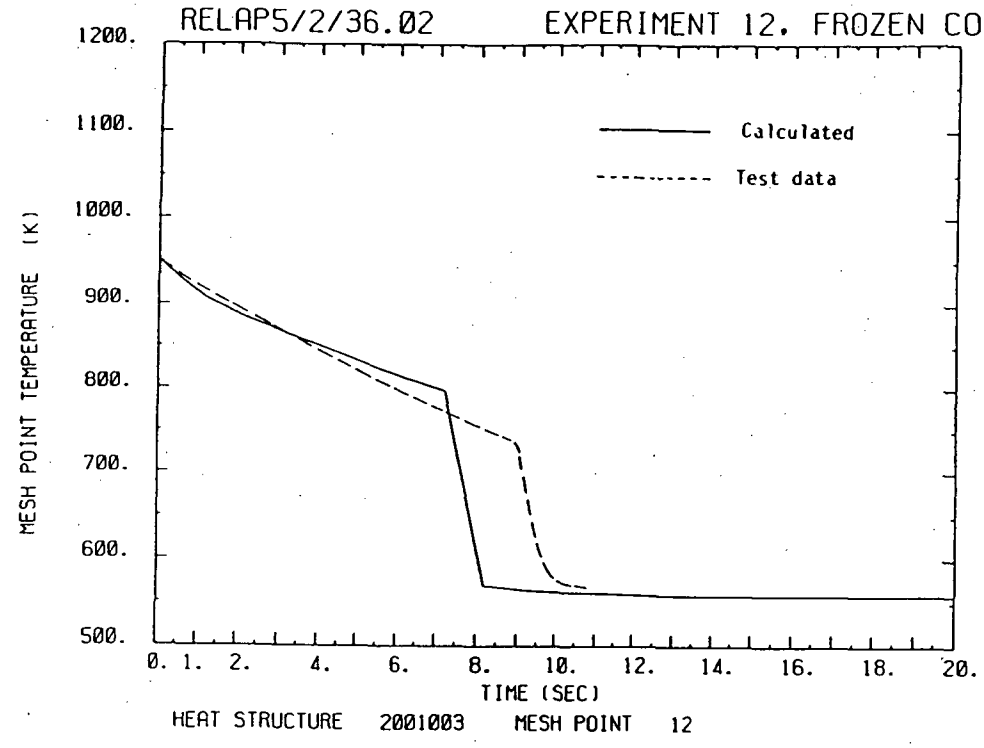


**Figure 19:** Comparison of RELAP5/Mod2 (frozen version) calculated cladding temperature with experimental data from the LTSF quench test No. 12 at level 1 (34.3 cm from inlet of the heated section).

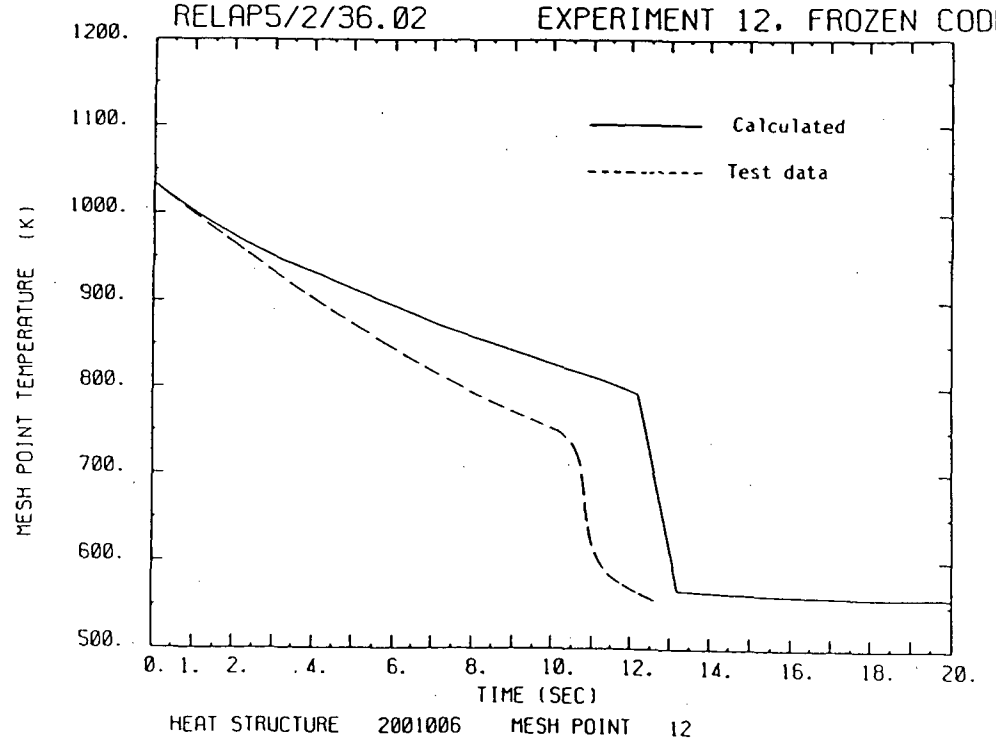


**Figure 20:** Comparison of RELAP5/Mod2 (frozen version) calculated cladding temperature with experimental data from the LTSF quench test no. 12 at level 3 (72.3 cm from the inlet of the heated section).

# TRAC AND RELAP5 CODE DEVELOPMENT WITHIN THE UK

by

I.Brittain (United Kingdom Atomic Energy Authority, Winfrith, Dorset)

and

M.Coney (Central Electricity Generating Board, Leatherhead, Surrey)

## SUMMARY

The UK is using the TRAC PF1 code for the assessment of licensing calculations for large break loss-of-coolant accidents in PWRs. The RELAP5 code is being used for small LOCAs and pressurized transients. The UK has participated in the International Code Assessment and Applications Program (ICAP) with respect to the assessment of TRAC PF1/MOD1 and RELAP5/MOD2 and some work is still on-going in this area. Since January 1988, the UK has also been collaborating with other ICAP members on the Code Improvement Plan, which seeks to remedy some of the code deficiencies identified in the assessment work.

The contribution to the Code Improvement Plan is in three areas. The largest effort is directed at the problem of post-CHF (critical heat flux) heat transfer and quenching. Although it is hoped that the proposed improvements will be adopted for both codes, the UK effort is aimed at implementation in the TRAC code, since this is seen mainly as a large LOCA phenomenon. The second area of UK involvement is that of interphase drag under wet wall conditions. The main purpose of this work is to obtain improved predictions of voidage and level swell in rod bundles, particularly during small break LOCA. The UK implementation is therefore aimed at RELAP5 for this case. The third area is the implementation of an improved off-take model in order to make better predictions of the flow and quality from a junction or break in a horizontal pipe, such as the PWR hot leg, where stratified conditions might exist. The paper describes the work in progress in the UK relating to these three areas.

## 1. INTRODUCTION

The TRAC PF1 code has been chosen by the Central Electricity Generating Board (CEGB) for the assessment of large break loss-of-coolant licensing calculations required for the Pre-Operating Safety Report for Sizewell B (1110MW PWR). The RELAP5 code has been chosen for the assessment of small break loss-of-coolant accidents and pressurized transients. The licensing calculations themselves will be carried out using proprietary Westinghouse codes (WCOBRA-TRAC, NOTRUMP and LOFTRAN) for large LOCA, small LOCA and pressurized transients respectively. This will be the first application of advanced best-estimate codes for licensing and assessment in the UK.

The UK has participated in the International Code Assessment and Applications Program (ICAP) with respect to the assessment of TRAC PF1/MOD1 and RELAP5/MOD2 and some work is still on-going in this area. Since January 1988, the UK has also been collaborating with other ICAP members on the Code Improvement Plan, which seeks to remedy some of the code deficiencies identified in the assessment work.

The UK programme of work under the ICAP Code Improvement Plan consists of three items:

1. Post-CHF heat transfer, with implementation in TRAC

2. Interphase drag under wet-wall conditions, with implementation in RELAP

3. Improved offtake model for horizontal pipes with implementation in RELAP

The programme of work, which includes implementation and documentation, is intended to take place over an 18 month timescale which began on January 1st 1988. The work is being undertaken at UKAEA Winfrith and at CERL, Leatherhead, which is one of the CEGB laboratories. Both sites are contributing to the post-CHF and quenching developments. The interphase drag work is being done at CERL and the offtake work is being done at Winfrith.

The paper outlines work relating to these areas. This includes the choice of a new set of post-CHF heat transfer correlations and the modelling of the hydraulic behaviour under post-CHF conditions. Studies undertaken to understand and quantify the role of external thermocouples in LOFT large break experiments are also briefly described. Also, the results of studies to determine the effect of the TRAC fine mesh nodalization on quench front propagation are outlined and the approach being taken to provide an option to calculate quench front propagation by an analytic method is described.

Concerning interphase drag, the paper states the recommended choice of void fraction correlations to be used to determine interphase drag coefficients in bubbly/slug flow regimes. The implementation of this approach is also outlined together with examples of the improvements in the accuracy of the predictions. The paper also mentions work done on the problem of counter-current flow in straight channels, indicating where there are deficiencies in the existing MOD2 version of RELAP5 and showing how improved predictions can be made. The improvements to the off-take model are also briefly summarised.

One of the objectives of the present paper is to explain the experimental evidence and the reasoning that has led UK workers in the LOCA area to their present perception of these complex phenomena. It is of course possible that some of the current plans are modified in the light of experience or additional experimental evidence. Also, since the ICAP Code Improvement Plan involves an international collaboration, it will be necessary to obtain the agreement of the other participants before provisional modifications which have been implemented in UK versions of the advanced codes are adopted for the mainstream versions.

The original intention of the Code Improvement Plan was that the improvements would be implemented into local versions of TRAC PF1/MOD2 and RELAP5/MOD3 as appropriate. However, there have been some difficulties and delays in implementing these new code versions on UK machines and so code development has been pursued using experimental versions of TRAC PF1/MOD1 and RELAP5/MOD2.

## 2. IMPROVEMENTS TO TRAC POST-CHF HEAT TRANSFER AND QUENCH MODELS

### 2.1 Scope of the Planned Improvements

The main emphasis of the UK work on TRAC is on large break LOCA analysis. Assessment studies carried out over a number of years, primarily on the LOFT large break tests, have led us to conclude that two of the most important uncertainties in TRAC are in the modelling of post-dryout heat transfer and quenching. This includes both the high pressure phase during blowdown, when surges of liquid into the core can occur, and the low pressure final reflood phase. Thus, topics covered by the UK programme include improvements to the post-dryout heat transfer package and improved modelling of the hydraulic behaviour under dry wall conditions. In addition, because of the importance of the LOFT tests, studies have been carried out to understand and quantify the role of the LOFT external thermocouples. It is planned to provide a simple representation in TRAC of external thermocouples. Finally, the importance of axial conduction on quenching has been examined by carrying out a mesh size sensitivity study. It is planned to provide, as an option, an analytic quench front propagation model for cases where a very fine axial conduction mesh would otherwise be necessary.

### 2.2 Previous UK Work on Post-CHF Heat Transfer and Quenching

There has been a long history of UK involvement in the fields of post-CHF heat transfer and quenching and a large number of experiments have been performed. In particular, the THETIS and ACHILLES reflood facilities have played a large part in this work. The 'hot patch' experiments at both Harwell and at Winfrith have also contributed significantly. In these experiments the quench front is prevented from entering the test-section by the use of large heated copper blocks at the inlet and outlet. The 'hot patch' experiments allow post-CHF heat transfer to be investigated (at pressures up to 20 bars) under steady-state conditions so that the hydraulic conditions in the dry wall region downstream can be more accurately known. Other experimental work at CERL, Winfrith and Harwell has focussed on the measurement of quenching behaviour both with falling films and with flooding up from the bottom of the test-section.

It will be seen below that reference is made to two separate effect codes, BERTHA and QFLOOD, which have been used by the UKAEA and CEGB for analyses of a number of post-CHF and reflood experiments. Indeed to a large extent, it is the experience with these two codes, applied to both UK and international data, that has helped form our understanding of these phenomena. The BERTHA code was developed at Winfrith to predict and interpret post-CHF heat transfer experiments in both blocked and unblocked geometries. QFLOOD is a reflood code, which has been developed at CERL. The approach to the modelling of post-CHF heat transfer is very similar in the two codes. Both codes have been compared quite widely with data and are believed to represent state-of-the-art modelling with respect to separate effect reflood and post-CHF heat transfer experiments.

## 2.3 Improved Post-Dryout Heat Transfer Correlations

An improved set of post-dryout correlations has been proposed, which are closely based on those used in BERTHA. The correlations explicitly represent both the inverted annular regime and the dispersed droplet regime, with a transition regime between them. An important feature of the model is that the heat transfer coefficient is calculated as a function of the distance from the quench front in the inverted annular flow regime. The correlation used in this regime is a Z-dependent modification of the original Bromley correlation, and is thus different from the modified Bromley correlation used in TRAC-PF1/MOD1. In the dispersed flow regime either the Kim or Dittus-Boelter correlation is used for heat transfer to the vapour, replacing the Dougall-Rohsenow correlation of MOD1. In addition, in both regimes radiation from wall to liquid is modelled. The Forslund-Rohsenow correlation is no longer used at all.

The selection of inverted annular, transition, or dispersed droplet regime is determined by considering the phenomena that cause the liquid core, in inverted annular flow, to break down. These are excessive voidage in the liquid core and high vapour flow in the vapour film. For upflow these are quantified by defining two core break-up factors $CB_{\alpha}$ and $CB_{We}$. Correlations have been proposed for the determination of these two parameters. For downflow, in the absence of specific correlations, the heat transfer in the inverted annular regime is assumed to be by vapour conduction across a film whose thickness is calculated by considering the acceleration of the liquid core due to gravity. The core break-up factor is restricted to a dependence on void fraction.

The proposed correlations have been implemented into a version of TRAC-PF1/MOD1 and some preliminary assessment has been performed. A comparison of the modified TRAC-PF1/MOD1 with LTSF data has indicated that there is an improvement in the prediction of the post-dryout heat transfer, but that quenching takes place too slowly (Figures 1 and 2). This is expected because the modification did not include any changes to the quench calculation. A comparison with a single Winfrith post-dryout (hot patch) experiment indicated that the transition from inverted annular to dispersed droplet flow was possibly too abrupt, causing an underprediction of the heat transfer (Figure 3).

## 2.4 Dry Wall Hydraulics Modelling

We have observed many times that in forced reflood calculations with TRAC the hydraulic behaviour is not smooth, and is likely to consist of intermittent pulses of liquid being thrown upwards. A number of factors contribute to this

behaviour including operation of the interface sharpener, filling of an hydraulic cell, the switching from bubbly to inverted annular flow and the quenching of structural material. The problem is further aggravated by the coarseness of the hydraulic mesh, which is used in order to limit computer running times.

The basis of the proposed modelling change is to superimpose on the existing hydraulics solution a more-detailed model of the quench front and post-dryout region. The detailed model will necessarily be based on a quasi-static approach, updated at each time-step. The objectives are to produce improved modelling of the heat transfer and interphase drag, and in particular to ensure that the interphase drag is continuous across the quench front. It will also be possible within this approach to define a local void fraction at the coarse mesh boundaries, thus achieving the effect of an interface sharpener.

The approach being taken is to implement modifications which are believed to represent the physical development of the flow from the quench front into the post-dryout region. The modelling approach is again based on the method used in the BERTHA code. An important feature of the method is that there is a calculation of the developing flow from the quench front on a mesh size of the order of one or two centimetres as compared to the 60 cm mesh size used in many TRAC calculations. Also the heat transfer is predicted to be quite a strong function of the distance from the quench front, because of the increase in the vapour film thickness and the steam temperature with increasing distance. The transition from inverted annular to dispersed flow is calculated in an identical fashion to that described in Section 2.3 above. The model also recognises annular flow below the quench front, if appropriate, with a transition to dispersed flow at the quench front.

The model described has been implemented in TRAC-PF1/MOD1. Further work needs to be carried out to tune the arbitrary features of the model by comparison with experiments, particularly those from the THETIS and ACHILLES bundle reflood tests, and to cater for downflow. However, preliminary results are encouraging. For instance, Figure 4 shows a snapshot of the void fraction profiles calculated for a THETIS reflood test by the standard TRAC-PF1/MOD1 and the development version. It can be seen that the unphysical pulse of liquid seen in the standard case is not present in the curve from the new version.

## 2.5 LOFT External Thermocouples

For large break LOCA, code validation is heavily dependent on the integral tests carried out in the LOFT facility. This is particularly so for the blowdown cooling and quenching phenomenon. The LOFT fuel rod cladding temperatures were measured using external thermocouples which were welded to the rod at intervals. There is the possibility that the thermocouples could behave independently of the clad, or induce early quenching of the clad, rather than being true indicators of the clad temperature behaviour. A study has been carried out at Winfrith in an attempt to establish which of these three possibilities is correct.

Experimental results from a SEMISCALE rod, with internal clad thermocouples, in the LOFT Test Support Facility (LTSF) have been used to give heat transfer coefficients under the relevant high pressure, high flow conditions. These heat

transfer coefficients have then been applied to a 3-dimensional, time-dependent, finite-element model of a similar rod with a LOFT-type external thermocouple attached, using the TAU code. The resistance paths between the thermocouple wire and the clad through both the weld metal and the vapour film were treated as tunable parameters, and results from similar experiments in LTSF on external thermocoupled SEMISCALE rods used to fix the values of these parameters. The TAU model had no representation of quenching, and the experimentally observed quench temperatures were used to trigger a large increase in heat transfer in the calculation. Results from the model are compared with LTSF data for both bare and LOFT-thermocoupled SEMISCALE rods in Figure 5. It can be seen that the temperature of the thermocouple initially falls very rapidly, but then stabilises some 200K below the bare rod temperature as the heat flow through the weld builds up.

Having shown that the model satisfactorily reproduces the features of the LTSF experiments, the next step is to apply the model to real LOFT fuel, ie fuel with a gas gap. This has been done by taking the heat transfer coefficients from a TRAC calculation of test L2-6 and applying them to a TAU model of LOFT fuel. The results are shown in Figure 6. This figure shows that the TAU model predicts that a bare rod, as in the TRAC calculation, does not quench, while a thermocouple attached to an identical rod does quench. The deviation between the TAU curves and the others towards the end of the calculation is due to the fact that TAU did not take account of decay heat.

An approximate lumped parameter model to represent external thermocouples, based on the TAU study, has been devised for TRAC but has not yet been tested.

This study leads us to conclude that the external thermocouples on LOFT fuel rods would quench under the blowdown conditions in LOFT. The study also shows that an unthermocoupled rod might not quench under the same conditions. According to our understanding of the physics, spontaneous quenching from temperatures well above the homogeneous nucleation temperature is not possible. The only available mechanisms for quenching from very high temperatures are for a quench front to become established in a cool zone (eg. at the bottom of the core or on a thermocouple cable) and then to propagate into the hot zone; or for there to be a transient dry wall heat transfer coefficient very close to the quench front, which is very much higher than that seen in steady-state experiments. Scoping calculations performed with QFLOOD, assuming a zircaloy rod with a gas gap and including an assumed surface layer of oxide, suggest that although the quench speeds are significantly higher than those on a 'solid' Semiscale-type rod, the predicted quench speeds are too low to explain the LOFT results in terms of propagation from the bottom of the core.

Thus the UK view is that the LOFT blowdown quenches were not as extensive as the measurements of the external thermocouples suggest. However, some quenching of the uninstrumented rods would have occurred. It is hoped that the improved heat transfer and quenching model being developed for TRAC will give some indication of the likely extent of this.

2.6 General Comments Concerning Modelling of Quenching

Assessment of TRAC PF1/MOD1 has shown that there is a tendency for the code to overpredict the heat transfer in the post-CHF regime, particularly at low void

fractions. This effect has been noted both in hot-patch experiments and in reflood experiments, where TRAC erroneously predicts a sudden improvement in heat transfer, when the void fraction falls below a critical value. Many workers now believe that TRAC PF1/MOD1 predicts too much heat transfer to the liquid phase directly. However, if the heat transfer to the liquid phase is reduced or eliminated, then it is found that the quench front does not progress quickly enough to match the experimental data.

The authors believe that there are two reasons why it has proved difficult to obtain satisfactory agreement with respect to both the post-CHF heat transfer and the quench progression simultaneously.

1. The modelling of the axial conduction of heat within the fuel cladding in the vicinity of the quench front is achieved in TRAC by the use of a special model which generates a fine mesh of temperature nodes. Nodes are created ahead of the quench front and deleted behind it, to cater for the movement of the quench front up (or down) the rod. However the user specifies what the minimum mesh size should be. In many instances, this mesh is not made fine enough and a converged result is not obtained.

2. In performing the fine mesh quench calculation, TRAC applies the same boiling curve and the same value of the critical heat flux (CHF) that is used to predict CHF under fully developed conditions. There is clear evidence that this will result in an under-prediction of the CHF value appropriate to quenching conditions.

## 2.7 TRAC Sensitivity Studies Relating to Quench Progression

Sensitivity studies performed at Winfrith have shown that if the specified minimum mesh size is reduced from a typical specified value of 2.5 mm down to 0.1 mm or even 0.05 mm, then there can be a significant change in the predicted quench time. This is seen in Fig.7 which indicates a 50% increase in quench speed resulting from the use of a very fine mesh for a low pressure reflood experiment. Fig.8 shows an even larger effect for the case of a single rod under blowdown conditions of 70 bars pressure and a ramped flow. In this case the quench velocity is increased by a factor of four by a change in mesh size from 2.5mm down to 0.025mm.

It is clear from these two figures that not only is the quench speed increased by the very fine nodalisation, but the apparent quench temperature is increased also. The explanation for this is that the point at which the temperature falls sharply is NOT the true quench temperature, which is constrained by the code to have a value close to the homogeneous nucleation temperature. The knee in the curve is caused by strong axial conduction effects which occur a very short distance ahead of the quench front itself.

The TRAC sensitivity study showed that the effect of a fine nodalisation was much greater if the temperature of the rod is high. However, if the rod is cooled by convective heat transfer mechanisms to temperatures below 650 deg.K, then a very fine mesh makes little difference to the quench speed.

TRAC automatically reduces the time-step when a finer mesh is used, however it was found that a reduction in the time-step, with a fixed mesh size also had

a substantial effect on the quench velocity and the apparent quench temperature. Indeed the effect of a reduced time-step had 70-80% of the combined effect of the reduced time-step and the reduced mesh.

The TRAC sensitivity study included an investigation of the magnitudes of the various components of heat transfer in the immediate vicinity of the quench front in the reflood example mentioned above. Figure 9 defines the various terms in the heat conduction equation. Figure 10 shows the values of these components on the surface nodes of the clad for the case of a minimum mesh siz of 0.05mm. It is seen that with this very fine mesh, the axial and radial heat transfer terms both have very large transient magnitudes. Figure 10 shows that the large radial heat flux spike, which represents heat transferred to the fluid, is mostly confined to an axial distance of 0.5 mm. The change in surface temperature is spread over a somewhat larger axial distance. Figure 10 shows that 90% of the change occurs in a distance of 2mm.

2.8 Applicability of CHF Correlations to the Prediction of Quench Behaviour

The assumption that the critical heat flux is determined by the local conditions of flow and heat transfer is only valid when the heated length is of the order of 80 hydraulic diameters (Collier, 1972, p269). This occurs because the mechanisms leading to critical heat flux require a certain development length. If the heated length is significantly reduced, with the flow and quality at the CHF point held constant, the value of the critical heat flux is increased.

The progression of a quench front along a hot surface is an extreme example of a non-uniform heat flux. This is clearly seen from Figure 10. For the case of a sharp heat flux spike, a much higher value of the critical heat flux might be expected.

Experimental support for this hypothesis has recently obtained from experiments at the CEGB laboratories at Berkeley, England (Hall, 1988). A surface thermocouple, 70 microns in diameter and a depth somewhat less than this was mounted in a heated block and used to measure the temperature transient following the collapse of film boiling of a single drop of water. Transient surface heat fluxes were calculated from the measured temperature traces using the theory for a semi-infinite solid suddenly exposed to a cooling medium. Peak heat fluxes of 60 $MWm^{-2}$ were inferred, as compared to critical heat flux values of 1 or 2 $MWm^{-2}$, which would be predicted on the basis of the correlation used in TRAC.

2.9 The Analytic Approach to the Prediction of Quenching Behaviour

The determination of boiling curves as a function of pressure, flow rate and quality has proved difficult even for the case of a uniformly applied heat flux. The physical understanding of the boiling phenomenon under the extreme conditions of a very sharp heat flux spike is not good enough to allow predictions of the quenching phenomenon from first principles. Instead it is necessary to use measurements of quench velocity under a wide variety of conditions together with somewhat simplified physical models in order to be able to make reliable predictions of quench behaviour.

The experience of CEGB workers in this field has been that a simple physical model in which it is assumed that there is a simple step change in heat transfer

coefficient from the dry to the wet-side of the quench front has proved very effective in the prediction of quench velocities over a wide range of conditions. Indeed the quench model in the QFLOOD code is of this type. The quench model is only assumed to apply over a very short axial distance, typically about 4mm, which is sufficient to include more than 90% of the temperature change. In this context, the fact that the model assumes that the wet-side heat transfer coefficient stays constant over an axial distance typically equal to 2 mm and the fact that the dry side heat transfer coefficient is assumed to be zero over a similar distance is unimportant.

Work is in progress to implement the QFLOOD analytic quench model in a version of TRAC PF1/MOD1. This model calculates the quench velocity as a function of the cladding temperature ahead of the quench front. The analytic quench model replaces the need for a very fine mesh axial conduction calculation, but it does not remove the need for a precursory cooling calculation ahead of the quench front. The method of implementation will be to modify the heat transfer selection logic such that if the analytic quench model predicts that a reflood node (typically 1 or 2 cms in length) to have quenched, a nucleate boiling heat transfer coefficient will be adopted for that time step. The critical heat flux limit will therefore be over-ridden.

The effect of this modification (considered in isolation from the planned changes to the post-CHF heat transfer correlations) is expected to be that TRAC will predict faster quenching and that the computer run time will be reduced, because a very fine mesh will no longer be needed.

## 3. INTERPHASE FRICTION MODEL IMPROVEMENTS TO RELAP5

### 3.1 Review of Void Fraction Correlations and Data

The ICAP assessment programme showed that there were systematic differences between the predictions of the advanced codes and experimental data concerning void-fraction, level swell and boildown, which adversely affected the prediction of some small LOCA transients. Also it had been noted that if the interphase friction relationships in the advanced codes were extracted and compared with well-established void fraction correlations within the framework of a simple steady-state 'driver code', again there were systematic differences, leading to an over-prediction of void fraction by the codes.

The UK programme of work in this area of code improvement began with a detailed survey of experimental void fraction data and the correlations that are often used to predict void fraction under steady state conditions in which a bubbly-slug flow regime existed (see Putney, 1988). Recommendations were made as to the most reliable correlations for particular conditions and a slightly modified version of these is summarised in Figure 11. It is seen that for modest flow rates, in the vertically upward or downward directions, different correlations are recommended for rod bundles, small pipes, medium-sized pipes and large pipes or vessels. At high flow rates, the same correlation is recommended for all these geometries and for both upflow and downflow. Another correlation is recommended for non-stratified horizontal flow. Putney (1988) also proposed that the recommended correlations for bubbly-slug flows should be used within the advanced codes to calculate appropriate interphase friction

coefficients, using an inverse calculation. This approach, which has been proposed and used by others in the recent past (eg. Analytis, 1986) is equivalent to assuming that the interphase friction coefficients applicable to a steady-state flow are also applicable to a transient condition which has the same instantaneous flow parameters. This does not mean that the predicted void fraction would be the same, because a certain relaxation time would be needed to achieve this. However this approach should ensure that there would be no discrepancies between the predictions of the advanced codes for steady-state conditions and the best available experimental data.

3.2 Implementation Experience and Preliminary Assessment

The interphase friction recommendations have been implemented in a provisional way in the CEGB's IBM version of RELAP5/MOD2. Preliminary assessments of the improvements have been done by comparison with two ORNL level swell tests, at high and low power. Calculations were done for two noding schemes, one with 24 vertical volumes representing the core and one with 6 volumes, which is the number usually used in plant calculations. As seen in Figures 12 and 13, the fine node scheme gives excellent agreement with the data for both the cases considered. In contrast it is seen that the unmodified RELAP5/MOD2 code gives a significant overprediction of the voidage in both tests. The fact that both code versions give a good prediction of the dryout point is a straightforward result of the heat balance that can be applied to this steady-state experiment. Separate calculations also confirmed that the fine node calculation is virtually indistinguishable from the result of a direct application of the EPRI correlation to the ORNL tests. This confirms that there is no significant loss of accuracy as a result of the numerical implementation. The coarse node calculation results in a small overprediction of the void fraction in the two ORNL experiments.

Although much improved agreement was observed in the comparisons of the above two tests, certain problems were identified, which occur with the standard code as well as the version with the new interphase friction model. These were overcome in the present calculations by reducing the time-step and switching off the vertical stratification model.

3.3 Avoidance of Negative or Infinite Interphase Friction Coefficients

In the method of implementation used for this preliminary study it was noted that there was the possibility of negative or infinite interphase friction coefficients arising in downflow and horizontal flow. A new formulation has now been proposed which avoids this. It is not expected that the good results for the ORNL upflow tests will be affected, but the new formulation should be much more satisfactory for downflow and horizontal flow.

3.4 Interphase Friction in Annular Flow

Work is in progress on the assessment of the RELAP5 interphase drag model applicable to annular flow and the flow regime transition criteria for annular flow are also being examined. The correlations from RELAP5 have previously been programmed into a small stand-alone code and the results of predictions of this code have been compared with data in the HTFS data bank at Harwell. Preliminary indications are that the interphase friction model presently in the code is

sufficiently accurate and does not require improvement. However the criterion for the occurrence of annular flow may require modification.

## 4 OFFTAKE MODEL IMPROVEMENTS IN RELAP5

The UK studies relating to improvements in the RELAP5 horizontal stratification entrainment model are described by Ardron and Bryce (1988). The study included reviews of available correlations and data for the 2-phase quality through an offtake from a horizontal pipe. Three basic geometries were considered, ie. with the offake upward, downward and horizontal respectively. The recommended correlations for offtake quality were expressed in terms of the depth ratio of liquid to a critical entrainment depth, which was also correlated.

The recommended correlations were implemented into a UK version of RELAP5/MOD2 and an assessment was performed. As might be expected, the agreement with the separate effect database was significantly improved.
Figure 14 shows the effect for the important case of the horizontal offtake. There was, in fact, a much larger effect for the case of an upward vertical offtake, but this figure is not included here.

In the standard RELAP5 model, homogeneous discharge conditions are assumed in flow regimes other than stratified flow. This assumption fails to recognise that partial separation of the phases occurs in plug, slug and annular flow in horizontal pipes. To allow for this, the revised model was applied in all horizontal regimes except dispersed flow, which is assumed to be entered when the main pipe flow exceeds 3000 $kgm^{-2}s^{-1}$. A transition zone of 2500 to 3000 $kgm^{-2}s^{-1}$ was assumed for which the offtake quality was interpolated . It should be noted that the above treatment is based on judgement, since no experimental data appear to be available for offtake flows when flow regimes other than stratified exist in the main pipe.

The modified model was also assessed by comparison to LOFT test LP-SB-02, which involved a 1% break in the side of the hot leg and which involved a long period of stratified flow. Figure 15 shows the experimental data for the density in the break line in comparison to both the modified and unmodified codes. The modified version gives significantly improved agreement after 850 s, when the hot leg mass velocity falls below the threshold value of 3000 $kgm^{-2}s^{-1}$. The agreement after 2000s is excellent, but prior to 850s the data indicates that there is preferential discharge of vapour even under the prevailing highly mixed conditions. It is believed that this effect is caused by inertial separation at the junction of the two pipes. This effect is not modelled in either the standard or the modified version of RELAP5.

## 5 MODELLING COUNTER-CURRENT FLOW LIMITATION WITH RELAP5

Although not formally part of the Code Improvement Plan, some relevant studies of the counter-current flow limitation as applied to RELAP5 are in progress at Winfrith. This work does not deal with the situation where there is a geometrical restriction, but with the case of a straight vertical or horizontal channel, where the CCFL limit should be governed by the interphase friction

relationships built into the code. This work is therefore very relevant to the interphase friction improvements described above.

In this study, RELAP5 was used to generate a curve representing the maximum liquid downflow in a pipe for a given steam upflow, known as the flooding curve. This curve has been compared with experimental data. It is found that the code overpredicts liquid downflows by more than an order of magnitude and this is shown to be mainly due to the so-called 'Reverse Void Profile' model, which reduces interphase friction when fluid density increases with height in a vertical section.

With the model removed, the code still overpredicts liquid downflows at lower gas flow rates because it assumes slug flow in the channel, when annular flow is appropriate. The problem is that the applied co-current flow regime transition criterion is inappropriate in a counter-current flow situation. The study shows that the code reproduces the experimental flooding curve well at all gas flowrate if it is forced to assume annular flow in the channel.

It has also been noted that although the modified code gives good predictions of the flooding curve for a finely noded simulation, there is a significant deterioration in the accuracy if a coarse mesh is used. Consideration needs to be given to the numerical method applied to the junctions between the nodes to see how the dependance on nodalisation can be minimised.

## 6 CONCLUDING REMARKS

1. The collaboration with the USA and other countries within the auspices of the International Code Assessment and Applications Programme (ICAP) forms an important part of the UK's activities on LOCA code development and validation.

2. UK studies relating to the ICAP Code Improvement Plan are focussed on three topics; post-CHF heat transfer and quenching, interphase friction under wet wall conditions in straight pipes and the modelling of offtake flows from a horizontal pipe.

3. It is considered that good progress has been made in all these areas. The improved modelling methods are mostly decided upon and implementation in UK versions of TRAC and RELAP is in progress. Some assessment work has started. The authors are hopeful that future assessment results will persuade our ICAP partners that the proposed improvements should be implemented in the mainstream versions of TRAC PF1/MOD2 and RELAP5/MOD3.

## 7 ACKNOWLEDGEMENTS

This paper is published by permission of the United Kingdom Atomic Energy Authority (UKAEA) and the Central Electricity Generating Board (CEGB).

## 8 REFERENCES


Analytis, G.Th., 1986, Effect of Bubbly/Slug Interfacial Shear on Liquid Carryover Predicted by RELAP5/MOD2 During Reflooding. Trans.Am.Nuc.Soc., Vol 53, pp 540-541.

Ardron, K.H. and Bryce, W.M., 1988, Assessment of RELAP5/MOD2 by Comparison with Separate Effects Experiments, 3rd International Topical Meeting on Nuclear Power Plant Thermal-Hydraulics and Operations, Seoul, Korea

Bryce, W. M., 1977, A New Flow-Dependent Slip Correlation which gives Hyperbolic Steam-Water Mixture Flow Equations. AEEW-R1099.

Chexal, B. and Lellouche, G., 1986, A Full-Range Drift-Flux Correlation for Vertical Flows (Revision 1). EPRI NP-3989-SR

Collier, J.G., 1972, Convective Boiling and Condensation, 2nd ed., McGraw-Hill International Book Co.

Gardner, G. C., 1980, Fractional Vapour Content of a Liquid Pool through which Vapour is Bubbled. Int. J. Multiphase Flow, Vol 6, pp 399-410.

Hall, C.M., 1988, Measurement of local transient temperatures and heat fluxes in film boiling collapse, AIChE/ASME National Heat Transfer Conference, Houston, Texas, USA.

Kataoka, I. and Ishii, M., 1987, Drift Flux Model for Large Diameter Pipe and New Correlation for Pool Void Fraction. Int. J. Heat Mass Transfer, Vol 30, No 9, pp 1927-1939.

Putney, J.M., 1988, Proposals for Improving Interphase Drag Modelling for the Bubbly and Slug Regimes in RELAP5. CEGB Report RD/L3306/R88 (Unrestricted).

Woodford, D. J. and Scriven, A. H., 1983, The Rise Velocity of Bubbles and the Distribution of Vapour in a Liquid Pool during Depressurization. TPRD/L/2413/N82 (CEGB Unrestricted).

Zuber, N. et al., 1967, Steady-state and Transient Void Fraction in Two-Phase Flow Systems. General Electric Report GEAP-5417.

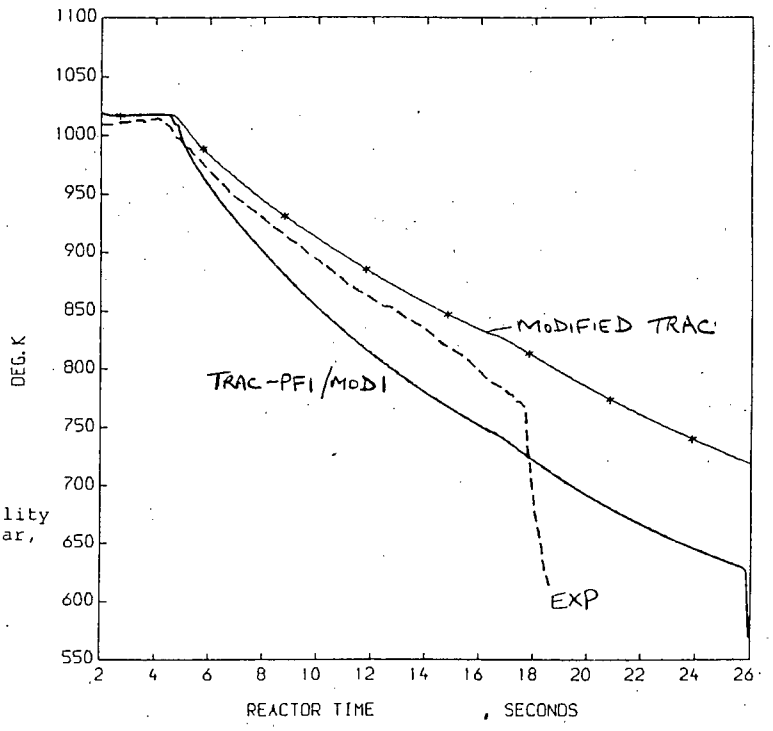


FIG 1 LOFT Test Support Facility Test at 69 bar, 0.45 m/s

COMPARISON OF CLAD TEMPERATURES TRAC & EXPT @ 72CMS

Winfrith

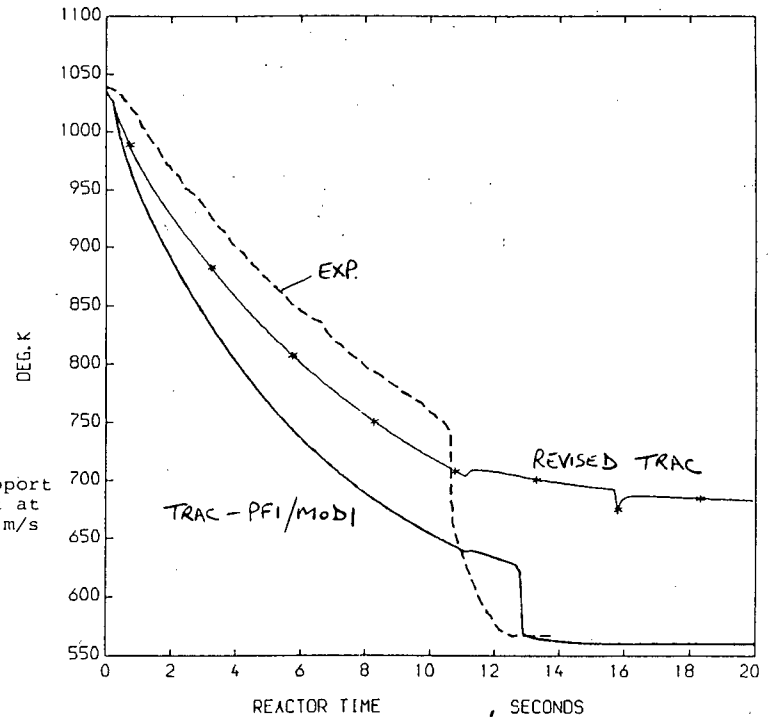


FIG 2 LOFT Test Support Facility Test at 69 bar, 3.75 m/s

COMPARISON OF CLAD TEMPERATURES TRAC & EXPT @ 72CMS

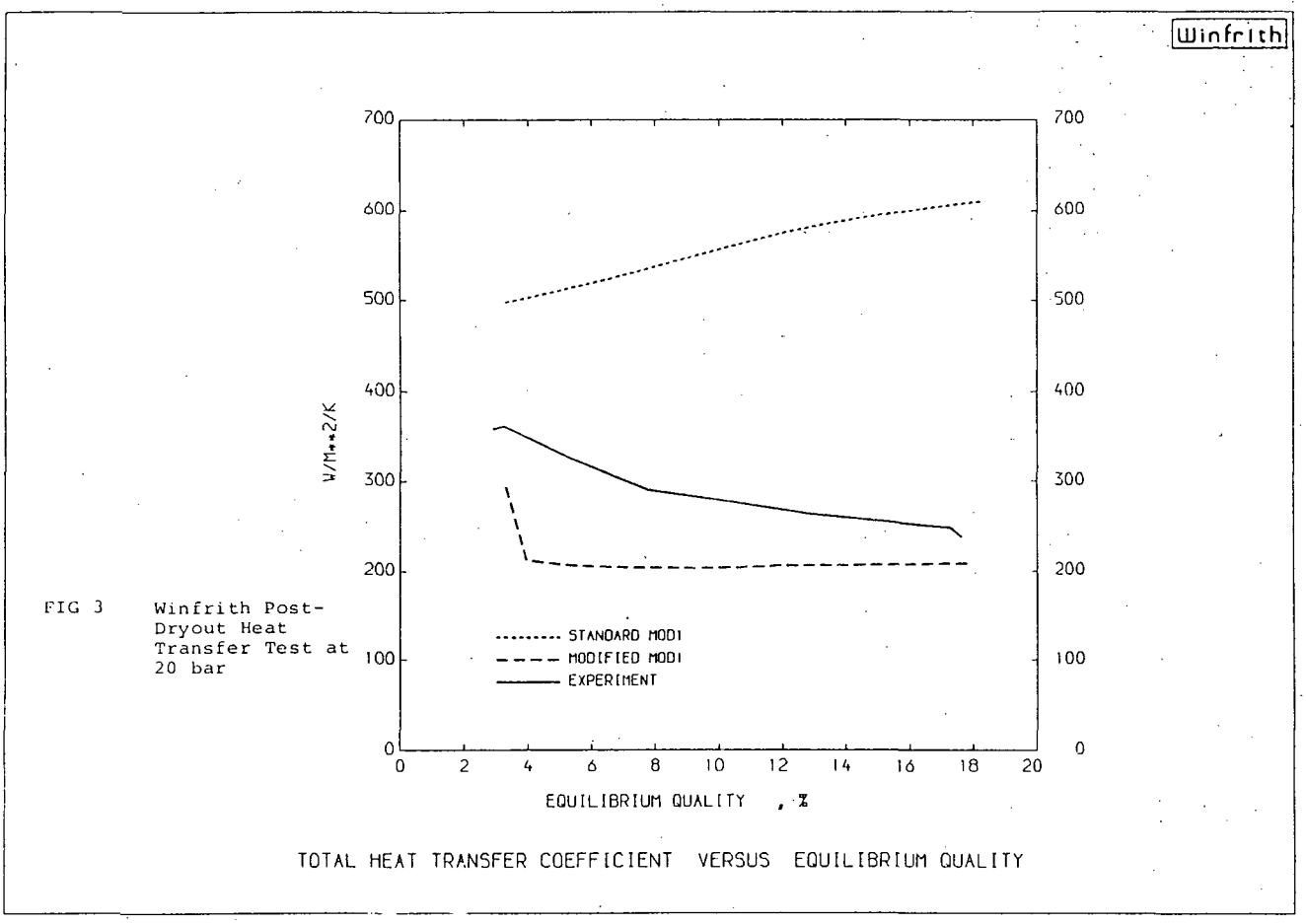


FIG 3 Winfrith Post-Dryout Heat Transfer Test at 20 bar

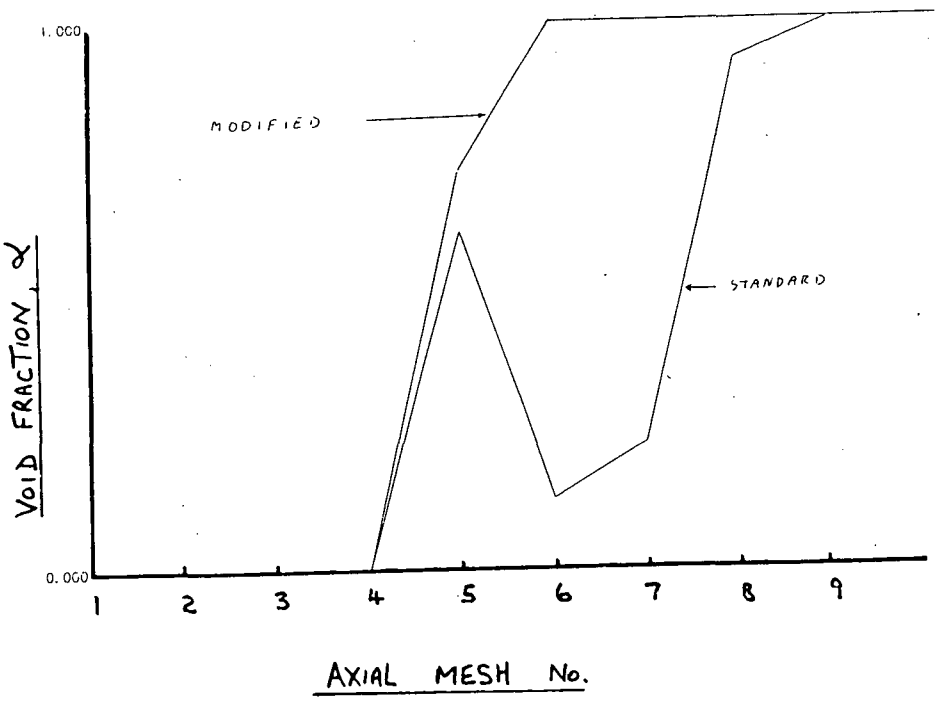


FIG 4 TRAC-PF1/MOD1 Calculations of THETIS Reflood Test

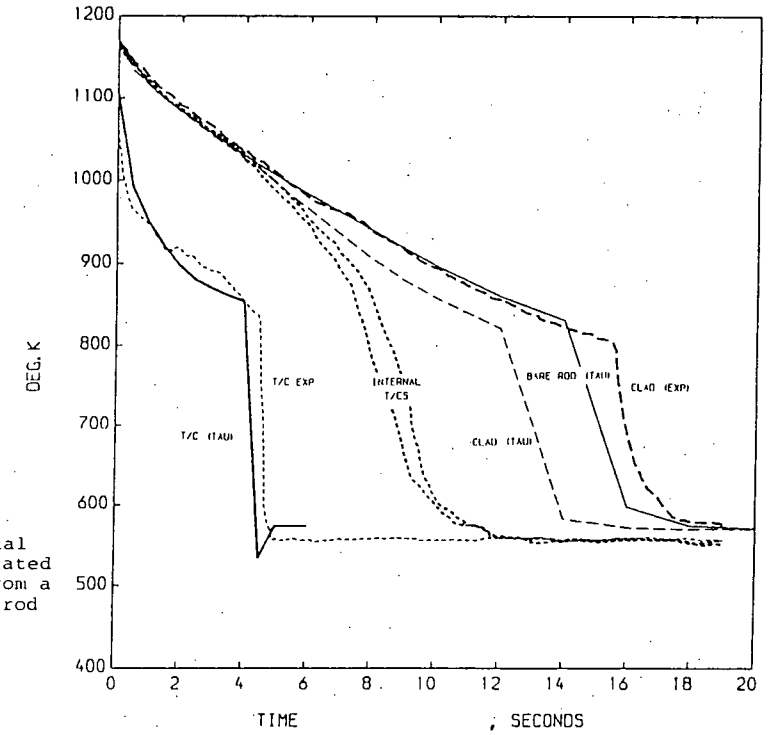


FIG 5 Experimental and Calculated Results from a SEMISCALE rod in LTSF

STEAM CONDUCTIVITY = 0.35 W/K.M

Winfrith

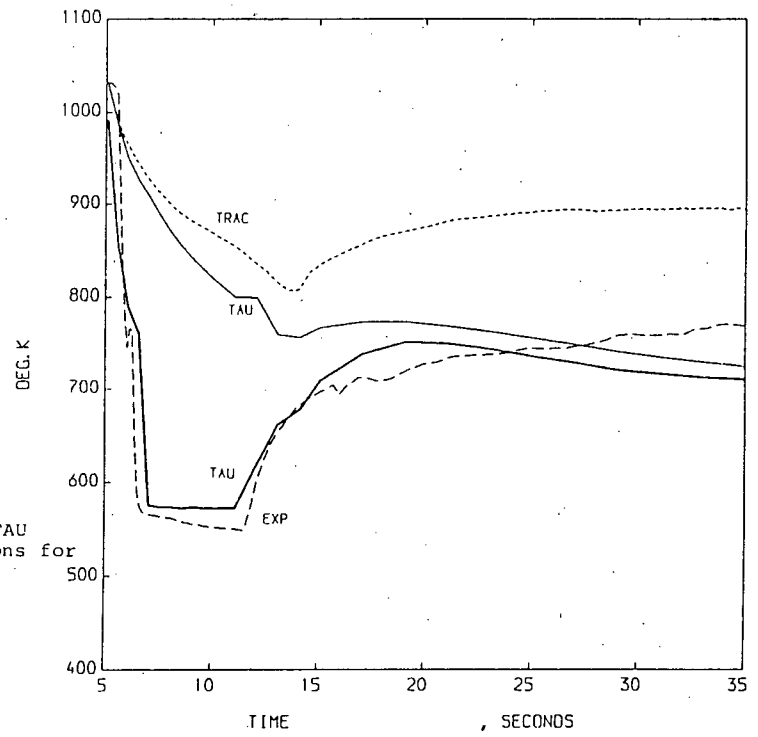


FIG 6 TRAC and TAU Calculations for LOFT Test L2-6

LOFT CALCULATION AND EXPERIMENTAL DATA - 21 IN.
ADDITIONAL HEAT TRANSFER BETWEEN 6.3 AND 11.8 S.

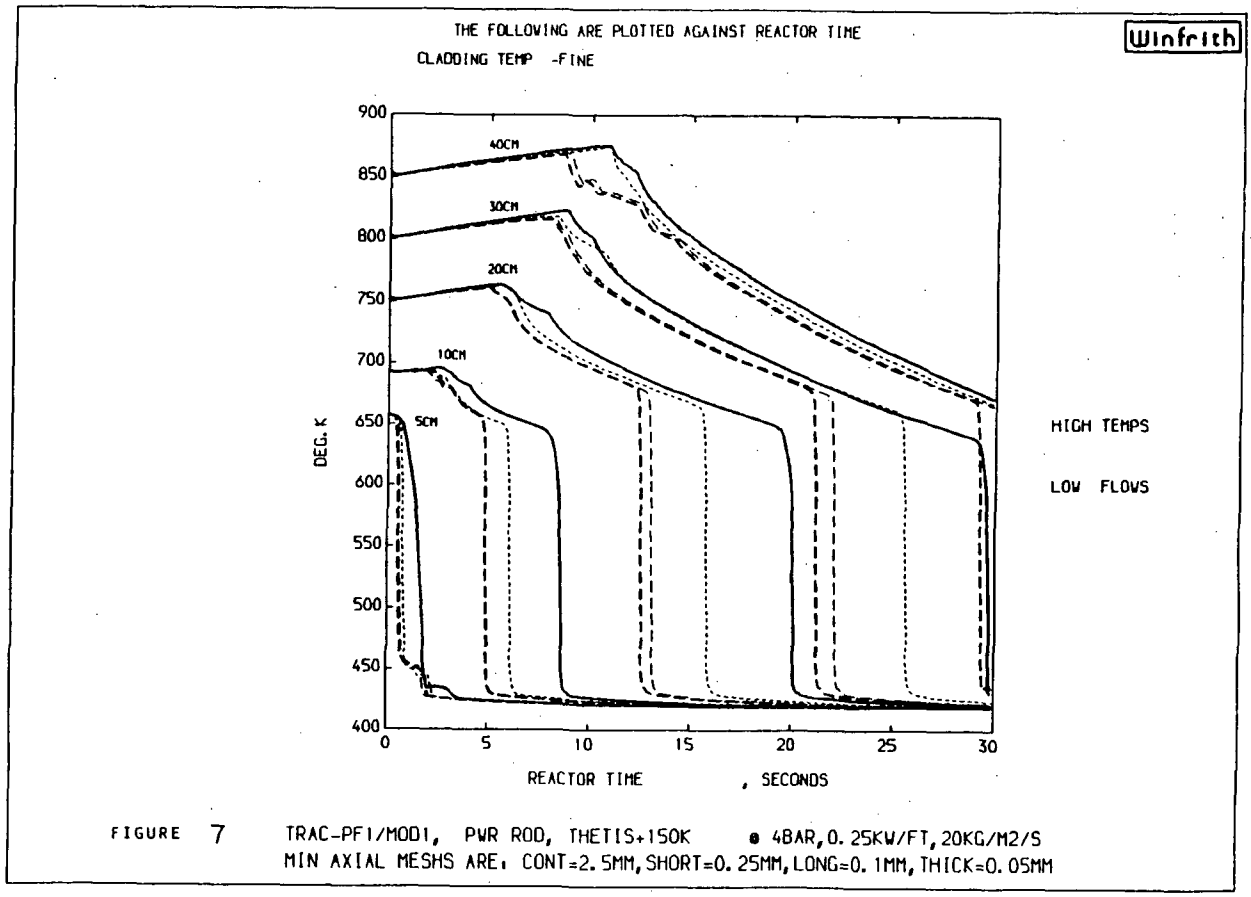


FIGURE 7 TRAC-PF1/MOD1, PWR ROD, THETIS+150K @ 4BAR, 0.25KW/FT, 20KG/M2/S
MIN AXIAL MESHS ARE: CONT=2.5MM, SHORT=0.25MM, LONG=0.1MM, THICK=0.05MM

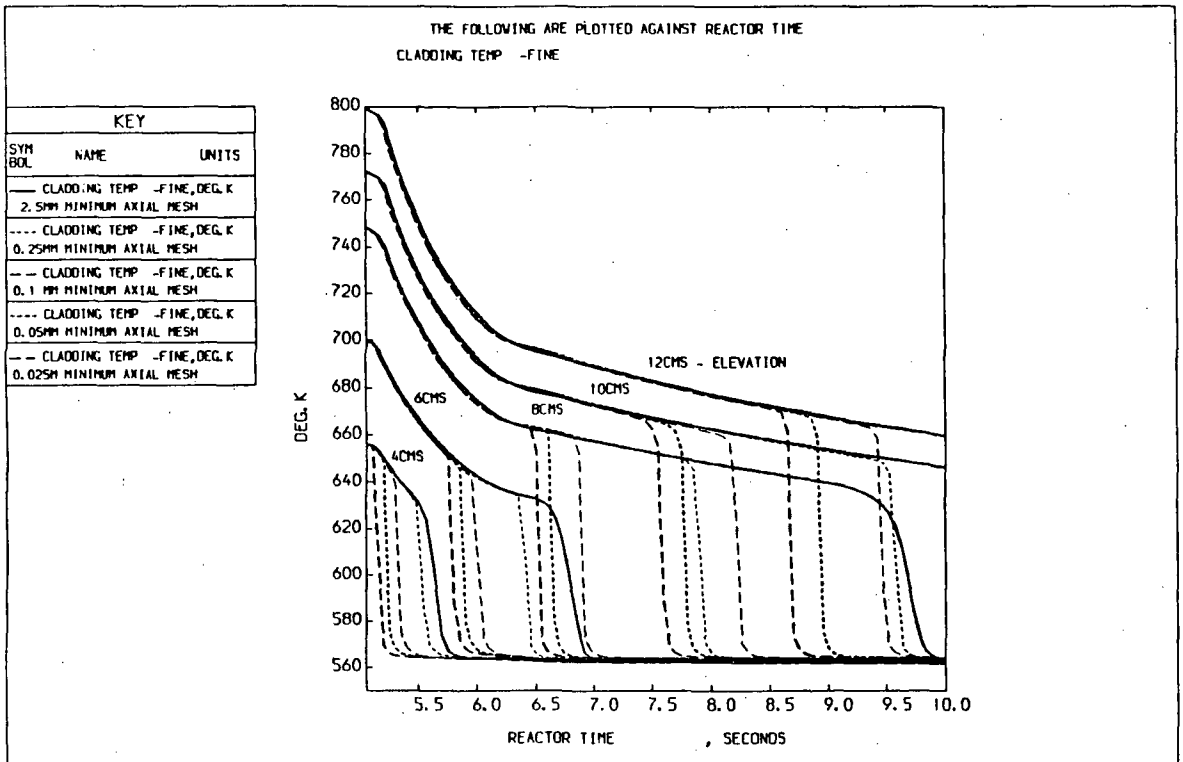


FIGURE 8 QUENCHING AT 70BAR, 0.37KW/FT, 960KG/M2/S RAMPED FLOW
TRAC-PF1/MOD1 LOFT L2-6 ROD SIMULATION FOR VARIOUS AXIAL MESH SIZES

THE TRAC ROD HEAT CONDUCTION EQUATION IS :-

$$\rho c_p \frac{\partial T}{\partial t} = \dot{q}''' + \frac{1}{r}\frac{\partial}{\partial r}\left(rk\frac{\partial T}{\partial r}\right) + \frac{\partial}{\partial z}\left(k\frac{\partial T}{\partial z}\right) \quad .$$

DIVIDED BY $\rho c_p$ THIS CAN BE WRITTEN IN THE FORM :-

TOTAL = GENERATION + RADIAL + AXIAL

WHERE EACH TERM IS IN °K/SEC

THE FOLLOWING FIGURES SHOW THE INDIVIDUAL TOTAL, RADIAL AND AXIAL TERMS FOR CLADDING SURFACE NODES. (THE GENERATION TERM IS ZERO FOR THE CLADDING).

THE FIGURES ALSO SHOW THE SURFACE NODE TEMPERATURES AND HEAT TRANSFER REGIMES.

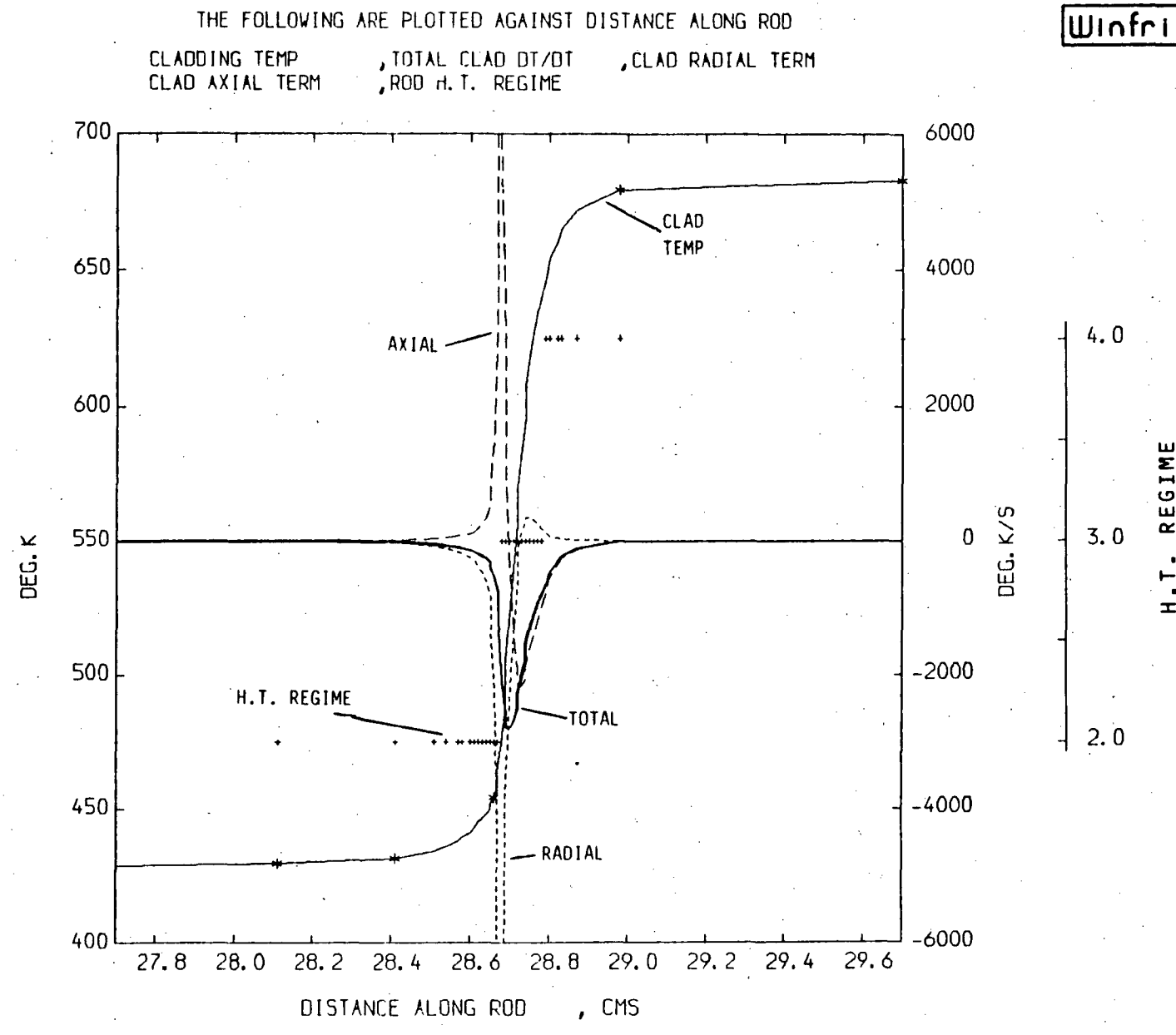


FIGURE 10. PWR ROD REFLOOD CALCULATIONS. 4BAR 20KG/M**2/S, HIGH TEMPS-LOW FLOWS
PWR123. 0.05MM MIN AXIAL MESH PROFILE AT 20.0 SECONDS

## FIG. 11 *Void Fraction Correlations used in New Interphase Drag Model*

| | Rod Bundles | Small Pipes<br>$D_h \leq 1.8cm$ | Intermediate Pipes | Large Pipes<br>$D_h \geq 24cm$ |
|---|---|---|---|---|
| High Upflow Rates<br>$G > 100$ $kg\,m^{-2}\,s^{-1}$ | EPRI | EPRI | | |
| Low Up, Down and Counter-Current Flow Rates<br>$G < 50$ $kg\,m^{-2}\,s^{-1}$<br>$G > -50$ $kg\,m^{-2}\,s^{-1}$ | EPRI | Zuber-Findlay Slug Flow | Kataoka-Ishii | Gardner |
| High Downflow Rates<br>$G < -100$ $kg\,m^{-2}\,s^{-1}$ | EPRI | EPRI | | |

Interpolation applied between different flow regions in pipes

The Gardner correlation is formulated as a drift flux model by taking $C_0 = 1$

***Horizontal Flow***

Bryce

***References***


EPRI - Chexal and Lellouche (1986)

Zuber-Findlay Slug Flow - Zuber et al. (1967)

Kataoka-Ishii - Kataoka and Ishii (1987)

Gardner - Gardner (1980) with modification proposed by Woodford and Scriven (1983) to extend validity to $\alpha \geq 0$

Bryce - Bryce (1977)

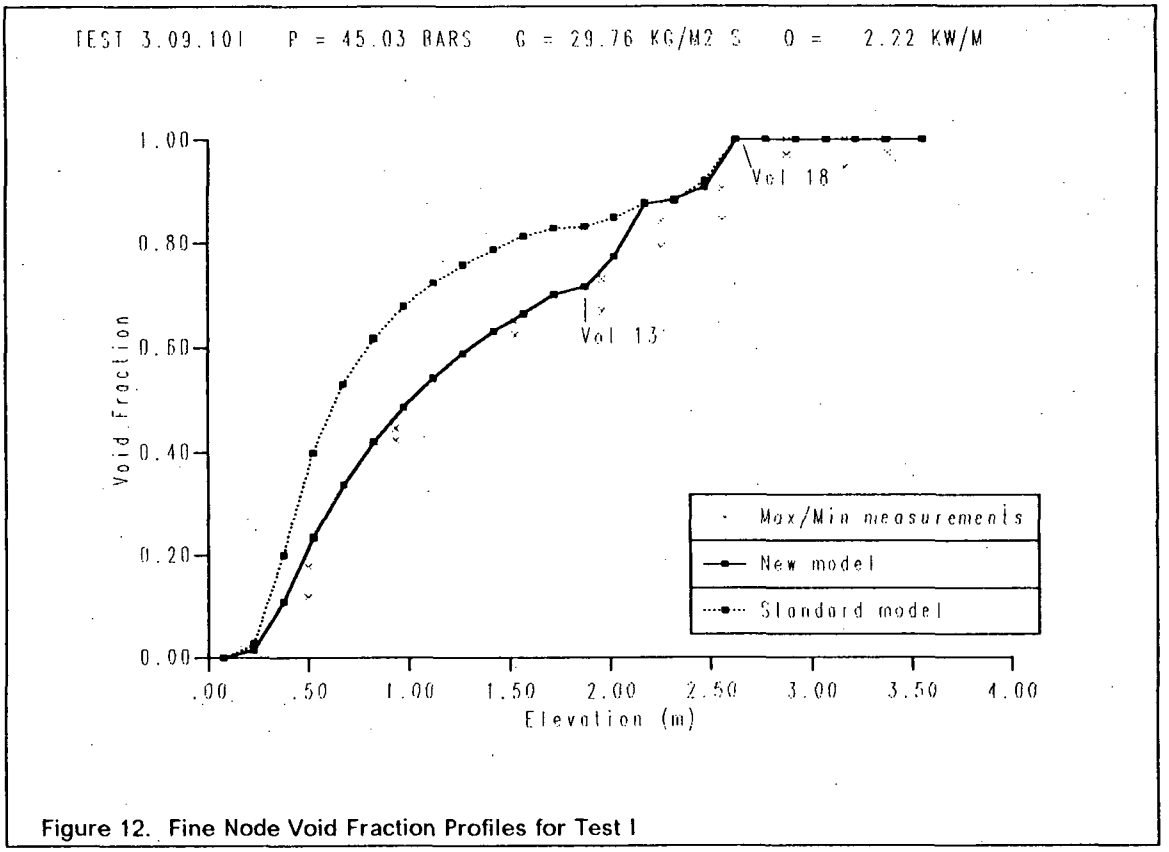


Figure 12. Fine Node Void Fraction Profiles for Test I

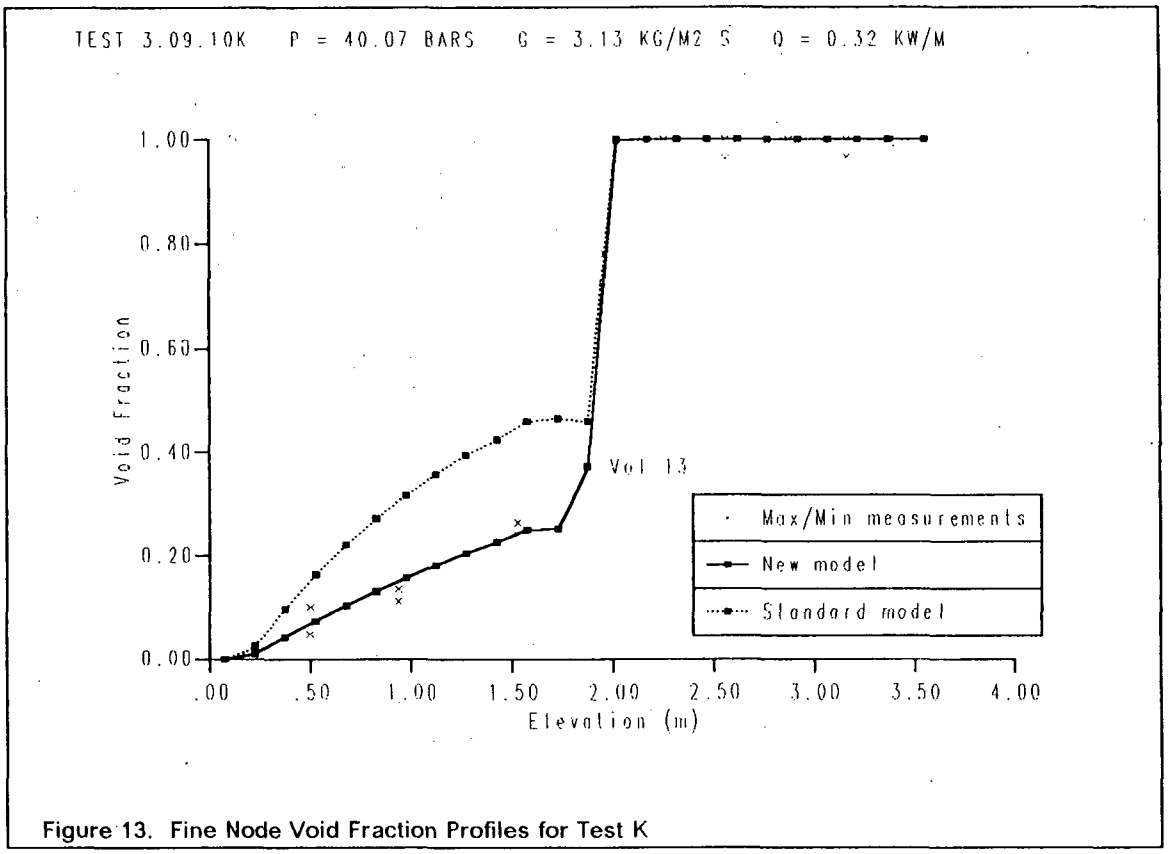


Figure 13. Fine Node Void Fraction Profiles for Test K

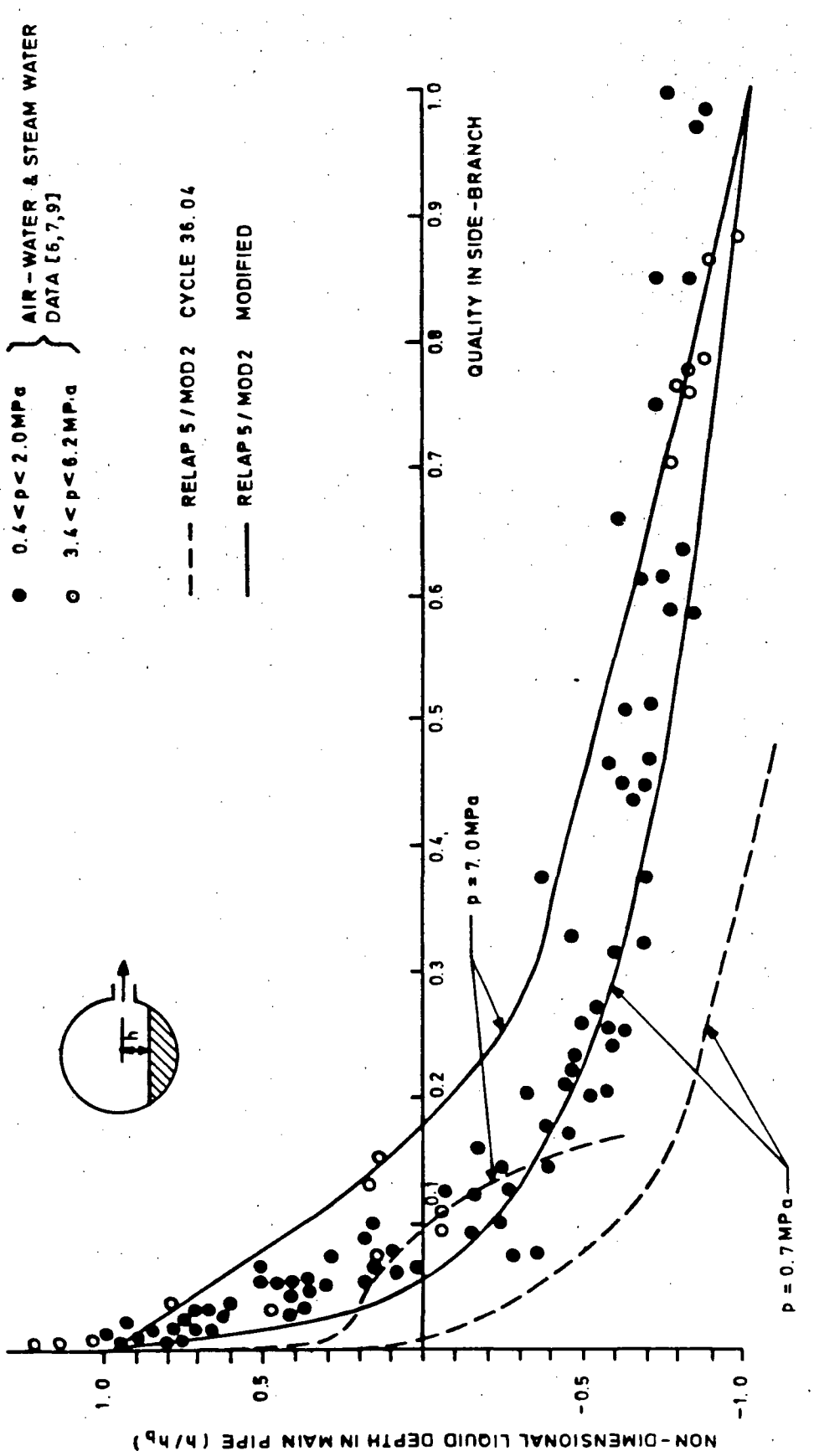


FIG 14 DISCHARGE FLOW QUALITY v LIQUID DEPTH: HORIZONTAL SIDE-BRANCH

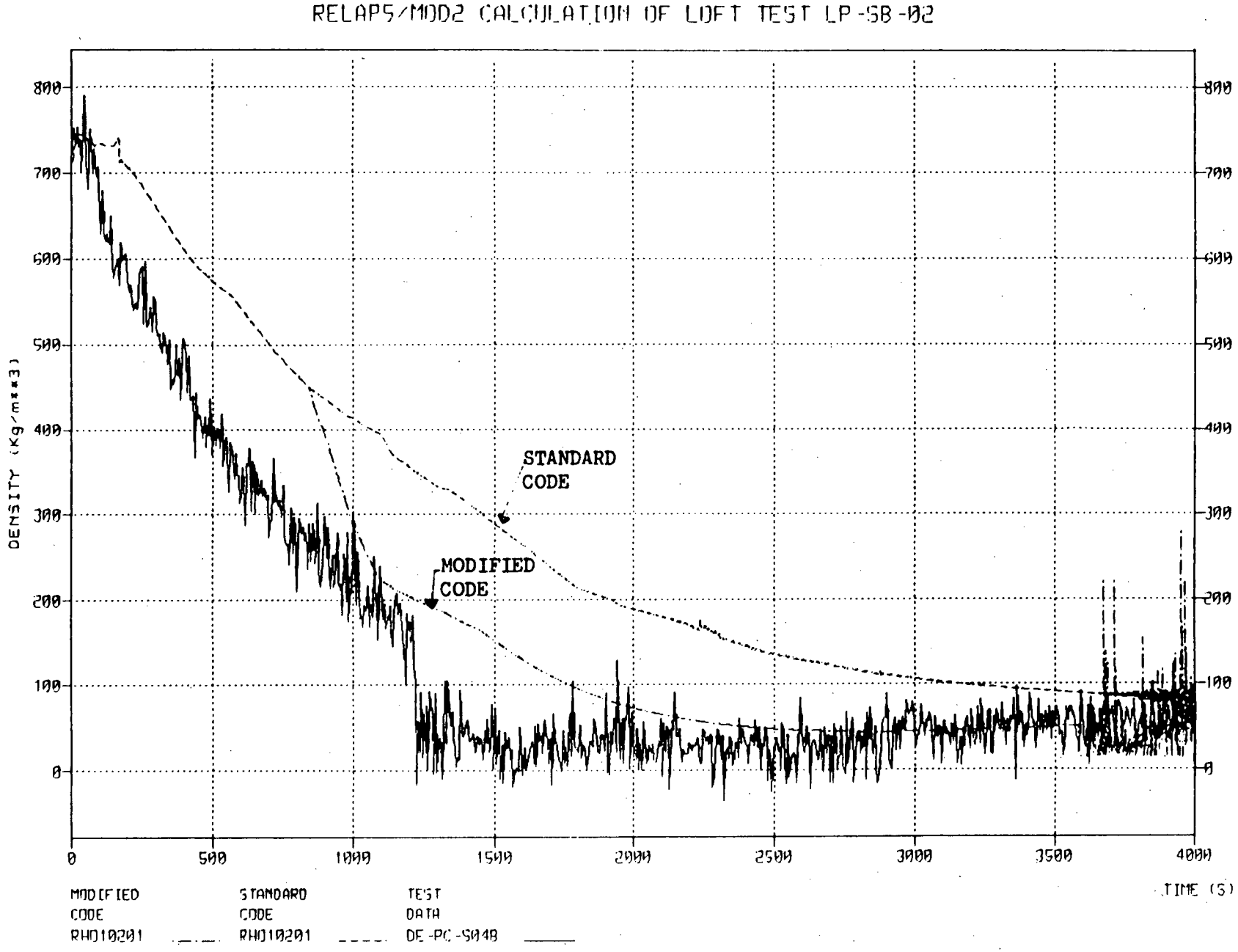


FIGURE 15 MEASURED AND CALCULATED BREAK LINE DENSITIES

# MIST PROGRAM: SUMMARY OF KEY RESULTS

J. R. Gloudemans
Babcock & Wilcox, Nuclear Power Division
Lynchburg, Virginia

and

D. P. Birmingham
Babcock & Wilcox, Research and Development Division
Alliance, Ohio

## ABSTRACT

The multiloop integral system test (MIST) was part of a multiphase program started in 1983 to address small-break loss-of-coolant accidents (SBLOCAs) specific to Babcock & Wilcox-designed plants. Data from MIST are used to benchmark the adequacy of system codes, such as RELAP5 and TRAC, for predicting abnormal plant transients.

In 1982, a Test Advisory Group (TAG) was formed to identify experimental data needs for the Babcock & Wilcox-designed nuclear steam system. The TAG developed a list of 17 issues perceived both to lack experimental data and to be of sufficient interest that such data were needed. The issues were grouped under four major topics: natural circulation, small-break loss-of-coolant accidents, feed and bleed, and steam generator tube rupture. The MIST facility was scaled, designed, and tested to address these issues.

The MIST tests addressed each of the 17 TAG issues. A wealth of consistent integral system data has been generated for each issue. An important issue under the topic of natural circulation was the ability of boiler-condenser mode natural circulation to remove core heat and effectively depressurize the reactor coolant. In this program, the viability of this mode of primary-to-secondary heat transfer was repeatedly observed. When the prerequisite conditions for boiler-condenser mode were met, the primary system tended to depressurize through vapor condensation and the accompanying primary-to-secondary heat transfer. The ability of the reactor vessel vent valves to augment primary system depressurization during the simulated SBLOCAs was also observed in MIST. MIST repeated exhibited system resiliency to imposed changes in the primary boundary conditions as a result of the steam venting capabilities of the reactor vessel vent valves. The ability of feed and bleed cooling to provide continual core cooling as well as system cooldown and depressurization was demonstrated in MIST, indicating the viability of this alternate method of plant cooldown. Finally, integral system interactions with multiple- and single-tube ruptures were characterized in MIST. The major observations regarding the test data are presented in this publication.

## INTRODUCTION

The multiloop integral system test (MIST) was part of a multiphase program to address small-break loss-of-coolant accidents (SBLOCAs) specific to the Babcock & Wilcox-designed nuclear steam system. MIST is sponsored by the U.S. Nuclear Regulatory Commission (NRC), Electric Power Research Institute (EPRI), the Babcock & Wilcox Owners Group, and Babcock & Wilcox (B&W). Test data from the MIST facility have been used to benchmark the predictive capabilities of several system codes – RELAP5 and TRAC – for predicting abnormal plant transients.

In 1982, a Test Advisory Group (TAG) was formed to identify experimental data needs for the B&W-designed nuclear steam system. The TAG developed a list of 17 issues perceived to lack experimental data and to be of sufficient interest that such data were needed. The issues were categorized into four major topics: natural circulation, small-break loss-of-coolant accidents, feed and bleed, and steam generator tube rupture.

Due to the unique features of the Babcock & Wilcox design, specifically the hot leg U-bend configuration that results with the once-through steam generator (OTSG), previous large integral system test facilities did not simulate the appropriate natural circulation conditions. There was uncertainty regarding the effects of non-condensible gases, high point vents, and the reactor vessel vent valves on natural circulation. The validity of the boiler-condenser mode of heat removal was also questioned. Since a major phenomenon in an SBLOCA in a B&W plant is the natural circulation mode of heat removal, the TAG recommended that the natural circulation phenomena be addressed on an integral system basis. Parameters such as break size and location, isolation of the break, sensitivity to emergency core cooling system (ECCS) operation, and the effects of reactor coolant pump operation were to be evaluated. This would also permit evaluation of the reactor vessel vent valves on an integral system basis. The group recommended that tests be performed to assess the computer code capability of predicting the feed and bleed mode of heat removal. Finally, since the once-through steam generator presents a significantly different configuration from a U-tube steam generator, it was concluded that integral system testing of tube ruptures would be beneficial. Both single- and multiple-tube ruptures were to be considered, along with a steam line break in conjunction with a tube rupture.

The MIST test matrix was designed to address these issues formulated by the TAG. As listed in Table 1, the MIST testing was divided into seven different groups.

**Table 1**

**MIST TEST GROUPS**

Test Group 30 - Mapping Tests
Test Group 31 - Boundary System Variations
Test Group 32 - Altered Leak and HPI Configurations
Test Group 33 - HPI-PORV Cooling
Test Group 34 - Steam Generator Tube Rupture
Test Group 35 - Non-Condensibles and Venting
Test Group 36 - Pump Operation and Core Uncovery

In the Group 30 - Mapping Tests, integral systems data were obtained during a measured, controlled traverse through the initial events governing an SBLOCA. Whereas these early SBLOCA events ordinarily occur rapidly, in the mapping tests these events were greatly prolonged in time by controlling

the rate of primary inventory depletion. Test Groups 31 through 36 were referred to as Transient Tests. In the boundary systems variations (Group 31), a single boundary system parameter was varied from their nominal condition to assess its effect. The boundary conditions so evaluated included reactor vessel vent valve control, heat loss control and augmentation, feed control and wetting, symmetry of steam generator secondary system depressurization for cooldown, an abnormal transient operating guideline (ATOG) operator-controlled test, and test repeatability. In altered leak and HPI configurations (Group 32), leak size, leak location, isolation status, and HPI capacity were varied singly from the nominal test condition. Feed and bleed, or HPI-PORV cooling (Group 33), was examined by interrupting feed to both steam generators and making inert the steam generator secondaries. Testing examined the timing of HPI actuation, HPI capacity, and the effects of surge line uncovery. In the steam generator tube rupture tests (Group 34), both single-ended rupture of one tube and double-ended rupture of 10 tubes were simulated. Methods of primary system depressurization, rupture elevation (top or bottom of generator), isolation status of the affected generator, and depressurization rate of the affected generator were varied from a nominal test condition. In the non-condensibles and venting tests (Group 35), the effects of non-condensible gases and venting on an SBLOCA were examined. Test variations included the effects of gas species, break location, and venting status. For the pump operation and core uncovery tests (Group 36), MIST was configured for forced flow. Test variations included a repeat of the nominal test with the new forced flow loop configuration, an ATOG operator test in which the pumps were available, pumps operation throughout an SBLOCA, pumps tripped at minimum inventory, and the effect of test initialization in forced flow. A core uncovery test involving pump operation was also tested.

Additional MIST testing beyond the above described program was performed in late 1987. This MIST follow-on program – referred to as Phase 4 – both extended the earlier (Phase 3) data base, and explored transients that were previously not addressed. A 100 $cm^2$ SBLOCA transient was performed, extending the range of break sizes in the MIST data base. A low-pressure injection (LPI) system added for Phase 4 testing provided a more realistic simulation of the emergency core cooling system (ECCS) during low reactor coolant system pressure than was previously available. A repeat of the MIST nominal test was performed, but with modified post-trip core power and steam generator cooldown rates. This test was to provide insight into the known scaling compromise of having excess primary fluid volume. A series of steady-state steam generator performance tests were performed to supplement the current understanding of high-elevation auxiliary feedwater, as well as provide data on main feedwater operation. The areas previously not addressed included two SBLOCA transients without high-pressure injection. The variation on these tests was different strategies on utilizing the steam generator for loop cooldown. A station blackout transient was also simulated in this phase of testing. One possible procedure for mitigating this postulated event was tested on the MIST facility. Finally, two plant transients were simulated on the scaled MIST facility. The Crystal River 3 loss-of-offsite power event of June 1981, and the Rancho Seco loss-of-ICS event of December 1985 were simulated. The intent of these scaling tests was to provide insight into the scaling compromises known to exist in the MIST facility, and to provide code benchmarking data. These tests were completed in December 1987 and are presently being reported. The major test observations noted in this paper include only those observations from the earlier (Phase 3) test program.

## FACILITY DESCRIPTION

The MIST Facility is a scaled physical model of a B&W lowered-loop, nuclear steam system. The test loop was designed to operate at typical plant pressures and temperatures, with emphasis on leak tightness and minimal heat losses. The MIST model includes all the major components of a plant reactor coolant system, including a full length electrically heated simulated core, two hot legs, two full length once-through steam generators, four cold legs, an external vessel downcomer, simulated reactor vessel vent

valves, and pressurizer. The boundary conditions include scaled high-pressure injection, core flood tanks, low-pressure injection, scaled leaks and vents, power-operated relief valve, and scaled feed and steam capabilities for the secondary side of the steam generator. A test facility schematic is shown in Figure 1.

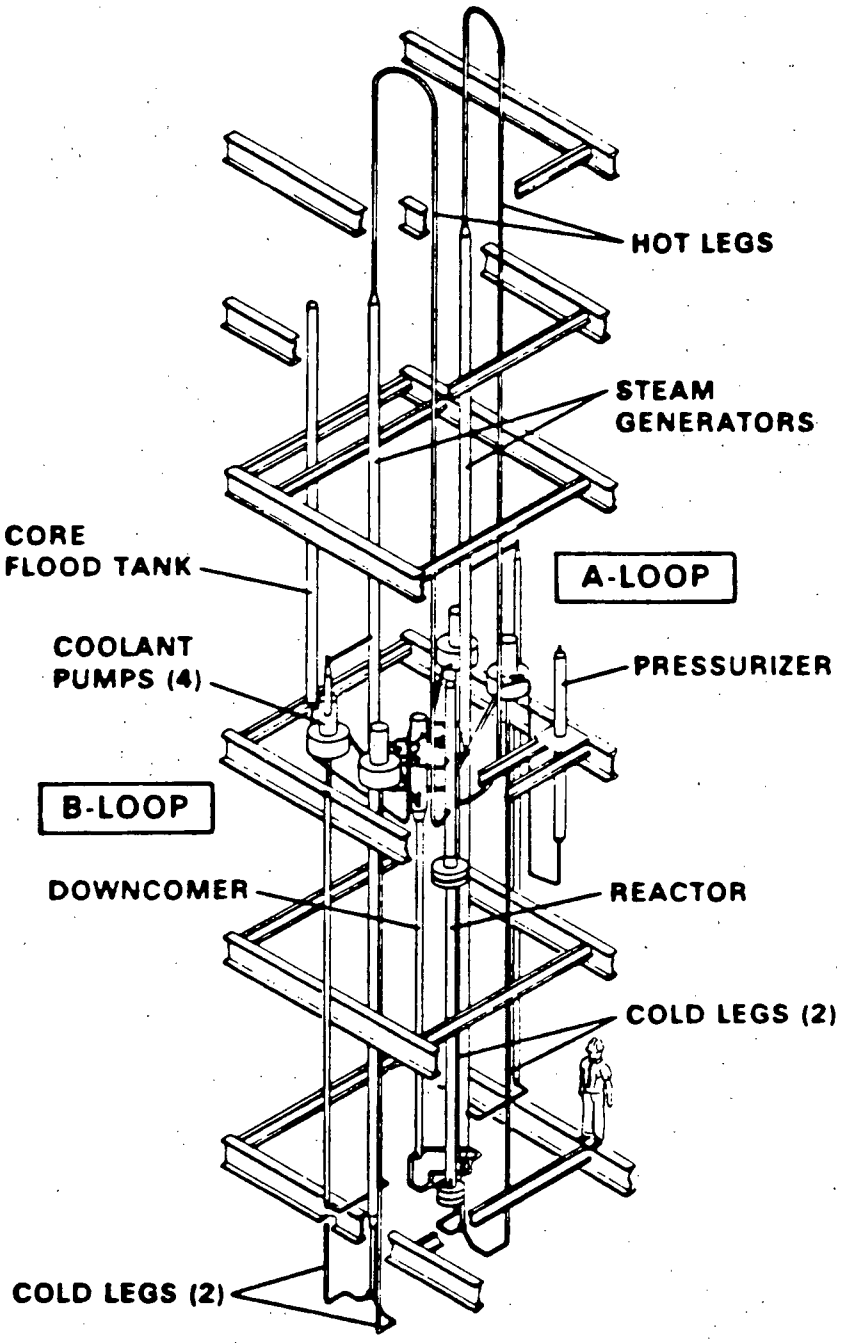


Figure 1. Reactor Coolant System – Multi-Loop Integral System Test (MIST)

Scaling priorities for MIST were elevation, post-SBLOCA phenomenon, component and piping volumes, and irrecoverable pressure losses. MIST is generally full-elevation scaled. The key interfaces maintained include the hot leg U-bend spillover, upper and lower tubesheets of the steam generator (secondary faces), cold leg low point, pump discharge, cold and hot leg nozzles, core, and points of emergency core cooling system injection. System two-phase behavior during voiding of the hot leg U-bend and flow interruption is sufficiently prototypical. Both the plant and the model will experience phase separation early in the post-SBLOCA transient. The model hot leg pipes are large enough to admit bubbly flow, and the model reactor vessel upper internals were designed to obtain prototypical phase separation. The model fluid volume is approximately 40% larger than that obtained using power-to-volume scaling. The hot legs, cold legs, and upper downcomer were oversized. This atypicality was imposed by the higher-priority model system characteristics and by the consideration of regional fluid irrecoverable pressure losses. System irrecoverable pressure losses were preserved in the MIST model. A complete description of the MIST facility is contained in Reference 1.

## MAJOR TEST OBSERVATIONS

MIST has generated an extensive data base and a correspondingly extensive set of observations. Selected observations are summarized in the following paragraphs. These observations are those perceived to be of most interest, especially as they provide insight into expected plant performance. Additional detailed information is provided in Reference 2.

The MIST observations involve certain key interactions, such as boiler-condenser mode (BCM), intermediate levels, and HPI-leak cooling. These interactions are defined as they arise in the discussions.

The following observations are addressed:

- Interruption of Loop Flow
- System Compliancy
- Reproducibility
- HPI-PORV Cooling
- Non-Condensible Gases (NCG) Effects
- Operation of the Reactor Coolant Pumps
- Operator Control

### Interruption of Loop Flow

The interruption of loop flow following a SBLOCA marked the transition from standard to non-standard methods of primary system heat removal. Subcooled forced or natural circulation preceded interruption. Following interruption, primary cooling was obtained by BCM, HPI-leak cooling, and HPI-PORV (feed and bleed) cooling. The timing of the transition among cooling modes, and the effectiveness of these modes, largely determined the course of the transients. Flow interruption was observed repeatedly in MIST and under a wide variety of settings. Two distinct types of flow interruptions were observed – those in which the primary system gradually depressurized following interruption, and those in which the primary abruptly repressurized. The depressurization versus repressurization tendency was governed by the ability of HPI to condense the steam generated in the core. Those tests in which the plant systems were simulated fell into the depressurization category.

The SBLOCA transients were conducted to be similar to plant transients. Core power was gradually reduced to simulate post-trip decay. HPI was controlled to obtain plant-typical head-flow response, and usually simulated the full-plant HPI flow capacity scaled to MIST. HPI-leak cooling was thus usually sufficient to offset all of the core power. When the downcomer level approached the elevation of the cold leg nozzles, HPI condensation began. Steam which was generated in the core passed through the reactor vessel vent valves (RVVVs) and was condensed in the downcomer and cold legs. Loop flow interrupted, but the primary system gradually depressurized in sharp contrast to the repressurization observed in the mapping tests (Group 30). Loop conditions at the time of flow interruption are illustrated in Figure 2.

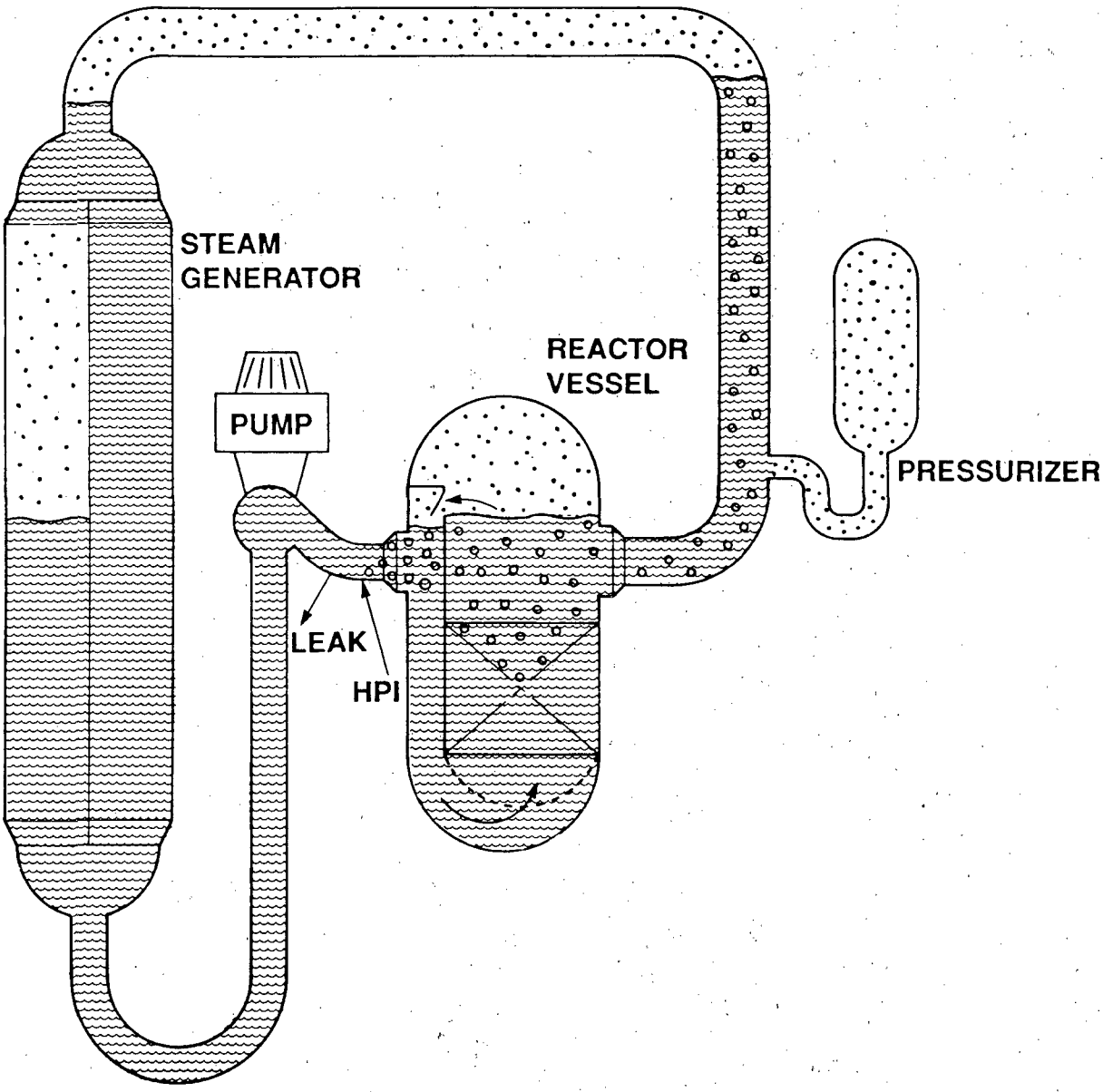


**Figure 2. Illustration of Test Loop Conditions at Flow Interruption During SBLOCA Transient**

In the mapping tests, the primary system fluid inventory was reduced very gradually. The transient interactions were deliberately prolonged to facilitate both their examination and their simulation in the computer codes. The method of inventory control altered these interactions, however. Inventory was controlled by throttling HPI – adjusting the HPI flow rate to create a small imbalance between the leak and HPI mass flow rates.

Because of this reduced HPI flow rate, HPI-leak cooling was insufficient to offset core power. As a result, primary system flow generally persisted until the hot leg nozzles were uncovered and the core-region fluid had saturated. The primary system repressurized quite rapidly upon the interruption of loop flow.

**System Compliancy**

MIST has been tested with a wide range of SBLOCA conditions. Break size was varied from 5 to 50 $cm^2$, break location was varied, and both full-capacity and half-capacity HPI flow rates were used. In each instance, MIST depressurized and attained mass equilibrium without uncovering the core. The key to this observed system compliancy was the RVVVs.

The RVVVs vented core-generated steam to the downcomer where it was condensed by HPI. Because (scaled) full-capacity HPI was sufficient to condense all of the core steam after only 10 minutes of post-trip decay, the primary system depressurization generally began early in the SBLOCA transient. With half-capacity HPI, the HPI condensing capacity remained less than the core output during the first several hours of post-trip decay. The excess steam led to cold leg voiding and saturation of the break-site fluid. Test loop conditions during the half-capacity HPI test are illustrated in Figure 3. Saturation of the break-site fluid in turn caused the break mass flow rate to decrease (towards the HPI mass flow rate), and caused the break volumetric flow rate to increase (augmenting HPI condensation). The system conditions thus inherently realigned to accommodate an imposed reduction of HPI flow rate. This system compliancy is illustrated in Figure 4 as a plot of primary system pressure and total primary system fluid mass during the full-capacity and half-capacity HPI 10 $cm^2$ SBLOCAs. In these tests, the system achieved similar minimum fluid mass inventory and primary system pressure.

A similar system adjustment occurred with the largest break size. In each case, the RVVVs were central to system compliancy. They not only vented core- generated steam to the region in which HPI condensation could occur, but also caused the cold leg break size fluid conditions to be responsive to the steam generation-condensation balance. A SBLOCA test with the MIST RVVVs held shut underscored their role. Rather than gradually depressurizing, the primary system cyclically repressurized for the duration of the test.

**Asymmetries**

The multi-loop configuration of MIST, like that of the plant, was prone to asymmetries. Indeed, MIST experienced a wide variety of asymmetries in every test. They were manifested, for example, by inter-loop inequalities of levels, fluid conditions, flow rates, cold leg flow directions, and steam generator activity. With few exceptions, these asymmetries served to mitigate the integral-system transient.

Inter-loop asymmetries were generally beneficial because of "intermediate levels" wherein primary-to-secondary heat transfer was inhibited. This range of levels was delineated by the elevations of the steam generator upper tubesheet and of the hot leg U-bend spillovers. Within this level band, BCM was precluded because the primary two-phase interface resided above the zone of condensation, but single-phase circulation was precluded because of U-bend voiding. If both hot leg levels resided within this

intermediate-level range, then primary-to-secondary heat transfer was precluded. But, if either hot leg level transcended the intermediate range, then heat transfer could be activated. Inter-loop asymmetries thus countered the effects of intermediate levels. Examples of specific asymmetries occurrences are described in the following paragraphs.

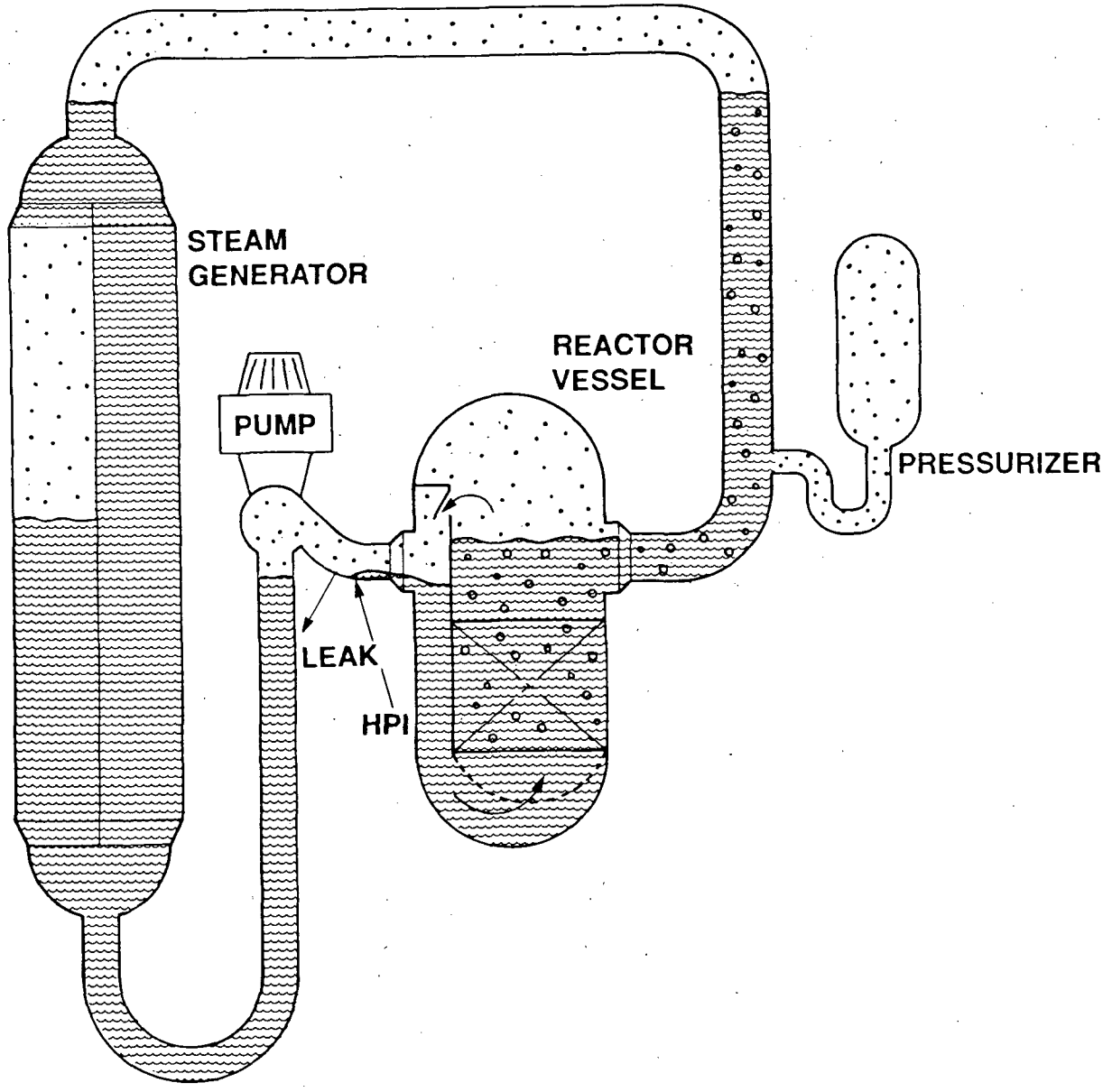


Figure 3. Illustration of Test Loop Conditions During 10 $cm^2$ SBLOCA With Half-Capacity HPI

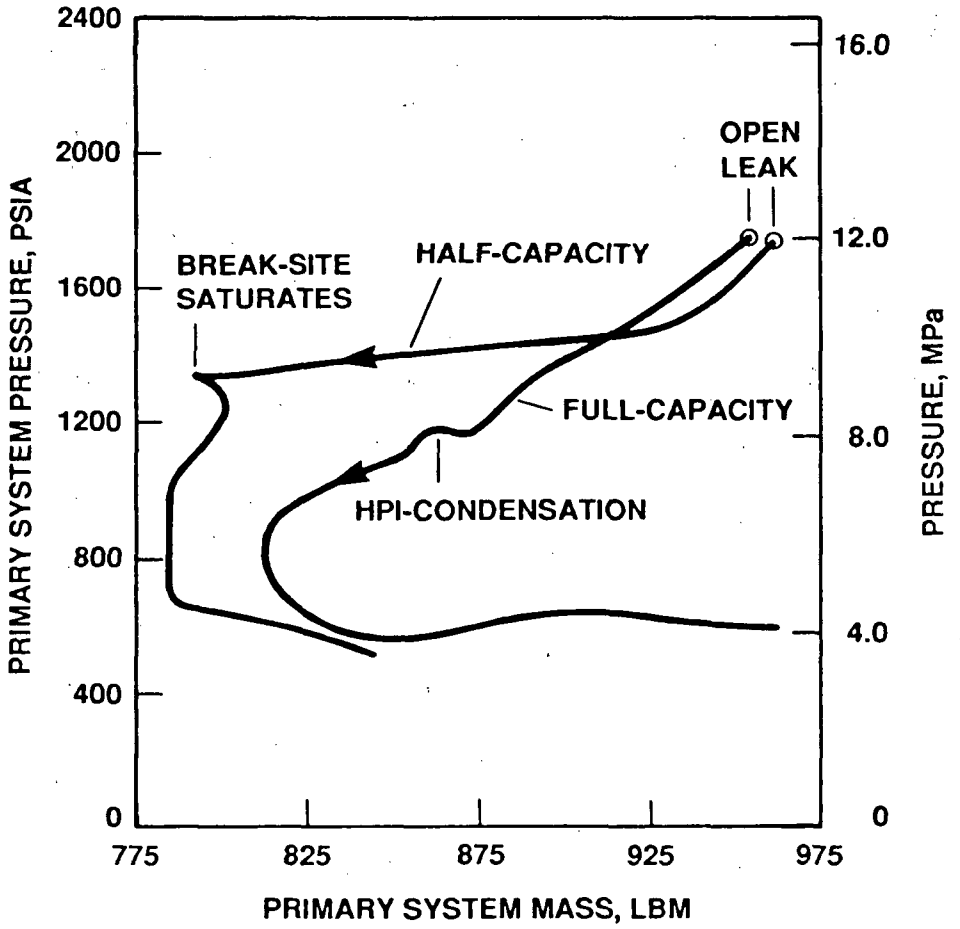


**Figure 4. Effect of Available HPI-Capacity on 10 $cm^2$ SBLOCA**

Early in the SBLOCA transients, an inter-loop hot leg level difference obtained a relatively early primary system depressurization. The depressurization mechanism was AFW BCM while AFW remained active to accomplish the initial increase of steam generator secondary level.

Late in the SBLOCA transients, as the hot leg risers began to refill, inter-hot leg level differences again hastened primary system depressurization. In this instance, a hot leg level achieved the U-bend spillover elevation. The resulting re-initiation of loop flow re-activated the associated steam generator, ultimately causing natural circulation cooling and the final reduction of primary system pressure.

Inter-loop asymmetries were the most pronounced in the tube rupture tests. With the larger simulated rupture size, the robust initial primary system depressurization quickly led to reverse heat transfer in the intact steam generator. That loop voided extensively, almost depleting its primary fluid inventory. The loop containing the ruptured steam generator, on the other hand, remained relatively full and highly albeit intermittently active. The primary system depressurized not only due to the tube-rupture discharge, but also through BCM-like activity between primary system vapor and the rupture effluent being discharged from the secondary side of the ruptured steam generator.

The smaller-rupture tests also exhibited marked inter-loop asymmetries, but of a quite different nature than those of the larger-rupture tests. The ruptured steam generator secondary was isolated after the requisite

depressurization. Primary-to-secondary heat transfer to the isolated steam generator consequently diminished, causing that loop to stagnate. As the primary system was depressurized in response to the continuing single-loop cooldown, the primary system saturation temperature approached that of the stagnant loop. That loop finally saturated and then voided, but the single-loop cooldown was virtually unaffected.

Another sort of system asymmetry occurred in the core uncovery test (Group 36). Whereas the previously discussed asymmetries had a beneficial or, at worst, benign impact on primary system cooldown and depressurization, this asymmetry was apparently detrimental. The test involved a loss of feedwater and an extensive reduction of primary system inventory. Early in the test transient, feed was restored to both steam generators, but the secondaries were controlled unequally. The more active steam generator apparently diverted primary fluid to that loop, causing the two-phase performance of an opposite loop pump to degrade abruptly. This sequence of increased, asymmetric steam generator activity followed by pump degradation was repeated later in the test. Still later, with the primary system average void fraction near 50%, steam generator activity apparently triggered excursions of the core fluid temperatures.

**Test Reproducibility**

Test reproducibility has been extensively examined. Not only were specific tests repeated, but also certain portions of several tests utilized nominally identical boundary conditions. For example, the break isolation test repeated the control of the nominal SBLOCA test until the break was isolated at 30 minutes. Three major conclusions have arisen from these repeatability studies:

- Slight variations of boundary system conditions can preclude certain system events.
- Inter-test differences which initially are almost indiscernible can, by integral system feedback, take on increasing significance.
- Inter-test differences notwithstanding, tests with like boundary conditions exhibited the same global trends, and generally converged during the later refill stages of the transients.

The nominal SBLOCA transient was repeated once in its entirety, and several times through the earlier stages of the transient (until imposed inter-test differences took effect). An early AFW-BCM depressurization occurred in some but not all of these comparably-controlled tests. This difference was caused by a slight (6%) change in the leak flow rate at comparable conditions, apparently due to a change of the physical characteristics of the critical-flow orifice used to control leak flow rate. In summary, integral system tests were not always reproducible in detail, but their global system trends – primary system pressure and total inventory, for example – were reproducible.

**HPI-PORV Cooling**

The viability of HPI-PORV cooling in MIST was demonstrated in a series of tests. HPI flow rate and delivery time were the major variables among these tests. A single HPI-PORV test was initiated in forced circulation. The primary system pressure stabilized as the PORV-site fluid changed state, rather than as the primary fluid saturated as had occurred in the tests without forced flow.

Surge line uncovery occurred in several of the HPI-PORV cooling tests. The hot leg A riser level descended sufficiently to expose the pressurizer surge line to two-phase fluid. This caused the quality of the PORV-site fluid to increase, thereby augmenting the primary system depressurization as well as

slowing the rate at which primary system fluid inventory was discharged by the PORV. In this way, surge line uncovery mitigated the system-condition trends during the HPI-PORV cooling. Primary test loop conditions at the time of surge line uncovery are illustrated in Figure 5; the response of the primary system pressure and fluid mass during a typical HPI-PORV cooling test (Group 33) is illustrated in Figure 6.

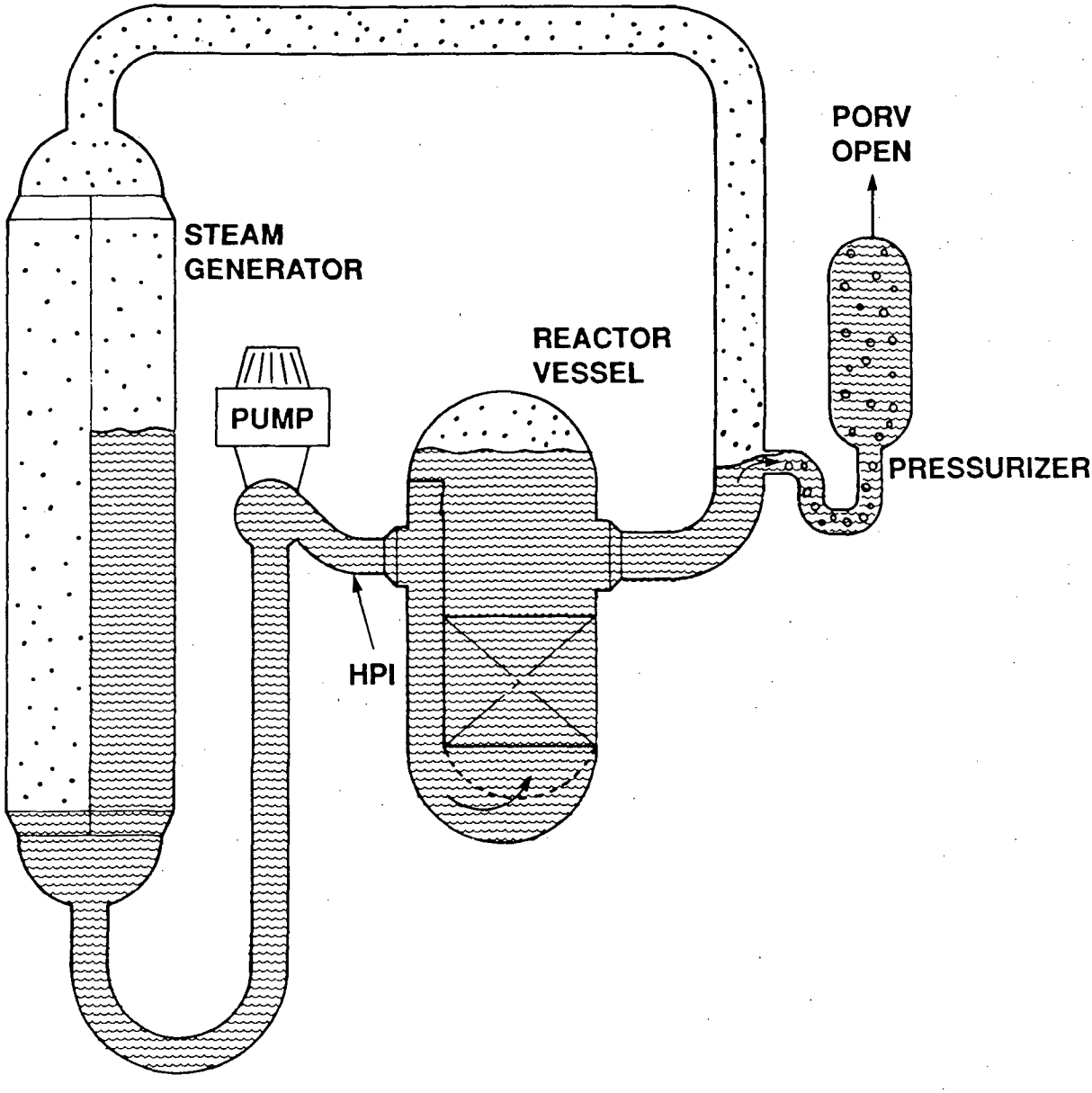


**Figure 5.** **Illustration of Test Loop Conditions During HPI-PORV Cooling – Surge Line Uncovery**

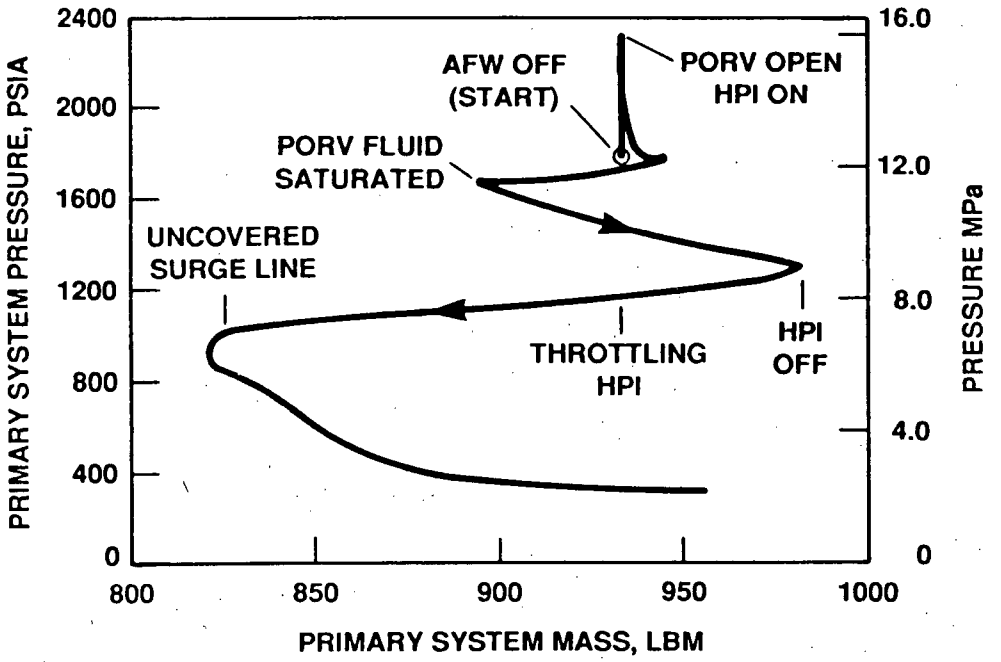


**Figure 6.** **Response of Primary System Pressure and Fluid Mass During Typical HPI-PORV Cooling Test**

### Effects of Non-Condensible Gases

The effects of non-condensible gases (NCG) were explored in a series of MIST SBLOCA tests conducted entirely without forced flow. Although BCM effects were diminished by NCG, the primary system cooldown and depressurization were affected. Hot leg venting was relatively ineffective, however.

Both hot leg vents were kept open throughout most of the NCG tests. Although the vents discharged NCG at first, the rate of discharge quickly dwindled. Rather than migrating up the hot legs from their lower-core injection location, the NCG was swept through the RVVVs and into the downcomer and cold legs. This diversion occurred as core-generated steam began to be condensed by HPI. As a result of this displacement of NCG to the downcomer, most of the injected gas remained within the system. A cold leg discharge leak discharged significant amounts of gas, however. Late in these transients as the hot legs were refilled, the cold legs sometimes voided. Whereas the relatively cold HPI fluid was customarily heated through mixing and condensation, these interactions were impaired in the NCG tests. The lower downcomer and lower reactor vessel fluid temperatures approached the HPI supply fluid temperature.

### Operation of the Reactor Coolant Pumps

Operation of the reactor coolant pumps mitigated the SBLOCA transients. Two mechanisms were operative. First, pump operation sustained primary-to- secondary heat transfer. Whereas this heat transfer was inhibited by intermediate levels (above the steam generators, but below the U-bend spill- overs) without forced flow, pump operation continued to transport even a two-phase mixture to the steam generators. The steam generator secondary systems remained active, thus condensing primary system vapor in a sort of forced-flow BCM.

The second major effect of pump operation involved the fluid conditions at the leak site. Even with a cold leg discharge piping break, this fluid generally remained subcooled without forced flow. The exceptions

occurred with reduced HPI flow and with a larger break. Then, the break fluid quality increased. The mass discharged flow rate decreased and both the discharged volumetric flow rate and the heat removal capacity of HPI-leak cooling increased. These responses without forced flow mitigated the transients and were due largely to the steam venting function of the RVVVs. With forced flows, of course, the RVVVs remained closed. But the pumps directly supplied two-phase fluid to the break site, if voids resided anywhere within the primary loop. Pump operation thus raised the enthalpy of the leak-site fluid, mitigating the transient just as it had occurred through RVVV operation in the natural-circulation transients.

The combined effects of the two mechanisms of mitigation were pronounced. With the pumps operating in a nominal SBLOCA test, the primary loop was refilled in just over 1 hour. Primary system pressure was then controlled by throttling HPI, and an orderly, two-loop forced circulation cooldown ensued. The response of primary system pressure and fluid mass during a 10 $cm^2$ SBLOCA, with and without reactor coolant pumps operating, is shown in Figure 7.

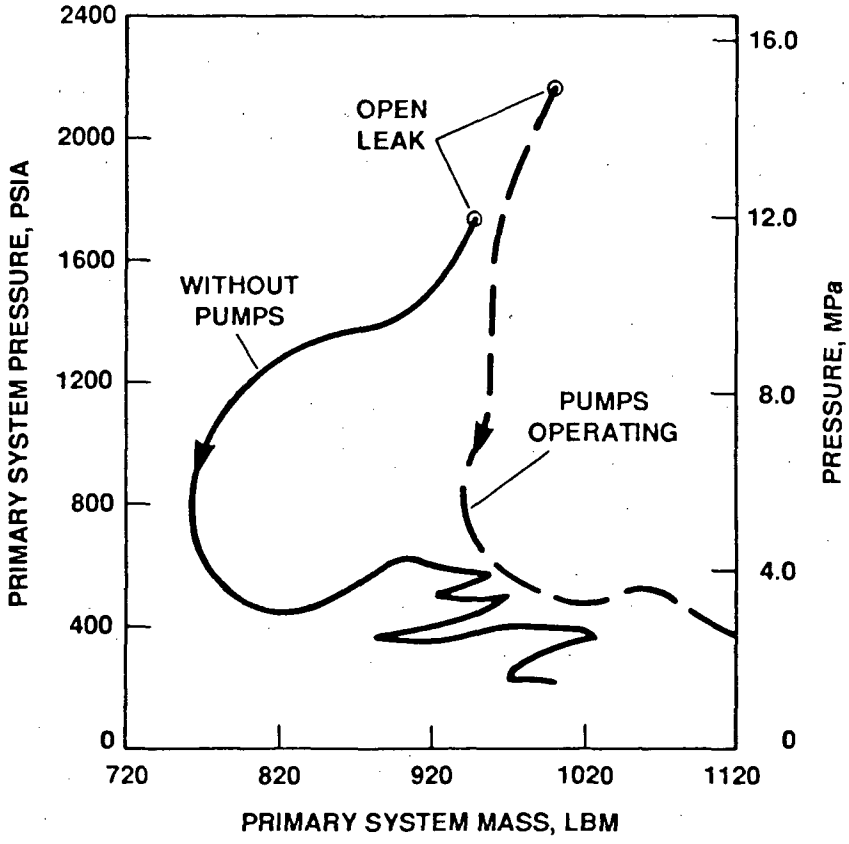


**Figure 7. Response of Primary System Pressure and Fluid Mass During 10 $cm^2$ SBLOCA – With and Without Pumps Operating**

### Operator Control

An operator versed in plant procedures controlled MIST throughout two otherwise-nominal SBLOCA transients. The model reactor coolant pumps were simulated to be unavailable in the first test, but available in the second. Notwithstanding this basic inter-test difference, the major progression of the two operator-controlled transients was surprisingly similar. Moreover, in both operator-controlled tests, the primary system was depressurized, refilled, and cooled much more rapidly and smoothly than in any other comparable test.

With the model reactor coolant pumps simulated to be unavailable, the operator used PORV actuations to counteract intermediate levels. The primary system then depressurized through both the PORV discharge and the re-activated primary-to-secondary heat transfer. More subtly, the operator also promoted loop refill by re-closing the PORV. The fluid inventory which had been displaced to the pressurizer then transferred to the loop, dramatically raising the hot leg levels. In the second operator-controlled tests, two pump bumps were used. Each bump momentarily re-activated primary-to-secondary heat transfer, obtaining a step-decrease of primary system pressure. Hot leg venting was also used to promote hot leg refill.

## SUMMARY

MIST testing was conducted to generate integral-system data with which to benchmark system computer codes. MIST fulfilled this mission admirably. A wealth of self-consistent and comprehensive integral system data was obtained over a wide range of conditions and interactions.

MIST was necessarily atypical of a plant in certain important respects. MIST interactions are, therefore, not to be applied directly to a plant. Nevertheless, MIST interactions provide insight into expected plant behavior; therefore, they are of intrinsic interest. Selected major observations have been discussed. Pervading these observations was a general tendency of MIST to depressurize and to attain a stable fluid inventory. Both BCM and HPI condensation were effective mechanisms of depressurization. The core remained covered and the core fluid temperatures remained at saturation or subcooled, except in those tests specifically designed to force core uncovery and superheating. MIST has, thus, demonstrated the compliancy and controlability of the B&W-designed system.

## REFERENCES


1. "Multi-Loop Integral System Test (MIST) Facility Specification," RDD:84:4091-01-01:01, November 1984. (To be published as an NRC Report in 1989.)

2. "MIST Final Report (Draft), Volume 1 – Summary," J.R. Gloudemans, BAW-2023, May 1988. (To be published as an NRC Report in 1989.)

# UMCP 2x4 Loop Observations Regarding the Behavior of an Integral System During SB-LOCA.

K. Almenas, Y.Y. Hsu, M. diMarzo, G. Pertmer and Z. Wang
University of Maryland, College Park, Md.

The test program at the UMCP 2x4 facility has conducted several series of SB-LOCA experiments. The accumulated data base is now sufficiently extensive that it is feasible to advance from the description of specific SB-LOCA transients to more generalized observations. The generality of the observations can be confirmed by comparison with the extensive data base generated by the OTIS and MIST programs and selected test results provided by experiments at the SRI integral facility.

A necessary initial step in the generalization of the extensive combined data base is a classification of the possible transient types and the identification of the observed flow modes. Several classification schemes have been employed. One divides the transient characteristics into the 'inherent' response of the integral system itself and the modification of this response imposed by boundary conditions such as HPSI, AFW flow, power modifications and others. Another scheme utilizes the observation that SB-LOCA transients can be divided into two dynamically different operational modes. These are: a. quasi-steady state modes For example, continuous two-phase natural circulation or BCM (boiling condenser mode), and b.transition modes. The later can occur between two sequential quasi-steady state modes, but can also occur repeatedly for operational states which exhibit a cyclical character. It has been shown that the most dependable parameter for correlating the operational characteristics is the inventory of the primary system.

The cyclical and oscillatory operational modes deserve special consideration. The accumulated data base has shown that for broad ranges of primary inventory levels, oscillatory behavior is common. The causes and characteristics of oscillations vary. Some are generic and are observed in all of the IST facilities, a few are facility specific and can be related to specific atypicalities. In most cases the ETC (Energy Transport Capacity) of the oscillatory operational modes is relatively high and can equal or even exceed the ETC of single phase natural circulation. Several oscillatory modes observed in the UMCP, MIST and SRI facilities are described and comparatively analyzed.

## INTRODUCTION

The activities of the past year have brought the IST experimental program to a new level of maturity. At the UMCP facility two additional test series investigating SB-LOCA transient response have been conducted, at the MIST facility the phase 3 tests have been finished and the SRI facility tests have been finalized. All this experimental activity has generated a wealth of data which when added to the previous experimental information (e.g. the OTIS, LOFT, Semiscale, PKL, ROSA etc tests) now forms a solid basis for predicting the transient behavior of integral systems which are undergoing a gradual loss of primary system inventory. The available data can provide benchmarks for system code verification which cover most phenomena that can be expected during an actual SB-LOCA in a prototypical plant.

This extensive data base also present a challenge. The challenge is how to apply it in an effective way and to ensure that the ability to interpret and utilize it is not lost after the groups which generated the data have gone on to other projects.

For the most part the experiments have been performed in order to address some specific issues. The questions that were raised by these issues have now, by and large, been answered. At this stage it is therefore appropriate to enquire if this data can remain useful for enhancing our knowledge of integral system behavior in general and for future, yet unforseen code verification purposes.

To enhance such a future usefulness, an effort must be made to classify the data base using a general classification method which will allow identification and recovery of desired data categories without undue effort. That is a large task which will require an effort especially dedicated to this goal. Such a task is beyond the scope of this report. In the past year the UMCP experimental and analytical team have been occupied by the performance of tests and the analysis of the resulting data. The experiment types which have been performed are listed in Table I and II. Documentation and analysis of the tests are presented in refs 1 to 7, additional background of the data is given in refs 8 to 10. In this presentation, rather then review the recent test data as has been customary in previous years, we want to emphasize the need for a more general data classification methodology. Several potential classification schemes are proposed and their use is illustrated by examples chosen from the recently generated UMCP and MIST data base.

## DATA BASE OVERVIEW

Presently the experimental data obtained in the IST programs is classified almost exclusively on the basis of nomenclature which was used to identify a given test or test series. These test designations are chosen by the various experimental groups to meet their internal identification needs. While they are useful to experimenters, they do not lend themselves to generalization. Classification solely on the basis of test designation incorporates identification difficulties on two levels:

1. In order to locate data having specific characteristics, first an overview of the test program and a thorough familiarity with the conditions for all the tests is required.
2. The data for a given test encompasses a wide range of operational states. It is thus in fact a small 'data base' in its own right.

These circumstances make the use of the data difficult even for persons having a familiarity with the test programs. The difficulty can be illustrated by noting the that the final reports summarizing the MIST data comprise 10 volumes (11,12,13,14) and the STR (Standard Data Reports) of the UMCP tests exceed 50 positions. The situation is alleviated somewhat by summary reports and by grouping of the tests according to some unifying characteristics (e.g. the 'Mapping', 'Boundary' or 'Nominal' test series for MIST experiments, the ITL, BSM or MSI series for UMCP). Nevertheless, the fact remains that the use of the IST data base requires an extensive investment of time and effort. In order to locate data of a certain type, the investigator must gain an overview of the characteristics of the test programs, the initial and boundary conditions that the experimental groups employed and only then can he proceed to the question whether the data will be suitable for his specific needs. Under such conditions it is almost certain that this accumulated information will be utilized only by the groups which have an intimate acquaintance with the details of its measurement.

## CLASSIFICATION METHODS

Several general classification schemes which have a potential for serving as a framework for data identification are considered. Illustrative examples are drawn primarily from the recent UMCP test program results. The examples are compared with test results from the MIST program in order to illustrate their facility independent generality.

The outlined classification methods are redundant, that is, the same test data could be classified according to several categories. This seems to be not just a shortcoming of this initial classification attempt, but reflects the complex nature of the data itself. It is probable that to enhance data accessibility not one but several classification schemes will be required. This would allow the grouping of data according to categories which address specific end use needs, for example such as code verification, accident mitigation or operator training.

1. Flow mode (phenomenological) classification.

A potentially fruitful method of data classification has been presented in several UMCP studies (3,7). Analysis of a range of SB-LOCA tests performed at UMCP led to the recognition that the transient can be separated into several sequential stages based on the prevailing dominant phenomena. Comparison of the data with MIST (13), SRI (15) and OTIS-GERDA (23) data showed that the analogous behavior has been observed also in these facilities. The flow mode classification method would thus be based on first identifying dominant phenomena and subsequently outlining the range of operational variables under which they occur. Tests (or rather data segments from various tests) would then be classified according to these defined phenomenological categories.

This approach is illustrated by Fig. 1 which shows the characteristics of the main flow modes in the UMCP facility. The early test series at the UMCP facility used boundary conditions which tend to emphasi the distinctive character of these modes, as a result right from the beginning analytical and experimental attention was directed towards analysis of individual operational states rather then complete transients. However, except for the increased emphasis towards this aspect of the test data, this approach is not new. It is rather the natural outcome of an attempt to understand an inherently complex series of phenomena and is to some degree practiced by all groups that deal with integral system data. For example, Fig 2 shows the pressure trace form an OTIS nominal test(23). The flow states of the system in this example are indicated are in a less formalized manner, but the general approach is similar.

Cautionary note is advisable before proceeding to specific illustrative examples. A multiloop integral facility is an inherently complex system and not all of its operational states can be identified by a single dominant phenomenon. Some states can, an example is single phase natural circulation, however dynamic flow states (cyclical or oscillatory) which encompass an entire sequence of phenomena also occur. To reflect this circumstance, the terminology of 'flow mode' introduced in ref(7) is employed.

The test series which is used for illustration (the BCM series) employed a constant power, a constant level in the secondary and no HPI. The only boundary condition driving the transient was a leak in the bottom of the B2 cold leg. These tests served to define the dominant flow modes that occur while the inventory is depleted from liquid solid to a level where the energy is transported by vapor in the BCM (Boiler Condenser Mode).

It was found that as inventory depletion progresses several flow modes which differ in ETC (Energy Transport Capacity) and dynamic characteristics occur. Fig. 3 presents the time history of total pressure for a fairly typical inventory loss transient for which the liquid level in the secondary is maintained at 50%. Transitions between the flow modes are indicated by the letters A,B,C. These transitions will be employed as reference points for comparing MIST and UMCP transients. They are in sequence:

A. Termination of the depressurization stage and initiation of 2-phase operation.

B. Initiation of a complex flow mode which includes a repetitive sequence of phenomena including the condensation of vapor in the upper downcomer-cold leg region. This mode has been given the name of IRM (Interruption Resumption Mode) and is analyzed in more detail in references 3,6 and 7.

C. Establishment of BCM (Boiler Condenser) and rapid depressurization because of the excellent ETC for this flow mode.

The flow modes and transition states listed above are observed in many of the SB-LOCA transients performed at the UMCP facility. During most of the MIST tests these system characteristics are obscured by the impact of time dependent power changes, time varying HPSI flows, changes in secondary liquid levels and so on. However, as shown by test data for which outside influences are reduced, fundamentally similar flow modes can be recognized. This is illustrated by the two pressure traces of two MIST tests shown in Fig. 4. The relative magnitude of the time dependent pressure variation is different the nature of some flow modes (e.g. the IRM flow mode) is altered, however, the main characteristics of the response observed during the UMCP tests can be readily recognized. This similarity leads to the proposition that a classification according to dominant phenomena (or flow modes) would be useful.

A phenomenological classification presupposes that the dominant phenomena have been identified and are understood. This is not always simple since as noted some operational modes have a dynamic character. The IRM (Interruption-Resumption Mode) which has been studied extensively by the UMCP analysis group is an example of a dynamic cyclical mode and will be used for illustration. This flow mode occurs after 12-18% of the inventory has been lost (this depends on the level maintained on the secondary side of the steam generator), and can persist till inventory loss exceeds 30% to 35%. System energy transport (ETC) during this flow mode can be relatively large and is usually equivalent or even exceeds ETC during single phase natural circulation.

The IRM flow mode is characterized by large amplitude oscillations of liquid levels, flow rates and pressures. A dominating feature is the rapid, periodic condensation of large vapor volumes in the upper downcomer region and the cold legs(4). Before experimental results from the IST facility tests were available, it was assumed that flow interruption is produced by vapor liquid separation in the upper region of the hot legs(17,18). The test data showed that most of the time this is not the case and that the termination of two-phase flow into the steam generators can be initiated by a condensation event in the cold leg-upper downcomer region. This condensation lowers local pressure and literally 'pulls' fluid both from the hot legs and the primary side of the steam generators. Such a flow termination is not dependent upon the physical conditions in the hot legs, therefore, after the available vapor volume is condensed, vapor generation in the core region refills the dome and two-phase flow over the hot leg candy canes is readily reestablished. The next termination cycle begins when a new 'condensation pull' event is initiated.

The initiation phase of this flow mode is schematically illustrated in Fig 5. The figure presents sequential time frames which illustrate the development of a vapor dome in the upper vessel region as the inventory is initially depleted. After the vapor level reaches the RVVV's (frame 2), it expands into the upper downcomer region and the cold legs. Initially the vapor is separated from the colder water coming from the steam generators by a layer of hot core water. The first condensation event therefore takes a relatively longer time to develop. After it has occurred (frame 4), liquid is drawn from the hot legs and the steam generators thus terminating hot leg two phase flow (frame 5). For the subsequent cyclical events the saturated layer of liquid is diminished and the condensations occur at a higher frequency. Fig. 6 presents selected measured data documenting the cyclical nature of the flow mode. Note that each cycle can be divided into two dynamically different phases: a relatively slow phase during which the pressure gradually increases and a pulse like, condensation collapse phase. For the UMCP facility the duration of the entire cycle approaches ~2 min.

Cyclical phenomena having a similar general character have been observed also in the SRI(15,24) and MIST(13) facilities. An example from the MIST mapping test series is presented in Fig 7. The two phases, a slowly developing one and a pulse like phase caused by the initiation of volume condensation phenomena can readily be recognized.

The presented examples illustrate that the flow mode (phenomenological) classification approach incorporates some difficulties. One is the directly illustrated circumstance that the flow modes can be quite complex and that the two-phase flow states can incorporate a stochastic component. This means that the transition between flow modes is not clear cut. An even more serious problem which has not been

confronted in the examples is that large multiloop integral systems operating at natural circulation conditions can have relatively long time constants (on the order of tens of seconds to several minutes). This makes the separation of flow modes in terms of operational conditions more difficult. It implies that a given flow mode depends not just on the complement of operational conditions (e.g. primary system inventory, power, pressure etc.) that exist at a given time but is influenced also by the sequence of events.

2. System-boundary condition response classification.

A potential universal classification method can be based on the widely used control theory practice of separating the 'inherent system' response from the response produced by 'imposed boundary conditions'. The advantage of such a method is its generality. Theoretically everything that happens to a system can be separated into an 'inherent system response' which is determined by the system itself and the initial conditions and the effect of boundary conditions. In practice for a complex 'system' like a multi-loop thermal-hydraulic facility complications do arise and such a separation requires a careful definition of terminology.

For the IST experiments 'boundary conditions' are taken to encompass all the operating condition changes that are imposed on the system once a test is initiated. This includes the energy sinks or sources which are altered during a test, for example HPI and break flow, changing power and secondary liquid levels and so on. By extension the 'inherent system' response is then the flow state that exists without such perturbing influences. In its ideal form this would be a steady-state flow mode (for example, natural circulation with steady state single phase or two-phase flow), while in actuality this includes flow modes which are inherently dynamic like the IRM mode illustrated in Figs 5 to 7. If the concepts of 'inherent' and 'boundary conditions' are not interpreted in a too formalistic manner, a distinction between the two categories can usually be recognized. An example of the impact of imposed boundary conditions during the MIST tests is illustrated by Fig. 8. The figure shows the variation of pressure vs primary system inventory for a so called 'mapping' test (the trace in the upper part of the figure) and three separate 'nominal' tests. Initially the system is full and pressure is ~2000 psi, thus to trace a time trajectory start at the right of the figure and follow the curve toward decreasing inventories.

The 'mapping' test protocol included a constant power and no HPI addition. The impact of boundary conditions on the trajectory of the transient is thus reduced and the developed trace approached an 'inherent' system response. On the other hand, the nominal tests incorporated the full complement of boundary conditions employed to simulate a 'plant typical' SB-LOCA trajectory. This includes the gradual reduction of power, changes in secondary liquid level and variable HPI flow. As the figure shows these boundary conditions dampen some of the flow modes apparent in the inherent trace and completely suppress others.

A potential advantage of this classification mode is that the inherent and boundary condition responses should be additive to some extent. That is, once the 'inherent' behavior is established, the impact of energy 'source' or 'sink' type boundary conditions can,to a certain degree, be inferred. For boundary conditions which impose a linear perturbation a quantitative superposition of 'inherent' and 'boundary' effects should be possible. However, the effect of most actual boundary conditions (e.g. HPI flow or PORV operation) is likely to be nonlinear. For those cases the achievement of a quantitative superposition is unlikely, but it should be possible to predict qualitative effects. An illustration of boundary conditions which have an almost linear to a clearly nonlinear effect is drawn from recent UMCP experiments and shown in Figs 9 to 11.

Fig 9 depicts a segment of the pressure trace after the IRM mode has terminated and before initiation of full fledged pool BCM. Auxiliary feed water is supplied by liquid level control thus it is intermittent in nature and the timing and location of delivery is dependent upon the level of secondary water in a given steam generator. On the other hand the effectiveness or 'impact' of this imposed boundary condition will be greatly dependent upon the liquid level that exists at the time of delivery on the primary side of the SG and the state of the balance of the loop. Such an impact can range from barely perceptible one, to a linear perturbation which disturbs the system but does not affect the trajectory in the transient in a general way and out

to a clearly nonlinear perturbation which pushes the transient along a different trajectory. A close to linear perturbation is illustrated in Fig. 10 which extends the time trace to include the transition to pool BCM (pool BCM has a high ETC and consequently produces a consistent pressure decrease). Fig. 11 depicts a clearly nonlinear impact of imposed boundary conditions. The phenomena which bring about these greatly different impacts of basically the same boundary condition have been analyzed in detail and will be reported in future studies.

3) Flow mode - transition state classification.

This classification scheme duplicates to some extent aspects of the two previous approaches, but has the advantage that it focuses on a feature which is of particular importance for code verification purposes. The state of the art system codes have reached a level of development at which their ability to reproduce most quasi-steady state flow modes is reasonably assured. The real challenge for the codes is now an adequate reproduction of the 'transitions' from one flow mode to another and the modeling of dynamic, that is oscillatory or cyclical, operation states.

The modeling of dynamic flow states by means of a finite difference systems code represents a formidable challenge. The code designer has to ensure that numerical stability is maintained and at the same time ascertain that oscillations which have a physical basis are not damped out. This challenge has been defined well in a survey paper by Ransom (25) where it is stated that:

"Development of a numerical rationale for maintaining numerical stability while retaining the ability to model physical instabilities has taxed the mental and computational abilities of man machine."

The finite difference systems codes presently are not able to simulate the onset of physical instabilities adequately, consequently data which can be used in the modeling and verification of the 'transition' states will have particular relevancy. This classification method therefore would focus on the identification and description of data segments which fulfill these requirements.

At this point a further note regarding dynamic operation states is in order. For normal operating conditions such operation modes are considered to be highly undesirable and design efforts are made to exclude them. As a consequence they are encountered relatively seldom and familiarity with them is limited. An integral system operating under conditions where a gradual loss of inventory occurs falls outside the normal design regime. As a result it should not be surprising that far from being seldom, dynamic operation modes now become practically the rule. A brief survey of available data shows that for such conditions the occurrence of dynamic operation states have been observed in all earlier test facilities including LOFT(26), Semiscale(27), ROSA(28) and others. They have also been observed for all of the UMCP, MIST and SRI tests, in fact, during most of the UMCP tests their duration usually represents the major time segment of the SB-LOCA transient. It can be concluded therefore that they are generic and for some transient types even dominant. Note that for accidental conditions dynamic operation modes are not necessarily detrimental. Under SB-LOCA conditions the main goal is to ensure adequate core cooling and some of the dynamic flow states have ETC values which exceed those of steady state flow modes at an equivalent system inventory.

Examples of dynamic and transition states have already been shown in the previous figures. A few additional examples are chosen to illustrate the wide variety of dynamic flow modes that can be present. Fig. 12 taken from the UMCP ITL test series shows sequential temperatures in a cold leg for the entire duration of an SB-LOCA transient. The figure illustrates well the initiation of a dynamic flow state from a basically quiescent, quasi-steady state flow mode, its persistence and the eventual transition to a flow mode for which the cold leg flow rate is significantly damped. The measured temperature swings are caused by alternate flow of cooler water from the S.G. or hotter water from the pressure vessel.

Fig 13 illustrates the changes that can be produced in the characteristic of dynamic flow modes by altering the flow geometry. Both of the depicted tests have equivalent system inventory, power, secondary coolant liquid level and other operational parameters. The only change is the closure of the vent valves for the RVVV test. As shown, this alteration of the flow geometry changes the prelevant flow mode from one

having a cyclical character where the cycles repeat roughly at 2 minute intervals, to an oscillatory flow state having a frequency of ~20 sec.

Finally Fig. 14 is taken from a MIST test and illustrates the development and termination of two well defined oscillatory modes characterized by completely different frequencies and amplitudes. In this case the sharp transition between the flow modes is caused by a drop in the pressure vessel liquid inventory from the vent valve to the hot leg entrance level. The oscillations are stabilized by the inertial resistance that exists in the cross over pipes which connect the pressure vessel with the downcomer region in the MIST facility.

The proceeding figures illustrate a generic characteristic of integral systems operating at two-phase flow conditions. The phenomenological details can vary, but for all integral facilities that have been operated, transitions between different flow modes, oscillations and/or cyclical behavior are observed. Such behavior must therefore be considered not as a perturbation of a quasi-steady operating state, but as an inherent characteristic of the system. This implies that system codes must either be able to simulate these flow modes directly or they should be able to evaluate a quantitatively acceptable time-averaged behavior. To achieve this a comprehensive data base covering the expected parameter range for SB-LOCA conditions must be made both available and accessible. The 'transition state' classification scheme would concentrate on documenting the experimental conditions for the flow modes during which flow state transitions become probable.

## SUMMARY

The past year has seen a further expansion of the experimental data base documenting the response of integral systems to a gradual loss of inventory (SB-LOCA). The data base is now sufficiently extensive that many if not most of the conditions that hypothetically can occur during an SB-LOCA transient have been simulated in facilities having a range of scaling relationships to the prototype. However, the increase in the scope and variety of this data has also increased the problem of data accessibility. To date no systematic classification scheme which would help to identify and locate experimental information within a specified parameter range has evolved. Experimental data continues to be classified according to individual tests and is identified by test nomenclature assigned to it by the various experimental groups. Such a system requires a large investment of time and effort in order to locate and extract specific information.

In this study three classification schemes having a broader generality are offered for further discussion. Their use is illustrated with examples drawn from recent UMCP facility measurements and from published MIST facility data. The evolution of a satisfactory, workable classification scheme is a sizable task and will require the ideas and efforts of the experimental groups which are generating the data and the analytical groups which are applying this information for code benchmarking and verification.

# Table I: Test Performances in 1987-88 at UMCP

| Test ID | Power (kw) | Sec. Level (% of full) | Break Size |
|---|---|---|---|
| STR/AFW1125 | 155 | 55 | 1/8 |
| STR/HPI1020 | 160 | 55 | 1/8 |
| STR/HPI1022 | 152 | 55 | 1/8 |
| STR/HPI1104 | 153.2 | 55 | 1/8 |
| STR/HPI1109 | 153 | 50 | 1/8 |
| STR/HPI1118 | 153 | 50 | 1/8 |
| STR/ITL0312 | 132 | 40 | 1/8 |
| STR/ITL0318 | 132 | 40 | 1/8 |
| STR/ITL0805 | 168 | 50 | 1/8 |
| STR/ITL0807 | 168 | 50 | 1/8 |
| STR/ITL1130 | 155 | 55 | 1/8 |
| STR/STP1111 | 141 | 55 | 1/8 |
| MIS092188 | 75 | 60 | 1/16 |
| MIS100588 | 75 | 60 | 1/16 |

| Test ID | Power (kw) | Sec Level (% of full) | Break Size |
|---|---|---|---|
| STR/BCM0715 | 141 | 50 | 1/8 |
| STR/BCM0731 | 142 | 50 | 1/8 |
| STR/BCM0915 | 141 | 75 | 1/8 |
| STR/BCM0917 | 141 | 50 | 1/8 |
| STR/BCM0922 | 142 | 55 | 1/16 |
| STR/BCM0924 | 141 | 55 | 1/16 |
| STR/BCM1006 | 141 | 50 | 1/8 |
| STR/BCM1008 | 142 | 75 | 1/8 |
| STR/BCM1013 | 141 | 50 | 1/8 |
| STR/BCM1015 | 143 | 75 | 1/8 |
| STR/BCM1219 | 140 | 75 | 1/8 |

AFW - Aux-Feed Water
BCM - Boiling Condensing Mode
ITL - Integral test
ITL - Integral Test
STP - Step-Wise Test
MIST - Counter-Part for MIST Test

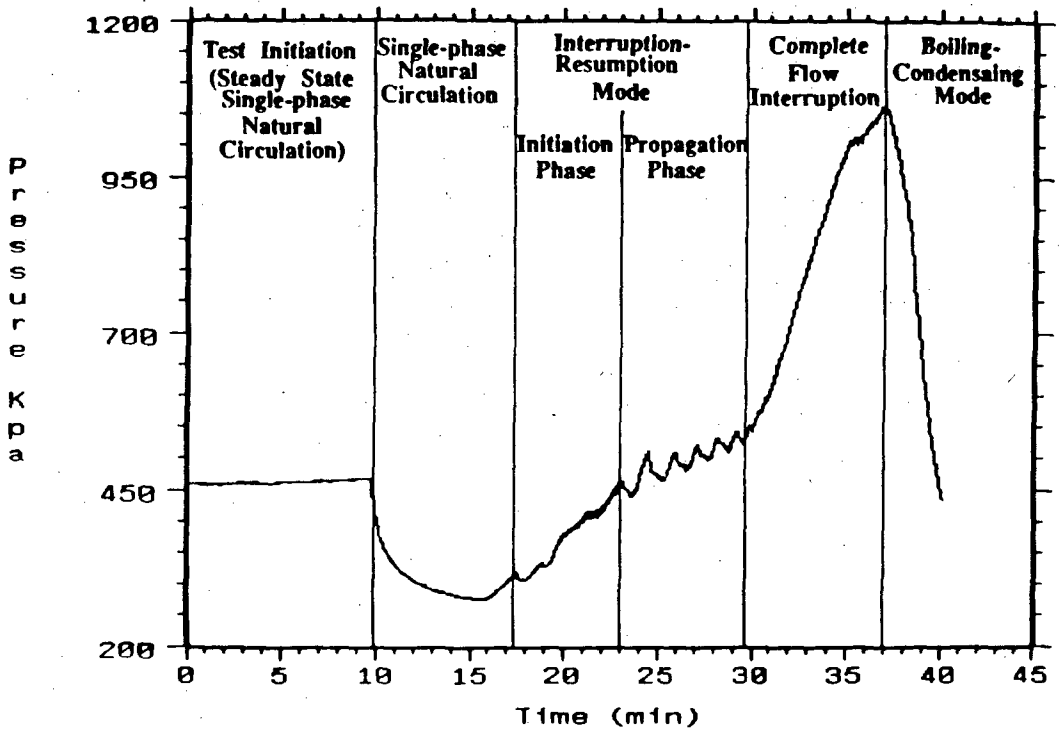


**Figure 1: Flow Modes During a Loss of Inventory Transient**

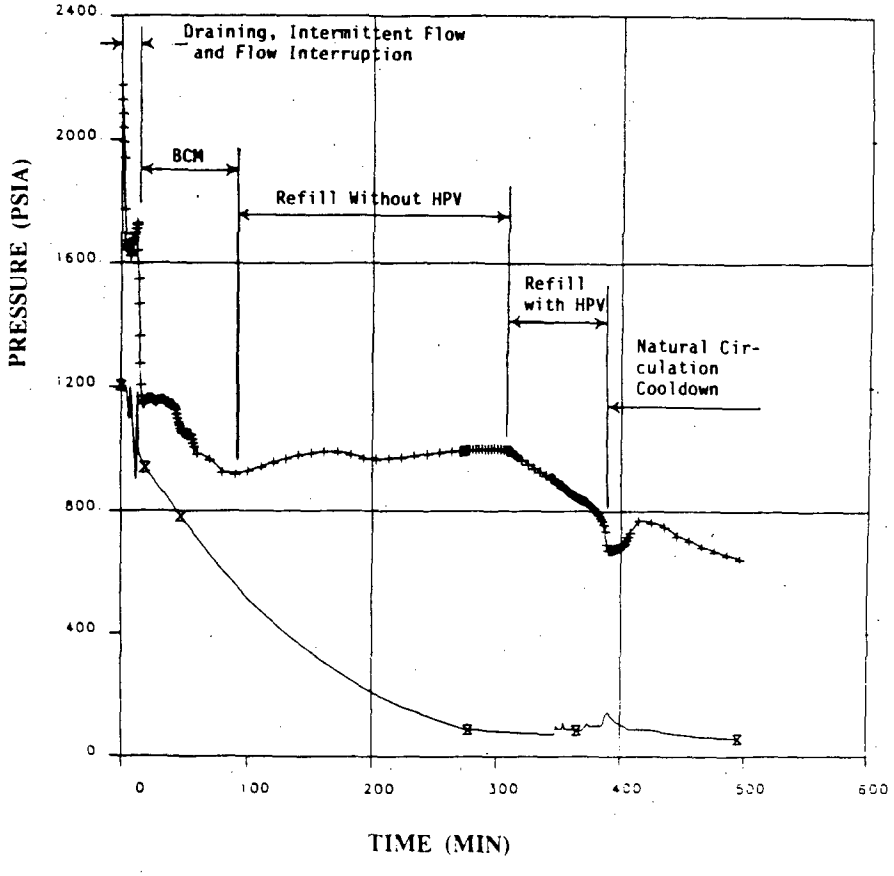


Figure 2: **Primary and Pressure for OTIS Test 220604**

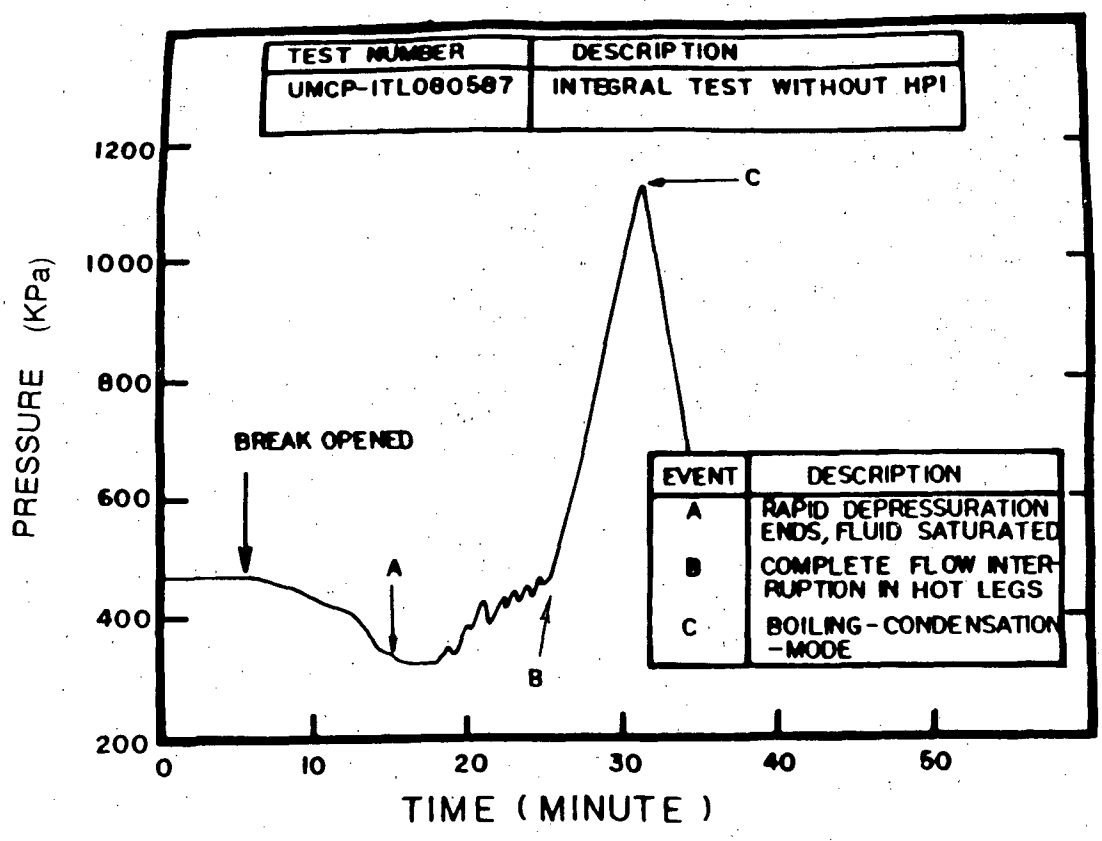


Figure 3: **The Vessel Pressure Versus Time for a UMCP SBLOCA Test Without High Pressure Injection**

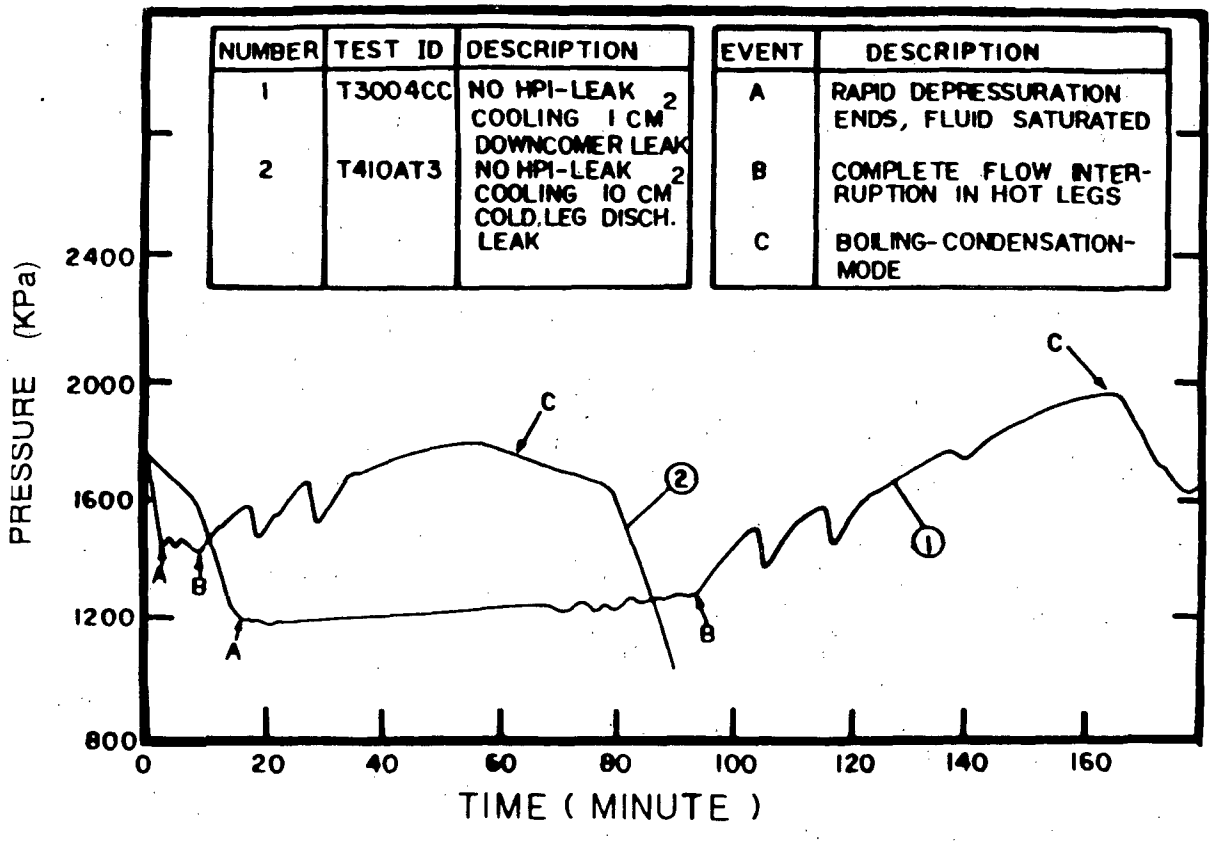


Figure 4: **The Vessel Pressure Versus Time for Two MIST SBLOCA Tests Without High Pressure Injection System (HPI)**

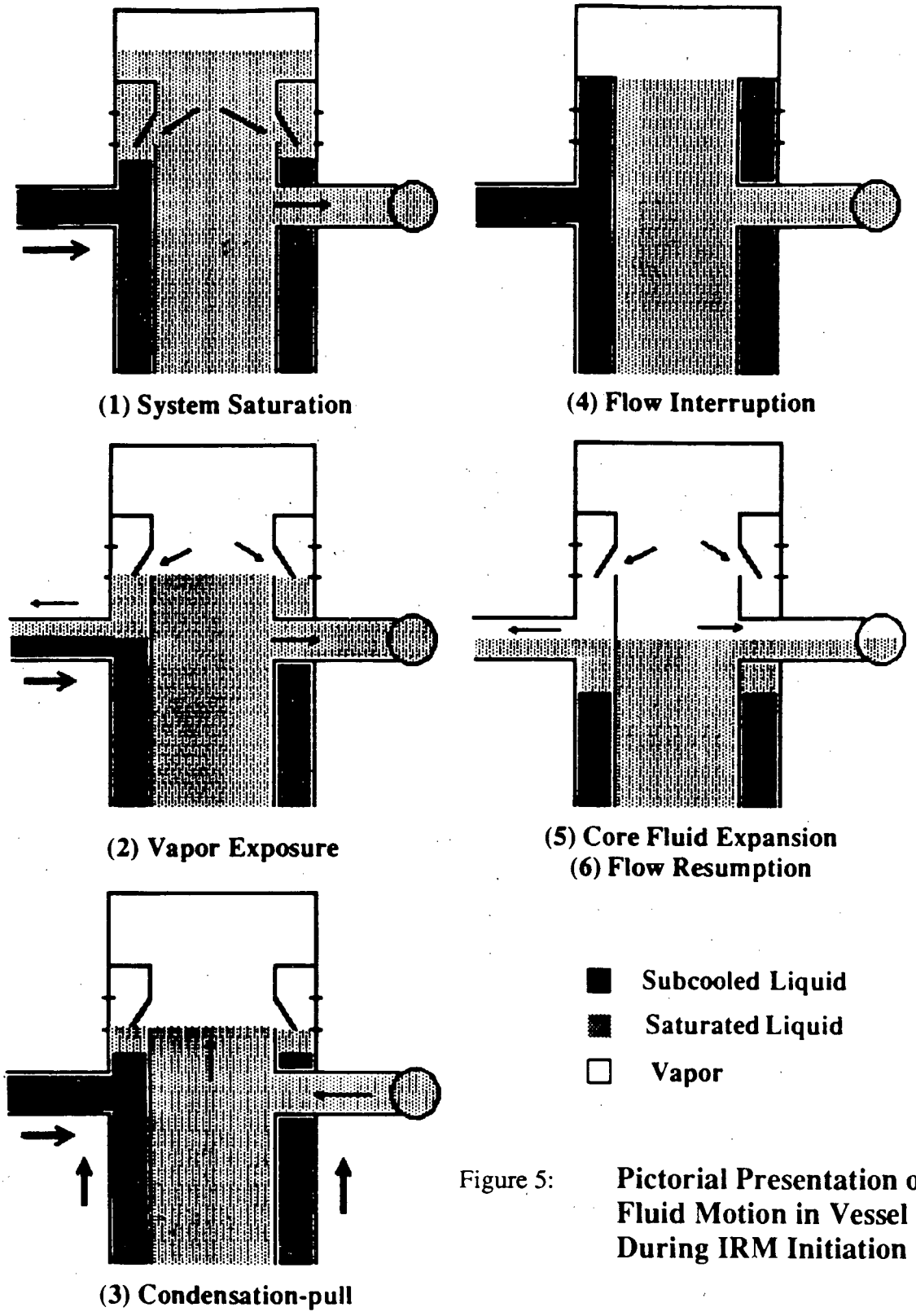


Figure 5: **Pictorial Presentation of Fluid Motion in Vessel Region During IRM Initiation Phase**

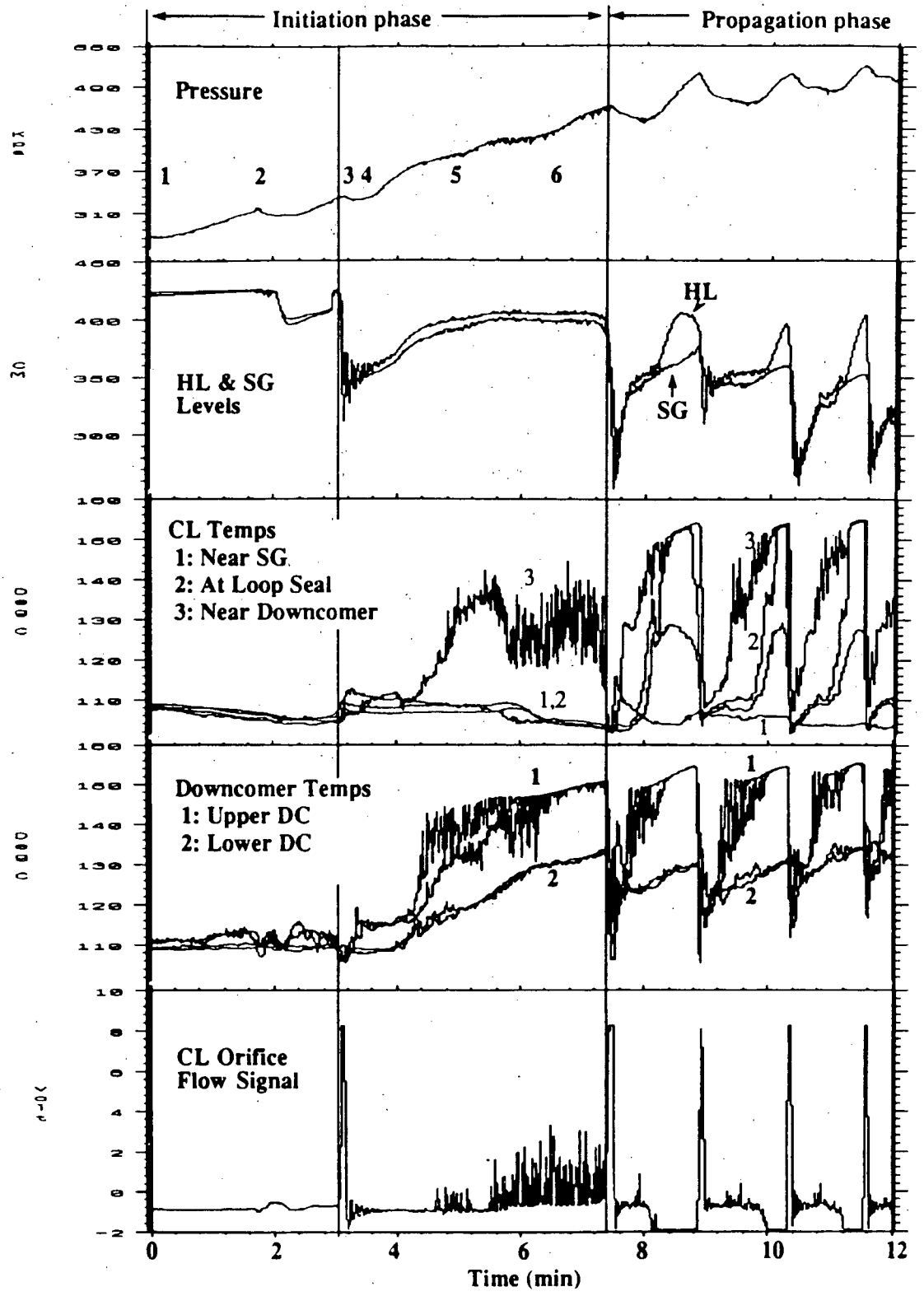


Figure 6: **Illustration of IRM Flow Mode (BCM0731 A Loop)**

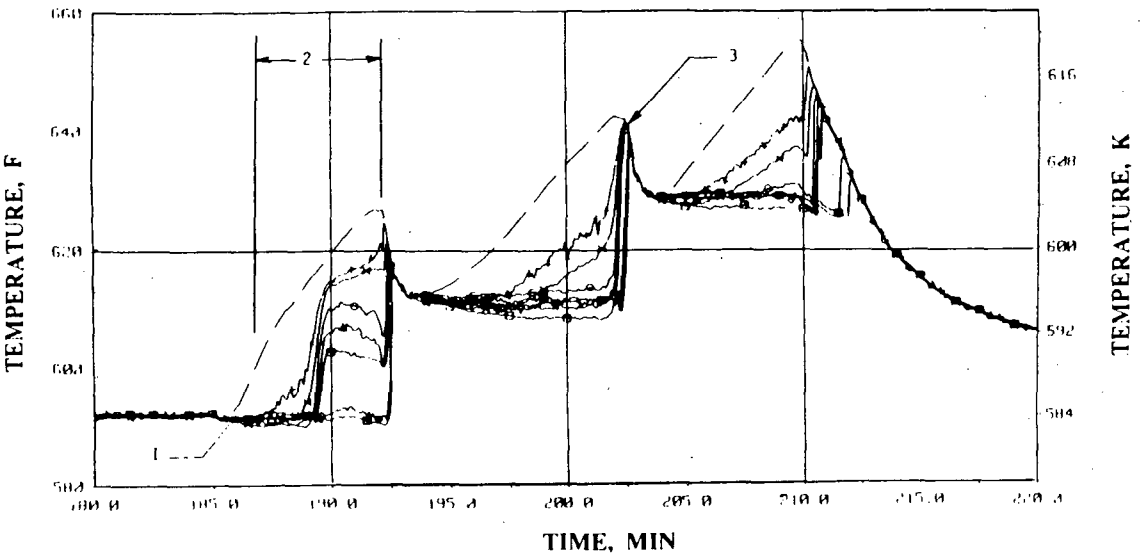


Figure 7: **Hot Leg A Lower-Elevation Riser Fluid Temperatures (HITCs)**

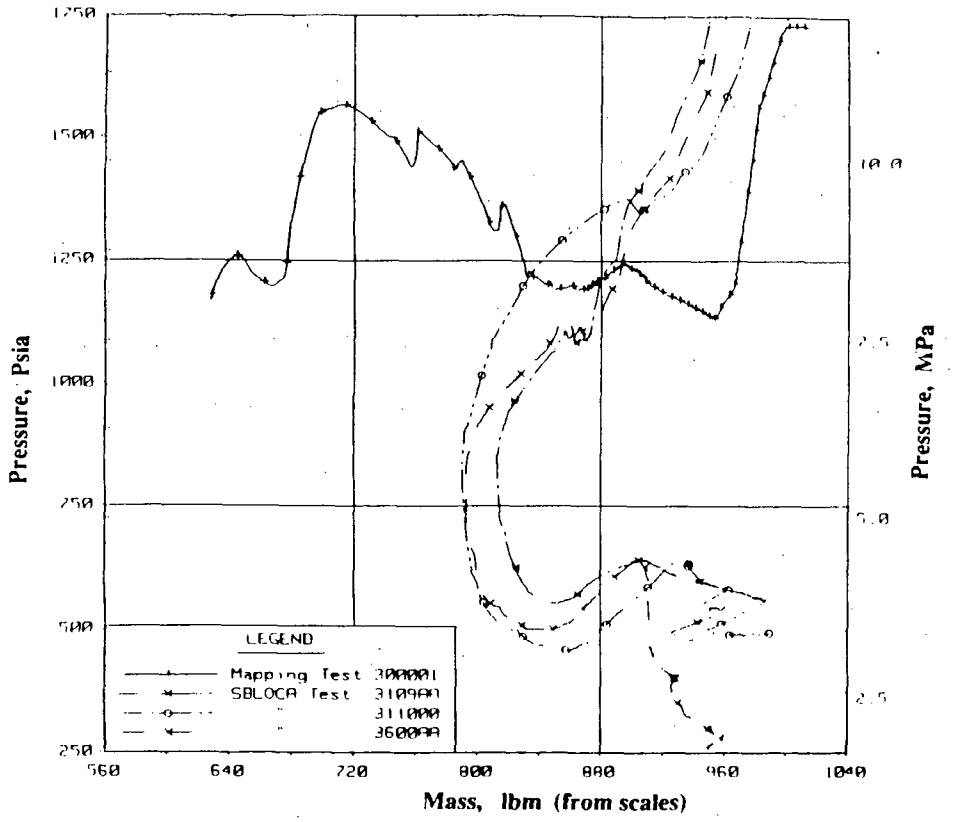


Figure 8: **Cold leg A1 Fluid Temperatures Test T3001B**

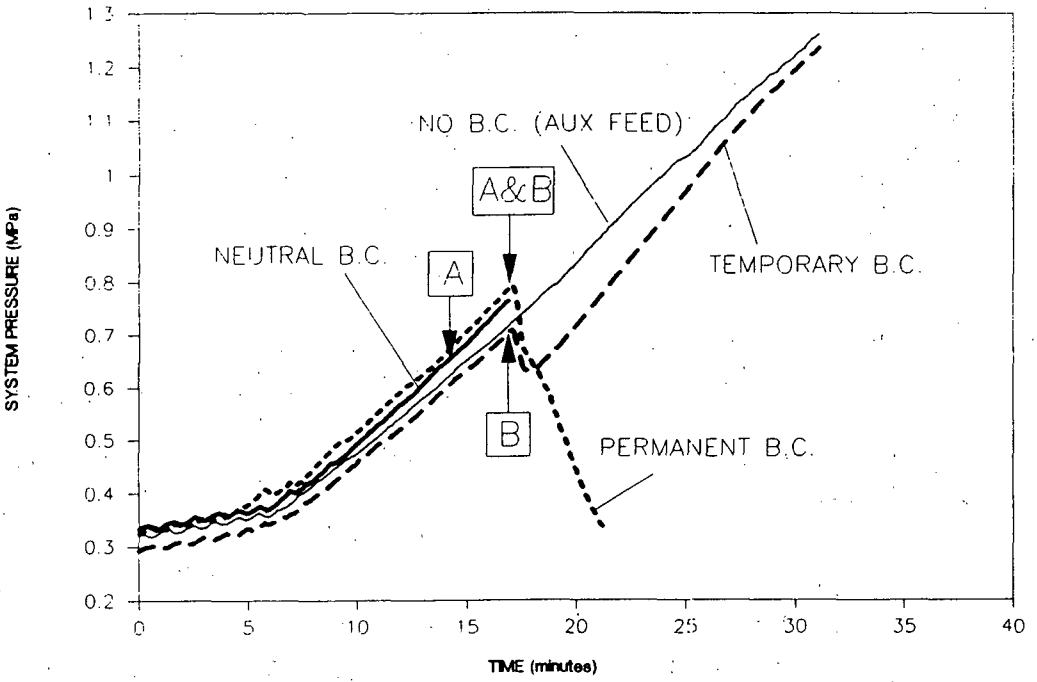


Figure 9: **Inherent and Boundary Condition Response**

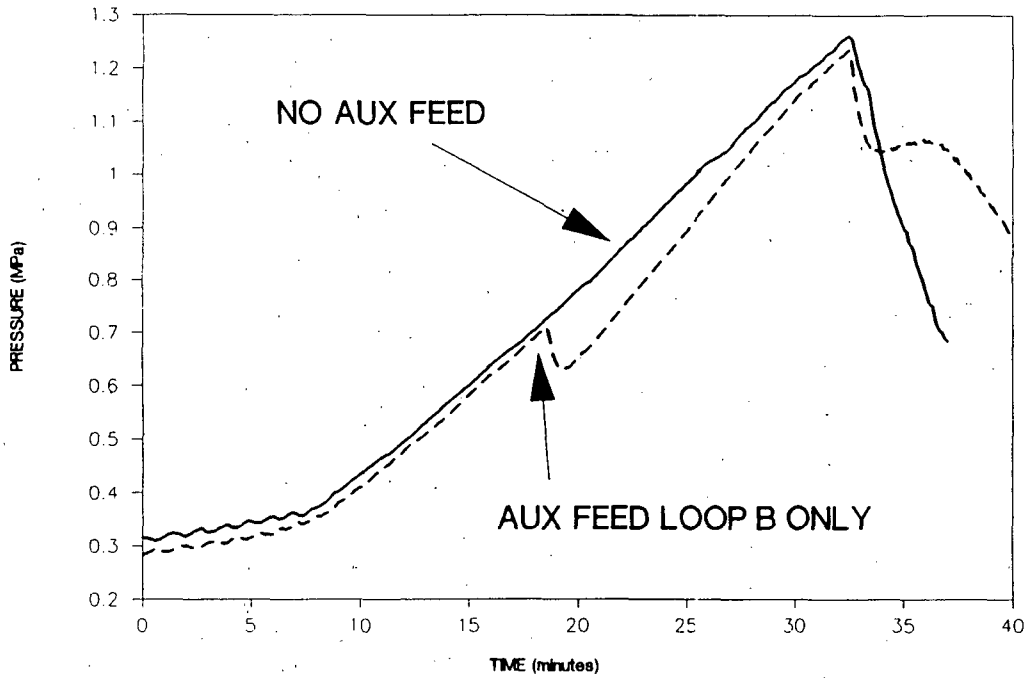


Figure 10: **Linear Boundary Condition Response**

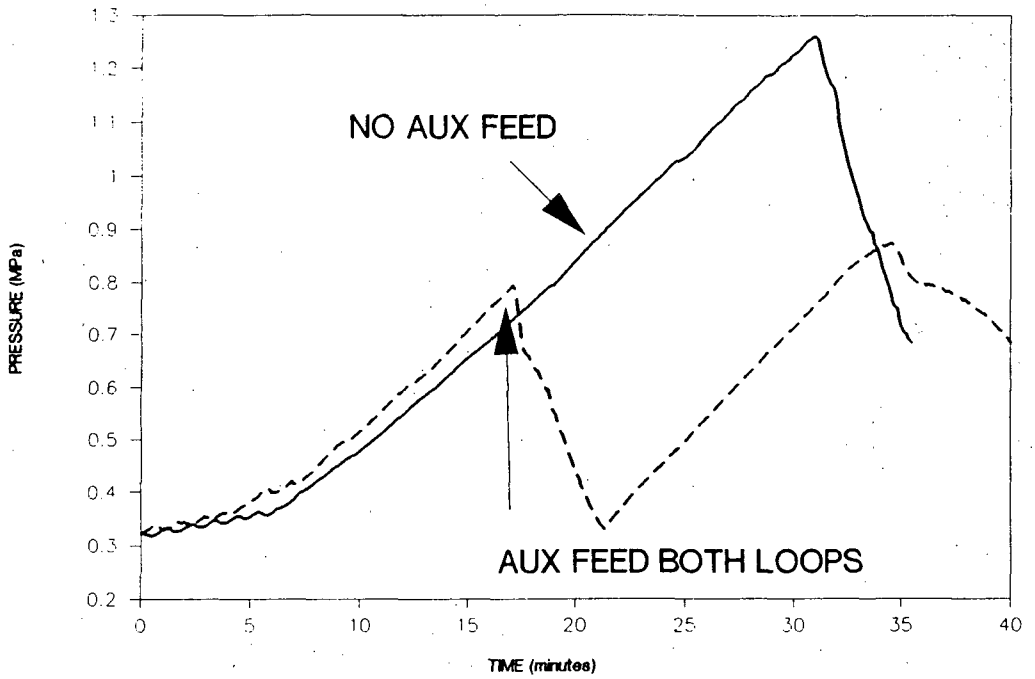


Figure 11: **Non-Linear Boundary Condition Response**

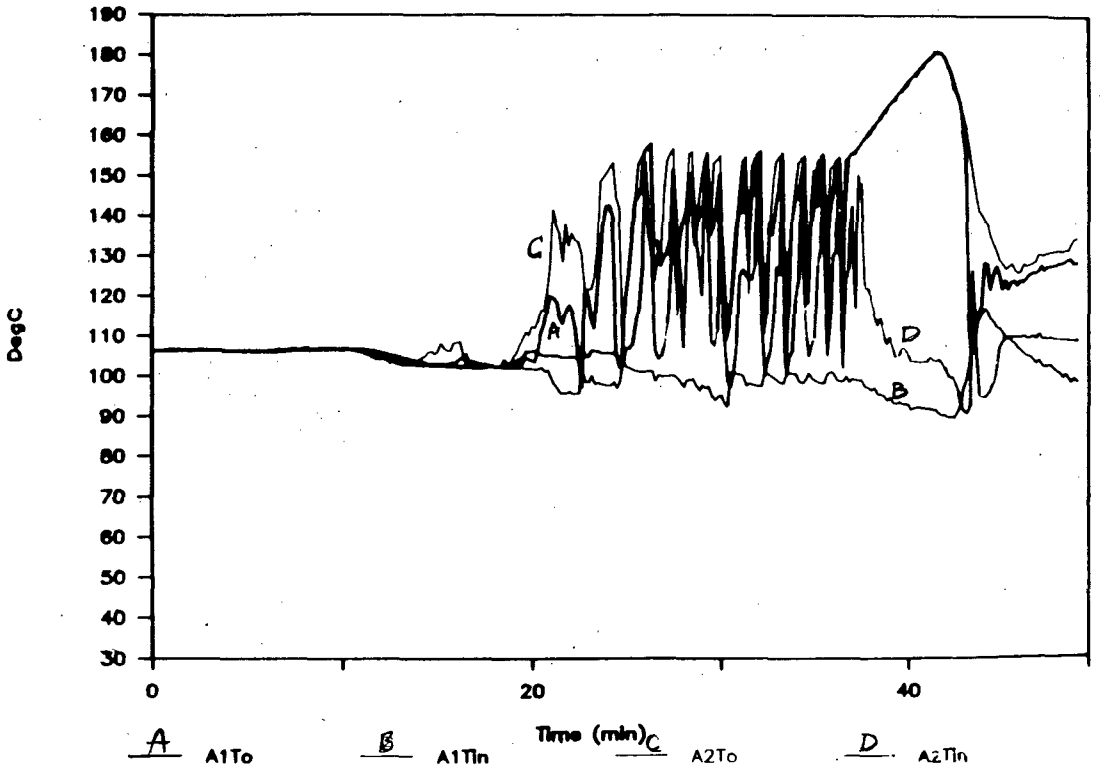


Figure 12: **Initiation and Termination of Flow Cycling Test BCM1218 Temperatures in Cold Leg A2**

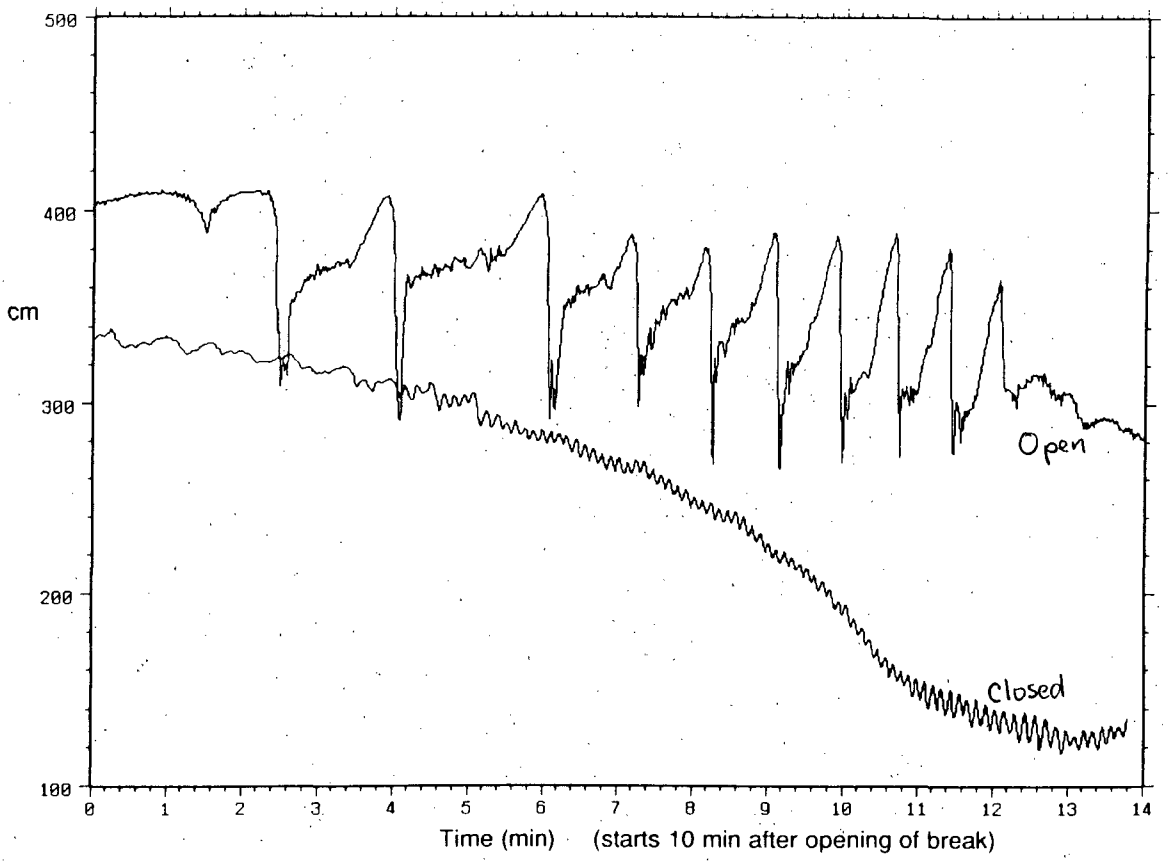


Figure 13: **Comparison of Loop A Hot Leg Levels for RVV Open and Closed Flow Geometry**

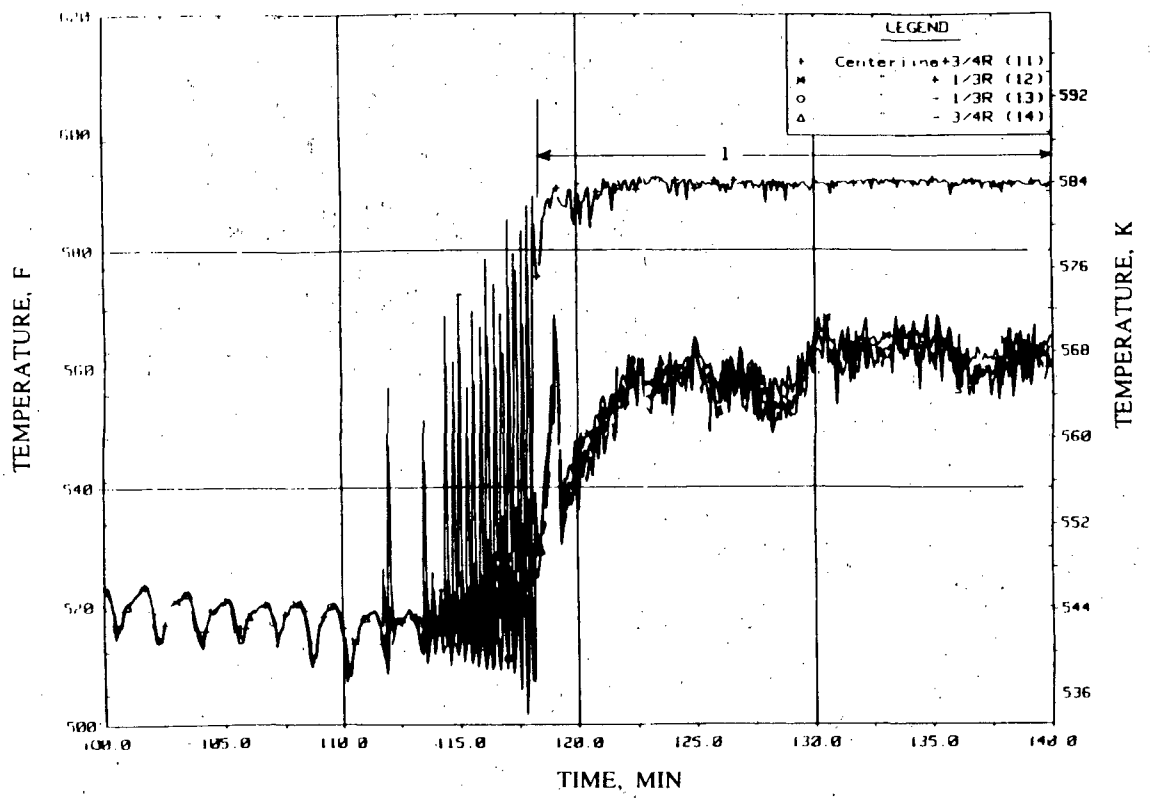


Figure 14: **Pressure vs. Primary System Inventory for SBLOCA Nominal**

*REFERENCES*


1. *Wang, Z. et.al, "Test Data Report, UMCP 2x4 Loop, The BCM Test Series (Boiling-Condensing Mode)," MDNE-88-L2, University of Maryland, College Park, Sept. 1988, NRC-NUREG report to be published.*

2. *Almenas, K. et.al, "Reproducibility in a Multi-Loop Thermal Hydraulic System," Nuclear Technology.,82, pp 341-354 (Sept. 1988)*

3. *Hsu, Y.Y., Z. Wang, C. Unal, M. diMarzo and K. Almenas, "Scaling for SB-LOCA Test Facilities," 3-d Int. Topical Meeting on Nuclear Power Plant Thermal Hydr. (Nov. 1988, Korea).*

4. *Wang, Z. et.al, "Impact of Rapid Condensation of Large Vapor Spaces on Natural Circulation in Integral Systems," Submitted to Nuclear Engr. and Design.*

5. *Wang, Z., Y.Y. Hsu, K. Almenas and M. diMarzo, "On the Applicabiliuty of Ishii's Similarity Parameters to Integral System Test Facilities," Submitted to Nuclear Engr. and Design.*

6. *Almenas, K., Y.Y. Hsu, "UMCP Observations on the Atypicality Issues," Pres. to ACRS Thermal-Hydraulic Subcommittee 7/21/'88.*

7. *diMarzo, M, K. Almenas, Y.Y. Hsu and Z. Wang, "The Phenomenology of a SB-LOCA in a Complex Thermal Hydraulic Loop," Nuclear Engineering and Design, in press.*

8. *Hsu, Y.Y., K. Almenas, M. diMarzo, C. Unal, Z.Y. Wang, "Observations of UMCP 2x4 Loop Test Result Simulating B&W Power Plant Behavior," Proc. of the 15-th Water Reactor Safety Info. Meeting, NUREG/CP-0091.*

9. *Hsu, Y.Y. et.al, "UMCp 2x4 Loop Test Results," Proc. of the 14-th WaterReactorSafety Info. Meeting, NUREG/CP-0081.*

10. *Hsu, Y.Y. et.al, "UMCP 2x4 B&W Simulation Loop Final Design Report," (Aug. 1984).*

11. *Gloudemans, J.R., "Mist Final Report Vol. 1 Summary," NRC- 04-83-168 (May, 1988).*

12. *Gloudemans, J.R., "Mist Final Report Vol. 9 Inter-Group Comparisons," NRC-04-83-168 (June, 1988).*

13. *Geissler, G.O. ed., "Group Report MIST Test Group 30 Mapping Tests," BAW-1950 (June 1987).*

14. *Geissler, G.O. et.al., "Group Report, Mist Test Group 30 Mapping Tests," Babcock and Wilcox Report, BAW-1950 (June, 1987).*

15. *Kiang, R.L. and P.R. Jeuck III, "Natural Circulation in a Scaled PWR Integral Test Facility," Proc. ASME Winter Annual Meeting, Boston, 1987.*

16. *Gloudemans, J.R., "Open Testing and Analysis Items," Pres. to PMG Meeting (January, 1988).*

17. *Larson, T.K., "Investigation of Integral Facility Scaling and Data Relation Methods," NUREG/CR-4531 (Feb. 1987).*

18. *Hashemi, A., A. Munis and J. Goodman, "TYYwo-Phase Regimes and Carry-over in a Large-Diameter Model of a PWR Hot Leg," EPRI NP-4530 (April, 1986).*

19. *Gloudemans, J.R., "Mist Phase 3 Versus the TAG Issues,"Presentation to the ACRS Subcommittee on Thermal-Hydraulics, July 21, 1988.*

20. *Wheatley, P.D. et.al., "Evaluation of Operational Safety at B&W Plants Vol. 2 Thermal-Hydraulic Results," NUREG/CR-4966 (Nov. 1987).*

21. *"Guidelines and Procedures for the International Code Assessment and Applications Program," NUREG-1271 (April, 1987).*

22. *Tasaka, K., Y. Kukita, H. Kunamaru, T. Yonomoto, M. Suzuki and Y. Koizumi, "The Results of 0.5% PWR SB-LOCA Tests in Rosa-IV STF Break Parameter Test Series," Proc. of the 15-th Water Reactor Safety Info. Meeting, NUREG/CP-0091.*

23. *Gloudemans J.R. et al "Once-Through Integral System()TIS): Final Report" NUREG/CR-4567 (Sept. 1986)*

24. *Sursock J. "SRI-2 Integral Test Project" ACRS prsentation (June 16, 1988) Washington D.C.*

25. *Ransom, V. H. and W. L. Weaver "Selective Review of LWR Thermal-Hydraulic Simulation Methods Used in the USA" Int. Top. Meeting on Advances in Reactor Physics (April 1987) Paris*

26. *Nalezny T. K. "Summary of NRC LOFT Program Experiments" NUREG/CR-3214 (July 1981)*

27. *Loomis G. G. and J. E. Streit "Results of Semiscale Mod-2C Small-Break LOCA Experiments S-LH-1 and S-LH-2" NUREG/CR-24438 (Nov. 1985)*

28. *Tasaka K., Y. Kukita and Y. Koizumi "The Results of 5% SB-LOCA Tests and Natural Circulation Tests at the ROSA-IV LSTF" 14-th Water Reactor Safety Info. Meeting, (Oct. 1986) NUREG/CP-0082*

# TRAC PF1/MOD1 CALCULATIONS AND DATA COMPARISONS FOR MIST FEED AND BLEED AND STEAM GENERATOR TUBE RUPTURE EXPERIMENTS*

by

D. A. Siebe, B. E. Boyack, and J. L. Steiner

Reactor Design and Analysis Group
Nuclear Technology and Engineering Division
Los Alamos National Laboratory
Los Alamos, New Mexico 87545

## ABSTRACT

Los Alamos National Laboratory is a participant in the Integral System Test (IST) program initiated in June 1983 for the purpose of providing integral system test data on specific issues/phenomena relevant to post-small-break loss-of-coolant accidents, loss of feedwater and other transients in Babcock & Wilcox (B&W) plant designs. The Multi-Loop Integral System Test (MIST) facility is the largest single component in the IST program. MIST is a 2 x 4 [two hot legs and steam generators (SGs), four cold legs and reactor coolant pumps] representation of lowered-loop reactor systems of the B&W design. It is a full-height, full-pressure facility with 1/817 power and volume scaling. Two other integral experimental facilities are included in the IST program: test loops at the University of Maryland, College Park, and at SRI International (SRI-2). The objective of the IST tests is to generate high-quality experimental data to be used for assessing thermal-hydraulic safety computer codes. Efforts are under way at Los Alamos to assess TRAC-PF1/MOD1 against data from each of the IST facilities.

Calculations and data comparisons for TRAC-PF1/MOD1 assessment are presented for two transients run in the MIST facility. These are MIST Test 330302, a feed and bleed test with delayed high-pressure injection; and Test 3404AA, an SG tube-rupture test with the affected SG isolated. Only MIST assessment results are presented in this paper.

The TRAC-PF1/MOD1 calculations completed to date for MIST tests are in reasonable agreement with the data from these tests. Reasonable agreement is defined as meaning that major trends are predicted correctly, although TRAC values are frequently outside the range of data uncertainty. We believe that correct conclusions will be reached if the code is used in similar applications despite minor code/model deficiencies.

* This work was funded by the US Nuclear Regulatory Commission (NRC), Office of Nuclear Regulatory Research, Division of Accident Evaluation.

## INTRODUCTION

Los Alamos National Laboratory has been involved with the Integral System Test program since 1984 and is currently performing code assessment of the Transient Reactor Analysis Code (TRAC) computer code against data from the Multi-Loop Integral System Test (MIST) facility. The MIST facility is a scale model of a Babcock & Wilcox (B&W) nuclear power plant. The facility is located in Alliance, Ohio, and is designed to experimentally investigate transients occurring after reactor trip and primary-pump coastdown. Data from the MIST facility are used to help resolve current plant licensing issues and also to assess and refine computer codes used to analyze plant thermal-hydraulic behavior.

A primary goal of our code assessment is to evaluate the adequacy of the correlations and models in TRAC. A related goal is to assist in developing an understanding of the phenomena occurring during the experiment. A secondary goal is to evaluate input modeling practices and develop user guidelines. In order to achieve these goals, it is necessary to understand the reasons for differences between test data and calculated values. These fall into three categories. First, a difference may exist because of an incomplete or inaccurate knowledge of the facility or its operation, including the instrumentation and the resulting data. Although this might seem to be a minor problem, it has not been for many facilities. Differences of this type may be difficult to isolate and can mask problems with the input model or the code. The documentation of the MIST facility, its operation, and data qualification are excellent, although there have been occasional problems as occur in any complex facility or test sequence. Second, the input model may be inadequate because of modeling compromises, noding, use of one-dimensional instead of three-dimensional models, etc. Third, inadequacies in the code closure models and correlations can cause differences. A major task of an analyst in code assessment calculations is to understand the differences between calculation and test within this framework, and in the case of code deficiencies, to identify the particular code model or correlation causing the difference.

Two assessment studies performed with TRAC-PF1/MOD1, version 14.3 (Ref. 1), are reported in this paper. Experimental data for MIST Tests 330302 (Refs. 2–3) and 3404AA (Refs. 4–5) are compared with code-calculated results. The complete TRAC posttest analysis of MIST Test 330302 is documented in Ref. 6.

Test 330302 was conducted to examine an extended period of pressure-operated relief-valve (PORV) actuation without makeup and with the steam generators (SGs) unavailable. In addition, high-pressure injection (HPI) was delayed to permit extensive voiding in the primary system to occur. It was anticipated that the HPI, when finally actuated, would perturb system conditions because of condensation and depressurization.

Test 3404AA was one of a series of Steam Generator Tube Rupture (SGTR) tests performed in the MIST facility. A double-ended rupture of 10 SG tubes in the top of the B-loop SG was simulated with the affected SG isolated when the primary pressure dropped to 6.55 MPa (950 psi).

## CODE DESCRIPTION

The calculations reported herein were performed with TRAC-PF1/MOD1, version 14.3, with a MIST-specific update. The TRAC-PF1/MOD1 code (Ref. 1) was developed at Los Alamos National Laboratory to provide best-estimate predictions of postulated accidents in light-water reactors. The code features a two-phase, two-fluid nonequilibrium hydrodynamics

model with a noncondensable gas field; flow-regime-dependent constitutive equation treatment; either one- or three-dimensional treatment of the reactor vessel; complete control-systems modeling capability; a turbine component model; and a generalized SG component model.

Code modifications were necessary for this application. We made changes in the TRAC-PF1/MOD1 code to improve the calculation of falling-film heat transfer on the secondary side of the SG tubes when the auxiliary feedwater (AFW) is active. The falling-film heat transfer from the AFW was calculated in the updated code version by redistributing the liquid in the single-channel secondary to the heat slabs connected to the three-tube primary channel. In addition to the liquid redistribution, a multiplier was applied to the Chen correlation heat-transfer coefficient for the wetted-channel heat slabs. These code changes resulted in a more accurate calculation of the heat-transfer distribution and the thermal-center elevation in the SGs. We note that the code update produced is specific to the MIST facility and not for general application.

## TRAC MODEL OF MIST FACILITY

The TRAC-PF1/MOD1 input model of the MIST facility is constructed entirely of one-dimensional components. The model consists of 77 components that have been subdivided into 276 fluid cells. Figure 1 is a MIST facility arrangement drawing. Figures 2 and 3 provide an overview of the TRAC MIST facility model. The model was initially based on preliminary information provided in the MIST Facility Specification (Ref. 7). It has progressed to its present form as available as-built facility information was received from B&W. The model is considered to be rather finely noded and has been shown to predict the dominant phenomena during MIST experiments.

## CALCULATION RESULTS

In this section we present and compare the TRAC-PF1/MOD1 calculated results with the measured and observed results for MIST Tests 330302 and 3404AA. We have attempted to develop an understanding of both the test and calculated results and will discuss these. The assessment descriptors appearing in Appendix A are used to characterize the degree of agreement between measured and calculated results.

### Test 330302 Transient Calculation.

The test was begun from steady-state conditions meeting prescribed tolerances. A steady-state calculation was run to 2000 s, corresponding to about five loop transits. At the end of the steady-state calculation, the primary- and secondary-system fluid conditions had stabilized within the uncertainties of the measured values.

Feed-and-bleed transient 330302 was initiated at time zero from the steady state by terminating all AFW to both SG secondaries. An overview of the resultant test and calculated transients is shown in Fig. 4.a–4.l. A summary of major events for Test 330302 is presented in Table I.

With the termination of AFW to the SG secondaries, the SG-secondary inventory began to boil off. However, this process removed only part of the core energy and the primary system began to heat up and pressurize as shown in Fig. 4.a. In the test the primary pressurized to the PORV set point of 16.20 MPa (2350 psia) at 942 s. The same primary-system pressurization

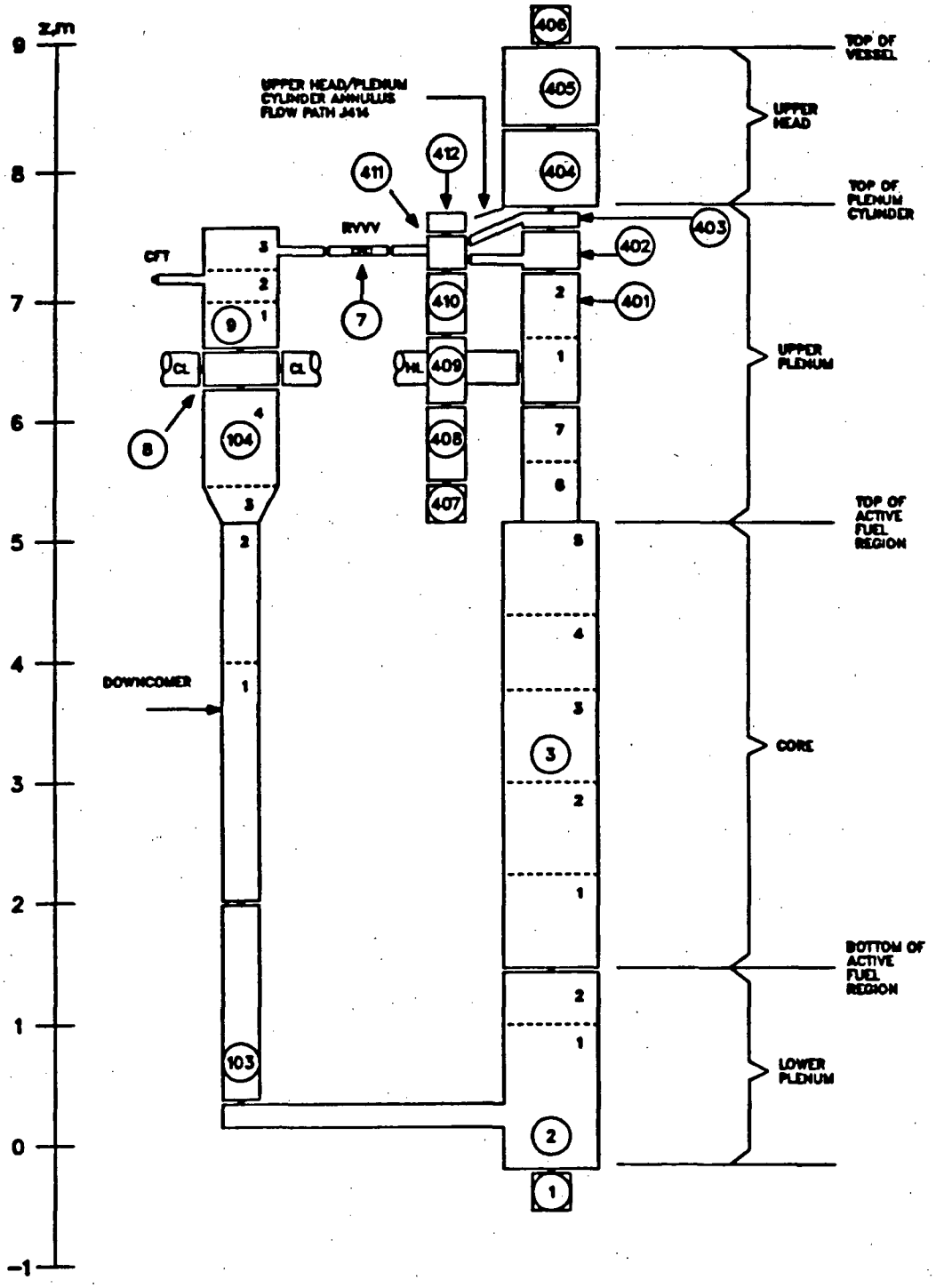


**Fig. 1.**
MIST facility isometric.

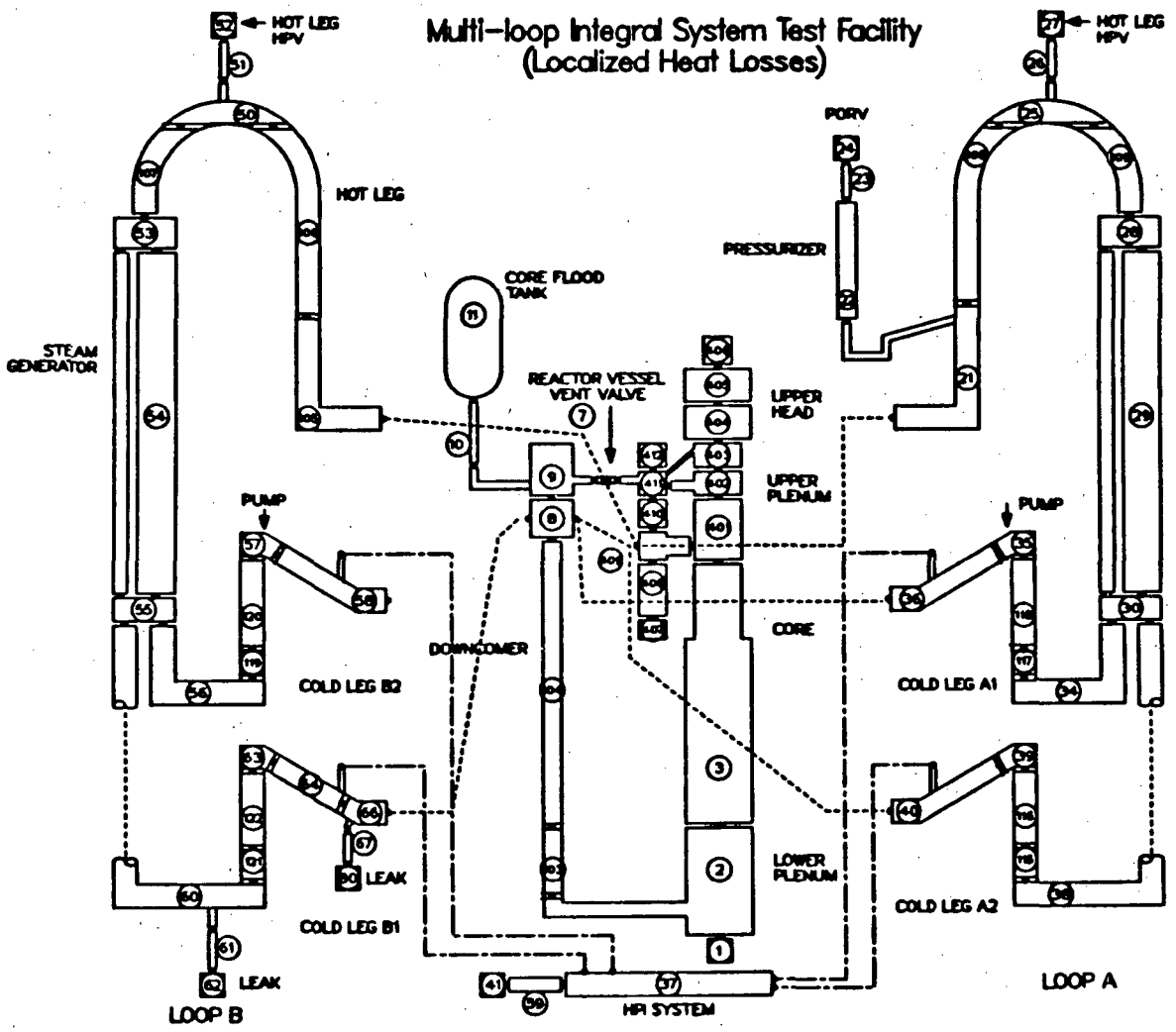


**Fig. 2.**
TRAC component noding schematic of MIST facility.

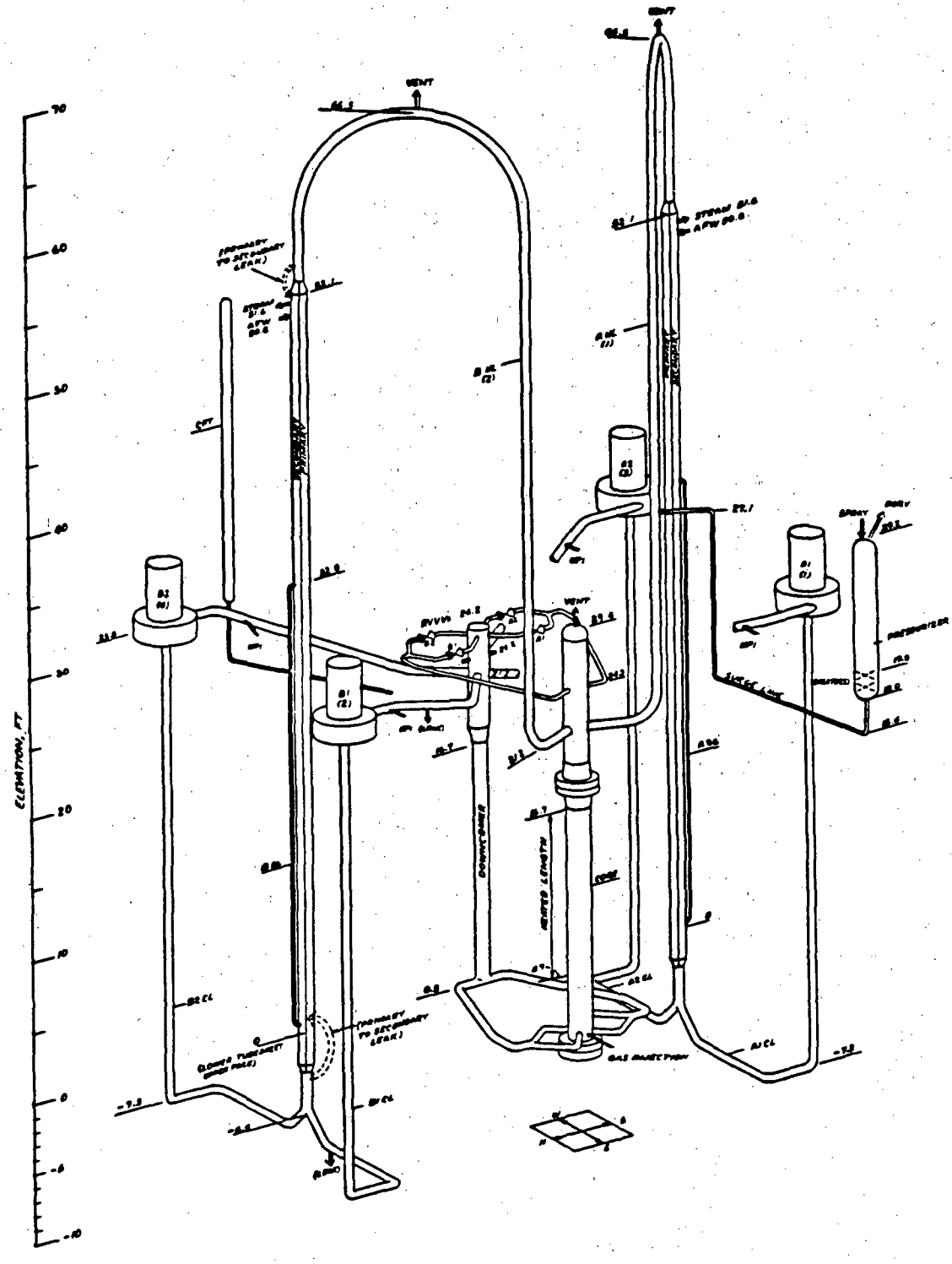


**Fig. 3.**
TRAC reactor-vessel noding schematic of MIST facility.

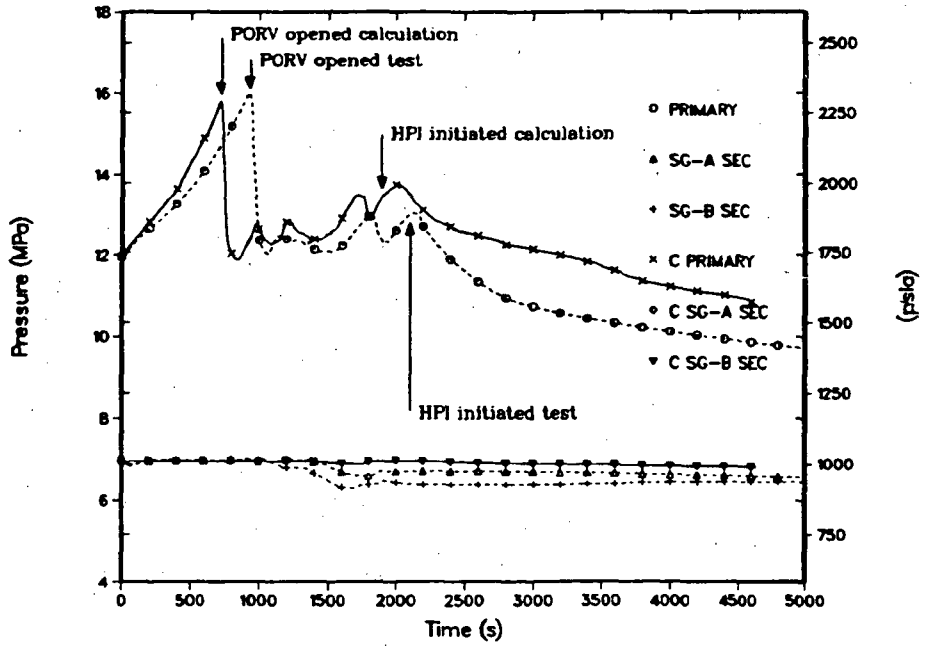


**Fig. 4.a.**

MIST Test 330302 primary and secondary pressure.

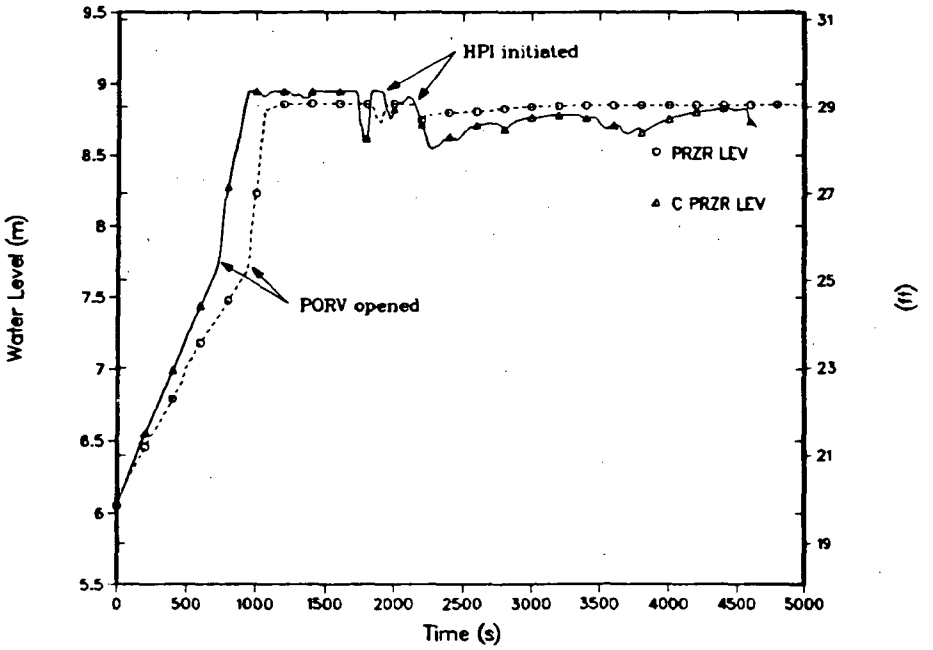


**Fig. 4.b.**

MIST Test 330302 pressurizer water level.

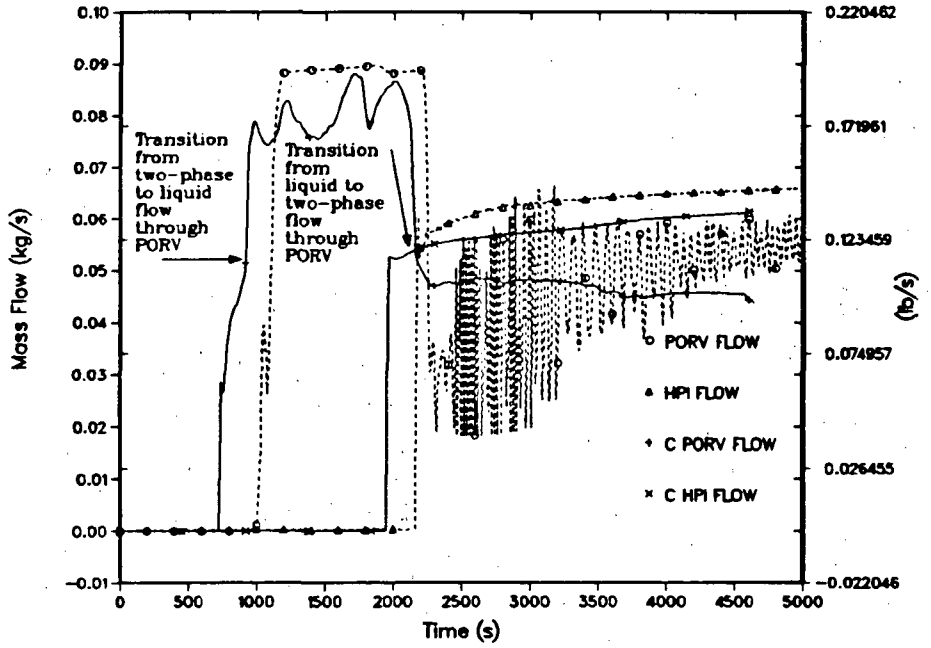


**Fig. 4.c.**

MIST Test 330302 PORV and HPI flows.

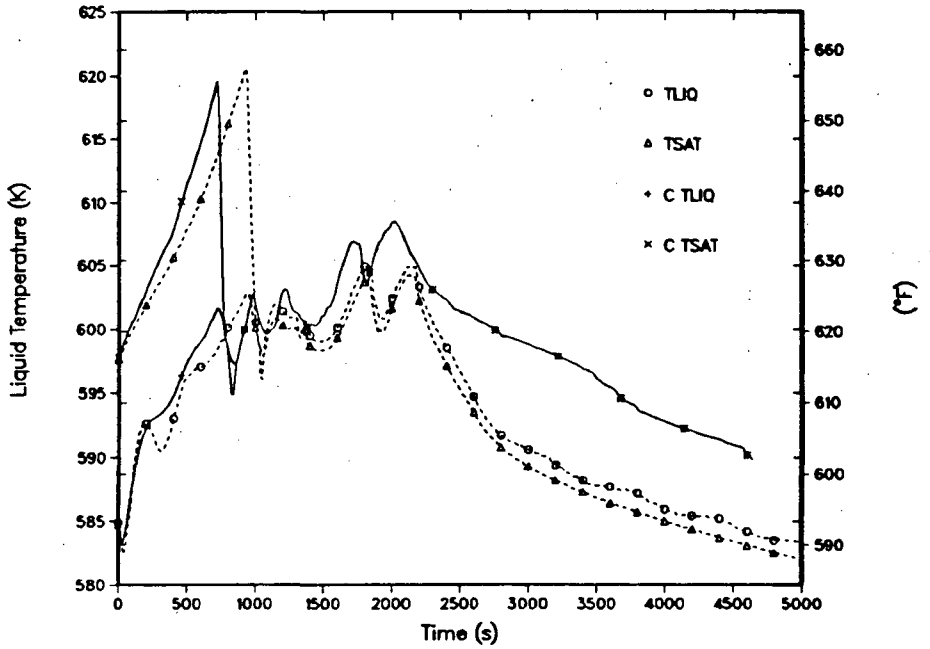


**Fig. 4.d.**

MIST Test 330302 core exit liquid temperature compared to saturation.

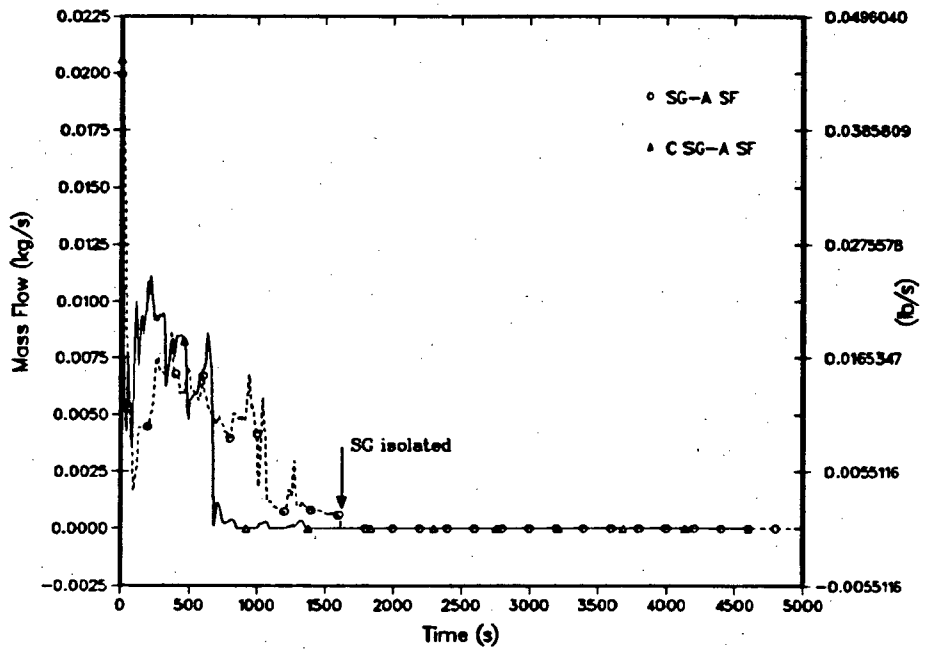


**Fig. 4.e.**
MIST Loop-A SG-secondary steam flow.

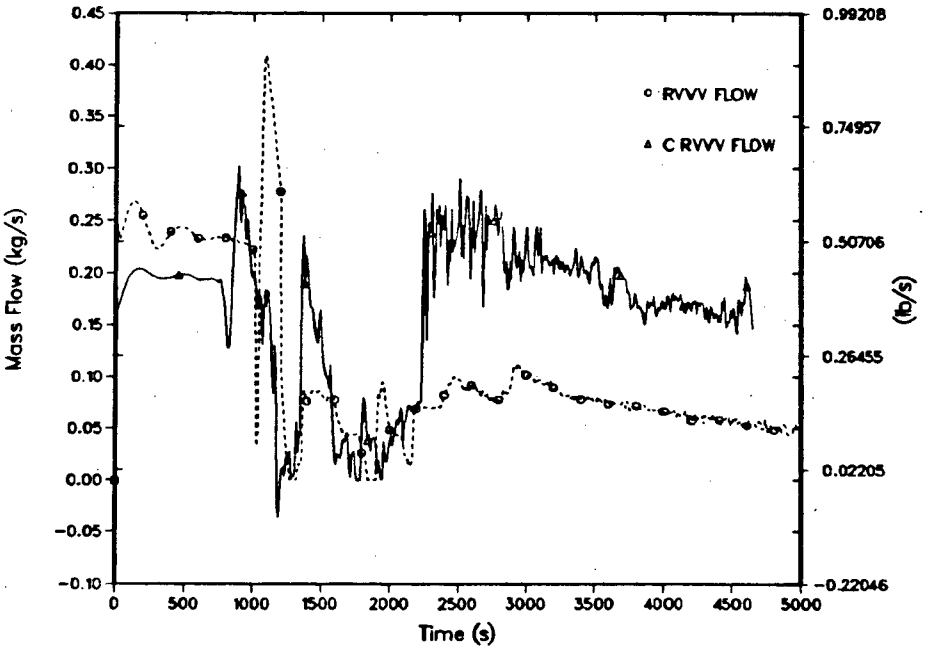


**Fig. 4.f.**
MIST Test 330302 reactor-vessel vent-valve flow (total of four valves).

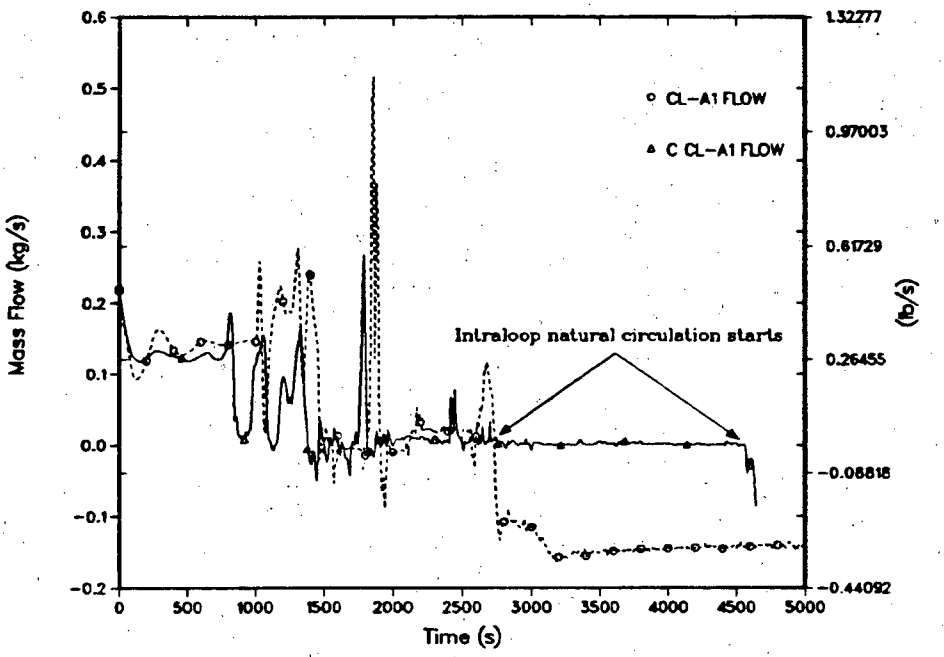


**Fig. 4.g.**

MIST Test 330302 Loop A1 cold-leg mass flow.

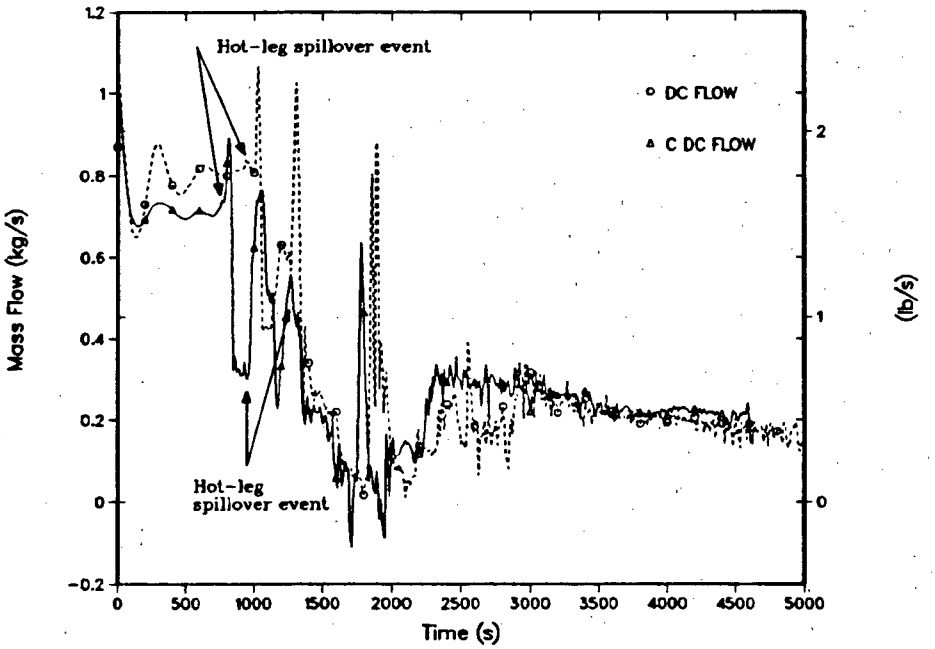


**Fig. 4.h.**

MIST Test 330302 downcomer mass flow.

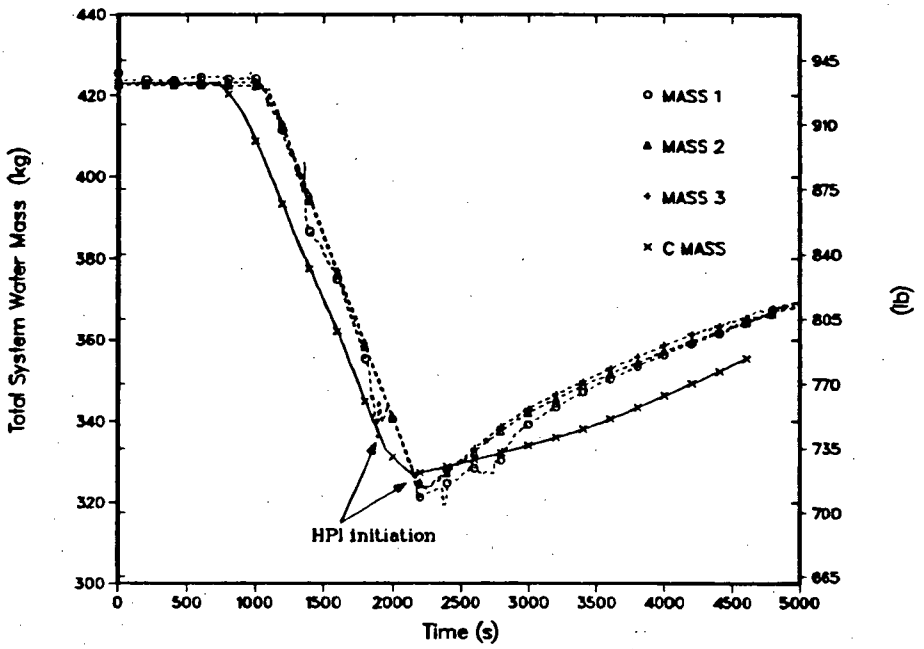


**Fig. 4.i.**

MIST Test 330302 primary-side water mass.

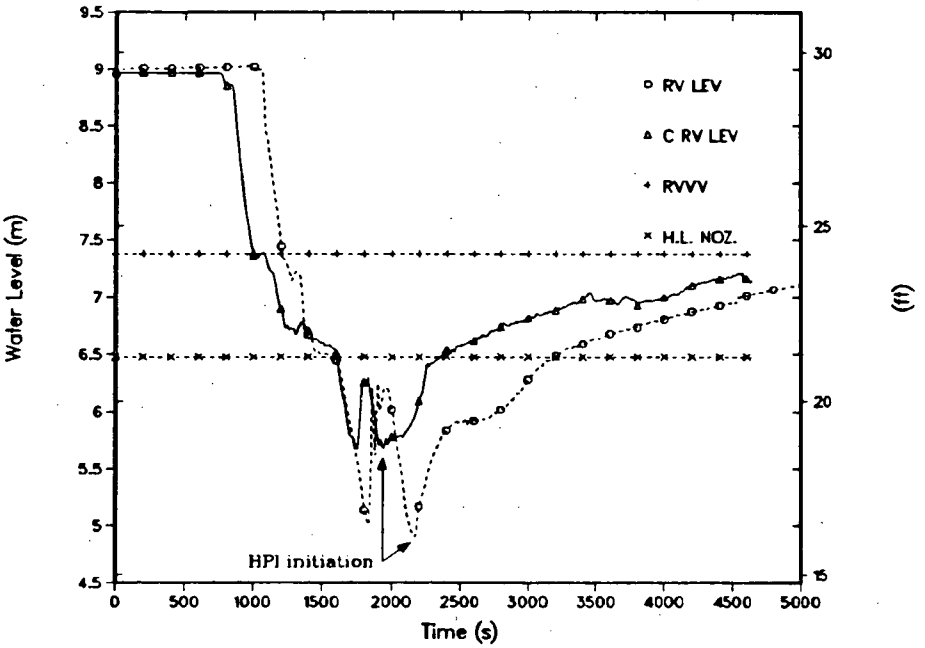


**Fig. 4.j.**

MIST Test 330302 reactor-vessel collapsed liquid level.

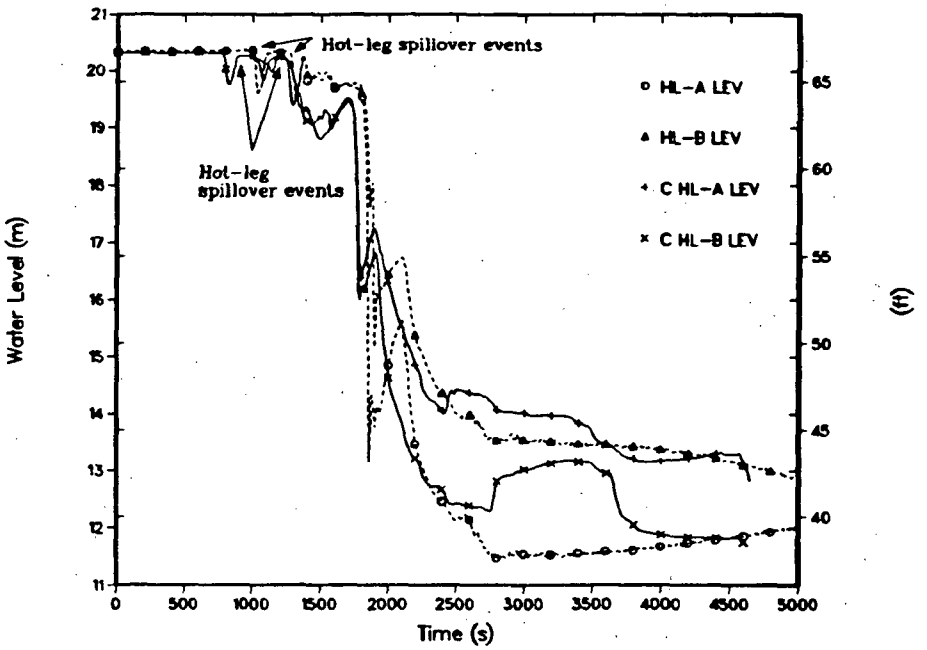


**Fig. 4.k.**

MIST Test 330302 hot-leg collapsed liquid level.

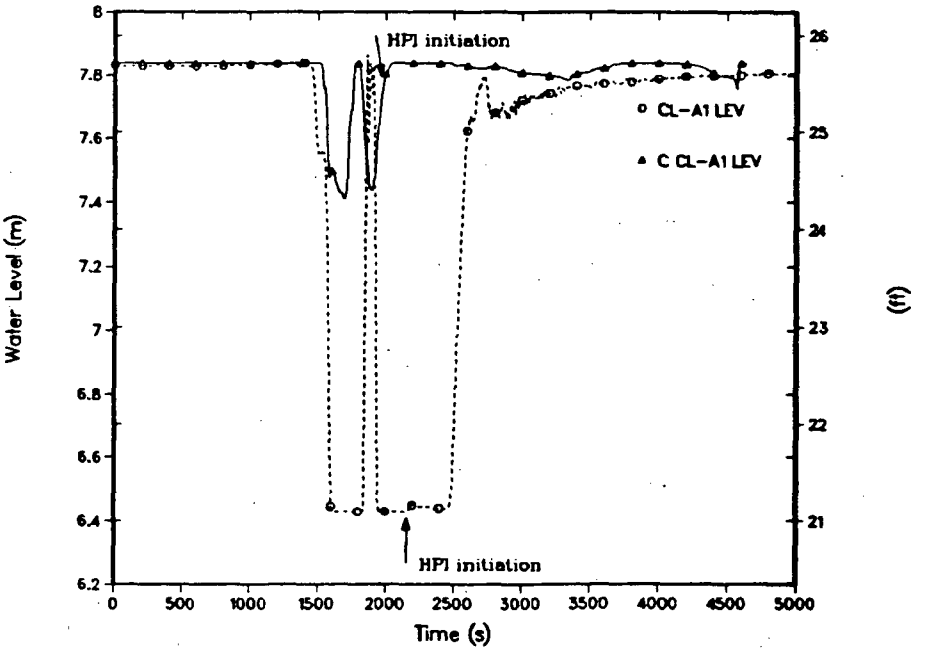


**Fig. 4.l.**

MIST Test 330302 Loop A1 cold-leg collapsed liquid level.

**TABLE I**

**EVENT TABLE FOR TEST 330302**

| Test Time (s) | Calculation Time (s) | Event Description |
|---|---|---|
| 0.0 | 0.0 | Start transient – loss of AFW to SG secondaries. |
| 942.0 | 730.0 | Primary system pressure increases to 16.20 MPa (2350 psia) and PORV lifted. PORV maintained open for remainder of test. |
| 942.0 | 730.0 | Core power decay ramp initiated. |
| 1025.0 | 860.0 | RVVVs first close. |
| 1080.0 | 935.0 | Pressurizer full. |
| 1680.0 | | SG secondary isolated |
| 2142.0 | 1930.0 | HPI started |
| | 4560.0 | Calculation terminated (vessel refilled to near RVVV level). |

and heatup phenomena were calculated, but the pressurization was more rapid than measured and the PORV set point was reached at 730 s. We believe that this discrepancy is related to our modeling of the pressurizer and surge line, specifically to the initial fluid temperature distributions in the surge line and pressurizer and the pressurizer noding. During this period the pressurizer liquid level was increasing as a result of primary-system swelling as shown in Fig. 4.b. The calculated rate of steam generation in the SG secondary during the boiloff was greater than measured as shown in Fig. 4.e. Thus, TRAC seemed to predict excessive heat transfer to the SG secondary during the SG-boiloff period. Primary-system mass flows were provided for the reactor-vessel vent valves (RVVVs), Loop-A1 cold leg, and downcomer in Figs. 4.f through 4.h. The early RVVV flow was underpredicted. The predicted loop and downcomer flows displayed the same trends as seen in the test but the magnitude of flow swings was underpredicted. The period from test initiation to PORV actuation was designated as Phase 1, SG dryout period.

Phase 2 of the transient covers the period between PORV actuation and HPI initiation 1200 s later. This period was a time of primary-system inventory depletion and covers the time between 942 and 2142 s in the test. The corresponding calculated times were 730 and 1930 s. Boiling began in the hottest regions of the primary following PORV actuation as shown in Fig. 4.d. Boiling was predicted to occur earlier than measured because the PORV was opened earlier, as previously discussed. Immediately following PORV actuation, the pressurizer-filling rate increased in both the calculation and test. Two-phase fluid was released through the PORV while the pressurizer filled and then liquid was released through the PORV. The PORV mass flow is shown in Fig. 4.c. Because HPI flow was delayed for 1200 s after PORV actuation and there was no other primary-coolant makeup, primary-system liquid levels began to decline. The reactor-vessel collapsed liquid level is shown in Fig. 4.j. The calculated and measured level trends display a similar character but the observed liquid levels were lower. This was a direct result of the underprediction of PORV mass flow during Phase 2, as shown in Fig. 4.c. Calculated and measured hot- and cold-leg collapsed liquid levels are shown in Figs. 4.k and 4.l, respectively. In both the calculation and the test, voiding occurred in the hot legs first and

was followed by several U-bend spillover events. The effect of the U-bend voiding and spillover events was observed in the Loop-A1 cold-leg and downcomer mass flows (see Figs. 4.g and 4.h). The Loop-A1 cold-leg mass flow stagnated following the hot-leg liquid spillover event that occurred in the test at approximately 1475 s and a similar stagnation was predicted, although it occurred slightly earlier. There was a subsequent short-lived hot-leg spillover event that occurred in the test at 1870 s and re-established flow in the Loop-A1 cold leg; this phenomenon was predicted. There was a marked difference between measured and calculated SG performance, as shown in Fig. 4.e. Dryout was predicted to occur at about 680 s while the SG was still steaming in the test when it was isolated at about 1600 s. We have determined that our initial specification of SG-secondary liquid level based on measured liquid levels was low. In addition, we have determined that the predicted primary-to-secondary heat transfer was too high.

Phase 3 of the transient covers the period between HPI initiation and about 4650 s, the end of the posttest assessment calculation. HPI was activated at 2142 s in the test. There were several direct consequences of the HPI activation. First, the primary-system pressure, which had slowly oscillated while generally trending upward during Phase 2, began to slowly decrease in both the test and the prediction, as shown in Fig. 4.a. Second, the PORV flow rate abruptly decreased, as shown in Fig. 4.c, indicating that two-phase flow was established through the PORV. The pressurizer liquid levels provided in Fig. 4.b show that a small vapor space was established at the top of the pressurizer. First the reactor vessel and then the cold legs begin to refill, as shown in Figs. 4.j and 4.l, respectively. In each case, the major test trends were predicted. Finally, an intraloop cold-leg circulation began at about 2770 s, as shown in Fig. 4.g. The predicted start of intraloop circulation was about 1900 s later.

MIST Test 330302 displayed many phenomena of interest. These included an SG-secondary boiloff, slow primary-system pressurization at constant primary-system inventory, single- and two-phase fluid flows through the PORV, hot-leg spillover events, cold-leg and downcomer flow interruptions and the flow recovery, the effects of late HPI injection into a voided primary system, and primary-system refill. In general, the TRAC-calculated results are in reasonable agreement with the observed phenomena. Thus, TRAC-PF1/MOD1 provides an acceptable prediction of the test. All major trends and phenomena were correctly predicted. Two areas of concern observable in Figs. 4.a–4.l were identified. First, the calculated PORV flow rate is less than measured. Because the MIST system behaviors are very sensitive to primary-system inventory, a more accurate prediction of the PORV flow rate is desirable. Second, TRAC predicted the too-rapid transfer of heat from the primary to the SG secondaries during Phase 1, SG dryout. This resulted in the too-rapid pressurization of the primary to the PORV setpoint.

**Test 3404AA Transient Calculation.**

The test was begun from steady-state conditions meeting prescribed tolerances. A steady-state calculation was run to 2000 s, corresponding to about five loop transits. At the end of the steady-state calculation, the primary- and secondary-system fluid conditions had stabilized within the uncertainties of the measured values.

An overview of the test and calculated transients is presented in Figs. 5.a–5.l. Major events are summarized in Table II. SGTR transient 3404AA was initialized at time zero from

the steady state by opening the valve in the SGTR line connecting the B-loop SG primary at the top of the SG to the top of the SG secondary. The tube rupture orifice represented a scaled 30.8 $cm^2$ double-ended break of 10 tubes at the top of the SG. After the primary-system subcooling dropped below 27.8 K (50°F), HPI was to have been initiated, the secondary fill of the A-SG was to have begun, AFW to the B-SG was to have been terminated, and a secondary cooldown of 55.6 K/hr (100°F/hr) was to have been initiated. These actions were taken late in the test but were still completed before the primary saturated. The test was judged acceptable as run.

An overview of the resultant test and calculated transients are shown in Figs. 5.a–5.l. With the opening of the SGTR, the subcooled primary system depressurized quickly (Fig. 5.a). The flow though the orifice was greater in the test than calculated by TRAC. The pressurizer emptied and the hot legs first saturated at about the same time, 70 s in the test and 80 s in the calculation. The hot-leg liquid level (Fig. 5.b) dropped quickly in the A-loop as inventory drained. The initial system voiding occurred in the A-loop because the liquid entering the A-loop from the pressurizer was warmer and flashed more readily. Natural-circulation flow interrupted in the A-loop at 80 s in the test and 120 s in the calculation (Fig. 5.c) as the hot-leg level dropped too low to allow spillover. The timing in the calculation was slower because the calculated flow rate through the SGTR orifice was smaller and calculated inventory greater.

The pattern seen in the B-loop flows (Fig. 5.d) was similar to the pattern seen in a number of other MIST Tests. The rate of depressurization slowed as voiding began in the upper head at 140 s in the test and 220 s in the calculation. B-loop natural-circulation flow increased to a peak at 190 s in the test and 270 s in the calculation and then declined rapidly as the liquid level fell away from the U-bend. Flow in the B-loop then ceased at 220 s in the test and 330 s in the calculation. Primary pressure (Fig. 5.a) reached a minimum at these times and started to increase. At 270 s in the test and 380 s in the calculation, the liquid level in the reactor vessel had drained to the RVVV elevation (Fig. 5.e). The downcomer contained cooler liquid than in the reactor vessel so that voiding was less extensive in the downcomer. The downcomer level did not drop as quickly. This exposed the ends of the RVVV lines in the reactor vessel to steam while the RVVVs were still below the liquid level in the downcomer. This condition caused the RVVVs (Fig. 5.f) to close. With the RVVVs closed, the voiding in the reactor vessel forced flow up the hot legs. This produced a spillover flow surge that peaked at 330 s in the test and 480 s in the calculation (Figs. 5.c and 5.d), and that ended at 360 and 580 s, respectively. Continued voiding, as inventory continued to drop rapidly, uncovered the RVVV elevation in the downcomer so that the RVVVs reopened allowing steam flow through them at 380 s in the test and 580 s in the calculation. This exposed steam from the core to cold HPI liquid draining down the cold legs into the downcomer, producing significant condensation and thus depressurization.

The repressurization that began at 220 s in the test and 330 s in the calculation ended at 290s and 470 s, respectively, because the increased flow through the broken hot leg provided sufficient cooling. After that time, the condensation on HPI and heat transfer to the SGs along with the inventory loss through the SGTR was sufficient to keep primary system depressurizing until the B-SG was isolated. After about 400 s, the SGTR line on the primary side uncovered allowing steam or two-phase flow out the break, increasing the volumetric flow rate while decreasing the rate of primary inventory loss.

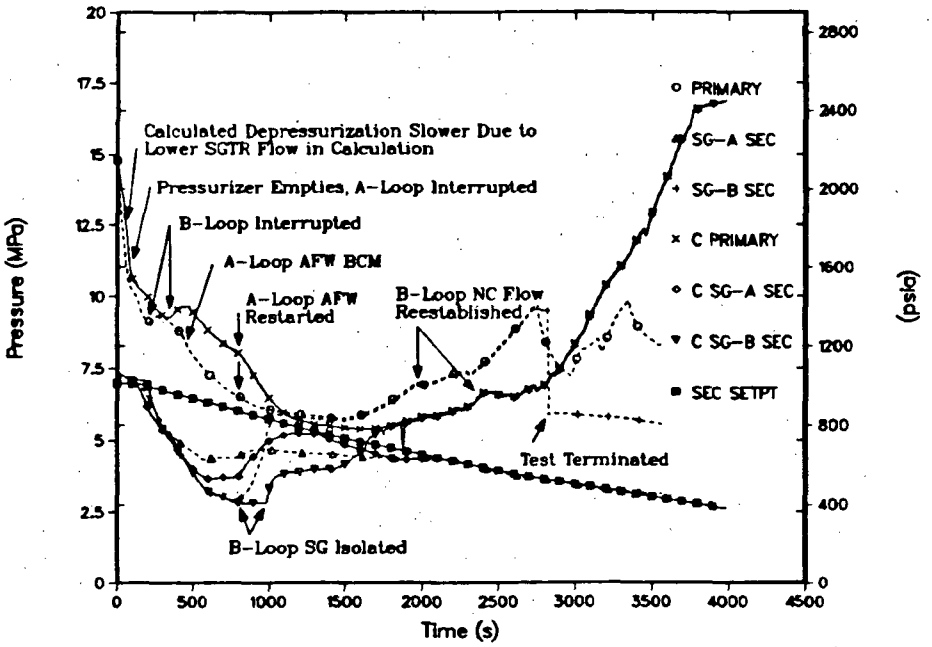


**Fig. 5.a.**

MIST Test 3404AA, primary and secondary pressures.

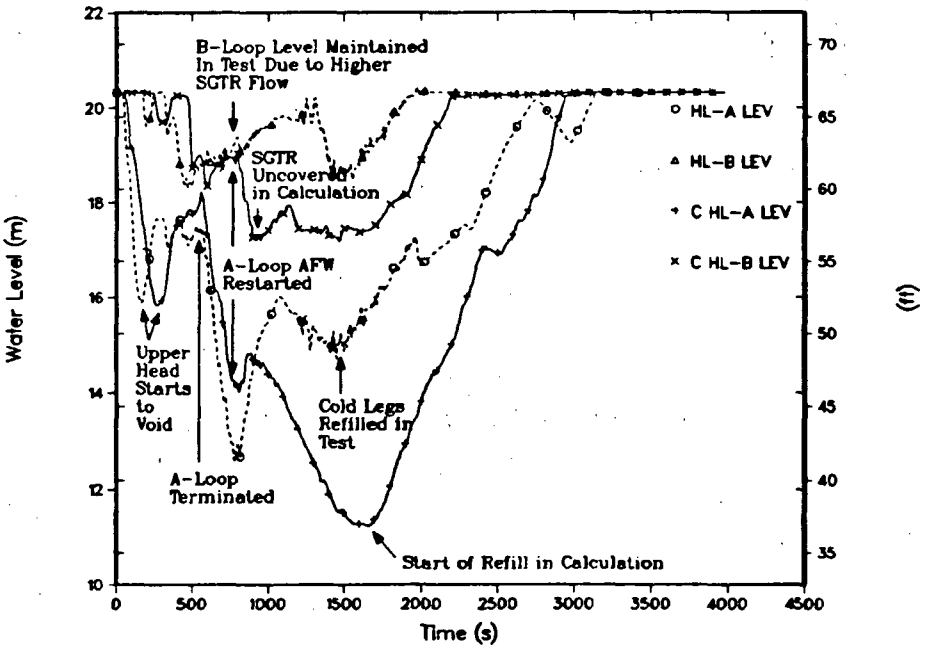


**Fig. 5.b.**

MIST Test 3404AA, hot-leg collapsed liquid levels.

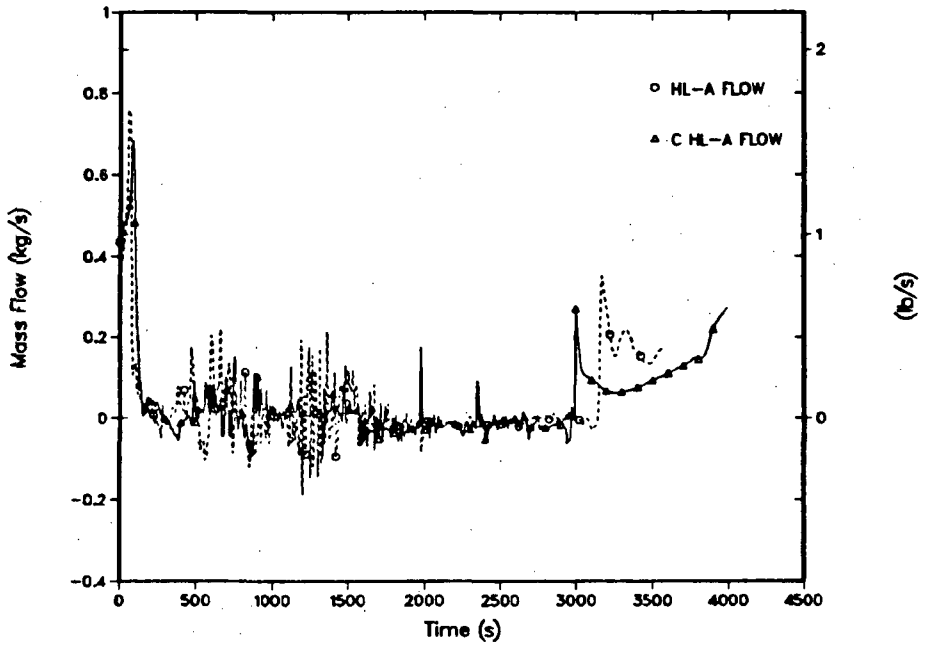


**Fig. 5.c.**
MIST Test 3404AA. SG-A primary mass flow.

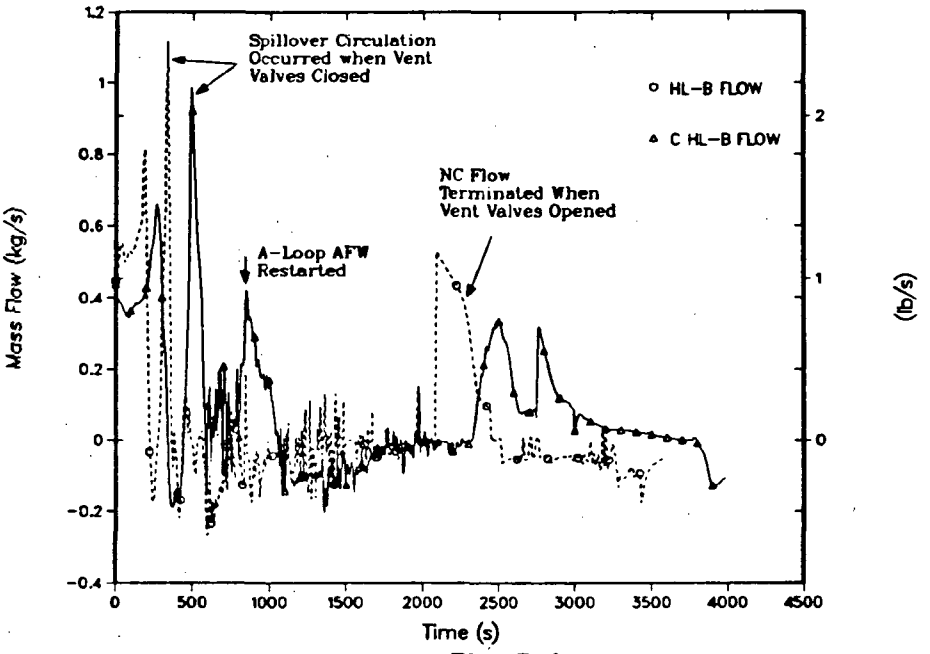


**Fig. 5.d.**
MIST Test 3404AA. SG-B primary mass flow.

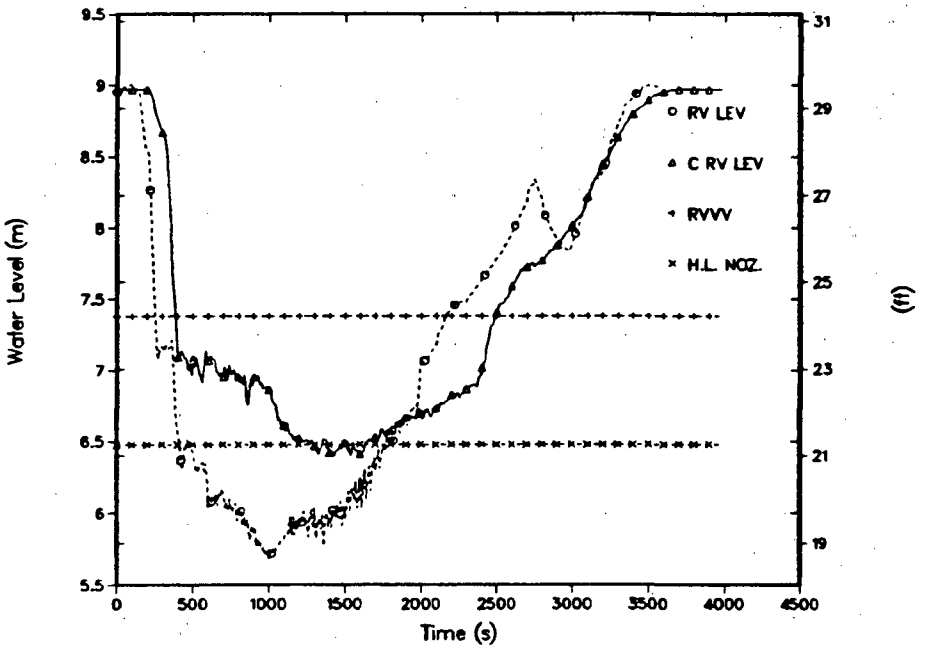


**Fig. 5.e.**

MIST Test 3404AA. reactor-vessel collapsed liquid level.

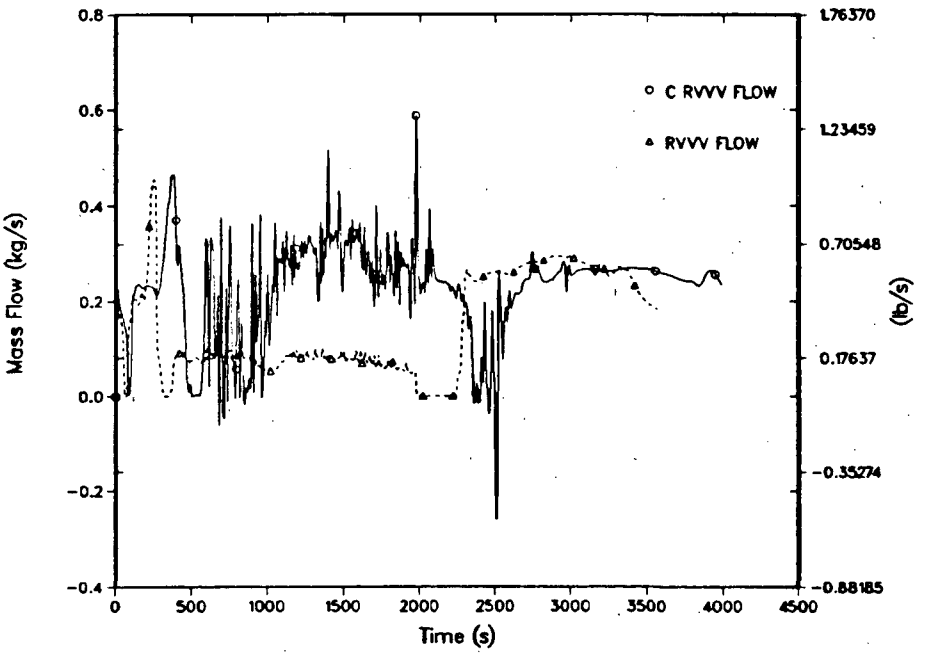


**Fig. 5.f.**

MIST Test 3404AA. RVVV mass flow.

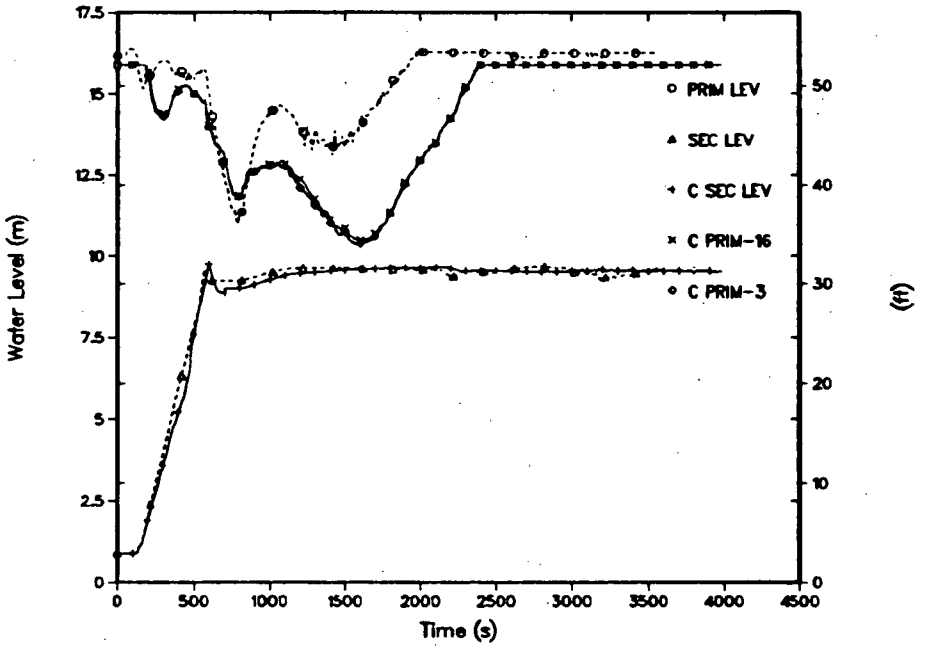


**Fig. 5.g.**
MIST Test 3404AA, SG-A collapsed liquid levels.

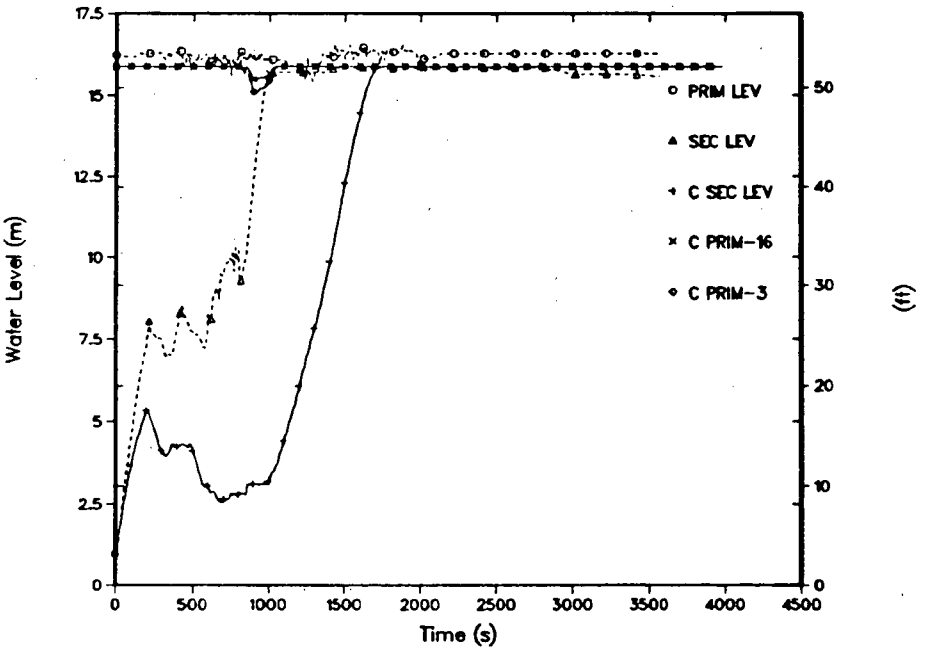


**Fig. 5.h.**
MIST Test 3404AA, SG-B collapsed liquid levels.

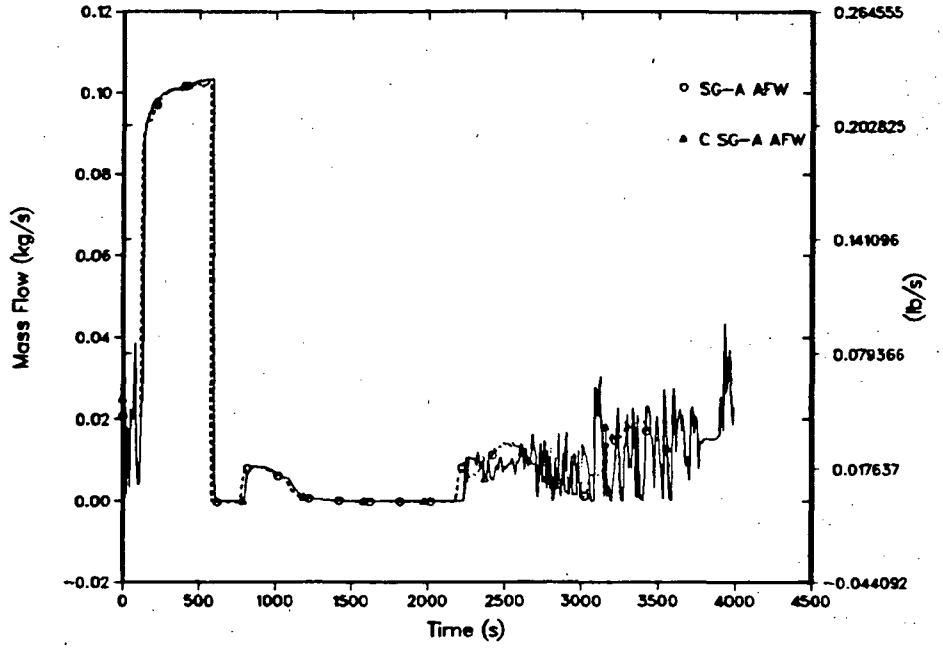


**Fig. 5.i.**
MIST Test 3404AA. SG-A AFW flow.

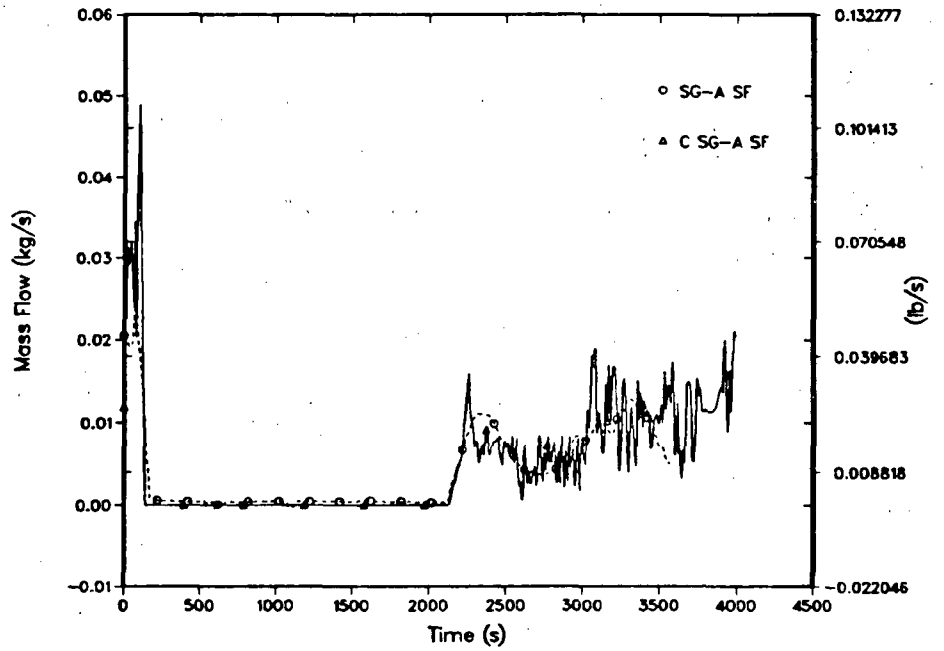


**Fig. 5.j.**
MIST Test 3404AA. SG-A steam flow.

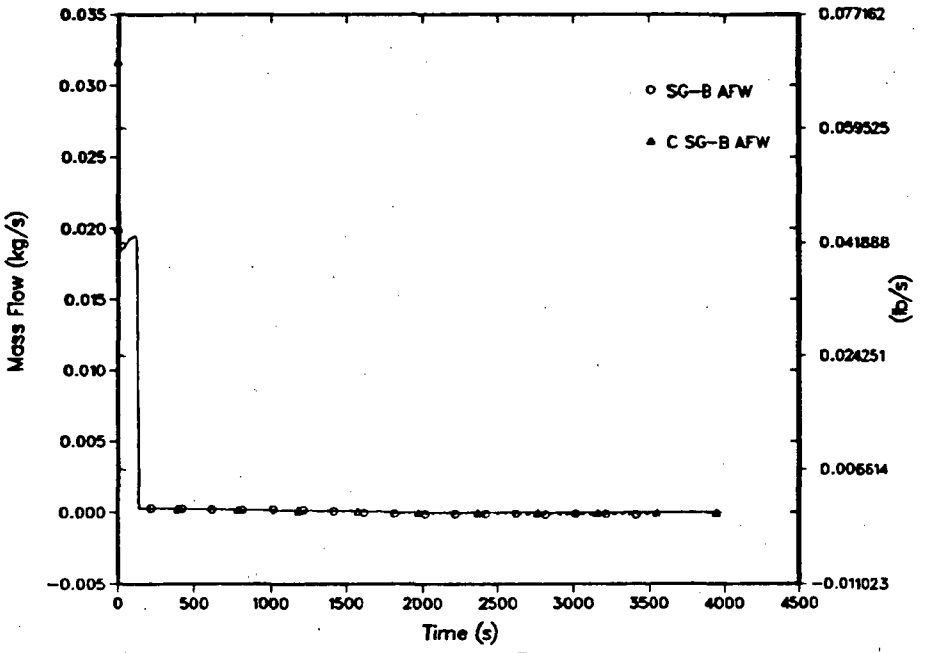


**Fig. 5.k.**
MIST Test 3404AA, SG-B AFW flow.

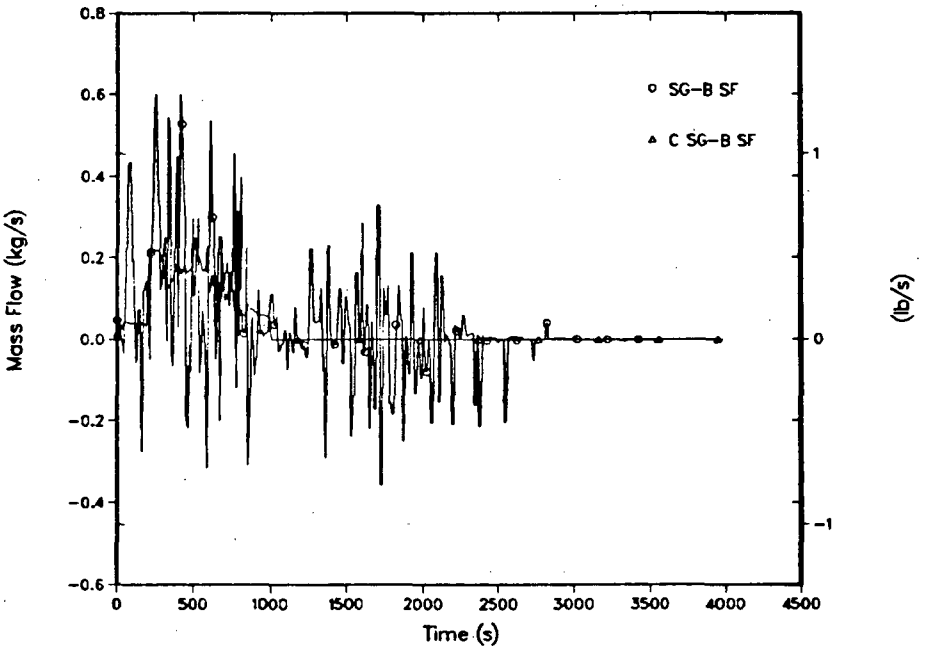


**Fig. 5.l.**
MIST Test 3404AA, SG-B steam flow.

**TABLE II**

**EVENT TABLE FOR TEST 3404AA**

| Test Time (s) | Calculation Time (s) | Event Description |
|---|---|---|
| 0.0 | 0.0 | Start transient – open SGTR valve. |
| 70.0 | 80.0 | Primary system saturates. |
| 80.0 | 120.0 | Natural circulation interrupts in A-loop. |
| 360.0 | 480.0 | Natural circulation interrupts in B-loop. |
| 800.0 | 990.0 | B-loop SG secondary isolated. |
| 2700.0 | | Test aborted on maximum SG pressure. |
| | 4560.0 | Calculation terminated (vessel refilled to near RVVV level). |

SG levels are given by Figs. 5.g and 5.h. AFW and steam flows for the SG secondaries are given by Figs. 5.i through 5.l. The B-loop SG provided a good heat sink for the natural-circulation flow ending at 360 s because steaming had been increased at about 200 s in the B-SG in response to the level increase caused by the SGTR flow (Figs. 5.h and 5.l). AFW boiler-condenser mode (BCM) heat transfer in the A-SG was also important for determining the depressurization rate. During the test, BCM occurred during refill from about 130 to 170 s and from 400 to 570 s. The corresponding times for the calculation were 200 to 350 s and 480 to 600 s. These were times when the level in the primary side of the A-SG (Fig. 5.g) was below the elevation of the AFW injection nozzle and AFW was on (Fig. 5.i). After the A-SG had refilled, AFW was off while control modes changed. Beginning at 770 s in the test and 800 s in the calculation, AFW came back on (Fig. 5.i) to maintain the level. This created AFW BCM in the A-SG from 770 to 1200 s when the AFW ended.

At 800 s in the test and 990 s in the calculation, the primary pressure (Fig. 5.a) dropped to 6.55 MPa (950 psi) and the B-SG was isolated. In the test, the B-SG then filled and the secondary pressure came to equilibrium with the primary by about 1000 s (Figs. 5.h and 5.a). In the calculation, the process was much slower because the initial level of the SG secondary was lower and because of the smaller leak flow rate. Equilibrium was not reached in the calculation until about 1700 s (Fig. 5.a).

The collapsed liquid level in the reactor vessel (Fig. 5.e) dropped below the hot-leg nozzle elevation at 490 s in the test and declined slowly until the B-SG was isolated and filled at 1000 s. In the calculation, the collapsed liquid level in the B-SG never dropped below the hot-leg nozzle elevation. System inventory in the calculation began increasing when the isolated SG came to equilibrium with the primary, at about 1700 s.

After isolation of the B-SG, the primary pressure in the test stabilized and the primary began to refill. At 1500 s, the cold legs, which had voids in the vicinity of the RCPs, refilled. Cold legs in both loops went into an intraloop circulation where flow is in the forward direction for one cold leg of a pair and in the reverse direction in the other. This brought warmer water to the downcomer and decreased the condensation of steam. With no strong depressurization mechanisms operating, the primary began to repressurize (Fig. 5.a). In the calculation this was delayed until about 1800 s.

At about 1950 s in the test, the downcomer had filled to the RVVV elevation closing the RVVVs. Steam generation from the core then forced some flow through the B-loop (Fig. 5.d) into the isolated, B-SG. This provided a weak heat sink, which reduced the repressurization rate. This flow lasted about 200 s, the time for the liquid level in the reactor vessel to rise to the RVVV level, causing the RVVVs to reopen. In the calculation, the same events occurred about 400 s later.

At about 2200 s, the control signal for SG-secondary pressure decreased to the pressure of the A-SG, and steaming began to further reduce the A-SG pressure (Fig. 5.a). AFW then came on in the A-SG to maintain the secondary level. This event occurred at about the same time in both test and calculation. In the calculation, the primary level (Fig. 5.g) was still low enough to produce some BCM heat transfer and reduce the repressurization rate. In the test, refill had been under way for about 700 s longer, so the A-SG primary level was higher, too high for BCM heat transfer to occur.

The A-SG was not coupled to the primary in any strong way in the test during the period after 2200 s, when the A-SG was being cooled. Also, when the RVVVs reopened at 2300 s, the flow through them was liquid so the path for vapor to contact HPI liquid was no longer available. This eliminated the major mechanisms for depressurization and the primary repressurized (Fig. 5.a) at a faster rate after 2300 s.

The test was aborted at about 2700 s when the pressure of the primary and the B-SG reached the maximum pressure for the model SGs of the MIST facility. At the time the test was aborted, the primary had nearly refilled. B&W believed (Ref. 4) that natural-circulation flow would have begun shortly in the A-loop, allowing a one-loop cooldown. Had the pressure continued to rise, PORV-HPI cooling could also have been used. Both of these phenomena had been demonstrated in other MIST Tests. Most of the phenomena of interest for an SGTR with isolation of the damaged SG had occurred prior to the termination of the test.

The calculation showed the phenomena and trends of the test. The SGTR line had been geometrically modeled but showed lower calculated flows than observed in the data. This may indicate that TRAC could be improved for this situation. Data for the tube rupture flows in the test were derived from component inventory data. Thus, flow rates do not give good instantaneous values for making detailed comparisons.

## CONCLUSIONS

Both Test 330302 and Test 3404AA showed many phenomena of interest. In both cases the overall level of agreement between test and calculation was judged to be reasonable; that is, that major trends are predicted correctly, although TRAC values are frequently outside the range of data uncertainty. We believe that correct conclusions will be reached if the code is used in similar applications despite minor code/model deficiencies.

**Test 330302.** Two areas were found where facility knowledge was inadequate. Transient data showed that the surge line and lower part of the pressurizer contained cold water at steady state. The few thermocouples in these components were located away from the low regions where this cold water was located and did not reveal its presence. The calculation was initialized with the pressurizer and surge line at the temperatures indicated by the thermocouples. The calculation shows considerable sensitivity to the pressurizer and surge-line conditions, and we believe that the differences in timing between test and calculation were

caused, at least in part, by inaccuracies in the initialization of the pressurizer and surge-line conditions in the model. Facility data also seem inconsistent between the amount of liquid initially in the SGs, as indicated by liquid levels, and integrated steam flows through the steam line. This may have contributed to the earlier predicted boil-off of the SGs in the calculation.

One area was found where the TRAC model of the MIST facility was inadequate for this transient and was modified. The bottom cell of the SG secondaries was subdivided into five cells. This improved the calculation of the SG boil-off rate.

Two areas were identified where code models and correlations might be improved. The primary-to-secondary heat transfer in the SGs during phase 1 appeared to be overpredicted. This may indicate a need for refinement of the TRAC heat-transfer package. Also, the critical flow from the PORV appeared to have a different sensitivity to subcooling than predicted by TRAC for single-phase liquid flow. With the differences between the temperature profiles that apparently existed within the pressurizer and surge line, and the values used in the calculation, it is difficult to draw a definitive conclusion about the critical flow model sensitivity to subcooling.

**Test 3404AA**. The differences between the test data and the calculation for Test 3404AA can be attributed primarily to the difference between the SGTR flow in the test and the calculation. Even though we judge the overall agreement between test and calculation to be reasonable, that is, the calculation showed the same trends as the test, the time shifts were of sufficient magnitude to prevent the isolation of secondary causes of differences between test and calculation. The SGTR line was geometrically modeled. Flow losses because of acceleration of the fluid as it enters the tube, and/or frictional losses predicted for the high velocity through the small tube, are too large. This was also observed for a calculation of MIST Test 320201, a scaled 50-$cm^2$ small-break loss-of-coolant accident test. In both of these tests, the leak orifice was located in a tube branching off a much larger pipe and with much larger velocities than the pipe. This is apparently a code problem that can be alleviated to some extent with noding changes. It is a deficiency that makes the accurate prediction of flow through leak orifice tubes difficult. We believe that the effect on calculations with plant decks is not significant.

The code/data analyses presented herein constitute part of an assessment matrix for the performance of the TRAC-PF1/MOD1 code, which will ultimately be used to extrapolate data from the MIST facility to full-scale plant behavior.

## REFERENCES


1. Safety Code Development Group. "TRAC-PF1/MOD1: An Advanced Best-Estimate Computer Program for Pressurized Water Reactor Thermal-Hydraulic Analysis." Los Alamos National Laboratory report LA-10157-MS, NUREG/CR-3858 (July 1986).
2. "Immediate Report. Test 330302: Group 33 (Feed and Bleed) Test 3, Delayed HPI." Babcock & Wilcox document BAW-1938 (October 1986).
3. J. R. Gloudemans (principal author). "Group Report. MIST Test Group 33. HPI-PORV Cooling." Babcock & Wilcox document BAW-1965 (July 1987).
4. "Immediate Report. Test 3404AA: Group 34 (SGTR) Test 4. Steam Generator Isolated." Babcock & Wilcox document BAW-1933 (November 1986).
5. J. R. Gloudemans (principal author). "Group Report. MIST Test Group 34. Steam Generator Tube Rupture." Babcock & Wilcox document BAW-1966 (August 1987).
6. B. E. Boyack. "Posttest Analysis of MIST Test 330302 Using TRAC-PF1/MOD1." Los Alamos National Laboratory report LA-UR-88-1937 (June 1988).
7. "Multi-loop Integral System Test (MIST) Facility Specification." Babcock & Wilcox document RDD:84:4091-01-01:01 (1984).

## Appendix A

## Code Assessment Descriptor Definitions

The descriptors will be used to provide an overall characterization of how TRAC predicted the thermal-hydraulic behavior in the MIST facility. Four descriptors are used to characterize the degree of agreement and the application consequences of either the agreement or lack of agreement. The four descriptors are **excellent agreement, reasonable agreement, minimal agreement**, and **insufficient agreement**. Each of these descriptions will be defined below along with the consequences for future application of the code in the given area being characterized and the perceived need for additional code development.

**Excellent agreement** is an appropriate descriptor when the code exhibits no deficiencies in modeling a given behavior. Major and minor phenomena and trends are correctly predicted. The calculated results are judged by the analyst to be close to the data with which a comparison is being made. If the uncertainty of the data has been identified and made available to the analyst, the calculation will, with few exceptions, lie within the uncertainty band of the data. The code may be used with confidence in similar applications. Neither code models nor the facility noding model require examination or change.

**Reasonable agreement** is an appropriate descriptor when the code exhibits deficiencies, but the deficiencies are minor; that is, the deficiencies are acceptable because the code provides an acceptable prediction of the test. All major trends and phenomena are correctly predicted. Differences between the test and calculated traces of parameters identified as important by the analyst are greater than those deemed necessary for excellent agreement. If uncertainty data are available, the calculation will frequently lie outside the uncertainty band. However, the analyst believes that the discrepancies are not sufficiently large to require a warning to potential users of the code in similar applications. The assessment analyst believes that the correct conclusions about trends and phenomena would be reached if the code were used in similar applications. The code models and/or facility noding model should be reviewed to see if improvements can be made.

**Minimal agreement** is an appropriate descriptor when the code exhibits deficiencies and the deficiencies are significant; that is, the deficiencies are such that the code provides a prediction of the test that is only conditionally acceptable. Some major trends or phenomena are not predicted correctly while others are predicted correctly. Some TRAC calculated values lie far outside the uncertainty band of the data with which a comparison is being made. The assessment analyst believes that incorrect conclusions about trends and phenomena may be reached if the code were used in similar applications. The analyst believes that certain code models and/or the facility noding model must be reviewed, corrections made, and a limited assessment of the revised code or input models made before the code can be used with confidence for similar applications. A warning should be issued to the TRAC user community that the user applying the code in similar applications risks drawing incorrect conclusions. This warning should stay in force until the identified review, modification, and limited assessment activities are completed and the resultant characterization descriptor is "reasonable" or better.

**Insufficient agreement** is an appropriate descriptor when the code exhibits major deficiencies; that is, the deficiencies are such that the code provides a prediction of the test that is unacceptable. Major trends are not predicted correctly. Most TRAC calculated values lie far

outside the uncertainty band of the data with which a comparison is being made. The assessment analyst believes that incorrect conclusions about trends and phenomena are probable if the code is used in similar applications. The analyst believes that certain code models and/or the facility noding model must be reviewed, corrections made, and a limited assessment of the revised code or facility noding model made before the code can be used with confidence for similar applications. A warning should be issued to the TRAC user community that the code must not be used for similar applications until the identified review, modification, and limited assessment activities are completed and the resultant characterization descriptor is "reasonable" or better.

# RESULTS AND ANALYSIS OF THE INEL ONCE THROUGH STEAM GENERATOR AIR-WATER AND STEAM-WATER EXPERIMENTS*

T. K. Larson, K. G. Condie and G. E. McCreery

Idaho National Engineering Laboratory
EG&G Idaho, Inc.
Idaho Falls, Idaho 83415

Experiments have been conducted in steam/air-water facilities that model B&W Once Through Steam Generator (OTSG) heat transfer and fluid flow behavior during auxiliary feedwater (AFW) injection. The experiments and analysis described in this paper examine the basic phenomena of AFW radial and axial flow distribution, tube support plate (TSP) flooding, and tube heat transfer. Flow distribution is studied visually and measured in an unheated multi-tube (625 tubes) full scale 1/8 sector of the OTSG that includes three TSP's. Heat transfer is examined in a heated single tube facility with either one or two broached hole support plates and either air or steam upflow. The flow distribution experiments indicate that radial, axial, and azimuthal spreading is a strong function of AFW flow rate and a weaker function of vapor upflow although liquid spreading becomes an increasingly stronger function of vapor upflow as the flooding line is approached. A semi-empirical model of AFW penetration without gas flow is presented. The model is extended to include the influence of gas flow by correlation. The heat transfer experiments indicate that heat transfer is highly dependent on AFW injection rate, and in particular on whether or not the water flows down the tubes as a continuous film or breaks into rivulets. A computer model of heat transfer has been developed, and is described. The data gathered during the experiments and the models developed from this data are currently being incorporated into the RELAP5 computer code.

## INTRODUCTION

During the last two decades, significant effort has been devoted to the study of light water nuclear steam supply systems (NSSS) during off-normal operating conditions. The major research efforts have been devoted to the design basis large break loss of coolant accident. Examples of such research programs supported by the United States Nuclear Regulatory Commission (NRC) included the LOFT[1], Semiscale[2], FIST[3], and THTF[4]. In the past few years, research emphasis has changed to more probable events such as small break loss of coolant accidents (SBLOCA) and operational transients. Emphasis of ongoing programs such as LOFT and Semiscale was changed and new programs such as MIST[5] and SRI-II[6] were initiated to

* Work supported by the U.S. Nuclear Regulatory Commission, Office of Nuclear Regulatory Research under DOE Contract No. DE-AC07-76ID01570.

examine details of particular reactor system designs. Development of analytical tools (e.g., RELAP5 and TRAC) used for the prediction of light water reactor response to off-normal conditions also was redirected to improve the analysis capabilities for the more probable events. In addition to the change in research emphasis, efforts are underway to allow better utilization of the research information gathered over the last two decades. In effect, both the experimental research and the analysis tool development research emphasis is becoming more "best estimate" oriented rather than "evaluation model" oriented. As a reflection of this research emphasis, analytical tools that contain a better physical basis have been developed or are being developed. New experimental programs have been initiated to provide data needed to support the development and help provide the data base necessary to assess and improve the analytical methods.

This paper describes a recently completed experimental program designed to provide separate effects information on the performance of once through steam generators (OTSG) commonly used in the Babcock and Wilcox (B&W) NSSS design. The program is funded by the United States Nuclear Regulatory Commission and is being conducted at the Department of Energy's Idaho National Engineering Laboratory. The objectives of the program are to develop an experimental data base that can be used to assess existing models and develop improved models for characterizing the behavior of OTSG during the auxiliary feedwater (AFW) injection portion of transients. The program is concentrating on studies of falling film heat transfer, flooding in single- and multiple-tube geometries representing the OTSG, and on characterization of the multi-dimensional aspects of AFW injection. This paper describes the results obtained from flooding, AFW penetration, and heat transfer experiments conducted and is organized as follows: first, the full scale OTSG geometry is described to provide information on the design features and the operating characteristics of the steam generator; then, the hardware features of the two OTSG facilities constructed at the INEL are described and more detailed objectives of the experimental program are given; third, results of experiments and analysis conducted to date are provided; and finally, conclusions of the program are given.

## FULL SCALE OTSG DESCRIPTION

Once through steam generators are used exclusively in B&W pressurized water reactors. The OTSG is a single-pass counter flow tube-in-shell heat exchanger consisting of 15531, 15.85 m (52 ft) long tubes contained inside a 3.5 m (138 in.) ID vessel. In the OTSG design, there are two tube sheets; an upper one for tube inlets (primary fluid inlet) and a lower one for tube outlets (primary fluid outlet). Forty-two, 2.22 cm (7/8 in.) diameter rods support 15, 3.8 cm (1-1/2 in.) thick tube support plates (TSP) between the tube sheets. The tube support plates maintain the 1.59 cm (5/8 in.) ID steam generator tubes on a 2.22 cm (7/8 in.) triangular pitch. Each TSP has broached flow passages adjacent to each tube through which secondary fluid passes. Figures 1 and 2 provide detail of the overall steam generator design and the TSP geometry, respectively.

In an OTSG, main feedwater is injected into a downcomer annulus. Steam

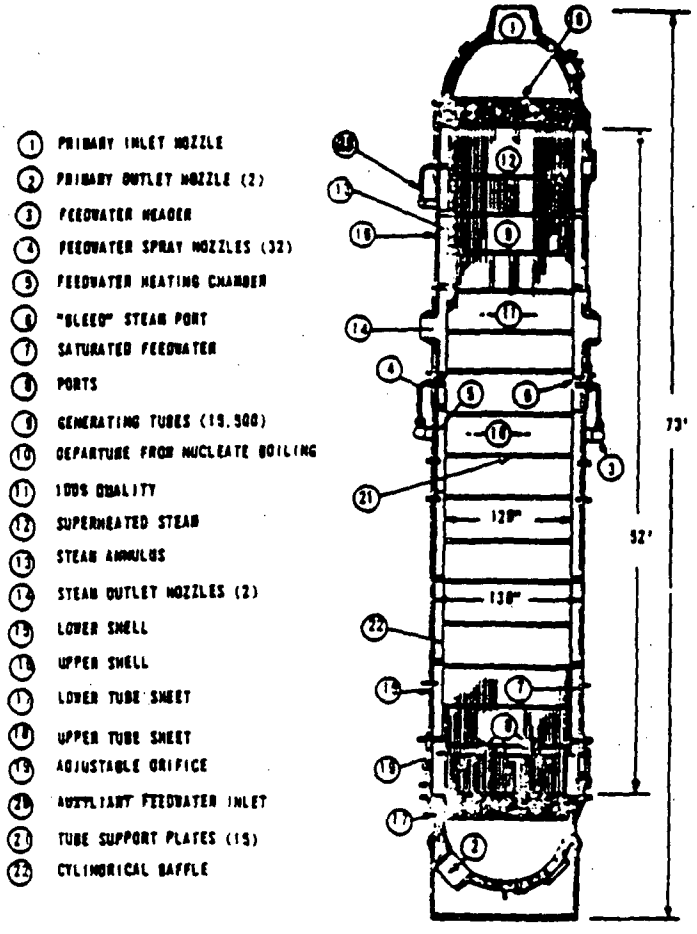


Figure 1. Schematic of a Once Through Steam Generator.

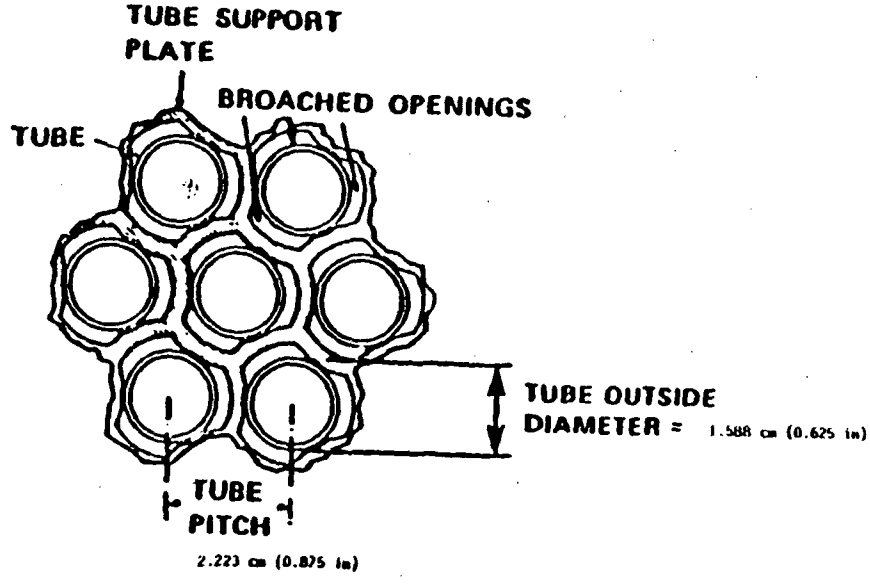


Figure 2. Broached hole tube support plate geometry.

from the boiler region is aspirated with the feedwater to raise the feed tempeature to near saturation conditions before the feed is introduced into the boiler region. Decay heat removal capability is provided by injection of AFW into the top of the steam generator boiler region through six 10.16 cm (4 in.) diameter nozzles. The six nozzles are located at $45^{0}$ increments on the bundle outer periphery. The injection occurs at the periphery of the tube bundle and just below the top of the cylindrical shroud separating the boiler and steam annulus regions (see Figure 1).

Injection of AFW in an OTSG results in a complex counterflow situation within the boiler. As AFW is injected it tends to fall downward due to gravity and spread inward due to its injection momentum and liquid level build-up. Characterization of the flow behavior is complicated, however, by the close proximity of the tubes and the horizontal tube support plates shown in Figures 1 and 2. These support plates present a restriction to downward AFW flow, and likely tend to pool the AFW, which promotes its spreading into the tube bundle. Furthermore, as the AFW falls and steam is produced, the upward flow of steam may produce a counter current flow limiting situation at the tube support plate, which further restricts the downward flow. Additional complicating factors concern the design of the top TSP. The outer four rows of holes in this TSP are not broached and there are flow holes around the outer periphery where the TSP and the shroud meet that provides an additional flow area. Other TSP's have slots around the outer periphery that provide additional flow area (considerably larger than that at the top TSP).

The B&W Company has conducted some limited experiments in an operating plant[7] and in an air-water facility[8] to investigate penetration of AFW. This data has been used to generate an empirical model for AFW wetting that describes the total number of tubes wetted as a function of AFW flow rate and distance below the AFW injection point. The limited conditions under which this model was developed have prompted the NRC to support design, construction, and testing in the separate effects facilities described below.

## INEL SEPARATE EFFECTS OTSG FACILITY DESCRIPTION

Two different scaled OTSG facilities have been built and operated at the INEL to generate a data base of information related to OTSG behavior during AFW injection. The hardware design and objectives of these two atmospheric pressure facilities are discussed below.

### Single Tube Facility

Two different configurations of the single-tube facility were used in the conduct of experiments. An adiabatic configuration was used for flooding and pressure drop investigations and a heated tube configuration was employed for heat transfer experiments. Figure 3 shows a schematic generally representative of both configurations.

The adiabatic experimental apparatus employs a clear 1.59 cm (5/8 in.)

OD polycarbonate tube, which passes through the TSP. The TSP is a 3.8 cm (1-1/2 in.) thick aluminum plate with accurately duplicated broached hole geometry (Figure 2). The tube and TSP are enclosed by a 10.16 cm (4 in.) O.D. clear polycarbonate shroud. AFW is supplied by a header that penetrates the shroud approximately 0.91 m (3 ft) above the TSP. The AFW falls down the inside of the shroud and accumulates on the TSP, where it may then flow through the broached hole and down the outside of the tube and eventually to a catch tank measuring system.

Steam generated by the evaporation of AFW flowing down the steam generator tubes and from the liquid pool on the bottom of the steam generator is simulated by air or steam flow. In the configuration used for flooding experiments, air is driven through the TSP holes by an air suction fan. The fluid passes through a phase separator upstream of the fan and flow measurement station to remove any entrained liquid. Air flow rate is regulated by means of a bypass valve. In an alternate configuration used to study the effects of steam condensation, either air or steam is forced under pressure into the bottom of the secondary side of the apparatus, and flows through the TSP holes.

Recorded parameters include temperature, pressure, air flow rate, water flow rate, and water head above the TSP. A standpipe is employed to maintain the water height above the TSP at a fixed level during flooding experiments using the suction fan. Direct observations of water level on the TSP are made using a borescope, which slides inside the clear polycarbonate tube.

The heated tube apparatus employs an actual 1.59 cm (5/8 in.) O.D. inconel steam generator tube provided by B&W. The primary fluid is pressurized and heated [typically 1.38 MPa (200 psi), and 420 K ($296^{o}$F)]. The AFW is controllable and can be heated to a maximum of 370 K ($205^{o}$F) before injection. The inside of the tube is instrumented with 36 thermocouples to measure primary bulk fluid temperature. In addition to temperature and flow measurements, video and still photography is used to record flow phenomena on the outside of the tube. Vapor generated at tube locations below the TSP (e.g., at the pool surface or on the tube surfaces below the TSP) can be simulated by steam provided by a small boiler.

The objectives of the single tube facilities were several fold and include: (a) determining the flooding characteristics for the single tube/broached hole TSP combination, (b) obtaining heat transfer regime and rate data for typical TSP flow and primary conditions, (c) investigation of measurement techniques potentially usable in the larger multitube facility.

## Multi-tube Facility

The multitube facility shown in Figure 4 represents a 1/8 radial sector of the top three TSPs in an OTSG. The facility contains a single AFW nozzle and 625 tubes placed in the 15 outermost rows directly in front of the AFW nozzle. (A typical operating OTSG would have approximately 1940 tubes in a 1/8 sector.) Each of the three TSPs includes typical broached holes for the

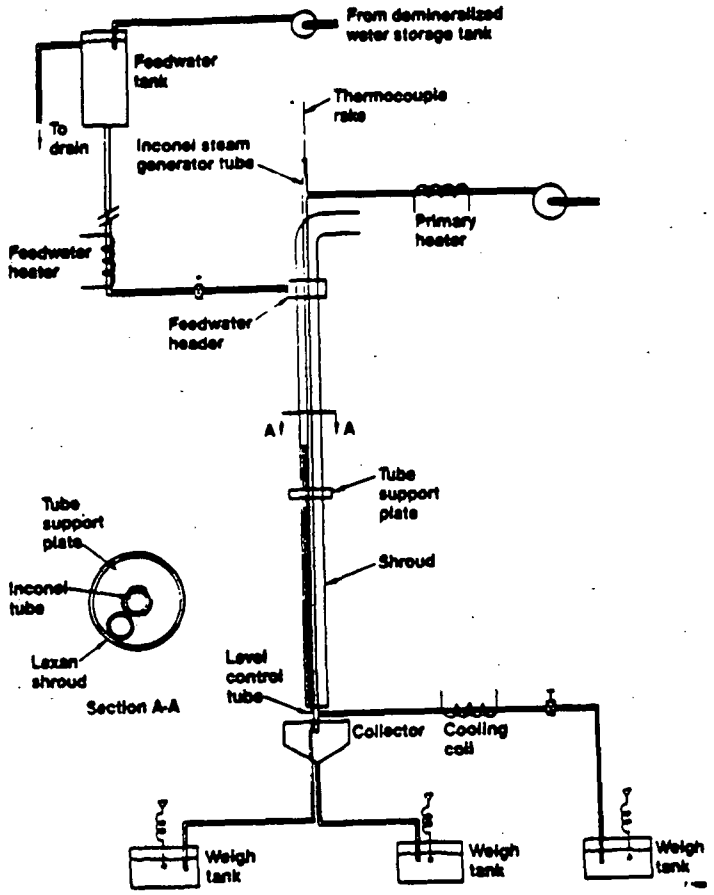


Figure 3. Schematic of the single tube heated once through steam generator apparatus.

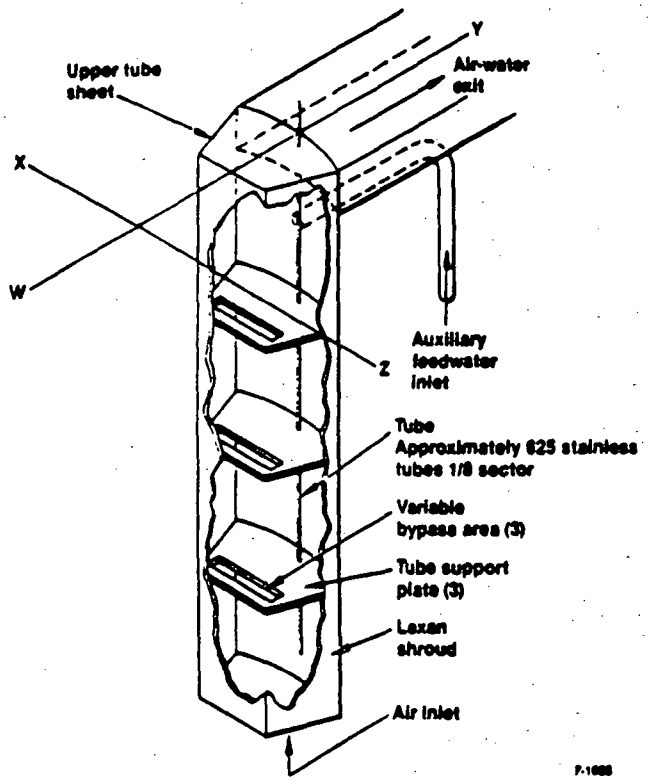


Figure 4. Schematic of the multi-tube once through steam generator facility.

625 tubes and a variable area bypass region, that can be adjusted to represent the axial flow resistance of the balance of the tubes in the 1/8 sector. Each TSP is constructed of 3.81 cm (1.5 in.) thick aluminum and accurately represents the full scale geometry. In particular, on the top TSP, the outer four rings of holes in the TSP do not include the broached flow passages around the tubes. The flow paths in the TSP between the outer row of tubes and the flow shroud (representing clearance fit in the full scale OTSG) are also represented. The sector is enclosed in a polycarbonate shroud to allow visual observation of the phenomena of interest. Flowrate controlled AFW is injected above the top TSP and collected in a large catch tank below the third TSP. Vapor upflow is simulated by air drawn through the test section by a suction fan connected to the top of the test assembly. The fan is capable of delivering an air flow of 2.4 $m^3$/min (5000 $ft^3$/min) at 51 cm (20 in.) of head.

Six-hundred fifteen of the tubes in the assembly were constructed of stainless steel and 10 were made of clear polycarbonate. Ten of the stainless tubes were fitted with film flow collection devices beneath the third TSP to allow individual tube flows to be measured. The ten polycarbonate tubes facilitated observation and measurement of the liquid level above each TSP via a borescope placed inside the tubes.

The objectives of the multitube facility include: (a) determination of the flooding characteristics of the multiple tube arrangement relative to the single tube; (b) examination of the axial, radial, and azimuthal penetration characteristics of the AFW as a function of both AFW and air flow rates; and (c) quantitative mapping of the tube flowrate and tube wetting profiles.

## FLOODING EXPERIMENT CONDUCT AND RESULTS

Flooding experiments were conducted in both the single tube facility and in the multitube facility. In the single tube test the standpipe was set at the selected elevation. After AFW flow was established, air suction was initiated. For very low suction, the water level would raise above the TSP but no air would flow. The air suction was increased until countercurrent flow was established (representing the first data point). Additional data points were taken with increased air flow until all the liquid was diverted through the standpipe i.e., no liquid passed through the TSP. This represented the critical flooding point. The air flow was then decreased and the data points were repeated until no air flow passed through the TSP. This process was repeated for several different standpipe settings. In the multitube facility, flooding was investigated for both the top TSP alone and with all three TSPs assembled in the facility. In these tests, experiments were initiated by setting an air flow rate with zero AFW flow. The AFW was then increased in a stepwise fashion to approach the flooding line. At the inception of flooding, a liquid level started to build up on the flooded TSP. Further increases in the AFW rate produced increasing liquid levels and a series of equilibrium points along the flooding line, along which liquid head plus pressure loss was matched by blower head, until the level exceeded the maximum head the air blower is

capable of sustaining. At this point, the air flow decreased to zero. The system was then reinitialized at a different initial air flow and the process was repeated to create a series of air flow/water flow points that follow the flooding line.

Figure 5 summarizes the single tube and the multitube (single TSP) flooding data, plotted in nondimensional superficial velocity coordinates and the liquid level on the TSP at flooded conditions for the multitube TSP. Also shown are typical trajectories of points for both increasing and decreasing liquid flow rates at a constant air flow setting taken in the multitube facility. These data were taken to examine hysteresis effects.

The single tube and multitube flooding data shown in Figure 5 can be correlated with either the Wallis[9] or Kutateladze[10] type formulations. For the Wallis correlation (see nomenclature for definition of terms),

$$\sqrt{j_g^*} + \sqrt{j_f^*} = C \qquad (1)$$

the C coefficient was determined to be 1.74 for the single tube data and 2.06 for the multitube data. The characteristic diameter used to compute the dimensionless superficial velocity was the hydraulic diameter [0.432 cm (0.17 in.)] of the broached hole. The data can also be correlated with the Kutateladze correlation,

$$\sqrt{K_g} + \sqrt{K_f} = K \qquad (2)$$

The constant K was determined to be 1.97 from the single tube data and 2.27 from the multitube data.

The data shown in Figure 5 is consistent with other researchers data in that the flooding line for multidimensional geometries is higher than that for a one-dimensional geometry. Bankoff, et al.[11] saw the same relationship during their investigation of the influence on flooding of the number and size of holes in a perforated plate. Following these authors conclusions, the lower flooding curve for the single tube TSP compared with the multi-tube is attributable to the formation of large vorticies above the comparatively large closed area of the single tube TSP. The vorticies contribute to turbulent mixing and therefore higher interphase drag compared with that in the multi-tube. The present data also indicate that the flooding line for the broached hole plate is considerably higher than that for flooding in a tube where the constant C in the Wallis correlation is generally of the order of 0.7. The data for the multi-tube facility are similar to the data reported by Sun[12] for a boiling water reactor tie plate. Sun reported a critical gas Kutateladze number of 4.3 (e.g., $K^2$) whereas the present data yield a $K^2$ of 5.15. This is interesting in light of the fact that the hydraulic diameter for the tie plate is considerably larger than that for the OTSG broached hole plate. In fact, the TSP has a hydraulic diameter in the range where the Wallis correlation is preferred. The Wallis correlation is applicable, according to Bankoff, et al.[11], when

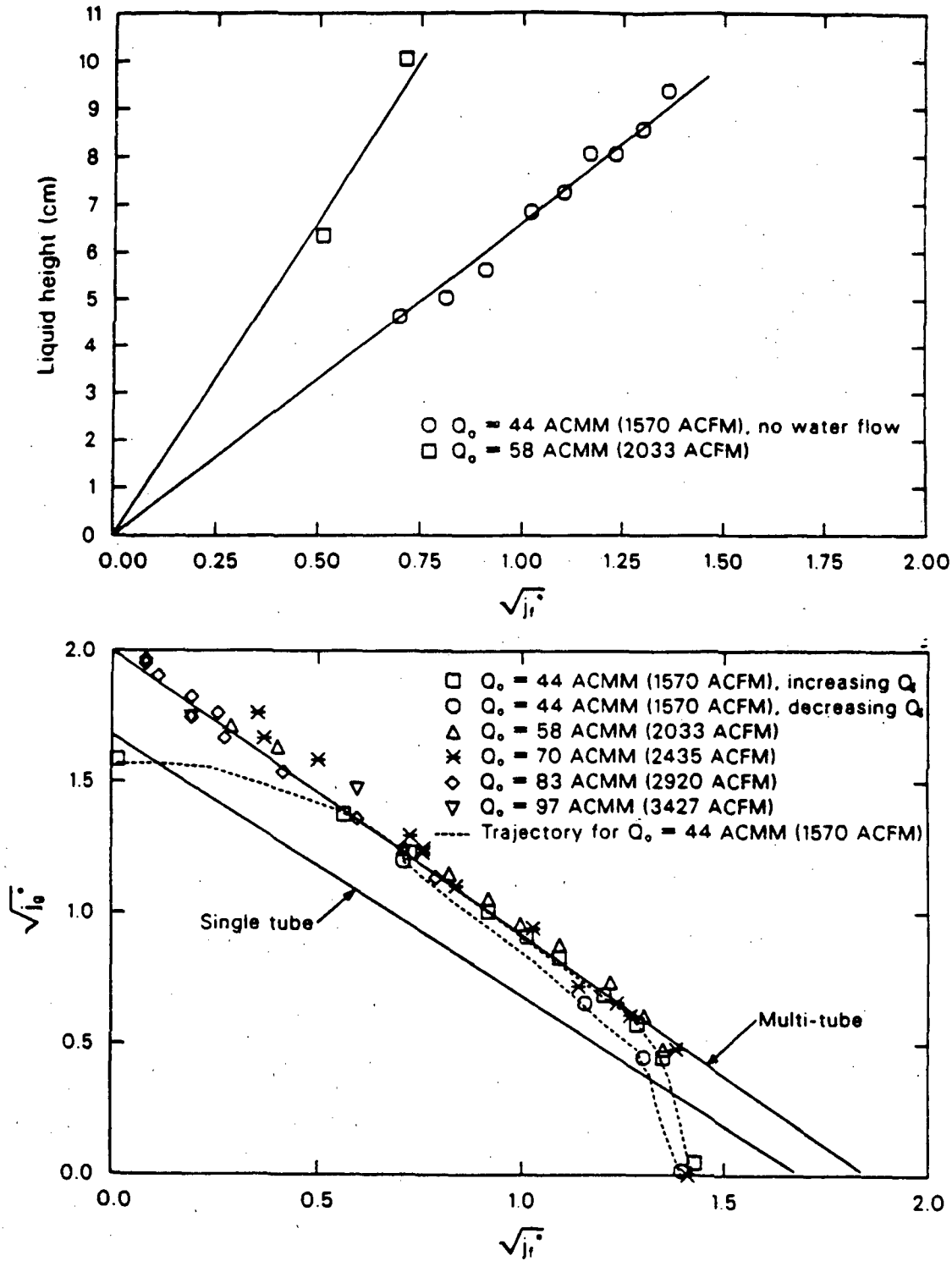


Figure 5. Flooding and liquid height data for the single- and multi-tube facilities.

CCMTL02-7

the hydraulic diameter is much less than the Laplace capillary distance.

For the TSP geometry, the hydraulic diameter is 0.43 cm and the Laplace capillary distance is approximately 6 cm at atmospheric pressure, and 2 cm at 6.89 MPa (1,000 psi).

Top TSP flooding data were also taken in the multitube facility with two TSP's installed and with three TSP's installed. In these experiments, the bypass valves (Figure 4) were opened to simulate the flow around the tubes not represented in the 1/8 sector. Details of the results of these experiments are given in Reference 13. The data obtained gives confidence that the bypass settings were correct for AFW penetration studies (discussed below) where distance from the flooding line is a primary variable.

## AFW FLOW DISTRIBUTION EXPERIMENT RESULTS AND MODELING

The multitube facility was used to map the AFW radial and azimuthal penetration as a function of AFW flow rate and air upflow rate. The mapping was accomplished via visual observations and film flowrate measurements for the 10 tubes fitted with film collection devices. Liquid or froth height was measured for some experiments using a borescope inserted into the transparent polycarbonate tubes. The experiments were performed first with the top TSP plus tubes in place, then with the top two TSP's in place, and finally with all three TSP's in place.

Figure 6 shows tube wetting profiles for various AFW flow rates and no air upflow. The number of tubes wetted is counted from the flow distribution maps and does not include tubes below the unbroached holes in the top TSP. A tube is considered wet if any continuous flow, either falling film or rivulet, is observed. These counts are somewhat subjective, and the accuracy is estimated to be approximately $\pm$10 tubes for liquid flow rates up to 18.9 l/s (300 gpm). Above this flow rate, AFW penetrates through the tube bundle and the number of tubes wetted includes an estimate of additional penetration. The accuracy decreases with increasing flow rate to perhaps only $\pm$50 tubes at 31.6 l/s (500 gpm).

The tube wetting profiles of Figure 6 illustrate that liquid penetration distance is maximum along the AFW injection axis. Liquid (and froth) height is also maximum along the injection axis as is shown in the three dimensional sketch in Figure 7. Above approximately 25 l/s the profile is chaotic and frothy, especially close to the injection location. Liquid (or froth) height is measured at the outside wall and represents the profile of maximum height as the water penetrates the tube bundle. Liquid or froth height falls off with penetration distance and initially with distance in the azimuthal direction and appears typically as bell shaped curves when viewed in either the radial-azimuthal plane or axial-azimuthal plane. The description of liquid height as a bell shaped curve is only approximate because of the occurrence of increasing liquid height at larger azimuthal distances. This occurs because of the formation of smooth waves at lower AFW flow rates, which transition to hydraulic jumps at intermediate flow rates (approximately 10 l/s to 19 l/s), and then transition back to

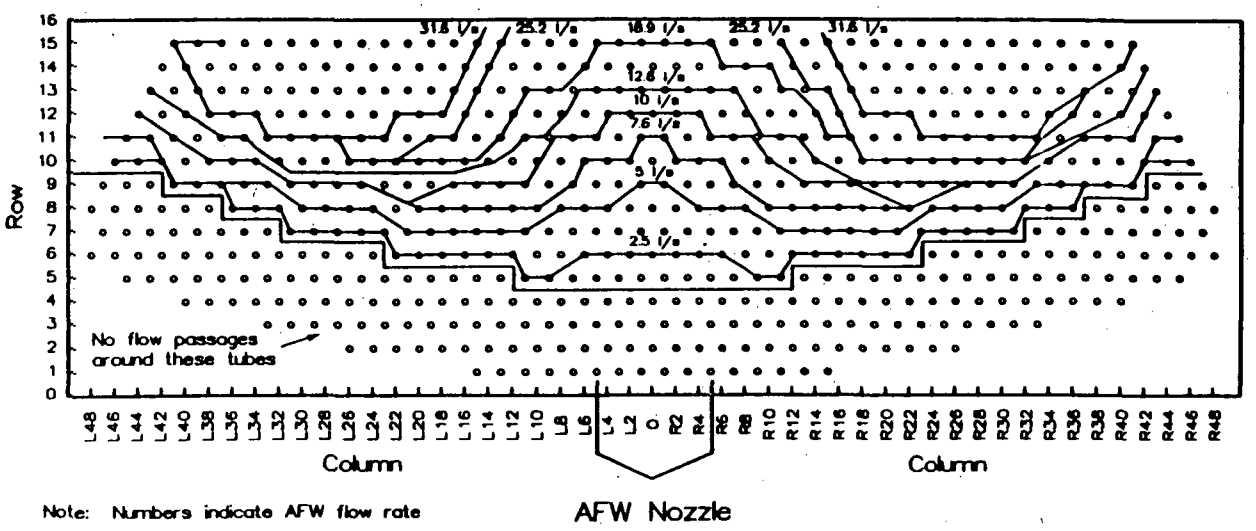


Figure 6. Auxiliary feedwater penetration map for various liquid flows and zero gas flow.

CCK00798

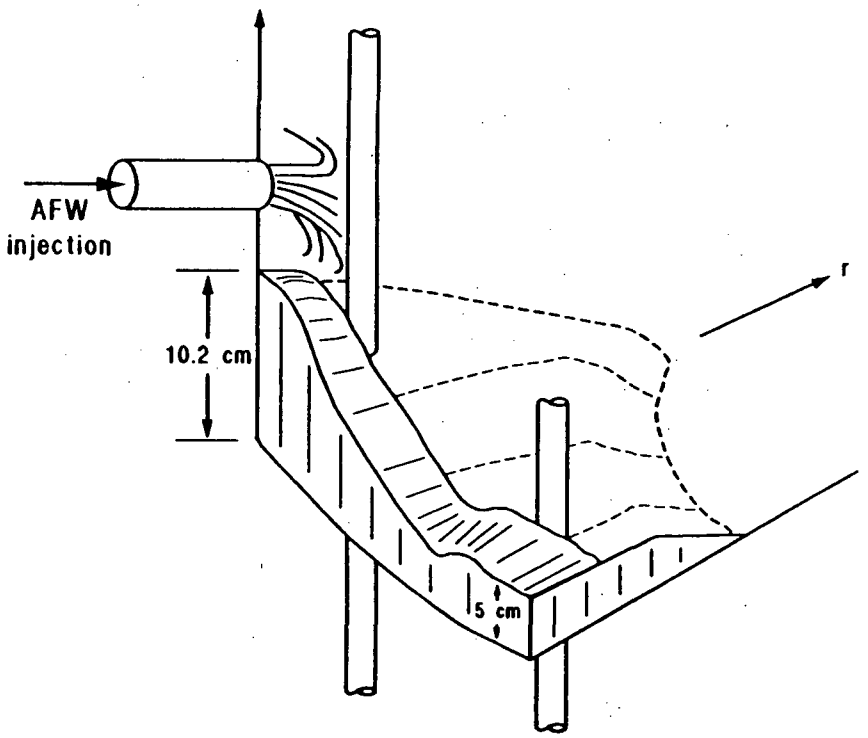


Figure 7. Liquid level profile on the top TSP in the multi-tube facility for 10 l/s AFW injection rate and zero air flow.

waves at higher flow rates. This same wave or hydraulic jump formation is expected in a steam generator, even though our apparatus is bounded by walls at the sector boundaries. Adjacent sectors in a steam generator with similar AFW flow rates should also bound the flow in the azimuthal direction since, from potential flow theory, a wall may be considered to mirror an equal strength source in an adjacent sector.

A fraction of the AFW [measured for several typical flow rates (5 l/s and 12.6 l/s) to be approximately 5%] does not penetrate the tube bundle, but runs down the outside wall through gaps in the TSP-to-wall spacers. The gaps are a feature duplicated from the actual steam generators. Except under flooding conditions, this water falls directly to the liquid pool at the bottom of the steam generator.

A significant feature of the flow distributions is that they are relatively unaffected by the number of TSP's, except for tubes below unbroached holes in the top TSP. Figure 8 shows that the difference in number of tubes wetted are of the order of experimental accuracy. On the other hand, the flow below unbroached holes is observed to be affected by at least the addition of a second TSP. This distribution of liquid spreading is due to the highest liquid flow rates occurring on tubes adjacent to the unbroached holes (spreading increases with flow rate) while the lowest flow rates occur on those tubes at the outer periphery of wetted tubes. The outer periphery defines the number of tubes wetted excluding those below the unbroached holes.

Liquid height is observed to decrease approximately linearly with penetration distance from the unbroached holes, at least away from positions close to the injection location where it is difficult to observe and measure the height directly under the injection nozzle due to air-water frothing and because of visual obstruction by the many rows of tubes. A linear decrease with distance has physical basis and is a result of the derivation of the simple steady-state model of flow distribution with zero gas flow. The model is derived in Reference 13 and is stated here.

The flow distribution model is derived by considering mass continuity and pressure losses for flow in the radial inward and axial downward (above and through tube support plate holes) directions. The final form of the model relates number of tubes wetted, $N_1$, to AFW flow rate, $Q_0$ by the simple expression

$$N_1 = 40.11\ (Q_0)^{2/3} \qquad (3)$$

where $Q_0$ has units of l/s. Equation 3 represents the data well, at least with $Q_0$ less than or equal to 25.25 l/s (400 gpm). Since the number of tubes wetted is based upon our 1/8 sector geometry, if the model is applied to an actual steam generator with injection nozzles in six of eight equally spaced sectors, then the constant in Equation 3 should be multiplied by 6.0.

The model may also be used to calculate the flow rate per tube $Q_t$, at which N tubes have a flow rate equal to or greater than $Q_t$ with the result

$$\frac{Q_t}{Q_o/N_1} = \frac{3}{2}\left(1 - \frac{N}{N_1}\right)^{1/2} = Q_t^* \qquad (4)$$

where

$Q_o/N_1$ = average flow rate per wetted tube

If the falling film-rivulet flow rate transition (which is of primary interest for heat transfer calculations, as discussed in the heat transfer analysis section) is given as $Q_t^*$ and is < 3/2, then the number of tubes, $N_T$, covered by a falling film is

$$\frac{N_T}{N_1} = 1 - \frac{4}{9} Q_T^{*2} \qquad (5)$$

## GAS FLOW INFLUENCE ON AFW FLOW DISTRIBUTION

Experiments were conducted to determine the influence of simulated steam flow on AFW flow distribution. Air flow simulated steam generated by evaporation and boiling from the water flowing down the tubes and from the liquid pool at the bottom of the steam generator. In the experiments an initial air flow rate without AFW injection was set. AFW flow was then increased in steps until the flooding curve was approached. At each point the flow distribution was measured at ten representative locations, and the tube wetting profile mapped. The number of tubes wetted versus AFW flow rate for various air flow rates (including zero air flow) is shown in Figure 8. These data, plus additional data for two TSP's, are shown in relationship to the flooding line in Figure 9.

The regions of influence of the gas and liquid flows on the number of tubes wetted is illustrated in Figure 9 The regions of influence are defined as gas-liquid flow combinations that result in an approximately 10% increase or greater in the number of tubes wetted relative to the zero gas flow experiments. The data shows only a small influence of increasing number of tube support plates on wetting. The majority of this effect occurs with adding the second TSP, with little effect of adding the third.

Figures 8 and 9 illustrate that the number of tubes wetted depends in an exponential fashion on two primary variables, the AFW flow rate, and the distance from the flooding line which in turn is a function of liquid and gas flow rates. These data and observations provide the basis for a non-dimensional correlation of the number of tubes wetted as a function of the two primary variables. The correlation is

$$\frac{N}{N_1} = \mathrm{EXP}\left\{0.1016 \left(\frac{j_f^{*1/2}}{j_{ff}^{*1/2} - j_f^{*1/2}}\right)\left(\frac{1}{j_{ff}^{*2.0}}\right)\right\} \qquad (6)$$

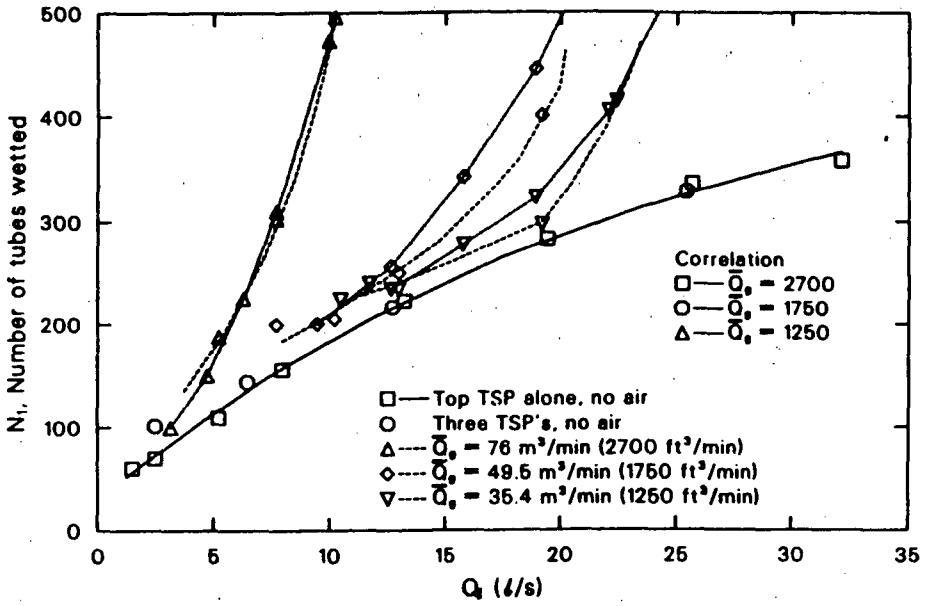


Figure 8. Number of tubes wetted versus AFW flow rate with all three TSPs in place and results of Equation 5.

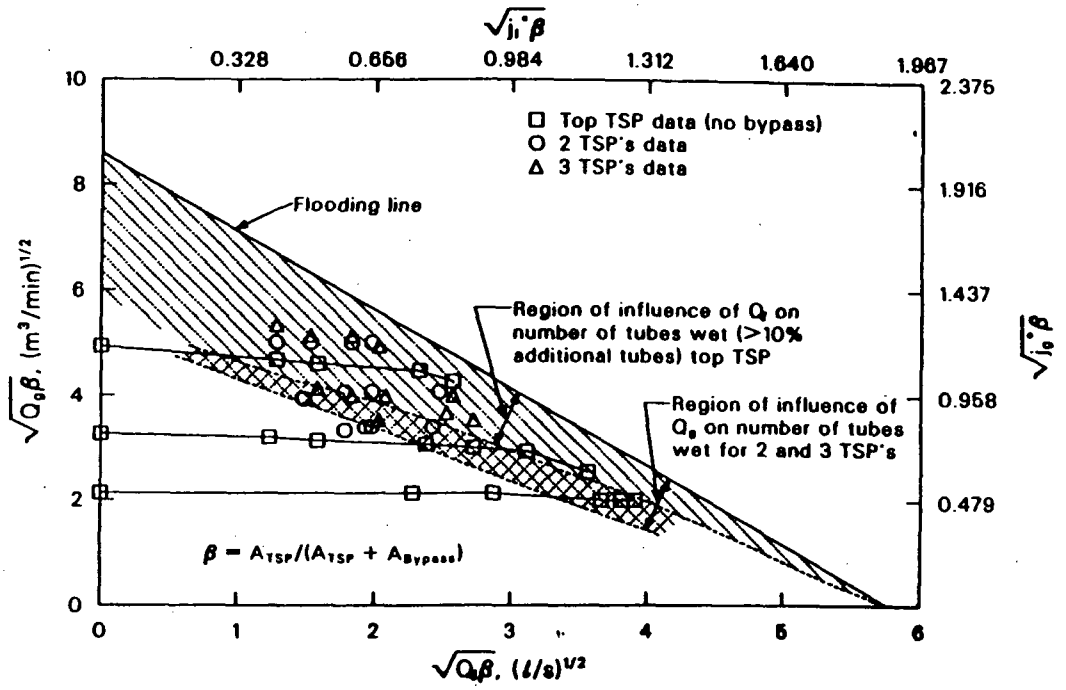


Figure 9. Influence of gas upflow on number of tubes wetted in the multi-tube facility.

where $j_{ff}^*$ is the non-dimensional liquid flooding rate corresponding to $j_j^*$ and $N_1$ is given in Equation 3. From our multitube flooding data (the flooding line in Figure 5),

$$j_{ff}^{*1/2} = 1.89(1 - j_g^{*1/2}/2.06) \quad (7)$$

The correlation is compared with the data for three TSP's in Figure 8. The correlation predicts the number of tubes wetted to within experiment accuracy. The correlation may be applied to an actual steam generator with probably a small underestimate of number of tubes wetted for 15 TSP's rather than 3.

## HEAT TRANSFER EXPERIMENTS

Experiments were performed using the single tube apparatus to determine the heat transfer characteristics of steam generator tubes under typical AFW flow conditions. Approximately 100 experiments were conducted with varying primary and secondary flow rates, inlet temperatures, and steam or air gas flow rates. The ranges of flow and temperature conditions were chosen to be as typical of actual steam generator conditions as possible. Primary flow rates were varied between 20 g/s to 70 g/s, and secondary flow rates between 1.6 g/s to 72 g/s. Primary fluid inlet temperatures were varied between 375 K (216 F) and 430 K (315 F), and secondary inlet temperatures between 296 K ($73^oF$) and 369 K ($205^oF$).

A primary flow rate of 22 g/s corresponds to a typical natural circulation velocity of 0.5 m/s in the hot leg. A secondary flow rate of approximately 28 g/s corresponds to the average flow per tube for a typical maximum AFW injection rate of 12.7 l/s (200 gpm) per injection nozzle spread over the 225 tubes wetted below broached holes in a 1/8 sector plus the 212 tubes below unbroached holes. The number of tubes wetted is calculated from Equation 3, or taken from Figure 8 for zero gas flow conditions. If the flow is spread evenly over the 1/8 sector by flooding, the flow rate per tube is reduced to approximately 6.5 g/s.

Additional experiments were performed to examine the influence of surface tension, gas flow, steam condensation, and flooding on tube heat transfer. The surface tension was reduced in several experiments to approximately that of water at 6.89 MPa (1,000 psi) by the addition of a wetting agent (Kodak Photoflow solution, diluted 1 ml per 1 of water). The effects of gas flow and steam condensation were investigated by first running heat transfer experiments with zero gas flow, and then repeating the experiments, first with steam flow and then with air flow. The steam or air flow rates used in the experiments were typically 50% to 75% of that required to flood the TSP hole. Increasing the gas flow rate to flooding provided the additional data on heat transfer under flooded conditions.

### Representative Heat Transfer Data

Data from three representative experiments without gas flow are presented in Figures 10, 11, and 12. The first figure shows data from a

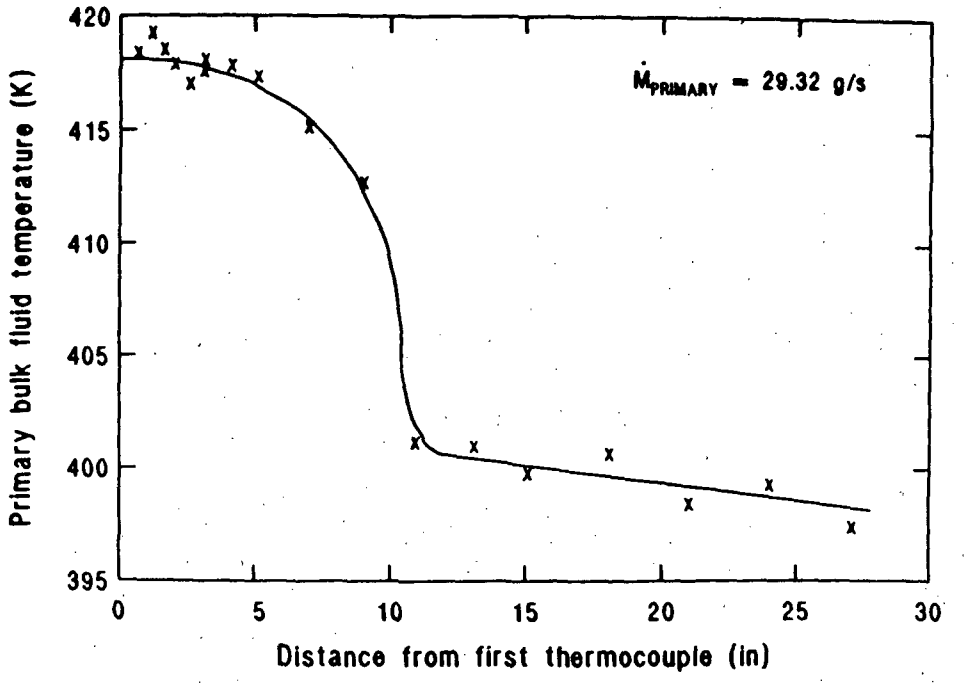


Figure 10. Primary fluid temperatures for a secondary flow rate of 30.3 g/s.

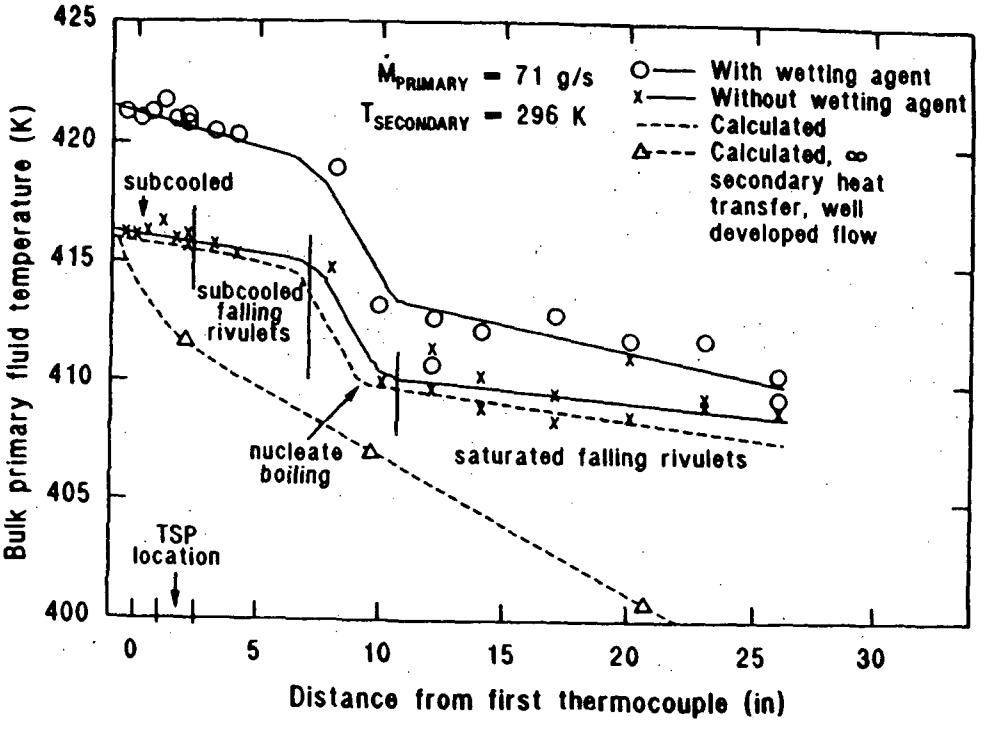


Figure 11. Measured and calculated primary fluid temperatures for a secondary flow rate of 12 g/s.

30.3 g/s secondary flow experiment, the second from a lower secondary flow (12 g/s) experiment, and the third from a low secondary flow experiment (1.7 g/s). Figure 11 also contains data from a similar experiment (with the exception of initial temperature) in which surface tension was reduced a factor of three by the addition of wetting agent.

The effects of gas flow, and therefore the effects of steam condensation, on heat transfer are illustrated in Figures 13 and 14. Figure 13 presents data from three otherwise similiar experiments that were performed with no gas flow (except that generated by evaporation), with steam flow, and with air flow respectively. Figure 14 illustrates the influence of flooding on heat transfer in comparison with an unflooded, but otherwise identical, experiment. The effects of flooding with air versus flooding with steam are also shown.

## Heat Transfer Phenomena Observed

The three experiments with no added gas flow shown in Figures 10, 11 and 12 are distinctly characterized by the secondary flow rate and distribution on the tube. The secondary water in the high flow rate experiment fully coats the outside of the tube and flows as a thin turbulent film. The water in the two lower flow rate experiments breaks into three rivulets at the TSP and snakes down the tube as shown in Figure 15, a photograph for a low flow experiment. The three rivulets correspond to the lobes of the broached holes and flow down below the positions of closest contact of the lobes with the tube wall since the water is attracted to these positions by surface tension forces. The rivulet flow thus provides significantly reduced heat transfer area to the secondary liquid compared with the fully wet tube.

Rivulet flow heat transfer is complicated by azimuthally varying wall temperatures and heat transfer rates. It is observed that a rivulet at one axial position may flow with no boiling while another rivulet at the same axial position will simultaneously boil. A simplified heat transfer analysis treating the wall as a rectangular fin confirms that the azimuthal conduction is small compared to the radial conduction. The conclusion reached is that there is a considerable variation in the tube wall temperature in the azimuthal direction and that the heat transfer can be treated as two parallel paths. One path is from the primary fluid through the wall to the area covered by rivulets and the other to the area covered by gas or vapor.

Typical heat transfer regimes observed in the no added gas flow experiments are (a) convection to low velocity subcooled or saturated water above the top TSP, (b) convection to subcooled or saturated water within the TSP holes augmented by conduction to the TSP at points of contact (the water may have steam from evaporated liquid bubbling upwards through it), (c) convection to falling film or rivulets below the TSP, transitioning to, (d) nucleate boiling, and changing back to (e) falling film or rivulet convection. If the nucleate boiling is sufficiently intense, the secondary fluid is observed to sputter from the tube. If boiling within and above the

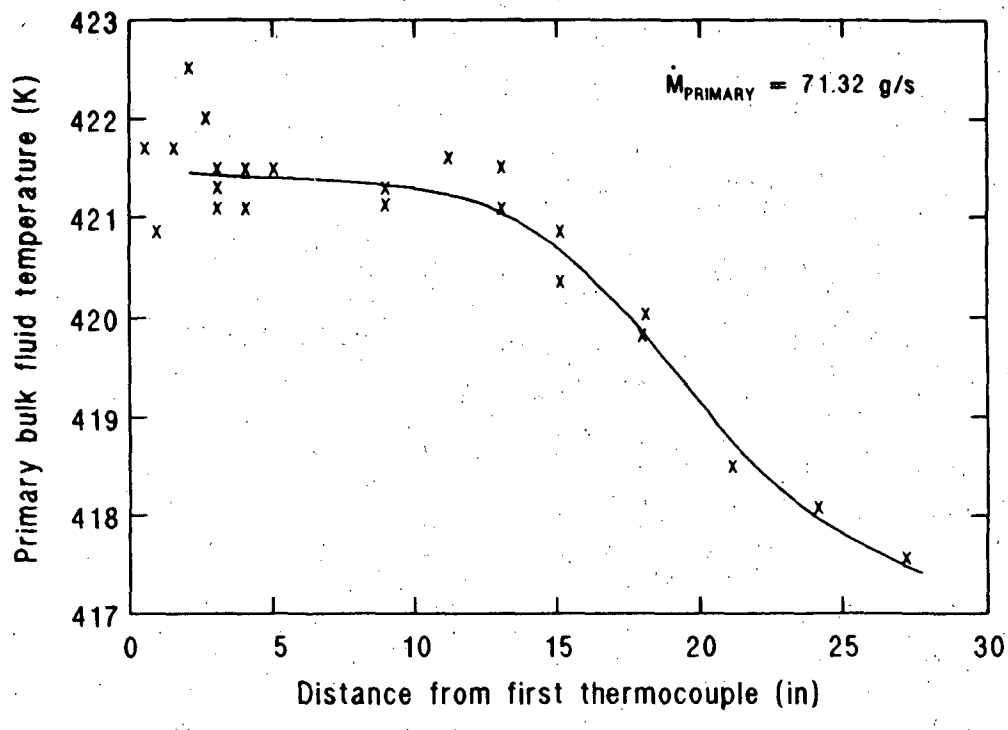


Figure 12. Measured primary fluid temperatures for a secondary flow rate of 1.7 g/s.

CK00637

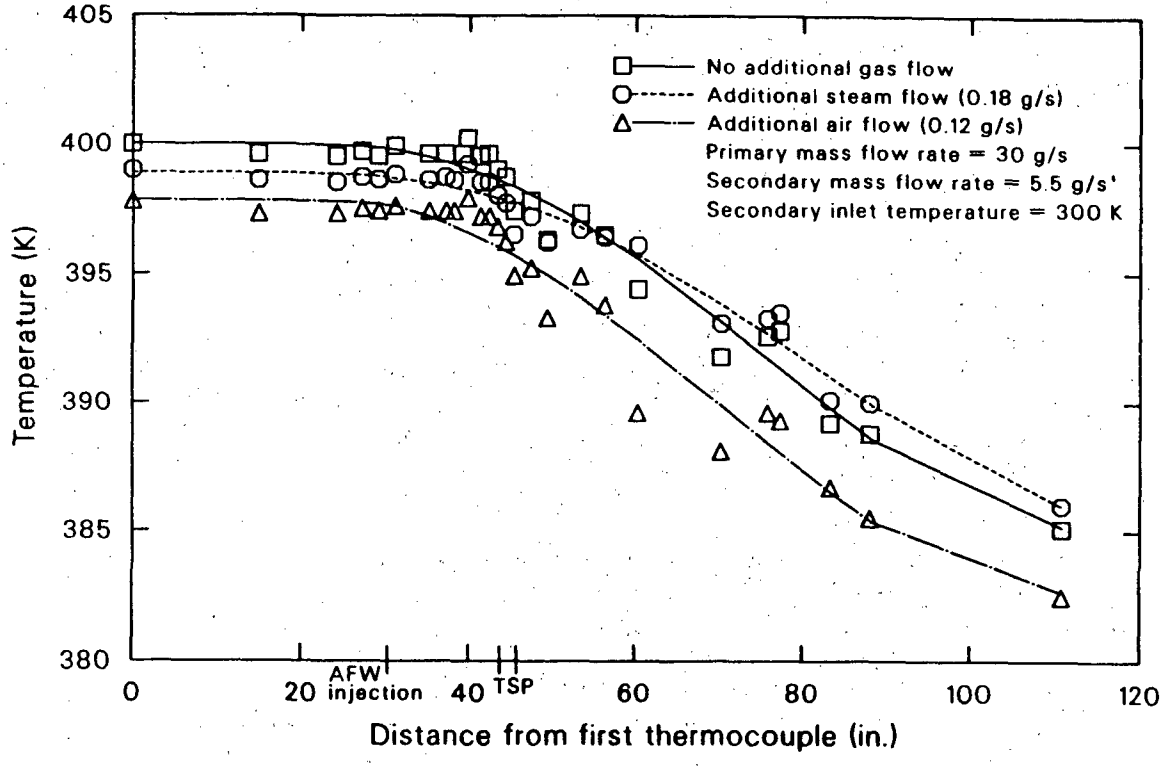


Figure 13. Measured primary fluid temperatures for the various conditions listed.

CCM8M01-4

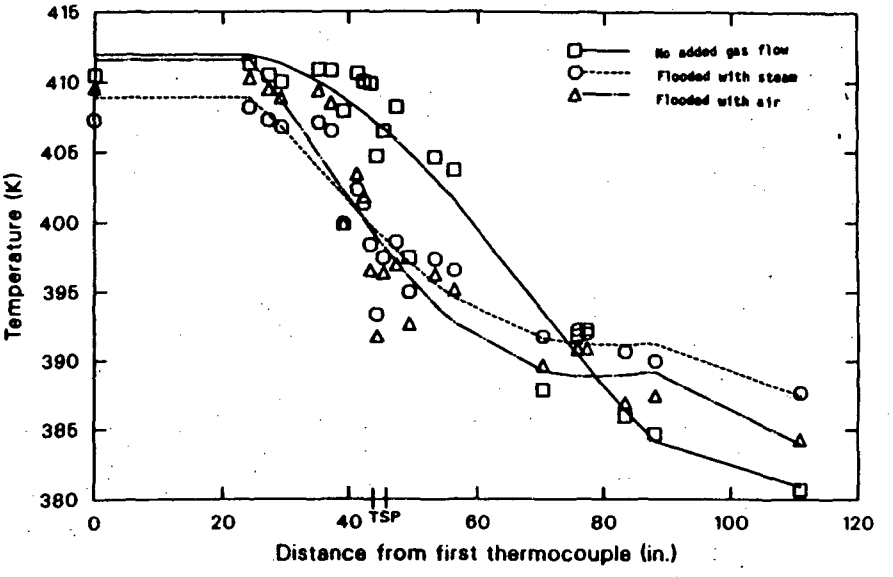


Figure 14. Measured primary fluid temperatures for unflooded conditions and for flooded conditions with air flow or steam flow.

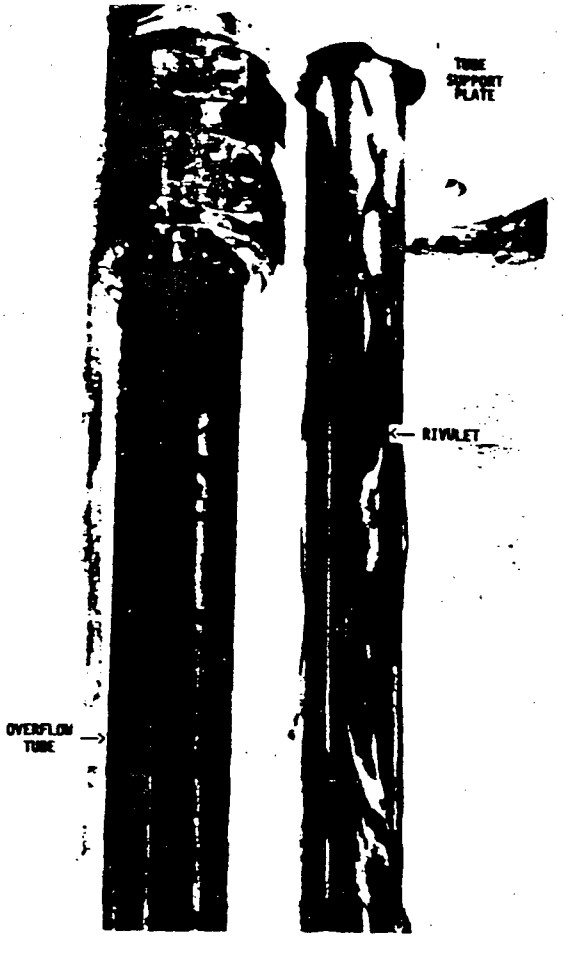


Figure 15. Photograph of rivulet flow down the steam generator tube.

TSP holes is sufficiently intense, the TSP may flood completely (zero liquid penetration) even without added gas flow or steam from evaporation below the TSP. This complete flooding condition is achieved in our experiments if the primary inlet temperature is above approximately 425 K (306$^{o}$F).

The addition of gas, either air or steam, does not significantly change tube heat transfer rates in our experiments if the gas flow rate is below that for flooding (and therefore, below that for liquid buildup above the TSP). This is illustrated in Figure 13, where primary bulk fluid temperature profiles are compared for zero added flow, for added steam flow, and for added air flow. Added gas flow is between 50% to 75% of that necessary for flooding, and is therefore not insignificant. The added steam flow was intended to increase condensation heat transfer in comparison with the zero added flow case, and the added air flow was intended to decrease condensation heat transfer. Because of the small effect of gas flow on heat transfer, it is concluded that steam condensation is not significant in these experiments. Condensation heat transfer is not significant because steam enthalpy flow rates from evaporated liquid or added steam flow rates up to and including those values for flooding, are typically much less than tube heat transfer rates (due in turn to much higher secondary liquid mass flow rates than steam mass flow rates), and because water on the majority of the tube surface below the top TSP is saturated rather than subcooled. Because of the predominately saturated conditions below the top TSP, evaporative cooling is expected to be a dominant heat transfer mechanism. The convection coefficient for an evaporating falling film is similar to that for a condensing falling film at the same Reynold's number since the outside film temperature in both cases is essentially saturation temperature, as investigated by Chun and Seban[14]. This correspondence is employed in the analytical modeling.

If flooding occurs above the top TSP, heat transfer to the subcooled fluid pool is significant (Figure 14). The difference in heat transfer for flooding with air flow versus flooding with steam flow is small. Therefore, although almost all of the added steam flow is condensed in the subcooled liquid pool above the TSP (few steam bubbles are seen to rise to the top liquid surface), the rate of addition of latent plus sensible heat from the steam is small compared with that from tube to liquid pool heat transfer.

The effect of reduced surface tension on rivulet flow is to enhance heat transfer (Figure 11). This occurs because the rivulets spread out and thin and cover a wider area if the surface tension is reduced. The height of a liquid rivulet varies with the square root of surface tension (Towell and Rothfeld[15]). In our comparative experiments, the surface tension was reduced by a factor of approximately 3, thereby providing a wetted area increase of approximately 1.7. This is close to the ratio of overall heat transfer rates in the two experiments (equal to the ratio of primary fluid enthalpy change of 1.6 in the two experiments).

Both surface tension and viscosity of the secondary fluid decrease with temperature. The result is increased rivulet spreading with increased temperature. The transition between rivulet flow and a falling film that fully covers the tube below the TSP (water is initially channeled into

three rivulets that then join to coat the tube) occurs at approximately 18 g/s secondary flow rate for an inlet temperature of 296 K (70°F). The transition flow rate decreases to approximately 11 g/s at 369 K (205°F), and will be lower yet at full temperature and pressure steam generator conditions. Simplified models exist for the rivulet/film flow transition, such as that of Hartley and Murgatroyd,[16] which formulates the transition flow rate per unit perimeter ($\Gamma$) as a function of liquid density ($\rho_f$), surface tension ($\sigma$), dynamic viscosity ($\mu$), and surface contact angle ($\theta$). Their equation is based on a force criterion with the assumption that the film flows isothermally, which appears not to be the case. The influence of wall heat flux is to increase the transition flow rate, as shown by Hsu et al.[17]. The initial channeling of flow below the TSP into rivulets and the elevated temperatures of dry patches on the tube result in an actual transition flow rate higher by at least a factor of four than calculated by the Hartley and Murgatroyd model using estimated contact angles of between 45° and 75°. The isothermal model does however, predict the correct trend of wetting flow rate decrease with secondary temperature increase for these experiments.

## Heat Transfer Analysis

A computer program that models steam generator tube heat transfer has been developed and is being used to analyze these experiments to test the applicability of various heat transfer models. The analysis work is directed toward the ultimate goal of developing fluid flow and heat transfer models for inclusion in the RELAP5 or TRAC system codes. In the model, the tube heat transfer is considered one dimensional and the flow is assumed to be steady state. For calculations, the tube, primary fluid, and secondary fluid are divided into evenly spaced axial increments represented by nodes with spacing of 2.54 cm along the tube length. At each node the local primary and secondary heat convection coefficients, primary and secondary bulk fluid temperatures, secondary liquid flow rate and evaporated steam flow rate, radial conduction heat transfer, and wall superheat are calculated. Heat transfer models used in the program include Dittus-Boelter (as given in Kays[18]) for the primary flow, and for falling film (evaporation or condensation), Labuntsov[19] for film Reynolds number less than 1280 and Chen[20] for Reynolds number > 1280 (the transition recommended by Chen).

For nucleate boiling, a primary side thermal entry length solution suggested by Kays[18] is used to account for the sudden increase in heat transfer rate (note that the temperature slope in the boiling region is steeper than the slope for the infinite secondary heat transfer with well developed primary temperature profiles). The onset of nucleate boiling is specified as the axial position where the secondary fluid reaches saturation.

For rivulet flow, the overall thermal conductance, defined as the reciprocal of the sum of primary convection resistance plus conduction resistance, plus secondary convection resistance (calculated on the basis of a fully wet periphery) is multiplied by an estimated fraction of rod

periphery wetted below the TSP (0.4 for the calculation shown in Figure 11). The heat transfer per unit perimeter (q) is then given by

$$q = U\,(T_{primary} - T_{secondary})\,\frac{P_{wet}}{P} \qquad (8)$$

where

$$U = \frac{1}{\frac{D_o}{D_i h_i} + \frac{D_o}{2k}\ln\frac{D_o}{D_i} + \frac{1}{h_o}}$$

Thermal conductance is plotted in Figure 16 as a function of tube outside convection coefficient for steady state flow with typical experiment and full pressure conditions. The figure illustrates the relative effectiveness and calculational sensitivity of the various heat transfer regimes. The results in the figure show that proper calculation of the falling film convection coefficient is more important than the heat transfer coefficient for nucleate boiling since, for nucleate boiling, the heat transfer coefficient $h_o$, over a broad range, has only a small effect on overall conductance.

The calculations in Figure 11 show good agreement with the data. The agreement is achieved by varying the wetted flow area ratio until the calculated temperature profile matches the measured data. The ratio chosen, 0.4, is reasonable since calculations also show good agreement with data from other experiments, including those for fully wetted tubes.

This simple heat transfer analysis indicates that a three region model of OTSG heat transfer is appropriate and reasonable for inclusion in RELAP5 or TRAC. The three regions would describe steam generator tubes that are (a) fully wet with falling film, (b) partially wet with rivulet flow, or (c) completely dry. This heat transfer model coupled with the flooding and AFW spreading models described above are presently being incorporated into the RELAP5 computer code.

## CONCLUSIONS

A series of experiments were completed to quantify and describe the phenomena of AFW flow distribution in a B&W type steam generator. Flooding experiments were conducted for the top TSP alone, and in conjunction with the second and third TSP's in place. The top TSP preferentially floods due to reduced flow area.

The flooding data is similar to that of other researchers for multi-hole plates with similar hydraulic diameter round holes. The data may be represented by either a Wallis or Kutateladze type correlation. The Wallis correlation is more appropriate due to the small hydraulic diameter of the broached holes.

Experiments were conducted to determine AFW distribution without air flow. Liquid penetration distance and liquid height are maximum along the

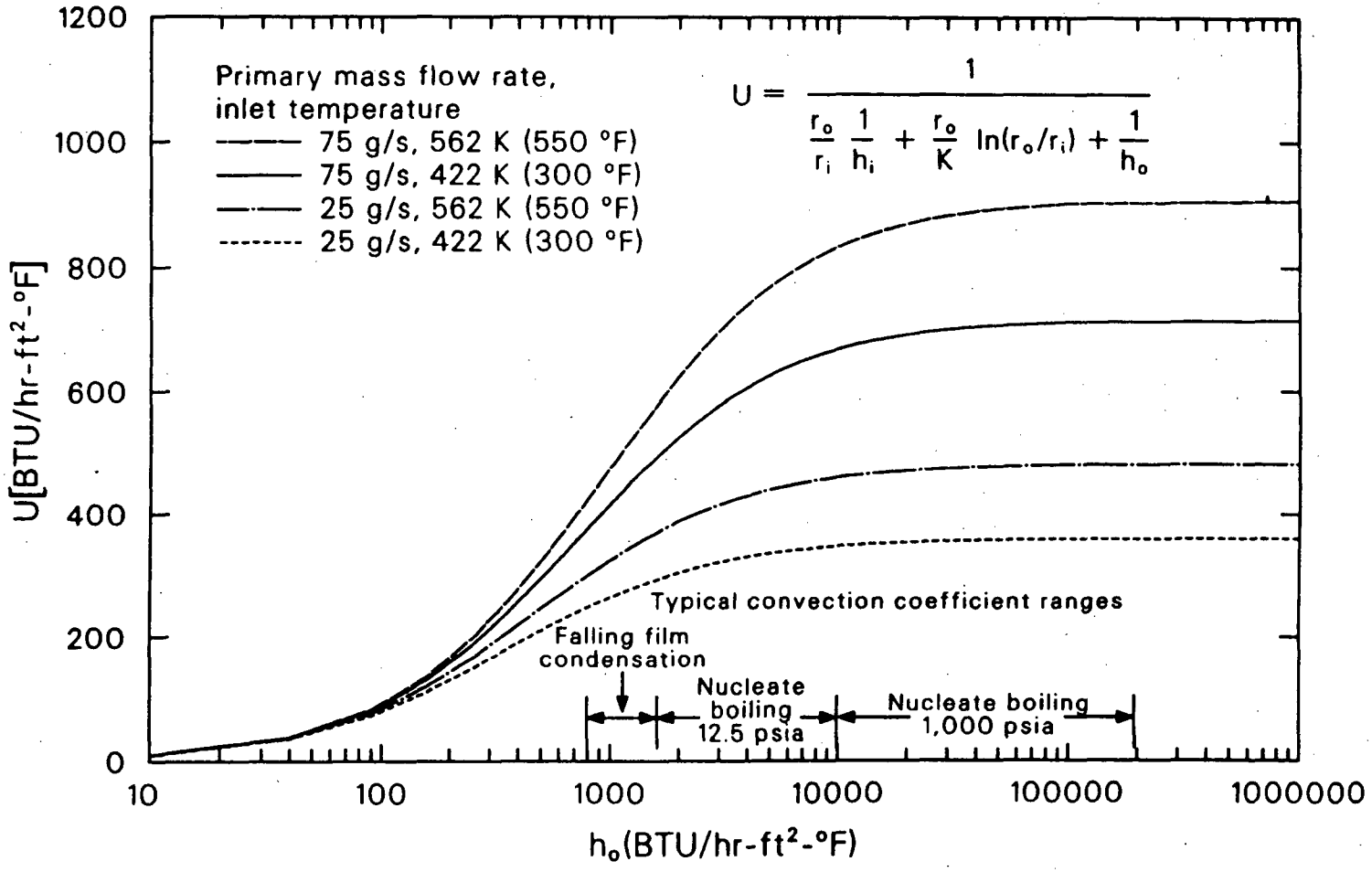


Figure 16. Steam generator tube thermal conductance as a function of outside convection coefficient for various conditions.

CCMGM01-1

AFW injection axis. Penetration falls off in the azimuthal direction, and is described by a bell shaped curve. Liquid height decreases approximately linearly with distance from the unbroached holes. The unbroached holes promote liquid spreading in the azimuthal direction. A small fraction of the AFW runs down gaps adjacent to the bundle outside wall and thus does not penetrate the bundle.

AFW penetration is unaffected by the number of TSP's for the zero air flow experiments for flow down tubes with broached holes in the top TSP. Some spreading with increased number of TSP's is noted for tubes below the unbroached holes in the top TSP.

A flow distribution model was formulated from mass conservation and pressure loss equations for steady-state flow. The model employs an empirical constant derived from the data.

The number of tubes wetted is primarily a function of liquid flow rate and the distance from the flooding line. More tubes are wetted as the flooding line is approached. An empirical correlation for the effects of gas flow rate has been developed.

Fluid flow and heat transfer experiments representing OTSG behavior during AFW injection were conducted in a single tube steam/air-water apparatus. Heat transfer data for typical primary flow and AFW flow conditions was obtained and the heat transfer regimes identified.

Tube wetting phenomena was investigated and described. Of primary interest is the formation of rivulets rather than a thin film at lower flow rates. The rivulet/falling film transition is being quantified.

Analysis of the heat transfer data shows that a one-dimensional model of steam generator tubes is capable of reasonable heat transfer calculations if appropriate models are employed. Modeling rivulet flow heat transfer can be accomplished by multiplying the overall thermal conductance calculated for a fully wet tube by the fraction of the tube perimeter wet. Models based on the results of this study are currently being implemented in the RELAP5 computer code.

## NOMENCLATURE

$A_{TSP}$ - flow area in the tubed region of the top tube support plate with tubes in place

$A_{BYPASS}$ - flow area in the bypass region of the top tube support plate with tubes in place

C - constant in Wallis flooding correlation

D - characteristic dimension for Wallis flooding correlation

$D_i$ - tube inside diameter

$D_o$ - tube outside diameter

$g$ - acceleration due to gravity

$h_i$ - tube inside wall convection coefficient

$h_o$ - tube outside wall convection coefficient

$j_g$ - gas superficial velocity

$j_g^*$ - nondimensional gas superficial velocity, $j_g [\rho_g/(gD\Delta\rho)]^{1/2}$

$j_f$ - liquid superficial velocity

$j_f^*$ - nondimensional liquid superficial velocity, $j_f[\rho_g/(gD\Delta\rho)]^{1/2}$

$k$ - wall thermal conductivity

$K$ - constant in Kutateladze flooding correlation

$K_g$ - nondimensional liquid superficial velocity, $j_g[\rho_g 2/(\tau g\Delta\rho)]^{1/4}$

$K_f$ - nondimensional liquid superficial velocity, $j_f[\rho_f 2/(\tau g\Delta\rho)]^{1/4}$

$N$ - number of tubes wet with gas flow

$N_1$ - number of tubes wet without gas flow

$P$ - tube perimeter

$P_{wet}$ - tube wetted perimeter

$Q_f$ - liquid volumetric flow rate

$Q_g$ - gas volumetric flow rate

$Q_{go}$ - initial gas volumetric flow rate

$Q_o$ - auxiliary feedwater total flow rate

$Q_t$ - flow rate per tube

$Q_t^*$ - non-dimensional flow rate per tube

$T$ - temperature

$U$ - thermal conductance

$\rho_g$ - gas density

$\rho_f$ - water density

$\Delta\rho$ - water density minus air density

$\Gamma$ - volumetric flow rate per unit perimeter

$\sigma$ - surface tension

$\mu$ - dynamic viscosity

$\theta$ - wetting angle

## REFERENCES


1. D. L. Reeder, LOFT System and Test Description (5.5 ft Nuclear Core 1 LOCE's, NUREG/CR-0247, TREE-1208, July 1978.

2. L. J. Ball, Semiscale Program Description, TREE-NUREG-1210, May 1978.

3. A. G. Stephens, BWR Full Integral Simulation Test (FIST) Program Facility Description Report, NUREG/CR-2576, September 1984.

4. D. K. Felde, et al., Facility Description, THTF MOD3 ORNL BCHT Separate Effects Program, ORNL/TM7842, September 1982.

5. Multi-Loop Integral System Test (MIST) Facility Specification, NRC-04-83-168, Babcock and Wilcox Company, Lynchburg, VA, October 1985.

6. J. P. Sursock and M. W. Young (eds), Coordination of Support Projects for the B&W Integral System Test Program, NUREG-1163, March 1987.

7. Supporting Data for AFT (EFW) Models - Auxiliary Feedwater Axial Flow Distribution, B&W Document #12-1132543-00, April 1982.

8. Supporting Data for AFW (EFW) Models - Auxiliary Feedwater Penetrations, B&W Document #12-1132513-00, April 1982.

9. G. B. Wallis, One-Dimensional Two-Phase Flow, McGraw-Hill, New York, 1969.

10. O. L. Pushkina and Y. L. Sorokin, "Breakdown of Liquid Film Motion in Vertical Tubes," Heat Transfer - Soviet Research 1, 56, 1969.

11. S. G. Bankoff, R. S. Tankin, M. C. Yuen, and C. L. Hsieh, "Countercurrent Flow of Air/Water and Steam/Water Through a Horizontal Perforated Plate," Int. J. Heat Mass Transfer, 24, 8, pp. 1381-1395, 1981.

12. K. H. Sun, "Flooding Correlations for BWR Bundle Upper Tieplates and

Bottom Side-Entry Orifices," Second Multiphase Flow and Heat Transfer Symposium - Workshop, Miami Beach, Florida, 1979.

13. K. G. Condie, T. K. Larson, and G. E. McCreery, "Flooding, AFW Penetration, and Visual Investigations in Scaled Once Through Steam Generator Facilities," to be presented at the 25th ASME/AIChE National Heat Transfer Conference, Houston, Texas, July 1988.

14. K. R. Chun, and R. A. Seban, "Heat Transfer Evaporating Liquid Filing," J. Heat Transfer, November 1971.

15. G. D. Towell and L. B. Rothfeld, "Hydrodynamics of Rivulet Flow," AIChE J., September 1966.

16. D. E. Hartley and E. Murgatroyd, "Criteria for the Breakup of Thin Liquid Layers Flowing Isothermally Over a Solid Surface," Int. J. Heat Mass Transfer, 7, 1964.

17. Y. Y. Hsu, F. F. Simon, and J. F. Lad, "Destruction of a Thin Liquid Film Flowing Over a Heating Surface," Chemical Engineering Progress Series, 61, 1965.

18. W. M. Kays, Convective Heat and Mass Transfer, New York, McGraw-Hill, 1966.

19. D. A. Labuntsov, "Heat Transfer in Condensation of Pure Steam on Vertical Surface and Horizontal Tubes," Teploenergetika, 4, 1957.

20. S. J. Chen, "Turbulent Film Condensation on a Vertical Plate," Proceedings of the Eight International heat Transfer Conference, 1966, Hemisphere, New York.

# Two-phase Flow Characteristic of Inverted Bubbly, Slug and Annular Flow in Post-Critical Heat Flux Region

by

M. Ishii
School of Nuclear Engineering
Purdue University
West Lafayette, Indiana

and

James P. Denten
Reactor Analysis and Safety Division
Argonne National Laboratory
Argonne, Illinois

## ABSTRACT

Inverted annular flow can be visualized as a liquid jet-like core surrounded by a vapor annulus. While many analytical and experimental studies of heat transfer in this regime have been performed, there is very little understanding of the basic hydrodynamics of the post-CHF flow field. However, a recent experimental study was done that was able to successfully investigate the effects of various steady-state inlet flow parameters on the post-CHF hydrodynamics of the film boiling of a single phase liquid jet. This study was carried out by means of a visual photographic analysis of an idealized single phase core inverted annular flow initial geometry (single phase liquid jet core surrounded by a coaxial annulus of gas). In order to extend this study, a subsequent flow visualization of an idealized two-phase core inverted annular flow geometry (two-phase central jet core, surrounded by a coaxial annulus of gas) was carried out. The objective of this second experimental study was to investigate the effect of steady-state inlet, pre-CHF two-phase jet core parameters on the hydrodynamics of the post-CHF flow field. In actual film boiling situations, two-phase flows with net positive qualities at the CHF point are encountered. Thus, the focus of the present experimental study was on the inverted bubbly, slug, and annular flow fields in the post dryout film boiling region.

Observed post dryout hydrodynamic behavior is reported. A correlation for the axial extent of the transition flow pattern between inverted annular and dispersed droplet flow (the agitated regime) is developed. It is shown to depend strongly on inlet jet core parameters and jet void fraction at the dryout point.

## INTRODUCTION

Inverted annular flow, which consists of a liquid core surrounded by a vapor annulus as shown in Fig. 1, is of considerable importance in the areas of LWR accident analysis, cryogenic heat transfer, and other confined, low quality film boiling applications. While many analytical and experimental heat transfer studies for this flow situation have been carried out, knowledge of the relevant hydrodynamics of the post-CHF flow field is still quite limited. Due to the coupled thermo-hydraulic nature of confined flow film boiling phenomena, the determination and characterization of the various two-phase flow regimes both before and after CHF become important in determining heat transfer (as well as mass and momentum transfer). While pre-CHF flow regimes may be predicted by using criteria developed by Ishii [1] and Mishima and Ishii [2], a more thorough understanding of the hydrodynamics of the post-CHF flow field is necessary in order to adequately assess post-CHF heat transfer.

The primary objective of this experimental study was to determine and characterize the various post-CHF two-phase flow regimes for a given inlet pre-CHF two-phase flow regime. A previous single phase core inverted annular flow experimental study [3] was carried out to determine the effects of inlet liquid jet core and annulus gas flow parameters on the flow regimes of the post-CHF region. To extend this work, and gain a more thorough understanding of the hydrodynamics of the post-CHF flow field, the present experimental study was carried out to determine the effects of liquid plus gas two-phase core inlet flow parameters on the resulting post-CHF two-phase flow regimes.

A detailed review of the state of the arts is given by DeJarlais and Ishii [3]. Some earlier reviews can be found in Refs. [4] to [13]. Flow visualization and hydrodynamic studies have been carried out by a number of researchers [14-39]. However, a reliable hydrodynamic model has not been developed previously. The present work, together with the results previously reported [3], has lead to a detailed two-phase flow regime transition criteria and hydrodynamic characterization for the post dryout region.

## POST DRYOUT TWO-PHASE FLOW EXPERIMENT

### Experimental Facility

An experimental test facility was previously constructed to study steady-state film boiling of liquid Freon 113 in a transparent quartz tube test section. The inlet of this test section was so designed as to initiate an idealized single phase core inverted annular flow geometry (single phase liquid core surrounded by a coaxial annulus of gas) with measurable steady-state inlet fluid and gas properties and flow rates at the entrance to the heated test section. This same apparatus was modified in order to initiate an idealized two-phase core inverted annular flow geometry (two-phase liquid plus gas central core, surrounded by a coaxial annulus of gas) with measurable steady-state inlet flow conditions at the heated test section entrance. Since a very elaborate description of the experimental apparatus is given elsewhere [3], following is a brief summary of the modified experimental facility.

A schematic of the modified steady-state film boiling facility is shown in Fig. 2. With the arrangement shown, pre-CHF two-phase flow regimes could be established in the jet core nozzle and subsequently injected into the heated test section. The result is an idealized two-phase core film boiling initial flow geometry, with measurable steady-state inlet flow parameters at the CHF or dryout point at the jet nozzle exit.

The heated portion of the test section, 1.0 m in length, consisted of two coaxial quartz tubes, fashioned in much the same manner as Liebig or West condensers (see Fig. 3). The dimensions of the inner and outer quartz tubes were 16x13.6 mm OD/ID and 35x31 mm OD/ID, respectively, giving an annular gap of 31x16 mm OD/ID through which a high temperature heat transfer fluid (Syltherm 800 by Dow Corning) was circulated. The inner quartz tube extended beyond the outer quartz tube to provide an unheated entrance length of 150 mm.

The two-phase jet core injection system consisted of a small bubbler chamber, a sight glass, and a circular jet core injection nozzle (Fig. 3). To establish pre-CHF two-phase flow regimes in the jet injection nozzle, a metered gas flow (nitrogen in all trials) was introduced through a 15 μm porous plate at the bottom of the bubbler chamber, while liquid Freon 113 (Trichlorotrifluoroethane) was introduced through four 0.25 inch holes drilled into a 0.50 inch liquid inlet tube entering the side of the chamber. A Jacoby-Turbox sight tube, 0.50 inch ID-window two inches long, directly above the bubbler chamber allowed visual and photographic analysis of the two-phase flow within the nozzle. The two-phase jet core (Freon 113 liquid/ nitrogen gas in up flow) was discharged into the heated test section through a thin-walled stainless steel injection nozzle (10.8 mm ID), the nozzle being precisely centered with respect to the inner diameter of the heated quartz tube. Annulus gas (nitrogen in all trials) was introduced into the heated test section via the annular gap between the stainless steel nozzle and the inner quartz tube of the test section.

Jet liquid flow rates were measured with a turbine flowmeter, while jet gas and annular gas flow rates were measured with rotameters. Pressure taps were located at the exits of the jet gas and the annular gas flowmeters, in the liquid Freon 113 bubbler inlet piping, in the piping at the start of the unheated length of the inlet quartz tubing, and in the piping at the outlet of the heated portion of the test section. Chromel-alumel thermocouples were inserted in the flow streams at the same locations as the above-mentioned pressure taps, and were also inserted into the flow of heat transfer fluid entering and leaving the heated portion of the test section.

Post-CHF flow could be established in the test section by heating the heat transfer fluid above minimum film boiling temperature and then introducing test fluids such as Freon 113 into the inner quartz tube directly. The drawback with this approach is one of lack of control of the annular gas and jet gas flow conditions. Setting up a simplified, idealized two-phase core film boiling flow geometry at the injection nozzle exit/heated test section inlet allowed accurate control of these inlet flow conditions. Thus, due to the unique injection design of the experimental facility used in this study, steady-state inlet flow parameters (core liquid and core gas flow rates,

annular gas flow rates) could be controlled, measured, and varied systematically.

Photographic observation of the post-CHF hydrodynamic behavior within the heated test section was accomplished using both still photograph and high-speed motion picture methods. Photographic observation of the pre-CHF two-phase flow within the jet core injection nozzle was made via the nozzle sight glass. Still photographs were taken with a Nikon FA-35 mm SLR camera, using a Nikkor 55 mm f/2.8 lens and Kodak Tri-X 400 ASA black and white film. Lighting was provided by a 3 μs strobe delivering a 0.5 w-s pulse of light bounced off a white background and onto the test section. For a selected series of trials, motion pictures were taken with a Teladyne DBM5-2 high-speed camera, using a Schneider 75 mm f/2.8 lens and 16 mm Kodak Ektachrome VNX 430, 400 ASA color reversal film. Film speed was 500 fps.

Experimental Parameters

The essential variables in this experimental study were the jet core liquid volumetric flux (or superficial velocity - $j_{fJ}$), the jet core gas volumetric flux (or superficial velocity - $j_{gJ}$), and the annulus gas velocity ($V_{gA}$). Once all actual volumetric flow rates were known, these steady-state inlet flow parameters were obtained from the following equations:

$$j_{fJ} = \frac{Q_{fJ}}{A_J} \tag{1}$$

$$j_{gJ} = \frac{Q_{gJ}}{A_J} \tag{2}$$

$$V_{gA} = \frac{Q_{gA}}{A_A} \tag{3}$$

Table 1 summarizes the range of inlet flow parameters studied. Two of the inlet jet core parameters, $j_{fJ}$ and $j_{gJ}$, along with fluid and gas properties, were used to determine the two-phase jet core theoretical void fraction at the jet nozzle exit/heated test section inlet. This will be discussed in the next section.

For the inlet jet nozzle flow of the present experimental study, two-phase jet core theoretical void fractions were calculated using correlations developed by Ishii [1]. The theoretical void fractions calculated, along with the flow regime transition criteria developed by Mishima and Ishii [2], were used to determine the pre-CHF flow regimes in the jet core injection nozzle. Visual and photographic analysis of the two-phase nozzle flow (through the nozzle sight glass) confirmed the type of pre-CHF flow present. The resulting post-CHF flow regimes, beginning from the jet nozzle exit/heated test section inlet, were the object of this experimental study.

Table 1. Summary of Inlet Flow Parameters

| $j_{fJ}$ (m/s) | $j_{gJ}$ (m/s) | $V_{gA}$ (m/s) |
|---|---|---|
| 0.069 | 0.028-5.125 | 0.029-1.120 |
| 0.172 | 0.040-8.736 | 0.072-1.281 |

Prior to experimental trial runs, initial values of 0.10 (pre-CHF bubbly flow), 0.35/0.50/0.65 (pre-CHF slug flow), and 0.80 (pre-CHF annular flow) were assigned to the jet void fraction. For the two jet core liquid volumetric fluxes $(j_{fJ})$ used in the present study, this pre-assigned $\alpha_J$ value, along with typical fluid and gas properties, was inserted into the corresponding theoretical $\alpha_J$ equation. The jet gas volumetric flux $(j_{gJ})$ and therefore the jet gas volumetric flow rate $(Q_{gJ} = j_{gJ} A_J)$ required to attain this pre-assigned $\alpha_J$ value was then calculated. The jet void fractions calculated, along with the flow regime transition criteria, were then used to determine the pre-CHF two-phase flow regime present in the nozzle for that series of trials (see Table 2). Visual and photographic analysis of the two-phase jet nozzle flow provided further information and confirmation of the type of pre-CHF flow present.

Table 2. Summary of Jet Core Theoretical Void Fractions

| Test Series | $j_{fJ}$ (m/s) | $j_{gJ}$ (m/s) | $\alpha_{J,b}$ | $\alpha_{J,s}$ | $\alpha_{J,c}$ | Pre-CHF Flow Regime |
|---|---|---|---|---|---|---|
| 1-10 | 0.069 | 0.028 | 0.119 | 0.120 | 0.106 | Bubbly |
| 11-20 | 0.069 | 0.137 | 0.464 | 0.380 | 0.350 | Slug |
| 21-30 | 0.069 | 0.255 | 0.616 | 0.510 | 0.480 | Slug |
| 71-80 | 0.069 | 0.602 | 0.739 | 0.658 | 0.636 | Slug |
| 81-90 | 0.069 | 5.125 | 0.825 | 0.812 | 0.807 | Annular |
| 31-40 | 0.172 | 0.040 | 0.107 | 0.109 | 0.100 | Bubbly |
| 41-50 | 0.172 | 0.198 | 0.394 | 0.356 | 0.337 | Slug |
| 51-60 | 0.172 | 0.424 | 0.569 | 0.514 | 0.494 | Slug |
| 61-70 | 0.172 | 0.974 | 0.703 | 0.657 | 0.643 | Slug |
| 91-100 | 0.172 | 8.736 | 0.821 | 0.813 | 0.810 | Annular |

A final comment should be made here concerning the inlet void fraction due to the annulus gas flow. For all trials in this study, the inlet annulus void fraction $(\alpha_A = A_A/A_T)$ for a nozzle ID of 10.8 mm and inner quartz tube ID of 13.6 mm was 0.37.

## EXPERIMENTAL OBSERVATIONS

In this section, an overview of the hydrodynamics of the post-CHF flow field is given. Graphical data for flow regime axial extents are also presented. Due to its dominance in the flow field, emphasis in the analysis is placed on the transition flow pattern between inverted annular and dispersed droplet flow. A predictive equation for the axial extent of this flow pattern transition regime, dependent on inlet two-phase jet core parameters only, is developed.

Still photographs taken with black and white film were analyzed by placing the developed negatives on a light table fitted with a binocular microscope. Initially, general flow field observations were made. Then a more careful and detailed analysis generated data on the axial extent of the various flow regimes present, using the image of the transparent ruler mounted alongside the test section as a reference. Motion pictures of the test section flow field were analyzed on a motion picture analyzer, with X-Y plotting cross hairs and film projection speeds from 48 fps down to zero.

### Hydrodynamic Behavior of the Post-CHF Flow Field

In the present film boiling experimental study, the post-CHF flow regimes are similar to the flow patterns established previously by DeJarlais and Ishii [3] and Obot and Ishii [35]. These flow regimes were observed using the same experimental apparatus as the present study, but with single phase liquid rather than two-phase core injection. For single phase liquid core injection, the post-CHF flow field contained four basic flow regimes: the smooth regime (stable inverted annular flow), the rough wavy regime, the agitated regime (transition flow between inverted annular and dispersed droplet flow), and the dispersed ligament/droplet regime. Mention should be made here that unlike the single phase core inverted annular study, for this two-phase core film boiling study the smooth flow regime does not exist; there is no smooth, stable inverted annular flow pattern when a two-phase core is injected into the heated test section. In general, flow patterns resembling the rough wavy regime and the transition between inverted annular and dispersed droplet flow (the agitated regime), along with the dispersed ligament/droplet regime were observed. Following is a description of the flow regimes encountered in the multiphase core film boiling study.

Rough wavy regime. The rough wavy regime, or inverted annular flow preliminary break down, is present only for pre-CHF bubbly flow ($\alpha_j \tilde{=} 0.1$) in the core injection nozzle. The dominant features of the rough wavy regime are the presence of a fairly stable, intact liquid plus gas central core, along with a very rough annular gas-core liquid interface. Small gas bubbles can be seen inside the multiphase core, while small disturbances on the surface of the core quickly grow to large amplitude roll waves. Shearing and entrainment of core liquid from roll wave crests result in a reduced diameter central core, along with fine structure liquid entrainment masses at the end of the rough wavy/beginning of the agitated flow regime. The axial extent of the rough wavy regime tends to increase with increasing jet liquid volumetric flux, and tends to decrease with increasing annular gas velocity.

Agitated regime. The agitated regime, which includes the inverted slug-churn flow field, is present for all pre-CHF flow regimes (bubbly, slug, and annular) established in the core injection nozzle. The agitated regime constitutes the unstable transition flow pattern between inverted annular flow film boiling and dispersed droplet flow. The dominant features of the agitated regime are the presence of thin, very fine structure skirt-like annular liquid sheets and small droplet clouds close to the heated wall. These sheets are not continuous. They appear with the cyclic chugging nature of the general flow field.

While the general appearance is essentially the same, the specific, underlying characteristics of the post-CHF agitated flow regime depend to a certain extent on the type of pre-CHF flow introduced into the heated test section. Therefore, following is specific descriptive summary of the agitated regime based on the pre-CHF flow regime established in the jet core nozzle and injected into the heated test section.

Agitated regime - pre-CHF bubbly flow. For pre-CHF bubbly flow in the jet core injection nozzle, the agitated flow regime follows directly after the rough wavy regime. The liquid entrainment masses of the post-CHF agitated regime consist of thin, very fine structure skirt-like annular sheets or droplet clouds in close proximity to the heated wall of the test section. The formation mechanism of these entrained liquid masses is similar to that reported by DeJarlais and Ishii [3] and DeJarlais [30]. Small roll wave disturbances on the central multiphase core, initially formed in the rough wavy regime, quickly transform to large amplitude roll waves. Extreme growth and distortion of these roll waves gives rise to core liquid entrainment from roll wave crests. This mechanism of roll wave entrainment is analyzed by Ishii and Grolmes [40] and DeJarlais [30]. The entrained liquid, sheared from roll wave crests by the annular gas flow, forms into the thin sheets and fine structure annular droplet clouds. The agitated annular mass structures formed accelerate as they move downstream, passing over and leaving undisturbed a reduced diameter two-phase core in the central portion of the test section. The reduced diameter core, initially in up flow, often stalls and falls back down the test section. Surface roughening results in some secondary ligament and droplet entrainment, while the bulk of the reduced core breaks into large ligaments and droplets. Generally, there is little agitated annular mass-intact reduced diameter core interaction. However, at times the next agitated mass in the cycle can be slowed or even broken up by the reduced core down flow.

Agitated regime - pre-CHF slug flow. For pre-CHF slug flow in the jet core injection nozzle, the agitated flow regime extends directly from the jet nozzle exit. The liquid entrainment masses of the post-CHF agitated regime for pre-CHF slug core flow also consist of thin, very fine structure skirt-like annular sheets and droplet clouds close to the heated wall of the test section. The liquid, flowing down along the sides of an initial slug bubble in the form of a thin annular ring film, is eventually forced to the sharp edged injection nozzle exit. As this liquid film, along with its slug bubble exits the injection nozzle, outward radial expansion towards the wall of the heated test section occurs. This expansion causes the liquid film in

the annulus region of the core injection nozzle to expand out into the annulus region of the test section. While the underlying physical situation is different from that for single phase liquid or two-phase bubbly core injection, the resulting flow is very similar.

The liquid slug collapses in behind the tail of the depleting slug bubble, forming a reduced diameter core in its wake, while the agitated mass structure continues to accelerate up the test section "riding" the slug bubble cap.

Agitated regime - pre-CHF annular flow. The agitated regime for pre-CHF annular flow consists only of liquid entrainment masses that emerge directly from the jet nozzle exit. Due to the limited availability of jet core liquid at pre-CHF annular nozzle flow, the post-CHF agitated regime is very small and depleted. The cyclic nature of the agitated flow field for pre-CHF annular core flow, i.e., agitated mass ejection followed by dispersed droplet ejection, results in a very unstable flow pattern with extreme fluctuations in axial extent. When averaged out, break up and depletion of the agitated masses to dispersed droplet flow usually occurs within 5-10 cm of the jet nozzle exit. However, for the two jet core liquid volumetric flow rates used in this experimental study, larger agitated masses have been observed to penetrate upwards of 25 cm into the heated test section.

Dispersed ligament/droplet regime. The dispersed ligament/droplet regime is present for all types of pre-CHF flow (bubbly, slug, and annular) established in the core injection nozzle. Beginning at the downstream edge of the agitated regime, the dispersed flow pattern extends to the test section exit (approximately 1 m from jet nozzle exit) for all trials in this experimental study. The dominant feature of this flow regime is the presence of fairly homogeneous dispersed liquid droplets and small ligaments.

Jet Void Fraction/Agitated Regime Trends

From the experimental observations, one can see that as the jet gas volumetric flux or jet void fraction is increased, the frequency and length of the agitated annular masses generally decrease, while the velocity tends to increase. As the jet void fraction is increased, the amount of liquid in the core is reduced. The decreased availability of liquid in the jet core results in less agitated mass formation (lower frequency), while those masses formed tend to be smaller, less coherent, and prone to more extensive depletion. Due to the decreased availability of core liquid as the jet void fraction is increased, the reduced diameter core associated with the agitated regime becomes progressively thinner, less stable, and less coherent, to a point where, for the high jet void fraction trials ($\alpha_J \cong 0.8$), no reduced core exists. As the jet void fraction is increased, any agitated regime reduced core down flow present becomes increasingly susceptible to quicker and more extensive surface roughening and break up to slugs, ligaments, and droplets.

## Axial Extent of Flow Regimes

Dimensional plots for the axial extent ($L_B$) of the rough wavy and agitated flow regimes versus the inlet annulus gas velocity are given in Figs. 4-8. The plots are presented in order of increasing jet core theoretical void fraction. The axial extent data for these plots were obtained by visual analysis of the still photographs taken with a 55 mm lens (30 cm field of view). The complex nature of the post-CHF flow field made it difficult to draw distinct, clear cut flow regimes. Boundaries between flow regimes were rarely, if ever, sharply defined. In spite of the subjectivity involved, every attempt was made to be consistent in the analysis. The quasi-periodic chugging nature of the agitated regime made for a very unstable flow field with fluctuating axial extents. Given the subjective determination of flow regimes and flow regime boundaries, and the fluctuating axial extents of those boundaries, the data points plotted in Figs. 4-8 represent average values determined by reviewing the 16 to 20 photographic frames taken for each trial run.

Note from the figures that for a jet core inlet void fraction of approximately 0.1, the agitated flow regime is preceded by the rough wavy regime, while for all other jet void fractions studied (approx 0.35 - 0.8) the agitated flow regime extends directly from the jet nozzle exit with no rough wavy flow regime present. Thus for the 0.1 jet void fraction trials, the axial extent of the agitated regime includes that of the rough wavy regime, while for the 0.35 through 0.8 jet void fraction trials, the axial extent of the agitated regime reflects the actual axial extent of that regime from the jet nozzle exit. For all test trials in this study, a dispersed ligament/droplet flow just downstream of the agitated regime extends beyond the exit of the heated portion of the test section (approximately 1 m from the jet nozzle exit).

Some general trends are apparent in Figs. 4-8. For a given value of inlet jet void fraction and annulus gas velocity, the axial extent of the various flow regimes is always greater for the high jet liquid volumetric flux trials relative to the low jet liquid volumetric flux trials. Also, for the 0.1 jet void fraction trial runs, the axial extent of the rough wavy flow regime tends to dop off with increasing annulus gas velocity. Most importantly, however, for a given jet liquid volumetric flux and fixed jet core inlet void fraction, the axial extent of the agitated flow regime remains relatively constant as the annulus gas velocity is increased. Thus, the axial extent of the agitated regime is essentially independent of the annulus gas flow. This applies only at the low ($\lesssim$ 1 m/s) annulus gas velocities used in this experimental study. In general, as the jet core void fraction is increased, the axial extent of the agitated regime decreases, and since the annulus gas velocity is negligible, the data reflect the true jet void fraction effect on the axial extent of the agitated flow regime.

## Predictive Equations for the Axial Extent of Flow Regimes

Correlations for Single Phase Jet Core. From a detailed study of an adiabatic, single phase (liquid) jet core inverted annular flow [30], it was

established conclusively that the correlated jet core break-up data followed two distinct trends; one for the region over which the jet break-up length was independent of the inlet annulus void fraction ($\alpha_A$), the annulus gas-liquid jet inlet relative velocity, and the gas density, with a marked sensitivity of the break-up to these variables for the second region. The break-up lengths for these two regions were closely approximated by the following equations:

$$\frac{L_B}{D_J} = 480\ Re_J^{-0.53}\ We_J^{0.5} \tag{4}$$

$$\frac{L_B}{D_J} = 685\ Re_J^{-0.53}\ We_J^{0.5}\left(\frac{We_{g,r}}{\alpha_A^2}\right)^{-0.645} \tag{5}$$

Since these two curves intersect at $We_{g,r}/\alpha_A^2 = 1.73$, this critical value of gas Weber number over the square of the inlet annulus void fraction provides a useful criterion for determining the validity range for each equation.

In a subsequent inverted annular flow film boiling study [35], it was determined that the break-up length, or axial extent ($L_B$), of the various post-CHF two-phase flow regimes could be correlated in terms of the nondimensional variables in Eqs. (4) and (5). For each flow regime the proposed correlation again followed two distinct trends, one for the $We_{g,r}/\alpha_A^2$ range over which $L_B/D_J$ depended only on the liquid jet parameters ($Re_J$ and $We_J$) and the other for the region where $L_B/D_J$ depended on the liquid jet parameters, the annulus gas parameters, and the annulus void fraction $Re_J$, $We_J$ and $We_{g,r}/\alpha_A^2$. For the first region, where flow regime axial extents depend solely on liquid jet inlet conditions, the maximum axial extent of each flow regime was approximated by the relation:

$$\frac{L_B}{D_J} \lessgtr A_i\ Re_J^{-0.53}\ We_J^{0.5}\ . \tag{6}$$

The regime dependent numerical values of constant $A_i$, together with approximate ranges of validity of Eq. (6) are summarized in Table 3. For the second region, where flow regime axial extents depend on both liquid jet core and annulus gas flow conditions at the inlet to the test section, the maximum axial extent of each flow regime was approximated by:

$$\frac{L_B}{D_J} = B_i\ Re_J^{-0.53}\ We_J^{0.5}\left(\frac{We_{g,r}}{\alpha_A^2}\right)^{m_i}\ . \tag{7}$$

Table 3. Predictive Equations for Single Phase Jet Core

| Flow Section | First Region+ | | Second Region+ | | |
|---|---|---|---|---|---|
| | $A_i$ | Validity Range for $We_{g,r}/\alpha_A^2$ | $B_i$ | $m_i$ | Range |
| Smooth | 80 | $\leq 10^{-2}$ | 25 | -0.27 | $>10^{-2}$ |
| Rough Wavy | 380 | $\leq 10^{-1}$ | 200 | -0.31 | $>10^{-1}$ |
| Agitated | 770 | $\leq 3.5$ | 1500 | -0.5 | $>3.5$ |
| Dispersed | 770 | $\leq 10$ | - | - | |

+Range for $Re_J$ and $We_J$: $1775 \leq Re_J \leq 13{,}280$ and $4.5 \leq We_J \leq 260$.

The appropriate regime dependent values for $B_i$ and $m_i$, along with the ranges of validity are also given in Table 3.

For the first region, where $L_B/D_J = f(Re_J, We_J)$, a further simplification of Eq. (6) was presented. Since $We_J/Re_J = \mu_f V_{fJ}/\sigma$ (= jet Capillary number, $Ca_J$), Eq. (6) could be rewritten as

$$\frac{L_B}{D_J} = \frac{A_i}{Re_J^{0.03}} \left(\frac{We_J}{Re_J}\right)^{1/2} \simeq C_i \sqrt{Ca_J} \,. \tag{8}$$

Recasting Eq. (6) in terms of $Ca_J$ resulted in the following simplified regime dependent correlations:

Smooth Regime: $$\frac{L_B}{D_J} \leq 60 \sqrt{Ca_J} \tag{9}$$

Rough Wavy Regime: $$\frac{L_B}{D_J} \leq 295 \sqrt{Ca_J} \tag{10}$$

Agitated Regime: $$\frac{L_B}{D_J} \leq 595 \sqrt{Ca_J} \tag{11}$$

Dispersed Regime: $$\frac{L_B}{D_J} > 595 \sqrt{Ca_J} \tag{12}$$

One should note that the simplified correlations given in Eqs. (9)-(12) apply only to the region where a given flow regime's axial extent is independent of the annulus gas flow, and thus is a function of liquid jet parameters only. However, most film boiling situations falls into this category.

Correlations for Two-Phase Jet Core. In this multiphase jet core film boiling study, the post-CHF flow field is dominated by the presence of the agitated flow regime. Since the agitated regime is the only flow pattern for which a significant amount of data is available, a jet parameter and inlet jet void fraction dependent predictive equation for the axial extent of this flow regime is provided.

In general, as the jet void fraction is increased, the axial extent of the agitated flow regime tends to decrease. As noted previously, at the low annulus gas velocities used in this study, the agitated regime axial extent ($L_B$) is essentially independent of the annulus gas flow. Thus, it was postulated that the axial extent is a function of the two-phase jet core parameters only. Certainly, this is the condition encountered in the standard film boiling condition. Accordingly, the agitated regime axial extent, scaled with the jet diameter and expressed as $L_B/D_J$, was correlated using a simplified equation of the form:

$$\frac{L_B}{D_J} = X_i \sqrt{Ca_{J,m}} \tag{13}$$

where $Ca_{J,m} = \mu_f j_J/\sigma$, the modified two-phase jet Capillary number based on the total jet volumetric flux $j_J$ ($= j_{fJ} + j_{gJ}$), and $X_i$ is a correlating factor. For each trial run, the value of the correlation factor $X_i$ ($= L_B/D_J\, Ca_{J,m}^{-0.5}$) was calculated. Thus, for each series of trials with constant inlet jet parameters (constant $j_{gJ}$, $j_{gJ}$, and $\alpha_J$), a mean value of $X_i$ was determined. The mean values of $X_i$, along with the standard deviation about the mean, are given in Table 4.

To maintain continuity with the single phase liquid jet core film boiling study, a correction factor to the agitated regime axial extent correlation given in Eq. (11) was evaluated. This correction factor simply consisted of the experimentally observed agitated regime axial extent for two-phase core injection over that predicted by Eq. (11) with $Ca_J = Ca_{J,m}$, thus:

Table 4. Correlation Constant and Correction Factor

| Test Series | $j_{fJ}$ (m/s) | $\alpha_{J,theo}$ | $\bar{X}_i$ | $\sigma_{\bar{X}_i}$ | $\bar{f}$ |
|---|---|---|---|---|---|
| 1-10 | 0.069 | 0.119 | 481.7 | 46.03 | 0.8096 |
| 31-40 | 0.172 | 0.107 | 580.6 | 47.82 | 0.9758 |
| 11-20 | 0.069 | 0.380 | 279.2 | 34.28 | 0.4692 |
| 41-50 | 0.172 | 0.356 | 328.3 | 30.20 | 0.5518 |
| 21-30 | 0.069 | 0.510 | 181.5 | 35.52 | 0.3050 |
| 51-60 | 0.172 | 0.514 | 207.5 | 31.11 | 0.3487 |
| 71-80 | 0.069 | 0.658 | 111.9 | 16.29 | 0.1881 |
| 61-70 | 0.172 | 0.657 | 102.3 | 13.48 | 0.1719 |
| 81-90 | 0.069 | 0.807 | 8.4 | 1.86 | 0.0141 |
| 91-100 | 0.172 | 0.810 | 14.8 | 1.92 | 0.0249 |

$$f = \frac{L_{B,experimental}}{L_{B,Eq.\ (11)}} = \frac{X_i\ D_J\ \sqrt{Ca_{J,m}}}{595\ D_J\ \sqrt{Ca_{J,m}}} = \frac{X_i}{595} \qquad (14)$$

For each series of trials with constant jet core inlet parameters, a mean value of the correlation correction factor $\bar{f} = \bar{X}_i/595$, was determined. These values are also given in Table 4. In Fig. 9 the mean correction factor is plotted against the inlet theoretical jet void fraction. Note that there is some slight dependence on the jet liquid volumetric flux $(j_{fJ})$, while the general tend is dominated by the jet void fraction. To obtain the functional relationship between $\bar{f}$ and $\alpha_J$, an equation of the form $\bar{f} = (1 - \alpha_J/\alpha_C)^n$ was assumed. Here $\alpha_C$ is the critical jet void fraction beyond which the agitated regime no longer exists, with the exclusive emergence of dispersed droplet flow at the jet nozzle exit. With an extrapolated value of 0.85 for the critical jet void fraction resulted in the following relation:

$$\bar{f} = \left(1 - \frac{\alpha_J}{0.854}\right)^{1.22} \qquad (15)$$

This curve is given by the dotted line in Fig. 9. When this correction factor is applied to Eq. (13), the proposed correlation for the axial extent of the agitated flow regime becomes:

$$\frac{L_B}{D_J} = 595 \sqrt{\frac{\mu_f j_J}{\sigma}} \left(1 - \frac{\alpha_J}{0.854}\right)^{1.22} \qquad (16)$$

Equation (16) gives estimates that are close to those observed experimentally, with a 7-30% error band for the $\alpha_J \cong 0.1$ through $\alpha_J \cong 0.65$ trials (pre-CHF bubbly and slug jet core flow). The error band for the $\alpha_J \cong 0.8$ trials (pre-CHF annular jet flow) is considerably higher due to the relatively small size of the agitated regime and the extreme fluctuations in the axial extent of this regime for these trials.

The experimental range of the modified jet Capillary number in this study was 0.0035 to 0.35, while the range of the modified relative gas Weber number over the square of the annulus void fraction was 0.0024 to 414. The extreme upper bound of the $We_{g,r,m}/\alpha_A^2$ term is due to the dominance of the jet gas volumetric flux in this term at the high ($\cong 0.8$) jet void fraction trials.

Some general comments should be made here concerning the proposed correlation in Eq. (16). The value of the critical jet void fraction, $\alpha_C = 0.854$, was not determined experimentally, but was extrapolated from the data. The actual critical void fraction could be anywhere in the range $0.82 \leq \alpha_C \leq 1.0$, and would have to be determined by further experimentation. Also, while Eq. (16) provides a good estimate of the axial extent of the agitated flow regime, the interpretation of $L_B$ needs further explanation. In this experimental study, the post-CHF flow field was very unstable, with extreme fluctuations in flow regime axial extents. Thus, the agitated regime axial extent values predicted by Eq. (16) will reflect these average values in what is an extremely fluctuating post-CHF flow field.

## SUMMARY AND CONCLUSIONS

A flow visualization study of a simplified two-phase core film boiling flow geometry was carried out with the objective of determining and characterizing the various post dryout flow regimes. For this idealized film boiling of a steady-state inlet, pre-CHF two-phase jet core, the post-CHF flow field basically consists of three flow regimes: the rough wavy regime, the agitated regime, and the dispersed ligament/droplet regime. The dominant characteristics of the rough wavy regime are an intact two-phase central jet core, with a rough and wavy core liquid-annulus gas interface. The agitated regime is dominated by the presence of a reduced diameter multiphase core, along with thin, fine structure agitated annular liquid entrainment masses. Break up and depletion of the reduced diameter multiphase core and liquid entrainment masses result in a dispersed ligament/droplet flow pattern just downstream of the agitated regime.

The axial flow pattern in the post-CHF region is dependent on the type of pre-CHF flow established in the two-phase jet core injection nozzle. The post dryout flow pattern for pre-CHF bubbly flow begins with the rough wavy regime, followed by the agitated regime, and then the dispersed ligament/droplet regime. For pre-CHF slug flow, the post-CHF axial flow pattern consists of

the agitated regime followed by the dispersed ligament/droplet regime. Pre-CHF annular core flow results in a small, depleted agitated flow regime at the jet nozzle exit, again followed by the dispersed ligament/droplet regime.

The most significant of the above-mentioned flow regimes, as far as the analysis of post-CHF heat transfer is concerned, is perhaps the agitated regime. The large interfacial surface area generated in the agitated region indicates large heat and momentum transfer rates. Large momentum transfer is manifested in the periodic formation and acceleration of thin, highly agitated annular liquid entrainment masses. The fine structure and large interfacial area of these agitated entrainment masses indicate high heat transfer rates as these annular mass structures accelerate up the test section in close proximity to the heated wall. Data are presented for the frequency, length, and velocity of the agitated masses for varying inlet pre-dryout flow conditions [41].

As reviewed by various researchers [7-12, 42-44], there are a number of correlations for heat transfer in the post dryout region. However, these correlations are developed without detailed knowledge of two-phase hydrodynamics. Therefore, their applicability beyond the data base is quite limited. Furthermore, often the postulated heat transfer mechanisms do not fit to the real two-phase flow characteristics observed in the present study.

In order to develop a reliable heat transfer model for the post CHF region, detailed flow characteristics such as the regime transitions, droplet size and existence of thin annulus sheet of liquid should be considered. Among them, probably the most important factor is to distinguish the agitated regime and dispersed ligament/droplet regime. The heat transfer mechanisms in these two regimes are completely different. The existence of the agitated regime explains the relatively high wall heat transfer immediately after the dryout point which has been observed experimentally [45].

Since most of the practical film boiling occurs with relatively low gas annulus (gas film) velocities, the flow regime transitions can be characterized by the two-phase jet core parameters only. Therefore, a general flow regime transition criteria between the agitated regime and the dispersed droplet regime can be given by

$$\frac{L_B}{D_J} = 595 \sqrt{\frac{\mu_f j_J}{\sigma}} \left(1 - \frac{\alpha_J}{0.854}\right)^{1.22}$$

where J refers to the values at the dryout point.

ACKNOWLEDGMENTS

The authors would like to express their sincere appreciation to Drs. Novak Zuber and Richard Y. Lee of NRC for their valuable discussions and support. This work was performed under the auspices of the U.S. Nuclear Regulatory Commission.

REFERENCES

1. Ishii, M., One-Dimensional Drift Flux Model and Constitutive Equations for Relative Motion Between Phases in Various Two-Phase Flow Regimes, Argonne National Laboratory report ANL-77-47, 1977.

2. Mishima, K. and Ishii, M., Flow Regime Transition Criteria Consistent with Two-Fluid Model for Vertical Two-Phase Flow, Argonne National Laboratory report NUREG/CR-3338, ANL-83-42, 1983.

3. DeJarlais, G. and Ishii, M., Inverted Annular Flow Experimental Study, Argonne National Laboratory report NUREG/CR-4277, ANL-85-31 (1985).

4. Jordan, D. P., Film and Transition Boiling, Advances in Heat Transfer, Vol. 5, 1968, pp. 55-128.

5. Clemments, L. D. and Colver, C. P., Natural Convection Film Boiling Heat Transfer, Ind. Eng. Chem., Vol. 62, #9, 1970, pp. 26-46.

6. Hsu, Y. Y., A Review of Film Boiling at Cryogenic Temperatures, Advances in Cryogenic Eng., Vol. 17, 1972, p. 361.

7. Bressler, R. G., A Review of Physical Models and Heat Transfer Correlations for Free-Convection Film Boiling, Advances in Cryogenic Eng., Vol. 17, 1972, p. 382.

8. Kalinin, E. K., Berlin, I. I., and Kostyuk, V. V., Film Boiling Heat Transfer, Advances in Heat Transfer, Vol. 11, 1975, p. 51.

9. Groeneveld, D. C. and Gardiner, S. R. M., Post CHF Heat Transfer Under Forced Convective Conditions, Proc. Sym. on the Thermal and Hydraulic Aspects of Nucl. Reactor Safety, ASME, Vol. 1, New York, 1977, p. 43.

10. Groeneveld, D. C., Post Dryout Heat Transfer: Physical Mechanics and a Survey of Prediction Methods, Nucl. Eng. & Design, Vol. 32, 1975, p. 283.

11. Collier, J. G., Post-dryout Heat Transfer - A Review of the Current Position, Proc. NATO Advanced Study Inst. on Two-phase Flows and Heat Trans., II, Istanbul, 1977, p. 769.

12. Mayinger, F. and Langner, H., Post-dryout Heat Transfer, Proc. 6th Intl. Heat Trans. Conf., Toronto, Canada, Vol. 6, 1978, p. 181.

13. Ishii, M. and DeJarlais, G., Hydrodynamics of Post CHF Region, Intl. Workshop on Fundamental Aspects of Post-dryout Heat Trans., Salt Lake City, April 2-4, 1984.

14. Westwater, J. W. and Santangelo, J. C., Photographic Study of Boiling, Ind. Eng. Chem., Vol. 47, #8, 1955, pp. 1605-1610.

15. Hsu, Y. Y. and Westwater, J. W., Film Boiling from Vertical Tubes, AIChE J., Vol. 4, #1, 1958, pp. 58-62.

16. Hsu, Y. Y. and Westwater, J. W., Approximate Theory for Film Boiling on Vertical Surfaces, Chem. Eng. Prog. Symp. Series, Vol. 56, #30, 1960, pp. 15-24.

17. Coury, G. E. and Dukler, A. E., Turbulent Film Boiling on Vertical Surfaces: A Study Including the Influence of Interfacial Waves, 4th Intl. Heat Trans. Conf., Paper B3.6, Paris, 1970.

18. Chi, J. W. H. and Vetere, A. M., Two-Phase Flow During Transient Boiling of Hydrogen and Determination of Nonequilibrium Vapor Fractions, Advances in Cryogenic Eng., Vol. 9, 1964, pp. 243-253.

19. Chi, J. W. H., Cooldown Temperatures and Cooldown Time During Mist Flow, Advances in Cryogenic Eng., Vol. 10, 1965, pp. 330-340.

20. Chi, J. W. H., Slug Flow and Film Boiling of Hydrogen, J. Spacecr. & Rockets, Vol. 4, #10, 1967, pp. 1329-1332.

21. Laverty, W. F. and Rohsenow, W. M., Film Boiling of Saturated Nitrogen Flowing in a Vertical Tube, ASME J. Heat Trans., Vol. 89, 1967, pp. 90-98.

22. Forslund, R. P. and Rohsenow, W. M., Dispersed Flow Film Boiling, ASME J. Heat Trans., Vol. 90, 1968, pp. 399-407.

23. Kalinin, E. K., et al., Heat Transfer in Tubes with Rod Regime in the Case of Film Boiling of a Subcooled Liquid, Cocurrent Gas Liquid Flow, Plenum Press, New York, 1969, p. 497.

24. Kalinin, E. K., et al., Investigation of Film Boiling in Tubes with Subcooled Nitrogen Flow, 4th Intl. Heat Trans. Conf., Paper B4.5, Paris, 1970.

25. Kalinin, E. K., et al., Investigation of the Crisis of Film Boiling in Channels, Proc. Two-Phase Flow and Heat Trans. in Rod Bundles, ASME Winter Annual Meeting, Los Angeles, California, 1969.

26. Cadek, F. F., Dominicis, D. P., and Leyse, R. H., PWR FLECHT Final Report, Westinghouse report WCAP-7665, 1971.

27. Lee, N., Wong, S., Yeh, H. C., and Hochreiter, L. F., PWR FLECHT SEASET Unblocked Bundle, Forced and Gravity Reflood Task Data Evaluation and Analysis Report, NUREG/CR-2256, 1981.

28. Ishii, M. and DeJarlais, G., Phenomenological Modeling of Two-phase Flow in Water Reactors at ANL (Inverted Annular Flow Modeling), presented at the NRC 10th Water Reactor Safety Research Information Meeting, Gaithersburg, Maryland, October 12-15, 1982.

29. Ishii, M. and DeJarlais, G., Inverted Annular Two-phase Flow Experiments and Modeling, 11th Water Reactor Safety Research Information Meeting, Gaithersburg, Maryland, 1983.

30. DeJarlais, G., An Experimental Study of Inverted Annular Flow Hydrodynamics Utilizing an Adiabatic Simulation, Argonne National Laboratory report NUREG/CR-3339, ANL-83-44, 1983.

31. DeJarlais, G. and Ishii, M., Hydrodynamic Stability of Inverted Annular Flow in an Adiabatic Simulation, Interfacial Transport Phenomena HTD 23, ASME Proc., 1983, p. 75.

32. DeJarlais, G. and Ishii, M., Hydrodynamics of Adiabatic Inverted Annular Flow - An Experimental Study, 3rd Multiphase Flow and Heat Trans. Sym., Miami Beach, Florida, April 18-20, 1983.

33. Ishii, M. and DeJarlais, G., Flow Visualization Study of Inverted Annular Flow of Post Dryout Heat Transfer Region, 3rd Intl. Topical Mtg. on Reactor Thermal Hydraulics, Paper 1.C, Newport, Rhode Island, 1985.

34. Ishii, M. and DeJarlais, G., Flow Visualization Study of Inverted Annular Flow of Post Dryout Heat Transfer Region, Nucl. Eng. & Design, Vol. 99, 1987, pp. 187-199.

35. Obot, N. T. and Ishii, M., Two-Phase Flow Regime Transition Criteria in Post-Dryout Region Based on Flow Visualization Experiments, Argonne National Laboratory report NUREG/CR-4972, ANL-87-27, 1987.

36. Costigan, G. and Wade, C. D., Visualization of the Reflooding of a Vertical Tube by Dynamic Neutron Radiography, Intl. Workshop on Post-dryout Heat Trans., Salt Lake City, Utah, April 1-4, 1984.

37. Ottosen, P., Experimental and Theoretical Investigation of Inverse Annular Film Flow and Dispersed Droplet Flow, Important Under LOCA Conditions, Riso National Laboratory report No. R-424, Denmark, 1980.

38. Kurilenko, A. A., Dymenko, S. R., and Kochelaev, Y. S., Phase Slip and Heat Transfer to the Liquid in Film Boiling of a Cryogenic Liquid in Piston Flow, J. Eng. Phys., Vol. 39, 1981, pp. 961-965.

39. Graham, R. W., Hendricks, R. C., Hsu, Y. Y., and Friedman, R., Experimental Heat Transfer and Pressure Drop of Film Boiling Liquid Hydrogen Flowing Through a Heated Tube, Advan. Cyog. Eng., Vol. 6, 1961, pp. 517-524.

40. Ishii, M. and Grolmes, M. A., Inception Criteria for Droplet Entrainment in Two-Phase Concurrent Film Flow, AIChE J., Vol. 21, #2, 1975, pp. 308-317.

41. Denten, J. G. and Ishii, M., Flow Visualization Study of Post Critical Heat Flux Region for Inverted Bubbly, Slug and Annular Flow Regimes, Argonne National Laboratory report NUREG/CR-5171, ANL-88-27, 1988.

42. Groeneveld, D. C., Inverted Annular and Low Quality Film Boiling: A State-of-the-Art Report, Keynote Paper, The 1st Intl. Workshop on Fundamental Aspects of Post-Dryout Heat Transfer, Salt Lake City, Utah, April 2-4, 1984, NUREG/CP-0060.

43. Chen, J. C., Review of Post-Dryout Heat Transfer in Dispersed Two-Phase Flow, Keynote Paper, The 1st Intl. Workshop on Fundamental Aspects of Post-Dryout Heat Transfer, Salt Lake City, Utah, April 2-4, 1984, NUREG/CP-0060.

44. Yadigaroglu, G. and Bensalem, A., Interfacial Mass Generation Rate Modeling in Non-Equilibrium Two-Phase Flow, Intl. Workshop on Two-Phase Flow Fundamentals, Gaithersburg, Maryland, Sept. 22-27, 1985.

45. Webb, S. W. and Chen, J. C., A Two-Region Vapor Generation Rate Model for Convective Film Boiling, The 1st Intl. Workshop on Fundamental Aspects of Post-Dryout Heat Trans., Salt Lake City, Utah, April 2-4, 1984, NUREG/CP-0060.

NOMENCLATURE

| | |
|---|---|
| $A$ | Cross-sectional area, m |
| $Ca_J$ | Single phase jet Capillary number, $\mu_f V_{fJ}/\sigma$ |
| $Ca_{J,m}$ | Two-phase jet Capillary number, $\mu_f j_J/\sigma$ |
| $D_J$ | Jet nozzle diameter, m |
| $g$ | Gravity acceleration, $m/sec^2$ |
| $j_{fJ}$ | Jet liquid volumetric flux (superficial velocity), m/s |
| $j_{gJ}$ | Jet gas volumetric flux (superficial velocity), m/s |
| $j_J$ | Total jet volumetric flux, $j_{fJ} + j_{gJ}$, m/s |

| | |
|---|---|
| $L_B$ | Axial extent of a flow regime, m |
| Q | Volumetric flow rate, $m^3/sec$ |
| $Re_J$ | Single phase jet Reynolds number, $\rho V_{fJ} D_J/\mu$ |
| $V_{fJ}$ | Jet fluid velocity, m/s |
| $V_{gA}$ | Annulus gas velocity, m/s |
| $V_r$ | Single phase jet relative velocity, $V_{gA} - V_{fJ}$, m/s |
| $V_{r,m}$ | Two-phase jet relative velocity, $V_{gA} - j_J$, m/s |
| $We_{g,r}$ | Single phase jet, gas Weber number, $\rho_g V_r^2 D_J/\sigma$ |
| $We_{g,r,m}$ | Two-phase jet, gas Weber number, $\rho_g V_{r,m}^2 D_J/\sigma$ |
| $We_J$ | Single phase jet Weber number, $\rho V_{fJ}^2 D_J/\sigma$ |

Greek Symbols

| | |
|---|---|
| $\alpha_A$ | Annulus void fraction at inlet to test section |
| $\alpha_C$ | Critical jet void fraction |
| $\alpha_J$ | Two-phase jet theoretical void fraction |
| $\mu$ | Viscosity, Pa•s |
| $\rho$ | Density, $Kg/m^3$ |
| $\Delta\rho$ | Density difference, $\rho_f - \rho_g$, $Kg/m^3$ |
| $\sigma$ | Surface tension, N/m |

Subscripts

| | |
|---|---|
| A | Annulus |
| a | Annular flow |
| b | Bubbly flow |
| C | Critical |
| c | Churn flow |
| f | Fluid |
| g | Gas |
| J | Jet nozzle |
| s | Slug flow |
| T | Test section, or at test section inlet |

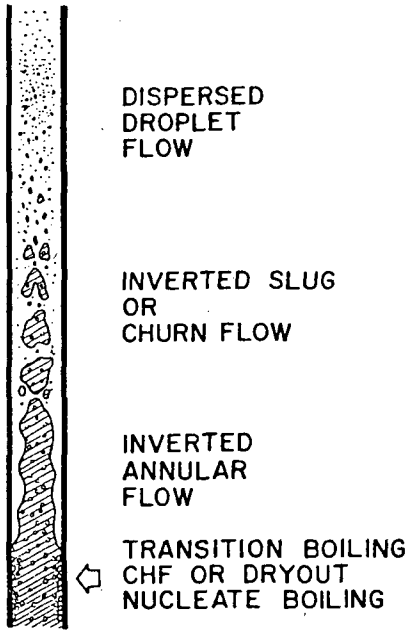


Figure 1. Possible Flow Regimes in Post Dryout Region

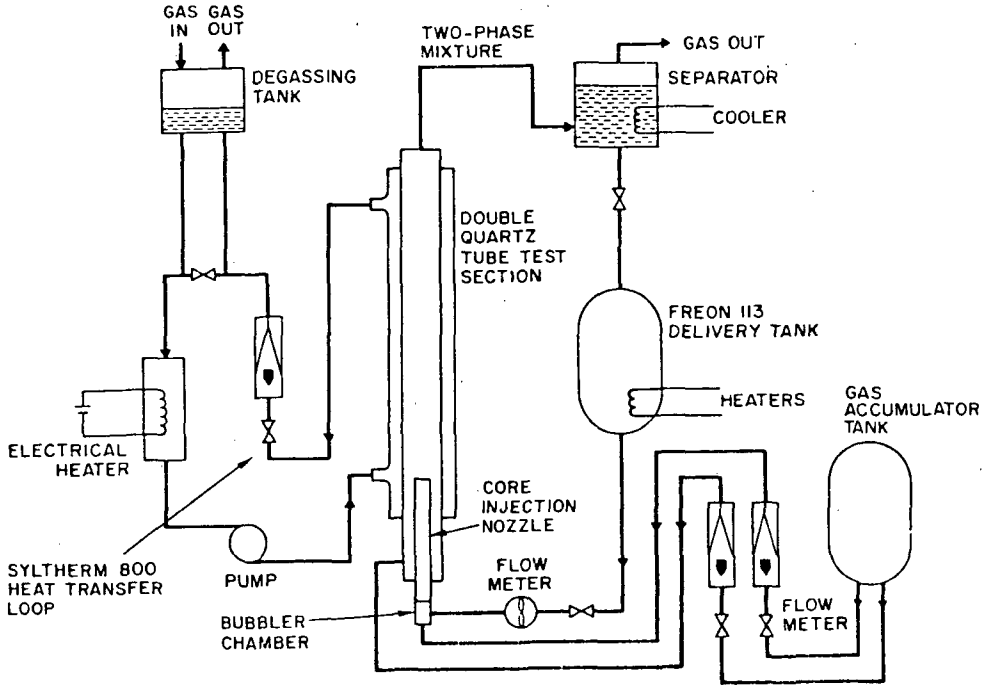


Figure 2. Schematic of the Experiment Facility

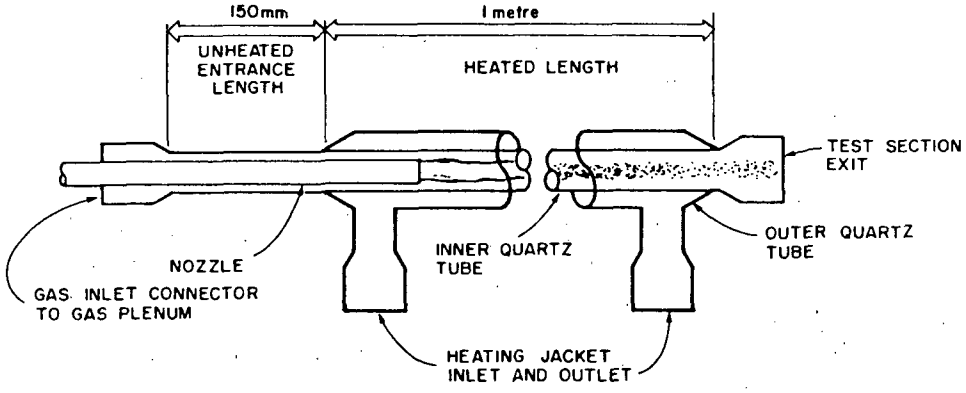


Figure 3. Sketch of the Test Section

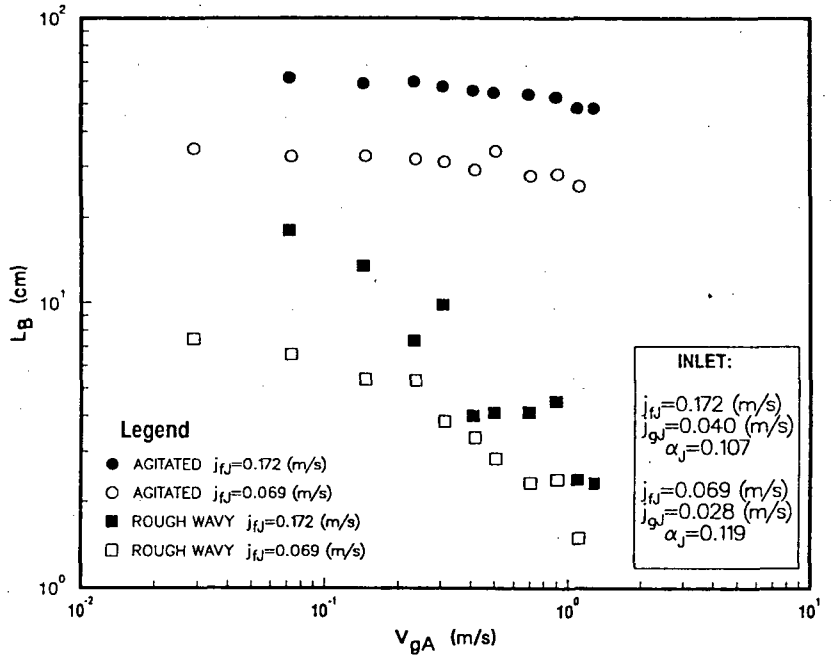


Figure 4. Post-CHF Regime Axial Extents, $\alpha_J \cong 0.1$

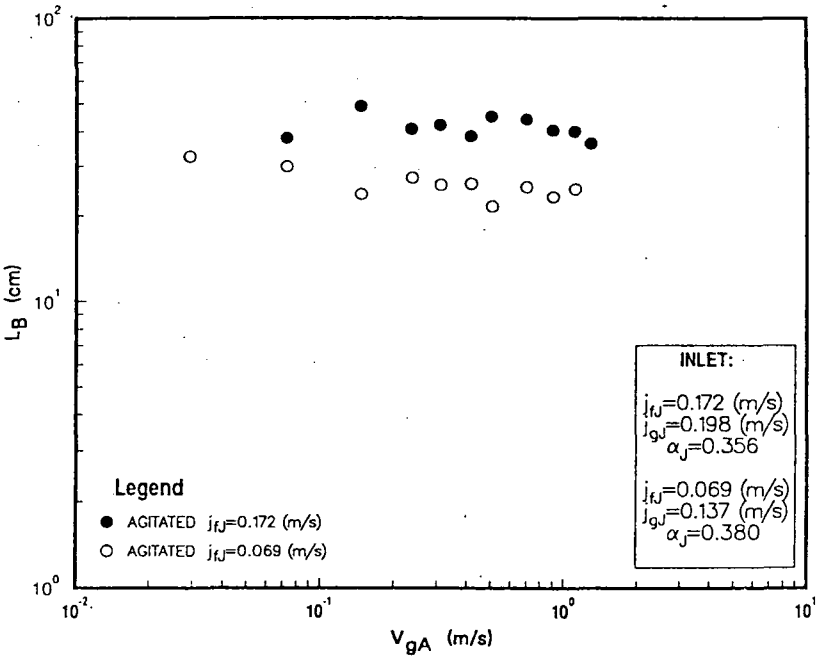


Figure 5. Post-CHF Flow Regime Axial Extents, $\alpha_J \cong 0.35$

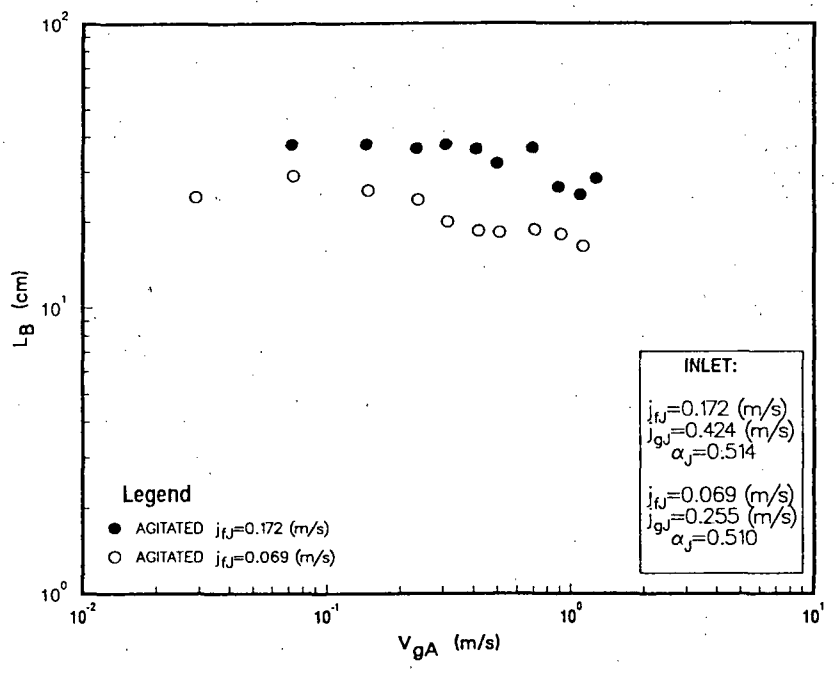


Figure 6. Post-CHF Flow Regime Axial Extents, $\alpha_J \cong 0.5$

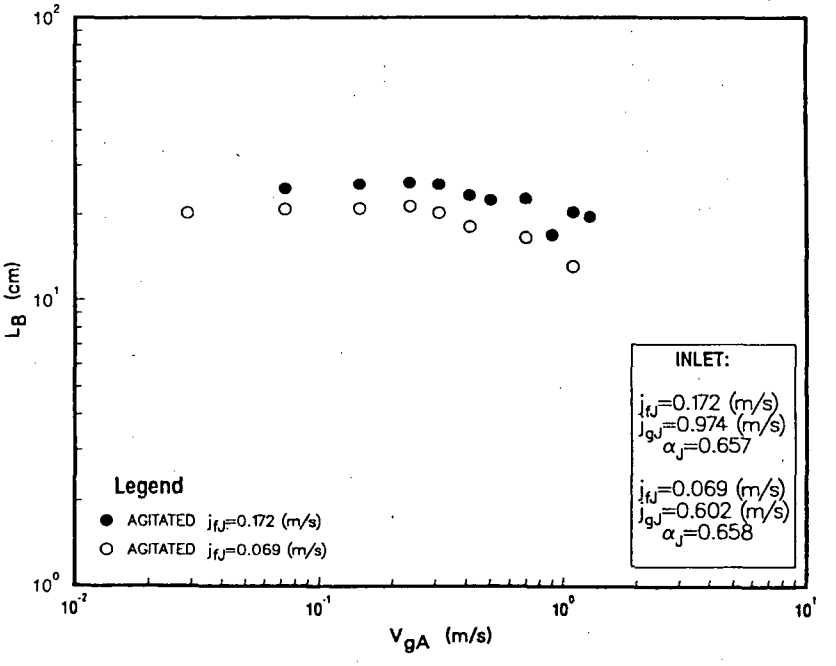


Figure 7. Post-CHF Flow Regime Axial Extents, $\alpha_J \cong 0.65$

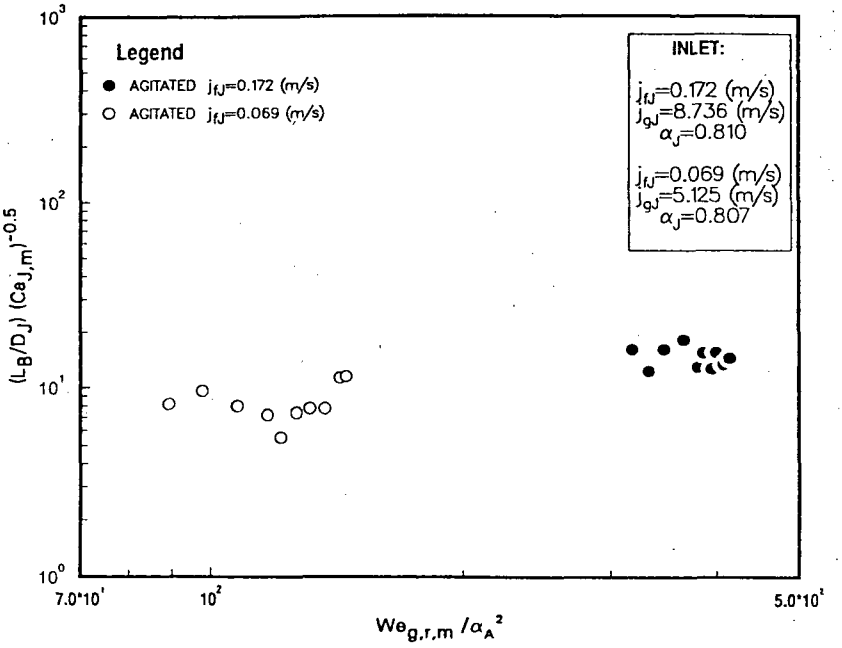


Figure 8. Post-CHF Flow Regime Axial Extents, $\alpha_J \cong 0.8$

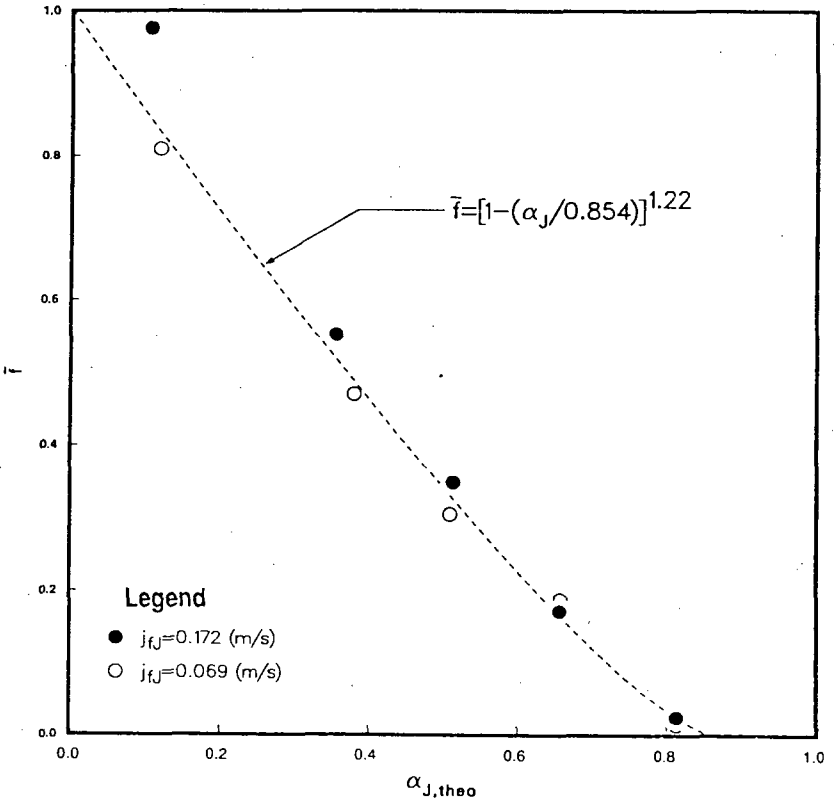


Figure 9. Correlation Correction Factor vs. Jet Void Fraction for Axial Extent of Agitated Flow Regime

# LOOP SEAL CLEARING AND REFILLING DURING A PWR SMALL-BREAK LOCA: RESULTS OF ROSA-IV LSTF EXPERIMENTS

K. TASAKA, Y. KUKITA, J. KATAYAMA
H. NAKAMURA, Y. KOIZUMI AND H. ASAKA

JAPAN ATOMIC ENERGY RESEARCH INSTITUTE

ABSTRACT

During a cold-leg small-break loss-of-coolant accident in a pressurized water reactor, the core collapsed liquid level is depressed when liquid in the loop seals is cleared by vapor toward the broken cold leg. Loop seal clearing and associated core level depression may occur again if the loop seals are refilled by water after clearing. This paper discusses experimental results on loop seal clearing and refilling obtained from loss-of-coolant experiments at the ROSA-IV Large Scale Test Facility (LSTF).

## I. INTRODUCTION

During a cold leg small-break loss-of-coolant accident (SBLOCA) in a pressurized water reactor (PWR), the core liquid level is not solely determined by the vessel liquid inventory but is dependent on the primary loop differential pressure (between the vessel hot-leg and cold-leg nozzles) which is created mainly by the liquid remaining in the loop seals (cross-over legs). Since the liquid in the loop seals prohibits the core-generated vapor from escaping through the break, the vapor will depress the loop seal downflow-side liquid level until the vapor eventually blows out the liquid toward the break. During this process (loop seal clearing), the loop differential pressure will maximize and depress the core collapsed liquid level down to the loop seal bottom elevation that is lower than the top of the core. Although this differential pressure will diminish as soon as the loop seals clear in one or more loops, there is a possibility that loop seals refill with liquid and this causes core liquid level depression again.

This paper is concerned with experimental results on loop seal clearing and refilling phenomena observed at the ROSA-IV Large Scale Test Facility (LSTF). It is shown that loop seal refilling can occur at primary pressures higher and lower than the secondary pressure due to different mechanisms.

## II. TEST FACILITY

The LSTF, shown in Fig. 1, is a 1:48 volumetrically-scaled full-height model of a Westinghouse-type 4-loop (3423 MWt) PWR. It is configured symmetrically with two primary loops. Each loop, representing two loops in the reference 4-loop PWR, includes an active steam generator (SG) which consists of 141 full-size U-tubes.

The LSTF hot legs (207 mm i.d.) are sized to conserve the length to square-root-of-diameter diameter ratio $L/\sqrt{D}$ as well as the scaled volumes. This scaling criterion was taken to simulate the flow regime transitions in the horizontal legs.[1] The loop seals (168 mm i.d.) are sized to scale the volume and height. The loop seal cross-sectional area is about 1/22 scale since each LSTF loop represents two PWR loops.

## III. LOOP SEAL CLEARING

Cold-leg break experiments have been conducted at the LSTF for scaled break areas of 0.1% (1 run, with HPI activated by the safety injection signal), 0.5% (5 runs, all without HPI), 2.5% (2 runs, both without HPI), 5% (3 run with HPI and 4 runs without) and 10% (1 run with HPI and 3 runs without). All the experiments used a sharp-edged orifice to simulate the break.

Loop seal clearing occurred in all these experiments except the 0.1% break experiment where the HPI flow rate balanced with the break flow rate before loop seals cleared. The number of cleared loops was dependent on the break area as summarized in Table 1: only one out of the two loops (the broken loop in all the cases) cleared for 0.5 and 2.5% breaks, and both loops cleared for 5 ad 10% breaks.

For 0.5% break experiments, loop seal clearing was incomplete, with a certain amount of liquid remaining in the loop seal upflow side, whereas it was complete for 2.5% break experiments. The broken-loop upflow leg differential pressure measured for one of 0.5% break experiment (Run SB-CL-12) is shown in Fig. 2. This figures also shows vapor flow rate through the loop seal predicted by the RELAP5/MOD2 (CY 36.05) code.[2] The predicted flow rate is zero before loop seal clearing, and increases quickly after the vapor starts to flow the upflow leg, taking a peak value that is several times greater than the steady-state value reached after loop seal clearing, This steady-state value is equal to the break flow rate. (The break flow is single-phase vapor after loop seal clearing.) The transient overshooting of the vapor flow rate may occur due to the "capacitance" effects of the primary volumes filled with vapor.

The completeness of liquid clearance appears to be related to flooding of the loop seal upflow leg. The vapor-phase Kutateladze number, $K_g$, calculated for the steady-state vapor flow rate was about 0.8 for 0.5% break and 4 for 2.5% break. These values are smaller and larger, respectively, than the flooding limit available in literature for large diameter vertical pipe of $K_g=3.2$[3]. Thus, it seems reasonable that clearing was complete for 2.5% and incomplete for 0.5%. (Note that the LSTF loop seal cross-sectional area is a factor of 48/22 greater than 1/48-scaled PWR loop seal cross-sectional area. The number of cleared loops may be dependent not only on the break flow rate (i.e., the total vapor flow rate through all the loops) but also on the upflow-leg flow resistance (primarily the pump resistance) that would determine the vapor flow partition among the loops.

## IV. HIGH-PRESSURE LOOP SEAL REFILLING

For all 0.5% cold leg break experiments (5 runs) conducted so far in the LSTF with assumed complete failure of HPI, the cleared loop (broken

loop) started to refill soon after clearing. At this time, the primary pressure was nearly in equilibrium with (but slightly higher than) the secondary pressure that was about 8 MPa.[4,5]

The loop seal refilling in these experiments occurred since the condensate, which formed in the SG downflow side, dropped into the loop seals and accumulated there. The SG condensation was continuing because the primary pressure remained higher than the secondary pressure even after loop seal clearing which enabled the vapor to discharge from the break. The vapor discharge rate out of the break (about 0.4 kg/s) was smaller than the core vapor generation rate (about 0.8 kg/s) at this stage of transient (about 2000 s after break).

The condensate in the broken-loop loop seal was not blown out by the vapor but formed a two-phase mixture which eventually filled the loop seal upflow side entirely, while the loop seal downflow side remained clear. The hydrostatic head of this two-phase mixture depressed the core liquid level, which had been already dropping due to vessel inventory boil-off, and thus accelerated the onset of core dryout. This situation is shown schematically in Fig. 3.

Loop Seal Void Fraction

These experiments have been analyzed using the RELAP5/MOD2 and TRAC-PF1/MOD1[6] codes. Both codes predicted the loop seal refilling behavior reasonably well, however, the timing of loop seal clearing was affected by the accuracy of break flow rate prediction which had been unsatisfactory for these codes before appropriate modifications[5,7] were made to the code's break flow models. Fig. 2 compares the measured and RELAP5-predicted broken-loop loop seal upflow-side differential pressures for Run SB-CL-12. RELAP5 predicts well the increase in the loop seal differential pressure after loop seal clearing, as well as the maximum loop seal differential pressure that was reached after the two-phase mixture filled the upflow leg to the pump inlet.

For a 0.5% break, the vapor flow rate through the cleared loop seal (that was equal to the break flow rate) was smaller than the flooding limit as has been discussed earlier, and thus it is reasonable that the loop seal mixture was not cleared by the vapor. The agreement between the predicted and measured loop seal void fractions (about 0.5) is somehow unexpectedly good considering that the code has been scarcely tested against void fraction data for high-pressure large-diameter flows.

## V. LOW-PRESSURE LOOP SEAL REFILLING

The U.S. Nuclear Regulatory Commission (USNRC) recently identified the possibility of core liquid level depression during long-term core cooling following a LOCA.[8] The level depression may occur if the loop seals refill, in all the loops, with the emergency core coolant (ECC), closing the vapor path to the break. During this level depression the core top region may uncover and heat up until at least one loop seal clears again.

This phenomenon has been simulated at the LSTF by conducting dedicated experiments for scaled break areas of 5, 10 and 75%. The break was located between the ECC injection port and the vessel cold leg nozzle, and was simulated using a sharp-edged orifice for the 5 and 10% breaks

and with a venturi for the 75% break. The orifice/venturi was mounted in a horizontal piping connected to the cold leg. These experiments did not simulate the whole LOCA transient but were initiated from a low primary pressure that was reached after conducting a SBLOCA integral experiment. The experimental conditions are summarized in Table 2. The secondary pressure was kept higher than the primary pressure, which was lower than 0.7 MPa in all the experiments, by leaving the secondaries isolated. The experiments were conducted by changing both the core power and ECC injection rate in steps. ECC was injected to the intact and broken cold legs at an intended ratio of 3:1, however, this ratio varied with variations in the cold leg pressures in the two loops.

The loop seal behavior in these experiments was governed by the vapor flow rate through the loop seal that was primarily dependent on the core power. The experimental results are summarized in Table 3 and are described as follows.

Loop Seal Clearing Limit

For core powers lower than about 0.5% of the scaled PWR rated power, both loops remained sealed, i.e., loop seal clearing did not occur. This happened because the core steaming was suppressed by heat loss to the downcomer. This heat was removed by a vessel crossflow, formed by the ECC injected into the intact loop, and was delivered toward the break (Fig. 4). A steady state was reached when the break flow equilibrated with the ECC injection rate.

Obviously, the core-to-downcomer heat loss in these experiments was much greater than scaled since the LSTF does not represent the core bypass region. The LSTF core and downcomer are separated only by a 10-mm thick core barrel. Thus the net core vapor generation rate needs to be evaluated considering this heat loss.

Loop Seal Refilling Limit

For core powers higher than about 1.5%, at least one of the two loops (mostly the broken loop) remained clear, i.e., refilling of both loops did not occur being prohibited by the vapor counterflow through the clear loop seal. The location at which countercurrent flow limitation (CCFL) occurred has not been defined yet, though it may be in the reactor coolant pump where the flow cross-sectional area is smaller than the leg piping (Fig. 5). The minimum cross-sectional area is located at the pump discharge side (0.0090 $m^2$) where the flow direction is horizontal. The pump discharge opens at the centerline elevation of the hot leg (0.0336 $m^2$ in area) The loop seal upflow leg (0.0222 $m^2$ in area) is connected to the pump suction which has the same diameter (0.168 m) as the loop seal. Since this loop seal refilling phenomenon was not taken into consideration in the LSTF design, the LSTF pump flow areas are not scaled at the PWR pump. Neither the pump flow geometry is representative of an actual PWR pump. Thus, quantitative extrapolation of the present experimental results to real plant transients will require considerable efforts.

Fig. 6 shows data points (pressure vs. core power) plotted against contour of the vapor-phase Kutateladze parameter evaluated for the pump minimum cross-sectional area. The plotted values of core power are not corrected for the core-to-downcomer heat loss that is about 0.5%

for the low-pressure loop seal refilling experiments. The high pressure (> 1 MPa) data points shown in Fig. 6 were taken from a 5% SBLOCA experiment. In this experiment, accumulator came on at a primary pressure of 4.51 MPa and LPI at 1.26 MPa, however, both loops remained clear until this test was terminated at a core power of 1.5%. This figure consistently shows that the cold leg ECC liquid is prohibited from falling into the loop seal for vapor flow rates greater than a certain limiting value. The limiting value of $K_g$ appears to lie between 5 and 10. (This uncertainty range will become smaller after the low pressure data are corrected for heat loss. ) This result appears reasonable, since $K_g$=8.0 at the pump discharge is equivalent to to $j_g^*$=1.0 at the same location, where $j_g^*$ is non-dimensional gas-phase superficial velocity (Wallis parameter)[9], and this also corresponds to $K_g$=3.2 at the loop seal upflow leg (i.e., pump suction). Namely, flooding limit may well be reached at both pump discharge (horizontal flow) and suction (vertical flow) for net core powers (excluding the core-to-downcomer heat loss) corresponding to $K_g$=8.0 at the pump discharge.

Repeated Refilling and Clearing

For the intermediate core powers, between 0.5 and 1.5%, loop seal clearing and refilling occurred cyclically. This involved cyclic variations of the primary pressure, break flow rate and core inlet subcooling. The mechanism of the cyclic loop seal clearing and refilling is described diagrammatically in Figs. 7 and 8.

This phenomenon was characterized by significant variation of the break flow. The variation of the difference between the ECC and break flow rates is shown in Fig. 9. This shows the net increase or decrease rate of the coolant inventory. The break flow rate varied so largely with the change in the primary pressure since the differential pressure across the break orifice (that determines the break flow rate) was small. The primary pressure was only slightly higher than the pressure in the simulated containment system, and this primary pressure was determined primarily by the balance between the ECC flow rate and the break flow rate that was dependent of pressure.

When all the loops were sealed, the core-generated vapor was no longer able to escape from the break, and this resulted in a primary pressurization which continued until the break flow rate exceeded the ECC injection rate causing a net decrease in the primary coolant inventory. This decrease in the coolant inventory resulted eventually in loop seal clearing. After the loop seal clearing, the vapor flow rate through the cleared loop seal was enough to sweep the liquid out of the upflow leg completely or almost completely.

Once loop seal clearing occurred, the primary pressure decreased due to vapor discharge. Then, the break flow rate decreased, due to both an increase in the break flow and a decrease in the primary pressure, resulting in a net increase in the primary coolant inventory. Since the vapor flow rate through the cleared loop seal decayed, due to the primary depressurization following loop seal clearing, and also due partially to a decrease in core vapor generation resulting from the penetration of ECC following loop seal clearing, CCFL broke down and the cold leg liquid was allowed to refill the loop seal.

The observed phenomena were qualitatively the same for the three

experiments which were conducted for different break areas (5, 10 and 75%). The influence of break area was appreciable only in the primary pressure; the time-averaged primary pressure tended to be lower for larger breaks.

Core Dryout Behavior

Fig. 10 shows core collapsed liquid level obtained from the measured core differential pressure. The level dropped to the loop seal lowest elevation (1.8 m above the core bottom) every time the loop seal cleared. Fig. 11 shows the core mixture level calculated by using the Cunningham-Yeh void fraction correlation[10] for the measured variation of core differential pressure. The calculated mixture level drops below the core top during the collapsed level depressions and the lowest mixture level depends on the core power. Experimentally, the core mixture level was not well defined from the rod temperature measurement because the core power was so low that the rod surface could be cooled by the existence of small amount of liquid.

Fig. 12 shows the calculated minimum core mixture level (during loop seal clearing) as a function of primary pressure and core power. This figure indicates the boundary of reactor conditions under which the core top region may uncover during loop seal clearing. Experimental observations, from both low-pressure loop seal experiments and transient SBLOCA experiments, are consistent with the calculated boundary.

The rod temperature excursions were generally small because of low core power. It is interesting to note that the maximum rod surface heatup above the saturation temperature (70 K) was recorded for a core power of 0.7%, close to the loop seal clearing limit (0.5%). The behavior of the peak cladding temperature for this case is shown in Fig. 13. For this case, the loop seal clearing progressed slowly. Thus the core top region remained uncovered for a relatively long time (more than 100 s) and continued to heatup although the heatup rate was small due to the small core power.

## VI. CONCLUSIONS

Clearing and refilling of loop seal during a cold-leg SBLOCA have been studied with regard to experimental results obtained at the ROSA-IV LSTF. Three dedicated experiments were conducted on low-pressure loop seal refilling phenomenon that may occur during PWR cooldown process following a LOCA. The primary observations obtained from this study are:

(1) The number of cleared loops depends on the size of break. When only one loop is cleared, the completeness of liquid clearing depends again on the size of break.
(2) When the break size is insufficient to relieve all the vapor generated in the core, the loop seal is refilled, after clearing with SG condensate. This causes a core liquid level depression.
(3) When the core power has decayed significantly, ECC in the cold leg will refill the loop seal against the vapor counterflow. The refilled loop seal will eventually cleared if boiling continues in the core, and this process will repeat.
(4) Loop seal clearing at low core power can result in a prolonged core

uncovery although the uncovered core heats up only slowly.

ACKNOWLEDGMENT

The low-pressure loop seal refilling concern was communicated by the USNRC to the Japan Atomic Energy Research Institute (JAERI) at the JAERI-USNRC ROSA-IV Program Review Group Meeting held in December 1987.

REFERENCES

1. Zuber, N., "Problems in Modeling Small break LOCA," NUREG-0724 (1980) U.S. Nuclear Regulatory Commission.
2. Ransom, V.H. et al., "RELAP5/MOD2 Code Manual," NUREG/CR-4312, EGG-2396 (1985) Idaho National Engineering Laboratory.
3. Richter, H.J., "Flooding in Tubes and Annuli," Int. J. Multiphase Flow, 7 (1981) 647-658.
4. Tasaka, K. et al., "The Results of 0.5% PWR Small-Break LOCA Tests in ROSA-IV LSTF Break Location Parameter Tests Series," Proc. 15th Water Reactor Safety Information Mtg., Gaithersburg, Maryland, Oct. 26-29, 1987.
5. Tasaka, K. et al., "The Effects of Break Location on PWR Small-Break LOCA," to be presented at the Third Int. Topical Mtg. on Nuclear Power Plant Thermal Hydraulics and Operations, Seoul, Nov. 14-17, 1988.
6. "TRAC-PF1/MOD1: An Advanced Best-Estimate Computer Program for Pressurized Water Thermal-Hydraulic Analysis", NUREG/CR-3858 (1986) Los Alamos National Laboratory.
7. Kukita, Y. et al., "Manometric Core Liquid Level Depression During a Small-Break Loss-of-Coolant Accident in a Westinghouse-Type Pressurized Water Reactor, Int. Conf. on Thermal Reactor Safety, ENS/ANS Topical Mtg., Avignon, Oct. 2-7, 1988.
8. Fletcher, C.D. and Callow, R.A., "Long Term Recovery of Westinghouse Pressurized Water Reactors Following a Large Break Loss of Coolant Accident," EGG-TFM-7993 (Feb. 1988) Idaho National Engineering Laboratory.
9. Wallis, G.B., One-Dimensional Two-Phase Flow, McGraw-Hill Book Co., New York, 1969.
10. Cunningham, J.P. and Yeh, H.-C., "Experiments and Void Correlation for PWR Small Break LOCA Conditions," Trans. Am. Nucl. Soc., 87 (1973) 453.

# Schematic of Large Scale Test Facility ( LSTF )

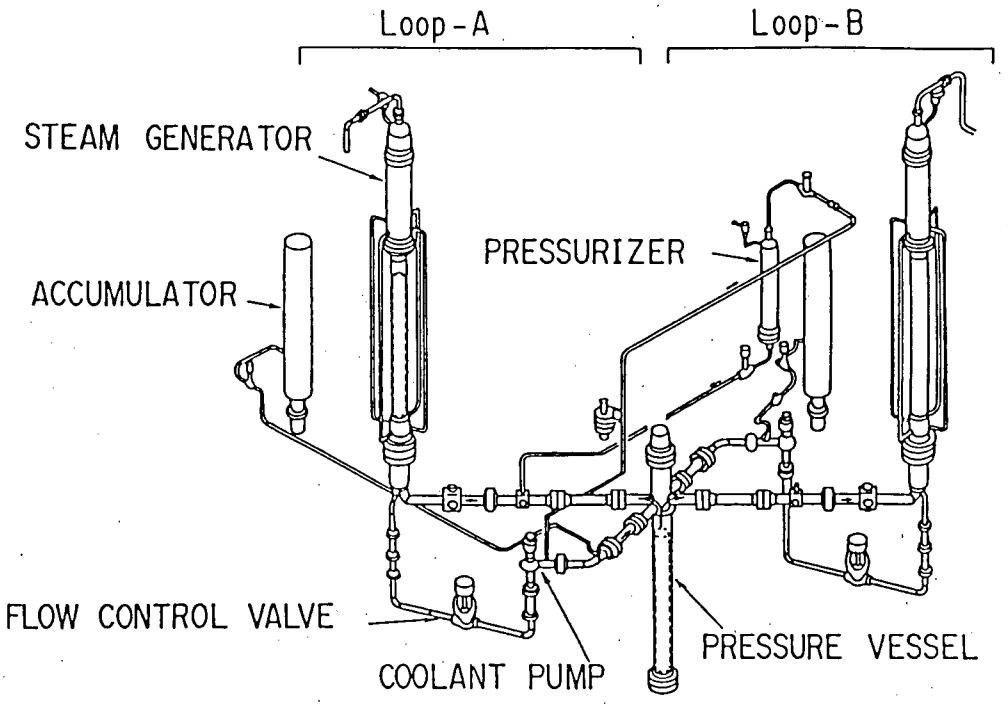


FIG. 1

TABLE 1

## Loop Seal Clearing

| | | | |
|---|---|---|---|
| 0.1% Break | w/ HPI | (1 run) | No Clearing |
| 0.5% Break | w/o HPI | (5 runs) | One Loop (Broken Loop) Cleared |
| 2.5% Break | w/o HPI | (2 runs) | One Loop (Broken Loop) Cleared |
| 5% Break | w/ and w/o HPI | (7 runs) | Two Loops Cleared |
| 10% Break | w/ and w/o HPI | (4 runs) | Two Loops Cleared |

Calculated and Measured Crossover Leg Up-Flow Side Differential Pressure, Liquid Fraction and Vapor Flow Rate during 0.5% Cold-leg Break Test

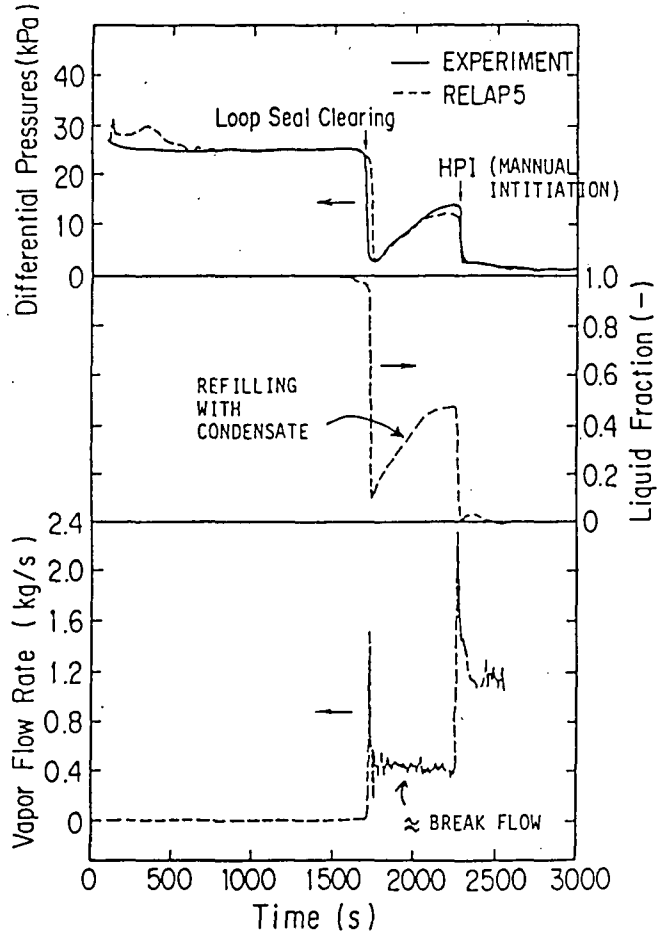


FIG. 2 High Pressure Loop Seal Refilling.

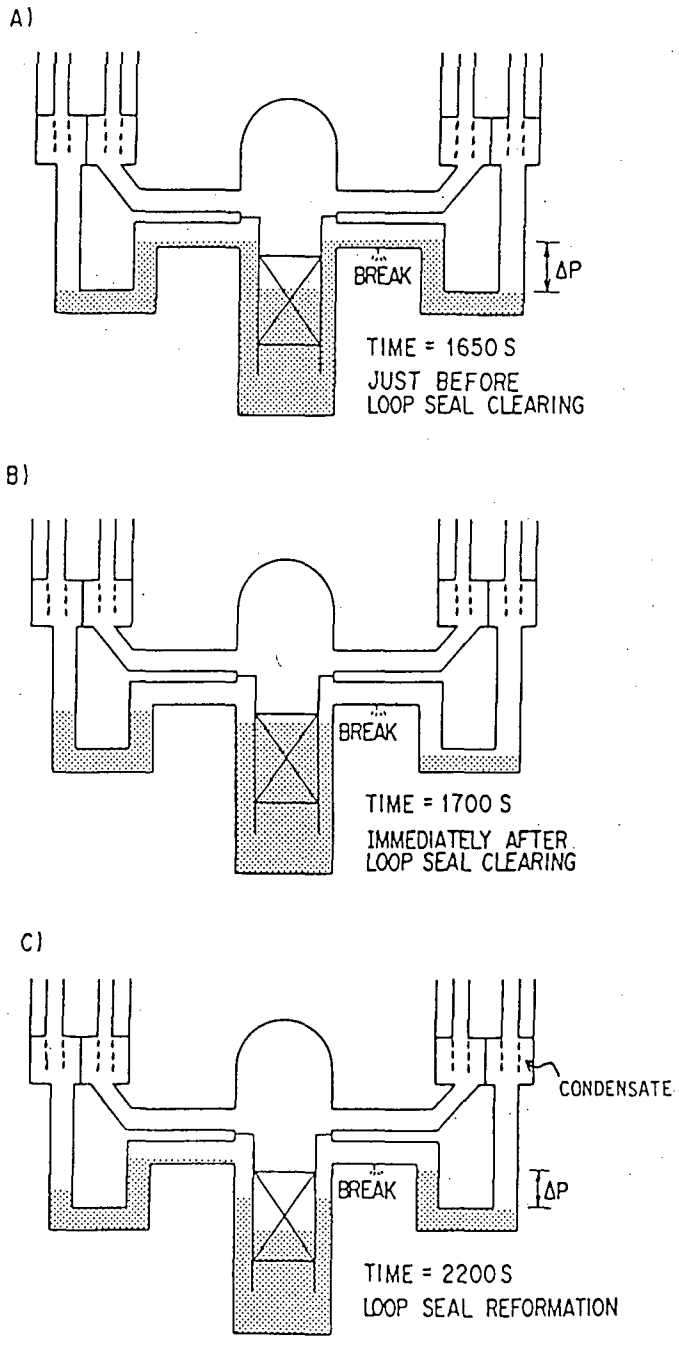


FIG. 3

Primary Coolant Distribution during Refilling.

TABLE 2

## Low Pressure Refilling Tests

- Conducted after the completion of blowdown tests.
- Initial conditions:
  - both loops sealed with water
  - zero core power
- Core power and LPI injection rate were changed in steps.
- Secondary pressure > primary pressure with secondaries isolated.

## Test Conditions

| | SB-CL-14 | SB-CL-18 | SB-HL-04 |
|---|---|---|---|
| Break | 10% Cold leg | 5% Cold leg | 75% Cold leg |
| Core Power | 0.14 - 1.40 % | 0.50 - 1.20 % | 0.20 - 1.50 % |
| Primary Pressure | ≈ 0.25 MPa ( Upper head ) | 0.22 - 0.48 MPa ( Upper head ) | ≈ 0.21 MPa ( Hot leg ) |
| ECCS | | | |
| HPIS | 0.0 kg/s | 2.0 kg/s | 0.0 kg/s |
| LPIS | 5.0 kg/s | 2.0 kg/s, 4.0 kg/s | 8.1 kg/s |

TABLE 3

Summary of Experimental Results

- All loops remained sealed for core powers < 0.5%
  - No loop seal clearing occurred.
- One loop kept clear for core powers > 1.5%
  - No refilling occurred.
- For core powers between 0.5 and 1.5%, loop seal clearing and refilling occurred cyclically.
- Core top region was uncovered and heated up during loop seal clearing.

No loop seal clearing for core powers < 0.5%

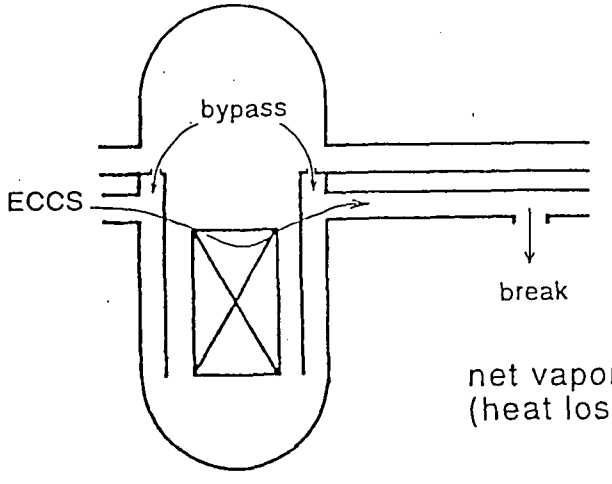


net vapor generation rate ≈ 0
(heat loss to downcomer ≈ core power)

Core heat was removed by the ECC injected into the intact loop which flowed to the broken loop through the downcomer.

The core-to-downcomer heat loss in LSTF is greater than scaled since the core bypass region is not represented.

FIG. 4

## Conditions for Loop Seal Refilling

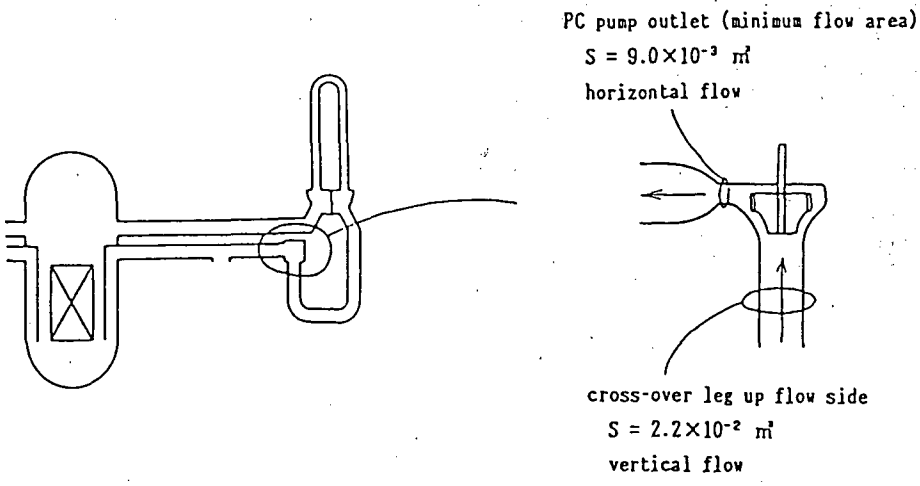


- CCFL controls the onset of refilling. The location of CCFL has not been defined yet.
- Vapor flow rate needs to exceed flooding limit to clear liquid from the loop seal upflow leg.

FIG. 5

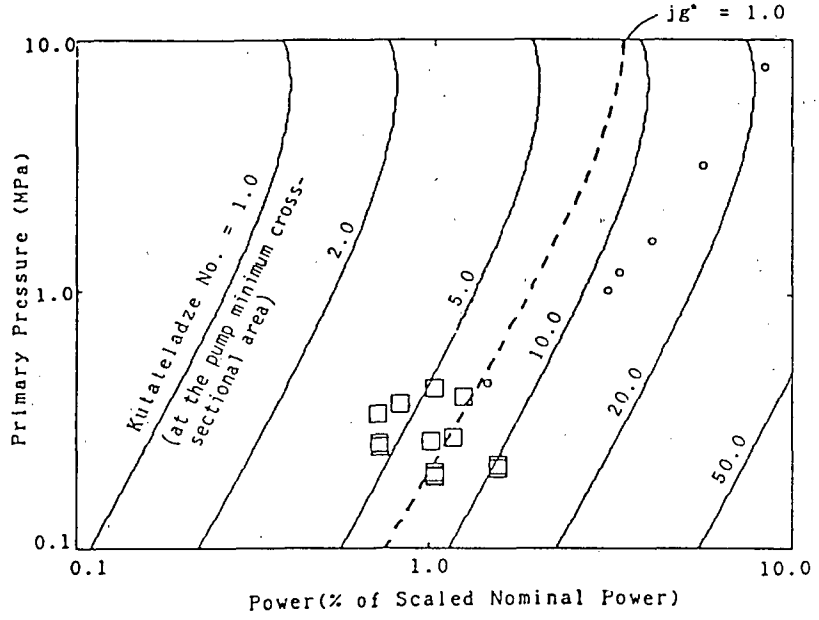


$$\text{Kutateladze No.} = \alpha V_g \left[ \frac{\rho_g^2}{(\rho_f - \rho_g)\,\sigma\, g} \right]^{\frac{1}{4}}$$

FIG. 6

Start of Loop Seal Refilling

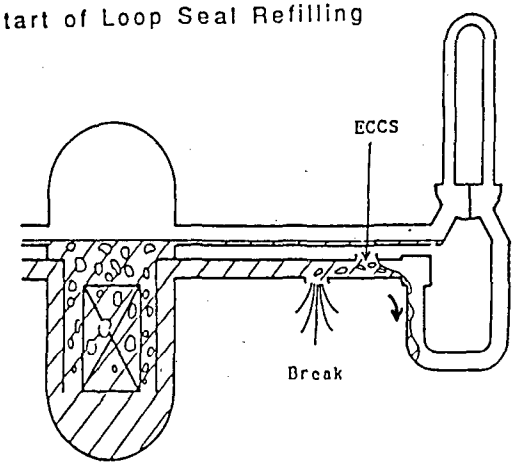


CCFL breakdown

↓

ECC water begins to fall into loop seal

↓

Loop seal is refilled

Loop Seal Clearing

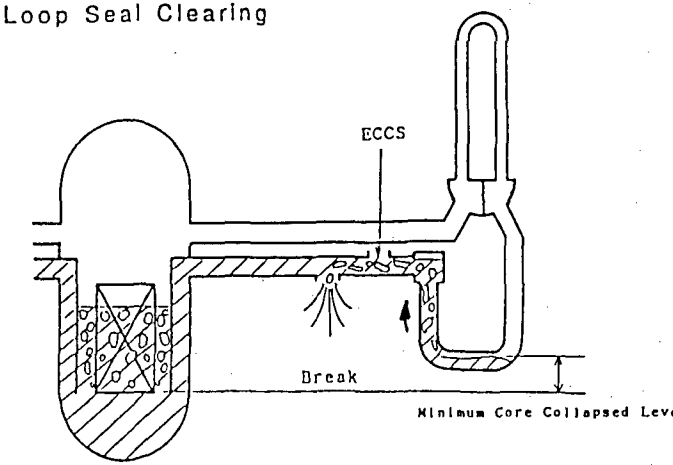


Liquid level depression in the loop seal downflow side.
( concurrent with level depression in the core. )

↓

Vapor starts to reach the break

↓

Liquid in the loop seal is blown out toward the break.

End of Loop Seal Refilling

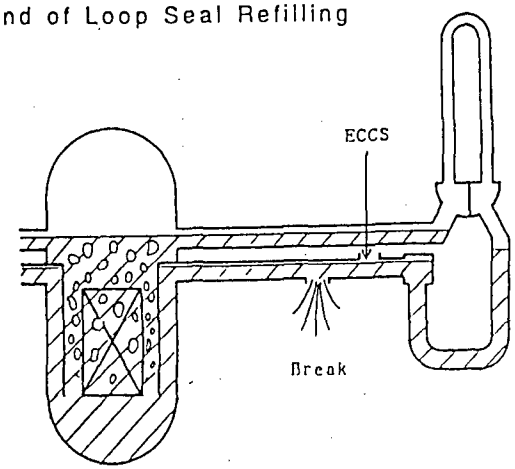


Water level in loop seal downflow side
= Core collapsed level

↓

Vapor cannot escape from the break

↓

the primary pressure increases

FIG. 7

Primary Coolant Distribution during Repeated Loop Seal Clearing and Refilling

Mechanisms for repeated loop seal refilling and clearing.

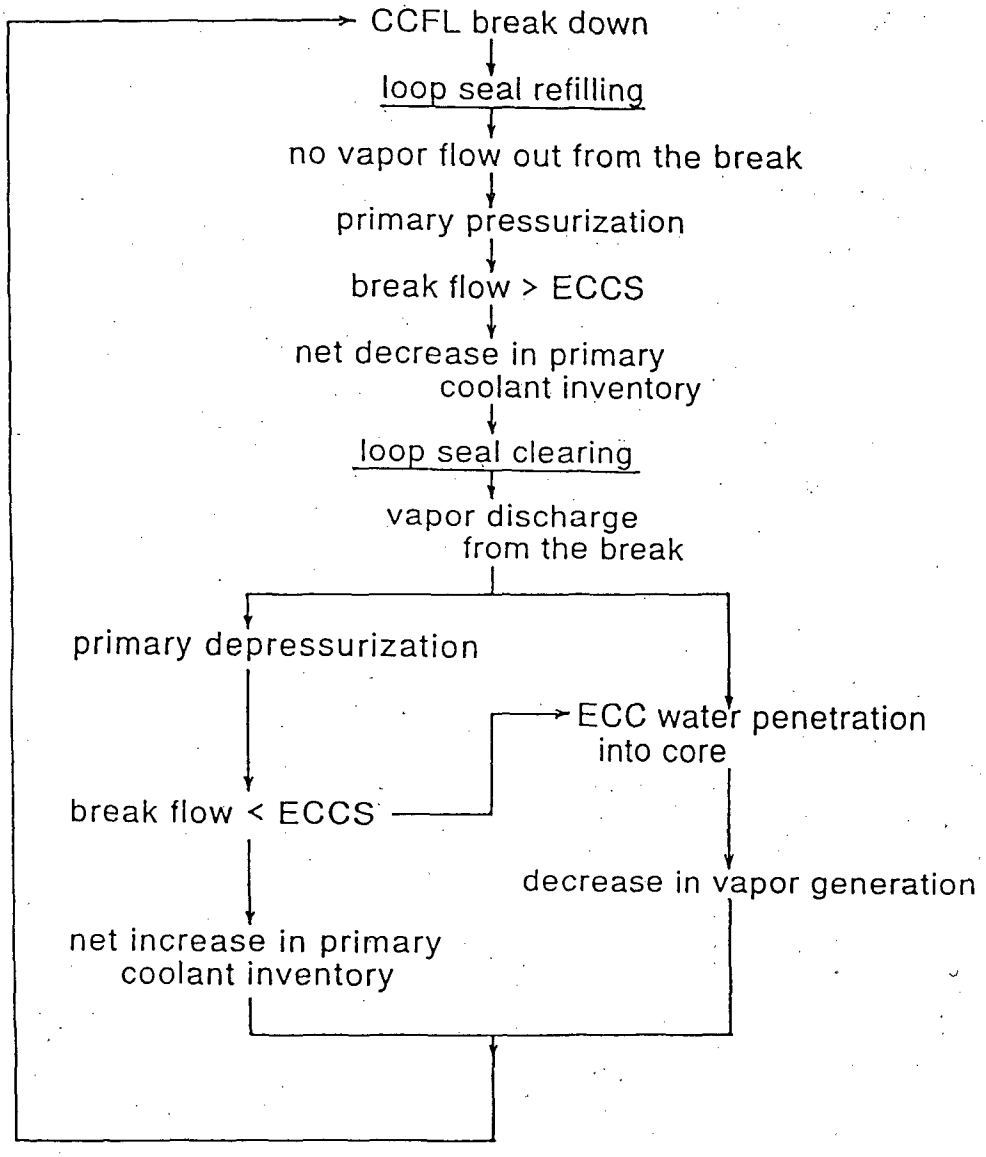


FIG. 8

ECCS > Break flow ... loop seal starts to refill
ECCS < Break flow ... loop seal starts to clear

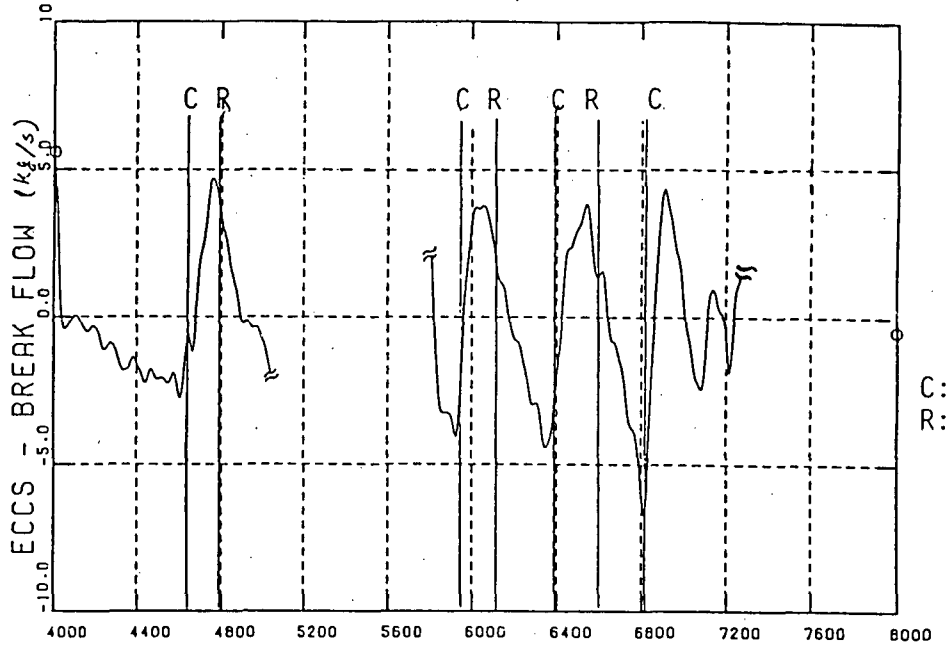


FIG. 9

Core collapsed level = loop seal bottom level
when loop seal clearing starts.

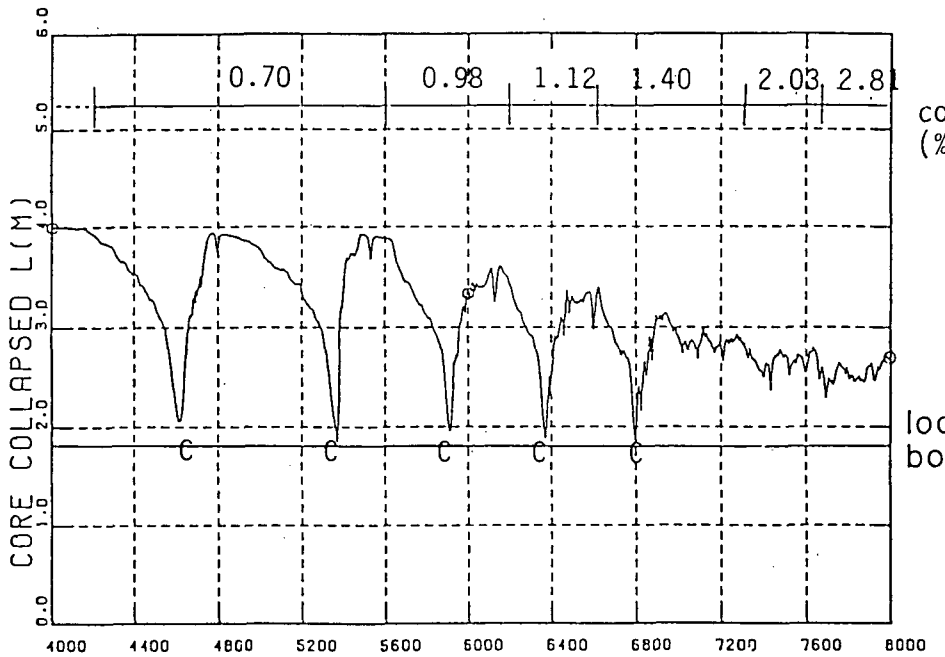


FIG. 10

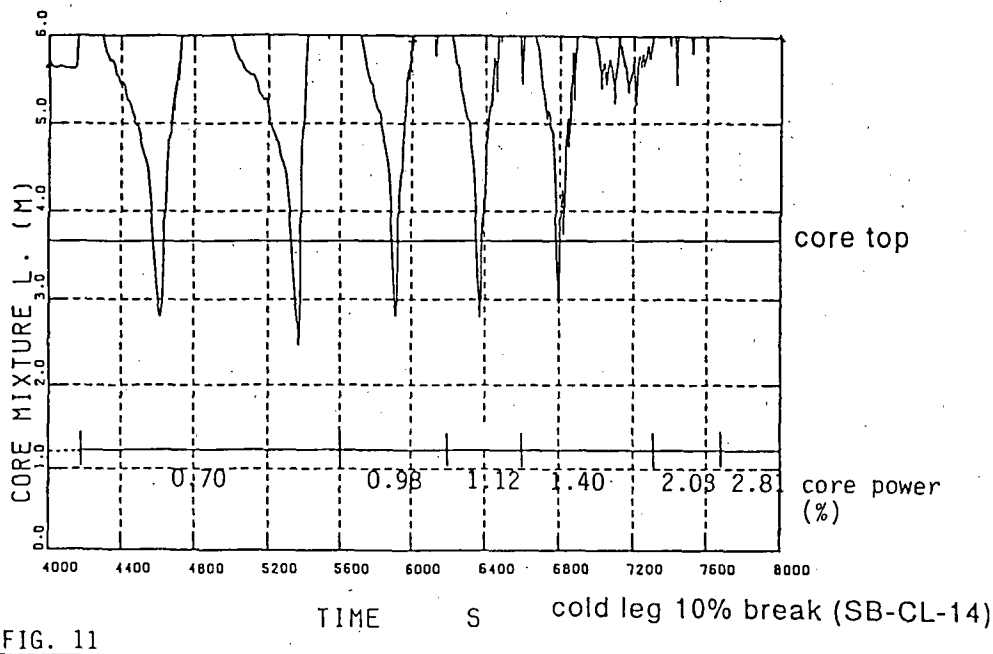


FIG. 11

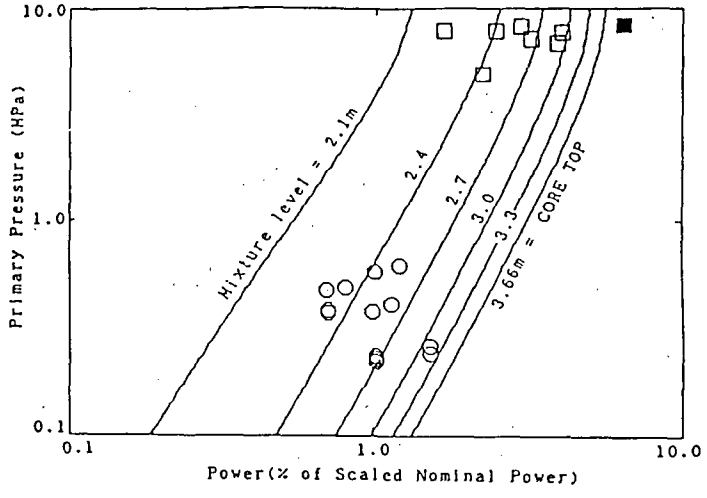


□ — loop seal clearing during blowdown process

( ■ — core uncovery was not detected )

○ — loop seal clearing after the loop seal was refilled

Core mixture level at loop seal clearing

- calculated with Cunningham - Yeh void fraction correlation for core collapsed liquid level = loop seal bottom elevation ( = 1.8m above the core bottom )

FIG. 12

Core heatup

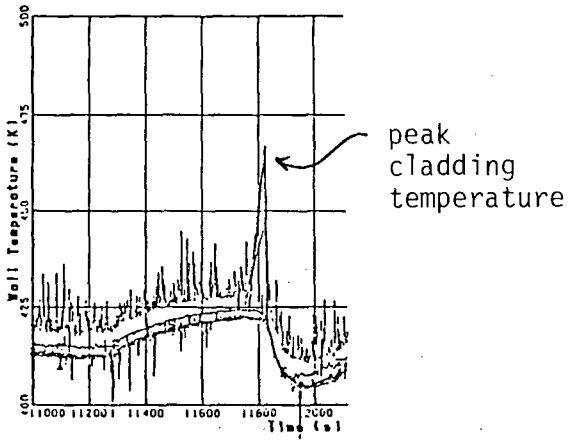


core power = 0.8%

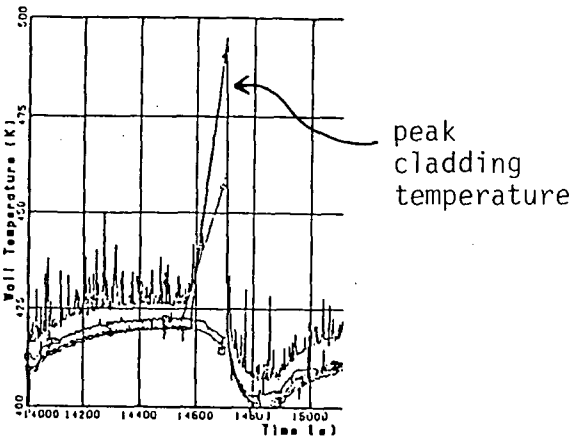


core power = 0.7%

The largest core heatup above the saturation temperature occurred at a low core power close to the loop seal clearing limit ( =0.5% ) because of a slow core level depression which resulted in core uncovery continuing a few hundred seconds.

FIG. 13

# PKL III INVESTIGATION OF PWR OFF-DESIGN CONDITIONS

R. M. MANDL, B. BRAND, K. UMMINGER

Siemens AG, UB KWU Erlangen

## ABSTRACT

A new programme aimed at experimentally investigating off-design transients with and without loss of coolant was startet in 1987.
This paper presents the overall programme objectives as well as test results obtained so far. Future plans are also discussed.

## INTRODUCTION

The increased interest in off-design transients and accident management measures forms the basis of the PKL III* experimental programme.
The PKL Test Facility, operated between 1975 - 85 with the aim to investigate Loss of Coolant Accidents (LOCA), was enlarged and equipped with additional subsystems in 1986/87. Since then an experimental programme has been under way which covers the area of off-design transients (excluding ATWS) and small breaks. The programme is a joint venture of the German Ministry of Research and Technology (BMFT), German Power Utilities (EVU) and the power plant manufacturerer Siemens/KWU-Group. This paper gives an overview of the general programme objectives, presents two tests in detail and outlines future plans.

## PKL III PROGRAMME OBJECTIVES

The objectives of the PKL III test programme focus on the following area:

### Verification of advanced computer codes

Current computer codes capable of analyzing transients or small breaks have reached relatively high standard. These codes can be verified only by using well instrumented integral test facilities.

---

*PKL (Primär-kreis-läufe)

Investigating optimum shutdown operating procedures following off-design plant conditions

A well constructed and instrumented test facility is capable of simulating extreme off-design conditions which cannot be reproduced in the real plant. In this way shutdown procedures can be optimized.
Small breaks on the primary or secondary side and non-availability of one or more subsystems fall into this category.
The experience thus gained will also contribute towards simplification and standardization of operating procedures.

Availability of the test facility for investigation of topical nuclear power plant problems

In a country where over 20 nuclear power plants are either on line or under construction, it is in utilities', manufacturers' and public interest to have a well instrumented test facility available at short notice. The time necessary, to construct a new facility and train a team to operate it takes several years. Recommissioning of an existing facility and assembling a new competent experimental team cannot be achieved in under one year. Continuing the PKL programme will not only produce useful experimental results, it also guarantees permanent availability of a relatively large test facility and of an experienced team.

Scope of Tests

The tests are subdivided into six subgroups, fig. 1.
A small number of characterisation tests are to be carried out. They include the experimental determination of pressure losses, heat losses and the facility's behaviour under natural circulation conditions (single and two-phase). Results of a shutdown at 50 K/h (120 F/h) with one or two RCPs operating lends itself to a comparison with data from the full size plant.
The second group covers tests simulating Loss-of-Offsite-Power conditions, i. e. a shutdown at 50 K/h ($\sim$ 120 F/h) using one or more steam generators but RCPs not in operation. Special attention is to be paid to formation of voids in the primary system and their effect on the ability to reduce the primary pressure.
The third group addresses the question of restarting the RCPs in the presence of a void in the upper plenum.
The fourth and fifth groups cover small breaks on the primary and secondary. They include various break locations such as the hot or cold legs, pressurizer, and steam generator tube(s) rupture.
The final group of tests deals with feedwater system failures.
Here it is of interest to determine the minimum water level required in a steam generator (the other three being isolated) at which there is no pressure increase on the primary operating in natural circulation mode. The effect of injecting emergency feedwater (cold) into a depleted steam generator is also to be investigated.

## TEST FACILITY DESCRIPTION

The PKL test facility was originally designed as an integral test facility to investigate the refill and reflood phases of large-break loss of coolant accidents (LB LOCA).

As the phenomena of interest in the current test series differ from those occurring during LB LOCAs it was necessary to modify and improve certain sections of the facility.

### Primary Side

As in all other comparable test facilities power/volume scaling with original elevations was used. The scaling factor was determined as the ratio of the numbers of heater rods in the test bundle to the number of fuel rods in the reactor - it is 1:145, fig. 2.
The core power of 2.5 MWe is equivalent to 10 % of nominal rating - sufficient for the proposed tests as reactor scram is postulated on accident detection. The limited maximum allowable pressure of 40 bar on the primary side means that certain types of tests (the faster transients) cannot be fully simulated. Counterpart tests with LOBI and LSTF test facilities in which test results at 40 and 80 bar are to be compared will provide information on the validity of extrapolating PKL results to higher pressures. A scaling study /1/ showed that thermodynamic properties and certain phenomena such as density, single and two-phase heat transfer do not change significantly between 40 and 80 bar.

In this relatively large test facility, distortions such as excessive heat losses or boundary effects on flow are of considerably lesser importance than they are in smaller facilities.

As shown in fig. 2 the reactor pressure vessel is modelled by volume - trically scaling the full height of the upper and lower plena. The downcomer is modelled as an annulus in the upper region and continues as two stand pipes connected to the lower plenum. This configuration permits reliable determination of flow rates, provides adequate access to the test bundle (instrumentation), and does not unacceptably distort the volume/surface (water/steel) ratio. This is of importance with respect to the removal of stored heat from the walls during cooldown.
This facility is the only large-scale test facility with 4 loops. Its configuration allows, among other things, to investigate the individual effects of multiple failures. The 4 loops are arranged symmetrically around the RPV which means that the requirement for identical piping lengths and hence recirculation period is fulfilled.
For these experiments active pumps are required; they are equipped with speed controllers to enable any pump characteristics to be simulated. Experiments on the behaviour of a 3-loop plant can also be conducted by simply isolating one loop.

Engineered Safety Systems

In the course of SB LOCAs and transients a large number of systems become effective. On the primary side these are:

- o high-pressure safety injection system
- o accumulators
- o low-pressure injection system
- o residual heat removal system
- o volume control system
- o pressurizer pressure control system (heating and spraying)

All these systems are integral part of the PKL facility and are fitted with appropriate control equipment, fig. 3.

Secondary Side

The secondary side, too, is simulated in accordance with the demands of the test matrix:
Each of the 4 steam generators is equipped with 30 U-tubes of original size.
Allowance has been made for the differing elevations (1.5 m) between the tube with the smallest and largest bending radius.
These different elevations affect the transition from natural circulation to reflux condenser operation (film condensation).

Since the secondary is the main and in many cases the only heat sink available in the postulated transients, special care was taken to ensure that the steam generator and the systems connected to it were simulated as correctly as possible. This included:

- o correct volume in the tube area
- o simulation of the downcomer by 2 stand pipes (instrumentation, symmetry)
- o water and steam dome volumes above the tube bundle
- o flow limiter at outlet
- o feedwater system
- o emergency feedwater system
- o main-steam lines with all control features of the original systems, fig. 4

The turbine and the condenser were not simulated in all cases the outflowing steam is dumped via silencers to atmosphere (open-loop system).

Instrumentation

Only extensive instrumentation of the test facility guarantees optimum use of the test results. The 1070 measuring points in PKL III are divided into three categories:

o PKL test instrumentation (860)
o PWR-identical instrumentation ( 60)
o PKL operational instrumentation (150)

The last mentioned will be used to run the facility. As the name implies, location and function of the PWR-idendical instrumentation in the PKL facility are identical with those in the PWR.
After analyzing a test using the extensive PKL instrumentation, the PWR identical instrumentation will be evaluated separately with the aim of finding out whether this information alone would have helped the operator to draw the correct conclusions about the phenomena and the course of the test.

## RESULTS

To date about half of the 23 planned tests have been carried out. Two of these, namely "Loss of Off-site Power" and "Restart of Reactor Coolant Pumps with a Steam bubble in the Upper Plenum" are described here in detail.
The salient points of the other experiments are summarized at the end of this section.

### Loss of Off-site Power

When the connection to off-site power is lost the plant depends on diesel generators for its power. This means that the cooling capability of the secondary is preserved, on the primary the RCPs are not operational. Under these conditions it is still possible to shutdwon the plant at the prescribed 50 K/h ( 120 F/h) as the energy is transferred from the core to the steam generators by means of natural circulation.
However, in this case there is no significant pressure difference between the downcomer and the upper plenum and no flow through the upper-head bypass. If follows that as the pressure and temperature are decreased throughout the plant the upper head and a part of the upper plenum where there is no flow soon reach the saturation temperature leading to formation of a steam bubble in this region, figs. 5, 7.
As the pressure is decreased the size of the steam bubble increases - heat losses are too insignificant to be able to remove energy from the bubble. The bubble reaches its maximal size about 0.3 m above the hot leg top edge and during further cooldown and depressurization the size of it does not change. The flow pattern in this region is such that the subcooled water entering the hot legs erodes the thin layer of saturated water which forms the boundary at the steam/water interface. The 0.3 m level (which turned out to be reproducible in all tests) is evidently the location where the energy removal from the bubble and its tendency to grow by depressurization is in equilibrium. In the long term (many hours) the steam bubble slowly diminishes in size - this is attributed to the natural cooldown of the upper head.

Restart of RCP with Steam Bubble in Upper Plenum

In the above scenario if half an hour after the bubble was formed the off-site power is restored, the operators are faced with the decision whether or not to restart the RCPs. Sudden mixing of subcooled water and steam could lead to violent condensation and endanger the structural integrity of the upper plenum.

The RCP restart was performed in PKL, fig. 6, 8. No violent condensation took place and the bubble started to diminish in size at a maximum rate of about 0.5 m/min. This is attributable mainly to the upper head bypass flow which after restarting the pump, amounted to about 0,5 % of the downcomer flow and was responsible for condensation not at the steam/water interface but at the location of the bypass overflow. When the diminishing bubble reached this location and the bypass flow started injecting into water instead of into steam the rate of the bubble decrease was slowed down to 2 cm/min. At this point a second RCP was turned on resulting in a changed pressure distribution within the primary but affecting the bubble in no way whatsoever.

Salient Points of other Experiments

The base line tests established these characteristics for which power plant data are available. The pressure losses and flow distribution in the individual loops with one or more RCPs operating were within a few percent of the power plant data. The maximum heat losses on the primary (50 kW), although proportionately higher than in a PWR, can be partly compensated and do not cause an undue distortion of test results. The heat losses on the secondary (ca. 18 kW per SG) are fully compensated.

Natural circulation is an important mechanism for cooling the reactor core and was investigated in detail. The mass flow as a function of coolant volume on the primary is shown in fig. 9.
The mass flow peaks at 83 %, at about 62 % natural circulation stops and reflux condensing becomes the only mode of heat transport from the core to the steam generators. The CCFL and water hold-up characteristics in the hot legs and SG tubes as a function of power will be investigated in future tests.

Yet another natural circulation (single-phase) test showed clearly that when under steady state conditions one steam generator is isolated but the other three are operating then flow also exists in the isolated steam generator. This fact is significant in avoiding unequal distribution of boron in the system.

Efficient depressurisation of an isolated steam generator without violent condensation and excessive temperature gradients on the secondary can be achieved by reducing the secondary side water level (using the letdown line) and exposing to steam mere 1 % of the primary tubing area. This procedure ensures that the secondary follows

closely the primary in pressure as well as temperature.
Injection of emergency feed water (cold) into a depleted secondary side of a steam generator was also investigated.
The injected water warmed up on the condensing steam and hot downcomer walls and by the time it reached the riser tubes and the tube sheet it was not more then 50 K (122 F) below the prevailing saturation temperature. No violent condensation occured in this test - the secondary pressure fell by not more than 2 bar/min before the injection ring was completely covered with water.

## OUTLOOK

The present test series will be continued by investigating small breaks on the primary and secondary as well as steam generator tube rupture.
A follow-up programme with following aims is under discussion:

- accident management measures
- investigation of CCFL phenomena in SGs
- tests involving $N_2$ in primary
- counterpart tests with ROSA IV and LOBI to investigate the effect of scale under otherwise identical conditions.

## CONCLUSIONS

The first results of the "PKL III Transients and Small Breaks" experimental programme are presented in this paper.
The characterization tests showed that where data for the pilot plant are available (e. g. pressure losses, flow distribution pump characteristics) the agreement with PKL data is within a few percent. A natural circulation test established the test facility's characteristics under single-phase, two-phase and reflux condenser conditions. In a simulated loss of off-site power test it could be shown that while shutting down the plant at 50 K/h under natural circulation conditions the steam bubble which is formed in the upper plenum does not enter the hot legs. Subsequent restarting of at first one and later of a second RCP did not lead to violent condensation in the upper plenum; a steady bubble decrease of max. 0.5 m/min was attributable to the upper head bypass flow. It could be demonstrated that exposing 1 % of the primary tubing area to steam on the secondary is sufficient to depressurize an isolated steam generator, when there is at least one RCP running. Yet another test revealed that cold emergency feedwater entering a depleted steam generator has warmed up to within 50 K of the prevailing saturation temperature by the time it reached the riser tubes and the steam generator tube sheet, while the secondary pressure fell by no more than 2 bar/min.

## REFERENCES

/1/ R. M. Mandl, B. Brand, "PKL III Small Breaks and Transients Experimental Programms", Fourteenth Water Reactor Safety Research Information Meeting, Gaithersburg, Maryland, 10/86.

SIEMENS

## 1) Base Line Tests

Characterisation i.e.
- Δp-losses
- heat-losses
- natural circulation

Shutdown with
- 2 RCPs and 4 SGs
- 1 RCP and 1 SG

## 2) Loss of Off-Site Power

RCPs not in operation,
shutdown with
3, 2 or 1 Steam Generator

## 3) Criteria for Restarting RCPs

Parameters:
- size of RPV Bubble
- degree of subcooling

## 4) Small Break on Primary Side. Operating Procedures

Break Location:
- Pressurizer
- Hot or cold leg
- SG tube(s)

## 5) Break on Secondary Side

- Main steam line break (200% or less)
- Feedwater line break

## 6) Feedwater System Failure

- Delivery of feedwater (hot or cold) at different water inventories on the secondary
- Delivery of feedwater from intact to isolated SG via blowdown line



**PKL III – Scope of Experiments**
Fig. 1

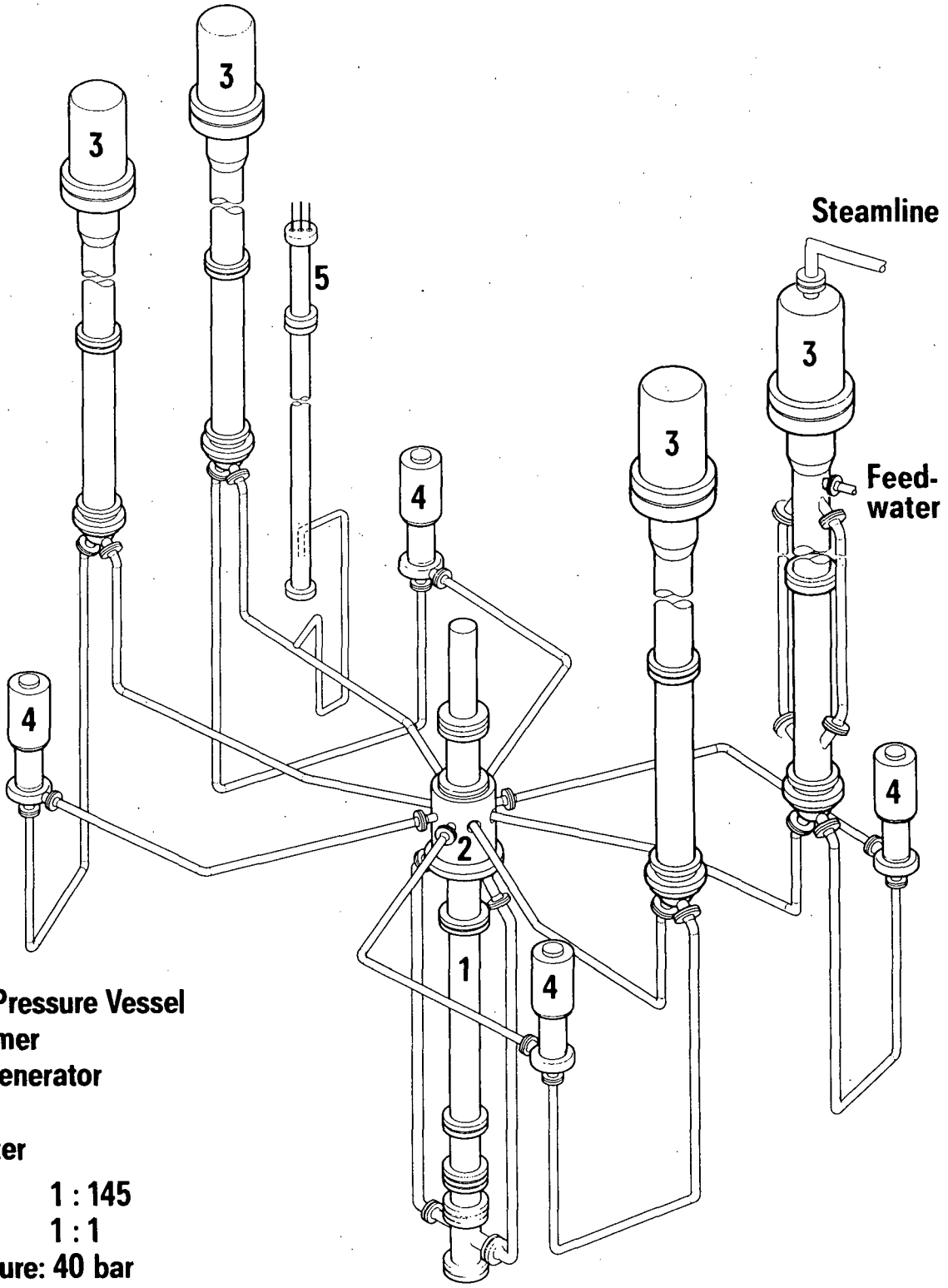


1 Reactor Pressure Vessel
2 Downcomer
3 Steam Generator
4 Pump
5 Pressurizer

Volume: 1 : 145
Elevations: 1 : 1
Max. Pressure: 40 bar
Max. Power: 2.5 MW (10%)

## PKL III Test Facility Primary Side

87 PWR 022e

Fig. 2

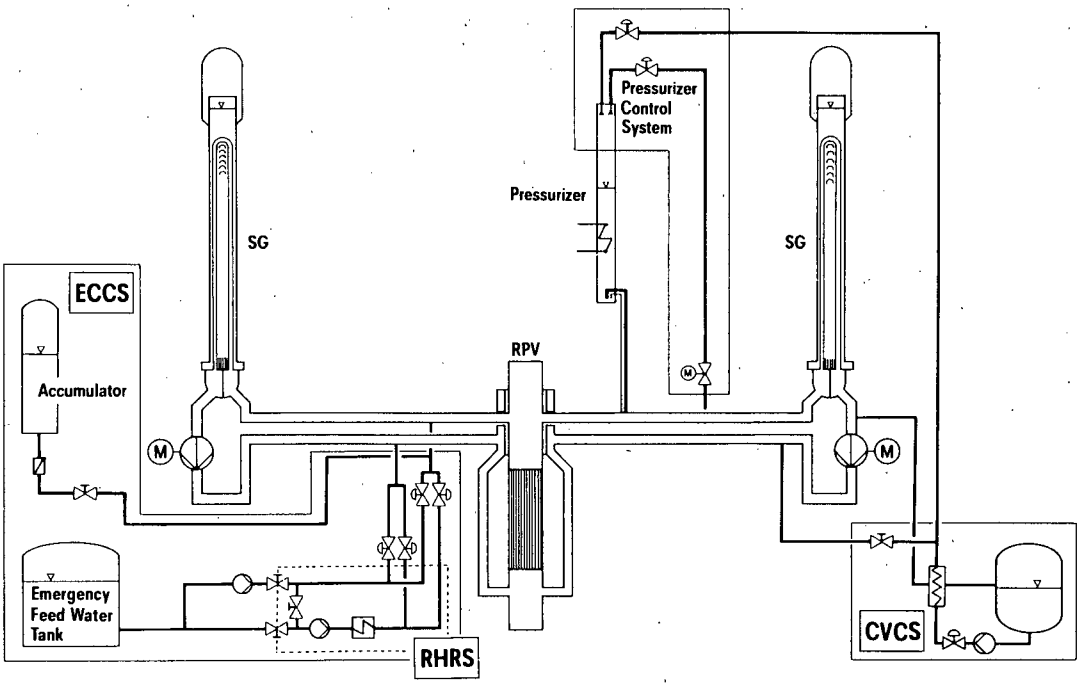


**PKL III Engineered Safety Systems,**
**Fig. 3**

86 PWR 063e
UB KWU

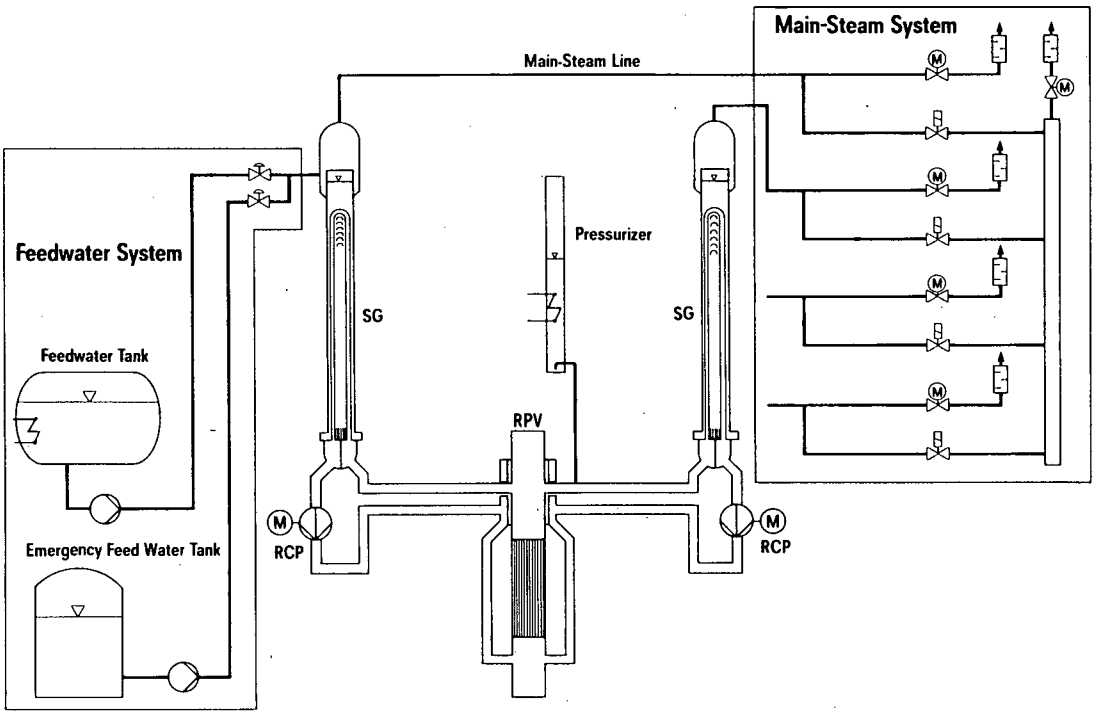


**PKL III Feedwater and Main-Steam Systems**
**Fig. 4**

86 PWR 064e
UB KWU

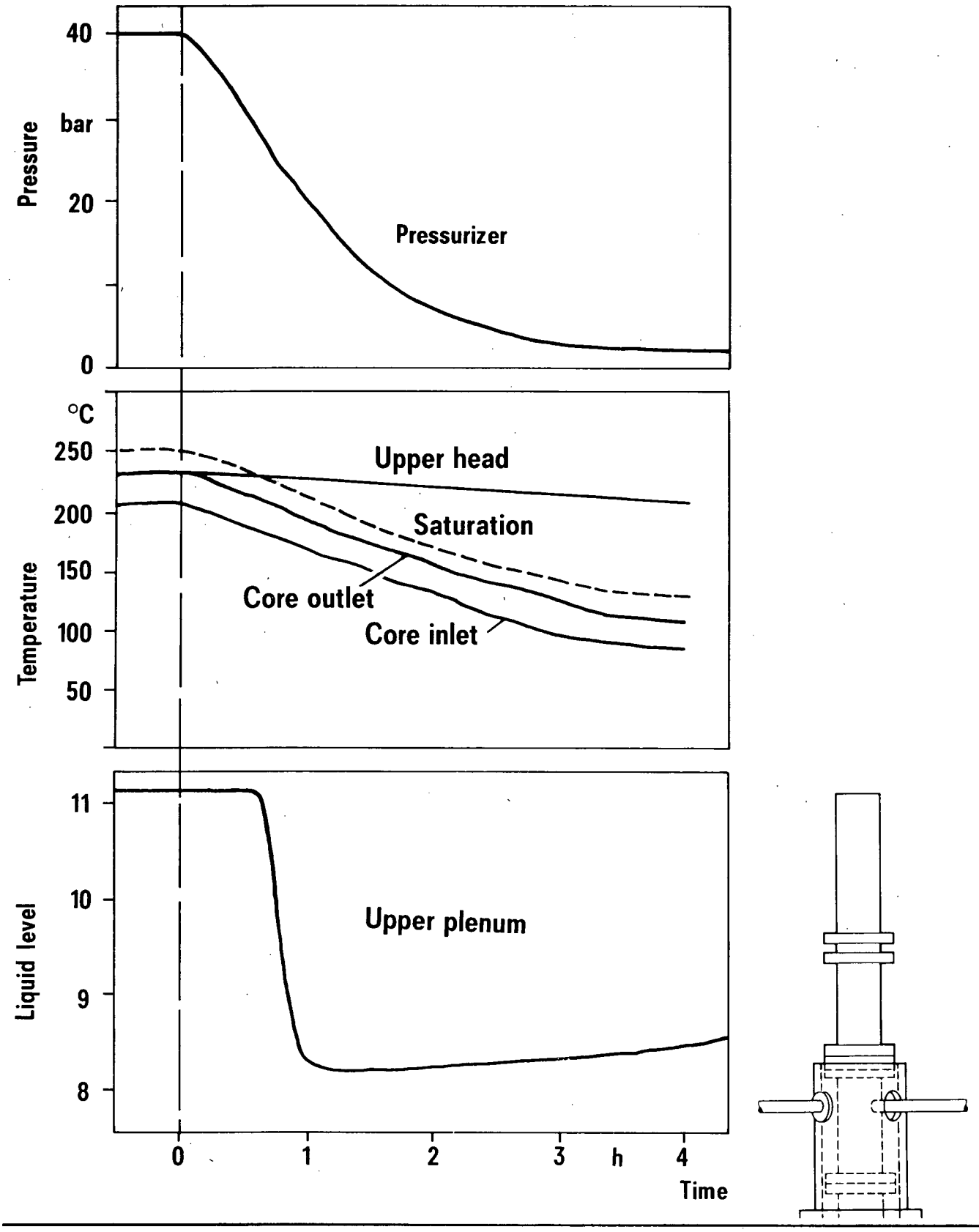


## Loss-of-Offsite Power Test

Fig. 5

88 PWR 342
UB KWU

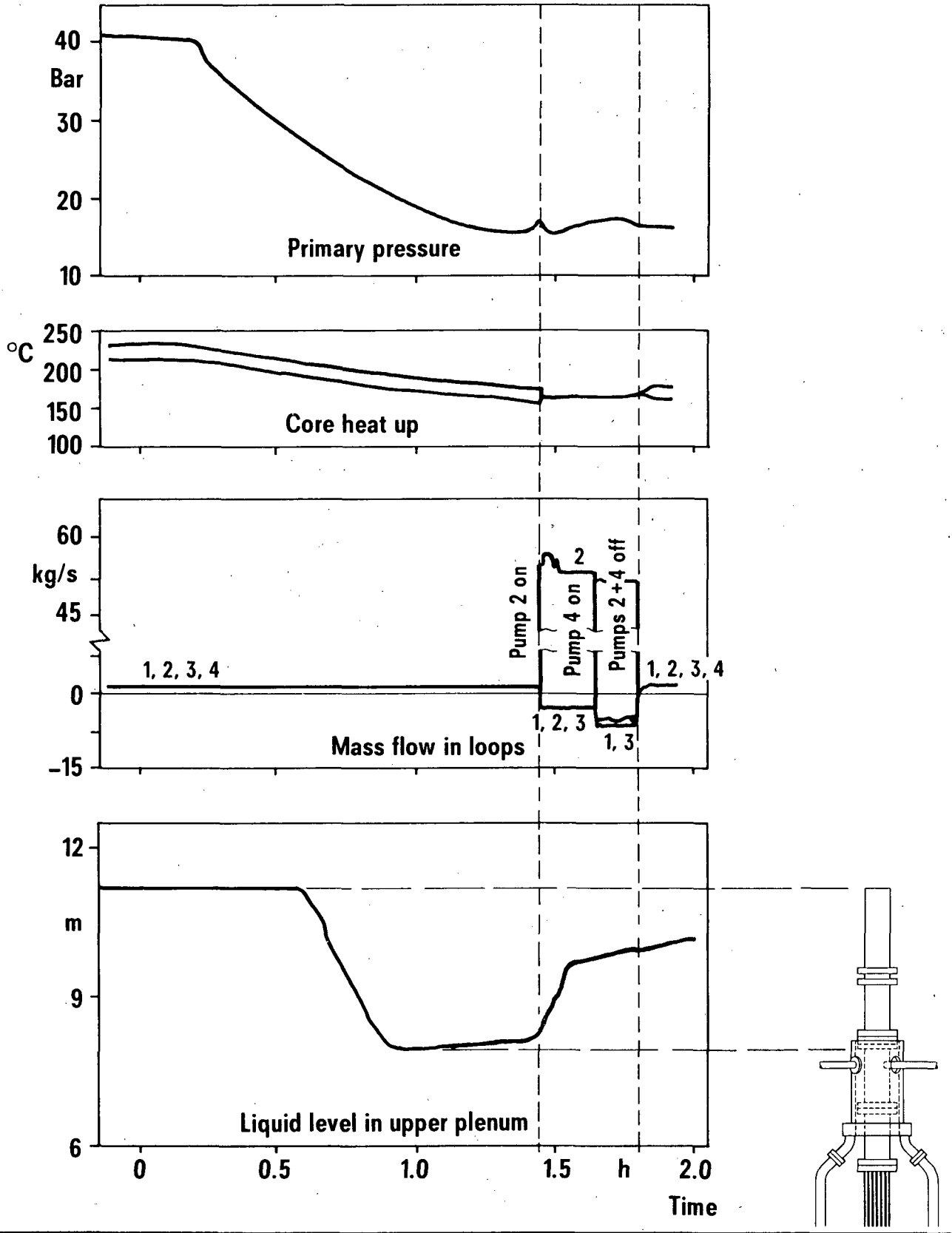


**Restart of RCPs.**
Fig. 6

88 PWR 335
UB KWU

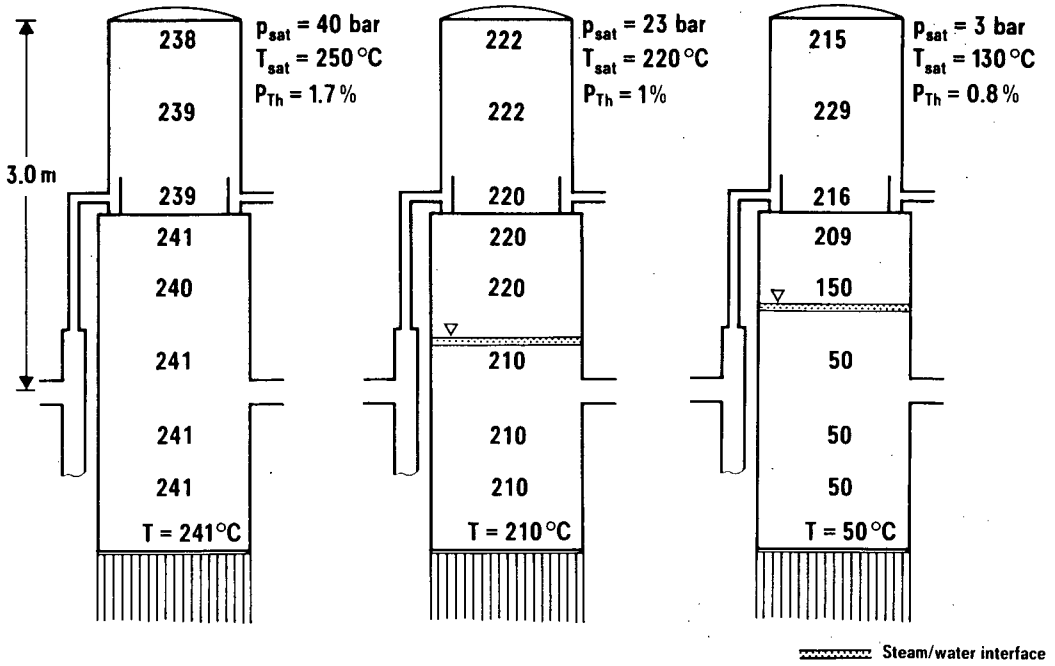


**Loss-of-Offsite Power Test**
**Temperature Distribution in RPV**
Fig. 7

88 PWR 337
UB KWU

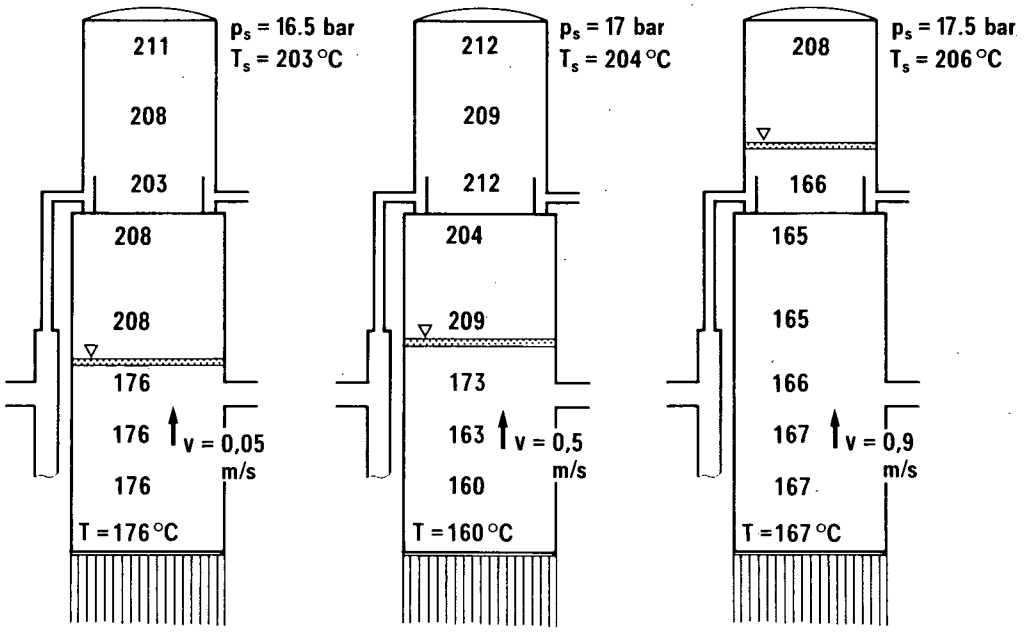


**Restarting RCPs**
**Temperature Distribution in RPV**
Fig. 8

88 PWR 338
UB KWU

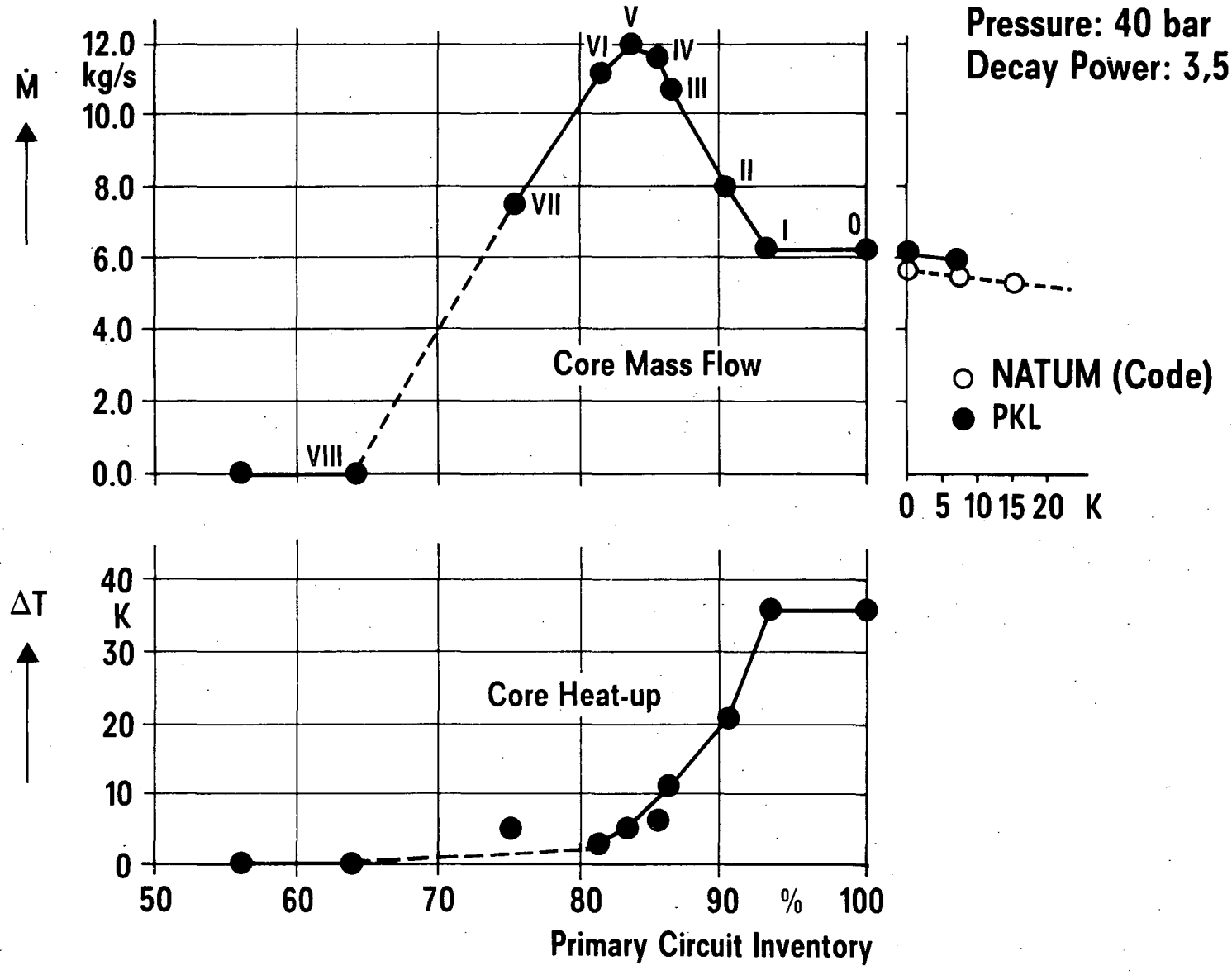


## PKL III – Natural Circulation Test
## Mass Flow, Core Heat-up

88 PWR 325
UB KWU

Fig. 9:

# BORON MIXING IN THE LOWER PLENUM OF A BWR

by

T.G. Theofanous and E.A. Shabana
Department of Chemical and Nuclear Engineering
University of California
Santa Barbara, CA 93106

## ABSTRACT

Current ATWS procedures are rather complicated because of uncertainties regarding the flow behavior of the liquid poison injected into the lower plenum for control. The concern, supported by some old small-scale experiments (at General Electric Co.), is that due to strong buoyancy forces the natural circulation flow (less than 30% of rated) would be insufficient to entrain and convect the cold boric acid solution upward and into the core area. On the other hand, the applicability of these experimental results is also in doubt. This is because Froude-number scaling becomes problematic at small scales. The purpose of this work is to bypass such concerns by carrying out a set of experimental simulations at full scale.

Such full-scale simulations are practical because of the high degree of compartmentalization of a BWR lower plenum by the control rod guides and the nearly longitudinal flow of coolant in the interstitial spaces. The experimental facility represents a lower plenum slice corresponding to 9 guide tubes in the neighborhood of the injection standpipe (also included at full scale). The structural material is acrylic, allowing full visualization. The base flow is created by recirculation from a 2,000-gal.-capacity (water) tank at velocities of up to the full natural circulation strength expected in the reactor. The injection flow consists of $NaC\ell$ or $CaC\ell_2$ solutions with $\Delta\rho/\rho$ values of up to 30%. In addition to visualization, the facility is instrumented for mapping out the local/instantaneous concentration (conductivity probes) and velocity (fibre optic laser doppler anemometer) fields.

Last year in this conference we sketched out the experimental facility and presented the initial qualitative (visualization) data on mixing with a 1-nozzle injection. In this presentation we present quantitative mixing information for a 3-nozzle injection. The injection orientation was also changed from impinging directly on the adjacent control rod guide to aiming in the interstitial space between two radial rows of them. Because of a sizeable dicontinuity in funding last year, this project had to be maintained as a low-level effort. We expect to carry out full simulations with a 7-nozzle injection, and complete the project during the next year.

# 1. INTRODUCTION

Many boiling water reactors (BWRs) rely on liquid poison (standby liquid control system or SLCS), injected into the lower plenum, to achieve shutdown from postulated ATWS (anticipated transients without scram) events. Due to the combination of solute (boric acid) and temperature effects, the injection solution is ~60% heavier than the primary fluid, and the potential for its stratification into the lower plenum (settling rather than entering the core region, where it is needed) under the relatively low natural circulation flow velocities has been recognized long ago. The General Electric (GE) Company has obtained mixing data in an 1/6-scale (geometric) simulation facility. These data remain proprietary, although the indications are that they exhibit a strong tendency to stratify for recirculation flows less than ~20% of rated. This is precisely the range of interest for the natural circulation flows relevant to postulated ATWS transients. This led to complicated operator procedures and an interest in modeling the mixing process in a form appropriate for use in system's codes (i.e., TRAC-BWR).

The complications arising from inadequate mixing can be understood in terms of Figure 1, obtained from a 1982 BWR Owner's Group letter to the Nuclear Regulatory Commission (NRC) (BWR Owner's, 1982). In it, mixing efficiency is seen to approach zero at ~5% of rated flow, while it seems to reach a nearly constant upper value of ~75% for flows higher than 20% of rated. On the other hand, the core power shows a linear decrease with recirculation flow, due to corresponding increases in core void (steam) fraction. The combined effect on an ATWS transient is to produce the strongly upward concave curve of suppression pool temperature, as shown in Figure 1. That is, at high flows the suppression pool overheats as the boron mixing cannot keep up with the steam production. At very low flows, on the other hand, the whole transient is prolonged such that suppression pool overheating is obtained even at the low power levels.

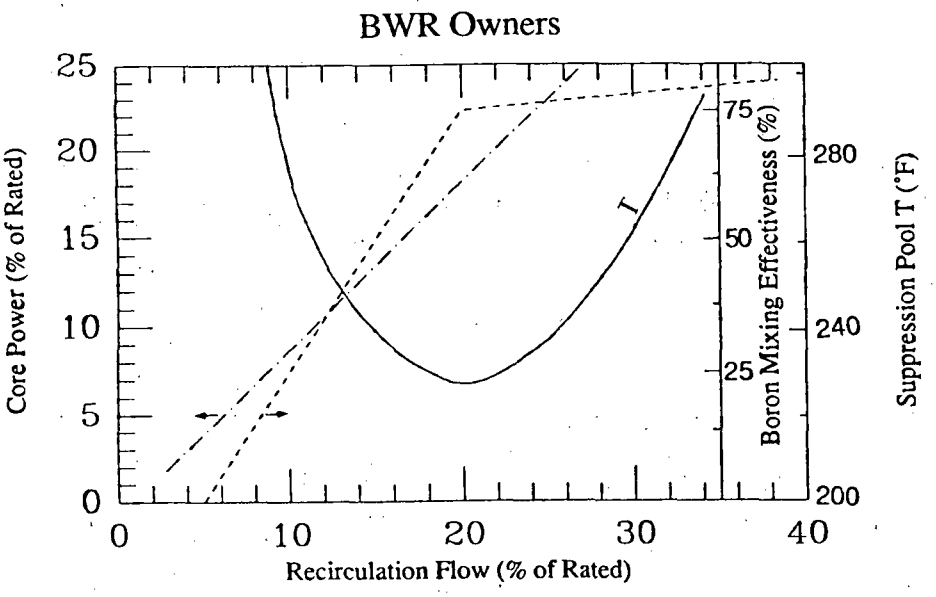


Fig. 1. *Boron mixing effectiveness, associated power, and supression pool overheating as a function of recirculation flow[1].*

Additional perspectives on the behavior can be obtained from Figures 2 and 3, reproduced from Chexal et al. (1984). The critical path in Figure 2 shows the decrease in core power and associated decrease in recirculation (natural) flow resulting from dropping the water level from the normal water level (NWL) to the top of active fuel (TAF) at normal operating pressure. The critical path in Figure 3 indicates the effect of depressurization on the same variables. It is clear from these figures that power reduction to sufficiently low levels can only come about by a combined and *decisive* reduction in both water and pressure levels. It is also clear that the relevant recirculation flows are in the rated range of 10 to 30%. Finally, in subjecting the plant to these low-power, low-flow conditions, one needs to be concerned about the potential occurrence and impact of coupled flow-power instabilities, as recently manifested in the La Salle incident.

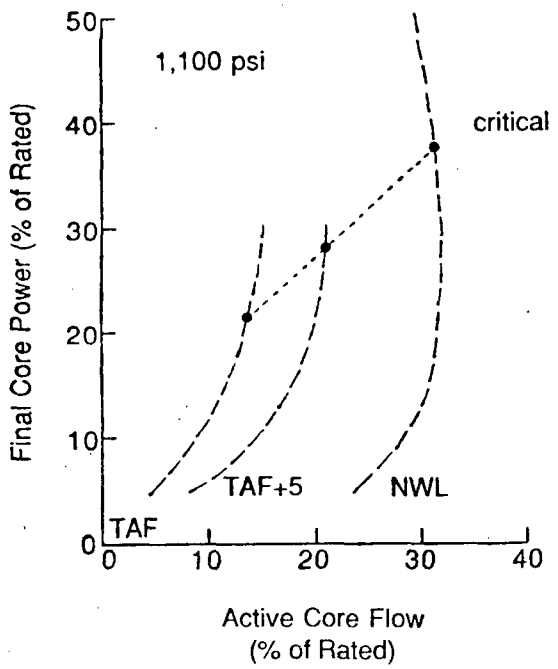


Fig. 2. *Final core power versus active core flow at various downcomer levels.*

Based on the above as an initial ATWS fin, the operators were instructed to reduce water levels to the top of the active core. More recently as an update to this procedure, there is a proposal in front of the NRC-licensing that the water level be dropped below the top of the active core in order to achieve an acceptable performance under such conditions. Clearly, such procedures are not particularly condusive to safety, indeed they result in a significant contribution to estimates of core melt frequency in current probabilistic risk assessments. These then provide a motivation for a closer examination of the boron mixing phenomena, which is the subject of this study.

In this report we provide a new experimental approach. The initial experimental data indicate considerable promise that mixing is complete and that the special procedures discussed above may not be necessary.

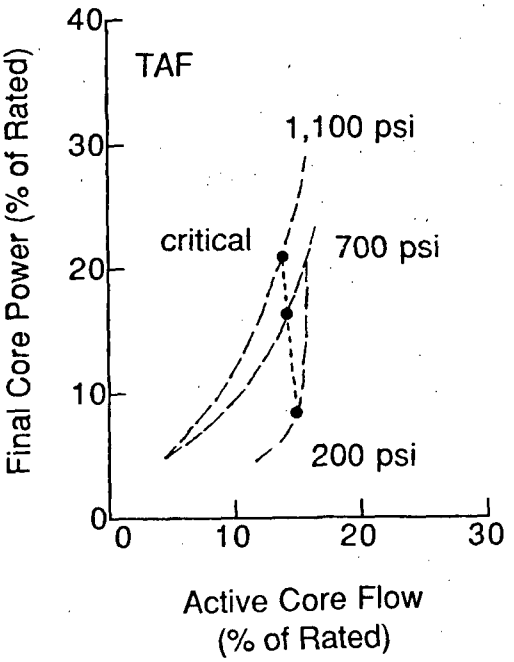


Fig. 3. *Final power versus total core flow at various system pressures.*

## 2. SCALING CONSIDERATIONS

The lower plenum geometry of interest is shown in Figure 4. The actual positioning of the injection line (SLCS standpipe) within the control rod guide array is indicated for two representative designs (BWR3s and BWR4s) in Figure 5. The key dimensions and characteristics are summarized in Table 1, below:

TABLE 1

Geometric Features of SLCS

| Plant | A | B | C | Pipe Size | # of Holes | Hole Diameter |
|---|---|---|---|---|---|---|
| BWR3 (Dresden 3) | 2.6" | 42" | 9.4" | 1" SCH40 | 8 | 0.25" |
| BWR4 (Peach Bottom 3) | 6.1" | 42" | 14.8" | 1" SCH40 | 8 | 0.25" |

Note: All dimensions in inches, holes directed towards vessel center

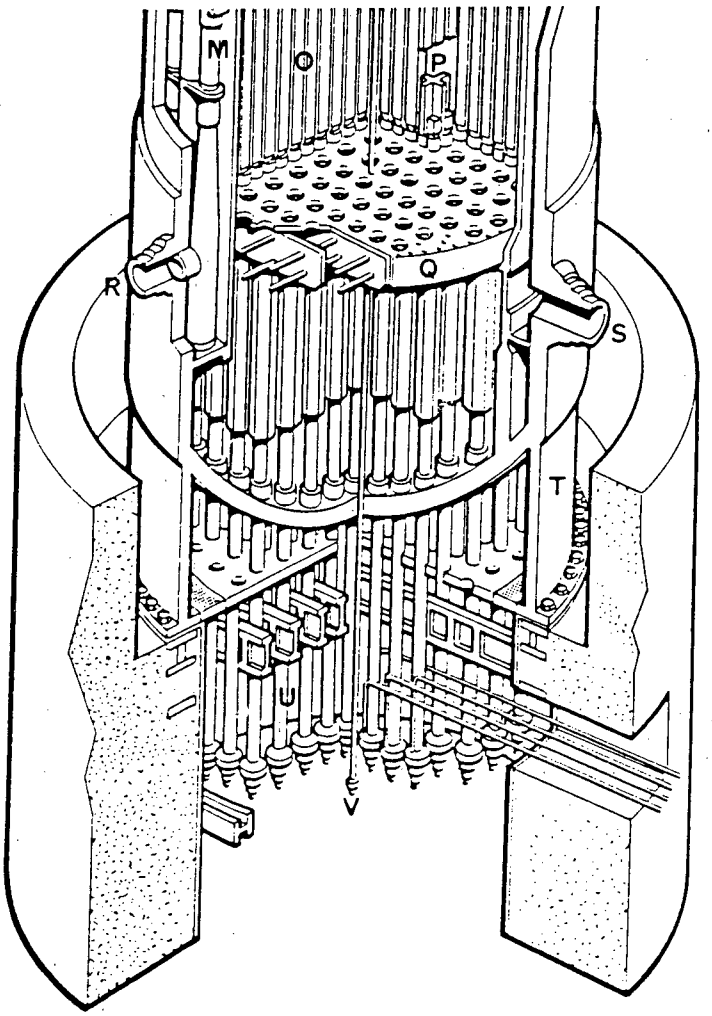


Fig. 4. *The lower plenum of a BWR.*

Typical injection rates are 60 to 80 gpm of borated (10% by weight sodium borate) 20 °C water. We are interested in determining the fraction of this injected flow that enters the core region, entrained by the buoyancy-driven recirculating coolant flow.

We can identify two mixing regimes. The first, or vertical mixing regime (VMR), is obtained as the mean flow streams along the control rod guide tubes while the injected solution jets in a direction cross to it, impinging between the nearest two control rod guides as illustrated in Figure 6. This figure also shows the entrainment due to the jet effect and the injection orientation. The second, or horizontal mixing regime (HMR), may be obtained in case some solution settles downward, having escaped entrainment from the VMR. It is characterized by the mean flow streaming across the guide tubes and the solution attempting to settle through it, as illustrated in Figure 7.

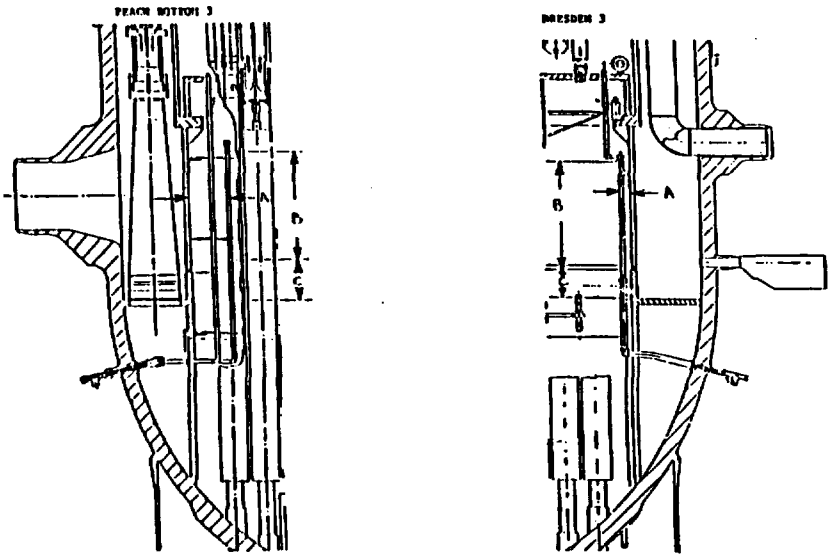

Fig. 5. *SLCS standpipe (injection) geometry.*

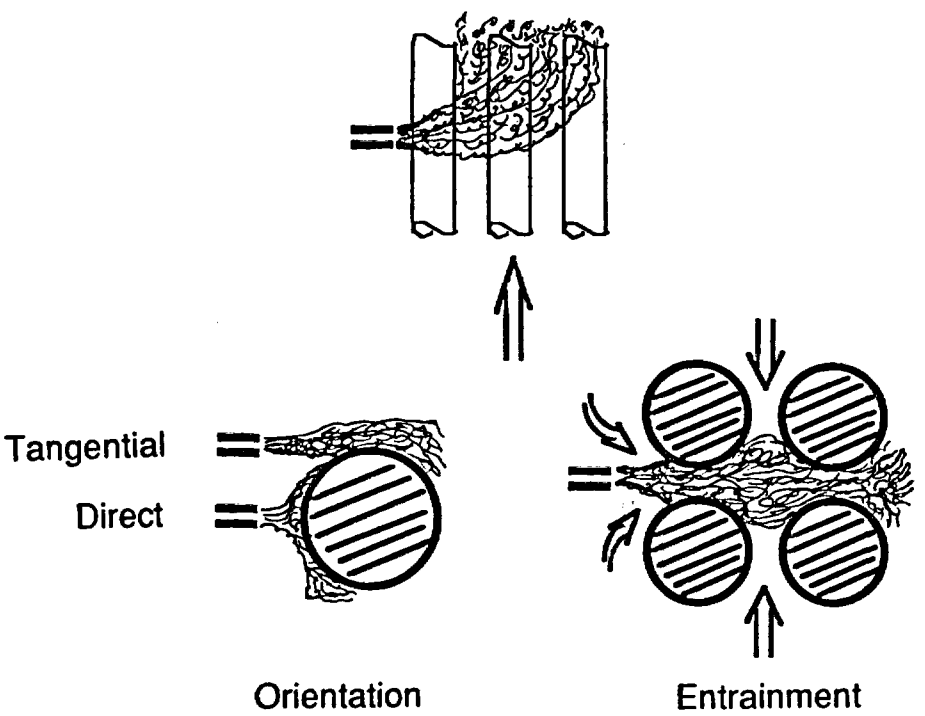


Fig. 6. *Illustration of the vertical mixing regime (VMR).*

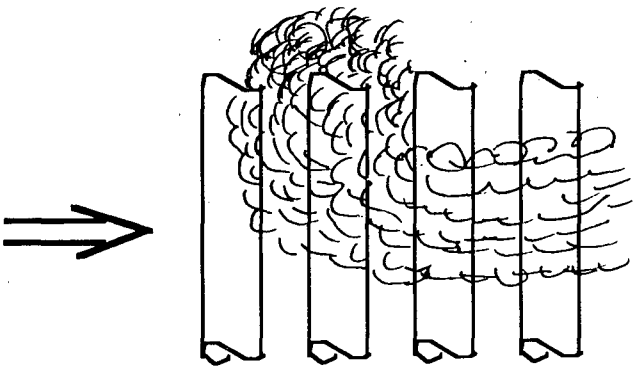

Fig. 7. *Illustration of the horizontal mixing regime (HMR).*

As it is customary for flows where gravitational effects are important, the GE experiments were scaled on the basis of the Froude number:

$$Fr = \frac{U}{\sqrt{gD\Delta\rho/\rho_I}}, \tag{1}$$

where $U$ and $D$ are the characteristic velocity and length scales, $g$ is the acceleration of gravity, and $\Delta\rho = \rho_I - \rho_m$, where $\rho_I$ and $\rho_m$ are the densities of the injected and mean flow, respectively.

The problem is that at small scales such scaling can lead to very large Reynolds numbers dissimilarities. Indeed, as may be seen from Eq. 1, at 1/6-scale the characteristic velocity must be reduced by a factor of $\sqrt{6} \sim 2.5$, and the combined effect is a Reynolds number dissimilarity by a factor of $6 \times 2.5 \sim 15$. The scaling can further deteriorate due to inabilities to achieve the full $\Delta\rho/\rho_I$, and also because of the considerably larger kinematic viscosity in the experiment (low pressure and temperature system) in relation to the reactor. For example, the use of a 10% solution in the experiment would yield another factor of $\sim \sqrt{5}$ reduction in velocity, i.e., together with the scale effect a total factor of $\sim$7. All of these effects are rather detrimental, especially when inertia and momentum flux effects are important, as is the case here due to the high injection Froude numbers and impinging (see Figure 6) geometry.

Based on the above, it is not difficult to surmise that small scale simulations, in this area, may significantly underestimate mixing behavior. We decided, therefore, to pursue the problem at full scale.

## 3. EXPERIMENTAL FACILITIES

### *3.1 Vertical Mixing Regime*

The UCSB VMR full-scale facility is shown in perspective in Figure 8. It represents a 3x3 array of control rod guide tubes in the vicinity of the SLCS standpipe. Axial flow is provided by a centrifugal pump, at up to 2,300 gpm, through a 2,000 gal recirculation stainless-steel tank, and it is controlled by a butterfly valve. The flow is distributed by means of deflector vanes, in the lower plenum, and straightened by honeycomb plates, prior to entering the subchannel space of the test section, and as it exits into the outlet plenum. The test section (overall dimensions 0.84 $\times$ 0.76 $\times$ 1.69 m) is accessible to full visualization—both guide tubes and pressure boundary are acrylic. All piping external to the test section is of PVC material. Injection flow is provided by a positive displacement pump (at flows up to 10 gpm per nozzle) from a 200-gal. storage tank into any number of the injection nozzles (corresponding to the SLCS standpipe holes) by opening the appropriate ball valves (Fig. 9(c)). The recirculating flow is measured by a nozzle insert and the injected flow by an orifice meter.

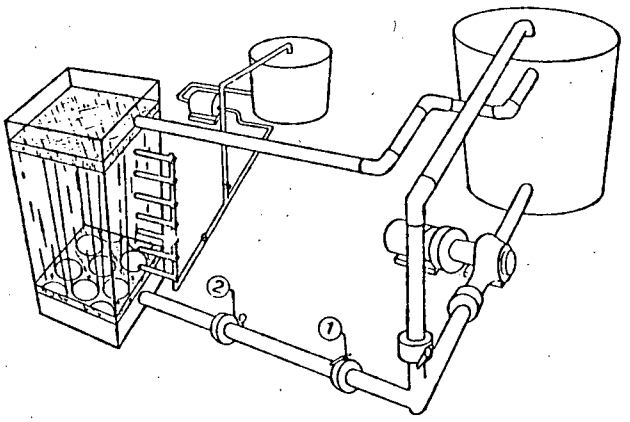


Fig. 8. *The UCSB VMR full-scale facility.*
*(1) flow butterfly valve; (2) flow measuring nozzle.*

Solutions are made with NaCl (up to 20% by weight) or $CaCl_2$ (up to 42% by weight); concentrations in the test section and inlet/outlet piping are measured by conductivity probes (Theofanous et al., 1984). Overall mixing performance can be determined from the difference between inlet and exit concentrations and appropriate mass balances. Local mixing performance can be determined from a large number of conductivity probes distributed throughout the subchannel space in the test section. The data are taken by a PDP-11 at a rate of 500 Hz and recorded at a rate of 5 Hz (averaged) and subsequently analyzed on the University VAX computer. Frequent calibrations indicate high reliability measurements with an estimated error of $\sim$2%.

Visualization data are also obtained by coloring the injection tank contents and using a video system. A secondary injection system (not shown) can provide short pulses of solution into the bottom of each subchannel to visualize and measure (from the time to traverse two axial probe positions) velocity distribution. A two-velocity fiber optic LDA is also available for local velocity measurements at latter stages of this study.

Pictorials of the overall experimental arrangement, the test section, the injection system, and the pump/recirculation-tank combinations are shown in Figure 9 (a-d).

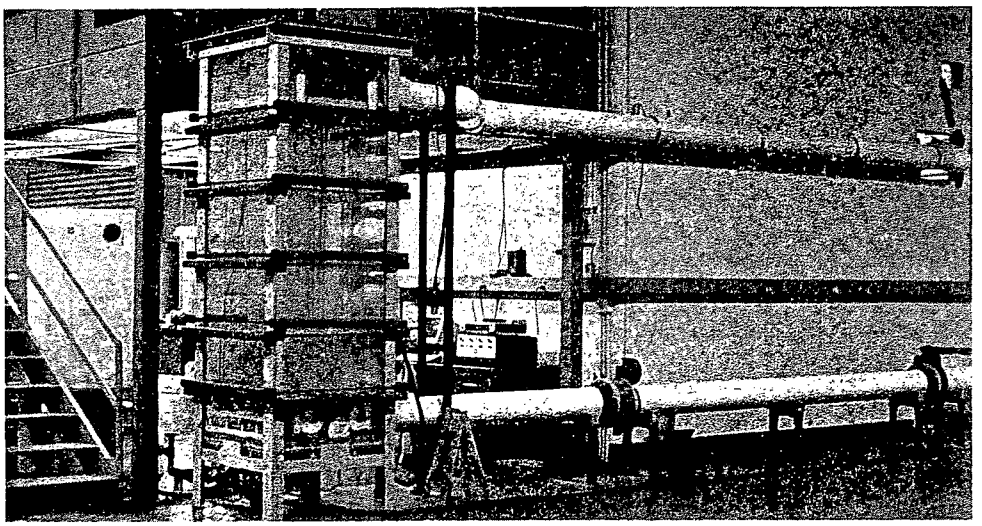

Fig. 9a. *Overall experimental setup.*

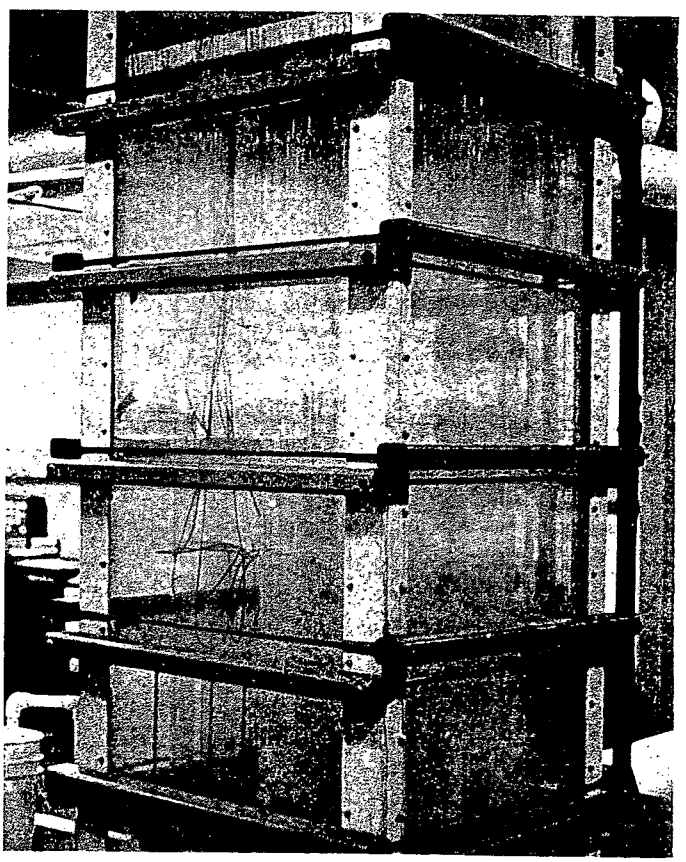

Fig. 9b. *Test section with conductivity probes in place.*

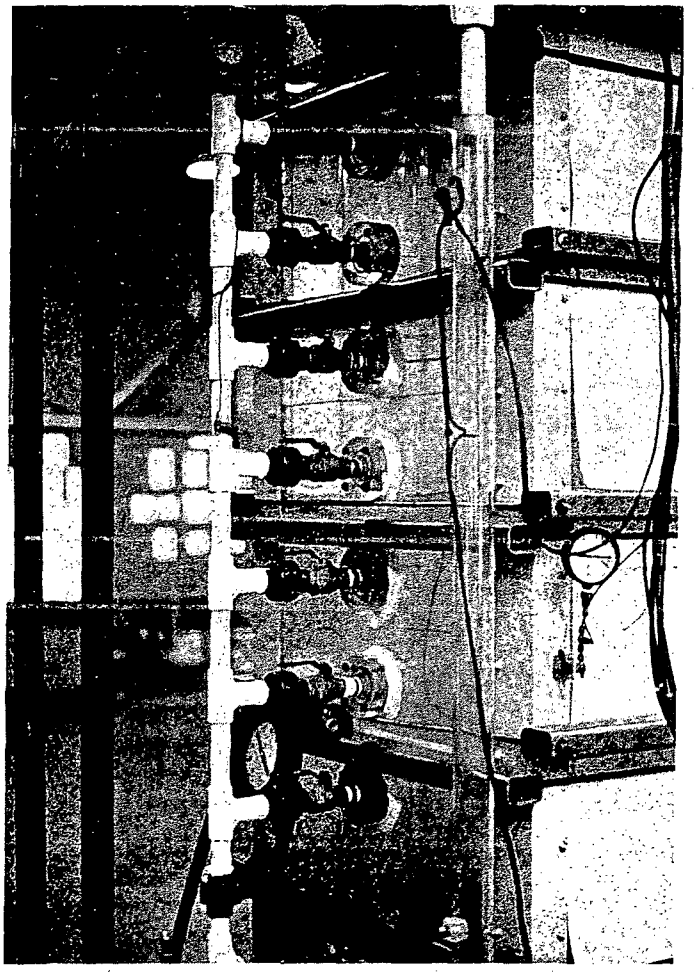

Fig. 9c. *The injection system.*

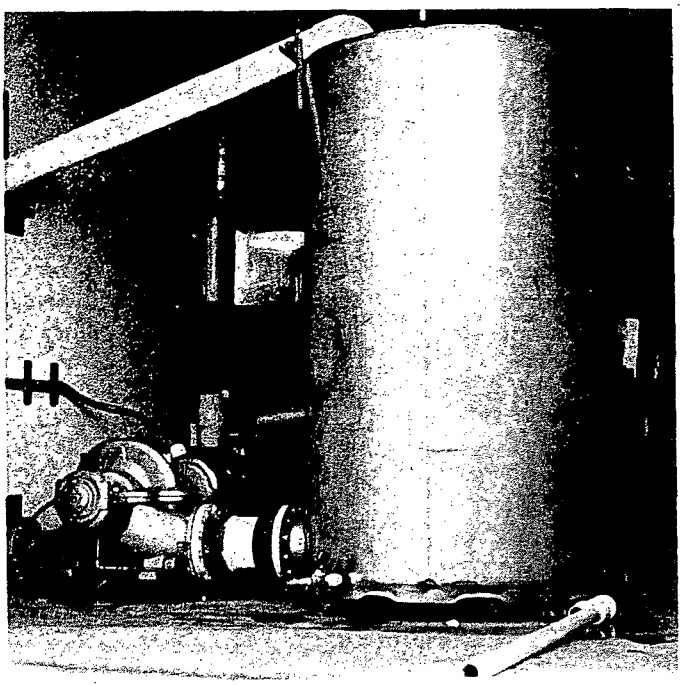

Fig. 9d. *The pump/recirculation-tank arrangement.*

*3.2 Horizontal Mixing Regime*

Here we make use of an existing flume in the adjacent Ocean Engineering Laboratory (Figure 10) fitted by the 3x3 array of control tube guides (Figure 11). The flume can provide up to 5,500 gpm over a flow cross section of 0.91 × 0.91 m. Here the solution is distributed (rather than forcefully injected) at the top of the subchannel space of the first one or two rows, and the mixing behavior as it is convected across the tube array is followed by conductivity probes and video recordings.

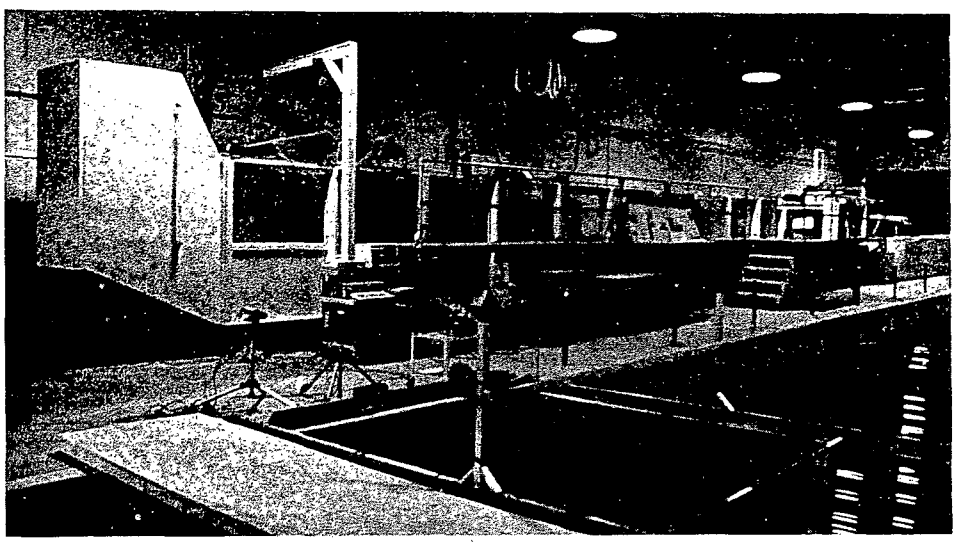

Fig. 10. *Flume utilized for studying the HMR.*

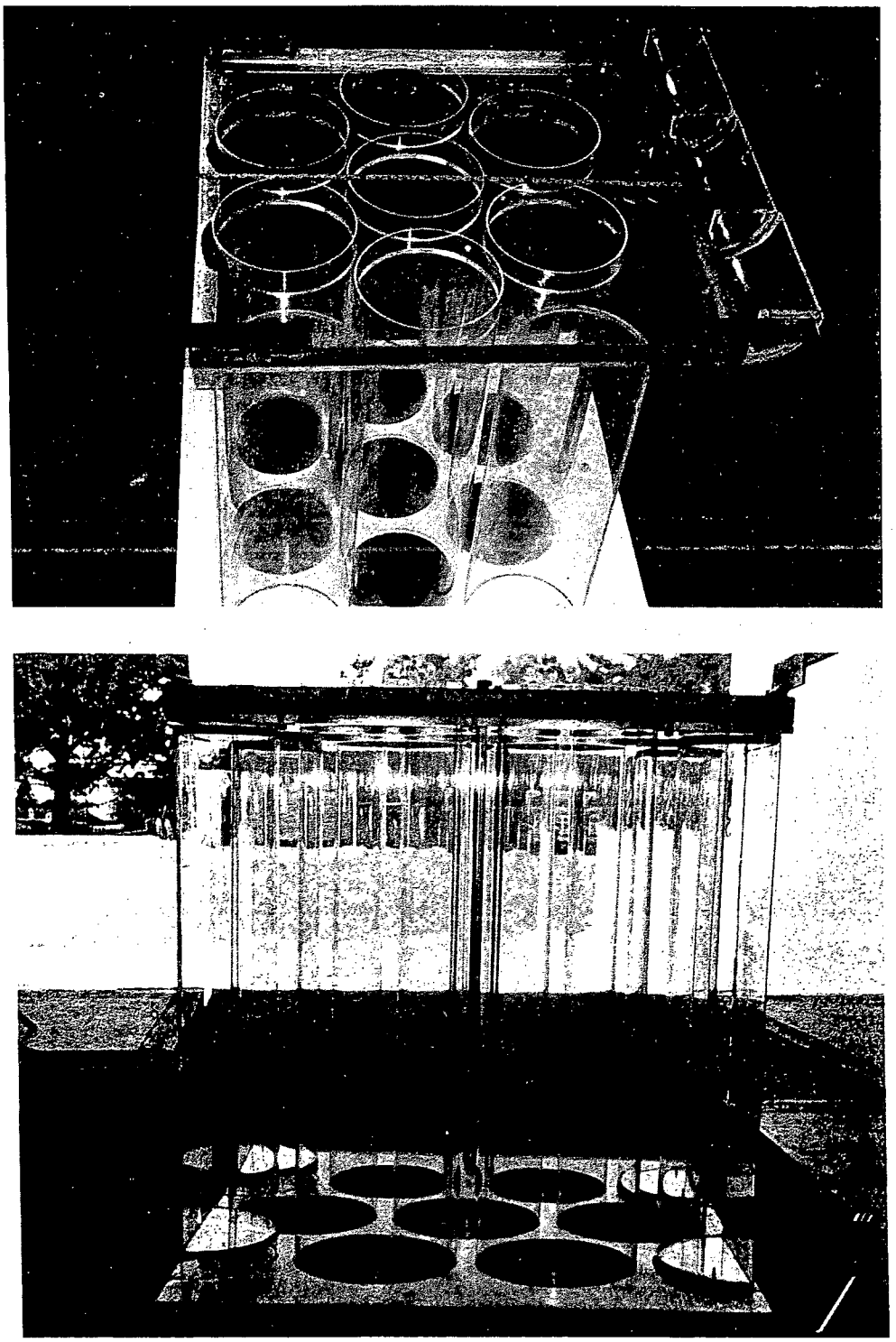

Fig. 11. *Test section for the HMR studies.*

## 4. EXPERIMENTAL RESULTS AND DISCUSSION

In conjunction with development of the experimental techniques, an extensive set of experiments were run in both the VMR and the HMR facilities. Visualization data indicated a strong tendency toward complete mixing. Based on this initial information, the program was directed, accordingly, towards establishing the minimum boundaries for complete entrainment and mixing. An indication of the kind of data obtained at this stage is given in Figures 12 and 13.

In the second stage, we sought to identify such minimum boundaries for the VMR with a 3-nozzle injection. In this first stage of quantification we would have preferred to work with a single nozzle injection (10 gpm); however, because of the large quantity of recirculating flow, from a measurement accuracy standpoint we felt more comfortable with a 3-nozzle, 30 gpm injection. Three sets of experiments were performed. In each set we exposed a single solution to a variety of recirculating flows. The three solutions were $CaCl_2$ ($\rho_I = 1.124$), NaCl ($\rho_I = 1.2$), and $CaCl_2$ ($\rho_I = 1.42$).

Typical data records for a fully-entraining (100% mixing) and a significantly-stratified behavior (40% mixing) are shown in Figures 14 and 15, respectively. These data may be analyzed by means of a mass balance, as follows

$$V\frac{d\bar{\rho}}{dt} = \dot{Q}_R(\rho_i - \rho_o) + \dot{Q}_I(\rho_I - \rho_o), \tag{2}$$

where $V$ is the volume of the subchannel space in the test section, $\dot{Q}_R$ and $\dot{Q}_I$ are the recirculating and injection flow rates, respectively, and $\rho_i$, $\rho_o$,, and $\bar{\rho}$ are the inlet, outlet, and test section average densities, respectively. A rough indicator of the test section time constant can be obtained by setting $\bar{\rho} = \rho_o$, i.e.,

$$\tau = \frac{V}{\dot{Q}_R + \dot{Q}_I}. \tag{3}$$

This yields 4.3 sec and 9.8 sec for the runs of Figures 14 and 15, respectively. Thus, if the injected flow is fully entrained, steady state is obtained in a very short time, and Eq. (2) yields

$$\rho_o(\dot{Q}_R + \dot{Q}_I) = \rho_i \dot{Q}_R + \rho_I \dot{Q}_I. \tag{4}$$

Conversely, measured values of flows and densities can be substituted in Eq. (4) to determine the extent of departure from perfect mixing as reflected by the transient term in Eq. (2). Then mixing efficiency can be defined as the fraction of injected salt mass that actually leaves the test section, i.e.,

$$\epsilon = \frac{\Delta\rho_o'}{\Delta\rho_I'} \quad \frac{\dot{Q}_R + \dot{Q}_I}{\dot{Q}_I}, \tag{5}$$

where

$$\Delta\rho_o' = \rho_o - \rho_i \quad \text{and} \quad \Delta\rho_I' = \rho_I - \rho_i. \tag{6}$$

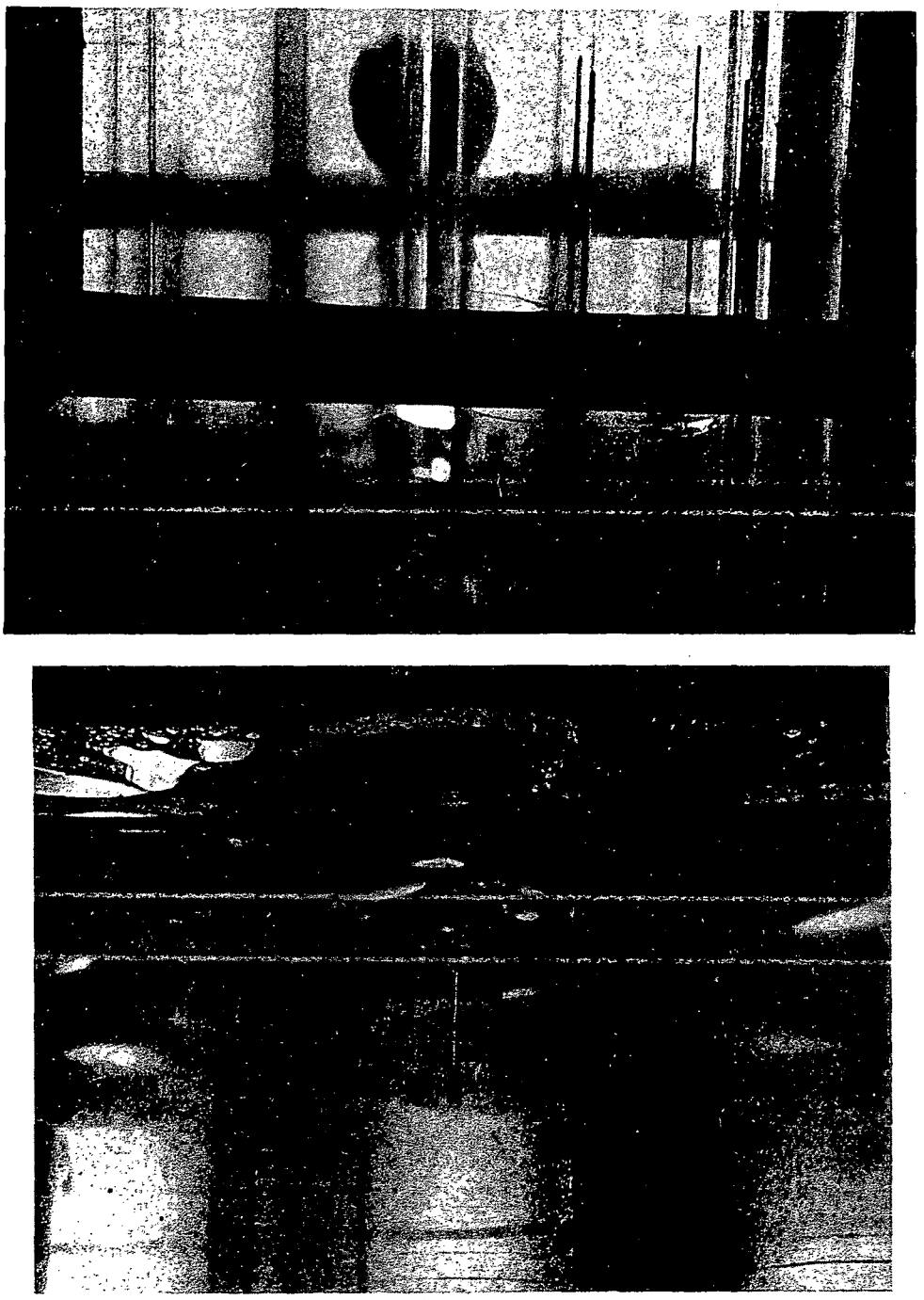

Fig. 12. *The mixing phenomena in the VMR.*

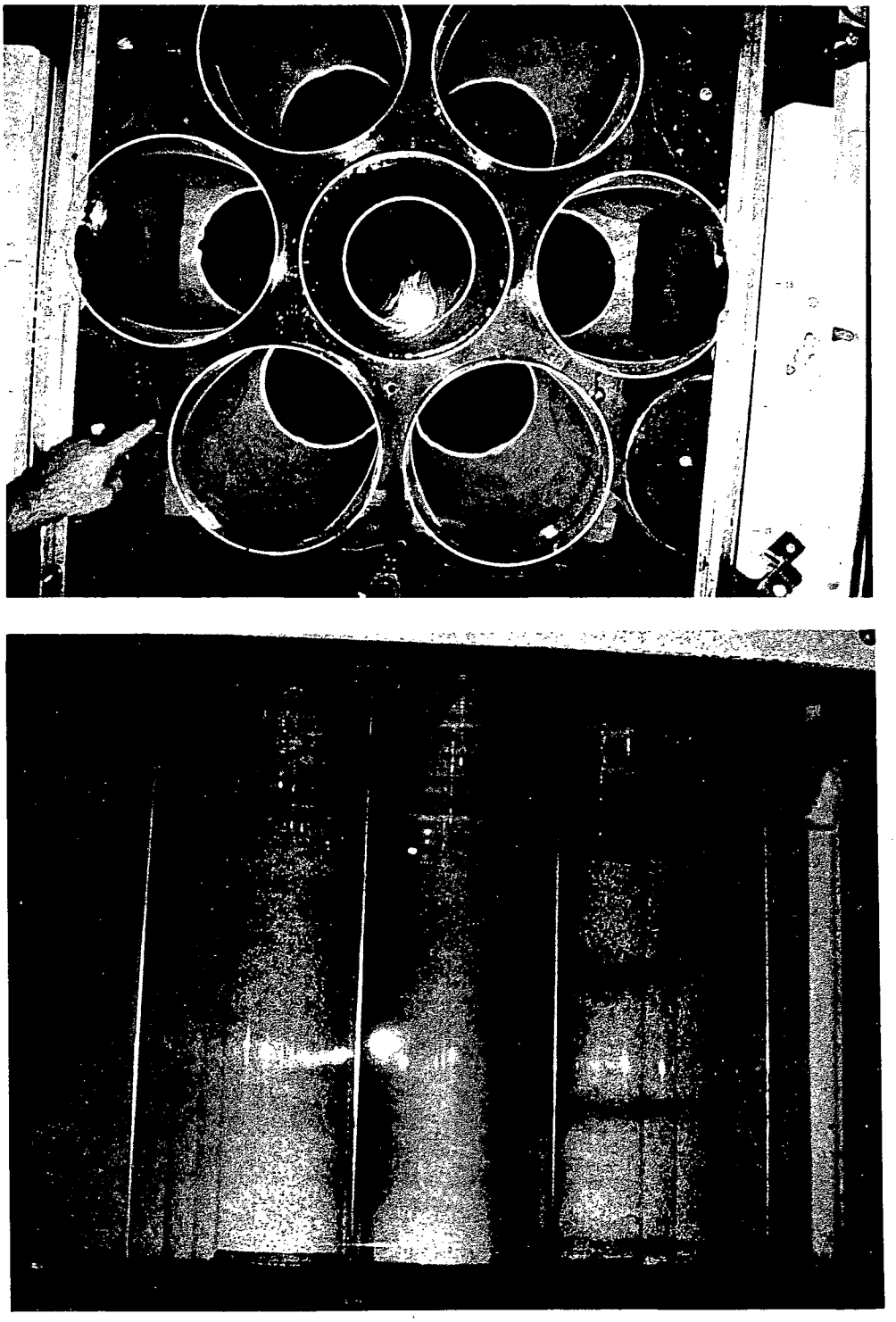

Fig. 13. *The mixing phenomena in the HMR.*

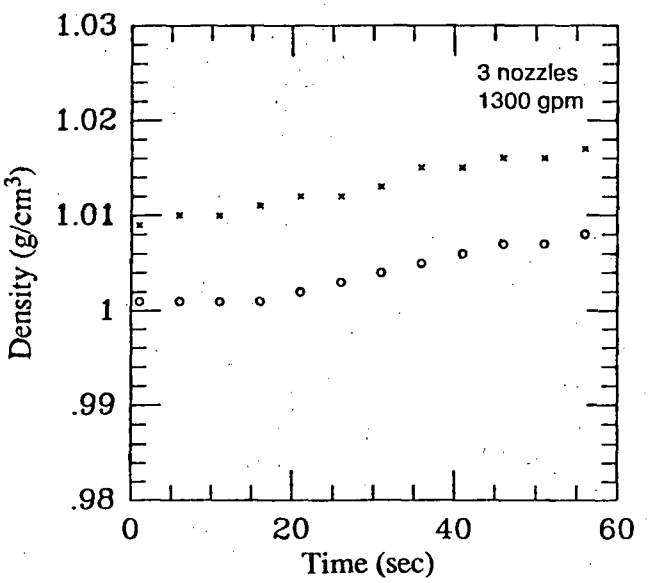


Fig. 14. *Inlet (o) and outlet (x) solute concentrations (3-nozzle injection).*

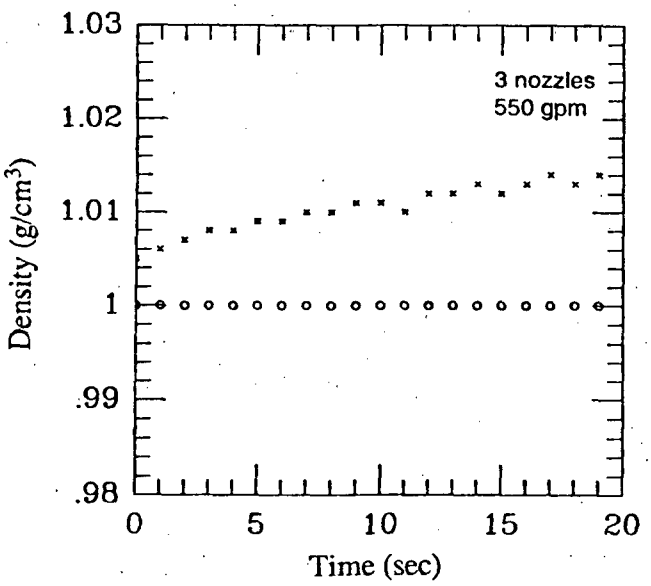


Fig. 15. *Inlet (o) and outlet (x) solute concentrations (3-nozzle injection).*

Thus, each pair of measured densities ($\rho_o$, $\rho_i$) corresponds to a mixing efficiency, as shown in Figures 16 and 17 for the runs of Figures 14 and 15, respectively. The results for all the runs can be found elsewhere (Theofanous and Shabana, 1989).

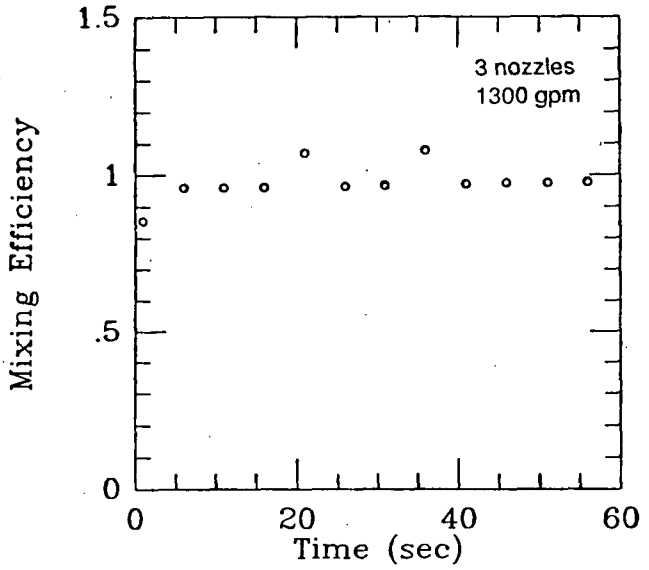


Fig. 16. *Mixing efficiency data for a typical fully-entraining run.*

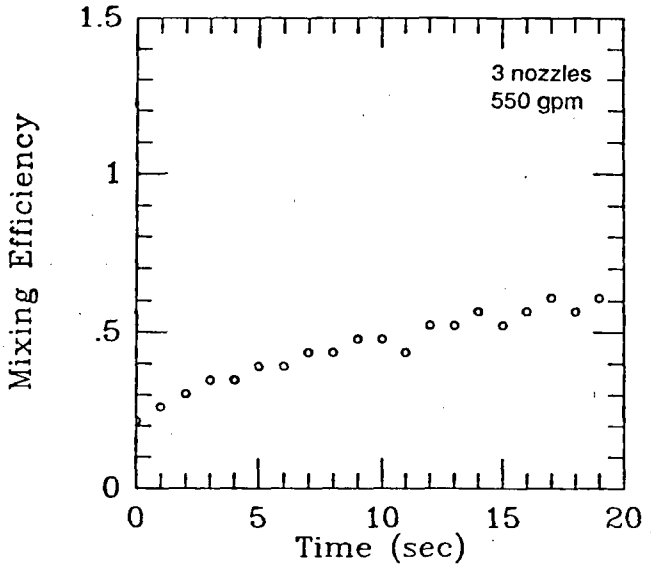


Fig. 17. *Mixing efficiency data for a run where entrainment is incomplete.*

An interesting discriminating feature between complete and partial entrainment may be noted in these figures. In those runs that reflect complete entrainment, the mixing efficiency rises, within a few seconds, to a well-defined plateau. In contrast, for those runs characterized by partial entrainment, the mixing efficiency rises slowly and more or less uniformly for the duration of the run. This, of course, is expected as the accumulation term in Eq. (2) is now controlled by a significantly longer time constant ($\bar{\rho} \neq \rho_o$). Eventually, in this case also, 100% efficiency will be reached; however, this long term behavior is not of interest to the practical problem addressed here. Transition to full entrainment occurs at ~400 gpm for the $\Delta\rho/\rho_I$ value of 0.3.

The prototypic $\Delta\rho/\rho_I$ value is 0.4 and Froude scaling, as above, yields ~500 gpm as the lower boundary of the full entrainment regime. This corresponds to ~7% of rated. What remains to be done is to establish such trends as function of the number of injection nozzles, and subject the imperfectly mixed behavior to the horizontal mixing regime.

## 5. CONCLUSIONS AND RECOMMENDATIONS

So far we have established a scaling rational and an experimental approach to assess boron mixing in the lower plenum of a BWR during ATWS. We have determined that with a three-hole injection full entrainment occurs at natural circulation flow of ~7% of rated. Clearly, it is important to pursue the effects of nozzle number (up to 7), and the multidimensional flows in the partially entraining regime. The latter will provide the boundary conditions for exploring the secondary entrainment in the horizontal mixing regime. Based on what we have seen, we believe it will be possible to demonstrate perfect mixing for the practical situation of interest under ATWS and to eventually effect a change of operator procedures to the benefit of real as well as perceived safety.

## ACKNOWLEDGMENTS

This work was performed for the U.S. Nuclear Regulatory Commission, under contract 0486-111. We appreciate the interest of Paul Hill and his help with system information.

## REFERENCES

1. BWR Owner's Group letter to the U.S. Nuclear Regulatory Commission, February 1982.
2. Chexal et al., NSAC/69, Electric Power Research Institute, May 1984.
3. T.G. Theofanous et al., "Decay of Buoyancy Driven Stratified Layer with Applications to Pressurized Thermal Shock (PTS)," NUREG/CR- 3700, February 1984.
4. T.G. Theofanous and E.A. Shabana, "Performance of Liquid Control Systems in BWRs," (to be published as a NUREG/CR report, 1989).

# ADMITTING COLD WATER INTO STEAM FILLED PIPES WITHOUT WATER HAMMER DUE TO STEAM BUBBLE COLLAPSE

**Yuanching Chou**
Institute of Nuclear Energy Research,
P.O. Box 3-3, Lung-Tan,
Taiwan, Republic of China

**Peter Griffith**
Department of Mechanical Engineering,
Massachusetts Institute of Technology,
Cambridge, Mass. 02139

## ABSTRACT

Water hammer due to steam bubble collapse when cold water is admitted to vertical upward flowing, vertical downward flowing, and nominally horizontal pipes has been studied both experimentally and analytically. The work in horizontal pipes included a study of the effect of a slight doward inclination, a slight upward inclination, and the length of the pipe on the initiation of water hammer. Stability maps showing the combinations of filling velocities and liquid subcooling that cause water hammer and those which don't for each flow geometry were obtained from experiments. Analytical models were developed to predict those stability boundaries in the stability maps. All these models were tested with experimental data. Based on the verified models, a step-by-step approach for each flow geometry is presented for plant engineers and designers to follow in avoiding water hammer induced by steam bubble collapse.

## NOMENCLATURE

$A_P$ Cross sectional area of the pipe used in experiments.
$A_{WA}$ Heat transfer area between steam and pipe wall.
$A_0$ Cross sectional area of initial water pool.
$A_1$ Cross sectional area of water behind the positive surge wave.
$A_2$ Cross sectional area of water behind the negative surge wave.
$aa$ As that defined in equation (11).
$bb$ As that defined in equation (11).
$C$ Sonic velocity in the water inside a pipe.
$C_L$ Specific heat of water.
$C_{WA}$ Specific heat of pipe wall material.
$C_0$ Constant in equation (14).
$C_1$ Constant in equation (14).
$D_P$ Diameter of the pipe used in experiments.
$e_S$ Internal energy of steam.
$g$ Gravitational acceleration.
$h_S$ Enthalpy of steam.
$h_{fg}$ Enthalpy of evaporation.
$h'_{fg}$ As that defined in equation (10).
$h_{WA}$ Heat transfer coefficient between steam and pipe wall.
$h_{INT}$ Specific heat of pipe wall material.
$k_L$ Thermal conductivity of water.
$k_{WA}$ Thermal conductivity of pipe wall material.
$L_P$ Length of pipe from ball valve to the end of the pipe.
$\dot{m}_C$ Mass condensation rate of steam.

$M_{air}$ Constant showing reduction in heat transfer rate due to presence of air in steam.
$P_d$ Driving pressure of the filling water.
$P_S$ Pressure of steam in the pipe.
$(\Delta P)_{spike}$ Pressure spike due to water hammer.
$(\Delta P)_f$ Pressure loss due to pipe wall friction.
$(\Delta P)_g$ Pressure loss due to liquid gravity.
$(\Delta P)_i$ Pressure loss due to liquid inertia.
$P_0$ Reference pressure in equation (12).
$\dot{q}_{WA}$ Heat flux from steam to pipe wall.
$\dot{q}_{INT}$ Heat flux at the steam/water interface.
$R$ Gas constant of steam.
$T_L$ Temperature of the filling water.
$T_S$ Temperature of steam in the pipe.
$T_{WA}$ Temperature of pipe wall.
$t$ Time variable.
$U_b$ Bubble rise velocity.
$U_w$ Phase velocity of surge wave.
$U_{gS}$ Vapor superficial velocity.
$U_{LS}$ Liquid superficial velocity.
$U_0$ Phase velocity of the initial water pool.
$U_1$ Phase velocity of water behind the positive surge wave.
$U_2$ Phase velocity of water behind the negative surge wave.
$V_S$ Volume of steam.
$x$ Distance traveled by liquid front in the pipe.
$Y$ Height of water pool in circular pipe.
$\bar{Y}_0$ Centroidal depth of the initial water pool.
$\bar{Y}_1$ Centroidal depth of water pool behind the positive surge wave.
$\bar{Y}_2$ Centroidal depth of water pool behind the negative surge wave.
$y_0$ The thickness of the pipe wall.

Greek Letters
$\mu_L$ Viscosity of water.
$\rho_f$ Density of saturated water.
$\rho_g$ Density of saturated steam.
$\rho_L$ Density of the filling water.
$\rho_S$ Density of steam.
$\rho_{WA}$ Density of pipe wall material.

## 1. Introduction

In the past two decades, a large number of water hammer events have been reported by licensees of operating nuclear power plants in the United States. Most of these events only resulted in damage to piping supports and restraints. However, a few cases caused cracks or ruptures in piping systems. Electric Power Research Institute (EPRI) has recently initiated a multi-year project to study water hammer events in nuclear power plants . According to the preliminary results of this project (Van Duyne and Yow, 1988), steam-water counter-flow in a horizontal pipe and subcooled water into a vertical steam filled pipe are the dominant initiating mechanisms for water hammer in PWR's and BWR's respectively. Both of these water hammers arise from the rapid condensation of steam bubbles in subcooled water.

The purpose of this work (and in greater depth by Chou, 1988) is to develope quantitative models which allow one to avoid steam bubble collapse induced water

hammer in piping systems. Stability maps showing the combination of filling velocities and liquid subcooling that cause water hammer and those that don't for vertical upward flow, vertical downward flow, and horizontal flow in a short pipe (i.e. $L/D \leq 48$) were obtained experimentally. Analytical models describing the limiting boundaries obtained in stability maps are presented. The analytical results describing these experiments agree with the experimental data very well. Strategies that can be used to avoid the water hammer events due to steam bubble collapse are identified by using the analytical models.

## 2. Vertical Pipes Filled From The Bottom

A schematic diagram of the experimental apparatus used in this study is shown in Figure 1A. The test section is made of a steel pipe with 6.0 cm outside diameter, 4.9 cm inside diameter, and 2 m in length. A Lexan pipe of essentially the same inside diameter and length was substituted for the visual tests. During a test, the test section is filled with steam saturated at one atmosphere first, then water with a specified subcooling is admitted by opening the ball valve. Water flow rates into the pipe are measured with differential pressure transducer installed across an orifice. Steam pressures measured by a piezo-electric type transducer installed at the top.

Figure 2 illustrates the time response of the orifice $\Delta P$ and the pressure in the pipe for tests with a water hammer. The pressure in the pipe dropped at the beginning of filling period due to transient condensation on the cold water immediately after the ball valve was opened. A pressure spike greater than the driving pressures was induced due to intensive condensation when the pipe was filled up. For tests without a water hammer, the steam pressure only went up to the level of the driving pressure. The orifice $\Delta P$ followed these pipe pressure fluctuations, but with the reverse sign.

For tests with a water hammer, the peak pressures scatter for different filling conditions. This makes the stability boundary for water hammer difficult to determine from the magnitude of peak steam pressure also. An alternative way is to use the maximum pressure which can be tolerated by the piping system as a safe limit. If we arbitrarily assume the maximum tolerable pressure to be 150% of the driving pressure of the filling water in our case, then a stability map can be worked out as that shown in Figure 3. It turns out that the subcooling of the filling water is not an important variable in determining the stability boundary.

Figure 4 shows the approximate flow regimes observed in the Lexan pipe. Following the opening of the ball valve, a turbulent water front moves up in the pipe. The profile of the water front becomes smoother as the front moves higher. If the water filling rates were sufficiently high, loud noises could be heard and pressure spikes appeared on the pipe pressure-time curves as the pipe filled up.

Figure 1B illustrate the model for the anlytical analysis. The assumptions for this model are: (a) the processes are one dimensional, (b) homogeneous properties are used in the steam space, (c) a constant water temperature is assumed, (d) a constant air pressure acts above the water in the tank, and, (e) the steam/water interface shape and area are constant.

Because no steam flow is introduced into the test section, the momentum equation is not needed in the steam space. The mass of steam is reduced by the condensation. The rate of condensation is:

$$\frac{d(\rho_S V_S)}{dt} = -\dot{m}_C \quad . \tag{1}$$

The steam volume is reduced by water insurge, thus,

$$\frac{dV_S}{dt} = -U_{LS}\,A_P - \frac{\dot{m}_C}{\rho_L} \quad . \tag{2}$$

The energy equation is:

$$\frac{d(\rho_S\,e_S\,V_S)}{dt} = -\dot{m}_C\,h_S - P_S\,\frac{dV_S}{dt} \quad . \tag{3}$$

The equations of state for the steam are:

$$e_S = h_S - P_S\,v_S \quad , \quad \frac{d\rho_S}{dt} = (\frac{\partial \rho_S}{\partial h_S})_{P_S}\frac{dh_S}{dt} + (\frac{\partial \rho_S}{\partial P_S})_{h_S}\frac{dP_S}{dt} \quad . \tag{4}$$

By manipulating the previous four equations, a relation for the steam pressure can be obtained. It is:

$$[\frac{1}{\rho_S} - (\frac{\partial h_S}{\partial P_S})_{\rho_S}]\frac{dP_S}{dt} = \frac{1}{V_S}(\frac{\partial h_S}{\partial \rho_S})_{P_S}(\rho_S\,U_{LS}\,A_P - (1 - \frac{\rho_S}{\rho_L})\dot{m}_C) \quad . \tag{5}$$

In the liquid side, the mass of steam condensed is negligible compared with the total water inventory. Therefore, only the water momentum equation is needed to calculate the filling velocity of the subcooled water.

$$(\Delta P)_i = (P_d - P_S) - (\Delta P)_g - (\Delta P)_f \quad , \tag{6}$$

where the $(\Delta P)$'s can be expressed as functions of liquid filling velocity $(U_{LS})$. When no air is present in the pipe, the condensation rate can be expressed as:

$$\dot{m}_C = \frac{\dot{q}_{INT}\,A_P + \dot{q}_{WA}\,A_{WA}}{h_{fg}} \quad . \tag{7}$$

The heat flux on the steam/water interface can be obtained from an investigation of direct-contact condensation of steam on turbulent, subcooled water. Sonin et al.(1986) have presented a correlation based on the comparison of turbulence distribution model and heat transfer data. Their correlation is expressed with an average turbulent velocity and a constant Staton number. It is, however, more convenient to use the liquid front filling velocity than turbulent velocity as the dependent variable. Since the latter is about an order of magnitude smaller than the former (Kowalchuk and Sonin, 1978), the heat flux on the steam/water interface in our case can be expressed as ;

$$\dot{q}_{INT} = (0.001)\rho_L\,C_L\,U_{LS}\,(T_S - T_L) \quad . \tag{8}$$

Heat flux from the steam to the pipe wall can be written as:

$$\dot{q}_{WA} = h_{WA}\,(T_S - T_{WA}) \quad , \tag{9}$$

where $h_{WA}$ is the film condensation heat transfer coefficient on the wall. For laminar film condensation on vertical plate, a formula for heat transfer coefficient averaged over a length of $(L_P - x)$ can be obtained by solving force and energy equations of the liquid film (Rohsenow and Hartnett),

$$h_{WA} = 0.943\left(\frac{g\rho_f(\rho_f - \rho_g)k_L^3 h'_{fg}}{(L_P - x)\mu_L(T_S - T_{WA})}\right)^{\frac{1}{4}} \quad , \quad h'_{fg} = h_{fg} + \frac{3}{8}C_L(T_S - T_{WA}) \quad . \quad (10)$$

Because the thickness of laminar films are of the order of magnitude of thousandths of an inch, this formula can be used in cylindrical tubes with internal diameters larger than $\frac{1}{8}$ inches.

The surface temperature of the pipe wall can be obtained by a one dimensional heat diffusion equation. By using the integral method developed by Saedi, the heat diffusion equation can be expressed in an ordinary differential equation with $T_{WA}$ and $T_S$ as the dependent variables:

$$(1 + aa)(bb)\frac{dT_{WA}}{dt} + h_{WA}T_{WA} = (aa)(bb)\frac{dT_S}{dt} + h_{WA}T_S \quad , \quad (11)$$

where

$$aa = \frac{y_0 h_{WA}}{3k_{WA}} \quad , \quad and \quad bb = \rho_{WA}C_{WA}y_0 \quad .$$

Finally, to correlate the saturation temperature and pressure of the steam, the following equation is derived from the Clapeyron equation.

$$\frac{1}{T_S} = \frac{1}{T_S(P_0)} - \frac{R}{h_{fg}}ln\frac{P_S}{P_0} \quad . \quad (12)$$

Equations (2), (5), (6), (7), (8), (9), (11), and (12) can be solved simultaneously to obtain steam pressure and liquid filling rate as functions of time. A computer program based on a forward difference numerical scheme was written to solve these equations.

It was found from the results of the model, that the total heat transfer rate (the product of the heat flux and the heat transfer area) from the steam to the wall is about one order of magnitude higher than that from the steam to the filling water. This is because the former has much larger heat transfer area in the begining and has higher heat flux due to high steam temperature later on. As a result, the steam pressure response is surprisingly independent of the subcooling of the filling water. Comparison with experimental data confirms the result calculated from the model.

The second thing to note is that air might be evolved from the filling water front as the water temperature increases, This effect reduces the heat transfer from the steam to both the pipe wall and the steam/water interface. To take this effect into account, heat fluxes from the steam to both the wall and the interface were divided by a constant $(M_{air})$ in the model. It was found that, the results with $M_{air}$ equal to 3 are better than the others.

Figure 5 shows the comparison between the results from this model with $M_{air} = 3$ and those from the corresponding experiments. They agree with each other pretty well except for the fast transients at the begining and at the end of the filling periods. In the initial period, the steam/water interface is disturbed due to valve opening in the

experiments. In the final period, the collapse of the steam bubble is governed by the competition between liquid inertia and the condensation heat transfer( Florschuetz and Chao,1965). Because of this, the oscillatory steam pressures and water flow rates which appear, could not be predicted with this model.

Alternatively, since the liquid filling rates could be predicted well before the final vapor collapse occurs, a conservative estimation of the pressure spikes due to the collapse can be obtained by using Joukowsky relationship (Rust, 1979),

$$(\Delta P)_{spike} = \rho_L C_L (\Delta U_{LS}) \quad . \tag{13}$$

With this conservative approach, an algorithm for avoiding water hammer in vertical up-flow is proposed as follows:

a. Determine the maximum pressure spike which can be tolerated by the piping system.
b. Calculate the maximum final impact velocity corresponding to the maximum tolerable pressure by using Joukowsky relationship.
c. Calculate the maximum filling velocity corresponding to the maximum final impact velocity by solving conservation equations of the whole system.
d. Install a flow restriction in the water solid region of the fill system such that the maximum tolerable fill velocity for zero steam bubble pressure is not exceeded.

## 3. Vertical Pipes Filled From The Top

The experimental apparatus for vertical downward flow test is similar to that for vertical upward flow test, except that the whole piping system was rearranged so that the subcooled water was introduced into the top of the test section. Typical response curves for the cases with a water hammer are shown in Figure 6. In these tests, the steam pressure didn't go up and sometimes dropped below the initial value until a spike occurred when the liquid filled up the pipe. The orifice $\Delta P$ fluctuated about some average value. Those large peaks and dips were caused by collapse of vapor bubbles inside the downward liquid stream during water insurge. For the tests without a water hammer, the response curves look very similar except that there is no spike in the steam pressure curve when the pipe filled up.

In those tests with a water hammer, the peak steam pressures are well above ($\geq$ 150%) the corresponding driving pressures of the filling water. Therefore, a well defined stability boundary could be worked out. The boundary is shown in Figure 7. The dashed line in this figure was obtained from a simple theory which will be described later.

The observed flow regimes are sketched in Figure 8. For the cases with sufficiently low filling rates, downward annular liquid flow dominated the filling period. Some liquid drops were dispersed through the vapor core but the volume of the drops was not large enough to block the vapor stream ( Figure 8A). On the other hand, radial bridging of the liquid layers appeared when the filling rates were large enough. When that happened, the trapped steam bubbles were washed down by the incoming liquid. As a result, pressure spikes and loud noises occurred when the bubbles eventually collapsed due to the increasing hydrostatic pressure near the bottom of the pipe ( Figure 8B). From these observations it can be inferred that the way of avoiding this type of water hammer is to restrict the liquid filling rates to a value that is lower than the flowrate which brings an ascending vapor bubble to rest in downward liquid flow.

Referring to the well known drift flux model, the bubble rise velocity relative to the flowing mixture can be expressed as (Wallis, 1969):

$$U_b = C_0(U_{LS} + U_{gS}) + C_1\sqrt{\frac{\rho_f - \rho_g}{\rho_f} g D_P} \quad , \tag{14}$$

where the coefficient $C_0$ reflects the flow and concentration profiles across the pipe, and $C_1$ is a factor that depends on pipe diameter, liquid density, liquid viscosity, and so on. It was found that, a fully developed upward turbulent flow in pipes with diameters of 5.1 cm or less, the bubbles always travel along the pipe axis, and therfore, propagate relative to the greatest liquid velocity in the pipe. As a result, the coefficient $C_0$ is equal to 1.2 in this case. The value of $C_1$ was found to be 0.35 both experimentally and theoretically for the same situation.

Martin (1976) measured the terminal velocity of ascending bubbles in downward flows. He found that, except for very small pipe diameters(less than 2.54 cm), bubbles in downward flow are unstable and are eccentrically located off the pipe axis. If equation (14) was used to correlate his experimental data, then due to the fact that the bubbles migrate off the pipe axis, $C_0$ should be reduced because the nose of the bubble is traveling in a region where the velocity is less than the maximum velocity in the pipe, and $C_1$ should be increased because the drift velocity increases due to the increased radius of curvature of the nose of the bubble as the bubble gets closer to the pipe wall. Table 1 shows the values of $C_0$ and $C_1$ obtained by Martin and those recommended in this study.

Table 1 $C_0$ and $C_1$ for Different Pipe Diameters

| | Martin's data | | | This study |
|---|---|---|---|---|
| Diameter(cm) | 2.54 | 10.2 | 14.0 | $\geq 5.1$ |
| $C_0$ | 1 | 0.9 | 0.86 | 0.9 |
| $C_1$ | 0.35 | 0.66 | 0.58 | 0.6 |

Solving equation (14) with $C_0 = 0.9$, $C_1 = 0.6$, and $U_{gS} = 0$, the superficial liquid velocity on the boundary can be expressed as :

$$U_{LS} = -0.67\sqrt{\frac{\rho_f - \rho_g}{\rho_f} g D_P} \quad . \tag{15}$$

The negative sign means the liquid flows down in the pipe. Results calculated with equation (15) are shown as dashed line in Figure 7, the deviations from the boundary obtained in experiments (shown as solid line in Figure 7) are within 20%.

Referring to the above discussion, the algorithm used to avoid water hammer when filling a pipe in vertical downward flow is as follows.

a. Calculate the liquid superficial velocity at the water hammer boundary by using equation (15).
b. Install a flow restriction in the water solid region of the filling system such that the filling velocity doesn't exceed 80% of that calculated in step a.

## 4. Filling a Short Horizontal Pipe From One End

To begin with, it is important to mention that a 'short' pipe in this context means a pipe with ($L/D \leq 48$). The same apparatus that was used in previous vertical flow studies was rearranged such that the subcooled water was introduced into the test section horizontally. Figure 9 shows the typical response curves for tests with water hammer events. It should be noted that several peaks and dips appeared in the orifice $\Delta P$ curves, and another spike occurred in the steam pressure curve at the end of the filling period. If the filling rate was increased to a sufficiently high level, noises and pressure spikes could only be detected at the end of the pipe. In order to distinguish between the two kinds of water hammer events, those that occurred at the orifice are called intermediate water hammer events, while those that occurred at the end of the pipe are designated as final water hammer events.

A stability map for the intermediate water hammer events in a short horizontal pipe is presented as shown in Figure 10. Three regions are divided by two boundaries in the map. Again the subcooling of the filling water is not an important factor on this map. The two dashed lines in the map are the results obtained from the appropriate analytical models which will be described later.

For the final water hammer events in this flow geometry, the mechanism of initiation is similar to that in vertical upward flow. Compared with those for a vertical upward flow, the stability boundary for this flow geometry is a little bit higher. However, the stability boundary for the final water hammer events is located between the lower and the higher boundary for the intermediate water hammer events, so that it is not considered a limiting criterion.

Three mechanisms of water hammer were observed in visual tests. At a low filling velocity, when the filling front hits the end of the pipe, a negative surge wave forms and travels back to the entrance. (see Figure 11B) If the surge wave is high enough to touch the top of the pipe, then the steam trapped at the far end of the pipe stays at about the same pressure as that when the surge forms, while the steam upstream of the surge wave front is depressurized by condensation onto the continually entering cold water. This pressure difference accelerates the surge wave toward the cold water entrance, which causes a water hammer when the wave hits the incoming liquid front.

As the liquid filling rate is increased to a higher level, intensive condensation occurs near the entrance due to high water insurge rate, while a large amount of evaporation is caused at the end portion by quick depressurization of the steam and the accompaning vaporization from the water pool in the bottom of the pipe. (see Figure 11C) The steam flow induced by this imbalance of condensation and evaporation gives rise to the possibility of water slug formation in the middle of the pipe. If a slug forms, the different condensation rates between the steam upstream and downstream of the slug result in a differential pressure across the slug, accelerating it back to the entrance and inducing a water hammer.

If the liquid filling rate is high enough for the pipe to run full, no steam can be trapped behind the liquid front. (see Figure 11D) Under these circumstance, a water hammer induced by a water slug or a surge wave cannot occur. However, the final collapse of the steam bubble when the liquid front hits the end of the pipe can still cause a water hammer.

For a pipe running full, the criterion of a Froude number equal to one is used as a conservative limit (Ruder, 1984). For a horizontal pipe of diameter $D_P$, the criterion can be expressed as:

$$U_{LS} = \sqrt{gD_P} \quad . \tag{16}$$

The calculated results are shown as the upper dashed line in Figure 10. The experimental data for pipe running full are within a range of ±13% about the line predicted by equation (16). From the view point of practical application, the boundary for pipe running full is probably not an important limit, because it is higher than the boundary for any other type of water hammer events in short horizontal pipes. For a piping system with sturdy supports, however, it might provide a safe limit for eliminating intermediate wate hammer events.

To find out the safe limit of intermediate water hammer events due to surge wave formation, the heights of both positive and negative surge wave are two essential parameters. The positive surge wave caused by valve opening in the pipe and the negative surge forming at the end of the pipe can be modeled by using a rationale similar to that of surge formation in open channel flow analysis (Chow, 1959). Figure 12 presents these concepts schematically.

Let the control volumes be the rectangles enclosed by the dashed lines in Figure 12. They travel with the waves. Mass conservation for positive surge case can be expressed as:

$$A_1(U_w - U_1) = A_0(U_w - U_0) \quad . \tag{17}$$

The momentum change is balanced by the difference of gravity forces.

$$\rho_L A_1(U_w - U_1)U_1 - \rho_L A_0(U_w - U_0)U_0 = A_1\bar{Y}_1\rho_L g - A_0\bar{Y}_0\rho_L g \tag{18}$$

Conservation of volume gives:

$$Q = A_1 U_1 \quad . \tag{19}$$

$A_0$ and $\bar{Y}_0$ can be expressed by using $Y_0$, while $A_1$ and $\bar{Y}_1$ can be expressed by using $Y_1$. The initial depth '$Y_0$' is known while $U_0$ is equal to zero. Therefore, the unknowns in equations (17) (18), and (19) are $Y_1$, $U_1$, $U_w$, and $Q$. For any assumed value of $Q$, the other three unknowns can be calculated by those three equations.

Referring to the drawing in the lower portion of Figure 12, the mass and momentum equations for negative surge are:

$$(U_w + U_2)(A_2 - A_0) = (U_w + U_1)(A_1 - A_0) \quad , \tag{20}$$

$$\rho_L(A_2 - A_0)(U_w + U_2)U_2 - \rho_L(A_1 - A_0)(U_w + U_1)U_1 = -A_2\bar{Y}_2\rho_L g + A_1\bar{Y}_1\rho_L g \quad . \tag{21}$$

At the end of the pipe, let $U_2 = 0$ and combine the previous two equations, we have:

$$\bar{Y}_2 = \frac{A_1\bar{Y}_1}{A_2} + \frac{(A_1 - A_0)(A_2 - A_0)U_1^2}{A_2 g(A_2 - A_1)} \quad , \tag{22}$$

where $U_1$ is the same as the wave velocity '$U_w$' obtained in positive surge calculation.

Solving equations (17), (18), (19), and (22) iteratively, different heights of both the positive and the negative surge waves can be obtained for each specified volumetric flowrate. The criterion for water hammer to occur is the minimum flowrate which causes the negative surge height be equal to or greater than the pipe diameter. According to these results, the boundary of intermediate water hammer due to surge formation for a pipe with a length of 2.45 m or less and an inside diameter of 5.1 cm ($L/D \leq 48$) is:

$$U_{LS} \simeq 0.14 \ \ (m/sec) \quad . \tag{23}$$

This boundary is shown as the lower dashed line in Figure 10. The difference between the experimental data and the results of calculation are within 13% with the latter being more conservative.

For a horizontal pipe with a slightly downward inclination, because there is no initial water pool trapped on the bottom, no steam can be generated by evaporation. This condition reduces the possibility of water slug formation in the middle of the pipe. However, the accumulation of liquid at the low end of the inclined pipe decreases the space above the water/steam interface, and therefore, increases locally the chance of water hammer due to surge wave formation. The net result is that avoiding water hammer in a slightly inclined pipe in down flow is more difficult than in a horizontal pipe.

Filling a slightly upward inclined pipe from the low end, the problems caused by both the initial water pool and the accumulation of water at the low end. are eliminated. Therefore, an upward flowing inclined pipe is better than truely horizontal or downward flowing inclined pipes in avoiding water hammer due to steam bubble collapse. If, however, the filling rate is sufficiently high, a water slug can still be induced by the coutercurrent flow due to condensation of the steam on the incoming water. Water hammer due to slug impact at the end of the pipe is then very possible.

For a longer horizontal pipe ($L/D \geq 96$) filled with steam, both the amount of steam in the pipe and the area of the steam/water interface become larger. Both these changes cause more intensive condensation and evaporation when filling a long pipe than filling a short pipe. As a result, a long pipe has greater tendency toward water hammer due to water slug formation than a short pipe does.

With these findings, the algorithm to avoid water hammer in a horizontal pipe is proposed as follows:

a. Avoid filling slightly downward sloping pipe from the high end.
b. Avoid filling long horizontal pipe (i.e. $L/D \geq 96$) from one end. Use multiple inlet ports for the liquid in this geometry.
c. For short horizontal pipes (i.e. $L/D \leq 48$), calculate the surge heights for different filling rates, and find out the maximum filling rate which won't cause the surge height to be greater than the pipe diameter. Then install flow restricting device in the water solid region of the fill system such that the maximum allowable filling rate is not exceeded.
d. If the piping and the piping support are sturdy enough to sustain the pressure spike due to bubble collapse at a filling velocity which causes pipe running full, use equation (16) to calculate the maximum filling velocity and insure that the fill flow will be greater than this velocity, but not so large that the resulting water hammer cannot be sustained.
e. Slightly inclined pipes of any length are best filled from the low end.

## 5. Application to Complex Piping Systems

Figure 13 shows a simplified flow diagram of a typical low pressure core injection (LPCI) system in BWR. The piping represented by BCDEFGH has been reported damaged by a water hammer. Suggestions for avoiding water hammer in this system are listed to demonstrate how the findings in the present work can be applied to complex piping system.

a. Change the loop in CDEF into a straight vertical run, if it is possible.
b. Incline the horizontal pipe runs upward in flow direction, if it is possible.
c. Reduce the length of horizontal pipe runs such that $L/D \leq 48$ for each section, if it is possible.

d. If neither step b nor c is possible, install multiple injection ports directly from the pump discharge to horizontal pipe runs, such that $L/D \leq 48$ in the pipe between any two adjacent ports.
e. Use the algorithm suggested for vertical upward flow to determine the safe filling rates for vertical and upward inclined pipe runs.
f. Use the algorithm suggested for vertical downward flow to determine the safe filling rates for vertical downward pipe runs.
g. Use the algorithm suggested for a short horizontal pipe to determine the safe filling rates for those modified horizontal pipe runs.
h. Use the lowest safe filling rate among those calculated in steps e, f, and g as a safe filling rate for the entire system.

The procedures recommended above have been developed and proven only on sections of pipe oriented in different ways. There is a possibility that the presence of fitting will modify these recommendations. However, it will not be possible to fill pipes any more rapidly than the most limited filling rate identified in the above algorithm.

## REFERENCES


1 Chou, Y., 'Avoiding Steam Bubble Collapse Induced Water Hammer in Piping Systems', Ph.D Thesis, Department of Nuclearing Engineering, M.I.T., July 1988.
2 Chow, V.T., 'Open-Channel Hydraulics', McGraw-Hill Book Company, 1959.
3 Florschuetz, L.W., and Chao, B.T., 'On The Mechanics Of Vapor Bubble Collapse', J. of Heat Transfer, May 1965, pp. 209-220, 1965.
4 Kowalchuk, W., and Sonin, A.A., 'A Model For Condensation In A Subcooled Water Pool', NUREG/CR-0221, June 1978.
5 Martin, C.S., 'Vertically Downward Two-Phase Slug Flow', J. of Fluid Engineering, pp.715-722, Dec. 1976.
6 Rohsenow, W.M., and Hartnett, J.P., 'Handbook Of Heat Transfer', McGraw-Hill Book Company, 1973.
7 Ruder, Z., 'The Influence of Two-Phase Flow Regimes on Circumferential Temperature Distribution in Horizontal, Steam Generating Tubes', Ph.D. Thesis, Department of Mechanical Engineering, Ben-Gurion University of the Negev, May 1984.
8 Rust, J.H., 'Nuclear Power Plant Engineering', Haralson Publishing Co., 1979.
9 Saedi, H.R., 'Insurge Pressure Response And Heat Transfer For PWR Pressurizer', Master thesis, Department of Mechanical Engieneering, M.I.T., November 1982.
10 Sonin, A.A., Shimko, M.A., and Chun, J.H., 'Vapor Condensation Onto A Turbulent Liquid-I. The Steady Condensation Rate As A Function Of Liquid-Side Turbulence', Int. J. Heat Transfer, Vol. 29, No. 9, pp. 1319-1332, 1986.
11 Van Duyne, D.A., and Yow, W., 'Water Hammer Prevention, Mitigation, And Accomodation -Task 1- Plant Water Hammer Experience', Stone and Webster Eng. Co., report prepared for EPRI, Jan. 1988.
12 Wallis, G.B., 'One Dimensional Two Phase Flow', McGraw Hill, 1969.

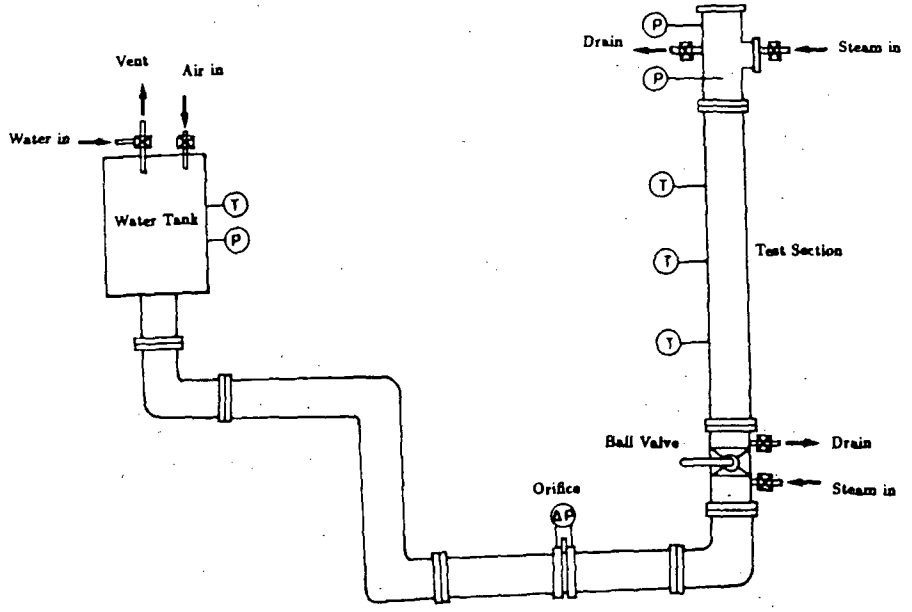


(A) Apparatus

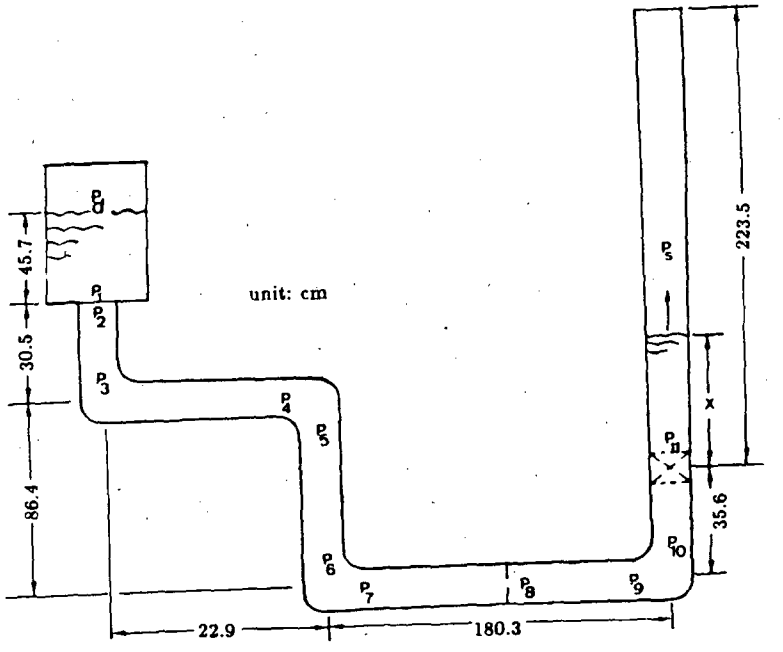


(B) Model

Fig. 1 The experimental apparatus and the corresponding model for vertical upward flow study.

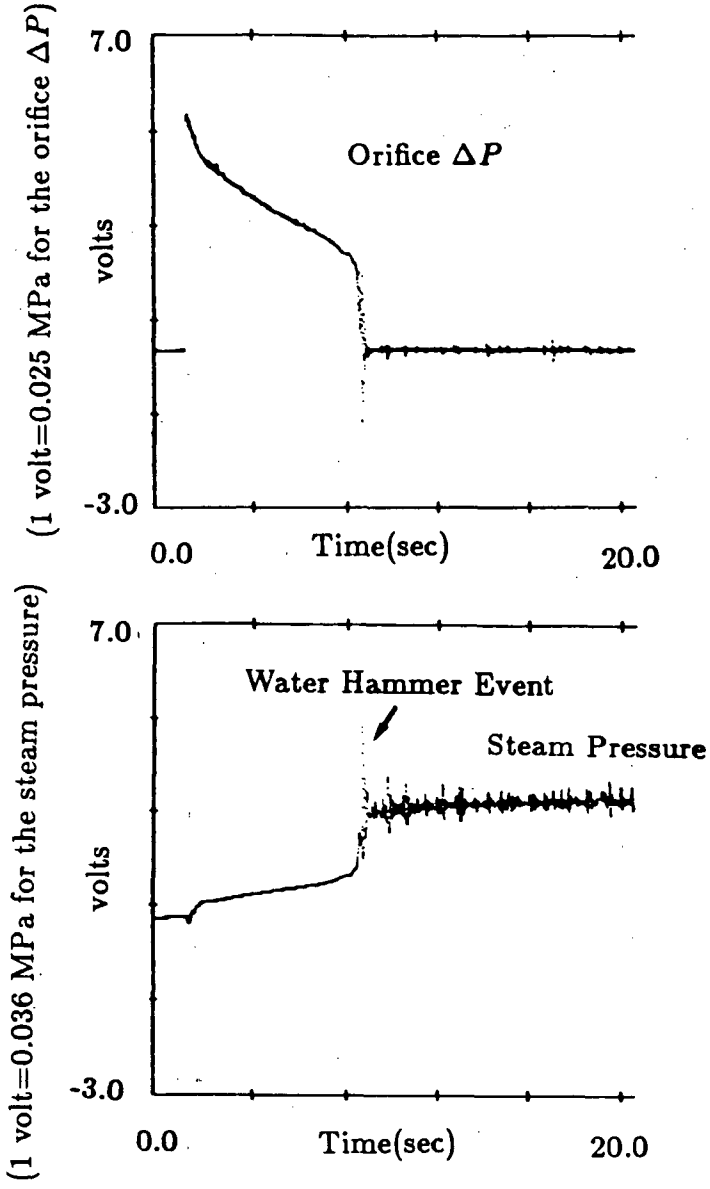


Fig. 2 Typical response curves in vertical upward flow. ($P_d = 0.22MPa$, $T_L = 82°C$)

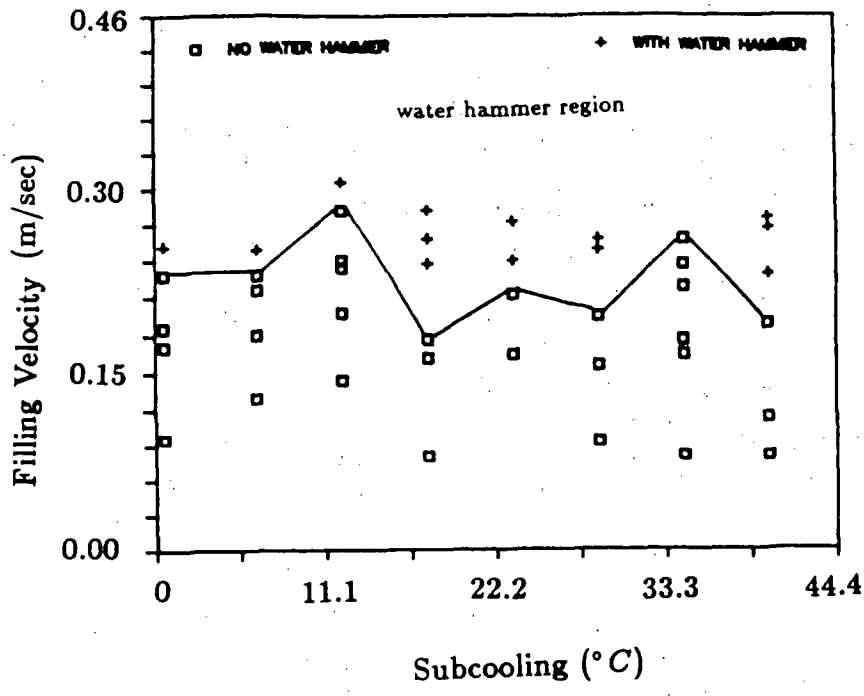


Fig. 3 Stability map in vertical upward flow.

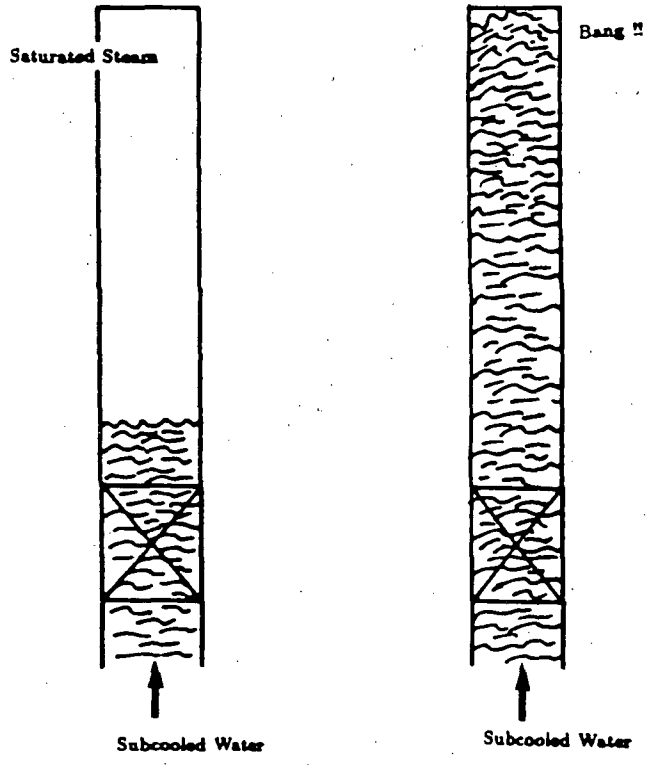


Fig. 4 Flow regimes in vertical upward flow.

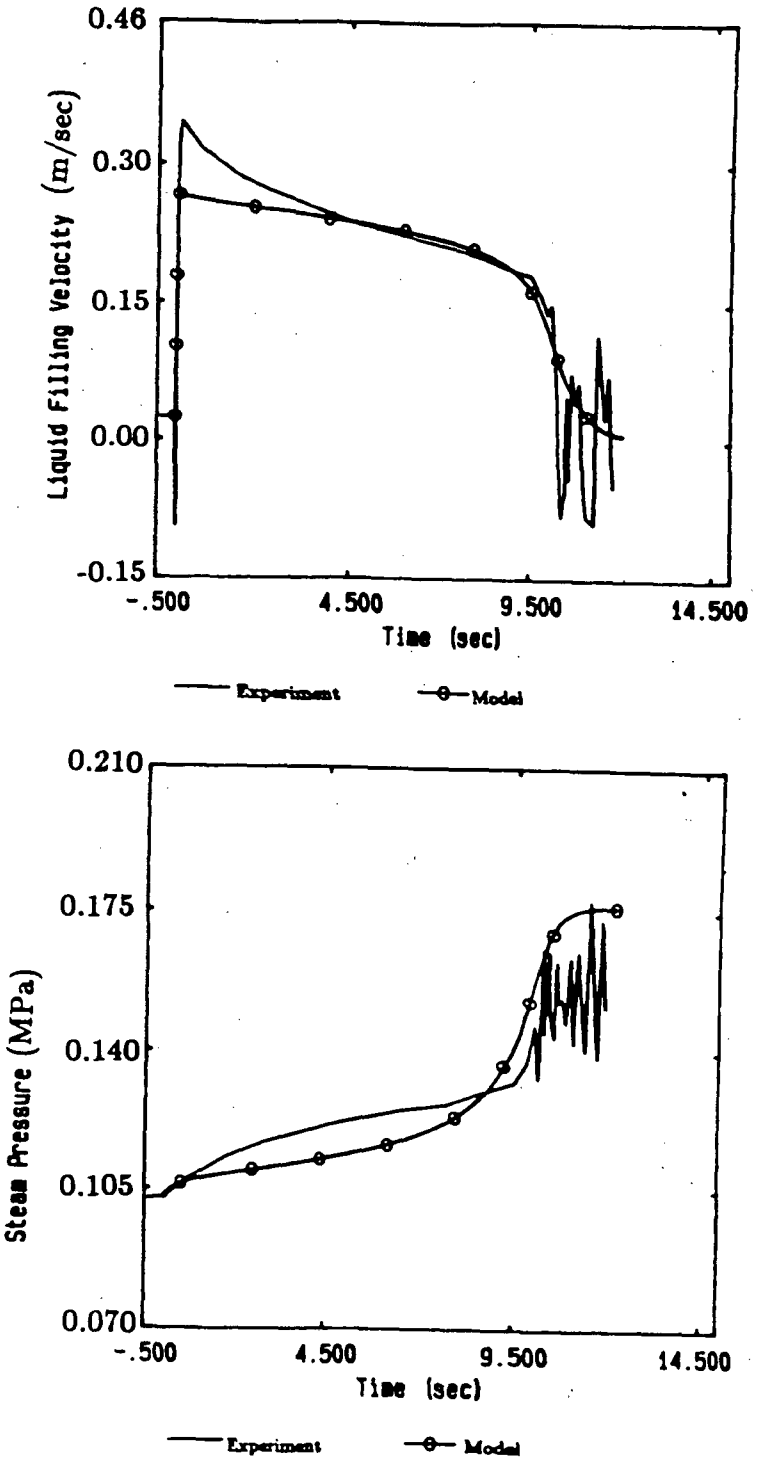


Fig. 5 Comparison between the experimental data and the analytical results in vertical upward flow. ($M_{air} = 3$ in model, $P_d = 0.18MPa$, $T_L = 82°C$)

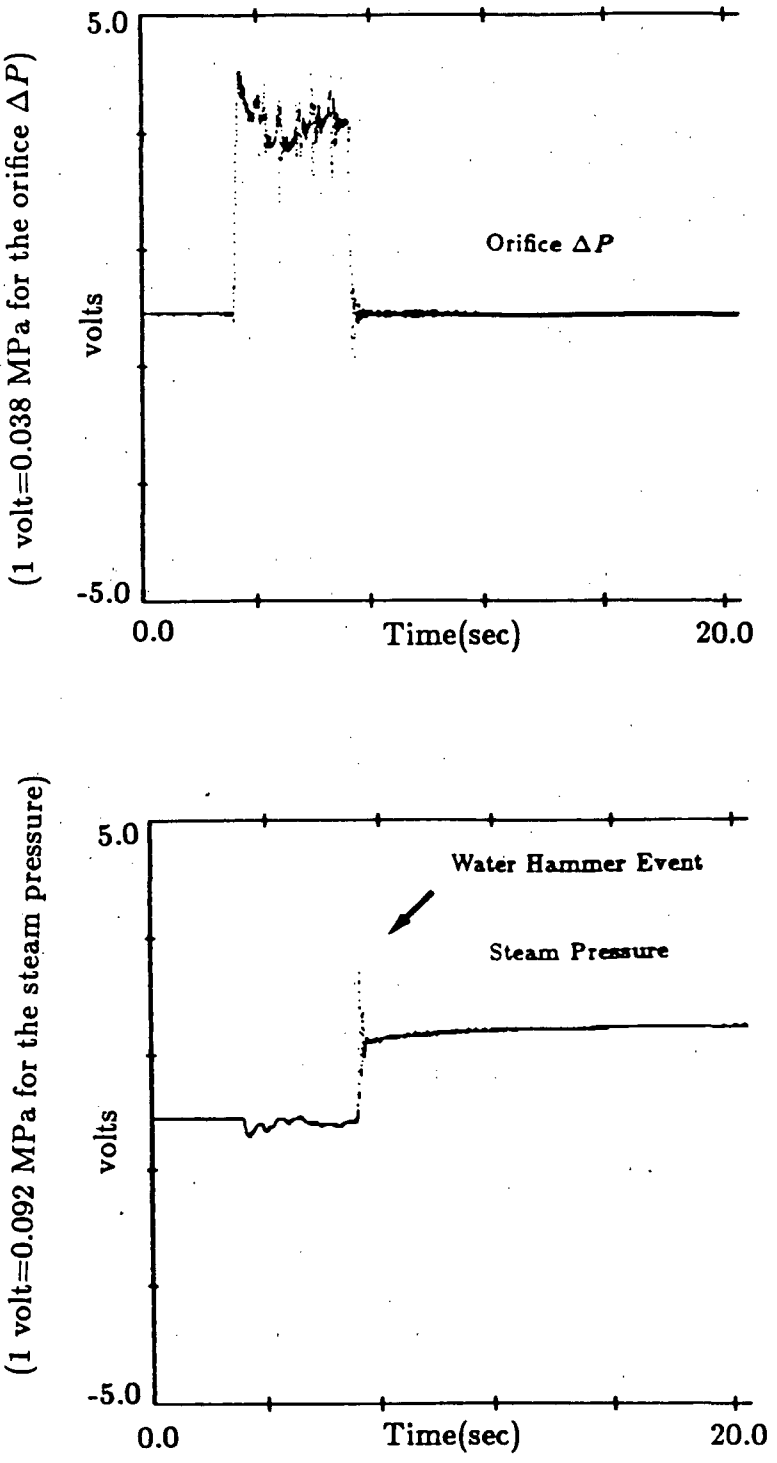


Fig. 6 Typical response curves in vertical downward flow. ($P_d = 0.24MPa$, $T_L = 49°C$)

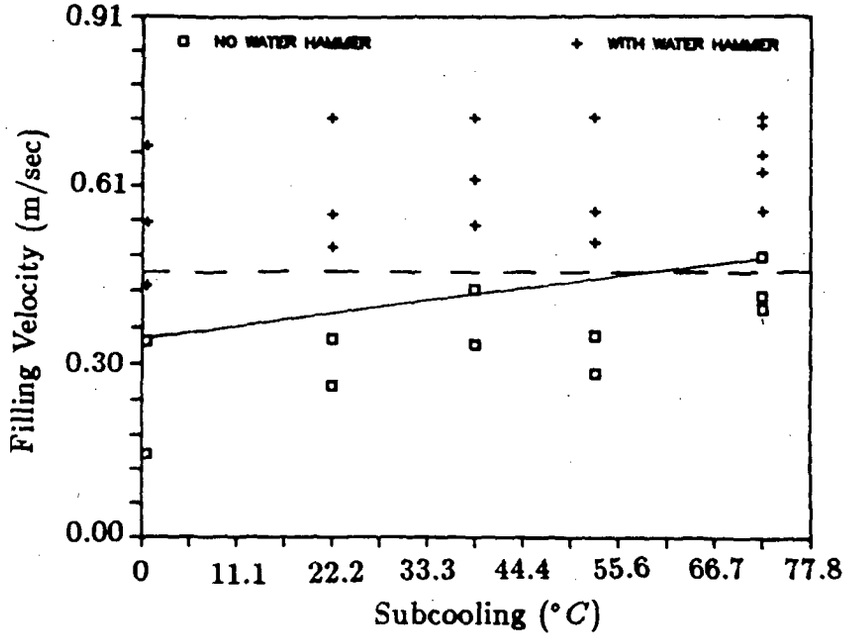


Fig. 7 Stability map in vertical downward flow.

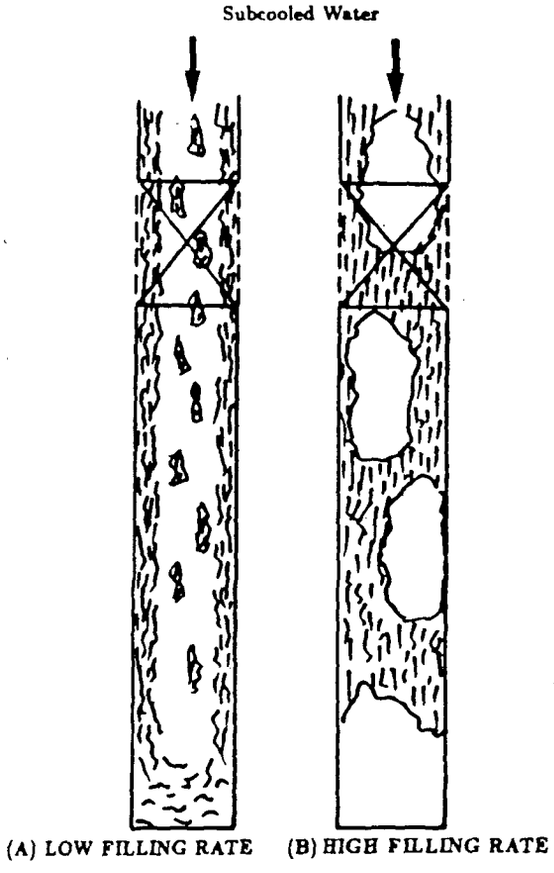


Fig. 8 Flow regimes in vertical downward flow.

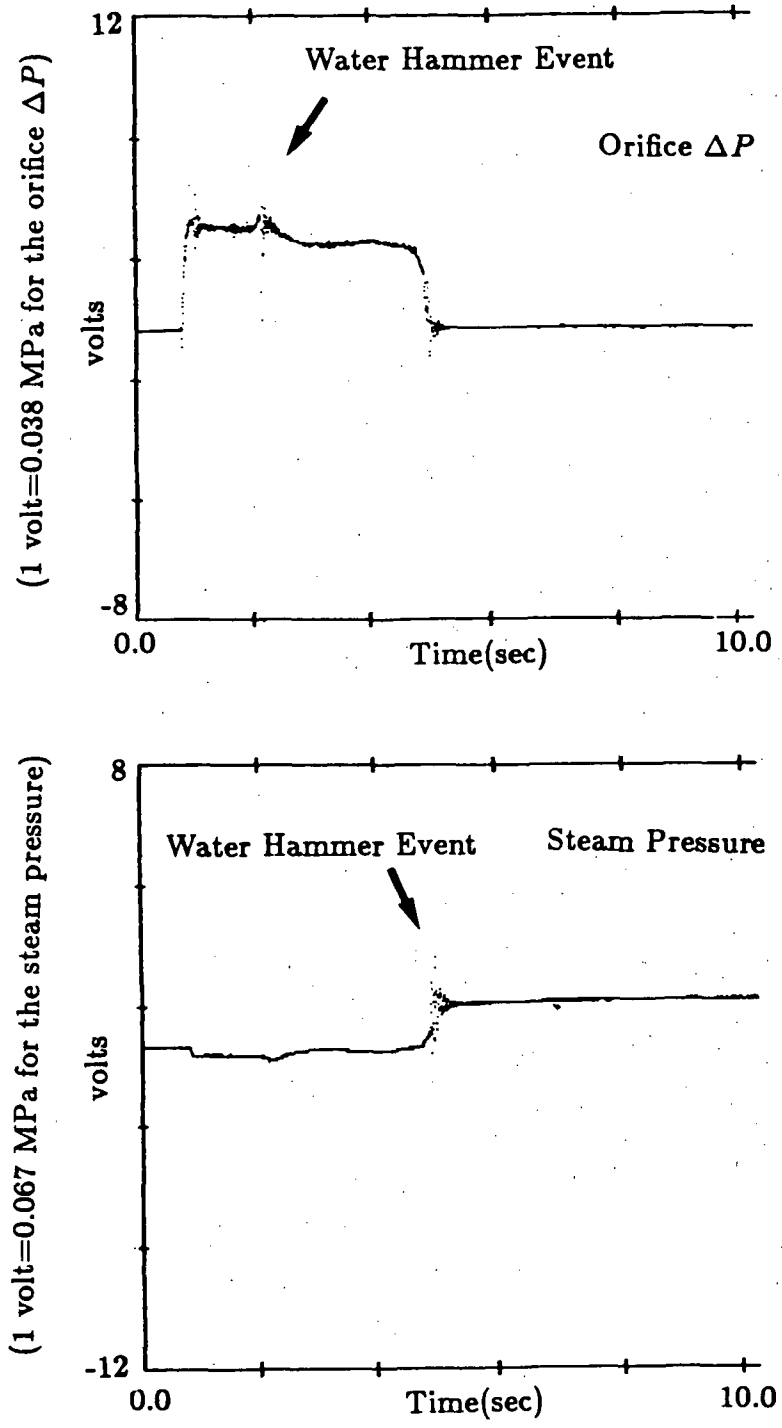


Fig. 9 Typical response curves in filling a short horizontal pipe. ($L/D \leq 48$, $P_d = 0.22MPa$, $T_L = 85°C$)

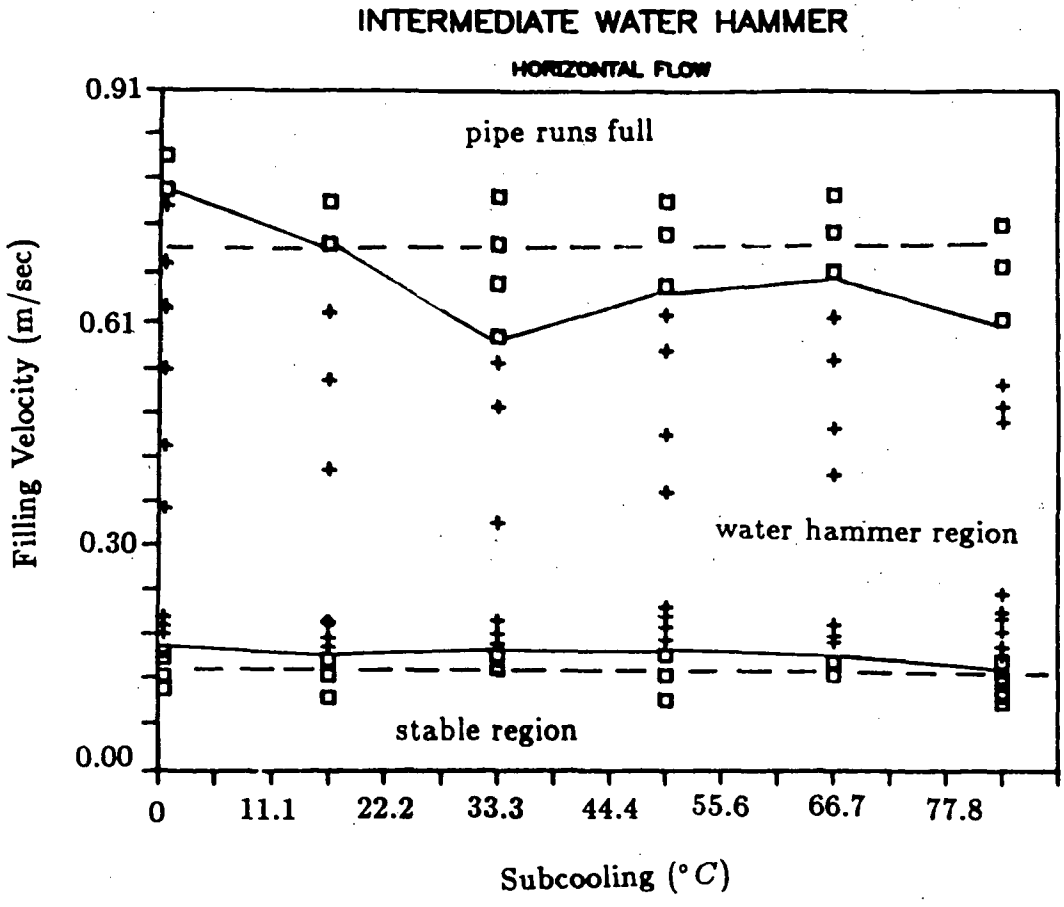


Fig. 10 Stability map of intermediate water hammer events in filling a short horizontal pipe. ($L/D \leq 48$)

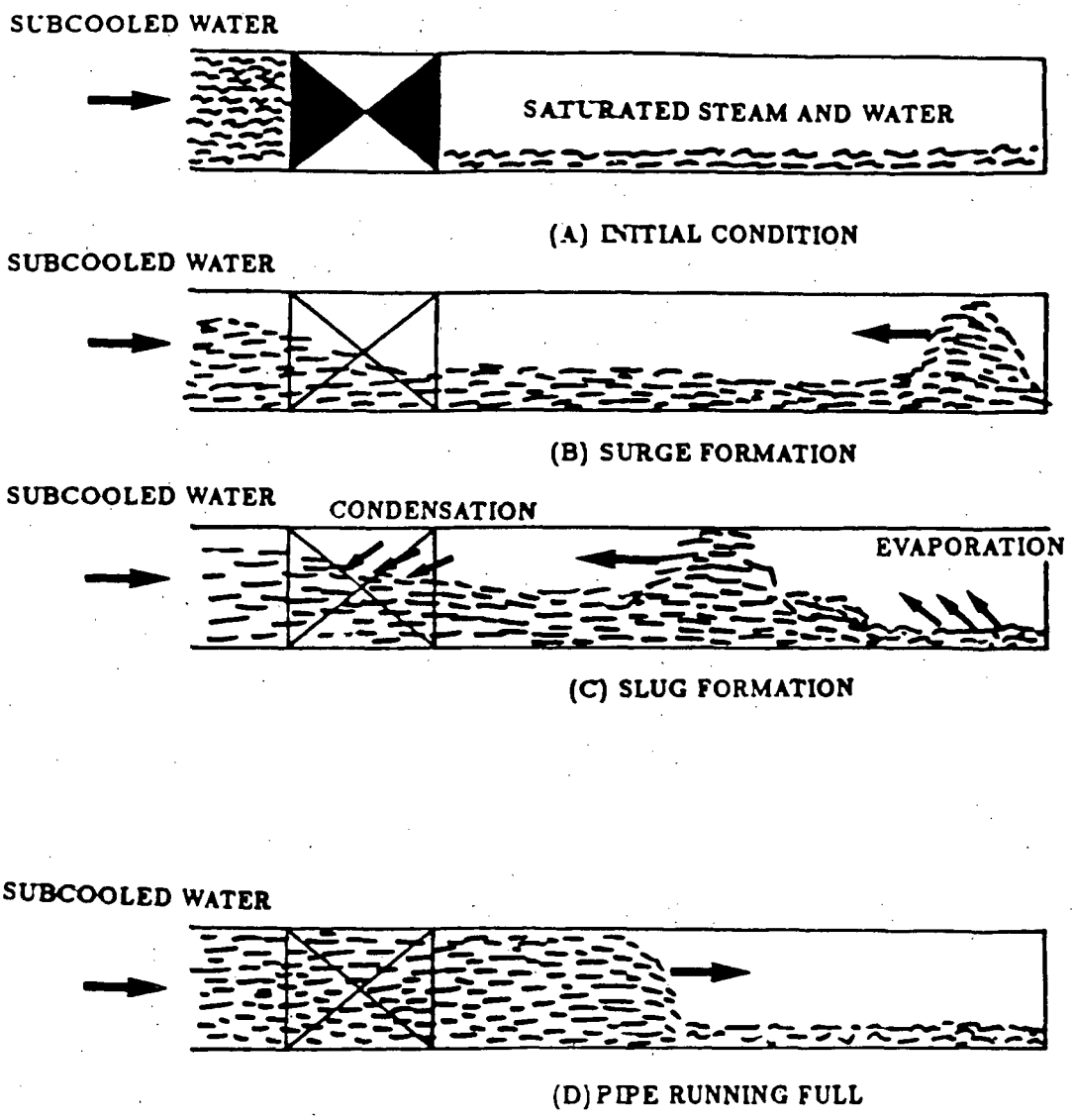


Fig. 11 Flow regimes in filling a short horizontal pipe. ($L/D \leq 48$)

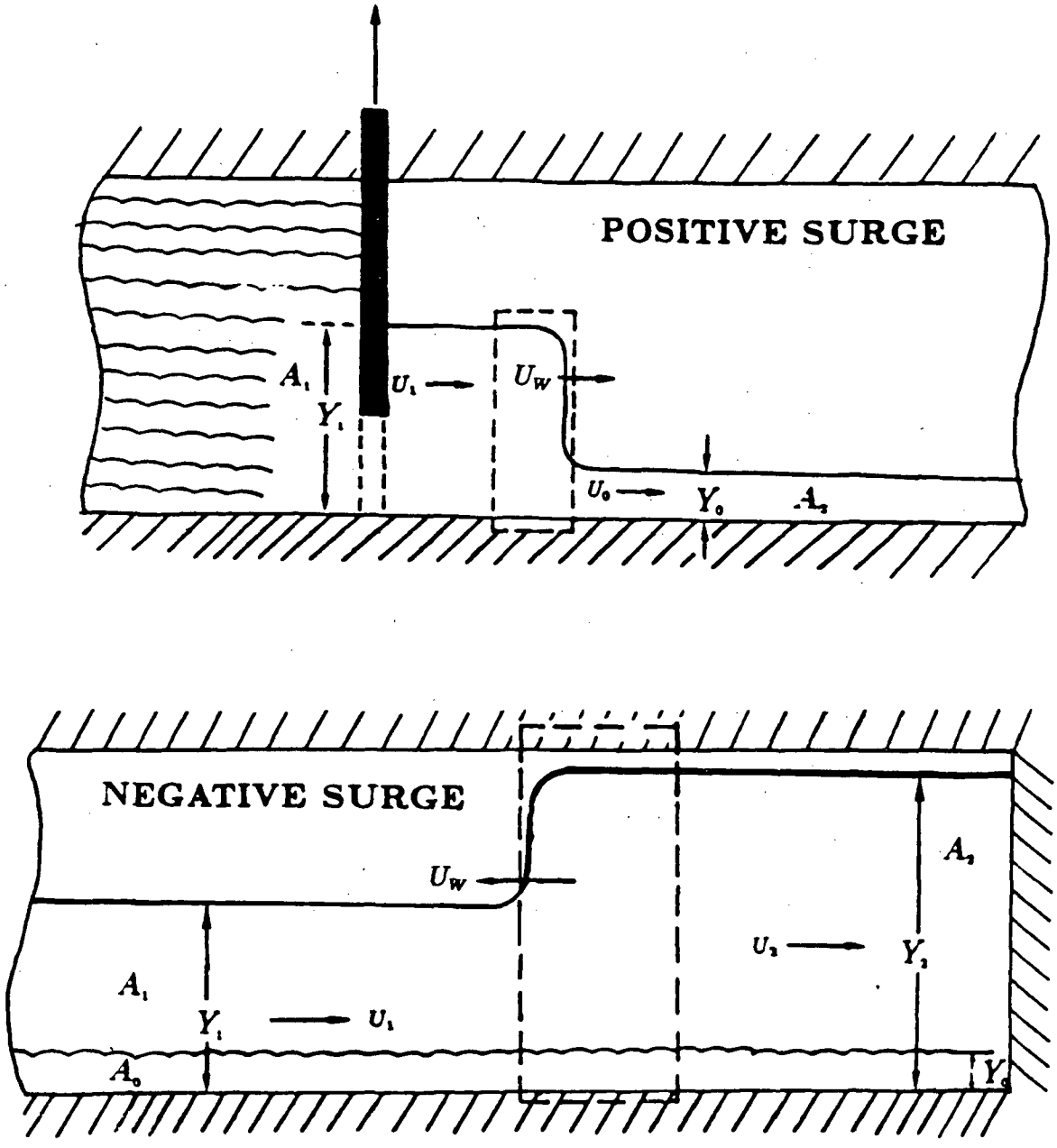


Fig. 12 Surge model for filling a short horizontal pipe. ($L/D \leq 48$)

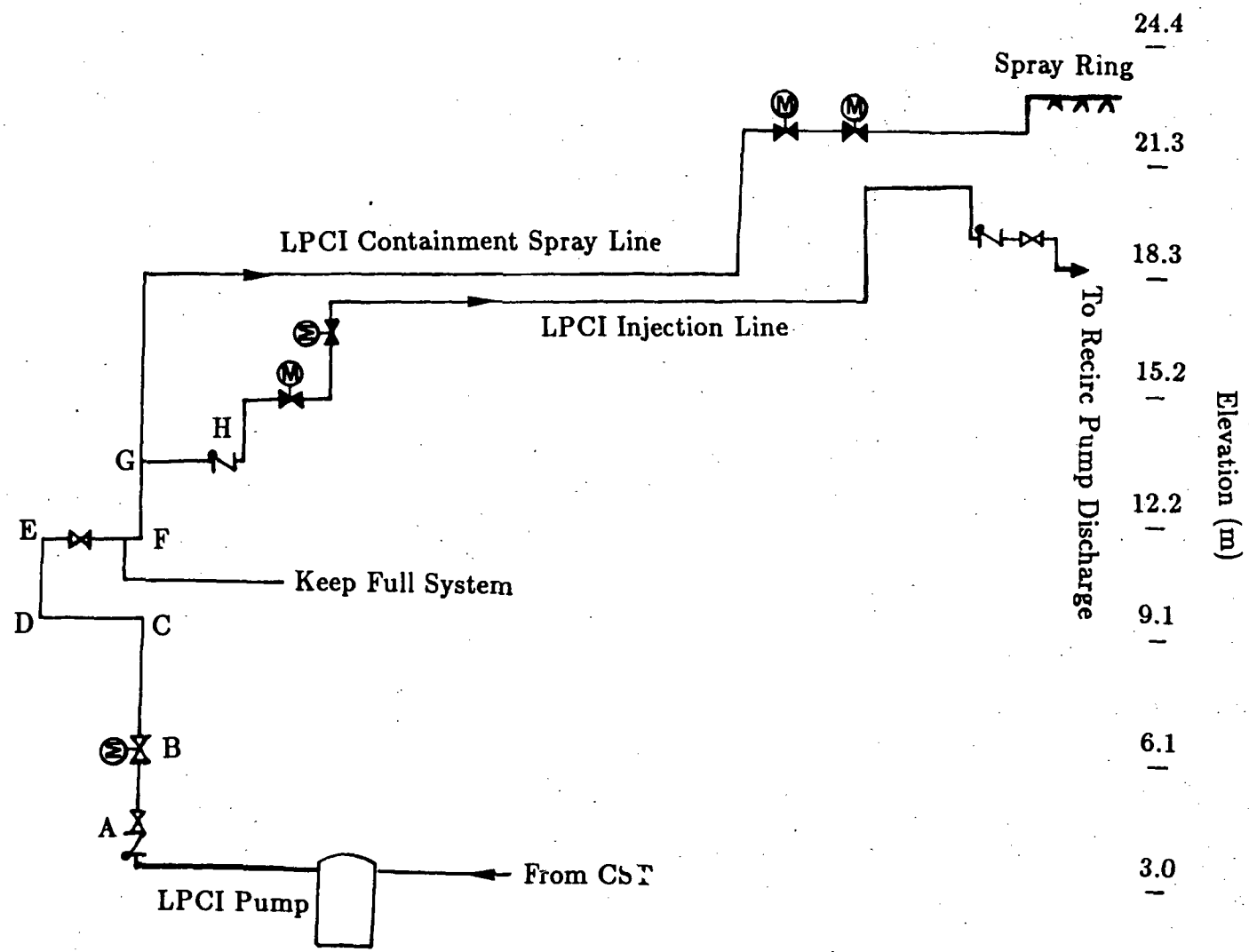


Fig. 13 Simplified flow diagram of a typical LPCI system in BWR.

# UPTF UPPER PLENUM INJECTION (UPI) TEST RESULTS AND APPLICATION TO PWR

A. Russell
P. Damerell
MPR Associates, Inc.
Washington, D. C.

G. Ahrens
Siemens/Battelle
Mannheim, FRG
P. Weiss
Siemens
Erlangen, FRG

## Abstract

The UPTF UPI test provides data on upper plenum and loop phenomena related to LOCA reflood in a UPI plant. The UPTF is about 2.1 times larger than a pressurized water reactor with UPI. Data from Semiscale, IDL, Dartmouth, CCTF, SCTF and UPTF now cover UPI phenomena at a range of scale from 1/600 to 2.1 relative to a UPI plant. The UPTF test included subcooled ECC injection into the upper plenum simultaneously with saturated steam/water flow from a simulated reactor core. There were three test phases, to parametrically study core steam flow and distribution. The UPTF results show major water delivery to the core in a very local region, rapid formation of an upper plenum pool, 100% condensation efficiency with 80% in the upper plenum and 20% in the core, and significant storage of carryover water in the hot legs. These phenomena show distinct trends with scale when compared to the results from scaled tests. Estimated UPI plant LOCA behavior is also determined from these comparisons. The inferred UPI plant behavior indicates that good core cooling is expected in the event of a large break LOCA.

## Introduction

In the United States there are six Westinghouse two-loop pressurized water reactors (PWRs). In these PWRs, the low pressure emergency core coolant (ECC) is piped directly to the reactor upper plenum, an arrangement referred to as upper plenum injection (UPI). The ECC system for a typical UPI plant is shown schematically in Figure 1. In the event of a hypothesized loss-of-coolant accident (LOCA), ECC would be injected directly into the reactor vessel upper plenum once the pressure drops below the discharge head of the low pressure ECC pumps. In a large break LOCA this occurs during the refill and reflood phases. The UPI is the primary source of water to reflood the core during a large break LOCA.

The phenomena associated with downward ECC penetration into the core and cooling of the core in a UPI plant are more complex than for most US PWRs, which use cold leg or downcomer injection and flood the core using a water pool rising from below. In the case of UPI, countercurrent steam/water interaction can strongly affect the water flow, and condensation, pooling and entrainment in the upper plenum are first-order phenomena influencing the LOCA behavior (Figure 2). Initially, plants with UPI were licensed based on simplified LOCA calculations which assumed that ECC injected in the upper plenum flows to the lower plenum without any heat transfer in the core. This approach was thought to be conservative. Later, the NRC indicated that because of the complexity of the phenomena involved, this non-mechanistic assumption was not necessarily conservative. Although strong action (e.g., shutting down plants) was determined not to be required, the NRC requested the utilities to perform improved LOCA calculations and embarked on a research effort to more adequately explain the UPI LOCA phenomena.

The experimental research effort included tests at several scaled facilities that investigated the effectiveness of UPI and the associated phenomena that occur during a LOCA. These facilities include:

- Semiscale (1/600 scale relative to UPI plant) [Ref. 1]
- Dartmouth (1/110 scale) [Ref. 2]
- Cylindrical Core Test Facility (CCTF, 1/11 scale) [Ref. 3]

Further, tests that were not designed to evaluate UPI but had conditions related to UPI have been carried out at:

- Instrument Development Loop (IDL; 1/30 to 1/90 scale) [Ref. 4]
- Slab Core Test Facility (SCTF; 1/11 scale)

Recently, a separate effects test simulating UPI flow conditions was carried out at the Upper Plenum Test Facility (UPTF) [Ref. 5]. The UPTF, which simulates a four-loop PWR at full scale, is about 2.1 times larger than a UPI plant. The total group of experimental results applicable to UPI now cover the range of scale from 1/600 to 2.1 and no more NRC-sponsored UPI tests are currently envisioned. Given the wide range of scale of the results, the effect of scale (up to full scale and above) can be evaluated. From these scale evaluations, several key phenomena which would occur in a UPI plant LOCA can be quantified directly, and that is the main emphasis of this paper. The UPTF test is described first, followed by an evaluation of scaling and expected PWR behavior.

## UPTF UPI Test -- Test Objectives

A detailed study of the UPTF and its capabilities to perform a test related to UPI was carried out. The conclusion of the study was that, because of several differences between a UPI plant and UPTF, it was not possible to carry out a UPTF test simulating integral LOCA transient behavior. However, it did appear feasible to perform a separate effects test in UPTF which would create flow conditions in the upper plenum like

those that would occur in a UPI plant LOCA. Accordingly, a test was specified with the objective of obtaining large scale data on the following phenomena:

- Pool formation and distribution in the upper plenum
- Mixing of subcooled and saturated water
- Steam condensation
- Water carryover to hot legs
- Water penetration to core

With regard to the last phenomenon, it was realized that UPTF would not precisely simulate a UPI plant because, as discussed below, UPTF does not have a heated core. Hence, the local enhancement of steam generation due to water downflow in the core was not simulated.

UPTF UPI Test -- Test Facility Configuration

The UPTF has been described elsewhere [Refs. 6 - 7] and a complete description will not be repeated here. Rather, the discussion below focuses principally on the configuration of the upper plenum, core and loops, and on the special manner in which UPTF was configured for this test.

The UPTF simulates the primary system of a German four-loop PWR. Included are a full scale (relative to the German four-loop PWR) reactor vessel, four 0.75-m (29.5-inch) diameter hot legs and cold legs, four steam generator simulators (steam/water separators) and four pump simulators (variable flow resistances). One loop has two break valves, each of which can direct flow from the primary system to a containment simulator tank. The reactor vessel upper plenum has internal structures (Figure 3) which are a precise simulation of the German four-loop plant. The reactor vessel core is simulated by a "core simulator" steam/water injection system consisting of 193 steam/water nozzles, one for each fuel assembly of the German PWR. The upper 25% of the core is simulated physically by 193 dummy (unheated) fuel assemblies, to create a realistic flow channel at the top of the core.

There are no upper plenum ECC injection pipes in UPTF similar to those in a UPI plant. However, there is an ECC injector (called a "Hutze") located in each hot leg approximately 1.5 m (4.9 ft) from the upper plenum. The detailed configuration of the hot leg injector is shown in Reference 8. For this test, the hot leg injector in Loop No. 1 was used to inject ECC and this loop was blocked at the pump simulator to prevent steam from flowing in the loop and potentially impeding ECC delivery to the upper plenum. This left two intact loops and one broken loop open to flow. The pump simulator K-factor in the intact loops was about 10; the total intact loop K-factor was 19. The total broken loop K-factor was approximately 29. These resistances roughly simulated the total loop flow resistance in a UPI plant with locked pump rotors. Precise loop

simulation was not needed due to the separate effects nature of this experiment.

UPTF UPI Test -- Test Conditions

The UPTF UPI test consisted of:

- Saturated steam/water injection in the core simulator
- Subcooled ECC injection in the Loop No. 1 hot leg injector
- Water drainage in the lower plenum

Further, there was a small steam injection in the steam generator simulator of Loop No. 1 to ensure smooth ECC delivery to the upper plenum. Finally, the containment simulator pressure (which is also the initial system pressure) was maintained at 2.5 bar (36 psia) throughout the test. Figure 4 shows an overview of the test approach.

The test conditions described above were applied in three separate phases, to allow parameter variation study. Table 1 summarizes the pertinent conditions of each phase. The two parameters varied in the test include the core steam flow rate (simulating the best-estimate and licensing heat release rates) and the core steam flow distribution (simulating uniform and power-shaped profiles). The three phases are referred to as A, B, and C.

UPTF UPI Test -- Comparison of Test Configuration and Conditions to UPI Plant

Table 2 shows a comparison of pertinent UPTF configuration and test parameters with corresponding UPI plant values. From the configuration comparison it can be seen that the "scale factor" of UPTF relative to a UPI plant is about 2.1. The significant distortions relative to this scale factor are:

- Total UPTF hot leg area is about 75% of the appropriately scaled value. This is because Loop No. 1 was blocked in this test for ECC injection. This results in hot leg velocities about 35% high in the test.
- UPTF ECC injection nozzle area is about 2.5 times the appropriately scaled value. This is because the German Hutze was the only possible choice for simulating UPI. This results in a wider, slower-moving ECC jet by a factor of 2.5.

In spite of these differences, the overall UPTF configuration dictated that a scale factor of about 2.1 should be used to develop test conditions. This approach can be seen in the test conditions shown in Table 2.

## UPTF Test Results

### Overall Mass Disposition

Mass balances were used to determine steam and water flows in each of the three phases of the UPTF test. The mass balances closed with good accuracy (1 to 5% of total injected mass). Of particular interest in the UPTF test is the behavior of injected ECC water. The results in all three phases showed generally similar behavior, as follows:

- A major delivery of water from the upper plenum to the core started essentially immediately after injection and persisted throughout the phase. The delivery ranged from 117% to 121% of the injected flow and from 92% to 95% of the total available water (injection plus condensation). As will be discussed below, this water downflow occurred in only a portion of the upper plenum.

- Water rapidly formed a pool in the upper plenum. This pool also had a multidimensional character, as will be discussed below. The mass stored in the pool was relatively small, equal to 2.5 seconds worth of ECC flow. The upper plenum collapsed level was about 0.06 m (2.5-inch), giving an average upper plenum void fraction of over 95%.

- After formation of the upper plenum pool, water which did not penetrate to the core was carried over to the hot legs. Some of this water de-entrained and was stored in the hot legs and steam generator inlet plena and some was carried into the steam generator simulator (representing the tube region of a PWR steam generator). The water stored in the hot legs was in a stratified pattern, with liquid fractions up to approximately 30%.

- After about 120 to 150 seconds, the hot legs and steam generator inlet plena became saturated with water and from that time on essentially all water not penetrating to the core was transmitted to the steam generator simulators.

Figure 5 shows a simplified mass balance for Test Phase A which demonstrates the behavior described above.

### Subcooling and Condensation

As expected, there was strong thermal interaction between steam and subcooled ECC water in the upper plenum. The initial subcooling of the ECC was 100 K (180°F). The maximum measured subcooling in the water penetrating to the core ranged from 20 to 25 K (36 to 45°F) and the average subcooling of water penetrating to the core was estimated from several measurements to be 14 K (25°F). No subcooled water was found in the water carryover to the hot legs or in the region below the core. This implies that the overall condensation efficiency was 100%, which was confirmed by steam mass flow input and output measurements. The upper plenum condensation efficiency was calculated from the data to be about 80%, with the remaining 20% occurring in the core.

Subcooling was measured in the upper plenum, but only in local areas, as will be discussed below. Most of the upper plenum pool was at saturation temperature.

Distribution and Multi-Dimensional Effects

Non-uniform distribution and multi-dimensional effects were observed in the flow to the core and in the upper plenum mass and energy storage. The observed patterns are described below:

- The mass flow from the upper plenum to the core occurred in a single region covering about 10% of the total area. This region was located near the hot leg where injection occurred, as shown in Figure 6. The existence, location and size of the breakthrough region was measured directly by several instruments, including thermocouples, turbine meters, and special "breakthrough detectors," which are small momentum flux detectors mounted at the tie plate. Figure 6 is based on breakthrough detector measurements.

- The upper plenum pool was non-uniform and had multi-dimensional character. Specifically, the pool had a somewhat higher collapsed level in the region above the breakthrough region, as shown in Figure 7. This distribution was measured by an array of 36 differential pressure measurements in the upper plenum. The observed result is intuitively understandable in that the ECC water appears to be delivered in a non-uniform manner through the upper plenum to the core.

- The subcooling was also distributed in a manner like the penetration and inventory discussed above, as would be expected. Figure 8 shows the subcooling distribution based on temperature measurements at the tie plate.

The multi-dimensional effects discussed above were observed to be formed rapidly in each test phase. Once established, each distribution persisted throughout the test and did not change significantly either in magnitude or location.

Parameter Effects

In general, effects of changing core steam flow and distribution in UPTF did not affect the phenomena described above in a first-order manner. An evaluation of the effect of steam flow (Phases B and C) showed that carryover to the hot legs was increased from 6% to 8% of injection, when steam flow out of the upper plenum increased by 41% from 41 to 58 kg/sec (90 to 128 lbm/sec).

An evaluation of the effect of core steam distribution (Phases A and C) showed that carryover to the hot legs decreased from 10% to 6% of injection, when steam flow distribution changed from uniform to peaked. Neither parametric change had a significant impact on upper plenum pooling, subcooling or breakthrough distribution.

Summary of Conclusions from UPTF Test

The results of the UPTF UPI test can be summarized as follows:

1. ECC water penetration to the core is the dominant water flow path. About 120% of the injected ECC flow, or 95% of the available water, penetrates to the core.

2. Penetration to the core occurs in a local region covering about 10% of the core cross-sectional area.

3. An upper plenum pool forms rapidly which contains about 2.5 seconds worth of ECC flow. The pool is uniform except for the region above the penetration zone, which indicates water levels about twice as high. The pool is saturated except for the region above the penetration zone which is subcooled.

4. Overall condensation efficiency is 100%, with 80% occurring in the upper plenum and 20% in the core. The subcooling of ECC penetrating to the core is about 14 K (25°F) average and 20 - 25 K (36 - 45°F) maximum.

5. The hot legs stored a significant amount of water carried out of the upper plenum (20 to 75%) in a stratified regime. The accumulation occurred mainly during the first two minutes of each phase. The remainder of the water flowed to the steam generator.

Comparison of Results at Different Scales

The principal phenomena described above were compared among tests at several different scales so that the effect of scale could be discerned. As a part of this comparison, it is important to recognize that the facility configuration and scaling, and the type of test in each facility were not the same. Table 3 summarizes a comparison of the configuration and scale of the several facilities and the UPI plant. Only the Dartmouth facility reproduced the UPI upper plenum geometry at scale; the other facilities typically simulated four-loop plants. However, the four-loop plant configuration is very similar to the two-loop plant. As seen in Table 3, the facilities cover a range of scale from 1/600 to 2.1.

Table 4 shows a comparison of test conditions covered in the various facilities, along with typical LOCA parameters for a UPI plant. As seen in this table, the tests generally produced vapor and liquid flows scaled in accordance with the overall scale factor. It should be noted that the tests in Semiscale, Dartmouth and CCTF were intended to simulate UPI plant behavior, whereas the tests in SCTF and IDL had different objectives but nonetheless developed conditions similar to those for UPI.

Figure 9 shows a comparison of normalized upper plenum collapsed water level from the facilities which had appropriate measurements. A general trend of decreasing upper plenum level with scale is apparent. This trend is consistent with the observation of very distinct multi-dimensional effects (e.g., downflow restricted to a small zone) in the large scale UPTF.

Figure 10 shows a comparison of the fraction of ECC penetrating to the core for similar conditions at different scales. Total upward gas momentum flux was the parameter used to determine similar conditions from the scaled facilities. A pattern of increasing penetration at larger scale can be readily observed. This pattern is consistent with expectation of the effect of size on countercurrent flow, i.e., increasing size leads to greater liquid penetration at a given average vapor flux.

Figure 11 shows a comparison of fractional breakthrough area as a function of scale. The water penetration occupies a smaller percentage of the entire area as size increases.

Finally, there are two other observed results of scale which are most conveniently summarized verbally rather than by graphical comparison:

1. Overall condensation efficiency was 100% for all scales. However, upper plenum condensation efficiency decreased from 100% at all subscale facilities to about 80% at scale 2.1 (UPTF).

2. There was no storage of water in the hot legs in any of the subscale facilities, but there was a significant storage in a stratified layer in the large scale UPTF. These results are consistent with void correlations obtained from previous UPTF hot leg separate effects tests [Ref. 8].

Application of Results to PWR

The comparisons of the scaled tests discussed above reveal the effects of scale on the principal phenomena. Because the scale ranged from 1/600 to 2.1 among the facilities, the UPI plant LOCA phenomena (scale = 1.0) are bounded by the scale tests results. A single exception is in the hot legs, where all of the tests had higher hot leg dimensionless velocity (j*) than expected in a UPI plant. However, in this case the UPTF results achieved close to the correct condition, and other UPTF tests provide a reliable basis to predict UPI plant behavior. The discussion below covers the expected UPI plant behavior in the major areas of UPI reflood phenomena.

Upper Plenum Pooling

The expected normalized upper plenum collapsed water level in a UPI plant is 0.1 based on Figure 9. This would result in a collapsed liquid level of 110 mm (4.4 inches) at the upper core support plate or a water inventory of about 600 kg (five seconds of ECC flow). This pool depth would not significantly increase the overall loop pressure drop to inhibit core cooling.

ECC Penetration

The expected penetration fraction to the core in a UPI plant is 0.9 of available water (ECC plus condensation), based on Figure 10 assuming ECC is 100 K (180°F) subcooled. This would result in a penetration of

130 kg/sec to the core assuming the condensation efficiency is 100% (discussed below). It should be noted that this is based on one of the two UPI nozzles being functional, i.e., the single active failure assumption applies. Other tests in CCTF [Ref. 3] showed the single failure is the most limiting LOCA reflood case.

Distribution

The expected ECC breakthrough area in a UPI plant is 15 to 20% of the core flow area based on Figure 11. The scaled tests indicated that this breakthrough area was stationary and that the breakthrough flow was steady with time. Thus, a steady, stationary breakthrough area is expected at a UPI plant as well.

Condensation

The expected overall condensation efficiency at UPI plant is 100% because the overall condensation efficiencies at all the scaled tests were 100%. The upper plenum condensation efficiency is expected to be between 80% and 100% which are the bounding values based on scale.

Hot Leg Water Storage

The expected water storage in the hot legs of a UPI plant is about 50% of the pipe volume, based on extrapolation of UPTF UPI test results and use of data from a special UPTF hot leg separate effects test [Ref. 8], as shown on Figure 12. As discussed above, the subscale tests had essentially no water storage in the hot legs, i.e., a hot leg void fraction of about 1.0, and so are generally not indicated on the figure. (The single CCTF data point shows how the scaled conditions were expected to have essentially no water in the hot legs.)

Overall LOCA Behavior at a UPI Plant

LOCA behavior expected in a UPI plant during the reflood phase can be summarized from the results above. This behavior is illustrated on Figure 13 which shows a pool in the upper plenum that forms quickly after low pressure ECC injection begins, storing about 600 kg of water. From this pool a steady downflow of about 130 kg/sec penetrates the core in a single channel covering about 15 to 20% of the core flow area. From the core, 34 kg/sec (best-estimate decay heat) of steam is produced and flows through the upper plenum pool where 24 kg/sec of the steam condenses (the steam cannot escape the bottom of the core because a water seal forms there at the start of the reflood phase). The remaining 10 kg/sec steam flow escapes through the hot legs (with flow roughly balanced between the two hot legs) carrying 14 kg/sec of water with it. This water de-entrains mainly in the hot legs and steam generator inlet plena until these locations become saturated at a void fraction of about 0.5. After these regions become saturated, the water carryover is carried into the steam generators where it vaporizes, adding to the loop steam flows in the cold legs. Steam in the broken loop flows out of the break into containment. Steam in the intact loop mixes with the high pressure ECC injection in the cold leg, completely condenses, and flows to the

downcomer. This flow to the downcomer and the core penetration flow cause the core to reflood and the downcomer level to rise such that eventually excess water spills out the cold leg break. Ultimately, two-phase mixture rises to cover and completely quench the core.

References


1. TREE-NUREG-1055, "Experimental Data Report for Semiscale MOD-1 Tests S-05-6 and S-05-7 (Alternate ECC Injection Tests)," June, 1977.

2. NUREG/CR-1078, "An Investigation of the Distribution and Entrainment of ECC Water Injected into the Upper Plenum," January, 1980.

3. Iguchi, T. and Y. Murao, "Experimental Study on Reflood Behavior in PWR with Upper Plenum Injection Type ECCS by Using CCTF," Journal of Nuclear Science and Technology, August, 1985.

4. NUREG/CR-3138 (ORNL/TM-8204), "Measurement of Two-Phase Flow at the Core/Upper Plenum Interface for a PWR Geometry under Simulated Reflood Conditions," August, 1983.

5. Siemens report U9 316/88/07, "Quick Look Report - UPTF-Test No. 20, Upper Plenum Injection Simulation Test," June, 1988. (This report is available only through the restrictions of the 2D/3D International Program.)

6. Hofmann, K., "Status of the German UPTF Program," presented at the 13th Water Reactor Safety Information Meeting, October 22 - 25, 1985.

7. Weiss, P., Sawitzki, M. and Winkler, F., "UPTF, a Full-scale PWR Loss-of-Coolant Accident Program," Atomkern-Energie Kerntechnik, Vol. 49, 1986.

8. Damerell, P., N. Ehrich and K. Wolfe, "Use of Full-Scale UPTF Data to Evaluate Scaling of Downcomer (ECC Bypass) and Hot Leg Two-Phase Flow Phenomena," presented at the 15th Water Reactor Safety Information Meeting, October 26 - 29, 1987.

TABLE 1

SUMMARY OF TEST CONDITIONS FOR
UPTF UPI TEST

| Parameter | Value |
|---|---|
| Containment Pressure | 2.5 bar (36 psia) |
| Initial Vessel Pressure* | 2.5 bar (36 psia)* |
| Initial Vessel Temperature | 403 K (266 °F) |
| Core Simulator Steam/Water Flow (Saturated) | |
| Phase A Steam | 87 kg/sec (191 lbm/sec) |
| Water | 24 kg/sec (53 lbm/sec) |
| Phase B Steam | 99 kg/sec (218 lbm/sec) |
| Water | 21 kg/sec (46 lbm/sec) |
| Phase C Steam | 83 kg/sec (183 lbm/sec) |
| Water | 24 kg/sec (53 lbm/sec) |
| Core Simulator Injection Profile (Peak/Average Factor) | |
| Phase A | 1.0 |
| Phase B | 1.13 |
| Phase C | 1.13 |
| ECC Flow Rate | 262 kg/sec (576 lbm/sec) |
| ECC Temperature | 306 K (91 °F) |
| Vessel Drain Flow Rate | 273 kg/sec (600 lbm/sec) |

*Vessel Pressurized to Approximately 2.7 bar (39 psia) During Test.

TABLE 2

COMPARISON OF SELECTED UPTF AND UPI PLANT PARAMETERS AND TEST CONDITIONS

| Parameter | UPTF | UPI Plant | Ratio of UPTF Value to UPI Plant Value |
|---|---|---|---|
| Full Power Thermal Rating-MW | 3,900 (Simulated) | 1,520-1,650 | 2.57-2.36 |
| Number of Fuel Rods | 45,548 | 21,659 | 2.10 |
| Core Flow Area-$m^2$ ($ft^2$) | 5.53 (59.5) | 2.47 (26.6) | 2.24 |
| Total Upper Plenum Area within Core Barrel ID[1]-$m^2$ ($ft^2$) | 14.0 (150.6) | 6.02 (64.8) | 2.32 |
| Area of One Hot Leg-$m^2$ ($ft^2$) | 0.442 (4.76) | 0.426 (4.59) | 1.04 |
| Area of All Hot Legs-$m^2$ ($ft^2$) | 1.33 (14.27)[2] | 0.852 (9.17) | 1.56 |
| UPI Nozzle Area-$m^2$ ($ft^2$) | 0.0407 (0.438) | 0.0081 (0.087) | 5.0 |
| Height of Hot Legs Above the Upper Core Support Plate-m (ft) | 1.4 (4.5) | 1.1 (3.7) | 1.22 |
| **Test Conditions** | | | |
| Core Steam Flow Rate kg/sec (lbm/sec) | 83-99 (183-218) | 30-40 (66-87)[3] | 2.5 |
| ECC Flow Rate - kg/sec (gpm) | 262 (4150) | 120 (1900) | 2.2 |
| Containment Pressure - bar (psi) | 2.5 (36) | 2.5-3.5 (36-51) | - |
| ECC Temperature - K (°F) | 306 (91) | 306 (91) | - |
| Vessel Temperature - K (°F) | 403 (266) | 400-560 (260-550) | - |

NOTES

1. Actual upper plenum flow area is dependent on internal configuration and is proprietary. The ratio of actual areas is similar to the value in this table.
2. Three loops only; one loop was isolated for UPI injection.
3. Core steam flow range is best estimate decay heat level to licensing estimate decay heat level. Actual LOCA flows would be slightly higher due to core stored energy removal simultaneous with decay heat removal during reflood.

TABLE 3

COMPARISON OF SELECTED UPI PLANT AND TEST FACILITY PARAMETERS

| Parameter | UPI Plant | UPTF | CCTF | Semiscale | SCTF | Dartmouth | ORNL |
|---|---|---|---|---|---|---|---|
| No. of Fuel Bundles, Array | 121, 14 x 14 | 193, 16x16 | 32, 8x8 | 1, N/A | 8, 16x16 | N/A | 1/3, 16x16 |
| No. of Heated Rods | 21659 | 45548 (Dummy) | 1824 | 36 | 1876 | N/A | 236/708 (Dummy) |
| Heated Length m (ft) | 3.66 (12.0) | N/A | 3.66 (12.0) | 1.68 (5.50) | 3.66 (12.0) | N/A | N/A |
| Core Flow Area $m^2$ ($ft^2$) | 2.47 (26.6) | 5.53 (59.5) | 0.22 (2.37) | 0.0048 (0.0513) | 0.22 (2.37) | N/A | 0.029/0.086 (0.31/0.92) |
| Tie Plate Flow Area $m^2$ ($ft^2$) | - | 3.78 (40.7) | .202 (2.17) | - | .204 (2.20) | .030 (0.32) | 0.016/0.055 (0.17/0.59) |
| Upper Plenum Flow Area $m^2$ ($ft^2$) | - | 10.2 (109.8) | 0.559 (6.02) | - | 0.53 (5.68) | 0.054 (0.585) | 0.054/0.19 (0.58/2.03) |
| Hot Leg Flow Area $m^2$ ($ft^2$) | 2x0.426 (4.59) | 3x0.442 (4.76) | 4x0.019 (0.205) | - | 0.011 (0.114) | 2x0.0045 (0.049) | 0.008/0.018 (0.087/0.196) |
| ECC Injection Nozzle Flow Area $m^2$ ($ft^2$) | 2x0.0081 (0.08) | 0.040 (0.438) | 2x0.0009 (0.0092) | 0.0001 (0.0016) | 8x0.0090 (0.097) | 7.0E-5 (8.0E-4) | 0.008/0.018 (0.087/0.196) |
| "Scale Factor" | 1.0 | 2.1 | 1/11 | 1/600 | 1/11 | 1/110 | 1/90-1/30 |

Note: N/A means not applicable. A dash (-) means the information was not readily attainable from the public domain.

TABLE 4

COMPARISON OF SELECTED UPI PLANT AND TEST CONDITIONS

| Operating Condition | UPI Plant | UPTF | | | CCTF | | | | | |
|---|---|---|---|---|---|---|---|---|---|---|
| | | Ph.A | Ph.B | Ph.C | Run 76 | Run 78 | Semiscale | SCTF | Dartmouth | ORNL |
| Test Vessel Pressure kPa (psi) | 300 (45) | 250 | (36) | | 200 (29) | 290 (42) | 240 (35) | 250-300 (36-45) | - | 105-129 (15.2-18.7) |
| Power, MWt Actual | 65.3-86.6 | - | - | - | 7.9 | 7.1 | 0.07 | 0-4 | - | - |
| Scale Factor Adjusted | 65.3-86.6 | - | - | - | 86.9 | 78.1 | 42 | 0-44 | - | - |
| Equivalent Steam Flow at 300 kPa kg/sec (lbm/sec) | 30-39 (65-87) | 87 (192) | 99 (218) | 83 (183) | - | - | - | 2-4.8 (4.4-10.6) | Air 0.0-0.52 (0.0-1.14) | Air 0.087-0.76 (0.19-1.68) |
| Scale Factor Adjusted | 30-39 (65-87) | 41 | 47 | 40 | - | - | - | 22.0-52.8 (48.4-116.6) | Air 0.0-57.0 (0-125) | Air 8.0-23.0 (17.5-154) |
| Power Profile (Uniform, Peaked) | Peaked | Uniform | Peaked | Peaked | Peaked | Uniform | Peaked | Uniform | Uniform | Uniform |
| ECC Flow Rate, kg/sec (gpm) Actual | 120 (2000) | 260 | (4300) | | 9.4-11.2 (160-190) | 10.4 (180) | 0.25 (4.2) | 12 (200) | 0.7-1.4 (11.9-23.7) | 0.63-50.5 (10-80) |
| Scale Factor Adjusted | 120 (2000) | 120 | (2000) | | 100-120 (1750-2080) | 110 (1940) | 150 (2520) | 130 (2240) | 77-150 (1300-2610) | 18.9-150 (300-2400) |
| ECC Water Subcooling K (°F) | 100 (180) | 100 | (180) | | 85 (153) | 96 (173) | 106 (190) | 5-85 (9-153) | N/A | N/A |

MPR ASSOCIATES
F-73-26-1865
10/5/88

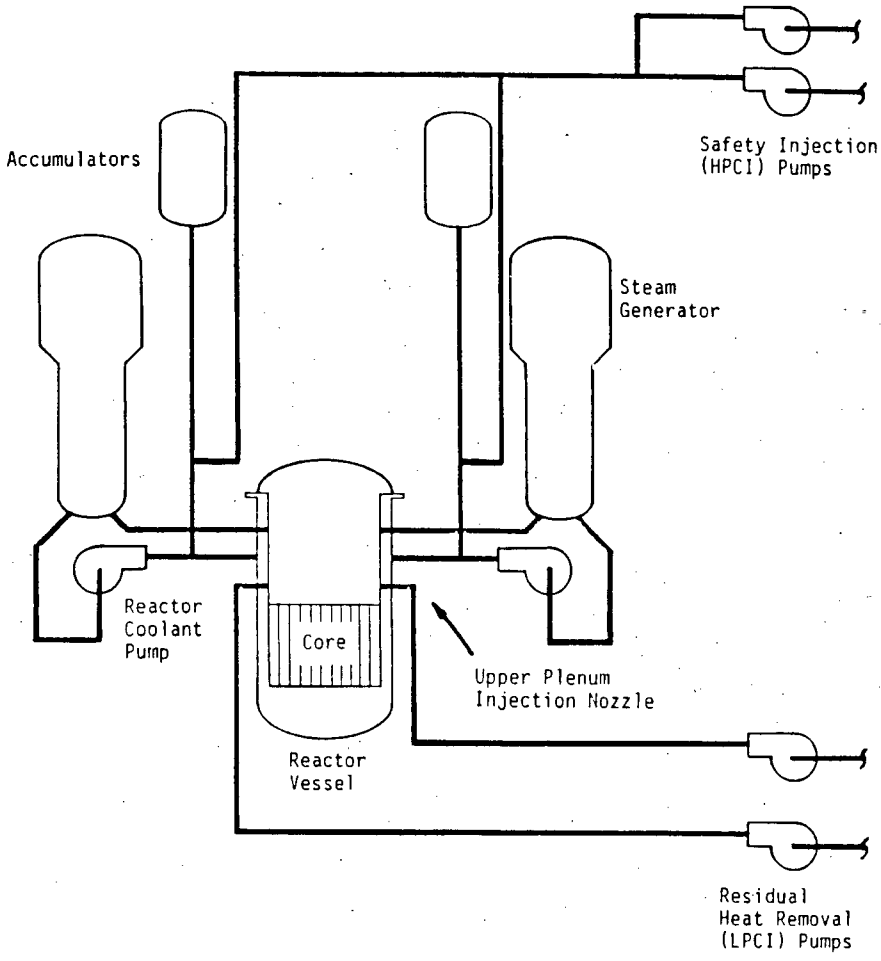




TYPICAL SCHEMATIC DIAGRAM
REACTOR COOLANT SYSTEM AND ECC SYSTEM
FOR PLANT WITH UPPER PLENUM INJECTION
FIGURE 1

MPR ASSOCIATES
F-73-26-1668
10/27/88

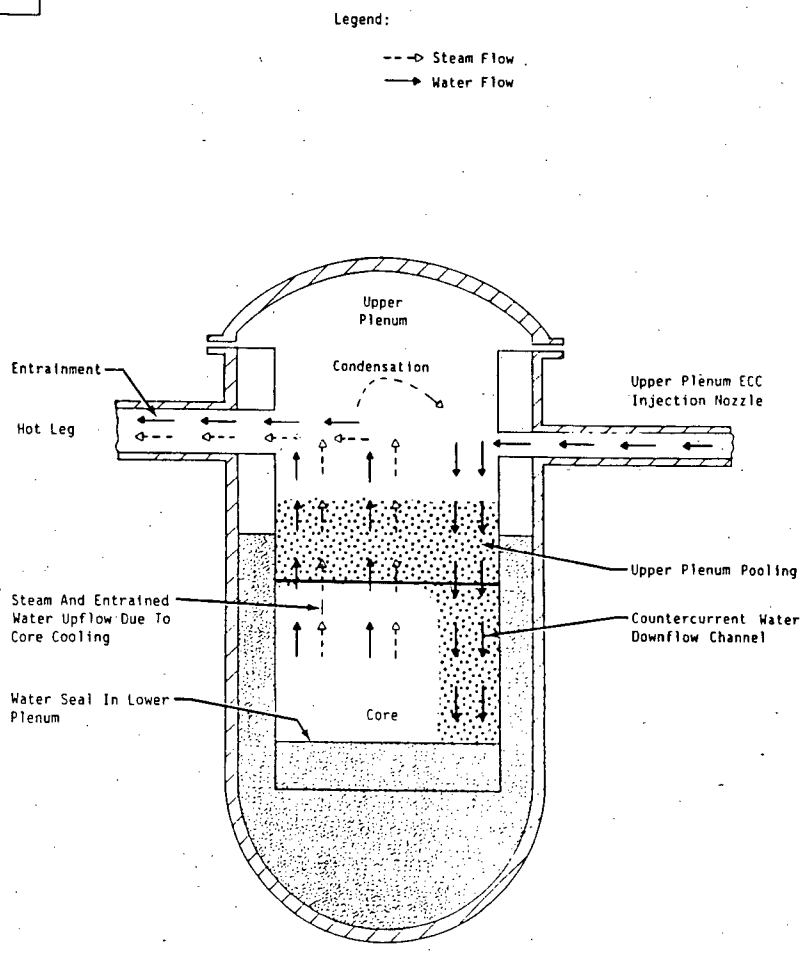


UPI VESSEL DURING REFLOOD STAGE OF LOCA
FLOW DIAGRAM
FIGURE 2

MPR ASSOCIATES
F-73-26-1664
10/28/88

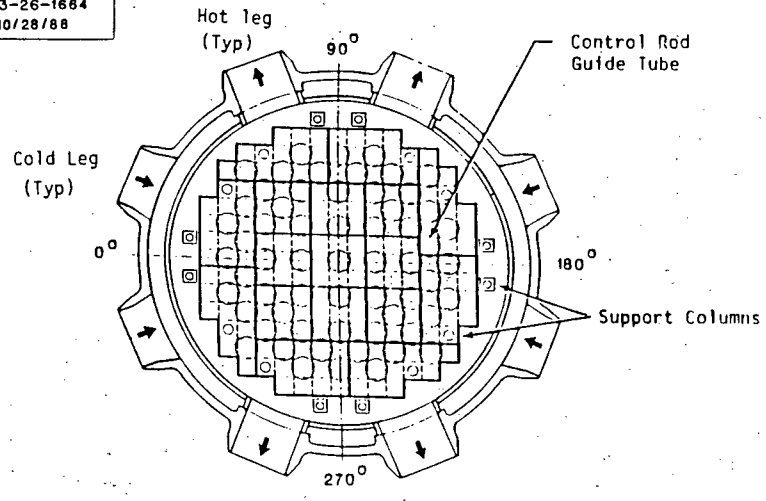


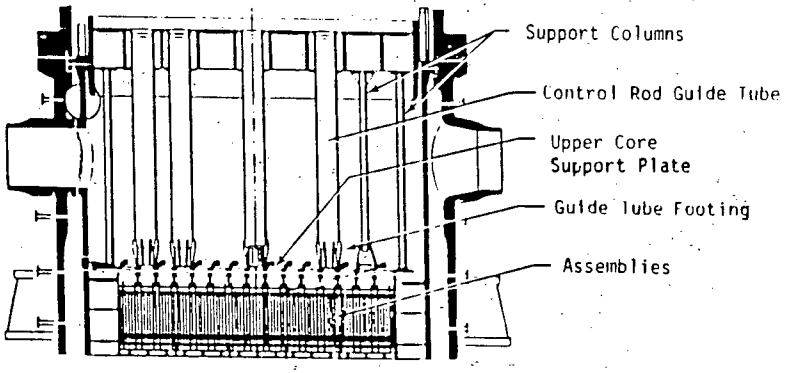


UPTF UPPER PLENUM STRUCTURE

FIGURE 3



MPR ASSOCIATES
F-73-26-1663
10/27/88

Note: For Simplicity, Cold Legs Not Shown

Legend: Steam Flow
Water Flow

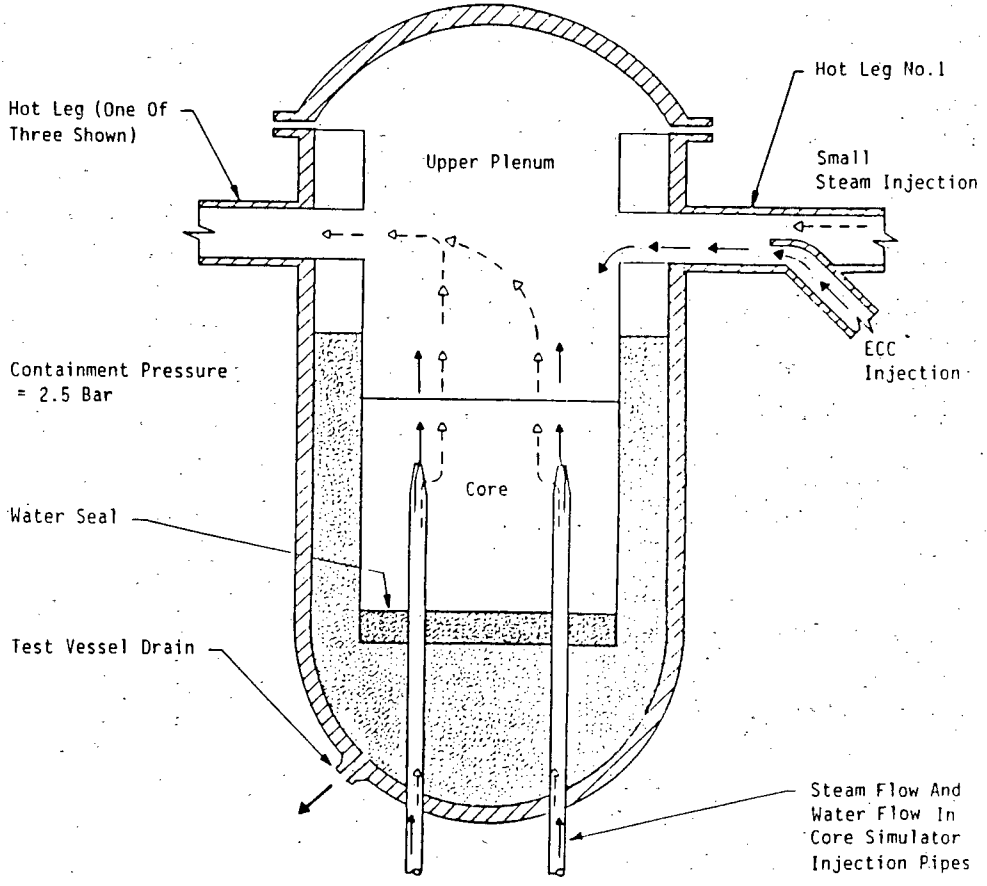


UPTF UPI TEST
OVERVIEW OF TEST APPROACH

FIGURE 4

MPR ASSOCIATES
F-73-28-1574
10/27/88

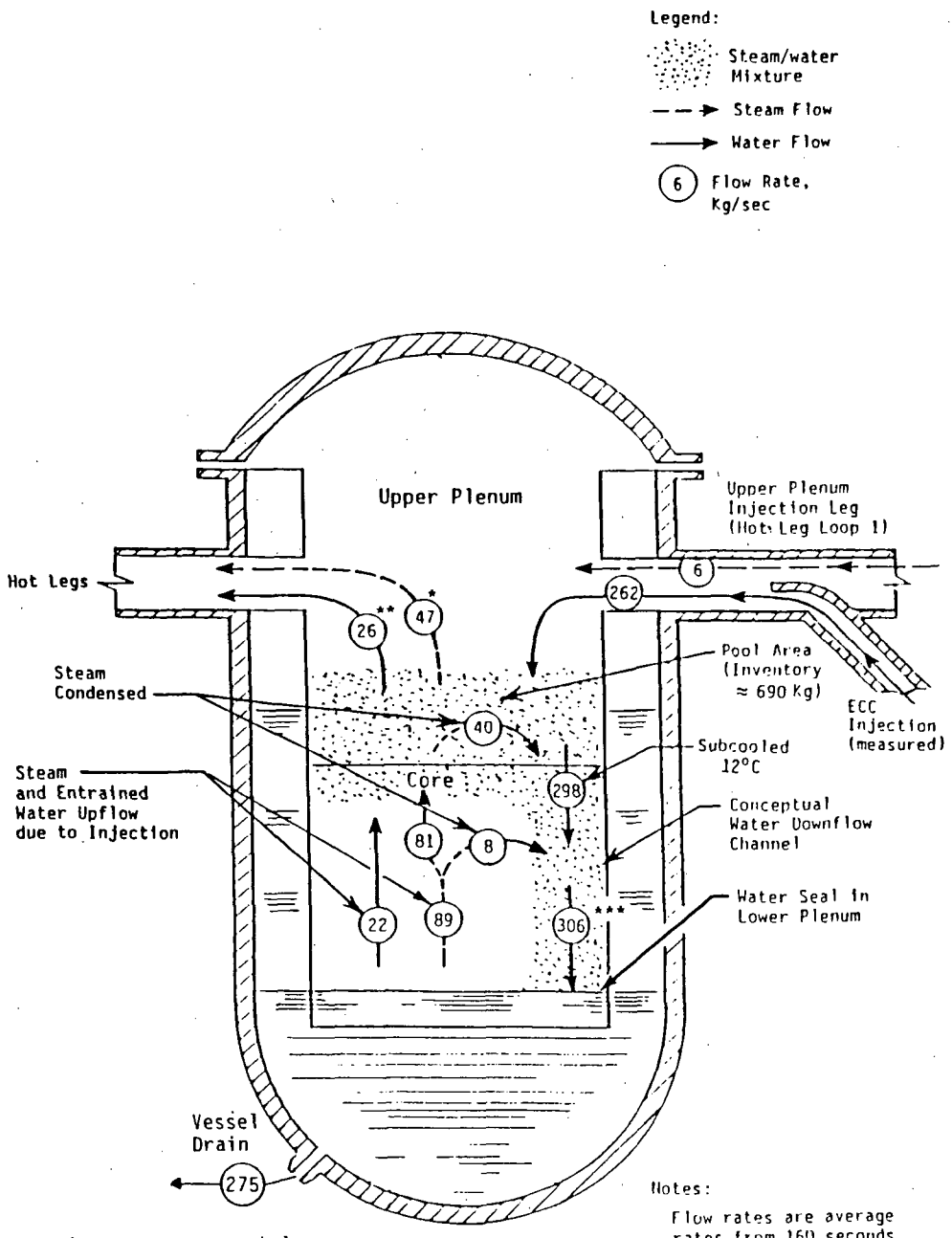


# PHASE A
# SEPARATE EFFECTS SIMULATION DURING REFLOOD
# UPTF VESSEL FLOW DIAGRAM

## FIGURE 5

MPR ASSOCIATES
F-73-28-1711
10/28/88

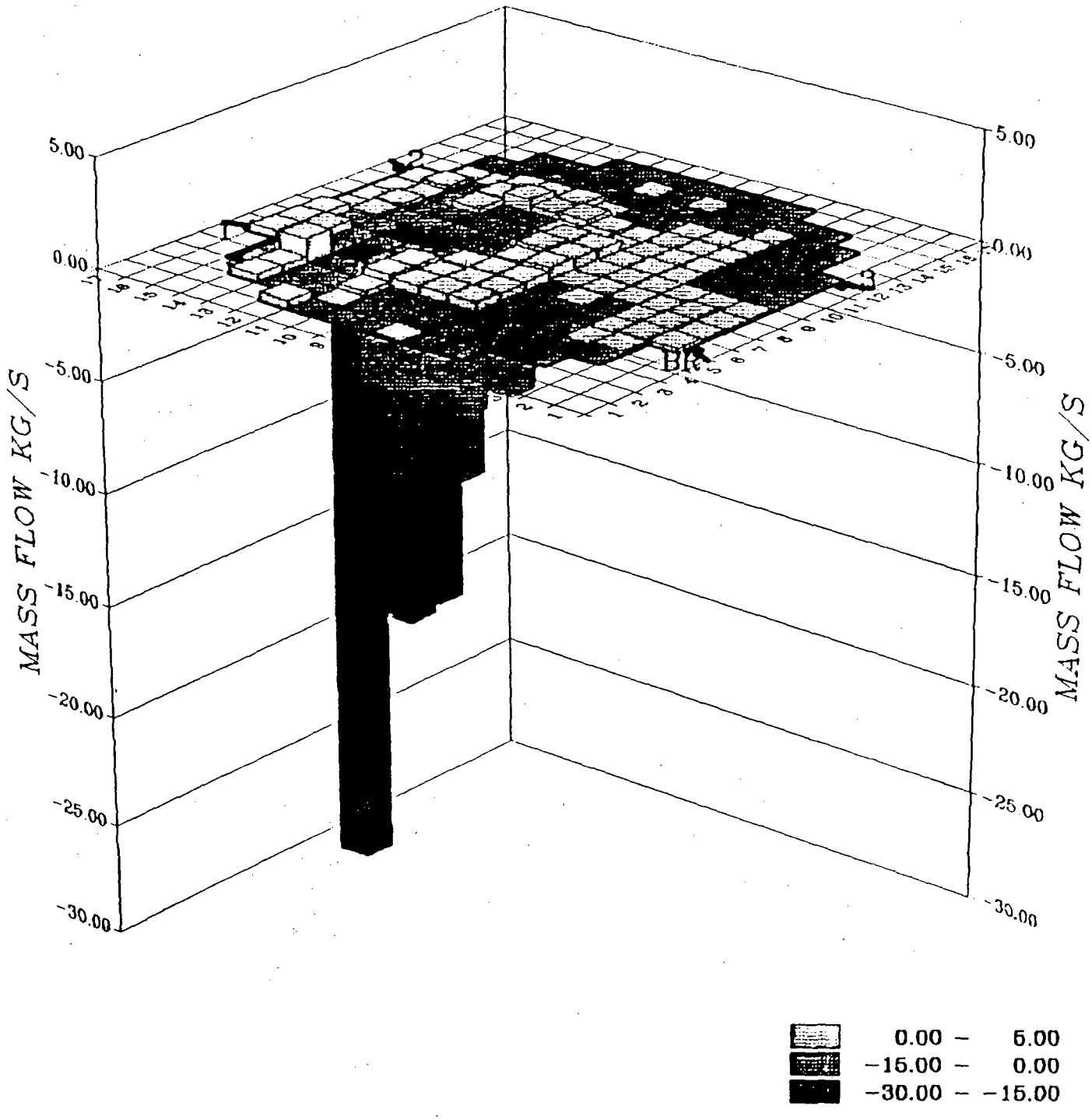


DISTRIBUTION OF WATER FLOW RATE AT
TOP OF CORE DURING PHASE A OF UPTF UPI TEST

FIGURE 6

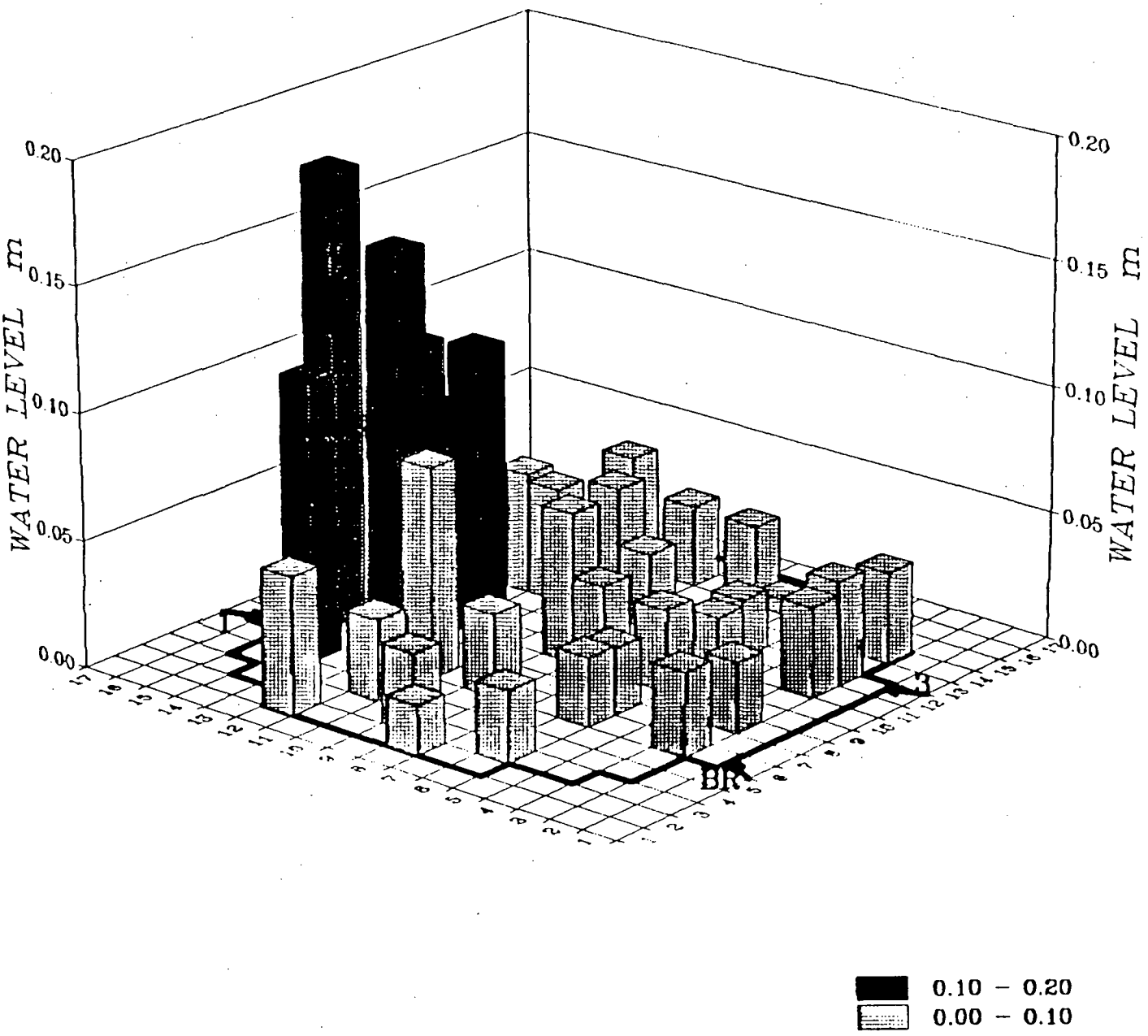


DISTRIBUTION OF UPPER PLENUM LEVEL
DURING PHASE A OF UPTF UPI TEST

FIGURE 7

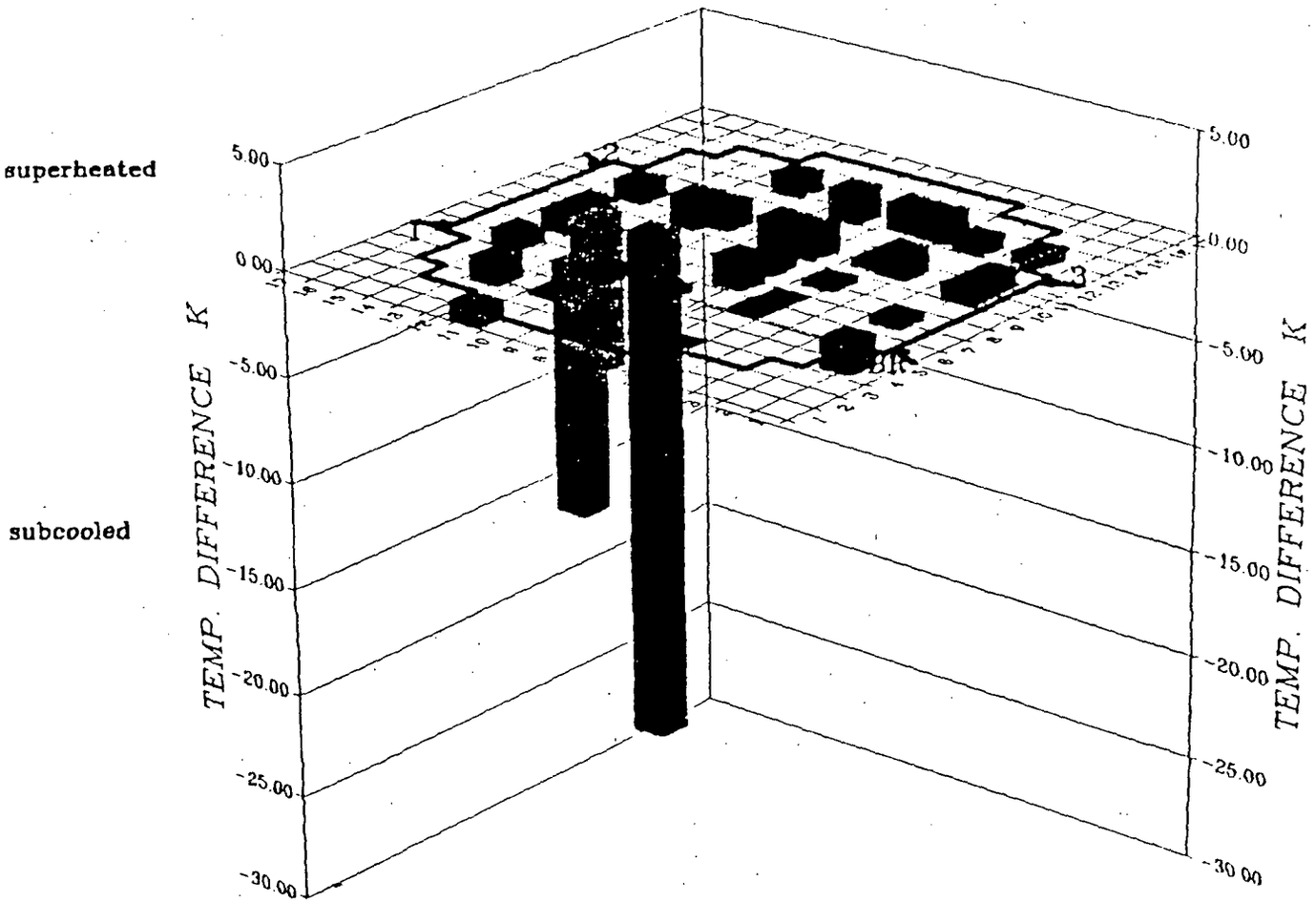


DISTRIBUTION OF FLUID TEMPERATURE AT
TOP OF CORE DURING UPTF UPI TEST

FIGURE 8

MPR ASSOCIATES
F-73-26-1714
10/27/88

Notes:
1. Semiscale (□): Test did not include Measurements to Determine the Pool Level.
2. *Dartmouth (X): Tests did not include Measurements to Determine the* Pool Level.
3. ORNL (◇):
   a. 1 Module: Data is for Core Steam Injection Facility Only.
   b. 3 Module: Runs had Air Flow Simulating Core Flow.
4. CCTF (▽): Data Point is from Run 76.
5. SCTF (△): Data Points are *from Runs* S2-04 and S2-05.
6. UPTF (○): Data Points are from Test No. 20.

Upward Gas Momentum
Flux Similar in all Tests

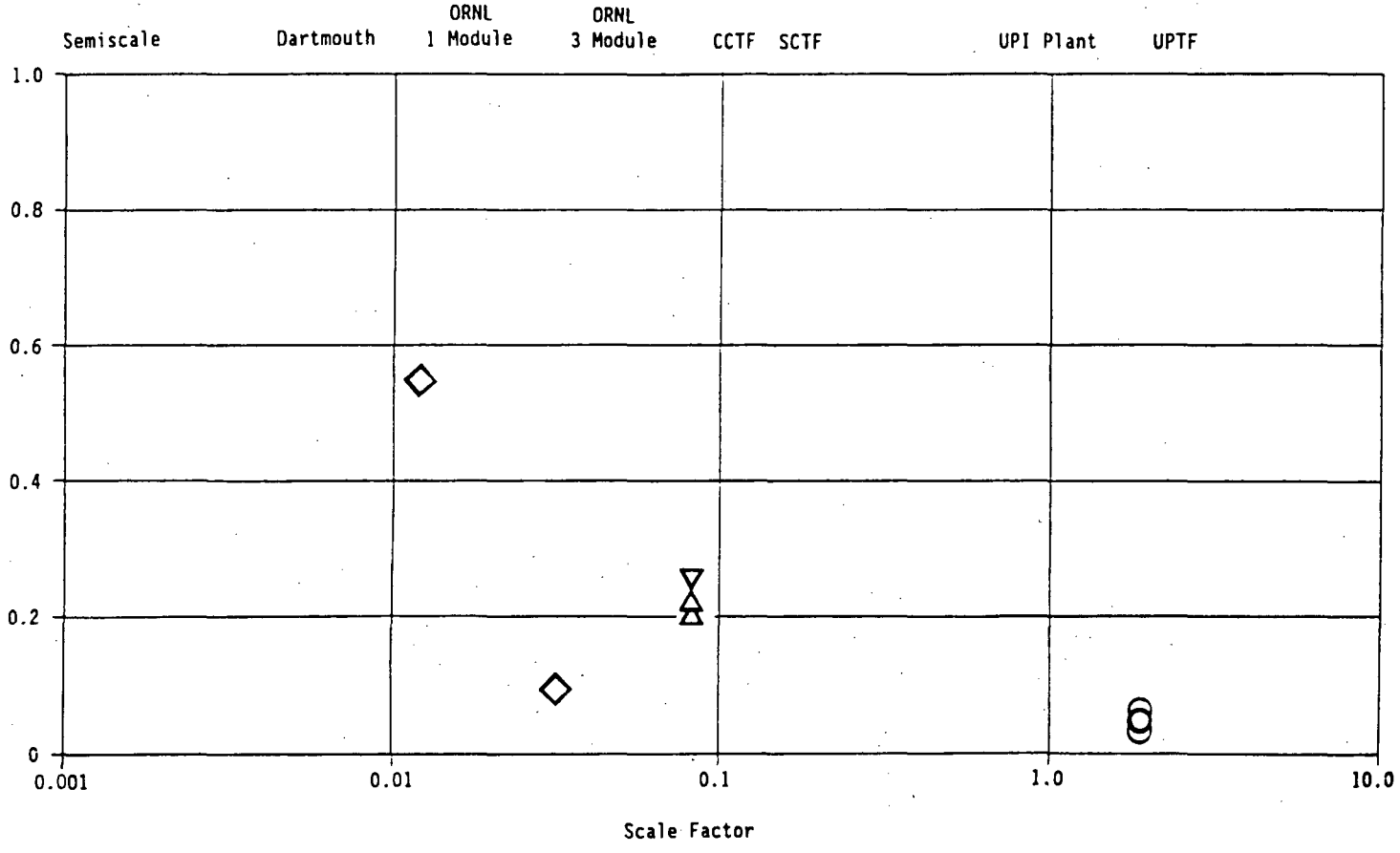


NON-DIMENSIONAL COLLAPSED LIQUID LEVEL IN UPPER PLENUM VERSUS UPPER PLENUM AREA SCALE FACTOR

FIGURE 9

MPR ASSOCIATES
F-73-26-1715
10/27/88

Notes:
1. Semiscale (□): Test did not include Measurements to Determine the Amount of Downflow.
2. Dartmouth (X): Runs had Air Flows Simulating Core Flow which is Equivalent to No ECC Subcooling.
3. ORNL (◇):
   a. 1 Module: Runs had Air Flows Simulating Core Flow which is Equivalent to No ECC Subcooling.
   b. 3 Module: Runs had Air Flows Simulating Core Flow which is Equivalent to No ECC Subcooling.
4. CCTF (▽): Data Point is Based on Run 76 where ECC is 85K Subcooled.
5. SCTF (△): Data Span is from 33% (ECC was not Subcooled) to 75% (when ECC was 80K Subcooled). Data is from Runs S2-04 and S2-05.
6. UPTF (○): Data is from Test No. 20 where ECC was 100K Subcooled.

*Upward Gas Momentum Flux Similar in all Tests*

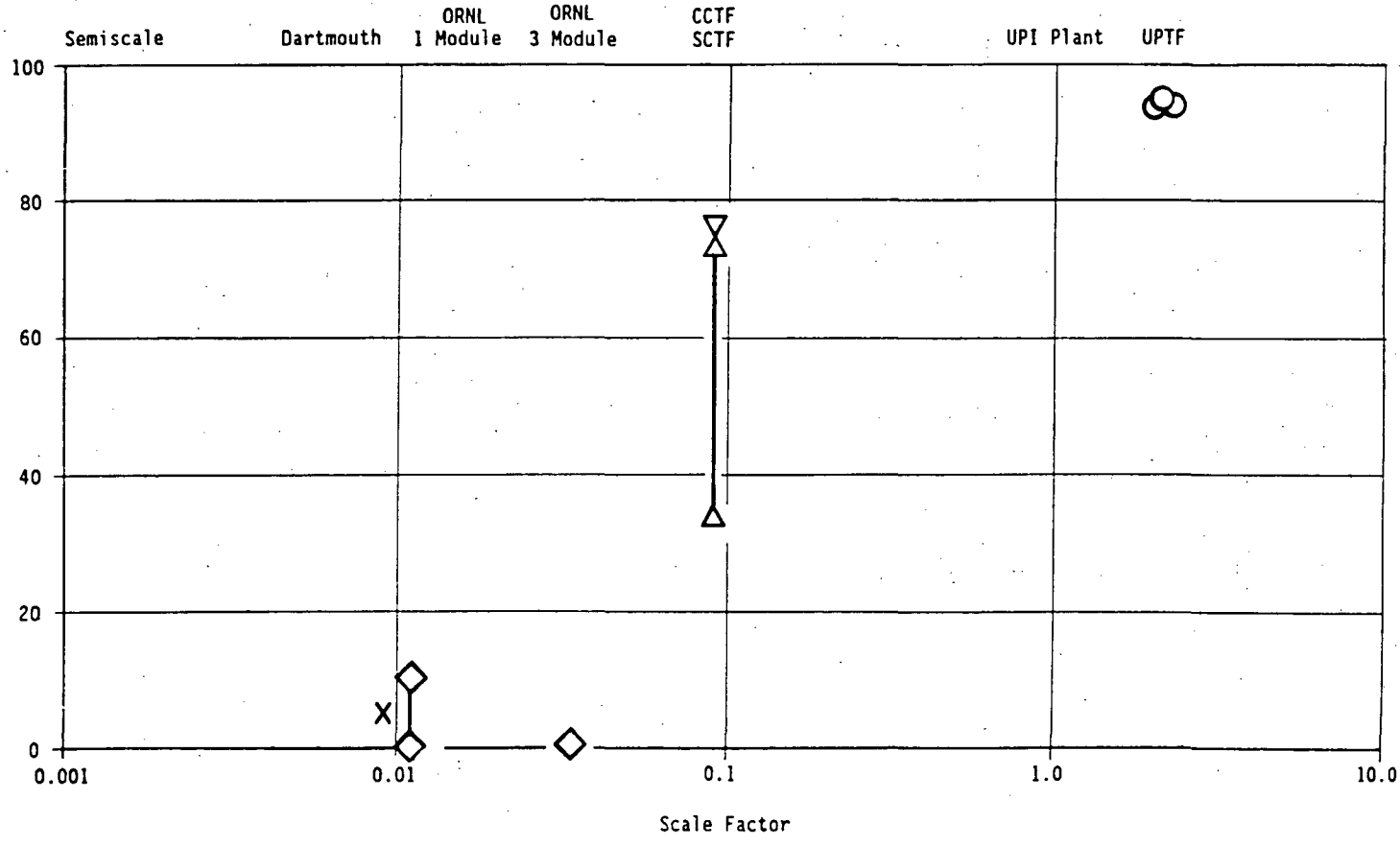


DOWNFLOW VERSUS SCALE FACTOR

FIGURE 10

Notes:
1. Semiscale (□): Data Point is from Run S-05-7.
2. Dartmouth (X): Data Span is from Runs that had no Core Air Flow. Runs that had Core Air Flows did not Measure Breakthrough Flow Area.
3. ORNL (◇):
   a. 1 Module: Tests did not include Measurements to Determine the Breakthrough Flow Area.
   b. 3 Module: Tests did not include Measurements to Determine the Breakthrough Flow Area.
4. CCTF (▽): Data Span is Based on Runs 59, 72, 76, and 78.
5. SCTF (△): Data Points are from Runs S2-04 and S2-05.
6. UPTF (○): Data Points are from Test No. 20.

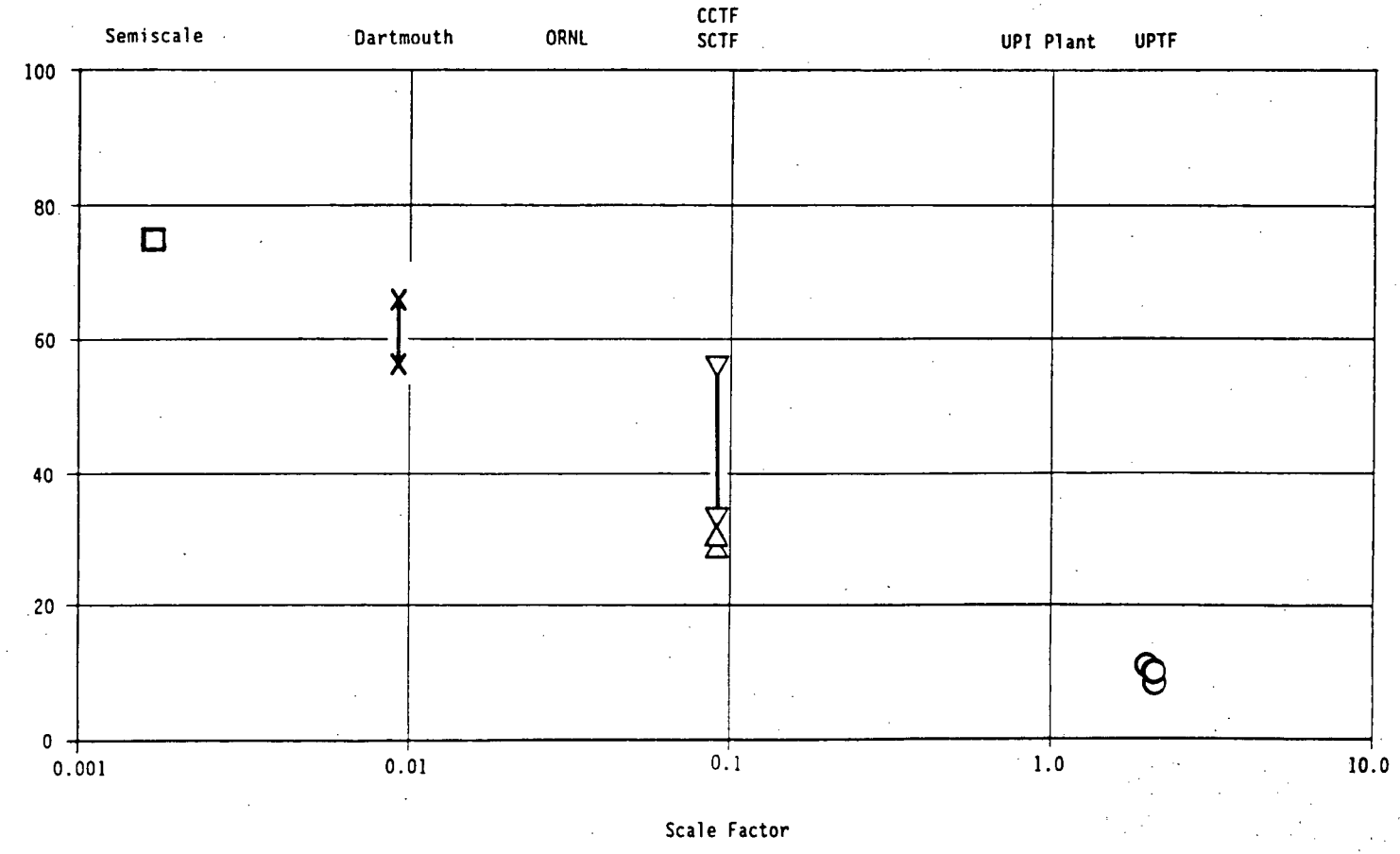


BREAKTHROUGH FLOW AREA VERSUS SCALE FACTOR

FIGURE 11

MPR ASSOCIATES
F-73-26-1717
10/27/88

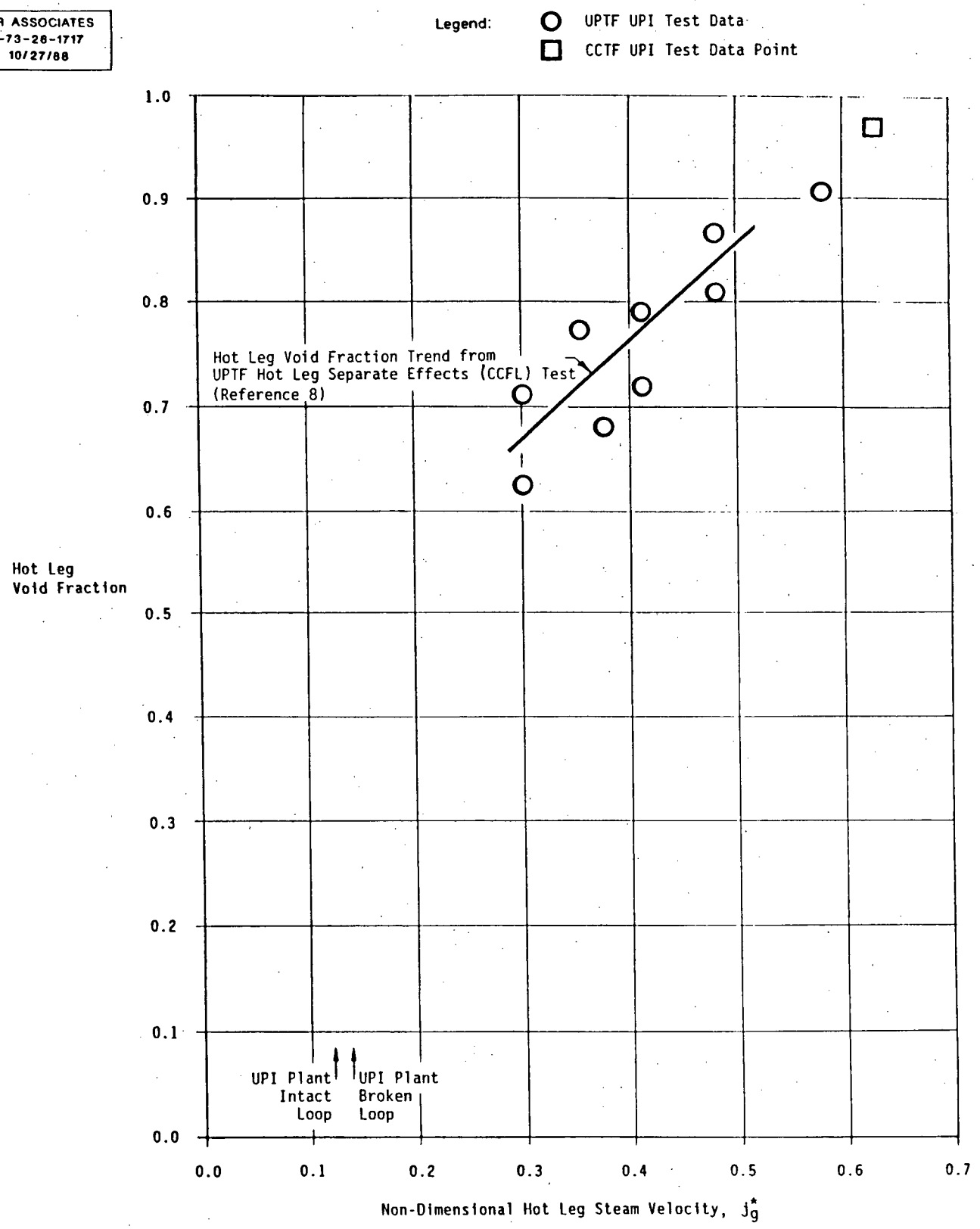


UPTF UPPER PLENUM INJECTION (UPI) TEST
HOT LEG VOID FRACTION VERSUS
NON-DIMENSIONAL HOT LEG STEAM VELOCITY

FIGURE 12

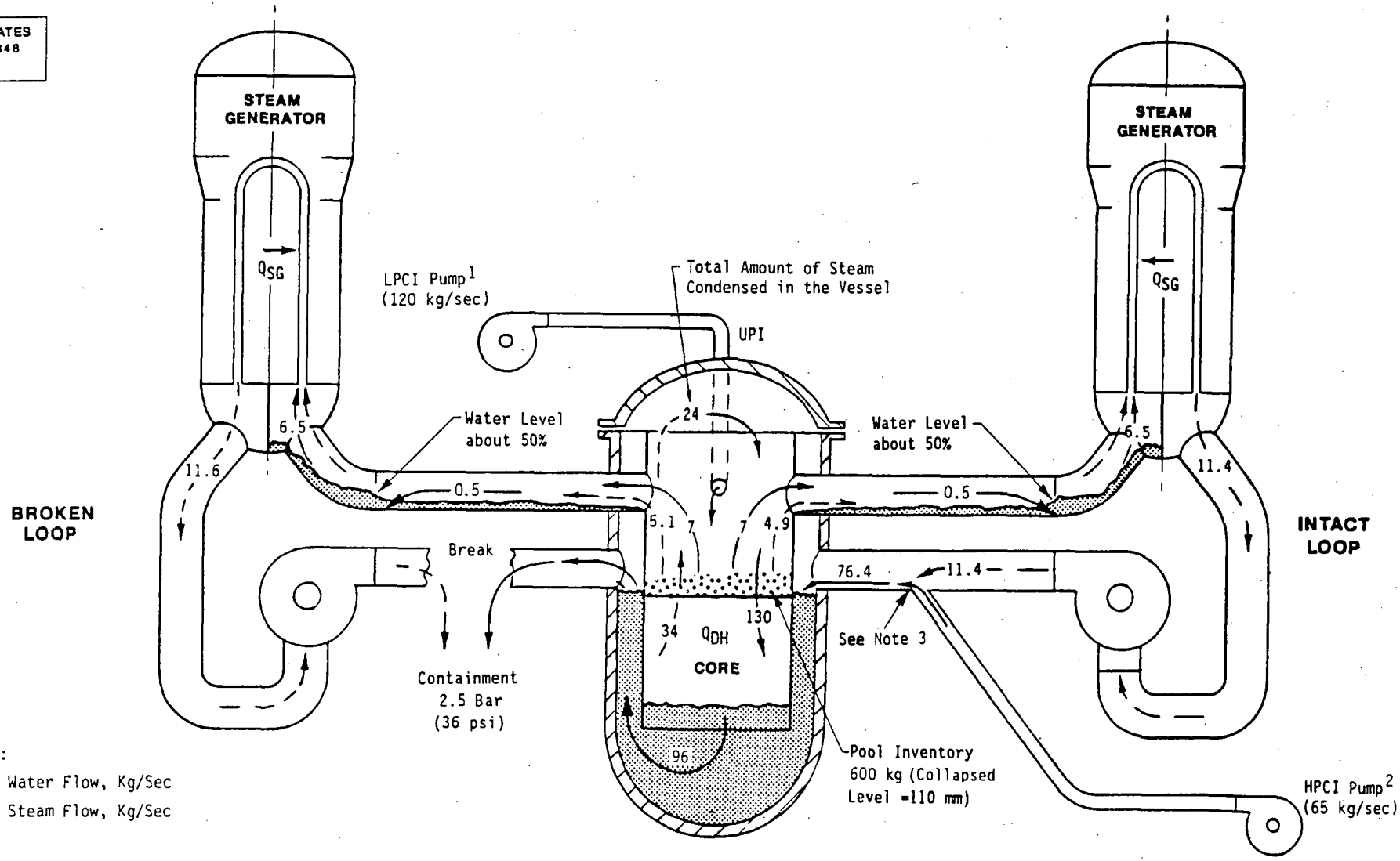


Notes:

1. LPCI Is Subject To A Single Active Failure (i.e., One LPCI Pump).
2. HPCI Is Assumed To Have No Active Failure. HPCI Into Broken Loop Is Not Shown Because The HPCI Flow Is Assumed To Be Lost Through The Break.
3. Assumes HPCI And Steam Completely Mix.

SCHEMATIC OF EXPECTED OVERALL UPI PLANT BEHAVIOR DURING REFLOOD (SINGLE LPCI INJECTION PORT)

FIGURE 13

# USE OF 2D/3D DATA TO SCALE UP LIQUID CARRYOVER/ DE-ENTRAINMENT (STEAM BINDING) BEHAVIOR TO A PWR

G. Rhee
USNRC
Washington, D. C.

P. Damerell
J. Simons
MPR Associates, Inc.
Washington, D. C.

## Abstract

The behavior of liquid water entrained out of the top of the core is important during a large break loss-of-coolant accident (LOCA) in a pressurized water reactor (PWR). The upper plenum, hot legs and steam generator inlet plena can de-entrain and accumulate water, which is generally beneficial because it reduces water carryover to the steam generator tubes. In the tubes, water vaporizes and contributes to steam binding. Full-scale UPTF tests provide information on the de-entrainment and carryover phenomena. The test results show the upper plenum and steam generator inlet plena act as delay volumes for water transport by storing water in frothy pools. The time delays are about 6 and 30 seconds, respectively. The hot legs store liquid water in a stratified flow regime, with the amount stored dependent on steam flow. The remaining water not stored in these volumes is carried over to the steam generator tube region. Based on the UPTF data, a "rule-of-thumb" for PWR liquid transport is determined. Application of this rule to a transient actually run in UPTF shows reasonable agreement with measured water carryover to the steam generator. The amount carried over is about one-half of the water exiting the core for this transient.

## Introduction

Loss-of-coolant accident (LOCA) experiments with a full-scale reactor are not practical from the standpoint of both cost and safety. Therefore, over the years numerous LOCA experiments have been performed in small-scale test facilities. In general, these scaled facilities were designed to satisfy specific scaling principles (e.g., power-to-volume ratio preserved) and many tests were carried out across a range of conditions. The intent of this testing approach was to ensure the major phenomena occurring in a LOCA were identified and investigated in a realistic regime, even if precise LOCA transients were not reproduced. In this regard, the scaled tests have provided useful data for identification and screening of phenomena, for development of models and correlations of phenomena, and for assessing computer codes. One of the residual issues with regard to nuclear power plant LOCA calculations is the uncertainty associated with scaling up to full-scale. Scale can have a major

influence particularly on two-phase flow, because of size effects on flow regime, countercurrent flow, steam/water separation, etc.

In the 2D/3D Program, a joint project by the Federal Republic of Germany, Japan and the United States to study the refill and reflood phases of a large break LOCA in a pressurized water reactor (PWR), full-scale steam/water test data which can be used to evaluate scale-up to a PWR have been obtained. This program involves two scaled, heated-core test facilities -- the Cylindrical Core Test Facility (CCTF) and Slab Core Test Facility (SCTF) in Japan, -- and one full-scale steam/water test facility -- the Upper Plenum Test Facility (UPTF) in Germany. UPTF provides the most significant information on full-scale, two-phase flow effects.

A previous paper (Reference 1) discussed the use of UPTF data to address scale-up of two specific phenomena: ECC delivery/bypass in a PWR downcomer at the end-of-blowdown stage of a large break LOCA, and countercurrent flow of water in a PWR hot leg, which is principally related to the reflux condensation stage of a small break LOCA but also has applications to the reflood stage of a large break LOCA. In both of these cases, positive effects of scale were noted, i.e., water penetrated to the reactor vessel through a downcomer or hot leg better than in scaled geometries. Since this previous paper, additional UPTF testing has been carried out, principally to address large break LOCA phenomena. For example, additional downcomer ECC delivery/bypass tests have been carried out. These additional data appear to confirm the previous conclusion but they are still being evaluated in detail and will be covered in a future paper. Also, UPTF tests related to water entrainment/carryover during reflood (steam binding issue) have been carried out and the evaluation of these phenomena is the subject of this paper. Based on these data, we can now summarize the expected full-scale phenomena and behavior associated with liquid carryover and de-entrainment in regions above the core. These phenomena cover three major PWR areas: upper plenum, hot legs, and steam generators. This paper discusses each of these areas, covering the following points:

- Significance of the behavior
- Findings of UPTF tests
- Conclusions on expected PWR behavior

The discussion starts with a brief overview of the UPTF, and then each of the three areas are discussed individually. An overall summary of the collective behavior is given at the end of the paper in terms of a "rule-of-thumb" for water carryover behavior. This summary includes a discussion of accuracy and a demonstration of the accuracy of the "rule-of-thumb" in predicting liquid carryover to the steam generators in an actual complex transient.

## Overview of UPTF and Comparison to US/Japanese PWRs

The UPTF has been previously described (References 2 and 3) and is briefly discussed here with emphasis on the reactor vessel upper plenum, the hot legs and the steam generator simulators.

The UPTF simulates the primary system of a German four-loop PWR which is similar to a US or Japanese four-loop (Westinghouse) PWR. A full-size reactor vessel and four 0.75-m (29.5-inch) diameter loops are included in the UPTF. Figure 1 shows the reactor vessel and a typical loop. Each loop contains a steam generator simulator (which is a steam/water separator) and a pump simulator (which is an adjustable flow resistance). One of the four loops contains break valves which are piped to a large containment simulator tank. The reactor vessel upper plenum has internal structures which are a precise simulation of the German four-loop plant. The reactor vessel core is simulated by a "core simulator" steam/water injection system consisting of 193 steam/water nozzles, one for each fuel assembly of the German PWR. The upper 25% of the core is simulated physically by 193 dummy (unheated) fuel assemblies, to create a realistic flow channel at the top of the core. The UPTF can operate at up to 18 bar (260 psia) pressure and 493 K (428°F) temperature.

The UPTF configuration in the core, upper plenum, hot legs and steam generators is compared to Westinghouse and Combustion Engineering (CE) PWRs on Figure 2. As shown in this figure, the UPTF configuration is slightly less restrictive in the upper plenum and steam generator inlet plena and slightly more restrictive in the hot legs, if core flow area is used for normalization. The effects of these differences will be discussed with the results; overall, the UPTF is of comparable scale and configuration to the PWRs.

### Upper Plenum

The two-phase flow behavior in the upper plenum is significant during a large break LOCA. Specifically, during the reflood phase steam and entrained water enter the upper plenum from the core. Since the upper plenum area is larger than that of the core, the flow velocity decreases; also, the flow must turn and pass over structures in the upper plenum on its way to the hot legs. These factors combine to potentially de-entrain some of the liquid flow, thereby creating a frothy pool in the upper plenum (Figure 3). This de-entrainment and storage of water is beneficial in that the water is not carried over to the loops and steam generators, where vaporization would contribute to steam binding. On the other hand, de-entrainment can be detrimental in that the hydrostatic head of water in the upper plenum adds a pressure drop which needs to be overcome by the steam flow out of the core, thereby tending to slightly depress core water level and inhibit core reflood. In general, for the types of flows and pressure drops associated with reflood, the beneficial effect predominates.

Upper plenum phenomena in UPTF have been investigated by both separate effects and integral tests. In these tests the phenomena are simulated by injecting steam and water through the core simulator. Steam/water flow enters the upper plenum from the core (Figure 4). In the separate effects tests steady flows are used. In the integral tests, transient flows determined from mass/energy balance analysis of scaled heated core facilities are used.

The results of the UPTF steady-state tests show that over a range of flow conditions typical of reflood, the upper plenum liquid inventory achieves a steady value proportional to the liquid flow rate entering the upper plenum from the core. The upper plenum liquid inventory is relatively independent of steam flow rate. Figure 5 shows the pertinent data; as shown in this figure the proportionality constant is about six seconds and there is an offset accumulation of about 200 kg (440 lbm). The six-second value represents a sort of "accumulation constant" for the UPTF upper plenum and the 200 kg value represents a "residual" accumulation which appears to be unaffected by liquid flow. The data point at the y-intercept of the plot in Figure 5 was found by terminating water flow to the upper plenum after water had already been permitted to accumulate.

During the steady-state tests, the water flow from the core to the upper plenum was changed abruptly a few times. In these transient conditions, the upper plenum inventory immediately starts to change toward its new equilibrium value, and the time required for the change is also approximately six seconds. This result suggests that the upper plenum behavior can be generally characterized as follows:

$$M_{UP} = \int_{t-t_u}^{t} \dot{M}_L \, dt + M_{UP,0} \qquad [1]$$

Where $M_{UP}$ is the upper plenum liquid mass, $\dot{M}_L$ is the core exit flow rate, $t_u$ is the upper plenum delay time (6.38 seconds in UPTF) and $M_{UP,0}$ is the offset upper plenum accumulation (211 kg in UPTF).

The accumulation behavior of UPTF (Equation [1]) is considered to be realistic of behavior that would occur in a PWR upper plenum during LOCA reflood. Because the time delay constant (about six seconds) is small compared to the duration of reflood (which can last about 200 seconds or more), it appears upper plenum water de-entrainment, by itself, has only a small beneficial impact on PWR reflood.

Hot Legs

The two-phase flow behavior in the hot legs is significant during the reflood phase of a large break LOCA and during a small break LOCA after significant inventory loss. Specifically, during the reflood phase of a large break LOCA, steam and water flow into the hot legs from the upper plenum. In the hot legs, the horizontal flow path can give rise to de-entrainment of liquid, storage of liquid in a layer on the bottom of the pipe and countercurrent flow of liquid back toward the upper plenum (Figure 6). All of these phenomena are beneficial for reflood core cooling in that they reduce water carryover to the steam generators, which would add to steam binding.

During the reflux condensation phase of a small break LOCA, steam flows from the vessel to the steam generator and condensate flows countercurrent to the steam through the hot legs back to the vessel, i.e., countercurrent flow is an inherent part of the cooling mode.

Hot leg phenomena in UPTF have been investigated by both separate effects and integral tests. A special hot leg separate effects test investigated principally the countercurrent flow behavior including the CCFL boundary. This test was viewed as being principally applicable to the small break LOCA scenario. The results and evaluation of this test were reported in previous papers (References 1 and 4). Specifically, it was found that flows typical of reflux condensation were well below the hot leg CCFL boundary (as expected) and that hot leg phenomena could be scaled reasonably reliably using the j* parameter. The results from this separate effects test also suggested that water storage and runback could be significant in large break LOCA reflood, and they successfully explained the observations of no storage or runback in CCTF (scaled height hot legs) and of significant storage/runback in SCTF (full height hot leg). However, this earlier UPTF test did not answer the question of how much water would be de-entrained and stored in the hot legs under typical reflood conditions. SCTF results in this regard were not considered completely definitive since the shape of the SCTF hot leg (oval) compared to PWR hot legs (round) could have led to unusual de-entrainment behavior.

Since this previous work, additional UPTF separate effects and integral tests have been carried out to address the question of typical hot leg behavior during LOCA reflood. These tests are the same ones as described above for the upper plenum phenomena, i.e., they involved core simulator steam/water injection, both steady and transient.

The results of the UPTF tests show that the hot legs are not highly effective at de-entrainment of water, but that they do store a significant amount of water which is de-entrained at the entrance (inlet plenum) of the steam generator. (A detailed discussion of the transient progression of these phenomena is contained in the next section.) The measured hot leg storages are slightly less than observed in the previous hot leg separate effects test, at corresponding values of dimensionless hot leg steam velocity ($j_g^*$). Figure 7 shows selected data of hot leg water storage (expressed as void fraction) and the comparison to the data trend observed in the previous hot leg separate effects test. The data on Figure 7 are from time periods after water has had a chance to collect, i.e., they are considered to represent "equilibrium" values of water storage. The lower inventories (higher voids) in the reflood type test are considered to be due to inherently slightly lower water storage in the reflood flow regime (cocurrent two-phase flow from vessel) compared to the previously tested CCFL regime. A least squares fit to the reflood type data on Figure 7 gives the following relationship for hot leg water storage.

$$\alpha = 0.493 + 0.679\ j_g^* \qquad [2]$$

were $\alpha$ is the hot leg void fraction measured near the bend and $j_g^*$ is the dimensionless steam velocity defined on Figure 7.

In the UPTF tests, hot leg water runback was not measurably observed. This is attributable to the UPTF hot legs being somewhat more restrictive (per unit core flow area) than US/Japanese PWR hot legs, and to the use of higher steam flows in UPTF, particularly the separate effects test. The UPTF hot legs are somewhat more restrictive than US/J PWR hot legs because of the presence of an internal hot leg injection pipe (Hutze) and the use of a larger core with similarly sized hot legs in German PWRs (which UPTF simulates). The dimensionless hot leg steam velocity in the UPTF tests was large enough that runback was expected to be prevented or nearly prevented. In the cases where small runback was expected, this runback was below the measurable range of the hot leg drag disks.

Direct comparison of UPTF hot leg water storage results to scaled tests is not feasible. CCTF reflood tests had essentially no hot leg water storage because the hot legs were flow area scaled round pipes. In Reference 1 it was shown this CCTF result is consistent with UPTF results. SCTF reflood tests had markedly different upper plenum behavior than UPTF, as previously discussed. Thus, the flow delivered to the hot leg was not closely matched. SCTF did have a full-height hot leg and stratified water accumulation was observed; however, the SCTF hot leg was shorter and had excess surface area (due to its oval configuration). Accordingly, comparison of the amount of water storage between SCTF and UPTF is not highly useful. Reference 1 showed the presence of stratified water storage and runback in SCTF is consistent with UPTF results.

In the hot legs of a US/Japanese PWR, the dimensionless steam velocity which occurs during large break LOCA reflood is less than that which occurs in UPTF. The result of this difference is that greater hot leg water level and greater potential water runback to the upper plenum are expected in US/J PWRs than occurred for similar LOCA conditions in UPTF. However, typical Westinghouse and CE hot legs are shorter than those in UPTF, which limits the total mass which can be accumulated. Figure 8 shows a graph of predicted total hot leg water storage in Westinghouse, CE, and UPTF hot legs during a large break LOCA, as a function of hot leg steam flow. This graph is based on Figure 7 and use of fluid properties at 3.5 bar (51 psia). Figure 8 shows that the total expected water storage in US/J PWRs is similar to values observed in the UPTF tests. Hence, we can reliably conclude this beneficial effect does occur in full-scale PWRs and the UPTF data provide a means to quantify the extent to which it will occur. Based on Figure 8, we estimate from 800 to 1200 kg (1760 to 2640 lbs) would be stored in typical PWR hot legs during reflood, which is a significant amount of water storage.

Steam Generators

Two-phase flow behavior in steam generators is important during the reflood stage of a large break LOCA. It has also been shown that this behavior is important during a small break LOCA (e.g., Reference 5);

however, due to inherent facility limitations, UPTF data address only the large break phenomena. During the reflood phase of a large break LOCA, steam and water flow into the inlet plenum of the steam generator from the hot leg. Because the flow area of the inlet plenum is considerably larger than the hot leg, the steam velocity decreases; also, the flow turns to vertical in this region. These factors combine to potentially de-entrain water and build up a frothy pool in the inlet plenum. Also, water can be entrained out of the inlet plenum into the tube region of the steam generator, and water can drain from the inlet plenum into the hot leg (Figure 9). The de-entrainment, pooling and drainback phenomena are beneficial as discussed earlier for the upper plenum and hot legs. Liquid carryover to the tube region of the steam generator is detrimental in that vaporization occurs, adding to steam binding.

Steam generator phenomena have been investigated in UPTF based on the same separate effects and integral tests described previously for the upper plenum and hot legs. Both steady and transient flows were covered. The results of UPTF steady state tests show that over a range of conditions typical of reflood, the inlet plenum inventory is proportional to the liquid flow rate and is relatively independent of steam flow rate, i.e., it is similar to the upper plenum behavior described above. Figure 10 shows the pertinent data; as shown in this figure the proportionality constant is observed to be about 30 seconds and there is negligible offset. When the water flow rate was abruptly changed, the inlet plenum inventory also started changing, after the several second delay period due to the upper plenum behavior. As in the case of the upper plenum, this suggests a generalized characteristic behavior of

$$M_S = \int_{t-t_S}^{t} \dot{M}_L' \, dt \qquad [3]$$

Where $M_S$ is the liquid mass in the inlet plenum, $\dot{M}_L'$ is the liquid mass flow rate entering the inlet plenum from the hot leg, and $t_S$ is the steam generator inlet plenum time constant (30 seconds in the case of UPTF).

The UPTF tests also showed that when the inlet plenum approached its equilibrium value of liquid inventory, two phenomena started to occur at about the same time: (1) carryover of liquid from the inlet plenum to the tube region of the steam generator; and (2) fallback of liquid into the hot legs. These two processes proceeded at approximately equal rates until the hot legs accumulated the maximum amount of water they could hold; at that point the net fallback to the hot legs stopped and liquid water was principally carried over to the steam generator tube region.

In a PWR, it is expected that similar behavior as observed in UPTF, in terms of inlet plenum void, would be expected to occur. PWR steam generator inlet plena are slightly more restrictive than UPTF, by about 20 - 30%. Accordingly, the PWR mass storage delay time in the inlet plenum would be expected to be on the order of 20 - 25 seconds, rather than 30 seconds.

Overall Summary of Water Transport Above Core

Based on the above discussion, entrained liquid transport above the core can be summarized as follows:

- First, liquid is de-entrained and stored in the upper plenum in accordance with the upper plenum delay time constant (six seconds in the case of UPTF).

- Next, liquid is de-entrained and stored in the steam generator inlet plena in accordance with its delay time constant (30 seconds in the case of UPTF).

- Next, liquid is delivered in approximately equal portions to the hot legs and to the tube region of the steam generator, until the hot leg reaches its equilibrium accumulation, which is a function of instantaneous hot leg steam flow.

- Following the delays mentioned above and the storage in the hot legs the remaining liquid is transported to the tube region of the steam generator (where the water would be vaporized in a PWR).

According to the above, an analytical equation summarizing the water transport is as shown in Table 1.

The information shown in Table 1 forms a "rule-of-thumb" for determining liquid transport and storage above the core during LOCA reflood. Since it is based on full-scale data it is considered to be a realistic indicator of reflood behavior. The full-scale data used in this evaluation were the UPTF system mass storages determined from instrumentation in the upper plenum (36 differential pressure instruments), hot legs (3-beam gamma densitometer in each hot leg), steam generator inlet plena (one differential pressure instrument in each loop) and steam generator simulator (one differential pressure instrument in each water separator). To determine the accuracy of the measured masses and hence of the overall result shown in Table 1, a mass balance was performed to compare total measured liquid mass with total injected liquid mass. The measured mass was 15% less, which is an indicator of the accuracy of the method in Table 1. A normal use of the method in Table 1 would be to calculate the upper plenum, hot leg, and steam generator inlet plenum storages based on the core exit liquid flow rate ($M_L$), and to assume the remaining water goes to the steam generator (tube region. Used in this way, the 15% inaccuracy indicated by the mass balance is essentially all put in the steam generator tube region. Hence, the calculated mass delivered to the steam generator tube region would be expected to be accurate within the bounds $+0, -(0.15)\left(\int M_L\right)$.

As additional check of the accuracy of the method in Table 1, which was determined principally from steady state data, the method was applied to a complex integral LOCA transient run in a UPTF integral test. The integral test had time variant core simulator steam and water flows. The predicted and actual results for water accumulated in the steam generator tube region are shown in Figure 11. This typical reflood transient showed that about one-half of the net liquid mass above the core made it

to the steam generator tubes. The agreement between predicted and actual results is reasonable, indicating both the validity and accuracy of the method.

References


1. Damerell, P. S., N. E. Ehrich and K. A. Wolfe, "Use of Full-scale UPTF Data to Evaluate Scaling of Downcomer (ECC Bypass) and Hot Leg Two-phase Flow Phenomena," presented at the 15th Water Reactor Safety Information Meeting, October 26 - 29, 1987.

2. Hofmann, K., "Status of the German UPTF Program," presented at the 13th Water Reactor Safety Information Meeting, October 22 - 25, 1985.

3. Weiss, P., Sawitzki, M. and Winkler, F., "UPTF - a Full-scale PWR Loss-of-Coolant Accident Program," Atomkern-Energie Kerntechnik, Vol. 49, 1986.

4. Weiss, P. A., and R. J. Hertlein, "UPTF Test Results -- First 3 Separate Effects Tests," presented at the 14th Water Reactor safety Information Meeting, October 27 - 31, 1986.

5. Kukita, Y. et al, "Flooding at Steam Generator Inlet and its Impact on Simulated PWR Natural Circulation," ASME FED Vol 61, HTD Vol 92, p. 111.

TABLE 1

ANALYTICAL SUMMARY OF LIQUID MASS TRANSPORT ABOVE CORE

| COMPONENT MASS | ANALYTICAL EXPRESSION |
|---|---|
| UPPER PLENUM | $\int_{t_2}^{t_3} \dot{M}_L \, dt + M_{UP,0}$ |
| + STEAM GENERATOR INLET PLENA | $+ \int_{t_1}^{t_2} \dot{M}_L \, dt$ |
| + HOT LEGS | $+ \frac{1}{2} \int_{t_0}^{t_1} \dot{M}_L \, dt - \frac{1}{2} \int_{t_0}^{t_1} \dot{M}_L \, dt - \sum_{1}^{n} M_{HL} \, (j_g^*)_n$ |
| + STEAM GENERATOR TUBE REGION | $+ \frac{1}{2} \int_{t_0}^{t_1} \dot{M}_L \, dt + \frac{1}{2} \int_{t_0}^{t_1} \dot{M}_L \, dt - \sum_{1}^{n} M_{HL} \, (j_g^*)_n$ |
| = TOTAL | $= \int_{0}^{t} \dot{M}_L \, dt$ |

Notes:

$\dot{M}_L$ = liquid flow rate out of top of core

$M_{UP,0}$ = upper plenum "offset" mass storage

$t_0$ is such that $M_{UP,0} = \int_{0}^{t_0} \dot{M}_L \, dt$

$t_1 = \langle t - t_u - t_s - t_0 \rangle + t_0$

$t_2 = \langle t - t_u - t_0 \rangle + t_0$

$t_3 = \langle t - t_0 \rangle + t_0$

$t_u$ = upper plenum storage delay constant

$t_s$ = steam generator inlet plenum storage delay constant

$n$ = number of hot legs

$M_{HL} \, (j_g^*)$ = liquid mass storage in hot leg as a function of dimensionless steam velocity

$\langle x \rangle = x$ if $x \geq 0$ $\quad \langle x \rangle = 0$ if $x < 0$.

MPR ASSOCIATES
F-73-26-1674
10/21/88

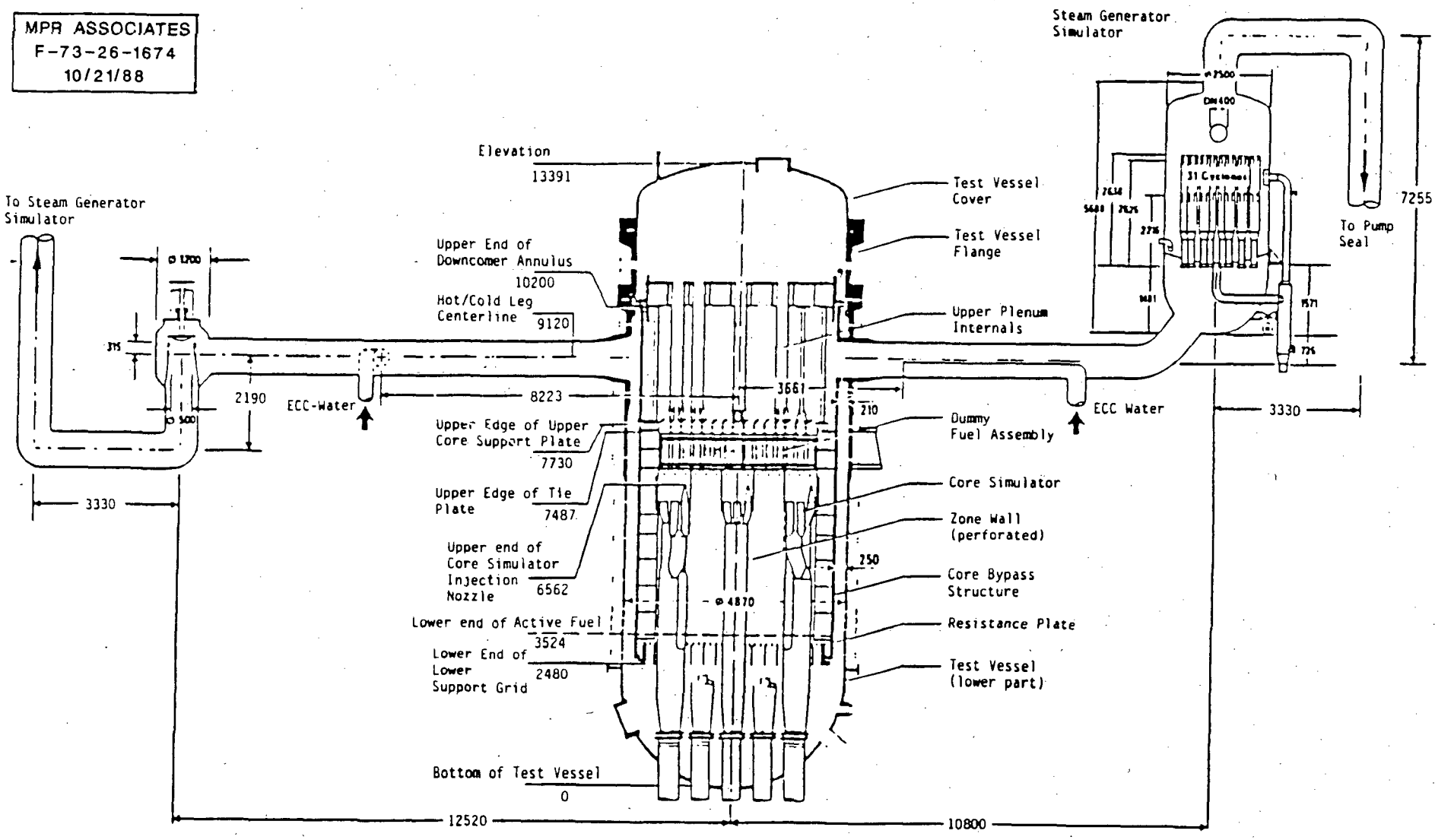


Note: All dimensions in mm

UPTF TEST VESSEL AND PRIMARY LOOP (ONE SHOWN)

FIGURE 1

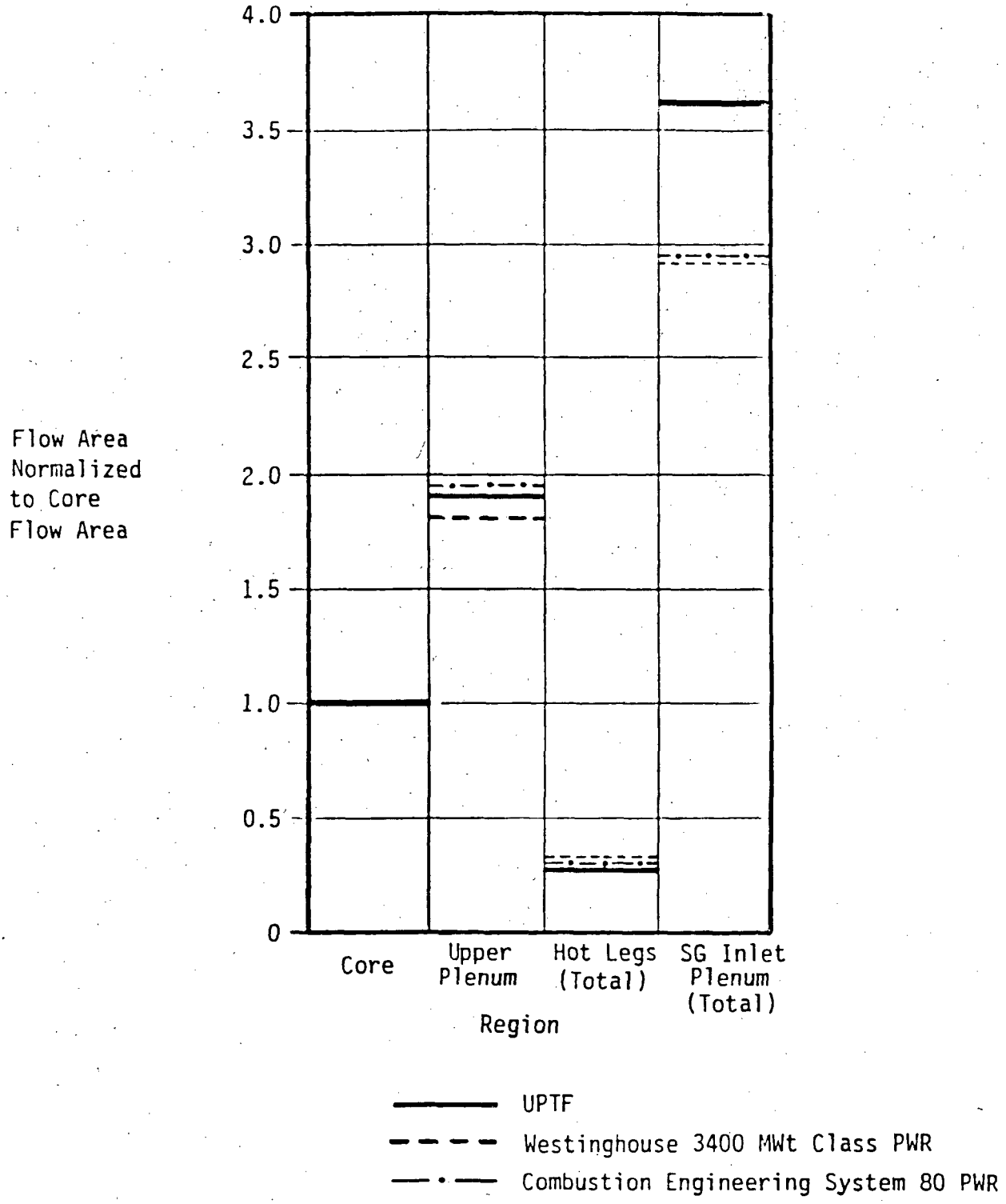


COMPARISON OF NORMALIZED FLOW AREAS FOR UPTF AND TYPICAL U.S. PWRS

FIGURE 2

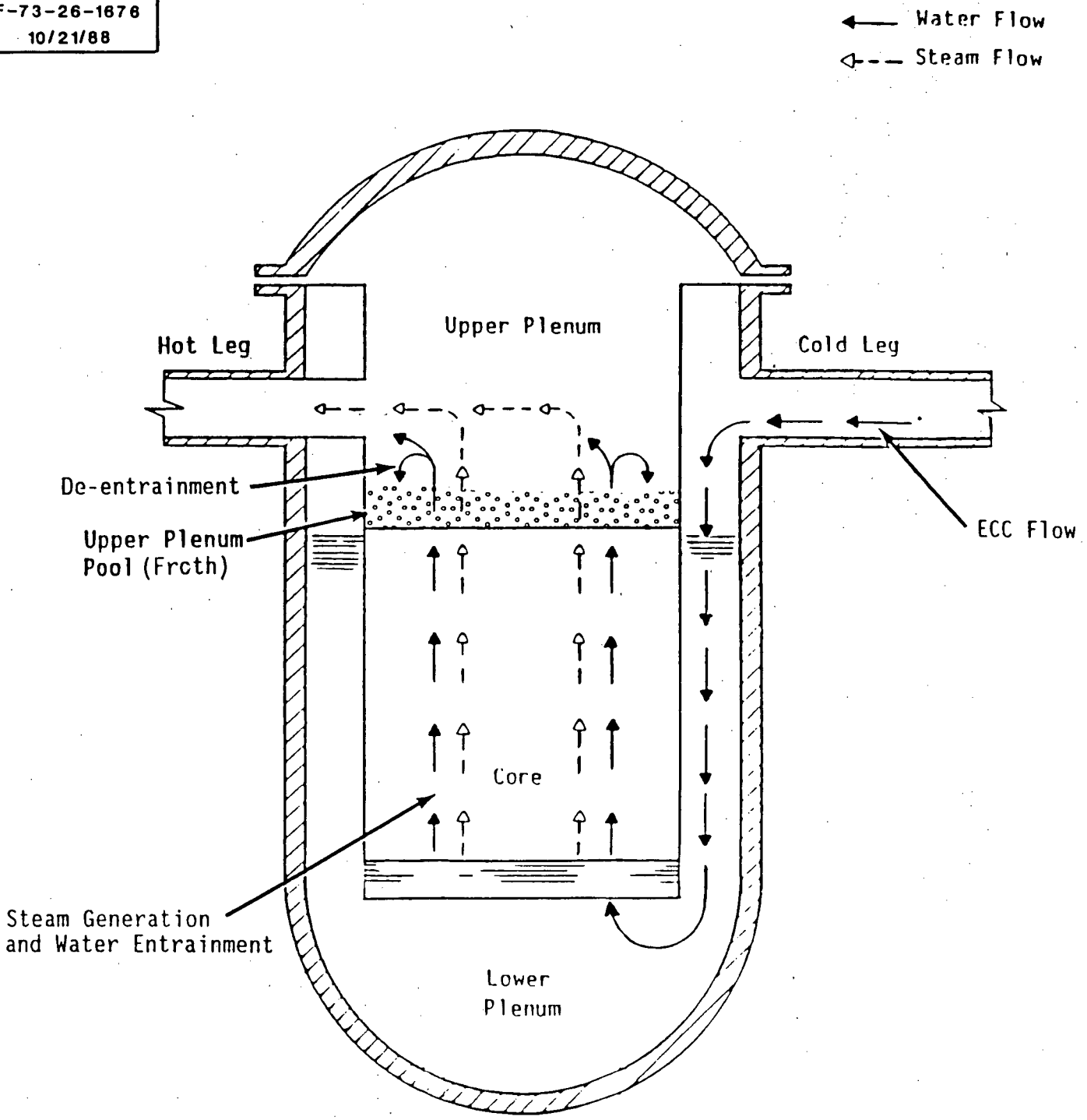


SCHEMATIC DIAGRAM OF LOCA REFLOOD PHENOMENA SHOWING FORMATION OF UPPER PLENUM POOL BY DE-ENTRAINED WATER

FIGURE 3

MPR ASSOCIATES
F-73-26-1677
10/21/88

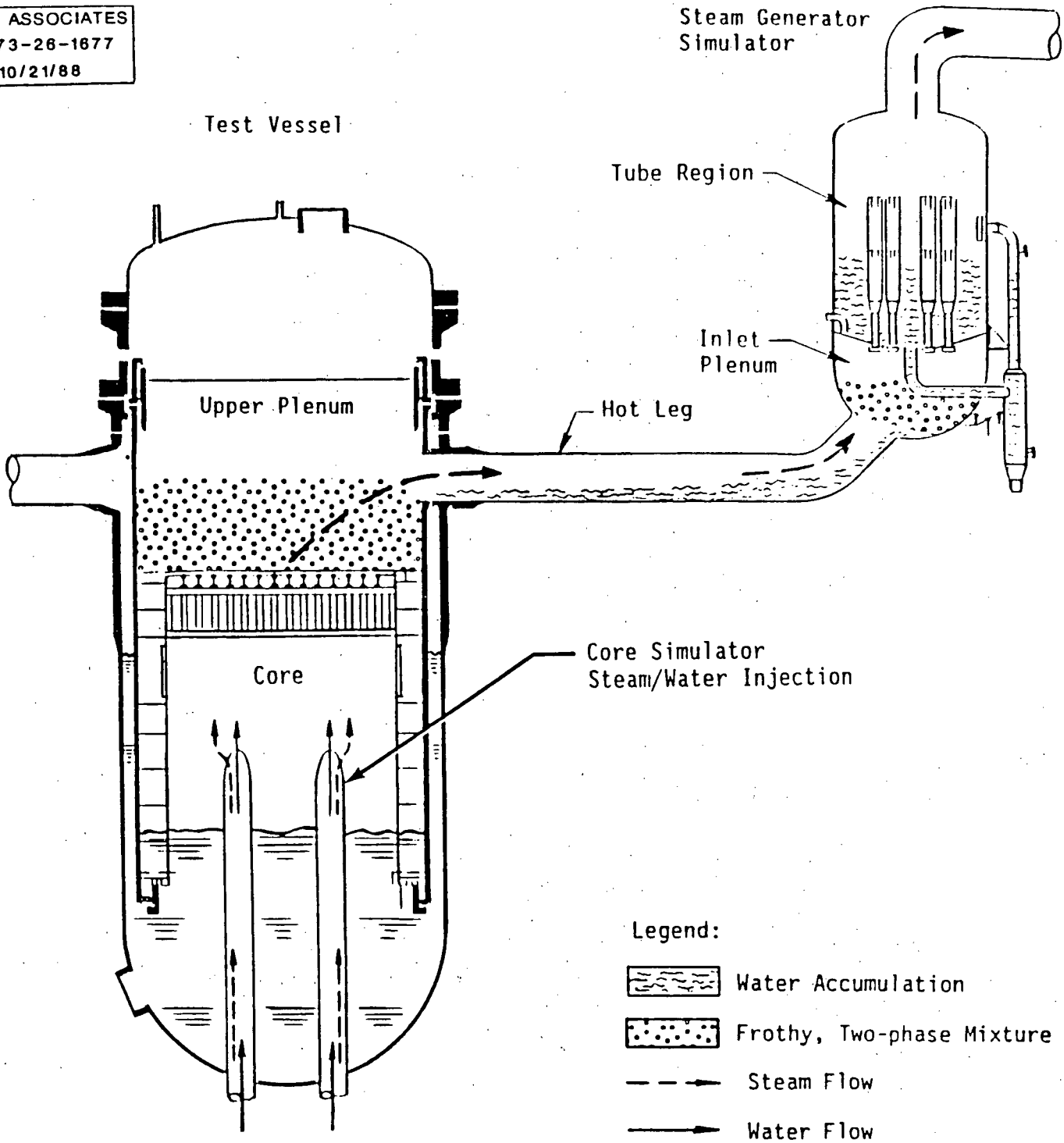


SIMULATION OF WATER DE-ENTRAINMENT
AND ACCUMULATION PHENOMENA IN THE UPTF

FIGURE 4

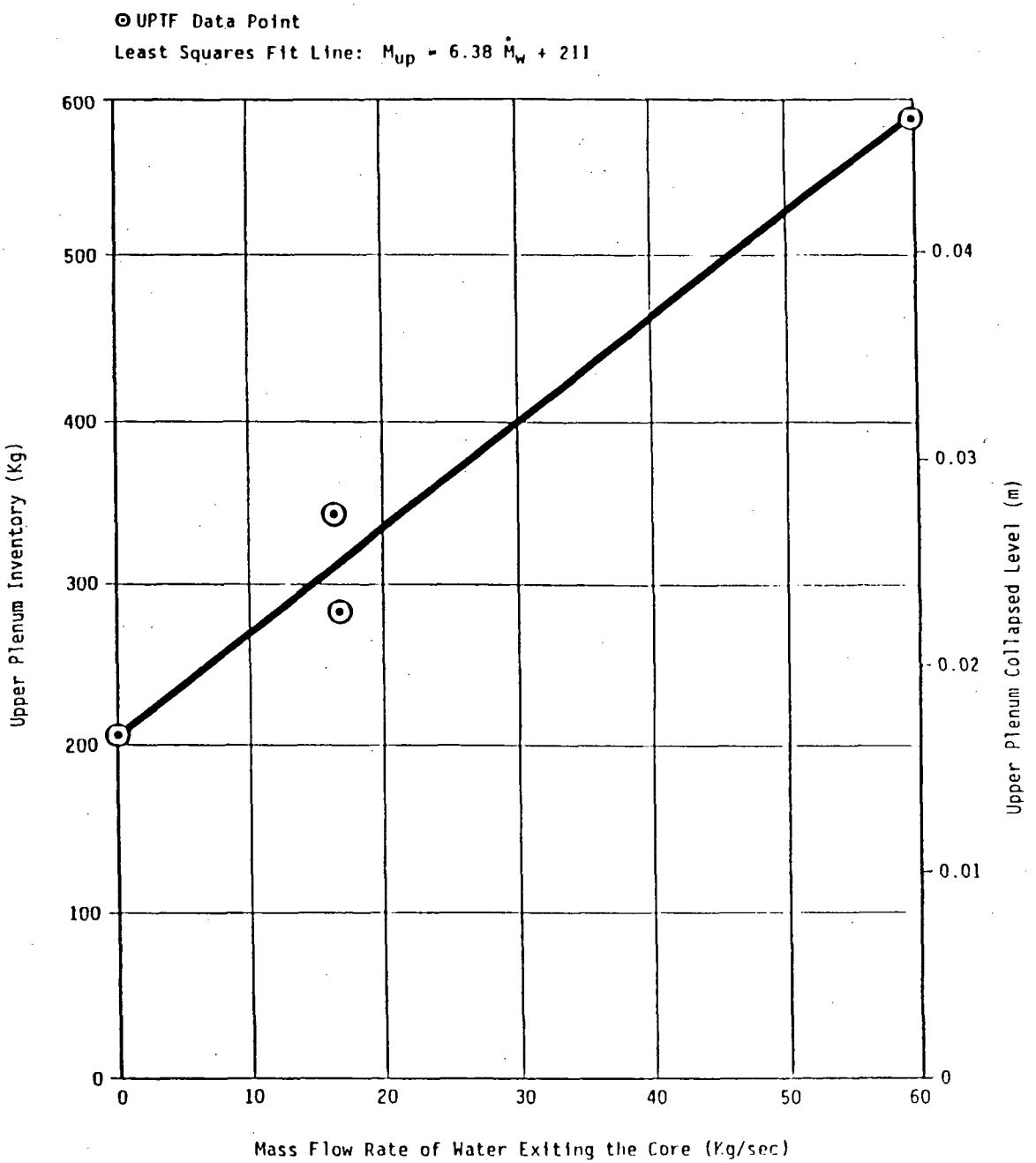


UPTF SEPARATE EFFECTS TEST
UPPER PLENUM INVENTORY AS A FUNCTION
OF WATER FLOW RATE EXITING THE CORE

FIGURE 5

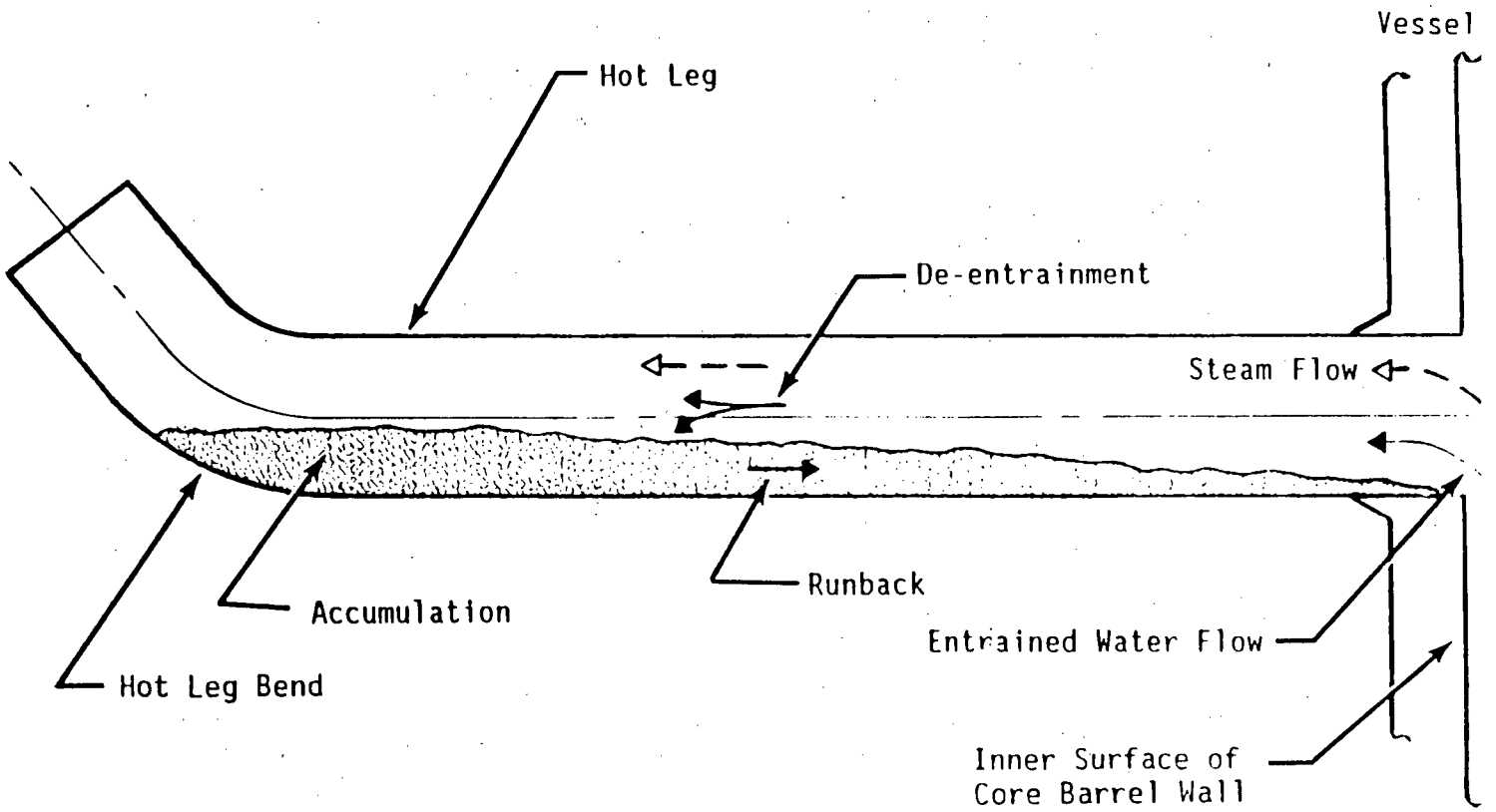


SCHEMATIC DIAGRAM OF
HOT LEG PHENOMENA DURING LOCA REFLOOD

FIGURE 6

$$j^* = \frac{M}{\rho A}\sqrt{\frac{\rho}{\Delta \rho g D}}$$

⊙ UPTF Data Point

Equation of Least Squares Fit Line: $\alpha = 0.493 + 0.679\ j_{g^*}$

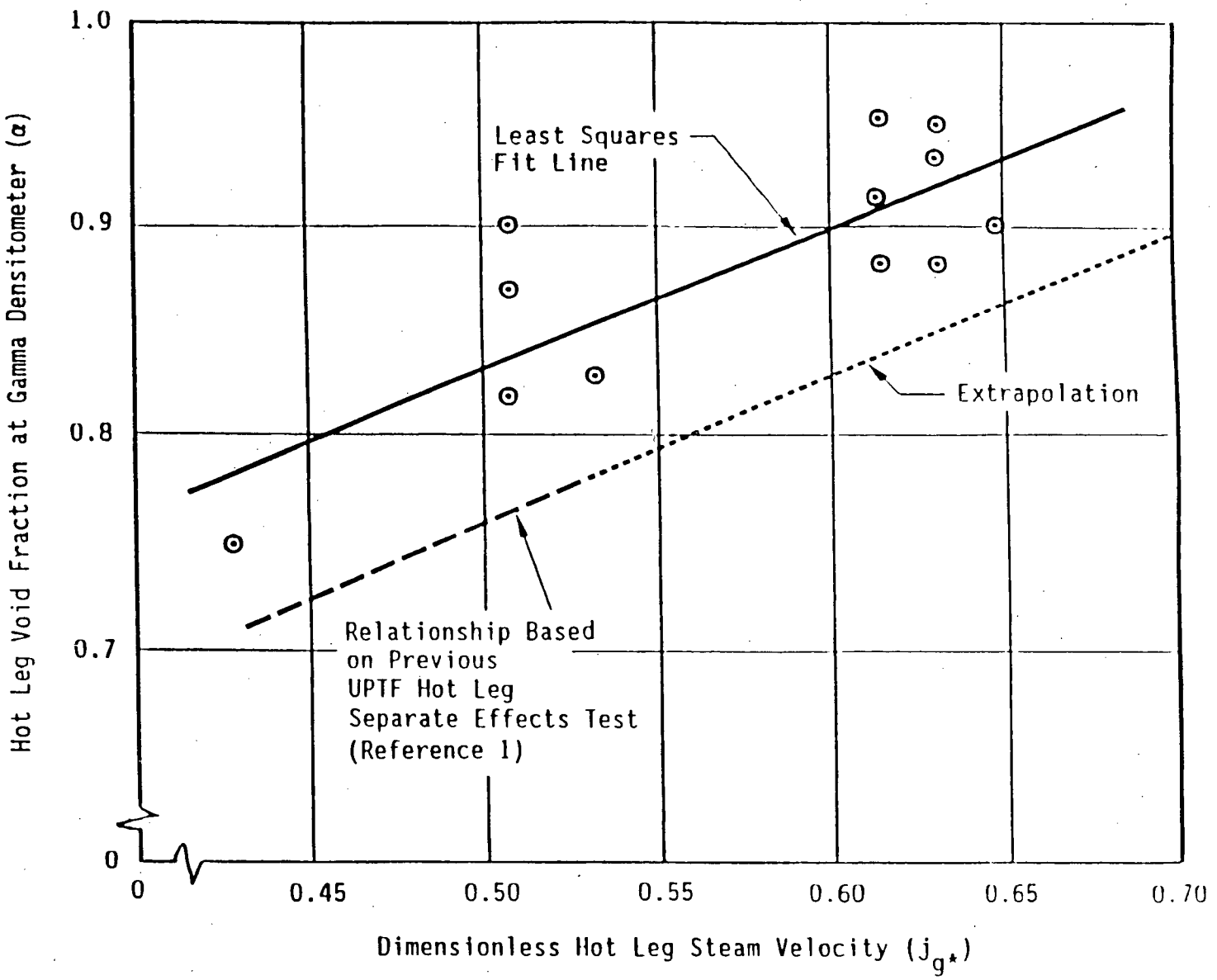


Notes:

1. This figure represents an individual hot leg.
2. The dimensionless steam velocity range for the UPTF Hot Leg Separate Effects Test data was 0.30 to 0.53.

UPTF SEPARATE EFFECTS TEST
HOT LEG WATER INVENTORY (EXPRESSED AS VOID FRACTION)
AS A FUNCTION OF DIMENSIONLESS STEAM VELOCITY

FIGURE 7

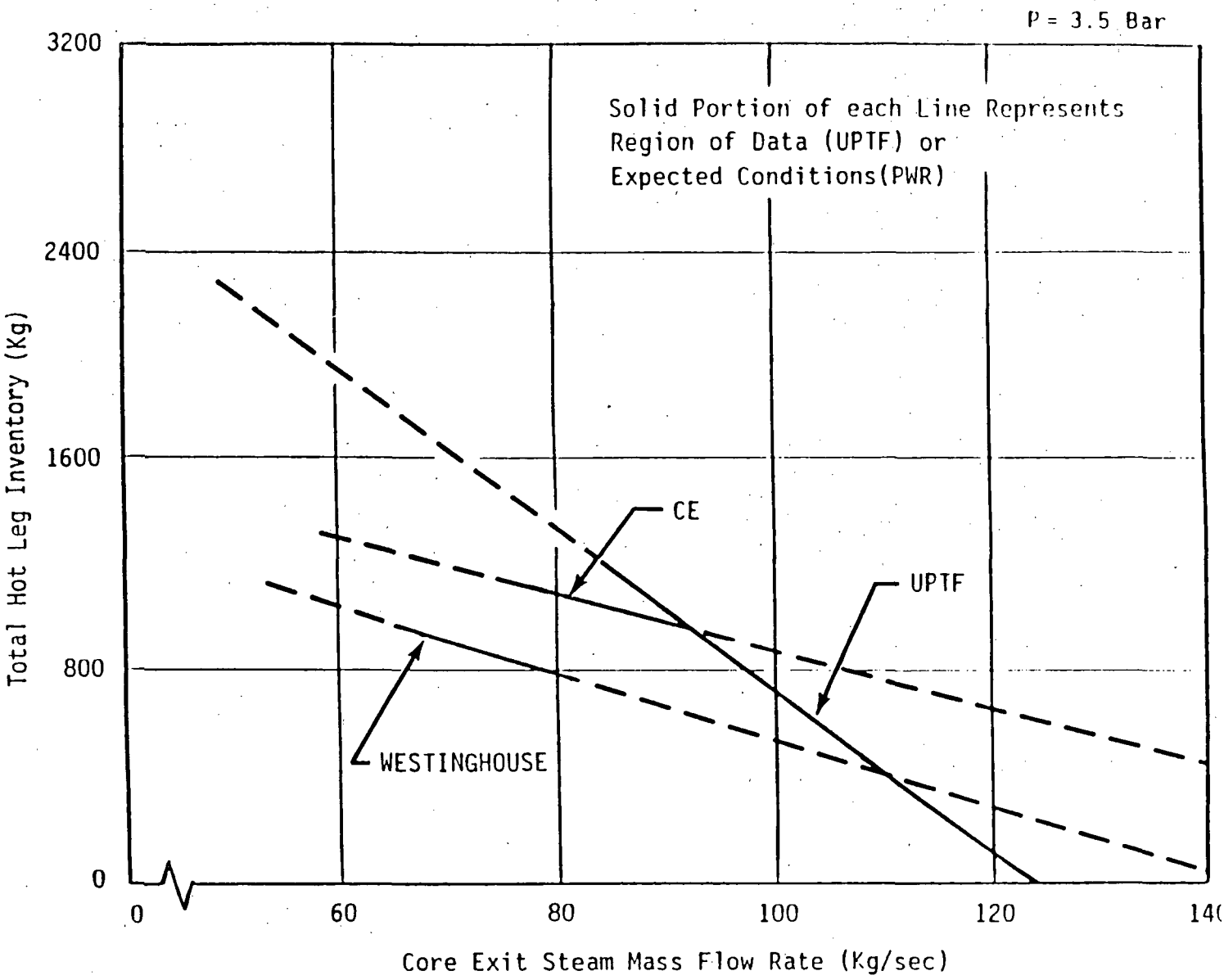


Notes:

1. This relationship was calculated from the void fraction - dimensionless steam velocity relationship (see Figure 7) for a reactor coolant loop pressure of 3.5 bar.
2. Hot leg inventory is calculated by multiplying the liquid fraction at the gamma densitometer by the hot leg volume, liquid density and a factor of 0.56 which accounts for a non-uniform water level profile.

HOT LEG INVENTORY AS A FUNCTION OF
HOT LEG STEAM MASS FLOW RATE FOR UPTF AND TYPICAL PWRS

FIGURE 8

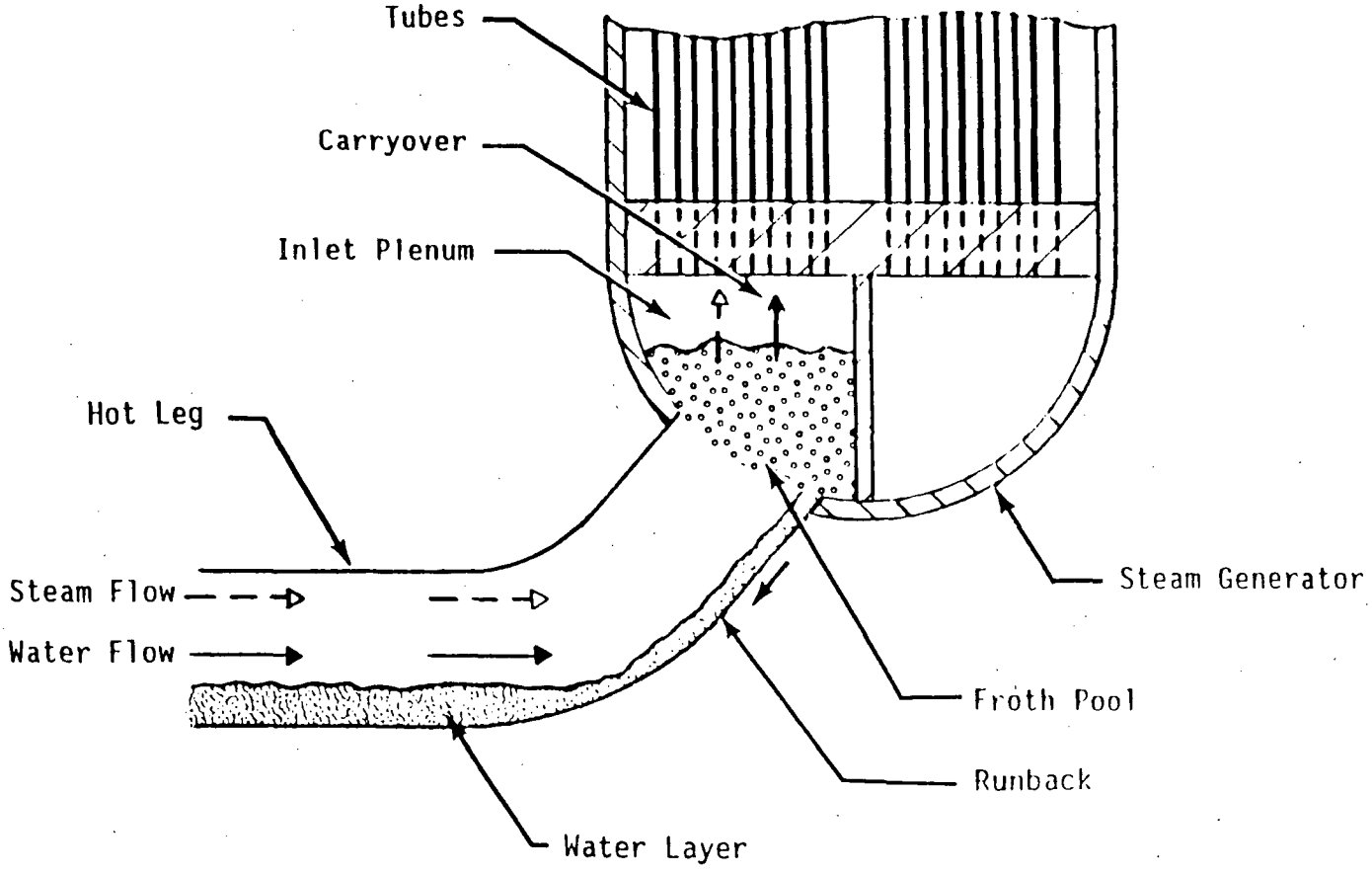


SCHEMATIC DIAGRAM OF
STEAM GENERATOR PHENOMENA DURING LOCA REFLOOD

FIGURE 9

MPR ASSOCIATES
F-73-26-1693
10/21/88

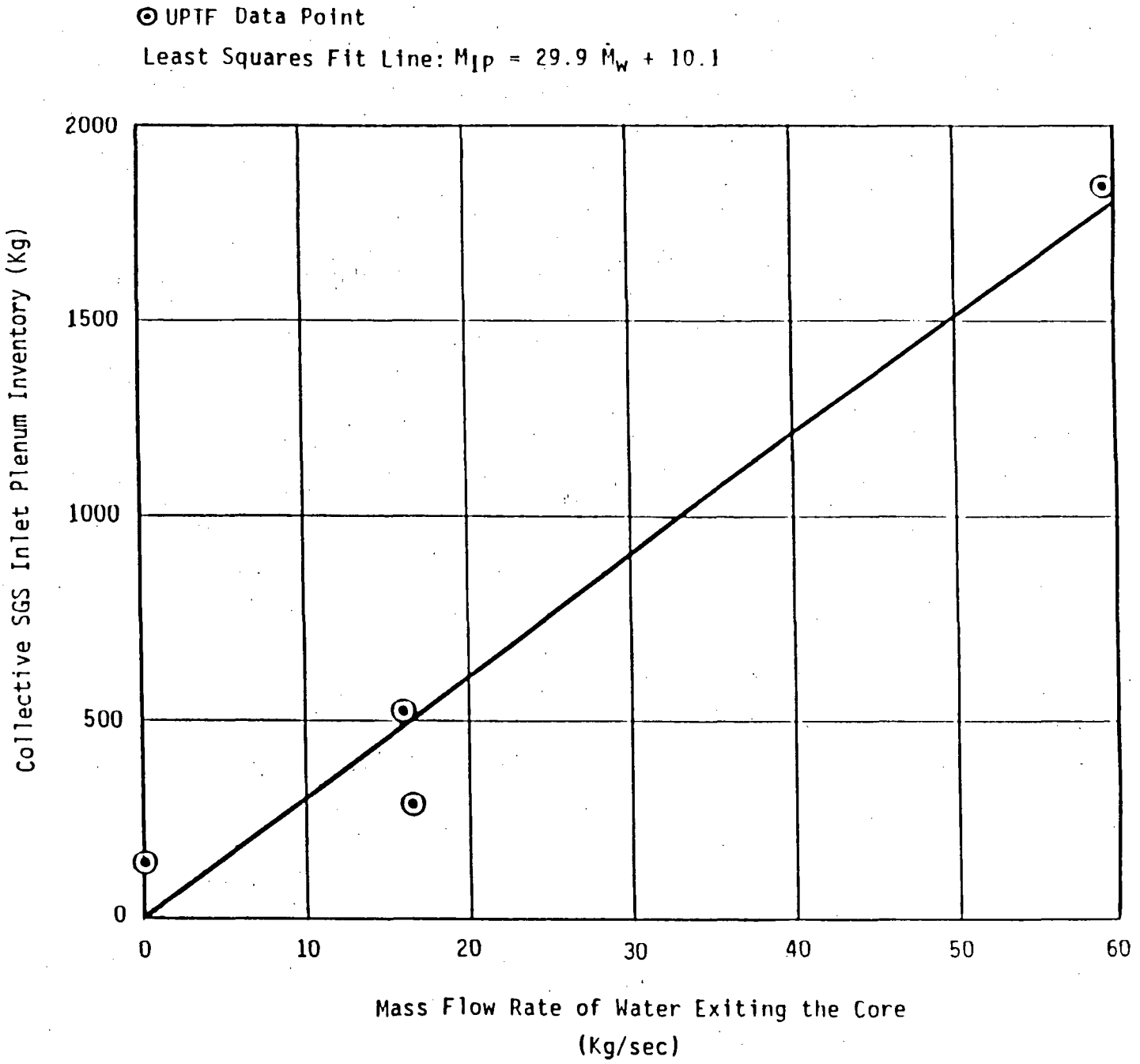


UPTF SEPARATE EFFECTS TEST COLLECTIVE STEAM GENERATOR INLET PLENUM INVENTORY AS A FUNCTION OF WATER FLOW RATE EXITING THE CORE

FIGURE 10

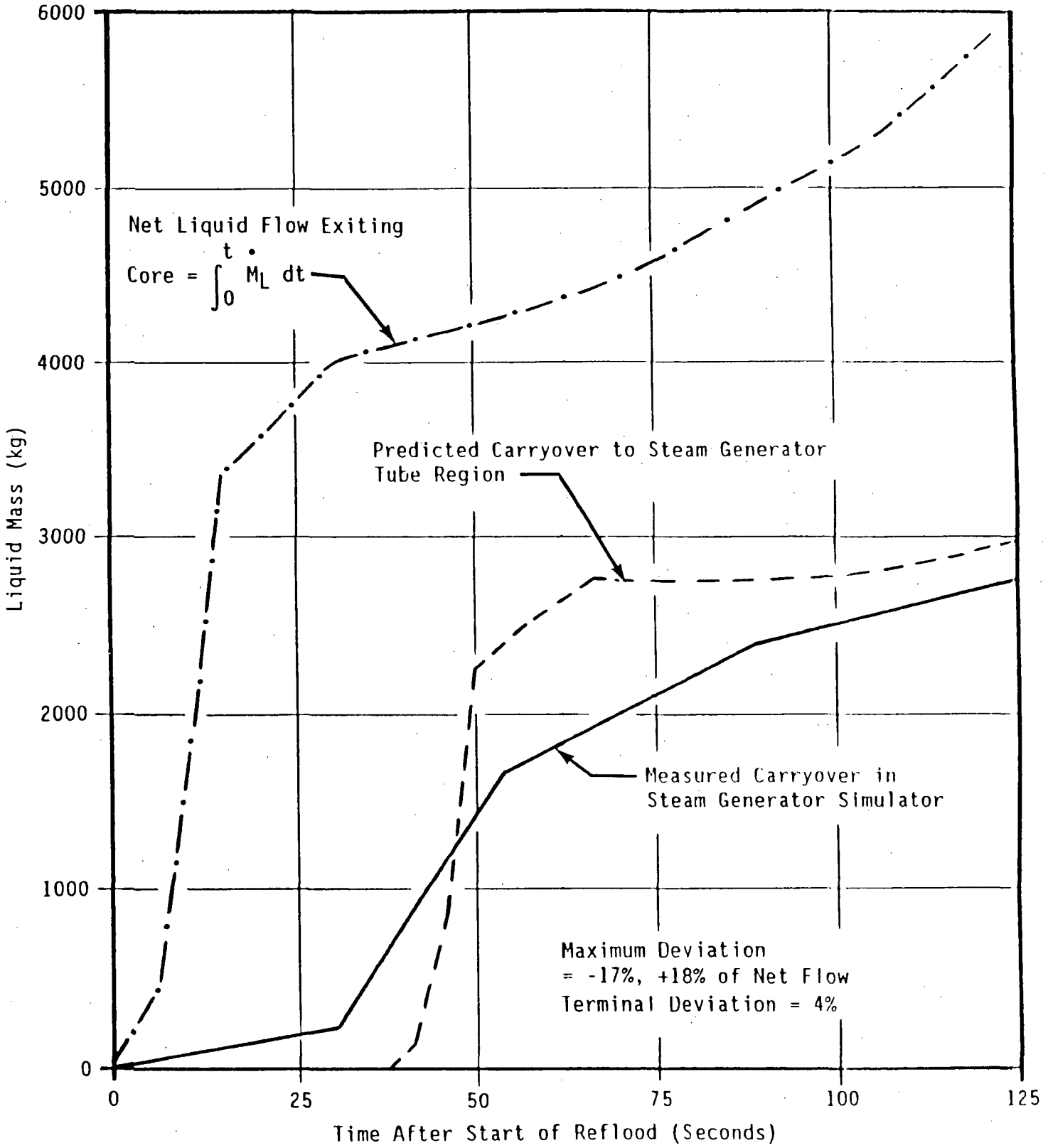


COMPARISON OF PREDICTED AND MEASURED CARRYOVER TO STEAM GENERATOR IN UPTF TRANSIENT INTEGRAL TEST

FIGURE 11

# USE OF 2D/3D DATA FOR PEAK CLADDING TEMPERATURE UNCERTAINTY STUDIES*

by

B. E. Boyack
Nuclear Technology and Engineering Division
Los Alamos National Laboratory
Los Alamos, New Mexico 87545

## ABSTRACT

In August 1988, the Nuclear Regulatory Commission (NRC) approved the final version of a revised rule on the acceptance of emergency core cooling systems. The revised rule allows emergency core cooling system analysis based on best-estimate methods provided uncertainties in the prediction of prescribed acceptance limits are quantified and reported. To support the revised rule, the NRC developed the Code Scaling, Applicability, and Uncertainty (CSAU) evaluation methodology. Data from the 2D/3D program have been used in a demonstration of the CSAU methodology in two ways. First, the data were used to identify and quantify biases that are related to the implementation of selected correlations and models in the thermal-hydraulic systems code TRAC-PF1/MOD1 as it is used to calculate the demonstration transient, a large-break loss-of-coolant accident. Second, the data were used in a supportive role to provide insight into the accuracy of code calculations and to confirm conclusions that are drawn regarding specific CSAU studies. Examples are provided illustrating each of these two uses of 2D/3D data.

## INTRODUCTION

In August 1988, the Nuclear Regulatory Commission (NRC) approved the final version of a revised rule on the acceptance of emergency core cooling systems (ECCS) entitled "Emergency Core Cooling System; Revisions to Acceptance Criteria" (Ref. 1). The revised rule contains three key features. First, the current acceptance criteria related to peak cladding temperature (PCT), clad oxidation, hydrogen generation, coolable core geometry, and long-term cooling are retained. Second, evaluation model (EM) methods based on Appendix K of Ref. 1 may continue to be used as an alternative to the best-estimate (BE) methodology. Third, an alternate ECCS performance analysis, based on BE methods, may be used to provide more realistic estimates of plant safety margins, provided the licensee quantifies the uncertainty of the estimates and includes that uncertainty when comparing the calculated results with prescribed acceptance limits.

To support the revised ECCS rule, the NRC and its contractors and consultants have developed and demonstrated a method called the Code Scaling, Applicability, and Uncertainty (CSAU) evaluation methodology. This methodology provides a formal, auditable, and traceable method for combining quantitative analysis and expert opinion in arriving at computed values of uncertainty. The objective of the selected demonstration is to quantify the uncertainty

* This work was funded by the US Nuclear Regulatory Commission (NRC), Office of Nuclear Regulatory Research, Division of Accident Evaluation.

in using TRAC-PF1/MOD1 (Refs. 2–3) to calculate the PCT for a Westinghouse four-loop pressurized water reactor (PWR) with 17 x 17 fuel experiencing a cold-leg large-break loss of coolant accident (LOCA).

The CSAU methodology consists of twelve interrelated steps. These are (1) scenario specification, (2) selection of the power plant, (3) phenomena identification and ranking according to importance for the selected scenario, (4) computer code selection, (5) collection and review of a complete set of code documentation, (6) determination of code applicability for the selected scenario, (7) establishing a code assessment matrix, (8) definition of nuclear power plant (NPP) nodalization, (9) determination of code accuracy using data from separate-effect and integral tests, including a statement of experiment accuracy, (10) determination of scale-up effects in both the code and data, (11) combination of biases and uncertainties, and (12) determination of total uncertainty. Steps 7, 9, and 10, above, are related to the review and use of experimental data. The objective of this paper is to describe the use of data collected within the 2D/3D program for the CSAU demonstration effort.

## 2D/3D FACILITIES

Three experimental facilities contribute data within the 2D/3D program. The Slab Core Test Facility (SCTF) is a separate-effect reflood facility located in Japan. It models a full-height 1/21-scale section of the core, one fuel element wide from core centerline to outer periphery; this is, in effect, a two-dimensional modeling a reactor core. The Cylindrical Core Test Facility (CCTF), an approximately 1/21-scale facility modeling the core in three dimensions, is also located in Japan. The Upper-Plenum Test Facility (UPTF), located in the Federal Republic of Germany, is a 1/1-scale integral test facility focusing on phenomena in the downcomer, lower plenum, upper plenum, and hot and cold legs of a PWR.

## USE OF 2D/3D DATA IN THE CSAU DEMONSTRATION

Data from the 2D/3D facilities identified above have played an important role in the CSAU demonstration effort; they have been used in two ways. First, they have been used directly to assess the degree to which the code models specific phenomena. Second, the data have been used in a supportive role to provide insight into the accuracy of code calculations and to confirm conclusions that are drawn regarding specific CSAU studies. Examples of each usage of 2D/3D data are provided below.

### Direct Application of 2D/3D Data

**SCTF Data.** Step 3 of the CSAU method leads to the identification of key phenomena that must be considered in the code uncertainty quantification process. For example, steam binding in the steam generators has been judged to be important during the reflood phase of a large-break LOCA (Ref. 4). Previous 2D/3D assessment activities have shown that the TRAC-PF1/MOD1 simulation of SCTF and CCTF phenomena that are directly related to steam binding are deficient. It has been determined that the code underpredicts the amount of liquid above the quench front during core reflood (Refs. 5–7). This is a consequence of an interface sharpener model (Rozen entrainment correlation) in the code that is implemented in the core region (Ref. 3). Outcomes of this deficiency propagate throughout the primary coolant loop. Specifically, too little liquid reaches the vessel upper plenum and, subsequently, too little liquid is transported through the hot leg and into the steam generators where it would be available for vaporization, which produces steam binding. The Technical Program Group (TPG), formed to develop the CSAU method and provide a demonstration, chose to deal with this code deficiency by treating it as a margin to be added to the combined uncertainty determined by probability distribution function and Monte Carlo techniques.

Using SCTF data, three code parameters were adjusted to improve the comparison to data. First, a multiplier was applied to the Rozen entrainment correlation to increase the amount of liquid leaving the interface sharpener model; the multiplier was ranged between 1 and 50. Second, a multiplier was applied to the interfacial shear predicted in the core; the multiplier was ranged between 2 and 100. Third, a multiplier was applied to the interfacial shear predicted in the upper plenum; the multiplier was ranged between 0.1 and 10. The TRAC-PF1/MOD1 code was then run and the multipliers adjusted to obtain improved agreement between calculated and measured values of the upper-plenum liquid level and hot-leg mass flow. The best overall improvement (upper-plenum liquid level, hot-leg mass flow, physically reasonable processes) was obtained with a multiplier of 20 on the Rozen entrainment correlation, 10 on the core interfacial shear, and 1 on the upper-plenum interfacial shear. Comparisons between measured and calculated values of upper-plenum liquid level with the nominal code and with the multipliers identified above are provided in Fig. 1a,b. Hot-leg mass flow was increased by about 20% with the selected multipliers but remained significantly less than measured. Additional attempts to produce improved hot-leg mass flows while retaining the improved upper-plenum liquid level were not successful; large fluid surges not seen in the data were predicted.

To quantify the margin in an NPP to defects in the core entrainment and interfacial shear models, the same multipliers were used and the resultant PCT change relative to the NPP base case calculated. The effect of the multipliers on the upper-plenum liquid level calculation for the NPP is shown in Fig. 2. The predicted upper-plenum liquid mass was markedly increased for the calculation with core entrainment and interfacial shear multipliers. The effect of the multipliers on PCT is shown in Fig. 3. The effect of the multipliers was to increase the PCT during the second reflood peak by 106 K and increase the cladding quench time by over 50 s.

**UPTF Data.** Data from the UPTF are being applied in several ways within the CSAU activity. First, the data are being used to evaluate the existence of potential bias to be quantified as a margin in the TRAC-PF1/MOD1 code; an example will be provided. Second, data from the UPTF facility are being used to provide information about scaling factors in both experimental facilities and within the TRAC-PF1/MOD1 code. The UPTF data are viewed as highly important because they uniquely address many important scaling issues. A calculation of UPTF Test 10B, a quasi-steady downcomer counter-current flow limitation (CCFL) test, has been performed at Los Alamos using TRAC-PF1/MOD1. For the given quasi-steady test conditions, it was found that TRAC predicted complete bypass of ECC liquid; no liquid was delivered to the lower plenum. The TPG noted, however, that in reduced-scale separate-effect tests, in large-break LOCA integral tests, and in the standard plant calculation, TRAC predicted delivery of ECC liquid to the lower plenum. Therefore, several conclusions were reached. First, the TRAC models for interfacial shear exhibited deficiencies at full scale, i.e., for a limited range of steam fluxes TRAC would levitate and bypass ECC liquid while downcomer penetration and lower-plenum filling would be observed in the test. Second, at lower steam fluxes, TRAC would predict delivery of ECC liquid to the lower plenum. Third, during a UPTF transient with prototypical large-break LOCA steam fluxes or during a large-break LOCA in standard plant, the steam flux would be reduced to the point TRAC would predict delivery. Fourth, the model deficiency displayed by TRAC would result in higher PCTs than would occur if ECC delivery could be more accurately predicted. The TRAC bias associated with modeling of ECC system bypass effects has been estimated to be -19 K.

The scale-related bias in TRAC-PF1/MOD1 prediction of the lower-plenum filling rate has been more fully examined at Brookhaven National Laboratory (BNL). BNL examined the data from Creare 1/15 and 1/5 scale downcomer tests, the Battelle Columbus Laboratory 2/15

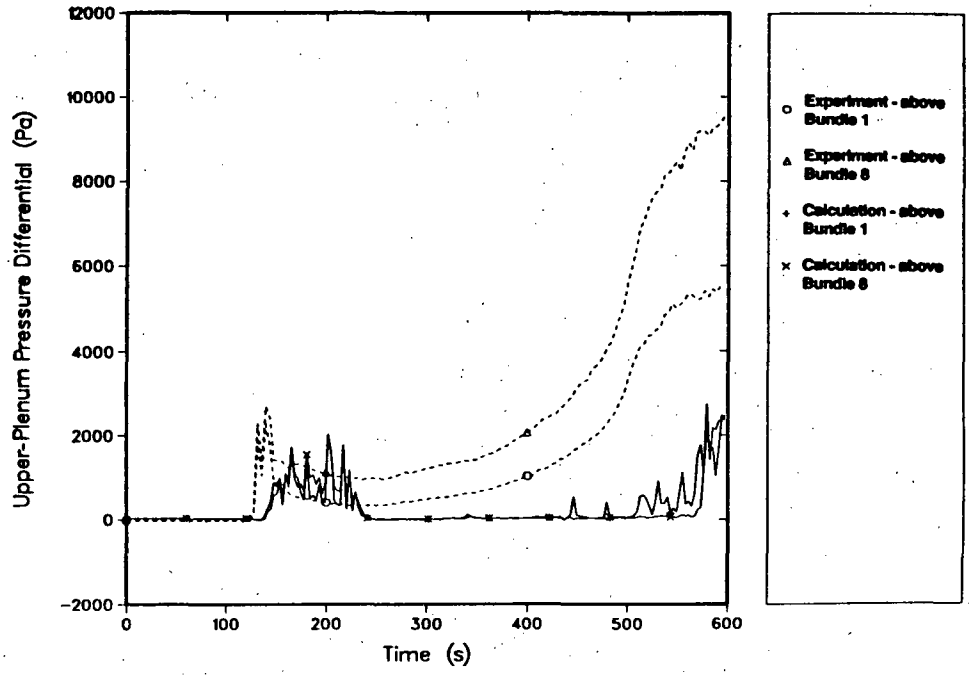


**Fig. 1.a.**
Upper-plenum liquid level for SCTF Run 601 nominal calculation.

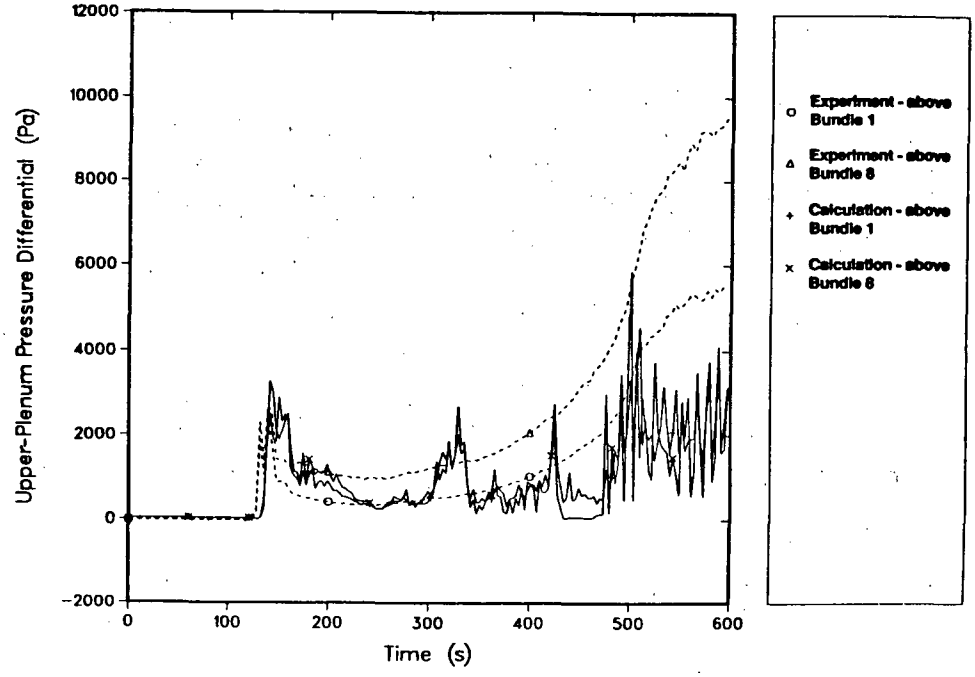


**Fig. 1.b.**
Upper-plenum liquid level for SCTF Run 601 calculation with entrainment and interfacial shear multipliers.

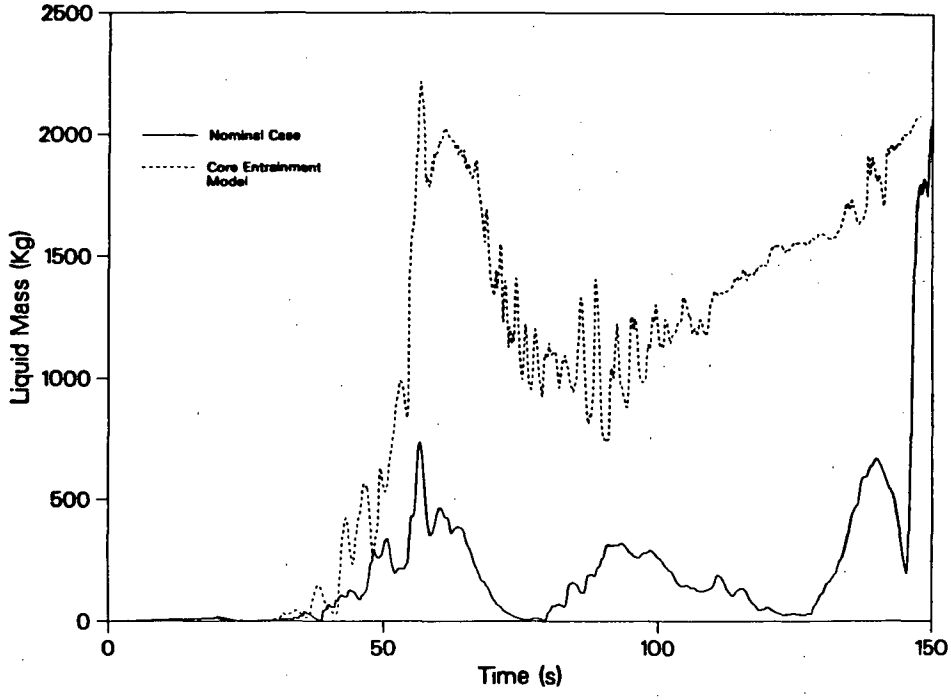


**Fig. 2.**
Calculated NPP upper-plenum liquid mass (nominal and with entrainment and interfacial shear multipliers).

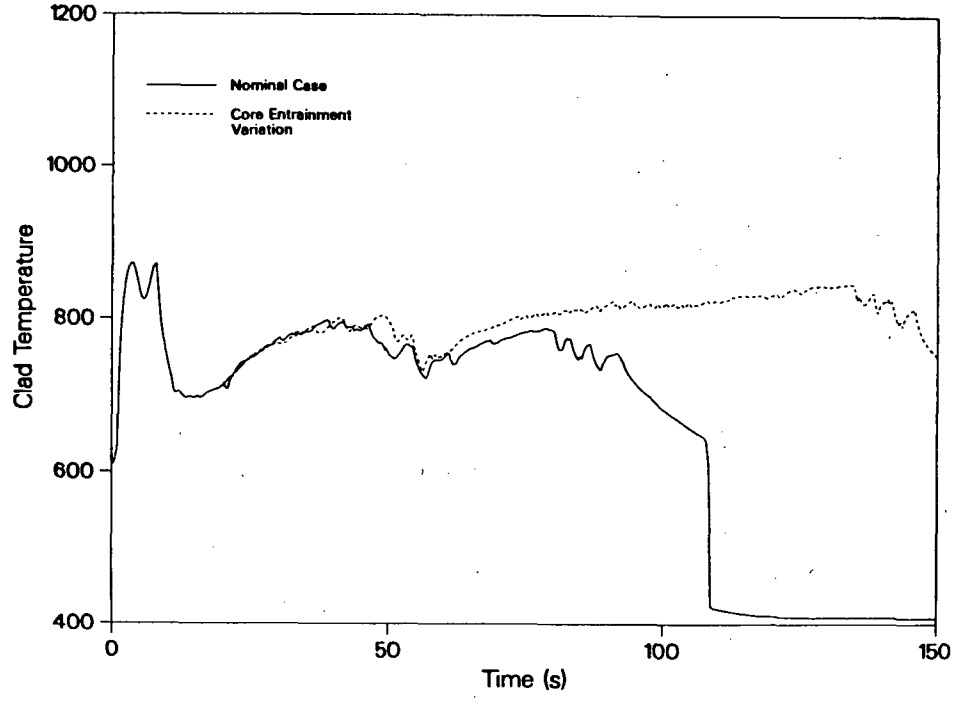


**Fig. 3.**
Calculated NPP PCT (nominal and with entrainment and interfacial shear multipliers).

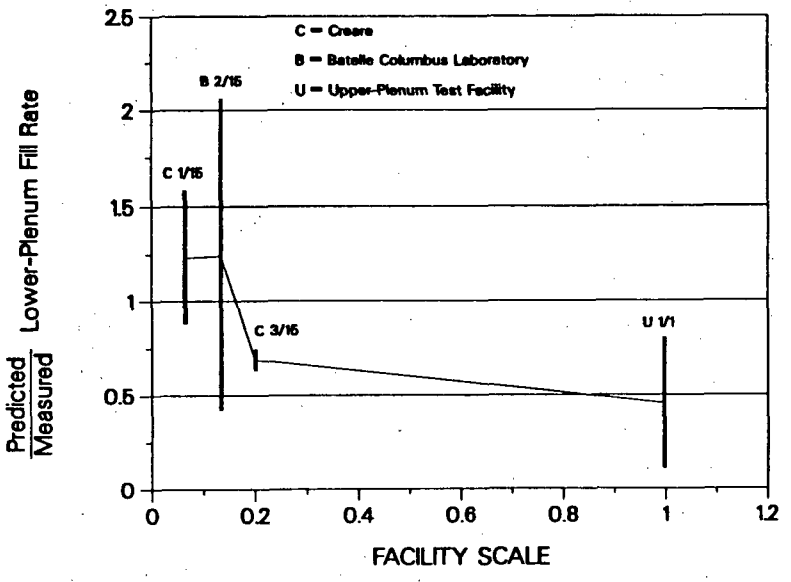


**Fig. 4.**
Bias in TRAC-PF1/MOD1 prediction of lower-plenum filling rate (reproduced from Ref. 8 by permission of Brookhaven National Laboratory.)

downcomer tests, and UPTF 1/1 scale downcomer tests (Ref. 8). Based on these studies it was demonstrated that scale effects exist in the code. TRAC was shown to overpredict the delivery of ECC to the lower plenum at smaller scales and underpredict the delivery of liquid at full scale (Fig. 4.) The BNL work provided convincing evidence of a scale-related bias in TRAC regarding the prediction of ECC bypass phenomena.

**Use of 2D/3D Data for Insight and Support**

If a large-break LOCA data base collected in a full-scale fully prototypic configuration were available, it would be possible to determine code uncertainty by direct comparison to data. However, this data base is not available; such facilities do not exist and no large-break LOCA has occurred in an operating plant. However, large-break LOCA transients have been run in reduced-scale integral and separate-effect facilities such as Semiscale, the Loss-of-Fluid Test Facility, CCTF, and SCTF. Numerous assessment calculations have been performed using the data from these tests. From such calculations it is possible to state that a given code, e.g., TRAC-PF1/MOD1, will predict a selected parameter in the sub-scale facility, such as PCT or cladding quench time, within a stated uncertainty band. In addition, the level of confidence related to such calculations can be provided. Although such results provide insight into the ability of the code to calculate similar phenomena in operating plants, they do not, in themselves, transfer directly to the full-size plant. Therefore, such results are considered to be supportive within the context of the CSAU methodology. It is important to emphasize, however, that the availability of such supportive results is important. In addition to increasing confidence that the dominant phenomena are modeled in the code, the quantified uncertainty

for full-size plants can be checked for both trends and magnitudes as insurance that problems in application of the CSAU method at full scale do not go unrecognized.

We have used data from several 2D/3D facilities in this manner. Data from SCTF and CCTF tests simulate the reflood phase of a large-break LOCA. Calculated and measured PCTs have been compared for 5 SCTF tests and 4 CCTF tests producing 204 comparison points. An additional 16 data points were obtained from other SCTF and CCTF assessments for a total of 220 comparison data points. As reported by BNL (Ref. 9), the mean difference (or bias) between the measured and calculated PCTs is 10.32 K and the standard deviation (1-sigma value) is 49.76 K. A scatter diagram displaying the TRAC-calculated PCT versus measured PCT is provided in Fig. 5. Similar studies have recently been performed at Los Alamos using data from the SCTF Core-III facility. A comparison of measured and calculated PCTs for eight SCTF Core-III tests is provided in Fig. 6. The mean difference is -19.4 K and the standard deviation (1-sigma value) is 59.8 K. A comparison of measured and calculated quench times for the same tests is provided in Fig. 7. The mean difference is -0.6 s and the standard deviation (1-sigma value) is 33.8 s. These results have been used to increase confidence that the dominant phenomena are modeled in the code.

## CONCLUSION

Data from the 2D/3D program have been used in the demonstration of the CSAU method for a large-break LOCA in a Westinghouse four-loop plant. The data have been used to provide insight into and support for the standard plant results developed during the CSAU demonstration. In addition, the data have been used directly to identify and quantify biases that are related to the implementation of selected correlations and models in the code. The UPTF data are of use in quantifying the effect of scale related to similar experiments in reduced-scale facilities and the implementation of specific correlations and models in TRAC-PF1/MOD1.

## ACKNOWLEDGMENTS

The work reported in this paper has been the result of the activities of many individuals. In particular, I acknowledge the considerable contributions of the members of the TPG formed to develop and demonstrate the CSAU method. The members of this group are P. Griffith (Massachusetts Institute of Technology), K. R. Katsma (Idaho National Engineering Laboratory), G. S. Lellouche (S. Levy, Inc.), U. S. Rohatgi (Brookhaven National Laboratory), G. E. Wilson (Idaho National Engineering Laboratory), W. Wulff (Brookhaven National Laboratory), and N. Zuber (United States Nuclear Regulatory Commission). Individuals from Los Alamos National Laboratory contributing to the CSAU effort are P. R. Shire and H. Stumpf.

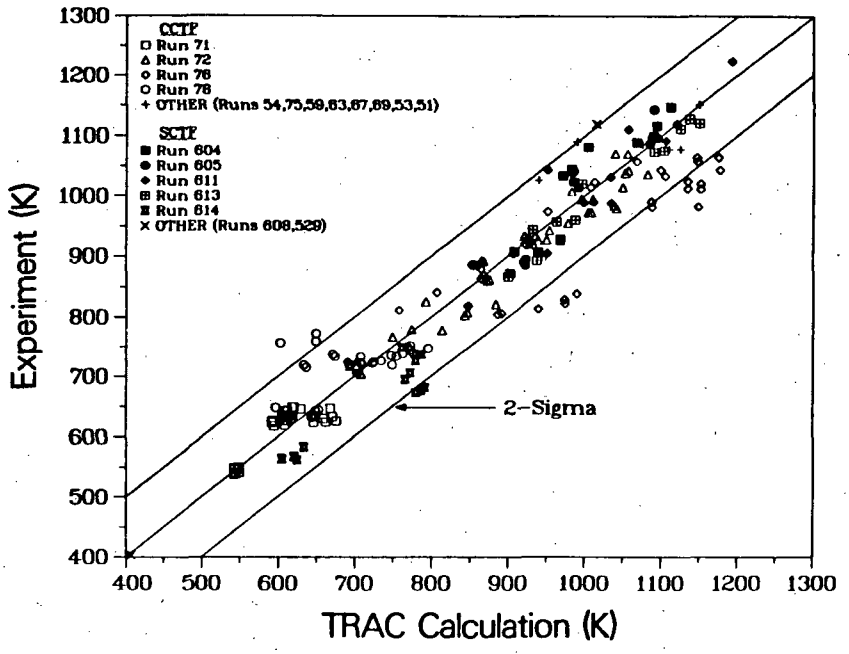


**Fig. 5.**
Comparison of measured and calculated PCTs for SCTF and CCTF tests.

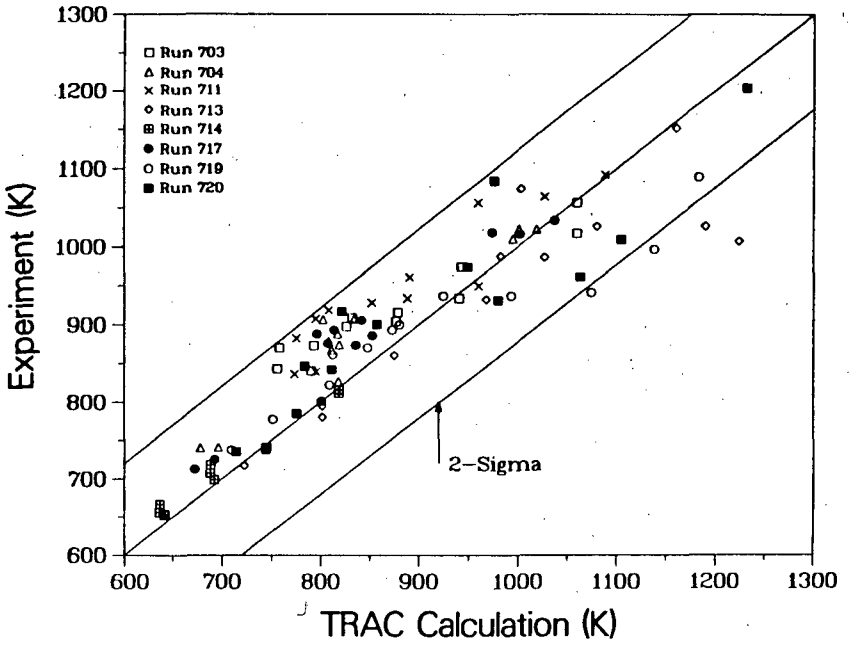


**Fig. 6.**
Comparison of measured and calculated PCTs for eight SCTF Core-III tests.

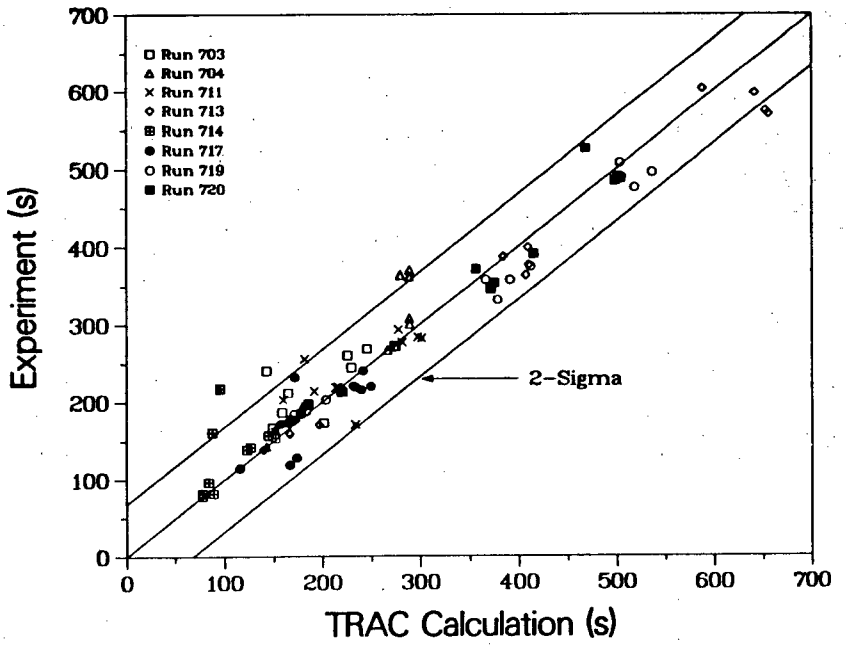


**Fig. 7.**
Comparison of measured and calculated cladding quench times for eight SCTF Core-III tests.

## REFERENCES


1. "Emergency Core Cooling Systems; Revision to Acceptance Criteria," Federal Register (to be published).
2. Safety Code Development Group, "TRAC-PF1/MOD1: An Advanced Best-Estimate Computer Program for Pressurized Water Reactor Thermal Hydraulic Analysis," NUREG/CR-3858 (July 1986).
3. Safety Code Development Group, "TRAC-PF1/MOD1 Correlations and Models," NUREG/CR-5069 (to be issued).
4. R. A. Shaw, T. K. Larsen, and R. A. Dimenna, "Development of a Phenomena Identification and Ranking Table (PIRT) for Thermal-Hydraulic Phenomena During a PWR LBLOCA," EG&G Idaho, Inc., NUREG/CR-5074 (August 1988).
5. F. Motley, "Research Information Report Results from TRAC Analysis of Cylindrical Core Test FAcility Core I Test Series," Los Alamos National Laboratory Group N-9 report LA-2D/3D-TN-86-10 (July 1986).
6. M. W. Cappiello, H. J. Stumpf, and B. E. Boyack, "CCTF Core-II Upper-Plenum Injection TRAC-PF1/MOD1 Analysis Summary," Los Alamos National Laboratory Group N-9 document LA-2D/3D-TN-86-16 (March 1987).
7. K. A. Williams, "Research Information Report on the TRAC Analysis and Experimental Results of the Core I Test Series at the Japan Atomic Energy Research Institute Slab Core Test Facility," Los Alamos National Laboratory document LA-CP-88-52 (March 1988).

8. U. S. Rohatgi, L. Y. Neymotin, and W. Wulff, "PCT Uncertainty from Downcomer Modelling and UPTF Experiments," presentation at TPG meeting held June 9–10, 1988, Campbell California.
9. W. Wulff, "Comparison of TRAC-PF1/MOD1 Calculated PCT Data with CCTF and SCTF Data, Extension of Scatter Diagram 1 (iii) in August 3, 1987 Memorandum from W. Wulff to TPG Members and Consultants," Brookhaven National Laboratory letter to TPG Members, Consultants to TPG (March 31, 1988).

# UPTF EXPERIMENT

## PRINCIPAL EXPERIMENTAL RESULTS

## TO BE USED FOR IMPROVED

## LB LOCA UNDERSTANDING

**P.A. WEISS**

**SIEMENS AG**

**Unternehmensbereich KWU**

**8520 Erlangen, FRG**

Abstract

A series of 21 tests has been performed at UPTF - a 1:1 scale test facility - to investigate the thermohydraulic phenomena in PWR primary systems during blowdown, refill and reflood phases. Based on test results a typical PWR-LOCA scenario applying combined hot and cold leg ECC injection for core cooling is developed. Special attention is given to transient two-phase flow phenomena in the cold legs, downcomer, the tie plate region, upper plenum and hot legs.

## 1. Introduction

The Upper Plenum Test Facility (UPTF) Experimental Program, sponsored by the Ministry for Research and Technology (BMTF) is the German contribution to the trilateral 2D/3D Project, and is performed within international cooperation among Japan (JAERI), USA (USNRC) and the Federal Republic of Germany (BMFT).

The UPTF simulates the primary cooling system of a KWU 1300 MW PWR. The system configuration of UPTF is shown in Figure 1, and major dimensions of the facility are depicted in Figure 2. The upper plenum including internals, the

downcomer and the four connected loops are represented in 1:1 scale. The core is simulated with controlled injection of steam and water supplied from external sources.

The three intact loops are equipped with flow restrictors to simulate the reactor coolant pumps, and with steam/water separators representing the steam generators. The hot and cold legs of the broken loop lead through steam water separators and break valves to the containment simulator. Breaks of variable sizes can be simulated in the hot and in the cold leg as well.

## 2. Objectives and Status of the UPTF Program

The objective of the test program is the full-scale investigation of the three-dimensional single and two-phase flow behaviour in the primary system of a PWR during the end-of-blowdown, refill and reflood phases of a loss-of-coolant accident.

The experimental program includes the simulation of various types of PWR's with different ECC systems as cold leg injection, hot leg injection, simultaneous hot and cold leg injection and downcomer injection. The influence of vent valves on core cooling will also be investigated.

Separate effect and integral tests are being performed to study thermohydraulic phenomena in the upper plenum, across the upper core tie plate, in the downcomer and in the hot and cold legs of the primary system.

According to the internationally agreed test matrix providing for a total of 30 tests, a series of 21 tests has been performed by October 1987. The focus of these tests was on the two-phase flow phenomena

- in the downcomer (4 tests)
- at the upper plenum/core interface (7 tests)
- in the loops - cold and hot side (2 tests)
- in the integral primary system (6 tests)

In addition, 2 tests referring to small break LOCA problems were performed to investigate

- fluid/fluid mixing phenomena in the cold leg and the downcomer area,

- countercurrent flow phenomena in the hot leg under reflux condenser conditions.

Fig. 3 shows ECC injection mode being investigated at UPTF. Three basic injection modes can be distinguished when ECC-water is to be delivered into the core region:

- the cold leg injection to deliver the ECC-water via the cold leg, the downcomer and the lower plenum into the core,

- the hot leg injection, to deliver the ECC-water via the hot leg, the upper plenum and through the upper tie plate into the core,

- the combined injection mode coupling both cold and hot leg injection modes.

These three ECC injection modes determine mostly the areas of interest and the scope of investigation in the UPTF Program. Therefore, principal UPTF experimental results to be used for improved LOCA understanding will be presented in accordance with these areas of interest.

Cold leg ECC injection

A total of 13 test runs has been performed to cover this subject (see Fig. 4). The goal of scaling oriented tests 6 and 7 was to determine a countercurrent flow limitation curve for a full-size PWR downcomer with a realistic geometry and to compare these results with findings from subscale experiments performed at CREARE [1] and BATTELLE [2].

The advantage of full-size downcomers in terms of ECC-water delivery results from strongly heterogeneous countercurrent flow conditions, which can develop to a greater extent in full-size than in subscale geometries.

A first indication of this important feature was given by UPTF Test No. 5 - a cold leg ECC delivery test performed with subcooled ECC injection under blowdown, refill and reflood conditions [3].

The major findings from this test were:

- water plugs were formed in all intact cold legs immediately after start of ECC injection. The water plugs existed throughout the ECC injection period and moved back and forth,

- the ECC delivery to the downcomer was consistent with the water plug movement,

- the test results showed highly heterogeneous conditions in the downcomer (see Fig. 5):

    - a marked immediate local breakthrough and downflow of the subcooled water from cold legs 2 and 3 for both steam and two-phase mixture flow was measured,

    - the subcooled ECC flowing out of cold leg 1 was prevented by the upflowing two-phase mixture from flowing over the shortest path to the lower plenum,

    - a water bypass via the cold leg was observed during the first part of the transient.

Hot side ECC injection

A total of 9 test runs has been carried out to study the flow phenomena at the tie plate for the hot side ECC injection (see Fig. 6).

Test runs with blocked loops provided information about the flow phenomena at the tie plate, when no fluid/fluid interaction in the loops was permitted.

Test No. 12 provided a consistent picture of the breakthrough behaviour at the tie plate, when steam flowed upwards through the tie plate and hot side injected water penetrated the tie plate into the core region [4].

The main findings were:

- immediately after start of ECC injection subcooled water reached the tie plate and started to break through into the core region,

- the breakthrough areas established in front of the ECC injection ports did not change their locations and remained stable (see Fig. 7),

- the tie plate flow area and the core region were split up into a water breakthrough and downflow area near the injecting hot legs and a steam upflow region,

- the fluid temperature measurements near the tie plate indicated strongly subcooled water in the breakthrough areas. A maximum subcooling of more than 70 K was measured.

Test Nos. 13, 15A and 10A provided information about the countercurrent flow limitations at the tie plate, when two-phase flow from the core or saturated ECC conditions were used.

The situation at the tie plate changed substantially, when fluid/fluid interaction at the hot leg injection port was permitted. This information was gained from the group of tests with unblocked loops.

It was observed, that

- the pressure difference between the upper plenum and the downcomer combined with condensation effects at the injection ports caused steam/water countercurrent flow conditions in the intact loop hot legs when ECC-water was injected in both legs,

- the countercurrent flow led to water flow reversal and plug formation in the hot leg; the ECC delivery into the upper plenum was temporarily

interrupted when the water plug was formed and/or moved towards the steam generator simulator,

- after the plug formation was completed a substantial ECC delivery into the upper plenum occured causing extensive breakthrough phenomena at the tie plate.

Combined ECC injection

A group of 3 tests was performed at UPTF to investigate the flow phenomena in a PWR primary system, when combined hot and cold side ECC injection was used, fluid/fluid interaction in all primary system components was permitted and transient conditions (depressurisation from 18 to 4 bar) were applied.

The main findings listed below were derived from UPTF Test No. 18.

- Almost immediately after start of the ECC injection a remarkably effective delivery of ECC-water into the lower plenum and core region was measured (Fig. 8).

- During the end-of-blowdown phase the collapsed water level increase was caused mainly by the hot side injected water.

- During this phase a fraction of the injected water was bypassed via the broken loop nozzle and did not contribute to the refill process in the lower plenum.

Regarding the Cold Leg and Downcomer Region it was observed, that

- after the start of the cold side ECC injection the pipe between injection nozzle and downcomer was completely filled with subcooled water; the ECC water entered the downcomer approximately 7s after start of the ECC injection (Fig. 9),

- owing to oscillations of the water plugs in the cold legs the water delivery into the downcomer was intermittent,

- the water flow in the downcomer can be characterized by the following three phases:

    - the ECC bypass phase, continuing for approx. 9 s after the first water had entered the upper part of the downcomer,

    - the complete delivery phase lasting for 17 s, when the total cold side injected ECC water contributed to the refill process,

    - the downcomer overflow phase, which started 35s after start of the test.

With respect to the Hot Leg and Upper Plenum Region it was observed, that

- the breakthrough zones were located in front of the injecting loops (see Fig. 10),

- the water breakthrough events at the upper tie plate occured intermittently because of the unsteady ECC delivery from the hot legs,

- these breakthrough processes were not stopped even when the core simulator feedback system increased the steam injection substantially.

References

[1] Crowley C.J. et al. - 1/5-Scale Countercurrent Flow Data Presentation and Discussion; NUREG/CR-2106, Creare, Jnc.

[2] Seger A., Collier R. P. - Development of a Mechanistic Model for ECC Penetration in a PWR Downcomer; NUREG/CR - 1426 BMI-2051, Battelle Columbus Laboratories

[3] Hertlein R.J., Weiss P.A. - PWR Downcomer Countercurrent Flow under Steam of Two-Phase Upflow Conditions, 15th Water Reactor Safety Information Meeting, Gaithersburg, Maryland, October 1987

[4] Weiss P.A., Hertlein R.J. - UPTF Test Results: First Three Separate Effect Tests, Nuclear Engineering and Design 108 (1988) 249 - 263.

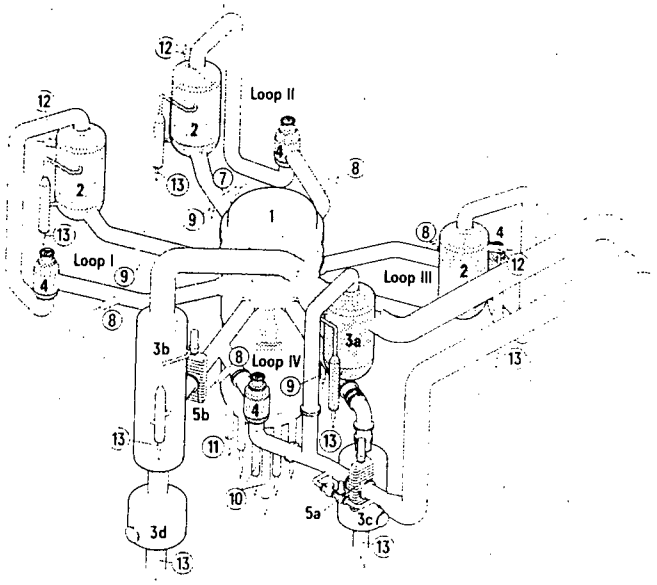


1 Test Vessel
2 Steam Generator Simulator (Intact Loop)
3a Steam Generator Simulator/ Water Separator (Broken Loop Hot Leg)
3b Water Separator (Broken Loop Cold Leg)
3c Drainage Vessel for Hot Leg
3d Drainage Vessel for Cold Leg
4 Pump Simulator
5a Break Valve (Hot Leg)
5b Break Valve (Cold Leg)
6 Containment Simulator

(7) Surgeline-Nozzle
(8) ECC-Injection Nozzles (Cold Leg)
(9) ECC-Injection Nozzles (Hot Leg)
(10) Core Simulator Injection Nozzle
(11) TV-Drainage Nozzle
(12) Steam Injection Nozzle
(13) Drainage Nozzle

Simulator

## Upper Plenum Test Facility-Primary System

86 PWR 039e
UB KWU

SIEMENS

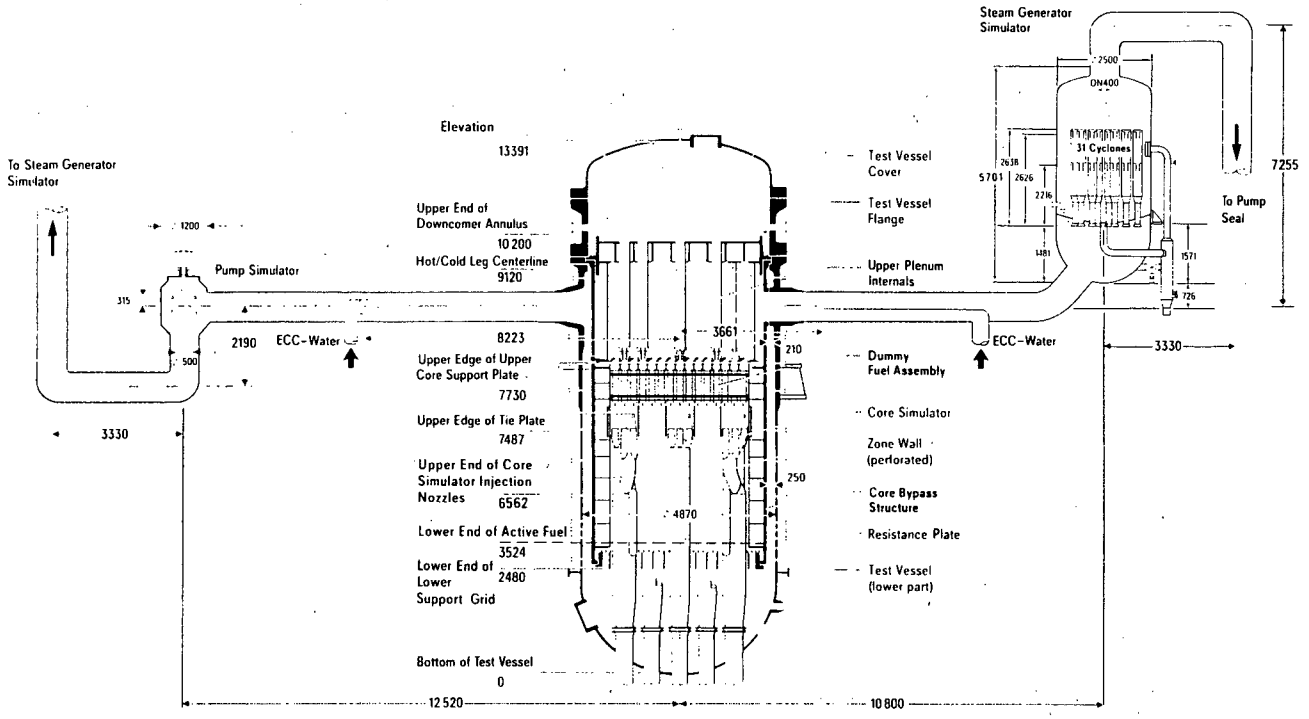


## Fig. 2 Major Dimensions of UPTF-Primary System



86 PWR 036e
UB KWU
a

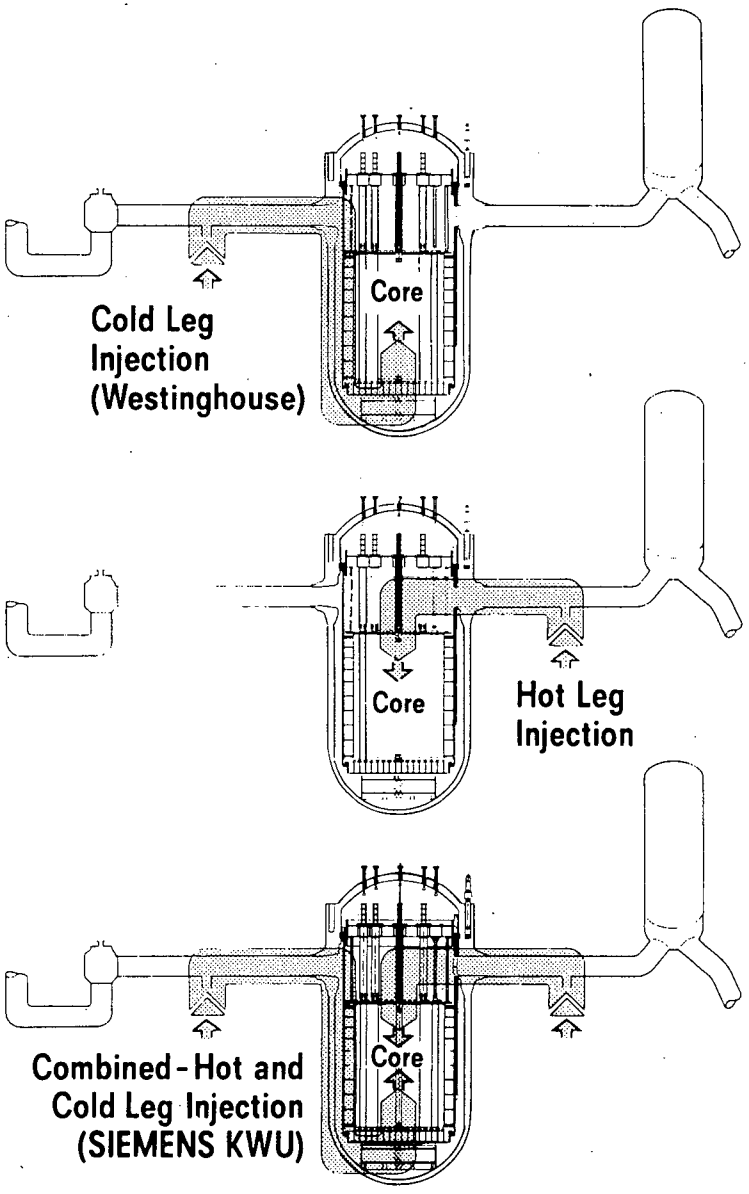


-551-

Fig. 3 UPTF-ECC Injection Modes being Investigated

88 PWR 112e
UB KWU

SIEMENS

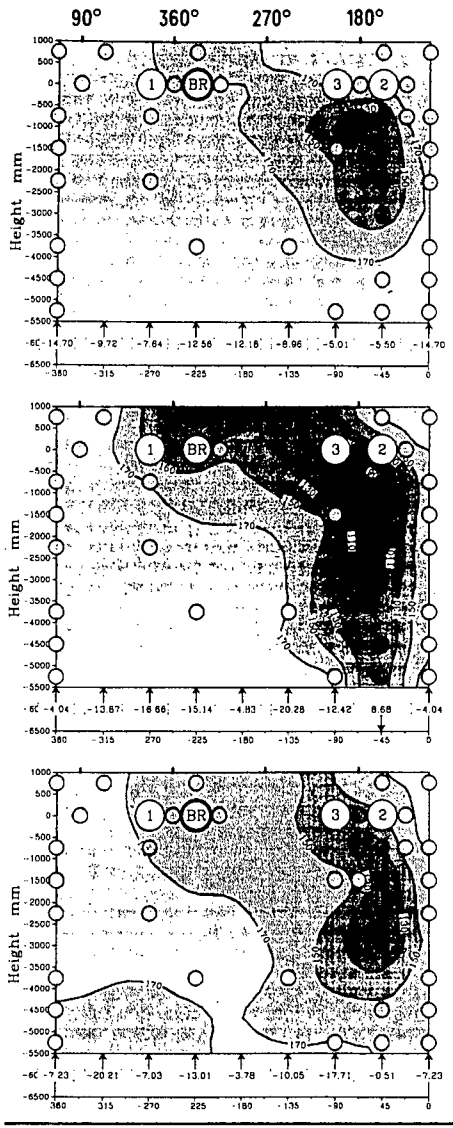


UPTF Test RUN 063 Downcomer CCF

Data averaged over 0.10 sec

x.xx

Turbine meter linear velocity [m/s]

Fluid temperature [°C]

Above 210
190 - 210
170 - 190
150 - 170
130 - 150
110 - 130
90 - 110
70 - 90
50 - 70
30 - 50
10 - 30
Below 10

Offset from DAS start: 32 sec

- Water downflow below cold legs 2 and 3

Offset from DAS start: 33 sec

Offset from DAS start: 34 sec

- No ECC delivery out of cold legs

Fig. 5: Contour Plots of Fluid Temperature Distribution in Downcomer (Test Phase A)

88 PWR 351
UB KWU

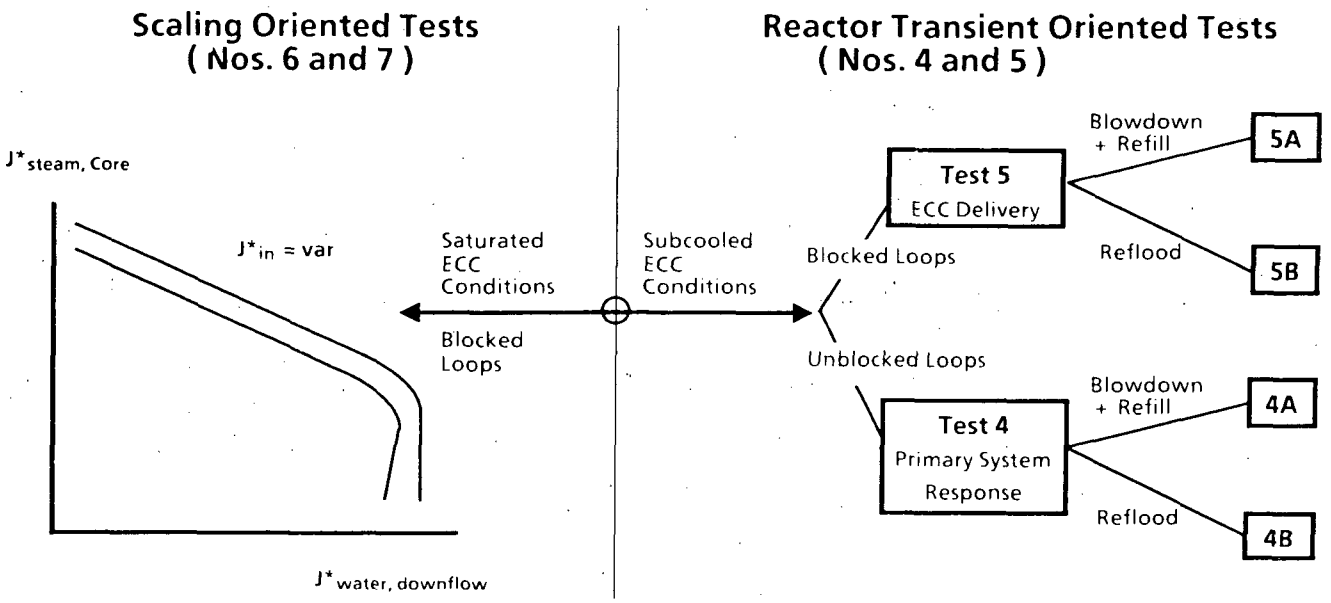


Fig.4: UPTF - Downcomer Separate Effects Tests ( Total of 13 Test Runs )

SIEMENS

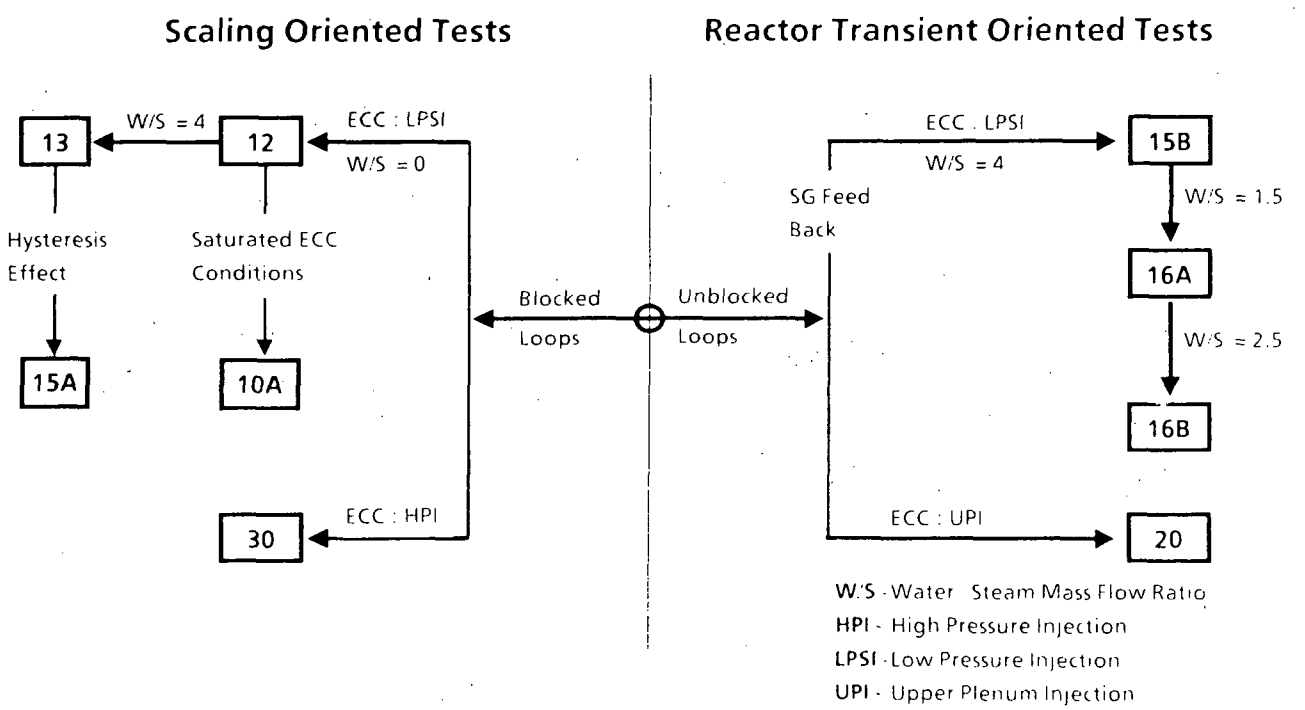


Fig 6: UPTF - Tie Plate Separate Effects Tests ( Total of 9 Test Runs )

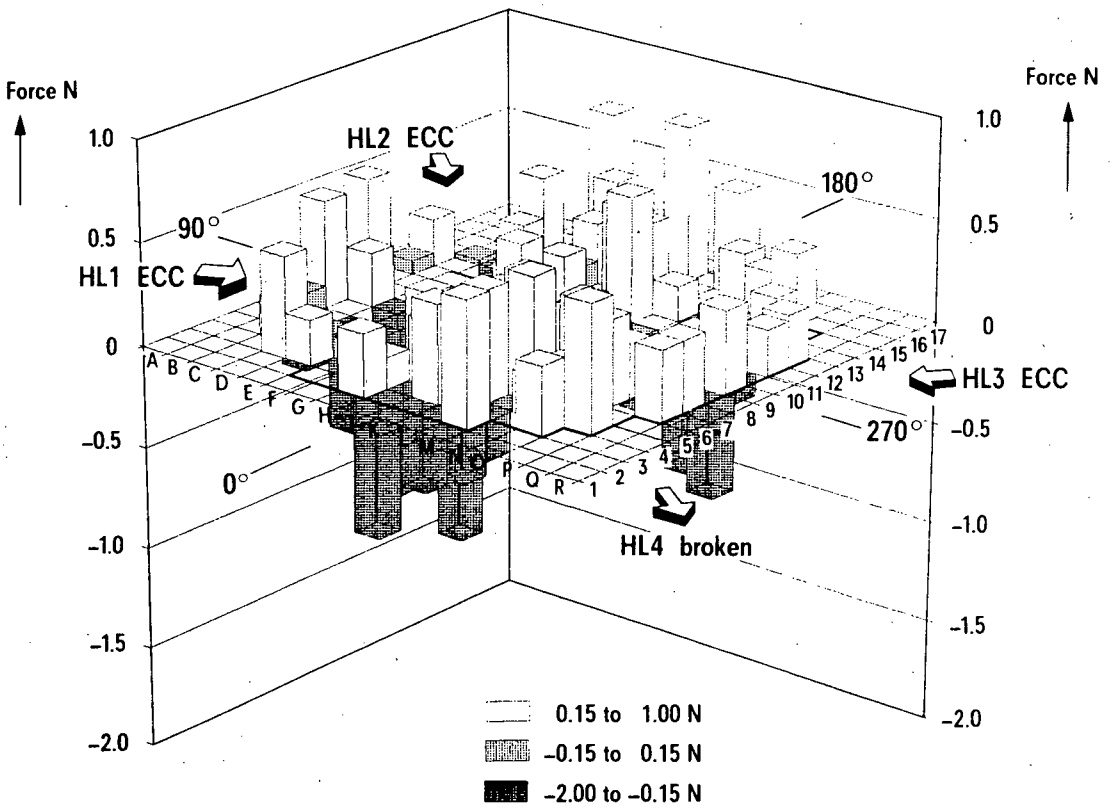


Fig. 7a **UPTF Test No. 12 (RUN 014) – Discrete Values of Corrected BTD Forces at 200 s**
(Set Tieplate JKF = 0 JNG = 1200 QH/. 05 = 45 kg/s)

86 PWR 088e
UB KWU



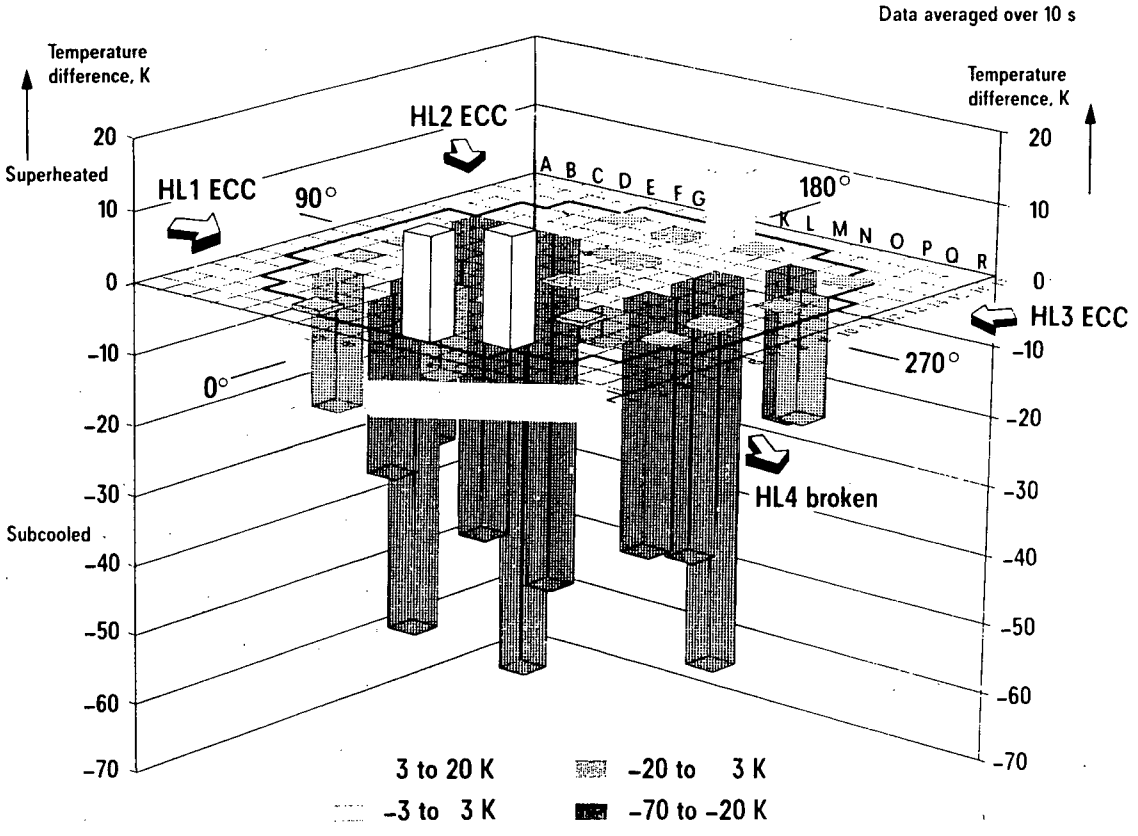


Fig.7b **UPTF Test No. 12 (RUN 014) – Discrete Values of Fluid Temperatures 10 mm below Tie Plate at 200 s**

86 PWR 090e
UB KWU

UPTF TEST RUN 169
INTEGRAL TEST 2A-BREAK 2HL+3CL ECC INJ.

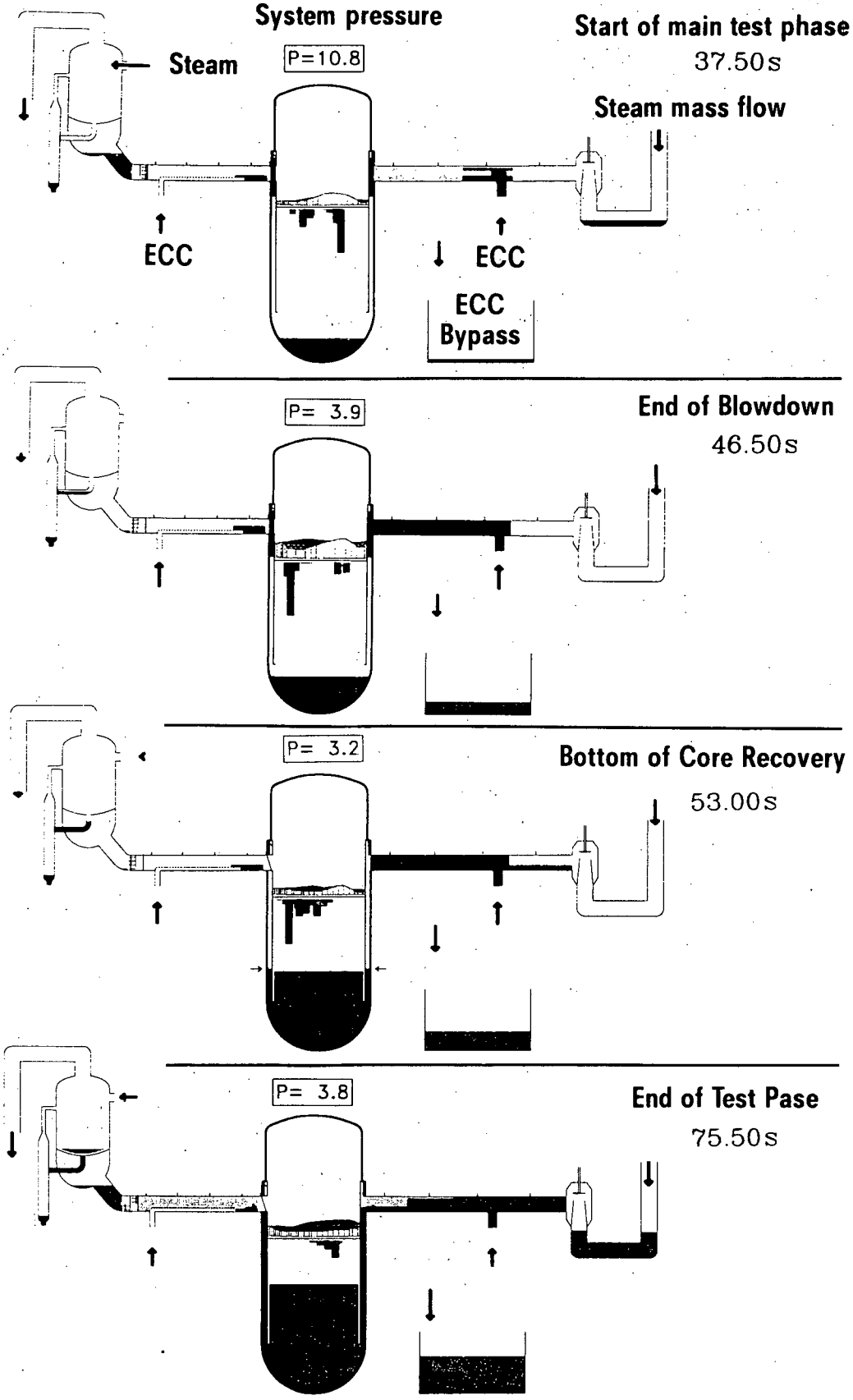


**Fig. 8 UPTF Test 18 – Overall System Behaviour**

88 PWR 341
UB KWU

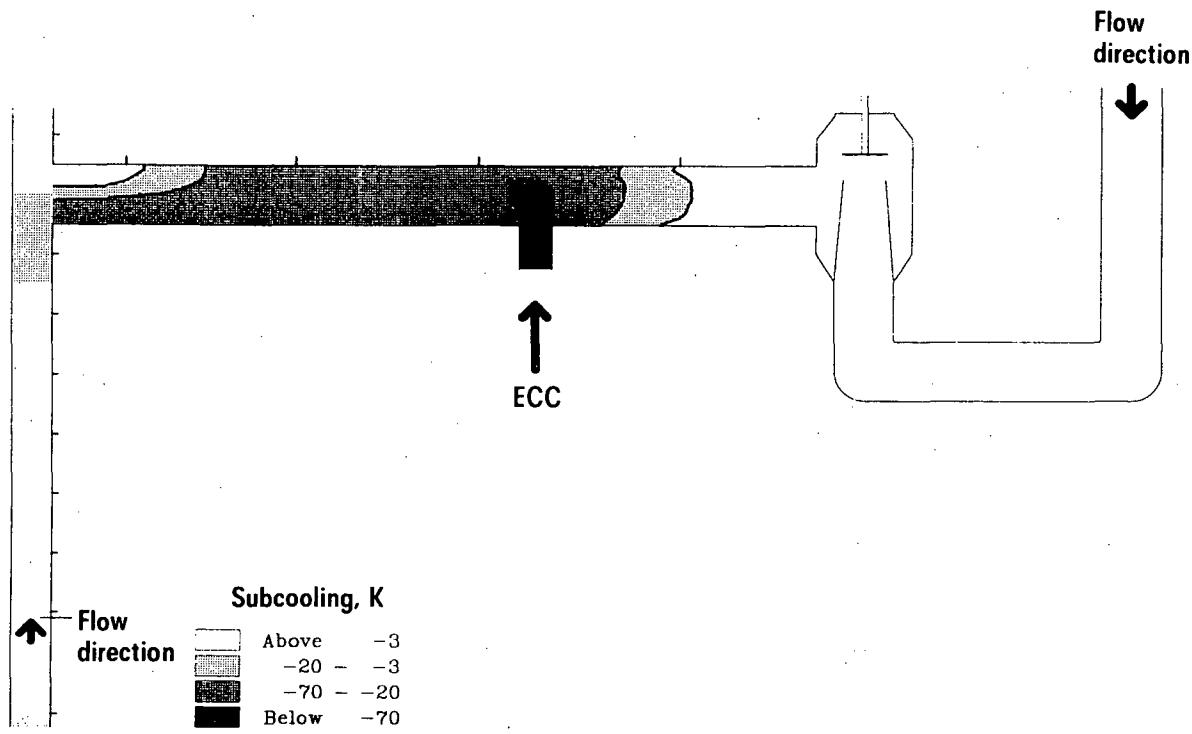


**Fig. 9 UPTF Test 18 – First Water Delivery from Cold Leg to Downcomer**

88 PWR 340
UB KWU



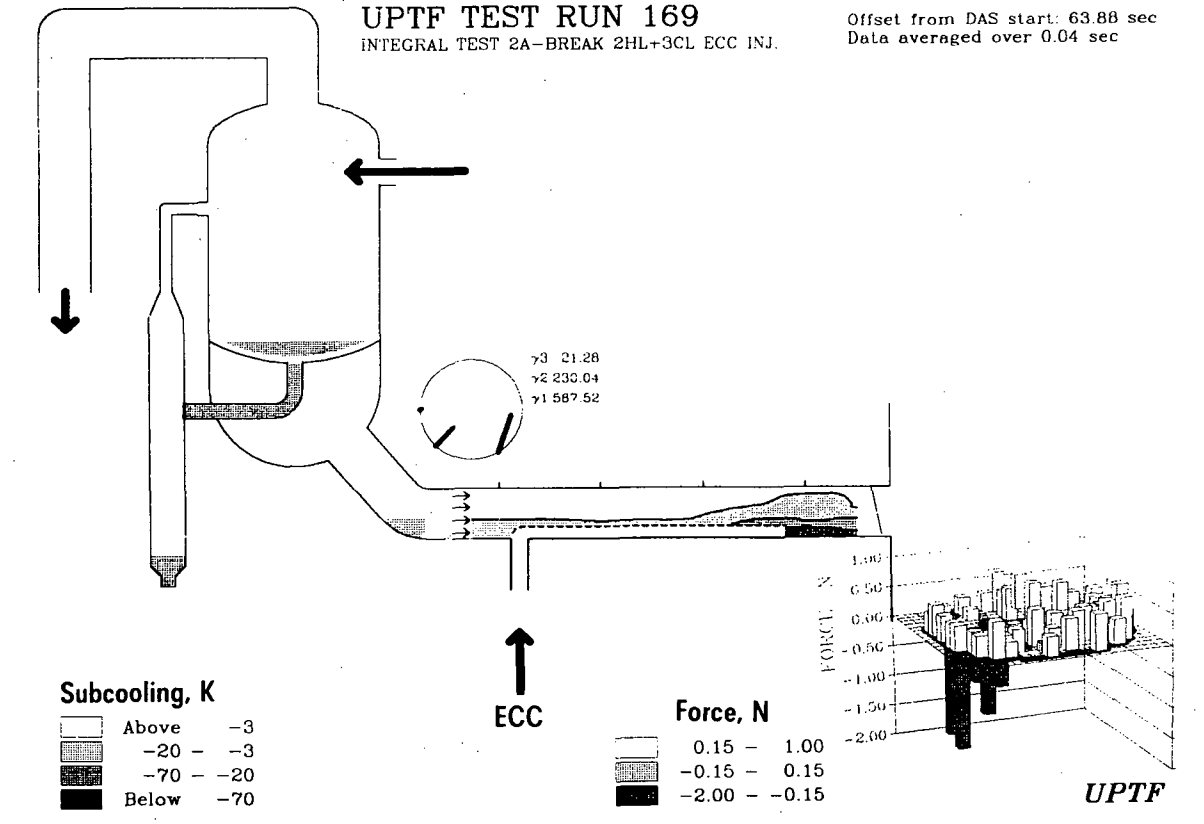


**Fig. 10 UPTF Test 18 – Flow Phenomena in Hot Leg and Tie Plate Area**

88 PWR 339
UB KWU

# Recent results of analytical study on SCTF-III tests for reflood phenomena of PWR with combined-injection-type ECCS under cold-leg-large-break LOCA

T. IGUCHI, H. ADACHI, J. SUGIMOTO, T. IWAMURA, H. AKIMOTO,
T. OKUBO, A. OHNUKI, Y. ABE, M. KIKUTA, Y. MURAO

Japan Atomic Energy Research Institute

Abstract

The reflooding behavior in a PWR with a combined injection type ECCS was studied based on test results with Slab Core Test Facility (SCTF). Important phenomena for core cooling were physically analyzed. They are flow circulation in pressure vessel, condensation in upper plenum, heat transfer from two-hase upflow region to water downflow region and heat transfer coefficient in two-phase upflow region. Based on these analyses, the clad temperature transient was successfully predicted. This supports the validity of the phenomenological understanding obtained in the present study.

## 1. Introduction

A reflood test program(1) for a large break loss-of-coolant accident (LOCA) of pressurized water reactor (PWR) has been conducted at Japan Atomic Energy Research Institute (JAERI), by using large scale test facilities, which are the Cylindrical Core Test Facility (CCTF) and the Slab Core Test Facility (SCTF). Thisprogram has been in a part of 2D/3D project performed by the cooporation among USNRC, BMFT in Federal Republic of Germany and JAERI.

The main objective of the CCTF tests is to study overall thermal hydraulics in primary system of PWRs during reflood phase. Therefore, the CCTF was designed to have a well-simulated primary system.

The main objective of the SCTF tests is to study two-dimensional effect on thermal hydraulics during reflood phase, especially in the core with full radius. Therefore, the SCTF was designed to have a full-height, full-radius and one-bundle width core and to be equipped with many kinds of instruments (clad temperature, fluid temperature, differential pressure and so on) distributed two-dimensionally in the pressure vessel.

The SCTF Core-I and Core-II test series have been performed and completed by July, 1985. In these tests, the reflood phenomena in PWRs with cold-leg-injection-type emergency core cooling system (ECCS) have been studied. Through the study, it
hasbeen demonstrated(2) that the heat transfer in high power bundles is enhanced due to the two-dimensional effects.

---

The work was performed under contract with the Atomic Energy Bureau of Science and Technology Agency of Japan.

Since January 1986, the SCTF tests with Core-III (SCTF-III tests) have been performed under the condition of PWRs with the cold-leg-injection-type and the combined-injection-type ECCSs. The main objectives of the SCTF-III tests for PWRs with the combined-injection-type ECCS are

(1) to attain physical understanding on reflood phenomena,
(2) to establish a quantitative prediction method for core cooling, and
(3) to provide data for coupling between the SCTF and the UPTF(9) and for verifying best-estimate analytical codes, for example TRAC code(5). In the following, the recent results of analytical study on SCTF-III tests for reflooding phenomena of PWRs with the combined-injection-type ECCS are presented.

## 2. Description of SCTF-III

### 2.1 Facility

The SCTF was originally designed to study two-dimensional effect on thermal hydraulics during reflood phase, especially in the core of full radius. Therefore, the SCTF has a slab shaped core of full-height, full-radius and one-bundle width. The core flow area scaling ratio against the typical 1300 MWe class PWRs is 1/22.

The flow diagram of the SCTF is shown in Fig. 1. The SCTF is simulating a 200 % cold-leg-large-break with a simplified primary system and can be operated at less than 0.6 MPa. It consists of the slab core with electrically heated rods, one hot leg, one intact loop, one steam-generator-side broken loop and one pressure-vessel-side broken loop. A steam/water separator in the SCTF simulates the steam generators in PWRs. The valves shown by V1 and V2 simulate a 200 % cold-leg-large-break.

The pressure vessel consists of upper plenum, core, lower plenum and downcomer, as shown in Fig. 1. Fuel rods are simulatedby heater rods in the core in the arrangement of eight 16x16 bundles. The dimension of a heated rod is 10.7 mm in diameter and 3613 mm in heated length, identical to a PWR one. The axial peaking factor of the heated rod is 1.39. The maximum available power for the heated rods is 10 MW.

### 2.2 Test method

The initial set-up of the SCTF for testing is shown in Fig. 1. Prior to a test, the valves (V1 and V2) are closed and the pressure vessel are pressurized with saturated steam. Heating power is supplied to heated rods. When the clad temperature of the heated rods reaches a specified value, the valves are opened.Thus, the blowdown behavior is simulated. The ECC water injection system is activated and the heating power starts to simulate decay heat.

The ECC water is injected into both the cold leg and the upper plenum in the SCTF, although it is injected into both the coldleg and the hot leg in PWRs.

By analyzing the UPTF data, it has been found that the ECC water from

the hot legs falls down locally in the concentrated regions from the upper plenum to the core and the ECC water is heated up in the upper plenum and the hot legs. Hence in the SCTF, the ECC water was injected radially ununiformly in the concentrated region into the upper plenum. The ECC water temperature was varied in each test to cover the temperature observed in the UPTF tests.

Figure 2 shows a test sequence of a typical SCTF test performed for simulating evaluation model condition, and Table 1 showsthe values of the test conditions.

## 3. Summary of test results

### 3.1 Major observed phenomena in pressure vessel(3)(4)

Figure 3 illustrates(3) the thermal hydraulic behavior in theprimary system, especially in pressure vessel, which has been derived from SCTF and CCTF test results. Two thermo-hydrodynamically different regions, i.e. water downflow region and two-phase upflow region, were identified in the core. In the water downflow region, the subcooled water flowed downward from the upper plenum to the core bottom. On the other hand, in the two-phase upflow region, the two-phase mixture flowed upward from the core bottom to the core top.

The water in the upper plenum flowed down to the core in locally concentrated region, i.e. water downflow region. The flow circulation was established in the pressure vessel due to the region separation mentioned above. The flow circulation increased the upward water flow rate in the two-phase upflow region.

The condensation mostly occurred in the upper plenum. This then increased the temperature of the water flowing down from the upper plenum into the water downflow region.

The water in the water downflow region can be possiblly heated up due to the heat release from the rods in the water downflow region as well as due to the heat transfer from the two-phase upflow region.

Figure 4 shows the clad temperature and the quench front propagation in both the water downflow and two-phase upflow regions. It is observed that in the water downflow region the significantly quick quenching occurred along the entire elevation of thecore while in the two-phase upflow region the rather slow bottomquenching occurred dominantly along the most elevation of the core. The maximum clad temperature is realized in the two-phase upflow region.

### 3.2 Physical investigation on major phenomena

(1) Flow circulation

Figure 5 shows the water downflow rate and the steam upflow rate between the upper plenum and the core across the entire cross section, which are measured with drag-body-flow-modules. Two tests were conducted with different temperatures of water flowing down from the upper plenum (cold water test and hot water test). When the steam upflow rate is high enough,

the water downflow rate is small, as observed in the first short period of the reflood phase. Generally after this short period, the water downflow rate increases and then gradually decreases. However in some case of the hot water test, the water downflow rate sometimes becomes nearly zero, as observed between 100 s and 150 s of hot water test. Since in this case the small steam upflow rate was detected even in the water downflow region, it is considered that the flow circulation is restrained if the uncondensed steam flows up in the water downflow region. Anyway, during most period the flow circulation continues.

Figure 6 shows the model for the prediction of the water downflow rate. This model (Prediction 1) is based on the natural convection due tothe density difference between the water downflow region and the two-phase upflow region. It is assumed that the water downflow region is filled with water. Figure 7 shows one example of the comparison between the measured and predicted water downflow rates. The prediction gives good agreement with the measurement for the later period. For the early period, the prediction is larger than the measurement and some modification is needed for a good prediction.

According to gamma ray densitometer installed at point A shown in Fig. 6 (3.2 m elevation in core), the density is 250-750 $kg/m^3$ until 65 s after reflood initiation and it is above 900 $kg/m^3$ after 70 s for the test shown in Fig. 7. From these data, it is considered that the water downflow region is almost filled with water after 70 s, when the prediction 1 gives good result. Before this time, however, it cannot be assumed that the water downflow region is filled with water. For such case, the water in the water downflow region can probably not support the water in the upper plenum, and therefore we assumed that the water in the upper plenum could flow down without any restriction. Based on this assumption (no restriction of water downflow), the water downflow rate was alternatively predicted. This prediction (Prediction 2) gives good agreement for early period as shown in Fig. 7.

(2) Condensation in the upper plenum

Figure 8 illustrates the upper plenum thermal hydraulic behavior, which has been derived from the SCTF and CCTF test results. Four thermal-hydraulically differnt regions were formed in the upper plenum, that is, the subcooled water pool, the saturated water pool with void, the steam flow region with saturated water droplets and steam flow region with subcooled water droplets.

The SCTF simulates the hot leg injection of PWRs by two injection systems, which inject ECC water into the top of the pressure vessel and into just above the upper core support plate. The SCTF test results showed that the efficiency of the condensation by ECC water injected from the top of the pressure vessel into steam flow was very high, on the other hand, the direct condensation by the ECC water injected into the water pool just above the water falling region was very small, and the condensation in the water pool was also high in the subcool area spreading over the water falling region shown by shadow in Fig. 8. These were lead from the result of the following calculation.

The total condensation in the upper plenum was calculated by the sum of the steam mass condensed by the subcooled ECC water injected into the steam

flow and the steam mass condensed in the subcooled water pool spreading over the water falling region. The former was calculated by assuming that the condensation efficiency by ECC water in steam flow was 1.0. The latter was calculated by assuming that steam flowing into the subcool pool condenses completely.

The comparison of condensation mass rate in the upper plenum between the above calculation and the mesurement results are shown in Fig.9. Good agreement of the calculation and the measurement resuls is obtained. This indicates that above mentioned overall behavior of condensation in the upper plenum is reasonable (High efficient condensation by ECC water in steam flow and also high efficient condensation of steam flowing into subcool water pool).

(3) Heat transfer from two-phase upflow region to water downflow region

Figure 10 shows the steam upflow rate from the two-phase upflow region to the upper plenum and the condensation rate of steam flowing from the two-phase upflow region to the water downflow region. They were obtained from direct measurement and energy balance calculation. The latter is very little in comparison with the former. Therefore, it is considered that the steam generated in the two-phase upflow region condensed little in the water downflow region.

Figure 11 shows the experimental data of the heat released from the rods in the water downflow region and the heat transferred from the two-phase upflow region to the water downflow region. Again the latter is little in comparison with the former.

From the above result, it is concluded that the temperature increase of the water in the water downflow region is evaluated only with the heat released from the rods in the region and the effect of the thermal interaction between the two-phase upflow region and the water downflow region is negligible.

Based on the above findings, the water temperature at the core bottom of the water downflow region was predicted. The prediction gives a fairly good agreement with the measurement as shown in Fig. 12.

(4) Heat transfer coefficient in two-phase upflow region

Murao et al. developed the heat transfer correlation(6) for reflood phase of a PWR with cold-leg-injection-type ECCS. It is not successful to predict the heat transfer coefficient in the two-phase upflow region with this correlation as shown in Fig. 13. The reason of unsuccessful prediction is probably due to high core flooding rate because the applicable range of the correlation for flooding velocity is too low for the PWR with the combined-injection-type ECCS.

Ohnuki modified the correlation for the condition under the high flooding velocity(7). The modified correlation gives good predicion as shown in Fig. 13.

## 4. Prediction on thermal hydraulics in two-phase upflow region

### 4.1 Schematic of prediction method

Using the above results (1) through (4) of Section 3.2 and additionally REFLA code(8), the prediction of the thermal hydraulics inthe two-phase upflow region was performed. Figure 14 shows the adopted schematic of the prediction method. The core was assumed to consist of two volumes (water downflow region and two-phase upflow region) and the interaction between two regions concerning mass, momentum, and energy transfer was assumed to be negligible.

In this prediction, the thermal hydraulics in the pressure vessel are focussed. Hence, the following parameters were selected to be the input boundary conditions, i.e. the flow rate and temperature of water injected into the upper plenum, the backpressure at the break point and the mass flow rate from the lower plenum to the downcomer, as shown in Fig. 15.

In addition, the simplicity shown in Fig. 15 was used based on the results indicated in (1) through (4) of Section 3.2.

### 4.2 Predicted result

Figure 16 shows the predicted and the measured clad temperatures in two-phase upflow region. The prediction gives a good agreement with the SCTF data except after 80 s in SCTF Run 722, in which atypically hot water was injected into the upper plerum.

Figure 17 shows the predicted and the measured core flooding rates at core bottom of the two-phase upflow region. Prediction gives a good agreement with the measurement in cold water test (SCTF Run 717). However the prediction is larger than the measurement after 80 s of hot water test (SCTF Run 722). This causes the lower clad temperature in two-phase upflow region shown in Fig. 16.

Thus, although in hot water case further improvement is neccessary for the better prediction of clad temperature transient, the thermal hydraulics in two-phase upflow region are successfully predicted. This supports the validity of the phenomenological understanding in Section 3.2.

## 5. Conclusion

Through this study, the following findings were obtained concerning the thermal hydraulics during the reflooding phase in the pressure vessel of PWRs with combined-injection-type ECCS.

(1) Flow circulation was predicted with a model based on no restriction for water downflow and/or density difference between the water downflow region and the two-phase upflow region.

(2) The amount of condensed steam in upper plenum was nearly equal to the sum of condensibilities of ECC water injected into steam flow and steam flowing into subcooled water pool on upper core support plate.

(3) Heat transfer from the two-phase upflow region to the waterdownflow region was negligible. Water temperature increase from the top to the bottom of the core in water downflow region was well predicted by only taking into account of heat release from rods in water downflow region to the water.

(4) Heat transfer coefficient in the two-phase upflow region was higher than that obtained in cold-leg-injection ECCS. The heat transfer coefficient was predicted well by Murao-Sugimoto correlation modified by Ohnuki.

The thermal hydraulics in the two-phase upflow region were successfully predicted with the present models. This supports the validity of the phenomenological understanding obtained in the present analyses.

References

(1) K. Hirano, Y. Murao; J. At. Ener. Soc. Japan, 22 (10), 681 686 (1980)
(2) H. Adachi, et al.; 15th WRSI Mtg. (1987)
(3) T. Iguchi, et al.; 14th WRSI Mtg. (1986)
(4) Y. Murao, et al.; 15th WRSI Mtg (1987)
(5) B. E. Boyack, et al.; 15th WRSI Mtg. (1987)
(6) Y. Murao, J. Sugimoto; J. Nucl. Sci. Technol., 18(4), 275 284 (1981)
(7) A. Ohnuki; Private communication
(8) Y. Murao, et al.; JAERI-M 84-234(1984)
(9) P. A. Weiss, R. J. Hertlein; 15th WRSI Mtg. (1987)

Table 1. Test condition of a typical SCTF test performed for simulating evaluation model condition

| Item | Value |
|---|---|
| Pressure (MPa)<br>Containment tanks<br>Pressure vessel (Initial) | <br>0.3<br>0.6 |
| Power<br>Initial power (MW)<br>Power decay curve<br>Time after scram (s)<br>Radial power profile | <br>7.5<br>ANS·1.03 + Act.<br>25<br>Uneven*1 |
| Clad temperature (K)<br>(Peak at ECC start) | <br>973 |
| ECC water inj. location | CL / UP*3 |
| Cold leg injection<br>ECC injection rate (kg/s)<br>ECC temperature (K) | <br>Transient*4<br>308 |
| Upper plenum injection<br>ECC injection rate (kg/s)<br>ECC temperature (K) | <br>Transient*5<br>308 |
| Initial water level (m)<br>(Lower plenum) | <br>0.4 |

*1 Bundle power ratio : 1.04:1.08:1.08:1.04:1.04:1.04:0.97:0.71
(Bundle 1~8)

*2 Cold leg

*3 Upper plenum

*4 3·Acc+2.6·LPCI

*5 2·Acc+1.4·LPCI

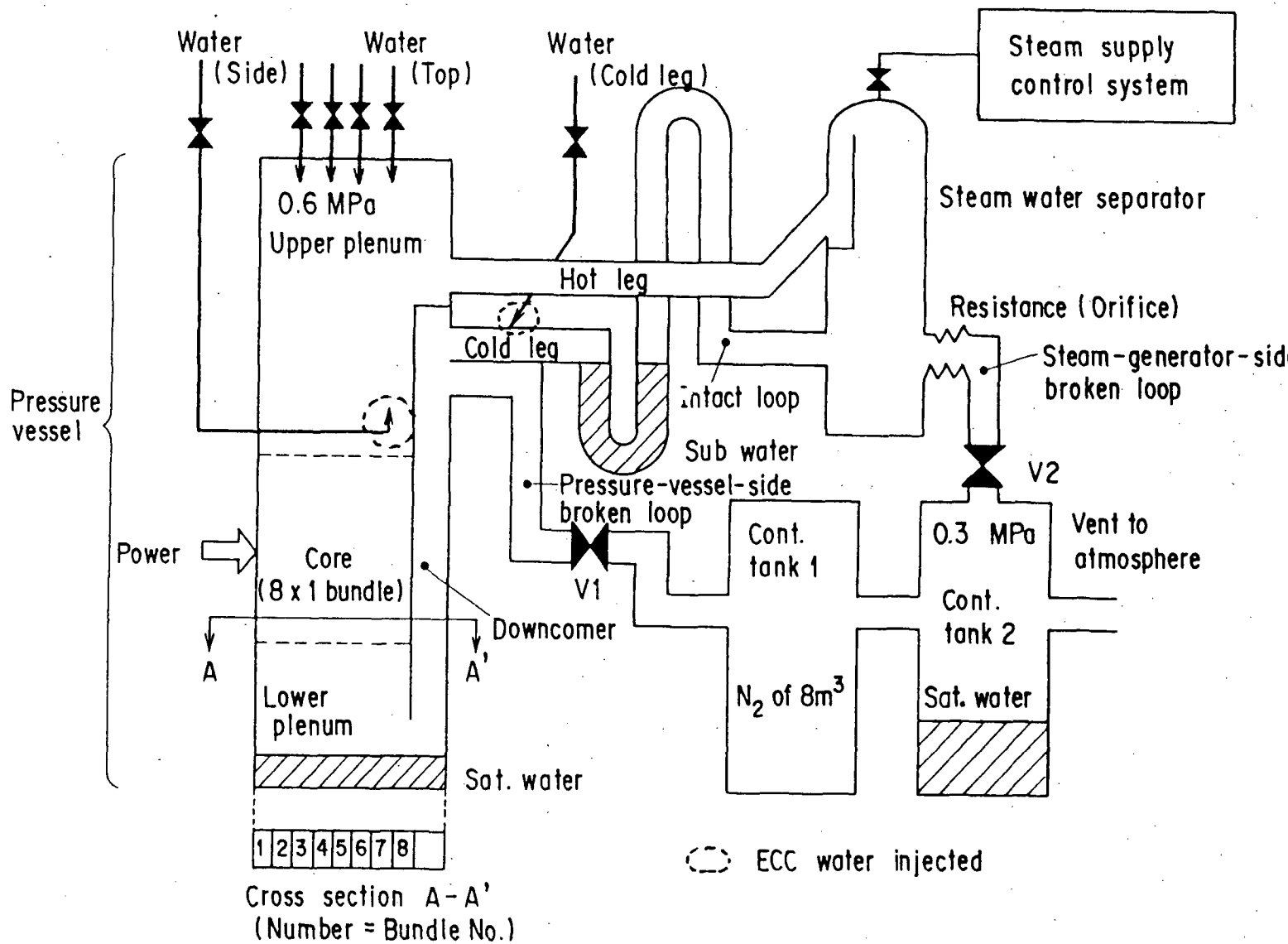


Fig. 1 Flow diagram and initial set-up of a typical SCTF test

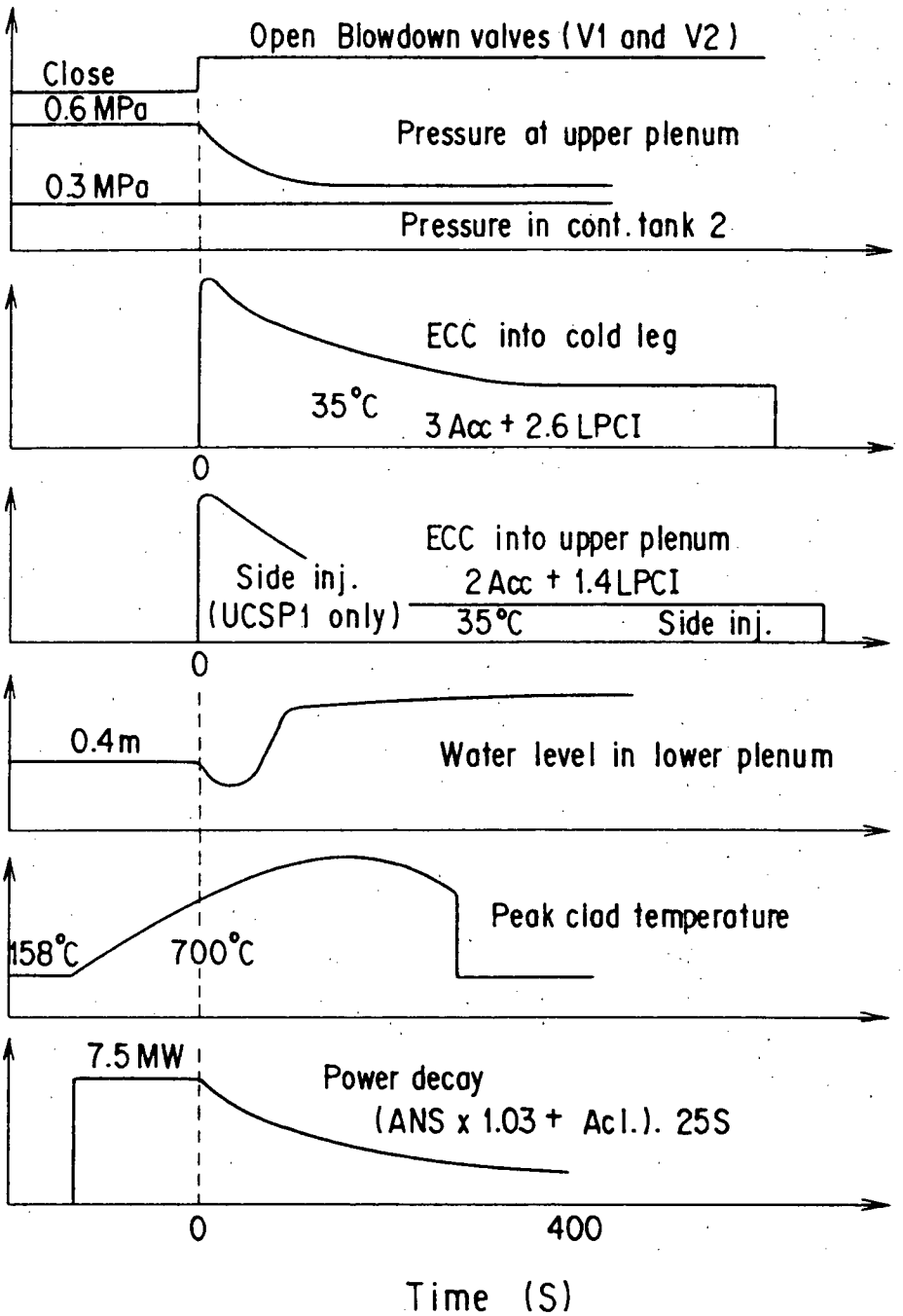


Fig. 2 Test sequence of a typical SCTF test

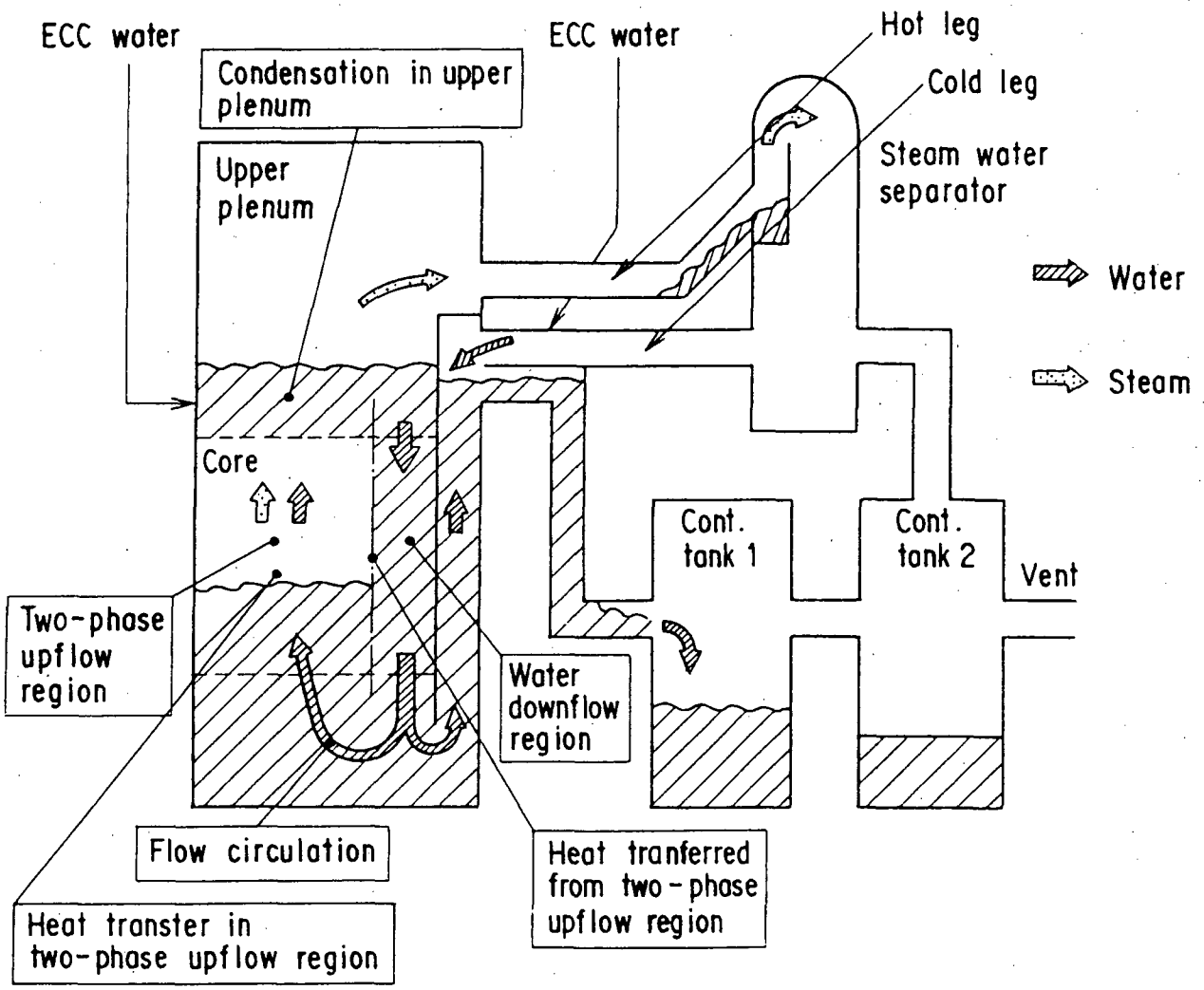


Fig.3 Illustration on thermal hydraulic behavior in primary system derived from SCTF and CCTF test results

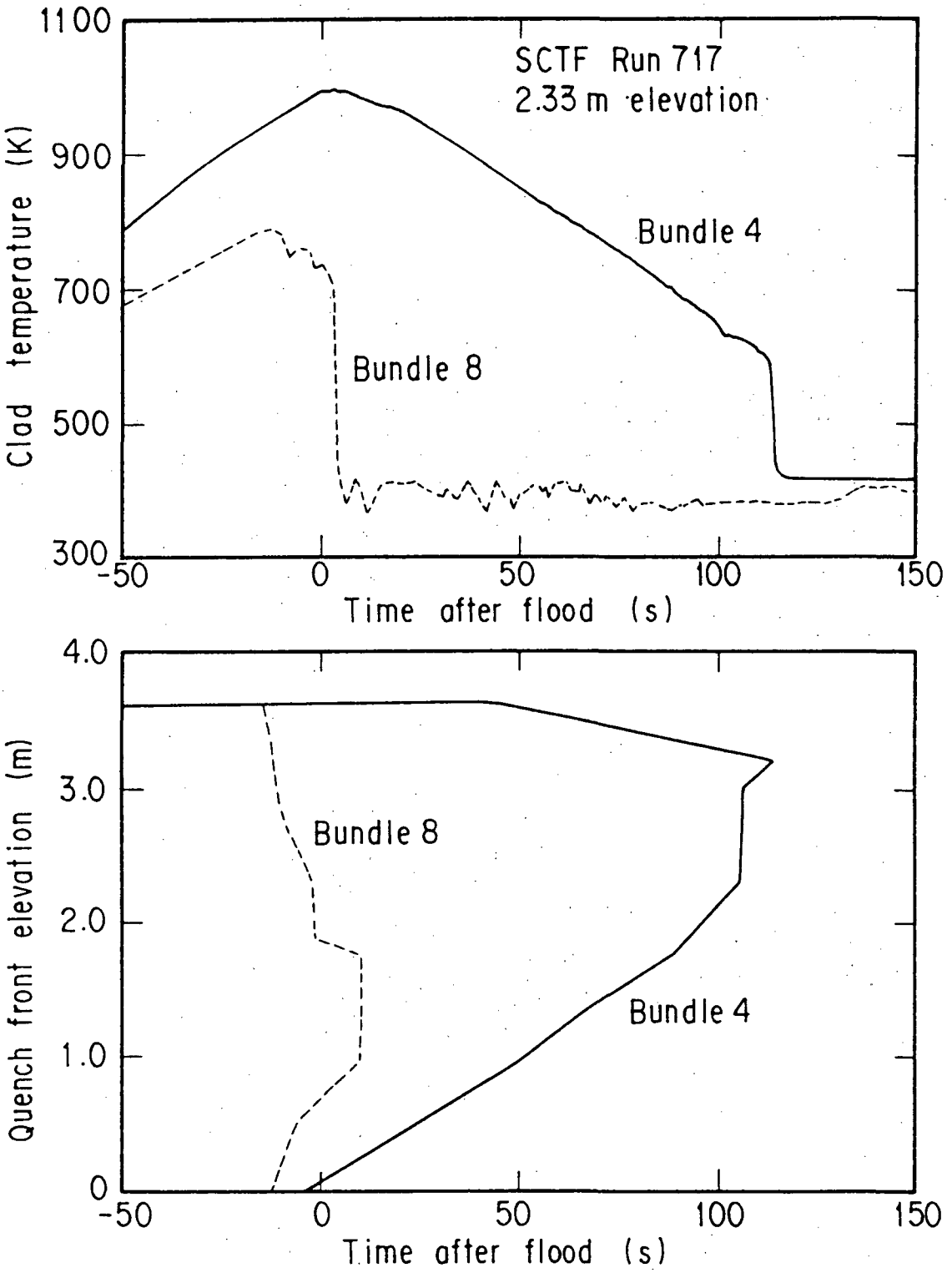


Fig. 4 Clad temperature and quench front propagation in water downflow and two-phase upflow regions

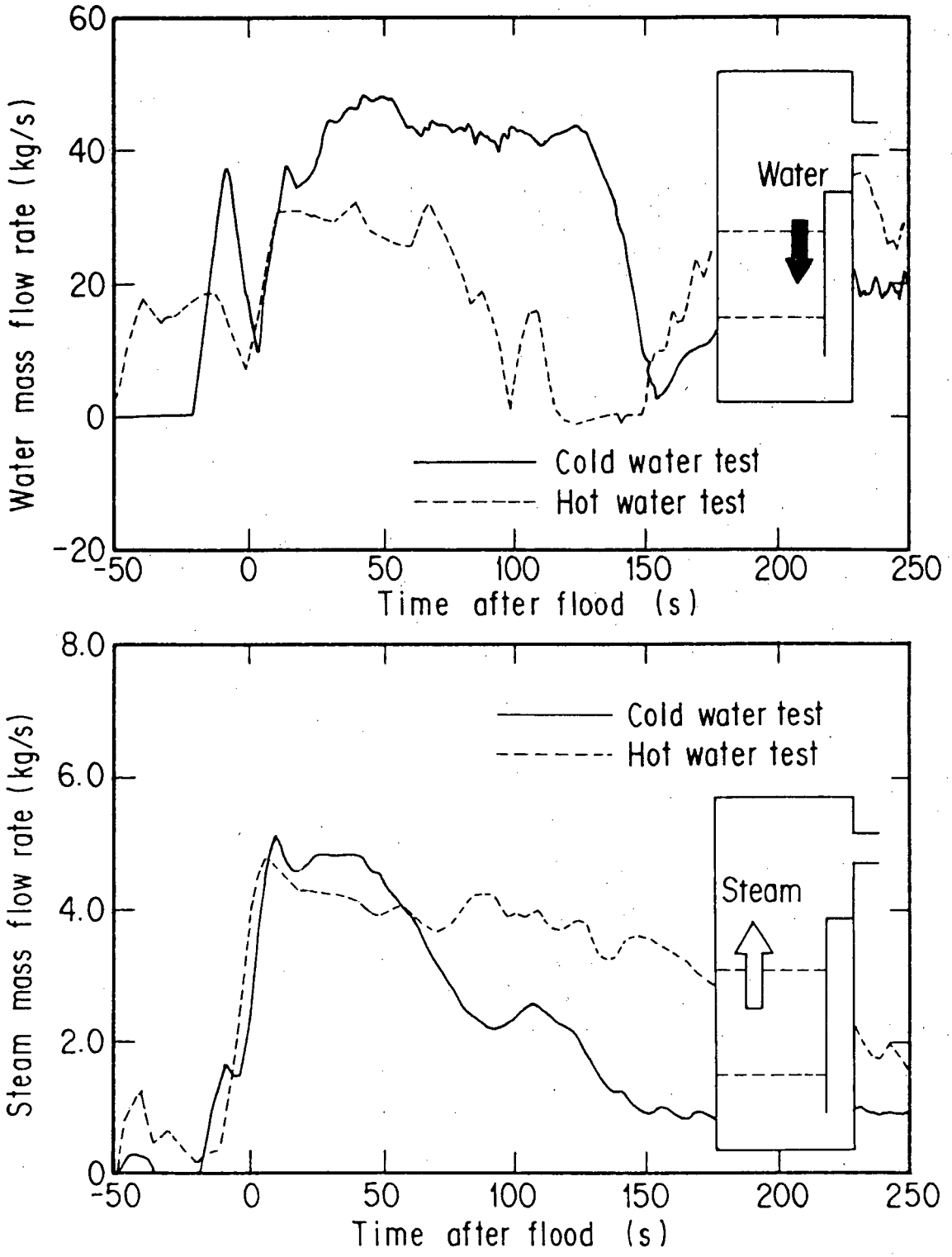


Fig. 5 Water downflow rate and steam upflow rate at the boundary of the upper plenum and the core in cases of cold and hot water

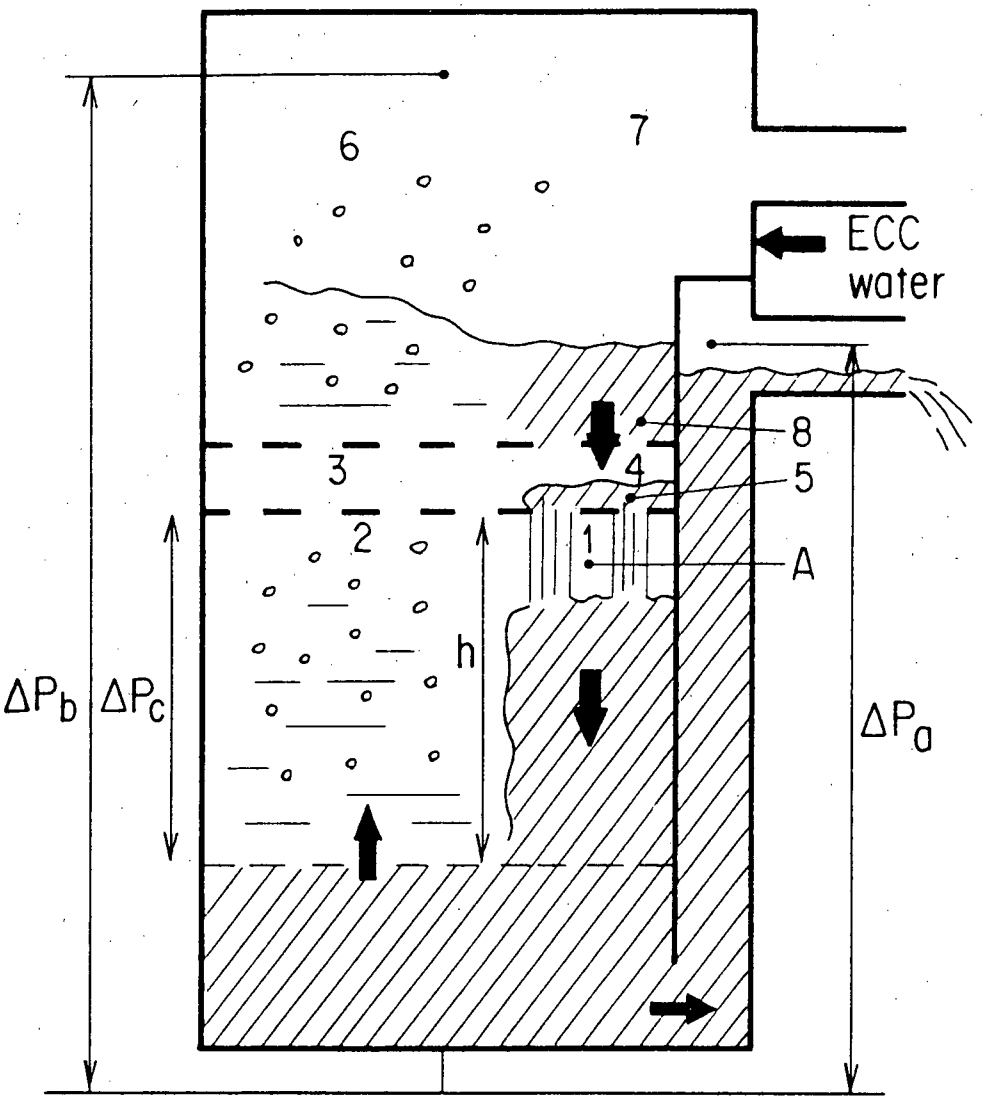


$$\Delta P_c = \rho_l g h - \frac{1}{2}\rho_l (u^2_{Bottom} - u^2_{Top}) - \frac{1}{2} K_c \rho_l \bar{u}_c^2$$

Fig. 6 Assumed model for the prediction on the water downflow rate

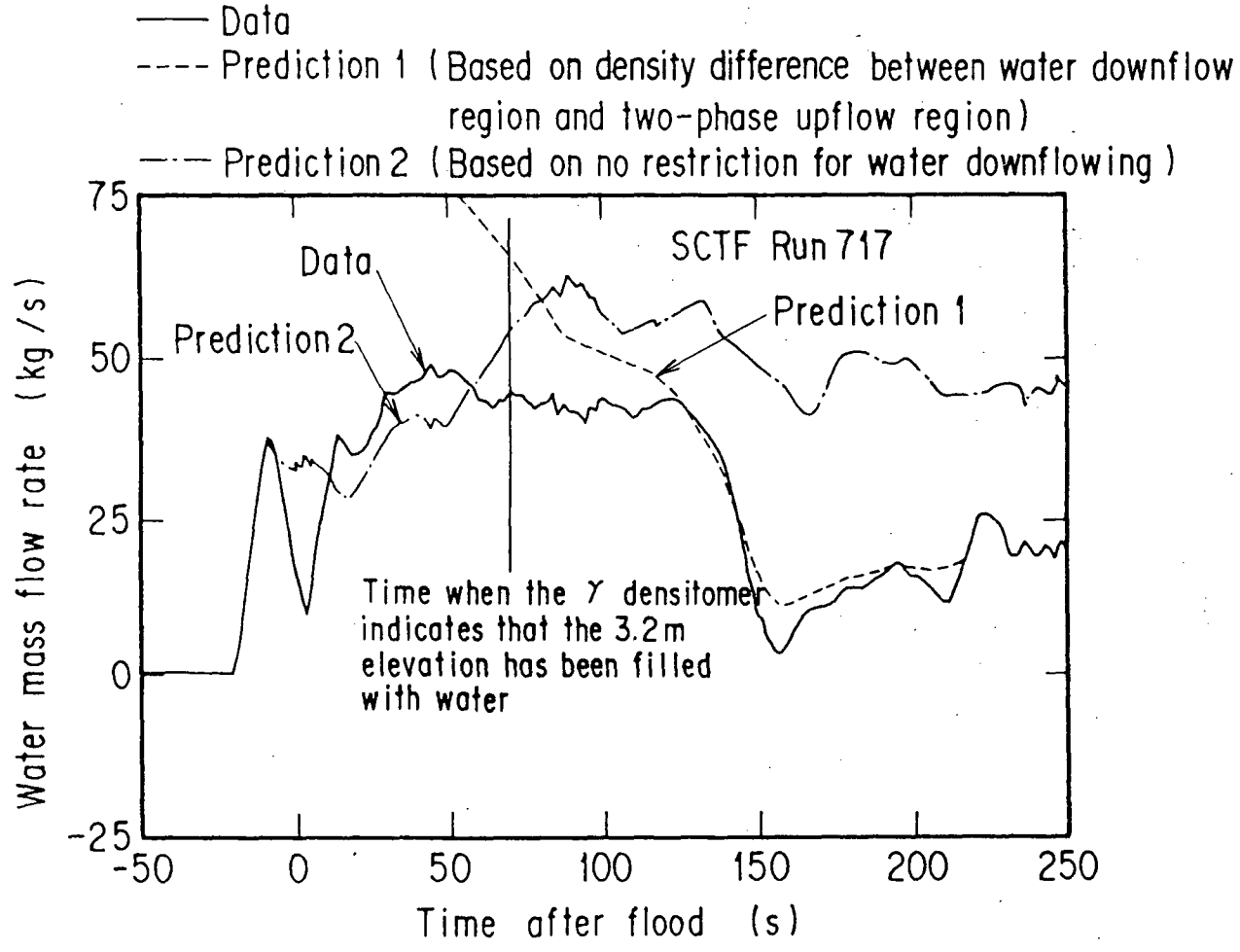


Fig. 7 The measured and predicted water downflow rates

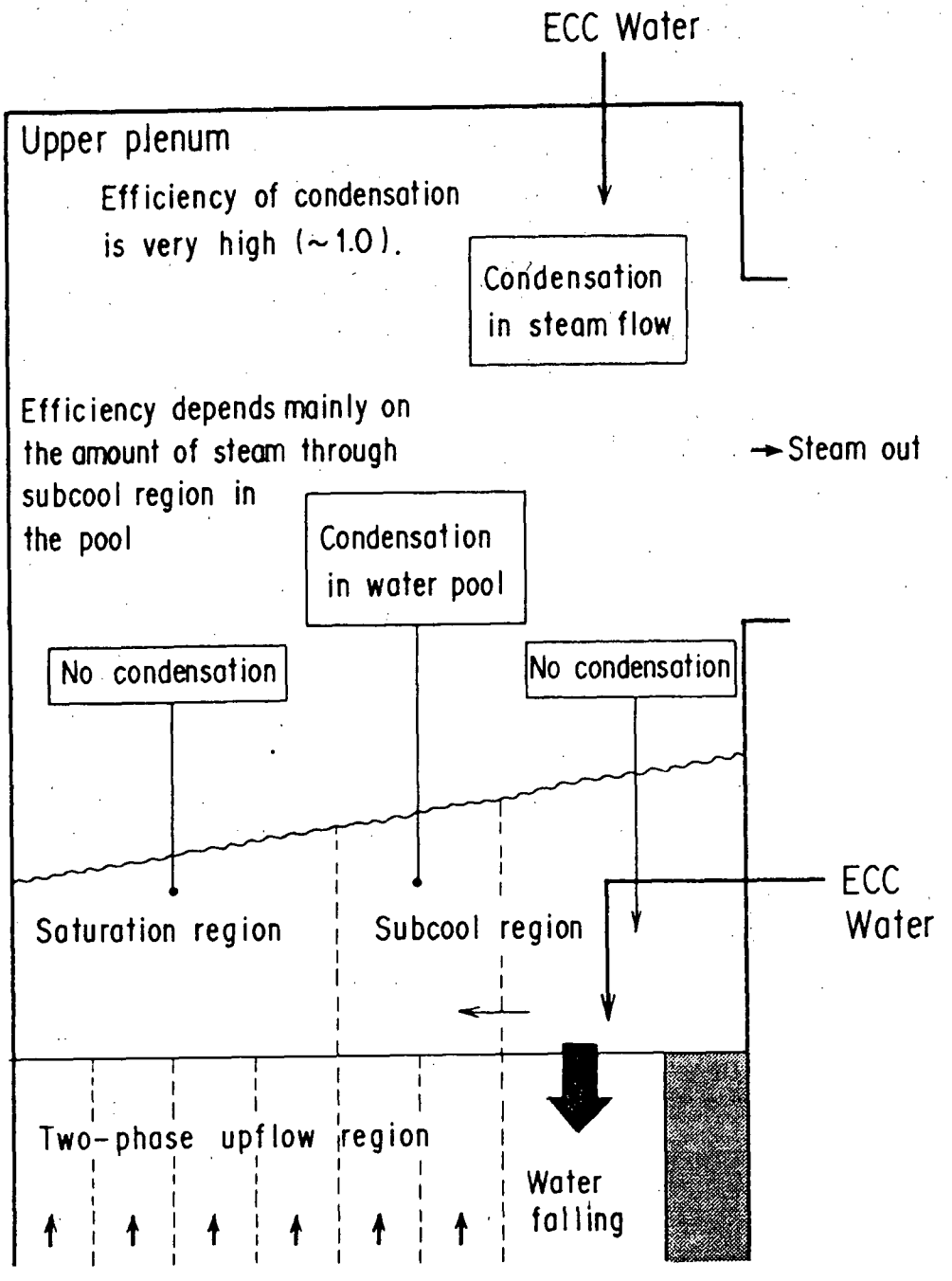


Fig. 8 The illustration on the upper plenum thermal hydraulic behavior derived from SCTF and CCTF test results

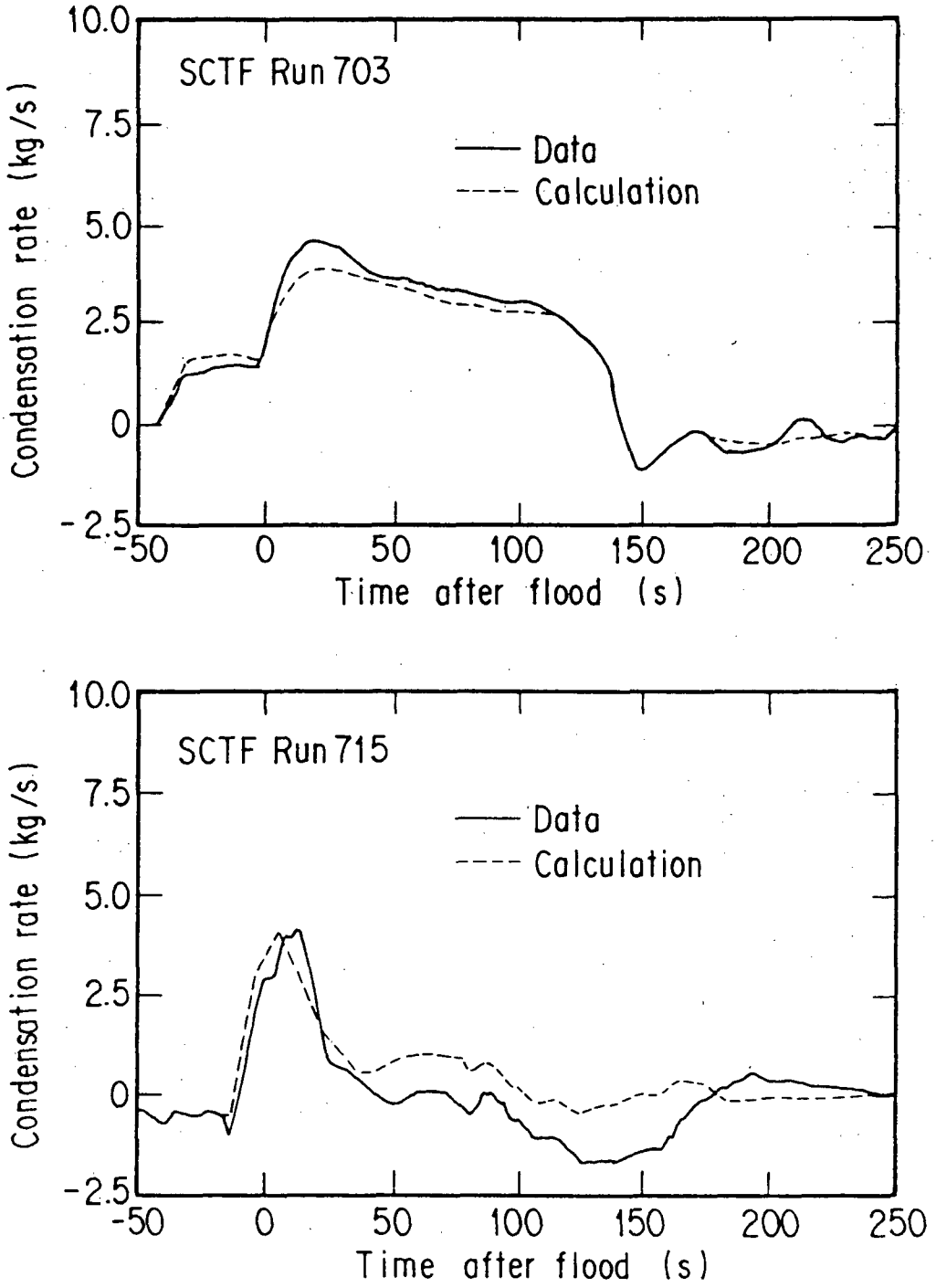


Fig. 9 Comparison of condensed steam in the upper plenum between the prediction and the measurement

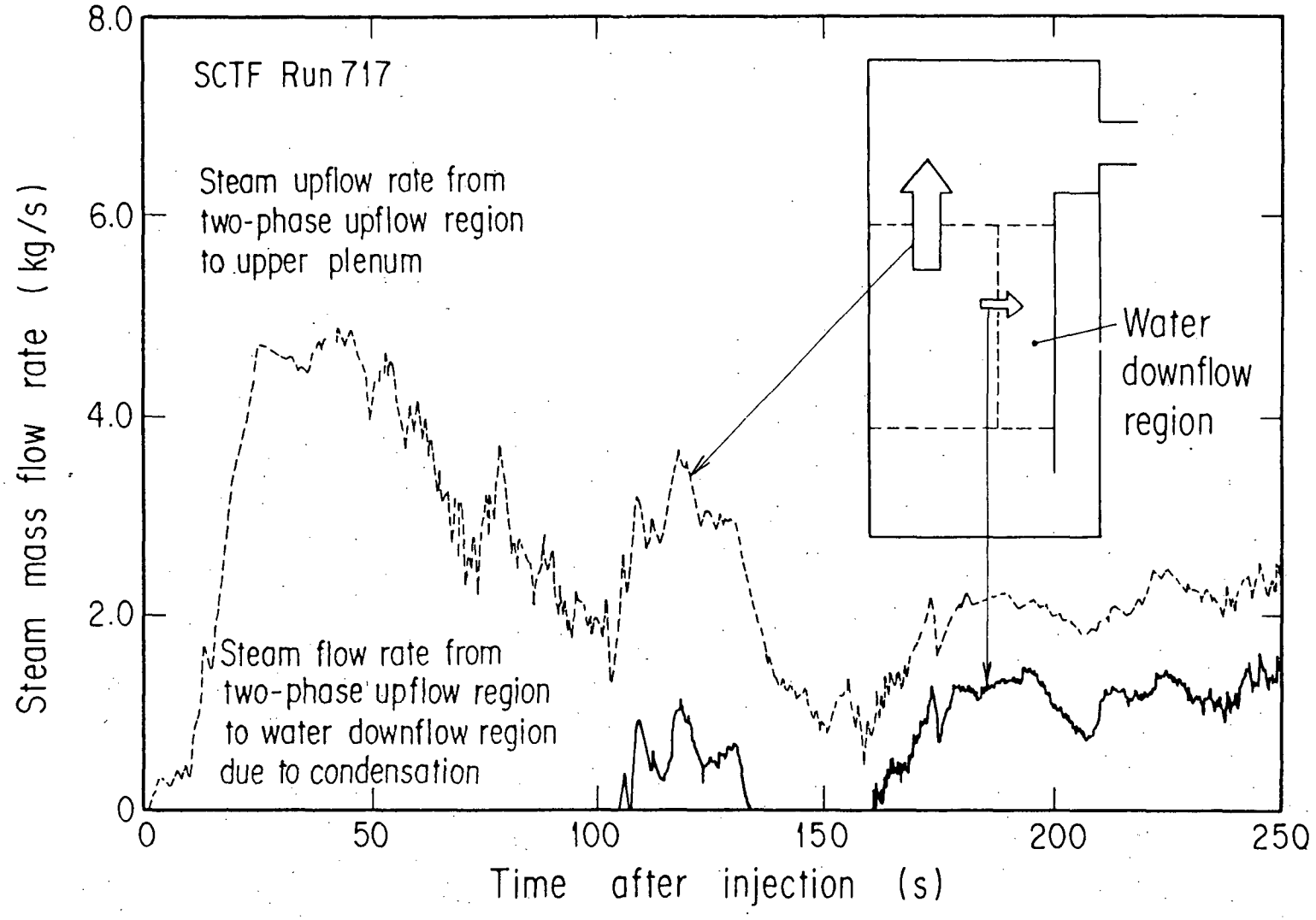


Fig. 10 Comparison of the steam upflow rate from the two-phase upflow region to the upper plenum with the steam flow rate from the two-phase upflow region to the water downflow region due to condensation

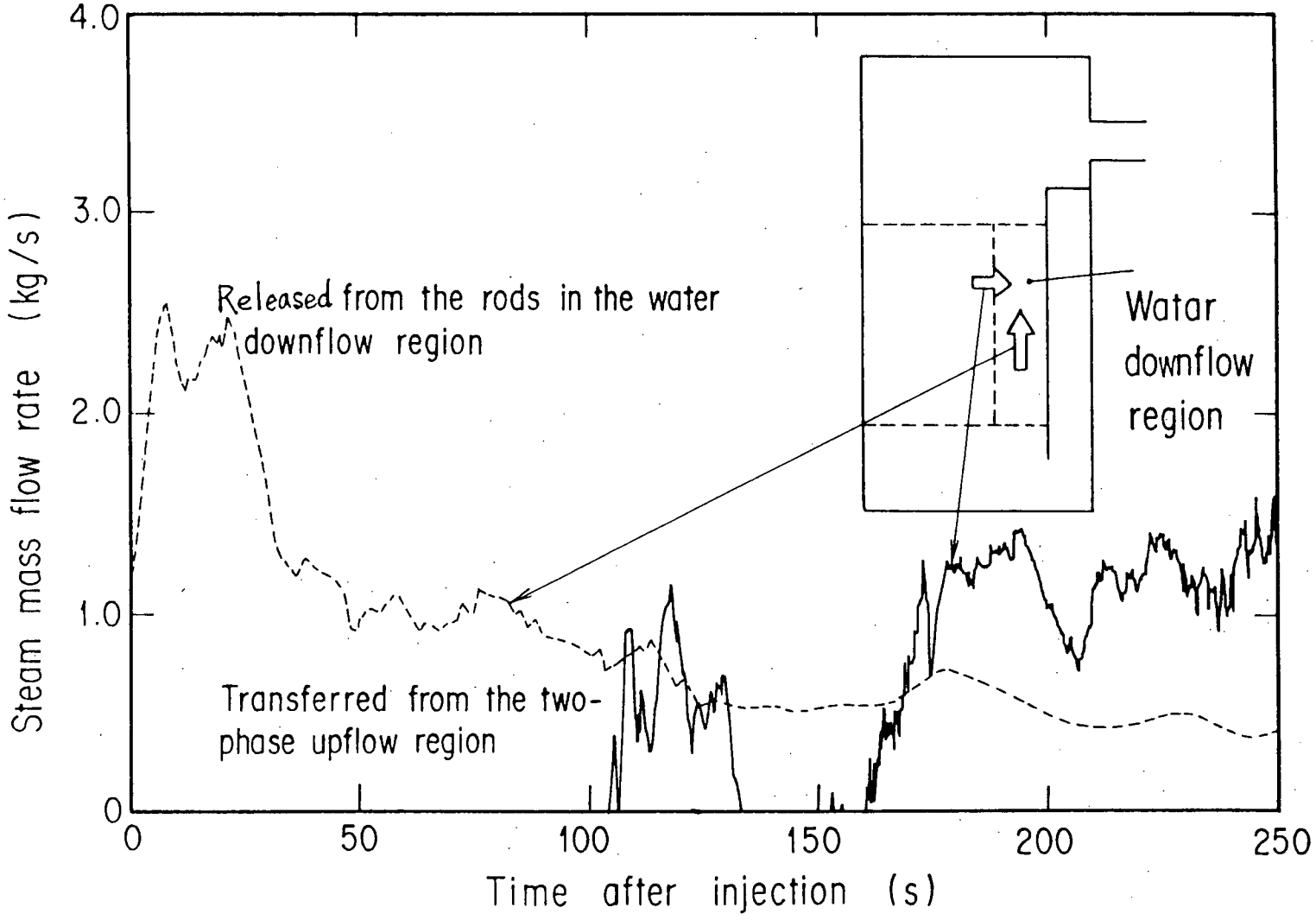


Fig. 11 Comparison of the heat transferred from the two-phase upflow region to the water downflow region with the heat released from the rods in the water downflow region
(Indicated by converting to steam mass flow rate)

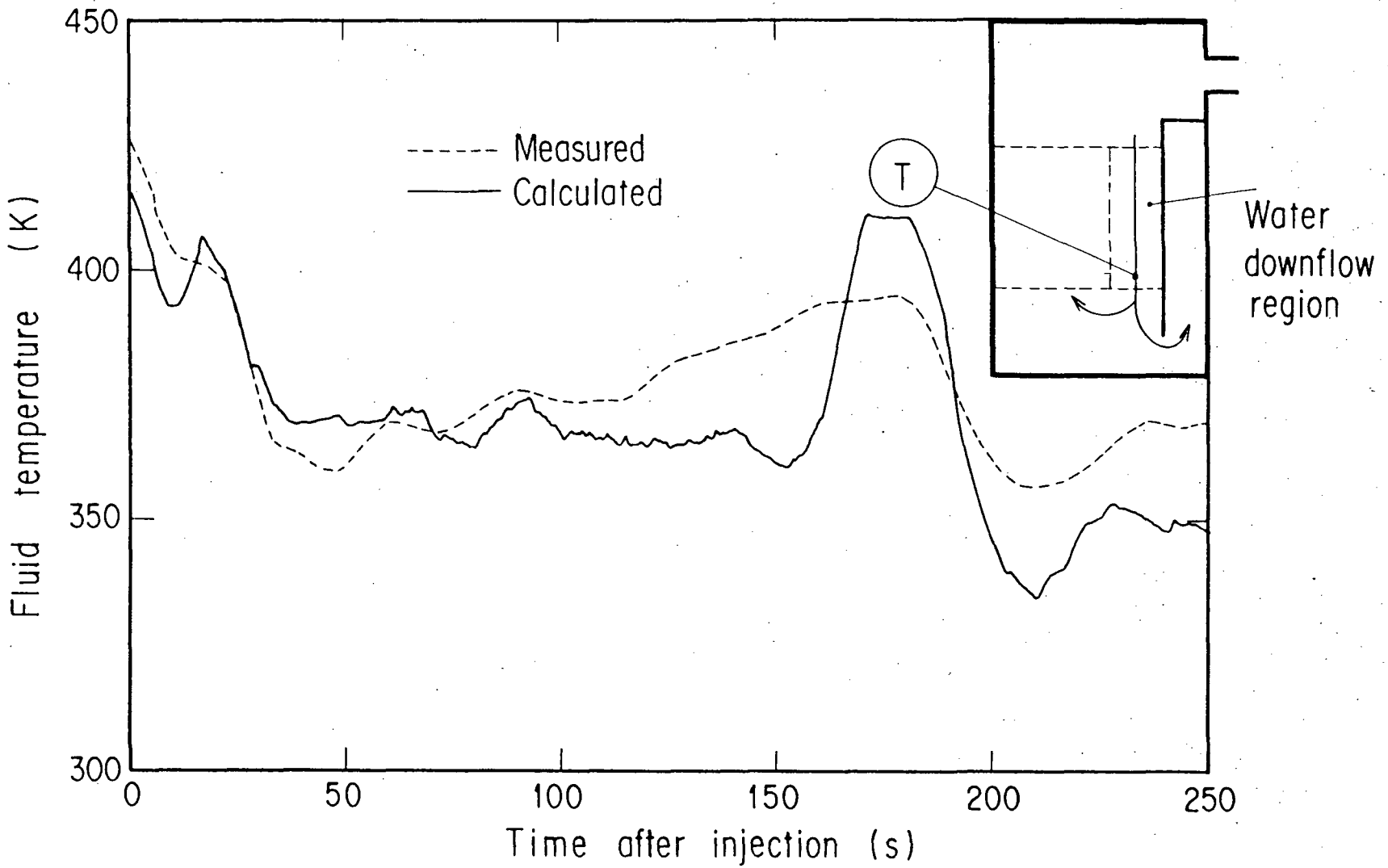


Fig. 12 The predicted and measured water temperature at core bottom of water downflow region

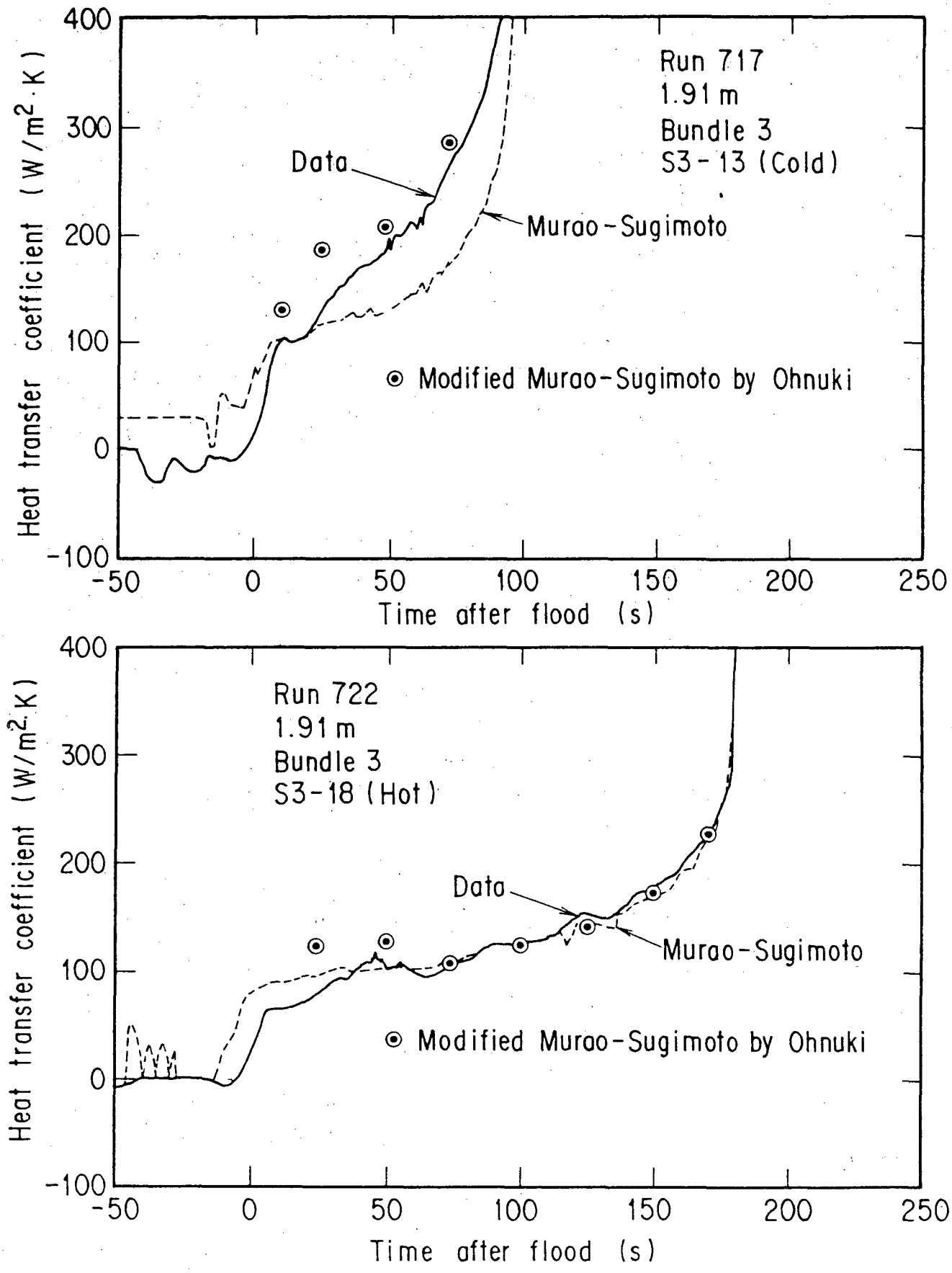


Fig.13 The measured heat transfer coefficient in the two-phase upflow region and the predicted ones

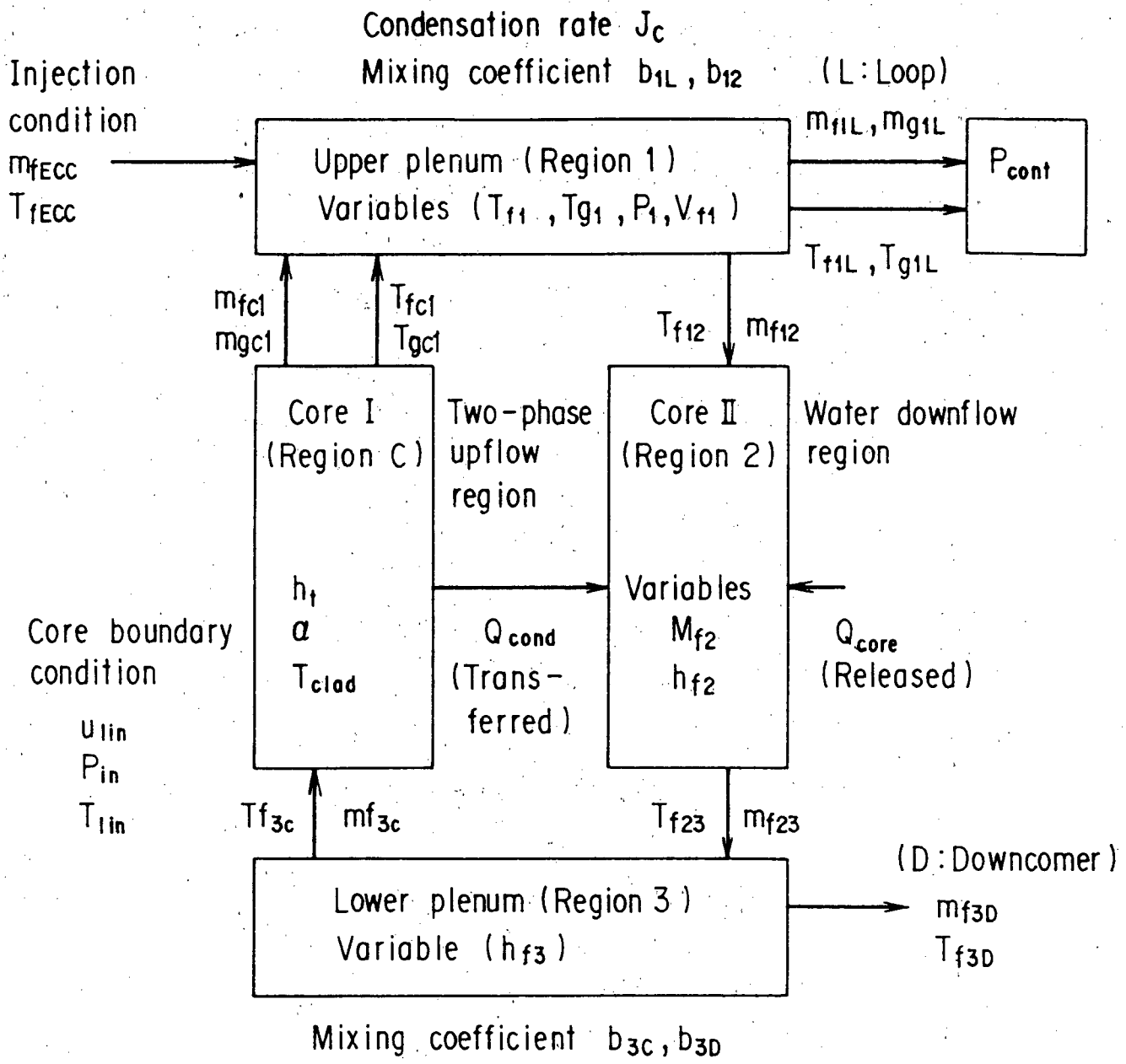


| | | | | | |
|---|---|---|---|---|---|
| f | : Water | | $T_{clad}$ | : Clad temperature | (K) |
| g | : Steam | | m | : Mass flow rate | (kg/s) |
| $P_{cont}$ | : Containment pressure | (Pa) | T | : Temperature | (K) |
| Q | : Heat | (Kcal) | M | : Mass | (kg) |
| $h_f$ | : Heat transfer coef. | ($W/m^2K$) | h | : Enthalpy | (Kcal/kg) |
| $\alpha$ | : Void fraction | (-) | | | |

Fig. 14 The adopted schematic of the prediction method for thermal hydraulics in pressure vessel

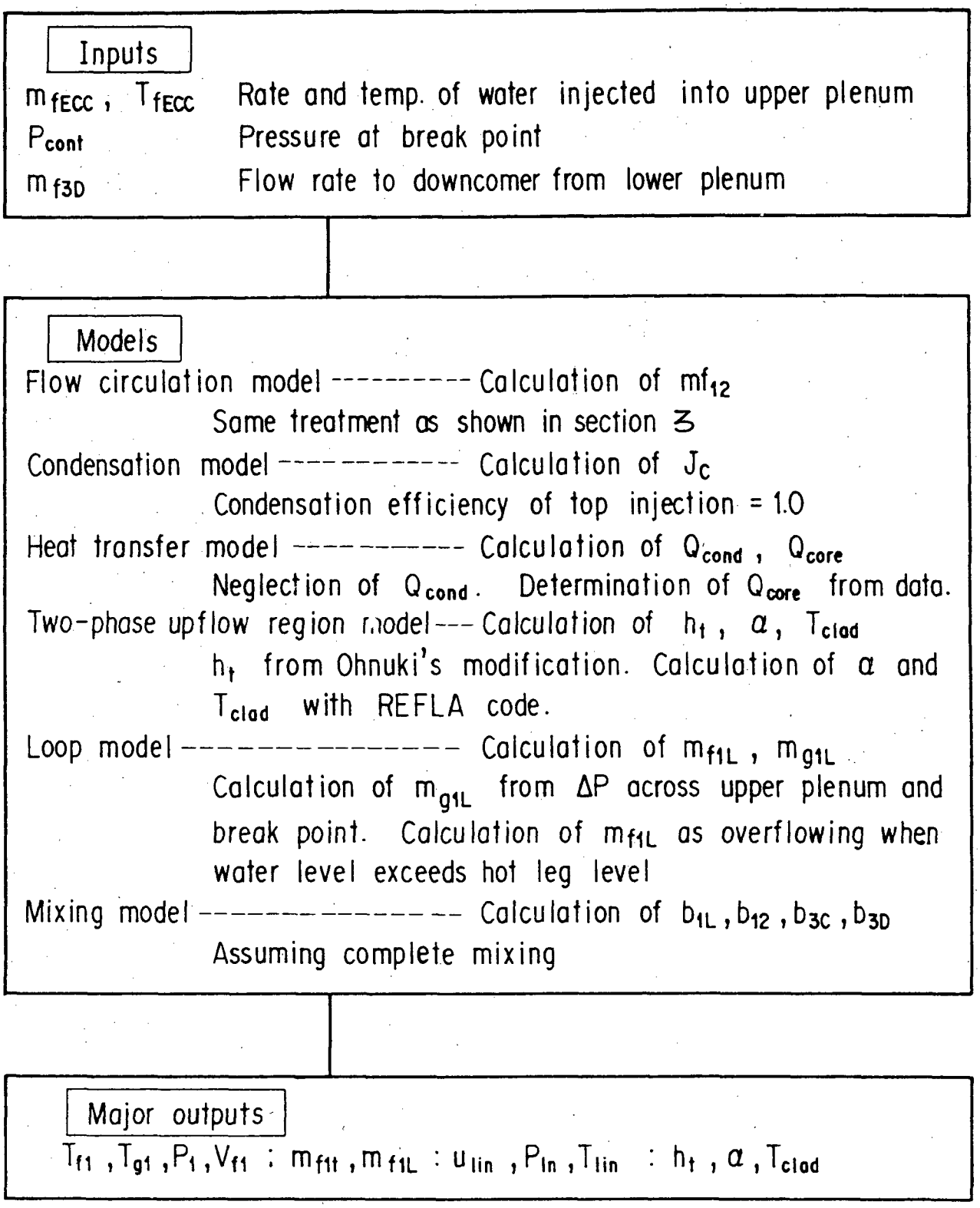


Fig.15 Sequence of the calculation of thermal hydraulics in pressure vessel

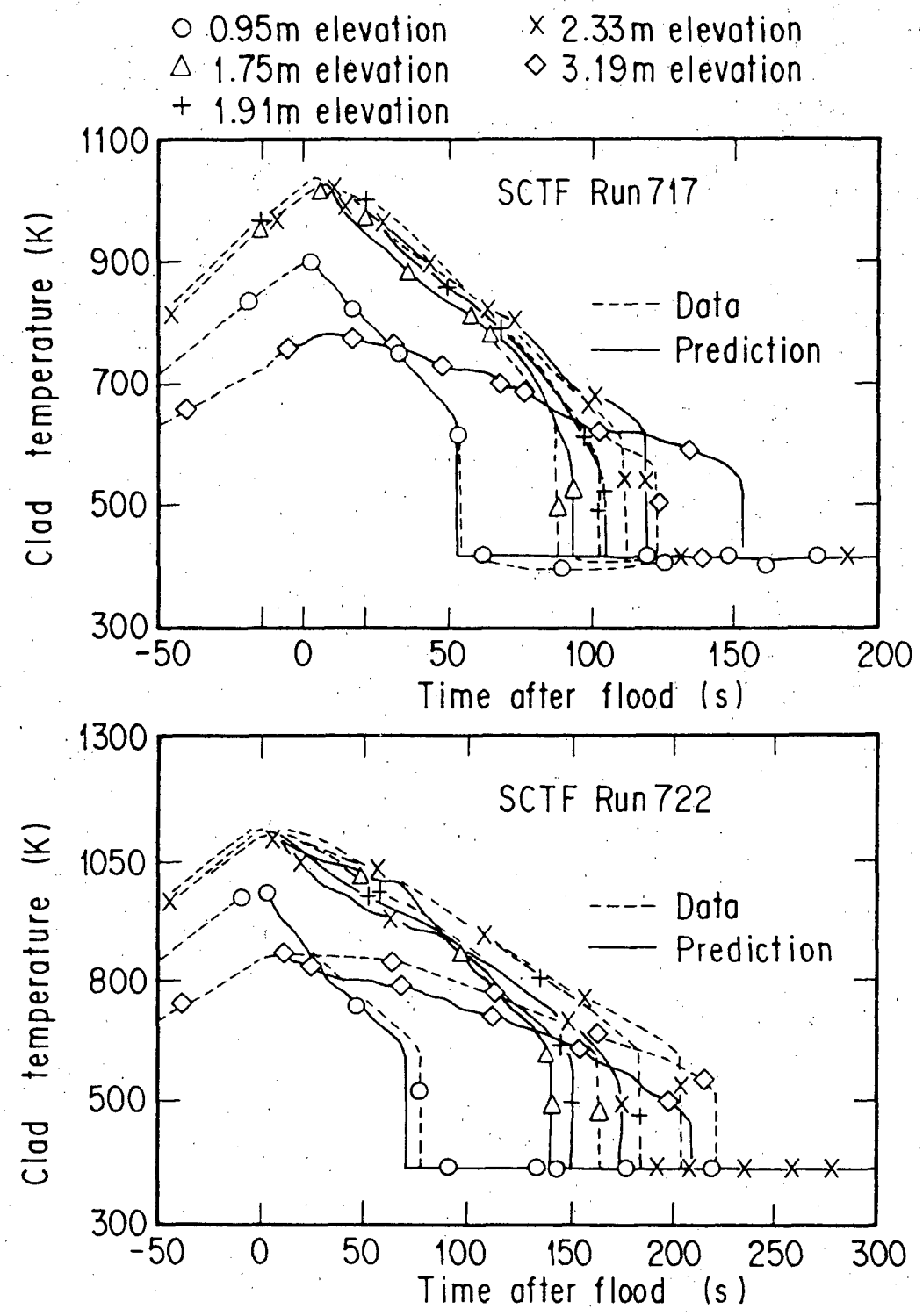


Fig. 16 The predicted and the measured clad temperature in two-phase upflow region

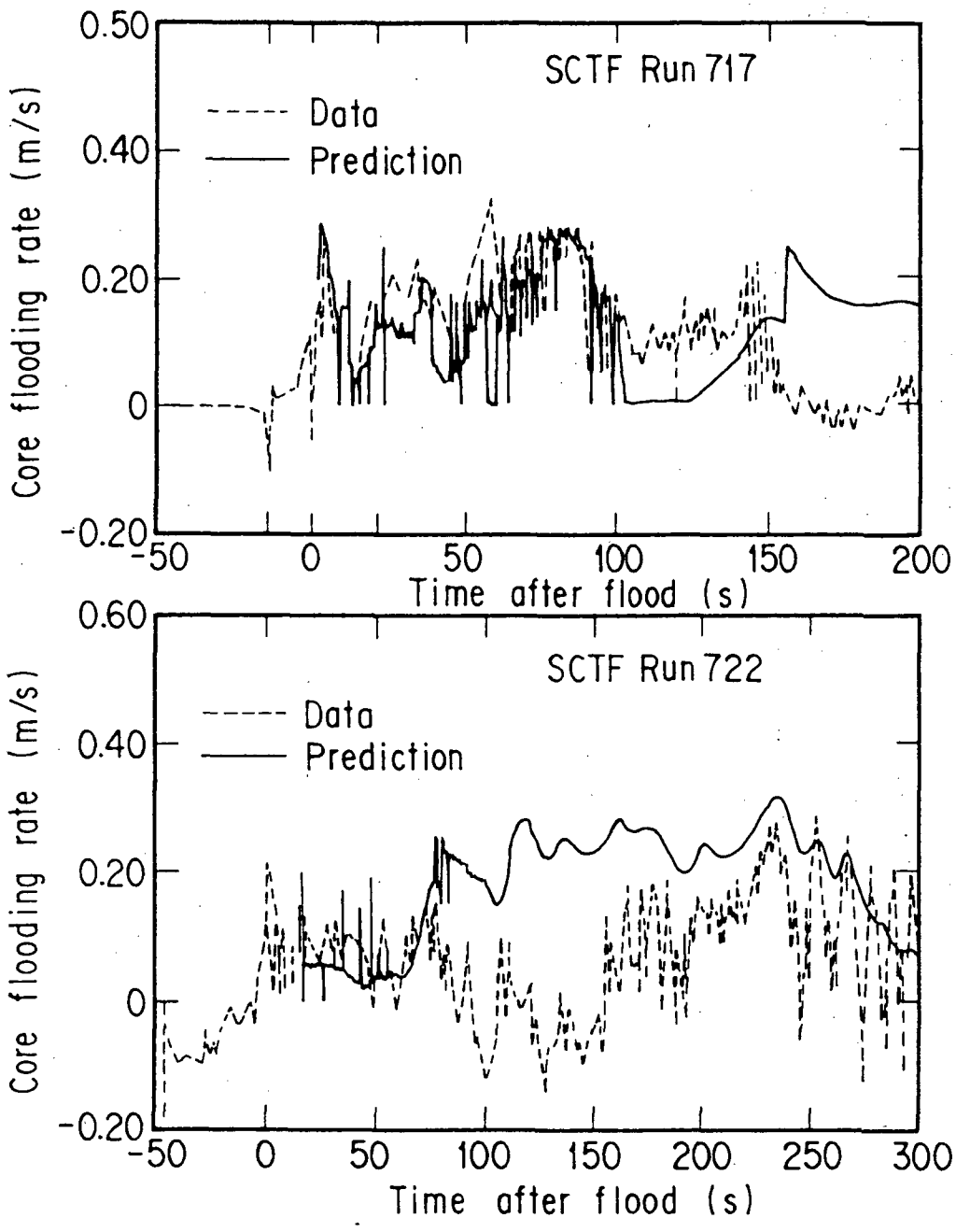


Fig.17 The predicted and the measured core flooding rate at core bottom of two-phase upflow region

# Assessment of J-TRAC code with CCTF/SCTF test data

Hajime AKIMOTO, Akira OHNUKI, Michitaka KIKUTA,
Yutaka ABE, Yoshio MURAO

Reactor safety laboratory II
Japan Atomic Energy Research Institute

The J-TRAC code has been developed at Japan Atomic Energy Research Institute (JAERI) to develop a standard code for reactor safety assessment. The J-TRAC code uses the TRAC-PF1/MOD1 code as the framework of the code and uses physical models at JAERI for refill and reflood phases of a PWR LOCA based on physical understanding of phenomena. This paper summarizes results of assessment calculations of the J-TRAC code with CCTF/SCTF test data. The assessment study confirms that the J-TRAC code can predict well core thermal hydraulic behaviors during reflood phase of a PWR LOCA including core void fraction profile and clad surface temperature. Several areas will be proposed for future improvements for exact prediction of clad temperature with 3D model and for stable system calculation.

## 1. Introduction

J-TRAC program is a code developmental program which started in 1984 at Japan Atomic Energy Research Institute(JAERI) to develop a standard code for reactor safety assessment. The J-TRAC code is being developed by using TRAC-PF1/MOD1[1] code as the framework of the code and by improving the physical models for the refill and reflood phases of a PWR LOCA based on the physical understanding of the phenomena. The J-TRAC code is expected to be used for the calibration of licensing codes or best-estimate oriented codes and for the simulation of the transients in PWRs.

Since 1984, the reflood model of the J-TRAC code is being developed by using the physical models in the REFLA code, which has been developed as a best-estimate code for the reflood analysis at JAERI.[2] As hydraulic models implemented into the J-TRAC code are an interfacial friction model equivalent to the Murao-Iguchi void fraction correlation, the droplet flow model and the relaxation model of the water accumulation in the core. For the heat transfer model, the Murao-Sugimoto correlation for the film boiling regime and the Murao correlation of the quench front velocity are implemented into the J-TRAC code.

To assess the predictive capability of the J-TRAC code and to grasp the application limit of the developed model, several assessment calculations were performed at JAERI. This paper summarizes results from these assessment calculations. In the followings, the code improvements performed at JAERI will be described briefly and results of the assessment calculation will be shown.

## 2. Outline of reflood model improvements at JAERI

In this section, the outline of reflood model improvements performed at JAERI will be described briefly. In model improvements, the physical models in the REFLA code, which has been developed as a best-estimate code for reflood analyses at JAERI, are adapted. The details of the physical models ate described in reference(2).

In reflood analyses with the TRAC-PF1/MOD1 code, the predicted void fraction showed poor agreement with CCTF test results although the predicted clad temperature showed good agreement with CCTF test results.[3] This result suggests that both of hydraulic and heat transfer models should be improved to describe precisely both of core water accumulation and core cooling behaviors because both behaviors coupled tightly during reflood.

For the hydraulic models, the following models were implemented into the J-TRAC code as interfacial friction models:

(1) Churn-turbulent flow model equivalent to the Murao-Iguchi void fraction correlation,[4]
(2) Dispersed flow model equivalent to that of the REFLA code,[2]
(3) Relaxation model for flow transition from a dispersed flow to a churn-turbulent flow.[2],[4]

For the heat transfer models, the following models were implemented into the J-TRAC code as interfacial or wall heat transfer models:

(1) Film boiling heat transfer correlation by Murao and Sugimoto[5] with a modification for liquid velocity effect proposed by Ohnuki, et al.[6]
(2) Quench velocity correlation by Murao,[2],[7]
(3) A dispersed flow model equivalent to that of the REFLA code.[2]

## 3. Assessment matrix and TRAC input

In order to understand the predictive capability of the J-TRAC code, systematic assessment calculations were performed with CCTF/SCTF test results.[8],[9] Table 1 shows major test conditions of CCTF/SCTF tests used in this assessment study. The conditions of the CCTF base case test were determined based on the licensing calculation of PWRs.[8] The core power of the CCTF base case test simulates the decay curve type of (1.2xANS + 1.1x Actinide (30s after scram)) in PWRs. The core power of the CCTF low power test simulates the decay curve type of (1.0 x ANS + 1.1 x Actinide (40s after scram)). Although the peak clad temperature at reflood initiation of the CCTF flat power test is lower than that of the CCTF low power test, the total core stored energy at reflood initiation is almost the same between both tests. The system pressure of the CCTF low and high pressure tests is 0.15 and 0.42 MPa, respectively. The pressure ranges cover the range of the pressure change predicted in the licensing calculations of PWRs during reflood. Two SCTF tests were performed under similar test conditions to those of CCTF. These tests were selected to cover test conditions appeared in licensing calculations of PWRs during reflood.

Table 1 Test conditions

| Test name | Peak clad temperature (K) | System pressure (MPa) | Core power (MW) | Radial peaking factor (-) |
|---|---|---|---|---|
| CCTF flat power test | 914 | 0.20 | 7.12 | 1.00 |
| CCTF base case test | 1073 | 0.20 | 9.35 | 1.37 |
| CCTF low power test | 1073 | 0.20 | 7.12 | 1.37 |
| CCTF high pressure test | 1073 | 0.42 | 9.35 | 1.37 |
| CCTF low pressure test | 1073 | 0.15 | 9.35 | 1.37 |
| SCTF flat power test | 922 | 0.20 | 7.12 | 1.00 |
| SCTF steep power test | 1160 | 0.20 | 7.12 | 1.20 |

Note) Values shown in Table 1 are those at reflood initiation.

In the assessment calculations, three types of input data were applied. In the first type of the calculations, only the core part of the facilities is modeled with a 1D CORE component as shown in Fig. 1. The measured core inlet mass flow rate, fluid temperature, core power and core outlet pressure were specified as boundary conditions. This type of calculations were planned to assess the predictive capability of the improved reflood model separately without interaction with the thermal-hydraulic behaviors in other components of the primary system. In the assessment calculation, investigated is the parameter effect such as the core radial power profile, system pressure, core power level and configuration of core.

In the second type of the calculation, only the pressure vessel of the facilities is modeled with a 3D VESSEL component as illustrated in Fig. 2. The improved reflood model ,described in chapter 2, was developed based on one-dimensional experiment with small scale tests such as JAERI small scale reflood test and FLECHT test. The second type of the calculations were planned to identify the problem areas in case that the model is extended to the large scale facilities with multidimensional thermal hydraulic behaviors. The second type of assessment calculations were focused on the SCTF tests with steep radial power profile in core.

In the third type of the calculations, full components of the primary system are modeled with 1D components as shown in Fig. 3. In the calculation, the improved reflood model was applied only at the core heated part in the CORE component. Because unrealistic depressurization was observed due to the condensation in cold legs and downcomer, particular modification was performed for the interfacial heat transfer model for the components which simulate intact cold legs, downcomer and broken cold leg of the pressure vessel side. The third type of calculations were planned to assess the cooperative characteristics of the improved reflood model with the original models in the TRAC-PF1 code. The third type of assessment calculation was performed for the CCTF base case test.

## 4. Results and discussion

### 4.1 Assessment calculations with 1D core model

Effect of facility size

Figure 4 shows void fractions and clad temperatures in the CCTF flat power test. The calculated results with the J-TRAC code show excellent agreement with CCTF test results for both core void fractions and clad temperatures. The reflood models of the REFLA code or the J-TRAC code were developed based on small scale reflood test facilities such as the (JAERI small scale test facility and the FLECHT-SET. The scaling factor is 1/21.4 in the CCTF based on the core flow area while it is 1/370 in the FLECHT-SET. Figure 4 shows that the reflood models can also be applied to large test facilities such as the CCTF.

The core radius is scaled to 1/4.5 of actual PWRs in the CCTF. To check the applicability of the reflood model to a full radius, an assessment calculation was performed for the SCTF flat power test because the SCTF has a full-radius, full-height and one-bundle-width core. Figure 5 shows core void fractions and clad temperatures in the SCTF flat power test. For the SCTF test, the calculated results also show excellent agreement with measured results. These results suggest that the J-TRAC code can predict well core water accumulation and core cooling behaviors in large scale facilities such as the CCTF and SCTF as well as in small scale test facilities under conditions with flat radial power profile in core.

Effect of core radial power profile

In actual PWRs, a steep power profile may exist in radial direction as well as in axial direction. To assess the applicability of the J-TRAC code for the cases with a steep radial power profile in core, the calculated results of the CCTF base case test were compared with measured results because a steep radial power profile was supplied in the CCTF base case test as shown in Fig. 6.

Figure 7 shows void fractions at various elevations of the core in the CCTF base case test. The calculated results show excellent agreement with measured results for the CCTF base case test. The core void fraction profile is predicted well with the J-TRAC code under the conditions with a steep radial power profile in the core. The result shows that one-dimensional model with the average power rod is applicable for predicting core void fractions in the axial direction even when a steep radial power profile exists.

Figure 8 shows clad temperatures along a low power rod (radial peaking factor 0.76) and a high power rod (radial peaking factor 1.36). The calculated clad temperatures along a low power rod show excellent agreement with measured results at various elevations. The calculated clad temperatures along a high power rod show slightly higher turnaround temperatures and later quench than measured results at elevations of 1.83 m and 3.05 m. Figure 9 shows a quench envelope along a low power rod and a high power rod in the CCTF base case test. The calculated results show excellent agreement with measured results along a low power rod, while the calculated results show slower quench propagation along a high power rod than measured results. These assessment results suggest that the model for the core heat transfer should include the effect of the core radial power profile to predict the entire transient of the clad surface temperature exactly. However, the calculated results along a high power rod show slightly higher peak clad temperature than measured

results. Because the J-TRAC code is expected to give the conservative results for the clad temperature of the peak power rod, the 1D model of the J-TRAC can be applicable to practical uses in reactor safety assessment.

Effect of system pressure

The system pressure is one of the most important parameters for thermal hydraulic behaviors during the reflood. In the assessment calculations of the CCTF low and high pressure tests, excellent agreement was obtained for the core void fractions as well as in the CCTF base case test. The calculated void fraction decreased with system pressure as observed in the CCTF test.

For the core cooling behavior, similar results were obtained in the CCTF low and high pressure tests as in the CCTF base case test. Figure 10 shows quench envelope in the CCTF low and high pressure tests. In both tests, the calculated results show excellent agreement with measured results along a low power rod while the calculated results show slower quench propagation along a high power rod than measured results. The J-TRAC code predicted slightly higher peak clad temperature in both tests.

These results show that the J-TRAC code can predict the system pressure effect precisely on core thermal hydraulic behaviors during the reflood.

Effect of core power level

The core power level is also one of the most important parameters for core thermal hydraulic behaviors during the reflood. In the assessment calculations of the CCTF low power test, excellent agreement was obtained for the core void fractions at various elevations. The calculated void fraction increased slightly with the core power level in the later period of the reflood as observed in the CCTF tests. The calculated peak clad temperature of the CCTF low power test slightly higher than the measured one and increased with the core power level as observed in the CCTF tests. Figure 11 shows quench envelope in the CCTF low and high power tests. The calculated results show excellent agreement with measured results along a low power rod in both tests while the calculated results show slower quench propagation along a high power rod than measured results. These results show that the J-TRAC code can predict the effect of core power level precisely on core thermal hydraulic behaviors during the reflood.

## 4.2 Assessment calculation with 3D core model

The reflood models of the REFLA code were also implemented into a 3D VESSEL component of the J-TRAC code. As a first approach, the improved hydraulic models were applied to models only in axial direction. In radial and azimuthal directions, original models of the TRAC-PF1/MOD1 code were used. For the heat transfer models, the same models as in the REFLA code were implemented into the 3D component as a first approach. In this improved model, the effect of the core radial power profile can be calculated through coupling between two-phase fluid and heat release from heater rods with various power and temperature values. No direct effect of the cross flow on core heat transfer is included in this model.

The assessment calculation was performed using results of the SCTF steep power test. In the SCTF steep power test, the radial peaking factors were 1.0, 1.2, 1.0 and 0.8 at bundles 1-2, 3-4, 5-6 and 7-8, respectively. Bundles 1, 2, 5 and 6 were named average power bundles. Bundles 3 and 4 were named

high power bundles. Bundles 7 and 8 were named low power bundles in this study. Figure 12 shows void fractions in average, high and low bundles at elevation between 2.03 and 2.57 m. The void fraction is nearly uniform in radial direction regardless of radial peaking factor in the SCTF steep power test. The calculated results with the J-TRAC code show nearly uniform void fraction as in the test. In quantity, the calculated results shows reasonable agreement with measured results. It is confirmed that the core void fraction can be predicted well by the installation of models of the REFLA code in axial direction.

Figure 13 shows clad surface temperature in each power bundle at elevation of 1.905 m. The J-TRAC code predicted slightly lower turnaround temperature in the low and high power bundles and shows good agreement with measured results for turnaround temperature in average power bundle. The J-TRAC code predicted slightly later quench than measured results.

In the SCTF tests, the core heat transfer enhancement was reported by Adachi, et al. arising from flow circulation in core resulting from radial power profile.(9) In such a situation, the flow distribution inside core is one of key phenomena to understand core heat transfer during the reflood. Figure 14 shows a calculated flow distribution with the J-TRAC code at 300 s after reflood initiation. The quench front was located about 1.78 m at the time.

The steam mass flow rate increases with elevation and is nearly uniform in radial direction except bundle 8. The water mass flow rates in bundles 3 and 4 are higher than those in the other bundles below the quench front. In the lower part of the core (below 1.20 m), a radial water flow toward bundles 3 and 4 is calculated by the J-TRAC code. On the other hand, a radial water flow from bundles 3 and 4 is calculated near the quench front (between 1.20 and 2.38 m). In bundles 7 and 8, downward water flow is predominant below the quench front. Water circulation is calculated below the quench front by the J-TRAC code. In the top part of the core (above 2.38 m), the water mass flow rate is nearly uniform except bundle 8. The concentrated water flow profile is quickly flattened by the radial water flow near the quench front.

In the SCTF test, the heat transfer coefficients in the high power bundle are higher than those in the average and low power bundles. The J-TRAC code predicted qualitatively the tendency, mentioned above. However, the calculated heat transfer enhancement due to flow circulation was smaller than the measured result. It seems that that the small heat transfer enhancement in the high power bundle is caused by the nearly flat profile of the water mass flow rate above the quench front in the J-TRAC calculation. The radial water flow seems to be too high above the quench front in the calculation. More study is necessary to be performed on hydraulic models such as water flow in radial direction.

## 4.3 Assessment calculation with 1D system model

To check the cooperative characteristics of the improved reflood model with the TRAC-PF1/MOD1 code, a system calculation was performed for the CCTF base case test using 1D component models. In the calculation, the improved model was applied only at the heated part in a CORE component. Because unrealistic depressurization was calculated due to the condensation in cold legs and downcomer, a simplified condensation model was applied for the

components which simulated intact cold legs, downcomer and broken cold leg of the pressure vessel side. For the other components and situation, original models of the TRAC-PF1 code were applied.

Figure 15 shows total loop mass flow rates through intact loops. Figure 16 shows clad temperatures at midplane of core in high power region. The top figures of Figs.15 and 16 show results from a base case calculation. In the base case calculation, geometry and boundary data were input as in the test. In the base case calculation, several spikes are predicted in the loop mass flow rate and a oscillation with a long period is predicted in the loop mass flow rate and the clad temperature. The spiky mass flow rate in the loop calculations was supposed to be related to vaporization of water in steam generators due to intermittent water carry-over from the upper plenum (U/P). The boiling at downcomer due to system pressure transients was supposed to result in a long period oscillation.

In order to understand the cause of oscillation, two sensitive calculations were performed by changing boundary and geometry data. In the first calculation, the initial downcomer wall temperature was set at saturation temperature to reduce the effect of boiling at downcomer although the downcomer wall was superheated in the CCTF base case test. In the second calculation, the volume at upper plenum was set at 10 times volume of actual one to reduce the effect of the intermittent water carry-over from the upper plenum to hot legs in the calculation. The results from the first sensitivity calculation are shown in the middle of Figs. 15 and 16, while the results from the second sensitivity calculation are shown in the bottom of Figs. 15 and 16.

In the first calculation, the oscillation with a long period is eliminated in the loop mass flow rate although spikes still exist. The result suggests that the oscillation with a long period is related to boiling phenomena in the downcomer. In the second calculation, spikes in the loop mass flow rate disappeared. The water from the core trapped at the upper plenum and almost no water was carried over to hot legs in the second calculation. These results suggest that more model improvements are required to get stable calculation result as in the test, especially for thermal hydraulic models in the upper plenum and the downcomer.

## 5. Conclusions

To assess the predictive capability of the J-TRAC code for thermal hydraulic behavior during the reflood, assessment calculations were performed with CCTF/SCTF test data. From this assessment study, following conclusions were obtained.

(1) Both core void fraction profile and core cooling behavior are predicted excellently with the 1D reflood model of the J-TRAC code although the clad temperature of the high power bundle was slightly higher than the measured results.

(2) The 1D reflood model of the J-TRAC code can predict precisely effect of system pressure and power level on core cooling behavior.

(3) With the extended model to 3D model, the J-TRAC code calculated flow circulation in the core. The calculated core heat transfer enhancement in high power bundle was smaller than the measured one. More study is required for core hydraulic models such as radial water flow .

(4) More model improvements are required for hydraulic models in upper plenum and downcomer to get stable system response as observed in CCTF tests.

## Acknowledgment

This work was performed under a contract with the Atomic Energy Bureau of the Science and Technology Agency of Japan. The authors appreciate Drs. M. Shiba and T. Shimooke of JAERI for their encouragements and arrangements. The authors also appreciate members of 2D/3D analysis group for valuable discussions.

## References

(1) Los Alamos National Laboratory : NUREG/CR-3567, LA-9944MS, February 1984.
(2) Murao, Y., et al. : JAERI-M 84-243, February 1985.
(3) Akimoto, H. : JAERI-M 85-117, August 1985.
(4) Murao, Y., Iguchi, T. : J. Nucl. Sci. Technol., 19(8), 613(1982).
(5) Murao, Y., Sugimoto, J. : J. Nucl. Sci. Technol., 18(4), 257(1981).
(6) Ohnuki, A., et al. : Proceeding of 1987 fall meeting of the Atomic Energy Society of Japan F51, September 1987, (in Japanese).
(7) Murao, Y. : JAREI-M 10000, March 1982, (in Japanese).
(8) For example, Murao, Y., et al. : 13th water reactor safety research information meeting, October (1985).
(9) Adachi, H., et al. : 15th water reactor safety information meeting, October (1987).

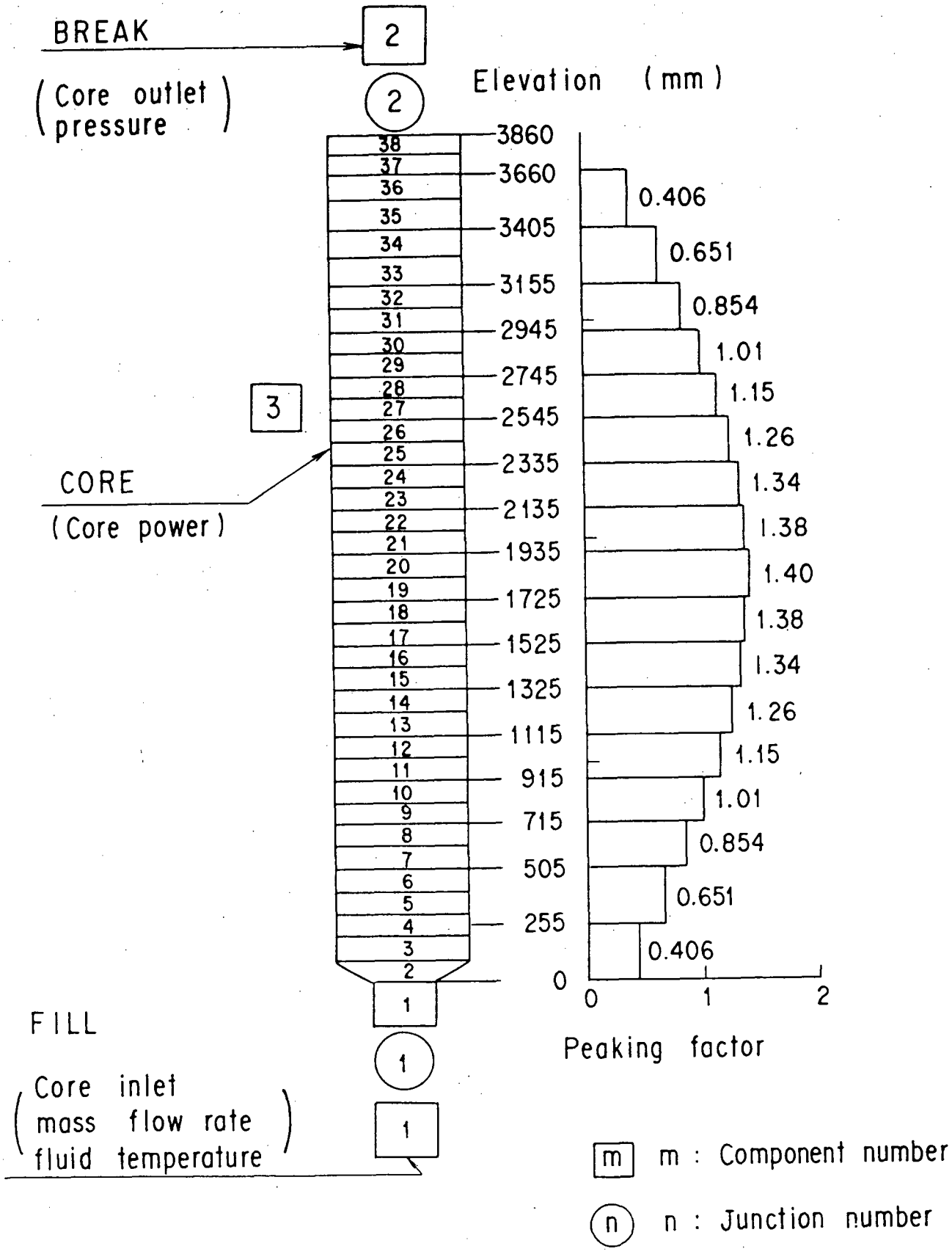


Fig.1 TRAC noding of CCTF 1D core calculation

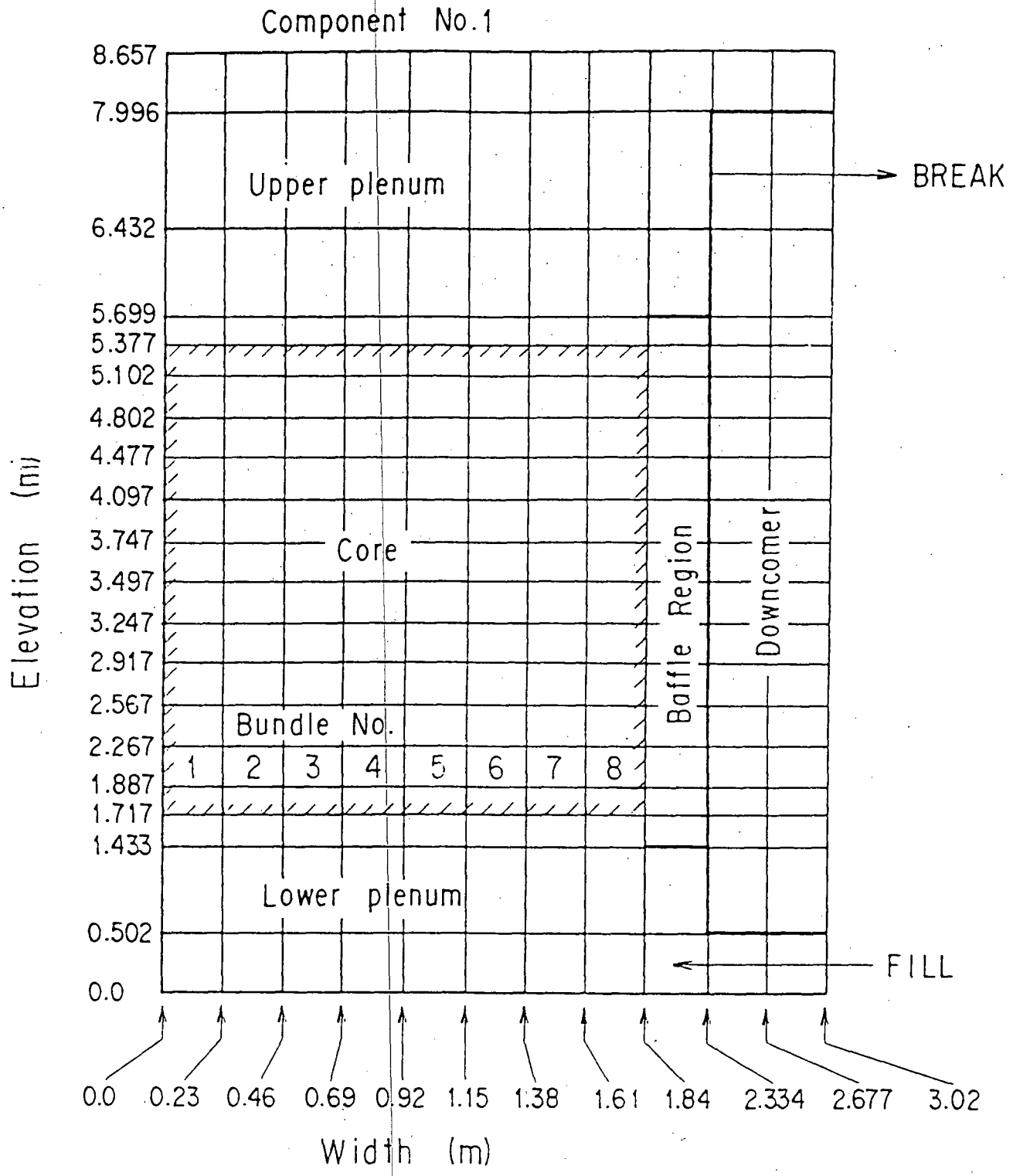


Fig.2 TRAC noding of SCTF 2D core calculation

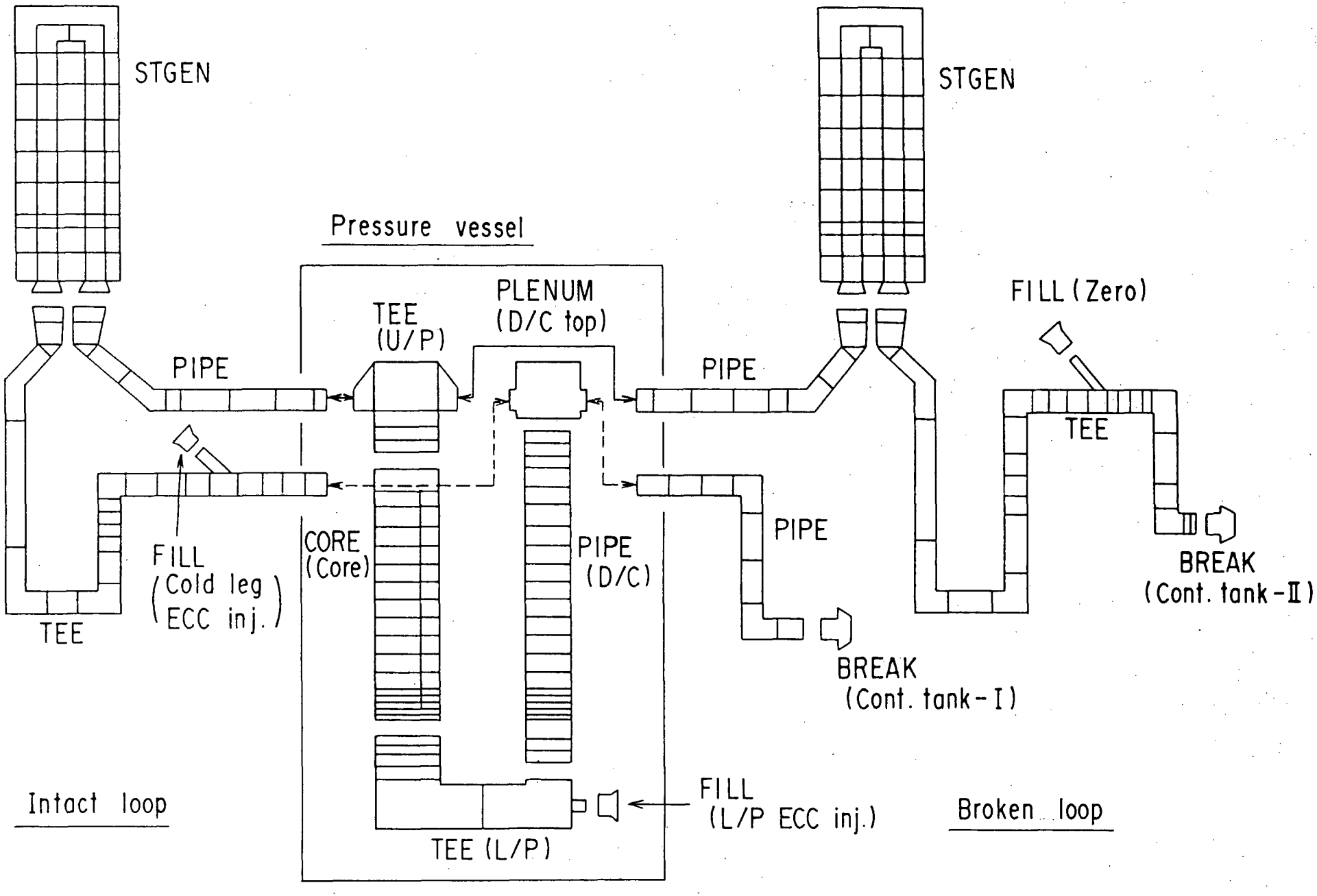


Fig.3 TRAC noding of CCTF system calculation

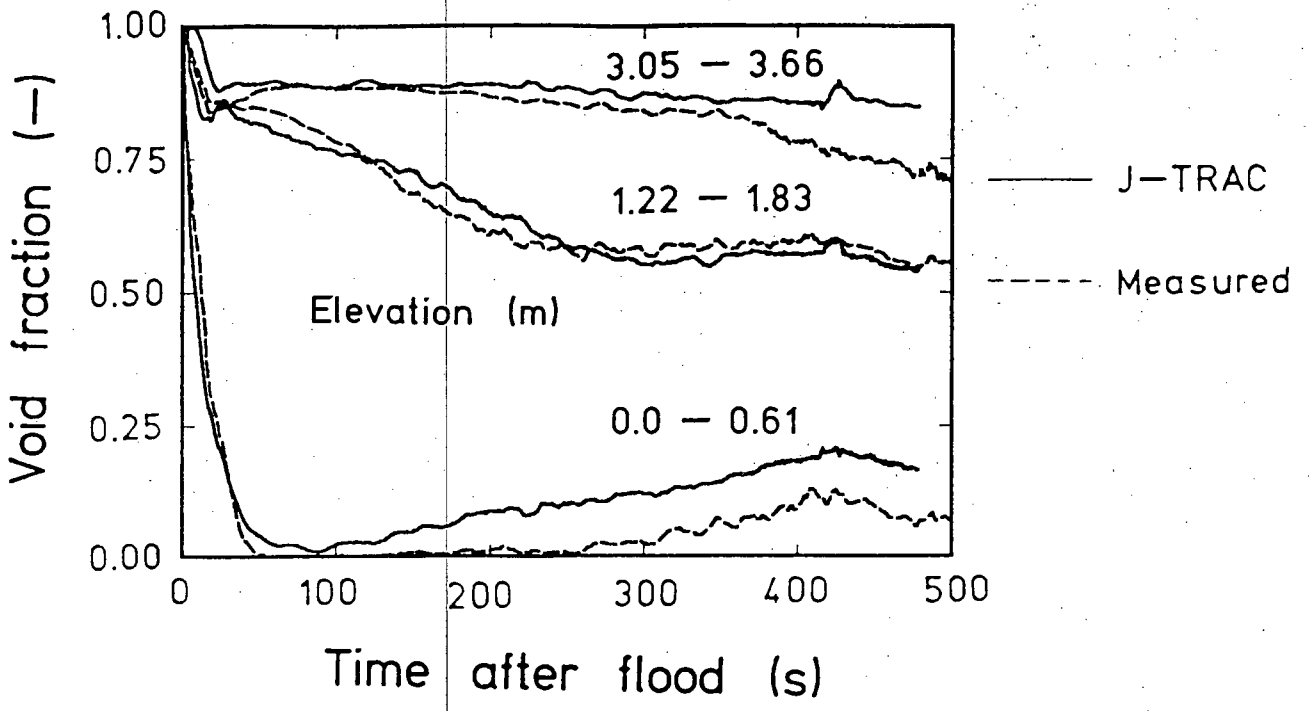


(a) Void fraction

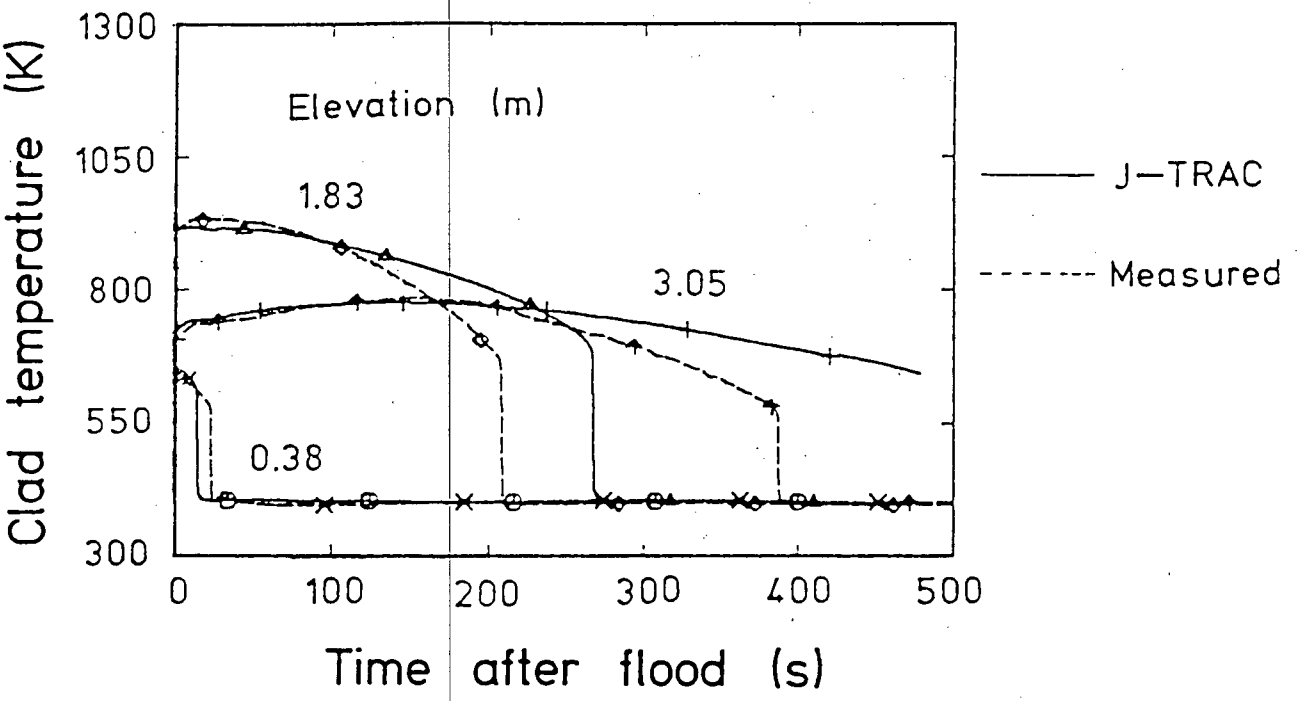


(b) Clad temperature

Fig.4 Comparison for CCTF flat power test

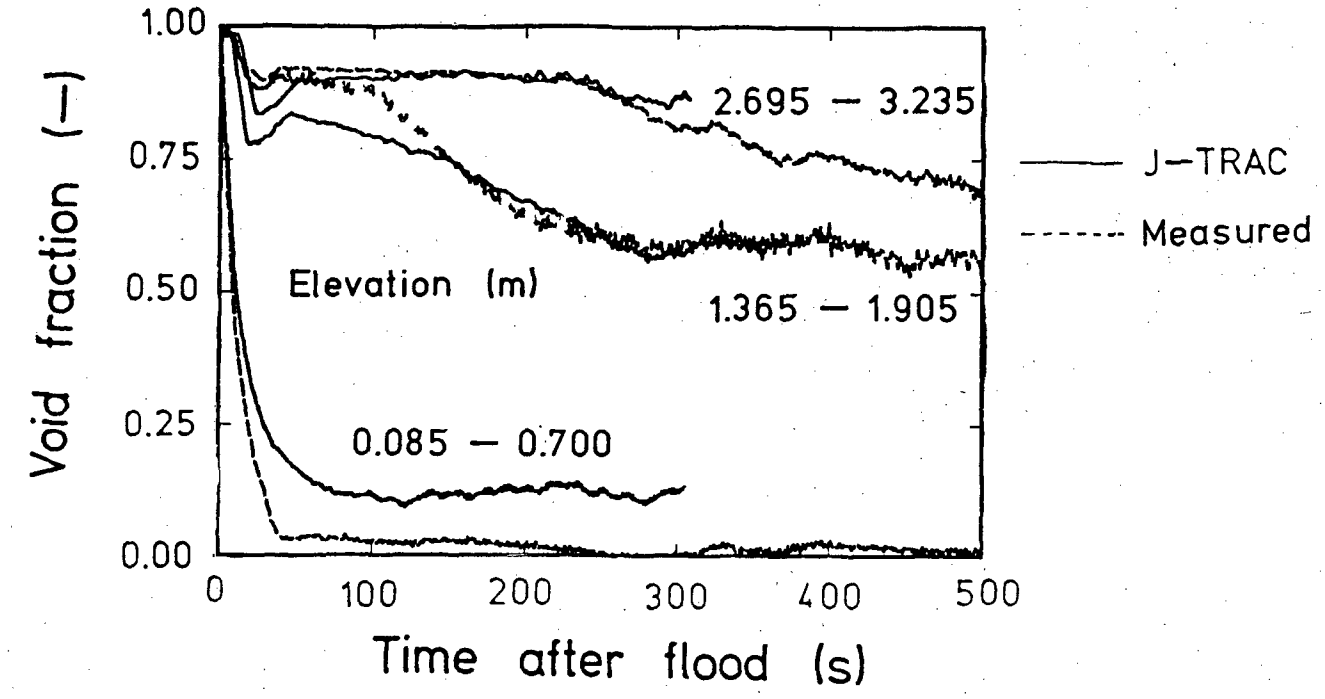


(a) Void fraction

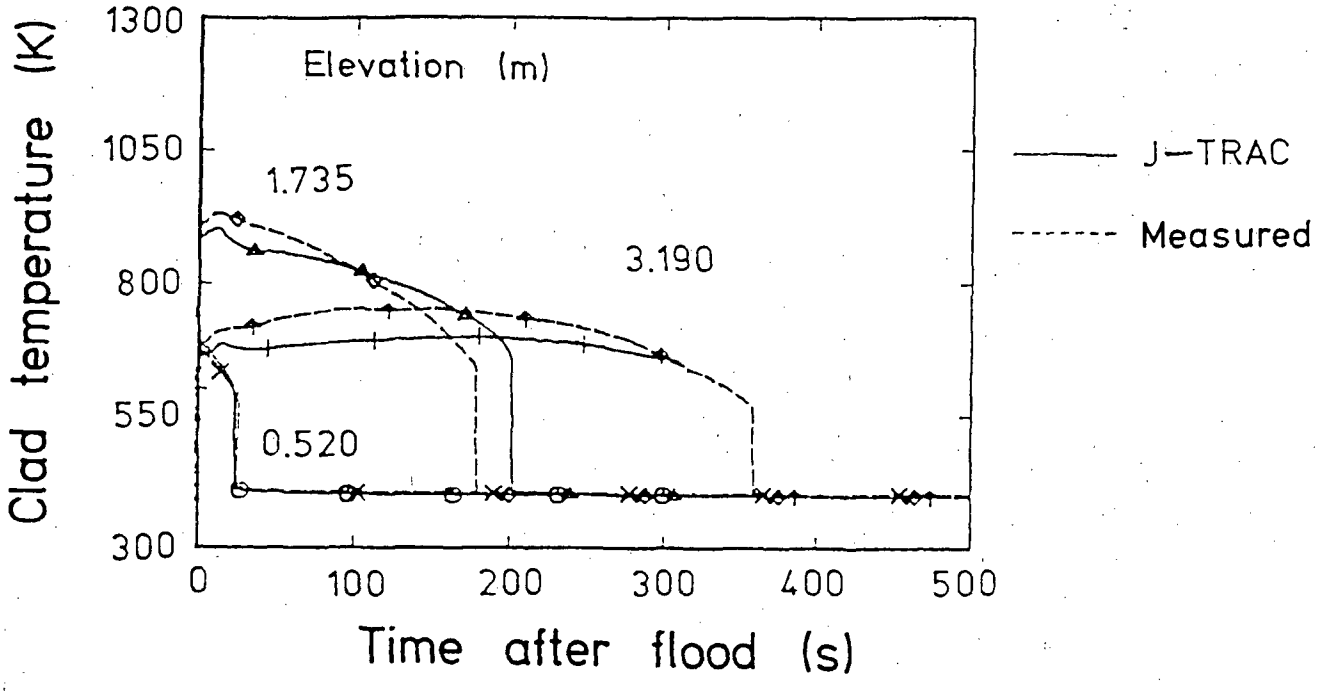


(b) Clad temperature

Fig.5 Comparison for SCTF flat power test

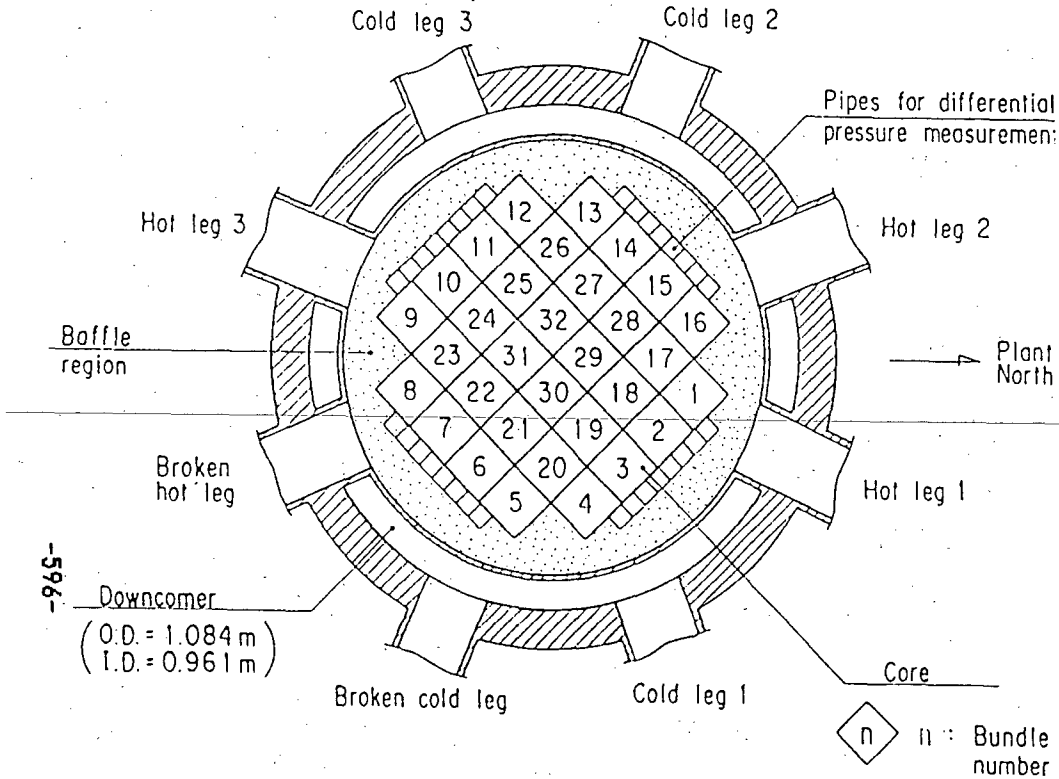


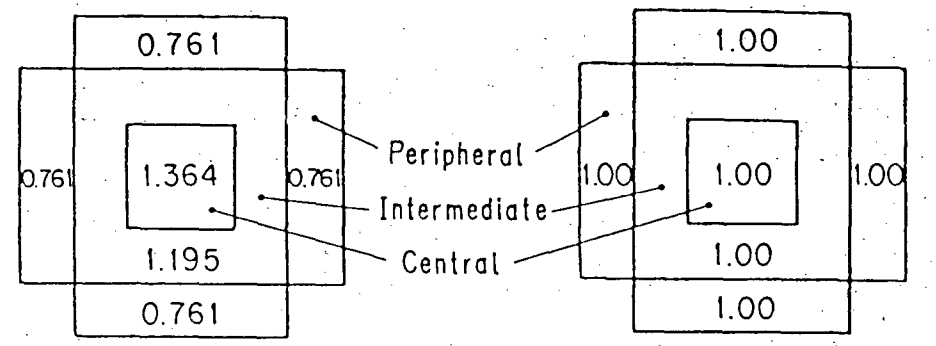


(1) Steep radial power test (2) Flat radial power test

(a) Radial peaking factor

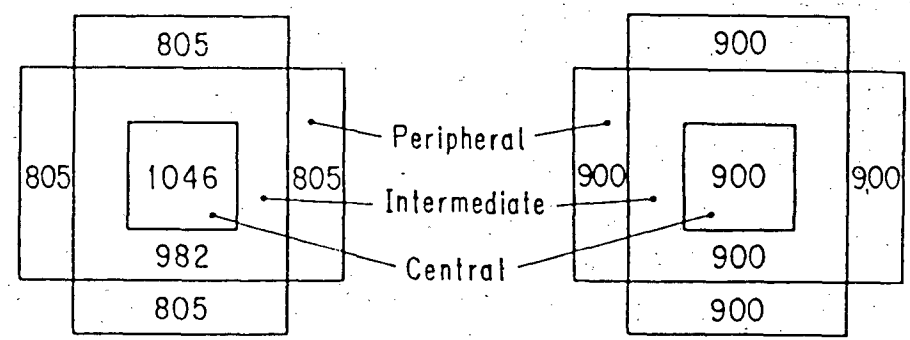


(1) Steep radial power test (2) Flat radial power test

(b) Initial clad surface temperature at midplane of core (in K)

Fig.6 Core radial power profile in CCTF

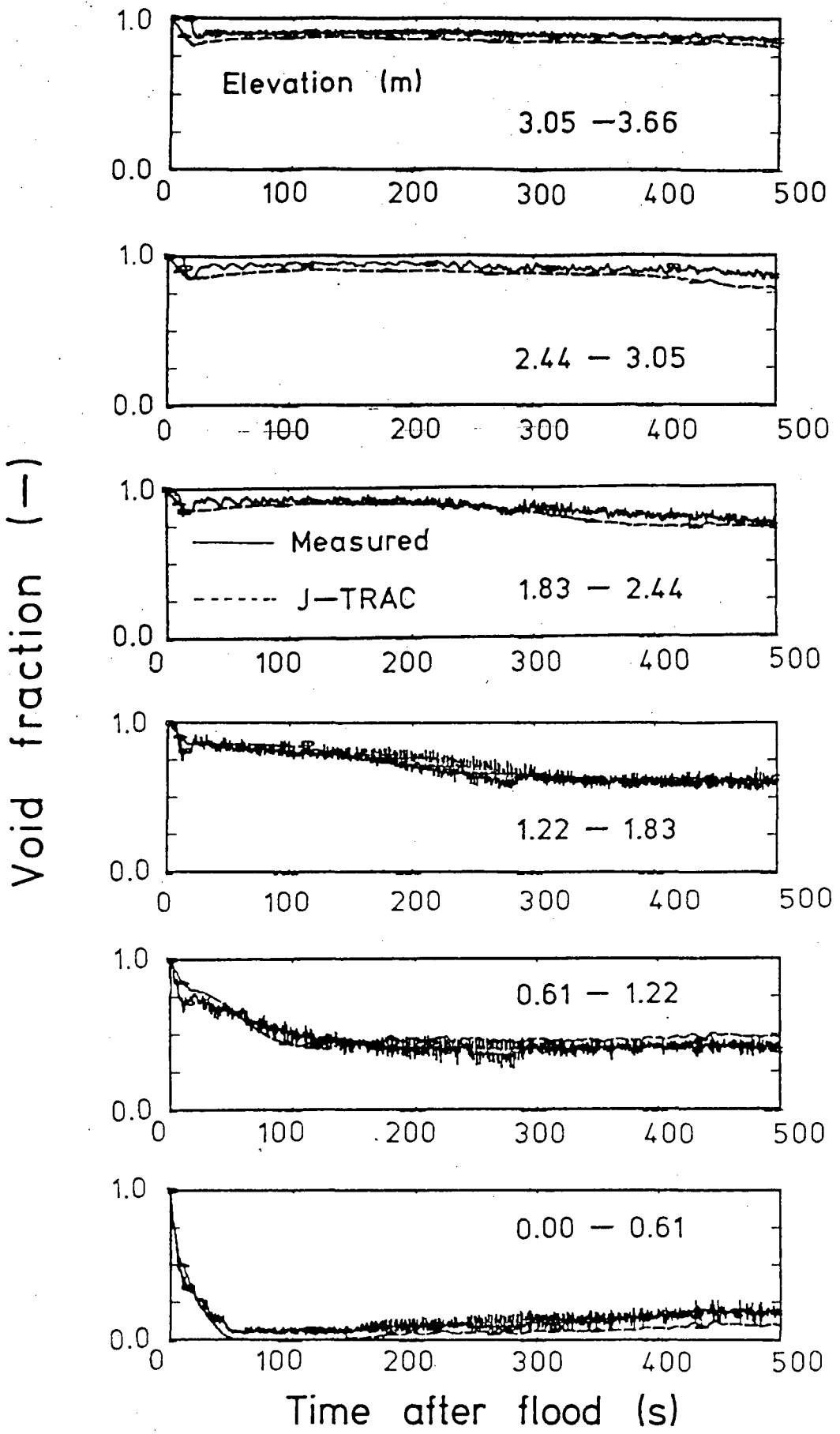


Fig.7 Core void fractions in CCTF base case test

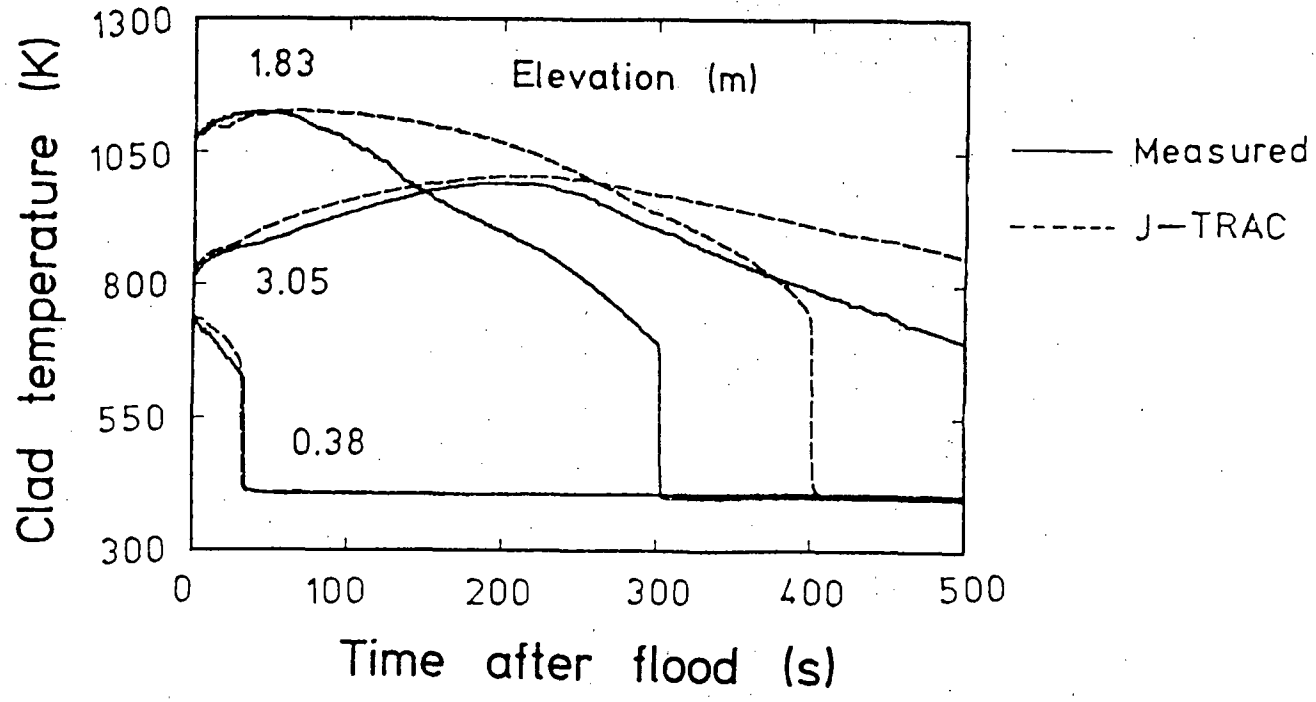


(a) High power rod

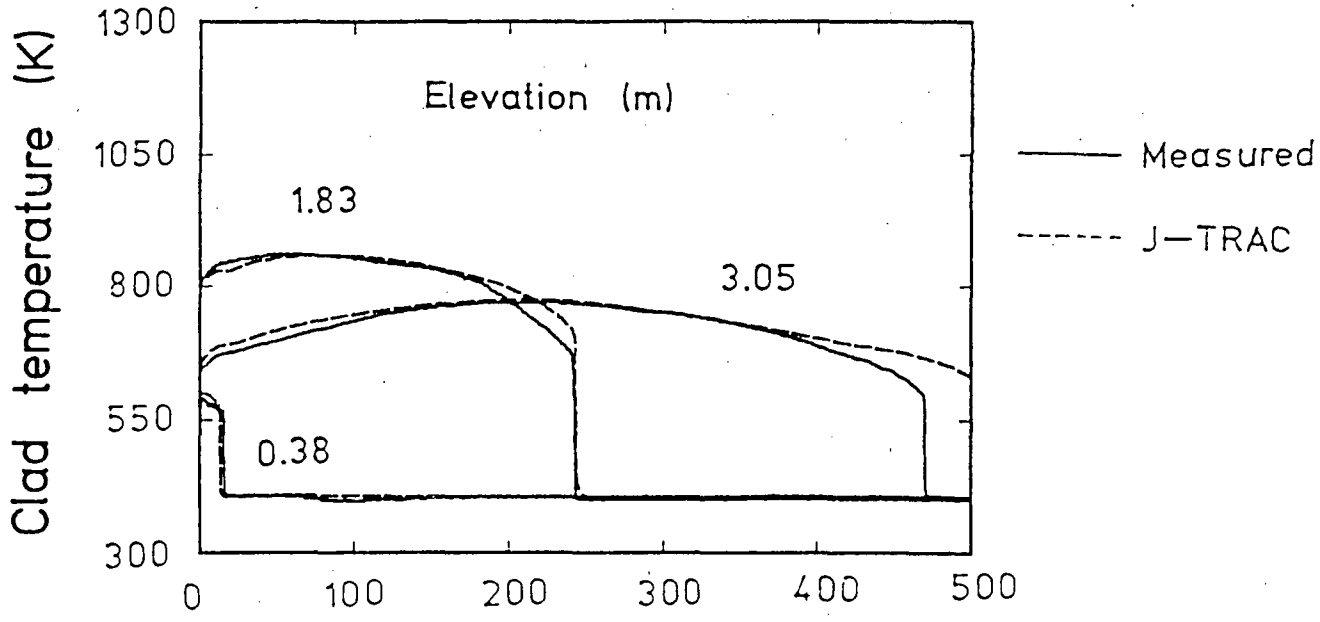


(b) Low power rod

Fig.8 Clad temperatures in CCTF base case test

| | J—TRAC | Measured |
|---|---|---|
| High power rod | ——— | ○ |
| Low power rod | ---------- | △ |

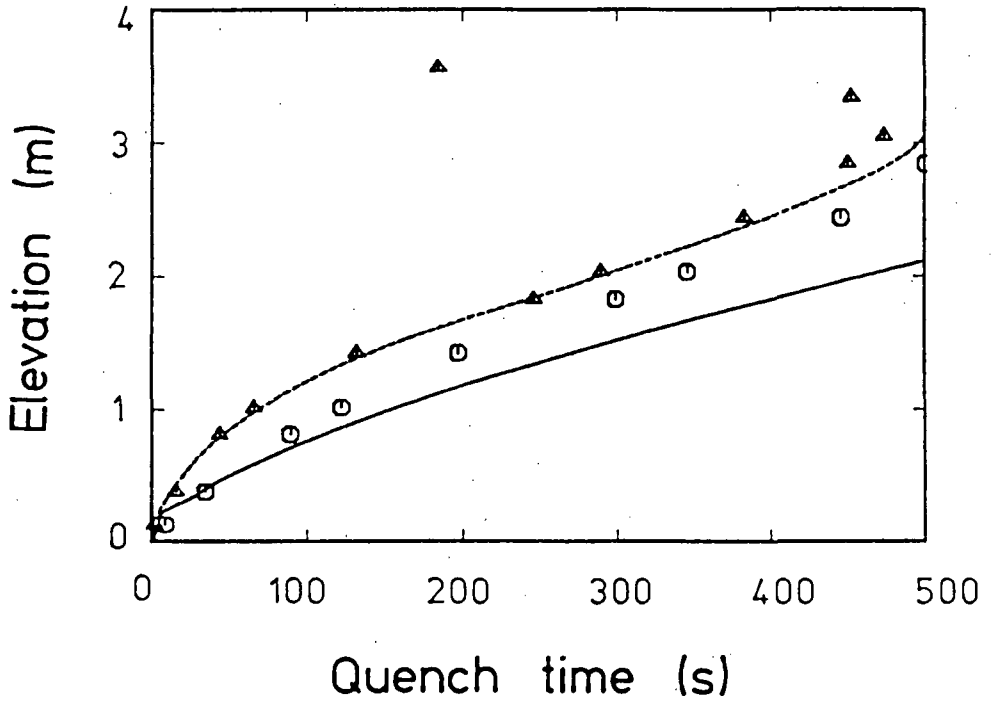


Fig.9 Quench envelope in CCTF base case test

| | J—TRAC | Measured |
|---|---|---|
| 0.42MPa | ——— | ○ |
| 0.15MPa | ---------- | △ |

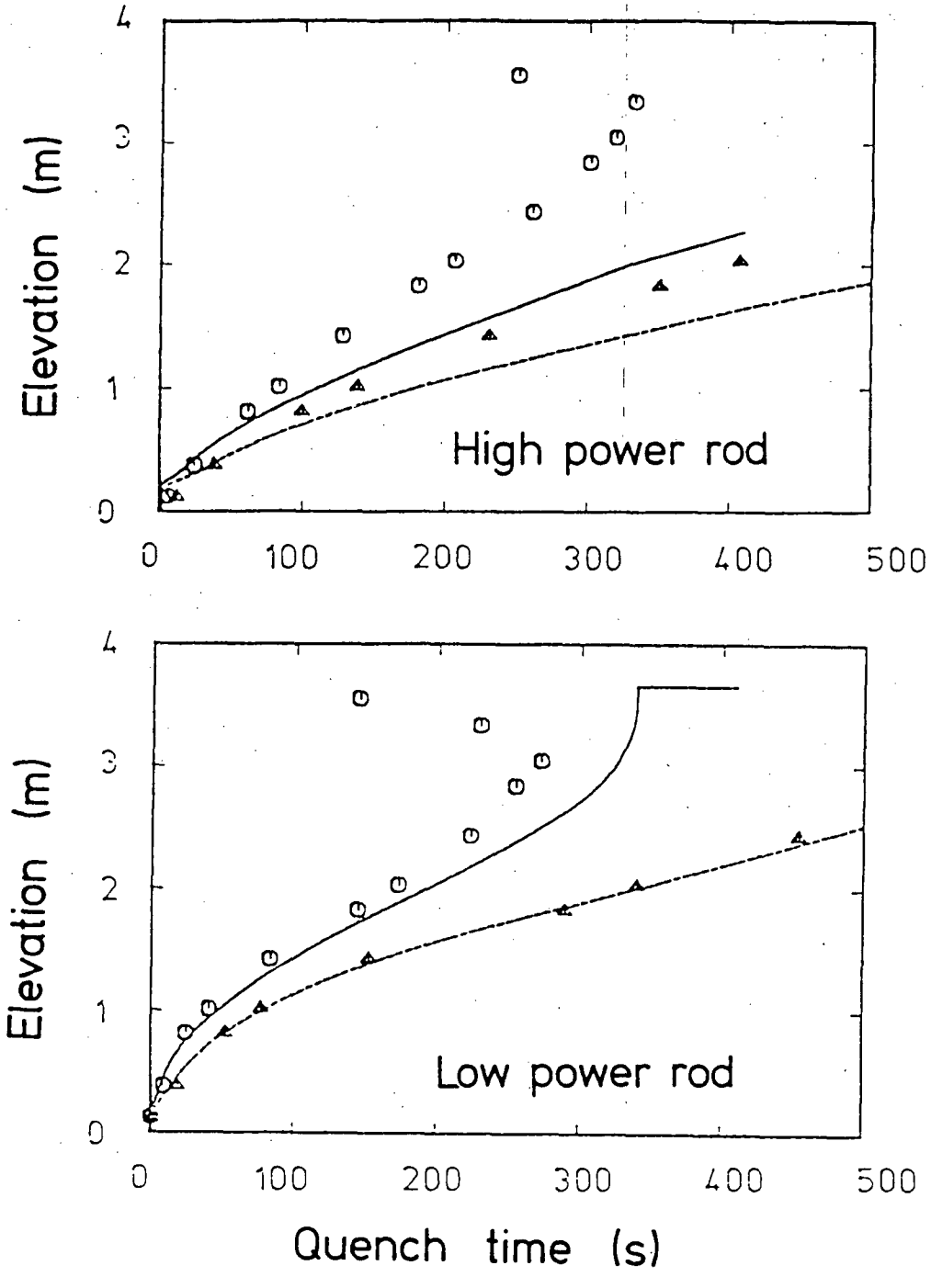


Fig.10 System pressure effect on quench behavior

| | J—TRAC | Measured |
|---|---|---|
| High power test | ——— | ○ |
| Low power test | ····· | △ |

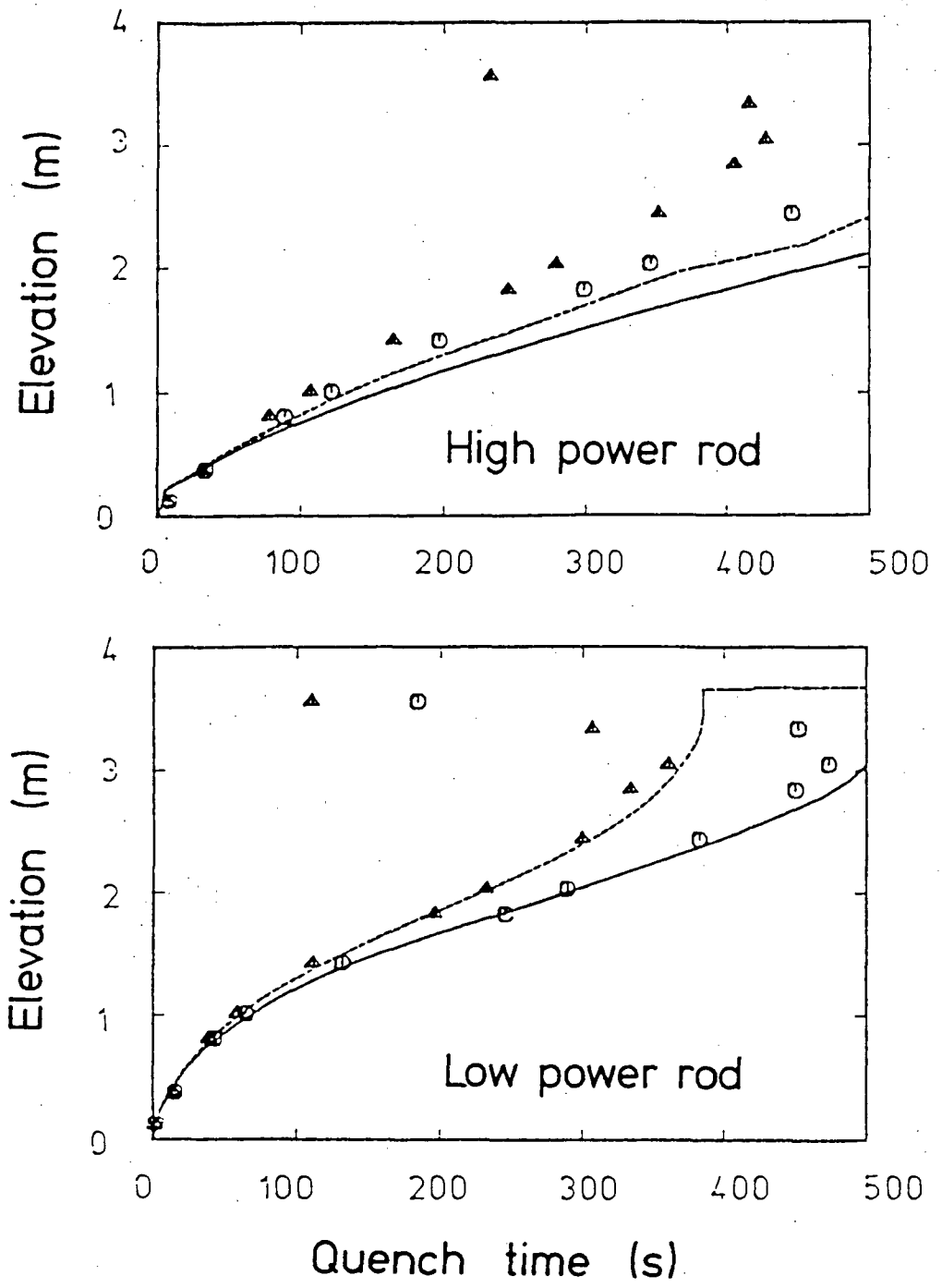


Fig.11 Core power effect on quench behavior

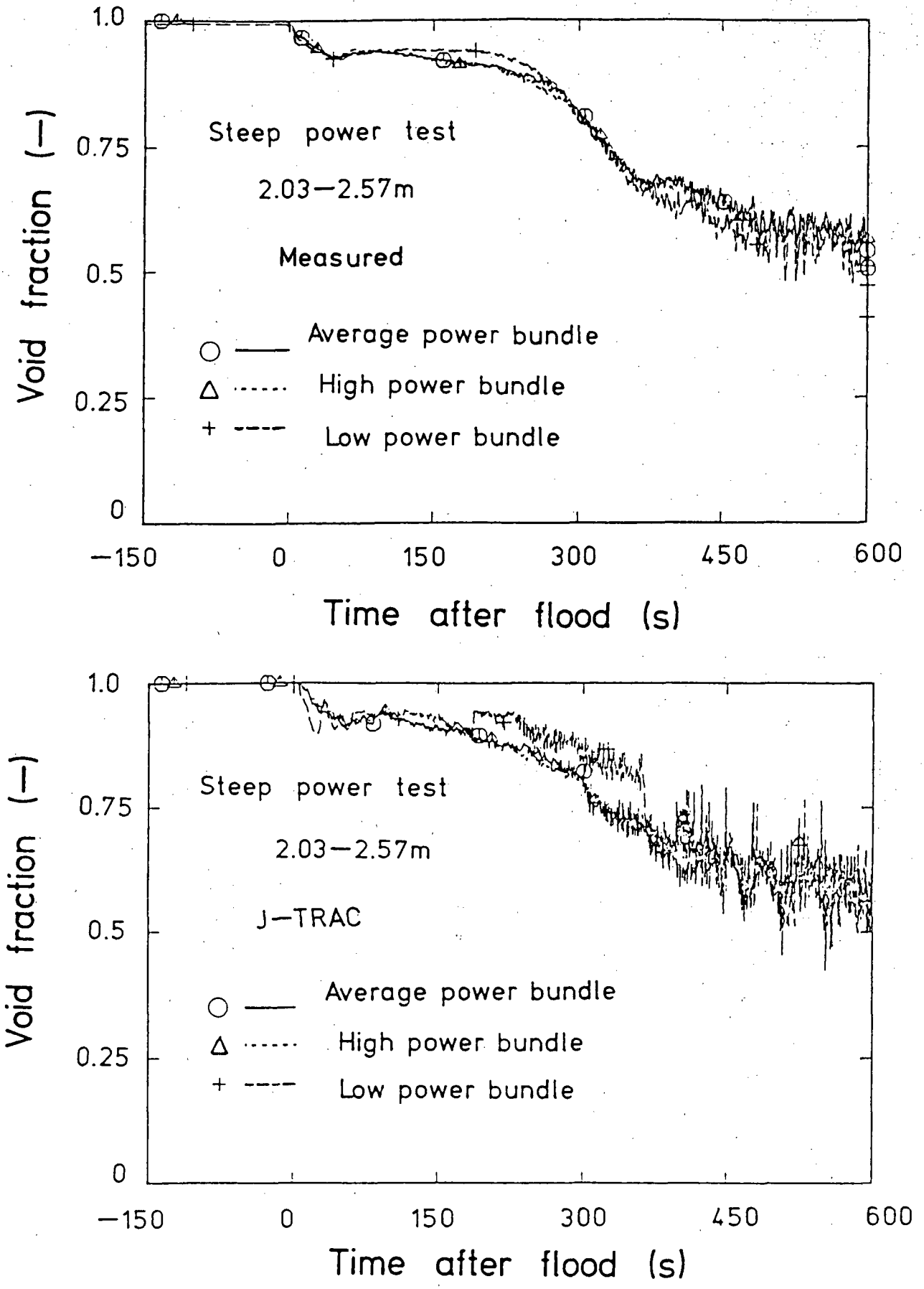


Fig.12 Radial profile of core void fraction in SCTF steep power test

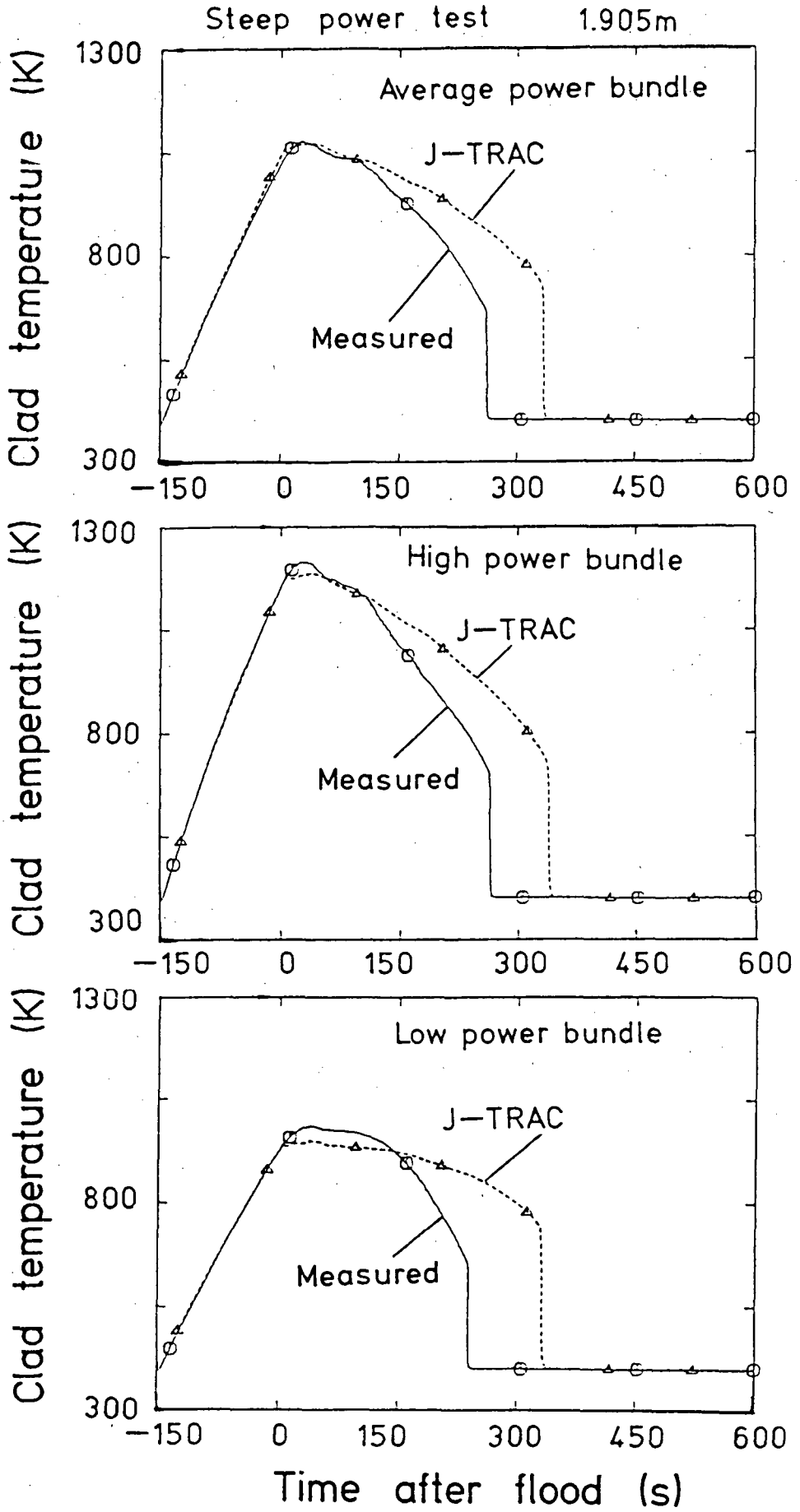


Fig.13 Clad temperature at elevation of 1.905m in SCTF steep power test

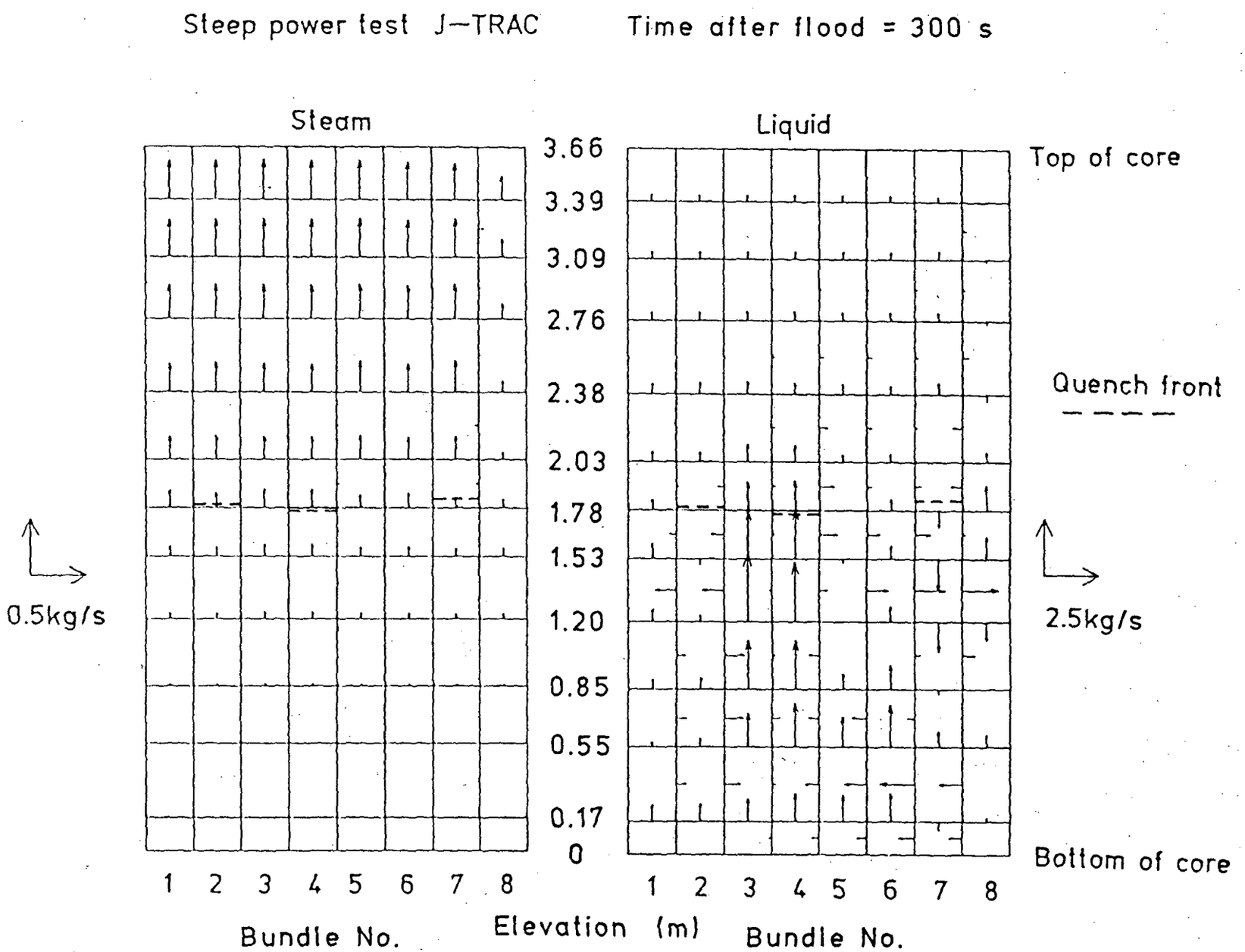


Fig.14 Steam and water mass flow rates in SCTF steep power test

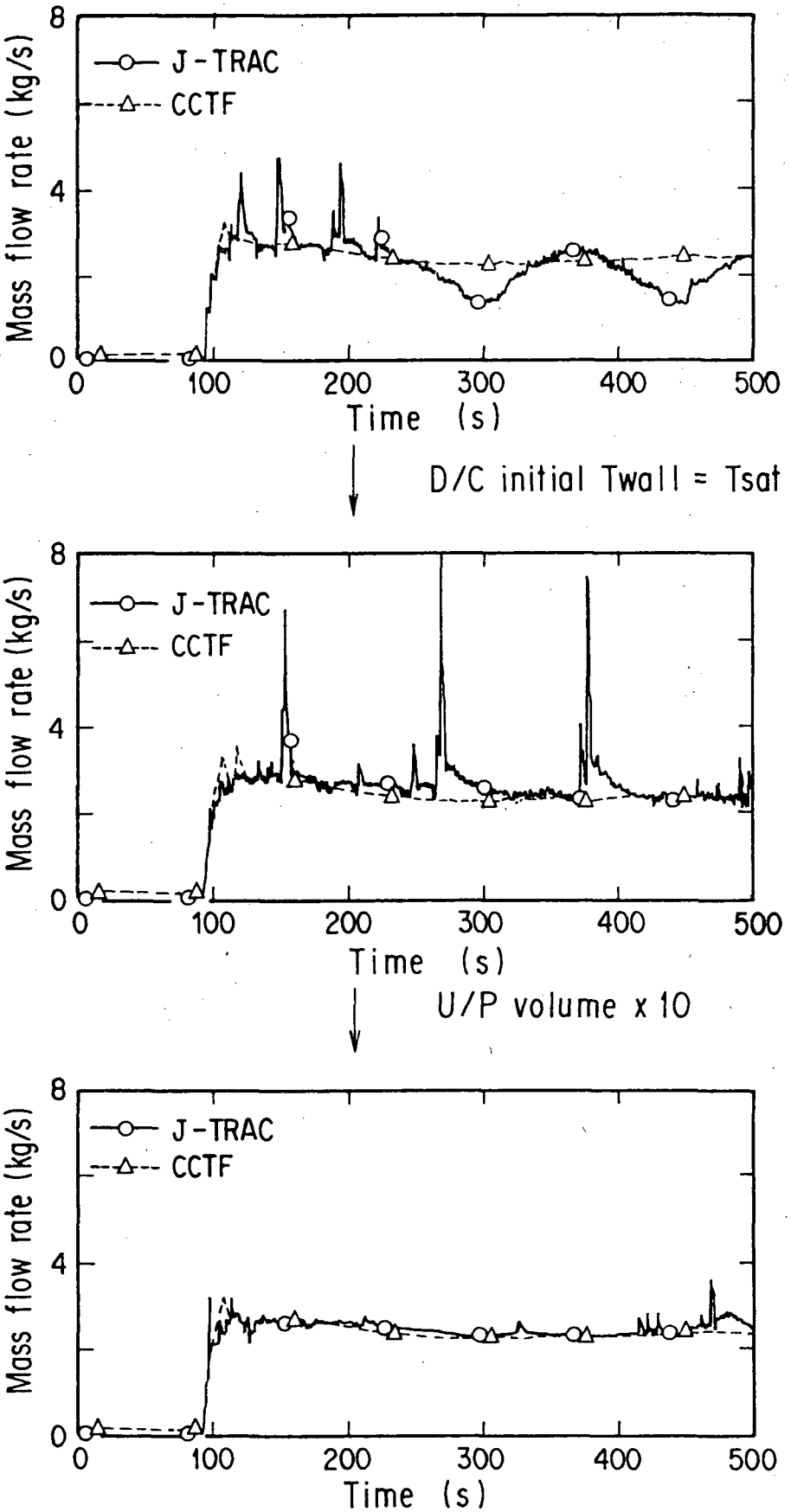


Fig.15 Loop mass flow rate in CCTF system calculation

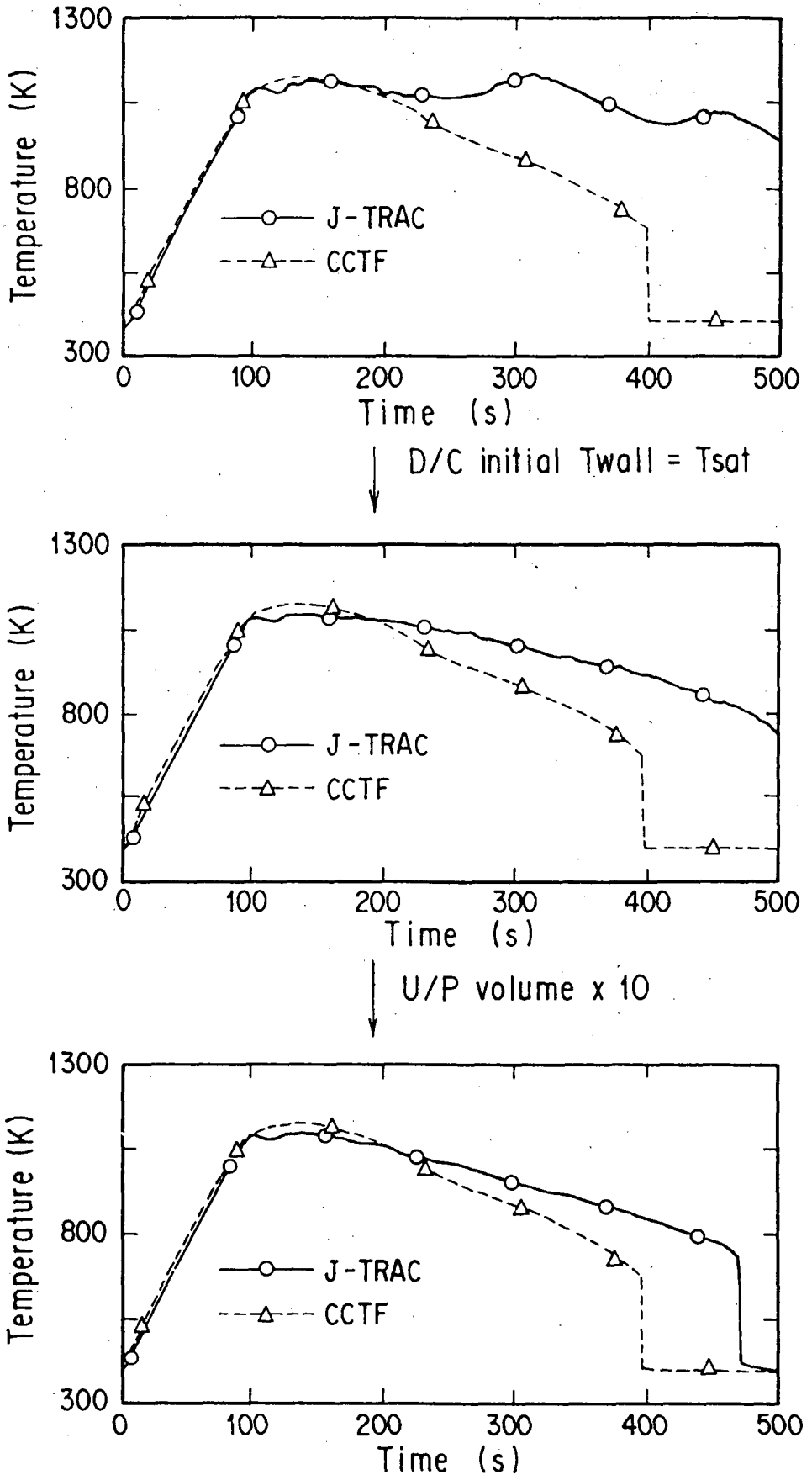


Fig.16 Clad temperature at midplane in CCTF system calculation

NRC FORM 335 (8-87) NRCM 1102, 3201, 3202

U.S. NUCLEAR REGULATORY COMMISSION

# BIBLIOGRAPHIC DATA SHEET

SEE INSTRUCTIONS ON THE REVERSE

1. REPORT NUMBER (Assigned by PPMB; DPS, add Vol. No., if any)

NUREG/CP-0097
Vol. 4

2. TITLE AND SUBTITLE

Proceedings of the Sixteenth Water Reactor Safety Information Meeting

3. LEAVE BLANK

4. DATE REPORT COMPLETED

| MONTH | YEAR |
|---|---|
| February | 1989 |

5. AUTHOR(S)

Compiled by Allen J. Weiss, BNL

6. DATE REPORT ISSUED

| MONTH | YEAR |
|---|---|
| March | 1989 |

7. PERFORMING ORGANIZATION NAME AND MAILING ADDRESS (Include Zip Code)

Office of Nuclear Regulatory Research
U. S. Nuclear Regulatory Commission
Washington, D. C. 20555

8. PROJECT/TASK/WORK UNIT NUMBER

9. FIN OR GRANT NUMBER

A-3282

10. SPONSORING ORGANIZATION NAME AND MAILING ADDRESS (Include Zip Code)

Same as Item 7 above

11a. TYPE OF REPORT

Proceedings of conference on safety research

b. PERIOD COVERED (Inclusive dates)

October 24-27, 1988

12 SUPPLEMENTARY NOTES

Proceedings prepared by Brookhaven National Laboratory

13. ABSTRACT (200 words or less)

This five-volume report contains 141 papers out of the 175 that were presented at the Sixteenth Water Reactor Safety Information Meeting held at the National Institute of Standards and Technology, Gaithersburg, Maryland, during the week of October 24-27, 1988. The papers are printed in the order of their presentation in each session and describe progress and results of programs in nuclear safety research conducted in this country and abroad. Foreign participation in the meeting included twenty different papers presented by researchers from Germany, Italy, Japan, Sweden, Switzerland, Taiwan and the United Kingdom. The titles of the papers and the names of the authors have been updated and may differ from those that appeared in the final program of the meeting.

14. DOCUMENT ANALYSIS - a. KEYWORDS/DESCRIPTORS

reactor safety research
nuclear safety research
decontamination and decommissioning

b. IDENTIFIERS/OPEN-ENDED TERMS

15. AVAILABILITY STATEMENT

Unlimited

16. SECURITY CLASSIFICATION

(This page)
Unclassified
(This report)
Unclassified

17. NUMBER OF PAGES

18 PRICE